



*proceedings*

# The 14th International Conference Interdisciplinarity in Engineering - INTER-ENG 2020

Târgu Mureș, Romania | 8–9 October 2020

---

Edited by

Liviu Moldovan and Adrian Gligor

Printed Edition of the Special Issue Published in *Proceedings*

**The 14th International Conference  
Interdisciplinarity in Engineering—  
INTER-ENG 2020**



# The 14th International Conference Interdisciplinarity in Engineering— INTER-ENG 2020

Editors

**Liviu Moldovan**

**Adrian Gligor**

MDPI • Basel • Beijing • Wuhan • Barcelona • Belgrade • Manchester • Tokyo • Cluj • Tianjin





*Editors*

Liviu Moldovan  
“George Emil Palade” University of  
Medicine, Pharmacy, Science, and  
Technology of Târgu Mureş  
Romania

Adrian Gligor  
“George Emil Palade” University of  
Medicine, Pharmacy, Science, and  
Technology of Târgu Mureş  
Romania

*Editorial Office*

MDPI  
St. Alban-Anlage 66  
4052 Basel, Switzerland

This is a reprint of articles from the Special Issue published online in the open access journal *Proceedings* (ISSN 2504-3900) (available at: <https://www.mdpi.com/2504-3900/63/1>).

For citation purposes, cite each article independently as indicated on the article page online and as indicated below:

LastName, A.A.; LastName, B.B.; LastName, C.C. Article Title. <i>Journal Name</i> <b>Year</b> , <i>Volume Number</i> , Page Range.
--

**ISBN 978-3-0365-0716-3 (Hbk)**

**ISBN 978-3-0365-0717-0 (PDF)**

© 2021 by the authors. Articles in this book are Open Access and distributed under the Creative Commons Attribution (CC BY) license, which allows users to download, copy and build upon published articles, as long as the author and publisher are properly credited, which ensures maximum dissemination and a wider impact of our publications.

The book as a whole is distributed by MDPI under the terms and conditions of the Creative Commons license CC BY-NC-ND.

# Contents

About the Editors . . . . . xiii

**Liviu Moldovan and Adrian Gligor**

Europe's Future Is Digital: A Broad Vision of the Industry 4.0 Concept beyond Direct Manufacturing in the Company  
Reprinted from: *Proceedings* 2020, 63, 29, doi:10.3390/proceedings2020063029 . . . . . 1

**Ferencz Peti and Petru Serban**

Coordinate Measuring Machine Probes Effect during Inner Thread Position Measurement  
Reprinted from: *Proceedings* 2020, 63, 55, doi:10.3390/proceedings2020063055 . . . . . 5

**Marius Tintelecan, Dana-Adriana Iluțiu-Varvara, Oscar Rodriguez-Alabanda, Ioana Monica Sas-Boca, Ionuț Marian and Aristides Santana Martinez Gustavo**

Achieving a Toothed Gear on Presses  
Reprinted from: *Proceedings* 2020, 63, 57, doi:10.3390/proceedings2020063057 . . . . . 11

**Dana-Adriana Iluțiu-Varvara, Marius Tintelecan, Claudiu Aciu and Ioana-Monica Sas-Boca**

Reuse of the Steel Mill Scale for Sustainable Industrial Applications  
Reprinted from: *Proceedings* 2020, 63, 14, doi:10.3390/proceedings2020063014 . . . . . 19

**Bogdan Bucur, Constantin Bucur and Gabriela Andronic**

Peculiarities Regarding the Reconstruction of a Broken Grooved Shaft  
Reprinted from: *Proceedings* 2020, 63, 65, doi:10.3390/proceedings2020063065 . . . . . 23

**Rami Alfattani**

Modeling and Simulating the Static Structural Response and Lift Off of a Preloaded Bolted Joint on a Flange  
Reprinted from: *Proceedings* 2020, 63, 10, doi:10.3390/proceedings2020063010 . . . . . 31

**Cristina Havadtöi**

Innovation of Pull and Torque Testing Device for Cable Cords  
Reprinted from: *Proceedings* 2020, 63, 28, doi:10.3390/proceedings2020063028 . . . . . 41

**Oscar Rodríguez-Alabanda, Esther Molero, Marius Tintelecan, Guillermo Guerrero-Vaca, Pablo E. Romero and Gustavo Aristides Santana Martinez**

Fine Electrolytic Tough Pitch Copper Multistage Wire Drawing Pass Schedule Design by Analytical and Numerical Methods  
Reprinted from: *Proceedings* 2020, 63, 12, doi:10.3390/proceedings2020063012 . . . . . 49

**Daniel Lateș, Laura Irina Vlașin and Alexandru Ianoși-Andreeva-Dimitrova**

Design of a Hybrid Two-Degree-of-Freedom Lower Limb Exerciser  
Reprinted from: *Proceedings* 2020, 63, 27, doi:10.3390/proceedings2020063027 . . . . . 61

**Marius-Ion Ghițescu, Marilena Ghițescu and Arina Modrea**

A New Light Aircraft and Its Design Method  
Reprinted from: *Proceedings* 2020, 63, 66, doi:10.3390/proceedings2020063066 . . . . . 67

**Djamel-Eddine Aizi and Meriem Kaid-Harche**

Mechanical Behavior of Gypsum Composites Reinforced with *Retama monosperma* Fibers  
Reprinted from: *Proceedings* 2020, 63, 40, doi:10.3390/proceedings2020063040 . . . . . 79

<b>Alexandra Coșa, Bogdan Hegheș, Camelia Negruțiu and Zoltan Kiss</b> Strain and Displacement Measurements in Reinforced Self-Compacting Concrete Beams with Openings Using Digital Image Correlation Technique Reprinted from: <i>Proceedings</i> 2020, 63, 39, doi:10.3390/proceedings2020063039 . . . . .	87
<b>Adrian-Victor Lăzărescu, Henriette Szilagyi, Cornelia Baeră and Andreea Hegyi</b> Parametric Studies Regarding the Development of Alkali-Activated Fly Ash-Based Geopolymer Concrete Using Romanian Local Raw Materials Reprinted from: <i>Proceedings</i> 2020, 63, 11, doi:10.3390/proceedings2020063011 . . . . .	97
<b>Brăduț Alexandru Ionescu, Adrian-Victor Lăzărescu and Andreea Hegyi</b> The Possibility of Using Slag for the Production of Geopolymer Materials and Its Influence on Mechanical Performances—A Review Reprinted from: <i>Proceedings</i> 2020, 63, 30, doi:10.3390/proceedings2020063030 . . . . .	107
<b>Elvira Grebenișan, Andreea Hegyi, Henriette Szilagyi, Adrian-Victor Lăzărescu and Brăduț Alexandru Ionescu</b> Influence of the Addition of TiO <sub>2</sub> Nanoparticles on the Self-Cleaning Performance of Cementitious Composite Surfaces Reprinted from: <i>Proceedings</i> 2020, 63, 42, doi:10.3390/proceedings2020063042 . . . . .	117
<b>Alexandra Olga Pinteă, Marta Ioana Moldoveanu and Daniela Lucia Manea</b> Behavior of Natural Organic Polymer-Based Plaster Mortars under the Influence of Water Reprinted from: <i>Proceedings</i> 2020, 63, 78, doi:10.3390/proceedings2020063078 . . . . .	129
<b>Marta Ioana Moldoveanu, Alexandra Olga Pinteă and Daniela Lucia Manea</b> Innovative Materials with Complex Applicability Reprinted from: <i>Proceedings</i> 2020, 63, 76, doi:10.3390/proceedings2020063076 . . . . .	137
<b>Gabriela Călătan, Andreea Hegyi, Elvira Grebenisan and Anamaria Cătălina Mircea</b> Possibilities of Recovery of Industrial Waste and By-Products in Adobe-Brick-Type Masonry Elements Reprinted from: <i>Proceedings</i> 2020, 63, 1, doi:10.3390/proceedings2020063001 . . . . .	145
<b>Tudor Panfil Toader and Anamaria Cătălina Mircea</b> Self-Healing Concrete Mix-Design Based on Engineered Cementitious Composites Principles Reprinted from: <i>Proceedings</i> 2020, 63, 5, doi:10.3390/proceedings2020063005 . . . . .	155
<b>Anamaria Boca, Tudor Panfil Toader and Călin Mircea</b> Romanesque Historical Monuments Reconstruction by Using Original Materials and Recycling of Those that Have Lost Their Historical Value Reprinted from: <i>Proceedings</i> 2020, 63, 7, doi:10.3390/proceedings2020063007 . . . . .	163
<b>Ligia Hanuseac, Marinela Barbuta, Liliana Bejan, Raluca Rosu and Alexandru Timu</b> Experimental Study on Hollow Blocks with Wastes Reprinted from: <i>Proceedings</i> 2020, 63, 79, doi:10.3390/proceedings2020063079 . . . . .	171
<b>Anamaria Cătălina Mircea and Tudor Panfil Toader</b> Fracture Energy of Engineered Cementitious Composites Reprinted from: <i>Proceedings</i> 2020, 63, 8, doi:10.3390/proceedings2020063008 . . . . .	177
<b>Ioana Miruna Tătaru, Elena Fleacă, Bogdan Fleacă and Radu D. Stanciu</b> Modelling the Implementation of a Sustainable Development Strategy through Process Mapping Reprinted from: <i>Proceedings</i> 2020, 63, 6, doi:10.3390/proceedings2020063006 . . . . .	185

<b>Ioan-David Legman and Manuela Rozalia Gabor</b> New Optimization Technique for Sustainable Manufacturing: The Implementation of the Spc Indicator (System of Evaluating Employee Performance Depending on Customer Satisfaction) as an Important Element of Satisfaction Measurement Reprinted from: <i>Proceedings</i> 2020, 63, 4, doi:10.3390/proceedings2020063004 . . . . .	195
<b>Karam Al-Akel and Liviu-Onoriu Marian</b> The Lean Six Sigma Algorithm—A Pathway for Decreasing the Continuous Improvement Projects Failure Rate Reprinted from: <i>Proceedings</i> 2020, 63, 47, doi:10.3390/proceedings2020063047 . . . . .	203
<b>Karam Al-Akel and Liviu-Onoriu Marian</b> The Lean Six Sigma Algorithm—A Roadmap for Implementation Reprinted from: <i>Proceedings</i> 2020, 63, 24, doi:10.3390/proceedings2020063024 . . . . .	209
<b>Narcis Sebastian Păvălașcu and Manuela Rozalia Gabor</b> A Case Study on the Particularities and Sustainability of the Concepts of TQM, Quality Control, and Risk Management in the Corporate Insurance Industry: Loss and the Incidence of Catastrophic Risks Reprinted from: <i>Proceedings</i> 2020, 63, 3, doi:10.3390/proceedings2020063003 . . . . .	219
<b>Flaviu Moldovan</b> Framework Specifications for Evaluation of Quality Improvement and Sustainable Development in Healthcare Facilities Reprinted from: <i>Proceedings</i> 2020, 63, 2, doi:10.3390/proceedings2020063002 . . . . .	229
<b>Razvan Cazacu</b> Matlab Framework for Image Processing and Feature Extraction Flexible Algorithm Design Reprinted from: <i>Proceedings</i> 2020, 63, 72, doi:10.3390/proceedings2020063072 . . . . .	235
<b>Fatmir Azemi, Roberto Lujic, Goran Šimunović and Daniel Tokody</b> Selection the Basic Lean Manufacturing Techniques in Developing the Model for Industry 4.0 in Kosovo Manufacturing Industry Reprinted from: <i>Proceedings</i> 2020, 63, 62, doi:10.3390/proceedings2020063062 . . . . .	243
<b>Mihaela Bucur</b> The Importance of Corporate Social Responsibility among Students in EUROPE Reprinted from: <i>Proceedings</i> 2020, 63, 75, doi:10.3390/proceedings2020063075 . . . . .	251
<b>Marius Miklos Veres, Cristina Veres, Antoaneta Maria Rauca, Liviu Onoriu Marian and Ancuta Sigmirean</b> Research on Qualified Vocational Training Development in the Context of Digitalization Reprinted from: <i>Proceedings</i> 2020, 63, 68, doi:10.3390/proceedings2020063068 . . . . .	257
<b>Ionuț-Cosmin Chiva, Marius Minea, Viviana-Laetitia Minea and Augustin Semenescu</b> Anonymous Detection of Traveler Flows Employing Bluetooth Technologies Reprinted from: <i>Proceedings</i> 2020, 63, 61, doi:10.3390/proceedings2020063061 . . . . .	263
<b>Edina Albininé Budavári and Zoltán Rajnai</b> Social Engineering—The Hidden Control Reprinted from: <i>Proceedings</i> 2020, 63, 60, doi:10.3390/proceedings2020063060 . . . . .	273
<b>Lucreția Dogaru</b> Green Economy and Green Growth—Opportunities for Sustainable Development Reprinted from: <i>Proceedings</i> 2020, 63, 70, doi:10.3390/proceedings2020063070 . . . . .	279

**Lucreția Dogaru**

About Sustainability between Responsible Production and Consumption  
Reprinted from: *Proceedings* 2020, 63, 69, doi:10.3390/proceedings2020063069 . . . . . 287

**Mihai Anitei, Cristina Veres and Adrian Pisla**

Research on Challenges and Prospects of Digital Agriculture  
Reprinted from: *Proceedings* 2020, 63, 67, doi:10.3390/proceedings2020063067 . . . . . 295

**Jozsef Boer and Petruta Blaga**

Streamlining the Work Process by Reducing Procedural Times in the Field of Electrostatic Powder Painting  
Reprinted from: *Proceedings* 2020, 63, 71, doi:10.3390/proceedings2020063071 . . . . . 301

**Petruta Blaga**

Making Production More Efficient Using Analysis and Continuous Improvement Methods  
Reprinted from: *Proceedings* 2020, 63, 73, doi:10.3390/proceedings2020063073 . . . . . 309

**Petruta Blaga**

Ways to Increase the Efficiency of Production Activity through the Active Involvement of the Human Factor  
Reprinted from: *Proceedings* 2020, 63, 74, doi:10.3390/proceedings2020063074 . . . . . 319

**Liviu Moldovan**

An Innovative Guide to Work-Based Learning in the Field of Industry 4.0  
Reprinted from: *Proceedings* 2020, 63, 58, doi:10.3390/proceedings2020063058 . . . . . 329

**Liviu Moldovan**

Good Practices and Results for the Implementation of a Framework of Sustainable Development in Higher Education  
Reprinted from: *Proceedings* 2020, 63, 59, doi:10.3390/proceedings2020063059 . . . . . 337

**Dana Rus**

English for Specific Purposes in the Context of the Shifting Educational Paradigm Triggered by Industry 4.0  
Reprinted from: *Proceedings* 2020, 63, 64, doi:10.3390/proceedings2020063064 . . . . . 345

**Bianca Han**

Translation, from Pen-and-Paper to Computer-Assisted Tools (CAT Tools) and Machine Translation (MT)  
Reprinted from: *Proceedings* 2020, 63, 56, doi:10.3390/proceedings2020063056 . . . . . 351

**Mihaela Bucur**

Studies on the Use of ISO 7730 in Romanian Companies  
Reprinted from: *Proceedings* 2020, 63, 63, doi:10.3390/proceedings2020063063 . . . . . 359

**Lucian Ioan Dulău and Dorin Bică**

Algorithm for Smart Home Power Management with Electric Vehicle and Photovoltaic Panels  
Reprinted from: *Proceedings* 2020, 63, 49, doi:10.3390/proceedings2020063049 . . . . . 365

**Rachid Herbazi, Youssef Kharchouf, Khalid Amechnoue, Ahmed Khouya and Adil Chahboun**

Solar Photovoltaic Cell Parameters Extraction Using Differential Evolution Algorithm  
Reprinted from: *Proceedings* 2020, 63, 43, doi:10.3390/proceedings2020063043 . . . . . 371

<b>Attila Albini, Edina Albininé Budavári and Zoltán Rajnai</b> Energetic Sustainability of Systems Reprinted from: <i>Proceedings</i> 2020, 63, 50, doi:10.3390/proceedings2020063050 . . . . .	379
<b>Adrian Gligor, Piotr Cofta, Tomasz Marciniak and Cristian-Dragoş Dumitru</b> Challenges for the Large-Scale Integration of Distributed Renewable Energy Resources in the Next Generation Virtual Power Plants Reprinted from: <i>Proceedings</i> 2020, 63, 20, doi:10.3390/proceedings2020063020 . . . . .	387
<b>Pavel Atănăsoae, Radu Dumitru Pentiuic and Eugen Hopulele</b> Considerations Regarding the Negative Prices on the Electricity Market Reprinted from: <i>Proceedings</i> 2020, 63, 26, doi:10.3390/proceedings2020063026 . . . . .	395
<b>Mariana Dumitrescu</b> Overview on Efficient Naval Power Architecture Reprinted from: <i>Proceedings</i> 2020, 63, 22, doi:10.3390/proceedings2020063022 . . . . .	405
<b>Mariana Dumitrescu</b> Isolated Power System Safety Analysis Reprinted from: <i>Proceedings</i> 2020, 63, 21, doi:10.3390/proceedings2020063021 . . . . .	413
<b>Zakia Ngadi and Mohamed Lhassan Lahlaoui</b> Coal and Biomass Co-Combustion: CFD Prediction of Velocity Field for Multi-Channel Burner in Cement Rotary Kiln Reprinted from: <i>Proceedings</i> 2020, 63, 18, doi:10.3390/proceedings2020063018 . . . . .	419
<b>Mihail Chira, Andreea Hegyi, Henriette Szilagyi and Horaţiu Vermeşan</b> Thermoelectric Generator Based on CuSO <sub>4</sub> and Na <sub>2</sub> SiO <sub>3</sub> Reprinted from: <i>Proceedings</i> 2020, 63, 35, doi:10.3390/proceedings2020063035 . . . . .	427
<b>Cezar Afilipoaei and Horatiu Teodorescu-Draghicescu</b> A Review over Electromagnetic Shielding Effectiveness of Composite Materials Reprinted from: <i>Proceedings</i> 2020, 63, 23, doi:10.3390/proceedings2020063023 . . . . .	435
<b>Hanae El Fakiri, Lahoucine Ouhsaine and Abdelmajid El Bouardi</b> Thermal Dynamic Behavior in Bi-Zone Habitable Cell with and without Phase Change Materials Reprinted from: <i>Proceedings</i> 2020, 63, 41, doi:10.3390/proceedings2020063041 . . . . .	445
<b>Marius Brănoaea, Andrei Burlacu, Vasiliică Ciocan, Marina Verdeş and Robert Ştefan Vizitiu</b> Numerical Investigation of a Novel Heat Pipe Radiant Floor Heating System with Integrated Phase Change Materials Reprinted from: <i>Proceedings</i> 2020, 63, 15, doi:10.3390/proceedings2020063015 . . . . .	453
<b>Roxana Pătraşcu, Constantin Ionescu, Mihai Rareş Sandu and Diana Ban (Tuţica)</b> Technical-Economic Analysis of a Hybrid Thermal Energy Supply System Based on Renewable Energy Sources Reprinted from: <i>Proceedings</i> 2020, 63, 19, doi:10.3390/proceedings2020063019 . . . . .	463
<b>Daniel-Cornel Balan, Sorina-Mihaela Balan and Juliana Szakacs</b> Technical-Economic Analysis of a Hybrid Energy Systems Composed of PV and Biomass Obtained from Municipal Solid Waste Connected to the Grid Reprinted from: <i>Proceedings</i> 2020, 63, 9, doi:10.3390/proceedings2020063009 . . . . .	473

<b>Youssra El Qasemy, Abdelfatah Achahbar and Abdellatif Khamlichi</b> Stochastic Models of Particle Trajectories in Turbulent Atmosphere Flows by Using the LANGEVIN Equations Reprinted from: <i>Proceedings</i> 2020, 63, 32, doi:10.3390/proceedings2020063032 . . . . .	483
<b>Amahjour Narjisse and Abdellatif Khamlichi</b> Computational Fluid Dynamics Simulation to Predict the Airflow and Turbulence in a Wind Farm in Open Complex Terrain Reprinted from: <i>Proceedings</i> 2020, 63, 33, doi:10.3390/proceedings2020063033 . . . . .	491
<b>Sabra Ahyaten and Jalal El Bahaoui</b> Modeling of Wind Turbines Based on DFIG Generator Reprinted from: <i>Proceedings</i> 2020, 63, 16, doi:10.3390/proceedings2020063016 . . . . .	501
<b>Lavinia Andrei, Doru-Laurean Baldean and Adela-Ioana Borzan</b> Designing an Artificial Intelligence Control Program Model to be Tested and Implemented in Virtual Reality for Automated Chevrolet Camaro Reprinted from: <i>Proceedings</i> 2020, 63, 44, doi:10.3390/proceedings2020063044 . . . . .	509
<b>Florin Covaciu, Persida Bec and Doru-Laurean Băldean</b> Developing and Researching a Robotic Arm for Public Service and Industry to Highlight and Mitigate Its Inherent Technical Vulnerabilities Reprinted from: <i>Proceedings</i> 2020, 63, 25, doi:10.3390/proceedings2020063025 . . . . .	519
<b>Daniela Popescu, Adela-Ioana Borzan and Doru-Laurean Băldean</b> Development of an Automated System for Fuel Tank Level Checking and Machinery Location Management to Optimize Remote Accessibility and Mobile Tracking Reprinted from: <i>Proceedings</i> 2020, 63, 17, doi:10.3390/proceedings2020063017 . . . . .	529
<b>Ionel Staretu</b> Robotic Arms with Anthropomorphic Grippers for Robotic Technological Processes Reprinted from: <i>Proceedings</i> 2020, 63, 77, doi:10.3390/proceedings2020063077 . . . . .	539
<b>Ana María Valdeón Junquera, Javier García González, Joaquín Manuel Villanueva Balsera and Vicente Rodríguez Montequín</b> A Wire Rod Rolling Mill Digital Twin for the Simulation of the Rolls Replacement Process Reprinted from: <i>Proceedings</i> 2020, 63, 13, doi:10.3390/proceedings2020063013 . . . . .	549
<b>Stefano Carrino, Jonathan Guerne, Jonathan Dreyer, Hatem Ghorbel, Alain Schorderet and Raphael Montavon</b> Machining Quality Prediction Using Acoustic Sensors and Machine Learning Reprinted from: <i>Proceedings</i> 2020, 63, 31, doi:10.3390/proceedings2020063031 . . . . .	559
<b>Mírcea Dulău</b> Control Strategies for Thermal Processes in Chemical Industry Reprinted from: <i>Proceedings</i> 2020, 63, 34, doi:10.3390/proceedings2020063034 . . . . .	569
<b>Mírcea Dulau and Stelian-Emilian Oltean</b> The Effects of Weighting Functions on the Performances of Robust Control Systems Reprinted from: <i>Proceedings</i> 2020, 63, 46, doi:10.3390/proceedings2020063046 . . . . .	577
<b>László Kovács</b> Concept Lattice-Based Classification in NLP Reprinted from: <i>Proceedings</i> 2020, 63, 48, doi:10.3390/proceedings2020063048 . . . . .	587

<b>Seyed Mahdi Sagheblian, Daniel Dragomir-Stanciu and Roghayeh Ghasempour</b> Assessing the Capability of KELM Meta-Model Approach in Predicting the Energy Dissipation in Different Shapes Channels Reprinted from: <i>Proceedings</i> 2020, 63, 45, doi:10.3390/proceedings2020063045 . . . . .	595
<b>Swathi Sambangi and Lakshmeeswari Gondi</b> A Machine Learning Approach for DDoS (Distributed Denial of Service) Attack Detection Using Multiple Linear Regression Reprinted from: <i>Proceedings</i> 2020, 63, 51, doi:10.3390/proceedings2020063051 . . . . .	605
<b>Moustapha El Bakkali, Said Elkhalidi, Intissar Hamzi, Abdelhafid Marroun and Naima Amar Touhami</b> UWB-MMIC Matrix Distributed Low Noise Amplifier Reprinted from: <i>Proceedings</i> 2020, 63, 52, doi:10.3390/proceedings2020063052 . . . . .	617
<b>Mustapha El Halaoui, Laurent Canale, Adel Asselman and Georges Zissis</b> Dual-Band 28/38 GHz Inverted-F Array Antenna for Fifth Generation Mobile Applications Reprinted from: <i>Proceedings</i> 2020, 63, 53, doi:10.3390/proceedings2020063053 . . . . .	625
<b>Faouzi Rahmani, Naima Amar Touhami, Abdelmounaim Belbachir Kchairi and Nihade Taher</b> Wideband Reconfigurable Antenna with Beams Switching for Wireless Systems Applications Reprinted from: <i>Proceedings</i> 2020, 63, 36, doi:10.3390/proceedings2020063036 . . . . .	635
<b>Aye Mint Mohamed Mostapha, Gamil Alsharahi, Ahmed Faize and Abdellah Driouach</b> Effect of the Variation in Humidity of the Medium on the GPR Radar Response Reprinted from: <i>Proceedings</i> 2020, 63, 37, doi:10.3390/proceedings2020063037 . . . . .	645
<b>Sanae Azizi, Laurent Canale, Saida Ahyoud, Georges Zissis and Adel Asselman</b> Design of Transparent Antenna for 5G Wireless Applications Reprinted from: <i>Proceedings</i> 2020, 63, 54, doi:10.3390/proceedings2020063054 . . . . .	653
<b>Florin Covaciu, Persida Bec and Doru-Laurean Băldean</b> Design and Development of a Low-Cost Automated All-Terrain Intelligent Robotic Vehicle for Detection to Study Its Faults and Vulnerabilities from SWOT Perspective Reprinted from: <i>Proceedings</i> 2020, 63, 38, doi:10.3390/proceedings2020063038 . . . . .	661





## About the Editors

**Liviu Moldovan**, Professor, has an M.S. (1984) in Engineering, a M.S. (2001) in Industrial Management, and Ph.D. (1996) in Robotics (modeling and control of parallel robots), Polytechnic Institute of Cluj-Napoca, Romania. His working experience is: 1986 to 1990, research engineer in industry; 1990 to present, professor in robotics, quality management, at George Emil Palade University of Medicine, Pharmacy, Science, and Technology of Targu-Mures. He is acting as the Dean of the Faculty of Engineering and Information Technology.

**Adrian Gligor** is associate professor at Department of Electrical Engineering and Information Technology, "George Emil Palade" University of Medicine, Pharmacy, Science, and Technology of Targu-Mures. He received his M.Sc. degree in Advanced Industrial and Energy Process Control Systems from the "Petru Maior" University of Targu-Mures, Faculty of Engineering (1999) and PhD degree in the field of Civil Engineering from the Technical University of Cluj-Napoca (2007). His professional career began in 1997 in industry and continued since 1999 in academia. His areas of expertise include: systems optimizations, intelligent processes control, optimal control, automation in power systems, power quality, real-time systems design and implementations and image processing. He is currently the vice-dean of the Faculty of Engineering and Information Technology.



Editorial

# Europe's Future Is Digital: A Broad Vision of the Industry 4.0 Concept beyond Direct Manufacturing in the Company <sup>†</sup>

Liviu Moldovan \* and Adrian Gligor 

Faculty of Engineering and Information Technology, "George Emil Palade" University of Medicine, Pharmacy, Science, and Technology of Târgu Mureș, 38 Gh. Marinescu Street, 540139 Târgu Mureș, Romania; adrian.gligor@umfst.ro

\* Correspondence: liviu.moldovan@umfst.ro; Tel.: +40-740-498-427

† Presented at the 14th International Conference INTER-ENG 2020 Interdisciplinarity in Engineering, Mureș, Romania, 8–9 October 2020.

Published: 17 December 2020

---

These proceedings contain research papers that were accepted for presentation at the 14th International Conference Inter-Eng 2020 "Interdisciplinarity in Engineering", which was held on 8–9 October 2020, in the city of Târgu Mureș, Romania. It is a leading international professional and scientific forum for engineers and scientists to present research works, contributions and recent developments as well as current practices in engineering, which is falling into a tradition of important scientific events taking place at Faculty of Engineering and Information Technology in the "George Emil Palade" University of Medicine, Pharmacy Science, and Technology of Târgu Mureș, Romania.

Inter-Eng marks this year seventeen years of existence, the first edition taking place in 2003. Meanwhile the conference prestige grew primarily organizational aspect of arousing the interest of national and international institutions in the country and abroad to become conference partners. Therefore, this year's edition is organized in cooperation with the Romanian Academy of Technical Sciences, McMaster University from Canada and Zagazig University from Egypt. The conference partners from Romania are Romanian General Association of Engineers in Romania, Mureș County Council and Târgu Mureș City Hall.

From another perspective, the international visibility of the conference results is an outstanding increase, the conference proceedings in the previous six editions Inter-Eng 2013, 2014, 2015, 2016, 2017, 2018 and 2019 being published as dedicated issues in Elsevier's *Procedia Technology*, *Procedia Engineering* and *Procedia Manufacturing* journals [1–3], that are made available in open access on Elsevier's Science Direct for researchers worldwide. These volumes are indexed in the Clarivate Analytics Conference Proceedings Citations Index.

Inter-Eng conference starts from the observation that today in full XXIst century, the era of high technology, without new approaches in research one cannot speak of a harmonious society. The theme of the conference proposing a new approach related to "Industry 4.0" the development of a new generation of smart factories grounded on the manufacturing and assembly process digitalization, is related to Advanced manufacturing technology, Lean manufacturing, Sustainable manufacturing, Additive manufacturing, Manufacturing tools and equipment.

The conference slogan in this year is "Europe's future is digital: a broad vision of the Industry 4.0 concept beyond direct manufacturing in the company".

Industry is a central pillar of the European economy, and the EU production sector represents more than 95 million jobs. Nowadays, the challenge is to ensure that all industrial sectors make the best use of new technologies and to manage their transition to higher value products and processes, commonly known as "Industry 4.0" [4].

Currently, manufacturing production is determined by international competition and the requirement to rapidly adapt production to market needs. But manufacturing companies are facing a huge challenge in implementing Industry 4.0 solutions. The concept of the industry is not only limited to the manufacturing system, but also comprises the supply system and the sales system of the enterprise, its entire value chain which constitutes a globalized system of links of all the enterprises including all their functions and services.

These demands can only be met through the radical advances of current manufacturing technology supported by Industry 4.0 which is integrating business and production processes, as well as integrating suppliers and customers into the company's value chain.

Through vertical networking of the smart factory's cyber physical systems, changes in stocks or demand or even faults in equipment are quickly addressed. Both production and maintenance management of the factory can be organised automatically and independently of each other. With real-time virtualisation of everything in the factory, parts and equipment can be located anywhere and the workflows are self-organised for optimum efficiency.

Horizontal integration brings the efficiency of the network to other outside organisations, such as subcontractors, suppliers, logistics service providers, distribution points and customers. As products become more integrated with the Internet of Things, through embedded electronics and communication technologies, the link with the manufacturer is maintained throughout its life cycle.

Exponential technologies represent one of the major characteristics of Industry 4.0 serving as a catalyst for improvements in the manufacturing process. These technologies are evolving and enabling change at an accelerating pace. Innovation through exponential technologies can help manufacturers develop faster, be more flexible and unlock new forms of value.

Governed by vertical and horizontal integration and enabled by cyber physical systems, as well as by the internet of things, the organisation of a factory of the future will be more flexible, changeable, decentralised, and not as deterministic as today's organisations.

Meeting these advances is different, because at present there are only a few "islands" of the Industry 4.0 concept.

Delays of manufacturing companies in adapting to the transformations produced by digitization will lead to low competitiveness, with adverse effects for their future. The better the new technologies of "Industry 4.0" are understood and applied in practice, the more these companies will gain a competitive advantage.

This year, the InterEng conference has distinguished keynote speakers:

- Prof.dr.habil. Laszlo Kovacs, University of Miskolc, Hungary;
- Prof.dr. Abdelazim M. Negm, University of Zagazig, Egypt;
- Prof.dr. Mo Elbestawi, McMaster University, Canada;
- Prof.dr. Ahmed Hussein Ibrahim, University of Zagazig, Egypt.

They are researchers with outstanding results in their field of activity, giving the scientific weight to the conference. On behalf of the scientific committee, we thank them for attending the Inter-Eng 2020 conference.

During this edition of the conference are listed 123 papers distributed in five sessions. It is remarkable the international participation with papers from 12 countries on five continents such as Romania, Hungary, Switzerland, Spain, Finland, Slovakia, Canada, Egypt, Morocco, Saudi Arabia, Algeria and India.

The Inter-Eng 2020 Conference submissions have been anonymously reviewed by two independent reviewers, to ensure the final standard of the accepted submissions. On behalf of the scientific committee of Inter-Eng 2020, we thank all reviewers for their hard work.

We are especially grateful to the authors who submitted their papers to this conference and to the presenters who provided the substance of the meeting.

These Proceedings book contain a rich experience of the academic and research institutions and the industry on diverse themes related to advances and innovation in technology. We do hope that researchers, knowledge workers and innovators both in academia and industry will find it a valuable reference material.

These conference proceedings are made available with the professional support from:

Răzvan CAZACU;  
Adrian-Vasile DUKA;  
Lucian DULĂU;  
Mircea DULĂU;  
Cristian-Dragoș DUMITRU;  
Stelian-Emilian OLTEAN;  
Liviu POP.

The Inter-EngConference has become a tradition, and we are optimistic that it will be maintained in future, contributing to the development of emerging technologies in various fields.

Last but not least, we hope that everybody had a good time in Târgu Mureș, and we invite participants to join us for next year's edition of the Inter-Eng Conference.

Târgu Mureș, Romania	Liviu MOLDOVAN	Adrian GLIGOR
11 October 2020	President of Scientific Committee	Executive Director

**Author Contributions:** Conceptualization, L.M.; Resources, A.G.; Writing—Original Draft Preparation, L.M.; Writing—Review & Editing, A.G. All authors have read and agreed to the published version of the manuscript.

**Funding:** This research received no external funding.

**Acknowledgments:** The authors gratefully appreciate the help of scientific committee as well as organizing committee.

**Conflicts of Interest:** The authors declare no conflict of interest.

## References

1. Moldovan, L. State-of-the-art analysis on the knowledge and skills gaps on the topic of Industry 4.0 and the requirements for work-based learning. *Procedia Manuf.* **2019**, *32*, 294–301. [[CrossRef](#)]
2. Moldovan, L. Review of legislation framework in the field of work-based learning. *Procedia Manuf.* **2019**, *32*, 302–308. [[CrossRef](#)]
3. Moldovan, L.; Gligor, A. "Industry 4.0" the development of a new generation of smart factories grounded on the manufacturing and assembly process digitalization. *Procedia Manuf.* **2020**, *46*, 1–3.
4. International Conference Inter-Eng 2020 "Interdisciplinarity in Engineering". Available online: <https://inter-eng.umfst.ro/2020/> (accessed on 11 October 2020).

**Publisher's Note:** MDPI stays neutral with regard to jurisdictional claims in published maps and institutional affiliations.



© 2020 by the authors. Licensee MDPI, Basel, Switzerland. This article is an open access article distributed under the terms and conditions of the Creative Commons Attribution (CC BY) license (<http://creativecommons.org/licenses/by/4.0/>).



# Coordinate Measuring Machine Probes Effect during Inner Thread Position Measurement <sup>†</sup>

Ferencz Peti <sup>1,\*</sup> and Petru Serban <sup>2</sup>

<sup>1</sup> Faculty of Engineering and Information Technology, “George Emil Palade” University of Medicine, Pharmacy, Science, and Technology of Targu Mures, 540088 Targu Mures, Romania

<sup>2</sup> CIEMatronic S.A., 540394 Targu Mures, Romania; serban.petru@yahoo.com

\* Correspondence: ferencz.peti@umfst.ro; Tel.: +40-740-289-436

<sup>†</sup> Presented at the 14th International Conference INTER-ENG 2020 Interdisciplinarity in Engineering, Mures, Romania, 8–9 October 2020.

Published: 28 December 2020

**Abstract:** Starting from the idea of improving Coordinate Measuring Machines’ (CMM) measurement strategy for inner thread locations, we developed a new method which increases the accuracy of measurements and takes us closer to the pitch diameter. This article will analyze this new method by testing different touching probes configurations for different thread sizes. The objective is to identify the best probe configuration to be used in the measurements of different inner thread sizes.

**Keywords:** CMM measurement strategy; thread true position measurement; increase measurement accuracy

## 1. Introduction

The evolution of technology creates the need to improve the response during production processes; to do this, the process control must be faster and have increased accuracy. In this research, we are focused on thread position measurement strategy solutions, because even if the CMM software developer elaborate solutions for regulated and non-regulated surfaces, the small inner threads (ex. M3 to M12) strategy were left behind. The actual measurement strategies that are used to measure inner threads on the CMM are divided in two categories. In the first, we can use the inner cylinder CMM strategy; here, we can chose different types of measurement, like more circles on different levels or an elliptical rotation with a pitch indexation/revolution or tangent lines to indicate the minimum or maximum diameter. In the second method, we use special pins, which will auto-center on the inner thread. Each method has pro and cons, and the actual paperwork is focused on the first measurement strategy, where improvements were made. The second strategy’s advantages are the accuracy and the repeatability, the disadvantages are that the pins are very expensive and, overtime, the auto-centering will decrease, and repeatability will decrease, which will give bad measurement results. The CMM measurement accuracy is composed of two important categories: correct measurement strategy and correct tool used [1]. To improve the measurement accuracy, we elaborate a method where the measurement tool will scan the inner thread. This method was developed to improve the measurement strategy for this type of measurement. The second approach is to identify the best tool that can be used for different thread dimensions.

## 2. Material and Methods

The measurements were performed on a Hexagon Global Advantage 122,210 Coordinate Measurement Machine edition 2018, Accuracy: 2.1  $\mu\text{m}$  + L/333, Drive Unit: HH-A-T-5 + (SP25M + SM25-3 + SH25-3)\*equipped with a steel probe with an active side made of a ruby ball with different



diameters: 2, 3, 4 and 5 mm. Software of CMM is PC-Dmis 2019R1. Measurement speed was set to 4 mm/s.

For the thread profile evaluation, a MahrMahrsurfXC2 Contour measurement machine edition 2017 with CD120 Drive unit was used, equipped with probe PCV 350 ± 9 with a 25 µm active side of the probe, with an accuracy of 0.35 µm. Measurement speed was set to 1 mm/s.

The method that we used to make this evaluation consisted of measuring the thread as close as possible to the pitch diameter; this can be done by evaluating the form of the inner surface of the thread and identifying the closest point to the pitch diameter. The measurement will begin from this point and will measure a cylinder with a revolution movement that follows the pitch of the thread; more details can be observed in Figure 1. In the actual research, we connected the measuring probe diameter and the measurement strategy to measure a specific thread size. The probe configuration and dimensions are standardized, and therefore it is possible to measure metric threads between M4 and M12 without a wide variety of probes. The dimensions of a probe are formed from an active area and inactive areas; examples are presented in Figure 2, where we can observe the active area represented by (D), the diameter of the probe, and inactive areas like M2, the metric thread used to assemble the probe, L, which represents the length of the probe that must be introduced in the CMM software to can make automatic calibrations, EWL, which is the length of the active ball support which, in combination with S, which represents the diameter of the EWL, will have a big impact when we chose the measurement probe. The measurement is done taking into consideration that characteristic “S” of the probe will not be in contact with the thread; the probe must be in contact only with the active side when measuring the inner thread.

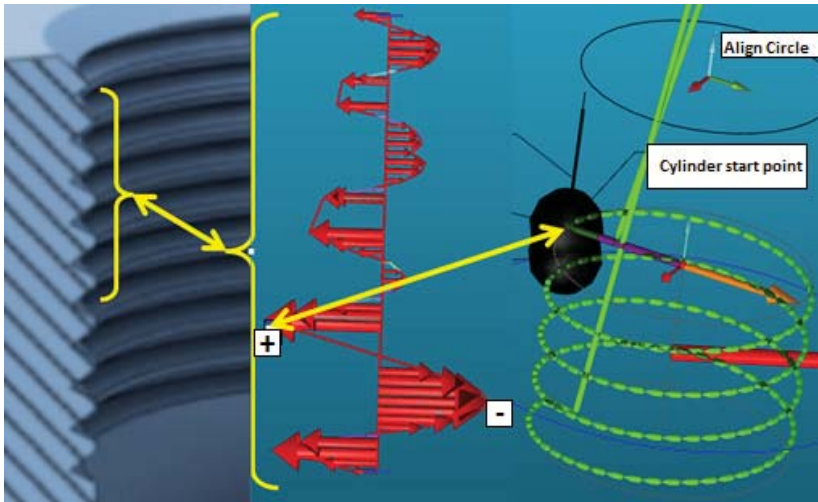


Figure 1. Evaluation steps to measure the inner thread.



Figure 2. Probe configuration and dimensions: (a) Probe characteristics; (b) Characteristic marked with yellow are inactive and with green are active. “Pitch diameter measurements of internal threads are more complicated than external threads [2] due to construction of internal thread which does not allow easy probing like external threads”.

### 3. Results and Discussion

Measurements were made for two metric threads, M6 and M8; for this, we used probes with an active sphere diameter from  $\varnothing 2$  to  $\varnothing 5$  mm. The results are focused on the pitch diameter and the repeatability and accuracy of thread location. Having all this information we investigate several issues and opportunities to do it right and here are some quotes from our references: “The basis of the direct method of measuring the position of the threaded holes was that the probe was led directly into the threaded hole and then were scanned the certain number of points, from these points cylinder by least-squares method was created. After that, the position of the axis of the cylinder to a reference hole was determined” [3]. “The methods presented apply only to determining the position of a threaded hole. The threads themselves, along with the minor diameter, should be checked with a thread gage with one exception. If they are large enough for a styli to fit inside and scan the surface, there are techniques discussed elsewhere that will help. None of the methods below will be able to calculate the size reliably (except scanning may get a reasonably close minor diameter) unless the pitch surface of the thread is accessible to a stylus” [4]. “Another problem measuring threads is if the threads on the CAD don’t match the physical part, you’ll have trouble finding the thread. Our part that we intended to measure threads on had a different start and end than what the model shows. So when I picked points along the major on the CAD, the CMM probed those points on the minor on the part. Not good. So we had to keep using threaded gages. Do the threads still work? yes they do, CAD is just the reference and I hear threads are a little difficult to model. Also we have multiple machines making the same part and there is start and end variation from those machines. So you’ll not be able to use the exact same program/routine across CNC machines. First thing you have to do is be able find the thread with the CMM” [5].

#### 3.1. Metric 6 Measurement Results

##### 3.1.1. Diameter Analysis

All diameter measurements are presented in Table 1. The results indicate that probe diameter  $\varnothing 2$  mm is the closest to the pitch diameter. If we consider going below this diameter, we risk that the part will be in contact with the inactive side of the probe.

**Table 1.** Diameters of the thread resulted by measuring using 3 probes and 5 measurements.

	M6X1/Min5.35/Max5.50				
Probe	1	2	3	4	5
$\varnothing 2$ mm	5.194	5.195	5.195	5.194	5.193
$\varnothing 3$ mm	5.134	5.133	5.135	5.134	5.134
$\varnothing 4$ mm	5.091	5.092	5.096	5.091	5.092

##### 3.1.2. Location Analysis

We calculate the true position (TP) for the measurement so that we have a simple interpretation of the results. Table 2 presents the measurement related to the diameter of the probe. Measurements made with probe  $\varnothing 2$  indicate the best results, next is probe  $\varnothing 3$  and the worst is probe  $\varnothing 4$ .

**Table 2.** TP of the thread resulted by measuring using 3 probes and 5 measurements.

		M6X1				
Probe	TP	1	2	3	4	5
$\varnothing 2$ mm	$\varnothing$ dev	0.014	0.016	0.016	0.016	0.016
$\varnothing 3$ mm	$\varnothing$ dev	0.020	0.019	0.019	0.018	0.019
$\varnothing 4$ mm	$\varnothing$ dev	0.130	0.125	0.123	0.126	0.124

### 3.2. Metric 8 Measurement Results

#### 3.2.1. Diameter Analysis

All diameter measurements are presented in Table 3. The results indicate that probe diameter  $\varnothing 2$  and  $\varnothing 3$  mm is the closest to the pitch diameter. If we consider going below to this diameter, we will risk being in contact with the inactive side of the probe.

**Table 3.** Diameters of the thread, found by measuring using 4 probes and 5 measurements.

M8X1/Min7.188/Max7.348					
Probe	1	2	3	4	5
$\varnothing 2$ mm	7.142	7.151	7.155	7.151	7.151
$\varnothing 3$ mm	7.082	7.083	7.083	7.083	7.083
$\varnothing 4$ mm	7.049	7.049	7.050	7.050	7.050
$\varnothing 5$ mm	7.001	7.003	7.021	6.987	7.021

#### 3.2.2. Location Analysis

We calculate the true position (TP) for the measurement so that we have a simple interpretation of the results. Table 4 presents the measurement related to the diameter of the probe. Measurements made with probe  $\varnothing 5$  indicate the best results, next is probe  $\varnothing 2$  and  $\varnothing 3$  and the worst is probe  $\varnothing 4$ .

**Table 4.** TP of the thread, found by measuring using 4 probes and 5 measurements.

M8X1						
Probe	TP	1	2	3	4	5
$\varnothing 2$ mm	$\varnothing$ dev	0.066	0.069	0.072	0.071	0.072
$\varnothing 3$ mm	$\varnothing$ dev	0.067	0.069	0.070	0.071	0.071
$\varnothing 4$ mm	$\varnothing$ dev	0.105	0.105	0.103	0.103	0.103
$\varnothing 5$ mm	$\varnothing$ dev	0.052	0.054	0.066	0.059	0.068

## 4. Conclusions

The measurement results indicated in Tables 1 and 3 show us that a small probe diameter can be a good solution to be closer to the pitch diameter; these results can also be seen in Tables 2 and 4. In these tables we measure the true position, and the evaluation indicates the same results as in Tables 1 and 2: a small probe is more accurate for this measurement strategy than a large probe. All the results presented above are made for a part where the machining tool is new. In the serial production, the regular measurement strategy remains the same for a CMM program, but the part will modify continuously during the cycle time of the project: wear of the mold, wear of the gages, wear of the machining tools, setup of new molds, etc., will all increase the chance of measurement errors. Knowing this, we created the variable strategy model where the thread is evaluated every time, and here the configuration of the probe also has a big impact on the final inspection of the part measurement. If we choose a probe with a small diameter, than we risk to measuring with the inactive part of the probe, whereas if we choose a probe with a large diameter, we will not measure the desired location. The wear of the machining tools (see Figure 3) facilitates the bad segment of thread and this will decrease the measurement availability area. The material defects can also facilitate a wrong measurement interpretation; the big porosity inside the threads must be identified before the measurement.

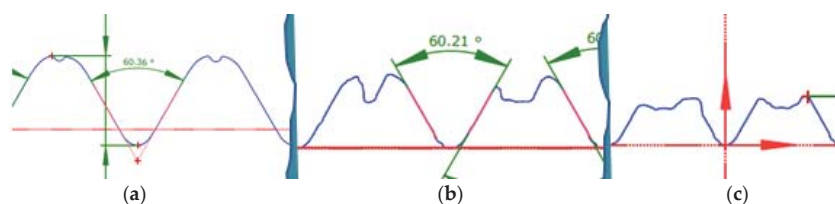


**Figure 3.** Thread section profile for a new tool (a), a used tool (b) and a broken tool (c).

If we use the correct measurement strategy and the correct measurement tool, we can increase the amount of correct measurements too. The pitch diameter gives us the most accurate and the most correct inner thread location and the axis given by this measurement indicates a correct location of the thread. We can find a false location of the threads if we are not focused on measuring these characteristics.

**Acknowledgments:** This work was partially supported by the UMFST “George Emil Palade” Quality Engineering and Digital Manufacturing Research Center.

**Conflicts of Interest:** The authors declare no conflict of interest.

## References

1. Serban, P.; Peti, F. Coordinate Measuring Machine thread position measurement analysis. In Proceedings of the IOP Conference Series: Materials Science and Engineering, Annual Session of Scientific Papers—IMT Oradea, Oradea, Romania, 28–29 May 2020; IOP Publishing Ltd.: Bristol, UK, 2020; Volume 898.
2. Ahmet Yüksel, İ.; OytunKılınç, T.; Berk Sönmez, K.; ÖnAktan, S. Comparison of internal and external threads pitch diameter measurement by using conventional methods and CMM's. In Proceedings of the 19th International Congress of Metrology, Paris, France, 24–26 September 2019; p. 09001.
3. Martikáň, P.; Drbúl, M.; Holubják, J.; Mrázik, J.; Joch, R. The issue of determining the geometric position deviation of the threaded holes. *Adv. Sci. Technol. Res. J.* **2016**, *10*, 47–52. [CrossRef]
4. Measuring a Pitch. Available online: <https://www.pcdmisforum.com/> (accessed on 25 June 2020).
5. How Do I Measure a Threaded Hole? Available online: [www.hexagon.com](http://www.hexagon.com) (accessed on 25 June 2020).



**Publisher's Note:** MDPI stays neutral with regard to jurisdictional claims in published maps and institutional affiliations.



© 2020 by the authors. Licensee MDPI, Basel, Switzerland. This article is an open access article distributed under the terms and conditions of the Creative Commons Attribution (CC BY) license (<http://creativecommons.org/licenses/by/4.0/>).



# Achieving a Toothed Gear on Presses <sup>†</sup>

Marius Tintelecan <sup>1,\*</sup>, Dana-Adriana Iluțiu-Varvara <sup>1</sup>, Oscar Rodriguez-Alabanda <sup>2</sup>,  
Ioana Monica Sas-Boca <sup>1</sup>, Ionuț Marian <sup>1</sup> and Aristides Santana Martinez Gustavo <sup>3</sup>

<sup>1</sup> Department of Materials Science and Engineering, Technical University of Cluj-Napoca, 100114 Cluj Napoca, Romania; dana.varvara@gmail.com (D.-A.I.-V.); monica.sas.boca@ipm.utcluj.ro (I.M.S.-B.); marianionut78@yahoo.com (I.M.)

<sup>2</sup> Department of Mechanical Engineering, University of Cordoba, Medina Azahara Avenue, 5, 14071 Cordoba, Spain; orodriguez@uco.es

<sup>3</sup> Engineering School of Lorena, University of São Paulo-USP, Lorena 12602-810, Brazil; gustavo.martinez@usp.br

\* Correspondence: marius.tintelecan@ipm.utcluj.ro; Tel.: +40-721-594-419

<sup>†</sup> Presented at the 14th International Conference INTER-ENG 2020 Interdisciplinarity in Engineering, Mureș, Romania, 8–9 October 2020.

Published: 28 December 2020

**Abstract:** This paper presents a device that, in final connection with presses, allows toothed gear (with a crown similar to a toothed wheel with right teeth) to be achieved by hot deformation starting from a cylindrical steel bar. For this, finite element simulations were performed in Forge software. The proposed device has 23 rollers, so for the simulation process, a slice representing a part (the 23rd) of a circle which simplifies the essential functionality of this device was taken into consideration.

**Keywords:** toothed gear <sup>1</sup>; hot deformation; presses; deformation roller; fibrous structure

## 1. Introduction

From the start of this research problem, it should be noted that the semi-finished product was obtained through a plastic forming process (pressing) by an equipment with 23 forming rollers [1]. The symmetry axis of the set is collinear to the symmetry axis of the final toothed gear, so we subjected a slice which is the 46th part from 360°, namely 7.8°, in the simulations. Additionally, we tried to quantify the implications of operating the press punch on the designed and assembled toothed gear wheel.

A mesh network was built for each slice, and the corresponding plastic deformation equations were applied in each of them. Through this research methodology, we noticed how each simulated slice of 7.8° was affected overall, so we reached the necessary conclusions that led us to make the necessary changes in the whole assembly, and finally we saw how the whole set behaved.

The technical parameters of this plastic deformation process were deduced. It was proven that the technical feasibility for the manufacture of toothed gear wheels through this method is clearly superior to the classical method which involves milling, especially due to the significantly higher productivity of the proposed process and the material saving, in addition to the advantage of toothed gear wheels obtained with continuous fiber, who are much more resistant from a mechanical point of view.

## 2. The Pressing

We started from the idea of making a toothed gear by pressing a cylindrical semi-finished product, made by drawing [2,3], through a roller device. In a specific case, we decided that the device should consist of 23 deformation rollers and a body (fixed) on which these rollers are assembled. The design was created using a CAD software: SolidWorks (see Figure 1). It must be noted that the device was made only for research, being intended for the realization of a gear with straight teeth having a certain number of teeth (23) and a certain circular pitch, respectively.

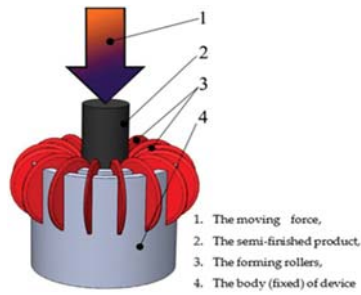


**Figure 1.** The principled sketch of the deformation mode with this device.

For practical, concrete cases, such a device can be built for each desired value of the number of teeth and the circular pitch “p” of the final toothed gear.

The toothed gear achieved device, built, has 23 deforming rollers, for simulation using the 46th part of a virtual circle, which has in the center the longitudinal axis of symmetry of the semi-finished product, thus being similar to a slice with peak angle of  $7.8^\circ$  as is shown in Figure 2.

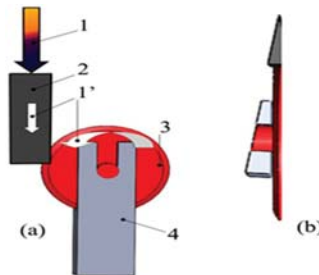


**Figure 2.** The aspect of the “slice” subjected to simulation ((a)—longitudinal view, (b)—cross-sectional view, 1—the moving force, 1’—the direction of movement, 2—the semi-finished product, 3—the deforming rollers, 4—the body of device).

This simplification was used to speed up the analysis time of the simulation process. We want to mention that the simulation of the deformation process was simplified to a “slice” because the process is axisymmetric.

### 3. The Device Description

The previously proposed device was actually made to confirm the simulation results and its design and real assembly is shown in Figure 3.

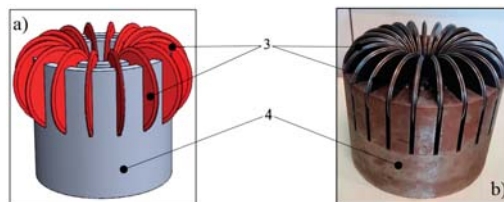


**Figure 3.** The device for achieving of a toothed gear on presses: (a) the proposed version, (b) the built version; the forming rollers 3 and the body (fixed) of device 4. The notations are in correspondence with those from Figure 1.

Starting from a cylindrical semi-finished product (see Figure 4a), the device manages to make toothed gears by hot forming, similar to that shown in Figure 4b.

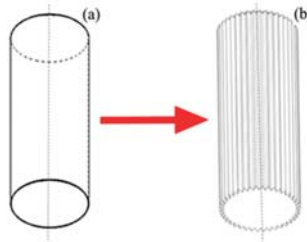


Figure 4. The initial semi-finished product (a); the final product (b).

In fact, the intermediate technical stages (viewed in cross section) are detailed in Figure 5.

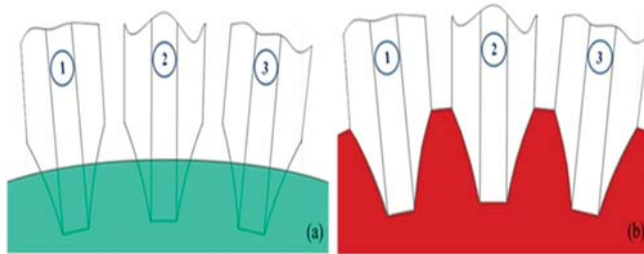


Figure 5. Cross-sectional view of the processed semi-finished product: (a) the initial semi-finished product (green) and (b) the final product (red); the forming rollers are numbered as 1, 2, 3.

#### 4. Simulation

The simulations were performed by finite element analysis (FEA), using FORGE software.

##### 4.1. The Dimension Assessment of the Initial Semi-Finished Product

Basically, the diameter  $D_s$  of the semi-finished product and its height  $H_s$  were determined. The mathematical calculation of the diameter  $D_s$  of the semi-finished product implies that the sum of the transverse areas of the portions displaced by the action of the forming rollers must be equal to the sum of the transverse areas of the tooth tips formed by the flow of the material [4] (see Figure 6).

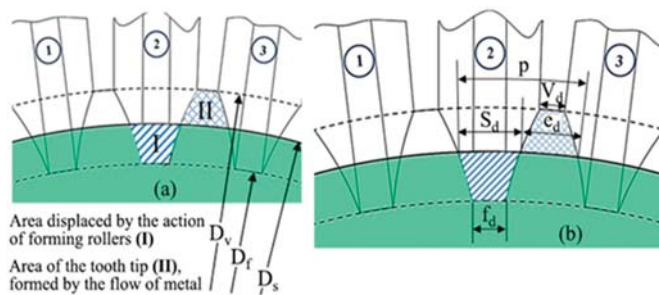


Figure 6. (a) Main view of the semi-finished product deformation and (b) the previous view enlarged with the dimensions that appear in the nomenclature.



We estimated the area affected by the forming rollers, corresponding to the area displaced by their action (I) and the area of the tooth tip, formed by the flow of the material (II), respectively, with two trapezoids [5] whose surfaces are:

$$S_I = \frac{f_d + s_d}{2} \cdot (D_s - D_f) \quad (1)$$

$$S_{II} = \frac{v_d + e_d}{2} \cdot (D_v - D_s) \quad (2)$$

$$\begin{aligned} \frac{(f_d + s_d)}{2} \cdot (D_s - D_f) &= \frac{(v_d + e_d)}{2} \cdot (D_v - D_s) \\ \frac{f_d \cdot D_s + s_d \cdot D_s}{2} - \frac{f_d \cdot D_f + s_d \cdot D_f}{2} &= \frac{v_d \cdot D_v + e_d \cdot D_v}{2} - \frac{v_d \cdot D_s + e_d \cdot D_s}{2} \\ \frac{f_d \cdot D_s + s_d \cdot D_s}{2} + \frac{v_d \cdot D_s + e_d \cdot D_s}{2} &= \frac{v_d \cdot D_v + e_d \cdot D_v}{2} + \frac{f_d \cdot D_f + s_d \cdot D_f}{2} \\ \text{so, } (f_d + v_d + s_d + e_d) \cdot \frac{D_s}{2} &= (v_d + e_d) \cdot \frac{D_v}{2} + (f_d + s_d) \cdot \frac{D_f}{2} \end{aligned} \quad (3)$$

The approximation of  $v_d \approx f_d$  and  $s_d \approx e_d$  results in:

$$(v_d + s_d) \cdot D_s = (v_d + s_d) \cdot \frac{D_v}{2} + (v_d + s_d) \cdot \frac{D_f}{2} \quad (4)$$

$$D_s = (D_v + D_f)/2 \quad (5)$$

- $S_I$  the area displaced by the action of the deforming rollers [mm<sup>2</sup>]
- $S_{II}$  the area of the tooth tip, formed by the flow of material [mm<sup>2</sup>]
- $D_s$  the diameter of the initial semi-finished product [mm]
- $D_f$  the diameter of the dedendum circle [mm]
- $D_v$  the diameter of the addendum circle [mm]
- $s_d$  tooth thickness [mm]
- $e_d$  tooth space [mm]
- $p$  circular pitch [mm]
- $f_d$  tooth space peak thickness [mm]
- $v_d$  tooth peak thickness [mm]

To correct the approximations from these calculations, FEA simulations were performed determining the von Mises stress and deducing the optimum dimensions of the initial semi-finished product: diameter,  $D_s$  (Figure 7), and height,  $H_s$  (Figure 8). The dimensions  $D_s$  and  $H_s$  are not specified as a value and are only relevant in correspondence with the dimensions of the device object of study. These dimensions were established so as to achieve the maximum degree of filling of the toothed gear by the flow of the material and a certain behavior in the process of its deformation.

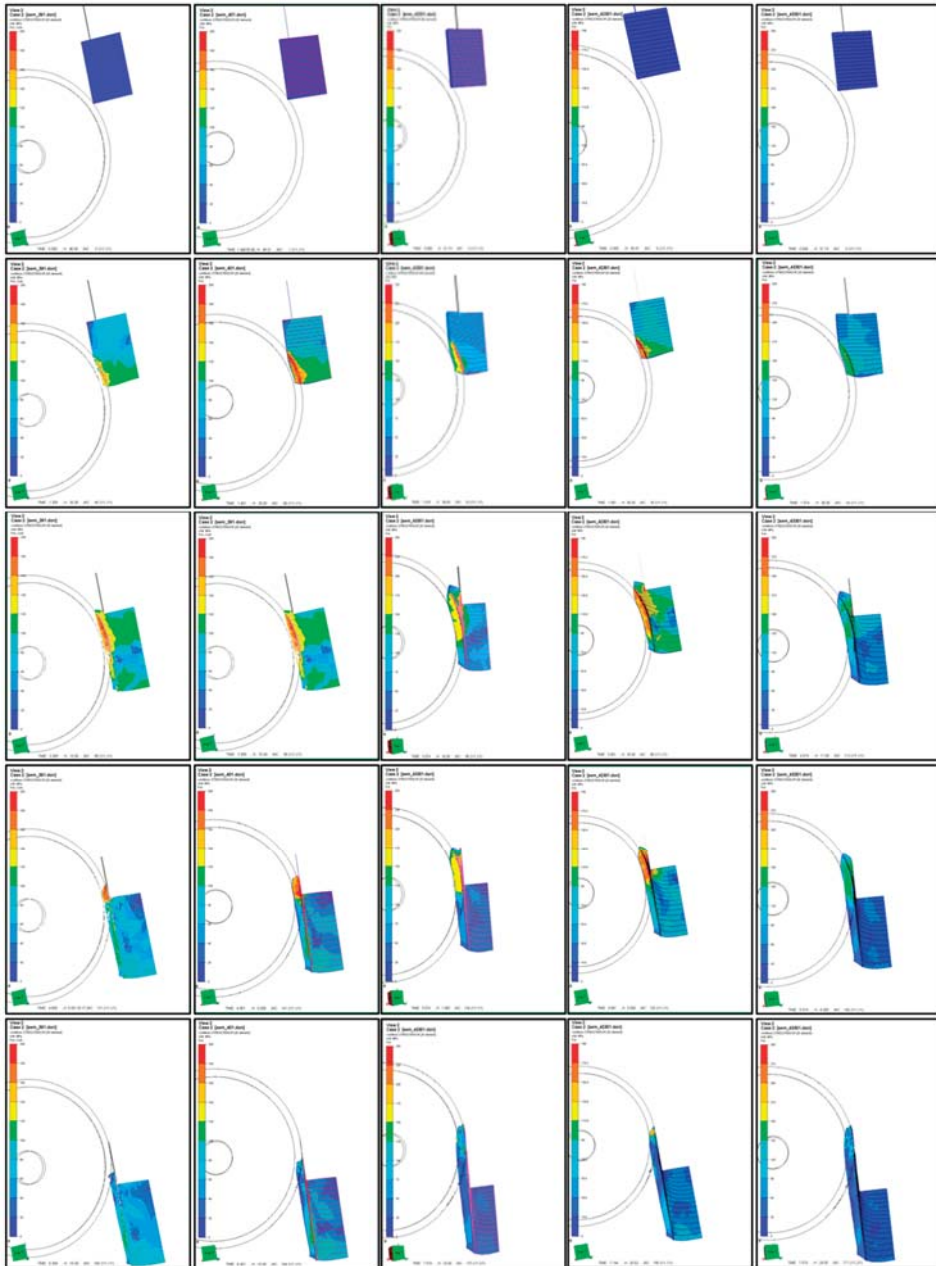


**Figure 7.** The deduction of the diameter  $D_s$  of the initial semi-finished product by finite element analysis (FEA) simulation.

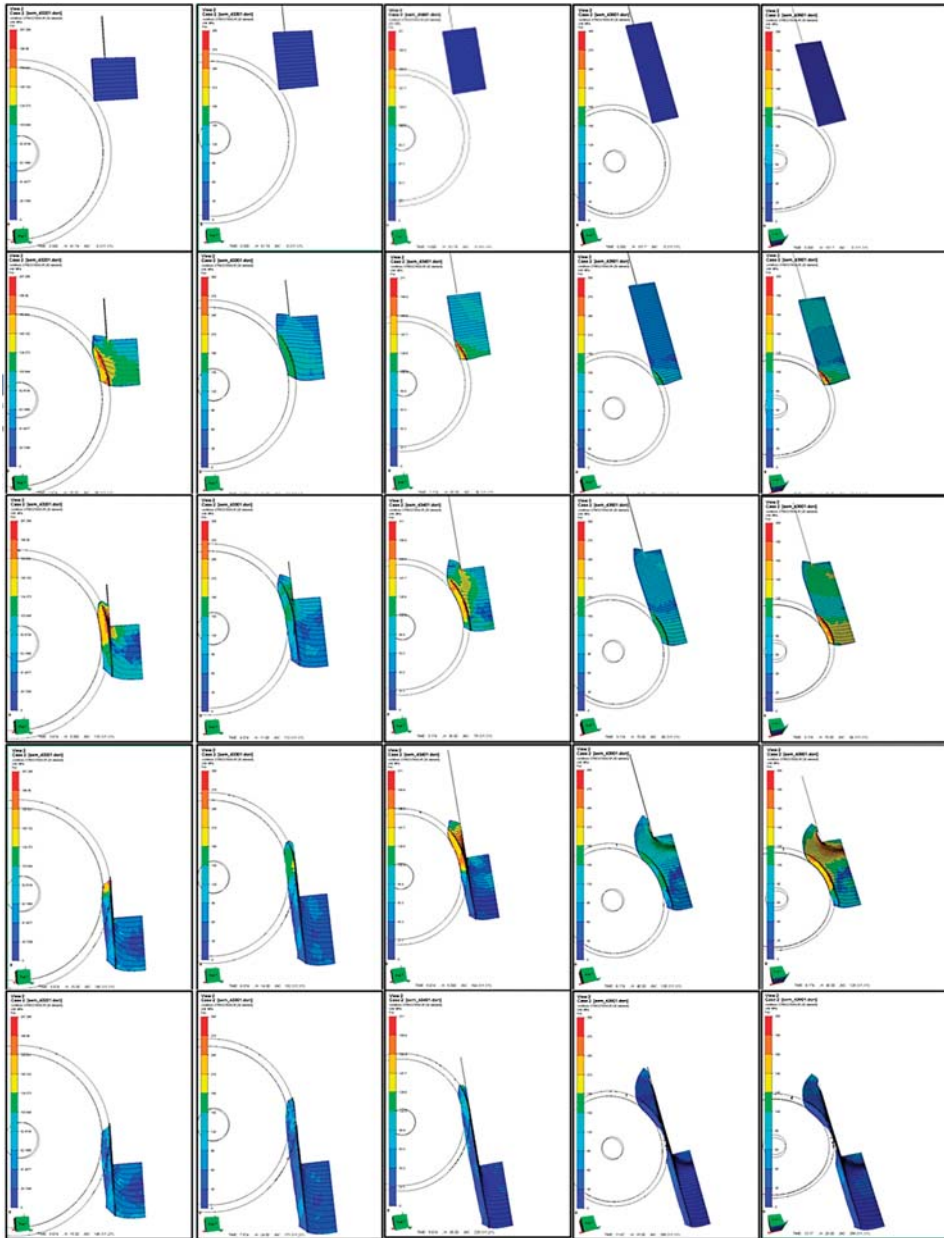
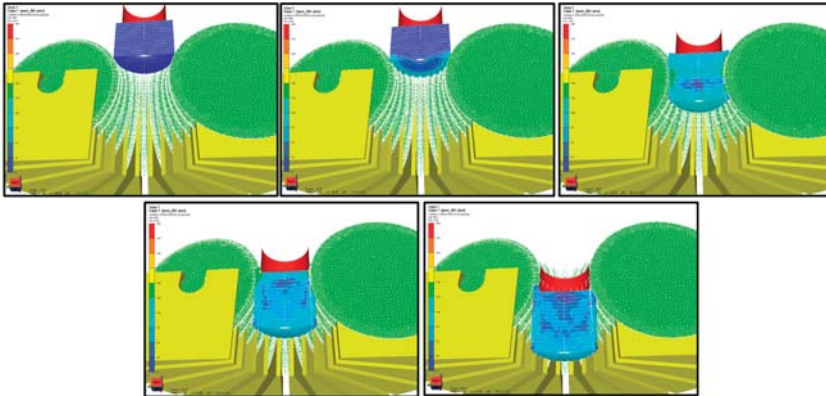


Figure 8. The deduction of the height  $H_s$  of the initial semi-finished product by FEA simulation.

#### 4.2. The Von Mises Stress Determination

In the second phase, with these correct dimensions, a mesh network was applied both for the semi-finished product and for the analyzed device. Thus, the final values of von Mises stress were deduced. Because both the semi-finished product and the analyzed device were involved in the simulation at this moment, a view was achieved in its longitudinal section, focused on the von Mises

stress that appeared at the deformation of the semi-finished product [6]. Figure 9 shows 5 figures made at various deformation moments: (a) corresponds to the deformation start time  $t = 0$  (initial deformation moment), (b) corresponds to the moment  $t/5$ , (c) moment  $(2/5) \cdot t$ , (d) moment  $(3/5) \cdot t$ , (d) moment  $(4/5) \cdot t$  and (e) the final moment ( $t = t$ ).



**Figure 9.** The von Mises stress involved in the whole process of plastic deformation of the semi-finished product (the duration of the deformation was symbolized by “t”).

#### 4.3. The Semi-Finished Product Deformations

This simulation is similar as aspect to the previous one, practically focusing on the amplitude of the deformations of the semi-finished product along the entire time interval ( $t$ ) of its deformation, as shown in Figure 10.

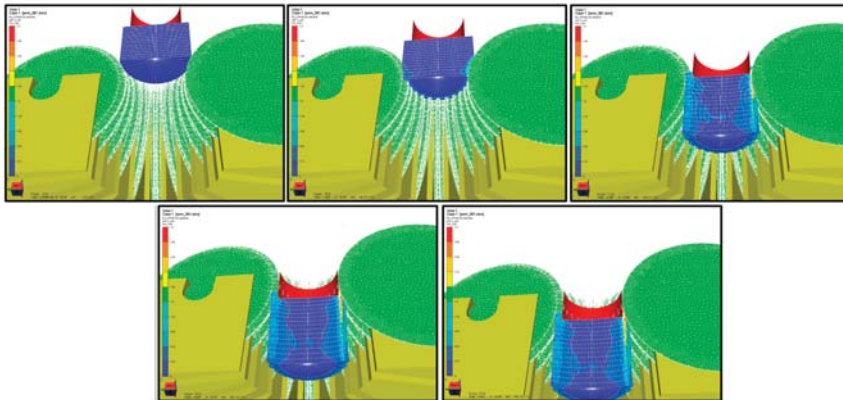


**Figure 10.** The deformations involved in the whole process of plastic deformation of the semi-finished product.

#### 4.4. The Flow of the Semi-Finished Material

Mesh network was no longer viewed. The whole system device-part was cut from the entire longitudinal section with the aim of analyzing only the evolution of the flow of the part material, as shown in Figure 11.

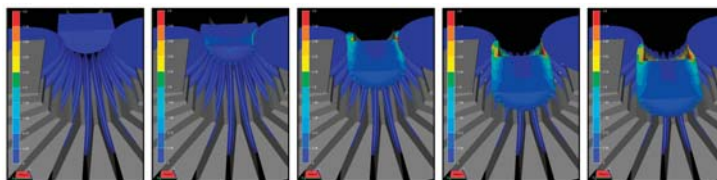


Figure 11. The flow of the semi-finished material, in the process of its plastic deformation.

## 5. Conclusions

In this research, it was proven that toothed gears with a certain circular pitch and number of teeth can be achieved by this method [7] of plastic deformation, and as with any process of plastic deformation, the fibrous structure being continuous, it results in a more resistant final product, able to respond more efficiently to various mechanical stresses [8]. During the practical hours of simulation, it was also observed that the flow of the material in the tooth formation imposes a certain regime of deformation speed. It was also observed that in the case of obtaining steel toothed gears, the respective deformation process will be performed hot, requiring only the heating of the cylindrical surface of the initial semi-finished product.

**Funding:** This research received no external funding.

**Conflicts of Interest:** The authors declare no conflict of interest.

## References

1. Pop, M. *Plastic Deformations*; Editura Mega: Cluj-Napoca, Romania, 2014; ISBN 978-606-543-509-4.
2. Wright, N.R. *Wire Technology. Process Engineering and Metallurgy*; Elsevier: Amsterdam, The Netherlands, 2011; ISBN 978-0-12-382092-1.
3. Rodriguez-Alabanda, O.; Guerrero-Vaca, G.; Romero, P. Machining time estimation using the geometrics features of the 2.5D pocket contour. *Procedia Manuf.* **2019**, *41*, 508–515. [[CrossRef](#)]
4. Neugebauer, R.; Putz, M.; Hellfritzschn, U. Improved Process Design and Quality for Gear Manufacturing with Flat and Round Rolling. *CIRP Ann.* **2007**, *56*, 307–312. [[CrossRef](#)]
5. André Weiß, A.; Liewald, M.; Weiß, A.; Missa, N. Manufacture of face gearing—A new production method by means of determined material pre-distribution. *Procedia Manuf.* **2018**, *15*, 511–518. [[CrossRef](#)]
6. Armentania, E.; Mattera, A.; Sepe, R.; Esposito, L.; Naclerio, F.; Bocchini, G.F. Dies for pressing metal powders to form helical gears. *Procedia Struct. Integr.* **2018**, *12*, 457–470. [[CrossRef](#)]
7. Linke, H.; Börner, J.; Heß, R. Manufacturing of Cylindrical Gearing. In *Cylindrical Gears*; Hanser: Munich, Germany, 2016; pp. 605–707. [[CrossRef](#)]
8. *ASM Handbook Volume 5: Surface Engineering*; ASM International: Novetty, OH, USA, 1994; ISBN 978-0-87170-384-2.

**Publisher's Note:** MDPI stays neutral with regard to jurisdictional claims in published maps and institutional affiliations.



© 2020 by the authors. Licensee MDPI, Basel, Switzerland. This article is an open access article distributed under the terms and conditions of the Creative Commons Attribution (CC BY) license (<http://creativecommons.org/licenses/by/4.0/>).

Article

# Reuse of the Steel Mill Scale for Sustainable Industrial Applications <sup>†</sup>

Dana-Adriana Iluțiu-Varvara <sup>\*</sup>, Marius Tintelecan , Claudiu Aciu and Ioana-Monica Sas-Boca

Department of Building Services Engineering, Faculty of Building Services Engineering, Technical University of Cluj-Napoca, 28 Memorandumului Street, 400114 Cluj-Napoca, Romania; mariust@ipm.utcluj.ro (M.T.); claudiu.aciu@ccm.utcluj.ro (C.A.); monica.sas.boca@ipm.utcluj.ro (I.-M.S.-B.)

<sup>\*</sup> Correspondence: dana.varvara@gmail.com or dana.adriana.varvara@insta.utcluj.ro

<sup>†</sup> Presented at the 14th International Conference INTER-ENG 2020 Interdisciplinarity in Engineering, Mureș, Romania, 8–9 October 2020.

Published: 11 December 2020

**Abstract:** The purpose of our paper is to assess the reuse potential of the steel mill scale for sustainable industrial applications. We have presented the experimental procedures for chemical and mineralogical characterizations. According to the results of the elementary chemical analysis, the steel mill scale contains the following predominant chemical elements: iron, aluminum, silicon, and magnesium. Due to its high iron content, the steel mill scale can be reused as a source of raw material in the sustainable steelmaking industry. The mineralogical phases identified in the steel mill scale are: wüstite (FeO), hematite (Fe<sub>2</sub>O<sub>3</sub>), magnetite (Fe<sub>3</sub>O<sub>4</sub>), silica (quartz) (SiO<sub>2</sub>), magnesioferrite (MgFe<sub>2</sub>O<sub>4</sub>), and aluminum oxide (corundum) (Al<sub>2</sub>O<sub>3</sub>). Silica, alumina, and hematite are the main compounds of the cement and contribute to the formation of the: dicalcium silicate (2CaO·SiO<sub>2</sub>), tricalcium silicate (3CaO·SiO<sub>2</sub>), tricalcium aluminate (3CaO·Al<sub>2</sub>O<sub>3</sub>), and tetra—calcium aluminoferrite (4CaO·Al<sub>2</sub>O<sub>3</sub>·Fe<sub>2</sub>O<sub>3</sub>). The results of the paper are promising and encourage the future research for establishing the optimal percentage for the reuse of the steel mill scale in the composition of concrete.

**Keywords:** reuse; sustainable industry; steel mill scale; mineralogical characterization; industrial wastes; cement; steelmaking; alloying elements

## 1. Introduction

Sustainable development was introduced in a widespread way by the Brundtland Commission, which defined it as development that “meets the needs of the present without compromising the ability of future generations to meet their own needs” [1]. Sustainability has been applied to many fields, including engineering, manufacturing, and design. Manufacturers are becoming increasingly concerned about the issue of sustainability. For instance, recognition of the relationship between manufacturing operations and the natural environment has become an important factor in the decision making among industrial societies [2].

Sustainable manufacturing focuses on both how the product is made as well as the product’s attributes. This includes the inputs, the manufacturing processes, and the product’s design. Sustainable manufacturing includes things such as making products using less energy and materials, producing less waste, and using fewer hazardous materials as well as products that have greener attributes such as recyclability or lower energy use [3].

The European steel industry generates an estimated 500,000 tones/yr of oily sludge and mill scales. More than 30% of this total is not valorised. The steelmaking by-products such as dust and mill scale are currently produced in large quantities and represent a potential of almost 5 million tons in the world [4,5].



Mill scale is a steelmaking by-product from the rolling mill in the steel hot rolling process. Mill scale can be considered a valuable metallurgical raw material for iron making, steelmaking, and construction industries because it contains valuable metallic minerals [6–8].

The chemical and mineralogical characterizations of steel mill scale play a key role for their reuse in sustainable industrial applications.

The aim of this paper is the assessment of the reuse potential of the steel mill scale for sustainable application, both in the steelmaking and building materials industries.

The objectives of the paper are:

- The chemical characterization of the steel mill scale;
- The mineralogical characterization of the steel mill scale;
- Identification of the mineralogical phases of the steel mill scale;
- Establishing the mineralogical phases of the steel mill scale that are also found in cement;
- Assessment of the steel mill scale potential for sustainable industrial applications.

## 2. Materials and Methods

The steel mill scale sample was taken from a metallurgical plant (Salaj County, Romania). The mill scale comes from the rolling process of the steel pipes. In order to identify the possibilities of reusing the mill scale, for sustainable industrial applications, the sample was subjected to chemical and mineralogical characterization. The chemical elements from the steel mill scale sample were determined using inductively coupled plasma. The mineralogical characterization of the mill scale sample was performed with the help of an X-ray diffractometer, Brucker Advance D8 type (Germany). The identification of the mineralogical phases was made with Match software from Crystal Impact. This software uses the PDF database from International Centre for Diffraction Data.

## 3. Results and Discussions

Table 1 shows the major and minor chemical elements contained in the steel mill scale.

**Table 1.** Major and minor chemical elements contained in the steel mill scale.

Chemical Element	Fe	Al	Si	Mg	Mn	Minor Elements (Cr, Ni, Mo, Cu, Zn, V, Cd, Ca, As etc.)
[%]	76.8	2.9	2.7	1.4	1.1	4.8

According to the results of the chemical analysis, the major elements in the steel mill scale composition are iron, aluminum, silicon, magnesium, and manganese. The main constituent of the mill scale is iron with 76.8%. Due to its high iron content, the steel mill scale can be reused as a source of raw material in the sustainable steelmaking industry. According to the reference [9], the reuse of iron, from the steel mill scale, as a raw or auxiliary material to the steelmaking, leads to natural resources conservation. The minor elements contained in the steel mill scale are chromium, nickel, molybdenum, copper, zinc, vanadium, cadmium, calcium, and, arsenic, etc. According to the references [9–11], the chromium, nickel, molybdenum, manganese, and vanadium can be reused as alloying elements to the stainless steelmaking in the electric arc furnace.

Figure 1 shows the diffractogram of the steel mill scale.

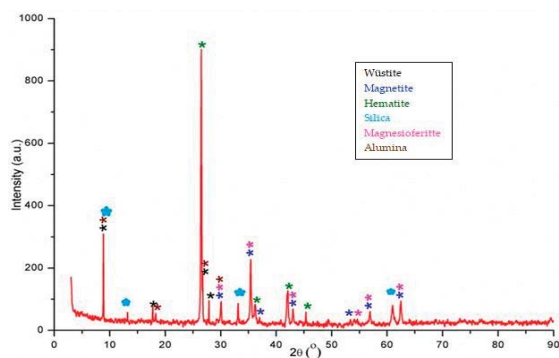


Figure 1. Diffractogram of the steel mill scale.

Table 2 shows the chemical formulas and powder diffraction files of the mineralogical phases identified in the steel mill scale sample, by X-ray diffraction.

Table 2. Mineralogical phases identified in the steel mill scale by X-ray Diffraction (XRD).

Name of the Mineralogical Phase	Chemical Formula	Powder Diffraction File (PDF)
Wüstite	FeO	46-1312
Hematite	Fe <sub>2</sub> O <sub>3</sub>	33-664
Magnetite	Fe <sub>3</sub> O <sub>4</sub>	19-629
Quartz (silica)	SiO <sub>2</sub>	46-1045
Magnesioferritte	MgFe <sub>2</sub> O <sub>4</sub>	36-398
Alumina (corundum)	Al <sub>2</sub> O <sub>3</sub>	43-1484

According to the data presented in the Figure 1 and Table 2, the mineralogical phases identified in the steel mill scale are: wüstite (FeO), hematite (Fe<sub>2</sub>O<sub>3</sub>), magnetite (Fe<sub>3</sub>O<sub>4</sub>), silica (quartz) (SiO<sub>2</sub>), magnesioferritte (MgFe<sub>2</sub>O<sub>4</sub>), and aluminum oxide (corundum) (Al<sub>2</sub>O<sub>3</sub>).

The results of the X-ray diffraction show that the mineralogical phases identified in the steel mill scale are also found in the mineralogical composition of the Portland cement. According to the references [12,13], the Portland cement consists mainly of lime (CaO), silica (SiO<sub>2</sub>), alumina (Al<sub>2</sub>O<sub>3</sub>), and iron oxide (Fe<sub>2</sub>O<sub>3</sub>). In conclusion, silica, alumina, and hematite are the main mineralogical phases both in steel mill scale and in the Portland cement.

Silica, alumina, and hematite are the main compounds of the cement and contribute to the formation of the dicalcium silicate (2CaO·SiO<sub>2</sub>), tricalcium silicate (3CaO·SiO<sub>2</sub>), tricalcium aluminate (3CaO·Al<sub>2</sub>O<sub>3</sub>), and tetracalcium aluminoferrite (4CaO·Al<sub>2</sub>O<sub>3</sub>·Fe<sub>2</sub>O<sub>3</sub>). According to the references [8,14], the steel mill scale can be reused in the cement and mortar compositions.

The mineralogical composition of the steel mill scale plays a key role in establishing the reuse domains.

#### 4. Conclusions

The main constituent of the mill scale is iron with 76.8%. Due to its high iron content, the steel mill scale can be reused as a source of raw material in the sustainable steelmaking industry.

The mineralogical phases identified in the steel mill scale are: wüstite (FeO), hematite (Fe<sub>2</sub>O<sub>3</sub>), magnetite (Fe<sub>3</sub>O<sub>4</sub>), silica (SiO<sub>2</sub>), magnesioferritte (MgFe<sub>2</sub>O<sub>4</sub>), and alumina (Al<sub>2</sub>O<sub>3</sub>). Silica, alumina, and hematite are the main mineralogical phases both in steel mill scale and in the Portland cement. These mineralogical phases contribute to the formation of the: dicalcium silicate, tricalcium silicate, tricalcium aluminate, and tetracalcium aluminoferrite. The results of the paper are promising and encourage the future research for establishing the optimal percentage for the reuse of the steel mill scale in the sustainable building materials.



**Author Contributions:** Conceptualization D.-A.I.-V., M.T., C.A. and I.-M.S.-B.; methodology D.-A.I.-V.; investigation D.-A.I.-V. and C.A.; writing—original draft preparation D.-A.I.-V., M.T., C.A. and I.-M.S.-B.; writing—review and editing D.-A.I.-V., M.T., C.A. and I.-M.S.-B.; visualization D.-A.I.-V.; supervision D.-A.I.-V.; project administration D.-A.I.-V.; funding acquisition D.-A.I.-V. All authors have read and agreed to the published version of the manuscript.

**Funding:** We acknowledge support by the Technical University of Cluj-Napoca.

**Acknowledgments:** This paper is written within the TUCN Internal Research Project Competition 2016 “Research concerning the characterization of the oily mill scale in order to identify an optimum method for reduction of the quantities of hazardous wastes landfilled”, internal competition for Research/Development/Innovation—Project 16362/07.07.2016, C.I. type 1.1-T4, Technical University of Cluj-Napoca (2016). The Internal Research Project Competition is funded by the Technical University of Cluj-Napoca in order to support the internal accredited research structures.

**Conflicts of Interest:** The authors declare no conflict of interest.

## References

1. World Commission on Environment and Development (WCED). *Our Common Future*; Oxford University Press: Oxford, UK; New York, NY, USA, 1987.
2. Rosen, M.A.; Kishawy, H.A. Sustainable Manufacturing and Design: Concepts, Practices and Needs. *Sustainability* **2012**, *4*, 154–174. [[CrossRef](#)]
3. Moldavska, A.; Welo, T. The concept of sustainable manufacturing and its definition: A content—Analysis based literature review. *J. Clean. Prod.* **2017**, *166*, 744–755. [[CrossRef](#)]
4. Houbart, M. *PLD-Erection of a Demonstrative De-Oiling Plant for Recycling Oily Steelmaking Sludge and Mill Scales*; LIFE11 ENV/LU/000855; Layman Report: Luxembourg, 2017.
5. Bienvenu, Y.; Rodrigues, S. *Manufacture of Metal Powders from Pulverulent Waste*, ENSMP; Centre des Matériaux, CNRS UMR 7633: Corbeil-Essonnes, France, 2007.
6. Saberifar, S.; Jafari, F.; Kardi, H.; Jafarzadeh, M.A.; Mousavi, S.A. Recycling evaluation of mill scale in electric arc furnace. *J. Adv. Mater. Process.* **2014**, *2*, 73–78.
7. Cartwright, D.; Clayton, J. Recycling oily mill scale and dust by injection into the EAF. *Steel Times Int.* **2000**, *24*, 42–43.
8. Murthy, Y.; Agarwal, A.; Pandey, A. Characterization of mill scale for potential application in construction industry. *Indian J. Eng.* **2017**, *35*, 71–76.
9. Iluțiu-Varvara, D.A.; Aciu, C.; Pică, E.M.; Sava, C. Research on the chemical characterization of the oily mill scale for natural resources conservation. *Procedia Eng.* **2017**, *181*, 439–443. [[CrossRef](#)]
10. Yang, Q.; Holmberg, N.; Bjorkman, B. EAF smelting trials of briquettes at Avesta works of Outokumpu stainless AB for recycling oily mill scale sludge from stainless steel production. *Steel Res. Int.* **2009**, *80*, 422–428. [[CrossRef](#)]
11. Iluțiu-Varvara, D.A.; Brândușan, L.; Arghir, G.; Pică, E.M. Researches about the characterization of metallurgical slags for landfilled wastes minimization. *Environ. Eng. Manag. J.* **2015**, *14*, 2115–2126. [[CrossRef](#)]
12. Soroka, I. Chemical and mineralogical composition. In *Portland Cement Paste and Concrete*; Palgrave: London, UK, 1979.
13. Lea, F.M. *The Chemistry of Cement and Concrete*; Edward Arnold: London, UK, 1970; p. 158.
14. Iluțiu-Varvara, D.A.; Aciu, C.; Tintelean, M.; Sas-Boca, I.M. Assessment of recycling potential of the steel mill scale in the composition of mortars for sustainable manufacturing. *Procedia Manuf.* **2020**, *46*, 131–135. [[CrossRef](#)]

**Publisher's Note:** MDPI stays neutral with regard to jurisdictional claims in published maps and institutional affiliations.



© 2020 by the authors. Licensee MDPI, Basel, Switzerland. This article is an open access article distributed under the terms and conditions of the Creative Commons Attribution (CC BY) license (<http://creativecommons.org/licenses/by/4.0/>).

# Peculiarities Regarding the Reconstruction of a Broken Grooved Shaft †

Bogdan Bucur \*, Constantin Bucur and Gabriela Andronic

“George Emil Palade” University of Medicine, Pharmacy, Science and Technology of Târgu Mures, Gh. Marinescu 38, 540142 Targu Mures, Romania; constantin.bucur@umfst.ro (C.B.); andronicgabriela86@gmail.com (G.A.)

\* Correspondence: bogdan.bucur@umfst.ro; Tel.: +40-721-498-449

† Presented at the 14th International Conference INTER-ENG 2020 Interdisciplinarity in Engineering, Mures, Romania, 8–9 October 2020.

Published: 22 January 2021

**Abstract:** The work remarks the peculiarities, which appeared in the reconstruction of a broken grooved shaft. The originality of the subject consists of the realization of a slotting tool, in material changing, which increased the reliability of the piece, and the total time of measuring the allocation to the work. The dimensional aspects specified include the adjustment, the tool making for profiling the groove, the choice of the material, and the required time to design and build the new spare part.

**Keywords:** splintering processing; grooved; CAD; slotting tool; semi-coupling

## 1. Introduction

Argument: for the machinery park to work with maximum, economic efficiency of mechanization and works automation, in addition to rational exploitation and the proper maintenance, the organization must be ensured and performing current and capitals repairs at a high technical level as well as of assemblies, [1].

The studied grooved shaft can be seen in Figure 1. The first findings on the damaged piece are as follows:

- the groove is made through injection up to the polyamide;
- contains two profiles, grooved and prismatic;
- has the number  $z = 12$  (channels);
- has two bores, the smallest being intended for fixing the coupling with an M5 screw.



Figure 1. Broken grooved shaft–plastic material/part.

## 2. Working Method

The construction stages of the new grooved shaft are as follows:

- determining the dimensions of the damaged piece;
- the execution of the drawings needed;
- material choosing;
- establishing the method of manufacturing the part;
- determining the time required for the manufacture;
- determining deviations of the new grooved shaft.

### 2.1. Dimensions of the Piece and Execution Drawing

The dimensions determining the defective piece are shown in Figure 2. It was achieved with some difficulty due to the advanced state of deterioration caused by impact. For dimensional detection it were used two micrometers of the exterior with an aperture of 0–25 and 25–50 mm were used for the measurements, having an accuracy of 0.01 mm and a caliper with a rod having an accuracy of 0.02 mm.

The CAD design media—Inventor Autodesk was used to elaboration on the drawings present in this paper. Groove assemblies are shaft-hub assemblies designed to transmit torque and rotational motion, [2].

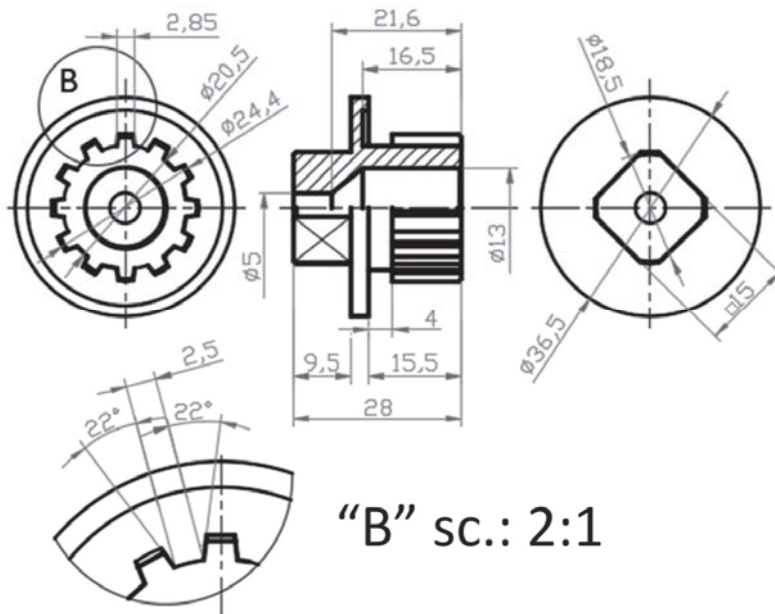


Figure 2. The execution sketch of the grooved shaft [3].

The shape of the groove protrusion is identified with the rectangular profile, but the piece which is made of polyamide, does not insist on the aspects related to the precision of execution (with external centering, with internal centering or with centering on the flanks). Argument: regardless of the category in which they fall, plastics have a high specific coefficient of expansion due to the Van der Waals bonds (weak bonds) between the chains and their conformation, [4,5].

The affected accuracy of the part in question is shown—Table 1.

**Table 1.** The coefficient of linear expansion [4].

Characteristic Properties	M.U.	Metal				Nylon 6.6	
		Steel	Al	Mg	Monowire	30% Fiberglass	30% Carbonfiber
The coefficient of linear expansion	$10^{-6}/K$	14	22	25	80	30	20

### 2.2. Choosing of the Material for the Grooved Shaft

The main framings of the polyamide are: Polyamide 6 (PA 6) and Polyamide 6.6 (PA 66). However by modifying the chemical structures (chain length and chemical organization), several other families of polyamides are obtained: PA 4.6; PA 6.10; PA 10.10; PA 11 and PA 12, [6]

Determining the type of polyamide that made up the defective piece was not insisted on, since another material will be chosen. The argument for this option as follows:

- it is desired to use a material with better properties in terms of impact/collision at breakage;
- since the piece will be machined by splintering, the newly chosen material must have technological and thermal properties superior to the original one;
- only one piece will be processed;

In order to improve the strength and hardness or of some technological properties (splintering, material castability, etc.), aluminum alloys with Mg, Cu, Mn, Ni, Zn, Ti, Li, Bi, Sb, etc. [7].

For the manufacturing process of the part was used the material: EN AW-6061/AlMg1SiCu (EN 573-3-2007) [5].

### 2.3. Machining of the New Grooved Piece

Of all technological processes necessary for execution of equipment, machinery, machines, the one of mechanical processing is most complex [8].

The notion of manufacture derives from two latin words *manus* (hand) and *factus* (to do), resulting combination meaning “hand made”. The formal term of “hand made” accurately described the manual methods used until the word “manufacture” was coined around 1567 [9], and it used as a verb, it first appears around 1683 [10]. Next, the piece will not be “hand made” totally, so we have the elements of technological process of mechanical processing are: operation, placement/position, phase, passage, handling and movement, [8]. The unique manufacturing system of the piece will use classic machine tools, a universal lathe SNB 400 × 750 [11] and a milling cutter machine FUS 22, [12].

### 2.4. Initial Turning of the Grooved Shaft

The processings performed on SNB 400 × 750, inside the machine tool laboratory of “George Emil Palade” UMFST of Târgu Mureş, are classic cutting operations, so this paragraph will not be developed, except for Figure 3, in order to argue the shape evolution of the semi-couple during its fabrication.



**Figure 3.** Cilindrical lathe of the semi-couple

### 2.5. Mortising the Grooved Profile

The manufacturing preparation of the FUS 22 machine (equipped with a slotter ram) takes into account the adjustment of MDPT system (machine, device, part and tool) as follows:

- design and construction, as well the related holder bar for the slotting tool;
- the piece centered in the universal of the index head and the axis centered of the slotter ram with respect to the axis of the piece, implicitly of the index head, can be observed in Figure 4.

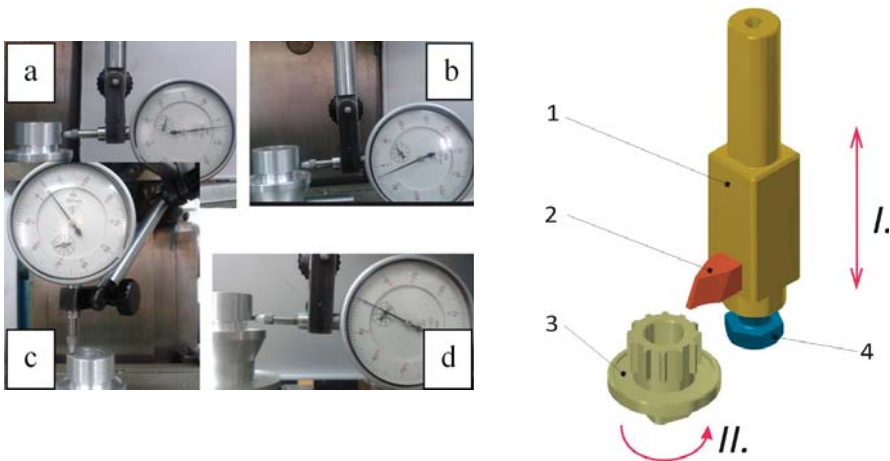


**Figure 4.** Measurement of deviations of fixing the part in the universal of the index head of FUS 22 machine tool: measuring the radial beat (a); axial deviation out of the X direction measurement (b); measuring frontal beat (c); axial deviation out of the Y direction measurement (d); Three-dimensional (3D) model of the slotting machine process: main cutting movement (I), indexing movement, executed by the part (II); mortising device (1) mortising knife-tool (2), part (3), screw for fixing the knife-tool (4).

When mortising, the main movement (alternating rectilinear) is performed vertically by the tool, and the feed movement (intermittent) is performed, at the end of each inactive stroke of tool [13,14], in the horizontal plane, also by the tool, however, in the transverse direction (particular case on—FUS 22 machine). By slotting, flat vertical surfaces can be generated with curvilinear profiles, channels of wedge, inner or outer grooves and teeth, etc. [13,14]. In the Figure 4, you can see the 3D model of the theoretical sintesis of the mortise process and the measurement of the deviations of fixing the piece in the universal slotter ram on the machine tool FUS 22:

- The measurement of the radial beat on surface “D” at a complete rotation of  $360^\circ$ , the result of dimensional deviation is exactly 0.03 mm;
- Axial deviation out of the X direction on surface “D” of the part, result of dimensional deviation is exactly 0.035 mm;
- Axial deviation out of the Y direction on surface “D” of the part, the result of dimensional deviation is exactly 0.00 mm;
- Measuring the frontal beat on surface “A” at a complete rotation of  $360^\circ$ , the result of dimensional deviation is exactly 0.045 mm.

After the mounting index head and slotter ram, both the semi-finished and the slotting tool, Kinematic adjustment parameters are established on the FUS 22 machine and after the positioning adjustments [15]: the main movement (alternative rectilinear) of the slotting tool  $n_{cd} = 50$  dr/min, the cutting advance  $s$  = manual, and an empirical calculation— $s = 0.0359$  mm/dr, is being determined

by knowing the timing (3'5''), to displacement at the cutting depth  $t = 1.95$  mm. About for the splintering knife-tool, the name is generally adopted for a wide range of single-tooth tools used in cutting processes, on universal lathes, revolver lathes, automatic, and semi-automatic, carousel lathes, on mortising, grinders, on boring machine, a.o. [16].

In Figure 5 you can see the scheme of the robot part that defines all the machined surfaces of the finished part.

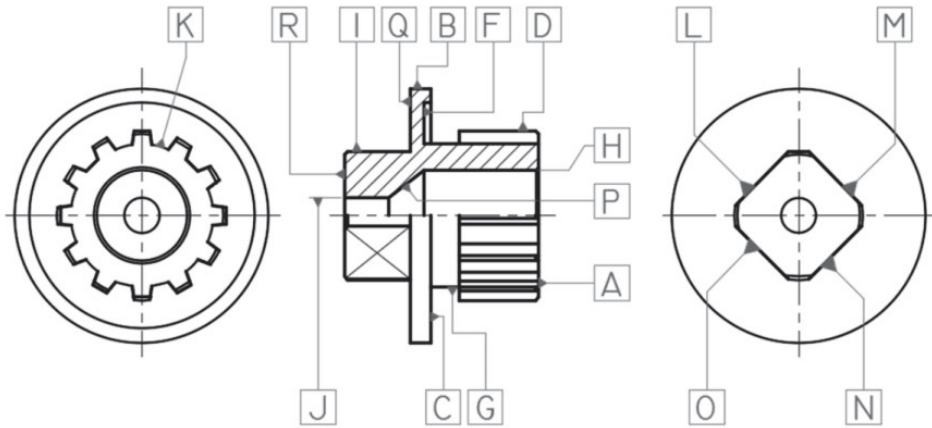


Figure 5. Letter of the surface on the piece [3,13].

Depending on temperature at they work, tools steels for cold processing, non-alloy and alloyed, with working temperature below 200 °C and tool steels for hot machining, alloyed, at which working temperature is over 200 °C, [7].

In Figure 6 you can see the details of the geometry of the active part of the mortising cutting tool, as well as the fixing in the mortising device.

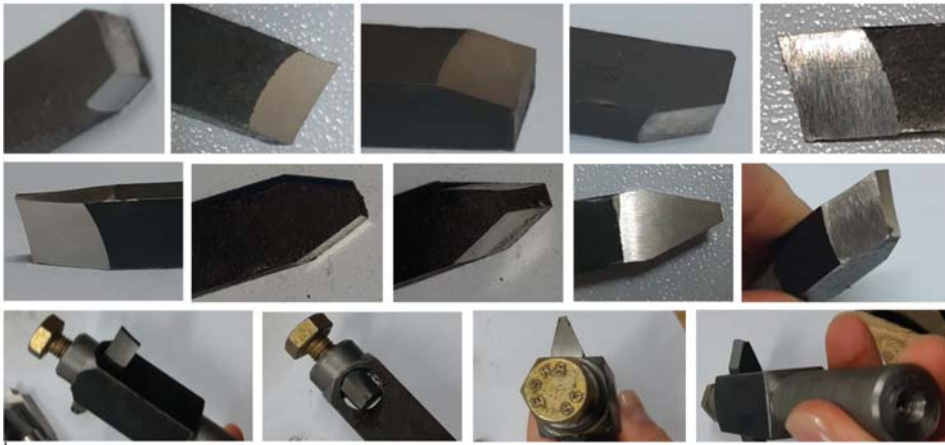
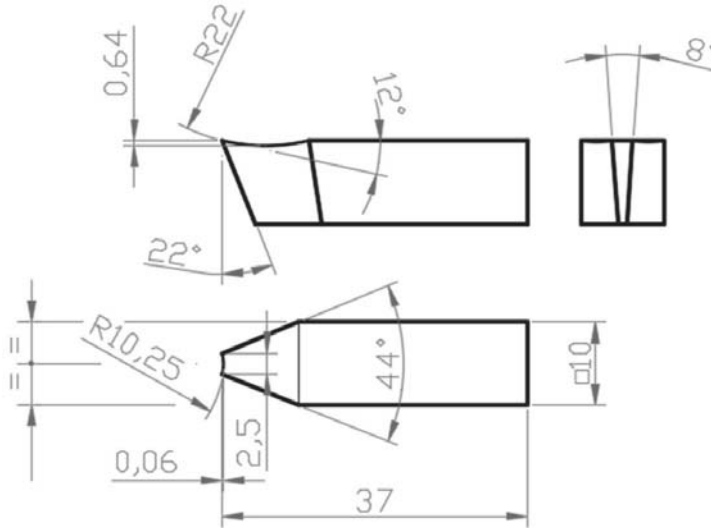


Figure 6. Shape evolution at the mortise knife manufacture.

Only one piece (aluminum) is fabricated, thus the chosen material for the mortise knife is C105U 1.1545 (SR EN ISO 4957:2002), [7].

According to the classification [15,17], the full name of the tool for cutting the groove is: Radial slotting tool of high-speed steel with a profile. In Figure 7 you can see all the geometric and constructive elements of the radial slotting cutting tool.



**Figure 7.** Geometric and constructive elements of the radial slotting tool and holder bar for cutting tool [3,15].

Following is the calculation of the simple indirect division [12,13] for the rotation of the index head axis at each executed channel (out of the 12 required channels):  $G_D$  is the number of holes on a circumference of disk  $D$ ;  $k$  is the number of traveled holes;  $Z_p$  is the number of divisions on the surface of the piece, relation (1). Therefore each channel will be divided, rotating the crank of the index head to three complete rotations, on a circle of  $G_D = 36$  holes plus  $k = 12$  additional holes displaced on  $G_D$ .

$$Z_p = \frac{k}{G_D} = \frac{40}{12} = 3 + \frac{40}{12} = 3 + \frac{12}{36} \quad (1)$$

In Figure 8 you can see practical aspects about manufacturing process of the grooved shaft.

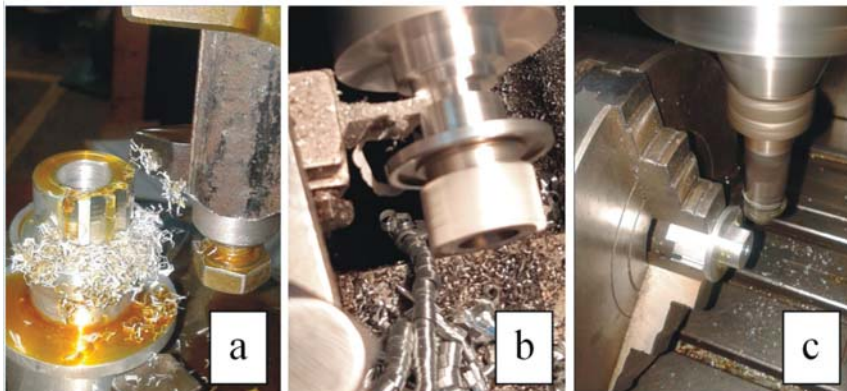


**Figure 8.** Slotting the groove (a), cutting the piece (b) and milling the square profile (c).



### 3. Results and Discussion

The total time includes: 1 h measurements + 1 h parametric modeling of three drawings + 1 h 55' slotting tool construction + 2 h 40' turning + 2 h 54' mortising + 1 h 19' turning again + 1 h 30' square profile milling, with a total of 11 h 38'. It is not possible to assess whether the realized time (11 h 38') is more or less, achieved. It would be desirable to conduct a theoretical calculation of time, for edification. Figure 9 shows the final result of the technological method approached for the manufacture of the grooved shaft, as well as the assembly whit conjugate part.

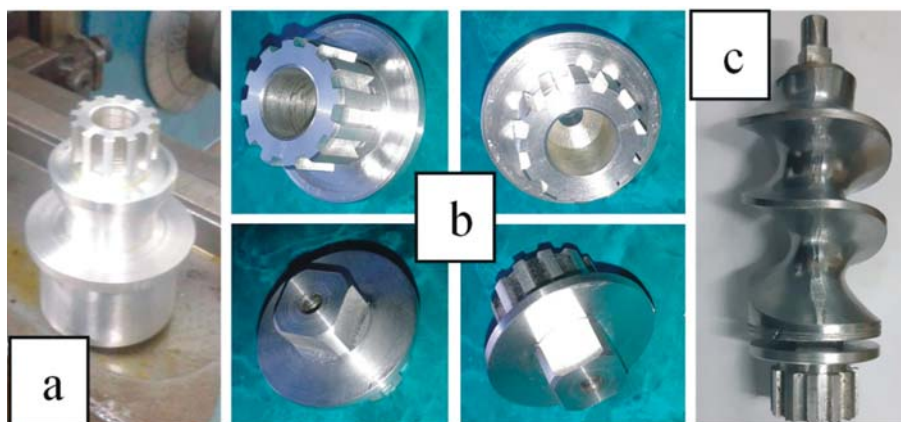


**Figure 9.** The piece after mortising (a), in four hypostases—the finished piece (b), the part-mounted piece on the worm (c).

For the working method presented, all the photo present in this paper are original and were taken in the laboratory M.U.—A014 of the “George Emil Palade” University of Medicine, Pharmacy, Science and Technologie of Targu Mures, Roomania.

### 4. Conclusions

The dimensions of the defective piece have been determined, in the Inventor-Autodesk enviroment. The necessary 2D and 3D drawings were designed, all the necessary technological steps, necessary tools, and adjustment of the machine tools were completed.

The slotting tool was conceived and built by the auto-endowment, and saving acquisition costs.

It was possible to piece the fabricate in required parameters, according to the endowment of the laboratory. Therefore, no other faster or cheaper fabricatiione ways are disputed (3D printing or CAD/CAM). In this sense, it would be interesting to have a comparison.

### References

1. Paraschiv, D. *Metal Surface Reconditioning and Processing of the Manufacturing Technologies (Tehnologii de Recondiționare și Procesări ale Suprafețelor Metalice)*; Junimea Publishing House: Iasi, Romania, 2005.
2. Jula, A.; Lateș, M. *Machine Parts (Organe de Mașini)*; Transilvania University Publishing House: Brașov, Romania, 2004.
3. Tero, M.; Bucur, B.; Bratu, G. *Descriptive Geometry and Technical Drawing (Geometrie Descriptivă și Desen Tehnic)*; Napoca STAR Publishing House: Cluj-Napoca, Romania, 2013.
4. Available online: <https://gsb-international.de/media/pdf/image/4C6A17BD7A044FB8B71D8F0108F4F21C.PDF> (accessed on 31 December 2020).
5. Available online: [https://metcenter.ru/t/en\\_573-3.pdf](https://metcenter.ru/t/en_573-3.pdf) (accessed on 31 December 2020).



6. Available online: <https://www.resinex.ro/tipurile-de-polimeri/pa.html> (accessed on 31 December 2020).
7. Socaciu, T. *Elements of the Materials Science and Engineering (Elemente de Știința și Ingineria materialelor)*; “Petru Maior” University Publishing House: Târgu Mureș, Romania, 2011.
8. Nae, I.; Petrescu, M.G.; Bucuroiu, R. *Modern Techniques in the Management and Supervision of the Technological Processes, Physics and Modern Technologies (Tehnici Moderne în Conducerea și Supravegherea Proceselor Tehnologice, Fizica și Tehnologiile Moderne)*; Society of Physics of Moldova: Chișinău, Moldova, 2008; Volume 6.
9. Frățilă, D. *Manufacturing Basics (Bazele Fabricației)*; UTPRESS Publishing House: Cluj-Napoca, Romania, 2019.
10. Groover, M.P. *Fundamentals of Modern Manufacturing, Materials, Processes, and Systems*, 4th ed.; John Wiley & Sons, Inc.: Hoboken, NJ, USA, 2010.
11. *The Machine Book—for Universal Lathes from Group B—Basic Type SNB 400 (Cartea Mașinii—Pentru Strungurile Universale din Grupa B—Tip de Bază SNB 400)*; Lathe Enterprise: Arad, Romania, 1979.
12. Available online: [https://kupdf.net/download/masina-de-frezat-universala-pentru-scularie-fus22-vol-1\\_5af5501fe2b6f5bb64666f16\\_pdf](https://kupdf.net/download/masina-de-frezat-universala-pentru-scularie-fus22-vol-1_5af5501fe2b6f5bb64666f16_pdf) (accessed on 31 December 2020).
13. Grama, L. *Manufacturing Technologies in Machine Construction (Tehnologii de Fabricare în Construcția de Masini)*; “Petru Maior” University Publishing House: Târgu Mureș, Romania, 1999.
14. Teodor, V. *Basics of Machining Processes (Bazele Proceselor de Prelucrare prin așchiere)*; “Dunarea de Jos” University Publishing House: Galați, Romania, 2008.
15. Dițu, V. *Basics of Metal Cutting. Theory and Applications (Bazele Așchierii Metalelor. Teorie și Aplicații)*; MatrixRom Publishing House: București, Romania, 2008.
16. Căpățînă, N. *Cutting Tools (Scule Așchietoare)*; “Dunarea de Jos” University Publishing House: Galați, Romania, 2008.
17. Rusu, Ș.; Rozsa, F. *Guide book for Mortising Processing. (Îndrumar Pentru Prelucrări Prin Rabotare și Mortezare)*; Technical Publishing House: București, Romania, 1983; Volume I.

**Publisher’s Note:** MDPI stays neutral with regard to jurisdictional claims in published maps and institutional affiliations.



© 2021 by the authors. Licensee MDPI, Basel, Switzerland. This article is an open access article distributed under the terms and conditions of the Creative Commons Attribution (CC BY) license (<http://creativecommons.org/licenses/by/4.0/>).

# Modeling and Simulating the Static Structural Response and Lift Off of a Preloaded Bolted Joint on a Flange <sup>†</sup>

Rami Alfattani 

Department of Mechanical Engineering, College of Engineering, Umm Al-Qura University, Makkah 24224, Saudi Arabia; rafattni@uqu.edu.sa

<sup>†</sup> Presented at the 14th International Conference INTER-ENG 2020 Interdisciplinarity in Engineering, Mureş, Romania, 8–9 October 2020.

Published: 11 December 2020

**Abstract:** The present paper describes the structural analysis performed on a preloaded bolted joint. The first joint modeled was comprised of a conventional cylindrical flange that was sliced to simplify the analysis for two bolts in lieu of four. This involved an L-shaped flat segment flange. Parametric studies were performed using elastic, large-deformation, non-linear finite element analysis to determine the influence of several factors on the bolted-joint response. The factors considered included bolt preload, contact surfaces, edge boundary conditions, and joint segment length in this first approach. The second model applied the previous preloaded torque on a complex flange to study the flange lift off. Joint response is reported in terms of displacements, gap opening, and surface strains. Most of the factors studied were determined to have minimal effect on the bolted joint response.

**Keywords:** static structural response; preloaded bolted joints; large-deformation analysis; non-linear finite element analysis

---

## 1. Introduction

In the International Journal of Mechanical Engineering, Welch argues that the preloaded (or pre-tensioned) bolted joints are sufficiently tightened to create joint closure while aligning the connecting components, which are tightened further to yield the required bolt preload and (more critically) a faying surface compressive load [1]. The faying face of a joint section is the prepared face (fabricated or ground) that connects with the faying face of a different joint component. Preloaded joints are essential in providing stiff joints that do not slip. The bolts possess substantial mean stress but have a lower range of working stress, which confers preloaded joints excellent fatigue functionality. Therefore, this research aims at analyzing the structural response and preloaded bolt joint lift off on flanges based on Welch argument [1].

We used elastic, large-deformation, non-linear finite element analysis to achieve this goal. We used two kinds of flanges to implement the technique: An L-shaped flat section flange and a sophisticated flange. The investigation was simulated using Ansys Workbench, while the Inventor Autodesk was used to build the geometry.

According to Oldfield and to Knight, eccentric loading to the fasteners greatly facilitates the separation of bolted joints. Such behavior of joints increases the possibility of bolt fatigue, principally because of the moments the bolts carry during lifting [2,3]. Thoppul and Somasundaram contend that many traditional flanges exert some quantity of eccentric weight on the fasteners [4,5].

Integrated Systems Research, Inc. analyzed the reaction of eccentrically loaded bolted joints by investigating the relative advantages of different features of joints on increasing separation resistance [6]. There was a presentation of the findings of surface analysis behavior of traditional cylindrical design

of a flange. Just like any vital bolted connection, finite element analysis should be used to finalize the preliminary design.

The study should integrate any safety issues, partial safety issues, and design factors, or allowable design stresses and loads requirement of the local regulations during the design of the equipment to satisfy specific needs and should precede any similar considerations that this paper proposes.

## 2. Materials and Methods

### 2.1. Joint Arrangement

Figure 1 illustrates the configuration of the preloaded bolted joint. It has two 5-inch flange sections of 0.656-inch-thick material. A 3/8-inch-diameter bolt in a large-diameter cylindrical casing is used to connect the flange specimens. It is normal not to know the exact preload force of the bolt. Nevertheless, the estimated preload torque was 300–600 ft-lb. The flanges were split for the simulation to be conducted using just two bolts to simplify the investigation.

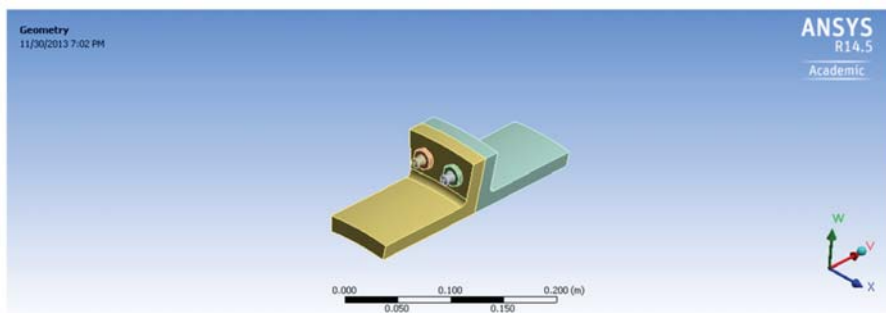


**Figure 1.** Two bolts were used to simulate the preloaded bolted joint of the flange.

### 2.2. Material Characteristics

It was assumed that the bolted joint material was (ABI 5L X52) carbon steel, which yielded 52 ksi of stress [7]. Because elastoplastic investigations were expected, it needed the material information as a type of actual stress being the function of plastic stress [8]. Medium carbon steel (SAE Grade 5), which yielded strain of 120 ksi, was assumed to be the material for the bolts and nuts [7]. The bolts and nuts in these investigations were postulated to have a linear elastic response and thus had no explicit modeling.

### 2.3. Stress Estimation in a Bolt

An evaluation of bolt stress depends on a simple material strength technique for the bolt and speculates a maximum use of bolt material before damage or failure, for instance, when the entire bolt cross-sectional area produces stress. The assumptions of bolt preload constitute a particular preload torque  $T$ . Preload Axial force,  $F$ , relates to the preload torque [9] as:

$$T = k \times F \times d, \tag{1}$$

where  $k$  is a nut factor to account for threads friction between nut and bolts [10].  $d$  is the bolt diameter. For permanent links:

$$F = 0.9 \times A_t \times S_p, \tag{2}$$

where  $S_p$  is the bolt's strength;  $A_t$ , the area of tensile stress, can be illustrated as:

$$A_t = 0.7854 \times (d - 0.9743/n)^2, \tag{3}$$

where  $d$  represents the nominal diameter in inches, while  $n$  is thread numbers in each inch (pitch).

A preloaded bolt with an axial force of 5927 lb produces a nominal preload torque of 444 ft-lb and a nut factor of 0.2. The force gives the initial bolt stress because of the preload of 92 ksi. Thus, the full stress of the bolt is calculated as the total of the stresses from the mechanical loads and preload stresses. Therefore, the total estimation of the bolt stress is 70 ksi. This result is entirely below the bolt material yield stress of 120 ksi. The definition of developing bolt yield force is a preload force capable of completing the cross-sectional yielding of a bolt (i.e., bolt yield stress multiplied by the cross-sectional area of the bolt), which equals 53,000 lb.

#### 2.4. Assumptions During Modeling

The development of these stress analysis models has several common assumptions. This simulation makes two key assumptions that should be discussed. First, the finite components did not have an explicit representation of the bolts and nuts; their effect was rather simulated. One-dimensional elastic beams represented the bolts. Second, the efforts to compute the finite element models were lowered by splitting the flange for the analysis of just two bolts as Figure 1 indicates. This reduced the CPU processing time and simplified the investigation.

### 3. Method of Analysis

A pipe with an internal pressure of 1 MPa was used to connect the flanges. Internal pressure was used as a second load in the simulation after the application of bolt pre-tension. Figure 2 shows the development of a non-linearity problem in connected areas. A 0.1 friction factor was assigned to the area of contact between the two flanges [11]. It sat asymmetrically, meaning the contacting regions will have a single side manifestation. The flanges were clamped by tightening the bolts and nuts.

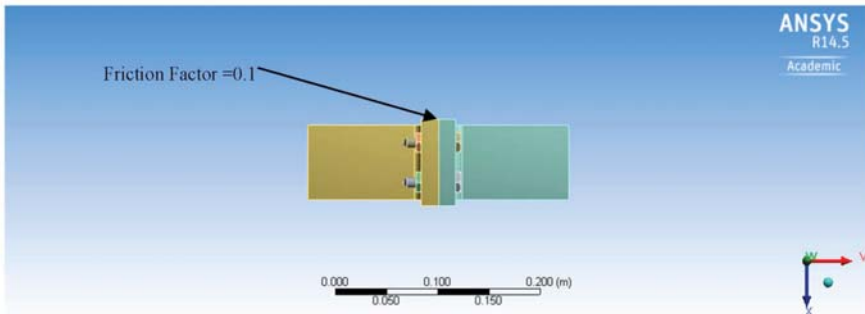


**Figure 2.** The friction factor at the area of contact between the two flanges that develops the non-linearity problem.

Meshing is an essential factor in modeling, with bolts being vital maximum stress areas. Figure 3 shows the mapping and meshing of geometry using a Hexahedron connection. After the experiment, the geometry was altered by making it stiffer to achieve a more complex geometry for the investigation and comparison of joint behavior; see Figure 4.

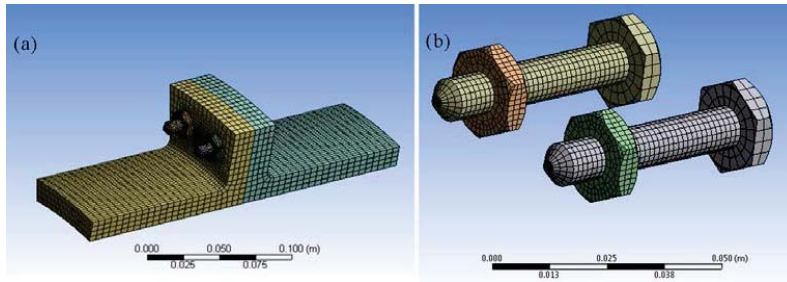


Figure 3. Hexahedron connection was used to map and mesh the (a) the flange (b) the bolts and nuts.

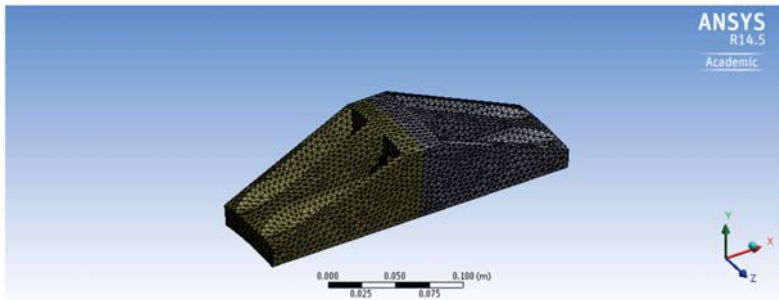


Figure 4. A complex geometry is generated to make a stiffer joint.

### Numerical Results

The utilization of various computer-assisted engineering investigation tools was needed in the engineering examination of the bolted joint arrangement. The tools included those that represented geometry, produced the models for infinite elements, performed analysis of the structure, and those that refined the computed findings. Besides this, system response was studied through analysis to determine modeling challenges to facilitate the precise bolted joint structure simulation and to offer pre-investigation predictions, should these need to arise. Various measures such as the bolt axial load function, fixed end reaction force, separation of flanges (or lift-off), lateral joint displacement, and strains were used to characterize the joint behavior.

Ansys Workbench 14.5 was used for all the analyses. There are two primary stages involved in the investigation. First was the application of bolt preload axial force at a particular value and watch local damage and stress response. Second, internal pressure application acted on the wall of the pipe. These were non-linear analyses as a result of explicit association modeling between the surfaces of the flanges.

### 4. Solutions for Static Structures

Figure 5 shows the structural behavior of a preloaded bolted joint. The bolt load is a function of the applied torque. The baseline analysis has two phases. Application of (5927 lb) preload onto the modeled flanges and monitoring its behavior to the initial stress is the first phase. This tightens them in a manner that simulates how a bolted joint tightens. Simulating water through a (1 Mpa) internal pressure pipe is the second phase.

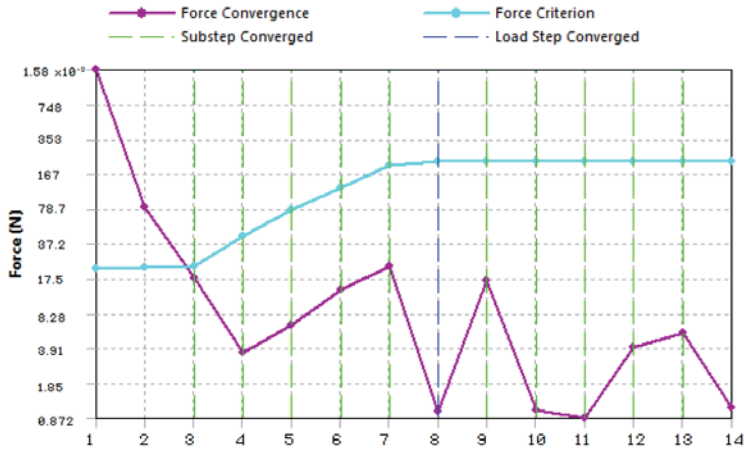


Figure 5. The phases of the structural behavior of a preloaded bolted joint.

Figure 6 shows flange separation (or lift-off) based on the reaction force. There is a non-linear increase of the lift-off, and the opening of the gap nearly reaches 0.005 inches with the application of the 5927 lb load. Nevertheless, there was no total separation of the flanges. Figure 7 shows flanges gliding atop and around the bolts.

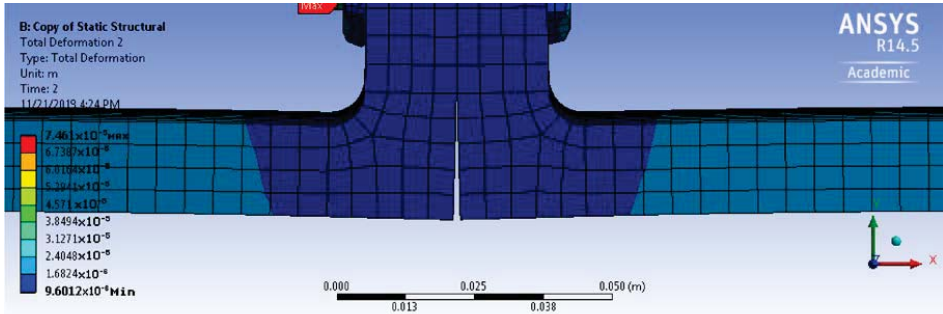


Figure 6. The flanges separation under load.

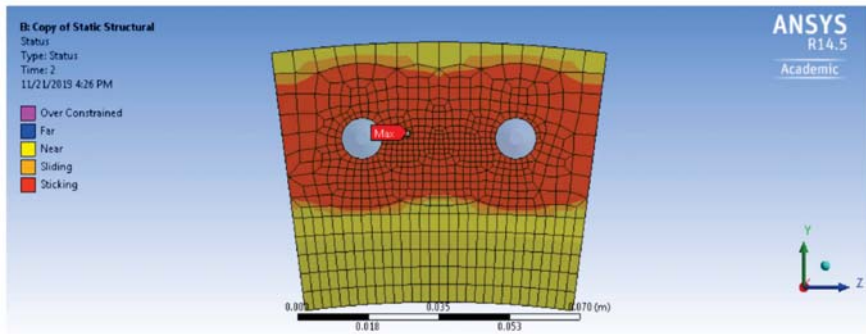


Figure 7. The flanges gliding atop and around the bolts.

Figure 8 shows the bolt equivalent static strains. The strains originate from the center of the bolt between the head of the bolt and the nut. The average value of the strain depicts the nominal stress of the membrane. The specimen has minimal surface strain extent at the design load locations. Besides this, these strain findings reveal significant joint bending behavior at the reaction load.

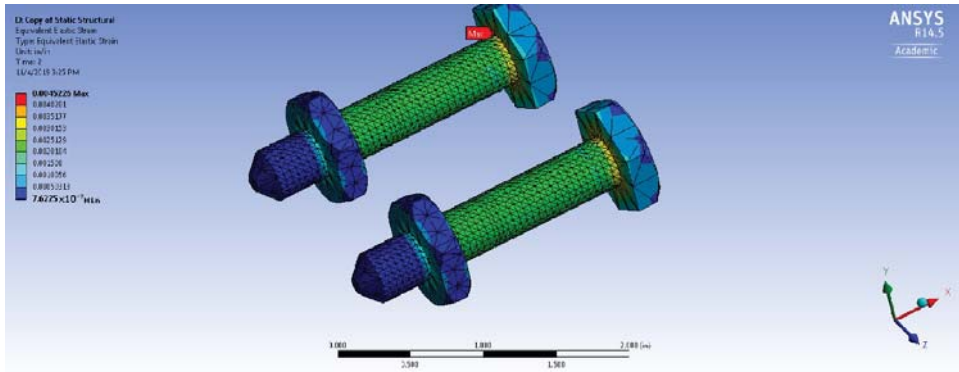


Figure 8. The bolt equivalent static strains as a function of the reaction load.

Figure 9 shows the joint's lateral displacement. The front surface is used to measure the lateral movement at the joint interface; it is uniform across the joint width. Positive measures show a standard direction displacement of the joint to the back surface, while negative results show a standard movement of the joint to the front surface. These findings indicate an outward displacement of the bolted joints (the front face direction).

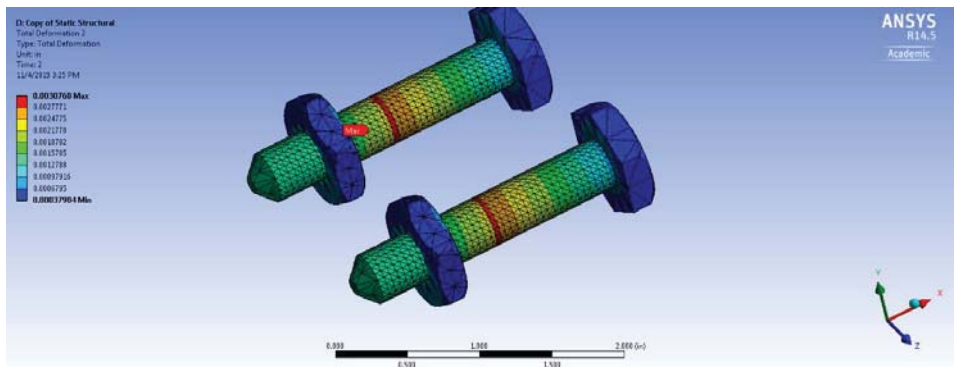


Figure 9. The joint's lateral displacement as a reaction force function.

Figures 10 and 11 show the axial deformation and the load von Mises stress  $\sigma_{vm}$ . These figures show the results for the 5927 lb load, including low von Mises levels of stress on the flanges. Many high-stress results are as a result of the flange bolts experiencing preload states. The corner of the head of the bolt also exhibits high stress as a result of the sharp model ends, which are absent in a real bolt.



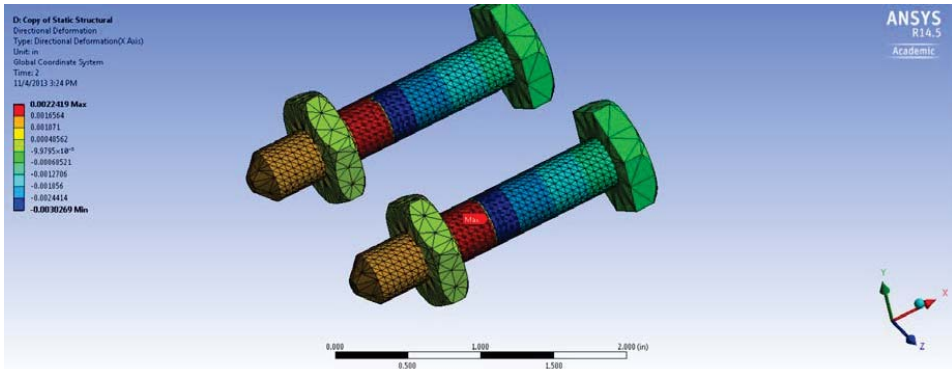


Figure 10. The axial deformation of a preloaded bolted joint.

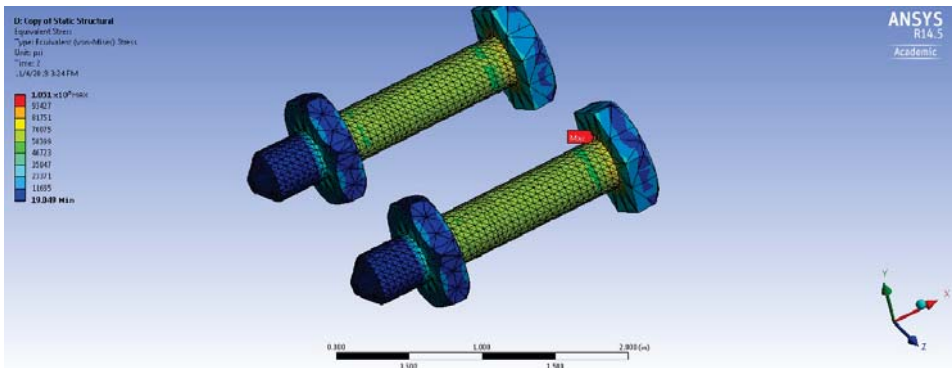


Figure 11. The equivalent stress (von Mises) of a preloaded bolted joint.

These findings show that it is easy to simulate the primary structural behavior of a preloaded joint. The technique is to first evaluate the condition of the preloaded joint, then to apply the external mechanical loads. In this investigation, a uniform internal loading pressure was imposed as the external loading. Next, parametric investigations are conducted to identify the factors that have significant effects on predicting the structural behavior of the joint.

Application of simple geometry (L-shape) bolt preload torque was the first modeling hypothesis to be considered. In the model for finite analysis, the preload axial force, computed using Equation (1), was specified instead of the preload torque. Nevertheless, in an ordinary bolted joint, a torque wrench is used to measure the preload torque. The joint structural behavior is indicated based on the bolt load and the induced internal pressure but assuming a 0.2 nut factor.

### *Influences of Complex Geometry*

Analyzing similar circumstances on a complex geometry that Figure 4 shows was the second hypothesis of modeling. It was to investigate the influence of increasing stiffness and reduce the lift-off behavior.

The findings show that there was an improvement in the primary structural behavior of the preloaded bolted joint. Both nut and bolt stresses were reduced; this facilitated the adjusted geometry to maintain a higher load, as shown in Figure 12. Figure 13 clearly shows that there was a reduction of the lift-off response, while the flanges stuck to each other.



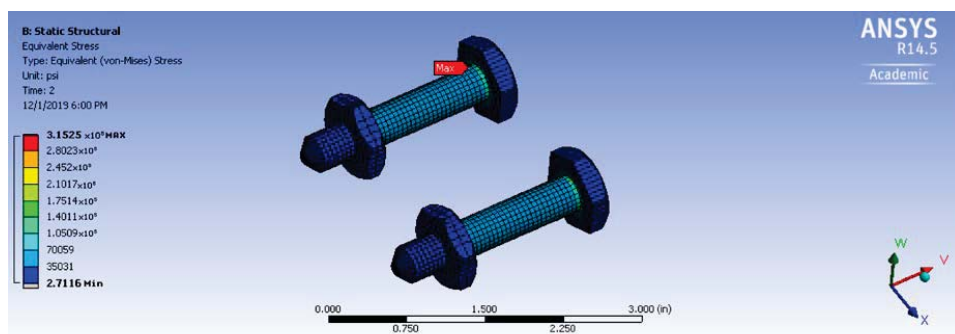


Figure 12. The equivalent stress (von Mises) of a preloaded bolted joint on the complex flanges.

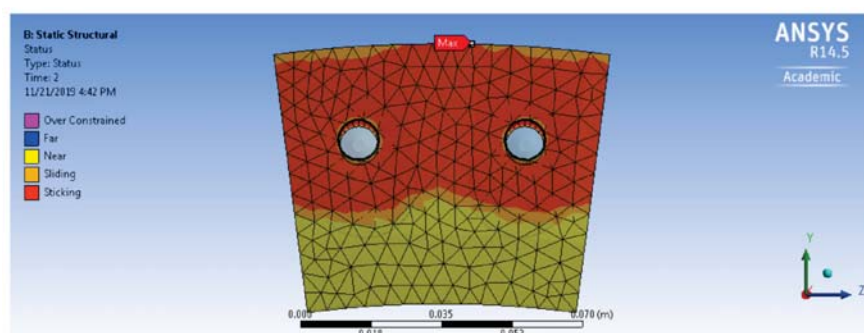


Figure 13. The complex flanges gliding atop and around the bolts.

## 5. Conclusions and Discussion

This paper explains the analysis of structural bolted joint arrangement to describe primary modeling and the requirements for investigations, and determines that the arrangement significantly influences the behavior. The Ansys Workbench 14.5 code was used to perform an elasto-plastic, large-deformation, non-linear finite element analysis. Various factor analyses were conducted, and it revealed that the bolts were the most significant factor affecting the response of the bolted joint. It was determined that modifying the flanges could diminish the response of the preloaded bolts. The parametric study results offer insights to lead future bolted flanges modeling and simulations. There are some uncertainties in the simulation of structural joint and connection behavior such as the ones in these experiment models, which can be averted by calibrating the results of this analysis with test findings.

**Funding:** This research received no external funding.

**Conflicts of Interest:** The author declares no conflict of interest.

## References

1. Welch, M. A Paradigm for the Analysis of Preloaded Bolted Joints. *Stroj. Časopis-J. Mech. Eng.* **2019**, *69*, 143–152. [\[CrossRef\]](#)
2. Oldfield, M.; Ouyang, H.J.; Mottershead, J.E.; Kyprianou, A. Modelling and Simulation of Bolted Joints under Harmonic Excitation. *Mater. Sci. Forum.* **2003**, *440–441*, 421–428. [\[CrossRef\]](#)
3. Knight, N.; Phillips, D.; Raju, I. Simulating the Structural Response of a Preloaded Bolted Joint. In Proceedings of the 49th AIAA/ASME/ASCE/AHS/ASC Structures, Structural Dynamics, and Materials Conference, Schaumburg, IL, USA, 7 April 2008.

4. Thoppul, S.D.; Gibson, R.F.; Ibrahim, R.A. Phenomenological modeling and numerical simulation of relaxation in bolted composite joints. *J. Compos. Mater.* **2008**, *42*, 1709–1729. [CrossRef]
5. Somasundaram, D.S.; Trabia, M.B.; O'Toole, B.J. A methodology for predicting high impact shock propagation within bolted-joint structures. *Int. J. Impact Eng.* **2014**, *73*, 30–42. [CrossRef]
6. Zeng, G.Y.; Zhao, D.F. Simulation and Experiment of Dynamics of Flange Structure with Bolted Joint. *Adv. Mater. Res.* **2011**, 335–336, 543–546. [CrossRef]
7. ToolBox, E. Bolt Stretching and Tensile Stress. Available online: [https://www.engineeringtoolbox.com/bolt-stretching-d\\_1164.html](https://www.engineeringtoolbox.com/bolt-stretching-d_1164.html) (accessed on 2 May 2020).
8. Fan, H.; Malsbury, J. Handbook for Bolted Joint Design, NCSX-CRIT-BOLT-00 14 February 2007. Available online: [https://ncsx.pppl.gov/NCSX\\_Engineering/Design\\_Criteria/BoltedJoint/NCSX-CRIT-BOLT-00-Signed.pdf](https://ncsx.pppl.gov/NCSX_Engineering/Design_Criteria/BoltedJoint/NCSX-CRIT-BOLT-00-Signed.pdf) (accessed on 3 May 2020).
9. Shigley, J.E. *Shigley's Mechanical Engineering Design*; Tata McGraw-Hill Education: New York, NY, USA, 2011.
10. Chambers, J.A. *Preloaded Joint Analysis Methodology for Space Flight Systems*; NASA Technical Memorandum: Cleveland, OH, USA, 1995.
11. Daniel, P.H. The Design and Fabrication of a Passive and Continuously Repositionable Joint. Ph.D. Thesis, Massachusetts Institute of Technology, Cambridge, MA, USA, 2013.

**Publisher's Note:** MDPI stays neutral with regard to jurisdictional claims in published maps and institutional affiliations.



© 2020 by the authors. Licensee MDPI, Basel, Switzerland. This article is an open access article distributed under the terms and conditions of the Creative Commons Attribution (CC BY) license (<http://creativecommons.org/licenses/by/4.0/>).



Article

# Innovation of Pull and Torque Testing Device for Cable Cords <sup>†</sup>

Cristina Havadtöi

Faculty of Engineering and Information Technology, “George Emil Palade” University of Medicine, Pharmacy, Science, and Technology of Targu Mures, Nicolae Iorga street, No. 1, RO-540088 Targu Mures, Romania; chila.cristina@yahoo.com

<sup>†</sup> Presented at the 14th International Conference INTER-ENG 2020 Interdisciplinarity in Engineering, Mureş, Romania, 8–9 October 2020.

Published: 16 December 2020

**Abstract:** The paper presents in the first part a diagnosis of the frequency per year of the pull and torque test followed by an analysis of the average time given to each attempt, a comparison of the average time spent on the torquing and pulling test and the average times to perform the other tests. In the second part there is a forecast of the times spent performing the test following the optimization. The optimization is performed in the first phase at project level in the Inventor Professional 2018 program. The testing method is not foreign to companies that produce cable cord, and is it described in at least two standards. The latest developments in the electronics field show an optimization on two separate devices for each stress, pull and torque. The goal of this paper is to present an optimization of the device for pull stress testing, in order to proceed with both of the stresses on one device. The optimization aims to reduce the time spent by the quality tester in the metrological laboratory on this test. Following the optimization, in the forecast it was found that the quality of work was improved by reducing working hours and removing human assistance as much as possible in order to eliminate the errors caused by it.

**Keywords:** cable cords; cable testing; pull and torque testing method; pull and torque testing equipment; reducing working time

---

## 1. Introduction

In modern industry, any company producing electrical cables must set its quality goals as paramount in order to remain a market leader [1]. In order to maintain its place on the market, the company must ensure the quality [2] of the products with a set of qualitative tests performed in the metrological laboratory. The tests must have a large scale to cover any possibility of premature failure and to ensure the efficiency of the product. Real attention should be paid to the potential for fires caused by wiring and its characteristics [3,4], and thermal aging [5], which reduces the safety of the electrical system [6].

One goal is the policy of continuous improvement [7], which aims to optimize the process, innovation, research and development as well as optimize working hours in the production process.

Optimization of the device aims to facilitate the work of the quality team in the metrological laboratory and to reduce the time used normally for this kind of test.

## 2. Innovation Need

Several analyses were carried out by the company in order to have a view of the entire time spent on the test in the metrological laboratory.

The method [8] helped to confirm the integrity of the product in the following four cases of application:

1. Stumbling on the cord cable when the socket is positioned at the bottom of the wall. For example, the cord is attached to a vacuum cleaner and the user moves the appliance, creating a tension of the cable through which it no longer sits on the floor but will be taut above the floor.
2. Pulling the product from its cable, in cases where the user tries to unplug the appliance by pulling directly on the appliance or pulling on the cable, instead of unplugging it by the plug.
3. Transporting or lifting the product by its cable. If the appliance is small, this includes appliances weighing 1 kg or less, such as hair dryers or curlers.
4. Attempting to move a product that is still electrically connected in cases where an appliance such as a vacuum cleaner is pulled from the cable.

The cables tested were the usual types, for daily use in house appliances.

The research was based on diagnosing the current condition of the cord to determine the level at which it operates. The diagnosis was based on three major points: (1) determination of the place of the test in relation to the other test performed in the laboratory, (2) determination of the average time spent on each test, and (3) determination of the time spent on the pull and torque test.

### 2.1. Frequency of The Test

Determination of the annual number of tests was made in order to ascertain its position in relation to the other tests performed in the metrology laboratory. In Figure 1 shows all the tests performed in the laboratory and their frequency during 2019.

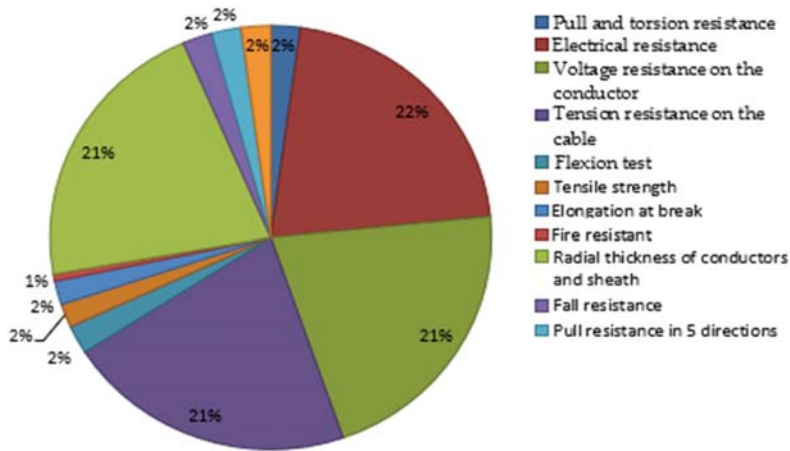


Figure 1. Frequency of laboratory tests during one year.

The diagram shows that routine or sample tests were performed at a higher frequency, routine tests being performed in the continuous flow of production and sample tests being performed on each sample to ensure product compliance. Type tests are tests that are performed on the product before delivery to ensure that the product is consistent with the requirements.

The pull and torque test is a type test performed at a frequency of 2% in a year; compared to the other tests performed, it had a much lower rate, but considering the time spent on this operation, it took longer than the sample ones. The sample test had a 21–22% rate, which was 118 times, compared to 12 times for the pull and torque test.

### 2.2. Time Spent on Each Test

When analyzing the average time of testing it was observed that the most time spent by the operator was on the test to determine the resistance to voltage in the cable and the resistance to falling

(Figure 2). For the pull and torque test, the laboratory technician spent 39 min to determine the conformity of the product.

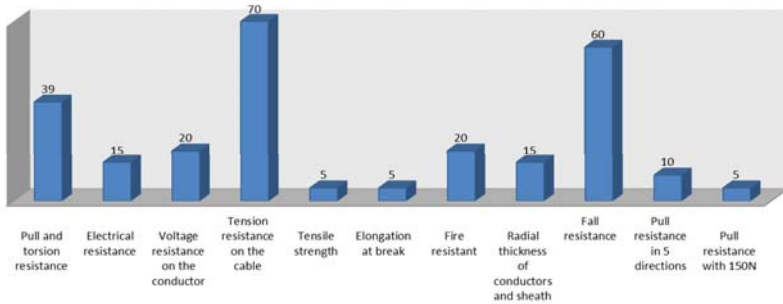


Figure 2. Average time in minutes given to each test.

Compared to other tests that were performed in the laboratory, this test required twice as much time as the electrical resistance, which was determined to be 15 min.

Routine or sample tests had a higher frequency but were performed in less time than the pull and torque tests; this was mainly due to the large number of operations involved in this test.

### 2.3. Average Time Provided for the Method

The relatively long time for the method was due to the two stresses to which the cord was subjected, the tensile stress and the torsional stress.

In this case the electrical resistance was determined as 15 min, the total time calculated for all operations taking place for this test.

In cases of determining the conformity of the cords in the test for pull and torsion, the average time of performance was divided by all the operations that took place, as we see in Figure 3. The preparation of the test piece, which consists in cutting it to size, stripping the jacket about 10 cm, stripping the conductors about 1.5 cm, and automatically measuring the electrical resistance, was carried out in an average time of 5 min. Preparing the device, which consists of measuring the weight required to perform the test using the scale, took an average of 3 min. Preparing the plug, which consists in marking it in order to have a comparison at the end of the tests, had a duration of 1 min. Preparing the device for the torsion test had a duration of 5 min, which consists in positioning in the vise. The weight measurement, which has to be accurate, was made in 3 min. Fixing the cord took place in 2 min, and the test itself lasted for 1 min. The electrical resistance has an important value because it shows the integrity of the plug within.

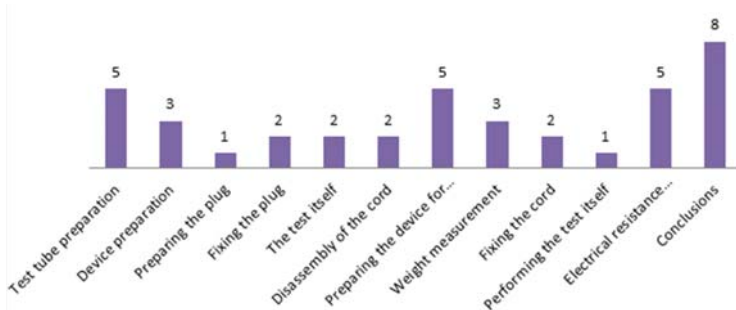


Figure 3. Average times of pull and torsion tests.

### 3. Optimization of the Device in Inventor Professional 2018

The latest developments in this field show that there are a series of electronic devices that can perform this test separately, which means that there is one device for the pull test and another one for the torque test, although between the two devices the most important role is played by the weight because it sets the hardness of the test. Researching the international market for the types of equipment used for this kind of test, there are limited options [9–12].

Optimization of the device has the goal to facilitate the work of the quality team in the metrological laboratory and to reduce the time used normally for this kind of test.

#### 3.1. Innovation of the Device

The version of the device that was used in the laboratory had manual actuation, which means that the 100 cycles were done by the staff manually, and the device for the torque test was separate from the device for the pull test. The staff had to walk every time from one operation desk to another, which was unnecessary time and could be reduced by an innovation of the device, so it could do both of the tests on one device.

Several measurements were carried out because the weight that rolls on the filleted bar could not roll to the minimal point, tangent to the body of the device, because of the fixing device for the cable. In order for the weight to roll and make a complete cycle, the bar that holds the weight was moved below, as Figure 4 shows. The prototype for this device was made in the Inventor Professional 2018 program.

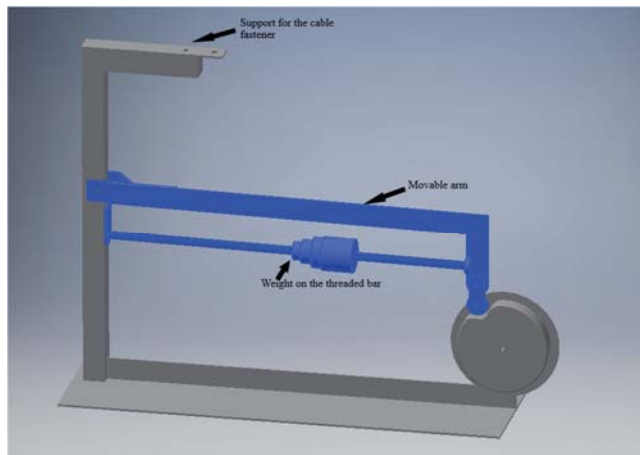


Figure 4. The pull device.

The basis of innovation was considered to be the last level at which the optimized product was located. Taking into account the latest research in this field, two separate, automated devices were used for that test.

The principle of use of the torsion device, following the innovation, changed completely. Despite the fact that the principle of operation remained identical to the previous one, the emphasis was on facilitating and excluding possible human errors that may occur as a result of the empirical use of the device.

The optimization of the device consisted in remodeling it so that both tearing and twisting requests could be executed on the same device. Taking into account the fact that a force of 100 N was applied in the pull-out test, which transformed into a unit of weight was 10,197 kg, and to the torsion test a force

of 12.5 N was applied, which, transformed, was 1275 kg, it was necessary to be able to slide the weight so that the margin of force on the glazing bar passed through the cable clamp.

For the tensile stress, the device was subjected to the optimization of the movable arm for the application of the weight; the position of the weight, as can be seen in Figure 4, was changed by placing the threaded bar at the bottom of it. At the top, the support for the cable fastener was kept, the initial bar being fixed by the support rods at the bottom.

For the pull-out and torsion test device, the force arm is of major importance because its optimization in terms of achieving a torque of less than 3 kg at the moment of force creates the possibility of using the weight for both tests. This optimization can be achieved only by constructing the arm so that the weight can slide over the entire arm to make a full stroke, but once it reaches the turning point its value is equal to 0.

Mathematically, the value of the moment of force is equal to the product of the value of the force arm and the value of the force [13].

$$M = b \times F \text{ N/m.} \tag{1}$$

In relation to the moment of force, the force is directly proportional to the force arm, so as the weight slides toward the fixing point, it decreases and the force arm will also decrease.

Both the force and the force arm are specified in IEC 66335-1 [8], as seen in Table 1.

**Table 1.** Torques applied to the pull-out and torsion test [8].

Couple	Section mm <sup>2</sup>
0.10 Nm	2 × 0.5
0.15 Nm	2 × 0.75
	3 × 0.5
0.25 Nm	3 × 0.75
F = 12.5 N	2 × 1.00
Bf = 2 cm	3 × 1.00
0.5 Nm	2 × 1.5
F = 25 N	3 × 1.5
Bf = 2 cm	

For torsional stress, the device used was remodeled and optimized so that it could be joined and fitted to the pull stress device. The questions underlying the determination of the appropriate location were closely related to the position of the cable fastener where the weight value is measured.

The optimized device for the torque test is presented in Figure 5, from front and rear view. The location in the upper part of the body allowed easy access to the cable entry hole for tensile stress and torsional stress when inserting the cord for the use of the same weight.

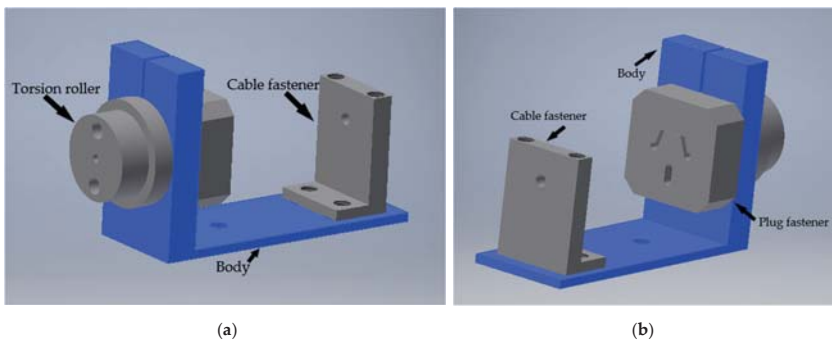


**Figure 5.** The torsion device. (a) Front view; (b) Rear view.



Compared to the original device, the optimized one, which is shown in Figure 6, was changed by moving the position of the cord fixing support, which was made for clamping, to the side of the device. To fix the cord in the initial device, a mobile fastening system was used that slid on the support but was fixed by screws, which in this phase is no longer possible, so the fixation was placed directly on the body of the traction device, and it will no longer be necessary to remove the traction device.

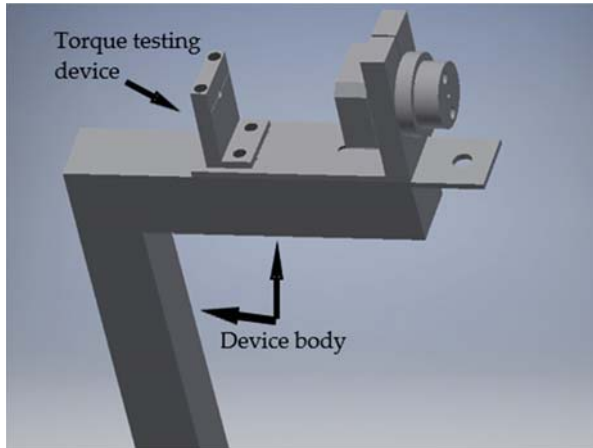


Figure 6. Position of the torsion device.

The cord that is attached to the torsion roller, and with which the device will be operated, will pass through the hole on the body of the device. The cord is fastened to the cable clamp used for the tensile stress.

### 3.2. Tests on the Device

The first tests on the new device took place in May and were recorded in metrological bulletins. Following the implementation, 12 trials were performed to establish the effectiveness of the optimization. As can be seen in Figure 7, in the determination of the conformity of the cords in the tensile and torsional test on the optimized device, the average performance time was divided for all operations taking place, the preparation of the specimen and the electrical resistance were performed in the same time, an average of 5 min.

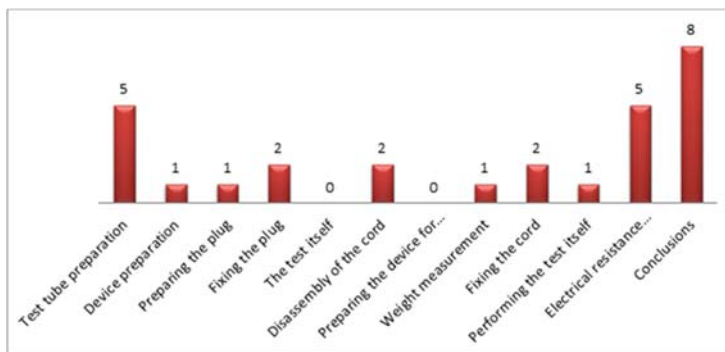


Figure 7. Average time of operation included in the pull and torsion test after optimizing the device.

The preparation of the device, which consisted in placing the weight necessary to carry out the test on the threaded bar next to the marking of the force provided in the standard, took on average 1 min.

The marking of the plug and the cord was performed in an average time of 1 min, after which its fixing between the clamping device on the arm of the device required on average 2 min. The test itself to perform the pull stress by rotating the eccentric of the device 100 times takes a total of 2 min but is no longer performed by the laboratory, thus allowing work such as, for example, the metrology bulletin to be completed at the end of the test and its disassembly for 2 min. The preparation of the device to perform the torsional stress was excluded because it no longer required time, but was kept in the diagram in order to have a vision of the optimization.

The measurement of the weight used in this test, which consists in positioning it in relation to the dimension on the bar indicating the appropriate weight, was carried out in 1 min. Fixing the plug in the device was done on average in 2 min. The test took an average of 1 min, measured with a stopwatch. The measurement of the electrical resistance, after the test, took on average 5 min, after which, following the observations of the test piece, the conclusions and possible discussions were made, which lasted on average 8 min. By summing up all the operations, it was observed that the average time to perform the operation was 28 min.

#### 4. Comparison between Test Results before Optimization and after Optimization

Following the implementation of the optimized device it was necessary to study the effectiveness of the device to conclude whether the proposed purpose was met and had a strong impact on the quality of working time of the staff in the metrology laboratory in a power plant.

The first step in the conclusion was a comparison between the durations of the operations that were part of the pull and torsion test before and after the optimization.

When overlapping the two average times obtained, as shown in Figure 8, from the beginning there was a decrease in times due to the presence of zero times when testing on the optimized device. Zero times were found in the first phase of the test itself, where the presence of the laboratory was no longer required. This was due to its automation, during which time staff could perform other tasks. This operation initially took 2 min. The second phase, the operation of preparing the torsion device, which consisted of fixing in the vise and lasted an average of 5 min, was completely excluded from the series of operations performed during the test on the optimized device because the vise was now attached to the device at a well-established, fixed place, not needing fixing in advance.

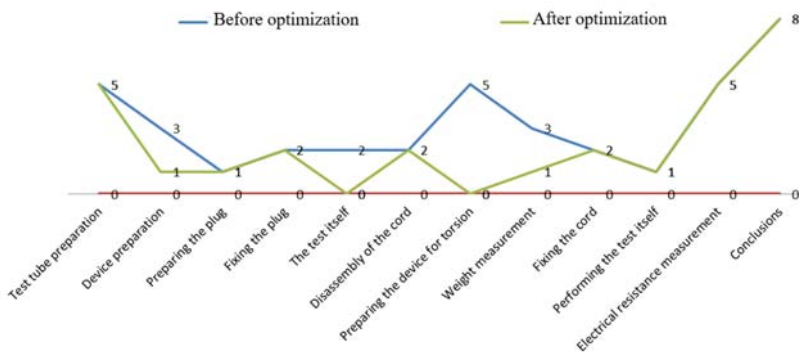


Figure 8. Comparison between the durations of the pull and torsion test operations before and after optimization.

#### 5. Conclusions

As the diagram shows, the average time allotted for sticking the device decreased considerably from 3 min to 1 min. This operation consisted of measuring the force required in placing the scale on

the upper surface of the plug fixing plate, after which the scale hook was fixed on the threaded bar, next to the cable fixing device. The force, N, in weight, was transformed to kg, then the weight was slid on the bar until the set force was reached. At the moment, the weight was slid on the bar next to the force marking on the plate.

Another decrease in working time due to optimization was found in the weight measurement operation for the torsional stress, which this time was performed on those devices so there was no need for measurement, as the location of the weight is next to the marking on the plate.

The efficiency of the device was distinguished by performing the test as quickly as possible, at the same quality as the previous one or at a higher quality. Excluding human intervention as much as possible raises the level of test quality by reducing errors such as manual traction, where lack of constant force and speed can cause involuntary jerks that damage the product.

**Conflicts of Interest:** The author declares no conflict of interest.

## References

1. Moldovan, L. *Managementul Calitatii (Quality Management)*; University “Petru Maior”: Targu-Mures, Romania, 2011; pp. 17–23.
2. Moldovan, L. *Certificarea Coformitatii (Certification of Conformity)*; University “Petru Maior”: Targu-Mures, Romania, 2011; pp. 3–5.
3. Andersson, P.; Rossell, L.; Simonson, M. Small and Large Scale Fire Experiments with Electric Cables under Well-ventilated and Vitiated Conditions. *Fire Technol.* **2004**, *40*, 247–262. [[CrossRef](#)]
4. Zhang, B.S.; Zhang, J.Q.; Li, Q.; Wang, L.F.; Xie, H.; Fan, M.H. Effects of Insulating Material Ageing on Ignition Time and Heat Release Rate of the Flame Retardant Cables. *Procedia Eng.* **2018**, *211*, 972–978. [[CrossRef](#)]
5. Šaršounová, Z. The Inconveniences Related to Accelerated Thermal Ageing of Cables. *Transp. Res. Procedia* **2019**, *40*, 90–95. [[CrossRef](#)]
6. Xie, H.; Zang, J.-Q.; Liu, Y.; Zhang, B.; Wang, L.; Fan, M. Study on Insulation Failure Time and Failure Temperature of the Aged Cables under External Heating. *Procedia Eng.* **2018**, *211*, 1012–1017. [[CrossRef](#)]
7. Moldovan, L. QFD employment for a new product design in a mineral water company. *Proc. Technol.* **2014**, *12*, 462–468. [[CrossRef](#)]
8. IEC 60335-1. *Household and Similar Electrical Appliances—Safety—Part 1*, 5th ed.; The International Electrotechnical Commission: Geneva, Switzerland, May 2010.
9. Huanyu Microcomputer Plug and Pull Force Tester. Available online: <https://www.amazon.com/Huanyu-Microcomputer-Force-Tester-Machine/dp/B01M6UYROH> (accessed on 15 July 2020).
10. Plug Socket Pull—Out Testing Machine. Available online: <http://www.bndtestequipment.com/plug-socket-and-switch-test-equipment/plug-socket-pull-out-testing-machine.html> (accessed on 15 July 2020).
11. Cord Grip Test Apparatus. Available online: <https://www.indiamart.com/proddetail/cord--grip-test-apparatus-5699994791.html> (accessed on 15 July 2020).
12. Horizontal Plug Insertion Force Tester Pull Off Tester. Available online: <https://www.labtestchamber.com/sale-10859663-horizontal-plug-insertion-force-tester-pull-off-tester.html> (accessed on 15 July 2020).
13. Pîrvulescu, L.D. *Fundamente de Inginerie Mecanică (Fundamentals of Mechanical Engineering)*; Editura: Timisoara, Romania, 2018; pp. 2–5.

**Publisher’s Note:** MDPI stays neutral with regard to jurisdictional claims in published maps and institutional affiliations.



© 2020 by the author. Licensee MDPI, Basel, Switzerland. This article is an open access article distributed under the terms and conditions of the Creative Commons Attribution (CC BY) license (<http://creativecommons.org/licenses/by/4.0/>).

# Fine Electrolytic Tough Pitch Copper Multistage Wiredrawing Pass Schedule Design by Analytical and Numerical Methods <sup>†</sup>

Oscar Rodríguez-Alabanda <sup>1,\*</sup>, Esther Molero <sup>1</sup>, Marius Tintelecan <sup>2</sup>,  
Guillermo Guerrero-Vaca <sup>1</sup>, Pablo E. Romero <sup>1</sup> and Gustavo Aristides Santana Martinez <sup>3</sup>

<sup>1</sup> Department of Mechanical Engineering, University of Cordoba, Medina Azahara Avenue, 5, 14071 Cordoba, Spain; esther.molero@uco.es (E.M.); guillermo.guerrero@uco.es (G.G.-V.); p62rocap@uco.es (P.E.R.)

<sup>2</sup> Department of Materials Processing Engineering, Faculty of Manufacturing and Materials Engineering, Technical University of Cluj-Napoca, 28 Memorandumului Street, 400114 Cluj-Napoca, Romania; marius.tintelecan@ipm.utcluj.ro

<sup>3</sup> Engineering School of Lorena, University of São Paulo-USP, Lorena, SP 12602-810, Brazil; gustavo.martinez@usp.br

\* Correspondence: orodriguez@uco.es

<sup>†</sup> Presented at the 14th International Conference INTER-ENG 2020 Interdisciplinarity in Engineering, Mures, Romania, 8–9 October 2020.

Published: 11 December 2020

**Abstract:** Electrolytic tough pitch copper is commonly used in electric and electronic applications while fine copper wires are widely used in electronic conductors. A multi-pass wiredrawing process was designed for the manufacturing of fine pure copper wire, from 0.50 mm to 0.10 mm in diameter. The analytical model and the finite element analysis (FEA) were performed to validate the pass schedule design. The initial wire was mechanically characterized, and the pass schedule design was established by the analytical method according to the specific criteria. The sequence of wiredrawing passes was modeled in the finite element method (FEM) software in order to analyze and validate the designed pass schedule. The combination of these methods allowed designing and validating the wiredrawing pass schedule to implement it in a real process with guaranteed results. This work contributes in showing a combined methodology for the design and virtual validation of the pass schedule in the case of multistage wiredrawing of ETP copper fine wires.

**Keywords:** multi-pass wire drawing process; Deform2D; fine ETP copper wire; slab method; finite element method

## 1. Introduction

Fine wire is manufactured with metals such as stainless steel, gold, magnesium, tungsten, rhodium and copper by a sequential multi-pass wiredrawing process [1–6]. Copper fine wires have a wide range of applications as semiconductors and bonding wire in electronics, medical devices, shielding applications or measurement sensors, as is shown in Figure 1.

Fine round section copper products are manufactured by wiredrawing with polycrystalline or natural single crystal diamond dies [7]. Its good formability allows to easily draw from rod into very fine wire sizes without intermediate annealing treatment. Usually, the area reduction of pure copper is limited to about 90% just before a first annealing. Beyond that level of reduction, metallurgical structure changes dramatically degrade the wire's mechanical properties. Fine copper wire is often produced by sequential multi-pass wiredrawing, the so-called “in line process”, which involves moderate advancing speed combined with continuous annealing.



Figure 1. Representative applications of fine pure copper wire.

The importance of die geometry is crucial in single-step and multi-step wire drawing process and the influence of the reduction and bearing zones affects directly on the drawing force ( $F_d$ ), drawing stress ( $\sigma_d$ ) and stress distribution in its radial ( $\sigma_{radial}$ ) and axial ( $\sigma_{axial}$ ) components, among other output variables [6,8–10].

On the other hand, analytical methods have long been used for modeling wire drawing. Rubio et al. demonstrated the feasibility of the combination of the slab method and numerical simulation for the single-step drawing process analysis [11–13]. Hassan et al. studied the influence of different process inputs, geometrical and technological, applying the free body equilibrium Equations (1) and (2) obtained by the slab method in the drawing process and evaluating the results by a comparison with those obtained in the numerical simulations [14]. Rodriguez-Alabanda et al. developed a software application for designing and optimization of multi-step wire drawing processes which is based in the implementation of the slab method [13,15]. The slab method analytical model and the finite element method (FEM) model of the single step process are shown in Figure 2.

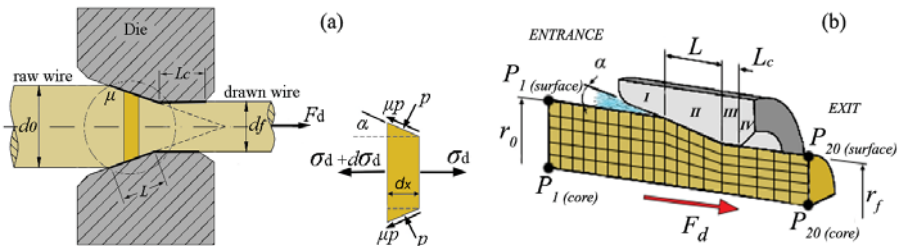


Figure 2. (a) The slab method in the drawing process: from free body equilibrium to Equation (1) to calculate the drawing stress; (b) the graphic of the finite element method (FEM) model used in the simulations.

Regarding the metal to be drawn,  $\sigma_y$  corresponds to the yield stress while  $\alpha$  is the semi-angle of the drawing die,  $d_0$  refers to the initial diameter of the wire and  $d_f$  is the diameter at the exit of the die. In the Figure 2,  $p$  is the normal die-wire pressure,  $L$  is the contact length of reduction cone,  $L_c$  is the bearing length and  $\mu$  corresponds to the friction coefficient at the die-wire interface.

$$\sigma_d = \sigma_y \cdot \frac{1+B}{B} \cdot \left[ 1 - \left( \frac{d_0}{d_f} \right)^{2B} \right] \quad (1)$$

where

$$B = \mu \cdot \cot \alpha \quad (2)$$

One of the most advanced analytical models for the calculation of the drawing stress ( $\sigma_d$ ) was developed by Avitzur [16,17] and later approached by Bitkov [6,18] from the implementation of the so-called upper bound method in the drawing process (Equation (3)), where  $r_i$  and  $r_f$  indicate the initial and final radius of the wire and  $f(\alpha)$  is a function of the die semiangle. Thus, in wire drawing,

the reduction ratio is noted as  $r$  and represents the degree of total area reduction possible without intermediate annealing as a function of the composition of the metal to be drawn (Equation (4)).

$$\frac{\sigma_d}{\sigma_y} = \frac{\frac{\sigma_{back}}{\sigma_y} + 2 \cdot f(\alpha) \cdot \ln \frac{r_0}{r_f} + \frac{2}{\sqrt{3}} \cdot \left( \frac{\alpha}{\sin^2 \alpha} - \cot \alpha \right) + 2\mu \cdot \left\{ \cot \alpha \cdot \left[ 1 - \frac{\sigma_{back}}{\sigma_y} - \ln \frac{r_0}{r_f} \right] \cdot \ln \frac{r_0}{r_f} + \frac{L_c}{r_f} \right\}}{1 + 2 \cdot \mu \cdot \frac{L_c}{r_f}} \quad (3)$$

$$r = 1 - \frac{d_f}{d_0} \quad (4)$$

As denoted from the above models, the friction factor has a great significance in the wiredrawing process. A negative effect of friction in the drawing process can have as a consequence non-uniform distribution of stress intensity on the metal into the reduction zone and may cause non-uniform distribution of mechanical properties on the final wire cross section. The friction coefficient ( $\mu$ ) can be calculated by using the Avitzur’s upper bound model equation [16,17,19], together with the data of the wire drawing force obtained empirically, and the most favorable value obtained under the different lubrication conditions used in the experiment has been used in the multi-step wiredrawing process modelization and FEM analysis.

Computer-aided numerical simulation of the wiredrawing process offers great potential in the sense of analysis and design of this type of process and previous works consulted [1,2,20], which demonstrated its viability for implementation in the case of multi-step wiredrawing case. The finite element method (FEM) has been implemented successfully in many previous research works consulted [5,21–24].

The present work constitutes an analytical-numerical study concerning the experimental procedure for the initial characterization of the metal and with the aim of determining the best tribological conditions of the wire drawing process object of study. The research is focused on the involvement and combination of both methods for the design and analysis of responses such as the drawing stress or the distribution of radial and axial stresses in the final drawn product in multi-step sequencing. It is a meaningful effort because the good implementation of this combined procedure allows to understand the process conditions leading the way for a specific product quality and functional properties improving the productivity. The structure of the paper is organized as follows: In the Materials and Methods section, we describe the copper properties and characteristics, in addition to all the specific methods and equipment used. The results from analytical as well as finite element method (FEM) simulations are presented in Results section and, finally, concluding remarks are mentioned in the Conclusions section.

## 2. Materials and Methods

The experimental procedure was applied to determine the plastic deformability of the commercial Cu-ETP (99.94% Cu) wire with 0.5 mm diameter and a length of 200 mm in the annealed condition implemented in the original industrial process. This wire is a semi-elaborated product that is annealed in a continuous induction system, just at the end of the production process. Since our objective was to study the possibilities of processing this material in a subsequent fine wiredrawing process, a tensile test was performed to obtain the mechanical properties of specimens.

Both Ludwik–Hollomon strain hardening model defined by Equation (5) and multilinear isotropic strain hardening (MLISH) rule were checked to simulate the material behavior in the FEM software. The MLISH was checked assigning a value of stresses equal to  $\sigma_y = 143$  MPa at  $\varepsilon = 0$  unitary true strain and  $\sigma_{UTS} = 349$  MPa when  $\varepsilon = 0.3706$  (Figure 3).

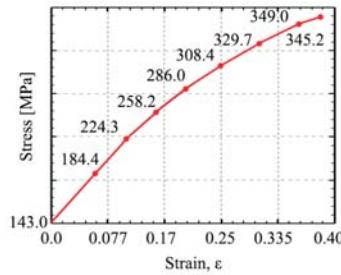


Figure 3. Multilinear strain hardening rule obtained from the tensile tests.

On the other hand, for the initial copper wire tested, the elastic modulus is  $E = 14001.92$  MPa, yield strength  $\sigma_{y,0.2\%} = 143$  MPa, break limit  $\sigma_{UTS} = 349.04$  MPa, constant  $K = 496$  MPa and strain hardening coefficient  $n = 0.34$ . Finally, the Ludwik–Hollomon strain hardening model was selected to analyze the results in the FEM simulations.

$$\sigma_{\epsilon(i)} = \sigma_{0(i)} + K \cdot \epsilon^n \tag{5}$$

$\epsilon$  is the unitary deformation in the step ( $i$ ),  $\sigma_{0(i)}$  in the initial yield strength of the metal to be drawn and  $\sigma_{\epsilon(i)}$  is the yield strength of the drawn metal after this drawing step.

In a second experimental phase, the single-step wiredrawing at different speeds were implemented with the aim of calculate the friction coefficient ( $\mu$ ) using a mineral oil lubricant and calculating the lower value for  $\mu$  from these experimental results. The experimental procedure was done using a single block drawing machine and a conical wiredrawing die with a core made of polycrystalline diamond (PCD) with  $2\alpha = 14^\circ$  and  $L_c = 50\% \cdot d_f$ , geometrical features and core material recommended by Esteves group [25], commonly used in the case of copper wiredrawing. The drawing stress  $\sigma_d$  was determined by a direct measure of the drawing load ( $F_d$ ) with a load cell and signal acquisition system installed on the machine (Figure 4). Finally, the optimal values of  $\mu$  were determined indirectly, analytically and by polynomial interpolation of the results.

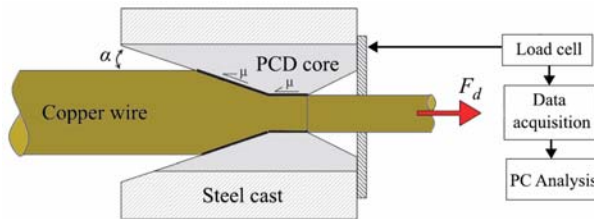


Figure 4. Experimental setup for the indirect determination of the friction coefficient  $\mu$ .

Next, and knowing the plastic behavior of the material, in addition to the minimum value of the friction coefficient obtained by the analytical-empirical method, the analytical method was applied to design the multi-step wiredrawing process for the manufacture of fine wire, using the PullWorks computer application developed for this purpose [26]. This software tool is friendly to use for a user with a certain experience since all the working input conditions must be introduced in the software interface: the material strain hardening is a function of its mechanical properties and the geometric and tribological parameters for each of the consecutive dies/steps constituting the sequential process. However, the software refers to a desired value for the shape coefficient  $\Delta$  in all the process for the multi-stage wiredrawing sequence design. A value  $1 < \Delta < 3$  reduces the effect of friction while lower values near to one  $1 < \Delta < 2$  minimize wear in the die contact surface, too [27]. In this specific work, the value of delta was fixed as  $\Delta = 1$  with aim of obtaining a short sequence of steps for the



designed wiredrawing process and, theoretically, minimizing friction and wear effects. This coefficient is geometrically defined as the quotient between the average diameter ( $d_m$ ) and contact length ( $L$ ), noted in the Equation (6).

$$\Delta = \frac{d_m}{L} = \frac{d_0 + d_f}{d_0 - d_f} \cdot \sin\alpha \tag{6}$$

Finally, numerical simulations were performed to analyze the proposed multi-step wiredrawing pass schedule using Deform2D FEM software [28]. The model of the initial wire consists of quadratic elements in a perfect plastic wire for the axisymmetric case and the three-dimensional system was simplified in a two-dimensional problem in terms of longitudinal as well as radial dimensions. This initial portion was considered as isotropic body of Ø0.5 mm per 2 mm long and meshed in a linear-quadratic array of 10 elements in the radial direction and 80 elements in the axial direction. For the subsequent simulations of the whole sequence of drawing passes, the accumulated stress and strain state was considered. The drawing dies were modelled as a perfectly rigid body since the interest of this work is focused on the deformation of the wire. It should be noted that, for the purpose of simplifying the design of the rows and the simulations, there was a constant distance from the entry point to the reduction cone to the exit point of the row equal to 1 mm (zones II to IV). The lower value of the friction coefficient  $\mu$ , obtained from the experimental measurements, was implemented in the simulations as Coulomb’s type friction. It must be noted that the effects of backward tension ( $\sigma_{back}$ ) and thermal increment generated during the process were neglected in the present approach. The friction coefficients were obtained for different drawing speeds and implementing the measurements of the drawing force in Equations (7) and (8), according to Avitzur’s Equation (3).

$$\mu = \frac{\sigma_0 \cdot \left[ \frac{\sigma_{back}}{\sigma_0} + 2 \cdot f(\alpha) \cdot \ln \frac{r_0}{r_f} + \frac{2}{\sqrt{3}} \cdot \left( \frac{\alpha}{\sin^2\alpha} - \cot\alpha \right) \right] - \sigma_d}{2 \cdot \left[ \left( \frac{L_c}{r_f} \cdot \sigma_d \right) - \left\{ \sigma_0 \cdot \left[ \cot\alpha \cdot \left( 1 - \frac{\sigma_d}{\sigma_0} - \ln \frac{r_0}{r_f} \right) \cdot \ln \frac{r_0}{r_f} + \frac{L_c}{r_f} \right] \right\} \right]} \tag{7}$$

$$f(\alpha) = \frac{\left\{ 1 - \cos\alpha \cdot \sqrt{1 - \frac{11}{12} \cdot \sin^2\alpha} + \frac{1}{\sqrt{11 \cdot 12}} \cdot \ln \frac{1 + \sqrt{\frac{11}{12}}}{\sqrt{\frac{11}{12} \cdot \cos\alpha + \sqrt{1 - \frac{11}{12} \cdot \sin^2\alpha}}} \right\}}{\sin^2\alpha} \tag{8}$$

In summary, in the presented procedural methodology, an experimental first phase is indispensable for the determination of the mechanical properties that define the behavior of the metal against cold deformation hardening using wiredrawing. The application of the analytical method implemented in software for the design of the desired sequence of steps for the multi-step process is proposed below, and it is demonstrated how the numerical method and the FEM simulations complement the procedure from the point of view of the analysis of different response variables of the same.

### 3. Results

#### 3.1. Experimental Determination of the Friction Coefficient

The experiments to determine the lower value of friction coefficient  $\mu$  were performed on a reduction from Ø0.50 mm to Ø0.45 mm using a die with a reduction angle  $2\alpha = 14^\circ$ , a bearing length  $L_c = 50\% \cdot d_f$  and a contact length in the conical zone  $L = 0.205$  mm which implies a total contact length of 0.43 mm. The drawing tests were done using 100% mineral oil as lubricant interfacial tribo-element [6]. The polynomial fitting, shown in the Figure 5, gives a minimum value of  $\mu = 0.127$ .



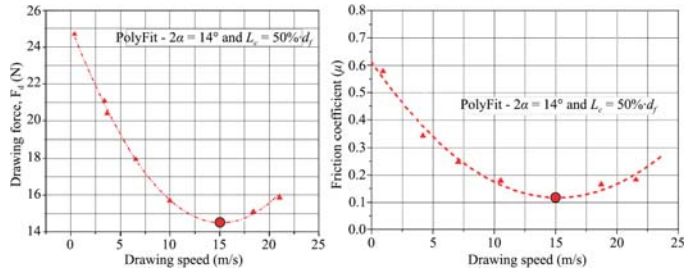


**Figure 5.** The polynomial fitted values of the minimum drawing force  $F_d$  and lower coefficient of friction  $\mu$  as a function of different values of drawing speed ( $v$ ) used in the experiments, for a die with  $2\alpha = 14^\circ$  and  $L_c = 50\% \cdot d_f$  lubricated with 100% mineral oil.

The results in the graph of Figure 5 show a lower friction when the drawing speed increases until a critical value of 15 m/s. Beyond this speed value, excess or lack of lubricant getting inside the wire/die interface may result in an increasing of the friction effect [29]. This minimum of  $\mu = 0.127$  was implemented in the analytical design and subsequent numerical analysis of the designed sequential wiredrawing process.

3.2. Analytical Definition of the Multi-Step Pass Schedule Design by PullWorks Software

Fine wiredrawing pass schedule design was calculated by PullWorks software and implementing Ludwik–Hollomon strain hardening law as shown in Equation (5), defining die geometry, the optimum friction coefficient  $\mu = 0.127$  and  $\Delta = 1$ , since this shape coefficient value minimizes friction and wear effects and allows a short relatively sequence for the designed wiredrawing process [27].

The selected conditions threw a seven-step wiredrawing sequence pointing out the convenience of annealing before each of them. This sequence was established as the aim of study by both analytical and numerical methods. Table 1 shows the multi-step wiredrawing pass schedule design.

**Table 1.** Multi-step fine wiredrawing pass schedule designed by PullWorks.

Step Nr.	Input, $d_{0(i)}$ [mm]	Output, $d_{f(i)}$ [mm]	Reduction Ratio, $r$	Unit Strain, $\epsilon$	Shape Factor, $\Delta$	Continuous Annealing
1	0.50	0.39	0.40	0.50	1	YES
2	0.39	0.31	0.40	0.46	1	YES
3	0.31	0.24	0.40	0.51	1	YES
4	0.24	0.19	0.40	0.47	1	YES
5	0.19	0.15	0.40	0.47	1	YES
6	0.15	0.12	0.40	0.45	1	YES
7	0.12	0.10	0.31	0.36	1.34	YES

Table 2 shows the wiredrawing sequence calculated with PullWorks software and the values obtained for the drawing force and drawing stress, analytical and FEM software applications.

**Table 2.** Drawing forces and drawing stresses obtained by the analytical (PullWorks/slab method) and numerical (FEM) software solutions in the multi-step fine wiredrawing sequence.

Step Nr.	Drawing Force, $F_d$ (PullWorks) [N]	Drawing Force, $F_d$ (FEM) [N]	Drawing Stress, $\sigma_d$ (PullWorks) [MPa]	Drawing Stress, $\sigma_d$ (FEM) [MPa]
1	45.9	53.2	384.5	445.3
2	27	30.1	357.2	398.8
3	17.9	19.4	394.4	428.8
4	10.3	10.7	363	377.4
5	6.5	7.3	366.9	413.1
6	3.9	4.5	348.7	397.9
7	2.5	2.6	321	331

The graph of Figure 6 shows that the difference obtained by both methods is smaller than 12.4% in the evolution of drawing stress calculated from a drawing force (Table 2).

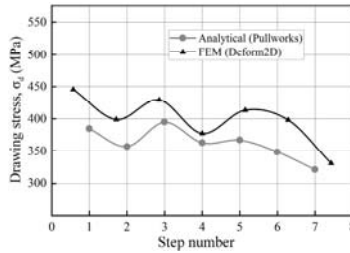


Figure 6. The evolution of the value of drawing stress  $\sigma_d$  (analytical vs. FEM).

3.3. Numerical FEM Study of the Proposed Multi-Step Pass Schedule

To understand the influence of the die geometry in each of the stages of the wire multi-step wiredrawing process, the numerical simulations allows to measure the axial (tractional) and radial (compressive) components of the drawing stress and their evolution while the copper wire is passing through the different zones inside of the dies.

The radial and axial stress distributions were simulated assuming the optimum value of the friction coefficient  $\mu = 0.127$  since this condition corresponds to the minimal tool wear and optimum drawing speed, as shown in Figure 5. The simulation snapshot in Figure 7 shows the differentiated zones in the standard geometry of the drawing die and the 23 tracked nodes in a displacement of 1 mm, from a fixed starting point of the reduction cone area (II) to the exit zone (IV).

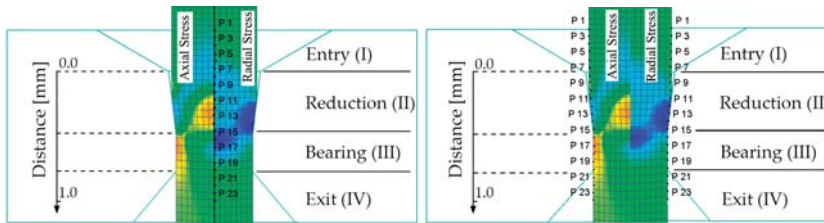


Figure 7. Tracking points and tracked displacement representation for the analysis distribution and evolution of the axial and radial stress when the wire goes through the die.

Figures 8–14 show the simulations allowed to obtain the compressive radial ( $\sigma_{radial}$ ) and axial ( $\sigma_{axial}$ ) data stress evolution when the wire goes to different zones through the die, in the surface and center of the wire (Figure 2b). Marks II, III, IV indicate the different zones trough the drawing die.

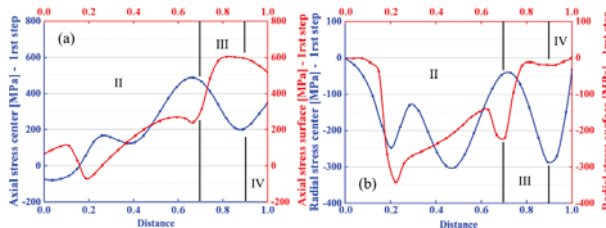


Figure 8. From FEM simulations: (a) axial and (b) radial stress (step 1); (blue) center, (red) surface.

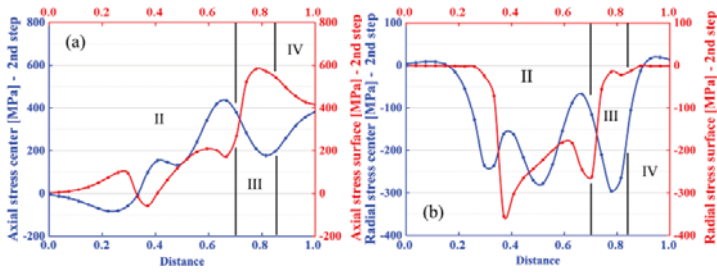


Figure 9. From FEM simulations: (a) axial and (b) radial stress (step 2); (blue) center, (red) surface.

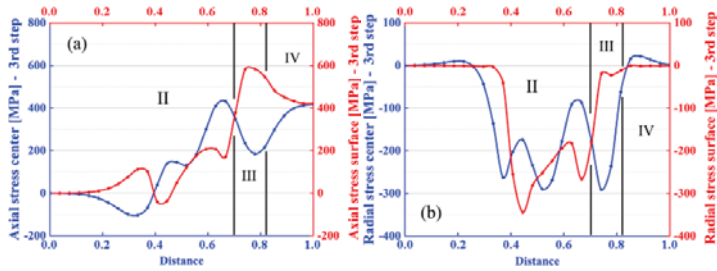


Figure 10. From FEM simulations: (a) axial and (b) radial stress (step 3); (blue) center, (red) surface.

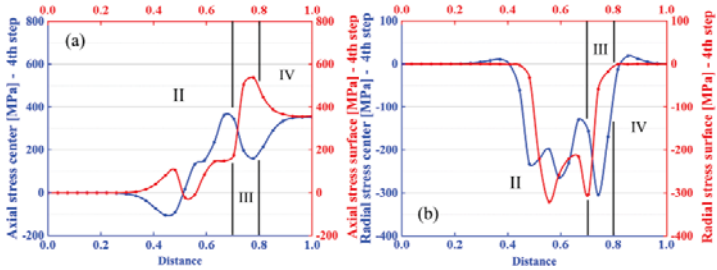


Figure 11. From FEM simulations: (a) axial and (b) radial stress (step 4); (blue) center, (red) surface.

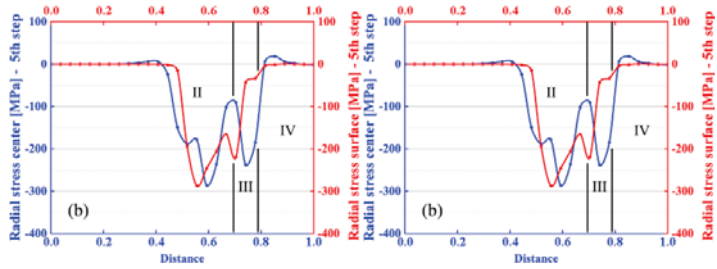


Figure 12. From FEM simulations: (a) axial and (b) radial stress (step 5); (blue) center, (red) surface.

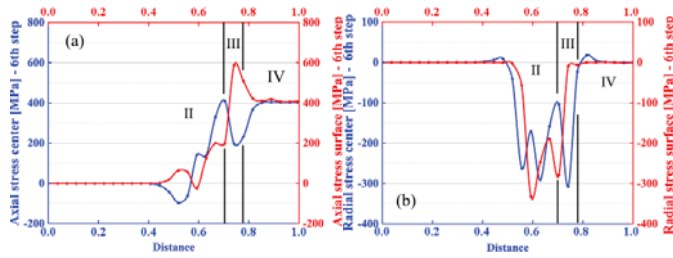


Figure 13. From FEM simulations: (a) axial and (b) radial stress (step 6); (blue) center, (red) surface.

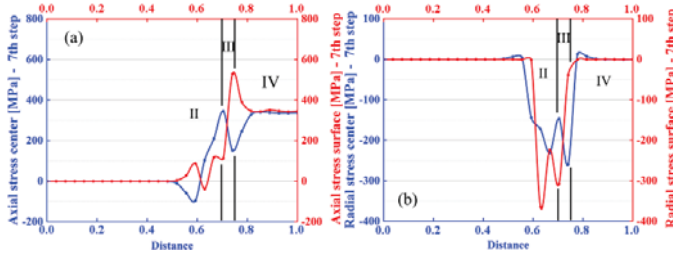


Figure 14. From FEM simulations: (a) axial and (b) radial stress (step 7); (blue) center, (red) surface.

The results demonstrate the internal die geometry’s influence in association with the traction force from capstan in the axial and radial values. In other words, it is possible to see the tensile stress that is necessary to apply by each of the machine capstans (steps) and the compression stress generated in the conical deformation zone into the die (II).

It has been observed that the results obtained by both methods for the values of drawing stress and drawing force shown a very similar evolution (Figure 6). The values obtained by the FEM simulations are slightly higher than those obtained from the calculations performed analytically by means of the software application PullWorks. This fact is in line with the conclusions obtained in the work of Luis et al. [30] and that is because the analytical method only considers the effects of homogeneous deformation and friction, unlike the numerical model, which takes into account the effects due to the additional energy required as a consequence of the non-homogeneous deformation that occurs in wiredrawing process.

As can be seen in Figure 7, the small dies were modelled in such a way that the 0.00 point is fixed, that is, while  $L_c$  decreases in the sequence, the length of the conical zone without contact increases just after the entry zone (I). This fact can be appreciated in the graphs (Figures 8–14): in the first step both radial (compressive) and axial stresses increase almost instantly with the wire contact with the conical zone, while in the last step (7th) the increase in values of  $\sigma_{radial}$  and  $\sigma_{axial}$  is appreciated a few tenths of a millimeter inside the cone. This is because the effective contact length  $L_{(i)}$  in this zone decreases as the area reduction increases in the wiredrawing sequence.

Compressive radial stresses ( $\sigma_{radial}$ ) show a maximum near 300 MPa in the surface points, in all the steps of the sequence, Figures 8b, 9b, 10b, 11b, 12b, 13b and 14b. This circumstance is in agreement with the results obtained by Martinez [30]. The evolution of this response parameter shows a marked increment in its value in a point just entering bearing length, in the case of surface radial stress  $\sigma_{radial} (surface)$ , while on the contrary, the radial stress in the center points decreases just in the same contact point.

As is shown in Figures 8a, 9a, 10a, 11a, 12a, 13a and 14a, axial stress ( $\sigma_{axial}$ ) evidences maximum values under 600 MPa and this maximum occurs at the exit of the die and on the surface points, just in the calibration zone (III) while the maximum of axial stress in the center points of the wire

( $\approx 400$  MPa) occurs punctually just at the entrance of the calibration zone (III) to drop lightly and reach this maximum again at the exit of the die (IV).

#### 4. Conclusions

In particular, by the experimental determination of the optimum value of the friction coefficient in the case of Cu-ETP commercial wire drawing process, the analytical designing of a multi-step wire drawing sequence and the corresponding numerical simulations have been performed in this work. This combined methodology development demonstrated that the effective complementation of the three methods, experimental, analytical, and numerical, allows the implementation of the real boundary conditions with the aim of process design and both analytical and FEM analysis. The work shows the results obtained by PullWorks software application, offering a proposal for a basic process of multi-step wire drawing to obtain fine copper wire and FEM software has allowed to understand the process conditions in terms of both the superficial and center radial and axial stress components derived from the effective stress associated to the process in each of the stages.

**Author Contributions:** Conceptualization, O.R.-A. and G.A.S.M.; methodology, O.R.-A.; validation, O.R.-A., E.M. and G.A.S.M.; formal analysis, G.G.-V.; investigation, O.R.-A. and G.A.S.M.; resources, O.R.-A. and G.A.S.M.; data curation, G.A.S.M. and O.R.-A.; writing—original draft preparation, O.R.-A.; writing—review and editing, O.R.-A., P.E.R., M.T. and G.G.-V.; visualization, E.M., P.E.R., M.T. and G.G.-V.; supervision, G.A.S.M. and M.T.; project administration, G.A.S.M. All authors have read and agreed to the published version of the manuscript.

**Funding:** This research received no external funding.

**Acknowledgments:** Thanks to Ana María Camacho López, PhD. in the Department of Engineering of Construction and Manufacture, E.T.S. of Industrial Engineering of UNED (Madrid, Spain), allowed us the use of the licensed FEM software Deform2D.

**Conflicts of Interest:** The authors declare no conflict of interest.

#### References

1. Parnian, P.; Parsa, M.H.; Mirzadeh, H.; Jafarian, H.R. Effect of Drawing Strain on Development of Martensitic Transformation and Mechanical Properties in AISI 304L Stainless Steel Wire. *Steel Res. Int.* **2017**, *88*, 1–10. [CrossRef]
2. Son, S.B.; Lee, Y.K.; Kang, S.H.; Chung, H.S.; Cho, J.S.; Moon, J.T.; Oh, K.H. A numerical approach on the inclusion effects in ultrafine gold wire drawing process. *Eng. Fail. Anal.* **2011**, *18*, 1272–1278. [CrossRef]
3. Kustra, P.; Milenin, A.; Byrska-Wójcik, D.; Grydin, O.; Schaper, M. The process of ultra-fine wire drawing for magnesium alloy with the guaranteed restoration of ductility between passes. *J. Mater. Process. Technol.* **2017**, *247*, 234–242. [CrossRef]
4. Schade, P. Wire drawing failures and tungsten fracture phenomena. *Int. J. Refract. Met. Hard Mater.* **2006**, *24*, 332–337. [CrossRef]
5. Lee, S.-K.; Lee, I.-K.; Lee, S.-Y.; Hwang, S.-K. Fabrication of 50.0  $\mu\text{m}$  Ultra-Fine Pure Rhodium Wire, Using a Multi-Pass Wire Drawing Process, for Probe Card Pins. *Materials* **2019**, *12*, 2194. [CrossRef]
6. Martinez, G.A.S.; Qian, W.-L.; Kabayama, L.K.; Prisco, U. Effect of Process Parameters in Copper—Wire Drawing. *Metals* **2020**, *10*, 105. [CrossRef]
7. Pops, H. The Metallurgy of Copper Wire. Copper Development Association Inc. 1997. Available online: <https://www.copper.org/publications/newsletters/innovations/1997/12/wiremetallurgy.html> (accessed on 9 December 2020).
8. Vega, G.; Haddi, A.; Imad, A. Investigation of process parameters effect on the copper-wire drawing. *Mater. Des.* **2009**, *18*, 3308–3312. [CrossRef]
9. Kabayama, L.K.; Taguchi, S.P.; Martinez, G.A.S. The Influence of Die Geometry on Stress Distribution by Experimental and FEM Simulation on Electrolytic Copper Wire Drawing. *Mater. Res.* **2009**, *12*, 281–285. [CrossRef]
10. Adamczyk, J.; Suliga, M.; Pilarczyk, J.; Burdek, M. The Influence of Die Approach and Bearing Part of Die on Mechanical-Technological Properties of High Carbon Steel Wires. *Arch. Metall. Mater.* **2012**, *57*, 12–14. [CrossRef]

11. Rubio, E.M.; Camacho, A.M.; Sevilla, L.; Sebastián, M.A.; Sevilla, L. Calculation of the forward tension in drawing processes. *J. Mater. Process. Technol.* **2005**, *162*, 551–557. [CrossRef]
12. Rubio, E.M. Analytical methods application to the study of tube drawing processes with fixed conical inner plug: Slab and Upper Bound Methods. *J. Achiev. Mater. Manuf. Eng.* **2006**, *14*, 119–130.
13. Rodriguez-Alabanda, O.; Romero, P.E.; Guerrero-Vaca, G.; Sevilla, L. Software implementation of a new analytical methodology applied to the multi-stage wire drawing process: The case study of the copper wire manufacturing line optimization. *Int. J. Adv. Manuf. Technol.* **2018**, *96*, 2077–2089. [CrossRef]
14. Hassan, A.K.F.; Hashim, A.S. Three Dimensional Finite Element Analysis of Wire Drawing Process. *Univers. J. Mech. Eng.* **2015**, *3*, 71–82. [CrossRef]
15. Rodriguez-Alabanda, O. PullWorks Software Application for the Analytical Study and Optimization of the Wire Drawing Process. Available online: <https://youtu.be/jawQDkiYvek> (accessed on 9 December 2020).
16. Avitzur, B. Analysis of Wire Drawing and Extrusion through Conical Dies of Large Cone Angle. *J. Eng. Ind.* **1964**, *86*, 305. [CrossRef]
17. Avitzur, B. *Handbook of Metal Forming*; John Wiley & Sons Inc.: New York, NY, USA, 1983.
18. Bitkov, V.V. Minimization of breaks during drawing thin wire of nonferrous metals. *Russ. J. Non-Ferrous Met.* **2010**, *51*, 134–139. [CrossRef]
19. Evans, W.; Avitzur, B. Measurement of Friction in Drawing, Extrusion, and Rolling. *J. Lubr. Technol.* **1968**, *90*, 72–80. [CrossRef]
20. Kovács, S.; Mertinger, V. Examination of Complex Optimization Objective Functions of Parameters of Multi-Step Wire Drawing Technology. *Acta Polytechnica Hung.* **2013**, *10*, 27–44.
21. Narayanan, K.R.; Sridhar, I.; Subbiah, S. Effect of cold work on the mechanical response of drawn ultra-fine gold wire. *Comput. Mater. Sci.* **2010**, *49* (Suppl. S1), S119–S125. [CrossRef]
22. Naga Teja, C.S.; Murty N, G.; Reddy Teja, P.S. Finite Element Analysis of Wire Drawing Process with different die contours. *Int. J. Sci. Eng. Adv. Technol.* **2016**, *4*, 134–143.
23. Sas-Boca, I.M.; Tintelean, M.; Pop, M.; Iluțiu-Varvara, D.-A.; Mihă, A.M. The Wire Drawing Process Simulation and the Optimization of Geometry Dies. *Procedia Eng.* **2017**, *181*, 187–192. [CrossRef]
24. Zottis, J.; Diehl, C.A.T.S.; Rocha, A.D.S. Evaluation of experimentally observed asymmetric distributions of hardness, strain and residual stress in cold drawn bars by FEM-simulation. *J. Mater. Res. Technol.* **2018**, *7*, 469–478. [CrossRef]
25. Esteves Group Hileras de Diamante Policristalino PCD. Available online: <http://www.estevesgroup.com/es/products/wire-drawing-dies/polycrystalline-dies> (accessed on 9 December 2020).
26. Rodriguez-Alabanda, O. PullWorks Software. Available online: <http://www.uco.es/grupos/prinia/oscar-rodriguez-alabanda> (accessed on 9 December 2020).
27. Wright, R.N. Mechanical analysis and die design. *Wire J. Int.* **1979**, *12*, 60–61.
28. Fluhner, J. *Deform2D Version 8.1 User's Manual*; Scientific Forming Technologies Corp.: Columbus, OH, USA, 2004.
29. Cheng, H.S. *Lubrication Regimes, ASM Handbook Vol.18, Friction, Lubrication, and Wear Technology*; ASM International: West Conshohocken, PA, USA, 1992.
30. Martinez Santana, G.A.; Ferro dos Santos, E.; Kabayama, L.K.; Siqueira Guidi, E.; de Azebedo Silva, F. Influences of Different Die Bearing Geometries on the. *Metals* **2019**, *9*, 1089. [CrossRef]

**Publisher's Note:** MDPI stays neutral with regard to jurisdictional claims in published maps and institutional affiliations.



© 2020 by the authors. Licensee MDPI, Basel, Switzerland. This article is an open access article distributed under the terms and conditions of the Creative Commons Attribution (CC BY) license (<http://creativecommons.org/licenses/by/4.0/>).



# Design of a Hybrid Two-Degree-of-Freedom Lower Limb Exerciser <sup>†</sup>

Daniel Lates <sup>1,\*</sup>, Laura Irina Vlaşin <sup>2</sup> and Alexandru Ianoşi-Andreeva-Dimitrova <sup>2</sup> 

<sup>1</sup> Department of Industrial Engineering and Management, Faculty of Engineering and Information Technology, Pharmacy and Science and Technology of Târgu Mureş, George Emil Palade University of Medicine, Tg. Mureş 540142, Romania

<sup>2</sup> Department of Mechatronics and Machine Dynamics, Faculty of Automotive, Mechatronics and Mechanical Engineering, Technical University of Cluj-Napoca, Cluj-Napoca 400114, Romania; Vlasin.IR.Laura@utcluj.didatec.ro (L.I.V.); Alexandru.Ianos@mdm.utcluj.ro (A.I.-A.-D.)

\* Correspondence: daniel.lates@umfst.ro

<sup>†</sup> Presented at the 14th International Conference INTER-ENG 2020 Interdisciplinarity in Engineering, Mureş, Romania, 8–9 October 2020.

Published: 16 December 2020

**Abstract:** Lower limb rehabilitation is an often-encountered need. This paper presents the design process of an exerciser that combines robot-assisted physiotherapy with functional electrical stimulation (FES) of the lower limb muscles. The exerciser features two degrees of freedom, one focuses on the rehabilitation of the muscles responsible for dorsiflexion and plantar flexion, the other one on the muscles responsible for the inversion and eversion of the foot. These motions might be accompanied by FES, if the physiotherapist so recommends. The presented exerciser constitutes a mechatronic device that seamlessly integrates mechanical design, electronics and control engineering.

**Keywords:** rehabilitation engineering; medical robotics; lower limb rehabilitation

## 1. Introduction

Lower limb rehabilitation is a subject which, among rehabilitation engineers, is not as popular as upper limb rehabilitation. A simple search query with the keywords “lower limb rehabilitation robot” returns less than half the results for the keywords “upper limb rehabilitation robot” on the popular science platform PubMed. This disparity can be explained by the fact that designing for the upper limb is more challenging from a technical point of view than designing for the lower limb, and consequently more palatable, yet there are many more situations that necessitate the rehabilitation of the lower limb (e.g., prolonged inactivity due to a certain illness impacts much more the lower limb). Lower limb orthoses are used to support the foot in a certain position and assist in recovery of gait; they are also used to redistribute forces that occur when the foot comes in contact with the ground while walking so as not to exert too much force on a specific affected area of the foot [1,2]. A robotized exerciser empowers a physiotherapist by providing a tool for repeatable and reproducible results, enabling more efficient and targeted procedures; moreover, provided the exerciser is affordable and meant to be also used in non-clinical environments, it facilitates rehabilitation for the patient in a prescribed way.

This paper describe the critical milestones in the design of a two-degree-of-freedom (DOF) hybrid lower limb exerciser [3]; the hybrid part is given by the fact that it combines the traditional physiotherapy assisted robotically with the functional electrical stimulation (FES) of the relevant muscle groups. The exerciser focuses on the ankle joint, namely, the dorsiflexion/plantar flexion and the inversion/eversion of the foot. The designed exerciser does not mandate the usage of FES in conjunction with the robotically assisted physiotherapy, it merely provides the option of simultaneously usage.



The paper provides a description of the state of the art, after which it focuses on the mechanical design and describes the electronics and coding involved in the control of the proposed exerciser.

## **2. State of the Art**

In this chapter several examples of rehabilitation equipment will be discussed that are in accordance with the object of the paper and which are considered representative.

In his patent [4], Stein presents an electronic stimulator with fixed electrodes attached to a textile tape. This band must be positioned correctly on the leg so that the electrodes are placed in an area over the nerve to be stimulated. The band also contains devices for monitoring body movement and a system that operates the electrodes at certain intervals to stimulate the nerve and activate latent muscles. This device can be used in the case of a person who suffers from "drop-foot" that may occur as a result of a stroke.

Gil et al. [5] describe a unilateral hybrid orthosis-type exoskeleton intended to assist and recover gait for patients who experience motor deficiencies due to central nervous system diseases. It consists of an orthosis at the knee, ankle and foot that supports the lower limb and a functional electrical stimulator that activates the affected muscles. The support part has the role of constraining the ankle and knee joint and stopping their involuntary movements in certain directions. This ensures a stable position of the lower limb while walking and while the patient is standing.

A platform presented by Liu et al. [6] is intended for patients who have suffered a stroke and experience motor deficiencies as a result. In order to recover the functions of the lower limbs, therapy based on exercises is needed, which has the role of strengthening the muscles and correcting the position of the leg. The device proposed in this example assists the patient in performing certain exercises that improve the ability to move the foot. The robotic platform consists of two symmetrical plates that have the role of foot support, each with 3 DOF and can perform internal and external rotation of the ankle, dorsal and plantar flexion and inversion and eversion of the foot. The patient can use the device in three ways depending on the rehabilitation stage: exercises that involve maintaining a constant speed, exercises that keep the motor speed constant and exercises that involve the proactive involvement of the patient in training.

Erhan and Mehmet [7] elaborate a study on the design and control of a robot for therapeutic exercises for the lower limbs of a patient who needs rehabilitation after a spinal cord injury. To control this robot, a "human-machine interface" with a rules-based control structure was developed. The robot manipulator can perform active and passive exercises, as well as learn specific exercise movements and perform them without the physiotherapist through the human-machine interface. Moreover, if a patient reacts against the robotic manipulator during an exercise, he may change position depending on the feedback data.

An interesting application of orthosis is the ability to assist the transfer from a sitting position to a standing one; Aroche et al. [8] proposed a computerized system for persons that suffer from complete paraplegia, arguing that widespread adoption of powered orthosis among this demographic is hampered by the fact that these orthoses does not provide equilibrium autonomy. Another system [9] blocks all but one DOF of the lower limb and makes use of mechanical linkages and automation for independent locomotion; it is not entirely clear if it can also provide the transfer function. Roula et al. [10] compared multiple operating conditions and concluded that PID controller might not perform well enough due to various uncertainties presented by the complex interaction between a subject, their orthosis and the environment.

## **3. Design Process**

From a structural standpoint, the designed exerciser is composed of three interconnected subsystems that are detailed in the following paragraphs. The integration of these parts makes the device a mechatronic product.

### 3.1. Mechanical Subsystem

The mechanical subsystem is designed to enable movement only in a predictive fashion; for a correctly executed exercise, a proper attachment to the foot is necessary that lines the bones, muscles, and tendons in an anatomically appropriate way. In order to achieve this goal, biomechanical data were taken into account, namely, it was hypothesized that the exerciser is used by a person 1.65 m tall with a mass of 50 kg; this gives a weight of the foot of 7.13 N and a position of the center of gravity (CG) by the following coordinates in relationship to the heel: 0.098 m horizontally and 0.039 m vertically (Figure 1a). The range of movement of the foot in relationship to the transverse plane allowed by the exerciser is  $-35^\circ$ ;  $20^\circ$  for the plantar flexion/dorsiflexion;  $-20^\circ$  and  $15^\circ$  for inversion and eversion, respectively. Given these data and using the geometrical relationship between the foot CG and the designed mechanism (Figure 1b), the result is a maximum necessary moment of 0.37 Nm for the first DOF, and 0.27 Nm for the latter.

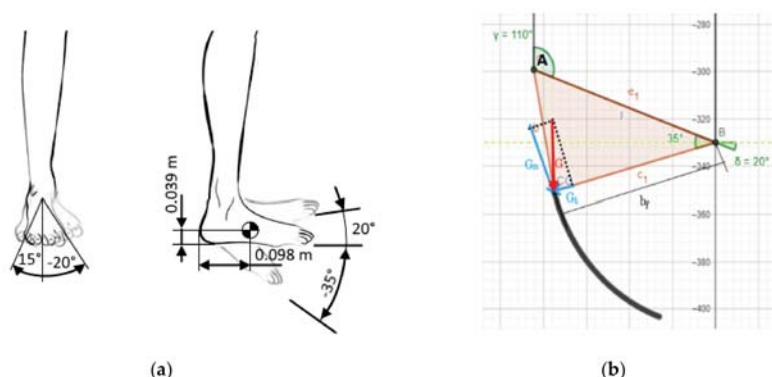


**Figure 1.** Input biomechanical data: (a) range of motion and position of the center of gravity of the foot (b) geometrical relationship between the center of gravity and exerciser.

The employed mechanism is a spatially stacked version of the well-known four bar linkage. Its main purpose is to provide a way of simultaneously actuating both degrees of freedom; 4 four-bar linkages are connected to form a parallelepiped, each vertex being formed out of two rotational joints, their axes perpendicular to each other and parallel to the other 3 sister joints axes (Figure 2a). The placement of a motor in one of the joints is trivial for actuating one DOF, but the second actuated DOF (Figure 2b dotted line) raises additional issues, as the linkage has to be connected to a fixed reference; if directly connected, the whole DOF is pinned. The designed solution was to incorporate in the power train an universal joint coupled to a sliding shaft with parallel splines; this allows the necessary tilt angle as well as accounting for the radial displacement. Due to the fact that the mobile part of the exerciser has considerable mass, additional support mechanism is employed: two gas cylinders, their ends connected by spherical joints add stability to the system (drawn with red on Figure 2c).

Referring to the aforementioned figure, the immovable part (drawn with blue) is attached to the leg by Velcro straps, which are not pictured, as to not overload the schematic. The foot is resting on a specifically designated platform. The design is modular, so that the footrest is easily changeable to accommodate various feet sizes by removing and reinserting the bottom U-shape shaft (drawn in magenta on Figure 2c). The normal operation of the exerciser presumed oscillatory movement, therefore the design does incorporate only plain bearings; the friction is dealt by using polytetrafluoroethylene bushing, the low speed nature of the real life use case scenario allowing sufficient time for cooling. The CAD model was designed using SolidWorks software package published by Dassault Systèmes.

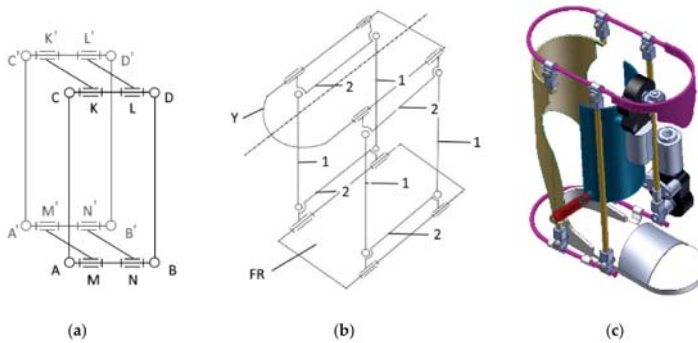


**Figure 2.** Design stages of the lower limb exerciser: (a) kinematic chain (b) mechanism, where FR is the foot resting plate, Y is the yoke, with 1 are designated the vertical linkages (0.330 m) and with 2—the horizontal linkages (0.143 m); dotted line represents the rotational axis (c) CAD model of the exerciser.

### 3.2. Electronics Subsystem

The electronics subsystem is built around an ATmega328-P microcontroller (refer to Figure 3a) that commands the actuation of the mechanical subsystem with two electrical motors, each powered by an H-bridge. Each electrical motor is encapsulated with a 210:1 gear ratio transmission, capable of delivering up to 3 Nm of torque, which is well above the computed necessary. The H-bridge is compatible with PWM signals and also provides a quick response disable input. The angular positioning of each DOF is monitored with a resistive absolute encoder that provides an accuracy of  $\pm 0.3^\circ$ . For additional safety, each DOF has 2 normally-closed limit switches, each of them controlling a normally-open relay in such a manner that if one of the limit switches is tripped, or the power to the switches is somehow interrupted (rusted connection, torn wire, etc.) only one direction is stopped; therefore, recovery of the system is still possible in normal operation and a high standard of safety is employed. Each faulty state is signaled to the microcontroller galvanically insulated through an optocoupler that drives the first interrupt pin to which an interrupt routine is attached.

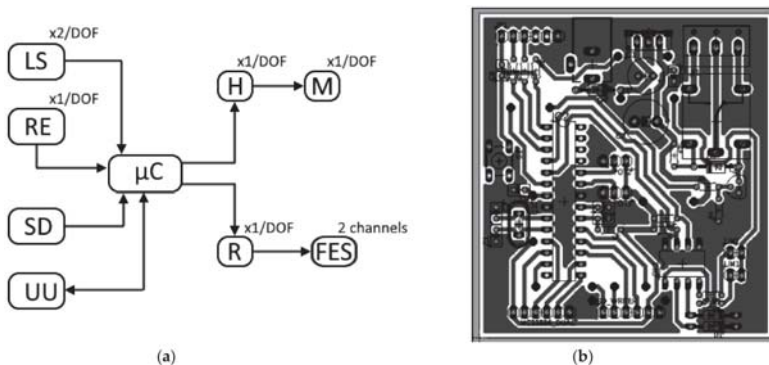


**Figure 3.** Electronics subsystem: (a) System architecture, where LS are limit switches, RE—resistive encoder, SD—SD read/write module, UU—USB to UART converter, H—H-bridge, M—motors, R—relays, FES—functional electrical stimulation unit and  $\mu\text{C}$ —the microcontroller; (b) PCB layout.

An SD-card module is included which allows for upload of different exercises; the file is a simple text string, each row containing one command that contain the desired position and maximum allowable speed for each motor as well as the necessary commands for the start/stop of FES system. The FES system used by the exerciser is a commercially available 2-channel device interfaced with by

relay; therefore, the pulse length, frequency and amplitude of the stimulation is manually dialed in before commencing the exercise, the microcontroller merely starts or stops the device. The placement for the FES electrodes on the skin is covered by the device user manual and might be performed either by a physical therapist or the patient after receiving a precursory instruction. The exerciser's main electrical circuit was implemented on a single layer printed circuit board (PCB), pictured in Figure 3b, using EAGLE (published by Autodesk); it is worth noting that this PCB is not entirely necessary if an Arduino board were to be used. Furthermore, for programming as well as testing purposes, communication over a USB to UART converter is employed.

### 3.3. Control Subsystem

ATmega328-P microcontroller is a popular microchip with the Arduino device family; therefore, the Arduino IDE was used in code design for its easy-to-use libraries. The motors were controlled using a PID algorithm implementation which reads the signal from the resistive absolute encoders through the microcontroller integrated 10-bit ADC and compares it to the target position provided by the exercise file that resides on the SD-card. The output from the PID controller is a PWM value that is proportionally to the motors speed; it is worth noting that if the value is negative, which correlate with the rotation in the opposite direction, a simple function remove the sign and invert the signal before further processing. The sign triggers a flag that signalize the H-bridge which combination is active, so that the motor can easily turn. In order to limit the speed in a safe range, the PWM value is capped before writing it in the appropriate PWM register with the value specified in the exercise file. The overall safely usage of the exerciser is ensured by the hardwired limiters described in the precedent subchapter, but as a first line of secure operation there are also software-defined limits which maintain a physiological range of motion.

Another mode of operation is by permanent connection via an USB-UART converter. At this stage a simple graphical user interface was designed in Matlab GUIDE, but further development was halted until prototype completion. If a limit switch is activated, an interrupt routine drives the H-bridge low and throws an error; putting the H-bridge on hold is redundant, as the wiring, described in subchapter 3.2, already cuts the power to the motor; as a result, the system has triple redundancy for emergency stop: software defined limits, external interrupt routine and hardware-defined limits, so even in case of end-user interference with the safety checks, it is reasonable to expect that at least one remains active.

## 4. Conclusions

This paper presented the design stages of a hybrid 2-DOF lower limb exerciser; although the work done so far is enough to grant the manufacture of a first prototype, several issues were identified and are taken into account for a future iteration. First of all, it is necessary to make sure that the exerciser is capable of serving a broader demographic; even though the selected motors have a 8-fold power margin, there was no rigorous calculation of the needed torque in order to cover at least the 95th percentile for height and mass of the population. A useful improvement would be the addition of strain gauges; not only would the operational safety increase (if an anomalous strain is detected, the exerciser stops and avoid potential injury), but it would also enable active and passive mode usage. Therefore, a patient might continue to use the exerciser for different stages of their rehabilitation; in the beginning, when the musculature is still weak, the system might work in a passive mode to maintain articular mobility; in the later stages, when the musculature begin to strengthen, the exerciser might switch to an active mode, opposing the movement with a certain force controlled by the strain gauges.

Another design requirement for a future iteration is the simplification of the actuating system; one of the DOF is directly connected to the motor, which makes the actuation very robust. The second DOF is connected with a quite complex transmission which is prone to failure. There are already several design solutions being investigated, but not fully explored at this time. Modern equipment tends to have implemented diverse communication protocols that use the radio spectrum; in this regard, a future development will be the addition of a Bluetooth module that will enable communication with

a smartphone app. Another idea worth investigating is implementing Wi-Fi functionality, but this direction must be carefully approached, as connecting a medical device to a computer network might expose the patient to malicious actors over the internet. Another planned improvement is related to multiple exercise selection: in preparation for the prototype, the designed code is capable of reading only one file; a file management system has to be implemented, which will allow multiple exercise files to be loaded on the SD card and chosen by the physical therapist or patient, presumably with a Bluetooth-connected smartphone. As soon as full activity in the Biomechanics Laboratory is allowed (currently reduced by measures taken to stop the spread of SARS-CoV2), a prototype will be build using the additive manufacturing technologies available; this prototype will be further used for preliminary testing, and, if found satisfactory, pre-clinical testing using healthy volunteers.

**Author Contributions:** Conceptualization, D.L. and A.I.-A.-D.; methodology, A.I.-A.-D.; software, L.I.V.; validation, A.I.-A.-D.; formal analysis, A.I.-A.-D.; investigation, L.I.V.; resources, L.I.V.; data curation, A.I.-A.-D.; writing—original draft preparation, D.L.; writing—review and editing, D.L.; visualization, A.I.-A.-D.; supervision, A.I.-A.-D.; project administration, A.I.-A.-D. All authors have read and agreed to the published version of the manuscript.

**Funding:** This research received no external funding.

**Conflicts of Interest:** The authors declare no conflict of interest.

## References

1. Farris, R.J.; Quintero, H.A.; Goldfarb, M. Preliminary Evaluation of a Powered Lower Limb Orthosis to Aid Walking in Paraplegic Individuals. *IEEE Trans. Neural Syst. Rehabil. Eng.* **2011**, *19*, 652–659. [[CrossRef](#)] [[PubMed](#)]
2. Quintero, H.A.; Farris, R.J.; Hartigan, C.; Clesson, I.; Goldfarb, M. A Powered Lower Limb Orthosis for Providing Legged Mobility in Paraplegic Individuals. *Top. Spinal Cord Inj. Rehabil.* **2011**, *17*, 25–33. [[CrossRef](#)] [[PubMed](#)]
3. Vlasin, L.I. *Design of a Hybrid Rehabilitation System Composed from an Orthosis and a Functional Electrical Stimulation Unit*; Technical University of Cluj-Napoca: Cluj-Napoca, Romania, 2020.
4. Stein, R.B. Assembly for Functional Electrical Stimulation during Movement. U.S. Patent No. 5,643,332, 1 July 1997.
5. Gil, J.; Sanchez-Villamanan, M.; Gomez, J.; Ortiz, A.; Pons, J.; Moreno, J.; Del-Ama, A. Design and Implementation of a Novel Semi-Active Hybrid Unilateral Stance Control Knee Ankle Foot Orthosis. In Proceedings of the 2018 IEEE/RSJ International Conference on Intelligent Robots and Systems (IROS), Madrid, Spain, 1–5 October 2018; pp. 5163–5168.
6. Liu, Q.; Wang, C.; Long, J.J.; Sun, T.; Duan, L.; Zhang, X.; Zhang, B.; Shen, Y.; Shang, W.; Lin, Z.; et al. Development of a New Robotic Ankle Rehabilitation Platform for Hemiplegic Patients after Stroke. *J. Health Eng.* **2018**, *2018*, 1–12. [[CrossRef](#)] [[PubMed](#)]
7. Akdoğan, E.; Adli, M.A. The design and control of a therapeutic exercise robot for lower limb rehabilitation: Physiotherabot. *Mechatronics* **2011**, *21*, 509–522. [[CrossRef](#)]
8. Aroche, O.N.; Meyer, P.-J.; Tu, S.; Packard, A.; Arcak, M. Robust Control of the Sit-to-Stand Movement for a Powered Lower Limb Orthosis. *IEEE Trans. Control. Syst. Technol.* **2019**, *28*, 2390–2403. [[CrossRef](#)]
9. Sunada, T.; Obinata, G.; Pei, Y. Active Lower Limb Orthosis with One Degree of Freedom for Paraplegia. In Proceedings of the 16th International Conference on Informatics in Control, Automation and Robotics, Prague, Czech Republic, 29–31 July 2019; SciTePress: Setúbal, Portugal, 2019; pp. 504–509. [[CrossRef](#)]
10. Roula, N.; Chemori, A.; Rizk, R.; Zaatari, Y. On Control Design for a Lower Limb Orthosis: A Comparative Study in Different Operating Conditions. *Adv. Mech. Mach. Sci.* **2018**, *58*, 81–97. [[CrossRef](#)]

**Publisher's Note:** MDPI stays neutral with regard to jurisdictional claims in published maps and institutional affiliations.



© 2020 by the authors. Licensee MDPI, Basel, Switzerland. This article is an open access article distributed under the terms and conditions of the Creative Commons Attribution (CC BY) license (<http://creativecommons.org/licenses/by/4.0/>).

# A New Light Aircraft and Its Design Method <sup>†</sup>

Marius-Ion Ghițescu <sup>1,\*</sup>, Marilena Ghițescu <sup>1</sup> and Arina Modrea <sup>2,\*</sup>

<sup>1</sup> Department of Mechanical Engineering, Faculty of Mechanical Engineering, Transilvania University of Brasov, 500036 Brasov, Romania; marilenaradu71@yahoo.com

<sup>2</sup> Department of Industrial Engineering and Management, Faculty of Engineering and Information Technology, University of Medicine, Pharmacy, Sciences and Technology, George Emil Palade of Tirgu-Mures, 540142 Tirgu-Mures, Romania

\* Correspondence: marius.ghitescu@unitbv.ro or m\_ghitescu@yahoo.com (M.-I.G.); arina.modrea@umfst.ro (A.M.)

<sup>†</sup> Presented at the 14th International Conference INTER-ENG 2020 Interdisciplinarity in Engineering, Mures, Romania, 8–9 October 2020.

Published: 22 January 2021

**Abstract:** The paper presents some aspects related to a new light aircraft that has as fields of use sports and leisure aviation. It also has a maximum capacity of two seats and a certain aerodynamic shape and which has on the wings mounted curved flaps for the flight board without hinges, as well as for gliding the plane in critical flight conditions or when it is necessary to save fuel. The paper presents an optimal design method of this new light aircraft.

**Keywords:** light aircraft; design method; optimal; symmetric geometry

## 1. Introduction

The activity of designing a product part uses knowledge acquired in the fields of mathematics, physics, strength of materials, technical drawing, study of metals, materials technology, tolerances and dimensional control, technology of machine construction.

Aircraft design is an information intensive engineering process full of evaluation and decision-making. Conceptual design phase, compared with the entire design process, consumes relatively less time and costs; however, many tasks should be carried out, and a lot of important decisions will have to be made during this period. It is estimated that as much as 80% of the life cycle costs of an aircraft is decided in the conceptual design and preliminary design phase [1–3].

The wing loading is the weight of the aircraft divided by the area of the reference (not exposed) wing. As with the thrust-to-weight ratio, the term “wing loading” normally refers to the takeoff wing loading but can also refer to combat and other flight conditions. Wing loading affects stall speed, climb rate, takeoff and landing distances and turn performance. The wing loading determines the design lift coefficient, and impacts drag through its effect upon wetted area and wing span. Wing loading has a strong effect upon sized aircraft takeoff gross weight. If the wing loading is reduced, the wing is larger. This may improve performance, but the additional drag and empty weight due to the larger wing will increase takeoff gross weight to perform the mission [4].

Aircraft sizing is the process of determining the takeoff gross weight and fuel weight required for an aircraft concept to perform its design mission.

It is known in the literature the light aircraft Extra 300 LT at which the force load of the direction reaches 90 kg [5]. The Extra 300 LT is a one- or two-seater acrobat aircraft produced by German manufacturer Extra Aircraft (Extra Flugzeugbau GmbH, today Extra Flugzeugproduktions- und Vertriebs-GmbH).

It is known the Zlin 142 light aircraft at which the load with forces reaches 200–250 N [6]. Zlin Z 142 is a single-engine aircraft with two seats for tourism and produced by Czechoslovak manufacturer Moravan Otrokovice (now ZLIN Aircraft Otrokovice, Czech Republic).

The new light aircraft has as its areas of use sports and recreational aviation with a maximum capacity of two seats [7].

The new light aircraft has a certain aerodynamic shape, symmetry geometry and good stability being made up of middle wings of rectangular shape and having in part an asymmetrical profile so that the profile rope forms an angle of incidence  $\varphi_{incidence} = 11^\circ$  with the direction of advance and a setting angle  $\varphi_{calaj} = 0^\circ$ , from a front fuselage with a certain aerodynamic shape, a central fuselage with a certain aerodynamic shape and having 2 parts of different shapes in the cabin area, a rear fuselage with a certain aerodynamic shape, propeller helmet, ailerons, flaps, cabin, depth, drift, direction, stabilizer with profiled shapes [8–10].

## 2. A New Light Aircraft and Optimal Design Method

The technical problem of a new light aircraft is the improvement of the dynamic behavior of the light aircraft through the control mechanisms of the flaps and the constructive form of the aircraft, in the conditions of low manufacturing costs and in a favorable time for the aircraft, increasing the surface of the flaps, increasing the wingspan to allow the aircraft to operate in critical flight conditions or when fuel economy is required, enabling the aircraft to glide in these situations.

The design of the aircraft took into account the fact that the components of the aircraft must be simple to manufacture and assemble and accessible for repair.

When establishing the aerodynamic shape and the constructive dimensions of the light aircraft, the optimal design of the light aircraft was taken into account, as were the parameters that influence the aerodynamic shape of the fuselage and wing (Figures 1–5), as well as the flap and aileron installations and mechanisms mounted in these areas.

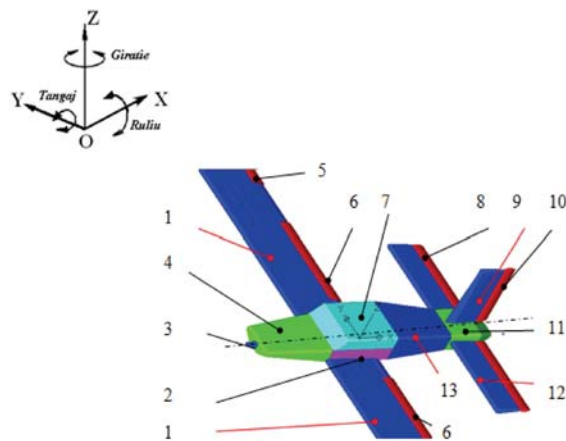


**Figure 1.** A new light aircraft. 1—the median wing of rectangular shape and having in part an asymmetrical profile so that the chord of the profile forms an angle of incidence with the direction of advance and an angle of choke of a certain length  $L$ , 2—the central plane of the fuselage, 3—the helmet of the propeller, 4—front fuselage (bonnets), 5—aileron, 6—curved flaps or single flaps (one on each wing) located on the trailing edge without hinges (without axes of rotation on the wings), 7—the cab, 8—the depth (the moving part of the horizontal tail), 9—the drift (the fixed part of the vertical tail), 10—the direction (the moving part of the vertical plumage), 11—rear fuselage, 12—stabilizer (fixed part of the horizontal tail), 13—central fuselage (2nd part).



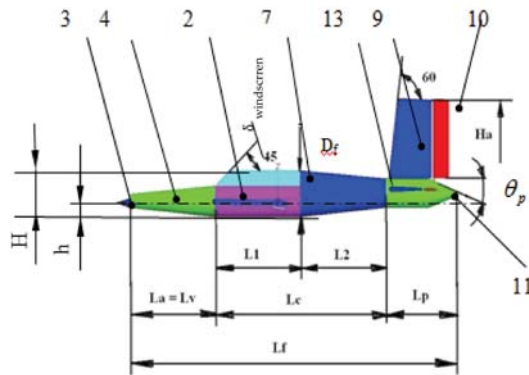


Figure 2. Lateral view of a new light aircraft.

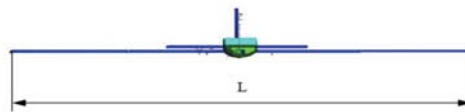


Figure 3. The frontal view of light aircraft.

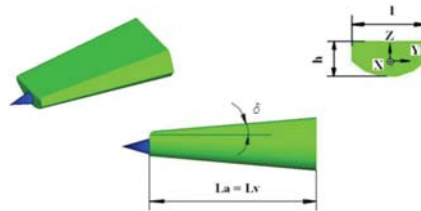


Figure 4. The first part of fuselage.

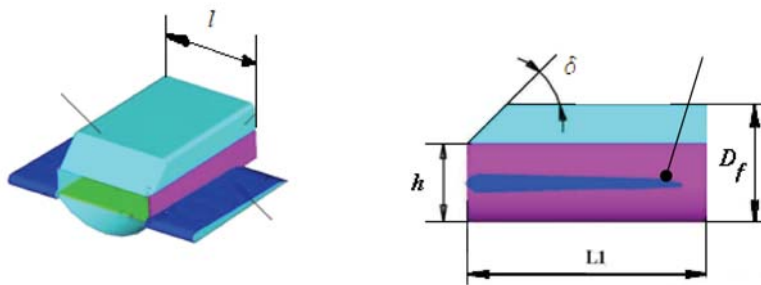


Figure 5. The central fuselage—Part 1.

The constructive solution of the new light aircraft consists of original components such as shape and dimensions to improve the aerodynamics of the aircraft and its stability, as follows: median wings, L-shaped, rectangular and having in part an asymmetrical profile so that the rope profile forms an angle with the forward direction, the central plane of the fuselage (Part 1 of the central fuselage), the propeller helmet, the front fuselage (hoods), ailerons and curves for the flight dashboard without



hinges (one on each wing), the cabin housing the crew, the depth, the drift, the direction, the rear fuselage, the stabilizer and the second part of the central fuselage.

The advantages of the light aircraft are the following:

(a) The light aircraft has a simple and fast response structure, is safe and reliable and has good flight control and lifting performance and good stability.

(b) The aerodynamic shape of the airplane and the constructive shape of the flywheel control mechanism imply an increased service life.

(c) In order to increase the lift capacity of the aircraft, during take-off and landing, as well as during the flight, two curved flaps for the flight board without hinge (without axes of rotation with respect to the wings) were mounted on the wings, one on each wing.

(d) By increasing the length of the wings, an increased load-bearing surface was obtained, increasing the wingspan  $L$  of the wings to a value greater than (1.1 ... 1.3) times the length of the fuselage  $L_f$ , which led to an increase in the surface of the flaps, which allows the aircraft be able to glide in critical flight situations when the engine is no longer running or when needed for fuel economy, which allows the aircraft to easily behave like a glider.

Figure 1 shows in axonometric view the constructive solution of a new light aircraft, which consists of original components as a shape and dimensions to improve the aerodynamics of the aircraft and its stability, as follows: 1—represents the median wing of rectangular shape and having in part an asymmetrical profile so that the chord of the profile forms an angle of incidence with the direction of advance and an angle of choke of a certain length  $L$  (2 pcs.), 2—the central plane of the fuselage, 3—the helmet of the propeller, 4—front fuselage (bonnets), 5—aileron (2 pcs., one on each wing), 6—curved flaps or single flaps (one on each wing) located on the trailing edge without hinges (without axes of rotation on the wings), 7—the cab, 8—the depth (the moving part of the horizontal tail), 9—the drift (the fixed part of the vertical tail), 10—the direction (the moving part of the vertical plumage), 11—rear fuselage, 12—stabilizer (fixed part of the horizontal tail), 13—central fuselage (2nd part) [7].

The aerodynamic shape and construction dimensions of this aircraft have been established by combining various geometric shapes for its components in order to obtain a good aerodynamic shape for the class of light aircraft and to fulfill the function of gliding when needed when fuel economy is needed or in critical flight conditions when the engine is no longer running.

The aerodynamic shape and constructive dimensions of the light aircraft shown in Figures 1–3 make this aircraft also fall into the category of glider, which means that the aircraft can glide as needed if the engine is no longer running or when the engine is stopped for fuel economy.

Figure 2 shows a side view of the light aircraft in which the important components and dimensions established in the design of the aircraft can be observed.

The aerodynamic shape of the light aircraft depends on the aerodynamics of the body systems of which the aircraft is composed. The fuselage being the supporting organ of the plane's transport load, its design starts from the interior partitioning necessary for the plane's mission.

The fuselage of a light aircraft consists of 3 large assemblies, namely, assembly 1 called the front fuselage 4 (front of the aircraft) in length, assembly 2 called the central fuselage which has 2 parts 1 and 2 (positions 2 and 13 lengths), and the last assembly being the rear fuselage 11 (from the tail of the plane) long.

The shape of the fuselage on light aircraft without special demands of an aerodynamic nature is imposed by technological considerations, manufacturing costs and useful volume.

The useful volume is the parameter that gives the available space inside where we can place the crew, luggage, equipment and fuel.

The payload depends on the carrying capacity of an aircraft which decreases with the reduction of the total length of the fuselage and the area of the maximum cross part.

A maximum useful aircraft volume means a lower than optimal aerodynamic shape.

The fuselage of the aircraft is located in a stream of air and it produces lift (very low) but especially forward resistance: Lateral aerodynamic forces and aerodynamic moments act on it; its construction takes over all the demands of the other organs and elements of the aircraft.

In addition, in the fuselage are arranged spaces for crew, propulsion system, fuel tank, equipment, etc., which implies the existence of a well-defined volume. For the fuselage, an optimal solution must be found both from an aerodynamic and constructive point of view: with a front surface as small as possible to “close” a large volume, but at the same time, the shape of the body volume obtained, to be as aerodynamic as possible.

The front fuselage of a light aircraft, Figures 2 and 4, has an aerodynamic profiled shape, being made up at the bottom of a surface arranged under a circular arc on a length  $L_a$ , the straight side surfaces on the length  $L_a = (1.2 \dots 1.5) * D_f$ , and the part of above is a flat surface that is inclined at a certain angle  $\delta = 20^\circ \dots 50^\circ$ .

The maximum equivalent part  $D_f = H$  [mm] for the center fuselage shall be determined according to the dimensions of the cab and of the installations which are contained in the fuselage.

For light aircraft with 2 adjacent seats, the area of the maximum rear fuselage part is recommended as  $S_f = 1.5 \dots 1.7 \text{ m}^2$ . Determining the total length of the fuselage with the relation:  $L_f = (6 \dots 10) * D_f$ , where  $L_f/D_f = l_f = 6 \dots 10$  represents the elongation of the fuselage.

At subsonic flight speeds, the pressure resistance in a laminar flow is relatively low compared to the frictional resistance, and there is no question of reducing it. As the forward resistance is mostly produced by the frictional resistance, it is recommended to use short (shorter) fuselages to reduce it.

The central fuselage has two aerodynamic parts (Figures 1, 2 and 5).

Part 1 of the central fuselage of a light aircraft has at the bottom a surface arranged under an arc of a circle on a length  $L_1 = L_2 = (1.7 \dots 2.0) * D_f$ , straight side surfaces; the top is straight, a front surface facing the cab inclined at a certain angle  $\delta_{windscreen} = 40 \dots 55^\circ$ , having in longitudinal part a profiled shape with dimensions  $h = 0.625 * D_f$ ,  $L_1, D_f, H = D_f = (1.5 \dots 1.7) * h$  and an inclined front surface which is the windscreen inclined at a certain angle  $\delta_{windscreen} = 40 \dots 55^\circ$  for optimum visibility, Figure 5.

Part 2 of the central fuselage of a light aircraft (Figures 2 and 6) has a profiled aerodynamic shape having at the bottom a surface arranged under an arc of a circle on a length  $L_2 = L_1$  and inclined at an angle  $\delta_1 = (10^\circ \dots 25^\circ)$ , the straight side surfaces, and the top is a flat and inclined surface at a certain angle  $\delta_1 = (10^\circ \dots 25^\circ)$ , having in longitudinal part a frustoconical shape with large base  $H = D_f$ , length and angle of inclination of the side edges  $\delta_1 = (10^\circ \dots 25^\circ)$ .

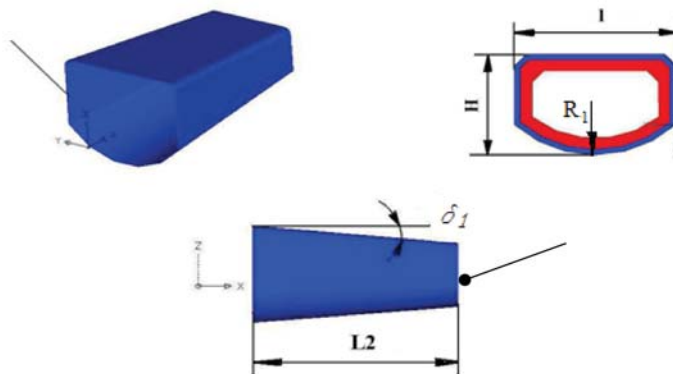


Figure 6. The central fuselage—Part 2.

The shape of the rear fuselage is shown in Figures 1 and 7. The rear fuselage of a light aircraft has a profiled aerodynamic shape, being formed at the bottom of a surface arranged under an arc of a circle on a certain length  $L_{p1} = 0.7 * L_p$ ; the left-right side surfaces are straight on a certain length  $L_{p1} = 0.7 * L_p$ ,

and the surfaces from the tail of the plane are inclined at a certain angle  $\theta_p = 20 \dots 50^\circ$  on a length  $L_p - L_{p1} = 0.3 * L_p$ , where  $L_p = (1.2 \dots 2.5) * D_f$ .

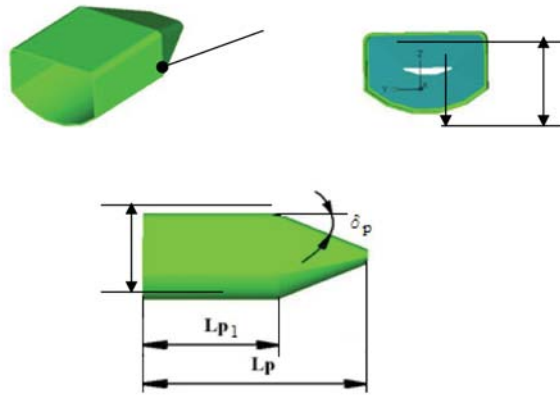


Figure 7. The rear fuselage.

The middle wing of a light aircraft (Figures 1–3) has a profiled aerodynamic shape, the wing having a rectangular shape and an asymmetrical profile in part so that the profile rope forms an angle of incidence  $\varphi_{incidence} = 11^\circ$  with the direction of advance and a right angle.  $\varphi_{chocking} = 0^\circ$ , and the wingspan  $L$  of the wing is greater than (1.1 ... 1.3) times the length of the fuselage  $L_f = (6 \dots 10) * D_f$ , ( $D_f = H$  [mm])—the maximum equivalent part for the central fuselage, for a non-circular profile) to allow the aircraft to behave like a glider due to the length of the wings and the aerodynamic shape, to glide when needed for fuel economy or in critical flight situations when the engine is no longer running.

The middle wing is advantageous in terms of interaction with the fuselage.

Figure 3 shows a front view of the light aircraft and the wingspan  $L$  of the wings.

When designing the fuselage of the aircraft, the operating conditions necessary for the fuselage were taken into account: maximum payload, access to all installations mounted in the fuselage, heating, ventilation, tightness, good visibility for the crew. The strength and rigidity of an aircraft are maximum at a minimum weight of the resistance structure.

The design of the aircraft took into account the fact that the components of the aircraft must be simple to manufacture and assemble and accessible for repair.

Increasing the length of the wings also increases the length of the flaps, which leads to increased lift during takeoff and landing of the aircraft slightly.

At subsonic flight speeds, a great influence on the aerodynamic characteristics has also the attack board of the wing profile, reason for which its sharp shape is avoided because it does not allow obtaining large lifting forces.

When the plane flies at relatively low speeds, the evolutions are made at high angles of incidence. The detachment of the boundary layer that begins with the increase of the angles of incidence is manifested with greater intensity in the area where the wing joins the fuselage. This detachment results in an increase in the forward resistance, a decrease in lift and a displacement of the center of pressure.

Upon landing, the pilot reduces engine traction and automatically reduces the lift. Volleyballs driven at negative downward angles ensure an increase in lift at this critical time, behaving like an aerodynamic brake.

At take-off, the traction of the engine increases successively, and the flaps as hypersuspension devices ensure an increase of the load-bearing force and the reduction of the take-off distance.

The optimal design method of the light aircraft is to establish the calculation steps that define the parameters of the fuselage and the wing and the aerodynamic shape of this aircraft depending on the maximum equivalent part  $D_f$  in the cabin area where the crew sits, the value of the magnitude  $L = (1.1 \dots 1.3) * L_f$ , of the installations that are mounted in these areas.

Figure 8 shows the logic diagram underlying the optimal design of the aerodynamic shape of a light aircraft with the steps to be followed.

1. Determining the maximum equivalent part  $D_f = H$  [mm] for the center fuselage for a non-circular profile.
2. Determining the total length of the fuselage with the relation:  $L_f = (6 \dots 10) * D_f$ , where  $L_f/D_f = l_f = 6 \dots 10$ , represents the elongation of the fuselage.
3. The establishment of the ratio between the sum of the lengths of the previous fuselage  $L_a$  and the length  $L_1$  of Part 1 of the central fuselage compared to the total length  $L_f$  of the is calculated with the relation:

$$(L_a + L_1)/L_f = 0.2 \dots 0.3$$

where  $L_a$  [mm] represents the length of the front fuselage,  $L_1$  [mm]—the length of Part 1 of the central fuselage (cabin area),  $L_f$  [mm]—the total length of the fuselage.

4. The determination of the elongation of the front fuselage is calculated with the relation:

$$L_a/D_f = 1.2 \dots 1.5 \text{ or } L_a = (1.2 \dots 1.5) * D_f \text{ [mm]}.$$

5. Setting the Peak Angle for the front fuselage  $\delta = 20^\circ \dots 50^\circ$ . It was adopted  $\delta = 30^\circ$ .
6. Determining the Length  $L_1, L_2$  of the two parts of the central fuselage, the total length  $L_c$  of the central fuselage, and the angle of inclination  $\delta_1$  of the edges with the relations:

$$L_1 = L_2 = (1.7 \dots 2.0) * D_f \text{ [mm]}, \delta_1 = 10^\circ \dots 25^\circ, \\ L_c = L_1 + L_2 = 2 * L_1 = 2 * L_2 = (3.4 \dots 4.0) * D_f \text{ [mm]},$$

where  $L_1$  [mm]—length of Part 1 of the central fuselage (in the cab area),  $L_2$  [mm]—the length of Part 2 of the central fuselage,  $L_c$ —the total length of the central fuselage, and  $\delta_1$ —the angle of inclination of the side edges.

7. The establishment of the lateral surface of the fuselage is approximated with the relation:

$$S_{lat} = K\pi D_f L_f = [0.734 + 14.5 \times 10^{-3} \times (6 \dots 10)] \pi D_f L_f, \text{ [mm}^2\text{]}$$

where  $K = 0.734 + 14.5 \times 10^{-3} \times (6 \dots 10)$ .

8. Determining the angle of the rear fuselage  $\theta_p = 20 \dots 50^\circ$ . It is adopted  $\theta_p = 30^\circ$ .
9. Determining the length of the rear fuselage  $L_p = (1.2 \dots 2.5) * D_f$  [mm].
10. Determining the inclination of the windshield (dome).  $\delta_{windscreen} = 40 \dots 55^\circ$ ,  $\delta_{windscreen} = 45^\circ$  was adopted for better visibility.
11. The determination of the height  $h$  [mm] is determined with the following relation:

$$h = 0.625 * D_f.$$

12. The determination of the width  $l$  [mm] of the cabin is determined with the following relation:

$$l = 1.0625 * D_f.$$

13. The determination of the height  $H$  [mm] is determined by the following relation:

$$H = D_f = (1.5 \dots 1.7) * h,$$

$D_f = 1.6 \cdot h$  was adopted.

14. The determination of the height  $H_a$  [mm] of the direction is determined by the following relation:

$$H_a = (1.2 \dots 1.3) \cdot D_f.$$

$H_a = 1.235 \cdot D_f$  was adopted.

15. Determination of the wingspan (distance between the extreme ends of the wings)  $L$  [mm], the angle of incidence  $\varphi_{incidence}$  [ $^\circ$ ] and the angle of offset  $\varphi_{chocking}$  [ $^\circ$ ],  $L = (1.1 \dots 1.3) \cdot D_f$ . We adopted  $L = 1.15 \cdot L_f$ ,  $\varphi_{incidence} = 11^\circ$  and  $\varphi_{chocking} = 0^\circ$ .
16. CAD modeling and optimization of the aerodynamic shape of the light aircraft.
17. Simulation of the plane with Adams software.
18. Practical execution and testing of light aircraft.

The optimal method of designing the light aircraft is to go through the following steps:

When the aircraft is operating lightly, the two flaps on the wings bend (rotate downwards) symmetrically, only at negative angles.

During the flight of the aircraft, the two identical ailerons on the wings brace anti-symmetrically to each other at positive and negative angles and generate the roll motion.

In the current stage of industrial development in conditions of high competition in the aero industry market, each manufacturer must develop its own strategy.

It seeks to reduce as much as possible the time interval between the conception (design) of an installation and its execution.

For this purpose, the use of the computer in all stages of design and production is a basic requirement. Thus, it is necessary:

- Real—time simulation of the dynamic behavior for these aircraft command and control installations.
- Virtual prototype optimization.

Aircraft must comply with special design and execution conditions. These apply to all subassemblies and components.

Computer modeling and virtual prototyping are valuable tools for creation.

The materials used for its execution also have an influence on the aerodynamics of the light aircraft and its minimum weight. The main components of the light aircraft (for example, fuselage, wings, tailings, throttle controls, ailerons) can be made of various materials (e.g., duralumin or composite materials) so as to obtain good aerodynamics and a minimum weight of plane.

By using composite materials, the weight of the aircraft is considerably reduced, the aerodynamics is improved, and its mechanical strength and reliability are increased.

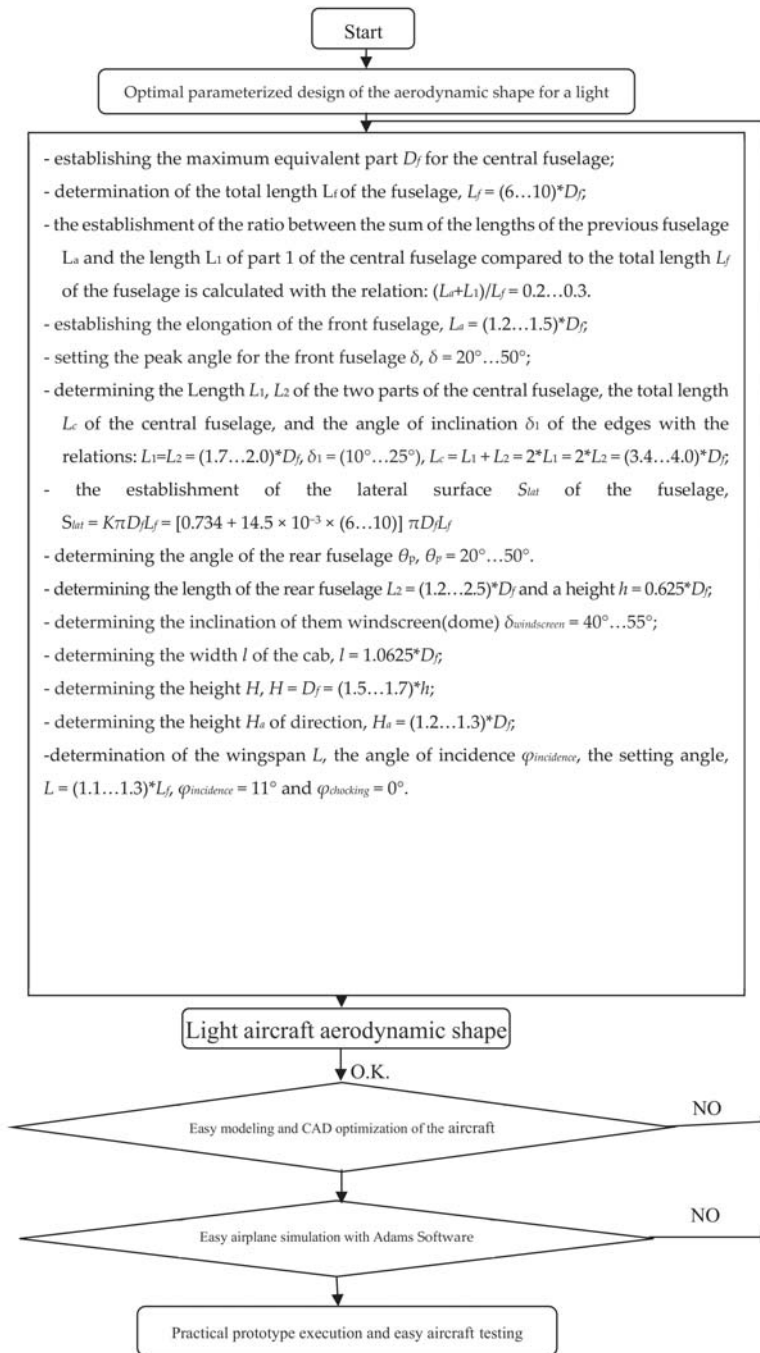


Figure 8. The logic diagram of optimal design method of light aircraft.

### 3. Conclusions

The process of aircraft conceptual design includes numerous statistical estimations, analytical predictions and numerical optimizations. However, the product of aircraft design is a drawing. While the analytical tasks are vitally important, the designer must remember that these tasks serve only to influence the drawing, for it is the drawing alone that ultimately will be used to fabricate the aircraft.

All of the analysis efforts to date were performed to guide the designer in the layout of the initial drawing. Once that is completed, a detailed analysis can be conducted to resize the aircraft and determine its actual performance.

This detailed analysis is time-consuming and costly, so it is essential that the initial drawing be credible. Otherwise, substantial effort will be wasted upon analyzing an unrealistic aircraft.

The design layout process generally begins with a number of conceptual sketches.

A good sketch will show the overall aerodynamic concept and indicate the locations of the major internal components. Once the design has been analyzed, optimized, and redrawn for a number of iterations of the conceptual design process, a more detailed drawing can be prepared.

The crew station will affect the conceptual design primarily in the vision requirements.

Requirements for unobstructed outside vision for the pilot can determine both the location of the cockpit and the fuselage shape in the vicinity of the cockpit. The pilot must be able to see the runway while on final approach, so the nose of the aircraft must slope away from the pilot's eye at some specified angle. While this may produce greater drag than a more streamlined nose, the need for safety overrides drag considerations. Similarly, the need for over-side vision may prevent locating the cockpit directly above the wing.

The vision angle looking upward is also important. Light Aircraft should have unobstructed vision forwards and upwards to at least 20 deg above the horizon.

By increasing the length of the wings, an increased load-bearing surface was obtained, increasing the wingspan  $L$  of the wings to a value greater than (1.1 ... 1.3) times the length of the fuselage  $L_f$ , which led to an increase in the surface of the flaps, which allows the aircraft be able to glide in critical flight situations when the engine is no longer running or when needed for fuel economy, which allows the aircraft to easily behave like a glider.

Computer modeling and virtual prototyping are valuable tools for creation.

By applying a virtual prototyping algorithm, we can shorten the distance between the creation and execution of the physical prototype. By increasing the length of the wing and the wingspan, the surface of the flaps is obtained. By increasing the surface of the shutters, the load is increased. By increasing the load and by increasing the steering angles, the take-off and landing of the aircraft is done in a shorter time and over a shorter distance.

### 4. Patents

The content of this paper is the subject of a patent application entitled "*Light aircraft and flap control mechanism*".

**Author Contributions:** Conceptualization, M.-I.G.; methodology, M.-I.G., M.G. and A.M.; software, M.-I.G. and M.G.; validation, M.-I.G.; formal analysis, M.-I.G., M.G.; investigation, M.-I.G.; resources, M.-I.G.; data curation, M.-I.G.; writing—original draft preparation, M.G.; writing—review and editing, M.G. and M.-I.G.; visualization, M.G.; supervision, M.-I.G. and A.M. All authors have read and agreed to the published version of the manuscript.

### References

1. Postelnicu, A. *Aerodynamic Profiles*; Transilvania University of Brasov: Brasov, Romania, 1997; pp. 27–54.
2. Roskam, J. *Airplane Design, Part I. Preliminary Sizing of Airplanes*; University of Kansas: Lawrence, KS, USA, 1985; pp. 44–100.
3. Raymer, D. *Aircraft Design: A Conceptual Approach*; Air Force Institute of Technology: Wright-Patterson Air Force Base, OH, USA, 1989; pp. 3–603.

4. Tomažič, T.; Matko, D.; Karba, R. Theoretical and practical approach to full-scale aircraft modelling. *IFAC Proc. Vol.* **2009**, *42*, 1223–1228. [[CrossRef](#)]
5. Maintenance Manual Extra 300 LT Aircraft. Available online: [https://www.extraaircraft.com/docs/tech-manuals/MM300LT/300LT\\_MM\\_20150612.pdf](https://www.extraaircraft.com/docs/tech-manuals/MM300LT/300LT_MM_20150612.pdf) (accessed on 22 July 2020).
6. Maintenance Manual Zlin 142 Aircraft. Available online: <http://aerodromclinceni.ro/wp-content/uploads/2012/07/Man-de-zbor-Z142-rev8-lb-eng.pdf> (accessed on 22 July 2020).
7. Ghitescu, I.-M.; Vlase, S.; Ghitescu, M. Light Aircraft and Flap Control Mechanism. Patent Application No. CBI A/00223, 27 April 2020.
8. Florescu, N. *Aerodynamics of the Airplane*; Scrisul Romanesc Publishing House: Craiova, Romania, 1984; pp. 34–94.
9. Gavrilă, J. *Aircraft Aerodynamics*; Dacia Foundation: Brasov, Romania, 2000; pp. 30–90.
10. Grosu, I. *Aircraft Calculation and Construction*; Didactic and Pedagogical Publishing House: Bucharest, Romania, 1965; pp. 18–80.

**Publisher's Note:** MDPI stays neutral with regard to jurisdictional claims in published maps and institutional affiliations.



© 2021 by the authors. Licensee MDPI, Basel, Switzerland. This article is an open access article distributed under the terms and conditions of the Creative Commons Attribution (CC BY) license (<http://creativecommons.org/licenses/by/4.0/>).





Proceedings

# Mechanical Behavior of Gypsum Composites Reinforced with *Retama monosperma* Fibers <sup>†</sup>

Djamel-Eddine Aizi \*  and Meriem Kaid-Harche

Laboratory of Plant and Microbial Production and Valorization (LP2VM),  
University of Science and Technology Mohamed Boudiaf, BP 1505, El M'naouar Oran 31000, Algeria;  
kaidharche@yahoo.fr

\* Correspondence: aizi\_djameledine@hotmail.fr; Tel.: +213-779922750

† Presented at the 14th International Conference INTER-ENG 2020 Interdisciplinarity in Engineering,  
Mureş, Romania, 8–9 October 2020.

Published: 21 December 2020



**Abstract:** In this pioneering study, *Retama monosperma* fibers were used in the preparation of a plaster composite dedicated to the field of civil engineering in order to find a substitute for fiberglass as a reinforcement material. *Retama monosperma* (Rtam) is one of the plant species abundantly available in Mediterranean regions. The localization of fibers at the organic level, the extraction procedure, physical and mechanical properties were studied to compare them with other vegetable fibers currently used in the manufacture of biocomposites. The results obtained show the possibility of improving the mechanical properties of plaster by using the fibers of *Retama monosperma*. The purpose of this paper is to promote the fibers of *Retama monosperma* as a building material in civil engineering in order to boost researchers' interests in this Mediterranean plant.

**Keywords:** gypsum; fiber; stems; *Retama monosperma*; concretes plaster; mechanical characteristics

## 1. Introduction

Plaster is a white powder produced by the calcination of gypsum. This material is extremely old—it was discovered by humanity in antiquity. Gypsum is a very abundant rock with varied crystalline forms. Gypsum has the formula  $\text{CaSO}_4 \cdot 2\text{H}_2\text{O}$ , and it is called calcium sulfate dehydrate, or, more simply, dehydrate. Due to its availability in subsoil, relatively low cost, ease of high usage and mechanical characteristics being suitable for many uses, plaster is a widely used construction material, and its use continues to grow, as does the use of prefabricated gypsum products such as tiles and plates. However, plaster appears to be permeable and too brittle [1]. Improving the crack resistance of gypsum is an essential problem which the science of composite materials has naturally responded to. The main idea is to introduce a material in the form of fibers into a binder, called a matrix. It is then possible to obtain extremely resistant materials from a fragile elastic fiber and matrix. Fiber glass first appeared in plaster, and a number of studies have shown that synthetic fiber reinforced plaster materials possess the best mechanical efficiencies [2,3], but it is an expensive reinforcement, and it makes the plates considerably heavier, making them less practical to use on larger sites; besides this, they have a harmful effect on the environment. Due to these kinds of fibers, scientists have been forced to look for a new material. Vegetable fibers are a potential source for a low-cost material from renewable resources, and are environmentally friendly, and they are less gluttonous regarding fossil energy. According to [4], the mechanical properties of plaster are enhanced by using natural fibers.

Nowadays, one of the current trends of the building industry is to develop “green materials”: the use of natural fibers as reinforcement of lime plasters plays a leading role in this transition towards renewable materials [5]. Generally, the application of natural fibers is attractive for four

main reasons: their specific properties, their price, their health advantages and their recyclability [6]. The fact that these natural fibers offer a low density and good specific properties is an important benefit. Furthermore, the fibers are renewable and have a CO<sub>2</sub>-neutral life cycle, in contrast to their synthetic opponents.

*Retama monosperma* (Rtam) is a shrub 1 to 4 m tall [7], belonging to the Fabaceae family. It grows in coastal regions [8,9]. *Retama monosperma* is able to tolerate salt spray, high temperatures and nutrient-poor soils [9]. Rtam is known for its very fiber-rich stems, but unfortunately until now there has been no study on the valuation of *Retama monosperma* fibers in building construction.

In the present study, the main objective is the modification of the mechanical behavior of gypsum by *Retama monosperma* stem fibers. For this, we attempted to study the influence of proportion and length of *Retama monosperma* stem fibers on the mechanical properties of plaster concretes.

## 2. Materials and Methods

### 2.1. Fibers

#### 2.1.1. Fiber Extraction

For this step (Figure 1), a procedure based on the combination of chemical and physical treatments was used [10].

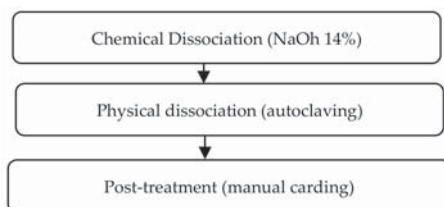


Figure 1. Fiber extraction procedure.

#### 2.1.2. Location of Fibers within the Stem of *Retama monosperma*

Freehand cuts were made on freshly harvested stems of *Retama monosperma*, which were colored with congo red and methyl green in order to reveal the different parts of the stem.

#### 2.1.3. Biometric Study of Fibers

A biometric study requires the separation of elementary fibers from one another. This was carried out according to the protocol of [11] by putting fragments of 1 cm of young stems in a solution of hydrogen peroxide and acetic acid with equal volume, before putting them in the oven at 70 °C for 24 h. Once the fibers were separated, microscopic observations were made using a light microscope with a micrometer incorporated in the eyepiece.

#### 2.1.4. Mechanical Characterization of Fibers

The mechanical properties (tensile strength, elongation and the modulus of elasticity of the fibers) were determined in accordance with standards NF EN ISO 5079(1996), under climatic conditions, T = 20 ± 2 °C, and a relative humidity, RH = 65 ± 2%, using an Instron universal testing machine equipped with a 250 N load sensor and two displacement transducers at a cross-head speed of 0.5 mm/min. Tests data were digitally recorded and the force/deformation curve was plotted.

### 2.1.5. Density

The density of fibers was determined by using a pycnometer (Figure 2).

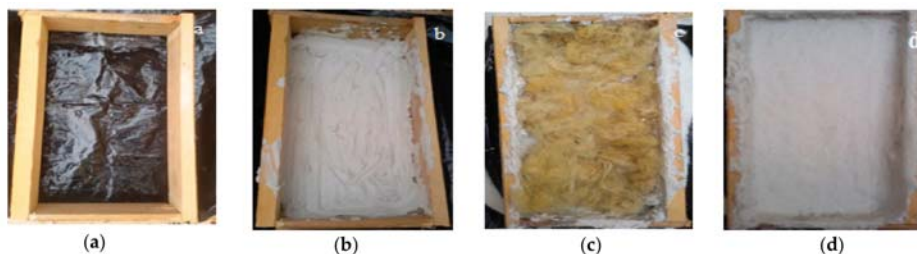


**Figure 2.** Illustration of the different steps of the composite preparation (plaster/fiber): (a) first step, (b) second step, (c) third step and (d) fourth step.

### 2.1.6. Thermogravimetric Analyses (TGA)

Thermogravimetric analyses (TGA) were carried out with an etaram TG/DTA 92 type device. The initial mass of the sample was approximately 10 mg. The heating rate was adjusted to 10 °C/min, with a temperature varying from 20 to 1000 °C.

### 2.1.7. Scanning Microscopy

A scanning electron microscope was used to examine the fibers' surface topographies and the section of fibers.

## 2.2. Plaster Concrete

The gypsum used comes from the Knauf factory of Oran in Algeria.

The steps of composite preparation:

1. The powdered gypsum was mixed with water until a slurry was obtained, which was then spread out in a mold.
2. Production of the composite by the gypsum fiber blend; the proportion of fibers in the composite was 1%.
3. Finally, the surface of each plaster brick was smoothed to have a regular brick surface of 30 cm length and 15 cm width.
4. Mechanical properties relate to flexural strength as well as compressive strength; the results were obtained on MPa.

## 3. Results and Discussion

### 3.1. Fiber

#### 3.1.1. Location of the Fibers at the Stems

The cross-section shows the distribution of fibers which go from the epidermis towards the medulla, grouping in clusters between each crypt (Figure 3). While the subepidermal fibers are colored green by methyl green, due to lignified walls, the fibers located in the direction of the phloem are colored in pink by the Congo red, which means that this cellulosic fibers are not lignified yet.

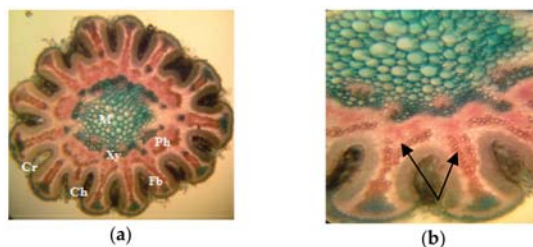


**Figure 3.** Cross-section in a stem of *Retama monosperma*. (a) Cross-section observed at (×100), FB: Fibers, Ph: Phloem, Xy: Xylem, M: Marrow, Ch: chlorenchyma; (b) cross-section observed at (×400); the fibers are indicated by arrows.

### 3.1.2. Fibers Extraction

Using the protocol of [10] allowed us to obtain an average fiber yield of 10.5% after manual carding (Figure 4).



**Figure 4.** *Retama monosperma* stem fibers. (a) Before manual carding; (b) after manual carding.

### 3.1.3. Physical and Mechanical Properties of *Retama monosperma* Fibers

Table 1 shows the density and mechanical properties of natural plant fibers commonly used in several sectors compared to *Retama monosperma* fibers. As can be seen from Table 1, the tensile strengths as well as Young’s modulus of *Retama monosperma* are lower than other fibers mentioned in this table. However, elasticity of *Retama monosperma* is 4.6% higher than other fibers. On the other hand, the *Retama monosperma* fibers show an interesting density of 1.3 g/cm<sup>3</sup>. The lower density is interesting where the weight of the structure needs to be reduced. Generally, the tensile strength and Young’s modulus of plant fibers increase with the increasing cellulose content of the fibers [15]. Additionally, the structure and microfibrillar angle determine the overall properties of the fibers [16].

**Table 1.** Mechanical characteristics of some vegetable fibers [11–14].

Fibers	Tensile Strength (MPa)	Elongation at Break (%)	Young’s Modulus (GPa)	Density (g/cm <sup>3</sup> )
<i>Retama monosperma</i>	110	4.6–4.7	13.3	1.3
Flax	345–1035	1.3–3.3	27.6	1.5
Sisal	600	3	12	1.5
Jute	396–773	1.5–1.8	26.5	1.3
Hemp	690	1.6	30–60	1.15
Cotton	287–597	7–8	5.5–12.6	1.5–1.6
<i>Raphia textilis</i>	148–660	2	28–36	0.75
<i>Raphia vinifera</i>	500	4	12.3	-
Kenaf	700	3	55	-

Plant fibers are more ductile if the fibrils have a spiral orientation to the fiber axis. Fibers are inflexible, rigid, and have a high tensile strength if the fibrils are oriented parallel to the fiber axis [17]. However, the origin place and climatic conditions affect the physical-mechanical properties of natural plant fibers. It is also important to note that natural plant fibers with poor mechanical properties may be suitable for nonstructural applications [17].

### 3.1.4. Geometric Features Including Fiber Length and Width

The fibers extracted from the stems of *Retama Monosperma* have an average length of 155.7 mm and a width of 0.116 mm. Each fiber is microscopically made up of several unitary fibers.

The *Retama monosperma* unitary fiber is 0.7 mm long and 20 μm wide. The comparison between the morphometry of *Retama monosperma* fibers and other fibers (Table 2) shows that the fibers of *Retama monosperma* are small.

**Table 2.** Morphological structure of some natural fibers [18–22].

Single Fiber	<i>Retama monosperma</i>	Cotton	Hemp	Kenaf
Length, mm	0.7	15–56	40–250	1.5–11
Width, μm	20	12–25	16–126	12–36

The morphological characteristics of the fibers, length and width, are important factors for the mechanical performance of fibers. In general, unitary fibers of short length give a fibrous bundle with limited resistance to mechanical traction, because the small unitary fibers need many interfibrillary bonds inside the fiber bundle compared to the long unitary fibers, which reduces the mechanical resistance of the entire bundle.

Microscopic observations with SEM show the appearance of the fibrous bundles of *Retama monosperma* (Figure 5a). The horizontal section of the fibers shows the presence of a triangular lumen in the center of each unitary fiber of *Retama monosperma* (Figure 5b), which gives the fiber a heat insulating capacity.

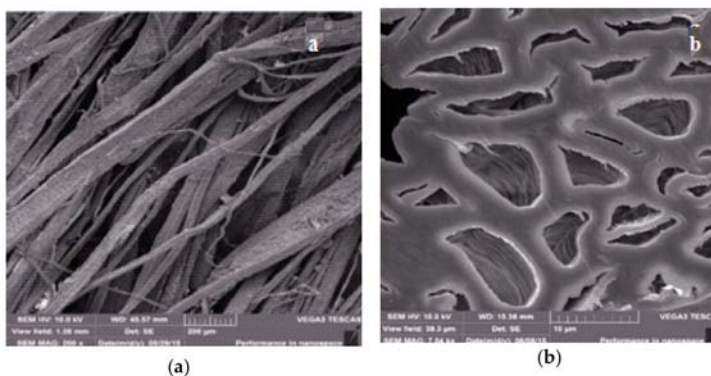


**Figure 5.** Observation of *Retama monosperma* fibers using an electron microscope. (a) Bundles of fibers (×50,000); (b) horizontal section (×100,000).

### 3.1.5. Thermal Stability

The obtained results show the evolution of the loss of mass fibers as a function of the temperature. In this study, the degradation of fibers started at a temperature of 66.57 °C, with an energy release of 1.55 J and a weight loss of 6.859% of the initial weight of the fibers (Table 3). The first mass loss is linked to the evaporation of water trapped inside the fiber [23]. The degradation continued with the increase in temperature until it reached its peak at the temperature of 312.40 °C where the weight

loss was 53.195%. More than half of the mass of the fibers was lost at 312.40 °C. This loss is linked to the cellulose mass loss; the numerous studies in the literature agree that cellulose degrades between 300 and 420 °C [24,25], while pectins and hemicelluloses degrade between 250 and 320 °C [24,25], and also indicate that breaks in glycosidic bonds in cellulose also occur from 200 °C. With regard to lignins, there remains a disagreement regarding their decomposition temperature which could be explained by the complexity of their chemical structure. [26] defined a very wide temperature range from 160 to 900 °C where the lignin degrades. The obtained results show a loss of 32.988% at 451 °C, before a total degradation of fibers at 568.21 °C.

**Table 3.** Fibers’ weight loss and energy released during the thermogravimetry test.

Temperature	Energy Released	Weight Loss (%)
66.57	1.55 J	6.859%
312.40	38.64 J	53.195%
451	35.18 J	32.988%
568.21	6.29 J	2.404%

### 3.2. Plaster Biocomposites Reinforced with *Retama Monosperma* Fibers

Use of natural fibers as a reinforcement in a cement matrix has also been practiced for making low-cost building materials such as panels, claddings, roofing sheets and tiles, slabs and beams [27,28]. Sisal and coir are two of the most studied fibers, but bamboo, jute, hemp, reeds and grasses have also been studied for making sheeting materials [29]. Many studies focused on natural fiber composite reinforcement concluded that the tensile strength and modulus of the rupture of composites increased up to a certain fiber length and volume fraction; further increase in fiber length or volume fraction induce a considerable decrease in the composite strength. In this study, two parameters were taken into account—the fibers’ lengths and their proportion in the plaster brick. Table 4 shows the obtained results.

**Table 4.** Mechanical properties of *Retama monosperma* fiber reinforced plaster composites.

Length (cm)	Test	Flexural Strength (MPa)	Compressive Strength (MPa)
0	control	0.7	7.51
10	0.5	1.33	8.75
	1	1.02	7.88
	1.5	1.04	7.91
15	0.5	1.09	10.49
	1	1.12	11.68
	1.5	1.01	9.21
20	0.5	0.51	6.54
	1	0.66	6.37
	1.5	0.47	5.98

Mechanical tests carried out on plaster samples reinforced with *Retama monosperma* fibers reveal that the fibers with a length of 15 cm and fraction of 1% gave the best performance in terms of the flexural strength, with an average of 1.12 MPa, as well as the compressive strength which was 11.68 MPa. According to these results, it is clearly noted that the flexural strength increases considerably with dosage and length of fibers. A clear improvement for different lengths was seen for a dosage of 1% fibers of 15 cm length, after which a loss of the flexural strength was recorded, owing to excess fibers and a bad distribution of the fibers in the matrix, which increased the porosity of the material and reduced the flexural strength. The plaster composite with a small amount of 0.5% *Retama monosperma* fiber has shown an improvement in the mechanical properties of the composite, this is in agreement with the results of [30] where it is reported that, even in small quantities, the behavior of the plaster changes.

Other studies have been conducted on different fibers, such as coconut fibers—Djoudi et al. [31] show that the best result is obtained with a volume fraction of 4% while Mathur [30] in a study on the strengthening of plaster concrete with date palm fibers has found that a fraction of 1.5% gives the best results in terms of tensile strength and bending. The length of the fibers and the optimal fraction in the composite are two parameters that differ from one fiber to another depending on their morphology and their chemical composition which are linked essentially to the organic fiber origin and of the plant itself. In general, the properties of a composite material result from the combination of several factors:

- (1) the length of the fibers;
- (2) fiber architecture;
- (3) the orientation of the fibers;
- (4) the fiber–matrix interface.

#### 4. Conclusions

One of the most widely used construction techniques is the use of fibers as a reinforcement in building materials. In Algeria, imported oakum are currently used for the creation of false plaster ceilings. Glass fibers and sisal are the most used reinforcements to date. Finding a replacement for the imported oakum using natural resources and, in particular, the local flora is necessary. Using *Retama monosperma* fibers as reinforcements for plaster is an objective which was demonstrated as being possible in this study by the results obtained in terms of the mechanical properties of the composite plaster/fiber. In order to guarantee the quality of the composite material produced, further research is required to complete this pioneering study.

**Conflicts of Interest:** The authors declare no conflict of interest.

#### References

1. Eve, S.; Gominaa, M.; Gmouhb, A.; Samdib, A.; Moussab, R.; Orangeç, G. Microstructural and mechanical behaviour of polyamide fibre-reinforced plaster composites. *J. Eur. Ceram. Soc.* **2002**, *22*, 2269–2275. [[CrossRef](#)]
2. Wu, Y.F. The structural behaviour and design methodology for a new building system consisting of glass fibre reinforced gypsum panels. *J. Constr. Build. Mater.* **2009**, *23*, 2905–2913. [[CrossRef](#)]
3. Çolak, A. Physical and mechanical properties of polymer-plaster composites. *J. Mater. Lett.* **2006**, *60*, 1977–1982. [[CrossRef](#)]
4. Dalmay, P.; Smith, A.; Chotard, T.; Sahay-Turner, P.; Gloaguen, V.; Krausz, P. Properties of cellulose fibre reinforced plaster: Influence of hemp or flax fibres on the properties of set gypsum. *J. Mater. Sci.* **2010**, *45*, 793–803. [[CrossRef](#)]
5. Le Troëdec, M.; Dalmay, P.; Patapy, C.; Peyratout, C.; Smith, A.; Chotard, T. Mechanical properties of hemp-lime reinforced mortars: influence of the chemical treatment of fibres. *J. Compos. Mater.* **2011**, *45*, 2235–2347. [[CrossRef](#)]
6. Bos, H.L. The Potential of Flax Fibres as Reinforcement for Composite Materials. Ph.D. Thesis, Eindhoven University of Technology, University Press Facilities, Eindhoven, Germany, 2004.
7. Selami, N. Etude des Associations Symbiotiques de *Retama monosperma*: Approches Morphologique, Anatomique et Ultrastructurale, Caractérisation Moléculaire des Isolats. Ph.D. Thesis, Université Mouhamed Boudiaf, Oran, Algiers, 2014.
8. Benmiloud-Mahieddine, R.; Abirached-Darmency, M.; Brown, S.C.; Kaid-Harche, M.; Siljak-Yakovlev, S. Genome size and cytogenetic characterization of three Algerian *Retama* species. *Tree Genet. Genom.* **2011**, *7*, 987–998. [[CrossRef](#)]
9. Muñoz Vallés, S.; Gallego Fernández, J.B.; Cambrollé, J. The Biological Flora of Coastal Dunes and Wetlands: *Retama monosperma* (L.) Boiss. *J. Coast. Res.* **2013**, *29*, 1101–1110. [[CrossRef](#)]
10. Aizi, D.E.; Kaid Harche, M. Extraction and characterization of *Retama monosperma* fibers. *Afr. J. Biotechnol.* **2015**, *14*, 2644–2651. [[CrossRef](#)]



11. Harche, M. Contribution à l'étude sur l'alfa (*Stipa tenacissima* L.): Germination croissance des feuilles différenciation des fibres. Ph.D. Thesis, 3eme Cycle Univ. Sciences et Techniques, Lille, France, 1978.
12. Bledzki, A.K.; Gassan, J. Composites reinforced with cellulose based fibers. *Prog. Polym. Sci.* **1999**, *24*, 221–274. [[CrossRef](#)]
13. Sandy, M.; Bacon, L. Tensile testing of Raffia. *J. Mater. Sci. Lett.* **2001**, *20*, 529–530. [[CrossRef](#)]
14. Béakou, A.; Ntenga, R.; Lepetit, J.; Téba, J.A.A.; Ayina, L.O. Physico- chemical and microstructural characterization of Rhextophyllum. *Compos. Part A* **2008**, *39*, 67–74. [[CrossRef](#)]
15. Elenga, R.G.; Dirras, G.F.; Goma Maniongui, J.; Djema, P.; Biget, M.P. On the microstructure and physical properties of untreated raffia texilis fiber. *Compos. Part A* **2009**, *40*, 418–422. [[CrossRef](#)]
16. Komuraiah, A.; Shyam Kumar, N.; Durga Prasad, B. Chemical composition of natural fibers and its influence of their mechanical properties. *Mech. Compos. Mater.* **2014**, *50*, 359–376. [[CrossRef](#)]
17. Mohanty, A.K.; Misra, M.; Drzal, L.T.; Selke, S.E.; Harte, R.B.; Hinrichsen, G. Natural fibers, biopolymers, and biocomposites: An introduction. In *Natural Fibers, Biopolymers, Biocomposites*; Mohanty, A.K., Misra, M., Drzal, T., Eds.; CRC Press: New York, NY, USA, 2005; Chapter 1.
18. Djafari Petroudy, S.R. Physical and mechanical properties of natural fibers. In *Advanced High Strength Natural Fibre Composites in Construction*; Woodhead Publishing: Sawston, UK, 2017; pp. 59–83.
19. Ramaswamy, G.N.; Ruff, C.G.; Boyd, C.R. Effect of bacterial and chemical retting on kenaf fiber quality. *Text. Res. J.* **1994**, *64*, 305–308. [[CrossRef](#)]
20. Ramaswamy, G.N.; Craft, S. Uniformity and softness of kenaf fibers for textile products. *Text. Res. J.* **1995**, *65*, 765–770. [[CrossRef](#)]
21. Rowell, R.M.; Young, R.A.; Rowell, J.K. *Paper and Composites from Agro-Based Resources*; Lewis Publishers: New York, NY, USA, 1997.
22. Batra, S.K. Other long vegetable fibers. In *Handbook of Fiber Science and Technology, Fiber Chemistry*; Lewin, M., Pearce, E.M., Eds.; Marcel Dekker, Inc.: New York, NY, USA, 1998; Volume 4, pp. 505–571.
23. Reddy, N.; Yang, Y. New long natural cellulosic fibers from cornhusks: Structure and properties. *AATCC Rev.* **2005**, *5*, 24–27.
24. Deepa, B.; Eldho, A.; Bibin, M.C.; Bismarck, A.; Blaker, J.J.; Pothan, A.L.; Leao, A.L.; Souza, S.F.; Kottaisamy, M. Structure, morphology and thermal characteristics of banana nano fibers obtained by steam explosion. *Bioresour. Technol.* **2011**, *102*, 1988–1997. [[CrossRef](#)]
25. Thi Thu Loan, D. Investigation on Jute Fibers and Their Composites Based on Polypropylene and Epoxy Matrices. Ph.D. Thesis, Dresden University, Dresden, Germany, 2006.
26. Yang, H.; Yan, R.; Chen, H.; Ho Lee, D.; Zheng, C. Characteristics of hemicellulose, cellulose and lignin pyrolysis. *Fuel* **2007**, *86*, 1781–1788. [[CrossRef](#)]
27. Albano, C.; Gonzalez, J.; Ichazo, M.; Kaiser, D. Thermal stability of blends of polyolefins and sisal fiber. *Polym. Degrad. Stab.* **1999**, *66*, 179–190. [[CrossRef](#)]
28. Gram, H.E. *Durability of Natural Fibres in Concrete*; Swedish Research and Concrete Research Institute: Stockholm, Sweden, 1983.
29. Swamy, R.N. *Natural Fibre Reinforced Cement and Concrete. Concrete Technology and Design*; Blackie: London, UK, 1988; Volume 1.
30. Mathur, V.K. Composite materials from local resources. *Constr. Build. Mater.* **2005**, *20*, 470–477. [[CrossRef](#)]
31. Djoudi, A.; Khenfer, M.M.; Bali, A.; Kadri, E.H.; Debicki, G. Performance of date palm fibres reinforced plaster concrete. *Int. J. Phys. Sci.* **2012**, *7*, 2845–2853. [[CrossRef](#)]

**Publisher's Note:** MDPI stays neutral with regard to jurisdictional claims in published maps and institutional affiliations.



© 2020 by the authors. Licensee MDPI, Basel, Switzerland. This article is an open access article distributed under the terms and conditions of the Creative Commons Attribution (CC BY) license (<http://creativecommons.org/licenses/by/4.0/>).

Article

# Strain and Displacement Measurements in Reinforced Self-Compacting Concrete Beams with Openings Using Digital Image Correlation Technique <sup>†</sup>

Alexandra Coșa \*, Bogdan Hegheș, Camelia Negruțiu and Zoltan Kiss

Department of Civil Engineering, Faculty of Civil Engineering, Technical University of Cluj-Napoca, 25 Baritiu Str., 400027 Cluj-Napoca, Romania; Bogdan.Heghes@dst.utcluj.ro (B.H.);

Camelia.Negrutiu@dst.utcluj.ro (C.N.); Zoltan.Kiss@dst.utcluj.ro (Z.K.)

\* Correspondence: alexandracosa89@yahoo.com; Tel.: +40-741-979-933

<sup>†</sup> Presented at the 14th International Conference INTER-ENG 2020 Interdisciplinarity in Engineering, Mureș, Romania, 8–9 October 2020.

Published: 23 December 2020

**Abstract:** In structural engineering, strain and displacement are critical parameters, and measuring these parameters outside of the laboratory is a challenge for concrete researchers. Recent advances have enabled digital image correlation (DIC) to calculate the concrete surface displacements of chosen targets in a series of images recorded during an experiment. This paper presents a comparison between traditional and optical measurements to evaluate the efficiency of the DIC technique in recording the deformations of reinforced concrete beams. Tests were performed on two small-scale reinforced self-compacting concrete beams with small circular openings in 3-point bending.

**Keywords:** digital image correlation; self-compacting concrete; strain; displacement; beams with openings

## 1. Introduction

Digital image correlation (DIC) is an optical high-resolution data acquisition method and a viable alternative technique to mechanical laboratory measurements of reinforced concrete element deformations. In the field of structural engineering, this technique is used for recording vertical and horizontal displacements, evaluation of changes in strain and crack development. The DIC method has the potential to become an efficient solution for field monitoring [1,2].

DIC uses mathematical correlation analysis to examine a digital image captured during a mechanical test on a reinforced concrete element. The principle of the method is to compare an initial reference image with a series of subsequent images of the element after deformation. With computer software, the displacements of the points in the “deformed” images are calculated relative to the initial “non-deformed” reference image [3]. Different areas, instead of just points, of the element can also be addressed. As a result, an analysis of a full field deformation of the target area can be performed by comparing the initial and final positions of its subareas [4,5]. Therefore, one of the main advantages of using an image processing technique is the possibility to monitor the entire element and determine the exact places where the destruction begins [6].

The provision of a small circular opening through a concrete beam changes the simple beam behavior, producing discontinuity in the normal distribution of stresses, leading to early cracking around the opening and reduction of the ultimate strength. In these types of beams, in some cases the collapse is originated from shear stresses [7]. The ability to monitor strain development and crack propagation near the opening can provide important information to prevent a sudden collapse.

The main purpose of the study is to perform a comparison between traditional and optical measurements in order to evaluate the efficiency of the DIC technique in recording the vertical displacements, evaluation of changes in strain and crack development of reinforced concrete beams.

## 2. Materials and Methods

### 2.1. Materials

The materials used were: cement CEM I 52.5 R, according to SR EN 197-1 [8]; fly ash originated from Govora Power Station, Romania; limestone filler produced by Holcim Turda Grinding Plant, Romania; natural aggregates with 16 mm maximum size; polyether carboxylates high range water reducer (HRWR), Sika ViscoCrete 20 HE.

### 2.2. Mix Proportions

Two concrete compositions were designed. One concrete composition was designed with a high volume of fly ash (SCC-CZ). The concrete class of the SCC-CZ composition was C50/60. The other composition was designed with limestone filler addition (SCC-FC), developing a concrete class of C55/67. The mix proportions are detailed in Table 1.

**Table 1.** Mix proportions of self-consolidating concrete compositions.

Material	SCC-CZ <sup>1</sup>	SCC-FC <sup>2</sup>
Cement CEM I 52.5R (kg/m <sup>3</sup> )	350	410
Fly ash (kg/m <sup>3</sup> )	220	0
Limestone filler (kg/m <sup>3</sup> )	0	160
Water (l/m <sup>3</sup> )	220	150
HRWA (l/m <sup>3</sup> )	14	13
Total aggregates (kg/m <sup>3</sup> )	1550	1550
Sand 0/4 (kg/m <sup>3</sup> )	930	930
Gravel 4/8 (kg/m <sup>3</sup> )	310	310
Gravel 8/16 (kg/m <sup>3</sup> )	310	310
Cement replacement by mineral addition (%)	63	39

<sup>1</sup> Self-consolidating concrete with fly ash addition; <sup>2</sup> Self-consolidating concrete with limestone filler addition.

### 2.3. Test Specimens

The experimental program analyzed the flexural and shear behavior of two reinforced self-compacting concrete beams with small circular openings with fly ash addition and limestone filler addition, exposed to 100 freeze–thaw cycles. The beams were 1.20 m long with two 75 mm diameter circular openings. The beams had the same cross-sections and reinforcement detailing (Figure 1).

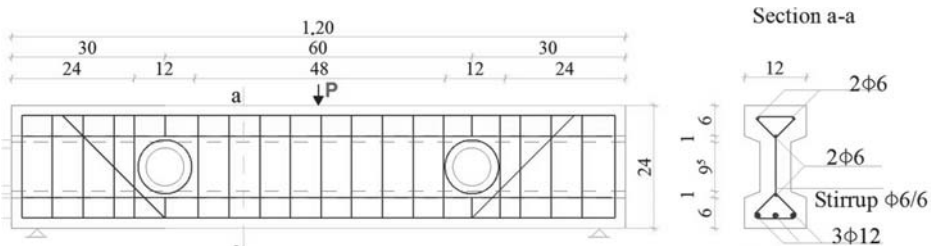


**Figure 1.** Reinforcement detailing of the beams.

## 2.4. Experimental Methods

The beams were cured for 90 days in laboratory conditions ( $RH = 65 \pm 5\%$  and  $T = 20 \pm 2\text{ }^\circ\text{C}$ ) and then exposed to 100 freeze–thaw cycles (17 days). At the end of the exposure time, the beams were subjected to a 3-point bending test. The beams were tested with a 300 ton hydraulic press and loaded with one concentrated load. The load was gradually applied in 5 kN incremental steps until failure. Cracks at each load increment were marked and mapped (Figure 2).



Figure 2. Marking and mapping cracks.

The concrete strain values at mid-span were measured using strain gauges with a 0.001 mm accuracy (Figure 3a). To measure the mid-span deflection, we used an LVDT (Linear Variable Differential Transformer) displacement transducer connected to a data acquisition system (Spider 8 basic device with 4.8 kHz carrier-frequency technology). The sensor type used was WA 300 mm.



Figure 3. Equipment for beams. (a) The set-up of the mechanical gauges and displacement transducer. (b) The equipment required to apply the optical method (DIC).

Half of each beam was analyzed with the DIC method. The equipment required to apply the optical method (DIC) consisted of a high-resolution digital camera (NIKON D3100, 14.2-megapixel DX format DSLR Nikon F-mount camera, AF-S DX NIKKOR 18-55mm f/3.5-5.6G VR lens, made in Thailand), computer software for image analysis (GOM Correlate 2016, developed by GOM Metrology, Braunschweig, Germany), white and black paint, and a light source (Figure 3b).

For the success of optical measurements, a good speckle pattern is essential (Figure 4). For this purpose, a thin layer of white paint (washable paint) was applied on half of the beam surface. When the white paint dried, we applied black matte spray paint (alkyd paint).



Figure 4. Speckle pattern on the surface of the analyzed area.

The camera was fixed on a tripod with its axis normal to the area of interest. External lighting was directed toward the region of interest to enhance the images. Before starting the test, a reference picture was taken (non-deformed image). While the specimen was subjected to the test, consecutive images were taken (deformed images) until the failure of the beam. The images were analyzed with GOM Correlate 2016 software.

### 3. Results and Discussion

#### 3.1. Load-Deflection Behavior

The moment-deflection curves of the fly ash beam (GR-3-CZ) and the limestone beam (GR-3-FC) are presented in Figure 5. Interpretation of results consisted of comparing the moment-deflection response of each beam according to the mechanical and optical method. In performing a comparison between the two methods used to record the displacement measurements, we noticed some differences. The mid-span deflection of the fly ash beam recorded with the DIC method was around 10% higher than the deflection recorded with the mechanical method. For the limestone beam, the increase was up to 25%. Joshi et al. (2018) performed a comparison between the load-deflection response of steel-fiber-reinforced prestressed concrete beams using DIC analysis and a conventional linear variable transducer. The authors concluded that the results from the DIC analysis showed a close agreement with the mechanical measurements [9].

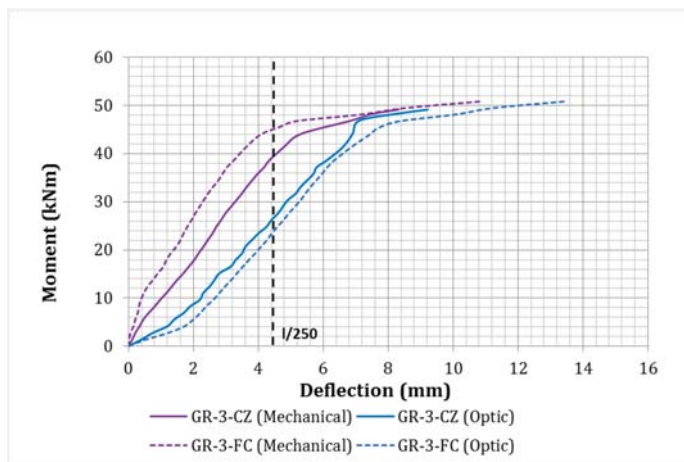


Figure 5. Moment-deflection curves according to mechanical and optical method.

A comparison was also performed in order to analyze the influence of using high-volume fly ash addition on the behavior of reinforced concrete beams with web openings exposed to freeze–thaw cycles. The fly ash beam (GR-3-CZ) exhibited a lower ductility and ultimate strength compared with the limestone beam (GR-3-FC) because, as other researchers concluded, the increase in the strength of concrete improves the general behavior of beams with small circular openings [10]. As well, other studies confirmed that dosages higher than 35% of fly ash decrease the compressive and mechanical strength of concrete [11,12].

The vertical displacements analyzed with GOM Correlate 2016 software are presented in Figures 6 and 7. The vertical displacement of Point 5 describes the mid-span deflection of the analyzed beams using the DIC method.

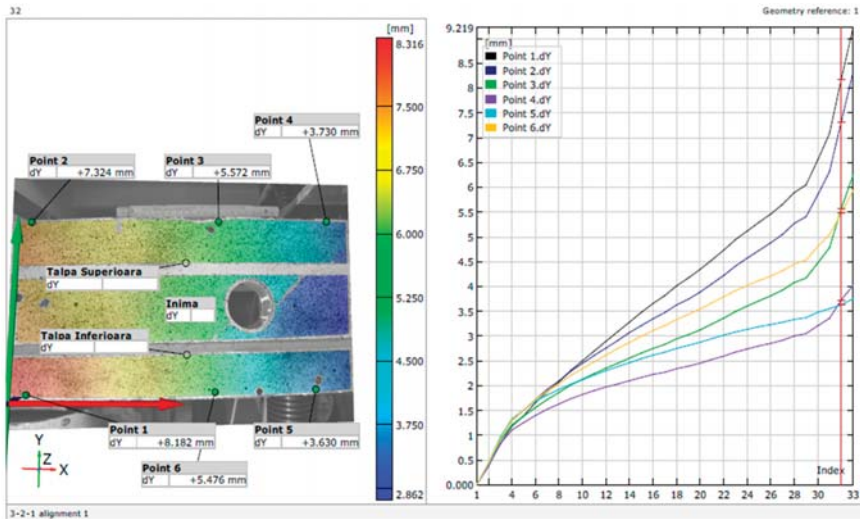


Figure 6. Vertical displacements of the fly ash beam (GR-3-CZ) analyzed with GOM Correlate.

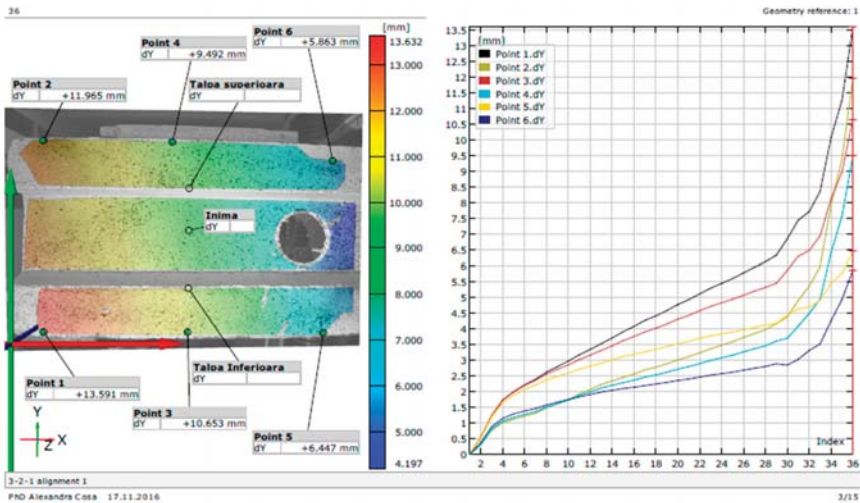


Figure 7. Vertical displacements of the limestone beam (GR-3-FC) analyzed with GOM Correlate.



### 3.2. Strain Distribution

To investigate the flexural behavior of SCC beams we analyzed the experimental strain distribution at mid-span section (Figures 8 and 9). For the fly ash beam (GR-3-CZ), the concrete strain at the top of the beam at failure was less than the crushing strain of concrete (3.5‰), the prescript value according to Eurocode 2 [13]. The limestone beam (GR-3-FC) recorded higher concrete strains at the top of the beam at the time of failure, exceeding the crushing strain of concrete. Strains in the longitudinal reinforcement were higher than the yielding strain of 2.615‰ (experimentally measured), indicating that longitudinal reinforcement yielded before the time of failure. Associating the ultimate strains in the longitudinal bars and the post-peak behavior shown in the load-deflection curves, it could be observed the ductile nature of the limestone beam. Similar results were obtained for beams containing pozzolanic fly ash, showing a less ductile behavior when compared to other beams with different mineral additions [14].

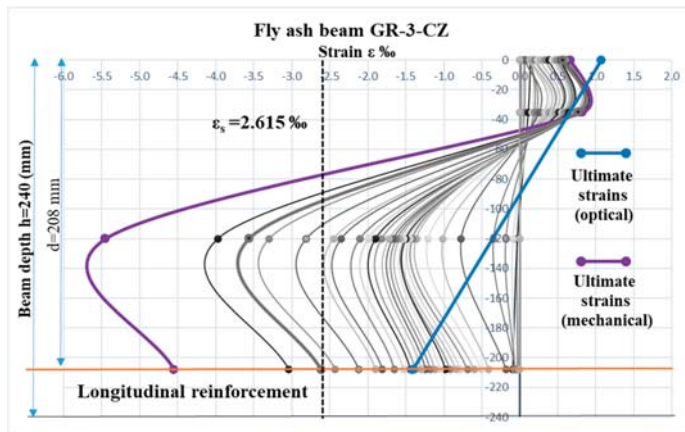


Figure 8. Experimental strains distribution at mid-span section according to mechanical and optical methods for fly ash beam (GR-3-CZ).

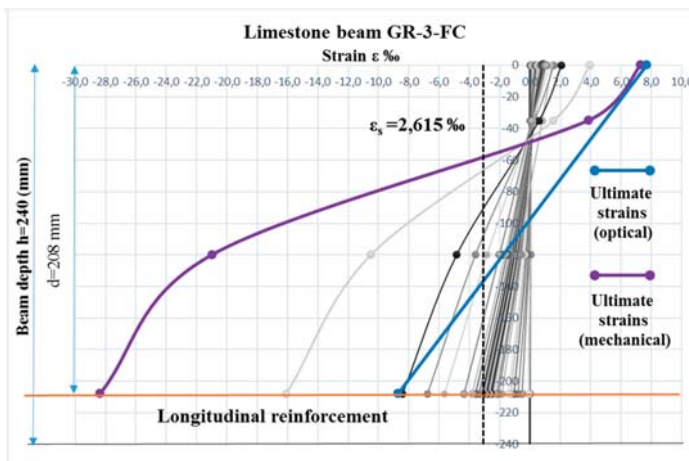


Figure 9. Experimental strains distribution at mid-span section according to mechanical and optical methods for limestone beam (GR-3-FC).

In the case of concrete strains at the top of the beam, the results obtained using the DIC technique were comparable with the conventional extensometer. The ultimate strains in the longitudinal reinforcement, measured with the DIC method, were around 70% lower, compared with the strains measured with strain gauges. The differences between the values obtained from the two measurement methods could be due to the imprecise location of the analyzed point at mid-span section. The 2D camera used to capture the images can also bring errors in the correlation, like distortion of the lens, as other researchers concluded [3,15]. On the other hand, Marcinczak et al. (2019) considered that the DIC method is a good alternative to strain gauges, allowing to determine the most stressed places of the element. Moreover, when using strain gauges, deformations of the element are difficult to clearly analyze because the strain gauge is in a specific, limited place and tends to break at the place of failure crack [6].

The strains measured with the DIC method and analyzed with GOM Correlate 2016 software are presented in Figures 10 and 11.

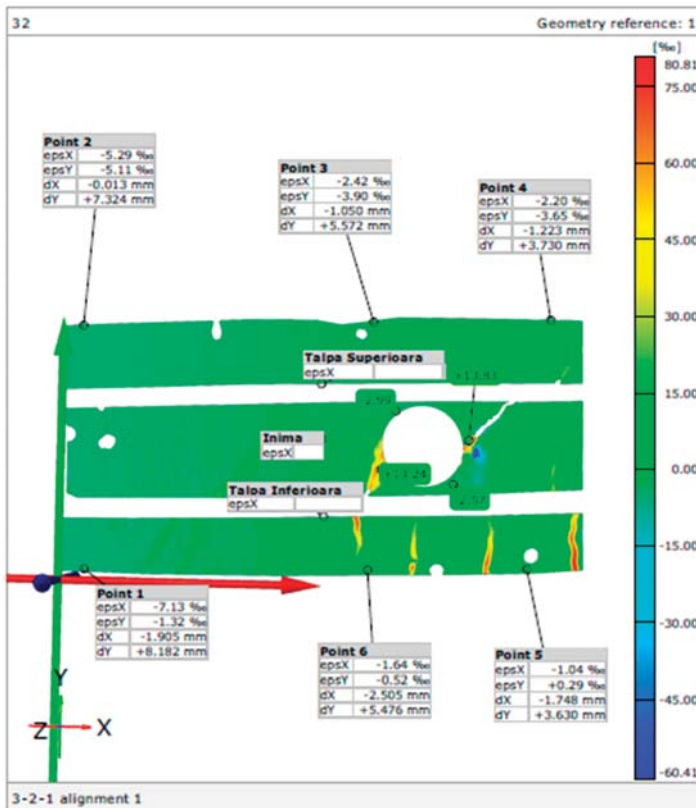


Figure 10. Experimental strains measured using the digital image correlation technique for fly ash beam (GR-3-CZ).



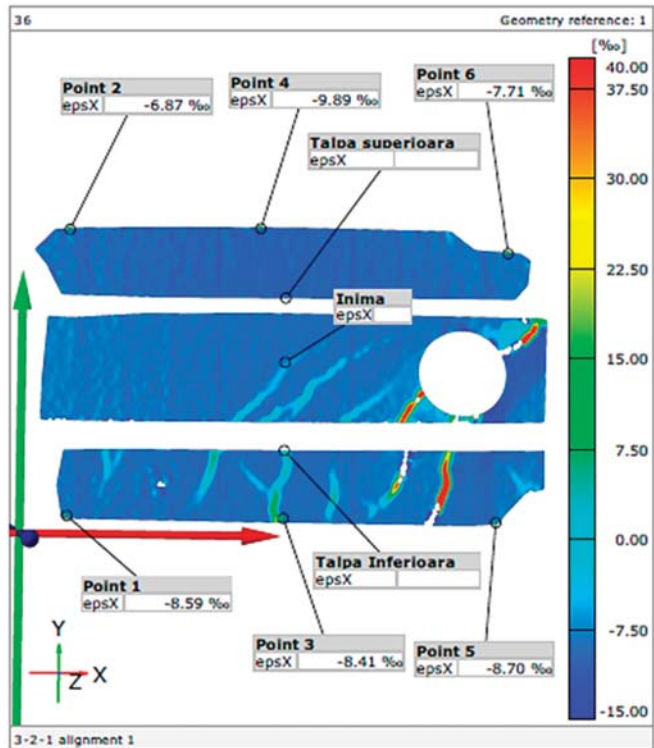


Figure 11. Experimental strains measured using the digital image correlation technique for limestone beam (GR-3-FC).

### 3.3. Cracking Pattern

To provide a comparison between the automated crack mapping obtained with the DIC method and the hand-drawn crack mapping, the longitudinal strain filed from the front face of the beam (left half) and the hand-drawn cracks at ultimate load (right half) are presented in Figures 12 and 13.

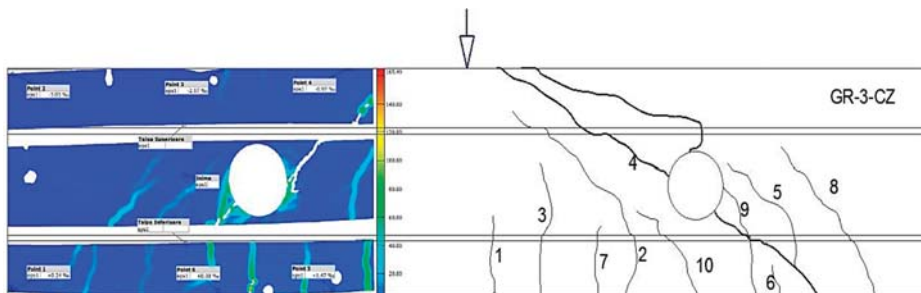
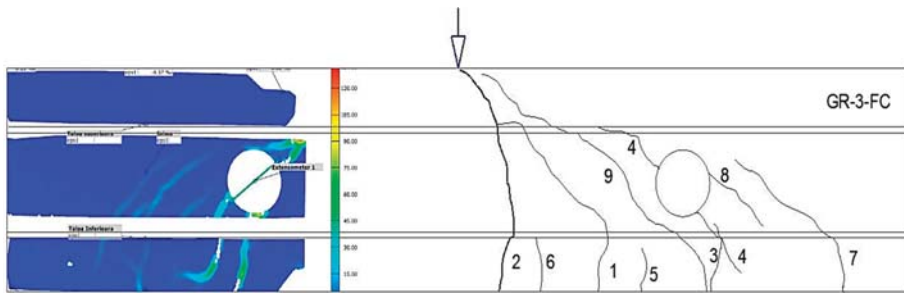


Figure 12. Cracking pattern at ultimate load for the fly ash beam (GR-3-CZ).



**Figure 13.** Cracking pattern at ultimate load for the limestone beam (GR-3-FC).

Both methods indicated that the first crack was a flexural crack and the fourth one was the first shear crack for both tested beams. The beams underwent beam type shear failure, having a ductile flexural behavior up to the ultimate load. As Tambusay et al. (2018) concluded, the longitudinal strain fields obtained from the DIC system are shown to compare well with hand-drawn crack maps [16].

#### 4. Conclusions

The current study presents a comparison between traditional and optical measurements to evaluate the efficiency of the DIC technique in recording the vertical displacements, evaluation of changes in strain and crack development of reinforced concrete beams. A comparison was also performed in order to analyze the influence of using high-volume fly ash addition on the behavior of reinforced concrete beams with web openings, exposed to freeze–thaw cycles.

Local materials were utilized to create a high-volume fly ash self-compacting concrete with a 63% cement replacement, applicable for the precast industry. For comparison, a similar self-compacting concrete was developed, but with the traditional limestone instead of fly ash.

Analyzing the general behavior of the tested beams, the fly ash beam exhibited a lower ductility and ultimate strength compared with the limestone beam because the increase in the strength of concrete improves the behavior of beams with small circular openings. Freezing and thawing dry cycles without de-icing salts did not majorly affect the self-compacted reinforced concrete beams.

Performing a comparison between the two methods used to record the displacement measurements, the mid-span deflection recorded with the DIC method was up to 25% higher than the deflection recorded with the traditional method.

In the case of concrete strains at the top of the beam, the results obtained using the DIC technique were comparable with the strain gauge measurements, but the ultimate strains in the longitudinal reinforcement, measured with the DIC method, were 70% lower.

The cause of the different values obtained from the two measurement methods could be due to the imprecise location of the analyzed point at mid-span section or the camera used to capture the images, which can bring errors in the correlation, like distortion of the lens.

The authors presented and verified a practical technique for utilizing digital image correlation to measure strain and displacement on a reinforced self-compacted concrete beam with circular openings. The experimental study gives useful information to create a non-contact measurement system that can provide information for field monitoring, but further studies are required to improve the correlation between the traditional and digital measurements.

**Author Contributions:** Conceptualization, A.C. and B.H.; methodology, A.C. and B.H.; software, B.H.; validation, A.C., B.H., C.N. and Z.K.; formal analysis, B.H.; investigation, A.C. and B.H.; resources, A.C. and B.H.; data curation, A.C. and B.H.; writing—original draft preparation, A.C.; writing—review and editing, A.C., C.N. and Z.K.; visualization, A.C. and C.N.; supervision, Z.K. All authors have read and agreed to the published version of the manuscript.

**Funding:** This research received no external funding.

**Acknowledgments:** The authors gratefully appreciate the assistance and the support from the Department of Central Laboratory of the Civil Engineering Faculty, where the experimental program was performed. The paper was developed in the first author's Ph.D. program in Civil Engineering, Eng. Coşa Alexandra, supervised by Eng. Kiss Zoltan.

**Conflicts of Interest:** The authors declare no conflict of interest.

## References

1. Dutton, M. Digital Image Correlation for Evaluating Structural Engineering Materials. Master's Thesis, Queens University, Kingston, ON, Canada, 2012; p. 122.
2. McCormick, N.; Lord, J. Digital Image Correlation. *Mater. Today* **2010**, *13*, 52–54. [[CrossRef](#)]
3. Cintron, R.; Saouma, V. Strain Measurements with Digital Image Correlation System Vic-2D. *System* **2008**, *106*, 1–22.
4. McCormick, N.; Lord, J. Digital image correlation for structural measurements. *Proc. Inst. Civ. Eng. Civ. Eng.* **2012**, *165*, 185–190. [[CrossRef](#)]
5. Fayyad, T.; Lees, J. Application of Digital Image Correlation to Reinforced Concrete Fracture. *Procedia Mater. Sci.* **2014**, *3*, 1585–1590. [[CrossRef](#)]
6. Marcinczak, D.; Trapko, T. DIC (Digital Image Correlation) method in the research of RC beams strengthened with PBO-FRCM materials. *E3S Web Conf.* **2019**, *97*, 03008. [[CrossRef](#)]
7. Mansur, M.A.; Tan, K.H. *Concrete Beams with Openings: Analysis and Design*; CRC Press: Boca Raton, FL, USA, 1999.
8. *BS EN 197-1:2011, Cement, Part 1: Composition, Specifications and Conformity Criteria for Common Cements*; European Committee for Standardization, British Standard Institution: London, UK, 2011.
9. Joshi, S.S.; Thammishetti, N.; Prakash, S.S.; Jain, S. Cracking and Ductility Analysis of Steel Fiber Reinforced Prestressed Concrete Beams in Flexure. *ACI Struct. J.* **2018**, *115*, 1575–1588. [[CrossRef](#)]
10. Amiri, J.V.; Hosseinalibygie, M. Effect of Small Circular Opening on the Shear and Flexural Behavior and Ultimate Strength of Reinforced Concrete Beams using Normal and High Strength Concrete. In Proceedings of the 13th World Conference on Earthquake Engineering, Vancouver, BC, Canada, 1–6 August 2004.
11. Bărbuță, M.; Bucur, R.; Serbănoiu, A.; Scuturasu, S.; Burlacu, A. Combined effect of fly ash and fibers on properties of cement concrete. *Procedia Eng.* **2017**, *181*, 280–284. [[CrossRef](#)]
12. Rujan, M.; Bărbuță, M. Influence of Fly Ash Addition on the Compressive Strength of Concrete. In Proceedings of the International Scientific Conference (CIBV 2014), Braşov, Romania, 7–8 November 2014.
13. *BS EN 1992-1:2004 Eurocode 2: Design of Concrete Structures—Part 1-1: General Rules and Rules for Buildings*; European Committee for Standardization, British Standard Institution: London, UK, 2004.
14. Aulia, T.; Afifuddin, M.; Opirina, L. Bending Capacity Analysis of High-Strength reinforced concrete Beams Using geopolymer Fly Ash and environmentally Friendly Slag as Fine Aggregate Substitution. In Proceedings of the 7th Civil Engineering Conference in the Asian Region (CECAR7), Waikiki, HI, USA, 30 August–2 September 2016.
15. Butean, C.; Heghes, B. Flexure behavior of a hybrid reinforced concrete beam. Strain correlation between mechanical gauges and optical measurement. *Procedia Manuf.* **2018**, *22*, 233–240. [[CrossRef](#)]
16. Tambusay, A.; Suryanto, B.; Suprobo, P. Visualization of Shear Cracks in a Reinforced Concrete Beam using the Digital Image Correlation. *Int. J. Adv. Sci. Eng. Inform. Technol.* **2018**, *8*, 573. [[CrossRef](#)]

**Publisher's Note:** MDPI stays neutral with regard to jurisdictional claims in published maps and institutional affiliations.



© 2020 by the authors. Licensee MDPI, Basel, Switzerland. This article is an open access article distributed under the terms and conditions of the Creative Commons Attribution (CC BY) license (<http://creativecommons.org/licenses/by/4.0/>).

Article

# Parametric Studies Regarding the Development of Alkali-Activated Fly Ash-Based Geopolymer Concrete Using Romanian Local Raw Materials <sup>†</sup>

Adrian-Victor Lăzărescu <sup>1,\*</sup>, Henriette Szilagyı <sup>1</sup>, Cornelia Baeră <sup>2</sup> and Andreea Hegyi <sup>1</sup>

<sup>1</sup> NIRD URBAN-INCERC Cluj-Napoca Branch, 117 Calea Florești, 400524 Cluj-Napoca, Romania; henriette.szilagyı@incerc-cluj.ro (H.S.); andreea.hegyi@incerc-cluj.ro (A.H.)

<sup>2</sup> NIRD URBAN-INCERC Timișoara Branch, 2 Traian Lalescu Street, 300223 Timișoara, Romania; baera.cornelia@gmail.com

\* Correspondence: adrian.lazarescu@incerc-cluj.ro

<sup>†</sup> Presented at the 14th International Conference INTER-ENG 2020 Interdisciplinarity in Engineering, Mureș, Romania, 8–9 October 2020.

Published: 11 December 2020

**Abstract:** Current research and development policies in the field of building materials, in the context of sustainable development, have the main objectives of increasing the safety and performance of the built environment at the same time as reducing pollution and its negative impact. Today, the idea that the sustainable city of the future should meet human needs and maintain a higher quality of life is worldwide unanimously accepted. The aim of this paper is to present results regarding the production of alkali-activated fly ash-based geopolymer concrete, a new, alternative material, produced using local available raw materials from Romania.

**Keywords:** fly ash; alkali-activation; geopolymer materials; sustainable development; advanced materials

## 1. Introduction

Both circular economy and sustainable development are concepts that focus on resource efficiency, which implies a complex waste management process with a high degree of recycling and recovery. Designing resilient, sustainable buildings, by using recycled materials that can replace some or all of the cement, leads to the development of a sustainable, low-carbon economy. Production of large volumes of cement/concrete is directly associated with environmental problems—cement production being responsible for about 5–8% of the total carbon dioxide emissions [1,2], therefore, awareness towards the possible production of alternative materials is rising. Demand for concrete, hence for cement, is constantly growing, especially in highly developed countries [3,4], which means that alternative binders are urgently needed to meet the needs of millions of people, without compromising the CO<sub>2</sub> levels of the atmosphere.

With the best available technologies for the production of Portland cement, industry estimates that currently, CO<sub>2</sub> emissions resulting from its production could decrease by a maximum of 17% (even through the use of alternative fuels, optimizing the amount of cement in concrete, recycling, etc.) [5]. As the population needs for energy continue to increase, it will lead, at global level, to an increase in the production of fly ash as by-product from the energy industry [4,6].

When partially used in the production of concrete, together with Portland cement, fly ash reacts with calcium hydroxide during the moisturizing process, in the presence of water. The use of materials derived from industrial by-products on a larger scale in the manufacture of concrete, has increased with the development and the increasing demand of producing special concrete (i.e., self-compacting concrete, high-strength concrete, high performance concrete, self-healing concrete) [7–10].

Studies shown that the large amount of fly ash resulting from the energy industry in Romania can create new opportunities to use this waste as a substitute for Portland cement in the production of new materials [11]. The alkaline activation of the fly ash as raw material represents a procedure able to generate its solidification when mixing it with a certain type of alkaline activator and creating a new binding material. When incorporating aggregates, new building materials could be obtained, as an alternative to traditional concrete and cement-based composites [12–14].

For a material used in the construction industry, mechanical behavior is a basic property, which makes it optimal for a specific application. Since geopolymer materials are a novelty in this area, and most of the studies are presented on a case-by-case situation, compressive strength is an important factor. The mechanical behavior of geopolymers varies depending on the used materials and the production methods they are subjected to [15]. In order to obtain a geopolymer material with a good compressive strength, the type and the molar ratios of the oxides in the source material, the pH of the alkaline solution, and the solubility of the source material in alkaline activator should be particularly taken into account [3,6,11,16].

It has been shown that the compressive strength of the alkali-activated geopolymer materials increases, in general, with the increase in the concentration of the specific alkaline activators [17–19]. A higher concentration of the NaOH solution may produce stronger Si-O-Si bonds and improve the dissolution of source materials in the presence of the activators [17,19,20]. The optimal alkaline concentration also varies by a large number of conditions and factors that must be taken into account in the mix-design.

The properties of alkali-activated geopolymer materials depend mainly on the important factors that could affect the development of this type of material and include: The characteristics of constituent materials, alkaline activators, heat treatment regimes, etc. It is obvious that, due to the multitude of factors that could influence the geopolymerization reaction, the specificity and conditions met for each proposed mixture generate case-by-case characteristics. However, in most cases, studies have shown that the properties of geopolymer materials were similar or even better than those of ordinary Portland cement concrete, when similar tests underwent [4,11,21,22].

Based on preliminary results obtained on alkali-activated geopolymer paste by using Romanian local raw materials [11,23], the aim of this paper is to present results regarding the production of alkali-activated fly ash-based geopolymer concrete, a new, alternative material, produced by using local available raw materials from Romania and to study the parameters that affect the mechanical properties of the material.

## 2. Materials and Methods

Worldwide, research on alkali-activated geopolymer materials exists, but their production differs greatly, due to factors that mainly influence this type of material. Alkali-activated geopolymer concrete mixtures were developed based on studying the literature and starting from a rigorous selection of source components that will be used to produce this type of material. By choosing relevant research in the literature, the preliminary mixtures were produced based on the variation of the parameters influencing them, from the point of view of the specific ratios, as well as their chemical composition. The evolution of the geopolymer concrete mix design was developed based on the observations collected in the experimental research and initial practical assessments, the fresh state appearance and the performance of the materials at a certain time. By modifying the variables and ratios of materials used in the production of geopolymer paste (alkaline liquid to fly ash ratio, molar concentration of the NaOH solution,  $\text{Na}_2\text{SiO}_3/\text{NaOH}$  ratio), several necessary data were obtained on the parameters that influence this type of material [11,23].

### 2.1. Fly Ash as Raw Material

Fly ash (FA) is the by-product obtained by electrostatic or mechanical precipitation of the pulverized particles resulting from the coal-fired combustion gases of the furnaces in power plants. As a fine

powder, consisting mainly of spherical shaped glass particles [24], some certain characteristics show significant differences when coming to their chemical composition. The high variation of the chemical composition, leading to different performance when it is used as binding material for producing alkali-activated fly ash-based materials and represents an essential aspect for the general development of the concept [11,23,24].

In order to study the transition from alkali-activated geopolymer paste to geopolymer concrete, low-calcium fly ash from a Romanian power plant was used in this study, focused on the development and the comparative analyses of the mechanical properties of the material [11]. Its chemical properties are presented in Table 1.

**Table 1.** Chemical composition of fly ash used in the production of alkali-activated geopolymer materials, measured by X-ray fluorescence [wt.%].

Oxide	SiO <sub>2</sub>	Al <sub>2</sub> O <sub>3</sub>	Fe <sub>2</sub> O <sub>3</sub>	CaO	MgO	SO <sub>3</sub>	Na <sub>2</sub> O	P <sub>2</sub> O <sub>5</sub>	TiO <sub>2</sub>	Mn <sub>2</sub> O <sub>3</sub>	L.O.I
FA	54.32	22.04	9.02	5.85	2.48	0.20	0.54	0.16	0.86	0.06	3.05

It can be seen from Table 1 that the fly used in the current study has low L.O.I. values, which means that it has low carbon content. As well, the Si/Al molar ratio of the fly ash batch is approximately 2, which makes it suitable for the production of alkali-activated geopolymer materials, due to the Si-O-Al-Si bonds that could be developed further in the mixture [25].

## 2.2. Alkaline Activator

The alkaline activator used for this experimental study was a combination of sodium hydroxide solution (NaOH) and sodium silicate solution (Na<sub>2</sub>SiO<sub>3</sub>). The sodium silicate solution was purchased from the local market with the following chemical composition: SiO<sub>2</sub> = 30%, Na<sub>2</sub>O = 14% and H<sub>2</sub>O = 56%. Two types of sodium hydroxide solutions were prepared by dissolving NaOH flakes (98% purity–SH1) and NaOH pearls (99% purity–SH2) into water until the desired concentration of the solution was achieved (8 M and 10 M).

## 2.3. Aggregates

Natural aggregates, granular class 0/4 mm (S) and 4/8 mm (CA), (sand and coarse aggregate) were used for the production of the alkali-activated geopolymer concrete.

## 2.4. Preliminary Design of Alkali-Activated Fly Ash-Based Geopolymer Concrete

Geopolymer concrete mixtures were developed based on studying the literature and starting from a rigorous selection of source materials that will be used to produce this type of material. The preliminary mixtures were produced based on the variation of the parameters influencing them, from the point of view of the specific ratios, as well as their chemical composition. The evolution of the geopolymer concrete mix design (Table 2) was developed based on the observations collected in the experimental research and initial practical assessments, the fresh state appearance and the performance of the materials at a certain time [11]. The raw materials (fly ash and aggregates) were conditioned at (20 ± 2) °C, until constant mass was reached. The alkaline activator (Na<sub>2</sub>SiO<sub>3</sub> and NaOH solutions) was prepared 24 h prior mixing. The mixing technology for the production of the AAGC samples included the following sequences (Figure 1): The sand (0/4 mm) and the coarse aggregates (4/8 mm) were mixed homogeneously for 30 s; the established amount of fly ash was then added and the raw materials (fly ash + aggregates) were mixed together for another 30 s; the alkaline activator was added during 90 s over the homogeneous mixture; after adding the total alkaline activator quantity, the mixing was continued at low speed for 3 min. During the entire mixing process, the workability of the mixture has been observed. The samples were then placed in 40 mm × 40 mm × 160 mm molds and heat cured at 70 °C for 24 h. A glass film was placed on top of every mold in order to prevent excessive water



release from the mixtures; after demolding, the specimens were stored in the climatic chamber at the temperature  $T (20 \pm 1) ^\circ\text{C}$  and relative humidity  $\text{RH} (60 \pm 5)\%$ .

**Table 2.** Alkali-activated geopolymer concrete mix-design (wt.%).

AA/FA	Fly Ash	Na <sub>2</sub> SiO <sub>3</sub> /NaOH	Na <sub>2</sub> SiO <sub>3</sub>	NaOH	NaOH Molarity	S 0/4 mm	CA 4/8 mm
1.0	1.0	1.0	0.25	0.25	8 M	0.5	0.5
		1.5	0.30	0.20			
		2.0	0.33	0.17			
		2.5	0.36	0.14			
1.0	1.0	1.0	0.25	0.25	10 M	0.5	0.5
		1.5	0.30	0.20			
		2.0	0.33	0.17			
		2.5	0.36	0.14			



**Figure 1.** Alkali-activated fly ash-based geopolymer concrete: (a) Fly ash; (b) Coarse aggregate—granular class 4/8 mm (CA); (c) Sand—granular class 0/4 mm (S); (d) Mixing of the aggregates; (e) Mixing of the raw materials (FA + aggregates); (f) Final mixing sequence; (g) Casting of the mixtures; (h) Geopolymer concrete samples after demolding.

### 2.5. Testing Methods

All the tests performed on the alkali-activated geopolymer samples were conducted at the age of 7 days. The flexural and compressive strength testing of the alkali-activated geopolymer concrete samples were performed using three prismatic specimens for each type of alkali-activated fly ash-based geopolymer mixtures; the mean value of the results was considered relevant for the data interpretation. The testing method was in accordance to EN 196-1 [26]. Early age testing at 7 days was considered

relevant for the comparative evaluation, as previously experiments proved that generally, the fly ash-based geopolymer binder reached most of its compressive potential by this age [11,23,24].

### 3. Results and Discussions

In order to study the physico-mechanical parameters, the grouping of the alkali-activated fly ash-based geopolymer concrete mixtures was made according to the type of raw materials used and is symbolized as follows: AAGC FA SHx yM SS, where AAGC–Alkali-Activated Geopolymer Concrete; FA–fly ash-based; SHx–type of sodium hydroxide solution; yM–molarity of the sodium hydroxide solution; SS–sodium silicate solution.

#### 3.1. AAGC Fresh-State Properties

The general observation was that when the  $\text{Na}_2\text{SiO}_3/\text{NaOH}$  solution ratio increased, the workability of the mixtures also increased. Instead, the functionality of the mixtures with NaOH solution 10 M was considerably lower than those using 8 M NaOH solution. The high content of NaOH solids in the solution directly affects the workability of the mixes. This does not mean that NaOH is the only parameter affecting the functionality of the fresh fly ash-based geopolymer material; however, it is of great importance. Another important observation during the preparation of the samples concerned their behavior during and after mixing. For the apparently dry mixtures, the ones with high  $\text{Na}_2\text{SiO}_3/\text{NaOH}$  ratios, at the beginning of the mixing, the material was not homogenous and the sample seemed to be an almost completely dry mixture. However, a significant aspect of these dry mixtures was that, by vibrations induced by a jolting table for compacting the samples, the mixtures formed a continuous and cohesive mixture.

#### 3.2. AAGC Hardened-State Apparent Density

The apparent density of the derived AAGC mixtures was carried out in accordance with the standard EN 12390-7 [27] at the age of 7 days. The results obtained are presented in Figure 2.

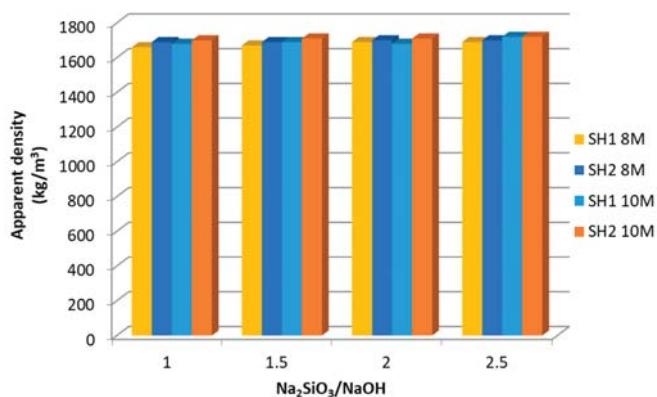


Figure 2. AAGC hardened-state apparent density.

Selection of the appropriate binder to aggregate ratio helps to ensure the proper workability and the performance characteristics of the hardened geopolymer material. As presented in Figure 2, the average values of geopolymer concrete apparent density are in the range between  $1690 \text{ kg/m}^3$  and  $1720 \text{ kg/m}^3$  for all the  $\text{Na}_2\text{SiO}_3/\text{NaOH}$  ratios, for both NaOH solution concentrations and for both NaOH types.



### 3.3. AAGC Mechanical Properties

The flexural strength, respectively the compressive strength, of the derived AAGC mixtures was carried out in accordance with the standard EN 196-1 [26]. The test age of the specimens was 7 days, as it has been shown that, due to the heat treatment to which the mixtures are subjected, they reach mechanical properties at young ages [11,23,24]. The results obtained are presented in Table 3.

**Table 3.** Alkali-activated geopolymer concrete mix-design (wt.%).

Mixture	Na <sub>2</sub> SiO <sub>3</sub> /NaOH	Flexural Strength (MPa)	Compressive Strength (MPa)
AAGC FA SH1 8 M SS	1.0	2.9	15.8
	1.5	3.0	17.7
	2.0	3.7	18.9
	2.5	4.2	20.3
AAGC FA SH1 10 M SS	1.0	3.0	16.9
	1.5	3.2	18.9
	2.0	3.9	21.8
	2.5	4.4	24.3
AAGC FA SH2 8 M SS	1.0	2.8	16.2
	1.5	3.1	17.9
	2.0	3.8	19.2
	2.5	4.1	20.5
AAGC FA SH2 10 M SS	1.0	3.1	17.6
	1.5	3.8	19.6
	2.0	3.8	22.4
	2.5	4.2	24.7

### 3.4. Influence of the Alkaline Activator on the Mechanical Properties

The alkaline activator plays a vital role in initiating the geopolymerisation process. Generally, a strong alkaline environment is required to increase the surface hydrolysis of the aluminosilicate particles present in the raw material, while the concentration of the chemical activator has a pronounced effect on the mechanical properties of geopolymers [28]. Results regarding the influence of the alkaline activator on the mechanical properties of the geopolymer concrete, in terms of NaOH solution type and concentration, but also in terms of Na<sub>2</sub>SiO<sub>3</sub>/NaOH ratio, are presented in Figure 3.

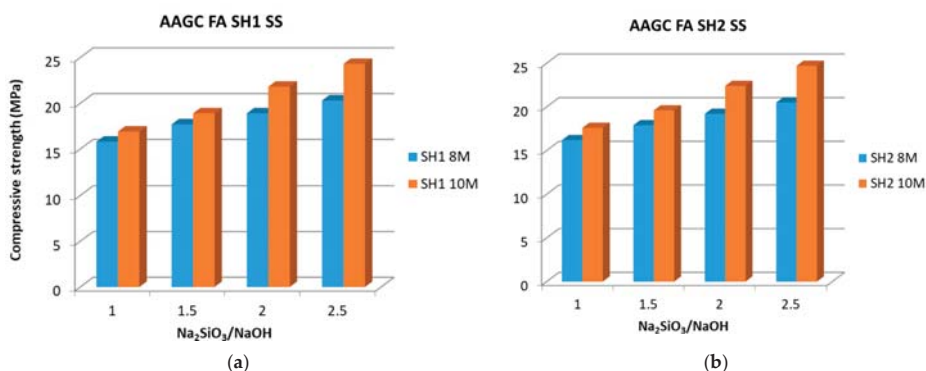


**Figure 3.** Influence of the alkaline activator on the compressive strength of the alkali-activated geopolymer concrete: (a) AAGC FA SH1 SS mixtures; (b) AAGC FA SH2 SS mixtures.

From the results obtained and presented in Table 3 and Figure 3, it can be seen that the compressive strength of the alkali-activated geopolymer concrete increased as the concentration of the NaOH solution increased, from 8 M to 10 M. In the case of AAGC FA SH1 SS mixtures, the increase in the

compressive strength of the samples, as the molar concentration of the NaOH solution increased was between 7% (for mixtures with  $\text{Na}_2\text{SiO}_3/\text{NaOH}$  ratio of 1.0 and 1.5) and 20% (for mixtures with  $\text{Na}_2\text{SiO}_3/\text{NaOH}$  ratio of 2.5). For AAGC FA SH2 SS mixtures, the increase in the compressive strength was between 9% (for mixtures with  $\text{Na}_2\text{SiO}_3/\text{NaOH}$  ratio of 1.0 and 1.5) and 21% (for mixtures with  $\text{Na}_2\text{SiO}_3/\text{NaOH}$  ratio of 2.5).

Results also show that the type of sodium hydroxide (NaOH) did not have a major influence on the final compressive strength of the alkali-activated geopolymer concrete mixtures. To the extent that their purity is comparable, the results are similar, with less than 1.5% for all the  $\text{Na}_2\text{SiO}_3/\text{NaOH}$  ratios, and they fall under the measurement uncertainty. One of the reasons users could choose a lower purity of sodium hydroxide might be the economic ones, with a lower purity sodium hydroxide being cheaper than a higher purity one.

As an influencing parameter of the mechanical properties of the alkali-activated geopolymer materials, the  $\text{Na}_2\text{SiO}_3/\text{NaOH}$  ratio, the results show that, as the ratio increases, the compressive strength of the AAGC mixtures increased. This is corroborated with the fact that, although the workability of the mixtures was lower, their mechanical properties increased. The result regarding the evaluation of the influence that this parameter has on the mechanical properties of the AAGC mixtures is presented in Figure 4.

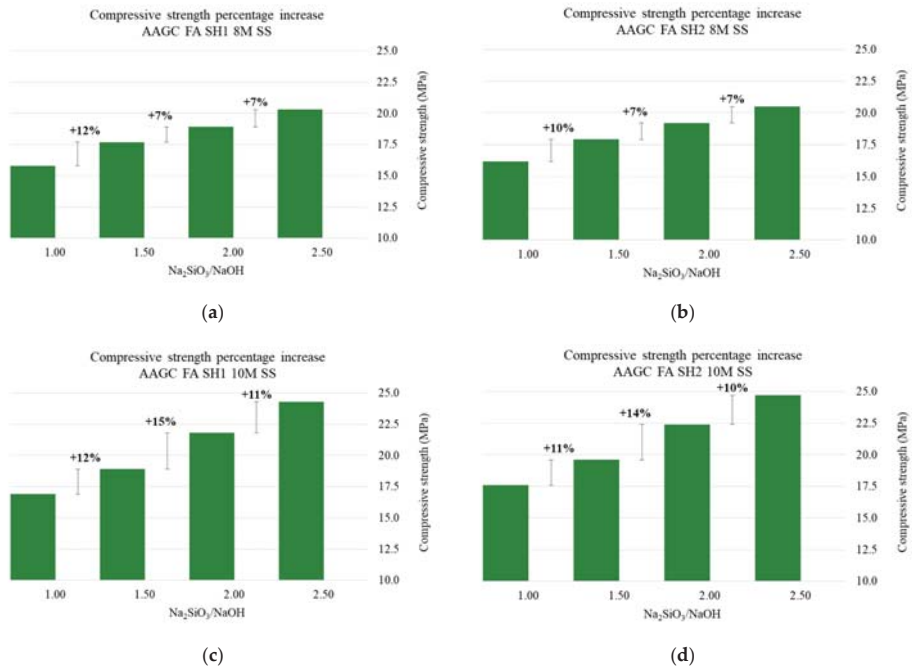


**Figure 4.**  $\text{Na}_2\text{SiO}_3/\text{NaOH}$  ratio influence on the compressive strength of the alkali-activated geopolymer concrete: (a) AAGC FA SH1 8 M SS mixtures; (b) AAGC FA SH2 8 M SS mixtures; (c) AAGC FA SH1 10 M SS mixtures; (d) AAGC FA SH2 10 M SS mixtures.

For all AAGC analyzed mixtures it can be seen that, for a  $\text{Na}_2\text{SiO}_3/\text{NaOH}$  ratio of 2.5, the highest compressive strength values are obtained with a percentage increase of 26–28% for AAGC FA 8 M SS mixtures and 40–44% for AAGC FA 10 M SS mixtures. The increase of the compressive strength of the samples can also be observed from the point of view of molar concentration of the NaOH solution. Results show that the increase in the compressive strength behavior is identical for a similar molar

concentration of the NaOH solution. This remark is corroborated with previous statements that have shown that, since purity of the NaOH used to produce the solution is comparable, not only the increase in the compressive strength is similar, but also the behavior in the increase of this parameter is similar.

#### 4. Conclusions

The aim of the current experimental research was to analyze the development of alkali-activated geopolymer materials produced by using raw materials from Romania and to study the parameters influencing the mechanical properties of the material, namely, the compressive strength. By using the same fly ash as raw material, by keeping the alkaline activator to fly ash mixing ratio constant and varying the  $\text{Na}_2\text{SiO}_3$  to NaOH solution ratio and also the NaOH solution concentration, the effect of the two main parameters on the compressive strength of the alkali-activated fly ash-based geopolymer binder could be studied.

The results obtained regarding the influence of the sodium silicate solution to sodium hydroxide solution ratio ( $\text{Na}_2\text{SiO}_3/\text{NaOH}$ ) highlight the importance of this parameter regarding the final results of the compressive strength of the alkali-activated fly ash-based geopolymer concrete. The evolution of the compressive strength values for the analyzed mixtures, at the age of 7 days, is different and, as this ratio increased, the values of the mechanical properties of the material also increased. For all AAGC mixtures that were analyzed, it can be seen that, for a  $\text{Na}_2\text{SiO}_3/\text{NaOH}$  ratio of 2.5, the highest values for the compressive strength were obtained.

Presented results also show that for the development of alkali-activated fly ash-based geopolymer materials, the influence of the sodium hydroxide solution concentration is a very important parameter, not only in the geopolymerization process, but also in the mechanical properties of the material. The solubility of fly ash increased as the concentration of the NaOH solution increased, therefore generating a denser material, with higher compressive strength results of the samples.

The workability of the mixtures was also assessed, considering the variation of the two studied parameters that influence the AAGC samples. Thus, it can be seen a clear interdependence between the variation of the workability and compressive strength of the mixtures. As the  $\text{Na}_2\text{SiO}_3/\text{NaOH}$  solution ratio increased, the workability of the mixtures also increased. Instead, the functionality of the mixtures with NaOH solution 10 M was considerably lower than those of 8 M NaOH solution, which, in the case of the compressive strength values, can be considered inversely proportional (higher ratio–lower workability–higher compressive strength).

As geopolymer concrete materials start to become more desirable in comparison to traditional OPC materials, both due to economic and ecological drivers and their demonstrated increased mechanical performances, the initial and long-term properties of these materials must be well understood, so they could be properly designed in order to obtain the effective mechanical properties. Results presented in the current paper emphasize that the specific evaluated parameters which could influence the compressive strength of the geopolymer materials, have an important effect on the behavior of the material.

Further studies will be performed using different types of raw materials and alkaline activators, in order to confirm the present conclusion. Furthermore, research regarding the viability of the material, through the optimization of the mixtures, will be carried out, thus opening up new opportunities for the development of this type of material in the future.

**Author Contributions:** Conceptualization, A.-V.L., H.S., C.B. and A.H.; methodology, A.-V.L. and H.S.; validation, A.-V.L., H.S. and A.H.; formal analysis, H.S. and C.B.; investigation, A.-V.L.; data curation, A.-V.L.; writing—original draft preparation, A.-V.L.; writing—review and editing, A.-V.L., H.S., C.B. and A.H.; visualization, H.S. and C.B.; supervision, H.S. All authors have read and agreed to the published version of the manuscript.

**Funding:** This research received no external funding.

**Conflicts of Interest:** The authors declare no conflict of interest.

## References

1. Aitcin, P.-C. Cements of yesterday and today; Concrete of tomorrow. *Cem. Concr. Res.* **2000**, *30*, 1349–1359. [[CrossRef](#)]
2. Malhotra, V.M. Making Concrete “Greener” with Fly Ash. *ACI Concr. Int.* **1999**, *21*, 61–66.
3. Malhotra, V.M. Introduction: Sustainable Structures in the 21st Century. *ACI Concr. Int.* **2001**, *23*, 57–63.
4. Ahmari, S.R.; Toufigh, X.; Zhang, L. Production of Geopolymer Binder from Blended Waste Concrete Powder and Fly Ash. *Constr. Build. Mater.* **2012**, *35*, 718–729. [[CrossRef](#)]
5. Damtoft, J.S.; Lukasik, J.; Herfort, D.; Sorrentino, D.; Gartner, E. Sustainable development and climate change initiatives. *Cem. Concr. Res.* **2008**, *38*, 115–127. [[CrossRef](#)]
6. Criado, M.; Fernandez-Jimenez, A.; Palomo, A. Alkali-activation of fly ash: Part III: Effect of curing conditions on reaction and its graphical description. *Fuel* **2010**, *89*, 3185–3192. [[CrossRef](#)]
7. Baeră, C.; Snoeck, D.; Szilagyi, H.; Mircea, C.; De Belie, N. Dynamic loading performance of fibre engineered cementitious materials with self-healing capacity (SH-FECM). *Int. Multidiscip. Sci. Geoconf. SGEM* **2016**, *2*, 91–98.
8. Szilagyi, H. *Special Concrete–Self-Compacting Concrete [In Romanian]*; Napoca Star: Cluj-Napoca, Romania, 2011; p. 258.
9. Szilagyi, H.; Baeră, C.; Hegyi, A.; Lăzărescu, A. Romanian resources of waste and industrial by-products as additions for cementitious mixtures. *Int. Multidiscip. Sci. Geoconf. SGEM* **2018**, *18*, 325–332.
10. Baeră, C.; Szilagyi, H.; Matei, C.; Hegyi, A.; Lăzărescu, A.; Mircea, A.C. Optimizing approach on Fibre Engineered Cementitious Materials with Self-Healing capacity (SH-FECM) by the use of slurry lime (SL) addition. *MATEC Web Conf.* **2019**, *289*, 01001. [[CrossRef](#)]
11. Lăzărescu, A.V.; Szilagyi, H.; Baeră, C.; Ioani, A. The Effect of Alkaline Activator Ratio on the Compressive Strength of Fly Ash-Based Geopolymer Paste. *IOP Conf. Ser. Mater. Sci. Eng.* **2017**, *209*, 012064. [[CrossRef](#)]
12. Duxon, P.; Provis, J.L.; Lukley, G.C.; van Deventer, J.S.J. The role of inorganic polymer technology in the development of ‘green concrete’. *Cem. Con. Res.* **2007**, *37*, 1590–1597. [[CrossRef](#)]
13. Palomo, A.; Grutzeck, M.W.; Blanco, M.T. Alkali-Activated Fly Ashes: A Cement for the Future. *Cem. Con. Res.* **1999**, *29*, 1323–1329. [[CrossRef](#)]
14. Bilodeau, A.; Malhotra, V.M. High-volume fly ash system: Concrete solution for sustainable development. *ACI Mater. J.* **2000**, *97*, 41–48.
15. Mehdi, B. Geopolymer technology, from fundamentals to advanced applications: A review. *Mater. Technol.* **2009**, *24*, 79–87.
16. Van Jaarveld, J.G.S.; van Deventer, J.S.J.; Lukey, G.C. The characterisation of source materials in fly ash-based geopolymers. *Mater. Lett.* **2003**, *57*, 1272–1280. [[CrossRef](#)]
17. Al Bakri Abdullah, M.M.; Kamarudin, H.; Binhussain, M.; Nizar, K.; Mastura, W.I.W. Mechanism and Chemical Reaction of Fly Ash Geopolymer Cement—A Review. *J. Asian Sci. Res.* **2011**, *1*, 247–253.
18. Dimas, D.; Giannopoulou, I.; Pnias, D. Polymerization in sodium silicate solutions: A fundamental process in geopolymerization technology. *J. Mater. Sci.* **2009**, *44*, 3719–3730. [[CrossRef](#)]
19. Kumar, S.; Kumar, R. Mechanical activation of fly ash: Effect on reaction, structure and properties of resulting geopolymer. *Ceram. Int.* **2011**, *37*, 533–541. [[CrossRef](#)]
20. Mishra, A.; Choudhary, D.; Jain, N.; Kumar, M.; Sharda, N.; Dutta, D. Effect of concentration of alkaline liquid and curing time on strength and water absorption of geopolymer concrete. *ARPN J. Eng. Appl. Sci.* **2008**, *3*, 14–18.
21. Panagiotopoulou, C.; Kontori, E.; Perraki, T.; Kakali, G. Dissolution of aluminosilicate minerals and by-products in alkaline media. *J. Mater. Sci.* **2007**, *42*, 2967–2973. [[CrossRef](#)]
22. Sofi, M.; van Deventer, J.S.J.; Mendis, P.; Lukey, G.C. Engineering properties of inorganic polymer concretes (IPCs). *Cem. Con. Res.* **2007**, *37*, 251–257. [[CrossRef](#)]
23. Lăzărescu, A.; Mircea, C.; Szilagyi, H.; Baeră, C. Mechanical properties of alkali activated geopolymer paste using different Romanian fly ash sources—experimental results. *MATEC Web Conf.* **2019**, *289*, 11001. [[CrossRef](#)]
24. Chindapasirt, P.; Rattanasak, U.; Jaturapitakkul, C. Utilization of fly ash blends from pulverized coal and fluidized bed combustions in geopolymeric materials. *Cem. Con. Comp.* **2011**, *33*, 55–60. [[CrossRef](#)]
25. Pacheco-Torgal, F.; Castro-Gomez, J.; Jalali, S. Alkali-activated binders: A review. Part 1. Historical background terminology, reaction mechanisms and hydration products. *J. Constr. Build. Mater.* **2008**, *22*, 1305–1314. [[CrossRef](#)]

26. ASRO. *SR EN 196-1 Methods of Testing Cement. Determination of Strength*; Romanian Standards Association: Bucharest, Romania, 2012.
27. ASRO. *SR EN 12390-7 Testing Hardened Concrete. Density of Hardened Concrete*; Romanian Standards Association: Bucharest, Romania, 2019.
28. De Vargas, A.S.; dal Molin, D.C.C.; Vilela, A.C.F.; Silva, F.D.; Pavao, B.; Veit, H. The effects of Na<sub>2</sub>O/SiO<sub>2</sub> molar ratio, curing temperature and age on compressive strength, morphology and microstructure of alkali-activated fly ash-based geopolymers. *Cem. Concr. Compos.* **2011**, *33*, 653–660. [[CrossRef](#)]

**Publisher's Note:** MDPI stays neutral with regard to jurisdictional claims in published maps and institutional affiliations.



© 2020 by the authors. Licensee MDPI, Basel, Switzerland. This article is an open access article distributed under the terms and conditions of the Creative Commons Attribution (CC BY) license (<http://creativecommons.org/licenses/by/4.0/>).

# The Possibility of Using Slag for the Production of Geopolymer Materials and Its Influence on Mechanical Performances—A Review <sup>†</sup>

Brăduț Alexandru Ionescu <sup>\*</sup>, Adrian-Victor Lăzărescu  and Andreea Hegyi

NIRD URBAN-INCERC Cluj-Napoca Branch, 117 Calea Florești, 400524 Cluj-Napoca, Romania; adrian.lazarescu@incerc-cluj.ro (A.-V.L.); andreea.hegyi@incerc-cluj.ro (A.H.)

<sup>\*</sup> Correspondence: bradut.ionescu@incerc-cluj.ro

<sup>†</sup> Presented at the 14th International Conference INTER-ENG 2020 Interdisciplinarity in Engineering, Mureș, Romania, 8–9 October 2020.

Published: 17 December 2020

**Abstract:** All industries produce wastes or byproducts, and if those are not properly managed, they will cause adverse effects on the environment. As the need for steel increases globally, waste from steel processing will also increase. Hazardous waste from steel processing is produced in the form of a coarse, dense aggregate, called steel slag. The aim of this paper is to present the possibility of using steel slag/blast furnace slag in the production of geopolymer concrete and to present the relevant results regarding the influence of this industrial byproduct on the mechanical properties of Geopolymer materials.

**Keywords:** geopolymer binders; industrial byproducts; sustainable development

---

## 1. Introduction

Industrial wastes generated by the various industries are a global problem with multiple social, financial and environmental effects. The efficient recycling of wastes and industrial byproducts is more than necessary in order to mitigate their negative effects, to reduce the consumption of other raw materials and to minimize at much as possible greenhouse gas emissions. Construction and demolition waste, fly ash, furnace/steel slag and mining waste can be recycled for reuse and to produce new, innovative materials in the civil engineering industry. Cement production raises major problems around the world through CO<sub>2</sub> pollution of the atmosphere. Cement production is considered to have a global pollution share of 5–8% by total emissions of CO<sub>2</sub> released into the atmosphere.

To reduce the high amount of carbon dioxide emissions released into the atmosphere during the production of Portland cement, alternative materials such as alkali-activated composites, or geopolymers, could provide a sustainable and durable approach. The most used raw materials in the production of alkali-activated geopolymer materials are fly ash and furnace/steel slag. Given the fact that the industries that produce these types of wastes are constantly growing, using these materials as raw materials offers the premises for producing alternative materials. As the need for steel increases globally, the waste produced by the steel processing industry will also increase. Hazardous waste from steel processing is produced in the form of a coarse, dense aggregate, called steel slag [1].

In 1999, Palomo proposed the possibility of activating puzzolanic materials such as furnace slag and fly ash “using alkaline liquids, to form a binder and completely replace the use of Portland cement in the production of concrete” [2]. Geopolymer concrete, known as alkali-activated cement [3], inorganic polymer concrete [4] or geocement [5], has emerged as an innovative way of new engineering materials, entirely replacing traditional Portland cement. In order to successfully produce geopolymer materials, the raw materials used in their production have to be rich in silicon (Si) and aluminum (Al).

Due to the chemical composition of the raw materials, geopolymers incorporating significant amounts of calcium-rich materials, such as slag, for example, may have different properties than those based only on low-calcium fly ash.

The industrial use of waste in the production of geopolymer concrete will not only have economic and environmental benefits but will also solve the problems associated with the removal of large amounts of waste materials, such as coal-fired power plant ash and slag from the production of metals, which otherwise could endanger the environment. Using different types of slag to produce alkali-activated geopolymer binders is important not only for saving metal resources but also for protecting the environment.

The aim of this paper is to present the relevant results from the literature on the influence of the use of this industrial byproduct on the mechanical properties of geopolymer materials and also the possibility of using steel slag/blast furnace slag in the production of geopolymer concrete, without the use of Portland cement. Studying the mechanisms that affect the properties of geopolymer materials, such as raw materials, mix-design ratio, testing procedures, etc., represents the current methodology of this study.

## 2. Results and Discussions

Slag is a byproduct obtained during the manufacture of cast iron and steel. Various slags are produced as byproducts in metallurgical processes or as residues in incineration processes [6]. Blast Furnace Slag (BFS) is a non-metallic (oxidic) byproduct, resulting from the process of obtaining cast iron in furnaces, where the melting of iron mixed with coke and fondants (for example dolomite) takes place [7]. In the furnace crucible, cast iron is obtained at the bottom and slag at the top. The emission of steel slag makes up 13–20% of steel production [8]. Steel Slag (SS) results from the process of obtaining steel by different processes: Martin furnace, converter, electric furnace. Ground Granulated Blast Furnace Slag (GGBFS) is a fine granular material, resulting from the cooling of the blast furnace in a lot of water. GGBFS has a high hydraulic activity potential and can be easily used in the preparation of geopolymer materials [9–11].

This industrial waste contains calcium, magnesium, manganese and aluminum silicates in various combinations along with iron oxide. The major difference between blast furnace slag and steel slag is the iron content [6–8]. For blast furnace slag, the FeO content is about 0.5%, while in the case of steel slag, the total iron content varies from 16 to 23% [12]. Chemical composition is an important parameter when producing alkali-activated materials. Depending on the raw materials used in the metallurgical industry, slag composition could vary drastically. These differences in raw materials lead to differences in how slag responds to alkaline activation [13,14].

In the case of slag blended systems, the geopolymerization reaction rate generally increases with higher amounts of slag and at higher activator amounts [15–17]. Although the good properties of alkali-activated slag-based geopolymer materials have been demonstrated, when using these types of blended systems, several parameters, such as workability, including relatively rapid slump loss, could become a major concern [8,15,16].

According to Shi Qian [18], the principle of alkali-activation of furnace slag has been known since the 1940s, when Purdon published several studies regarding the use of this raw material in the production of alkali-activated geopolymer [19]. However, it was only in the 1960s that systematic exploratory studies on this topic were conducted, especially by Gluhovsky and Pakhovmov. Industrial applications include 9-storey buildings (~1960), 20-storey buildings (~1987), sewer pipes (~1966), irrigation canals (~1962), road sidewalk (~1984), railway sleepers (~1989) as well as fire doors (~2000) [20].

Most of the research regarding the use of slag in the production of alkali-activated geopolymer material refer to fly ash–blast furnace slag/steel slag blended systems in various mixtures, with or without heat treatment [15–17]. Moreover, research includes most of the time results regarding

compressive strength under conditions of chemical attack (sulfuric acid, sodium sulfate and sodium chloride) [21–27].

Ng and Foster [28] reported that for the production of slag–fly ash-based geopolymer systems, the mass ratio between them varies according to the reactivity of the fly ash and slag. These parameters are important in order to obtain an optimum compressive strength of the material.

The properties of alkali-activated geopolymer materials depend mainly on the important factors that could affect the development of this type of material and include the characteristics of constituent materials. The mechanical properties of the geopolymer materials are directly affected by the way in which the rich Al-Si materials dissolve in the alkaline activator and their microstructural reorganization when the reaction occurs [29–31].

In practice, on a case-by-case basis, an analysis is required regarding the chemical composition of the byproducts used as raw materials in the production of geopolymer material [6–8,29,30]. Studies conducted worldwide show that the chemical composition of the raw materials used in the production of geopolymer materials has an important influence on the final mechanical properties of the material.

Table 1 summarizes the chemical composition of fly ash and blast furnace slag/steel slag, according to different authors, used for the production of these materials. It can be seen in the table below that Fe<sub>2</sub>O<sub>3</sub> is higher for fly ash. Moreover, it is noted that for steel slag, FeO has a very high percentage, between 10–40%, compared to furnace slag 0.26–1.1%.

**Table 1.** Chemical composition of raw materials used in the production of alkali-activated geopolymer materials, measured by X-ray fluorescence [wt%].

Oxide	SiO <sub>2</sub>	Al <sub>2</sub> O <sub>3</sub>	Fe <sub>2</sub> O <sub>3</sub>	CaO	MgO	SO <sub>3</sub>	L.O.I.	Ref.
Fly Ash	21.94	8.46	6.05	45.4	6.06	0	6.65	[21]
Blast furnace slag	37.33	12.49	0.26	43.3	5.31	0	0	
Fly Ash	65.81	22.17	3.23	1.24	1.01	0.47	1.57	[22]
Slag	37.25	10.24	1.1	42.17	3.82	2.13	0.81	
Fly Ash	52.0	33.9	4.0	1.2	0.81	0.28	6.23	[23]
Steel Slag	10–19	1–3	10–40 (FeO)	40–52	5–10	-	-	
Fly Ash	61.81	19.54	7.01	1.77	2.56	0.31	2.20	[24]
Ground Granulated Blast Furnace Slag	36.7	5.20	0.98	32.61	10.12	0.99	2.88	
Fly ash	51.11	25.56	12.48	4.3	1.45	0.24	0.57	[25]
Slag	32.76	12.37	0.54	44.64	5.15	4.26	0.09	
Fly Ash	63.53	27.40	3.67	1.26	0.35	0.01	-	[26]
Slag	34.26	11.32	0.61	38.34	7.94	3.84	-	
Fly Ash	48.3	28.3	11.8	3.97	1.51	0.22	1.74	[27]
Slag	32.9	14.3	0.47	41.2	5.42	2.40	0.36	

When using slag-fly ash blended systems, an increased amount of fly ash delays the setting time, reduces the compressive strength modulus of elasticity and Poisson’s ratio and results in high ductility and toughness [16,32,33] but helps the geopolymer system to have an enhanced homogeneity and also contributes to a limited microcracking phenomenon [33].

The summarized details presented in Table 1 of several raw materials used in the literature to produce alkali-activated geopolymer materials show that due to their different chemical composition, this parameter needs to be carefully taken into account as it could provide a guide line to evaluate later possible reactions and outputs for the improvement of the mechanical properties of the final material.

To attain a similar or even higher compressive strength when compared to OPC concrete, geopolymer materials require heat treatment. This type of curing process is beneficial for the dissolution and geopolymerization process of the aluminosilicate gel and also results in early-age strength gain of the material [34–36]. As shown in the literature, adopting the proper curing treatment



for the production of alkali-activated geopolymer materials must be appropriate in order to provide an ideal condition for the dissolution and precipitation of dissolved silica and alumina species [34].

### 2.1. Development of Geopolymer Materials without Heat Treatment

It is well known that typical fly ash-based geopolymer concrete requires high temperature curing treatment in order to develop sufficient early mechanical strength properties, which can be considered a severe limitation for on-site applications. However, in recent years, methods of producing geopolymer concrete without using heat treatment have been exploited. In order to achieve this, extensive experimental investigation on the mechanical and microstructural properties of geopolymer concrete mixes prepared using a combination of fly ash and slag and cured under ambient temperature to produce “user-friendly” geopolymer mixes have been researched.

Hyumjung et Yootak (2012) [21] carried out tests regarding the mechanical properties of alkali-activated geopolymer concrete, without heat treatment by using as binder, a combination between fly ash and blast furnace slag, in different ratios. It can be seen in Table 2 that the compressive strength increased with the increase in the percentage of furnace slag in the mix-design of the geopolymer. The highest compressive strength was achieved for a geopolymer mortar produced only by using blast furnace slag, without fly ash (44 MPa—at 28 days), almost double that of a geopolymer mortar produced using blast furnace slag-fly ash with a 50:50 ratio.

**Table 2.** Geopolymer mortar compressive strength of, without heat treatment, depending on the fly ash/blast furnace slag ratio [21].

Mixture	FA/BFS Ratio	Compressive Strength [MPa]	Binder/Water Ratio	NaOH Molarity
I	100:0	2.81		
II	50:50	23.51	100:40	2.78
III	0:100	44.41		

Luga et al. (2017) [24] also presented the compressive strength obtained for geopolymer materials using a fly ash–ground granulated blast furnace slag binding system, without heat treatment. Results are presented in Table 3.

**Table 3.** Geopolymer mortar compressive strength, without heat treatment, depending on the fly ash/ground granulated blast furnace slag ratio [24].

Mixture	FA/GGBFS Ratio	Compressive Strength at 28 Days [MPa]
I	100:0	3.1
II	80:20	8.4
III	60:40	18.2
IV	40:60	39.3
V	20:80	57.6
VI	0:100	74.8

It can be also seen in Table 3 that the compressive strength increased with the increase in the percentage of furnace slag in the mix-design of the geopolymer. The highest compressive strength was achieved for a geopolymer mortar produced only by using blast furnace slag, which also confirms previous studies in the field.

Other studies show that Steel Slag can be also used as addition to fly ash in order to produce the alkali-activated geopolymer binder. Premalta (2017) [23] also presented the results obtained regarding the compressive strength of a geopolymer concrete with steel slag addition between 2 ÷ 3.5%, at different ages. According to the data in the Table 4, it is observed that the compressive strength of

geopolymer concrete increased to a percentage of 2.5% steel slag, after which it decreases, showing that the behavior of the geopolymer binder should be analyzed on a case-by-case situation.

**Table 4.** Compressive strength at different ages and different percentages of steel slag addition [23].

Mixture	Steel Slag [%]	Compressive Strength [MPa]			
		2 Days	7 Days	14 Days	28 Days
I	2.0	3.5	8.5	13.3	21.3
II	2.5	4.8	9.3	14.7	23.9
III	3.0	3.3	7.8	12.9	18.6
IV	3.5	3.6	7.2	11.9	16.6

In another study, Nematollahi (2017) [25] presented the results regarding the compressive strength obtained for a fly ash–blast furnace slag-based geopolymer material with a constant ratio FA:BFS of 75:25 and different activator ratios, cured at ambient temperature. As shown in Table 5, it is noted that the compressive strength increases with the increase in the alkali-activator chemical properties, which also demonstrates that the chemical composition of the raw material is only one of the important parameters that affect the mechanical properties of the material. Careful selection of the alkali-activator and the ratio of the component materials should be taken into account.

**Table 5.** Compressive strength of non-heat-treated FA–BFS Geopolymers [25].

Mixture	FA:BFS	Na <sub>2</sub> SiO <sub>3</sub> -Anhydrous Activator	Water	W/GP Solid Ratio	Compressive Strength [MPa]
I			0.394	0.36	18.4
II	75:25	0.120	0.400	0.36	30.5
III			0.300	0.27	37.3

## 2.2. Development of Geopolymer Materials with Heat Treatment

The effect of the curing temperature on the alkali-activated geopolymer materials has been demonstrated by numerous studies which have shown that by using this type of treatment, improvements were observed in the geopolymerization reaction and also increases in the mechanical properties of the material, at very young ages [29,30,37].

Puertas et al. investigated the mechanical properties of alkali-activated fly ash/slag-based geopolymers by using an alkaline activator a combination between Na<sub>2</sub>SiO<sub>3</sub> solution and NaOH solution with 2 and 10 M molarity and subjected to heat treatment at 25 and 65 °C. According to the results, the ratios of fly ash/slag and of activator are the most important factors that influence the mechanical performance of the material since the hardening temperature has less effects compared to the two previous factors [38].

In another study, Ghosh and Ghosh (2018) [22] made different tests on geopolymers produced using fly ash and ground granulated blast furnace slag (GGBFS) as raw materials in different ratios: 100:0, 90:10, 85:15, 70:30, 50:50, 40:60. Geopolymers were subjected to heat treatment for 48 h, at a temperature of 85 °C. The samples were tested after 7 days.

As shown in Figure 1, the compressive strength of the mixtures increased with the addition of slag content. There was an increase in the compressive strength of the 90:10 mixtures by 19.99% over the 100:0 mixtures. Moreover, the compressive strength of the 85:15 mixture was 15.97% higher compared to the 90:10 mixture. The 70:30 mixtures showed an increase in compressive strength of 14.75% over the 85:15 mixtures. The highest compressive strength was obtained for the 70:30 mixtures.

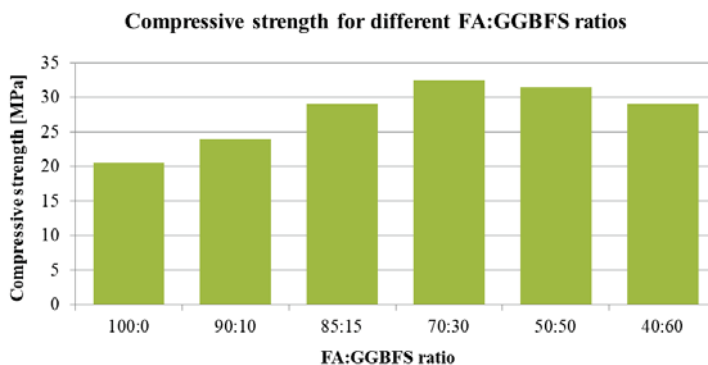


Figure 1. Effect of slag ratio variation on the compressive strength of the geopolymer material [22].

Decreases of 3.43% and 6.33% in the compressive strength were also observed for the 50:50 and 40:60 mixtures when compared to the 70:30 mixtures and the 50:50 mixtures, respectively. This phenomenon could be a sign of a low geopolymerization process; therefore, lower mechanical properties have been achieved.

Luga et al. (2017) [24] presented the compressive strength of a geopolymer mortar based on fly ash and granulated blast furnace slag (GGBFS), with a heat treatment of 72 h at a temperature of 100 °C. Results presented in Table 6 regarding the compressive strength of the alkali-activated geopolymer material are in accordance with the literature [22,39] showing that with the increase in the GGBF content in the mixture, the compressive strength of the material increased.

Table 6. The effect of the variation of the compressive strength of some geopolymers mortars based on fly ash and ground granulated blast furnace slag, with heat treatment (72 h/100 °C) [24].

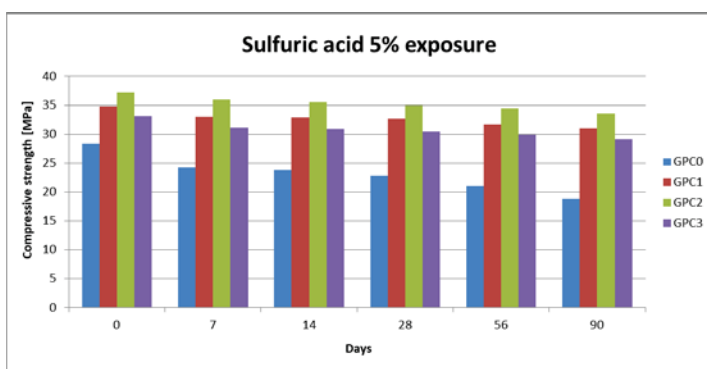
Mixture	FA/GGBFS Ratio	Compressive Strength [MPa]
I	100:0	15.4
II	80:20	13.7
III	60:40	12.1
IV	40:60	46.6
V	20:80	45.7
VI	0:100	42.7

Based on the results presented above, it can be said that the curing temperature is one of the most important factors affecting the mechanical properties of alkali-activated geopolymer materials when subjected to this type of treatment. For the heat curing regimes, there are a lot of possibilities both for their duration and temperature in order to achieve the desired mechanical properties of the geopolymer material.

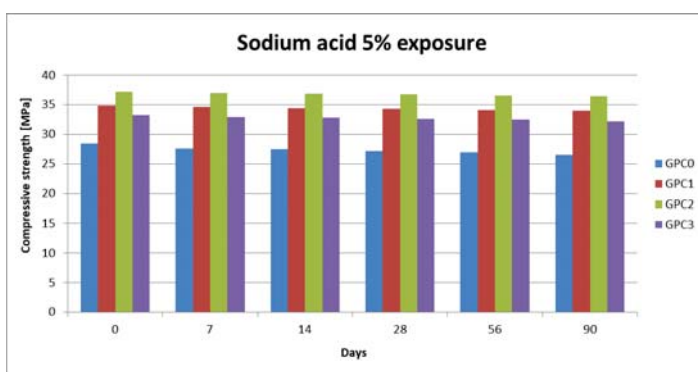
### 2.3. Development of Geopolymer Materials with High Chemical Attack Properties

Kartik et al. (2017) [26] studied the resistance of geopolymers based on coal fly ash and blast furnace slag after the test pieces were exposed to an acidic medium (5% sulfuric acid) for 7, 14, 28, 56 and 90 days, respectively, to a sodium sulphate attack and sodium chloride.

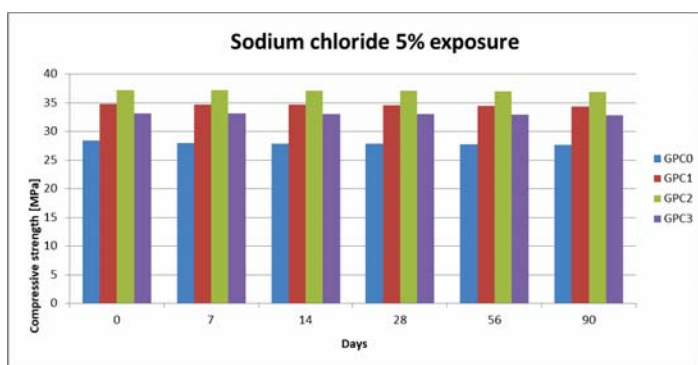
It can be seen in Figure 2a that the compressive strength decreases with the increase in the duration of immersion in sulfuric acid. The decrease in compressive strength is not significant given the extreme aggressive environment and the long immersion duration of 90 days. For the geopolymers GPC1, GPC2 and GPC3 there was a decrease of only 3–4 MPa, about 10%. For GPC0 there was a considerable decrease in compressive strength, from 28 MPa to 18 MPa, almost 34%.



(a)



(b)



(c)

**Figure 2.** Geopolymer materials compressive strength when exposed to chemical attack: (a) sulfuric acid exposure; (b) sodium acid exposure; (c) sodium chloride exposure.

Moreover, Kartik et al. (2017) studied the behavior of geopolymers compression, after having previously been subjected to an attack with sodium sulfate 5% (Figure 2b) and sodium chloride 5% (Figure 2c), respectively.

After long-time exposure to a sodium sulphate attack, the compressive strength decreased over time (Figure 2b). In comparison with the test pieces subjected to sulfuric acid immersion, those immersed in sodium sulphate showed better results. For the geopolymer GPC0, the lowest resistances and the greatest resistance decrease were obtained, as well as those immersed in sulfuric acid. If for the Geopolymers GPC1, GPC2, GPC3 were obtained decreases of 3–4 MPa (approx. 10%) for samples immersed in sulfuric acid, for those subjected to attack with sodium sulfate were obtained decreases of approx. 1 MPa (approx. 2.5%). Specimens long exposed for 90 days to a 5% sodium chloride attack suffered the least. They showed the lowest losses of compressive strength, i.e., approx. 1%.

### 3. Conclusions

Geopolymer technology is gaining quite a lot of ground due to the successful implementation of this type of material in certain countries, in different areas. This aspect is mainly due to the need to align with the principles of the circular economy by harnessing waste materials and byproducts and to also prevent generating new ones. The possibility of producing geopolymer building materials using slag as raw material was demonstrated, but only by compositional optimization due to the multitude of influences affecting this type of material.

Geopolymers materials have shown better properties when subjected to heat treatments to (accelerated) heat hardening, since geopolymerization and polycondensation reactions would occur faster. Moreover, the addition of slag at an optimum level of 30% increased the mechanical properties of heat-treated geopolymer composites, e.g., increasing compressive strength.

Studies have also shown that fly ash–slag based geopolymer materials have a very good resistance to chemical attacks (sulfuric acid, sodium sulphate or sodium chloride) over a long period.

Therefore, producing geopolymer concrete based on blast furnace slag/steel slag and fly ash will lead to long-term environmental protection, obtaining very good compressive strength from an early age and is an alternative to traditional concrete based on Portland cement in the future.

The need to continue existing studies is identified due to the many unknowns in the field regarding the geopolymerization process and the properties of the geopolymer concrete as well as the products derived from this process when using different raw materials to produce the geopolymer binder. Thus, the approach of this research direction falls within the current complex theme, aligned to worldwide research on innovative ways of harnessing byproducts or wastes in the development of new building materials.

**Funding:** This research received no external funding.

**Conflicts of Interest:** The authors declare no conflict of interest.

### References

1. Ashadi, H.W.; Aprilando, B.A.; Astutiningsih, S. Effects of Steel Slag Substitution in Geopolymer Concrete on Compressive Strength and Corrosion Rate of Steel Reinforcement in Seawater and an Acid Rain Environment. *Int. J. Technol.* **2015**, *2*, 227–235. [[CrossRef](#)]
2. De Silva, P.; Sagoë-Crenstil, K.; Sirivivatnanon, V. Kinetics of geopolymerisation: Role of Al<sub>2</sub>O<sub>3</sub> and SiO<sub>2</sub>. *Cem. Concr. Res.* **2007**, *37*, 512–518. [[CrossRef](#)]
3. Bosoaga Masek, O.; Oakey, J.E. CO<sub>2</sub> capture technologies for cement Industry, Energy. *Procedia* **2009**, *1*, 133–140.
4. Barcelo, L.; Kline, J.; Walenta, G.; Gartner, E. Cement and carbon emissions. *Mater. Struct.* **2014**, *47*, 1055–1065. [[CrossRef](#)]
5. Duxson, P.; Provis, J.L.; Lukey, G.C.; van Deventer, J.S.J. The role of inorganic polymer technology in the development of ‘green concrete’. *Cem. Concr. Res.* **2007**, *37*, 1590–1597. [[CrossRef](#)]
6. Shen, H.; Forssberg, E. An Overview of Recovery of Metals from Slags. *Waste Manag.* **2003**, *23*, 933–949. [[CrossRef](#)]

7. Liu, J.; Dongmin, W. Application of Ground Granulate Blast Furnace Slag-Steel Slag Composite Binder in a Massive Concrete Structure under Severe Sulphate Attack. *Adv. Mater. Sci. Eng.* **2017**, *2017*, 9493043. [[CrossRef](#)]
8. Furlani, E.; Tonello, G.; Maschio, S. Recycling of steel slag and glass cullet from energy saving lamps by fast firing production of ceramics. *Waste Manag.* **2010**, *30*, 1714–1719. [[CrossRef](#)]
9. El-Sayed, H.A.; El-Enein, S.A.A.; Khater, H.M.; Hasanein, S.A. Resistance of alkali activated water-cooled slag geopolymer to sulphate attack. *Ceram. Silik.* **2011**, *55*, 153–160.
10. Yang, H.F.; Dang, C.G.; Xu, W. Preparation of geopolymer using the slag from direct reduction-magnetic separation of refractory iron ore (SDRMS). *Manuf. Sci. Technol.* **2012**, *383*, 911–915. [[CrossRef](#)]
11. Kashani, A.; Provis, J.L.; van Deventer, J.S.J. Effect of ground granulated blast furnace slag particle size distribution on paste rheology: A preliminary model. *AIP Conf. Proc.* **2013**, *1542*, 1094–1097.
12. *Indian Minerals Yearbook 2012 Part- II: Metals & Alloys, 51st Edition, Slag-Iron and Steel*; Government of India, Ministry of Mines, Indian Bureau of Mines: Nagpur, India, 2012.
13. Bakharev, T.; Sanjayan, J.G.; Cheng, Y.-B. Effect of elevated temperature curing on properties of alkali-activated slag concrete. *Cem. Concr. Res.* **1999**, *29*, 1619–1625. [[CrossRef](#)]
14. Wang, S.-D.; Scrivener, K.L.; Pratt, P.L. Factors affecting the strength of alkali-activated slag. *Cem. Concr. Res.* **1994**, *24*, 1033–1043. [[CrossRef](#)]
15. Bijen, J. Benefits of slag and fly ash. *Construct. Build. Mater.* **1996**, *10*, 309–314. [[CrossRef](#)]
16. Nath, P.; Sarker, P.K. Effect of GGBFS on setting, workability and early strength properties of fly ash geopolymer concrete cured in ambient condition. *Construct. Build. Mater.* **2014**, *66*, 163–171. [[CrossRef](#)]
17. Provis, J.L. Geopolymers and other alkali activated materials: Why, how, and what? *Mater. Struct.* **2014**, *47*, 11–25. [[CrossRef](#)]
18. Shi, C.; Qian, J. High Performance Cementing Materials from Industrial slags—A review. *Resour. Conserv. Recycl.* **1999**, *29*, 195–207. [[CrossRef](#)]
19. Purdon, A.O. The action of alkalis on blast furnace slag. *J. Soc. Chem. Ind.* **1940**, *59*, 191–202.
20. *Recommended Practice- Geopolymer Concrete 2011*; Concrete Institute of Australia: Sydney, Australia, 2011.
21. Kim, H.; Kim, Y. Characteristics of the Geopolymer using Fly Ash and Blast Furnace Slag with Alkaline Activators. In Proceedings of the 4th International Conference on Chemical, Biological and Environmental Engineering, Phuket, Thailand, 1–2 September 2012; IPCBEE: Singapore, 2012; Volume 43, pp. 154–159.
22. Ghosh, K.; Ghosh, P. Effect of variation of slag content on chemical, engineering and microstructural properties of thermally cured fly ash-slag based geopolymer composites. *Rasayan J. Chem.* **2018**, *11*, 426–439.
23. Premalatha, P.V.; Rhema Rose, C.; Aboorvaraj, K.A. A Comparison of Geopolymer Concrete Blended with Steel Slag under Sunlight and Ambient Curing. *AJAST* **2018**, *2*, 55–62.
24. Luga, E.; Atis, D.C.; Karahan, O.; Ilkentapar, S.; Gorur, E.B. Strength properties of slag/fly ash blends activated with sodium metasilicate. *GRADEVINAR* **2017**, *69*, 199–205.
25. Nematollahi, B. Investigation of Geopolymer as a Sustainable Alternative Binder for Fiber-Reinforced Strain-Hardening Composites. Ph.D. Thesis, Faculty of Science, Engineering and Technology, Swinburne University of Technology, Hawthorn, Australia, 2017.
26. Karthik, A.; Sudalaimani, K.; Vijayakumar, C.T. Durability study on coal fly ash-blast furnace slag geopolymer concretes with bio-additives. *Ceram. Int.* **2017**, *43*, 11935–11943. [[CrossRef](#)]
27. Neupane, K.; Sriravindrarajah, R.; Baweja, D.; Des Chalmers, I. Effect of curing on the compressive strength development in structural grades of geocement concrete. *Construct. Build. Mater.* **2015**, *94*, 241–248. [[CrossRef](#)]
28. Hassan, A.; Arif, M.; Shariq, M. Use of Geopolymer Concrete for a Cleaner and Sustainable Environment—A Review of Mechanical Properties and Microstructure. *J. Clean. Prod.* **2019**, *223*, 704–728. [[CrossRef](#)]
29. Lăzărescu, A.; Szilagy, H.; Ioani, A.; Baeră, C. Parameters Affecting the Mechanical Properties of Fly Ash-Based Geopolymer Binders-Experimental Results. *IOP Conf. Ser. Mater. Sci. Eng.* **2018**, *374*, 012035. [[CrossRef](#)]
30. Lăzărescu, A.V.; Szilagy, H.; Baeră, C.; Ioani, A. The Effect of Alkaline Activator Ratio on the Compressive Strength of Fly Ash-Based Geopolymer Paste. *IOP Conf. Ser. Mater. Sci. Eng.* **2017**, *209*, 012064. [[CrossRef](#)]

31. Nergis, D.D.B.; Abdullah, M.M.A.; Sandu, A.V.; Vizureanu, P. XRD and TG-DTA study of new alkali activated materials based on fly ash with sand and glass powder. *Materials* **2020**, *13*, 343. [[CrossRef](#)]
32. Lee, N.; Lee, H. Setting and mechanical properties of alkali-activated fly ash/slag concrete manufactured at room temperature. *Construct. Build. Mater.* **2013**, *47*, 1201–1209. [[CrossRef](#)]
33. Lee, N.; Lee, H. Reactivity and reaction products of alkali-activated, fly ash/slag paste. *Construct. Build. Mater.* **2015**, *81*, 303–312. [[CrossRef](#)]
34. Diaz, E.I.; Allouche, E.N.; Eklund, S. Factors affecting the suitability of fly ash as source material for geopolymers. *Fuel* **2010**, *89*, 992–996. [[CrossRef](#)]
35. Fernandez-Jimenez, A.; Palomo, A.; Sobrados, I.; Sanz, J. The role played by the reactive alumina content in the alkaline activation of fly ashes. Microporous Mesoporous. *Materials* **2006**, *91*, 111–119.
36. Khale, D.; Chauldhary, R. Mechanism of geopolymerization and factors influencing its development: A review. *J. Mater. Sci.* **2007**, *42*, 729–746. [[CrossRef](#)]
37. Dutta, D.; Chakrabarty, S.; Bose, C.; Ghosh, S. Evaluation of geopolymer properties with temperature imposed on activator prior mixing with fly ash. *Int. J. Civ. Eng.* **2012**, *3*, 205–213.
38. Puertas, F.; Martinez-Ramirez, S.; Alonso, S.; Vazquez, T. Alkali-Activated Fly Ash/Slag Cement Strength Behaviour, Hydration Products. *Cem. Concr. Res.* **2000**, *30*, 1625–1632. [[CrossRef](#)]
39. Provis, J.L.; Myers, R.J.; White, C.E.; Rose, V.; van Deventer, J.S.J. X-ray microtomography shows pore structure and tortuosity in alkali-activated binders. *Cem. Concr. Res.* **2012**, *42*, 855–864. [[CrossRef](#)]

**Publisher's Note:** MDPI stays neutral with regard to jurisdictional claims in published maps and institutional affiliations.



© 2020 by the authors. Licensee MDPI, Basel, Switzerland. This article is an open access article distributed under the terms and conditions of the Creative Commons Attribution (CC BY) license (<http://creativecommons.org/licenses/by/4.0/>).

Article

# Influence of the Addition of TiO<sub>2</sub> Nanoparticles on the Self-Cleaning Performance of Cementitious Composite Surfaces <sup>†</sup>

Elvira Grebenișan, Andreea Hegyi <sup>\*</sup>, Henriette Szilagyı <sup>†</sup>, Adrian-Victor Lăzărescu <sup>†</sup> and Brăduț Alexandru Ionescu

NIRD URBAN-INCERC Cluj-Napoca Branch, 117 Calea Florești, 400524 Cluj-Napoca, Romania; elvira.grebenisan@incerc-cluj.ro (E.G.); henriette.szilagyı@incerc-cluj.ro (H.S.); adrian.lazarescu@incerc-cluj.ro (A.-V.L.); bradut.ionescu@incerc-cluj.ro (B.A.I.)

<sup>\*</sup> Correspondence: andreea.hegyi@incerc-cluj.ro

<sup>†</sup> Presented at the 14th International Conference INTER-ENG 2020 Interdisciplinarity in Engineering, Mureș, Romania, 8–9 October 2020.

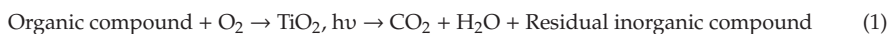
Published: 21 December 2020

**Abstract:** The presence of TiO<sub>2</sub> nanoparticles in a cementitious matrix induces self-cleaning capacity in the presence of UV radiation by combining two mechanisms: surface hydrophilicity and degradation of the stain agent molecules. Experimental results indicate an increase in surface water absorption and, indirectly, in the degree of hydrophilicity, with the increase in the concentration of TiO<sub>2</sub> nanoparticles in the matrix. Degradation of organic molecules, rhodamine B, is dependent on the duration of action and intensity of UV rays and the concentration of nanoparticles in the cementitious matrix. An addition of 3–6% TiO<sub>2</sub> is effective and sufficient for a good self-cleaning capacity of cementitious surfaces.

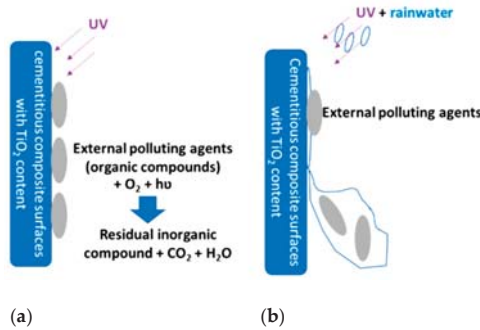
**Keywords:** self-cleaning; hydrophilicity; TiO<sub>2</sub> nanoparticles; photocatalytic activation; cementitious composites

## 1. Introduction

One of the most common causes of structural degradation is the accumulation of polluting materials, organic or inorganic, on the surface [1–4]. Nanotechnology could offer a solution by producing materials with self-cleaning capacities. A cementitious composite containing TiO<sub>2</sub> nanoparticles, under the influence of UV rays, has a specific behavior: a photocatalysis of redox reactions is manifested that allow the oxidation and decomposition of organic particles on the cementitious surface (particles that produce the staining effect) into smaller particles, molecules with a simpler structure, which can either be more easily taken up by rainwater and removed (washing phenomenon). On the one hand, the organic particles continue to decompose until the final reduction (Equation (1)) [5–14]; on the other hand, the hydrophilicity of the cement composite surface increases (Figure 1). The two mechanisms together realize the self-cleaning capacity of cementitious composites containing TiO<sub>2</sub> nanoparticles [1,15–22]. According to the literature [14], TiO<sub>2</sub> nanoparticles, alone, lose their property of influencing hydrophilicity and oxidation of organic molecules as soon as the UV action ceases, but in combination with SiO<sub>2</sub> in cement, this photoactivated capacity is prolonged even with more days of darkness (total lack of UV radiation).

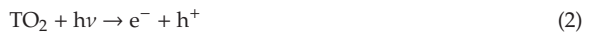






**Figure 1.** Schematic representation of the self-cleaning capacity by combining the two mechanisms: (a) photocatalytic oxidation process of organic substances; (b) removal of foreign substances with the help of rainwater by increasing surface hydrophilicity.

The mechanism underlying this property of cementitious composite surfaces containing TiO<sub>2</sub> nanoparticles, under conditions of exposure to the action of UV rays, can be explained by the increase of hydroxyl groups (OH<sup>-</sup>), a phenomenon identified by X-ray photoemission spectroscopy (XPS), Fourier-transform infrared spectroscopy (FTIR) or nuclear magnetic resonance (NMR), and shown schematically in Figure 2 [15,23–26]. The transition of the surface, under the influence of UV radiation, into a metastable thermodynamic state is the result of the coexistence of the forms of molecular water and dissociated water. Under the action of UV rays, titanium dioxide is a semiconductor with a band gap of about 3.0 eV that in the presence of UV light, through energy absorption, generates electrons (e<sup>-</sup>) and holes (h<sup>+</sup>) (Equation (2)). Electrons tend to reduce the cation Ti(IV) to the ion Ti(III) (Equation (3)), and voids oxidize O<sub>2</sub><sup>-</sup> anions (Equation (4)). This process will release oxygen and thus form gaps on the surface of titanium dioxide, giving the possibility of binding water molecules with the release of hydroxyl groups (OH<sup>-</sup>). The oxidation capacity of holes (h<sup>+</sup>) is higher than the electron reduction capacity (e<sup>-</sup>); on the surface of the photocatalyst is a single layer of adsorbed H<sub>2</sub>O molecules, and hydroxyl groups are formed (OH<sup>-</sup>). These hydroxyl groups are strongly oxidizing and react with molecules of organic nature producing free radicals of peroxy type, which will react with molecular oxygen in a chain of reactions to the final products CO<sub>2</sub> and H<sub>2</sub>O. On the other hand, electrons (e<sup>-</sup>) reduce oxygen to the free radical O<sub>2</sub><sup>-</sup> which will react with the peroxide molecules resulting during the reaction between hydroxyl groups and organic molecules, ultimately leading to a chain of reactions to the final products CO<sub>2</sub> and H<sub>2</sub>O [5–13]. Photogenerated holes (h<sup>+</sup>) increase the length of the links within the TiO<sub>2</sub> network (Figure 2), bringing the surface to a metastable state that allows the adsorption of molecular water, simultaneously with the formation of new hydroxyl groups and the release of a proton [15,27].



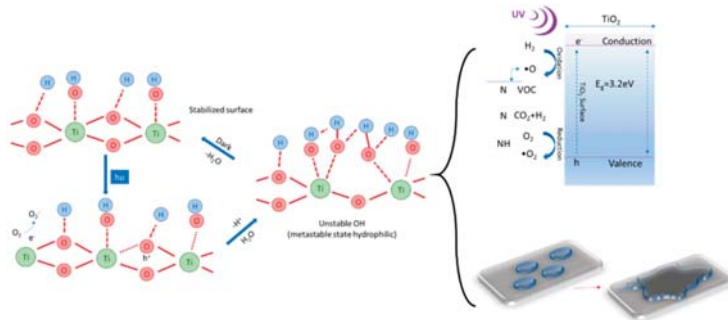


**Figure 2.** Schematic representation of the transition of the surface to a metastable state by photoactivation in the presence of UV rays [13,15,26].

Regarding the hydrophilicity assessment, the literature indicates that, in principle, the two methods of measurement—direct method of measuring the contact angle of the droplet of the liquid to the surface [1,28,29] and the indirect method for the determination of the water absorption on the surface [1,14,28] which states that there is a high potential of water absorption on the surface—are indicated by a high level of wettability. To highlight the ability of self-cleaning, research in the literature indicates several test methods, of which the method of staining with rhodamine B (RhB) is the most common.

Photocatalyzed degradation of RhB in the presence of  $\text{TiO}_2$  is a process that is based on the formation of molecular ions  $\text{RhB}^{+\bullet}$  and the formation of  $\text{O}_2^{-\bullet}$ , highly reactive species that will cause the degradation of the organic molecule [30–32]. The principle of this method is relatively simple: the surface of the test specimen is smeared with an aqueous solution of rhodamine B, after which it is exposed to the action of UV rays by combining or not with additional actions, for example, artificial rain. Measurable indicators expressing the degree of staining/cleaning of the surface are then identified and compared [30,33–36]. The UNI 11259 standard regulates this test by indicating the amount of aqueous solution of rhodamine B applied to the surface  $0.05 \text{ g/dm}^2$  and, as a measurable indicator, the measurement of the degree of staining [36]. In the literature, there are reports that comply with this standard, as well as reports of tests performed with deviations from UNI 11259, especially with regard to the concentration of rhodamine B solution ( $0.5 \text{ g/L}$  and  $1 \text{ g/L}$ , respectively) [36].

Using the standardized method or modified methods, the results of the conducted research indicate discoloration by 20% after exposure for 1 min and by 75–95% after exposure for 4 h to the action of UV rays [36]; the dependence of self-cleaning performance on characteristics of titanium dioxide used—granule size, granulometric distribution, type, crystalline structure and ratio of the three crystalline structures (rutile-tetragonal crystalline structure, anatase-tetragonal crystalline structure and brookite-orthorhombic crystalline structure) [30,34,35]; and non-alteration of the photocatalytic efficiency of  $\text{TiO}_2$  nanoparticles following accelerated aging cycles performed on cementitious composites [36]. After the exposure of samples to accelerated aging cycles simulating a period of five years in climatic conditions typical of northern Denmark, good behavior and durability of this property were observed [30,34]. Increased self-cleaning performance with increased  $\text{TiO}_2$  nanoparticle content in the range 0–3% was also observed [33]. Zhang et al. [37] indicated an increase of the self-cleaning effect with the increase of the time of action of the UV rays and a long-term efficiency of this performance for cement composites with the content of up to 6%  $\text{TiO}_2$ ; however, they recommended maintaining the dosage of  $\text{TiO}_2$  to a maximum of 2%. They also indicated a possible reduction in performance with the increase of the irradiation duration, performances that are subsequently recovered as soon as the specimen is subjected to the action of wet-dry cycles, artificial rain and therefore the removal by the washing of reaction products from the surface [37].

Until recently it was considered that these cementitious composites are intended exclusively for outdoor use because of the need for solar radiation and the UV content to activate the TiO<sub>2</sub> nanoparticles. Currently, research has shown that even in indoor conditions, minimum radiation of 1 μW/cm<sup>2</sup> from a fluorescent tube is sufficient to achieve the photocatalytic effect [15].

The aim of this research was to analyze the influence of the addition of TiO<sub>2</sub> nanoparticles in the cementitious composite matrix on the surface hydrophilicity and photochemical degradation capacity of the organic staining agent molecule, as well as to identify an optimal dosage for the TiO<sub>2</sub> nanoparticles in the cementitious matrix, thus providing valuable information for obtaining the self-cleaning capacity as best as possible.

## 2. Materials and Methods

### 2.1. Materials

In order to carry on the tests, prismatic specimens (plates) with an exposed surface of 0.085 m<sup>2</sup> were produced using white Portland cement (CEM I 52.5R) and Degussa P25 TiO<sub>2</sub> nanoparticles in different ratios: 1% (P2), 2% (P3), 3% (P4), 3.6% (P5), 4% (P6), 5% (P7), 6% (P8) and 10% (P8), percentage relative to cement quantity. One mixture was prepared without the addition of TiO<sub>2</sub> nanoparticles, which was considered the control sample (P1). For all cases, the ratio of water/dry powder material of 0.5 was maintained constant, where dry powder material represented the sum of the amounts of cement and TiO<sub>2</sub> nanoparticles in each mixture. After mixing the materials, the test samples were kept for 28 days for aging, according to EN 196 conditions.

### 2.2. Hydrophilicity

The 28 days age test samples, dried until constant mass, were exposed with an inclination of 10° from the vertical. From a constant distance of 30 cm, 5 mL of distilled water were sprayed every 2 min until a cumulative volume of 50 mL was reached. After each test step (after each spray of 5 mL distilled water), the samples were weighted, and the surface water absorption was calculated. After the test, the specimens were dried until constant mass and exposed for 1 h to the action of UV rays with a wavelength in the UVA field and luminous intensity of 405 lux, after which the test was repeated. Subsequently, the samples were dried again until constant mass and exposed to UV for another 24 h, and the test for determination of surface water absorption was repeated [38].

The surface water absorption was calculated as an indirect indicator of the degree of hydrophilicity of the surface of the cementitious composite (Equation (5)):

$$Q_t = (m_t - m_0)/A \text{ (kg/m}^2\text{)} \quad (5)$$

where  $m_t$ —test specimen mass at time  $t$  (2, 4, 6, 8, 10, 12, 14, 16, 18, 20 min) from the start of spraying, which corresponds to sprayers with a volume of (5, 10, 15, 20, 25, 30, 35, 40, 45, 50 mL) distilled water;  $m_0$ —the initial mass of the dry specimen at constant mass;  $A$ —the surface of the specimen exposed to spraying.

For each instance of activation by UV exposure or without UV exposure, the efficiency indicator of the addition of TiO<sub>2</sub> in the cementitious matrix was defined on the surface water absorption property (EIN) representing the percentage variation (increase) of the total surface water absorption (time 20 min, volume of water 50 mL) of the test piece of cementitious composite with the addition of TiO<sub>2</sub> nanoparticles, total surface water (time 20 min, water volume 50 mL) from cementitious composite without the addition of TiO<sub>2</sub> nanoparticles (Equation (6)):

$$EIN = (Q_{20}^{xUV} - Q_{20}^{\text{control sample } xUV})/Q_{20}^{\text{control sample UV}} \cdot 100 \text{ (\%)} \quad (6)$$

where  $Q_{20}^{xUV}$ —surface water absorption of the cementitious composite specimen with TiO<sub>2</sub> nanoparticles addition at time 20 min after the start of the test (50 mL water);  $Q_{20}^{\text{control sample } xUV}$ —surface

water absorption of the control specimen (without TiO<sub>2</sub> nanoparticles addition) at time 20 min after the start of the test (50 mL water); x—number of UV exposure hours (0 h, 1 h or 1 + 24 h).

Thus, indirectly, it can be said that the higher the efficiency index of nanoparticles, the more hydrophilicity increased, the cementitious mixture was more efficient, and the addition of nanoparticles was more effective in improving the performance of the composite.

### 2.3. Self-Cleaning Capacity

The principle of the method consisted of controlled staining, exposure to conditions of activation of the self-cleaning property and determination of the degree of whiteness of the stained surface (GA) as an indirect indicator of the self-cleaning capacity of cementitious composites containing TiO<sub>2</sub> nanoparticles. Thus, the test samples were stained by dripping, using as stain agent an aqueous solution of rhodamine B (1 g/L), applied in equal amounts on the surface of the samples. Subsequently, the samples were subjected to a cycle of action of UV rays, water through artificial rain and drying, according to the test diagram presented in Figure 3. After each step of the test diagram, the degree of whiteness (GA) was measured, and at predetermined intervals, the stained surface of the specimen (AM) was analyzed microscopically.

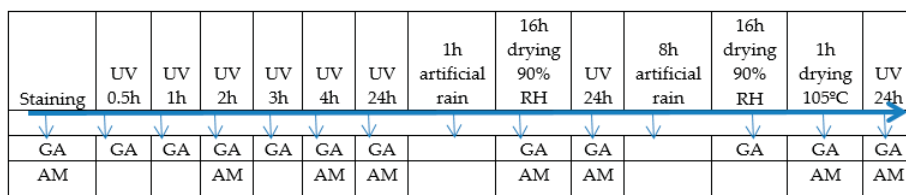


**Figure 3.** Self-cleaning capacity test diagram. GA: the degree of whiteness; AM: the stained surface of the specimen (\*RH - relative humidity).

Photoactivation of the surface was performed using a UV light source with emission in the spectrum 315–400 nm, corresponding to the UVA band. To assess the influence of UV radiation intensity on self-cleaning capacity, the irradiation source was placed at a distance of 10 cm and 20 cm for the second phase, above the surface of the specimens, which resulted in a luminous flux intensity of 860 lux and 405 lux, respectively. Exposure to artificial rain and drying were carried out in the absence of any light source.

The test equipment was composed of the following individual stations: UVA source exposure enclosure; artificial rain exposure enclosure; visual analysis area; microscopic analysis area and whiteness degree recording area. The degree of whiteness was measured with a WSB-1 leukometer.

The efficiency of the addition of TiO<sub>2</sub> nanoparticles on the self-cleaning character of the cementitious composite was analyzed visually and through two measurable parameters:

- Degree of the whiteness of the sample, determined in the stained area;
- Degree of the ability to recover the whiteness—represents, as a percentage, how much of the whiteness degree of the stained sample was recovered in relation to the initial whiteness degree, after going through one or more steps in the test diagram (Equation (7)):

$$CR = ((GA_t - GA_0)/GA_c) \cdot 100 (\%) \tag{7}$$

where CR = ability to recover the degree of whiteness, GA<sub>t</sub> = the degree of whiteness of the specimen in the stained area at test chart time t, GA<sub>0</sub> = the initial degree of whiteness of the stained sample but not yet exposed to UV light activation or washing, and GA<sub>c</sub> = the initial degree of whiteness of the unstained sample.

On the basis of these measurable indicators, it was thus assessed that the greater the whiteness degree and the recovery capacity of the whiteness degree increase from one step of the test diagram to another, the more pronounced the self-cleaning effect.

### 3. Results and Discussion

#### 3.1. Hydrophilicity

The results obtained from the point of view of the measurable parameters identified for the indirect measurement of the hydrophilicity of the surface of the cement compounds and with respect to the kinetics of the process are shown in Figures 4 and 5.

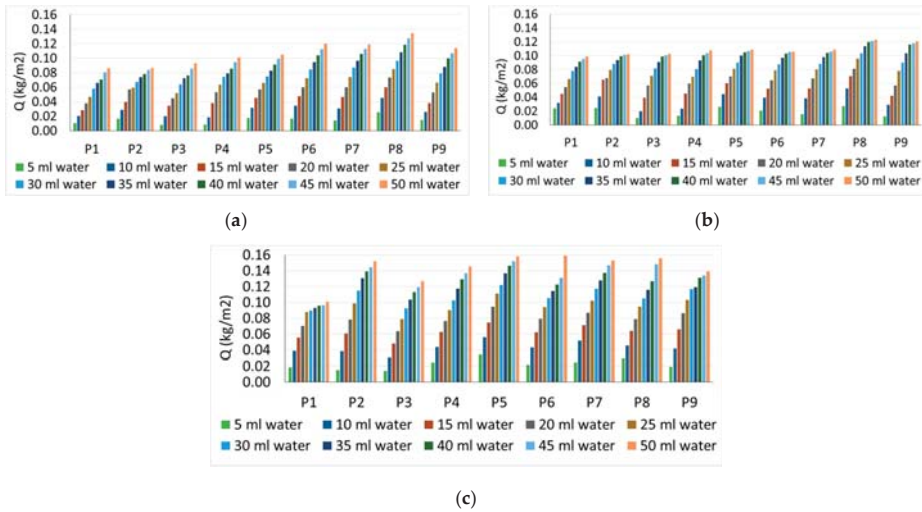


Figure 4. Surface water absorption: (a) non-UV specimens; (b) 1 h UV specimens; (c) 1 + 24 h UV specimens.

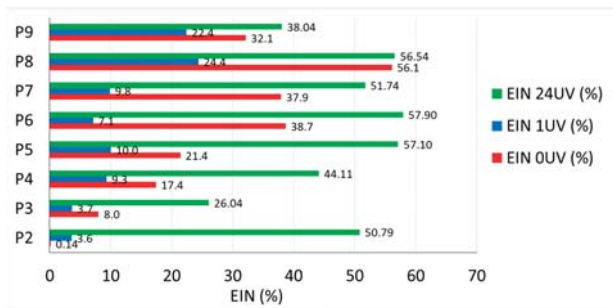


Figure 5. Efficiency Index of Nanoparticles (EIN): non-UV test specimens (red), 1 h UV test specimens (blue), 1 + 24 h UV test specimens (green).

Surface water absorption (Figure 4) increases continuously and steadily for all analyzed cases with the increase in the amount of water sprayed. This increase can be expressed mathematically by a Grade 1 equation according to the amount of water sprayed, in the form of  $ax + b$ , for each case analyzed. It is noted that the maximum water absorption is in the case of P8 composition with 6% TiO<sub>2</sub>, for all situations of the amount of water sprayed, therefore it is appreciated that this composite matrix has the highest hydrophilicity in conditions not exposed to UV, respectively exposure for 1 h to the action

of UV rays. In the case of samples exposed 1 + 24 h to UV action, the maximum water absorption is initially in the case of composition P5 (3.6% TiO<sub>2</sub>), followed very closely by P8 (6% TiO<sub>2</sub>), but with the advance of the test (increasing the amount of water sprayed, there is an increase in water absorption for all specimens in the range P2–P8 (1% TiO<sub>2</sub>–6% TiO<sub>2</sub>). Increasing the amount of TiO<sub>2</sub> over 6% causes a reduction of water absorption on the surface, which indicates a reduction of hydrophilicity (P9–10% TiO<sub>2</sub>). Sample P2 (1% TiO<sub>2</sub>) in the case of test specimens not exposed to UV action and samples P2 (1% TiO<sub>2</sub>) and P3 (2% TiO<sub>2</sub>) in the case of test specimens exposed for 1 h to UV action indicate rather small changes in hydrophilicity, compared to the control. It can thus be considered that the addition of 1–2% TiO<sub>2</sub> in the cementitious matrix is insufficient. The slight flattening of the curve, with the increase of the amount of water sprayed, can be considered as a measure of the tendency of stabilization of the phenomenon to achieve a maximum of the amount of water absorbed on the surface, after which the excess water has a chance to slip on the existing.

In all cases, as expected, the control sample (P1) shows a much-reduced evolution of the process of water absorption on the surface, compared to the composite samples with nanoparticles content, a sign that this surface is less hydrophilic, most of the amount of water remaining, probably, as drops that fail to form a film and fall easily.

In general, it can be said that at the beginning of the process (small amounts of water sprayed), the evolution of water absorption on the surface from one spray to the next is more strongly influenced by the amount of TiO<sub>2</sub>. As the amount of water sprayed increases, the absorption process on the surface stabilizes, the percentage of water added by each spray generally decreasing.

As seen in Figure 5, for samples tested without UV exposure and those tested with 1 h UV exposure, respectively, sample P8 (6% TiO<sub>2</sub>) shows the highest efficiency in terms of the influence of the addition of TiO<sub>2</sub> on surface hydrophilicity compared to the control sample, but sample P9 (10% TiO<sub>2</sub>) indicates a reduced efficiency of the addition of nanoparticles on surface hydrophilicity, even though the quantity of nanoparticles in the matrix is the highest. In the case of test specimens tested after 1 + 24 h exposure to UV rays, samples P6 (4% TiO<sub>2</sub>) and P5 (3.6% TiO<sub>2</sub>) have the highest efficiency in terms of the influence of the addition of TiO<sub>2</sub> on the surface hydrophilicity, compared to the control sample.

### 3.2. Self-Cleaning

Visually, evolution according to expectations was observed: discoloration of the stained area, both for exposure to UVA with the intensity of 860 lux and for the intensity of 405 lux, as shown, for example, for the control specimen made of the cementitious composite without TiO<sub>2</sub> content and for the specimen made of cementitious composite with 4% TiO<sub>2</sub> content in Figures 6 and 7, respectively.

The results obtained from the point of view of the measurable parameters identified for measuring the self-cleaning capacity are shown in Figures 8 and 9.



**Figure 6.** Discoloration of test specimens following the test diagram, example P1—control specimen made of the cementitious composite without TiO<sub>2</sub> content: before (a) and after (b) the test diagram, with luminous intensity 860 lux; before (c) and after (d) the test diagram, with luminous intensity 405 lux.

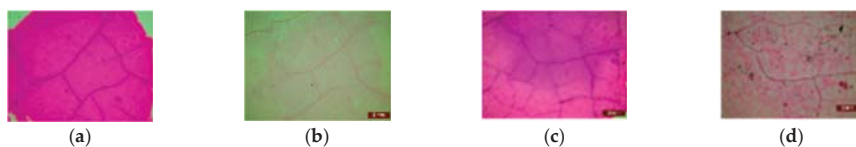


**Figure 7.** Discoloration of test specimens following the test diagram, example P5—test specimen made of the cementitious composite with 4% TiO<sub>2</sub> content: before (a) and after (b) the test diagram, with luminous intensity 860 lux; before (c) and after (d) the test diagram, with luminous intensity 405 lux.

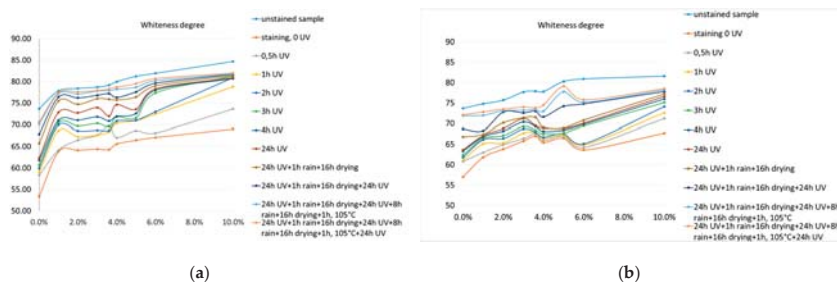


**Figure 8.** Whiteness degree: (a) test diagram with the luminous intensity 860 lux; (b) test diagram with the luminous intensity 405 lux.

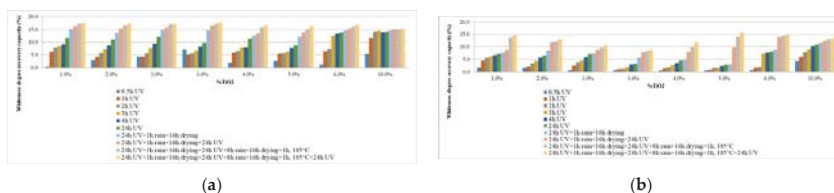


**Figure 9.** Whiteness degree recovery capacity: (a) test diagram with light intensity 860 lux; (b) test diagram with light intensity 405 lux.

Immediately after staining, the degree of whiteness of the specimens is significantly reduced, as expected (Figure 8), thus obtaining a degree of staining, expressed as a percentage reduction of the degree of whiteness, within the range (18.0–27.6%). By exposing stained specimens to the photocatalytic action of UV, the degree of whiteness increases steadily (Figure 8) with each evaluation after the preset exposure ranges (0.5 h, 1 h, 2 h, 3 h, 4 h, 24 h). Visually the discoloration of the spots is observed, and the microscopic analysis showed that there is a discoloration especially of the surface in the immediate vicinity of the micro-cracks that appeared during the ripening process. An exception is the control specimen made without the addition of TiO<sub>2</sub> nanoparticles: in this case, only a slight discoloration is observed, a phenomenon explained, on the one hand, due to the chemical degradation of the staining agent under the influence of UV, and on the other hand, due to the existence, from the manufacturing process, of a quantity of TiO<sub>2</sub>, even if not much. Analyzing the evolution of the degree of whiteness of the test specimens throughout the course of the test diagram, a significant jump is observed, in most cases, with the introduction of the washing agent, artificial rain, both in the case of high-intensity and low-intensity UV radiation.

The evolution of the control specimen is the least satisfactory, remaining intently stained throughout many stages of the test diagram, undergoing a cleaning process, probably more mechanical by the action of water droplets, its discoloration being more evident after the last two steps of the test diagram.



From the point of view of the mathematical modeling possibility of the evolution of the degree of whiteness, depending on the amount of nanoparticles added in the cement matrices, one can identify polynomial functions of degree 3 that provide a precision rate  $R^2$  minimum 0.8.

If analyzing, from the point of view of the ability to recover the degree of whiteness (Figure 9), the behavior of cementitious matrices in the presence of UV radiation with the intensity of 860 lux, but without the action of rain, one could say that content of  $\text{TiO}_2$  nanoparticles, in relation to the amount of cement, of around 6% is desirable. With the introduction of artificial rain/drying agents into the test diagram, the behavior of the test specimens' changes, suggesting a concentration of max. 4%  $\text{TiO}_2$  nanoparticles in the cementitious matrix. The same cannot be said about test specimens tested at an incident UV radiation of lower intensity (405 lux), where a higher concentration of  $\text{TiO}_2$  nanoparticles in the cementitious matrix would be desirable.

Tests carried out by the method of staining with rhodamine B provide evidence of the self-cleaning ability of cementitious matrices enriched with  $\text{TiO}_2$  nanoparticles by photoactivation under the influence of UVA rays. However, the experimental results obtained cannot provide the basis for a documented selection of the optimal nanoparticle content, so that the cost–benefit balance is the most favorable. It is considered, therefore, that further research is needed, as well as a correlation between the results obtained by experiments, on the one hand, with the other results reported in the literature and, on the other hand, the results obtained by experiments on the evolution of the physical-mechanical properties of the cementitious matrix based on the content of the nanoparticles, together with an analysis from the point of view of whether or not the field is intended to be used.

#### 4. Conclusions

The aim of this experimental study was to analyze the influence of the content of nanoparticles in the cement matrix on the two mechanisms that together realize the property of self-cleaning.

After analyzing, as an indirect indicator of hydrophilicity, the surface water absorption of all specimens, tested in all three conditions of exposure to the action of UV rays, it can be said that regardless of the content of  $\text{TiO}_2$  nanoparticles, in all cases, exposure to UV increases the hydrophilicity of the surface, compared to the situation of a lack of this exposure and the increase. The satisfactory behavior of P8 samples (6%  $\text{TiO}_2$ ) and the unsatisfactory behavior of P9 samples (10%  $\text{TiO}_2$ ), as well as the behavior strongly dependent on the UV exposure conditions of cementitious matrices with a low content of  $\text{TiO}_2$  nanoparticles, can easily be observed.

From the point of view of the decomposition capacity of the organic molecule rhodamine B, it can be said that the increase of the amount of  $\text{TiO}_2$  introduced in the cementitious matrix increases the degree of whiteness but also the self-cleaning capacity of the specimens. The self-cleaning capacity is also influenced by the intensity of the incandescent UV light flux on the surface of the sample, better results being recorded for a higher UVA intensity. In the absence of the action of rain (without accumulating the effect of increasing the hydrophilicity of the surface), it can be said that in case of a lower incident UV radiation a higher concentration of nanoparticles in the cementitious matrix is desirable. This need, however, can be reduced either by increasing the intensity of UV radiation or by combining with the action of washing water (the jump of the cleaning index being significant with the first step of artificial rain in the test diagram). However, it can be assessed that, from a cost-benefit point of view, a concentration of 10%  $\text{TiO}_2$  nanoparticles is not justified because the improvement of quantifiable parameters compared to those recorded for the 6%  $\text{TiO}_2$  composition is not proportional to the consumption of nanoparticles.

**Author Contributions:** Conceptualization, A.H. and E.G.; methodology, A.H., E.G., H.S., A.-V.L. and B.A.I.; formal analysis, A.H., E.G., H.S., A.-V.L. and B.A.I.; investigation, A.H., E.G., H.S., A.-V.L. and B.A.I.; writing—original draft preparation, A.H. and E.G.; writing—review and editing, A.H., E.G., H.S. and A.-V.L.; visualization, A.H., E.G., H.S. and A.-V.L.; supervision, H.S. All authors have read and agreed to the published version of the manuscript.

**Funding:** This research received no external funding.



**Acknowledgments:** Authors would like to thank Evonik Industries AG Hanau, Germany, for the donations of the necessary materials used in the current study.

**Conflicts of Interest:** The authors declare no conflict of interest.

## References

1. Graziani, L.; Quagliarini, E.; Bondioli, F.; D’Orazio, M. Durability of self-cleaning TiO<sub>2</sub> coatings on fired clay brick façades: Effects of UV exposure and wet & dry cycles. *Build. Environ.* **2014**, *71*, 193–203.
2. Cucek, L.; Klemes, J.J.; Kravanja, Z. A review of footprint analysis tools for monitoring impacts on sustainability. *J. Clean. Prod.* **2012**, *34*, 9–20. [[CrossRef](#)]
3. Chiarini, A. Designing an environmental sustainable supply chain through ISO 14001 standard. *Manag. Environ. Qual. Int. J.* **2012**, *24*, 16–33. [[CrossRef](#)]
4. Chiarini, A. Strategies for developing an environmentally sustainable supply chain: Differences between manufacturing and service sectors. *Bus. Strat. Environ.* **2014**, *23*, 493–504. [[CrossRef](#)]
5. Fox, M.A.; Chen, C.C. Mechanistic features of the semiconductor photocatalyzed olefin-to-carbonyl oxidative cleavage. *J. Am. Chem. Soc.* **1981**, *103*, 6757–6759. [[CrossRef](#)]
6. Cunningham, J.; Srijaranai, S. Isotope-effect evidence for hydroxyl radical involvement in alcohol photo-oxidation sensitized by TiO<sub>2</sub> in aqueous suspension. *J. Photochem. Photobiol. A Chem.* **1988**, *43*, 329–335. [[CrossRef](#)]
7. Brezová, V.; Stasko, A.; Lapcik, L., Jr. Electron paramagnetic resonance study of photogenerated radicals in titanium dioxide powder and its aqueous suspensions. *J. Photochem. Photobiol. A Chem.* **1991**, *59*, 59–115. [[CrossRef](#)]
8. Kamat, P.V. Photochemistry on nonreactive and reactive (semiconductor) surfaces. *Chem. Rev.* **1993**, *93*, 267–300. [[CrossRef](#)]
9. Courbon, H.; Formenti, M.; Pichat, P.J. Study of oxygen isotopic exchange over ultraviolet irradiated anatase samples and comparison with the photooxidation of isobutane into acetone. *Phys. Chem.* **1977**, *81*, 550–554. [[CrossRef](#)]
10. Anpo, M.; Chiba, K.; Tomonari, M.; Coluccia, S.; Che, M.; Fox, M.A. Photocatalysis on Native and Platinum-Loaded TiO<sub>2</sub> and ZnO Catalysts —Origin of Different Reactivities on Wet and Dry Metal Oxides. *Bull. Chem. Soc. Jpn.* **1991**, *64*, 543–551. [[CrossRef](#)]
11. Sun, L.; Bolton, J.R. Determination of the Quantum Yield for the Photochemical Generation of Hydroxyl Radicals in TiO<sub>2</sub> Suspensions. *J. Phys. Chem.* **1996**, *100*, 4127–4134. [[CrossRef](#)]
12. Grela, M.A.; Coronel, M.E.J.; Colussi, A.J. Quantitative Spin-Trapping Studies of Weakly Illuminated Titanium Dioxide Sols. Implications for the Mechanism of Photocatalysis. *J. Phys. Chem.* **1996**, *100*, 16940–16946. [[CrossRef](#)]
13. Fujishima, A.; Rao, T.N.; Tryk, D.A. Titanium dioxide photocatalysis. *J. Photochem.* **2000**, *1*, 1–21. [[CrossRef](#)]
14. Quagliarini, E.; Bondioli, F.; Goffredo, G.B.; Cordoni, C.; Munafo, P. Self-cleaning and de-polluting stone surfaces: TiO<sub>2</sub> nanoparticles for limestone. *Constr. Build. Mater.* **2012**, *37*, 51–57. [[CrossRef](#)]
15. Irie, H.; Hashimoto, K. Photocatalytic Active Surfaces and Photo-Induced High Hydrophilicity/High Hydrophobicity. *Hdb. Environ. Chem.* **2005**, *2*, 425–450.
16. Chen, J.; Poon, C.-S. Photocatalytic construction and building materials: From fundamentals to applications. *Build. Environ.* **2009**, *44*, 1899–1906. [[CrossRef](#)]
17. Fujishima, A.; Zhang, X. Titanium dioxide photocatalysis: Present situation and future approaches. *CR Chim.* **2006**, *9*, 750–760. [[CrossRef](#)]
18. Guan, K. Relationship between photocatalytic activity, hydrophilicity and self-cleaning effect of TiO<sub>2</sub>/SiO<sub>2</sub> films. *Surf. Coat. Technol.* **2005**, *191*, 155–160. [[CrossRef](#)]
19. Lee, Y.C.; Hong, Y.P.; Lee, H.Y.; Kim, H.; Jung, Y.J.; Ko, K.H. Photocatalysis and hydrophilicity of doped TiO<sub>2</sub> thin films. *J. Colloid Interf. Sci.* **2003**, *267*, 127–131. [[CrossRef](#)]
20. Graziani, L.; Quagliarini, E.; Osimani, A.; Aquilanti, L.; Clementi, F.; Yéprémian, C. Evaluation of inhibitory effect of TiO<sub>2</sub> nano-coatings against microalgal growth on clay brick façades under weak UV exposure conditions. *Build. Environ.* **2013**, *64*, 38–45. [[CrossRef](#)]
21. Li, C.; Chang, S.J.; Tai, M.Y. Surface chemistry and dispersion property of TiO<sub>2</sub> nanoparticles. *J. Am. Ceram. Soc.* **2010**, *93*, 4008–4010. [[CrossRef](#)]

22. Yu, J.; Low, J.; Wei, X. Enhanced photocatalytic CO<sub>2</sub>-reduction activity of anatase TiO<sub>2</sub> by Co-exposed {001} and {101} facets. *J. Am. Chem. Soc.* **2014**, *136*, 8839–8842. [CrossRef]
23. Wang, R.; Hashimoto, K.; Fujishima, A.; Chikuni, M.; Kojima, E.; Kitamura, A.; Shimohigoshi, M.; Watanabe, T. Photogeneration of Highly Amphiphilic TiO<sub>2</sub> Surfaces. *Adv. Mater.* **1998**, *10*, 135–138. [CrossRef]
24. Wang, R.; Sakai, N.; Fujishima, A.; Watanabe, T.; Hashimoto, K.J. Studies of Surface Wettability Conversion on TiO<sub>2</sub> Single-Crystal Surfaces. *Phys. Chem. B.* **1999**, *103*, 2188–2194. [CrossRef]
25. Nosaka, A.Y.; Kojima, E.; Fujiwara, T.; Yagi, H.; Akutsu, H.; Nosaka, Y.J. Photoinduced Changes of Adsorbed Water on a TiO<sub>2</sub> Photocatalytic Film As Studied by 1H NMR Spectroscopy. *Phys. Chem. B* **2003**, *107*, 12042–12044. [CrossRef]
26. Shen, W.; Zhang, C.; Li, Q.; Zhang, W.; Cao, L.; Ye, J. Preparation of titanium dioxide nano particle modified photocatalytic self-cleaning concrete. *J. Clean. Prod.* **2015**, *87*, 762–765. [CrossRef]
27. Sakai, N.; Fujishima, A.; Watanabe, T.; Hashimoto, K.J. Enhancement of the Photoinduced Hydrophilic Conversion Rate of TiO<sub>2</sub> Film Electrode Surfaces by Anodic Polarization. *Phys. Chem. B* **2001**, *105*, 3023–3026. [CrossRef]
28. Aslanidou, D.; Karapanagiotis, I.; Lampakis, D. Waterborne Superhydrophobic and Superoleophobic Coatings for the Protection of Marble and Sandstone. *Materials* **2018**, *11*, 585. [CrossRef]
29. Manoudis, P.N.; Tsakalof, A.; Karapanagiotis, I.; Zuburtikudis, I.; Panayiotou, C. Fabrication of super-hydrophobic surfaces for enhanced stone protection. *Surf. Coat. Technol.* **2009**, *203*, 1322–1328. [CrossRef]
30. Folli, A.; Jakobsen, U.H.; Guerrini, G.L.; Macphee, D.E. Rhodamine B Discolouration on TiO<sub>2</sub> in the Cement Environment: A Look at Fundamental Aspects of the Self-cleaning Effect in Concrete. *J. Adv. Oxid. Technol.* **2009**, *12*, 126–133. [CrossRef]
31. Wu, T.; Liu, G.; Zhao, J.; Hidaka, H.; Serpone, N.J. Photoassisted degradation of dye pollutants. V. Self-photosensitized oxidative transformation of rhodamine B under visible light irradiation in aqueous TiO<sub>2</sub> dispersions. *Phys. Chem. B* **1998**, *102*, 5845–5851. [CrossRef]
32. Chen, F.; Zhao, J.; Hidaka, H. Highly selective deethylation of rhodamine B: Adsorption and photooxidation pathways of the dye on the TiO<sub>2</sub>/SiO<sub>2</sub> composite photocatalyst. *Int. J. Photoenergy* **2003**, *5*, 209–217. [CrossRef]
33. Khataee, R.; Heydari, V.; Moradkhannejhad, L.; Safarpour, M.; Joo, S.W. Self-Cleaning and Mechanical Properties of Modified White Cement with Nanostructured TiO<sub>2</sub>. *J. Nanosci. Nanotechnol.* **2013**, *13*, 5109–5114. [CrossRef] [PubMed]
34. Folli, A. TiO<sub>2</sub> Photocatalysis in Portland Cement Systems: Fundamentals of Self-Cleaning Effect and Air Pollution Mitigation. Ph.D. Thesis, University of Aberdeen, Department of Chemistry, Aberdeen, UK, 2010.
35. Bianchi, C.L.; Gatto, S.; Nucci, S.; Cerrato, G.; Capucci, V. Self-cleaning measurements on tiles manufactured with micro-sized photoactive TiO<sub>2</sub>. *Adv. Mater. Res.* **2013**, *2*, 1–10. [CrossRef]
36. Carmona-Quiroga, P.M.; Martínez-Ramírez, S.; Viles, H.A. Efficiency and durability of a self-cleaning coating on concrete and stones under both natural and artificial ageing trials. *Appl. Surf. Sci.* **2018**, *433*, 312–320. [CrossRef]
37. Zhang, S.M.-H.; Tanadi, D.; Li, W. Effect of photocatalyst TiO<sub>2</sub> on workability, strength, and self-cleaning efficiency of mortars for applications in tropical environment. In Proceedings of the 35th Conference on Our World in Concrete & Structures, Singapore, 25–27 August 2010; Available online: <http://cipremier.com/100035009> (accessed on 8 February 2020).
38. Hegyi, A.; Szilagyí, H.; Grebenişan, E.; Sandu, A.V.; Lăzărescu, A.-V.; Romila, C. Influence of TiO<sub>2</sub> Nanoparticles Addition on the Hydrophilicity of Cementitious Composites Surfaces. *Appl. Sci.* **2020**, *10*, 4501. [CrossRef]

**Publisher's Note:** MDPI stays neutral with regard to jurisdictional claims in published maps and institutional affiliations.



© 2020 by the authors. Licensee MDPI, Basel, Switzerland. This article is an open access article distributed under the terms and conditions of the Creative Commons Attribution (CC BY) license (<http://creativecommons.org/licenses/by/4.0/>).



# Behavior of Natural Organic Polymer-Based Plaster Mortars under the Influence of Water <sup>†</sup>

Alexandra Olga Pintea <sup>1,\*</sup>, Marta Ioana Moldoveanu <sup>1</sup> and Daniela Lucia Manea <sup>2</sup>

<sup>1</sup> Faculty of Civil Engineering, Technical University of Cluj-Napoca, C. Daicovicu Street 15, 400020 Cluj-Napoca, Romania; Marta.Moldoveanu@ccm.utcluj.ro

<sup>2</sup> Faculty of Civil Engineering, Technical University of Cluj-Napoca, Memorandumului Street 28, 400411 Cluj-Napoca, Romania; Daniela.Manea@ccm.utcluj.ro

\* Correspondence: alexandra\_pintea91@yahoo.com

<sup>†</sup> Presented at the 14th International Conference INTER-ENG 2020 Interdisciplinarity in Engineering, Mures, Romania, 8–9 October 2020.

Published: 3 February 2021

**Abstract:** The influence of polymers upon building materials has been present since ancient times, but it was neglected for a long period. The present research discusses the effect of natural organic polymers (casein, rice, egg) in the formula of classical plastering according to the experimental research aiming at finding out the water absorption coefficient and the softening coefficient. The main objective of this work lies in identifying the most performance-related natural polymer which can determine the most efficient impermeability that can lead to the best values for the plaster mortar formula.

**Keywords:** plaster mortar; water absorption; casein; rice; egg

## 1. Introduction

Our research has identified a large variety of additives to be found in historical buildings, such as casein, beer, and master oils. Various additives have been applied to historical buildings, including polysaccharides, used either as powder or glue, proteins originating in animal glues, and casein. The research established that the use of such additives leads to the improvement of mechanical properties and the increase of resistance to water [1].

Due to the capillary rise of water in the ground or from infiltration, there comes out the issue of humidity in masonry leading to wall damaging and worse building materials properties. The phenomenon manifests in the poor adherence of paint, and in worse cases in plaster detaching. Humidity rise remains a constant issue in time which has a high impact on the costs for all of the building's life.

According to the findings of Dorin-Victor POPA in the book "Contributions to the theory and practice of historical and social cultural buildings foundations and walls drainage" [2], there is a direct infiltration when the foundation masonry is in direct contact with the underground water when the material of the masonry is saturated with water which rises through capillarity phenomena in the masonry weight.

When the surfaces of the foundations are not in direct contact with the underground water, it however reaches the surfaces due to the capillary forces in the pores (the smaller the soil grains and pores, the stronger such forces). In general, the liquid does not maintain the same level, but it rises more with a smaller column section. This is the reason for which the water rise level is inversely proportional to the pore diameter [3].

When the masonry is made with rocks that do not have the capacity of capillary absorption, the humidity capillary rise will be diminished and the means of getting to the member surface lies only in the mortar layers. This is the reason for which the Romans used, in masonry elevations, porous

materials such as volcanic rock which has a high water absorption capacity and also a good thermal insulation property, while for the foundations, they used solid and compact materials such as granite. The thicker the masonry member, the higher the vertically transmitted humidity [4].

The research established that the use of natural polymers as additives in the plaster mortar improves the mechanical properties and the property of resistance to water, as well as the differing speeds of carbonation and textures. The natural polymers, in compatible traditional building materials, are utilized in the restoration of the architectural heritage and modern architecture [5–8]. Starch alters the air content, the density, the water retaining capacity, the setting time, and other properties. The cactus extract increases plasticity, water absorption, and stabilizes resistance to salt. Using jaggery in concrete mixtures improves workability and reduces segregation. Animal glue in mortars improves mechanical strength. Olive oil ameliorates mortar imperviousness. Jelly rice paste, the gluey liquid made from elm wood chips, other additions, the dark brown glue from the sugar stems and leaves, oils, egg whites, liquid resins, cactus sticky liquid, latex from natural rubber are proteins and natural polymers identified in mortars [9–13].

The softening coefficient is defined as the ratio between the resistance to compression of the water-saturated material and of the dry material. It is the property of the materials of not destroying or essentially modifying properties under long-term water saturation influence.

## **2. Materials and Methods**

### *2.1. Materials*

Our formulae contained grade CEM I 42.5 R cement, which is a pure cement used for not affecting the properties at all and surveying only the influence of the polymer amount in the mixture. The aggregates used in the formulae were taken from a gravel pit from the Someş riverbank and were of size 0–4 mm. The water used in the tests was taken from the local water distribution network in Cluj-Napoca. The polymers under question were casein, rice, and egg. Casein is a protein extracted from milk, dried, and then milled. The rice grains were ground, for one formula being boiled and the water strained after boiling was used. The egg used was uncooked and fresh [1]. For more details regarding the materials used in the formulae, see the article “Influence of Natural Organic Polymers upon Plaster Mortar Workability” [14].

### *2.2. Methods*

The tests were carried out in the Building Materials Laboratory of the Faculty of Civil Engineering in Cluj-Napoca. The research methodology required the elaboration of our own plaster mortar formulae, to which natural polymers were added as additives and the determination of the water absorption content and softening coefficient according to SR EN 1015-18:2004 [15].

#### **2.2.1. Determination of the Water Absorption Coefficient**

The water absorption coefficient caused by capillary action was measured in prismatic mortar specimens, in well-defined conditions, at atmospheric pressure. After drying up to the constant weight. A face of the specimen was immersed in 5–10 mm water, for a specified time interval. In this way, the weight increase was determined.

For this determination, one requires a vessel with a minimum height of 20 mm and a plane surface large enough to contain the immersed specimens. The vessel should be provided with a device to maintain a constant water level. In order to put the specimen at an acceptable distance from the vessel bottom, one needs four supports or similar elements for each specimen that allow only a minimum contact surface with the specimen. For sealing purposes, paraffin or a reactive synthetic resin with a melting point higher than 60 degrees Celsius can be used.

The preparation and drying of the specimens were done in accordance with SR EN 1015-11 [16]. The sealing material was applied to the four long faces of the specimen and then they were crushed into

two pieces. They were dried until getting to a constant weight in a ventilated dry kiln, at a temperature of 60 degrees Celsius  $\pm$ 5 degrees Celsius. The constant weight is reached when, after two successive measurements made in an interval of 24 h during drying, the amount of water loss is smaller than or equal to 0.2% of the total weight.

The specimens are placed in the vessel with the fractured prism surface towards the bottom of the vessel, fitted onto the four supports so that the vessel bottom is not touched and the depth of immersion is 5–10 mm during testing. (See Figure 1). Air bubble formation under the specimens should be avoided.



Figure 1. Immersed specimens.

After 10 min, the specimens were taken out of the vessel, quickly dried with a wet cloth, weighted, and replaced in the vessel. The procedure was repeated 90 min later (Equation (1)). After 24 h, they were weighted again, then specimens were broken along their length so that prisms of the approximate size of 80  $\times$  40  $\times$  20 mm were obtained. The water penetration height at the specimen center was measured parallel to the length of 80 mm, with a deviation of a maximum of 1 mm.

$$C = 0.1(M_{90} - M_{10}) \text{ kg}/(\text{m}^2 \text{ min}^{0.5}), \quad (1)$$

The capillarity caused water absorption coefficient was by definition equal to the straight line slope uniting the significant points of the measurements performed at 10 and 90 min, respectively (Equation (2)). For repair mortars, the water absorption at 24 h was calculated as follows [15].

$$C = 0.625(M_{24} - M_0) \text{ kg}/\text{m}^2, \quad (2)$$

### 2.2.2. Determination of the Softening Coefficient

This coefficient reflects the property of the materials of not destroying or essentially modifying their property under the effect of long-term water saturation. This property is estimated through the softening coefficient ( $K$ ), defined as the ratio between the resistance to compression of the water-saturated material ( $R_s$ ) and the resistance of the dry material ( $R_u$ ) (Equation (3)).

$$K = \frac{R_s}{R_u}, \quad (3)$$

For the purpose of this determination, it is necessary to use a minimum of three samples. The determination was carried out on the halves of three broken specimens, after performing the flexural tensile stress. Three prism halves were preserved by immersing them in a vessel with water, in accordance with the conditions stipulated in the norm SR EN 1015, and the other three prism halves were immersed in a vessel with water where water passed by 1 cm the prisms (See Figure 2). The samples were left in water until they reached a constant weight. No protecting cover was applied onto the surface of the samples.



**Figure 2.** Fully water-soaked specimens.

After these wet samples reached a constant weight, they were tested for compression. The dry samples were also tested for compression on the same day. The ratio between the resistance to compression of the wet samples and the resistance to compression of the dry samples gives the softening coefficient (*K*).

### 3. Results and Discussion

#### 3.1. Determination of the Water Absorption Coefficient

In order to study the water absorption level, six specimens of size 160 × 40 × 40 mm were made for each formula. They were tested to the flexural tensile stress and then the prism halves were tested for water absorption.

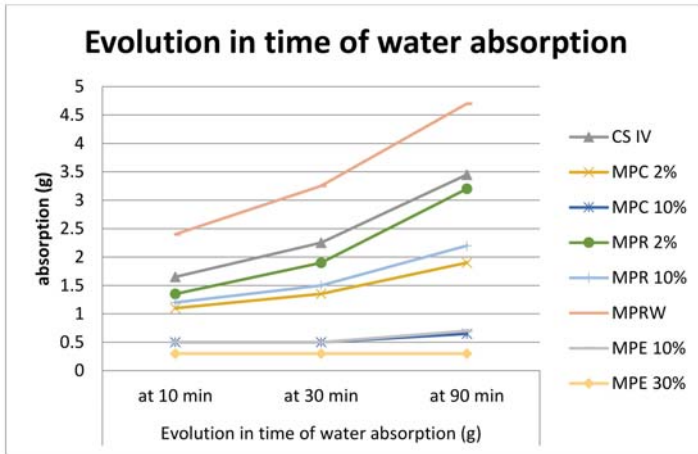
Table 1 presents the average values for water absorption (g) in the case of the mortars under investigation for the purpose of the present article.

**Table 1.** Average values for water absorption.

Formula	Evolution in Time of Water Absorption (g)		
	at 10 min	at 30 min	at 90 min
CS IV	1.65	2.25	3.45
MPC 2%	1.1	1.35	1.9
MPC 10%	0.5	0.5	0.65
MPR 2%	1.35	1.9	3.2
MPR 10%	1.2	1.5	2.2
MPRW	2.4	3.25	4.7
MPE 10%	0.5	0.5	0.7
MPE 30%	0.3	0.3	0.3

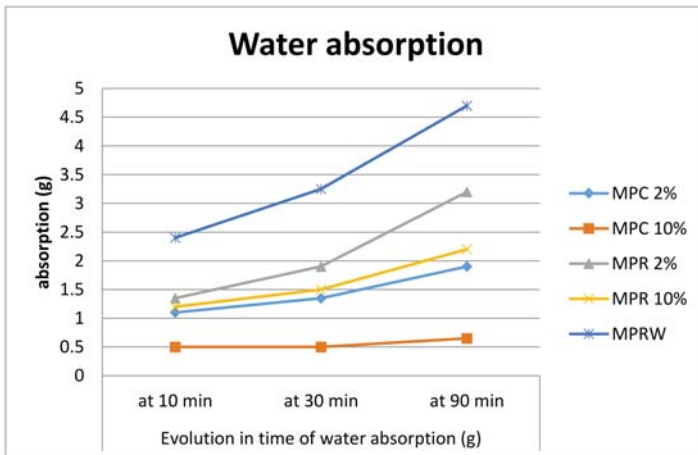
The name of the formulae has the following meaning: CS IV—cement plaster mortar (no additives); MPC 2%—CS IV mortar with 2% casein; MPC 10%—CS IV mortar with 10% casein; MPR 2%—CS IV mortar with 2% rice; MPR 10%—CS IV mortar with 10% rice; MPRW 2%—CS IV product with rice water; MPE 10%—CS IV mortar with 10% egg white; MPE 30%—CS IV mortar with 30% egg white.

Figure 3 shows that the conventional plaster mortar formula (CS IV) absorbs the highest amount of water, immediately after the rice water formula (MPRW). In the rest of the formulae, it is also visible that the polymer has a positive influence in so far as water absorption is concerned. Formula MPC 10% is thus one of the best formulae for water absorption, placed in the second position together with MPE 10%. The formula MPE 30% lies in the first place. It is noticed that the polymer has an influence through its low water absorption, which diminishes by adding polymers.



**Figure 3.** Graphical representation of water absorption at 10, 30, and 90 min for the mortars included in the experimental program.

Figure 4 presents water absorption at 10, 30, and 90 min for the formulae MPC 2%, MPC 10%, MPR 2%, MPR 10%, MPRW. In Figure 4, one can notice that the rice effect is not so beneficial as casein influence is, for water absorption. The values of the mortars containing rice increase with time, while in the mortars with casein, these values come to a standstill or the rise is very small. All the rice-based mortar formulae present higher values of water absorption than casein-based mortar formulae. Formula MPRW exhibits the highest water absorption level. Probably as the rice water left many capillary pores when evaporating. The higher the rice content in the mortar formulae, the lower water absorption. Mortar formulae with casein exhibit the lowest level of water absorption. At 10 min, formulae MPR 2%, MPR 10%, MPC 2% absorb approximately the same amount of water.



**Figure 4.** Graphical representation of water absorption at 10, 30, and 90 min for the mortars MPC 2%, MPC 10%, MPR 2%, MPR 10%, MPRW.

Figure 5 presents water absorption at 10, 30 and 90 min for formulae MPR 2%, MPR 10%, MPRW, MPE 10%, MPE 30%. In Figure 5, one can notice that similar to the previous case, rice-based mortars (MPR 2%, MPR 10%, MPRW) have higher values for water absorption as compared to egg white



based mortars (MPE 10%, MPE 30%). The higher the egg white content in mortars, the smaller the water absorption. The influence of the egg is obvious by comparison with that of the rice. The water absorption values of the rice-containing mortars increase in time, while those containing eggs stagnate or increase very poorly. Mortar MPE 10% has water absorption during the first 10 minutes, after 30 min it stops absorbing water and after 90 min it absorbs water very little. Mortar MPE 30% absorbs water during the first 10 min and then it stops absorbing water. In so far as water absorption is concerned, the best formulae is MPE 30%, followed by both MPE 10% and MPC 10%. The presence of the egg white in the mortar composition interrupts capillarity.

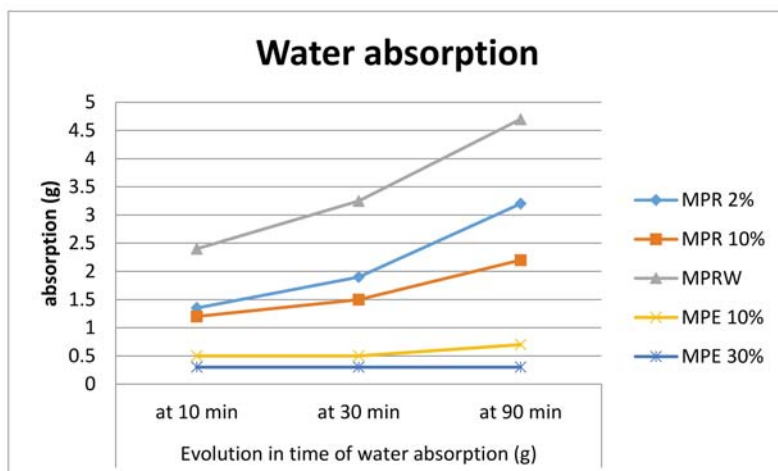


Figure 5. Graphical representation of water absorption at 10, 30, and 90 min for the mortars MPR 2%, MPR 10%, MPRW, MPE 10%, MPE 30%.

### 3.2. Determination of the Softening Coefficient

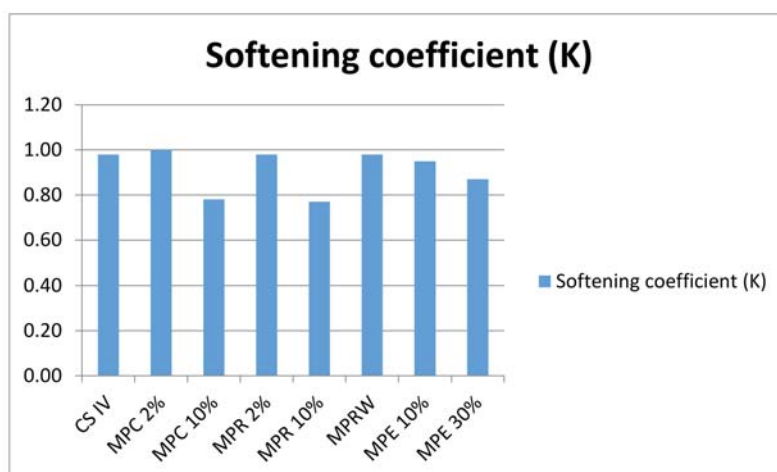
For the study of the softening coefficient, six specimens of size 160 × 40 × 40 mm were produced for each formula. The specimens were used for the flexural tensile tests, the resulting half prisms being tested for the softening coefficient.

Table 2 summarizes the average values of the softening coefficient (K) for the mortars under research for the purpose of the present article.

Table 2. Average values of the softening coefficient.

Formula	Softening Coefficient (K)
CS IV	0.98
MPC 2%	1.00
MPC 10%	0.78
MPR 2%	0.98
MPR 10%	0.77
MPRW	0.98
MPE 10%	0.95
MPE 30%	0.87

Figure 6 includes all the mortars subjected to tests for the softening coefficient in our experiment. One can notice that the higher the polymer content in the mortar, the more diminished the softening coefficient. The best softening coefficient is in MPC 2%, followed by CS IV, MPR 2%, and MPRW. Adding polymers (casein, rice, egg white) in small amounts, improves the softening coefficient of the mortars.



**Figure 6.** Average softening coefficient values at 28 days for the mortars investigated in the research program.

#### 4. Conclusions

This research established that natural polymers used as additives in plaster mortars contribute to diminishing water absorption and even to impermeability.

The influence of the polymer (casein) is made evident as water absorption decreases as compared to the normal plaster mortar. With an increase in the polymer amount, water absorption diminishes.

The formula with a 10% casein addition to the plaster mortar is one of the best performing formulae for water absorption, ranked second with the 10% egg white addition mortar.

Rice does not have such a beneficial influence as casein. The values of water absorption in the rice-based mortars increase in time, while those with casein and egg white standstill or increase very little.

Following the experimental program, it was found that adding egg to the mortar formula leads to a very low water absorption level. The formula with 30% egg absorbs the smallest amount of water in the first 10 min and then it absorbs water in such small quantity that it can be said to become almost impermeable.

As for the softening coefficient, it shows that the higher the polymer percentage in the mortar, the stronger the softening effect is. The best softening coefficient concerns the mortar formula with 2% casein.

The objective of our paper was reached. Of the three polymers tested in the experimental program (casein, rice, egg), the best behavior belongs to the mortar with egg white additions in so far as water behavior is concerned: regarding the water absorption and the softening coefficient.

#### References and Notes

1. Pinte, A.O.; Manea, D.L. Influence of natural polymers upon cement-based plastering mortars. In Proceedings of the C65 International Conference, Cluj-Napoca, Romania, 12–17 November 2018; pp. 69–70.
2. Popa, D.V. *Contribuții la Teoria și Practica Asanării Fundațiilor și Pereților Pentru Construcții Istorice și Social Culturale*; Casa Cartii de Știință: Cluj-Napoca, Romania, 2007.
3. Popa, A. *Consolidarea Fundațiilor*; UTPress: Cluj-Napoca, Romania, 2009.
4. Farcas, V. *Reabilitarea Fundațiilor Construcțiilor Social Culturale și Industriale*; UTPress: Cluj-Napoca, Romania, 2014.

5. Istudor, I. Detalii Tehnice ale Picturii de la Voroneț: Art Conservation Support. Available online: <http://acs.org.ro/ro/conservare/255-detalii-tehnice-ale-picturii-de-la-voronet> (accessed on 3 February 2021).
6. Anonymous. Secretele “Albastrului de Voroneț” și “Albului de Humor”. Available online: <http://www.gandul.info/reportaj/secretele-albastrului-de-voronet-si-albului-de-humor-3197351> (accessed on 3 February 2021).
7. Anonymous. “Tainele Mănăstirii Voroneț. Zece Lucruri Mai Puțin Știute Despre Capela Sixtină a Estului și Despre Cum a Apărut Superba Culoare Albastru de Voroneț”. Available online: <https://identitatea.ro/tainele-manastirii-voronet-zece-lucruri-mai-putin-stiute-despre-capela-sixtina-a-estului/> (accessed on 3 February 2021).
8. Anonymous. Manastirea Humorului. România Montană. Available online: <http://romania-montana.ro/en/proprietate/judet/suceava/manastirea-humorului/> (accessed on 3 February 2021).
9. Acharya, A.; Archroy, S.; Gokhale, V.A. Role of Additives in Mortars: Historic Precedents. *Int. J. Eng. Res. Appl.* **2017**, *7*, 7–12. [CrossRef]
10. Sekar, S.K.; Thirumalini, S. Review on Herbs used as Admixture in Lime Mortar used in Ancient Structures. *Int. J. Appl. Eng. Res.* **2013**, *3*, 295–298.
11. Yang, F.; Zhang, B.; Pan, C.; Zeng, Y. Traditional mortar represented by sticky rice mortar—One of the great inventions in ancient China. *Sci. China E Technol. Sci.* **2008**, *52*, 1641–1647. [CrossRef]
12. Vintilă-Bolchiș, O. Marele Zid Chinezesc a Rezistat Sutelor de ani, Datorită ... Orezului. Available online: <http://jurnalul.ro/afla-ce-e-nou/marele-zid-chinezesc-a-rezistat-sutelor-de-ani-datorita-orezului-545810.html> (accessed on 3 February 2021).
13. Pinteau, A.O.; Manea, D.L. New types of mortars obtained by aditivng traditional mortars with natural polymers to increase physico-mechanical performances. In Proceedings of the International Conference INTER-ENG 2018, Targu Mures, Romania, 4–5 October 2018.
14. Pinteau, A.O.; Manea, D.L. Influence of natural organic polymers upon plaster mortar workability. In Proceedings of the International Conference INTER-ENG 2019, Targu Mures, Romania, 3–4 October 2019.
15. Partea 18: Determinarea coeficientului de absorbtie a apei datorată acțiunii capilare a mortarelor întărite. In *Metode de Încercare a Mortarelor Pentru Zidărie*; SR EN 1015-18:2004; ASRO: Bucharest, Romania, 2004.
16. Partea 11: Determinarea rezistenței la încovoiere și compresiune a mortarului întărit. In *Metode de Încercare a Mortarelor Pentru Zidărie*; SR EN 1015-11:2002/A1:2007; ASRO: Bucharest, Romania, 2007.

**Publisher’s Note:** MDPI stays neutral with regard to jurisdictional claims in published maps and institutional affiliations.



© 2021 by the authors. Licensee MDPI, Basel, Switzerland. This article is an open access article distributed under the terms and conditions of the Creative Commons Attribution (CC BY) license (<http://creativecommons.org/licenses/by/4.0/>).

# Innovative Materials with Complex Applicability<sup>†</sup>

Marta Ioana Moldoveanu \*, Alexandra Olga Pinteau and Daniela Lucia Manea

Department of Civil Engineering and Installations, Faculty of Civil Engineering, Cluj Napoca Campus, Technical University of Cluj Napoca, Cluj-Napoca 400 114, Romania; Alexandra.Pinteau@infra.utcluj.ro (A.O.P.); Daniela.Manea@ccm.utcluj.ro (D.L.M.)

\* Correspondence: Marta.Moldoveanu@ccm.utcluj.ro; Tel.: +4-0264-401-200

† Presented at the 14th International Conference INTER-ENG 2020 Interdisciplinarity in Engineering, Mures, Romania, 8–9 October 2020.

Published: 28 January 2021

**Abstract:** This article represents necessary research, adopting an interdisciplinary approach and a combination of methodologies, in order to better describe the evolution of the physical and mechanical characteristics of mortars. This was done employing modern methods and modern equipment, such as the Bohme equipment for wear tests. Compression and bending test equipment were also used, as well as methods for testing adhesion to the support layer. The purpose of this research is represented by the need to optimize mortar recipes, based on cement and organic and/or synthetic polymers. We focused on how they can be optimized in order to obtain recipes that best meet the needs of today's construction.

**Keywords:** polymers; casein powder; mechanical strength; mortar recipes; rubber powder; complex applicability

## 1. Introduction

As expected, the knowledge about mortars is scarce, due to the fact that each company holds on to its own recipe in order to capitalize its investment. Usually company recipes are patented. Not knowing the composition of mortar recipes based on cement and polymers available on the market, we set out to create new recipes. The Technical University of Cluj-Napoca, namely, the Construction Materials Department, has been involved in this type of research for several years already, testing different mortars with organic polymers and having obtained remarkable results in recent times.

## 2. Materials and Methods

With conventional methods we can describe only the physical-mechanical characteristics of materials. Modern investigation methods, however, describe the various processes that occur inside the structure of the materials, analyzing distribution and pore size. In our research for organic materials [1] (pp. 456–462), the return to the traditional methods of obtaining construction materials was considered.

The polymers were introduced in the standard recipe of cement mortars: organic (casein) 2% compared to the amount of cement. In the following, we will name each recipe with an abbreviation, so that we can easily identify them in the text and graphs. The abbreviations are as follows: Standard Mortar—*MS*; 2% Casein Mortar—*MC 2%*; 2%, 5%, and 10% Rubber Powder Mortar—*MPC 2%, 5%, and 10%*; 2%, 5%, and 10% Rubber Powder Mortar and Casein 2%—*MPC 2%, 5%, and 10% C2%*.

The main objective of this article is to emphasize the contribution of polymers, in various forms, in mortar recipes [2] (pp. 37–40). Obtaining a mortar with an organic polymer recipe and also with a complex applicability is our goal. The research was performed using modern methods highlighting the contribution of polymers in increasing the physical and mechanical performance of the studied mortars. Along with our main objective, we also had these secondary objectives:

- Analyzing the current situation regarding mortars and polymers used in construction.
- Making rubber mortar recipes with a concentration of 2%, 5%, and 10% by weight of cement and testing them in order to determine their physical and mechanical characteristics.
- Making rubber mortar recipes with a concentration of 2%, 5%, and 10% by weight of cement with an additional casein concentration of 2% by weight of cement. Investigating them by traditional methods and highlighting the contribution of casein.
- Determination of the physical and mechanical characteristics of the standard mortar and all mortar recipes, maintaining the standards in force, and also testing the mortar recipes at 3, 7, and 28 days.

Studying the chemical properties of cement by testing the standard mortar recipe, but also the organic and synthetic polymer mortar recipes at 3, 7, and 28 days, we can obtain results that will further our research.

The steps for the standard mortar recipe and testing equipment are shown in Figures 1–3. We can observe that every single component was carefully selected, measured, mixed, placed in proper sample boxes, depending on which testing was to follow, and, eventually, tested.

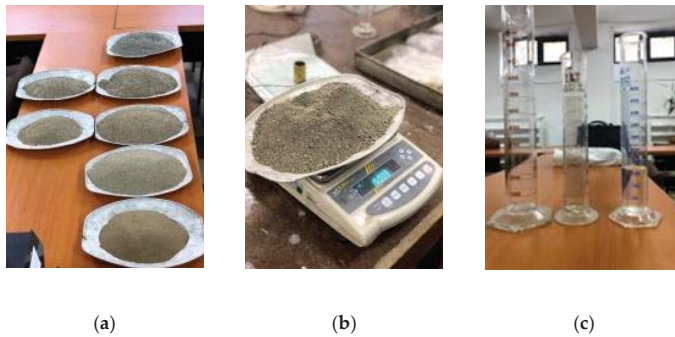


Figure 1. (a–c) Precise measuring of solid components.

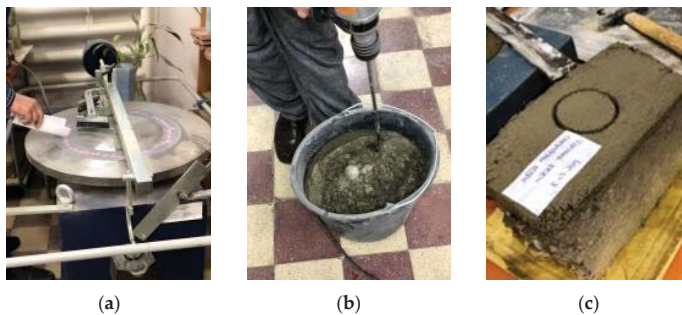


Figure 2. (a–c) Material preparation and Bohme equipment.

Step one is picking the right materials and precise measuring, as shown in Figure 1a–c. The higher the quality of the materials, the more qualitative the result will be, but in the field of construction, we must take into account another very important aspect—the cost.

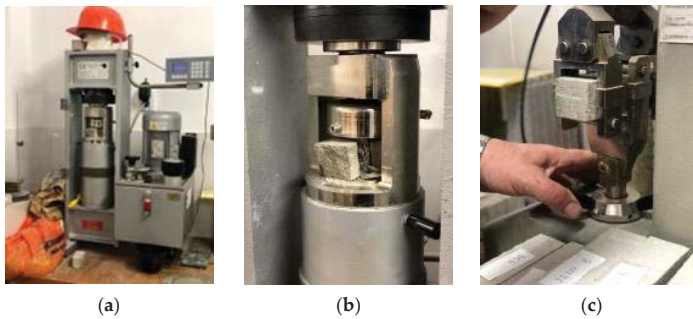


Figure 3. (a–c) Sample testing equipment.

The water concentration in the mortar recipe is very important because it dictates the consistency of the final result, therefore, it is very important to measure it carefully and with maximum accuracy, as shown in Figure 1b.

The next important step is mixing them together, as shown in Figure 2a, with the help of a mixer, so we can obtain a homogeneous compound. The material is usually tested with a testing cone.

Figure 2b showcases the adhesion to the main substrate and in Figure 3c we can see the equipment by which the compressive strength of the material sample is measured. Figure 3a highlights the bending equipment. In both situations, the material sample will break when the load is too high, thus establishing the maximum tolerability value. The pink abrasion sand is used for abrasion testing with the Bohme equipment. The Bohme equipment, as shown in Figure 2c, is in accordance with EN standards EN 1338, 1339, 1340, EN 13748-2, 13892-3, EN 14157. The machine is used to determine the volume loss of a sample subjected to the abrasion test.

Three standard mortar samples were prepared, which were tested for bending and compression, as we can see in Figure 3a–c, obtaining the results pointed out in Figure 4. The prepared samples for the bending and the compression tests are placed in  $4 \times 4 \times 16$  cm molds.

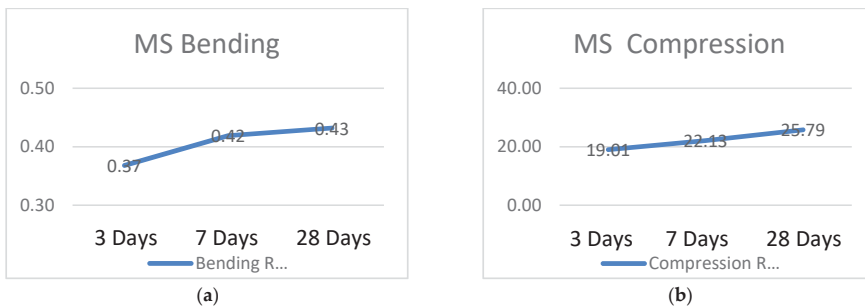


Figure 4. Three, 7, and 28 day bending (a) and compression (b) tests for MS,  $4 \times 4 \times 16$  samples.

### 3. Results

The results presented in Figure 4 highlight the evolution over time at 3, 7, and 28 days in terms of bending and compressive strength. One can easily observe the evolution of these values due to the hydration processes of the cement.

Figure 5a–d shows images from the adhesion testing of the standard mortar to the support layer (concrete element), which will represent future research directions.

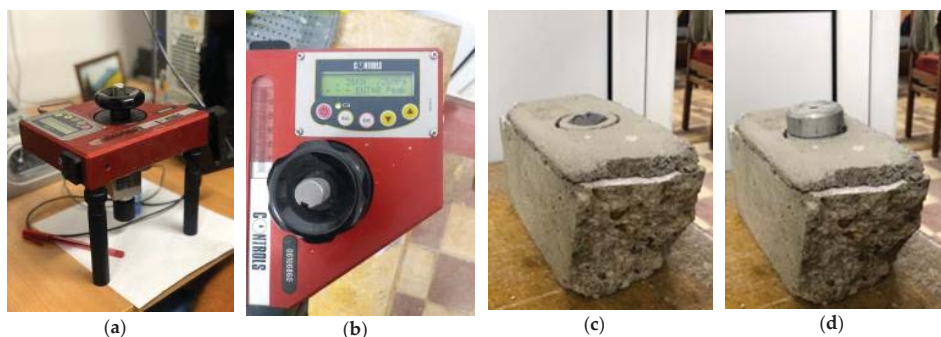


Figure 5. (a–d) Twenty-eight day adhesion test on the screed.

In order to improve the workability of a mortar, a natural polymer casein in a proportion of 2% by weight of cement [3] was added. Studying the specialty literature and studying the articles on the subject, it was found that the percentage of organic material used in researched recipes behaves best at a percentage of 2% [4]. Thus, we will discuss and later compare the recipes with 2%, with the 5% and 10% only used as examples. Therefore, the experimental program involved the study of three samples of  $4 \times 4 \times 16$ , in which casein was introduced in a percentage of 2% of the overall amount of cement in the recipe of the initial standard mortar. Figure 6 calls attention to the results from the three test samples of standard mortar with 2% casein, namely MC2%, using the equipment provided by the Technical University of Cluj-Napoca; namely, the bending test device and the hydraulic press. We will structure the abbreviations in Table 1, in order to have better readability.

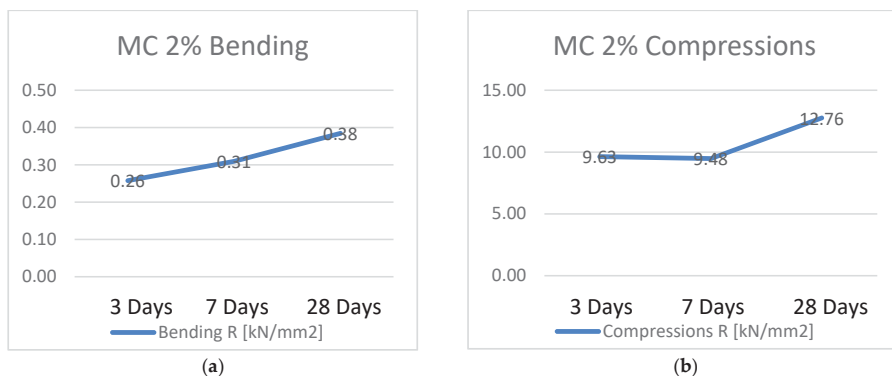


Figure 6. Three, 7, and 28 day bending (a) and compression (b) tests for MC2%,  $4 \times 4 \times 16$  samples.

Table 1. Mortar sample abbreviations.

Abbreviation	Percentage	Detailing
MS	2–10%	Standard Mortar
MCx%	2–10%	Standard Mortar with x% Casein Polymer
MPCx%	2–10%	Standard Mortar with x% Rubber Powder and x% Casein Polymer
MPCx%Cy%	2–10%	Standard Mortar with x% Rubber Powder and y% Casein Polymer

In the following study, we analyzed another three samples of  $4 \times 4 \times 16$  in which casein and rubber powder were introduced in a percentage of 2% to 10% of the amount of cement (rubber powder)



and a constant percentage of 2% of casein polymer [4]. Figure 7 shows the results from the three test samples of standard mortar with 2–10% rubber powder and 2% casein powder, namely, MPC2-10% C2%.

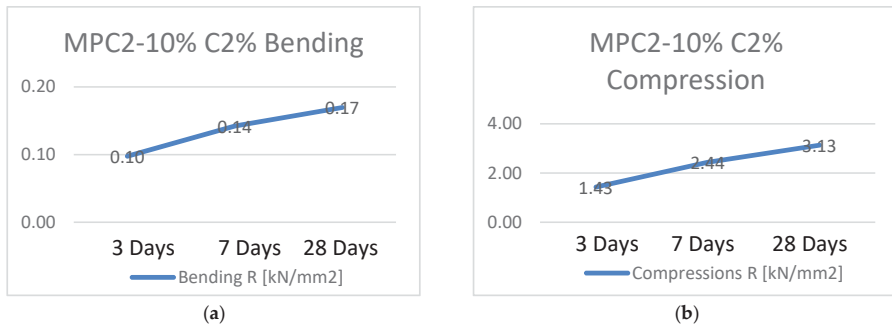


Figure 7. Three, 7, and 28 day bending (a) and compression (b) tests for MPC5-10% C2%, 4 × 4 × 16 samples.

The results presented in Figure 7 highlight the evolution over time at 3, 7, and 28 days of bending strength and compressive strength for the rubber and casein powder mix recipe. Here we can see the evolution of these values due to the hydration processes of the cement and also the use of polymers increases the handling of the product [5].

#### 4. Conclusions

The general conclusions of this paper, which summarizes all discussions on the methods of investigation used, as well as personal input on the subject, represents all the knowledge learned so far and all the tests done on the proposed mortar recipes, concerning the bending strength and compressive strength, the resistance to permeability [6], all those test were made in the Technical University of Cluj-Napoca labs [7,8].

As specific conclusions on the methods of investigation used [9], we can mention that as time passes, the standard mortar samples at 28 days are usually much more resistant to compression than 3 days old samples; this can be seen in Figure 4, Figure 6, and Figure 7. This happens with all recipes, as we can see in Figure 8. The comparison is made between the three types of recipes at the same time of measurement at odds with the standard mortar. What is noticeable is the fact that both the casein and the rubber powder and casein recipes are less resistant to compression and bending at 3 days, 7 days, and at 28 days, which is why the next stage of the research will involve recipes in which both polymers will not be used, but only one of them. We also propose a microscopic investigation, in order to study how the structure of the mortar evolves using these polymers. When comparing them, one can observe a better compressive strength of the mixed recipe of 10% rubber powder and 2% casein, also known as the abbreviation MPC10% C2%, compared to the benchmark—the standard mortar MS; the compressive strengths are completely different. Even with lower strength results, one thing stands out; namely, the fact that the handling was clearly superior through the use of polymers [10]. All research has been carried out in accordance with the relevant European standards [11–24].

We leave the discussions open, in terms of adhesion tests, as these will be performed on the support layer alongside the abrasion tests in the near future in one of our next research papers. The recipes with the related interpretations should not be neglected as they are very important towards obtaining a material with the minimum necessary mechanical strength, but with a superior resistance to permeability [6], which is of the utmost importance in terms of usage.



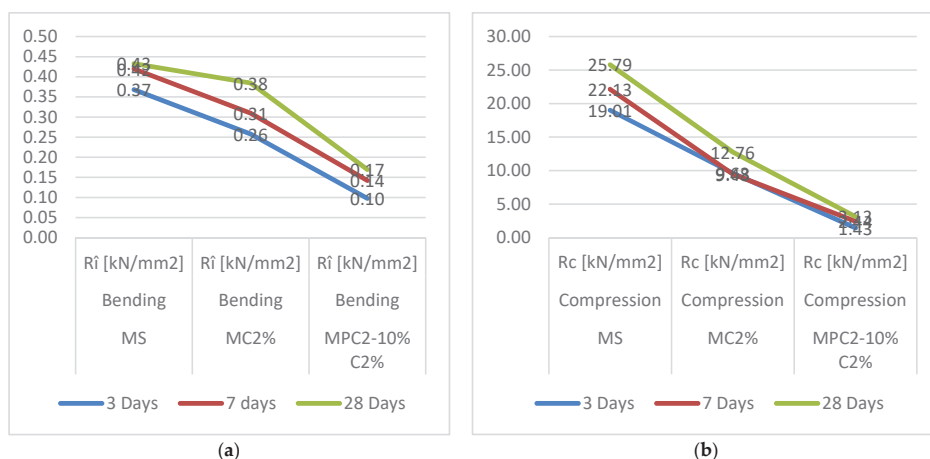


**Figure 8.** Three, 7, and 28 day bending and compression tests for MS, MC2%, and MPC5-10% C2%, 4 × 4 × 16 samples.

## References

1. Cantor (Andres), D.M.; Manea, D.L. Innovative building materials using agricultural waste. *Proc. Technol.* **2015**, *19*, 456–462. [CrossRef]
2. Saikhede, S.R.; Satone, S.R. An Experimental Investigation of Partial Replacement of Cement by Various Percentage of Phosphogypsum and Flyash in Cement Concrete. *Int. J. Eng. Res. Appl.* **2014**, *4*, 37–40.
3. Jumate, E.; Manea, D.L.; Moldovan, D.; Fechete, R. The effects of Hydrophobic Redispersible Powder Polymer in Portland Cement Based Mortars. *Proc. Technol.* **2017**, *181*, 316–323.
4. Pintea, A.O.; Daniela Manea, D.L. Influence of Natural Polymers upon Cement-Based Plastering Mortars. In Proceedings of the C65 International Conference, Cluj-Napoca, Romania, 15–17 November 2018.
5. Pintea, A.O.; Manea, D.L. New types of mortars obtained by aditivng traditional mortars with natural polymers to increase physico-mechanical performances. In Proceedings of the International Conference INTER-ENG 2018, Targu Mures, Romania, 4–5 October 2018.
6. Pintea, A.O.; Manea, D.L. Influence of Natural Organic Polymers upon Plaster Mortar Workability. In Proceedings of the International Conference INTER-ENG 2019, Targu Mures, Romania, 3–4 October 2019.
7. EN 934-6:2002/A1:2006 Additives for Concrete, Mortar and Paste. Part 6: Sampling, Control and Conformity Assessment. Available online: <https://vdocuments.site/sr-en-934-2-aditivi-pentru-beton.html> (accessed on 29 November 2020).
8. EN 13139:2003 Aggregates for Mortars. Available online: <https://standards.iteh.ai/catalog/standards/cen/d1169c31-b23e-41fa-8f1d-cf3a9b0ce8dd/en-13139-2002> (accessed on 29 November 2020).
9. STAS 790-1984 Water for Mortars and Concretes. Available online: <https://magazin.asro.ro/ro/standard/21638> (accessed on 29 November 2020).
10. EN 196-1:2016 Methods of Testing Cement. Determination of Strength. Available online: <https://www.en-standard.eu/bs-en-196-1-2016-methods-of-testing-cement-determination-of-strength/> (accessed on 29 November 2020).
11. EN 196-2:2013 Method of Testing Cement. Chemical Analysis of Cement. Available online: <https://standards.iteh.ai/catalog/standards/cen/47283941-90a2-43dc-8b2c-dea6208712a6/en-196-2-2013> (accessed on 29 November 2020).
12. EN 196-3:2016 Methods of Testing Cement Determination of Setting Times and Soundness. Available online: <https://standards.iteh.ai/catalog/standards/cen/e4921eca-8101-4261-b066-25d19b9b8e8a/en-196-3-2016> (accessed on 29 November 2020).
13. EN 196-4:2007 Methods of Testing Cement. Quantitative Determination of Constituents. Available online: <https://standards.iteh.ai/catalog/standards/cen/d55093fb-4c58-46c6-a91c-150121867625/cen-tr-196-4-2007> (accessed on 29 November 2020).

14. EN 196-6:2018 Methods of Testing Cement. Determination of Fineness. Available online: <https://standards.iteh.ai/catalog/standards/cen/9feaed91-485e-4e0b-93c6-36357e1580ec/en-196-6-2018> (accessed on 29 November 2020).
15. EN 197-1:2001. Cement Part 1. Composition, Specifications and Conformity Criteria for Common Cements. Available online: <https://standards.iteh.ai/catalog/standards/sist/00e7c857-98b1-4132-b9ec-9cf156a8dfc3/sist-en-197-1-2001-opra2-2006> (accessed on 29 November 2020).
16. EN 197-2:2020 Cement—Part 2: Assessment and Verification of Constancy of Performance. Available online: <https://standards.iteh.ai/catalog/standards/cen/49c9299e-9123-42eb-92d2-19b6461f41ad/en-197-2-2020> (accessed on 29 November 2020).
17. EN 197-3:2001 Cement—Part 3: Composition, Specifications and Conformity Criteria for Low Heat Common Cements. Available online: <https://standards.globalspec.com/std/1347120/din-en-197-3> (accessed on 29 November 2020).
18. EN 197-4:2004 Cement. Composition, Specifications and Conformity Criteria for Low Early Strength Blastfurnace Cements. Available online: <https://standards.iteh.ai/catalog/standards/cen/83a154a8-c2fc-4b4a-a408-8b46d6834132/en-197-4-2004> (accessed on 29 November 2020).
19. EN 197-5:2000. Cement. Part 5. Portland-Composite Cement CEM II/C-M and Composite Cement CEM VI. Available online: <https://standards.iteh.ai/catalog/standards/cen/69d3b559-4114-43b3-bfed-05787fc839a2/pren-197-5> (accessed on 29 November 2020).
20. EN 1338:2003 Concrete Paving Blocks. Requirements and Test Methods. Available online: <https://standards.iteh.ai/catalog/standards/cen/c0ceb4fd-ff66-437d-b05c-c62974d4ab41/en-1338-2003-ac-2006> (accessed on 29 November 2020).
21. EN 1339:2003 Concrete Paving Flags. Requirements and Test Methods. Available online: <https://standards.iteh.ai/catalog/standards/cen/19c0de8e-9430-4961-8d97-a1c6b70d041c/en-1339-2003-ac-2006> (accessed on 29 November 2020).
22. EN 1340:2003 Concrete Kerb Units. Requirements and Test Methods. Available online: <https://standards.iteh.ai/catalog/standards/cen/84647ce9-386d-4a39-8406-47d56f64692b/en-1340-2003> (accessed on 29 November 2020).
23. EN 13748-2 Terrazzo Tiles Part 2: Terrazzo Tiles for External Use. Available online: <https://standards.iteh.ai/catalog/standards/cen/db14b22d-212a-4aba-916f-62f32cf64bbe/en-13748-2-2004> (accessed on 29 November 2020).
24. EN 14157:2017 Natural Stone Test Methods. Determination of the Abrasion Resistance. Available online: <https://standards.iteh.ai/catalog/standards/cen/248b629a-b8ea-4c98-9554-0a5c2355def2/en-14157-2017> (accessed on 29 November 2020).

**Publisher's Note:** MDPI stays neutral with regard to jurisdictional claims in published maps and institutional affiliations.



© 2021 by the authors. Licensee MDPI, Basel, Switzerland. This article is an open access article distributed under the terms and conditions of the Creative Commons Attribution (CC BY) license (<http://creativecommons.org/licenses/by/4.0/>).



# Possibilities of Recovery of Industrial Waste and By-Products in Adobe-Brick-Type Masonry Elements <sup>†</sup>

Gabriela Călătan, Andreea Hegyi \*, Elvira Grebenisan and Anamaria Cătălina Mircea

NIRD URBAN-INCERC Cluj-Napoca Branch, 117 Calea Florești, 400524 Cluj-Napoca, Romania; gabriela.calatan@incerc-cluj.ro (G.C.); elvira.grebenisan@incerc-cluj.ro (E.G.); anamaria.mircea@incerc-cluj.ro (A.C.M.)

\* Correspondence: andreea.hegyi@incerc-cluj.ro

<sup>†</sup> Presented at the 14th International Conference INTER-ENG 2020 Interdisciplinarity in Engineering, Mureș, Romania, 8–9 October 2020.

Published: 9 December 2020

**Abstract:** The purpose of this study is to search for possibilities to capitalize on industrial waste, which occupies huge storage spaces. This paper presents an experimental study on the possibility and efficiency of this industrial waste in the composition of clay mixtures suitable for making unburned clay bricks. Living in harmony with nature is part of sustainable development. For this purpose, six compositions based on clay and industrial waste were made. The studied industrial wastes were: ash from the Mintia thermal power plant, Romania, limestone sludge, gypsum sludge, and damped waste from the processing of imported ore.

**Keywords:** adobe bricks; thermal power plant ash; dumped waste; limestone sludge; plaster sludge

## 1. Introduction

It is known that the cement industry produces air pollution due to CO<sub>2</sub> emissions, which constitute 4–8% of total greenhouse gas emissions. Other non-negligible emissions that occur in the cement industry are dust emissions and emissions of N<sub>2</sub>O, CH<sub>4</sub>, SO<sub>x</sub>, NO<sub>x</sub>, NH<sub>3</sub>, and CO [1]. All this results in a depletion of the ozone layer and, therefore, global warming. Under these conditions, the elimination or substantial reduction of cement consumption is desirable. By replacing classic building materials with environmentally friendly materials wherever possible, a considerable contribution is made to protecting the environment. The possibilities of recycling, reuse, reintegration in nature, environmental protection, and efficient management of natural resources are essential indicators in the context of sustainable development. Living in harmony with nature is part of sustainable development. Products that successfully meet all these requirements are the elements of unburned clay masonry.

Another important quality of ecological materials is the fact that they offer a healthy and pleasant climate to users. Clay-based building materials used in construction allow a natural and efficient ventilation of the walls, permeability to water vapor, thermal constancy, and a constant humidity of the indoor environment. In addition, these walls made of clay-based bricks have no toxic emissions, a factor that plays a very important role in reducing the risk of respiratory diseases, allergies, and more. Studies are presented in the specialized literature that demonstrate the durability of constructions made with local materials and local techniques in different geographical and climatic conditions [2–4].

Nine thousand years ago, construction techniques with clay bricks were used. Clay bricks were discovered in Turkistan, dating from 8000–6000 BC. Clay was used as a building material in all ancient cultures for religious buildings and houses; 5000-year-old foundations were discovered in Assyria [5].

Houses made of ecological materials have started to become more and more known and pleasant in Romania, and more and more specialists are interested in this type of construction [6,7]. The specialized literature presents the results of some research carried out in view of the possibility of realizing such

constructions from clay. These results, in addition to the many benefits, also point out some drawbacks due to the clay [1,8–10]. The main drawbacks are that, in order to obtain the minimum conditions of mechanical and thermal resistance, a large wall thickness is required. There is also a high risk of cracking during drying due to significant axial contractions. The ideal clay soil to be used in construction must contain at least 15–16% clay because it has the right plasticity and workability to obtain a quality finished product [9,10]. In order to obtain a workable mixture, a certain amount of water is needed to induce the phenomenon of thinning of the clay sheets, but it must be dosed so as not to reach significant axial contractions and the appearance of cracks during drying. Thus, a linear contraction between 3% and 12% is accepted for bricks from soft mixtures or between 0.4% and 2% in the case of drier mixtures [1,8,9,11].

In order to obtain a good thermal insulation, the specialized literature indicates an apparent density of the material between 1600 and 2000 kg/m<sup>3</sup> [1,8,11,12].

The studies presented until now in the literature do not adequately show the influence of various additives on the physical–mechanical characteristics of products made of clay (mechanical strength, thermal resistance, water behavior and water vapor, etc.). Among the additives that could be used for the clay matrix, but which have been insufficiently studied until now, is industrial waste. Every year, after burning coal in order to obtain thermal energy, large quantities of power plant ash are produced. The use of coal in the thermal energy production process in Romania has a share of over 38% of the entire electricity production in the country [13,14].

The ash resulting from the burning of coal can be of two types: fly ash, which is evacuated with the flue gases, and coarse ash, which is collected centrally and transported to specially arranged places in dumps. Both types of ash have a major impact on pollution; flying ash pollutes the air, and coarse ash occupies huge areas of land. In Romania, over 80% of industrial waste is stored in places arranged in nature; this is the main method for so-called ash disposal. A single thermal power plant in Romania produced almost 650,000 tons of ash, 50,000 tons of slag, and 50,000 tons of gypsum in 2017. Of the total industrial waste produced at the national level, only 0.06% is currently recovered [13,15].

In addition, within the technological process of the processing of natural stones and marble (limestone blocks), there are significant quantities of sludge—an average of 20 tons/day [13]. The resulting limestone sludge, which is partially dry, is stored in heaps in the form of cakes, drying naturally.

Another category of industrial waste is gypsum sludge resulting from the processing of imported ore. This plaster slime is stored in heaps, occupying large spaces as well. Therefore, studies and research are needed for the possibility of recovering this waste. One way of recovery of industrial waste can be by using it as an additive in clay mixtures intended for the manufacture of unburned clay bricks. The aim of this study is to establish optimal clay-based mixtures for the manufacture of unburned bricks, using four types of industrial waste as an addition to clay, as follows: power plant ash and limestone sludge on the one hand, and scrap waste from the processing of imported ore and gypsum sludge on the other.

The purpose of these experimental studies is to find sustainable ways to capitalize on industrial waste.

## 2. Materials and Methods

The raw materials used to make the experimental mixtures were: clay that was extracted from Valea Draganului, Cluj Napoca, Romania, ash from the Mintia thermal power plant, Romania, limestone sludge from limestone processing, scrap waste from imported ore processing, and gypsum sludge. These wastes were used simultaneously, two by two: ash with limestone sludge and scrap waste with gypsum sludge. The sandy clay used was characterized by particle size distribution (Figure 1) and oxide composition (Table 1) [16,17].

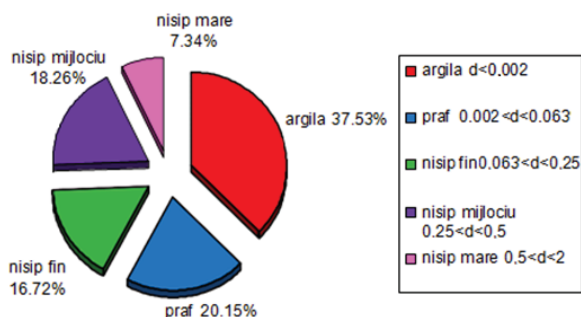


Figure 1. Granulometry of sandy clay [16].

Table 1. Oxide composition of clay, determined according to romanian standard STAS 9163.

Oxides	SiO <sub>2</sub>	Al <sub>2</sub> O <sub>3</sub>	Fe <sub>2</sub> O <sub>3</sub>	CaO	MgO	K <sub>2</sub> O	Na <sub>2</sub> O	TiO <sub>2</sub>	PC
Content [%]	74.17	12.74	4.38	0.7	1.0	1.43	0.73	0.05	4.78

The power plant ash was characterized by the oxide composition presented in Table 2, the particle size distribution of limestone is presented in Table 3, and the apparent density in Table 4 [18].

Table 2. The composition of the ash from the Mintia thermal power plant, determined by XRF (X-ray fluorescence) analysis.

Oxides	SiO <sub>2</sub>	Al <sub>2</sub> O <sub>3</sub>	Fe <sub>2</sub> O <sub>3</sub>	CaO	MgO	SO <sub>3</sub>	Na <sub>2</sub> O	K <sub>2</sub> O	P <sub>2</sub> O <sub>5</sub>	TiO <sub>2</sub>	Cr <sub>2</sub> O <sub>3</sub>	Mn <sub>2</sub> O <sub>3</sub>
Content [%]	53.75	53.75	26.02	7.91	2.54	1.54	0.35	0.59	2.57	0.12	0.05	0.09

The fineness of the ashes from the Minthia thermal power plant, determined on a sieve of 0.045 mm, was 39.20%.

The limestone sludge used had the particle size composition shown in Table 3 and the apparent density shown in Table 4 [18].

Table 3. Particle size distribution of limestone sludge.

Sieve Size (mm)	0.063	0.125	0.250	0.500	1
Through the sieve (%)	69	93	95	99	100

The apparent densities of all wastes used in this study, determined in the laboratory, are shown in Table 4 [18].

Table 4. Apparent density of the filler materials used.

Type of Industrial Waste	Ashes from the Mintia Thermal Power Plant	Landfilled Waste from Imported Ore Processing	Gypsum Sludge	Limestone Sludge
Apparent density (Mg/m <sup>3</sup> )	1.67	1.26	1.26	1.78

Three compositions of clay, ash, and limestone sludge were made in different proportions, as well as another three compositions of clay, scrap waste, and gypsum sludge in other three proportions. The dumped waste and gypsum sludge came from the same working point for processing the imported ore, and the ash and limestone sludge came from the same area. The compositions of the six mixtures made, as well as that of a control sample (made of clay material without additives), are presented in

Table 5. Prismatic specimens measuring 40 × 40 × 160 mm were made from each mixture and kept until the equilibrium humidity was reached. The parameters that were examined on these specimens, after a visual control of possible cracks appearing in the specimens that reached the equilibrium humidity, were:

- Axial contractions according to romanian standard STAS 2634;
- The apparent density in the hardened state when the equilibrium humidity is reached according to european standard harmonized in Romania SR EN 1015-10;
- Mechanical strengths according to european standard harmonized in Romania SR EN 1015-11.

The equilibrium humidity is considered to be reached when the constant mass is reached. From previous experiences, it has been found that it occurs about 40 days after making clay-based specimens.

**Table 5.** Compositions of experimentally tested mixtures.

Nr. of Test	Materials Age Test	Clay (%)	Mintia Thermal Power Plant Ash (%)	Limestone Sludge (%)	Dumped Waste from Imported Ore Processing (%)	Gypsum Sludge (%)
1	40 days	100	0	0	0	0
2	40 days	60	20	20	0	0
8	1 year					
3	40 days	50	25	25	0	0
9	1 year					
4	40 days	40	30	30	0	0
10	1 year					
5	40 days	70	0	0	15	15
11	1 year					
6	40 days	60	0	0	20	20
12	1 year					
7	40 days	50	0	0	25	25
13	1 year					

These compositions were tested at 40 days and at one year in order to appreciate the variation of the parameters over time. Samples 1 to 7 were tested at 40 days, and samples 8 to 13 were tested at one year.

### 3. Results and Discussion

Analyzing the appearance of the specimens at 40 days and at one year, the lack of surface cracks can be noticed, which is a very important aspect for clay-based mixtures, but it must be taken into account that the dimensions of the specimens are small (Figure 2).



**Figure 2.** Appearance of the surface of the hardened specimen.

The results of the axial contractions recorded are represented in Figure 3.

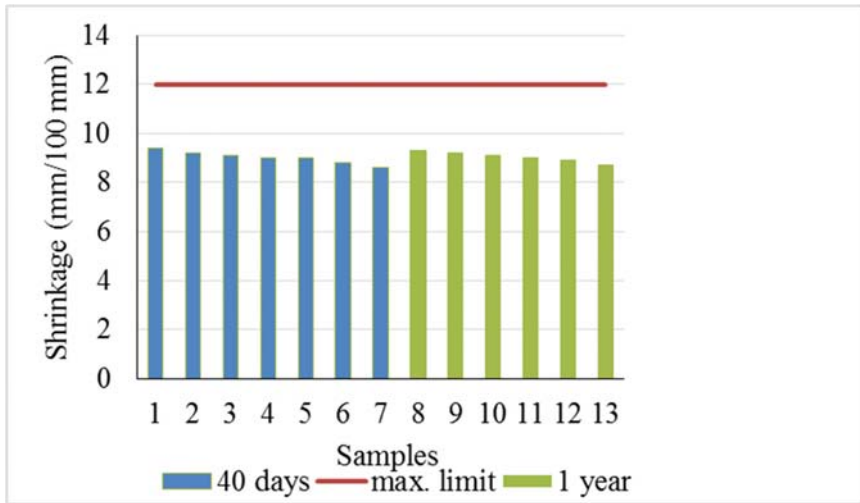


Figure 3. Axial contractions of dry mixtures at equilibrium humidity.

It was found that, from the point of view of the axial contractions, all the tested mixtures fell within the limits indicated as being admissible in the specialized literature [1,7,13,18]. Although the results obtained for drying shrinkage and crack evolution were satisfactory on these specimens, it can be stated that for the manufacturing of bricks from these compositions, the dimensions of the elements made must not exceed certain dimensions to avoid cracks. In order to be able to establish a correlation between the maximum permissible dimensions of the elements made from these types of clay mixtures with additions of industrial waste and the absence of cracks, a further study is needed.

Based on the results shown in the graph in Figure 3, it is observed that the additives used in the mixture had a small influence on the axial contractions compared to the control specimen made only of clay. The specimens were checked 40 days (mixtures 1 to 7) and one year (samples 8 to 13) after manufacturing, as shown in Table 5. It was observed that the waste obtained from the processing of the imported ore, as well as the dumped waste and the gypsum sludge added into the clay matrix, induced a more accentuated decrease of the axial contractions compared to when the Mintia ash and the limestone sludge were added in the same proportions.

The most accentuated decrease of the axial contractions was presented by the mixture with 50% clay, 25% dumped waste, and 25% gypsum sludge (sample no. 7), which was from 9.4 mm/100 mm of the control specimen up to 8.6 mm/100 mm. Axial contractions after one year remained constant. There was no significant decrease or increase in axial contractions from 40 days to one year after manufacturing.

The values of the apparent densities are presented in Figure 4.

According to the specialized literature, the materials whose apparent density is between 1600 and 1690 kg/m<sup>3</sup>, as shown in the graph, have the ability to store heat, which then yields when the temperature drops [1,7,12,13,18]. According to the graph, all compositions fall within this limit. Materials with densities between these values have a good thermal index, which causes a room to have constant temperature. This is an important quality of natural materials.

The mixtures with the lowest values of apparent density at 40 days, 1650 kg/m<sup>3</sup>, were samples 2 and 5. Sample 2 contained 60% clay and 40% waste (20% ash and 20% limestone sludge), and sample 5 contained 70% clay and 30% waste (15% waste and 15% gypsum sludge).

The sample with the highest apparent density was sample 4, which contained the maximum percentage of added waste (40% clay and 60% other additives). This composition probably had the



highest density due to the addition of limestone sludge, which has the highest bulk density compared to other raw materials.

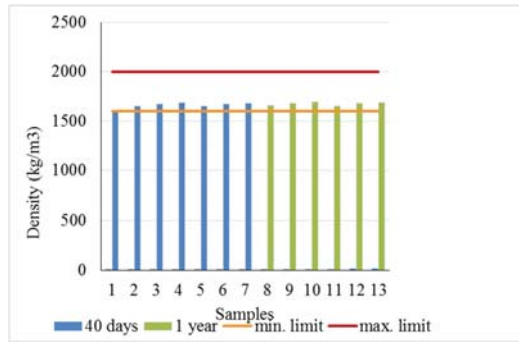


Figure 4. Apparent density of mixtures.

After one year, the sample with the highest apparent density was sample 10 which contained 40% clay and 60% waste (30% ash and 30% limestone sludge). In all mixtures, after one year, a small increase of the values of bulk density could be observed, probably due to the reaction between Ca and CO<sub>2</sub> from the air that formed the limestone.

The mechanical resistances determined on hardened prisms at the equilibrium humidity after one year are presented in Figure 5. In Figure 6, the appearance of the specimen after breaking can be observed.

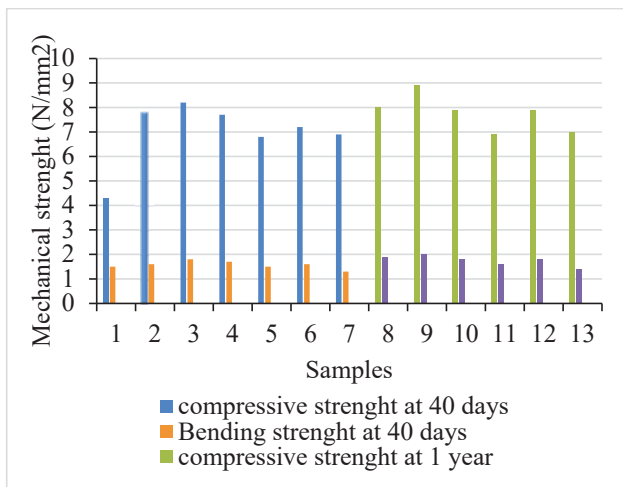


Figure 5. Mechanical resistance of samples.

A first observation is that all mixtures with added waste have increased mechanical strength compared to the control sample, which was made only with clay. Another important observation is that mechanical strength increases over time. All values of one-year resistance are higher than 40-day resistance.

In the case of the addition of ash and limestone sludge, samples 3 and 9 (25% ash, 25% limestone sludge, and 50% clay) had the highest mechanical strength at 40 days and one year, with 8.2 N/mm<sup>2</sup>

(sample 3) and  $8.9 \text{ N/mm}^2$  (sample 9), respectively. With a greater or lesser addition of this type of waste, the strengths are lower compared to that of this mixture. There is an increase in mechanical strength by 47% compared to the control sample at 40 days and by 8% at one year, compared to the same mixture tried at 40 days. For sample 2 (addition of 20% ash and 20% limestone sludge) as well as at sample 4 (30% ash and 30% limestone sludge), there was a small decrease in resistance compared to sample 3, but nevertheless, the mechanical strengths were higher than the strength of the clay without addition.



**Figure 6.** Appearance of test specimens after breaking.

In the case of the addition of dumped waste and gypsum sludge, the sample with the best mechanical resistance at 40 days was sample 6 with 20% dumped waste, 20% gypsum sludge, and 60% clay. The value of the mechanical strength of sample 6 was with 40% higher than that of the control sample. The same mixture tested at one year (sample 12) had a value of compressive strength 10% higher than at 40 days. A higher proportion of piled waste and gypsum sludge reduced the mechanical strength compared to sample 6 when tested 40 days after manufacture. The same mixture tested at one year, sample 12, also had the highest mechanical strength among mixtures with this type of waste. The samples with the addition of 30% and 50% mixtures of dumped waste and gypsum sludge had mechanical strengths of approximately 6% lower than that of sample 6.

The best mixtures analyzed from the point of view of mechanical strength were the mixtures marked with 3 or 9 (50% clay, 25% Mintia ash, and 25% limestone sludge) and samples 6 or 12 (20% dumped waste, 20% plaster sludge, and 60% clay).

#### 4. Conclusions

After this study, the following conclusions can be drawn.

All mixtures have a good workability, which allows a necessary homogenization.

Axial shrinkage is not negatively influenced by the addition of industrial waste, and no mixtures showed cracks when drying. The largest length of a side of the specimens made was 160 mm, so it can be stated that when making bricks with a side of 160 mm, no cracks appear, but for a brick with a larger side, there is a probability of cracks; therefore, an additional study to establish the maximum possible dimensions without cracks is necessary. Due to the results obtained at 40 days and at one year, it can be stated that the axial contractions remain constant over time.

All the values obtained for the densities in the hardened state were within the interval of  $1600\text{--}2000 \text{ kg/m}^3$ . According to the literature, this range is satisfactory in terms of thermal efficiency, so the addition of industrial waste does not negatively influence the values of apparent densities in the hardened state. The apparent density increases very slightly over time.

The mechanical strengths were positively influenced by the addition of waste. The composition with the addition of 25% ash and 25% limestone sludge had the highest mechanical strength of all mixtures. The mechanical strength of this mixture increased by 8% after one year.

The mechanical strength of the sample with the addition of 20% bulk waste and 20% gypsum sludge was also higher than the mechanical strength of the control sample. This mixture had the highest resistance in the case of dumped waste and gypsum sludge.

The resistance value of this sample was 12% lower compared to the sample with 25% ash and 25% limestone sludge. In the test with the addition of 20% dumped waste and 20% plaster sludge, the value of the resistance after one year increased by 10%.

All the conclusions confirm the fact that, in terms of physical–mechanical characteristics, industrial waste can be successfully used as an addition in clay matrixes intended for the production of unburned clay bricks, and it is very welcome to capitalize on industrial waste in this way, resulting in ecological and healthy materials at the same time.

The bricks made according to the studied recipes can be successfully used to make constructions that are environmentally friendly and energy efficient, and that provide a pleasant and healthy climate for the inhabitants; at the same time, nature is protected from pollution by reducing cement consumption. This also preserves the basic principles of traditional vernacular architecture that is modeled according to current technological progress.

**Author Contributions:** Conceptualization, G.C., A.H., E.G., and A.C.M.; methodology, G.C. and A.H.; validation, G.C., and A.H.; formal analysis, A.H. and A.C.M.; investigation, G.C.; data curation, G.C.; writing—original draft preparation, G.C.; writing—review and editing, G.C., A.H., E.G., and A.C.M.; visualization, A.H. and A.C.M.; supervision, A.H. All authors have read and agreed to the published version of the manuscript.

**Funding:** This research received no external funding.

**Conflicts of Interest:** The authors declare no conflict of interest.

## References

1. Minke, G. *Building with Earth: Design and Technology of a Sustainable Architecture*; Walter de Gruyter: Berlin, Germany, 2005; pp. 15–47, 55–68, 92–103.
2. Baskar, R.; Meera Sheriffa Begum, K.M.; Sundaram, S. Characterization and Reuse of Textile Effluent Treatment Plant Waste Sludge in Clay Bricks. *J. Univ. Chem. Tech. Met.* **2006**, *41*, 473–478.
3. Bui, Q.B.; Morel, J.C.; Venkataram Reddy, B.V.; Ghaya, W. Durability of rammed earth walls exposed for 20 years to natural weathering. *Build. Environ.* **2009**, *44*, 912–919. [[CrossRef](#)]
4. Ciurileanu, G.T.; Bucur Horvath, I. The new vernacular based architecture. *JAES Sect. Civil. Eng. Inst.* **2011**, *1*, 27–34.
5. Ciurileanu, G.T.; Bucur Horvath, I. Modular Building Using Rammed Earth. *Acta Tech. Napoc. Civ. Eng. Archit.* **2012**, *55*, 173–181.
6. Suciu, M.C.; Suciu, N. Sustainable development—The key issue of the XXI century. *Bul. Agir.* **2007**, *1*, 124–125.
7. Moquin, M. Ancient Solutions for Future Sustainability: Building with Adobe, Rammed Earth, and Mud. *Adobe J.* **1994**, *4*, 543–552.
8. Bui, Q.B.; Morel, J.C.; Hans, S. Compression behaviour of non-industrial materials in civil engineering by three scale experiments: The case of rammed earth. *Mater. Struct.* **2009**, *42*, 1101–1116. [[CrossRef](#)]
9. Kiroff, L.; Roedel, H. Sustainable Construction Technologies: Earth Buildings in New Zealand. In Proceedings of the Second Internatiol Conference of Sustenable Constructions Materials and Technologies, Ancona, Italy, 28–30 June 2010; Volume 1, pp. 349–360.
10. Vural, N.; Vural, S.; Engin, N.; Sumerkan, M.R. Eastern Black Sea Region. A sample of modular design in the vernacular architecture. *Build. Environ.* **2007**, *42*, 2746–2761. [[CrossRef](#)]
11. Jayasinghe, C.; Kamaladasa, N. Compressive strength characteristics of cement stabilized rammed earth walls. *Constr. Build. Mater.* **2007**, *21*, 1971–1976. [[CrossRef](#)]
12. Karim, M.d.R.; Zain Muhammad, F.M.; Jamil, M.; Lai Fook, C.; Islam, M.d.N. Use of Wastes in Construction Industries as an Energy Saving Approach. *Energy Proc.* **2011**, *12*, 915–919. [[CrossRef](#)]
13. Lazarescu, A.; Szilagyi, H.; Baera, C.; Hegyi, A. Alternative concrets—Geopolymer concrete. *Emerg. Res. Opp. Ed. Napoca Star* **2020**, *1*, 152.

14. Feuerborn, H.-J.; Harris, D.; Heidrich, C. Global aspects on coal combustion products. *Proc. Eurocoalash Conf. Univ. Dundee/Scottl. Great Br.* **2019**, Volume XXVI, 1–17.
15. CEPROCIM. C50—*Study on Possibility of Capitalization in the Romanian Economy of Products Resulting from the Energy Industry (Gypsum, Calcium Sulphite, Ash)*; Ministry of economy and finance-Sector Plan: Bucharest, Romania, 2007–2008.
16. Călătan, G.; Hegyi, A.; Dico, C. Adobe bricks constructions. Past experience, the base of the contemporary buildings. In *Proceedings of the International Multidisciplinary Scientific GeoConference: SGEM 2016*, Albena, Bulgaria, 30 June–6 July 2016; pp. 17–24, ISBN 978-619-7105-69-8.
17. Călătan, G.; Hegyi, A.; Dico, C.; Mircea, C. Additives influence on the earth characteristics used in vernacular construction. *Ecoterra J. Environ. Res. Prot.* **2015**, *12*, 7–20.
18. Călătan, G.; Hegyi, A.; Mircea, A.; Grebenisan, E. Experimental research on the use of industrial waste as addition to the realization of the bricks from unburned clay. *Rev.Constr.* **2020**, *XVII*, 13–20.

**Publisher’s Note:** MDPI stays neutral with regard to jurisdictional claims in published maps and institutional affiliations.



© 2020 by the authors. Licensee MDPI, Basel, Switzerland. This article is an open access article distributed under the terms and conditions of the Creative Commons Attribution (CC BY) license (<http://creativecommons.org/licenses/by/4.0/>).



Article

# Self-Healing Concrete Mix-Design Based on Engineered Cementitious Composites Principles <sup>†</sup>

Tudor Panfil Toader <sup>1,2,\*</sup> and Anamaria Cătălina Mircea <sup>2</sup>

<sup>1</sup> NIRD URBAN-INCERC Cluj-Napoca Branch, 117 Calea Florești, 400524 Cluj-Napoca, Romania

<sup>2</sup> Faculty of Civil Engineering, Technical University of Cluj-Napoca, 15 Constantin Daicoviciu Street, 400020 Cluj-Napoca, Romania; anamaria.mircea@incerc-cluj.ro

\* Correspondence: tudor.toader@incerc-cluj.ro

<sup>†</sup> Presented at the 14th International Conference INTER-ENG 2020 Interdisciplinarity in Engineering, Mureș, Romania, 8–9 October 2020.

Published: 10 December 2020

**Abstract:** Concrete is the most used material in the construction industry, being prone to cracking. Following the action of aggressive external agents, through cracks, access routes to the embedded reinforcement are created. By enclosing in concrete various materials that can induce the self-healing property, by taking actions when the cracks appear, the access of the external aggressive agents to the reinforcement can be stopped, therefore creating more durable materials. The aim of the research is to design a micro concrete with self-healing properties, based on Engineered Cementitious Composites principles from the literature and using local raw materials.

**Keywords:** micro concrete; self-healing; innovative materials; sustainable development; waste management

## 1. Introduction

Concrete is currently the most used material for in the civil engineering field. Depending on the type of the element and the desired and designed strength, concrete can be used in three different forms: simple concrete, reinforced concrete and reinforced/precompressed concrete. As a porous material, prone to microcracking/cracking, the retrieve of tensile efforts by the concrete are most of the time neglected, having very good properties in retrieving compression efforts, giving rigidity to the structure, and protecting the reinforcement. The retrieve of tensile efforts from the concrete sections is carried out by the reinforcement embedded in the concrete mass [1].

Cracking/microcracking of concrete does not implicitly lead to the failure of the infrastructure/suprastructure of the buildings of which it belongs, but leads to the formation of pathways for aggressive factors from the external environment, to the reinforcement embedded in the concrete, which in time lead to the decrease in the capacity of the reinforcement to retrieve the tensile efforts of the concrete sections, due to its possible corrosion [2]. Without blocking the access routes of external aggressive factors, structural failure can occur by the loss of the bearing capacity of the elements.

Literature highlights several of the main parameters that can generate the self-healing mechanism of concrete [3], namely:

- Subsequent hydration of un-activated cement in concrete mass;
- Filling cracks due to the action of outside water by transporting particles inside the cracks;
- Formation of calcium carbonate or calcium hydroxide;
- Extension of the hydrated cement matrix into the crack.

The application of the embedded microcapsule approach as a self-healing agent has been carried out and demonstrated by Withe et al. [4]. When the crack reaches and breaks the embedded microcapsules,

the healing agent is released into the cracks through the phenomenon of capillary (Figures 1 and 2). Then the self-healing agent comes into contact with the built-in catalyst, triggering the polymerization reaction and as a result closing the cracks nearby.

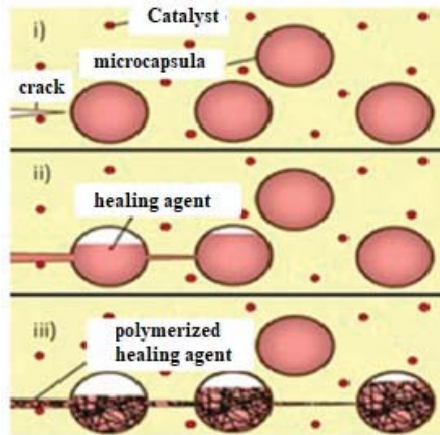


**Figure 1.** Basic method of approaching microcapsules: (i) formed in the matrix; (ii) crack breaks the microcapsules, releasing the healing agent into the plane of the fissure by capillary action; (iii) the healing agent comes into contact with the catalyst, triggering polymerization thus ensuring the closure of the close cracks [4].

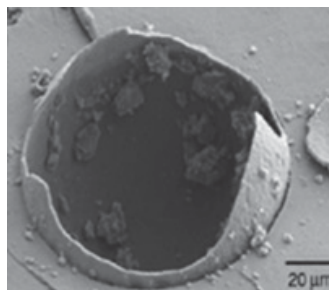


**Figure 2.** Expansion agents and mineral mixtures—eSEM image showing a broken microcapsule [4].

In another study [5], a geopolymer with a  $\text{SiO}_2$  content of 71.3% and an  $\text{Al}_2\text{O}_3$  content of 15.4% was added together with the expansive agent. Geopolymers were found to be formed by polymerization of individual species of alumina and silicate, which were dissolved from their original sources at high pH in the presence of alkaline metals. Detailed studies showed that the size of the geopolymeric gel was less than 2  $\mu\text{m}$  and that the interface phases of the cracks of the initial cracking area formed several phases of hydrogarnet. It indicated that the phases of hydrogarnets or phases Aft, (Figure 3) were formed of an expansive agent and therefore played an important role in the cracked materials. The EDS analysis also showed that most of the modified geopolymeric gel was structured by dense phases compared to the hydrogarnate phases. Chemical admixtures have also been studied in this research series [5,6]. It was concluded that the addition of carbonates such as  $\text{NaHCO}_3$ ,  $\text{Na}_2\text{CO}_3$  and  $\text{Li}_2\text{CO}_3$  to normal concrete contributed to increased recrystallization of cementitious particles and precipitated particles into concrete. In particular, when using the appropriate dosages of carbonates and the expansive agent, the self-healing capacity of the cracks could be improved.

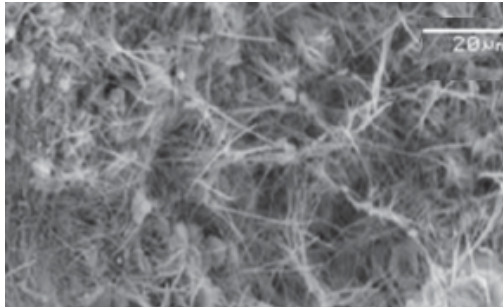


**Figure 3.** Microscopic image of healing products—formation of hydrogarnet phases [6].

Microbial precipitation of calcium carbonate ( $\text{CaCO}_3$ ) is determined by factors that include the concentration of inorganic carbon dissolved, the concentration of calcium ions and the presence of nucleic shales. The first three of these factors are veneered by the metabolism of bacteria while cell walls of bacteria action as nuclear sites [7].

Since the cell wall of bacteria is negatively charged, bacteria are able to extract cations from the environment, including positively charged calcium ions, which are deposited on the surface of the cell wall. With this method that induces bacterial precipitation of  $\text{CaCO}_3$  localized, cracked faces could be filled. Scenario of the process of self-healing of cracks by bacteria immobilized in concrete is illustrated in Figure 4.

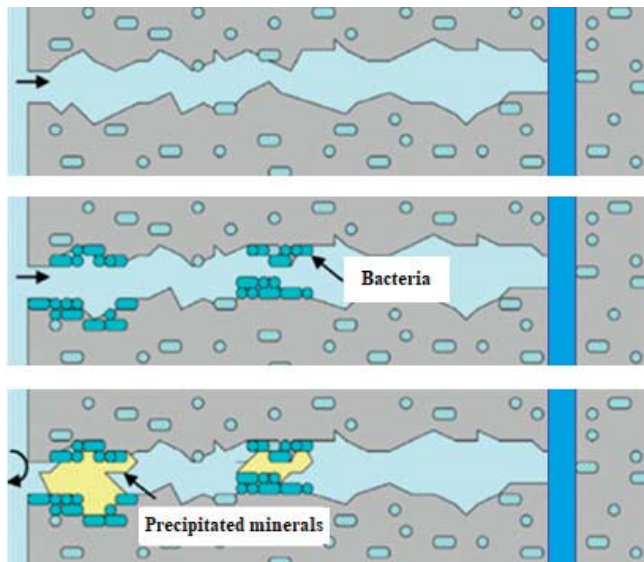


**Figure 4.** Schematic scenario of healing cracks by bacteria immobilized in concrete. Bacteria on the fresh surface of the fissure become activated due to water ingestion, begin to multiply and precipitate minerals such as calcite, seal the crack and protect the steel reinforcement from external chemical attack [8].

Self-healing concrete could solve the problem of concrete structures deteriorating well before the end of their service life. The success of a knowledge-based society depends on the interaction with the business environment and the sources available in order to generate new products and processes [9] Besides the production of materials with self-healing properties, the use of materials derived from



industrial by-products, is constantly increasing, therefore demand for special concrete is also increasing (i.e., geopolymer concrete, self-healing concrete) [10,11].

The aim of this research is present preliminary results regarding the mix-design of a new, innovative material, namely micro concrete, with self-healing properties, by using local sources materials (fly-ash, limestone slurry, fibers and aggregates), some of them being considered wastes after several industrial processes.

## 2. Materials and Methods

The design of the micro concrete with self-healing properties is based on the results obtained in the literature on cementitious composite materials, namely on their self-healing property [12]. For the first stage of the study, a micro concrete was designed, by replacing the type of sand used in the production of cementitious composite materials. Two mixtures were studied in which the silica sand with a maximum size of 0.3 mm used in previous studies [13] was replaced with CEN-Standard Sand (Mixture T1) and with river sand (Mixture T2).

The design of the materials studied in this paper started from the design studied in the literature about Engineered Cementitious Composites [11] and by using the following materials: Portland cement: CEM 42.5 R, fly-ash, sand, polymeric PVA fibers (with a density of 1300 kg/m<sup>3</sup> and 8 mm length), slurry paste and a highly water-reducing superplasticizer. The ratios for the mixture T1 and T2 and SS-L-PVA are presented in Tables 1 and 2. It can be seen that by changing the type of the sand, an optimization of the water used in the mix took place. For both mixtures, with washed river sand and with CEN-Standard Sand, the same quantity of water was used.

**Table 1.** Mixed design ratios of SS-L-PVA- FA/C used as a model from the literature [13].

Mixtures	CEM <sup>2</sup>	FA <sup>3</sup>	Sand	Water	PVA	LS <sup>4</sup>	Superplasticizer
SS-L-PVA- FA/C	1.00	1.20	0.76	0.65	2.0%	0.18	0.02

values reported to cement quantity, <sup>2</sup> CEM—cement; <sup>3</sup> FA—fly-ash, <sup>4</sup> LS—limestone slurry.

**Table 2.** Mix-design ratios for T1 and T2.

Mixtures	CEM <sup>2</sup>	FA <sup>3</sup>	Sand	Water	PVA	LS <sup>4</sup>	Superplasticizer
T1, T2	1.00	1.20	0.76	0.58	2.0%	0.22	0.02

values reported to cement quantity, <sup>2</sup> CEM—cement; <sup>3</sup> FA—fly-ash, <sup>4</sup> LS—limestone slurry.

Starting from the initial mixture of Engineered Cementitious Composite from the literature (Table 1), because of the workability of the new mixtures where the type of sand was changed, silica sand (maximum size of 0.3 mm) changed with washed river sand (maximum granule of 4 mm) and CEN-standard Sand, an optimization of the quantity of water was made, and decreased from 0.65% (for SS-L-PVA-FA/C) to 0.58% (for T1 and T2). As well, the quantity of limestone slurry was increased from 0.18% (for SS-L-PVA-FA/C) to 0.22% (for T1 and T2) in the mixtures.

The raw materials used in the production of the concrete were pre-conditioned in laboratory conditions at (20 ± 2) °C and (50 ± 3)% relative humidity and the two types sand were also conditioned until constant mass.

In order to obtain the desired self-healing properties, the ratios in which the materials were used, was carefully monitored in terms of mix-design of the new material. In addition, in the design of the micro concrete, the mixing sequences used for the preparation of the engineered cementitious composites were based on relevant studies in the literature [14]. Two types of mixtures were tested: Mixture T1- with CEN-Standard Sand and Mixture T2—with river sand with maximum size of 4 mm (Figure 5).

Tests regarding the mechanical properties of the material were performed at 28 days, on 40 × 40 × 160 mm samples to obtain flexural and 1600 mm<sup>2</sup> samples for compressive strength (Figure 6).

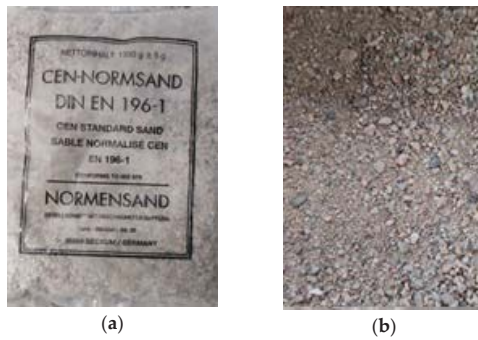


Figure 5. Sand used in the mixtures: (a) T1—CEN-standard Sand; (b) T2—River sand.

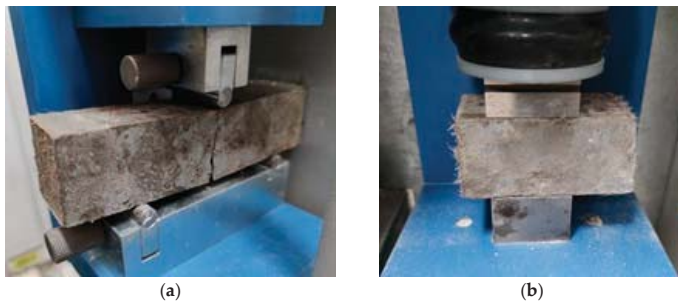


Figure 6. Mechanical parameters of the mixtures: (a) 3PB test; (b) compressive strength.

Three specimens were cut in halves and tested for the evaluation of the microcracks (Figure 7). To evaluate the self-healing capacity of the micro-concrete, the specimens after being tested were microscopically analyzed using a LEICA DMC 290 Microscope. The specimens after being tested [15] at 28 days were microscopically evaluated with measuring the microcracks and were subjected to 28 cycles of wet/dry. The wet/dry cycles were 12 h immersed in water and 12 h in air in laboratory conditions ( $(20 \pm 2) ^\circ\text{C}$  and  $(50 \pm 3)\%$  RH) and after 28 days were microscopically reanalyzed. The microcracks width was measured before and after the conditioning of the specimens in order to evaluate the self-healing capacity.

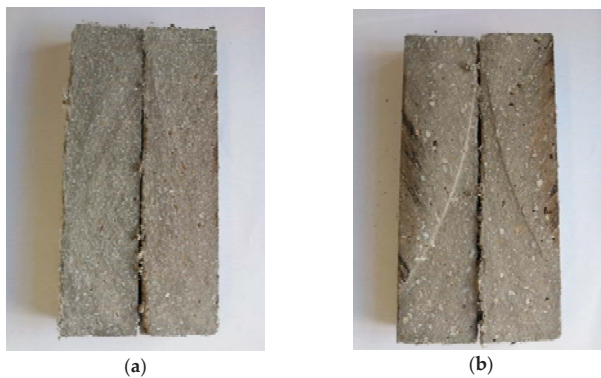


Figure 7. 3PB section samples for self-healing preparation: (a) T1; (b) T2.

Figure 8 represents microscopic images of the prismatic specimens made according to recipes T1 and T2.

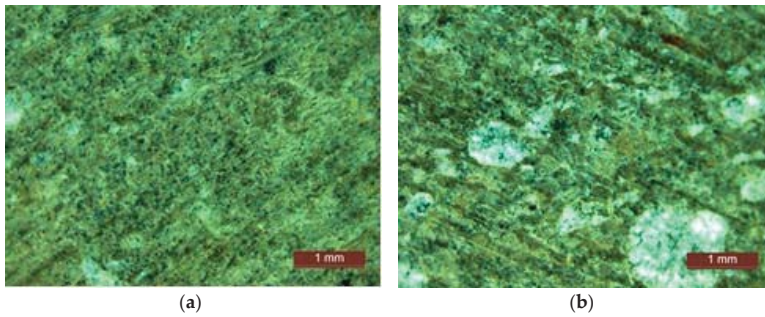


Figure 8. 3PB section samples microscopical analysis at 28 days: (a) T1; (b) T2.

### 3. Results and Discussions

The mechanical properties of the samples and the initial cracking analyses were carried on at 28 days after being conditioned in water at  $(20 \pm 2)$  °C. Result obtained on the flexural and compressive strength of Mixtures T1 (CEN-Standard Sand) and T2 (River sand) are presented in Table 3.

Table 3. Mechanical properties of the mixtures.

Mixture ID	Compressive Strength (MPa)	Flexural Strength (MPa)
T1	51.2	17.2
T2	51.3	18.1

Test results show that both the flexural strength and the compressive strength of the micro-concrete mixtures are not significantly influenced by the type of the sand used in the production of the samples, with less than 1% differences in the compressive strength.

The self-healing capacity of the samples was also tested by subjecting the samples presented in Figure 7 to a 3PB test in order to generate cracks on the surface of the samples, after which the samples were microscopically analyzed. After that, the samples were subjected to 28 wet/dry cycles (12 h immersed in water/12 h in air) and resubjected to microscopical analysis (Figures 9 and 10). Consequently, for all the samples, at each stage, the mean width of the microcracks ( $w_{med}$ ) was measured as a parameter of the self-healing capacity (Table 4).

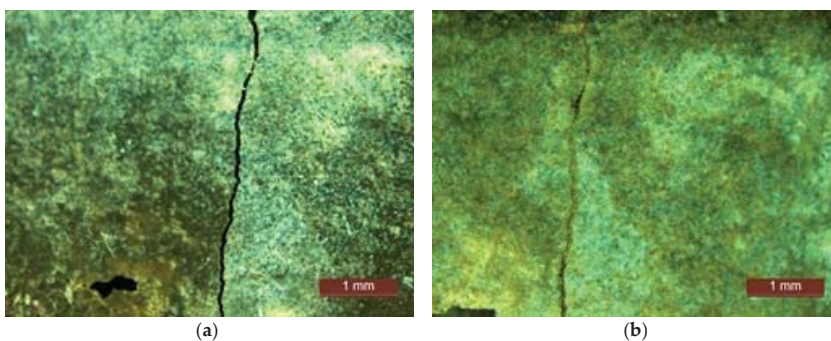
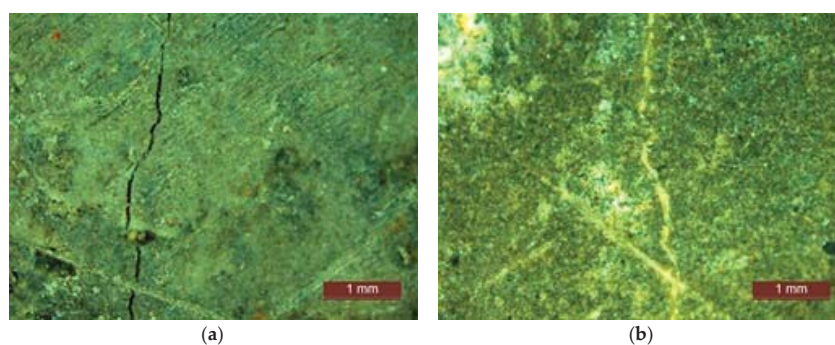


Figure 9. T1 microcrack evaluation: (a) 28 days initial evaluation; (b) evaluation after 28 wet/dry cycles.



**Figure 10.** T2 microcrack evaluation: (a) 28 days initial evaluation; (b) evaluation after 28 wet/dry cycles.

**Table 4.** Evaluation of the microcracks for T1 and T2 at 28 days and after 28 wet/dry cycles.

Mixture ID	Microcracks Width ( $\mu\text{m}$ )		Microcracks Healing (%)
	$W_{\text{med}}$ 28 Days	$W_{\text{med}}$ after 28 Cycles	
T1	48	6	80
T2	44	5	88

Results shown in Table 4 and Figures 9 and 10 show that the analyzed microcracks presented a self-healing potential, after being subjected to 28 wet/dry cycles with potential closing of the crack exceeding 80%, for the analyzed cases.

#### 4. Conclusions

As fly-ash and limestone slurry are considered by-products from their specific industrial processes and pollutants of the surrounding environment, using them in the production of new, innovative materials could become an important step in the production of sustainable materials for the construction industry.

Based on the above presented test results for compressive and flexural strength, the type of sand used in the mixtures did not significantly influence the mechanical properties of the material.

When comparing the results regarding the self-healing phenomenon with the ones presented in the literature, the microcracks self-healing potential exceeded 80% for the mixtures designed and studied in this paper and 90% for the mixtures from the literature.

Current results regarding both the mechanical properties of the analyzed material and the possible self-healing property opens new perspectives regarding the use of local raw materials in order to develop these types of materials. Future studies focus on the optimization of the mixtures, by using other types of fibers (mainly local), developing a mix-design by using larger size aggregates and by using new types of admixtures in order to study the possibility of producing micro-concrete with self-healing properties.

**Author Contributions:** Conceptualization, T.P.T. and A.C.M.; methodology, T.P.T. and A.C.M.; validation, T.P.T. and A.C.M.; formal analysis, T.P.T.; investigation, T.P.T.; data curation, T.P.T.; writing—original draft preparation, T.P.T.; writing—review and editing, T.P.T. and A.C.M.; supervision, T.P.T. All authors have read and agreed to the published version of the manuscript.

**Funding:** This research received no external funding.

**Conflicts of Interest:** The authors declare no conflict of interest.

## References

1. Wu, M.; Johannesson, B.; Geiker, M. A review: Self-healing in cementitious materials and engineered cementitious composite as a self-healing material. *Constr. Build. Mater.* **2012**, *28*, 571–583. [[CrossRef](#)]
2. Mircea, A.C.; Toader, T.P. Self-healing concrete. *Sci. B Adv.* **2020**, *5*, 324–337.
3. Li, V.C.; Herbert, E. Robust Self-Healing Concrete for Sustainable Infrastructure. *J. Adv. Concr. Technol.* **2012**, *10*, 207–218. [[CrossRef](#)]
4. White, S.R.; Sottos, N.R.; Geubelle, P.H.; Moore, J.S.; Kessler, M.R.; Sriram, S.R. Autonomic healing of polymer composites. *Nature* **2001**, *409*, 794–797. [[CrossRef](#)]
5. Ahn, T.H.; Kishi, T. The effect of geomaterials on the autogenous healing behavior of cracked concrete. In *Concrete Repair, Rehabilitation and Retrofitting II: 2nd International Conference on Concrete Repair, Rehabilitation and Retrofitting, ICCRRR-2, 24–26 November 2008, Cape Town, South Africa*; CRC Press: Cambridge, UK, 2008; pp. 235–240.
6. Ahn, T.H.; Kishi, T. Crack self-healing behavior of cementitious composites incorporating various mineral admixtures. *J. Adv. Concr. Technol.* **2010**, *8*, 171–186. [[CrossRef](#)]
7. Tittelboom, K.V.; De Belie, N.; Muynck, W.D.; Verstraete, W. Use of bacteria to repair cracks in concrete. *Cem. Concr. Res.* **2010**, *40*, 157–166. [[CrossRef](#)]
8. Jonkers, H.M.; Thijssen, A.; Muyzer, G.; Copuroglu, O.; Schlangen, E. Application of Bacteria As Self-Healing Agent for the Development of Sustainable Concrete. In *Proceedings of the 1st International Conference on BioGeoCivil Engineering-Delft, Delft, The Netherlands, 23–25 June 2008*.
9. Rus, M.-I. *The Knowledge Triangle in a Knowledge-Based Society*; Annals of Faculty of Economics, University of Oradea, Faculty of Economics: Oradea, Romania, 2013; Volume 1, pp. 942–947.
10. Lăzărescu, A.; Szilágyi, H.; Baeră, C.; Hegyi, A.; Meită, V. Experimental Investigation on the Development of Geopolymer Paving Blocks by Using Romanian Local Raw Materials. *IOP Conf. Ser.: Mater. Sci. Eng.* **2020**, *877*, 012034. [[CrossRef](#)]
11. Hegyi, A.; Szilágyi, H.; Grebenişan, E.; Sandu, A.V.; Lăzărescu, A.-V.; Romila, C. Influence of TiO<sub>2</sub> Nanoparticles Addition on the Hydrophilicity of Cementitious Composites Surfaces. *Appl. Sci.* **2020**, *10*, 4501. [[CrossRef](#)]
12. Piscoiu, D.N.; Mircea, A.C.; Toader, T.P. Engineered composites materials a new sustainable approach. *Sci. B. Adv.* **2020**, *5*, 345–348.
13. Mircea, A.C.; Mircea, C.; Szilágyi, H.; Baeră, C.; Hegyi, A. Experimental study regarding the influence of fibre to matrix compatibility on general performance of Fibre Engineered Cementitious Materials (FECM). *MATEC Web Conf.* **2019**, *289*, 04005. [[CrossRef](#)]
14. Snoeck, D.; Dewanckele, J.; Cnudde, V.; De Belie, N. X-ray computed microtomography to study autogenous healing of cementitious materials promoted by superabsorbent polymers. *Cem. Concr. Compos.* **2016**, *65*, 83–93. [[CrossRef](#)]
15. ASRO. *SR EN 196-1 Methods of Testing Cement. Determination of Strength*; Romanian Standards Association: Bucharest, Romania, 2016.

**Publisher's Note:** MDPI stays neutral with regard to jurisdictional claims in published maps and institutional affiliations.



© 2020 by the authors. Licensee MDPI, Basel, Switzerland. This article is an open access article distributed under the terms and conditions of the Creative Commons Attribution (CC BY) license (<http://creativecommons.org/licenses/by/4.0/>).



# Romanesque Historical Monuments Reconstruction by Using Original Materials and Recycling of Those that Have Lost Their Historical Value <sup>†</sup>

Anamaria Boca <sup>1,\*</sup>, Tudor Panfil Toader <sup>2</sup> and Călin Mircea <sup>1</sup>

<sup>1</sup> Faculty of Civil Engineering, Technical University of Cluj-Napoca, 15 Constantin Daicoviciu Street, 400020 Cluj-Napoca, Romania; calin.mircea@dst.utcluj.ro

<sup>2</sup> NIRD URBAN-INCERC Cluj-Napoca Branch, 117 Calea Florești, 400524 Cluj-Napoca, Romania; tudor.toader@incerc-cluj.ro

\* Correspondence: ana\_boca\_18@yahoo.co.uk

<sup>†</sup> Presented at the 14th International Conference INTER-ENG 2020 Interdisciplinarity in Engineering, Mureș, Romania, 8–9 October 2020.

Published: 10 December 2020

**Abstract:** The aim of this paper is to present the way of reconstruction of historical monuments of Romanesque architecture by reusing and highlighting the original component materials, related to the subassemblies of the construction, respectively the recycling of those components that have lost their historical value. The Romanesque buildings are part of Romanian national cultural heritage and have been through controversial historical periods, and therefore have undergone important modifications or structural losses. The reconstruction or rehabilitation of the Romanesque historical buildings is a way of sustainable development by adapting the buildings to the new conditions of use.

**Keywords:** Romanesque architecture; cultural heritage; reconstruction; rehabilitation

## 1. Introduction

Romanesque architectural style developed in the first period of Middle Ages and spread over the whole Catholic Europe between 9th and 13th centuries. Romanesque style presents significant regional variations because of the availability of materials, technologies and the aesthetic tastes. It became the first international ecclesiastical architectural style; therefore, the greatest number of surviving Romanesque buildings are churches. Romanesque style was introduced to Transylvania from Hungary in the 12th and 13th century. The influence on architectural style was initially from Hungary and Germany, and later from France and Italy. Romanian Romanesque churches are generally small and modest churches, compared to the cathedrals from Europe or the following Gothic churches. The construction material was brick or stone depending on the local availability. In Italy, Poland, part of Germany and Netherlands, brick was used on a larger scale. In other areas, the churches were made of stone in small, irregular pieces bedded in thick mortar. In Transylvania, the builders of the period used preponderant quarry and river stones because of the local availability and numerous stone quarries and Roman ruins. Brick was used in the northeast of Transylvania where stone was not available. While a small number remain substantially intact, many churches were sympathetically restored, being extended and altered in different styles. We will take into consideration some examples of rehabilitation of these historical monuments.

If today's buildings are built with a clear differentiation between their architecture and structure, when talking about Romanesque historical monuments the relationship between the shape and structure of a building appears in a mutual conditioning. The massive load-bearing structure of the Romanesque building gives the stability of these building over decades. Therefore, this study will

include complex aspects related to the reconstruction and rehabilitation of the load-bearing structures of the Romanesque buildings, at the interface between history, art, architecture and structural engineering. Preliminary study on the structural problems of Romanesque churches will be carried out in order to define adequate techniques of interventions following the preservation and restoration principles. The use of traditional, modern and innovative materials and techniques is also discussed.

## **2. Structural Diagnosis**

The reconstruction and rehabilitation of the load-bearing structures of Romanesque buildings require the knowledge of conception, of technical details or the materials and traditional technologies used. A deep understanding of the construction is mandatory when choosing the method of intervention based on the minimal intervention concept of historical monuments.

This research is carried out in two stages:

- structural diagnosis stage (identification of structural degradations);
- the stage of reconstruction and structural rehabilitation.

The structural diagnosis is based on the knowledge of each component of the load-bearing structure. The architectural components with impact on the structural subassemblies are also important, such as: door or window frames, details of floors or installations, the water-canal networks, the characteristics of the foundation land and its mechanical properties, etc. This phase requires collaboration of specialists in the field of architecture, engineering, topography, archeology or restoration. The common concern is to identify the characteristics of the Romanesque structures and to propose the optimal rehabilitation solutions.

The load bearing structure of a Romanesque church is composed by: thick walls made out of brick or stone, foundations, columns/piers, floors, barrel or groin vaults and roof trusses. These structural subassemblies are connected to each other in subunits with different spatial rigidities, which work together and give the mechanical behavior of the entire structure. The empirical-intuitive conception of the load-bearing structures, the quality of the interventions carried out during the utilization period, the extensions or modifications made during the exploitation, the quality of the used materials, the depth of the foundations and the geological conditions have an important influence on the mechanical behavior of Romanesque structures.

The most common deficiencies of the Romanesque structures are: vulnerability to horizontal loads, low anti-seismic conformation, lack of effective connections among the structural elements, presence of horizontal structures (floors and roofs) with poor in-plane stiffness; lack of longitudinal bracing subunit of the roof structure, lack of rigidity of the infrastructure compared to the need to embed the superstructure; stiffness asymmetries and irregular morphology, due to continuous modifications, stratifications and extensions occurring during the time; and low capacity for stretching and shear efforts (Figure 1).

The presence of curved elements along with the massiveness of the walls and pillars/pilasters generates gravitational actions, thrusts that produce significant bending stresses on the main load-bearing system (walls, pilasters, columns). The main structural degradations of the Romanesque ensembles are mostly due to these thrusts, being followed by the other causes like landslides, earthquakes and fires. A part of the Romanesque churches from Transylvania have one or two towers attached on the west end of the church. They produce distortions of seismic response that can lead to the detachment of the church tower and then to the danger of a collision of the two oscillating subunits: tower-nave. Examples can be found at the Evangelical churches from Roades and Rotbav where the towers collapsed in 2016. At Rotbav, the collapse of the tower led to the collapse of a part of the nave walls. Cracking or separation in the rigid bodies "tower-ship-altar" may also appear due to the differentiated settlements of the foundation land. It was found that the consolidation of the joint areas of these bodies with different rigidities and different pressures under the foundations would lead to those degradations in their vicinity.

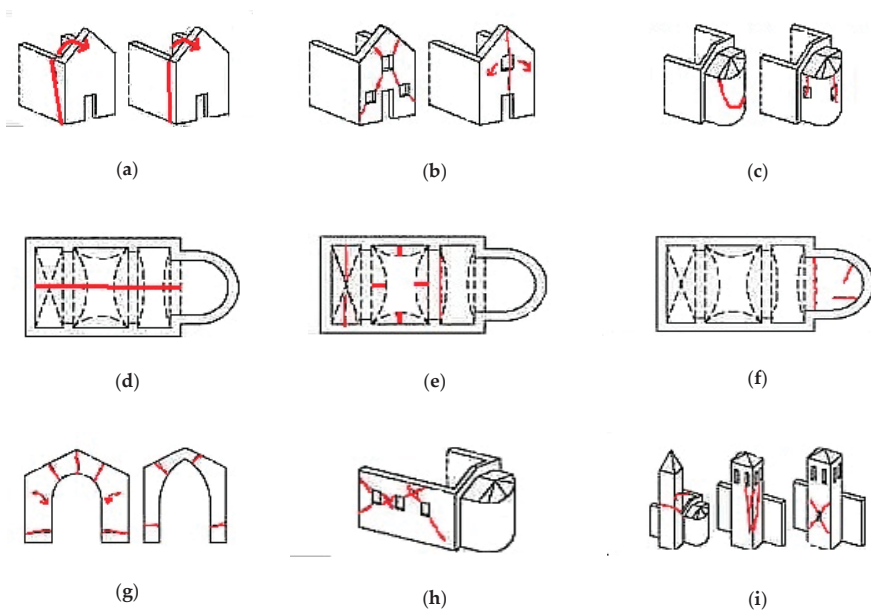


**Figure 1.** Failure mechanisms in Romanesque churches: (a) overturning of the facade; (b) shear mechanisms in the facade; (c) overturning of the apse; (d) transversal vibration of the nave; (e) vaults of the nave; (f) vaults in the presbytery or the apse; (g) triumphal arch; (h) shear failure of the walls; (i) bell tower.

### 3. Structural Consolidation

The structural consolidation on the Romanesque churches must be made with the main purpose of safeguarding the original structure through the use of compatible materials and traditional techniques that can be supplemented with scientifically grounded modern techniques. If the stability of a building is affected or there is the need of a change in destination's building, the structural modifications will be implemented through reversible solutions with the condition that the new elements have the same reliability with the original ones and they must be distinguishable.

#### 3.1. Roof Structure

Preserved in a relatively small number, Romanesque roof structures are characterized by a structural concept limited to the construction of trusses, without any longitudinal bracing systems. On the longitudinal direction, the trusses are stabilized through the roofing support system. The transmission of the loads carried by the trusses to the supporting subunits is made through the simple wall-plates placed over the longitudinal walls [1].

Both Romanesque roof structures are in a good state of stability but there is need of rehabilitation in order to maintain and increase their durability. There are some subsequent interventions on these roof structures. For example, in the case of Vurpar church, temporary consolidations of the marginal north-western area have been made. The biological degradations have made the rafter tie-beam (nodurile caprior-coarda) nonfunctional; therefore, the decision was to place a metal band for carrying the load resulted from the tie-beam between the rafter and the tie-beam. Also, several reinforced concrete rings were placed below the wall plates (centura de beton armat sub cosoroaba). At Toarcla, the observed intervention method on the roof structure is the integrations of bracings made out of a single piece of wood in the rafters (Figure 2).





**Figure 2.** Romanesque roof structures: (a) roof structure Lutheran church in Vurpar; (b) roof structure Lutheran church in Toarcla.

### 3.2. Arches and Vaulting System

The early Romanesque builders developed the science of vaulting when they wanted to replace the wooden ceilings with vaulting structures with better resistance for fire danger. The most common vaults in Romanesque churches are the barrel (semicircular) vaults and the groin vaults—intersection of two barrel vaults (Figure 3). In the later Romanesque period, the ribbed and pointed vaults were also introduced. Vaults constructed of numerous blocks of material pressing against one another exert not only the accumulated downward weight of the material and of any superimposed load, but also a side thrust or tendency to spread. To avoid collapse, adequate resistance against this thrust must thus be concentrated at the haunches (lower portions) of the vault. The resistance may take the form of thickened walls at the haunches; of buttress placed at points of concentrated thrust as in Romanesque and Gothic architecture; or of vaults so placed that their thrusts oppose and counteract. This necessity has controlled the evolution of masonry vaulting and its use in buildings.

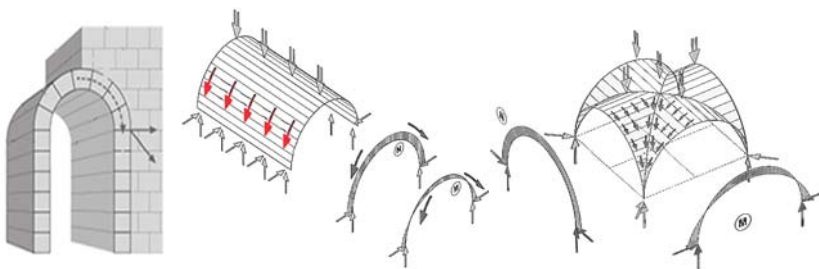


**Figure 3.** The thrusts of a barrel vault and a groin vault.

The structural deficiencies of Romanesque vaults occur mostly as a result of: subsequent faulty interventions, lateral buckling/displacements of the vault’s supports, the lack of horizontal connecting elements on the slabs level, the subsidence of the foundations and the decays of the masonry caused by moisture [2].

The structural consolidation of the vaults and the supporting elements system is mostly done through interventions that are meant to enhance the load-bearing capacity of the structure. This can be done through the increase of the cross-section of the deteriorated elements (encasement). Additional elements compatible with the original elements can be also introduced with the same purpose. Found in Romanesque churches are metal tension bars meant to take over the abutment loads from arched and vaulted structures. Metal tension bars/tie rods (tiranti) placed on the springing lines of the triumphal arches that separate the altar from the nave can be found in many churches of Transylvania (Herina, Avrig). In other cases, reinforced concrete ring-beams were placed on the slab’s level. Indirect

consolidations with additional structures may be also carried out with the purpose to discharge the weak original load-bearing structure of a part of the vertical loads.

The cross ribbed vault of brick at the Calvinist church in Sic was in bad condition due to the lack of a roof structure for the choir for a long period, which led to maceration of bricks on a considerable depth and cracks in the walls. Therefore, the intervention taken consisted of the replacement of macerated bricks, bonding-wedging-grouting and protective plaster on the backs of arches reinforced with geogrid [3].

### *3.3. System Walls-Piers-Columns*

Historical load-bearing support structures such as load-bearing walls, columns and piers have a deficiency in taking over the efforts of stretching and shearing in the console. The walls of Romanesque churches are one of the most important components for the load-bearing structure. The thickness of the walls allows to carry the weight of the vaults. Otherwise, the wall could become unstable if the loads exceed the strength of the masonry, causing structural collapse.

Stone masonry walls have considerable vulnerability to horizontal seismic action, due to their weak mechanical properties and extensive irregularities. In brick masonry, the problem of long-term sustained loads (creep) acting on massive structures (towers, curtain walls, heavy pillars) may induce sudden unexpected collapse [4].

The alternation of columns and piers together with the walls are a very important structural feature of the Romanesque architecture, but sometimes they are used as decoration as well.

At the Evangelical church of Herina, after the 1886 earthquake, the walls were presenting multiple cracks. The adopted solution for consolidations was the insertion of reinforced concrete beams at the upper level of the walls under the roof line and grouting of cracks with lime paste. The same solution was adopted at the church of Strei. In the case of the Calvinist church in Sic, where the degradations in walls occurred due to unprofessional subsequent interventions and improper treatment of fissures (with cement mortar), the cracked walls needed rehabilitation on 80% of their surfaces. The adopted solutions have focused on reassuring continuity by bonding-wedging-grouting plus reinforcing with stainless helical bars [3].

### *3.4. Foundations*

The subassemblies of foundations were made according to an empirical-intuitive conception and have the role of transmitting to the foundation ground the loads of the load-bearing structures. They were made mainly of stone or brick masonry, with lime mortar (up to M10) or clay mortars, with no protection against underground agents. The geometry of the foundations follows the plan design of the building and its construction was influenced by the nature of the foundation land or by the geographical position of the building. In Romanesque buildings, rigid surface foundations and continuous or isolated foundations were made. They were connected to each other by masonry arches through bonding-wedging technique. A major technological aspect that leads to the degradation of a Romanesque edifice is the deficient cooperation of the foundations made in different epochs that lead to unequal settlements. Foundations are exposed to aggressive soil moisture conditions. The problems that arise are related to the depth of foundation, which is often insufficient in relation to the depth of frost of the site and the depth of wetting of the clay with high contractions and swellings and in relation to the foundation ground. Thus, the foundations of the Romanesque structures do not ensure, most of the time, a rigid level of embedding in Romania.

Degradations in foundations of the church in Sic were due to the soil conditions (uneven settling), unprofessional previous interventions or insufficient foundations depth. For the consolidation, the underpinning and micro-piles system was used [3].




Interventions like sub base grouting were carried out at many of the Romanesque churches due to the degradations over time of the material or the insufficient depth. At Strei, the durations of this

intervention had caused cracks in the masonry and movement of the vault with dislocation in the ribs (Table 1).

#### 4. Case Studies

Case Studies—Three Romanesque Churches from Transylvania and Interventions Applied over Time.

**Table 1.** Summary of applied interventions.

	Reformed Church Santamarie-Orlea, HD	Orthodox Church of Strei, HD	Evangelical Church of Herina, BN
Date	1270–1280	End of 13th century	End of 12th century–beginning of 13th century
Model	Central Europe and Italy (cistercian style)	Santamarie-Orlea, HD	Hungary: Akos, Lébény, Jak and Zsambék; Transylvania: Acas and Capleni (Benedictine basilica)
LMI Code	HD-II-m-A-03445	HD-II-m-A-03452	BN-II-m-A-01661
Actual state	It is open to visit but not for liturgical services	Liturgical services are not performed (exception September 8)	It belongs to the Bistrita-Nasaud Museum Complex
Plan	 -hall church-rectangular -rectangular nave with square choir and bell tower	 -hall church-rectangular -rectangular nave with square choir and bell tower	 -basilical plan with central nave and two lateral naves, semicircular apse and two towers at the west end
Material	Rough stone and waist stone bound with thick mortar Facing stones at the corners	Rough stone masonry mixed with bricks Cut facing stones for the exterior intersections of the nave walls	Brick masonry Pillars of shaped stone Foundation-stone
Load-bearing structure	-load-bearing walls made out of stone -wooden roof timber -pointed vault (choir) -groin vault (tower) -octagonal piers cu cubic capitals -stone foundations	-load-bearing walls made out of stone (thickness 85–99 cm) and bricks bound with lime mortar for door areas -wooden floor -pointed vault (choir) with stone ribs -groin vault (tower) -rough stone foundations with lime mortar	-load-bearing brick walls (thickness 1.00–1.30 m) -wooden roof timber (naves) -cross vault (choir) -barrel vault -octagonal, circular, square, cross-shaped pillars (shaped stone) -stone foundations
Interventions history	Early 20th century -restoration works: -the decorative elements carved from stone and were replaced by rigid and unsightly concrete elements; -the stone pyramid of the initial covering of the tower was replaced with a hybrid roof sieve helmet on a wooden frame; -raising the floor level; 1957-repair project 1974-general restoration project to restore the monument to its original appearance and iconographic restoration Repairs: -eaves repair -gutters and downspouts -restoration of the tower roof -plastering the facades while preserving the painted layer -floor restoration -repair of the enclosure wall Consolidation: -sub base grouting for the wall church and for the enclosure wall -concrete topping of the vaults -bounding of the timber frame [4]	Restoration 1895 1969–1972 DMI—mural painting restoration; restoration and consolidation for the monument and for the protected area (prior archeological research) Maintenance/repair interventions: -replacing the shingle roof with one with tiles -rehabilitation of the stone floor at the original level -ditches for rainwater -protection of the area: drainage ditches + underground sewerage -interior and exterior lighting (with provisions for painting protection) Consolidation works: 1966–1972: -sub base grouting at the apse of the altar (because of the long duration resulted: cracks in the masonry + movement of the vault and dislocation and damaged in the ribs); -consolidation of the ribs of the altar vault (through U-shaped steel bracelets, fixed in the reinforced concrete used to consolidate the vault) -consolidation of walls by using concrete bracelets [5] -execution of a new wooden ceiling with moving his position to a upper level according to the level of the old floor) -injecting cracks with fluid mortar -2000-archaeological research	1692/1748: the roofs of the naves were replaced 1886: the church was closed—danger of collapse 1887–1989: -the elevation of the southern tower -interventions for consolidation with metal tie rods for the efforts that led to the cracking of the building; -metal tie rods were placed at the superior part of the nave's walls and the choir But the cracks were not injected -restoration of portals 1994–1999 DSMAI- consolidation-repair interventions -the cracks were injected with cement paste; wedging the wall -repair of metal tile roofing (tower) and roof tile roofs (ship) + eaves (50 cm) -gutters and downspouts -redone of the plasters with lime mortar Structural consolidation: -reinforced concrete bracelets at the top of the walls of the central nave, anchored by the walls of the towers through metal tie rods -metal tie rods on the east wall -braces on the supporting beams of the ships floors anchored in reinforced concrete bracelets and connected diagonally with metal tie rods or wooden cabinets (horizontal washer) [6]

## 5. Conclusions

The restoration of historical monuments has become a very important issue in the preservation of cities and communities. Well-preserved and maintained historical buildings improve the quality of community life with which they coexist. The Historic Monuments List drafted by the Ministry of Culture and National Heritage of Romania in 2015 lists 110 monuments built in the 12th–13th centuries [7,8]. Most of these monuments were built initially in Romanesque style but they have undergone additions or transformations in the following centuries; therefore, it is challenging to find the monuments that have kept their originality. The reconstruction and rehabilitation of the evangelical church of Herina was a necessity after the 1886 earthquake. The church of Sic was in an advanced state of degradation due to unprofessional subsequent interventions [9]. Even if the solutions adopted are questionable in correlation with today's principles, nowadays these churches stand as some of the most representative monuments for Romanesque architecture. Following these examples, we would like to raise awareness about the need of conservation or reutilization of the abandoned medieval churches. For example, in Cluj County, the actual state of the church of Nima (uncovered) affects the valuable mural paintings that can be seen on the walls [10]. Even if the monument was cleared out of the vegetation from inside and a roof over the altar was realized in 2006, a complex restoration of the monument was not possible yet due to lack of financial resources.

We should also look into the importance of the reconstruction of the several fortresses built between the 13th–15th centuries. A major reconstruction project for the Bologa Fortress was begun in 2016. The restorations of the stone churches of Santamarie Orlea and Strei have had an important impact on increasing tourism in this area. An approach on the research of small village churches in Romania may reveal the importance of including these almost abandoned churches on a so-called Romanesque Route (following the example of Germany, Portugal, Spain, France) and later on, their insertion on the TRANSROMANICA-The Romanesque Route of European Heritage, along with the St. Michael's Cathedral from Alba Iulia.

The reconstruction and the reutilization, along with some modern intervention techniques, are raising divisive opinions but we must take into consideration that reconstruction is motivated by an interest in value preservation and, in some cases, is imposed by functional needs.

**Conflicts of Interest:** The authors declare no conflict of interest.

## References

1. Suătean, H. The Historic Roof Structures of the Main Naves in the Romanesque Churches in Vurpar and Toarcla. *Transsylvania Nostra J.* **2013**, *1*, 34–42.
2. Bucur-Horvat, I. Structural Strengthening of Historic Buildings. *Transsylvania Nostra J.* **2013**, *2*, 49–60.
3. Makay, D.; Sandor, B.; Bordas, B.; Hari, J. The utility of valid standards and norms in what pertains to structural rehabilitation; Case study: The research, design and implementation of the calvinist churches in the village of Sic. *Transsylvania Nostra J.* **2015**, *4*, 20–36.
4. Arhiva INP, fond DMI, dosar 8465/1957-1982. In *Biserica reformată Sântămăria-Orlea, jud. Hunedoara*; National Institute of Heritage: Bucharest, Romania, 1982.
5. Arhiva INP, fond DMI, dosar 8624/1960-1972. In *Biserica din Strei, Calan, jud Hunedoara*; National Institute of Heritage: Bucharest, Romania, 1972.
6. Arhiva INP Fondul DMASI, nr proiect 163/1995. In *Lucrari de consolidare reparatii la biserica evanghelică Herina, jud. Bistrita-Nasaud*; National Institute of Heritage: Bucharest, Romania, 1995.
7. Boca, A. The influence of Romanesque structural elements over the development of architecture. In Proceedings of the 14th International Scientific Conference VSU'2014, Sofia, Bulgaria, 5–6 June 2014.
8. Ministry of Culture and National Heritage of Romania. *List of Historical Monuments*; Ministry of Culture and National Heritage of Romania: Bucharest, Romania, 2015. (In Romanian)

9. Boca, A.; Toader, T.P.; Mircea, A.C. Rehabilitation of “romanesque” structures, The Scientific Buletin Addendum, No. 5/2020. In *The Official Catalogue of the “Cadet INOVA” Exhibition, Research and Innovation in the Vision of Young Researchers, The International Student Innovation and Scientific Research Exhibition—“CadetINOVA’20”–“Nicolae Bălcescu” Land Forces Academy*; Editura Academiei Forțelor Terestre “Nicolae Bălcescu”: Sibiu, Romania, 2020; pp. 195–198.
10. Boca, A.; Toader, T.P.; Mircea, A.C. Managementul de protecție a clădirilor istorice. Studii de caz—biserici romanice din județul Cluj, România. In *Conferința de cercetare în construcții, economia construcțiilor, urbanism și amenajarea teritoriului. Lucrările Conferinței de Cercetare în Construcții, Economia Construcțiilor, Urbanism, Amenajarea Teritoriului*; Editura INCĐ URBAN-INCERC: Bucharest, Romania, 2020; pp. 73–80.

**Publisher’s Note:** MDPI stays neutral with regard to jurisdictional claims in published maps and institutional affiliations.



© 2020 by the authors. Licensee MDPI, Basel, Switzerland. This article is an open access article distributed under the terms and conditions of the Creative Commons Attribution (CC BY) license (<http://creativecommons.org/licenses/by/4.0/>).

# Experimental Study on Hollow Blocks with Wastes <sup>†</sup>

Ligia Hanuseac \*, Marinela Barbuta \*, Liliana Bejan, Raluca Rosu and Alexandru Timu

Faculty of Civil Engineering and Building Services, Department of Concrete, Materials, Technology and Management, “Gheorghe Asachi” Technical University of Iasi, 700050 Iasi, Romania; lilbejan@yahoo.com (L.B.); ana-raluca.rosu@academic.tuiasi.ro (R.R.); alexandru.timu@gmail.com (A.T.)

\* Correspondence: ligyahanuseac@gmail.com (L.H.); barbuta31bmc@yahoo.com (M.B.)

<sup>†</sup> Presented at the 14th International Conference INTER-ENG 2020 Interdisciplinarity in Engineering, Mures, Romania, 8–9 October 2020.

Published: 7 February 2021

**Abstract:** The article presents an experimental study on concrete blocks prepared by using waste types such as fly ash as a cement substitution, waste of plastic bottles and wood waste as replacements for sand and polyester fibers waste as a dispersed reinforcement. The mechanical characteristics of concrete with fly ash and polyester fibers were determined. The influence of the type and dosage of waste on the mechanical strength is discussed. The concretes with fly ash and different dosages of waste were used for manufacturing hollow blocks that were tested in compression, and the behavior under load was analyzed. Failure in compression of hollow blocks was gradual and ductile.

**Keywords:** eco concrete; fly ash; waste

## 1. Introduction

Concrete is one of the most used materials in construction and engineers have worked to ensure concrete responds to the new requirements related to environment protection [1,2]. Production of cement, an important component of concrete, is a cause of CO<sub>2</sub> emission (7%), and the huge quantities of natural aggregates used in the concrete composition result in important changes in the natural environment. Non-conventional concretes, with different types of materials in the mix, have emerged just for partially eliminating the above ecological problems. The cement is replaced partially or totally by different materials, such as fly ash, silica fume, slag, rice husk and banana leaves ash [3–8]. Aggregates have been replaced by steel slag, chopped plastic bottles, polystyrene granules, recycled aggregates, chopped sunflower, etc. [9–13]. Fibers of diverse types have also been added in the concrete mix: steel, polyester, hemp, etc. [14–18]. The main objective of the article was to analyze the behavior of hollow blocks manufactured with concrete prepared with a cement substitution with fly ash and waste types such as chopped plastic bottles and wood waste as replacements for sort 0–4 mm and polyester fibers as a dispersed reinforcement. The hollow blocks manufactured with non-conventional concretes will be used to make a non-load-bearing masonry wall. In the next stage, this masonry wall will be built and tested.

## 2. Experimental Program

### 2.1. Materials

In the research, a control mix of concrete (C<sub>0</sub>) was used for preparing hollow blocks which had the following components: cement type CEM I 42.5 R [19] in a dosage of 360 kg/m<sup>3</sup>; and river aggregates in three sorts, namely 0–4 mm, 4–8 mm and 8–16 mm, which were in the following dosages: 803 kg/m<sup>3</sup> of sand, 384 kg/m<sup>3</sup> of sort 4–8 mm and 559 kg/m<sup>3</sup> of sort 8–16 mm. We used water in a dosage of 172 L/m<sup>3</sup>, and 10% of the cement dosage was replaced with fly ash, from CET Holboca Iasi. Fly ash

was used before in other experimental tests and presented by the authors in [15,20]. Waste types PET bottles and wood waste were chopped into sorts of 0–4 mm and used as replacements for 20% by volume of the dosage of aggregate sort 0–4 mm in the case of PET and 40% by volume of the dosage of the same aggregate sort in the case of wood. The chopped PET and wood waste had sizes between 0 and 4 mm. Waste from polyester fibers was used, which was cut into 30 mm-long filaments and dispersed as a replacement reinforcement in the concrete, in a dosage of 0.25% of the concrete weight. In the mixture, we used a superplasticizer (Master Glenium SKY 617 from BASF) in a dosage of 1% of the cement volume.

2.2. Samples

The control mix of concrete (noted C<sub>0</sub>) and the mixes with fly ash and chopped PET (noted C<sub>1</sub>), fly ash and wood waste (noted C<sub>2</sub>) and fly ash and polyester fibers (noted C<sub>3</sub>) were prepared by mixing all the components. The wood waste was moistened before being added to the mix. The samples were poured: cubes of 150 mm in size for determining the compressive strength  $f_c$ , and prisms of 100 × 100 × 500 mm in dimension for determining the flexural strength  $f_{ti}$  and split tensile strength  $f_{td}$  [21–23]. The hollow blocks, one of which is shown in Figure 1, labeled HBF1–HBF3 were manufactured only for the concretes with waste (concretes C<sub>1</sub>–C<sub>3</sub>). After 24 h, the specimens were removed from the formwork and kept in the laboratory at a temperature of 20 °C until testing.

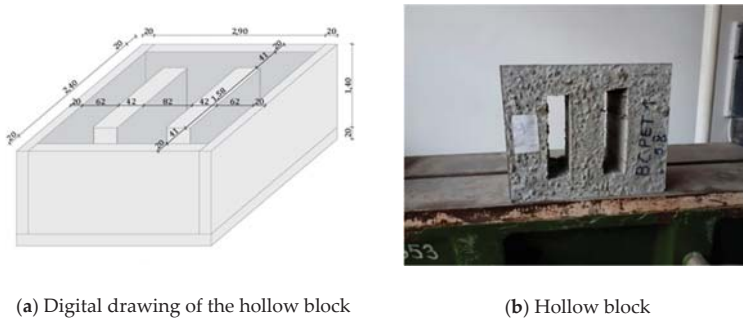


Figure 1. The experimental hollow blocks.

3. Testing Result and Discussion

3.1. Mechanical Strength of Concrete Mixes

The control mix and the concretes with waste were tested at 28 days for mechanical strength. The values are given in Table 1.

Table 1. Mechanical characteristics of experimental concretes.

Concrete Sample	$f_c$ N/mm <sup>2</sup>	$f_{ti}$ N/mm <sup>2</sup>	$f_{td}$ N/mm <sup>2</sup>
Control C <sub>0</sub>	33.45	1.82	1.72
C <sub>1</sub>	25.27	1.74	1.82
C <sub>2</sub>	13.63	1.30	1.24
C <sub>3</sub>	29.80	2.01	1.94



### 3.1.1. Compressive Strength

The value of  $f_c$  for concretes with waste was influenced by the type of waste. All values of  $f_c$  were lower than that of the control mix. The replacement of sort 0–4 mm with chopped plastic in a dosage of 20% had reduced  $f_c$ , with 24.5%, in comparison with the control mix. In the case of the replacement of sand with 40% sawdust,  $f_c$  was reduced, with 52%, and mix C<sub>3</sub> (only with fly ash and polyester fibers) presented a decrease in  $f_c$  of only 11% in comparison with the control mix. For  $f_c$ , the highest value was obtained for concrete C<sub>3</sub>.

### 3.1.2. Flexural Strength

The value of flexural strength was influenced by the type and dosage of waste. When the aggregates of sort 0–4 mm were replaced, a decrease in flexural strength was obtained. The addition of polyester fibers increased the flexural strength by 10% in comparison with the control mix. For  $f_{ti}$ , the highest value was obtained for concrete C<sub>3</sub>.

### 3.1.3. Split Tensile Strength

The value of split tensile strength was influenced by the type and dosage of waste. The waste type chopped PET as a replacement for sort 0–4 mm in a dosage of 20% resulted in an increase in the strength. The waste type wood waste as a replacement for sort 0–4 mm in a dosage of 40% resulted in a decrease in the strength. The dispersed polyester fibers increased the split tensile strength in comparison with the control mix by 12.8%.

The mechanical strengths of concretes with different waste types as replacements for aggregates were lower than those of the control mix. In the case of concrete with fly ash and polyester fibers, the compressive strength was lower than that of the control mix, but the flexural strength and split tensile strength were highest.

## 3.2. Hollow Blocks Experimental Test

The blocks of concrete were subjected to axial compression. The compression force was applied along with the height of the block. The maximum value of the compression load was divided by the gross contact area of the block, including holes, noted  $f_{cb1}$ , and by the net area, noted  $f_{cb2}$ .

The indirect tension stress, according to [24], was computed with the following relation (1):

$$f_{tb} = 2P/\pi Lh, \tag{1}$$

where P is the value of the maximum compression load, h is the height of the block (140 mm) and L is the split length (82 mm) if the holes are neglected, or 240 mm if the total length is considered.

The results of the experimental tests are given in Table 2.

**Table 2.** Experimental results of the compression test on the hollow blocks.

No.	Block	Sizes of Blocks mm	Maximum Compression Force kN	$f_{cb1}$ N/mm <sup>2</sup>	$f_{cb2}$ N/mm <sup>2</sup>	$f_{tb1}$ N/mm <sup>2</sup>	$f_{tb2}$ N/mm <sup>2</sup>
C <sub>1</sub>	HBF1	240 × 290 × 140	815.00	11.71	14.29	4.53	1.54
C <sub>2</sub>	HBF2	240 × 290 × 140	390.42	5.71	6.85	2.17	0.74
C <sub>3</sub>	HBF3	240 × 290 × 140	925.21	13.3	16.21	5.13	1.75

The compressive strengths  $f_{cb}$  of the blocks had different values, depending on the type of concrete. According to [24], the minimum compressive strength must be 7 N/mm<sup>2</sup> and the blocks with fly ash and PET waste (HBF1) and those with fly ash and polyester fibers (HBF3) satisfy this condition for their use in masonry also in seismic areas, as a self-weight masonry for realizing partitioning walls [24]. The block HBF2 can be used for self-weight masonry.



The split tensile strength  $f_{tb}$  of blocks also had good values which are in concordance with values given by other authors [11].

The mechanical characteristics of hollow blocks recommend them to be used in construction for realizing masonry walls.

### 3.3. Failure Mode

During the tests in compression, the blocks failed gradually, and vertical cracks developed throughout the entire depth, especially near holes. The blocks had a ductile failure until the complete damage, as shown in Figure 2.



(a) HBF1



(b) HBF2



(c) HBF3

**Figure 2.** Failure of hollow blocks HBF1, HBF2 and HBF3.

## 4. Patents

For manufacturing the blocks, the following types of waste were used for preparing concrete: fly ash that replaced 10% of cement in all mixes with waste, chopped plastic bottles (PET) that replaced aggregate sort 0–4 mm in a dosage of 20% by weight, waste of wood that replaced aggregate sort 0–4 mm in a dosage of 40% by weight and waste of polyester fibers that was added in the mix with fly ash.

The compressive strength, tensile strength and split tensile of the concretes with waste were determined. The type and dosage of waste influenced the mechanical properties. For all types of concrete, the value of compressive strength was lower than that of the control mix without waste. In the case of concrete with polyester fibers, the flexural strength and split tensile strength were higher than those of all others mixes. For concretes with saw dust, the lowest values of all mechanical strengths were obtained.

When tested in compression, the hollow blocks presented values of compressive strength and tensile strength comparable with other types of blocks, which means we can recommend their use for realizing walls.

**Author Contributions:** Conceptualization, L.H.G. and M.B.; methodology, M.B.; formal analysis and investigations, L.H.G., L.B., R.R., A.T., resources L.H.G., M.B. and A.T.; data curation, L.H.G. and M.B.; writing—original preparation, L.H.G.; writing—review and ending, L.H.G., M.B., L.B., R.R. and A.T.; supervision, M.B.; project administration, M.B. All authors have read and agreed to the published version of the manuscript.

**Funding:** This research received no external funding.

**Conflicts of Interest:** The authors declare no conflict of interest.

## References

1. Khan, R.; Jabbar, A.; Ahmad, I.; Khan, W.; Khan, A.N.; Mirza, J. Reduction in environmental problems using rice-husk ash in concrete. *Constr. Build. Mater.* **2012**, *30*, 360. [[CrossRef](#)]
2. Eun, O.J.; Monteiro, P.J.M.; Sun, J.S.; Sejin, C.; Clark, S. The evolution of strength and crystalline phase of alkali-activated ground blast furnace slag and fly ash-based geopolymers. *Cem. Concr. Res.* **2010**, *40*, 189.
3. Gencil, O.; Koksall, F.; Ozel, C.; Brostow, W. Combined effect of fly ash and waste ferrochromium on properties of concrete. *Constr. Build. Mater.* **2012**, *29*, 633. [[CrossRef](#)]
4. Harja, M.; Barbuta, M.; Gavrilesu, M. Study of morphology for geopolymer materials obtained from fly ash. *Environ. Eng. Manag. J.* **2009**, *8*, 1021. [[CrossRef](#)]
5. Zoum, K.S.; Moon, J.; Cho, J.Y.; Kim, J.J. Experimental study on strength and durability of lightweight aggregate concrete containing silica fume. *Constr. Build. Mater.* **2016**, *114*, 517.
6. Garg, C.; Khadwal, A. Behavior of ground granulated blast furnace slag and limestone powder as partial cement replacement. *Int. J. Eng. Adv. Technol.* **2014**, *3*, 93.
7. Van, V.T.A.; Rößler, C.; Bui, D.D.; Ludwig, H.M. Mesoporous structure and pozzolanic reactivity of rice husk ash in cementitious system. *Constr. Build. Mater.* **2013**, *43*, 208. [[CrossRef](#)]
8. Kanning, R.; Portella, K.; Braganca, M.; Bonato, M.; dos Santos, J.C.M. Banana leaves ashes as pozzolan for concrete and mortar of Portland cement. *Constr. Build. Mater.* **2014**, *54*, 460. [[CrossRef](#)]
9. Yu, X.; Tao, Z.; Song, T.Y.; Pan, Z. Performance of concrete made with steel slag and waste glass. *2016 Constr. Build. Mater.* **2016**, *114*, 737. [[CrossRef](#)]
10. Islam, M.J.; Meherie, M.S.; Rakinul, A.K.M. Effects of waste PET as coarse aggregate on the fresh and hardened properties of concrete. *Constr. Build. Mater.* **2016**, *125*, 946. [[CrossRef](#)]
11. Xu, Y.; Jiang, L.; Xu, J.; Li, Y. Mechanical properties of expanded polystyrene lightweight aggregate concrete and brick. *Constr. Build. Mater.* **2012**, *27*, 32. [[CrossRef](#)]
12. Gonzalez-Corominas, A.; Etxeberria, M. Effects of using recycled concrete aggregates on the shrinkage of high performance concrete. *Constr. Build. Mater.* **2016**, *115*, 32. [[CrossRef](#)]
13. Helepciuc Gradinaru, C.M.; Barbuta, M.; Serbanoiu, A.A. Characterization of a lightweight concrete with sunflower aggregates. *Proc. Manufac.* **2018**, *22*, 154. [[CrossRef](#)]
14. Serbanoiu, A.A.; Barbuta, M.; Burlacu, A.; Gradinaru, C.M. Fly ash cement concrete with fibers-comparative study. *Environ. Eng. Manag. J.* **2017**, *16*, 1123.
15. Barbuta, M.; Marin, E.; Cimpeanu, S.M.; Paraschiv, G.; Lepadatu, D.; Bucur, R.D. Statistical analysis of the tensile strength of coal fly ash concrete with fibers using central composite design. *Adv. Mat. Sc. Eng.* **2015**, *15*, 24. [[CrossRef](#)]
16. Awada, E.; Mabsoud, M.; Hmad, B.; Farran, M.; Khatib, H. Studies on fiber reinforced concrete using industrial hemp. *Constr. Build. Mater.* **2012**, *35*, 710. [[CrossRef](#)]
17. Carroll, J.C.; Helming, N. Fresh and hardened properties of fiber-reinforced rubber concrete. *J. Mater. Civ. Eng.* **2016**, *28*, 15. [[CrossRef](#)]
18. Urkhanova, L.; Lkhasaranov, S.; Buiantuev, S. Fiber-reinforced concrete with mineral fibers and nanosilica. *Proced. Eng.* **2017**, *195*, 147.
19. SR EN 197-1:2011 *Cement, Part 1: Composition, Specifications and Conformity Criteria for Common Cements*; Romanian Standard Association: Bucharest, Romania.
20. Timu, A. *Effects of Using Additions on the Properties of Concrete*; Universitatea Tehnica Gheorghe Asachi: Iasi, Romania, 2018.
21. SR EN 12390-3: 2011 *Testing Hardened Concrete. Part 3: Compressive Strength of Test Specimens*; Romanian Standard Association: Bucharest, Romania.

22. SR EN 12390-4:2010. *Testing Hardened Concrete. Part 6: Flexural Strength of Test Specimens*; Romanian Standard Association: Bucharest, Romania.
23. SR EN 12390-4:2010. *Testing Hardened Concrete. Part 7: Split Tensile Strength of Test Specimens*; Romanian Standard Association: Bucharest, Romania.
24. SR EN 771-4:2004 *Specifications for Masonry. Part 4: Blocks for Masonry of Cellular Aerated Concrete*; Romanian Standard Association: Bucharest, Romania.

**Publisher's Note:** MDPI stays neutral with regard to jurisdictional claims in published maps and institutional affiliations.



© 2021 by the authors. Licensee MDPI, Basel, Switzerland. This article is an open access article distributed under the terms and conditions of the Creative Commons Attribution (CC BY) license (<http://creativecommons.org/licenses/by/4.0/>).

# Fracture Energy of Engineered Cementitious Composites<sup>†</sup>

Anamaria Cătălina Mircea<sup>1,\*</sup> and Tudor Panfil Toader<sup>1,2</sup>

<sup>1</sup> Faculty of Civil Engineering, Technical University of Cluj-Napoca, 15 Constantin Daicoviciu Street, 400020 Cluj-Napoca, Romania; tudor.toader@incerc-cluj.ro

<sup>2</sup> NIRD URBAN-INCERC Cluj-Napoca Branch, 117 Calea Florești, 400524 Cluj-Napoca, Romania

\* Correspondence: anamaria\_catalina\_mircea@yahoo.com

<sup>†</sup> Presented at the 14th International Conference INTER-ENG 2020 Interdisciplinarity in Engineering, Mureș, Romania, 8–9 October 2020.

Published: 10 December 2020

**Abstract:** The aim of this paper is to present preliminary results regarding Engineered Cementitious Composites (ECC) and their behavior when experimentally assessing their fracture energy, by measuring the flexural tensile strength (limit of proportionality, residual). As a characteristic of a ductile material, fracture energy is an important parameter when assessing ECC post-cracking residual stresses. With 2% fibers addition in the mixtures, the crack width can be controlled and the material's ability to bear a tensile strain-hardening capacity has been assessed. Ninety days flexural tensile strength tests were performed in order to obtain preliminary results on ECC prismatic specimens.

**Keywords:** fracture energy; engineered cementitious composites; limit of proportionality; residual strength; fly ash

## 1. Introduction

Using 2% of fibers well distributed, Engineered Cementitious Composites (ECC), with the ability to undergo the tensile strain-hardening capacity with over 300 times that of normal concrete, allow cracks to form and control the crack width [1]. Those materials with high ductility and damage tolerance under tensile and shear loadings [1,2] have a distinguished design compared to Fiber Reinforced Concrete (FRC) based on micromechanics of first crack initiation, fiber bridging and steady-state flat-crack propagation mode [3].

Kanda and Li, in 1998 [4], established two conditions of Engineered Cementitious Composites in order to achieve the strain-hardening behavior and to induce the multiple cracking behavior. The first condition is defined by the first crack stress as a strength criterion and the second one is the steady-state cracking defined as energy criterion. Responsible for initiating the micro cracks, the strength criterion ensures the tensile load that allows the micro cracks to be less than the maximum capacity of the fiber fringing. The energy criterion that prescribes switching the Griffith-type crack is the second condition. As the crack length extends, the opening of the crack increases as for FRC to steady-state flat-crack propagation mode in the case of tension-softening behavior [3].

The fracture energy is the amount of energy that is necessary to generate a crack of one unit of area. For concrete, the fracture energy can be determined experimentally by applying flexural tensile strength loading on a notched concrete specimen [5] and can be calculated as the area under the load-deflection curve divided with the net cross section of the specimen situated above the notch. It is shown that the method of determining the fracture energy by means of stable three-point bend tests on notched beams seems suitable for concrete and similar materials [6]. In order to generate the area under the load-deflection curve, the first step is to experimentally evaluate the flexural tensile strength of the concrete by means of Limit of Proportionality (LOP) and residual strength.

The importance in studying fracture energy is to determine the formation of multiple cracks in the material in order to achieve high tensile ductility similar to ductile materials.

According to Mehta and Monteiro [5], the fracture energy increases when the aggregate size increases, among other factors. Delivering dimensional stability and wear resistance, aggregates can also affect negatively the tensile performances due to the increasing of the tortuosity of the fracture path, which leads to a tough Engineered Cementitious Composites matrix [3]. The propagation of the cracks after they occur leads dramatically to the damage of the steady-state flat-crack propagation process in Engineered Cementitious Composites and the sacrifice of the multiple-cracking behavior [7]. Therefore, in order to generate this effect, fine aggregates should be used in the mix-design, such as micro-silica sand with maximum grain size of 250  $\mu\text{m}$  and a mean size of 110  $\mu\text{m}$  instead of coarse aggregates.

To reduce the environmental impact [8–11], fly ash considered pozzolans and by-product materials and are added to concrete as a cement replacement for economic reasons and to improve the workability of the material as well as prevent their waste disposal. Studies have shown that industrial by-products can be successfully used as partially replacing OPC in concrete, but also as raw material by their chemical activation in the production of new, innovative materials [12,13].

To obtain the residual strength curve, the relationship between the fracture strength and the crack length are needed. The residual strength depends on the crack size. For the structures where the cracks grow slow like monolithic and single load paths, the residual strength capability is simple. For build-up structures, multiple load paths and fail-safe structures where the crack grow slow, due to the geometric construction of the components, the residual strength analysis is complicated. The residual strength for a given structure is a function of the service time.

The main objective of the current research is to explore the development of ECC materials and analyze their mechanical properties, as well as to explore initial experimental methods and testing procedures in order to assess the fracture energy (by means of flexural tensile strength) and the potential approach regarding concrete delay of cracks growing when the material present defects under certain loads, in accordance with fracture mechanics.

## **2. Experimental Program**

Engineered Cementitious Composite mixtures presented in this study were developed based on available literature [14] and starting from a rigorous selection of materials that will be used. The initiation of fracture at pre-existing cracks is affected by the residual stresses in structural materials and can modify the intensity of the crack tip stress field [15]. Depending on the crack opening or crack closure, residual stress can promote or inhibit the initiation of fracture. Residual stress affects the fracture initiation behavior of the materials and their resistance to subsequent crack growth [16]. These parameters can be affected by the raw materials and their specific mix-design ratio.

### *2.1. Raw Materials and Mix-Design Ratios*

In order to produce the ECC samples, Portland cement CEM I 42.5R, Class F fly ash from a local source, silica-sand (maximum size of 0.3 mm) and river sand (maximum size 4 mm), polyvinyl alcohol fibers (PVA), limestone slurry and a water reducing superplasticizer admixture were used. The characteristics of the PVA fibers used have the length of 8 mm, are chemical resistant, have UV-stability, are hydrophilic and previous studies have shown that they meet the requirements of strain-hardening performance of the Engineered Cementitious Composites [14]. The limestone slurry paste was obtained from a local source and, since water is an important parameter that influences the fresh and hardened state of concrete, the water content was measured (19.7%).

Two types of sand were used in the production of the samples in order to study the influence of this material. One mixture was produced using silica-sand (T1E) and one mixture was produced using normal river sand (T2E).

The mix-design ratio was developed based on ECC developed mixtures used in the literature (Table 1) [14] and are presented in Table 2.

**Table 1.** Engineered Cementitious Composites (ECC) base mix-design [14].

Mixtures	CEM <sup>2</sup>	FA <sup>3</sup>	Sand	Water	PVA	LS <sup>4</sup>	Admixture
SS-L-PVA-FA/C	1.00	1.20	0.76	0.65	0.05	0.18	0.02

values reported to cement quantity, <sup>2</sup>CEM—cement; <sup>3</sup>FA—fly-ash; <sup>4</sup>LS—limestone slurry.

**Table 2.** Engineered Cementitious Composites mixture proportions.

Mixture	Type of Sand	Ingredients (wt.%)						
		CEM <sup>2</sup>	FA <sup>3</sup>	Sand	Water	PVA	LS <sup>4</sup>	Admixture
T1E	Silica Sand	1.00	1.20	0.76	0.58	0.05	0.22	0.02
T2E	Normal Sand	1.00	1.20	0.76	0.56	0.05	0.22	0.02

values reported to cement quantity, <sup>2</sup>CEM—cement; <sup>3</sup>FA—fly-ash; <sup>4</sup>LS—limestone slurry.

## 2.2. Testing Methods

The mechanical properties (flexural and compressive strength) of the ECC samples were determined using 40 × 40 × 160 mm prismatic specimens for each of the proposed mixtures; the mean value of the results was considered relevant for the data interpretation. The testing method was in accordance to EN 196-1 [17] and the samples were tested at 28 and 90 days, under laboratory conditions ((20 ± 2) °C and (50 ± 3) % RH).

In order to investigate the 90 days flexural tensile strength (LOP and residual strength) of the mixtures, 150 × 150 × 600 mm samples were produced in the same conditions. The tensile behavior of the samples is evaluated in terms of the residual tensile strength values when subjected to bending, determined by the load-displacement curve of the crack edge, obtained by applying a point load centered on a notched prism. The loading scheme for the test is presented in Figure 1.

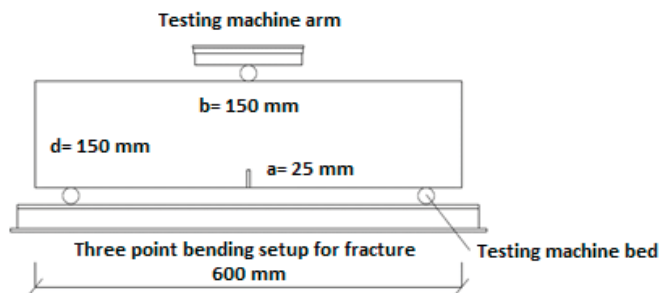


**Figure 1.** ECC flexural tensile strength loading scheme.

Tests to determine the stress displacement (CMOD) diagram, and to determine the values obtained for the displacements of 0.5, 1.5, 2.5 and 3.5 mm, were carried out according to SR EN 14,651 + A1 [18]. The Limit of Proportionality (LOP) was determined according to Equation (1) and the residual strength was determined according to Equation (2) [17].

$$f_{ct,L}^f = (3F_L l)/(2bh_{sp}^2) \text{ (N/mm}^2\text{)} \tag{1}$$

where,  $f_{ct,L}^f$  is the Limit of Proportionality;  $F_L$  is the corresponding stress;  $l$  is the length between the rollers;  $b$  is the width of the sample and  $h_{sp}$  is the distance between the lower part of the notch and the upper part of the sample.

$$f_{Rj} = (3F_j l)/(2bh_{sp}^2) \text{ (N/mm}^2\text{)} \tag{2}$$

where,  $f_{Rj}$  is the residual resistance, which corresponds to  $CMOD_j$  ( $j = 1, 2, 3, 4$ );  $F_j$  is the corresponding stress, which corresponds to  $CMOD_j$  ( $j = 1, 2, 3, 4$ );  $l$  is the length between the rollers;  $b$  is the width of the sample and  $h_{sp}$  is the distance between the lower part of the notch and the upper part of the sample. In Figure 2, the specimens equipped, ready to be tested, are presented.



**Figure 2.** Flexural tensile strength: (a) loading scheme of the samples; (b) transducer used for the displacement measurement.

### 3. Results and Discussions

#### 3.1. Mechanical Properties

The flexural and compressive strength test results of Engineered Cementitious Composites mixtures with different types of sand are presented in Figures 3 and 4.

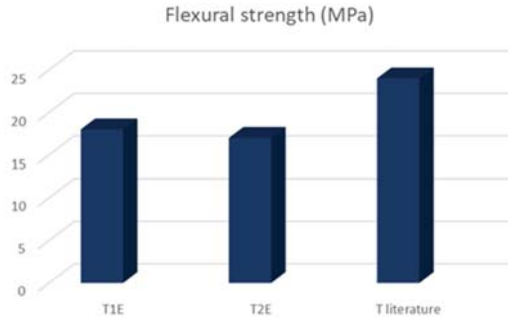


**Figure 3.** Flexural strength of ECC mixtures at 90 days.

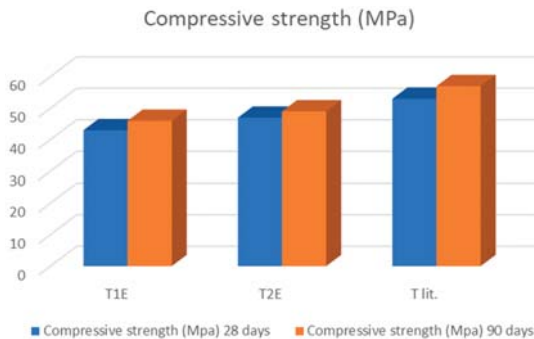


**Figure 4.** Compressive strength of ECC mixtures at 28 and 90 days.

### 3.2. Flexural Tensile Strength (LOP and Residual Strength)

Three point bending tests (3PB) performed at 90 days on the 150 × 150 × 600 mm samples and experimental results and curves concerning the nominal stress and Crack Mouth Opening Displacement (CMOD) are depicted in Figures 5 and 6. Results regarding the LOP are presented in Table 3 and results regarding the residual strength are presented in Table 4. The mean of the individual specimens' curves is also depicted.

Based on the graph curves above, the residual strengths  $f_{R,j}$  (evaluated at four different CMOD values), and the flexural tensile strength (LOP)  $f_{ct,L}^f$  were presented for both of the ECC mixtures proposed. It can be noticed that the post-cracking flexural behavior of samples is generally exhibiting the desirable high residual strength and toughness performance. T2E samples show a much higher post-cracking flexural behavior than T1E samples. A constant CMOD loading rate was maintained until the end of the test. The end point of the test is at 3.5 mm and that is the point where the fracture energy should be calculated.

To find the fracture energy of the specimens, the areas under the curves need to be calculated based on mathematical formulas that are dependent on the geometrical characteristics of the samples [19].

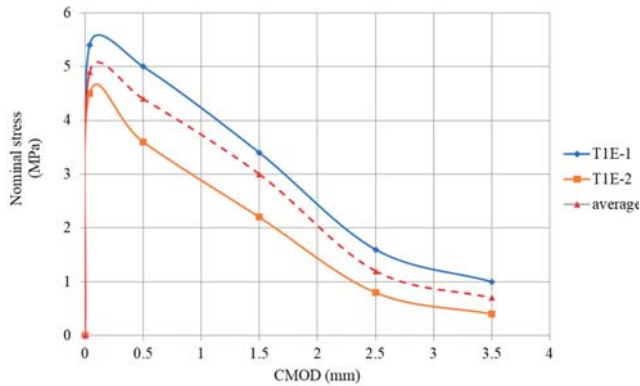


Figure 5. Flexural tensile strength (limit of proportionality, residual)—T1E (90 days).

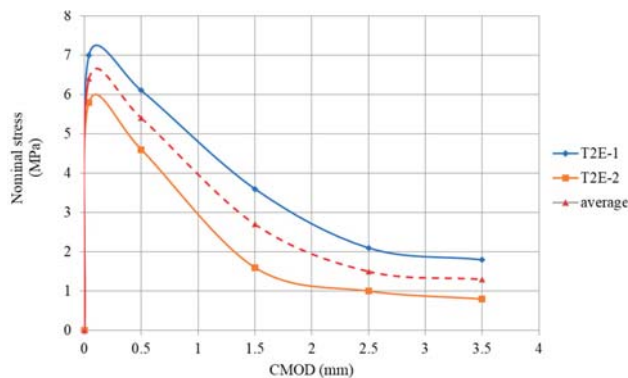


Figure 6. Flexural tensile strength (LOP, residual)—T2E (90 days).



**Table 3.** ECC mixtures Limit of Proportionality.

Mix	F <sub>L</sub>	l	b	h <sub>ps</sub>	f <sub>ct,L</sub>	f <sub>ct,Lmed</sub>	
T1E	T1E-1	16844	500	150	125	5.4	4.9
	T1E-2	14018				4.5	
T2E	T2E-1	21832				7.0	6.4
	T2E-2	18073				5.8	

**Table 4.** ECC residual strength.

Mixture ID	CMOD (mm)	f <sub>R,j</sub> (MPa)	
T1E	T1E-1	0.5	5.2
		1.5	3.8
		2.5	1.6
		3.5	1.0
	T1E-2	0.5	3.6
		1.5	2.2
		2.5	0.8
		3.5	0.4
T2E	T2E-1	0.5	6.1
		1.5	3.6
		2.5	2.1
		3.5	1.8
	T2E-2	0.5	4.6
		1.5	1.7
		2.5	1.0
		3.5	0.8

#### 4. Conclusions

In the present paper, an experimental study was presented aiming at evaluating the cracking behavior in terms of flexural tensile strength of ECC samples produces using local raw materials.

Comparing the test results for compressive and flexural strength with the results obtained in the literature, it was noticed that the mixtures from the literature have a higher compressive strength: 53 MPa at 28 days compared to 45 MPa for the mixtures from this paper, and for flexural strength, 24 MPa at 28 days compared to 18 MPa for the mixtures from this paper.

Post-cracking flexural behavior of the tested samples was generally exhibiting the desirable high residual strength and toughness performance expected for the mix-design of ECC mixtures.

As the fracture energy is tightly bound with the obtained results regarding the flexural tensile strength (LOP, residual) and it can be obtained based on mathematical formulas, further studies will be carried on regarding the output of the presented results in terms of fracture energy and evaluating the parameters that affect this characteristic.

**Author Contributions:** Conceptualization, A.C.M. and T.P.T.; methodology, A.C.M. and T.P.T.; validation, A.C.M.; formal analysis, A.C.M. and T.P.T.; investigation, A.C.M.; data curation, A.C.M.; writing—original draft preparation, A.C.M.; writing—review and editing, A.C.M. and T.P.T.; visualization, A.C.M.; supervision, A.C.M. All authors have read and agreed to the published version of the manuscript.

**Funding:** This research received no external funding.

**Conflicts of Interest:** The authors declare no conflict of interest.

## References

1. Li, V.C. On Engineered Cementitious Composites (ECC) A Review of the Material and Its Applications. *J. Adv. Concr. Technol.* **2003**, *1*, 215–230. [[CrossRef](#)]
2. Li, V.C. Engineered Cementitious Composites (ECC)—Tailored Composites through Micromechanical Modeling Volume 2164. *CSCE* **1997**, 1–38.
3. Sherir, M.A.A.; Houssain, K.M.A. Fracture Energy Characteristics of Engineered Cementitious Composites Incorporating Different Aggregates. **2014**, *2982*, 293–302.
4. Kanda, T.; Li, V.C. Multiple Cracking Sequence and Saturation in Fiber Reinforced Cementitious Composites. *Concr. Res. Technol.* **1998**, *9*, 19–33. [[CrossRef](#)]
5. Mehta, P.K.; Monteiro, P.J.M. *Concrete: Microstructural Properties and Materials*, 3rd ed.; McGraw Hill: New York, NY, USA, 2006.
6. Petersson, P.E. Fracture Energy of Concrete: Method of Determination. *Cem. Concr. Res.* **1980**, *10*, 78–89. [[CrossRef](#)]
7. Sahmaran, M.; Lachemi, M.; Hossain, K.M.A.; Ranade, R.; Li, V. Influence of Aggregate Type and Size on Ductility and Mechanical Properties of Engineered Cementitious Composites. *ACI Mater. J.* **2009**, *106*, 308–316.
8. Mehta, P.K. Influence of Fly Ash Characteristics on The Strength of Portland-Fly Ash Mixtures. *Cem. Concr. Res.* **1985**, *15*, 669–674. [[CrossRef](#)]
9. Mindess, S.; Young, J.F.; Darwin, D. *Concrete*, 2nd ed.; Pearson Education, Inc.: Upper Saddle River, NJ, USA, 2003.
10. Li, V.; Wu, C.; Wang, S.X.; Ogawa, A.; Saito, T. Interface Tailoring for Strain-Hardening PVA-ECC. *ACI Mater. J.* **2002**, *99*, 463–472.
11. Rus, M.-I. The knowledge triangle in a knowledge-based society. *Univ. Oradea. Șt. Ec Tom XXII* **2013**, *1*, 942–947.
12. Szilágyi, H.; Baeră, C.; Hegyi, A.; Lăzărescu, A. Romanian resources of waste and industrial by-products as additions for cementitious mixtures. *Int. Multidiscip. Sci. Geconf. SGEM* **2018**, *18*, 325–332.
13. Lăzărescu, A.; Mircea, C.; Szilágyi, H.; Baeră, C. Mechanical properties of alkali activated geopolymer paste using different Romanian fly ash sources—Experimental results. *MATEC Web Conf.* **2019**, *289*, 11001. [[CrossRef](#)]
14. Mircea, A.C.; Mircea, C.; Szilágyi, H.; Baeră, C.; Hegyi, A. Experimental study regarding the influence of fibre to matrix compatibility on general performance of Fibre Engineered Cementitious Materials (FECM). *MATEC Web Conf.* **2019**, *289*, 04005. [[CrossRef](#)]
15. Withers, P.J. Residual stress and its role in failure. *Rep. Prog. Phys.* **2007**, *70*, 2211–2264. [[CrossRef](#)]
16. Coules, H.E.; Horne, G.C.M.; Abbur Venkata, K.; Pirling, T. The effects of residual stress on elastic-plastic fracture propagation and stability. *Mat. Des.* **2018**, *143*, 131–140. [[CrossRef](#)]
17. ASRO. SR EN 196-1. *Methods of Testing Cement. Determination of Strength*; Romanian Standards Association: Bucharest, Romania, 2016.
18. ASRO. SR EN 14651+ A1. *Method of Testing a Concrete with Metal Fibers. Measurement of Bending Tensile Strength (Proportionality Limit (LOP), Residual Strength)*; Romanian Standards Association: Bucharest, Romania, 2008.
19. Wang, S.; Li, V.C. Engineered Cementitious Composites with High-Volume Fly Ash. *ACI Mater. J.* **2007**, *104*, 233–241.



© 2020 by the authors. Licensee MDPI, Basel, Switzerland. This article is an open access article distributed under the terms and conditions of the Creative Commons Attribution (CC BY) license (<http://creativecommons.org/licenses/by/4.0/>).



# Modelling the Implementation of a Sustainable Development Strategy through Process Mapping <sup>†</sup>

Ioana Miruna Tătaru <sup>\*</sup>, Elena Fleacă, Bogdan Fleacă and Radu D. Stanciu 

Department of Entrepreneurship and Management (DEM), Faculty of Entrepreneurship, Business Engineering and Management (FAIMA), University POLITEHNICA of Bucharest, 060042 București, Romania; elena.fleaca@upb.ro (E.F.); bogdan.fleaca@upb.ro (B.F.); radu.stanciu@upb.ro (R.D.S.)

<sup>\*</sup> Correspondence: tataru.miruna@gmail.com

<sup>†</sup> Presented at the 14th International Conference INTER-ENG 2020 Interdisciplinarity in Engineering, Mureș, Romania, 8–9 October 2020.

Published: 10 December 2020

**Abstract:** Industry 4.0 implies sustainable production by providing green products created through environmentally responsible processes. This paper aims to analyze the two main business processes responsible for energy innovation in a telecommunications company: “develop property strategy and long-term vision” and “evaluate environmental impact of products, services, and operations”. The processes will be introduced using an initial set of key-performance indicators (KPIs) and American Productivity & Quality Center (APQC) Process Classification Framework activities. Through value stream analysis, the non-value-added activities will be eliminated. Ultimately, to provide an overview for the stakeholders, a new set of KPIs will be proposed and the processes will be modeled using Event-Driven Process Chain (EPC) and Suppliers-Inputs-Process-Outputs-Customers (SIPOC) methods.

**Keywords:** sustainable development strategy; energy innovation; telecommunications; business process; event-driven process method; value stream analysis; Industry 4.0

## 1. Introduction

Sustainability, lean manufacturing, and Industry 4.0 are important concerns nowadays.

The concept of sustainability has been developed as a solution to the ecological crisis caused by the intense exploitation of resources and the continuous degradation of the environment. Sustainable development is defined as “development that meets the needs of the present without compromising the ability of future generations to meet their own needs” [1].

Lean manufacturing implies reducing all activities that do not bring value for end customers. It is an ongoing effort to eliminate or reduce all waste in design, manufacturing, and distribution, ensuring quality improvement, reducing processing time and overall costs [2].

Industry 4.0 implies real-time connectivity between suppliers, departments, machines and products, and it aims to revolutionize all industries in terms of technology, business processing and digitalization [2].

Research shows that Industry 4.0 has made the public aware of the challenges present in the Triple Bottom Line, which covers the three pillars of sustainability: economic, environmental and social [3].

Lean manufacturing will decrease energy consumption of non-renewable energies and industrial waste and increase interest in renewable energy and the collaboration between environmentally responsible companies [3].

Cyber-Physical Systems (CPS) introduced by Industry 4.0 will digitalize the relations between suppliers, producers and consumers, creating a smart manufacturing process. This transformation

will lead to an increase in productivity, reducing industrial costs (i.e., production, logistic, quality management), providing better quality of products and reducing errors [3].

Industry 4.0 will lead to a decrease in energy consumption and waste reduction through optimization of logistics and warehousing [3,4].

The Industry 4.0 technological framework consists of the Internet of Things (IoT) and Internet of Services (IoS), which connect the industry through their supply chain network [5].

Research shows that the IoT might have a positive impact on the environment by increasing collaboration with partners that follow good environmental practices and decreasing resource consumption [2].

On the other hand, another research shows that the IoT might increase the demand for massive data centers, which would lead to an increased energy flow. Automation and digitalization might have a negative impact on the environment as it might lead to increased equipment demand, which would increase raw material flow, energy flow and fuel flow in their manufacturing [5]. Digitization and integration would lead to more raw materials and energy required, as well as the disposal or recycling of outdated equipment [6].

The telecommunications industry (i.e., ITC) ensures the communication framework for Industry 4.0, the network and the inter-connection between Internet of Things devices, and therefore their sustainability practices and efforts to create sustainable business processes are objects of concern.

On the European market, the main telecommunications competitors, their revenue, digital programs and climate change actions are explored by the European Telecommunications Network Operation's Association [7].

In this paper, sustainable development data will be used to measure business processes and give examples of programs and initiatives developed by Vodafone (primarily, as their annual report contains a data sheet with useful information), Telekom and Orange.

Previous research addressed sustainability in supply chain systems and proposed a decisional model for evaluating suppliers, under the following criteria: environmental (green corporate social image, environmental management system), social (work safety and labor health) and economic (cost, quality, service) sustainability [8].

Another study extends the Business Process Management concept, focusing on optimizing costs, quality, time and flexibility of the business process with the Green Business Process Management (BPM) concept, which focuses on the environmental consequences of business processes. Green BPM implies reducing greenhouse gas emissions and energy consumption as optimization objectives for business processes [9].

Although there are a multitude of studies on business process in the literature, they cover either other production industries, lean manufacturing, or are focused on certain types of business processes (Green BPM). The processes that will be analyzed in this study are not addressed in the literature.

In the context of Industry 4.0, this study might be relevant to companies operating in the ITC industry thanks to the provided values stream analysis, which may give valuable insights to the implementation of sustainable development strategies and related processes key-performance indicators (KPIs).

## **2. Research Methodology and Input Data**

### *2.1. Categories of Business Processes*

A first step is to identify the input data, meaning the business processes responsible for the sustainable development strategy. The Process Classification Framework (PCF) from APQC in a telecommunications company will be used as a methodology [10].

Developing sustainable, innovative products and solutions that help customers save energy implies conducting business processes from the C2, C3 and C4 categories. A sustainable office uses renewable energy, has intelligent lighting or heating systems, with business processes from the C9

category being responsible from creating it. To drive energy innovation, environmental, health and safety programs should be put in place, and the business processes responsible for creating them are from the C10 category. A sustainable development strategy cannot be achieved without the support of governments, non-governmental organizations and the mass media, and the responsible processes reside in the C11 category. The C13 category is responsible for the adaptation of technology centers.

## 2.2. Groups of Business Processes

The next step is to identify programs implemented by the studied organizations that are directly correlated with the APQC groups of business processes [10]. In Table 1, the following notation will be used P(category\_number).(process\_number) Group of processes. The programs are extracted from the Corporate Social Responsibility (CSR) reports of the targeted companies [11–13].

For each group of processes, the authors identified and extracted the data reported in the CSR reports and date sheets [12–14].

**Table 1.** Groups of business processes.

Programs Claimed in CSR Reports	APQC Process	Process Data	APQC Category Number
Smart City Alba Iulia (Orange), Smart City Piatra Neamt (Telekom)	P2.2: Develop products and services	Purchased goods and services: 4.000.000 tonnes CO <sub>2</sub> (Vodafone)	C2
Supplier Performance Management Program (Vodafone), Supplier Code of Conduct (Telekom)	P4.8: Develop and manage supply chain	-	C4
Code of Ethical Purchasing (Vodafone), Certification in responsible purchasing (Orange)	P9.1: Design and construct/acquire non-productive assets	Energy consumed (GWh): 5582 (Vodafone) Energy consumed (GWh): 9928 (Orange)	C9
	P10.1: Determine health, safety, and environment impacts	3% reduction (Vodafone) 2% emission (Telekom)	
Regular company audits (PwC audits for Telekom, JAC audits for Vodafone)	P10.5: Ensure compliance with regulations	JAC audits for suppliers: 79, Vodafone audits for suppliers: 6, Number of stations evaluated using employee questionnaires: 12 (Vodafone)	C10
	P10.2: Develop and execute health, safety, and environmental program		
#RedLovesGreen, thrive (Vodafone) Certification OHSAS 18001:2007, Employees Forum, Plaza Hobbies Community (Orange), HSE Management System (Telekom)	P10.3: Train and educate employees	90% of employees completed the Code of Conduct training (Vodafone)	
	P10.4: Monitor and manage health, safety, and environmental management program		
Regular company audits	P10.6: Manage remediation efforts	Quarterly verification by JAC (Vodafone)	
GRI G4 Reporting	P11.2: Manage government and industry relationships	GRI Reports (Vodafone, Orange)	
Conflict Materials Report (Vodafone), Ethical code (Orange)	P11.4: Manage legal and ethical issues	90% of employees completed the Code of Conduct training (Vodafone)	C11

The table above contains both measurable data, percentages of the impact or progress of the company towards sustainable development objectives and data that cannot be measured. Also, not all processes have substantial and direct action on the sustainable development strategy.

Using the data from the previous table, the most relevant processes are identified as follows:

P1: Develop property strategy and long-term vision

P2: Evaluate environmental impact of products, services, and operations

P3: Develop IoT products in accordance with the sustainable development strategy

P4: Inform employees about the adoption of socially responsible behavior

P5: Manage relations with government, quasi-government bodies, trade or industry groups.

Based on previous authors' experiences, the following processes has been selected to be analyzed through value stream mapping and modelled, being considered the most relevant for any company operating in the ITC industry and/or other socio-economic sectors:

**P1: Develop property strategy and long-term vision**

**P2: Evaluate environmental impact of products, services, and operations.**

### 3. Mapping the Initial State of Business Processes and Value Stream Analysis

To improve business processes, it is necessary to know the initial state of the performance indicators. Different types of performance can be measured by key-performance indicators (KPIs), for example: energy, raw materials, control, operation [15]. The reason for low performance is waste in different forms, such as transport, inventory, movement, waiting, over processing, overproduction, and defects [16]. Waste does not add value to the product as defined by the customer [17]. From a lean perspective, each activity is classified as an activity that brings value (VA) or activity that brings no value (NVA). However, there are some activities, called ENVA, that are perceived as NVA but may be necessary to the process.

The activities within the processes have been taken from the PCF and divided by their value-added and the justification for their categorization [10].

Table 2 presents the initial state of the P1 process: "develop property strategy and long-term vision". The responsible units are Procurement department and Financial department.

**Table 2.** P1 process-initial state.

No.	Activity	KPI	Value	Justification
A1.1	Confirm alignment of property requirements with business strategy	Requirements list completed 70%	VA	Prevents repetition of next activities
A1.2	Assess the external environment	External environment analysis completed 70%	VA	Necessary for the smooth process execution
A1.3	Analyze the budget for acquiring/renting properties	Financial analysis completed 70%	NVA	Can be carried out along with the decision-making activity
A1.4	Determine build or buy decision for properties	Decision document completed 100%	VA	Decision to take
A1.5	Analyze requirements for workspace assets	Requirements list completed 70%	ENVA	To learn how to create "an environmentally responsible business"
A1.6	Analyze the budget for acquiring/renting workspace assets	Financial analysis document completed 70%	NVA	Can be carried out along with the decision-making activity
A1.7	Determine build or buy decision for assets	Decision document completed 100%	VA	Decision to take
A1.8	Analysis and evaluation	Lists analyzed and completed 90%	ENVA	Alignment and prevents repetition of next activities
A1.9	Improve the organization's sustainable development strategy	Sustainable development strategy completed 90%	ENVA	To include the property strategy

Table 3 provides the initial state of the P2 process: “evaluate environmental impact of products, services, and operations”. To exemplify, Vodafone reported a 3% emission reduction [11], whereas Telekom reported a 2% emission reduction [13]. Each company can set their own KPI. The responsible unit for the process activities is the CSR department.

**Table 3.** P2 process-initial state.

No.	Activity	KPI	Value	Justification
A2.1	Evaluate environmental impact of products, services, and operations	Emission reduction by 3%	VA	Prevents repetition of next activities
A2.2	Conduct health and safety and environmental audits	Renewable energy use 15%	NVA	To identify the regulations
A2.3	Identify regulatory and stakeholder requirements	Regulatory document completed 80%	NVA	To avoid repetition of activities
A2.4	Assess future risks and opportunities	List of risks completed 80%	VA	Necessary for the next activity
A2.5	Create emergency response program	Emergency plan completed 80%	VA	The result is the basis for the CSR plan
A2.6	Create pollution prevention program	Prevention plan completed 80%	VA	The result is the basis for the CSR plan
A2.7	Create health, safety, and environmental (EHS) program	EHS plan completed 80%	VA	The result is the social responsibility program-the purpose of this process
A2.8	Implement EHS program	Success rate 80%	VA	To implement the CSR program
A2.9	Record and manage EHS events	Database completed 80%	VA	To report CSR results
A2.10	Analyze EHS information	Analysis document completed 90%	NVA	The data can be analyzed in relation to the cost and benefit of implementing the program
A2.11	Perform cost-benefit analysis	Favorable cost-benefit ratio 70%	VA	To evaluate the progress
A2.12	Monitor compliance with regulations	Compliance rate 90%	VA	To ensure compliance with regulations
A2.13	Manage remediation efforts	Corrections applied 90%	VA	Activity required only if the company is not compliant
A2.14	Report social responsibility performance	Annual report delivered 100%	VA	To evaluate the progress from year to year

#### 4. Mapping the Future State of the Business Processes

To project the future status of the processes, NVA activities will be removed and new KPI values will be proposed. Each company can set their own KPIs. To exemplify, Telekom would like to achieve 100% renewable energy usage by 2021 [13], whereas Vodafone set the same goal for 2025 [11]. Vodafone would like to reduce 50% of their emissions by 2025 [11], and Telekom reported the objective to reduce by 25% from one year to another (2017 to 2018) [13].

Table 4 provides the future state of the P1 process: “develop property strategy and long-term vision”.



**Table 4.** P1 process-future state.

No.	Activity	KPI (Name)	KPI (Unit of Measurement)
A1.1	Confirm alignment of property requirements with business strategy	Requirements list completed	100%
A1.2	Assess the external environment	External environment analysis document completed	100%
A1.3	Determine decision for properties	Decision document completed	100%
A1.4	Analyze requirements for assets	Requirements list completed	100%
A1.5	Determine decision for assets	Decision document completed	100%
A1.6	Analysis and evaluation	Lists analyzed and completed	100%
A1.7	Improve the organization's sustainable development strategy	Sustainable development strategy completed	100%

Table 5 provides the future state of the P2 process: “evaluate environmental impact of products, services, and operations”.

**Table 5.** P2 process-future state.

No.	Activity	KPI (Name)	KPI (Unit of Measurement)
A2.1	Evaluate environmental impact of products, services, and operations	Emission reduction	50%
A2.2	Conduct health and safety and environmental audits	Renewable energy use	100%
A2.3	Identify regulatory and stakeholder requirements	Regulatory document completed	100%
A2.4	Assess future risks and opportunities	List of risks completed	100%
A2.5	Create emergency response program	Prevention plan completed	100%
A2.6	Create pollution prevention program	Prevention plan completed	100%
A2.7	Create health, safety, and environmental (EHS) program	EHS plan completed	100%
A2.8	Implement EHS program	Success rate	100%
A2.9	Record and manage EHS events	Database completed	100%
A2.10	Perform cost-benefit analysis	Cost-benefit ratio	100%
A2.11	Monitor compliance with regulations	Compliance rate	100%
A2.12	Manage remediation efforts	Corrections applied	100%
A2.13	Report social responsibility performance	Annual report delivered	100%

## 5. Modelling the Business Processes

To provide a view of the processes needed to be managed to achieve energy innovation, Suppliers-Inputs-Process-Outputs-Customers (SIPOC) and Event-Driven Process Chain (EPC) methods are used. SIPOC is a graphical process representation method outlining the entities that provide the necessary data for the execution of the organizational process (Supplier), the data needed for process execution (Input data), the sequence of activities (Process), the results of the process execution (Output), and the entities that use the result (Customer) [18–20].

To provide a strategical view of organizational processes for stakeholders, the sequence of process activities will be represented using the EPC method [21].

For the “develop property strategy and long-term vision” (P1) process, the input data are:

- The Corporate Social Responsibility (CSR) strategy or the sustainable development strategy, available at management level and in CSR and Procurement departments.
- External data, such as rental offices information and sustainable office tools (cooling/heating devices, intelligent lighting, etc.), available through specialized agencies and market research.

The process execution will generate a corporate social responsibility report, updated with the property strategy and long-term vision, that will be used by Management, Procurement and in the “manage relations with government, quasi-government bodies, trade or industry groups” (P5) process. Figure 1 outlines the “develop property strategy and long-term vision” (P1) process.

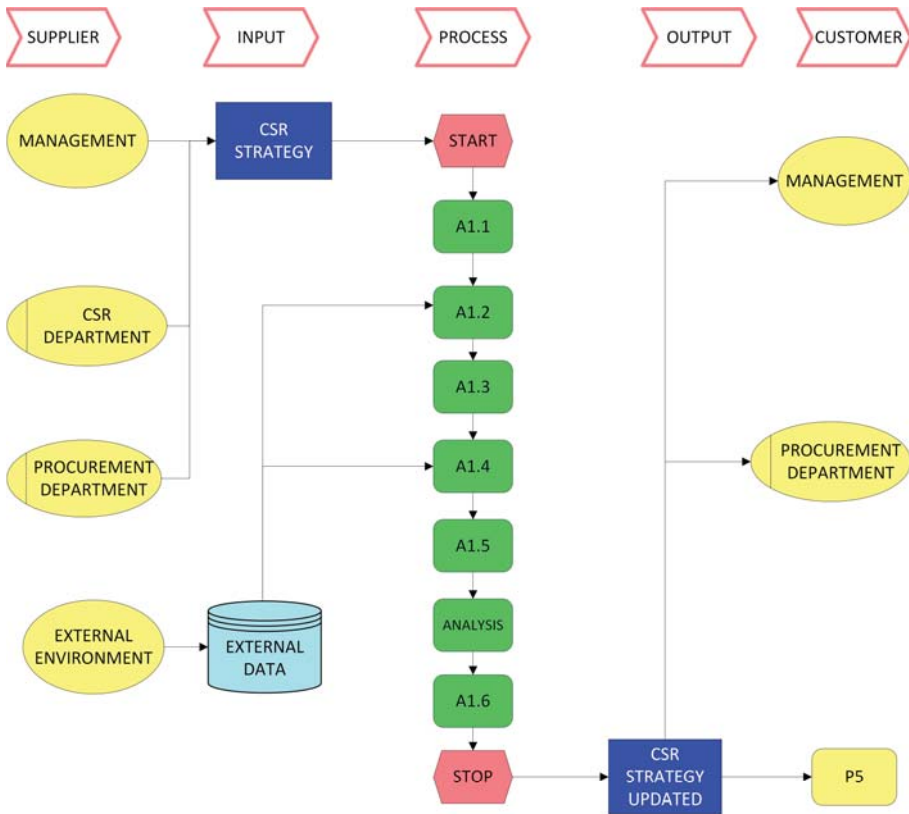


Figure 1. Future state for P1 process.

For the “Evaluate environmental impact of products, services, and operations” (P2) process, the input data are:

- External requirements—generated through market research and collaboration with specialized agencies. For example, an agency knows how to report social responsibility performance, the applicable rules and how the organization can create a favorable cost-benefit ratio by implementing environmental, health and safety measures.
- CSR impact requirements—measured by the CSR department and known by management.

The process execution will generate the CSR program, the updated CSR database, the cost-benefit report and the CSR report, which will be used by management and the CSR department, as well as being made public in the external environment and the “manage relations with government, quasi-government bodies, trade or industry groups” (P5) process. Figure 2 outlines the “evaluate environmental impact of products, services, and operations” (P2) process.

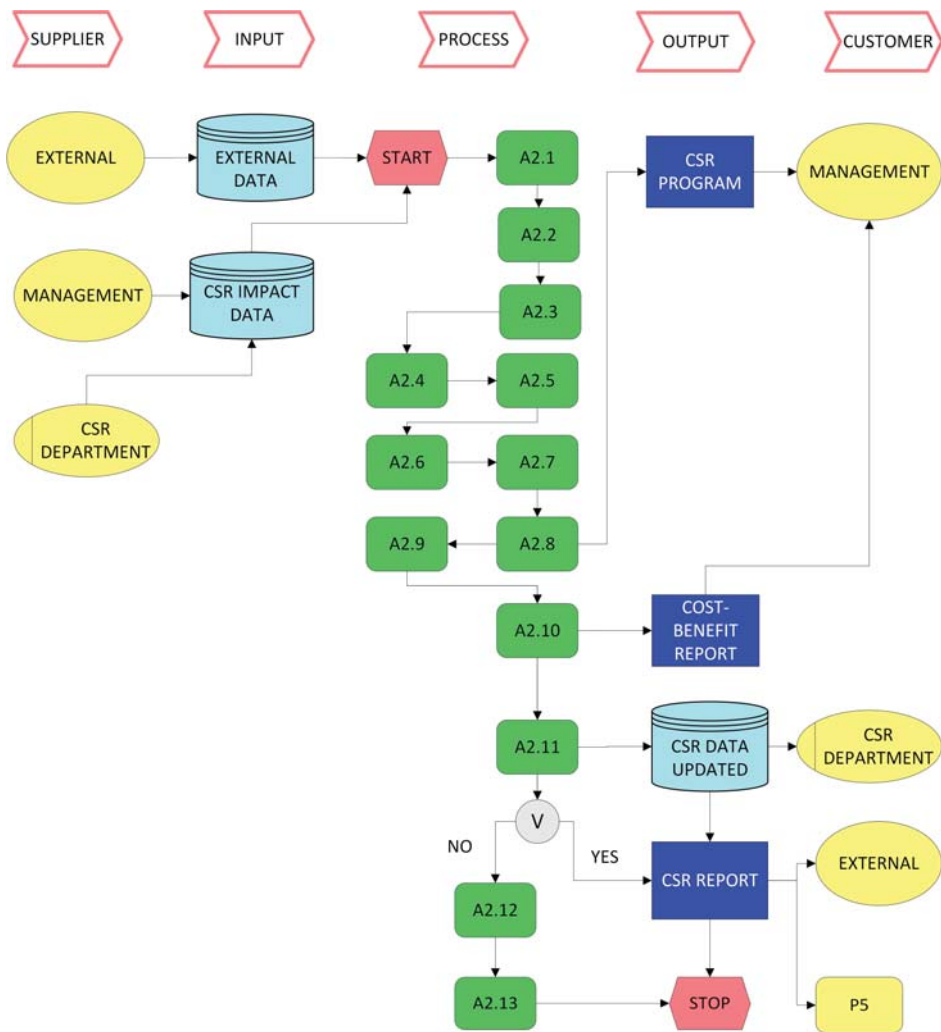


Figure 2. Future state for P2 process.

## 6. Conclusions

In the context of Industry 4.0, sustainable production implies environmentally responsible business processes. This paper, through problematic, approach and results, models the implementation of a sustainable development strategy through process mapping.

Despite numerous contributions to Industry 4.0, lean manufacturing and sustainability, there are few studies on business process modeling, and the two processes analyzed in this study are not addressed in the literature.

This paper addresses two business processes responsible for energy innovation, namely “develop property strategy and long-term vision” and “evaluate environmental impact of products, services, and operations”.

By mapping their initial state with an initial set of KPIs, the authors discovered that some activities can be eliminated or executed along with another activity. To provide an overview for the stakeholders,

a new set of KPIs for the processes has been proposed, and the processes have been modelled using EPC and SIPOC methods.

To create a sustainable business, the management team should improve the two mapped business processes. By developing a sustainable property strategy, the management team ensures that all their properties (offices, plants, factories) are environmentally friendly. Collaboration with specialized agencies and market research is needed to discover the latest trends in sustainability.

All companies should evaluate the environmental impact of their products, services and operational processes to provide an overview for governmental agencies and ensure their progress towards creating a sustainable business.

The study demonstrated that not only the CSR department is responsible for executing the processes and using their outcomes, but also the procurement department and the whole management team. Therefore, sustainability is a joint effort from the key departments in a company.

The study has some limitations. Firstly, the classification of the activities (value-added, non-value added and essential non-value added) is based on the authors' experience. Secondly, the business model is not executed or tested, it is just a proposal. The next step for the study would be to test the model to validate the feasibility of the proposed solution.

To further develop this research, the study can be further expanded by designing appropriate business process control measures in order to provide a complete Six Sigma cycle.

**Author Contributions:** All authors contributed to writing and completing the research paper. All authors read and approved the final version of the manuscript.

**Funding:** This research received no external funding.

**Conflicts of Interest:** The authors declare no conflict of interest.

## References

1. Brundtland, G. Report of the World Commission on Environment and Development: Our Common Future. In *United Nations General Assembly Document A/42/427*; 1987. Available online: <https://sustainabledevelopment.un.org/content/documents/5987our-common-future.pdf> (accessed on 5 July 2020).
2. Varela, L.; Araújo, A.; Ávila, P.; Castro, H.; Putnik, G. Evaluation of the Relation between Lean Manufacturing, Industry 4.0, and Sustainability. *Sustainability* **2019**, *11*, 1439. [[CrossRef](#)]
3. Brozzi, R.; Forti, D.; Rauch, E.; Matt, D.T. The Advantages of Industry 4.0 Applications for Sustainability: Results from a Sample of Manufacturing Companies. *Sustainability* **2020**, *12*, 3647. [[CrossRef](#)]
4. García-Muiña, F.E.; Medina-Salgado, M.S.; Ferrari, A.M.; Cucchi, M. Sustainability Transition in Industry 4.0 and Smart Manufacturing with the Triple-Layered Business Model Canvas. *Sustainability* **2020**, *12*, 2364. [[CrossRef](#)]
5. Bonilla, S.H.; Silva, H.R.O.; Da Silva, M.T.; Gonçalves, R.F.; Sacomano, J.B. Industry 4.0 and Sustainability Implications: A Scenario-Based Analysis of the Impacts and Challenges. *Sustainability* **2018**, *10*, 3740. [[CrossRef](#)]
6. Oláh, J.; Aburumman, N.; Popp, J.; Khan, M.A.; Haddad, H.; Kitukutha, N. Impact of Industry 4.0 on Environmental Sustainability. *Sustainability* **2020**, *12*, 4674.
7. European Telecommunications Network Operators' Association Facts & Figures about European Telecoms Operators. Available online: [https://etno.eu/datas/ETNO%20Documents/Facts%20%20Figures\\_final.pdf](https://etno.eu/datas/ETNO%20Documents/Facts%20%20Figures_final.pdf) (accessed on 26 June 2020).
8. Ahmadi, H.B.; Petrudi, S.H.H.; Wang, X. Integrating sustainability into supplier selection with analytical hierarchy process and improved grey relational analysis: A case of telecom industry. *Int. J. Adv. Manuf. Technol.* **2016**, *90*, 2413–2427. [[CrossRef](#)]
9. Couckuyt, D.; Van Looy, A. Green BPM as a Business-Oriented Discipline: A Systematic Mapping Study and Research Agenda. *Sustainability* **2019**, *11*, 4200. [[CrossRef](#)]
10. APQC Telecommunications Process Classification Framework. Available online: [https://ebpm.ir/wp-content/uploads/2018/05/PCF\\_Telecom\\_Ver\\_5.0.2.pdf](https://ebpm.ir/wp-content/uploads/2018/05/PCF_Telecom_Ver_5.0.2.pdf) (accessed on 26 June 2020).

11. Vodafone Sustainable Business Report 2019. Available online: <https://www.vodafone.com/content/dam/vodcom/sustainability/pdfs/sustainablebusiness2019.pdf> (accessed on 26 June 2020).
12. Orange Raport de Sustenabilitate 2016–2017. Available online: <https://www.orange.ro/responsabilitate-sociala/rapoarte-csr/2016-2017-raport-csr.pdf> (accessed on 26 June 2020).
13. Deutsche Telekom Corporate Responsibility Report 2018. Available online: [https://www.cr-report.telekom.com/site19/sites/default/files/pdf/cr\\_en\\_2018\\_dt\\_final.pdf](https://www.cr-report.telekom.com/site19/sites/default/files/pdf/cr_en_2018_dt_final.pdf) (accessed on 26 June 2020).
14. Vodafone Sustainable Business Report 2019-Data Supplement. Available online: <https://www.vodafone.com/content/dam/vodcom/sustainability/pdfs/data-supplement-2019.pdf> (accessed on 26 June 2020).
15. Lindberg, C.-F.; Tan, S.; Yan, J.; Starfelt, F. Key Performance Indicators Improve Industrial Performance. *Energy Procedia* **2015**, *75*, 1785–1790. [CrossRef]
16. Value Stream Mapping: Definition, Steps, and Examples. Available online: <https://tallyfy.com/value-stream-mapping/> (accessed on 26 June 2020).
17. Womack, J.P.; Jones, D.T. *Lean Thinking*; Free Press: New York, NY, USA, 2003.
18. Furterer, S. *Lean Six Sigma in Service: Applications and Case Studies*; CRC Press: Boca Raton, FL, USA, 2009.
19. Michael, L.G. *Lean Six Sigma for Service: How to Use Lean Speed and Six Sigma Quality to Improve Services and Transactions*; McGraw-Hill: New York, NY, USA, 2003.
20. Fleacă, E.; Fleacă, B.; Maiduc, S. Aligning Strategy with Sustainable Development Goals (SDGs): Process Scoping Diagram for Entrepreneurial Higher Education Institutions (HEIs). *Sustainability* **2018**, *10*, 1032. [CrossRef]
21. ARIS Community Event-Driven Process Chain (EPC). Available online: <https://www.ariscommunity.com/event-driven-process-chain> (accessed on 26 June 2020).

**Publisher's Note:** MDPI stays neutral with regard to jurisdictional claims in published maps and institutional affiliations.



© 2020 by the authors. Licensee MDPI, Basel, Switzerland. This article is an open access article distributed under the terms and conditions of the Creative Commons Attribution (CC BY) license (<http://creativecommons.org/licenses/by/4.0/>).

Proceedings

# New Optimization Technique for Sustainable Manufacturing: The Implementation of the Spc Indicator (System of Evaluating Employee Performance Depending on Customer Satisfaction) as an Important Element of Satisfaction Measurement <sup>†</sup>

Ioan-David Legman  and Manuela Rozalia Gabor <sup>\*</sup> 

“G.E. Palade” University of Medicine, Pharmacy, Sciences and Technology of Târgu Mureş, 540142 Târgu Mureş, Romania; daveione@yahoo.com

<sup>\*</sup> Correspondence: manuela.gabor@umfst.ro or rozalia\_gabor@yahoo.com

<sup>†</sup> Presented at the 14th International Conference INTER-ENG 2020 Interdisciplinarity in Engineering, Mureş, Romania, 8–9 October 2020.

Published: 10 December 2020

**Abstract:** Customer satisfaction as an indicator involves the entirety of employees of the company with direct connection with customers. It motivates employees to reach the highest standards and to constantly increase labor productivity. This paper proposes a new and innovative tool based on: analysis of the evolution of customer satisfaction, determination of mechanisms for evaluating customer satisfaction by applying our own new and innovative method (Spc—System of Evaluating Employee Performance Depending on Customer Satisfaction) in correlation with economic indicators (profit, productivity, cost), elaboration and proposal of solutions for growth and economic development at company level by increasing customer satisfaction based on the results of this research.

**Keywords:** Spc indicator; ITA Method; SIM Program; sustainable manufacturing; optimization technique

## 1. Introduction

The philosophy of any company should be the customer first. This statement should be based on the continuous improvement of both the products and the services offered on the market. From here, we can deduce the importance of analysis and customer satisfaction. Research in recent years has deduced several approaches that reflect the assessment of customer satisfaction from different perspectives. Measuring customer satisfaction is one of the most important elements that retain the attention of companies in all fields of the industry [1]. Customer satisfaction as an indicator involves the entirety of employees of the company with direct connection with customers. It motivates employees to reach the highest standards and to constantly increase labor productivity.

Nowadays, the optimization techniques need some improvement for services and products offered by the manufacturing companies from a sustainable and efficient point of view.

The main purpose of this research was to systematize theoretical concepts of how various aspects of increasing and assessing customer satisfaction in business activities, carried out at the level of society, can be improved. The research objectives were thus:

- analysis of the evolution of customer satisfaction,
- determining mechanisms for assessing customer satisfaction by applying our own methods in correlation with economic indicators (profit, productivity, cost),
- developing and proposing solutions for growth and economic development at the level of society by increasing customer satisfaction based on the results of this research.

Based on these objectives, we have tried to bring a new system to the forefront in the form of an indicator Spc (System of Evaluating Employee Performance Depending on Customer Satisfaction) that includes both classic elements of customer satisfaction and economic elements measuring the activities.

This research is intended to be a relevant research in the field, as no such study has been carried out in the area of customer satisfaction assessment. The main theoretical contribution is the design of a new efficiency measurement indicator, i.e., the Spc. In practical terms, research has a major impact in this area, namely the application of the SIM program (abbreviations from Spc and ITA) translated into the context of a case study: the introduction of a new Spc indicator and a new, innovative ITA method (training, testing of employees, application of knowledge), both components of the SIM program.

The application of these indicators and the method that the authors have ordered has led to increased labor productivity, followed by an increase in the number of contacts taken over by employees, an improvement in the company's management process, which has been reflected in the increase in the company's economic and financial indicators, and an improvement in the relationship between employees and customers, leading to an increase in their satisfaction, the reorganization of the employees' program, which means an increase in staff efficiency, and better control over the operating parameters of each employee, of the entire sector of activity by introducing a SIM program.

These efforts have resulted in an economic indicator: Profit, which is crucial for any market economy society. In the context where the customer is based on any successful economic activity, the focus of the entire analysis of this work was on his satisfaction and how to increase this satisfaction [2].

In this work, after a theoretical deepening of some elements underlying the creation of the Spc indicator and the ITA method, and a practical implementation of the SIM program, I have come to the conclusion that many aspects of the six Sigma method [3] generally used in industry also applies to the services sector. Setting goals, implementing a program, continuously educating employees, along with maintaining a professional environment within the company can be successful elements at the company level [4].

## **2. Theoretical Background**

Our theoretical background for this paper was based on: analysis of the evolution of customer satisfaction, determination of mechanisms for evaluating customer satisfaction by applying our own new and innovative method (Spc) in correlation with economic indicators (profit, productivity, cost), elaboration and proposal of solutions for growth and economic development at company level by increasing customer satisfaction based on the results of this research.

The inductive method was used in this work, and observations made at the level of the commercial service field could be extended to other areas. The analysis and synthesis method was carried out by studying basic concepts that make up different indicators or which form the basis for the formulation of methods and programs. Thus, we are talking about the creation of the Spc indicator based on economic indicators of productivity and cost. It started from the company model that was based on the NRR (Negative Response Rate) indicator and adapted the new indicator, which takes into account contact resolution time, labor productivity, number of contacts resolved and, not least, customer satisfaction. To improve this indicator, we have designed a new method, the ITA method, which refers to employee training, testing and applying knowledge. The employee training process should be a continuous process based on regular testing. The way in which it can apply the theoretical knowledge acquired is diverse, but I have chosen the Mystery Shopper method for this operation. All these activities were carried out under a program called the SIM program, the abbreviation from the Spc indicator, the ITA method and the Mystery Shopper evaluation mechanism.

The ITA method involves training, testing and applying the knowledge accumulated by employees as a result of the process. This method is based on the basic management functions. For the first time in 1916, Henry Fayol [5] formulated functions as essential qualities of management: provision, organization, command, coordination and control.



Any producer will seek to obtain the lowest possible cost for his product, based on supply and demand [6]. Even in the services sector, firms will try to reduce costs by making employees work more efficiently. Given the activity of the firm in this study, the market demand for the services provided by the firm is growing. The improvements needed for the work are aimed at the qualitative side of the work, with supply being of a high standard as regards to the services provided [7].

### 3. Methodology

Key elements of the Six Sigma method have been applied to support the improvement of this process: definition, measurement, analysis, improvement and control. Combining this method with applying a new employee performance measurement indicator has achieved positive results. This new indicator is Spc. The Spc indicator consists of several elements: average labor productivity (WmL), weighted arithmetic mean of satisfaction (Maps), cost per hour/employee (Cha), average contact resolution time—in minutes (t), total contact sum ( $\sum c$ ). The formula for calculating the indicator shall be in the form:

$$Spc = \frac{WmL * Maps}{Cha * t} \times \frac{\sum c}{1000} \tag{1}$$

The Map (weighted arithmetic average of satisfaction) is a way of assessing customer satisfaction after having contacted one of the company representatives. More specifically, the Map is presented in the form of a short questionnaire in which the customer will award from 1 to 5 stars depending on the satisfaction of the service received in connection with the problem resolution.

There has been much discussion on this customer satisfaction tool in the sense that these responses may not fully reflect reality. It is indicated, for the highest performance of the employee’s work, that the Map is as high as possible. This indicator also contributes to the output of the Spc.

Our research has two research hypotheses:

**Hypothesis 1 (H1).** *The current customer satisfaction assessment systems adopted by some companies are not always able to provide an optimal solution for economic growth and development.*

**Hypothesis 2 (H2).** *The current stage of evaluation systems and methods requires improvements and adaptations by applying new, innovative methods that take into account other indicators/parameters/aspects/etc.*

The case study applied to 32 employees where the Spc indicator was introduced. For the firm, a system of customer satisfaction assessment already exists, namely the NRR. This was a rather subjective instrument because the other aspects of the work carried out were not analyzed.

If within 3 consecutive weeks, the NRR is above the 13% ceiling, the employee will receive a warning, which will inform the employee of the situation and then be allocated a supervisor as a way to help to improve their statistics. Together with the supervisor, they will look at more sensitive cases with negative response so that they can determine the mistakes they made when handling specific cases.

Thus, when a representative receives negative feedback, in practice to restore the NRR to a positive value, 10 positive responses are needed. Of course, getting a customer to respond to feedback can be a problem, because the vast majority of customers do not attach too much importance to this assessment service. By assessing employees, an attempt is made to improve the quality of the services provided by the company. Of course, employees are in continuous personal development, with each employee having 30 min a day for training, provided with training material.

We present, in Table 1, an example of the starting dates for calculating the Spc indicator, with the business of employees within the company, and with the activity going on in practice on 2 levels: chat and phone. We have the percentages of how much each of these elements represents in the work done. The average productivity of a factor shall be the ratio of output obtained to the quantity consumed in that production factor. In other words, productivity is determined as the ratio between the results obtained and the efforts made to achieve them.



**Table 1.** The situation of the employees based on the company’s data for December 2018.

Agent Department	Agent Manager	Agent	NRR	Total	% Chat	% Phone
1502VCC	CAN	roberts	6.33%	481	74.03%	0.00%
1502VCC	CAN	angelrem	5.44%	339	8.40%	65.82%
1502VCC	CAN	costinm	11.78%	680	14.68%	66.24%
1502VCC	CAN	geainat	7%	277	0.00%	100.00%
1502VCC	CAN	mateif	<b>21.33%</b>	650	23.93%	48.91%
.....	.....	.....	.....	.....	.....	.....
1582VNAC	CAN	giurgiui	7.99%	122	88.13%	11.87%

Source: Data collected from the company.

The short-term analysis of the behavior of the producer in relation to one of the production factors shows the variation in productivity of this factor and the relationship between production, average productivity and marginal productivity. Work efficiency is usually identified with labor productivity [8]. The disutility attributed to work explains why—in line with the gradual increase in physical labor productivity, resulting from technological innovation and a higher volume of capital—there has generally been a reduction in working hours [9].

The Maps element has a direct influence on the Spc indicator and is directly proportional. It is normal when a customer’s satisfaction increases and the positive result is also increasing. Another important element of Spc calculation is cost.

Cost was described in the light of the company’s own indicator of NRR. 34% of the employees were in the red zone, i.e. the NRR was more than 13%, which, in the company’s view, was outside the target area. This is the starting point with the ITA method and the Spc indicator. In this case, those employees who have not fulfilled their fair share are monitored by following, if the situation is not remedied, to be dismissed.

#### 4. Results

In December 2018, the implementation and testing of the SIM program, named after the initials of the three elements—the Spc indicator, the ITA method and the Mystery Shopping evaluation site—was started. The objective of this program is primarily to develop the company across all sectors. This will aim to increase employee performance, increase labor productivity, increase company economic indicators, increase customer satisfaction, etc. This was the decision that this program should be applied to the entire company. This program was started from the idea that customer satisfaction is an effective indicator, but not sufficient. This should take into account employee productivity, hourly cost per employee, time to resolve a contact, i.e., the whole issue of resolution and satisfaction that is being taken into account to increase the efficiency of the activity.

In this abovementioned respect, I believe that the Spc indicator is best placed to meet these requirements. This indicator consists of all of these elements presented: It takes into account both customer satisfaction and other indicators needed to achieve the efficiency required to perform an economic activity. The application of the ITA method started by identifying the elements pursued in the action. That is, it started with *the training of personnel*. To start the training work, a few questionnaires were implemented from which some elements were derived. First, around 60% of the respondents indicated that the satisfaction with monthly pay was low. In particular, these employees were disturbed by the fact that the monthly fee was influenced by customer satisfaction. In this regard, some issues were discussed in the training process about the customer’s perception of the company’s promises. Some employees promised different services to customers without knowing whether they could be performed, how long they were started or when they were implemented. Employees were also informed about the company’s design, objectives, and how the company wants to be seen in the customer’s eyes. The major problem on the part of employees was the degree of disagreement with the customer satisfaction assessment model applied at the company level.

This training has sought to educate employees to move from a fast-based system with a strong focus on the intuitive side—often impulsive—to a reflective, contemplative system with a strong emphasis on empathy—which really listened to the customer, to understand his needs, and ready for continuous improvement.

Testing is the second element/step of the ITA method, which is an assessment method that involves measuring and assessing the effects of training quantitatively following the performance over time. This monitoring was carried out for 3 months. While in January, the percentage of employees who had difficulties in doing business reached 31%, i.e., the Spc indicator fell below 0.10 points for them, the percentage of employees with a score below 0.10 dropped to 9.38% in the following month (Table 2).

**Table 2.** Presentation of the Spc (System of Evaluating Employee Performance Depending on Customer Satisfaction) indicator at firm level during the period January to March 2019.

	January	February	March
Spc < 0.10	31.25%	9.38%	12.50%
0.10 < Spc < 0.20	46.87%	37.50%	34.37%
0.20 < Spc < 0.30	9.38%	34.37%	34.37%
0.30 < Spc < 0.40	9.38%	15.62%	12.50%
Spc > 0.40	3.12%	3.13%	6.26%
Total (Σ)	100.00%	100.00%	100.00%

Source: Own calculations based on data collected from the company.

The third element of the ITA method was the application of knowledge. The application of the knowledge was made by the “spy” (Mystery Shopper) method. This is also the last phase of the completion of the SIM program.

Each agent in the MS assessment was tested across several sectors: First, the response time of the contact retrieval was analyzed: the customer welcome, the weighted arithmetic mean of satisfaction, the number of contacts resolved, and the average time taken to resolve the problem. It can be seen, in Table 3, how the lowest Spc indicator has the most problems in the rest of the items analyzed.

**Table 3.** The status of employees as a result of the application of the MS (Mystery Shopper) method.

Agent Department	Agent Manager	Agent	Average Contact Pick Reaction Time (s)	How to Welcome the Customer	Maps	Number of Contacts resolved	How to Contact Chat/Phone (%)	Average of the Problem Resolution Time/Contact (min)	Spc—Jan 2019
1502VCC	CAN	roberts	11.9	satisfied	2.1	12	35/65	9	0.09
1502VCC	CAN	angelrem	4.1	good	4.7	28	75/25	4.1	0.23
1502VCC	CAN	costinm	4.5	very good	4.5	31	80/20	3.6	0.45
1502VCC	CAN	geaninat	3.9	excellent	4.7	27	80/20	3.9	0.34
1502VCC	CAN	mateif	6.3	satisfied	3.8	23	30/70	3.9	0.19
1502VCC	CAN	mesarovs	5.9	good	3.5	29	70/30	3.6	0.16
1502VCC	CAN	mirabela	5.8	satisfied	3.8	27	70/30	4.2	0.15
1502VCC	CAN	petricar	4.8	very good	3.9	36	80/20	4.1	0.22
1502VCC	CAN	samoilae	10.1	unsatisfied	1.7	15	55/45	6.1	0.02

Source: Own calculations based on data collected from the company.

For example, the *giurgiu* agent had the average reaction time at contact acquisition greater than 12.1 s. If we were to analyze against the *Spc* indicator, it can be seen that this agent has the lowest score of 0.02 points (Figure 1).

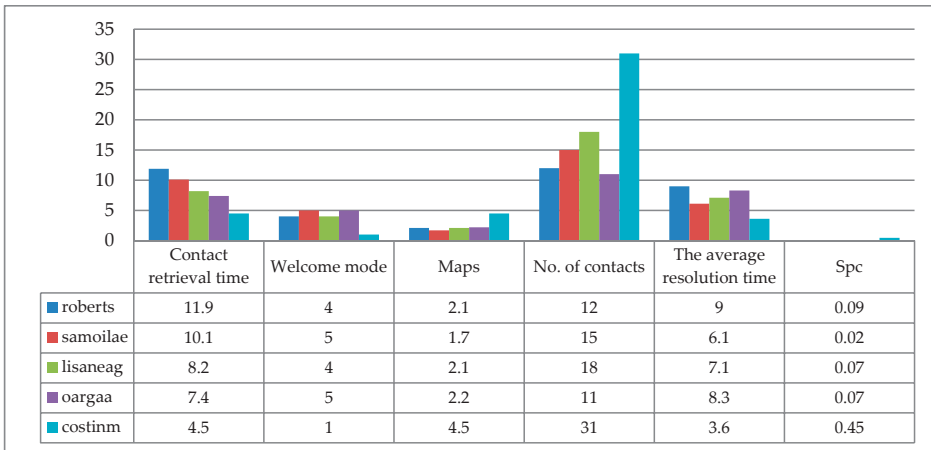


Figure 1. Status of the MS assessment of employees related to the best Spc obtained.

The same agent obtained, by applying the MS method, the average of how to welcome the customer as unsatisfactory, and, in terms of productivity, he also has less than 20 contacts, which places him in the weak area; this also because the average contact resolution time is 7.1 min per contact. When the agent has an average high contact resolution time, the number of contact retrieval is reduced. These correlations can be seen in Figure 2.

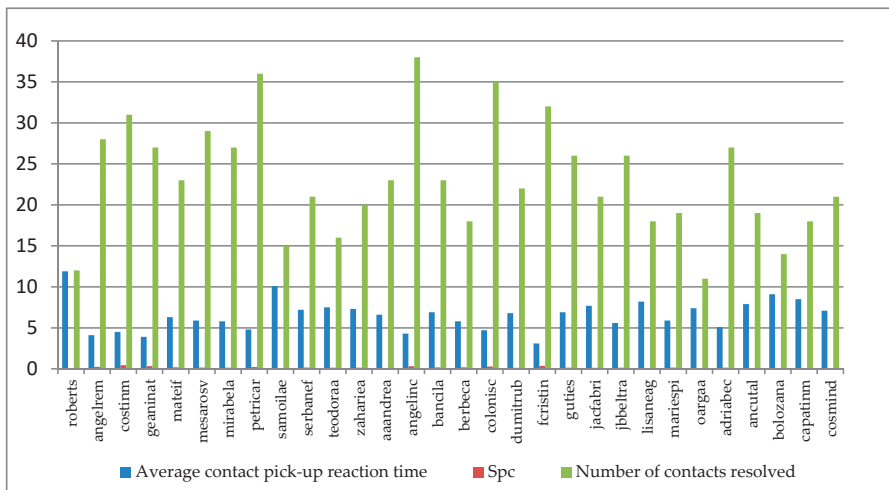


Figure 2. January benchmarking.

### 5. Discussions

This research was done by analyzing the situations and ways in which response times are reduced when dealing with contacts, especially those with high media. Why did some employees have the average time to react to take such high contacts? It seems that, in the case of the company analyzed in this work, there is an aversion to risk. This experiment revealed that only 3 out of the 32 employees were willing to take the risk. It follows that a narrow framework would prevent the managers of firms from achieving maximum efficiency, as employees do not take risks. Perhaps a solution to this problem

would be if groups of 8 people were formed, with the Spc indicator being taken as the average of the 8 employees, without individuality.

This MS method applied within the company has managed to bring, to the forefront, all these aspects which, in December, contributed to the reduction in the efficiency of the company’s staff. These evaluations have resulted in several problems that have been addressed. If we were to look at the changes that occurred over the 3 months individually, we can see, for example, the Spc for Roberts increased from 0.09 points in January to 0.17 points in March. While the resolution time of a contact was not reduced by keeping it to 10 min per contact, the other indicators have undergone various changes, i.e., labor productivity has increased and customer satisfaction has increased.

At company level, as a whole, total employee productivity increased and the number of contacts taken over since January 2019 increased (Table 4).

**Table 4.** Number of contacts taken over by employees between December 2018 and March 2019.

Month	December 2018	January 2019	February 2019	March 2019
Total contacts	12,223	12,557	15,281	14,292

Source: Own calculations based on data collected from the company.

Thus, in January 2019, compared to December 2018, for example, the total number of contacts taken over by employees increased by 2.73%; in February 2019, the number of contacts increased by 25% compared to December 2018.

As a result of the application of the SIM program within the company, economic efficiency has undergone some changes. Between December 2018 and May 2019, the economic and financial situation of the firm was presented in the following manner (Table 5).

**Table 5.** The economic situation of the firm in the period December 2018–May 2019.

Month	December 2018	January 2019	February 2019	March 2019	April 2019	May 2019
Turnover	97,470	96,248	101,744	106,988	100,223	99,309
Profit	13,182	12,967	22,123	29,889	21,659	19,742
Total costs	84,288	83,281	79,621	77,099	78,564	79,567
Number of employees	39	39	41	41	44	44
Eerfp	1.16	1.16	1.28	1.39	1.28	1.25
Eecfp	0.86	0.87	0.78	0.72	0.78	0.80
Rate of return	15.64	15.57	27.79	38.77	27.57	24.81
Commercial rate	13.52	13.47	21.74	27.94	21.61	19.88

Source: Own calculations based on data collected from the company.

If we were to look at the economic situation of the firm, we can see that the turnover of the company in December 2018 compared to January 2019 is down by −1.25%. Looking at the other economic indicators in the same range, it can be seen that the profit is also down by −1.63%; also, a positive thing is that we have a decrease in costs, but overall, the situation is not exactly positive. For example, the commercial rate and the rate of return are decreasing.

## 6. Conclusions

With the start of the implementation of the SIM program within the firm, there have been some visible changes both in the human resources sector and in the economic and financial sector. As regards to the economic efficiency indicator of output factors, it is on the increase that aspect is good, the higher the economic efficiency of the firm.

With regard to the rate of return indicator, which is the ratio between the profit achieved and total costs, we can say that it is growing steadily, which strengthens the claim that the SIM program has been really successful. The relative change in the rate of return is the most pronounced in February, in which it increased from January by 12.22 percentage points. The same trend is also the rate of trade which is also on the rise from one month to the next.

As a conclusion of the case study, we can infer that there is risk aversion [10] on the part of employees due primarily to their fears of failing or losing their jobs. A solution to improving business at the firm level would be to apply the ITA method consistently, along with the Spc indicator, and also to group the way employees are assessed. As a result, it has been noted that to reduce the risk of employee aversion, a solution would be to set up groups of 8 employees so that the analysis results are no longer individual but group.

The main objective of applying the six Sigma method is to improve and increase business activity in companies by reducing defects and increasing productivity [11]. Many of the principles underlying this method are also found in the SIM program used in this work. The very operating mechanism of the Spc indicator is developed on the application model of the six Sigma method. The implementation of this program aims at improving the results in terms of customer satisfaction, while at the same time, improving the results of the indicators presented.

In the case of the study presented, economic and financial indicators can be seen as increasing, which shows a positive aspect of the company's economic situation. The increase in the number of contacts taken at company level is clear to add productivity. From the point of view of the Spc indicator, it can be said that customer satisfaction has been continuously increasing according to the analysis carried out.

**Author Contributions:** Conceptualization, I.-D.L. and M.R.G.; methodology, I.-D.L.; validation, I.-D.L. and M.R.G.; formal analysis, I.-D.L.; investigation, I.-D.L.; writing—original draft preparation, I.-D.L.; writing—review and editing, M.R.G.; supervision, M.R.G. All authors have read and agreed to the published version of the manuscript.

**Funding:** This research received no external funding.

**Conflicts of Interest:** The authors declare no conflict of interest.

## References

1. Hill, N. *Customer Satisfaction*; Cogent: London, UK, 2007; p. 3.
2. Anghel, M. *Economie*; Niculescu: Bucharest, Romania, 2001.
3. Bhale, N.P.; Srividhya, P.K.; Mariappan, V.; Sony, M.; Belokar, V. Six Sigma in Service: Insights from Hospitality Industry. *Int. J. Adv. Res. Sci. Eng.* **2017**, *6*, 1–10.
4. Carroll, C.T. *Six Sigma for Powerful Improvement*; CRC Press: Boca Raton, FL, USA, 2013.
5. Fayol, H. General and Industrial Management. *Acad. Manag. Rev.* **1986**, *11*, 454–456. Available online: <https://www.jstor.org/stable/258475?seq=1> (accessed on 20 February 2020).
6. Angelescu, C. *Economie*; Economică: Bucharest, Romania, 2000.
7. Bauer, T. An Introduction to Organizational Behavior. 2012. Available online: <https://2012books.lardbucket.org/pdfs/an-introduction-to-organizational-behavior-v1.1.pdf> (accessed on 20 February 2020).
8. Gabor, M.R. *Prospectarea Pieței prin Metoda Statistică*; C.H. Beck: Bucharest, Romania, 2013.
9. Von Mises, L. *Actiunea Umana-Tratat de Teorie Economica*; Henry Regnery: Chicago, IL, USA, 1966; p. 99.
10. Kahneman, D. *Gândire Rapidă, Gândire Lentă*; Publică: Bucharest, Romania, 2012.
11. Legman, I.D.; Blaga, P. Six Sigma Method Important Element of Sustainability. *Acta Marisiensis. Ser. Oecon.* **2019**, *13*, 37–68. [CrossRef]

**Publisher's Note:** MDPI stays neutral with regard to jurisdictional claims in published maps and institutional affiliations.



© 2020 by the authors. Licensee MDPI, Basel, Switzerland. This article is an open access article distributed under the terms and conditions of the Creative Commons Attribution (CC BY) license (<http://creativecommons.org/licenses/by/4.0/>).

Proceedings

# The Lean Six Sigma Algorithm—A Pathway for Decreasing the Continuous Improvement Projects Failure Rate <sup>†</sup>

Karam Al-Akel \* and Liviu-Onoriu Marian

Faculty of Machine Building, Technical University of Cluj-Napoca, 400114 Cluj-Napoca, Romania; liviu.marian@yahoo.com

\* Correspondence: karam.alakel@gmail.com

<sup>†</sup> Presented at the 14th International Conference INTER-ENG 2020 Interdisciplinarity in Engineering, Mureş, Romania, 8–9 October 2020.

Published: 23 December 2020



**Abstract:** Even if Lean and Six Sigma tools are available for large audiences, many of the continuous improvement projects fail due to the lack of a pathway that ensures appropriate results in a timely manner. We would like to address this universal issue by generating, testing and validating an algorithm that improves manufacturing processes in a controlled manner. With a selection of the most valuable set of tools and concepts implemented in a specific order, a guideline for successful project implementation is proposed. Decreasing the overall number of continuous improvement project failures is the main scope of our algorithm and suggested methodology.

**Keywords:** lean manufacturing; Six Sigma; pharma industry; algorithm; roadmap; project structure; failure

## 1. Introduction

The continuous improvement of ongoing processes is a natural target for any company that aspires to maintain a competitive advantage on the market. Lean Six Sigma is one of the main methodologies preferred to be implemented with this scope and it maintains a continuous improvement culture and proper results [1]. Even if the Lean and Six Sigma tools are available for the larger public, many of the projects fail due to the lack of a pathway that ensures appropriate results in a timely manner [2,3]. We would like to address this universal issue by generating, testing and validating an algorithm that improves manufacturing processes in a controlled manner. As per our knowledge, an algorithm which addresses this general issue in such detail is not yet available. Decreasing the number of continuous improvement projects failures is the main scope of our algorithm.

## 2. Theoretical Background

Lean Six Sigma is a continuous improvement culture applied all across the world in several industries, with the deepest roots in automotive [4]. Even if the Lean principles have been available for over 30 years [5], many of the continuous improvement projects using its tools fail by missing a proper roadmap for applying them [1,2]. By starting to implement a project without the satisfaction of seeing its results in a timely manner, the project leaders will lose hope and motivation and will abandon the journey. Losing time and money without obtaining results is a no-go for any company. Lean Manufacturing and Six Sigma tools fusion has been proven to have beneficial effects in several companies and industrial fields [6–8]. Nevertheless, the missing link of a detailed implementation algorithm for the manufacturing area does not exist according to our knowledge. With high achievements reported

across the world [9–14], the rate of Lean Six Sigma projects abandoned or failed is kept behind the curtains. Short-term goals and achievements are key aspects in change management and a successful continuous improvement project implementation [15].

### 3. Materials and Methods

In order to generate the proposed algorithm, several studies have been conducted to reveal the most used and efficient Lean Six Sigma tools across several global industries, and the obtained results have been embedded in the suggested structure [16,17]. According to analysis made in various fields, such as automotive, aeronautical, steel and pharmaceutical, a resemblance regarding the challenges faced in manufacturing areas defines four generic issues marked in the algorithm as P1–P4, with the assigned improvement projects: *cycle time decrease (P1)*, *changeover time reduction (P2)*, *output increase (P3)*, *defective parts decrease (P4)*. A pilot project has been conducted in the pharmaceutical industry in the original form of the algorithm to be able to adapt it to the needs and shop floor reality of the manufacturing area [18]. The lessons learned, key take-aways, best order and timing for the LSS tools' usage have been embedded in the final form of the algorithm [19–24].

The ultimate form of the generated algorithm, represented in Figure 1, has been implemented in the pharmaceutical industry, at a manufacturing site. The designated manufacturing line for applying the algorithm was the bottle packaging line for suspensions where the *Overall Equipment Effectiveness (OEE, internally treated as OAE—Overall Asset Effectiveness)* needed to be increased as customer demand has been forecasted to continue growing over time and capacity constraint has already been reached. The algorithm, represented in Figure 1, has been validated by positively affecting the OAE KPI (Key Performance Indicator) which includes several additional CTQs (Critical To Quality), such as weekly unplanned stoppages time, weekly planned stoppage time and weekly/monthly output. Under the umbrella of OAE, challenges regarding P1–P4 were proposed to be solved. An OAE increase of 10% from a baseline of 25% to the new value of 35% would increase productivity by over 30%.

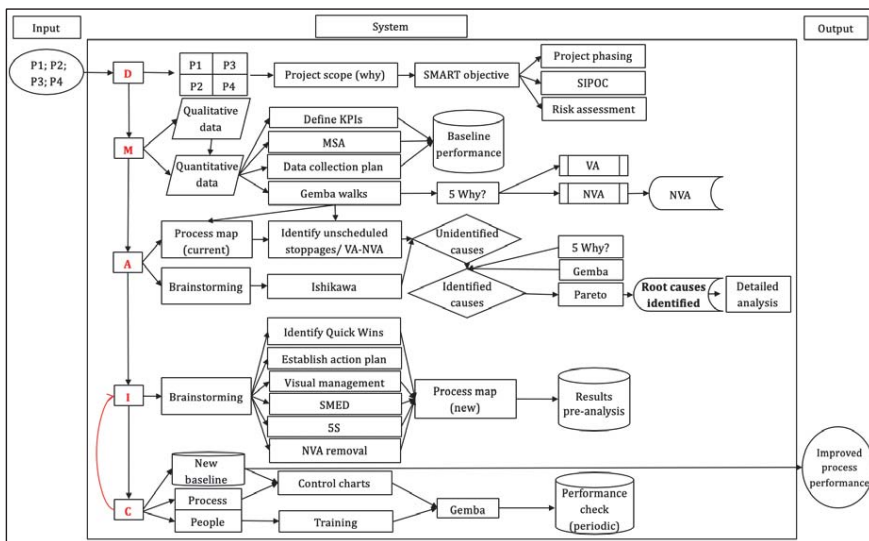


Figure 1. The Lean Six Sigma algorithm.

The main methodology for implementing the algorithm is revealed in a separate paper and states explicit examples of using the Lean Six Sigma tools and tips for applying them. The detailed results for the OAE components, such as planned and unplanned stoppage time, decrease, weekly output increases and waste (muda) removal results are presented in a related paper.

### 4. Results

The Lean Six Sigma algorithm has been implemented for the presented project with a total analyzed timeframe of 18 months, out of which the core implementation period for most of the actions was six months. First, significant results could be noticed after a period of only two months from starting to implement the initial actions and discipline into the process. All the results have been obtained by following the algorithm.

With OAE being a complex KPI with several components, we tracked the daily, weekly and monthly performance, along with one of its components, on a weekly basis: changeovers, packaging line speed, unplanned stoppages, weekly output. As represented in Figure 2, OAE has been improved by 9% from 25% to a new baseline of 34%.

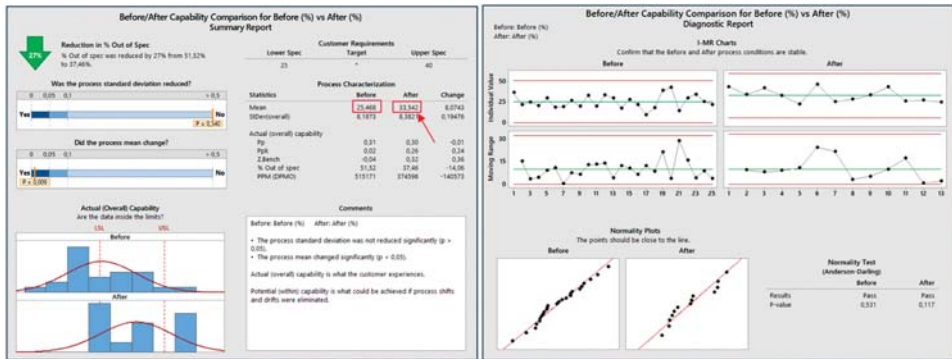


Figure 2. Overall Asset Effectiveness improvement.

The OAE Loss Tree presented in Figure 3 considers the losses from a time perspective, deliberately ignoring good count and asset net running speed. Nevertheless, both factors were included in the OAE calculation. We suggest targeting the OAE Loss Tree components as goals for smaller projects, and approaching them as a whole, in a structured manner according to the suggested algorithm, for the more complex ones.

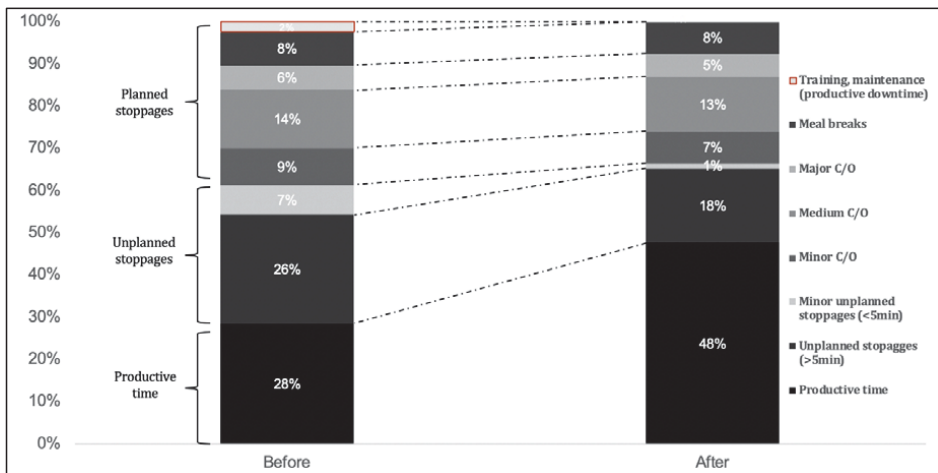


Figure 3. OAE Loss Tree.



## 5. Discussion

The suggested Lean Six Sigma algorithm is structured on the standard DMAIC phases with the specific Lean Manufacturing and Six Sigma tools and suggestions for guidance, organized in the appropriate order for proper implementation. Following the *Define, Measure, Analyze, Improve* and *Control* project phases, the actions have been implemented in the manufacturing area of one pharmaceutical company. This current paper's purpose is not to offer specific details regarding the implementation of each tool used; those key aspects are covered in a separate material.

The main scope of the algorithm is decreasing the failure rate of the continuous improvement projects in the manufacturing areas. We addressed this universal issue by generating, testing and validating through results, an algorithm that improves the manufacturing processes in a controlled manner. The algorithm has been applied, tested and validated in the manufacturing area of a pharmaceutical company, yet conceived to enhance the improvement project's results in multiple batch manufacturing environments. Through improving the complex OAE KPI and its components, we consider the algorithm as a successful pathway in decreasing the failure rate of Lean Six Sigma continuous improvement projects. Through generating and testing a Lean Six Sigma algorithm for process improvement, using specific tools and techniques, we dispatch a validated roadmap for a general issue unaddressed in such detail until today.

**Funding:** This research received no external funding to be disclosed.

**Acknowledgments:** The paper would not have been created without the exceptional support of my guide and advisor, Liviu-Onoriu Marian. I would also like to express my deep gratitude to the company that allowed me to implement, test and validate the algorithm in the manufacturing area. I would like to thank the kind and knowledgeable support of the entire team who aided my efforts.

**Conflicts of Interest:** The funders had no role in the design of the study; in the collection, analyses, or interpretation of data; in the writing of the manuscript, or in the decision to publish the results.

## References

1. Bhuiyan, N.; Baghel, A. An overview of continuous improvement: From the past to the present. *Manag. Decis.* **2005**, *43*, 761–771. [[CrossRef](#)]
2. Gerger, A.; Firuzan, A.R. Reasons of failure in Lean Six Sigma projects. *Int. J. Multidiscip. Res. Dev.* **2012**, *2*, 123–130.
3. Antony, J.; Lizarelli, F.L.; Fernandes, M.M.; Dempsey, M.; Brennan, A.; McFarlane, J. A Study into the Reasons for Process Improvement Project Failures: Results from a Pilot Survey. *Int. J. Qual. Reliab. Manag.* **2019**, *36*, 1699–1720. [[CrossRef](#)]
4. Womack, J.; Jones, D.; Roos, D. *The Machine That Changed the World*; MacMillan Publishing: New York, NY, USA, 1990.
5. Womack, J.; Jones, D. *Lean Thinking*; Simon and Schuster: New York, NY, USA, 1996.
6. Asli, Y.A.-B.; Jaideep, M.; Everett, M.S. When Lean and Six Sigma converge: A case study of a successful implementation of Lean Six Sigma at an aerospace company. *Int. J. Technol. Manag.* **2012**, *57*, 18–32.
7. Pepper, M.P.J.; Spedding, T.A. The evolution of lean Six Sigma. *Int. J. Qual. Reliab. Manag.* **2010**, *27*, 138–155. [[CrossRef](#)]
8. Jirasukprasert, P.; Garza-Reyes, J.A.; Kumar, V.; Lim, M.K. A Six Sigma and DMAIC application for the reduction of defects in a rubber gloves manufacturing process. *Int. J. Lean Six Sigma* **2014**, *5*, 2–21. [[CrossRef](#)]
9. McIntosh, R.I.; Culley, S.J.; Mileham, A.R.; Owen, G.W. A critical evaluation of Shingo's 'SMED' (Single Minute Exchange of Die) methodology. *Int. J. Prod. Res.* **2010**, *38*, 2377–2395. [[CrossRef](#)]
10. Ram, K.; Kumar, S.; Singh, D.P. Industrial benefits from a SMED methodology on high speed press in a punching machine: A review. *Adv. Appl. Sci. Res.* **2015**, *38*–41.
11. Rahman, S.; Laosirihongthong, T.; Sohal, A.S. Impact of lean strategy on operational performance: A study of Thai manufacturing companies. *J. Manuf. Technol. Manag.* **2010**, *21*, 839–852. [[CrossRef](#)]
12. Haleem, R.M.; Salem, M.Y.; Fatahallah, F.A.; Abdelfattah, L.E. Quality in the pharmaceutical industry—A literature review. *Saudi Pharm. J.* **2015**, *23*, 463–469. [[CrossRef](#)] [[PubMed](#)]

13. Faccio, M.; Cohen, Y.; Bevilacqua, M.; Ciarapica, F.E.; De Sanctis, I.; Mazzuto, G.; Paciarotti, C. A Changeover Time Reduction through an integration of lean practices: A case study from pharmaceutical sector. *Assembly Autom.* **2015**, *35*, 22–34.
14. Kumar, B.S.; Abuthakeer, S.S. Implementation of lean tools and techniques in an automotive industry. *J. Appl. Sci.* **2012**, *12*, 1032–1037. [[CrossRef](#)]
15. Kesterson, R.K. *The Intersection of Change Management and Lean Six Sigma*; CRC Press: Boca Raton, FL, USA, 2018; pp. 3–50.
16. Al-Akel, K.; Marian, L.; Harea, C. Analysis of Global Japanese Management Methods. Use and Efficacy. RMEE. Review of Management and Economic Engineering. No. 5. Ulrich's Periodicals Directory. 2018. Available online: [http://www.rmee.org/abstracturi/67/11\\_studii\\_si\\_cercetari\\_Articol\\_406\\_Karam%20Al-Akel%20-%20RMEE%202018%20%20ANALIZAREA%20EFICACITATII%20GLOBALE%20A%20METODELOR%20JAPONEZE%20DE%20MANAGEMENT.pdf](http://www.rmee.org/abstracturi/67/11_studii_si_cercetari_Articol_406_Karam%20Al-Akel%20-%20RMEE%202018%20%20ANALIZAREA%20EFICACITATII%20GLOBALE%20A%20METODELOR%20JAPONEZE%20DE%20MANAGEMENT.pdf) (accessed on 23 December 2019).
17. Al-Akel, K.; Marian, L.; Veres (Harea), C.; Gavrilaş, V. DMAIC importance and effectiveness in continuous improvement mindset. In Proceedings of the Review of Management and Economic Engineering, Cluj-Napoca, Romania, 20–21 September 2018.
18. Al-Akel, K.; Marian, L.; Veres (Harea), C.; Horea, R. *The contribution of Lean Manufacturing tools to Changeover time decrease in the pharmaceutical industry. A SMED project.* *Proc. Manuf. J.* **2018**, *22*, 886–892.
19. Shingo, S. *A Revolution in Manufacturing: The SMED System*; Productivity Press: Stanford, CA, USA, 1985.
20. Cakmakci, M. Process improvement: Performance analysis of the setup time reduction-SMED in the automobile industry. *Int. J. Adv. Manuf. Technol.* **2009**, *41*, 168–179. [[CrossRef](#)]
21. Ulutas, B. An application of SMED Methodology. *World Acad. Sci. Eng. Technol.* **2011**, *79*, 101.
22. Perinić, M.; Ikonić, M.; Maričić, S. Die Casting Process Assessment Using Single Minute Exchange of Dies (SMED) Method. *Metalurgija* **2009**, *48*, 199–202.
23. Dave, Y.; Sohani, N. Single Minute Exchange of Dies: Literature Review. *Int. J. Lean Think.* **2012**, *3*, 27–37.
24. Mali, Y.R.; Inamdar, K.H. Changeover Time Reduction Using Smed Technique of Lean Manufacturing. *Int. J. Eng. Res. Appl.* **2012**, *2*, 2441–2445.

**Publisher's Note:** MDPI stays neutral with regard to jurisdictional claims in published maps and institutional affiliations.



© 2020 by the authors. Licensee MDPI, Basel, Switzerland. This article is an open access article distributed under the terms and conditions of the Creative Commons Attribution (CC BY) license (<http://creativecommons.org/licenses/by/4.0/>).



# The Lean Six Sigma Algorithm—A Roadmap for Implementation<sup>†</sup>

Karam Al-Akel\* and Liviu-Onoriu Marian

Faculty of Machine Building, Technical University of Cluj-Napoca, 400114 Cluj-Napoca, Romania; liviu.marian@yahoo.com

<sup>†</sup> Presented at the 14th International Conference INTER-ENG 2020 Interdisciplinarity in Engineering, Mureş, Romania, 8–9 October 2020.

Published: 15 December 2020

**Abstract:** In competitive environments, such as batch manufacturing, Lean and Six Sigma offer the proper tools as a paramount advantage to the companies who choose to adopt their principles. With the main purpose of decreasing the failure rate of continuous improvement projects due to high abandon levels across the globe, a Lean Six Sigma algorithm has been generated, tested and validated in the pharmaceutical industry. The present paper will reveal the core implementation steps regarding the suggested algorithm, the critical tools used and results obtained through implementing the proposed roadmap.

**Keywords:** Lean manufacturing; Six Sigma; pharma industry; algorithm; roadmap; project structure; failure

## 1. Introduction

Continuous improvement culture may be referred to as the pillar for enhanced results and superior work ethics over time. Lean Manufacturing and Six Sigma reveal the proper tools to be used for starting and sustaining a continuous improvement culture across an organization. While the Lean Six Sigma tools are already available, a detailed roadmap for applying the most result-oriented ones in batch manufacturing areas is missing, according to our knowledge [1,2]. An algorithm for implementing the Lean Manufacturing and Six Sigma tools in a batch manufacturing environment has been suggested in a separate paper.

The generated algorithm was tested and validated in the pharmaceutical industry at the bottle packaging line of suspensions, a secondary packaging area. The purpose of the current paper is to reveal the methodology used for the implementation and results obtained through the algorithm. With validation taking place in the pharmaceutical industry, the main scope of the algorithm is to decrease the failure rate of continuous improvement projects in several batch manufacturing industries by offering a clear roadmap to solve universally faced issues in these fields. Having an algorithm to follow, the missing dedicated time for projects, the lack of next steps to adhere to and continuous roadblocks will affect a continuous improvement project until failure.

## 2. Theoretical Background

Lean Manufacturing (LM) and Six Sigma (SS) are continuous improvement methods that seek process improvement in a structured manner, using specific tools to obtain results [3,4]. Many of the continuous improvement projects using Lean Six Sigma tools fail due to a lack of a clear roadmap to apply their tools [1,2]. Process standardization and waste (*Muda*) removal from the process in order to enhance work efficiency are the main focus areas of Lean Manufacturing and Six Sigma [5,6]. Both LM and SS pursue the same scope, the tools and methodologies for achieving the results being specific for each of them, with a few exceptions such as *Pareto* charts, Control Charts, and *5Why* [6]. Having the

same scope of enhancing the status quo of processes through using different tools, the two methods present a potent synergism when combined [7–12].

### 3. Materials and Methods

#### 3.1. A Helicopter View

For the continuous improvement project and validation of its results, the proposed algorithm was implemented in the pharmaceutical industry in the secondary packaging area of suspensions. For obtaining the overall results of the project, the algorithm presented in a separate paper was entirely followed, relying on the DMAIC (Define Measure Analyze Improve Control) structure and following the suggested tools and techniques. Only the highlights of the key project parts are emphasized in the present paper.

##### 3.1.1. Process Mapping and Value-Added Activities

Following the *Define* phase, where the SMART (Specific Measurable Achievable Realistic Time-Bound) project scope, objectives and benefits are set, the *Analyze* phase should include, in a compulsory manner, the process of mapping and defining the value-added activities, as represented in Figure 1. By being able to establish the process map, the likely constraints will arise and guide the root cause investigation in the proper direction [13–18]. Process mapping is not as accurate or detailed as *Value Stream Mapping*; nonetheless, it represents a key and straightforward step to identifying the quick wins. Relying on the process map, the value-added activities were effortlessly identifiable, and we could establish the steps that were not adding value to the process and could be tagged or treated as *Muda* [19].

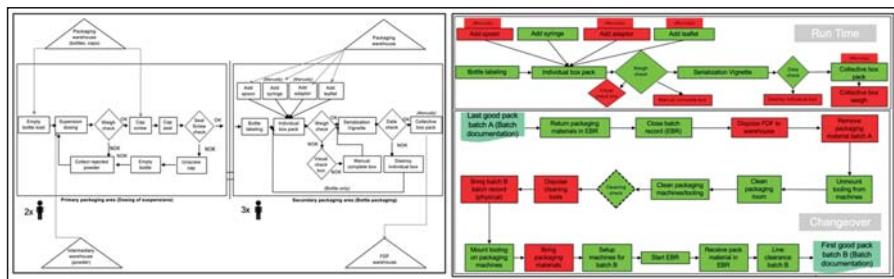


**Figure 1.** Process mapping (left) and Value-added activities (right). Legend: OK (OK, Good process step); NOK (Not OK, Failed process step); FDF (Finished Dosage Form); EBR (Electronic Batch Record).

##### 3.1.2. Changeover Standardization

In a batch manufacturing setup, the changeovers absorb a significant part of the planned production time. Any improvement of the changeover times will directly translate into additional uptime for the production asset. In the *Analyze* and *Improvement* phases, the changeover types had to be clearly identified and separated for a leaner standardization and improvement process. The establishment of a changeover ramp, such as the one represented in Figure 2, supported the proper understanding of the process. By thoroughly understanding the overall process and its key aspects in the *Analyze* phase, a detailed task list with target times for each process step (or category) could be defined in the improvement phase, as exemplified in Figure 2. For assuring an optimal acceptance from the directly productive personnel, quickly understandable visual representations were used, which incorporate figures, schemes and target times in a colorful and approachable manner. Any scheme, graph or work instruction should include color-coding in order to enhance the approachability for operators and supervisors, leading to increased openness in adhering to a newly established workflow.

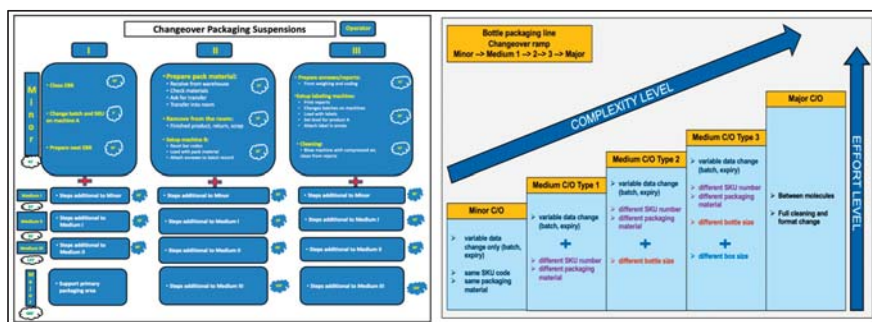


**Figure 2.** Changeover scheme (left) and Changeover ramp (right). Legend: SKU (Stock Keeping Unit); C/O (Changeover).

### 3.1.3. Visual Control

In the *Improvement* phase of the project, under the umbrella of *Visual Management*, a dispatch list was generated, see Figure 3, which reflected the production plan for the entire week. The list was displayed weekly in the production area and contained, for each batch, the critical information to be identified: target and actual run and changeover times, upcoming changeover types and issues faced for each batch. The list leveraged the responsibility among operators, traced the manufacturing issues per batch, and displayed the production status on a shift basis. The target values were set by the planner or project responsible and the actual values, shift issues and signatures were filled in by operators.

SKU	Production name	Quantity	Date	Industrial line size (SKU)	Planned production time (hours)	Actual production time (hours)	Stoppage reason	Stoppage time (min.)	Operator signature	Opening C/O type	Planned C/O time (min.)	Actual C/O time (min.)	Stoppage reason	Stoppage time (min.)	Operator signature
0014	A	1000	06/01/2019	75 x 50 x 100	8,3					Minor	45				
0006	B	8000	06/01/2019	75 x 50 x 100	8,3					Medium type 1	65				
0008	C	8000	07/01/2019	75 x 50 x 100	8,6					Medium type 1	65				
0004	D	4000	07/01/2019	75 x 50 x 100	10,6					Medium type 1	95				

**Figure 3.** Dispatch list.

The OAE (Overall Asset Effectiveness) tracking sheet, represented in Figure 4 and displayed on the shop floor, raised the awareness among operators and shift supervisors, color coded each shift’s status and output, increased productive competition between teams and highlighted key issues faced in every shift. For each molecule (A or B) a target OAE was established, which determined the color code (red or green) for the manual input of the operators. For a visual process control purpose, every team of operators manually calculated the OAE value on the shop floor tracking sheet. The weekly and daily averages were discussed at shift handover to identify possible corrective actions.

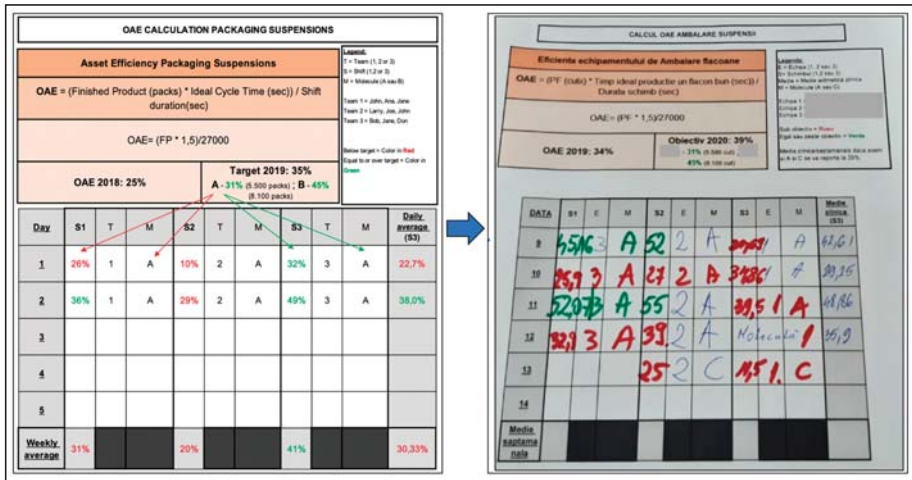


Figure 4. OAE tracking sheet. Legend: OAE (Overall Asset Effectiveness); FP (Finished Product).

3.1.4. Externalization Process

The SMED (Single Minute Exchange of Dies) technique enforces the use of externalization to execute parallel process steps whenever possible, preferably while the machine is still running to reduce processing time [20–24]. After determining, in a written form, the detailed process steps and assigning standard execution times to each of them, the non-value-added steps have to be identified, marked and removed, in addition to externalizing the non-critical ones. We managed to identify five steps that could be externalized and one that has been removed. As seen in Figure 5, preparing the packaging material near the manufacturing room for the next batch while the current batch is still running is one example of applied step externalization contributing to the overall SMED process.



Figure 5. Externalization process [25].

3.1.5. 5S Basics

Basic 5S concepts rely on creating an ergonomic and clean workplace as steps toward standardization and decreasing changeover times. Shadow boards are a common practice to create a clean and organized workplace and improve setup times and tooling stock adherence. In Figure 6, we exemplified some of the practices implemented at the suspension packaging line, where the tooling locker (left) and standard toolbox (right) have been transformed with the use of shadow board principles.





Figure 6. Shadow board.

### 3.1.6. The Power of Brainstorming

Brainstorming sessions were used to generate improvement ideas for the current process. Having material flow issues in the machine feeding system, which cause several small stoppages during the process for one type of the packaging materials, one improvement idea suggested installing a vibrating system on the feeder to mitigate the negative outcome of the packaging material quality (as the supplier could not be changed). A vibrating system was identified in stock and adapted by the technical department to fit the suggested purpose. The 2-sample *T*-test outcome represented in Figure 7 confirms the process improvement by increased output and average machine running speed (+3 packs/min, +15%) with a *p*-value of 0.002. Additionally, to improve packaging material flow in the feeding system, an increased number of individual boxes could be loaded in the stacker (almost double), decreasing the operator workload.

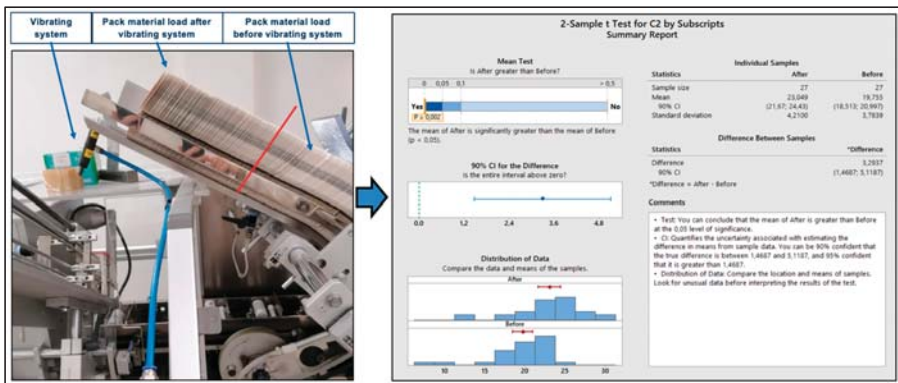


Figure 7. Brainstorming session outcome.

### 3.1.7. Removing the Muda

By removing a non-value adding component (*Muda*) previously aligned with the customers from the individual box of product A, which was causing false-positive rejects in the individual box-weighing step, we obtained a 37% packaging time/batch improvement. By cutting the *Muda*, additional reprocessing steps were removed and the process debottlenecked. The average run time/batch improved by 1.49 h, see Figure 8. In order to validate the results, we used a 2-sample *T*-test and compared the before and after performances. The *p*-value of 0.001 confirms the process improvement.



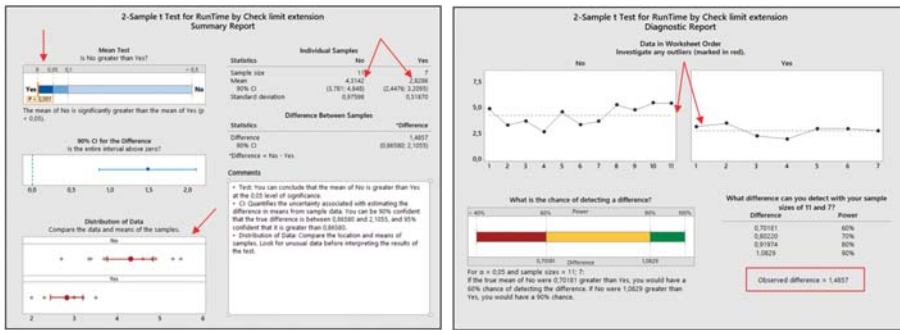


Figure 8. Run time decrease after *Muda* removal.

#### 4. Results

All the results presented below have been obtained by following the algorithm. A 9% difference in OAE value, from 25% to 34%, comparing the pre- and post-performances of the process, were considered a significant difference for validating the algorithm. We will focus below on the OAE components that were improved by using the Lean Six Sigma algorithm.

The implementation of SMED and 5S techniques, involving the steps of externalization and shadow board usage, according to the suggested algorithm, managed to decrease all in-scope changeover times. In Figure 9, we represent one type of medium changeover that was decreased by 25%, along with the overall standardization of the process.

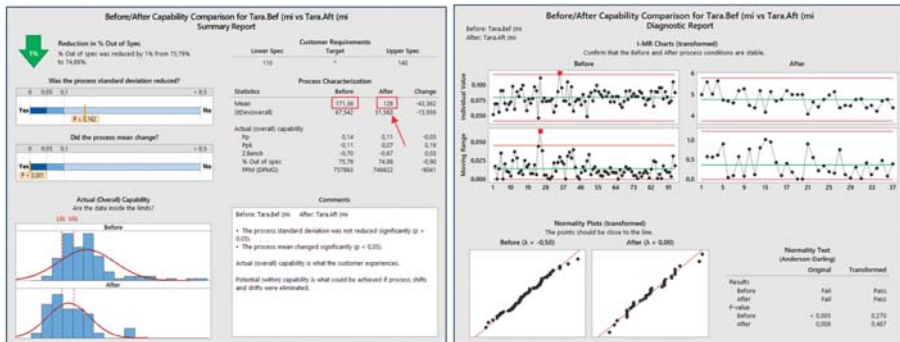


Figure 9. Medium changeover time improvement. Legend: I-MR (Individual-Moving Range), Pp (Process performance), Ppk (Process performance value), Z. Bench (Benchmark value), PPM (Parts Per Million), DPMO (Defects Per Million Opportunities), LSL (Lower Specification Limit), USL (Upper Specification Limit).

Weekly unscheduled stoppages also decreased from 33.6 h to 20.6 h. By decreasing the unscheduled elements in a certain timeframe, additional volume may be absorbed. Process standardization and awareness increase could be seen in the unscheduled breakdown results, represented in Figure 10, on a weekly basis.

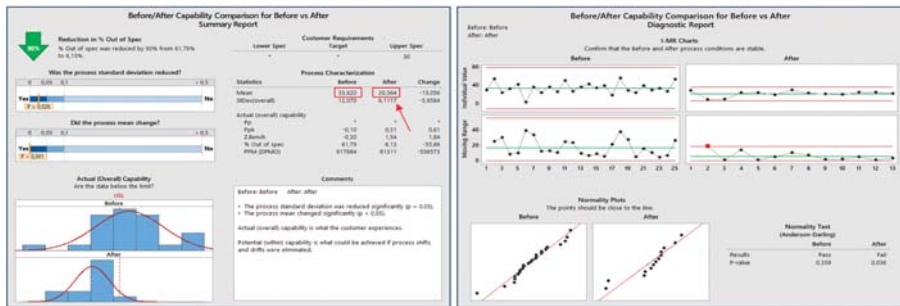


Figure 10. Weekly unscheduled breakdowns decrease.

The manufactured output for the involved packaging line increased by a weekly average of 13%, or 10,525 packs, see Figure 11, compared with the initial baseline. The output is the overall result of affecting the previous OAE components, such as changeovers and unscheduled stoppages.



Figure 11. Weekly output improvement.

The results obtained and detailed in the above graphical representations by applying the suggested algorithm are summarized in Table 1 for an optimal overview of the Lean Six Sigma implementation influence regarding the packaging process. In order to be able to influence the final CTQ (Critical to Quality), that is, the OAE, we targeted the KPI (Key Performance Indicator) components and implemented the optimal tools in a strategic manner for reaching the best results in the shortest amount of time possible.

Table 1. LSS (Lean Six Sigma) algorithm implementation results.

Key Performance Indicator	Baseline	Target	Result
OAE	25%	35%	34% (↑ 9%)
Weekly output	79,968 packs	-	90,493 (↑ 10,525 packs)
Minor changeover	86 min	-	66 min. (↓ 20 min)
Medium changeover type 1	171 min	-	128 min. (↓ 43 min)
Medium changeover type 2	240 min	-	147 min. (↓ 93 min)
Medium changeover type 3	257 min	-	198 min. (↓ 59 min)
Weekly unscheduled stoppages	33.6 h	-	20.6 h (↓ 13 h)
Average run speed	18.3 packs/min	-	19.9 (↑ 1.6 packs/min)
Savings	-	X\$ (dollar)/year *	Y\$ (dollar)/year *

\* The financial savings figures are non-disclosable.

## 5. Discussion

Having the framework structured on a DMAIC principle and following the *Define, Measure, Analyze, Improve* and *Control* project phases, each of the above actions were implemented in a batch manufacturing area. The periodic Gemba walks, SMED technique implementation, along with the tools and approaches detailed in the paper, are key aspects for the success of the project. We addressed this universal issue by generating, testing and validating through results an algorithm that improves the manufacturing processes in a controlled manner. The algorithm was applied, tested and validated in the manufacturing area of a pharmaceutical company; nevertheless, it was conceived to enhance improvement project results in multiple batch manufacturing environments. By improving the complex OAE KPI and its components, such as unscheduled stoppages, run time, changeovers and production output, we consider the algorithm to be successful in decreasing the failure rate of continuous improvement projects. By guiding the implementation methodology of the generated algorithm, and using specific tools and techniques, we have dispatched a validated pathway for a general issue that has been unaddressed, until today, in such detail, according to our knowledge.

**Funding:** This research received no external funding which may be disclosed.

**Acknowledgments:** The paper would not have been created without the exceptional support of my guide and advisor, Liviu-Onoriu Marian. I would also like to express my deep gratitude to the company that allowed me to implement, test and validate the algorithm in the manufacturing area. Without the kind and knowledgeable support of the entire team, all the efforts would have been increased.

**Conflicts of Interest:** The funders had no role in the design of the study; in the collection, analysis, or interpretation of data; in the writing of the manuscript, or in the decision to publish the results.

## References

1. Bhuiyan, N.; Baghel, A. An overview of continuous improvement: From the past to the present. *Manag. Decis.* **2005**, *43*, 761–771. [\[CrossRef\]](#)
2. Gerger, A.; Firuzan, A.R. Reasons of failure in Lean Six Sigma projects. *Int. J. Multidiscip. Res. Dev.* **2012**, *2*, 123–130.
3. Antony, J.; Lizarelli, F.L.; Fernandes, M.M.; Dempsey, M.; Brennan, A.; McFarlane, J. *A Study into the Reasons for Process Improvement Project Failures: Results from a Pilot Survey*; International Journal of Quality&Reliability Management; Emerald Publishing Limited: Bingley, UK, 2019. [\[CrossRef\]](#)
4. Womack, J.; Jones, D.; Roos, D. *The Machine That Changed the World*; MacMillan Publishing: New York, NY, USA, 1990.
5. Womack, J.; Jones, D. *Lean Thinking*; Simon and Schuster: New York, NY, USA, 1996.
6. Asli, Y.A.-B.; Jaideep, M.; Everett, M.S. When Lean and Six Sigma converge: A case study of a successful implementation of Lean Six Sigma at an aerospace company. *Int. J. Technol. Manag.* **2012**, *57*, 18–32.
7. Pepper, M.P.J.; Spedding, T.A. The evolution of lean Six Sigma. *Int. J. Qual. Reliab. Manag.* **2010**, *27*, 138–155. [\[CrossRef\]](#)
8. Jirasukprasert, P.; Garza-Reyes, J.A.; Kumar, V.; Lim, M.K. A Six Sigma and DMAIC application for the reduction of defects in a rubber gloves manufacturing process. *Int. J. Lean Six Sigma* **2014**, *5*, 2–21. [\[CrossRef\]](#)
9. McIntosh, R.L.; Culley, S.J.; Mileham, A.R.; Owen, G.W. A critical evaluation of Shingo's 'SMED' (Single Minute Exchange of Die) methodology. *Int. J. Prod. Res.* **2010**, *38*, 2377–2395. [\[CrossRef\]](#)
10. Ram, K.; Kumar, S.; Singh, D.P. Industrial benefits from a SMED methodology on high speed press in a punching machine: A review. *Adv. Appl. Sci. Res.* **2015**, *6*, 38–41.
11. Rahman, S.; Laosirihongthong, T.; Sohal, A.S. Impact of lean strategy on operational performance: A study of Thai manufacturing companies. *J. Manuf. Technol. Manag.* **2010**, *21*, 839–852. [\[CrossRef\]](#)
12. Haleem, R.M.; Salem, M.Y.; Fatahalla, F.A.; Abdelfattah, L.E. Quality in the pharmaceutical industry—A literature review. *Saudi Pharm. J.* **2015**, *23*, 463–469. [\[CrossRef\]](#) [\[PubMed\]](#)
13. Faccio, M.; Cohen, Y.; Bevilacqua, M.; Ciarapica, F.E.; De Sanctis, I.; Mazzuto, G.; Paciarotti, C. A Changeover Time Reduction through an integration of lean practices: A case study from pharmaceutical sector. *Assembly Autom.* **2015**, *35*, 22–34.
14. Kumar, B.S.; Abuthakeer, S.S. Implementation of lean tools and techniques in an automotive industry. *J. Appl. Sci.* **2012**, *12*, 1032–1037. [\[CrossRef\]](#)

15. Kesterson, R.K. *The Intersection of Change Management and Lean Six Sigma*; CRC Press: Boca Raton, FL, USA, 2018; pp. 3–50.
16. Al-Akel, K.; Marian, L.; Harea, C. Analysis of Global Japanese Management Methods. Use and Efficacy. 2018. Available online: [http://www.rmee.org/abstracturi/67/11\\_studii\\_si\\_cercetari\\_Articol\\_406\\_Karam%20Al-Akel%20-%20RMEE%202018%20-%20ANALIZAREA%20EFICACITATII%20GLOBALE%20A%20METODELOR%20JAPONEZE%20DE%20MANAGEMENT.pdf](http://www.rmee.org/abstracturi/67/11_studii_si_cercetari_Articol_406_Karam%20Al-Akel%20-%20RMEE%202018%20-%20ANALIZAREA%20EFICACITATII%20GLOBALE%20A%20METODELOR%20JAPONEZE%20DE%20MANAGEMENT.pdf) (accessed on 1 March 2020).
17. Al-Akel, K.; Veres (Harea), C.; Gavrilaş, V. DMAIC importance and effectiveness in continuous improvement mindset. In Proceedings of the RMEE, Review of Management and Economic Engineering, ISI Proceedings, Cluj-Napoca, Romania, 20–22 August 2018.
18. Karam, A.A.; Liviu, M.; Cristina, V.; Radu, H. The contribution of Lean Manufacturing tools to Changeover time decrease in the pharmaceutical industry. *A SMED project. Proc. Manuf. J.* **2018**, *22*, 886–892. [[CrossRef](#)]
19. Shingo, S. *A Revolution in Manufacturing: The SMED System*; Productivity Press: Stanford, CA, USA, 1985.
20. Cakmakci, M. Process improvement: Performance analysis of the setup time reduction-SMED in the automobile industry. *Int. J. Adv. Manuf. Technol.* **2009**, *41*, 168–179. [[CrossRef](#)]
21. Ulutas, B. An application of SMED Methodology. *World Acad. Sci. Eng. Technol.* **2011**, *79*, 101.
22. Perinić, M.; Ikonić, M.; Maričić, S. Die Casting Process Assessment Using Single Minute Exchange of Dies (SMED) Method. *Metalurgija* **2009**, *48*, 199–202.
23. Dave, Y.; Sohani, N. Single Minute Exchange of Dies: Literature Review. *Int. J. Lean Think.* **2012**, *3*, 27–37.
24. Mali, Y.R.; Inamdar, K.H. Changeover Time Reduction Using Smed Technique of Lean Manufacturing. *Int. J. Eng. Res. Appl.* **2012**, *2*, 2441–2445.
25. Available online: <http://www.lowgif.com/view.html> (accessed on 1 March 2020).

**Publisher's Note:** MDPI stays neutral with regard to jurisdictional claims in published maps and institutional affiliations.



© 2020 by the author. Licensee MDPI, Basel, Switzerland. This article is an open access article distributed under the terms and conditions of the Creative Commons Attribution (CC BY) license (<http://creativecommons.org/licenses/by/4.0/>).



# A Case Study on the Particularities and Sustainability of the Concepts of TQM, Quality Control, and Risk Management in the Corporate Insurance Industry: Loss and the Incidence of Catastrophic Risks <sup>†</sup>

Narcis Sebastian Păvălașcu and Manuela Rozalia Gabor <sup>\*†</sup> 

“G.E. Palade” University of Medicine, Pharmacy, Sciences and Technology of Târgu Mures, 540142 Târgu Mures, Romania; narcis@pavalascu.com

\* Correspondence: manuela.gabor@umfst.ro

† Presented at the 14th International Conference INTER-ENG 2020 Interdisciplinarity in Engineering, Mureș, Romania, 8–9 October 2020.

Published: 10 December 2020

**Abstract:** The development of quality control and risk management systems is a priority for any industry and especially for the corporate insurance industry. Defective product and work incidents represent 14% of the total number of insurance claims, serving as the main loss of liability for businesses. According to a Allianz Global Corporate and Specialty press release, the cyber risks and impact of new technologies will have an increasing influence on the landscape of corporate losses in the coming years. Our results from this study conclude that the emerging business risks for the next 3–4 years are as follows: cyber incidents, 48%; new technologies, 30%; and changes in legislations/regulations, 28% (i.e., the present pandemic cause by COVID-19, the Brexit, trade wars, and tariffs etc.).

**Keywords:** cyber risk; loss adjustments; corporate insurance industry; risk management; quality control

## 1. Introduction

The development of quality control and risk management systems is a priority [1] for any industry and especially for the corporate insurance industry. The Allianz Global Corporate and Specialty (AGCS) report [2] highlights the ascension of defective products in 2018 compared to 2014 [3] (Table 1). Defections rose from the ninth to the fifth largest loss incurred by companies worldwide. Defective products and work incidents account for 14% of the aggregate value of claims paid out to businesses, and are as such a root cause of liability losses. Risk management involves the assessment of risks facing an organization. Some risks can be avoided, but what remains must be borne by the organization or transferred through insurance [4].

The core causes of products being defective include, according to the Allianz Report 2018 [2]: product recalls, costs of defect repairs in the car-making industry, revenue loss due to businesses shutting down as a result of a significant percentage of defective products being delivered, food contamination, allergens etc.

Trends such as globalization and industry consolidation are conducive to growing claims on insurance policies covering multiple jurisdictions, according to the Allianz Report 2014 [3]. According to European Insurance [5], the insurance sector is the single largest institutional investor in the EU with more than EUR 10 bn in managed assets invested across the economy in 2017, which equals to 63% of the EU's GDP [5].

**Table 1.** The top causes for business losses in 2018 (a) and 2014 (b).

Top Causes of Loss by Total Value of Claims (2013–2018) (a)			Top Causes of Loss by Total Value (2009–2013) (b)		
1	Fire/explosion	24%	1	Grounding	
2	Aviation collision/crash	14%	2	Fire	
3	Faulty workmanship/maintenance	8%	3	Aviation crash	
4	Storm	7%	4	Earthquake	
5	Defective products	6%	5	Storm	
6	Damaged goods (including handlings/storage)	5%	6	Bodily injury (including fatalities)	
7	Machinery breakdown (including engine failure)	5%	7	Flood	
8	Water damage	3%	8	Professional indemnity	
9	Ship sinking/collision	2%	9	Product defects	
10	Professional indemnity (e.g., negligence/bad advice)	2%	10	Machinery breakdown	

Further causes that result in big business losses in various industries include:

- Business disruption as a result of natural disasters (flood, earthquake, fire etc.).
- Business disruption because of terrorist acts. Products sold in the insurance industry also include policies that cover losses caused by acts of terrorism.
- Business disruption because of cyberattacks, as products sold in the insurance industry also include policies that cover losses caused by cyberattacks.
- Environmental liability insurance and losses from industrial accidents, which affect the environment [6].
- Third party liability insurance for nuclear, oil, and gas operations [6], with Romania yet to develop this sector as its experience/expertise in the area is limited.
- Other business sector insurance covers losses caused by [7] a loss of key personnel, risk management, green business [8], terrorism, insurance against kidnapping of a company’s managing team or key personnel, etc.

The latest business insurance packages included terrorism insurance [9].

According to a press release issued by AGCS, which from 2013 to 2018 covered 470,000 global insurance claims from more than 200 countries, cyber risks and new technologies’ impact will increasingly affect the landscape of corporate losses over the coming years. However, fire and explosion incidents cause the highest claims to insurers, according to recent AGCS research. Most corporate insurance claims arise from technical or human factors rather than natural disasters, such as hurricanes, that inflicted devastating losses over the past two years.

The top perils for companies in 2019 include the following hierarchy (in terms of criticality):

1. Business interruption (discontinuation of business because of various causes), 37% down from 2018 (42%)
2. Cyber incidents, 37% down from 2018 (40%)
3. Catastrophes attributable to natural causes, 28% down from 2018 (30%)
4. Changes in laws and regulations, 27% up from 2018 (21%)
5. Market development, 23% slightly up from 2018 (22%)
6. Fires and explosion, 19% very similar to 2018 (20%)
7. New technologies, 19% up from 2018 (15%)
8. Climate changes/increasing volatility of weather, 13% up from 2018 (10%)
9. Loss of reputation or brand value, 13% as high as in 2018
10. Lack of a skilled labor force, 9% highlighted by AGCS as a new risk cause in insurance in 2019 as compared to previous years.

Technology creates new threats and business models. Traditional risks such as natural disasters still occur, whereas other threats, such as cybercrimes, are on a par with business interruption and top the

Allianz risk chart. For the first time, there have been daily rises in reputational risk, increasing exposure to intangible assets, and volatility and consolidation in the corporate environment. Yet, looking at the future, new technologies bring businesses benefits, risks, and liabilities. However, new technologies also provide an opportunity to prevent and minimize losses and to improve the claim settlement process for corporate customers. The analysis reveals that corporate insurance claims usually are originated by technical or human factors—or non-natural catastrophic events—accounting for 87% of the value of total claims.

**2. International Trends in Occurrence of Catastrophic Risks–Statistics and Facts**

In the opinion of the National Union of Insurance and Reinsurance Companies in Romania (UNSAR) [6], the rate of penetration for catastrophe insurance in the EU differs across countries, with legislation on natural disaster insurance and people’s education in risk awareness acting as major causative factors. Due to the patchiness of the EU Member States, more thorough research is required to comprehend the specific traits of each country in order to create suitable risk coverage, or coverage layers better suited to the needs of each individual country.

The past 20 years have seen a significant rise in both frequency and impact of disaster type events, which raised concerns in the world insurance industry. Significant (both material and human) losses have been in the public eye and generated governmental efforts to have them covered up, particularly when losses were not insured/insurable. Earthquakes, fires, landslides, or floods all resulted in a financial, social, economic, and political impact in the affected areas [10].

An analysis of the economic losses and insured losses from 1950–2018 worldwide were conducted by Radu and Naghi [11]. The analysis is presented in Table 2, which contains the statistical data supporting this analysis.

**Table 2.** Analysis of 10-year periods of natural disaster impacts (USD billion in 2018).

	1950–1959	1960–1969	1970–1979	1980–1989	1990–1999	2000–2009	2010–2018
Number of events	292	547	839	1653	2577	3861	2988
Economic losses	6058	18,445	17,181	53,845	746,015	892,312	1,354,014
Insured losses	0.033	0.066	0.113	0.239	98.8	479	739
Damage rate of economic losses	0.54	0.36	0.66	0.44	13.24	53.68	54.58
Average damage on the event	0.020747	0.0337203	0.0204779	0.0325741	0.28949	0.231109	0.453151
Average insured damage on the event	0.000113	0.0001207	0.0001347	0.0001446	0.038339	0.124061	0.247323

Source: [11].

A Munich Re research combined with the AON Report 2018 revealed that during 1988–1997, the global economy incurred USD 700 bn as a result of catastrophic events in the region, while such costs amounted to approximately USD 4000 bn over the last two decades (2000–2018), as opposed to the numbers in 2018. The second half of the 20th century saw 250 large scale natural disasters. As shown by the data in Table 1, the loss coverage rate provides a measure of how economic losses are recovered due to insurance coverage. During the periods under review, this rate has seen a notable rise (doubling in value), indicating that the insurance transfer method has seen steady rises; therefore, this supports specialist companies’ acknowledgment of natural disaster events.

Because there are a visible number of increasing events and values for the variables in Table 1, we used a statistical method (Student’s t-test) with SPSS statistical software the mean of values by grouping: after/before 1990 and after/before 2000. The results from Tables 3 and 4 show that there are statistically significant differences for these variables grouped from the years 1990 and 2000.



**Table 3.** ANOVA for the group before/after 1990.

		Sum of Squares	df	Mean Square	F	Sig.
Number of events	Between Groups	9,141,660.964	1	9,141,660.964	23,971	0.004
	Within Groups	1,906,814.750	5	381,362.950		
	Total	$1.105 \times 10^7$	6			
Economic losses	Between Groups	$1.625 \times 10^{12}$	1	$1.625 \times 10^{12}$	40,080	0.001
	Within Groups	$2.027 \times 10^{11}$	5	$4.054 \times 10^{10}$		
	Total	$1.828 \times 10^{12}$	6			
Insured losses	Between Groups	330,108.865	1	330,108.865	7961	0.037
	Within Groups	207,336.051	5	41,467.210		
	Total	537,444.916	6			
Coverage rate for economic losses	Between Groups	2742.857	1	2742.857	12,299	0.017
	Within Groups	1115.117	5	223.023		
	Total	3857.974	6			
Average damage per event	Between Groups	0.152	1	0.152	28,498	0.003
	Within Groups	0.027	5	0.005		
	Total	0.179	6			
Average damage insured per event	Between Groups	0.032	1	0.032	7230	0.043
	Within Groups	0.022	5	0.004		
	Total	0.054	6			

Source: own calculations with SPSS program based on data from [10].

**Table 4.** ANOVA for the group before/after 2000.

		Sum of Squares	df	Mean Square	F	Sig.
Number of events	Between Groups	7,186,572.014	1	7,186,572.014	9.304	0.028
	Within Groups	3,861,903.700	5	772,380.740		
	Total	$1.105 \times 10^7$	6			
Economic losses	Between Groups	$1.302 \times 10^{12}$	1	$1.302 \times 10^{12}$	12.403	0.017
	Within Groups	$5.251 \times 10^{11}$	5	$1.050 \times 10^{11}$		
	Total	$1.828 \times 10^{12}$	6			
Insured losses	Between Groups	495,853.553	1	495,853.553	59.610	0.001
	Within Groups	41,591.363	5	8318.273		
	Total	537,444.916	6			
Coverage rate for economic losses	Between Groups	3727.672	1	3727.672	143.040	0.000
	Within Groups	130.301	5	26.060		
	Total	3857.974	6			
Average damage per event	Between Groups	0.099	1	0.099	6.165	0.056
	Within Groups	0.080	5	0.016		
	Total	0.179	6			
Average damage insured per event	Between Groups	0.045	1	0.045	25.798	0.004
	Within Groups	0.009	5	0.002		
	Total	0.054	6			

Source: own calculations with SPSS program based on data from [10].

This trend in conjunction with the rising economic losses led us to conclude that, within the 70 years under review, the difference between the insured losses and uninsured losses decreased steadily, which confirmed that insurance covered these economic losses.

### 3. Particularities and Applications of the Corporate Insurance Industry: Total Quality Management (TQM) and Quality Control Globally and in Romania

Total quality management (TQM) has a host of definitions [12] but it is basically a quality management system that provides support for the continued improvement of products or services with zero defects. The advantages and benefits of implementing TQM in the insurance industry include [12] an increased market share, improved profitability, long-term cost-cutting [13], skilling and retaining company employees [14], heightened productivity, an innovative work environment, and a value-added difference.

The service and financial sector have been slow to implement the TQM principles for several reasons [15]:

- Quality and productivity policies are less clear than in the production sector.
- Service and financial companies are often shielded against international competitors under regulations, protection legislation, and cultural barriers.
- Financial institutions, particularly insurance companies, make promises that often are made good on only after a significant amount of time.

TQM is capable of defining, spotting, and prioritizing exceptional conditions that require a management decision [15]. This is the most compelling reason why a company's Actuarial Department should be the most informed and active participants in any TQM effort [15].

Big damage reports amount to a successful approach to this issue, yet they come with the downside of dealing only with cases that have already occurred. In this case, TQM's imperative is to limit management changes that may affect the claim settlement workflow to those changes that are required and supported by proof or are simply inevitable. The Actuarial Department is faced with the challenge of needing to interpret and use the monitoring data provided by the claim department to improve the accuracy and dynamic reaction of the actuarial projections [15].

There are countries in the world, such as Palestine [16], which have conducted research on key activities to ensure that the TQM concept is successfully implemented by insurance companies across the country [16]. A second example is Oman [17], which put together a "manual guide for minimal quality assurance standards for services provided to clients of brokers and insurance companies", which contains precise provisions for each individual aspect. It puts forth several quality standards based on the type of service provided by the insurance firm [17]. Another specific example of how to implement the TQM concept in the insurance industry is what has occurred in Indonesia [12], where an emphasis is placed on the fact that the insurance industry increasingly uses new channels for new technologies and tools. Authors have reviewed how TQM has been implemented in an insurance company that offered the following services: worker compensation, defective machinery, all-risk contractors, safe cash, cash-in-transit, and third-party liability.

Experience of insurance loss adjusters shows that insurance companies often use their QA (Quality Assurance) audit mission aggressively to deter what auditors describe as "inflated payments". In other words, one of the things sought by a QA auditor is the amount of money paid by a loss adjuster for a claim, irrespective of whether that amount is too small, fair, or too big [18].

Another insurance expert, Sandquist [19], focused on the implementation of Kaizen and TQM in the insurance industry. Sandquist claimed that focus on product quality, when used in insurance marketing, implies seeing beyond a product's features to better understand customers' insurance needs. Telematics is a means used by leading insurers to achieve this.

Examples of top ISO-certified insurance companies that successfully implemented TQM should include the US global Crawford and Company, which represents 70 countries, including Romania, who periodically uses press releases to inform which of its branches or representative offices has become ISO 9001:2000 certified (i.e., entities in the Netherlands [20] or Australia [21] for ISO 27001 for information security management system (ISMS) in the wake of an audit work by Lloyd's Register Quality Assurance).

As far as the concept of risk management is concerned, it is internationally recognized that, in the insurance industry, wide principles that should be embedded into a risk management framework are provided covering the strategy, organizational structure, policies, and procedures related to the management of the implicit risks in such business [11]. To achieve this, the Monetary Authority of Singapore [22] has proposed an entire process to address those risks generated by core insurance activities, including product development, pricing, underwriting, claim handling, and reinsurance management. Moreover, with regard to risk evaluation, the consulting firm KPMG offers the following recommendations [23]: understanding the entity; a plan to engage in-house and third party experts; internal audit; service providers and other auditors as required; evaluation of the relevant designs and implementation of the relevant controls; arranging talks to evaluate and plan risks; identification of audit strategy; and planning the required audit approach.

**4. Conclusions**

Over the last few years, natural catastrophic events have inflicted more losses upon economies around the world. Global climate changes, whether or not as a result of human activities, and the growing population density, mostly in the exposed areas, are the top causes responsible for the growing volume of economic losses both in developed countries and in those with an emerging economy. The more developed the economy of a region, the bigger the economic losses caused by catastrophes.

In terms of how a market can recover from such economic losses, a significant role is played by insurance, reinsurance, and capital market. The insurance and reinsurance industry is therefore faced with an enormous challenge: to identify solutions to manage issues posed by the growing impact of natural disasters around the world. This is clarified by one of the proposals in the TQM–quality control–risk management consolidation.

Thus, the seven conventional quality control tools can also be used in the corporate insurance industry, i.e., Pareto charts, cause-and-effect diagrams (fishbone diagram), histograms, control diagrams, scatter diagrams, inspection checklists, and the stratification method. Moreover, J. Chen and J.-H. Chen proposed, in 2011 [24], a model for risk management (Figure 1), which can be also applied in the insurance industry.

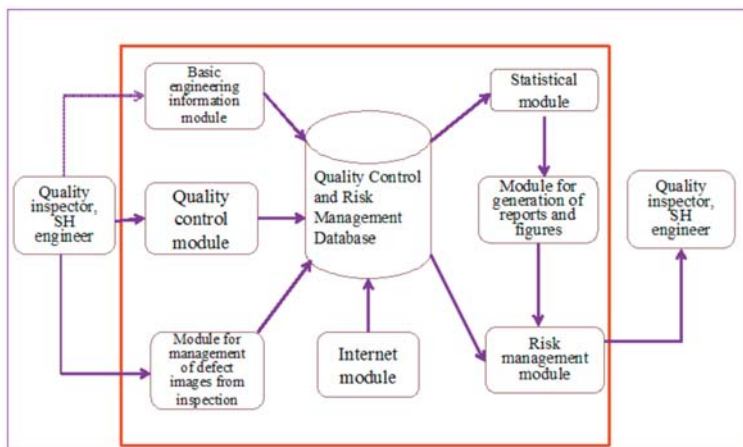


**Figure 1.** Model suggested by J. Chen and J.-H. Chen [24] for risk management.

An innovative solution contributed by UNSAR (The National Association of Insurance and Reinsurance Companies in Romania) is parametric index-based weather insurance for risk management caused by/originating from natural disasters [10]. Another risk management tool in the corporate

insurance industry put forth by UNSAR is insurance pricing as a market incentive for promotion of prevention and risk awareness and minimization [10].

Ongoing evaluation of the quality of services provided to customers to promote it, based on the insured's expectation and satisfaction, is one of the key methods in fostering a competitive environment in the insurance market to ensure a better performance level, as well as a better capacity to cope with a volatile market exposed to local and global economic changes [17].

Over the last few years, a growing trend of claims has arisen from quality control issues [25]. Several methods to mitigate this risk using corporate insurance should include:

1. Implementation of the following elements for a company's quality control policies, which guarantees for professional liability and general liability: alpha and beta testing, formal client acceptance procedure, prototype development, statistic quality control, supplier check process, TQM, writing and documenting quality control program, and a client's consent to each individual stage of the project.
2. Meeting one or more widely accepted industry standards: UL/CSA, ISO 9000, CE MARK, ANSI etc.
3. Performing pre-launch/pre-dissemination tests to protect clients against malicious codes and/or other security vulnerabilities in the company's services.
4. Availability of a plan to maintain documents/agreements for no less than 7 years.
5. Firms must create business continuity plans to manage this risk [26].

Lastly, we should mention several reasons to introduce TQM, quality control, and risk management in the corporate insurance industry [27]: prevent E&O; follow the existing workflow/procedure; allow for an effective workflow/procedure; monitor the workload; and maintain customer service quality.

**Author Contributions:** Conceptualization, N.S.P. and M.R.G.; methodology, M.R.G.; software, M.R.G.; validation, N.S.P. and M.R.G.; formal analysis, N.S.P. and M.R.G.; investigation, N.S.P.; resources, N.S.P.; writing—original draft preparation, N.S.P.; writing—review and editing, M.R.G. All authors have read and agreed to the published version of the manuscript.

**Funding:** This research received no external funding.

**Conflicts of Interest:** The authors declare no conflict of interest.

## References

1. Chen, J.; Chen, J.-H. Research in Establishment of Quality Control and Risk Management Systems. In Proceedings of the 28th International Symposium on Automation and Robotics in Construction (ISARC), Seoul, Korea, 29 June–2 July 2011; Available online: <http://www.iaarc.org/publications/fulltext/S09-4.pdf> (accessed on 20 August 2019). [CrossRef]
2. Allianz Global Corporate and Specialty. Global Claims Review 2018—The Top Causes of Corporate Insurance Losses. 2018. Available online: <https://www.agcs.allianz.com/news-and-insights/reports/claims-in-focus.html> (accessed on 20 August 2019).
3. Allianz Global Corporate and Specialty. Global Claims Review 2014—Loss Trend and Emerging Risk for Global Business. 2014. Available online: <https://www.agcs.allianz.com/content/dam/onemarketing/agcs/agcs/reports/AGCS-Global-Claims-Review-2014.pdf> (accessed on 20 August 2019).
4. Thomas, D. Risk management in NDT. *Insight* **1998**, *40*, 352.
5. Insurance Europe. European Insurance—Key Facts. 2018. Available online: <https://www.insuranceeurope.eu/sites/default/files/attachments/European%20insurance%20-%20Key%20facts%20-%20October%202018.pdf> (accessed on 20 August 2019).
6. UNSAR—Uniunea Națională a Societăților de Asigurare și Reasigurare din România. Gradul de Penetrare Pentru Asigurările de Catastrofă. 2013. Available online: [https://ec.europa.eu/finance/consultations/2013/disasters-insurance/docs/contributions/non-registered-organisations/unsar\\_ro.pdf](https://ec.europa.eu/finance/consultations/2013/disasters-insurance/docs/contributions/non-registered-organisations/unsar_ro.pdf) (accessed on 22 August 2019).

7. Allianz Global Corporate and Specialty. Allianz Risk Barometer—Top Business Risk for 2019. 2019. Available online: <https://www.agcs.allianz.com/content/dam/onemarketing/agcs/agcs/reports/Allianz-Risk-Barometer-2019.pdf> (accessed on 22 August 2019).
8. Insurance Information Institute. Available online: <https://www.iii.org/article/insurance-options-for-green-businesses> (accessed on 22 August 2019).
9. Insurance Information Institute. Available online: <https://www.iii.org/article/infographic-business-interruption-insurance> (accessed on 22 August 2019).
10. Allianz Global Corporate and Specialty. Press Release—Fires and Explosions Cause Largest Losses for Business: Allianz Global Claims Analysis. 2018. Available online: <https://www.agcs.allianz.com/news-and-insights/news/global-claims-review-2018.html> (accessed on 22 August 2019).
11. Radu, N.; Naghi, L.E. Evoluția internațională a Incidentei Riscurilor Catastrofale. *Rev. Stud. Fin.* **2019**, *IV*, 68–82. Available online: [https://revista.isfin.ro/wp-content/uploads/2019/05/5.4\\_Nicoleta-Radu\\_RO.pdf](https://revista.isfin.ro/wp-content/uploads/2019/05/5.4_Nicoleta-Radu_RO.pdf) (accessed on 2 September 2019).
12. Bawab, F.A.; Abbassi, G.Y. An application of Total Quality Management for the Insurance Companies Sector—A Case Study. *Am. Soc. Eng. Manag. J.* **1996**, 207–214. Available online: <http://www2.ju.edu.jo/sites/Academic/abbasi/Lists/Published%20Research/DispForm.aspx?ID=26> (accessed on 2 September 2019).
13. Surange, V.G. Implementation of Six Sigma to Reduce Cost of Quality: A Case Study of Automobile Sector. *J. Fail. Anal. Prev.* **2015**, *15*, 282–294. [[CrossRef](#)]
14. Jozsef, B.; Blaga, P. A more efficient production using quality tools and human resources management. *Procedia Econ. Financ.* **2012**, *3*, 681–689.
15. Heckman, P.E. Total Quality Management in Property/Causality Insurance: An Actuarial Respective. Discussion Papers—The Actuary as Business Manager. 1993. Available online: <https://www.casact.org/pubs/dpp/dpp93/93dpp073.pdf> (accessed on 2 September 2019).
16. Fataftah, S.K. The implementation of Total Quality Management (TQM) for the Insurance Companies in Palestine. Centre International de Hautes Etudes Agronomiques Mediterraneennes, Chania (Greece), Institut Agronomique Mediterraneean. 2012. Available online: <http://agris.fao.org/agris-search/search.do?recordID=QC2013200828> (accessed on 6 September 2019).
17. CMA (Capital Market Authority). Guiding Manual for the Minimum Standards of Quality Assurance for the Services Provided to the Customers of Insurance Companies and Brokers. Available online: <https://www.cma.gov.om/Home/InsurancePublicationFileDownload/I019> (accessed on 6 September 2019).
18. Terry, D. How Do Insurance Companies Track “Quality” Claim Handling? 2018. Available online: <https://www.badfaithinsider.com/2018/02/insurance-companies-track-quality-claim-handling/> (accessed on 6 September 2019).
19. Sandquist, E.J. Kaizen and TQM also Have Roles to Play in Insurance Marketing. 2019. Available online: <https://insuranceblog.accenture.com/kaizen-and-tqm-also-have-roles-to-play-in-insurance-marketing> (accessed on 6 September 2019).
20. Crawford and Company. Crawford Netherlands Receives ISO Renewal again. 2019. Available online: <https://www.claimsjournal.com/news/international/2005/09/16/59717.htm> (accessed on 6 September 2019).
21. Crawford and Company. Press Release: Crawford and Company@Australia achieves ISO 27001 Certification. 2018. Available online: <https://au.crawfordandcompany.com/media/2369287/013218-crawford-australia-achieves-iso27001-certification-final.pdf> (accessed on 6 September 2019).
22. Monetary Authority of Singapore. Guidelines on Risk Management Practices for Insurance Business—Core Activities. 2013. Available online: [https://www.mas.gov.sg/-/media/MAS/Regulations-and-Financial-Stability/Regulatory-and-Supervisory-Framework/Risk-Management/Risk-Management-Guidelines\\_Insurance-Core-Activities.pdf](https://www.mas.gov.sg/-/media/MAS/Regulations-and-Financial-Stability/Regulatory-and-Supervisory-Framework/Risk-Management/Risk-Management-Guidelines_Insurance-Core-Activities.pdf) (accessed on 6 September 2019).
23. KPMG International. Our Relentless Focus on Quality—2016 Transparency Report. 2016. Available online: [www.kpmg.com/transparency](http://www.kpmg.com/transparency) (accessed on 6 September 2019).
24. Ferguson, J. 4 Quality Control Tips That Can Reduce Claims. Available online: <https://www.sadlerco.com/quality-control/> (accessed on 16 September 2019).
25. Alexander, P. Best Practices Quality Management—Part I. 2011. Available online: <https://www.insurancejournal.com/blogs/patalexander/2011/06/01/200428.htm> (accessed on 6 September 2019).

26. Zsidisin, G.A.; Melnyk, S.A.; Ragatz, G.L. An institutional theory perspective of business continuity planning for purchasing and supply management. *Int. J. Prod. Res.* **2005**, *43*, 3401–3420. [[CrossRef](#)]
27. Pryor, J. Why Risk Management and Quality Management Must Converge. 2014. Available online: <https://www.irmi.com/articles/expert-commentary/risk-and-quality-management-convergence> (accessed on 16 September 2019).

**Publisher's Note:** MDPI stays neutral with regard to jurisdictional claims in published maps and institutional affiliations.



© 2020 by the authors. Licensee MDPI, Basel, Switzerland. This article is an open access article distributed under the terms and conditions of the Creative Commons Attribution (CC BY) license (<http://creativecommons.org/licenses/by/4.0/>).



Article

# Framework Specifications for Evaluation of Quality Improvement and Sustainable Development in Healthcare Facilities <sup>†</sup>

Flaviu Moldovan

“George Emil Palade” University of Medicine, Pharmacy, Science, and Technology of Târgu Mureș, Doctoral School, 540139 Târgu Mureș, Romania; moldovan.flaviu95@yahoo.com; Tel.: +40-754-671-886

<sup>†</sup> Presented at the 14th International Conference INTER-ENG 2020 Interdisciplinarity in Engineering, Mureș, Romania, 8–9 October 2020.

Published: 14 December 2020

**Abstract:** The purpose of this paper is to establish the specifications of an analysis and evaluation model in the form of a reference framework for the design, development, implementation, periodic evaluation, and continuous improvement of quality management systems based on the application of national and international standards for sustainable development in healthcare facilities. It integrates the existing legal requirements, standards, and quality assessment indicators from actual frameworks. Its structure is based upon the Plan-Do-Check-Act quality cycle, on the three pillars of sustainable development—social, economic, and environmental—incorporated in the seven basic topics of social responsibility mentioned in ISO26000.

**Keywords:** healthcare facility; quality improvement; sustainable development; reference framework

---

## 1. Introduction

A lot of research has been performed on quality improvement methods over the last decade, which developed a wide range of evaluation instruments, statistical tools, and methods of improvement. There are a large number of clinical and non-clinical interventions that have the effect of improving the quality of care. However, this reality is inconsistent with the continuous variations in quality and safety, which are constantly reported by media and scientific literature. For quality professionals that are responsible for planning, implementing, maintaining, and control of quality management in healthcare facilities at the organizational level, the abundance of information on quality and safety approaches is a complication.

The large number of quality improvement interventions is overwhelmingly high. The main decision is: what to begin with, but also how to integrate a multitude of tools into a coherent approach?

The motivation of this research is to support the management of health units in the alignment and use of these strategies and tools. Importance is accorded on cross-cutting matters such as supervision and guidance, the construction of assistance systems for quality improvement, and the provision of the adequate resources assuring high quality care. Healthcare specialists, quality professionals, and general managers can use this approach to periodically assess and continually improve the quality of their organization.

The general objective of the research is to establish the specifications of an analysis and evaluation model in the form of a reference framework for the design, development, and implementation, periodic evaluation, and continuous improvement of quality management systems based on the application of national and international standards for sustainable development in healthcare facilities.



## 2. Materials and Methods

The research methodology considers the study of the specialized literature, relevant for the research topic, which allows the creation of an adequate framework for the development of the empirical study.

The foundations of high quality healthcare systems must include: (a) a population and their health needs and expectations, (b) the governance of the health sector, and (c) partnerships between sectors, healthcare platforms, the number and skills of the workforce involved, as well as the tools and resources used, from medicines to data. High quality healthcare systems should adopt four values:

- (a) Be for people;
- (b) Be fair;
- (c) Resilient; and
- (d) Efficient.

Sustainability can be considered an area of the quality of healthcare, extending the responsibility of health services provided to patients from now to the future. A sustainable approach extends the definition of the value of healthcare to measure healthcare outcomes in terms of social and environmental impact, but also in terms of financial costs. Mortimer et al. [1] established a practical framework for including these new dimensions in an already well-defined quality improvement model. The current trend is to collaborate between actors involved in healthcare, called collaborative healthcare, which has the capacity to address challenges such as improving the social sustainability of the system. Maghsoudi et al. [2] developed a new model of medical organization in which collaboration between medical networks plays a central role in improving social sustainability.

Improving quality can promote the association between health security and healthcare systems; through integration of quality improvement approaches addresses global health security priorities and has the effect of improving health results at in all structures of the healthcare system [3]. Marimuthu et al. [4] explores the scope of sustainability practices in healthcare by highlighting three main conceptual aspects: the dimensions of sustainability practices in healthcare, the drivers of sustainable health practices, and strategies for implementing sustainability effectively in healthcare. Smith [5] highlights three levels of sustainability in which he describes the levels of healthcare with the appropriate measurement of performance through audit techniques.

Pantartzis et al. [6] highlight issues that can lead to small sustainable health institutions, such as energy saving and efficiency, that could be used to assess the viability of healthcare facilities. In a study, Glasgow [7] identified 539 potential articles on quality improvement methodologies and found that the true impact of this approach is difficult to assess, given that the lack of a rigorous evaluation or clearly supported improvements offers little evidence supporting widespread adoption. There is still a need for future research to improve the evidence base to understand more.

Currently, health facilities face major challenges, as patients demand continuous improvement in the quality of care, and health insurance companies demand the lowest possible prices. There are quality improvement programs from the industry, such as lean manufacturing, which is an excellent tool to meet current health challenges [8]. Some hospitals tend to adopt lean quality improvement programs, which require a lean assessment from a much more critical perspective [9] and quantification of sustainability effects [10]. A theoretical framework for sustainable health improvement developed by Hovlid et al. [11] is based on four main themes: (a) the question, (b) the decision, (c) the relationship, and (d) the interpretation.

In Romania, the national legislation on quality assurance in health has important references: Law no. 185/2017 on quality assurance in the healthcare system [12]; Standards, procedure, and methodology for evaluation and accreditation of hospitals [13]; and Legislation on the functioning [13] and working tools [14] used by the National Authority for Quality Management in Health. Hospital accreditation standards [15] comprise three references: Strategic and organizational management; Clinical management; Medical ethics and patient rights, which are supplemented by 64 checklists.

### 3. Results

This research proposes the development of a SANitary Quality (SANQ) reference framework containing a series of indicators addressed to health units that have implemented/are implementing quality management systems in their organizations and want to continuously improve the effectiveness of the quality management system by establishing quality indicators to monitor and promote their sustainable development. The conceptual model of the SANQ reference framework is presented in Figure 1, which integrates the existing legal requirements, standards, and quality assessment indicators from actual frameworks.

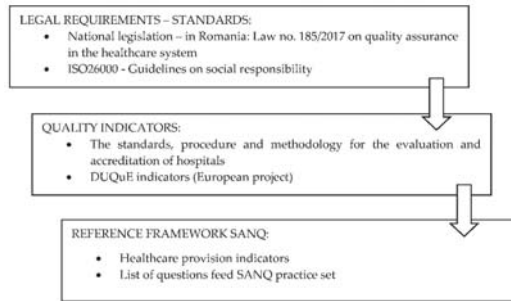


**Figure 1.** SANQ framework conceptual model.

In terms of quality cycle references, and in order to simplify its relationship with the already developed quality frameworks, the SANQ quality reference framework has to be structured based upon the Plan-Do-Check-Act (PDCA) quality cycle: planning, implementing, evaluating, and review. It should be developed also taking into consideration that the healthcare system can and should have a key role in the promotion of social cohesion and should also pursue financial sustainability and environmental responsibility.

The reason to adopt this conceptual model lies on the principles stated in ISO 26000, in regards to the definition of sustainable development and social responsibility—sustainable development is the “development that meets the needs of the present without compromising the ability of future generations to meet their own needs” [16]. Social responsibility is “the responsibility of an organization for the impacts of its decisions and activities on society and the environment, through transparent and ethical behavior that: contributes to sustainable development, including health and the welfare of society; takes into account the expectations of stakeholders; is in compliance with applicable law and consistent with international norms of behavior; and is integrated throughout the organization and practiced in its relationships” [17].

For this reason, the SANQ reference framework has to be structured on the three pillars of sustainable development—social, economic, and environmental—incorporated in the seven basic topics of social responsibility mentioned in ISO26000—Guidelines on social responsibility [17], adapted to the context of healthcare provision: Organizational governance, Human rights, Labor practices, Environment, Fair operating practices, Consumer issues, Community involvement and development, as shown in Figure 2.

In this way, the SANQ quality reference framework will be structured in four main phases, each of them corresponding to the four phases of the PDCA quality cycle, regarding healthcare: design of healthcare services, provision of healthcare services, evaluation of healthcare services, continuous improvement.

The extended applicability of the reference framework requires a correspondence between the SANQ indicators and the Standards for the evaluation and accreditation of hospitals provided in Order no. 446/2017 issued by the Ministry of Health [13].



**Figure 2.** Pillars of sustainable development and ISO 26000 social responsibility core subjects.

The reference framework should consist of several matrix assessment tools that will be structured in line with the DUQuE project results [18]: (1) Accreditation of healthcare services, (2) The effectiveness of the organization’s management, (3) Continuing medical education, (4) Patient safety culture, (5) Computerized support systems for clinical decisions, (6) Dissemination and implementation of guidelines, (7) Actions to improve transfers, (8) Patient-centered care actions, (9) Six Sigma and Lean, (10) Performance information, (11) Audit and feedback, (12) Reporting incidents to the hospital, (13) Safety checklists, (14) Documentation internships etc.

SANQ evaluation indicators are of a qualitative and/or quantitative type—which are described by formulas.

The SANQ quality reference framework will be accompanied by the Implementation Guide—The self-assessment tool, which will have three parts: (1) The SANQ reference framework, (2) The self-diagnosis tool, (3) The implementation guide.

The self-diagnosis tool will consist of a system of questions derived from the SANQ reference framework, whose assessment is made on the basis of a qualitative (poor to excellent) and/or quantitative grid (0 to 3 points). It will facilitate easy use by quality professionals in healthcare facilities.

#### 4. Conclusions

This research provided the specifications for a reference framework that aims to evaluate and improve quality and safety in healthcare facilities. The elaboration of the indicators of the reference framework requires state-of-the-art research, the use of the results of large-scale scientific studies, systematic reviews, and specialized knowledge.

Such research does not cover all quality strategies, but rather provides a perspective to support managers in reflecting on organization-wide approaches to ensure quality, safety, and sustainable development.

The widespread use of the assessment tool requires interactive links to specific assessment tools from the literature as well as those generated in this research.

**Conflicts of Interest:** The author declares no conflict of interest.

#### References

1. Mortimer, F.; Isherwood, J.; Wilkinson, A.; Vaux, E. Sustainability in quality improvement: Redefining value. *Future Healthc. J.* **2018**, *5*, 88–93. [[CrossRef](#)] [[PubMed](#)]
2. Maghsoudi, T.; Cascon-Pereira, R.; HernandezLara, A.B. The Role of Collaborative Health care in Improving Social Sustainability: A Conceptual Framework. *Sustainability* **2020**, *12*, 3195. [[CrossRef](#)]
3. Mensah, A.N.; Syed, S.B.; Hirschhorn, L.R.; Nambiar, B.; Iqbal, U.; Garcia-Elorrio, E.; Chattu, V.K.; Devnani, M.; Kelley, E. Quality improvement and emerging global health priorities. *Int. J. Qual. Health Care* **2018**, *30*, 5–9. [[CrossRef](#)] [[PubMed](#)]

4. Marimuthu, M.; Paulose, H. Emergence of Sustainability Based Approaches in Health care: Expanding Research and Practice. *Procedia Soc. Behav. Sci.* **2016**, *224*, 554–561. [CrossRef]
5. Smith, M.E. Sustainable Healthcare. A path to sustainability. Master's Thesis, Policy & Management Lund University, Lund, Sweden, 2012. Available online: <https://lup.lub.lu.se/luur/download?fileOid=3126182&func=downloadFile&recordOid=3126175> (accessed on 17 August 2020).
6. Pantartzis, E.; Edum-Fotwe, F.T.; Price, A.D.F. Sustainable health care facilities: Reconciling bed capacity and local needs. *Int. J. Sustain. Built Environ.* **2017**, *6*, 54–68. [CrossRef]
7. Glasgow, J.M. Guiding In patient Quality Improvement: A Systematic Review of Lean and Six Sigma. *Jt. Comm. J. Qual. Patient Saf.* **2010**, *36*, 533–540. [PubMed]
8. Van Den Heuvel, J.; Does, R.J.M.M.; DeKoning, H. Lean Six Sigma in a Hospital. *Int. J. Six Sigma Compet. Advant.* **2006**, *2*, 377–388. [CrossRef]
9. De BrandaoSouza, L. Trends and Approaches in Lean Healthcare. *Leadersh. Health Serv.* **2009**, *22*, 121–139. [CrossRef]
10. Kruk, M.E.; Gage, A.D.; Arsenault, C.; Jordan, K.; Leslie, H.H.; Roder-DeWan, S.; Adeyi, O.; Barker, P.; Daelmans, B.; Doubova, S.V.; et al. High-quality health systems in the Sustainable Development Goals era: Time for a revolution. *Lancet Glob. Health* **2018**, *6*, e1196–e1252. [CrossRef]
11. Hovlid, E.; Bukve, O.; Haug, K.; Aslaksen, A.B.; von Plessen, C. Sustainability of Health care Improvement: What Can We Learn from Learning Theory? *BMC Health Serv. Res.* **2012**, *12*, 235. [CrossRef]
12. Legea, nr. 185/2017 privind asigurarea calității în sistemul de sănătate (Law no. 185/2017 on Quality Assurance in the Health System). Available online: [http://www.spitalvn.ro/documente/legislatie/legea\\_185\\_2017.pdf](http://www.spitalvn.ro/documente/legislatie/legea_185_2017.pdf) (accessed on 17 August 2020).
13. Standardele, procedura și metodologia de evaluare și acreditare a spitalelor, aprobate prin Ordinul ministrului sănătății nr. 446/2017 (The standards, procedure and methodology for the evaluation and accreditation of hospitals, approved by the Order of the Minister of Health no. 446/2017). Available online: [https://anmcs.gov.ro/web/wp-content/uploads/2017/04/OrdinMS-446-2017-StandardeEd.IL\\_.pdf](https://anmcs.gov.ro/web/wp-content/uploads/2017/04/OrdinMS-446-2017-StandardeEd.IL_.pdf) (accessed on 17 August 2020).
14. Hotărârea Guvernului nr. Hotărârea Guvernului nr. 629/2015 privind componența, atribuțiile, modul de organizare și funcționare ale Autorității Naționale de Management al Calității în Sănătate (Government Decision no. 629/2015 on the composition, attributions, organization and functioning of the National Authority for Quality Management in Health). Available online: <https://lege5.ro/Gratuit/g42donrzg4/hotararea-nr-629-2015-privind-componenta-atributiile-modul-de-organizare-si-functionare-ale-autoritatii-nationale-de-management-al-calitatii-in-sanatate> (accessed on 17 August 2020).
15. Ordinul nr. 35 din data de 20.02.2018 pentru modificarea Ordinului Președintelui Autorității Naționale de Management al Calității în Sănătate nr. 8/2018 privind aprobarea instrumentelor de lucru utilizate de către Autoritatea Națională de Management al Calității în Sănătate în cadrul celui de al II-lea Ciclu de acreditare a spitalelor (Order no. 35 of 20.02.2018 for the amendment of the Order of the President of the National Authority for Quality Management in Health no. 8/2018 on the approval of the working tools used by the National Authority for Quality Management in Health within the Second Cycle of Hospital Accreditation). Available online: <https://anmcs.gov.ro/web/2018/02/20/> (accessed on 17 August 2020).
16. Shah, M.M. Sustainable development. In *Encyclopedia of Ecology*; Jorgensen, S.E., Fath, B.D., Eds.; Imprint Elsevier Science: Philadelphia, PA, USA, 2008; pp. 3443–3446.
17. ISO26000—Guidelines on Social Responsibility. Available online: <https://www.iso.org/iso-26000-social-responsibility.html> (accessed on 17 August 2020).
18. Groene, O.; Kringos, D.; Sunol, R.; on behalf of the DUQuE Project. Seven ways to improve quality and safety in hospitals. An evidence-based guide. *DUQuE Collab.* 2014. Available online: [http://www.duque.eu/uploads/DUQuE\\_Seven\\_Ways\\_To\\_Improve\\_Quality\\_And\\_Safety\\_2014.pdf](http://www.duque.eu/uploads/DUQuE_Seven_Ways_To_Improve_Quality_And_Safety_2014.pdf) (accessed on 17 August 2020).

**Publisher's Note:** MDPI stays neutral with regard to jurisdictional claims in published maps and institutional affiliations.



© 2020 by the author. Licensee MDPI, Basel, Switzerland. This article is an open access article distributed under the terms and conditions of the Creative Commons Attribution (CC BY) license (<http://creativecommons.org/licenses/by/4.0/>).



# Matlab Framework for Image Processing and Feature Extraction Flexible Algorithm Design <sup>†</sup>

Razvan Cazacu 

Faculty of Engineering, Department of Industrial Engineering and Management, University of Medicine, Pharmacy, Sciences and Technology “George Emil Palade” of Targu Mures, 540142 Targu Mures, Romania; paul.cazacu@umfst.ro

<sup>†</sup> Presented at the 14th International Conference INTER-ENG 2020 Interdisciplinarity in Engineering, Mures, Romania, 8–9 October 2020.

Published: 24 January 2021

**Abstract:** Image processing and the analysis of images in order to extract relevant data is an ever-growing topic of research. Although there are numerous methods readily available, the task of image preprocessing and feature extraction requires developing specific algorithms for specific problems by combining different functions and tweaking their parameters. This paper proposes a framework that allows the flexible construction of image processing algorithms. Its user interface and architecture are designed to ease and speed up the process of algorithm creation and testing as well as serve as an application for the use of these algorithms by end users. The framework was built in Matlab and makes use of its integrated Image Processing toolbox.

**Keywords:** image processing; feature extraction; Matlab; framework; algorithm design

## 1. Introduction

Enhancing and extracting useful information from digital images plays an important role in most scientific and engineering fields. There are numerous tools and software packages available for pure image processing. However, feature extraction requires the development of specific algorithms depending on image particularities and the type of data that needs to be retrieved from the images. Matlab is the leading platform for technical computing and is one of the most widely used languages for the creation of feature extraction algorithms. Its Image Processing toolbox [1] contains almost a thousand of the most common functions related to this field [2–4], allowing for the preprocessing, analysis, segmentation, registration, and postprocessing of digital images.

In addition to the core language and its plethora of toolboxes, Matlab also benefits from a very large community of programmers and researchers constantly extending its rich bank of tools and assets. They are all drawn by the versatility of the integrated computing environment, the volume of available resources, and the multitude of possibilities to share the created content with both programmers and end users, inside or outside the Matlab application. One of the methods for extending Matlab core functionality is the creation of frameworks, some based on available toolboxes, which can be used to program or solve problems in specific areas of interest, such as conducting behavioral and neuroimaging experiments [5], processing of digital elevation data [6], or the implementation of genetic algorithms for optimization problems [7].

Automatic characterization of materials and material structures is an essential tool for the speed and accuracy of their quality assessment. Algorithms such as those built for analyzing the cupping profiles of laminated wood products [8], the identification of fission gas bubbles [9], or for the extraction of information from SEM micrographs of nanotube structures [10] fall into this category. Developing, testing, tweaking, extending, and improving such algorithms is an iterative process that could be greatly sped up and eased by using a dedicated framework for flexible algorithm design.

The main drive behind building the framework proposed in this paper is the need for automatic characterization of highly ordered titanium oxide nanostructures (nanotubes/nanopores) formed on titanium-based surfaces as a result of an optimized electrochemical anodization process [11]. This technology has applications in the production of solar energy harvesting cells [12] and, most importantly, in medicine [13]. The formation of nanoscale tubes on the surfaces of dental or orthopedic implants [14] can be used as a tool for releasing drugs at the tissue level [15] and can help osteogenesis at the bone-implant interface for a better osseointegration of the implants [16]. The size, shape, and uniformity of nanotubes are important factors that determine the nanolayer quality and its capacity to favor osseointegration; thus, accurately extracting and interpreting these data from associated digital images is an essential process.

## 2. Materials and Methods

The framework for Image Processing Algorithm Design (IPADesign) was built with the nanotube micrograph interpretation in mind such as to allow the development and inclusion of most processing scenarios for this particular application. However, its structure was designed for maximum flexibility and should be suitable for most other feature extraction algorithms. This section describes the architecture of the framework and its underlying data while the next section deals with the graphical user interface and the actual implementation in Matlab.

The framework consists of a graphical user interface, part of which is dynamically generated; the engine running the algorithms; a base abstract class used to derive the classes encapsulating image processing functionality; and a number of predefined such classes (IPAFunctions) implementing the most common functions.

The general structure of the application and its associated files is schematized in Figure 1. The data it uses is grouped into 3 categories: metadata, document data, and algorithm data.

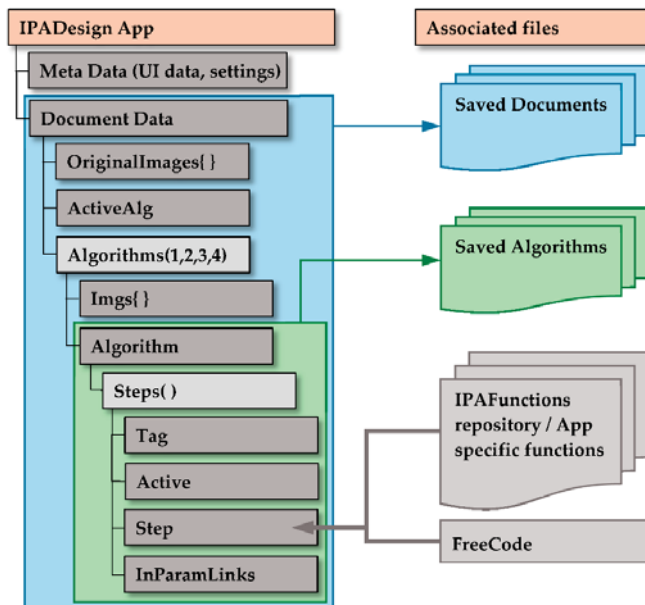


Figure 1. Application architecture and its associated files.

The metadata are the data used to keep track of the dynamic part of the user interface, the settings of the application, and the list of folders containing files associated with the framework. Only part of these data is saved and thus is persisted between sessions.

The document data are the structure and all the data associated with a specific image processing problem. They contain the original image or images requiring processing and a collection of up to 4 algorithm structures. These are each composed of an object containing algorithm data and a cell array with processed images from all intermediate steps. In a typical scenario, only one image will be processed with a single algorithm. However, it is possible to load more original images for batch processing or to be used in functions requiring multiple image input. At the same time, a document allows for working with more algorithms at once for comparison purposes or even have the same algorithm cloned in order to assess in parallel the intermediate results obtained during its execution. The data of a document can be saved as a workspace (.mat file) and later reloaded in the application for editing. Alternatively, the workspace can be loaded in Matlab and analyzed or postprocessed outside the application.

The algorithm data are all the information associated with a developed algorithm and can be saved separately as a workspace (.mat file) or loaded in a document. They contain all data required to build an image processing procedure but do not hold any information about the actual processed images. An algorithm consists of a succession of steps, each representing a certain image processing transformation or inquiry. A step has three properties that define how it will be treated by the algorithm running engine:

- Tag: unique identifier of a step, typically the name of the function associated with this step, followed by a numeric index accounting for possible multiple uses of the same function;
- Active: a Boolean (true/false) value indicating if this step is to be considered or not when running the algorithm (to allow maximum flexibility in testing algorithms);
- InParamLinks: a list of strings linking this step function's parameters to values returned by functions in previous steps, wherever the case (not a typical situation, but implemented for flexibility).

The most important component of a step is the actual image processing function. This part of the framework was implemented using the Object Oriented Programming paradigm. Each function is encapsulated in a class inheriting from an abstract class (IPAFunBase) as shown on Figure 2.

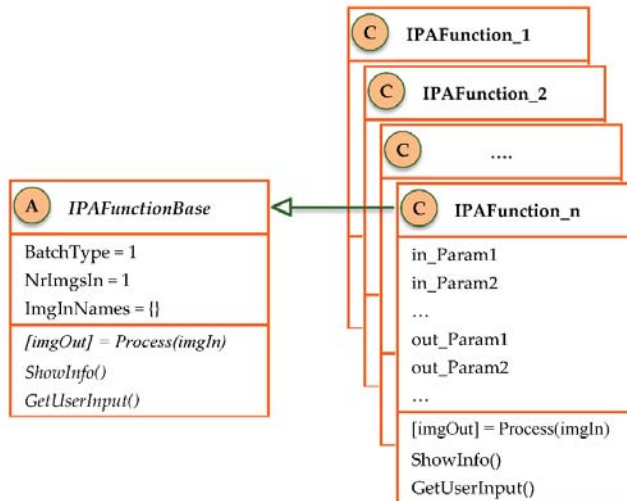


Figure 2. Diagram of the abstract base image processing function class and its derived classes.

The abstract class has the role of a template, allowing the algorithm running engine to communicate with the image processing functions using an agreed communication protocol. It consists of 3 properties:



- **BatchType (ReadOnly):** the default value (1) indicates the function will treat input images as a batch, processing each of them separately. A value of 2 should be set in the derived classes for the functions that aggregate all input functions and return a single output.
- **NrImgsIn (ReadOnly):** number of image inputs. The default value of 1 means the function processes images resulted from only 1 of the previous steps (or the original images), while greater values can be used in cases where input images originate from multiple previous steps.
- **ImgInNames:** a list of strings containing the tag(s) of the previous step(s) providing the input images. It should have a number of elements equal to *NrImgsIn* or be empty. If empty, the engine assumes only 1 input image, the one provided by the previous step (most common scenario).

and 3 methods:

- **Process:** abstract method that needs to be overridden in the derived classes, implementing the logic of the image processing function. It has only 1 argument, the input image(s), and 1 output, the processed image(s). Possible additional arguments and results are implemented in the derived classes as public properties.
- **ShowInfo:** implemented in derived classes only in the case of functions returning information other than images. It typically outputs feature extraction data in a visual form (GUI, graphs). It can optionally be called by the Process method to show the information when the algorithm runs; however, it is a separate method and can be accessed from the application GUI at any time.
- **GetUserInput:** used in the case of functions requiring the user to provide coordinates of points from the original image(s). Useful for functions extracting scale data from images providing such information and in some other fringe scenarios.

All classes implementing image processing or feature extraction functionality need to inherit from the *IPAFunctionBase* abstract class. *NrInImage* and *BatchType* have to be set in the constructor if they have other values than the default (1 for both). Besides overriding the main method (*Process*) and possibly the other 2 methods, the class can define additional parameters in the form of public properties. By convention, these are grouped into 2 categories and should follow the following name conventions:

- **in\_ParamName** parameters: properties whose names begin with the “in\_” particle are considered input arguments for the image processing function. These can be set on the app GUI at algorithm construction time.
- **out\_ParamName** parameters: properties whose names begin with the “out\_” particle are results returned by the function other than images. They can be end results (feature extraction information) or intermediate data used by the “in\_” parameters of subsequent steps.

For maximum flexibility, the *Step* field of a given step can either be an instance of an image processing class or, alternatively, it can simply contain Matlab code (*FreeCode*) that will be executed by the engine. This can be a series of commands separated by semicolons (;) or the name of a script to be called.

### 3. Results and Discussion

The framework is implemented in Matlab as an application that can be used directly as it is or extended with more image processing functionality by complying to the framework’s structure and tools. The abstract class along with the derived classes implementing core image processing functions are stored in a subfolder of the application called *IPAFunctions*. Classes specific to certain problems can be added and stored in different locations. The application keeps a list of paths where these classes are located, similar to Matlab’s built-in search paths. When building an algorithm, the user can choose from the list of all available image processing classes in the specified locations.

The graphical user interface (GUI) presented in Figure 3 consists of three main parts:

- Tools area. Fixed interface area with menus and controls for all operations except algorithm creation: saving and loading documents and algorithms, managing function paths, running algorithms, and controlling and navigating the image display area.
- Algorithm area. Dynamically generated and managed part of the interface, consisting of a list of controls associated with algorithm steps. Each line contains a control for the selection of the step, a checkbox associated with the Active field, a static text specifying the tag of the step (containing the name of the associated class), and a button opening the parameters window. Steps can be added, deleted, or reordered using the controls in the upper area.
- Image display area. Main panel for displaying the original and transformed images. It can show a single image belonging to the active algorithm, four images from different steps of the active algorithm, or four images from specified steps on each of the four algorithms in a document.

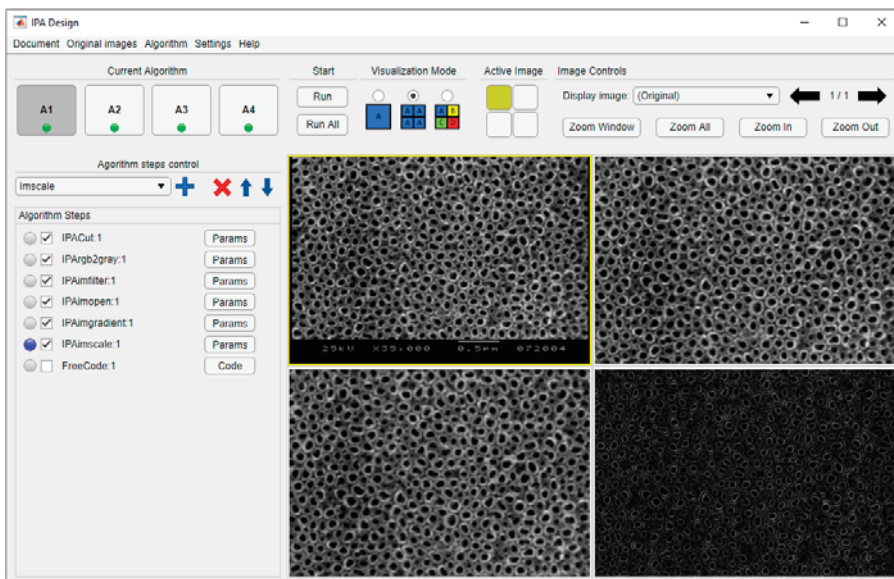


**Figure 3.** Main GUI of the application. Tools area—upper zone; algorithm area—left, image display—right.

For each step of the algorithm, the class parameters are specified in a dedicated window (Figure 4), accessed via the respective buttons as depicted in Figure 3. The parameters window is generated dynamically by the application. Depending on the `NrImgsIn` property of the respective class, the window offers a number of drop-down controls listing all previous tags for choosing the steps providing input images for this step. The chosen values are saved in the `ImgInNames` property of the class. The default value (previous step) is for the most common case when the input image is taken from the previous step, no matter which function that represents. In this case, `ImgInNames` is left empty. Below the choice of input images, the window lists all “in\_” parameters. The user can set static values for the parameters, enter expressions to be evaluated at run time (by convention, the engine treats the entered text as an expression if it starts with the equal sign “=”), or choose from the “out\_” parameters of previous steps (this is recorded as an entry in the `InParamLinks` field of the Step object). At the bottom of the window, two buttons allow the user to call the class methods to visually show the results (only available after running the algorithm) and to obtain user input.

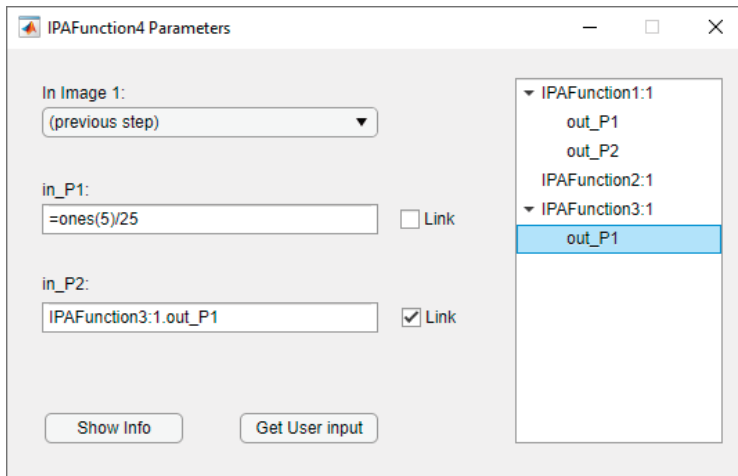


Figure 4. Example of a “Parameters” window.

In addition to the main graphical interface and the parameters dialogs, each image processing function has the option to output its specific results in a distinct window by overriding the ShowInfo method of the base abstract class. This functionality can be accessed from the parameter window of a step by clicking the respective button (shown in Figure 4).

An algorithm can be tested or used at any time by accessing the Run (current algorithm) or Run all (all algorithms in document) buttons. This will trigger the main engine of the framework, which uses all setup steps and parameter data, along with the associated files to output all intermediate and final results—images and extracted information. The images are shown in the image display area and can be navigated with the respective GUI buttons while the non-image data can be visualized or exported using the ShowInfo method.

#### 4. Conclusions and Further Research

The framework described in this paper can be a useful tool in the development of image processing and feature extraction algorithms, offering a flexible environment for speeding up the design, testing, and ultimate use of such algorithms. It was created to cover most scenarios involved in the automatic characterization of nanotube layers, but the generality of its architecture makes it a suitable tool for most other image processing applications.

Besides its core functionality, the framework’s versatility also depends on the number of available classes. Each such class implements a specific image processing function, either from Matlab’s dedicated toolbox or user-defined. The framework’s repository of classes can easily be extended by deriving from the abstract base class. This establishes the template, ensuring compatibility between new content and the algorithm running engine.

The user interface and application structure were designed to ensure maximum flexibility in the addition of new components, the construction of algorithms, and their use by final users. However, this power and flexibility comes with an overhead in execution time. The implication of running the algorithms from a superior programming layer was not studied in this paper. Although the extra computational effort introduced by the application itself should not have a significant weight compared to the execution time of the computationally intensive image processing functions themselves, a further study could establish the actual relative impact of the extra added layer.

The main purpose for creating the framework is its use in the assessment of TiO<sub>2</sub> nanotube structure quality by extracting statistical data regarding nanotube uniformity, shape, and size from SEM micrographs. Future research will focus on the issue of developing, testing, tweaking, and improving algorithms that can optimally achieve this task.

**Funding:** This research was supported by the University of Medicine, Pharmacy, Science and Technology “George Emil Palade” of Târgu Mureș, research grant number 292/2/14.01.2020.

**Acknowledgments:** The author would like to thank the University of Medicine, Pharmacy, Sciences and Technology “George Emil Palade” of Târgu Mureș and the team involved in researching the production of nanostructures on titanium-based surfaces. The idea and resources for this paper are based on the work and results of this team. A special mention goes to its leader, Strnad Gabriela, for her vision and support.

**Conflicts of Interest:** The author declares no conflict of interest. The funders had no role in the design of the study; in the collection, analyses, or interpretation of data; in the writing of the manuscript; or in the decision to publish the results.

## References

1. The MathWorks, I. MATLAB Image Processing Toolbox (R2019a), Natick, MA, USA. Available online: <https://www.mathworks.com/products/image.html> (accessed on 20 June 2020).
2. Gonzalez, R.C.; Woods, R.E. *Digital Image Processing*, 4th ed.; Pearson: New York, NY, USA, 2018.
3. Nixon, M.S.; Aguado Gonzalez, A.S. *Feature Extraction & Image Processing for Computer Vision*, 4th ed.; Academic Press: London, UK, 2020.
4. Petrou, M.M.P.; Petrou, C. *Image Processing: The Fundamentals*, 2nd ed.; John Wiley & Sons Ltd.: Chichester, UK, 2010.
5. Schwarzbach, J. A simple framework (ASF) for behavioral and neuroimaging experiments based on the psychophysics toolbox for MATLAB. *Behav. Res.* **2011**, *43*, 1194–1201. [[CrossRef](#)] [[PubMed](#)]
6. Pan, F.; Xi, X.; Wang, C. A MATLAB-based digital elevation model (DEM) data processing toolbox (MDEM). *Environ. Model. Softw.* **2019**, *122*, 104566. [[CrossRef](#)]
7. Cazacu, R.; Grama, L.; Mocian, I. An OOP MATLAB Extensible Framework for the Implementation of Genetic Algorithms. Part I: The Framework. *Procedia Technol.* **2015**, *19*, 193–200.
8. Li, L.; Gong, M.; Chui, Y.H.; Schneider, M. A MATLAB-based image processing algorithm for analyzing cupping profiles of two-layer laminated wood products. *Measurement* **2014**, *53*, 234–239. [[CrossRef](#)]
9. Collette, R.; King, J.; Keiser, D.; Miller, B.; Madden, J.; Schulthess, J. Fission gas bubble identification using MATLAB’s image processing toolbox. *Mater. Charact.* **2016**, *118*, 284–293. [[CrossRef](#)]
10. Caudrová Slavíková, P.; Mudrová, M.; Petrová, J.; Fojt, J.; Joska, L.; Procházka, A. Automatic characterization of titanium dioxide nanotubes by image processing of scanning electron microscopic images. *Nanomater. Nanotechnol.* **2016**, *6*. [[CrossRef](#)]
11. Strnad, G.; Cazacu, R.; Chetan, P.; German-Sallo, Z.; Jakab-Farkas, L. Optimized anodization setup for the growth of TiO<sub>2</sub> nanotubes on flat surfaces of titanium based materials. *MATEC Web Conf.* **2017**, *137*, 02011. [[CrossRef](#)]
12. El Ruby Mohamed, A.; Rohani, S. Modified TiO<sub>2</sub> nanotube arrays (TNTAs): Progressive strategies towards visible light responsive photoanode, a review. *Energy Environ. Sci.* **2011**, *4*, 1065–1086. [[CrossRef](#)]
13. Ribeiro, A.; Gemini-Piperni, S.; Alves, S.A. Titanium dioxide nanoparticles and nanotubular surfaces: Potential applications in nanomedicine. In *Metal Nanoparticles in Pharma*, 1st ed.; Rai, M., Shegokar, R., Eds.; Springer International Publishing: Basel, Switzerland, 2017; pp. 101–121.
14. Strnad, G.; Portan, D.; Jakab-Farkas, L.; Petrovan, C.; Russu, O. Morphology of TiO<sub>2</sub> surfaces for biomedical implants developed by electrochemical anodization. *Mater. Sci. Forum* **2017**, *907*, 91–98. [[CrossRef](#)]
15. Gulati, K.; Saso, I. Dental implants modified with drug releasing titania nanotubes: Therapeutic potential and developmental challenges. *Expert Opin. Drug Deliv.* **2017**, *14*, 1009–1024. [[CrossRef](#)] [[PubMed](#)]

16. Gulati, K.; Maher, S.; Findlay, D.; Lotic, D. Titania nanotubes for orchestrating osteogenesis at the bone–implant interface. *Nanomed. J.* **2016**, *11*, 1847–1864. [[CrossRef](#)] [[PubMed](#)]

**Publisher’s Note:** MDPI stays neutral with regard to jurisdictional claims in published maps and institutional affiliations.



© 2021 by the author. Licensee MDPI, Basel, Switzerland. This article is an open access article distributed under the terms and conditions of the Creative Commons Attribution (CC BY) license (<http://creativecommons.org/licenses/by/4.0/>).

# Selection the Basic Lean Manufacturing Techniques in Developing the Model for Industry 4.0 in Kosovo Manufacturing Industry <sup>†</sup>

Fatmir Azemi <sup>1</sup>, Roberto Lujic <sup>2</sup>, Goran Šimunović <sup>2</sup> and Daniel Tokody <sup>3,\*</sup>

<sup>1</sup> Mechatronics Management Department, University for Business and Technology, Lagjja Kalabria, 10000 Prishtinë, Kosovo; fatmir.azemi@ubt-uni.net

<sup>2</sup> Mechanical Engineering Faculty in Slavonski Brod, JJ Strossmayer University of Osijek, Trg Ivane Brlić Mažuranić 2, 35000 Slavonski Brod, Croatia; rlujic@sfsb.hr (R.L.); goran.simunovic@sfsb.hr (G.Š.)

<sup>3</sup> Doctoral School on Safety and Security Sciences, Óbuda University, Népszínház utca 8., 1081 Budapest, Hungary

\* Correspondence: tokody.daniel@dosz.hu; Tel.: +36-309-507-193

<sup>†</sup> Presented at the 14th International Conference INTER-ENG 2020 Interdisciplinarity in Engineering, Mures, Romania, 8–9 October 2020.

Published: 31 December 2020

**Abstract:** Recently, there have been done numerous investigations related to lean manufacturing techniques. However, very little has been reported about the implementation and selection of lean manufacturing in the Kosovo manufacturing industry. This article presents the application of lean tools through Kosovo manufacturing industries and the selection of the most useful lean techniques for developing a model for an innovative smart Kosovo enterprise which is our initiative in the process of preparing Kosovo enterprises for the new age of industry—Industry 4.0. After several visits through Kosovo enterprises, the literature review has noticed that there is no investigation in the selection and implementation of lean techniques and tools in Kosovo enterprises. The purpose was to understand how Kosovo manufacturing enterprises use lean techniques and which are the most useful techniques. Analyses have been done based on interviews and questionnaires. Seven basic lean techniques are selected based on the response from the questionnaire and representing basic lean tools for developing a model of a production system regarding Industry 4.0.

**Keywords:** Industry 4.0; innovative smart enterprises; Kosovo manufacturing industry; lean manufacturing techniques

## 1. Introduction

Origination in Japan, particularly at Toyota, a carmaker in the 1960s developed the principles of lean production/manufacturing. The lean manufacturing approach is about the reducing or elimination of waste or activities which add no value to the manufacturing process. Therefore, lean manufacturing is a management philosophy based on the Toyota Production Systems (TPS) [1].

In this paper, the investigation is to continue the work of our initiatives for developing a model for innovative smart enterprise in the Kosovo industry regarding Industry 4.0 [2,3]. Specifically, which are the most useful lean techniques for innovative smart Kosovo enterprises is the main issue of this investigation. The questionnaire is used to collect data from manufacturers on the use of lean methods and implementation within Small and Medium Enterprises (SMEs) in the Kosovo manufacturing industry. From questionnaires and interviews with experts in the industry, the aim is to understand common challenges that companies face when implementing or have implemented lean manufacturing techniques/practices in their facilities and select the most useful lean tools for Kosovo enterprises.

Many investigations have been done all around the world in the field of lean manufacturing and many of the authors have given solutions, but in the Kosovo manufacturing industry, a gap exists in this direction.

This study provides a brief description and explanation of which lean principles are used within SMEs of the Kosovo manufacturing industry, provides approaches on how to select the best lean tools for Kosovo enterprises, and identifies the most useful lean tool implications on systems by producing exactly what the customer wants, at the minimum cost with minimum or zero defects. So, the main reason of this study is to fulfil gaps in the developing model for smart enterprises in the aspect of the organization. Each manufacturing company has a unique system of manufacturing and recently some countries are in the process of developing their model for the new era of industry, such as Industry 4.0 in Germany. In Kosovo, there are no initiatives in this direction and the selection of lean manufacturing principles is too important for developing a model of the enterprise regarding Industry 4.0. The developed model could be implemented and will be unique and original for Kosovo enterprises, especially in SMEs.

Since the main objective of the investigation is to select the most useful lean techniques for developing the model for innovative smart enterprises, the following questions are presented:

- For Kosovo SME manufacturers that are not using lean manufacturing techniques, do they plan to use them?
- For Kosovo SME manufacturers that are not using them and do not plan to use LMTs, why not?
- For Kosovo enterprises that are using lean manufacturing techniques, which ones do they use and when did they start using them?
- For Kosovo enterprises that are using lean manufacturing techniques, which of them are helping the most?

## 2. Literature Review and Theoretical Background

To be successful in a competitive business environment, managers and staff need to know how to organize as well as how to develop product and manufacturing. Lean product development is an approach to organize product development according to a set of techniques/principles and existing different lean manufacturing techniques that are reported by different authors. Studies on the most used and helpful techniques can be found for different countries, but for the Kosovo manufacturing industry, it is not reported. Very little has been reported about the implementation and use of lean manufacturing in the Kosovo manufacturing industry; there are few papers specifically related to the administrative processes.

### 2.1. Lean Manufacturing

The term lean manufacturing was first used by Womack et al. [4] as a 'secret weapon' responsible for quality improvement and elimination of waste, so, the lean manufacturing contributes to cost reduction within organizations. Lean manufacturing according to Detty and Yingling [5] is a comprehensive philosophy for operating, structuring, managing, controlling, and continuously improving industrial production systems. The aim of lean manufacturing is to reduce the waste in inventory, human effort, time to market and manufacturing area to become responsible to demand of the customer while producing products with the highest quality, most economically and efficiently [6].

Shah and Ward [7] supported the above statements while pronouncing that lean production is a multi-dimensional technique that encompasses a wide diversity of management practices, involving quality systems, just-in-time, cellular manufacturing, work teams, and supplier management.

The lean manufacturing goal is to produce just what is needed and when the product is needed. The process of production is pulled according to the downstream processing workstation so that each of the workstations have only produced what is required by the next workstation. Lean manufacturing concentrates on defect-free lines of production [8]. It aims to avoid defects at the beginning and



for inspection of quality to be performed by the labourers as part of the process in-line production. Lean manufacturing requires attempting perfection by regularly removing layers of waste as they are uncovered. This, on the other hand, requires high level involvement of a worker in the continual improvement process.

According to Melton (2005) [9], the main improvements related to lean were time reduction to customers, efficient usage of processes, less utilization of inventory, improvement of knowledge management, cost savings, and rework reduction. Additional benefits of lean are improving the financial position, achieving competitive advantage, improving services, process standardization, and increasing quality. Some other positive factors are the increasing competence of employees, reducing disappointments with increasing satisfaction of customers, financial benefits to the organization, and faster work completion. In addition, lean manufacturing helps organizations in changing their approach to problem-solving abilities and standardization [10,11]. Moreover, it enables organizations to accomplish competitive advantage concerning high quality and encourages the empowerment of employees, delivery reliability, and faster delivery time.

## 2.2. Lean Manufacturing Techniques

To transform a traditional organization [12] into a lean organization should be made continually essential and take numerous efforts. Several elements have been discussed by researchers and manufacturing organizations have adopted them in the process of production to increase competitiveness in the market by reducing response time to customers, reducing product manufacturing cost, and improving productivity and quality. The following presents key elements which have been used in different research papers.

The 5S is a systematic philosophy (approach) aimed at organizing, standardizing, cleaning, ordering, and continuously improving a workplace area. Furthermore, the 5S according to Johansson is identified as part of the technique of green productivity [13].

Six Sigma is a program of management designed to decrease waste and increase productivity. Six sigma, according to Chakravorty [14], has a strong focus on customer satisfaction and meeting customer requirements.

TPM—the technique total productive maintenance (TPM) contributes to the basic preventative maintenance of machines, the breakdown time of equipment and machines is reduced. It also increases the efficiency of operation of the machine as a worker cleans, along with the inspection, lubrication, tightening activity of his machine.

Kanban is a shop floor tool used as an indication to control the release of the materials in operation and communicates customer requirements from downstream to the upstream worker. In such a manner, organizations know to provide more materials from suppliers [15]. Once the product is taken from finished parts against customer requests to recharge the moved quantity, it is replaced by coloured cards or with electronic devices.

SMED/setup time reduction—lean manufacturing aims to reduce setup time and changes over time because it spends critical working time and decreases the operator time and appropriate utilization of the machine.

Kaizen is a method which means small improvement. To keep activities continuously improving throughout the organization, the Kaizen method culture has to be created and preserved. Kaizen commonly is done by the personnel who are directly in the process of production mainly by operators for improvement in working circumstances, safety, productivity, quality, reduction of set up time, or some other small change for improvement.

Value stream mapping is a technique that visually displays the stream of materials and information along the production process. The main aim of value stream mapping is to put side by side activities for both added-value activities and non-added-value activities.



### 3. Methodology

This investigation project was designed as a questionnaire-survey and interviews with managers to evaluate the most useful lean manufacturing techniques within SMEs in the Kosovo industry. There were 186 questionnaires delivered to companies through email and by hand. Ninety-five questionnaires were answered completely and in the right way and are accepted as the sample size.

So, of the 186 questionnaires sent out, 95 were received as regular or completely answered, the response rate is 51.07%.

The questionnaire was divided into three parts: the general questions, background information about the organization, the usage of lean, benefits, and barriers in the implementation of the LMT (which LMT has helped the most, how important is for a company to use LMT, etc.). In Figure 1, the size of the company is presented (according to the choices presented in the questionnaire).

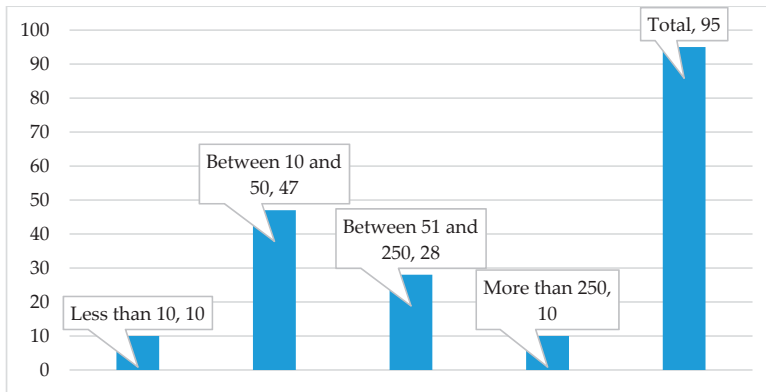


**Figure 1.** The size of the companies that are included in the survey.

According to the position in the company, the respondents who answered the questionnaires are as below:

- 56.25% of them are top managers,
- 37.50% of them are middle managers, and
- 6.25% of them are employees that have worked on the project.

Whereas, the type of industries which are included in the survey are presented as follows: civil industry (9 companies), food industry (11 companies), metal manufacturing industry (16 companies), general machinery and appliances manufacturing (13 companies), electrical machinery and appliances manufacturing (9 companies), transportation equipment manufacturing—other than automobiles (6 companies), transportation equipment manufacturing—automobiles (2 companies), plastic products and/or rubber products manufacturing (11 companies), construction (10 companies), lumber/wooden products manufacturing (14 companies), other manufacturing industries (11 companies).

### 4. Results and Discussion

To summarize data, the descriptive and inferential statistical analyses are done. The basic features of the data are described with descriptive and inferential statistics, spreadsheet and SPSS packet program are used to analyze collected data. The main purpose of this investigation was to determine which are the most used lean techniques and helpful for Kosovo SMEs, which lean tools (techniques) are used by the companies or are still used and so on.

For the companies that are not using lean manufacturing techniques, do they plan to use them? In Figure 2, the percentage of companies is presented that did not use LMTs but were planning to use or

not to use in the future. The percentage of those who said they did not use LMTs but were planning to was 63.49% (40 of 63 total), and companies that have not planned to use LMTs was 36.51% (23 of 63 total).

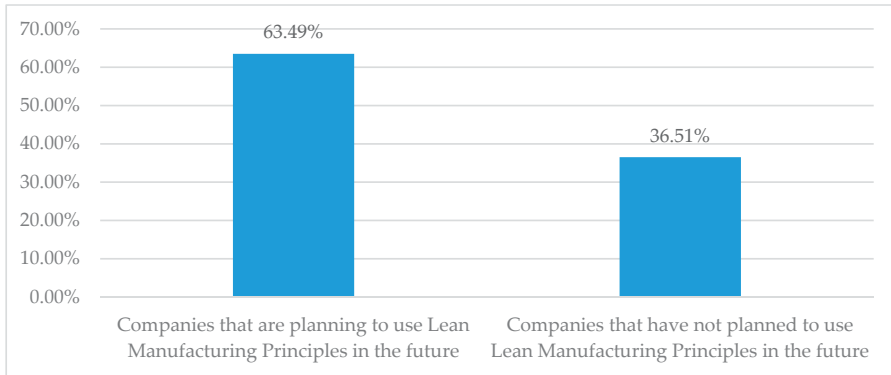


**Figure 2.** The percentage of companies that plan to use/not planned to use lean manufacturing principles in the future.

For the companies that are not using LMT and do not have a plane to use them, why not? Here are the “reason” percentages for the 23 companies that are both not using LMTs and are not planning to use in the future, the responses are as below:

- We are not informed much about lean manufacturing techniques: 43.48% (10 companies),
- We understand lean manufacturing techniques but we are not informed how to use them: 39.13% (9 companies),
- We consider that adopting lean manufacturing techniques will not be beneficial: 17.39% (4).

Figure 3 below presents lean tools that companies currently are using or have used in their process of manufacturing.

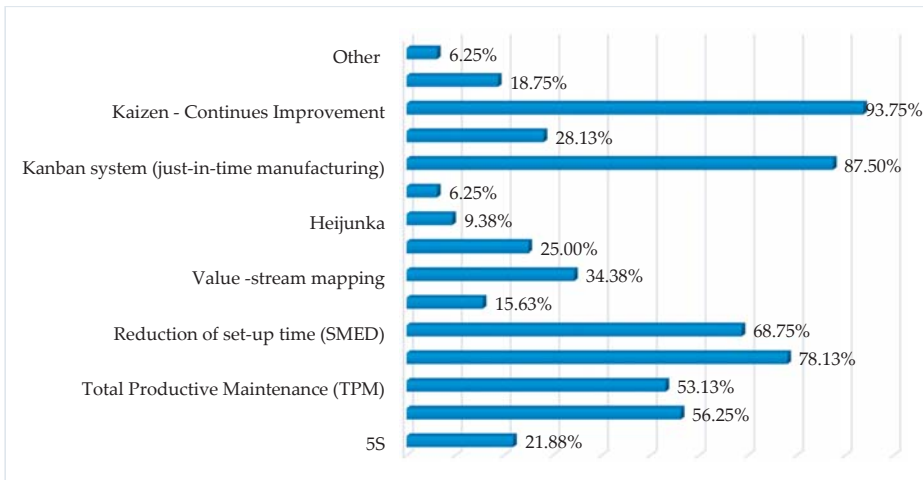


**Figure 3.** Lean tools that companies are using or have used.

For companies that use LMTs, when did they start using them? Based on the responses of 32 companies that are using LMTs, the first question was: how long the companies have been using LMTs. Below are given the choices of respondents on the questionnaire along with percentages:

- About six months ago: 3.13% (1 company),
- Between six months and a year ago: 6.25% (2 companies),
- Between a year and one and a half year ago: 12.50% (4 companies),
- Between one and a half year and two years ago: 9.38% (3 companies),
- Between two and three years ago: 25% (8 companies),
- Between three and five years ago: 21.80% (7 companies),
- More than five years ago: 21.80% (7 companies).

For companies that use them, which LMTs are helping them the most? The question was: “Which lean manufacturing techniques have helped (or are helping) you the most?”

Figure 4 presents the average of all numbers about lean manufacturing techniques that have helped the most companies in their process of production, such as money, time, number of workers, inventory, etc.

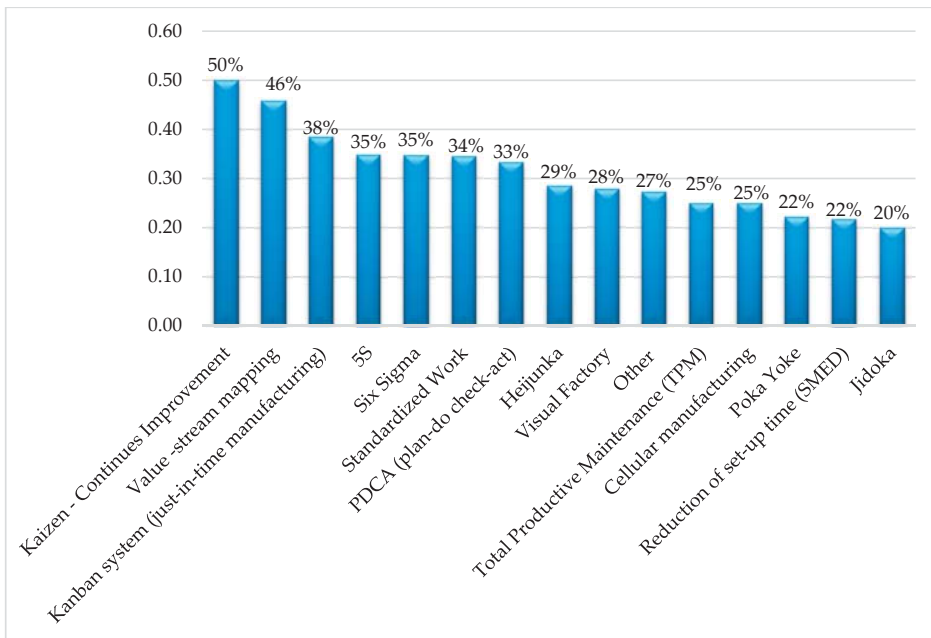


**Figure 4.** The average of all numbers about Lean Manufacturing Techniques (LMTs) that have helped the most companies.

The most helpful LMTs based on respondents are: Kaizen, value stream mapping, Kanban system, 5S, Six Sigma, standardized work, and so forth.

*Selection of Basic Lean Tools for the Development of the Kosovo Model Regard to Industry 4.0*

From a technological point of view, lean production can be regarded as a compliment to automation, some of the lean tools have more importance in those processes. Zuehlke [16] suggested that the complexity of the production system should be reduced by lean practices and stated that relying too much on technology cannot always improve the performance but may make the system

more complicated. Some research has been performed to emphasize the interaction between lean manufacturing and Industry 4.0. Models have been proposed to integrate lean manufacturing and Industry 4.0 concerning supplier, customer, and process as well as human and control factors. Veza et al. [17] carried out an analysis of global and local enterprises based on a literature review and questionnaires to develop a Croatian model of the innovative smart enterprise (HR-ISE model). In that study, a selection of six basic lean tools were made and foundations of the generic configuration of the HR-ISE model were defined.

In general, to successfully implement any management practice should often rely on organizational characteristics. Often, the most uncovered practices usually connected with lean production are: cellular manufacturing, bottleneck removal (production smoothing), continuous improvement programs, competitive benchmarking, cross-functional workforce, focused factory production, cycle time reductions, lot size reductions, just-in-time/continuous flow production, new process equipment/technologies, preventive maintenance, maintenance optimization, planning and scheduling strategies, pull system/Kanban, process capability measurements, quick changeover techniques, quality management programs, safety improvement programs, self-directed work teams, total quality management, re-engineered production process [7].

As mentioned earlier, the main reason for this investigation was to establish certain phases and steps for process and structural reorganization of Kosovo enterprises based on lean principles. Just-in-time, continuous improvement—Kaizen, flow orientation, standardized work, value stream management, pull system are the six most important lean tools for Croatian enterprises based on a synthesis of green application analysis and lean tools in Croatian enterprises [17] and application of Lean tools in 30 global enterprises [18]. Similarly, which lean tools are most used and helpful in Kosovo enterprises were investigated. From 95 enterprises, which have been analyzed, only 32 of them using lean manufacturing techniques. As is seen from Figure 4, the most used and helpful lean tools based on the response from the questionnaires are:

1. Kaizen—continuous improvement,
2. Kanban system—just-in-time,
3. Standardized work,
4. Six Sigma,
5. Total productive maintenance—TPM,
6. Value stream mapping,
7. Reduction of set-up time—SMED.

These seven lean tools are the most helpful and used in Kosovo enterprises, and represent basic tools for the Kosovo model of production system regard to Industry 4.0 and innovative smart enterprises.

## 5. Conclusions

As mentioned at the beginning, this investigation is the continuing process of our initiatives in preparation of Kosovo enterprises for the new age of industry—Industry 4.0. For that, the main purpose of this study was to select the most used and helpful lean tools. After analyses of data collected from companies, some conclusions have been drawn:

- The main reasons that companies do not use LMTs are: they are not much informed about lean manufacturing techniques (43.48% of responses), they understand lean manufacturing techniques but they are not informed how to use them (39.13% of responses), they consider that adopting lean manufacturing techniques will not be beneficial (17.39% of responses).
- The most helpful LMTs based on the response of respondents are Kaizen, value stream mapping, Kanban system, 5S, Six Sigma, standardized work.
- None of the companies has completely implemented principles, but in partial and limited level.

These facts represent the main problem in the journey of Kosovo manufacturing industries toward Industry 4.0. Industry 4.0 will not solve problems of mismanaged and weakly organized manufacturing

systems. Its tools should have been applied to lean activities that are successfully performed before automatizing. Kaizen—continuous improvement, Kanban system—just-in-time, standardized work, Six Sigma, total productive maintenance—TPM, value stream mapping, and reduction of set-up time—SMED are the most used and helpful lean principles in Kosovo enterprises based on the respondents' answers (Figures 3 and 4). These seven basic lean tools are approximately the same as lean tools in Croatia [17]; according to research there are six lean tools: just-in-time, Kaizen, flow orientation, standardized work, value stream management, and pull system.

Therefore, the selection of seven basic lean tools was made, and foundations of the generic configuration of the Kosovo model regarding industry 4.0 (innovative smart enterprise) model are defined.

## References

1. Holweg, M. The genealogy of lean production. *J. Oper. Manag.* **2007**, *25*, 420–437. [\[CrossRef\]](#)
2. Azemi, F.; Lujic, R.; Šimunović, G.; Maloku, B. Utilization and impact of ict on smes: The case study of the kosovo private sector at furniture and metalworking industry. In Proceedings of the International Multidisciplinary Scientific GeoConference Surveying Geology and Mining Ecology Management, Sofia, Bulgaria, 29 June–5 July 2017; Volume 17, pp. 751–758. [\[CrossRef\]](#)
3. Azemi, F.; Šimunović, G.; Lujic, R.; Tokody, D. Intelligent Computer-Aided resource planning and scheduling of machining operation. *Procedia Manuf.* **2019**, *32*, 331–338. [\[CrossRef\]](#)
4. Womack, J.P.; Jones, D.T.; Roos, D. The machine that changed the world. *Bus. Horiz.* **1992**, *35*, 81–82. [\[CrossRef\]](#)
5. Yingling, J.C.; Detty, R.B.; Sottile, J. Lean manufacturing principles and their applicability to the mining industry. *Miner. Resour. Eng.* **2000**, *9*, 215–238. [\[CrossRef\]](#)
6. Kumar, R.; Kumar, P.S. Strategy development for lean manufacturing implementation in a selected Manufacturing company. *Int. J. Eng. Sci.* **2014**, *3*, 51–57.
7. Shah, R.; Ward, P.T. Lean manufacturing: Context, practice bundles, and performance. *J. Oper. Manag.* **2003**, *21*, 129–149. [\[CrossRef\]](#)
8. Singh, B.; Garg, S.K.; Sharma, S.K. Lean can be a survival strategy during recessionary times. *Int. J. Product. Perform. Manag.* **2009**. [\[CrossRef\]](#)
9. Melton, T. The Benefits of Lean Manufacturing. *Chem. Eng. Res. Des.* **2005**. [\[CrossRef\]](#)
10. Morgen, J.M.; Liker, J.K. *The Toyota Product Development System*; Productivity Press: New York, NY, USA, 2006.
11. Liker, J.K.; Morgan, J.M. The toyota way in services: The case of lean product development. *Acad. Manag. Perspect.* **2006**, *20*, 5–20. [\[CrossRef\]](#)
12. Azemi, F.; Šimunović, G.; Lujic, R.; Tokody, D.; Rajnai, Z. The Use of Advanced Manufacturing Technology to Reduce Product Cost. *Acta Polytech. Hung.* **2019**, *16*, 115–131. [\[CrossRef\]](#)
13. Johansson, L. *Handbook on Green Productivity*; Azian Productivity Organization: Tokyo, Japan, 2006.
14. Chakravorty, S.S. Six Sigma programs: An implementation model. *Int. J. Prod. Econ.* **2009**. [\[CrossRef\]](#)
15. Slack, A.; Ho, S.; Forni, L.G. The management of acute renal failure. *Medicine* **2007**. [\[CrossRef\]](#)
16. Zuehlke, D. SmartFactory—Towards a factory-of-things. *Annu. Rev. Control* **2010**, *34*, 129–138. [\[CrossRef\]](#)
17. Veza, I.; Mladenio, M.; Gjeldum, N. Selection of the basic lean tools for development of Croatia model of innovative smart enterprise. *Teh. Vjesn.* **2016**, *23*, 1317–1324.
18. Netland, T.H. Exploring the phenomenon of company-specific Production Systems: One-best-way or own-best-way? *Int. J. Prod. Res.* **2012**, *54*, 1084–1097. [\[CrossRef\]](#)

**Publisher's Note:** MDPI stays neutral with regard to jurisdictional claims in published maps and institutional affiliations.



© 2020 by the authors. Licensee MDPI, Basel, Switzerland. This article is an open access article distributed under the terms and conditions of the Creative Commons Attribution (CC BY) license (<http://creativecommons.org/licenses/by/4.0/>).

# The Importance of Corporate Social Responsibility among Students in EUROPE †

Mihaela Bucur 

Department of Industrial Engineering and Management, “George Emil Palade” University of Medicine, Pharmacy, Science and Technology of Târgu Mureș, 540142 Târgu Mureș, Romania; mihaela.bucur@umfst.ro; Tel.: +40-074-239-4396

† Earlier versions of this paper have been presented at the research workshops “Islamist Armed Conflicts and the Prospects for Conflict Resolution,” 28–30 September 2018, Schwarzenberg, Switzerland, and “Sunni–Shia Relations in Europe: How to Study Them?”, 13–14 December 2018, Turku, Finland.

Published: 26 January 2021

**Abstract:** This document addresses the issue of awareness and involvement in Corporate Social Responsibility (CSR) by students from all over Europe. The purpose of the document is to investigate the involvement and the knowledge of students in Social Responsibility and to obtain results that can confirm or invalidate the proposed hypotheses, presenting a real situation regarding their involvement. Social responsibility has a major impact on communities, and awareness of this concept is needed for involvement in CSR actions. The aim of the research is to study the knowledge and development of Corporate Social Responsibility (CSR) in Europe.

**Keywords:** CSR; students; initiatives; knowledge; CSR benefits

## 1. Introduction

The concept of CSR has been debated in several contexts [1,2]. The following definitions are to be retained:

- CSR is the concept through which organizations integrate social and environmental concerns into their business operations and interact with stakeholders on a voluntary basis (European Commission, 2001);
- CSR is “the process by which managers within an organization think about and discuss relationships with stakeholders as well as their roles in relation to the common good, along with their behavioral disposition with regard to the fulfillment and achievement of these roles and relationships” [3].

Most studies in this field have identified a relationship between CSR activities and the benefits to their organization [4,5]. Whether we are talking about reducing direct costs, increasing labor productivity, applying risk management, image enhancement, or improving environmental management [6], the importance and application of the concept of CSR in the strategy and activities of any type of organization are indisputable.

The quest of this subject in Romania started shyly but in the course of time attracted some followers. Lungu et al. (2009) [7] integrated the studies on social and environmental reporting in Europe and worldwide and the financial reporting experience in this area, Șendroiou et al. referred to EMA principles in Romanian entities, Crisan-Mitra analyzes the context in which companies in Romania should use CSR practices [3]. There are also more concrete pieces of research regarding the involvement of CSR in the profession of accountants [6], Kork M. studies whether the concept of CSR is transposed from theory to practice [2,8] and even aspects related to public relations as a component of public [6].

The results of the Romanian research show that an integrated approach of corporate reports is needed as the CSR trends are set by the big companies. In this context, we believe that in order to change

things for the better, little initiatives, organizational awareness, insistence from the stakeholders are needed. This study considers that it was an awareness first and then an empirical analysis, its results have a number of conclusions and recommendations about that society is becoming more involved in more branches and fields. In 2007, a survey was carried out by the Forum for International Communications through its CSR Romania program on a sample of 250 corporations active in the Romanian business environment [7], followed by research in the field of CSR communication, [8] conducted a survey between 2006 and 2008 focused on the evolution and the quality of the environmental reports from the Romanian companies listed on the Bucharest Stock Exchange. The research was resumed to cover 46 companies with an environmental impact.

Corporate Social Responsibility (CSR) is a useful tool for any organization that wants to be renowned. Even if it is not a mandatory mechanism, ignorance of this concept and its neglect may have effects on the image and implementation of future strategies of any type of organization. Through this article, the authors emphasize the Romanian context in which companies need to implement and develop CSR practices, with empirical qualitative research based on questionnaires. The research tool used is a questionnaire drafted by the authors and the respondents were the representatives of the most important companies in the technical and industrial field present at the face-to-face event with the employers organized by the Association of ESTIEM Mures and the Faculty of Engineering of "George Emil Palade" University of Medicine, Pharmacy, Science and Technology of Târgu Mureș, Romania. The ongoing research provides a detailed picture not only of the perception of CSR but also of the reasons that have led companies to invest in CSR.

## 2. Materials and Methods

The parameters of the study consisted of:

- Target group: students and graduates of the ESTIEM network, from all over Europe;
- Sample: 59 samples;
- Sample type: ad-hoc sampling (probability);
- Data collection for the CSR study took place in March 2020.

The objectives of this study are closely related to the importance of the concept of CSR. Social responsibility has a major impact on communities, hence the awareness of the need to get involved in CSR actions. The aim of the research is to study the knowledge and development of Corporate Social Responsibility (CSR) in Europe. Among the objectives set by the research, we highlight four that are directly related to this paper: determining the level of knowledge on the concept of CSR, identifying ways to involve and organize CSR activities, implementation of CSR strategy, and implementation of CSR initiatives within organizations in the area of each respondent.

The questionnaire is based on the knowledge of the concept of Social Responsibility, which aims to identify the involvement of respondents in activities carried out by companies across Europe, the initiatives most often encountered in the communities they belong to, and the identification of reasons why participants were not involved in such activities. Depending on the purpose of the research and the literature, the structure of the CSR questionnaire was developed to verify the following hypotheses:

**Hypothesis 1.** *People with university studies know the concept of CSR, they have contact with this concept through non-governmental organizations present in universities.*

Figure 1a,b refer to questions 3 and 4, show that 49 of the participants completing this questionnaire have university degrees, they are aware of the existence of this concept in a proportion of 62.7%. A fairly large number, 37.3%, are not familiar with this concept, which demonstrates that society needs to be more involved in such activities. Thus, Hypothesis 1 is confirmed.

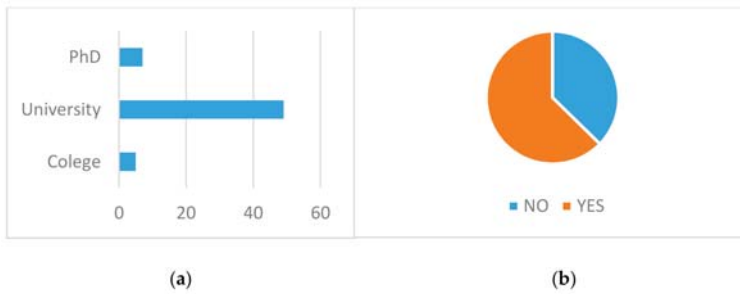


Figure 1. (a) Level of education of respondents; (b) Did you hear about CSR?

**Hypothesis 2.** *The concept of CSR is often encountered in companies.*

Figure 2 is representative of question number 5, which refers to where this concept of CSR is often encountered. As we can see from the chart above, the participants in this study consider that this concept is often found in companies, in a percentage of over 50%, and less common in NGOs, a percentage of 20%. Hypothesis 2 is confirmed.

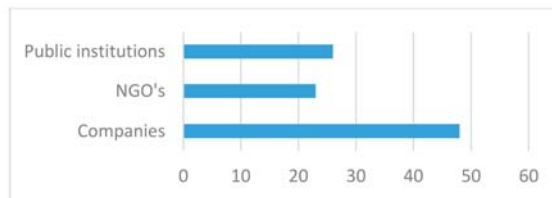


Figure 2. Where you can find this topic applied?

**Hypothesis 3.** *The field of involvement of companies in CSR projects is mainly for activities that cover initiatives towards the local community, environment, and business ethics.*

Figure 3 refers to question number 6, a question related to the initiatives that are most often applied/encountered in the country of which the respondents are part. The average of the answers is quite balanced, the first three positions being environmental protection, business ethics, and initiatives towards the local community. The hypothesis is confirmed.

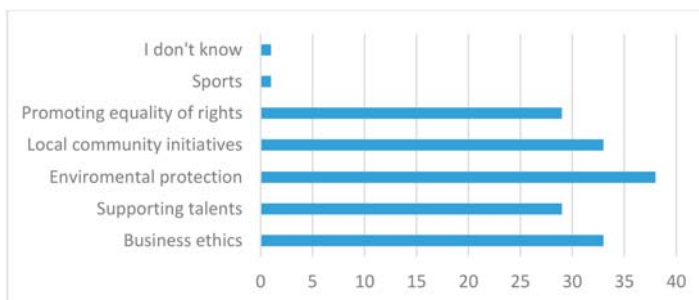
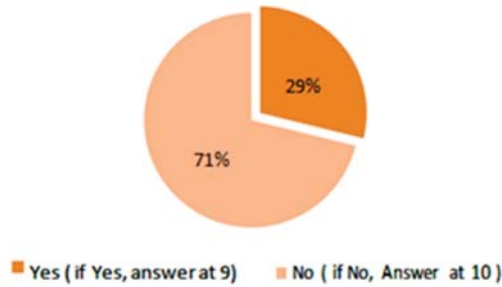


Figure 3. Which of these initiatives are usually applied in your country?



**Hypothesis 4.** *Universities and organizations support the involvement of students in CSR programs; therefore they are familiar with the concept of CSR.*

Figure 4, refers to question number 8, a question related to the involvement and participation of respondents in CSR actions. It can be seen that a very large number of them did not participate in such activities at 71%. Only 29% were involved in CSR actions. The hypothesis is not confirmed.



**Figure 4.** Have you ever participated in social responsibility actions?

**Hypothesis 5.** *The reason for students' non-involvement is related to the fact that they were not given the opportunity to be part of such projects.*

Figure 5 shows the reasons why the participants were not part of CSR projects (question number 10). The most common reason is related to the fact that they were not offered this opportunity, which shows the lack of presentation and introduction of several CSR projects. The hypothesis is confirmed.

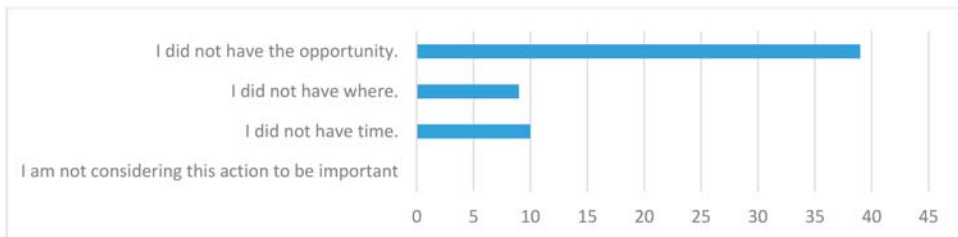


**Figure 5.** Specify your reasons for not being involved in CSR actions.

**Hypothesis 6.** *Social responsibility is practiced following the emergence of legal provisions.*

A relevant question in this study is to find out the reason for the involvement of companies in such actions. Why do participants believe organizations participate in such actions? The results highlight an interesting situation, following the data in Figure 6—most respondents believe that this involvement is due to the company's need to protect its reputation, followed by the option legal provisions. These two reasons are followed to a lesser extent by reasons such as investor relations, pressure from NGOs. It can be seen that these implications are due to the desire to increase the image by remedying certain problems. Pressure from local communities, customers and suppliers ranks last in this survey. The hypothesis is confirmed.

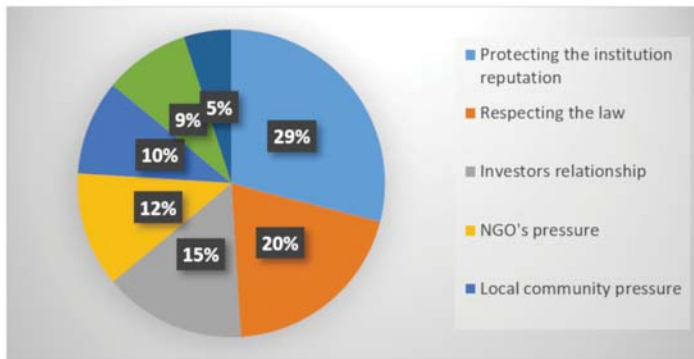


Figure 6. Which are the main actions in case your organization is using CSR practices?

**Hypothesis 7.** *The type of program/cause supported by most companies should be related to the predominant problem in each country.*

One last question refers to a more sensitive point, the situations in which these projects offer a chance and hope to only certain categories of people (Figure 7). The chart above reflects the need to involve people in CSR projects, in situations where people suffer from certain incurable diseases, or in situations where people are victims of sexual exploitation, homeless people, and people subjected to domestic violence. The hypothesis is confirmed.

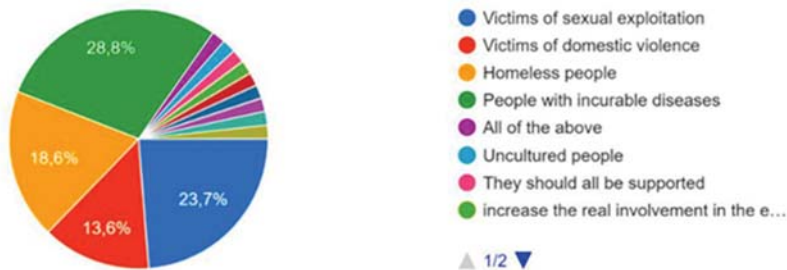


Figure 7. Which causes should be supported by companies from your country?

### 3. Conclusions

Following the interpretation of the study, it can be seen that the field of corporate social responsibility in Europe is an area that is taking shape and is constantly evolving. The respondents included in the study have general/minimal knowledge and notions on what this field entails and are eager to be involved in CSR activities.

The study shows that society is becoming more and more involved in more branches and fields, which is a very positive thing, and we tend to believe in continuous growth in the coming years.

Respondents believe that lately, companies are trying to create and maintain a pleasant image among society through CSR actions. The main purpose of the private sector is to generate profit and value. Through such activities, the private sector contributes to economic growth and social development. In the long run, it is in the interest of both society and companies to have a private sector that works responsibly and develops products and services that help solve social and environmental problems. Practicing the concept of Social Responsibility brings added value to organizations due to the easier implementation of legal provisions and the betterment of the company's image in the community, NGOs, and other stakeholders.

**Funding:** This research was funded by the University of Medicine, Pharmacy, Science and Technology “George Emil Palade” of Târgu Mureş Research Grant number 293/1/2020.

## References

1. Boubakary, A.; Moskolai, D.D. The influence of the implementation of CSR on business strategy: An empirical approach based on Cameroonian enterprises. *Arab Econ. Bus. J.* **2016**, *11*, 162–171. [CrossRef]
2. Michelon, G.; Pilonato, S.; Ricceri, F. CSR reporting practices and the quality of disclosure: An empirical analysis. *Crit. Perspect. Account.* **2015**, *33*, 59–78. [CrossRef]
3. Bucur, M. A study on business communication on Corporate Social Responsibility in Romania. *Procedia Technol.* **2015**, *19*, 996–1003.
4. Ban, A.; Bucur, M. What Does Engineering Ethics Involve? *Sci. Bull.* **2018**, *15*, 31–35.
5. Bucur, M.; Moica, S.; Ardelean, F.; Oțel, C.C. The importance of Corporate Social Responsibility among organizations in the Centre Development Region of Romania. *Procedia Manuf.* **2019**, *32*, 309–317. [CrossRef]
6. Fifka, M.S.; Kühn, A.-L.; Stiglbauer, M. One size fits all? Convergence in international corporate social responsibility communication-A comparative study of CSR mission statements in the United States and India. *J. Public Aff.* **2017**, *18*, e1670. [CrossRef]
7. Lungu, C.I.; Caraiani, C.; Dascălu, C. Corporate Social Responsibility Research on Corporate Social Responsibility Reporting. *Amfiteatru Econ. J.* **2011**, *29*, 117–131.
8. Bucur, M. The CSR implementation. *Sci. Bull.* **2013**, *10*, 70–74.

**Publisher’s Note:** MDPI stays neutral with regard to jurisdictional claims in published maps and institutional affiliations.



© 2021 by the author. Licensee MDPI, Basel, Switzerland. This article is an open access article distributed under the terms and conditions of the Creative Commons Attribution (CC BY) license (<http://creativecommons.org/licenses/by/4.0/>).

# Research on Qualified Vocational Training Development in the Context of Digitalization <sup>†</sup>

Marius Miklos Veres <sup>1,\*</sup>, Cristina Veres <sup>2</sup>, Antoaneta Maria Rauca <sup>1</sup>, Liviu Onoriu Marian <sup>1</sup> and Ancuta Sigmirean <sup>1</sup>

<sup>1</sup> Department of Management and Economic Engineering, Technical University of Cluj-Napoca, 400114 Cluj-Napoca, Romania; tonia\_0204@yahoo.com (A.M.R.); liviu.marian@yahoo.com (L.O.M.); ancuta\_sigmirean@yahoo.com (A.S.)

<sup>2</sup> Department of Industrial Engineering and Management, University of Medicine, Pharmacy, Science and Technology of Tirgu Mures, 540142 Tirgu-Mures, Romania; harea.cristina@yahoo.com

\* Correspondence: mariusveres@yahoo.com

<sup>†</sup> Presented at the 14th International Conference INTER-ENG 2020 Interdisciplinarity in Engineering, Mures, Romania, 8–9 October 2020.

Published: 21 January 2021

**Abstract:** From a strategic point of view digitalizing the economy in the near future means that it's necessary, from now on, to change the focus on digital skills because at the moment almost all jobs require some level of digital knowledge from employees. Although digitalization brings a lot of advantages, the vocational education and training cannot be entirely digitalized as qualified vocational development has to maintain its traditional approach in order remain efficient and most importantly attractive. This paper describes the results of a focus group conducted in Mures County, Romania on the topic of digitalization with the aim to offer an overview image on vocational education and training challenges in the current context.

**Keywords:** challenges; digitalization; training development; vocational education and training

## 1. Introduction

Digitalization is a hot topic in the context of the current pandemic, we are at the dawn of the digital age in which the fundamental systems of society are changing radically in a fast time. Digitalizing the economy in the near future means that from a strategic point of view it is necessary, from now on, to change the focus on digital skills because at the moment almost all jobs require some level of digital knowledge from employees. Moreover, the human resource will have to be trained in such a way that it can collaborate with robots and artificial intelligence. Moving the focus is a challenge of great importance and immediate relevance. The transformation of the economic system will be complex, so the appropriate adaptation of the qualified vocational training system to the new conditions will be essential.

The fourth industrial revolution represents the reorganization of society, more precisely a superior collaboration between humanity and digital technologies that will lead to a superior dynamic of organizations in general. This dynamic can be characterized by flexibility, reaction speed, infinite analysis and simulations, intelligent decisions, control.

It is therefore clear that the labour market is already feeling the wind of change, a change brought about by rapid technological innovations, on the one hand, and by human resources, the development and training of which is required to be much more dynamic, on the other. The level of expectations regarding the skills and individual values of employees will increase. Currently, the challenges of combining these two factors of change are very significant. The transformation of the economic system

will be complex, so the appropriate adaptation of the qualified vocational training system to the new conditions will be essential.

This article aims to highlight the strategic importance of digitalization in professional development, the challenges posed by it but also its limitations, offering an overview image on vocational education and training challenges in the current context.

## 2. Digitalization: Factors, Challenges and Limitations

Digital age learning represents a series of concerns which have to be addressed by policymakers, who attempt to plan education and training in such a way as to improve competences imperative for employment, personal development or social inclusion. *“A new skills agenda for Europe”* emphasized the difficulties of the employers in hiring skilled people with an appropriate level of digital competences, entrepreneurial and innovative capabilities. Almost 40% of European enterprises are facing a shortage of highly skilled personnel able to use digital technologies in the context of globalized economy.

The European Commission with its multi annual plan named *“A new skills agenda for Europe”* predicts a change of paradigm as skill needs will vary across different sectors of the economy which emerge or radically change as a result of technological developments. The just-in-time supply of the right skills will empower competitiveness and innovation. Investments will also utterly depend on the availability of high-end skills [1].

The accessibility of the digital technologies is the key to reduce the learning gap between education and the challenges of a dynamic and interconnected world. *“The Digital Education Action Plan”* underlines that digital innovation in education systems will improve the quality of education systems. The education must use more efficiently the digital technology for teaching and learning, to develop digital skills and competences relevant for the digital transformation of Europe, and to improve education [2].

More than ever people started to realize that digitalization is a solution and even though statistics show that the degree of digital literacy is very low in Romania, the adaptability and the employability provided by digital skills and competences in general should ensure that extra motivation from all beneficiary to work harder to overcome this drawback. Nevertheless, the digitalization projects and qualified vocational training systems must consider the digital literacy of our country to produce long-term change. Digital solution can only work if the systems that we have in operation make them functional. Without strong training systems we will not be able to achieve superior sustainable performance. No solution will work unless run in a suitable environment. The economic environment imposes new and updated requirements, norms, rigors and standards, therefore close collaboration and immediate communication between economic and educational organizations is imperative in order to upgrade the vocational training system so that it can meet the challenges.

In the short term, the field of health and education are a priority for digitalization, so the reaction speed of the institutions involved will be essential. Human resource skills and digital infrastructure are key factors in implementing digitalization. Digitalization ensures adaptability and employability for the masses. Digitalization is a huge opportunity for all value-producing areas, but this opportunity can only be exploited through the early implementation of comprehensive, long-term strategies and programs that focus on training the professional skills of human resources, that is, adapting them to new requirements.

The adoption of technologies has not led to the abolition of jobs but has created new opportunities that have harnessed creativity and human potential in a more satisfying and motivating way. The new hybrid skills not only capitalize on technology but combine it with the human dimension. The result is a new type of contribution, responsibility and leadership [3].

In this time of crisis some institutions have completely cut off budgets destined for education and training, including the digital one; however, it's obvious that the economy resets and as a result there will be many professional reconversions in the next period with an emphasis on digital skills and competences.

Vocational education and training need to be heavily funded through investment programs where all stakeholders must assume part of the financing. In this regard, effective co-financing system for these programs must be implemented, the lack of such systems may lead to major dysfunctions in their activity. Qualified vocational training infrastructure is deficient, but positive steps can be made. The stakeholders should develop regional or local heavily digitalized technologic workshops in which the professional training of the human resource is based on hybrid methodology and where the digital and the hands-on approach are harmoniously combined. In these smart centres various activities such as collaboration with robots, 3D technologies or virtual reality must be applicable.

A strong political signal, an ambitious answer and financial impulse materialized through a major recovery plan called “Europe’s moment: Repair and Prepare for the Next Generation”. European Commission President Ursula von der Leyen said that this crisis represents a good opportunity to invest in Europe’s future, also emphasizing that the European Green Deal and digitalization will boost jobs and growth [4].

Funds will be channelled through various EU Programmes like A Skills Agenda for Europe and A Digital Education Action Plan, which will ensure digital skills for E.U citizens.

Because this is a new, recently introduced field, digitalization has its limitations and challenges; we need to clarify its operating principles so that we can take full advantage of its advantages and potential. Vocational training institutions, including Romanian ones, are still failing to sufficiently prepare human resources for this new industrial revolution, also called digitalization, and companies are failing to take full advantage of the benefits that digitalization can generate. The reasons for this situation are many, but the most important factor that generates this desolate situation is that no one fully understands what skills and abilities ensure success in an era that is expected to be dominated by digital technologies and artificial intelligence.

Although digitalization brings a lot of advantages, the vocational education and training cannot be entirely digitalized as qualified vocational development has to maintain its traditional approach in order remain efficient and attractive. Vocational training must remain a hands-on experience otherwise it risks becoming abstract and distant, and the pleasure for learning will be partially lost. Physical contact and social interaction strengthen working relationships, help people learn from one another by sharing experience and knowledge which helps the company to progress. These aspects cannot be achieved in a digital environment [5].

Researchers have concluded that human labour, even after the introduction of digitalization, is better suited to perform certain processes and are more qualified to make certain decisions than the cyber system [6,7]. It is important to exploit the potential of digitalization, but it must only be introduced with and through people, as people must take full responsibility for, manage and supervise the machines.

There is a great fervour in discussing digitalization, especially in the current context. The pandemic initiated an extensive and dramatic digital transformation in the society, forcing a digital leap in our everyday life, business and education [8].

There is a sophistication and coolness about it. We believe that things must be seen separately, there are situations in which technology helps a lot, as detailed above, but when we talk about virtual education and training done via Zoom or similar platforms, all this communication between teacher and student is completely broken. Many public figures argued against distance learning and training. Even though the technical conditions are met, the act of training and education is badly altered. That non-verbal language matters a lot. No technology can replace interpersonal relationships yet. Moreover, there is a solemnity of the act of education that cannot be preserved through digitalization and has an extremely important role in the process itself, in the trust that students have in the teachers and trainers. The whole process can turn into a cold and impersonal act. It is therefore impossible to give up the classic approach, but many educational activities can be performed via digitalization. Digital technology is clearly helping the process of education; therefore, it has to remain a complementary component of the educational and training system, not an alternative.

### 3. Focus Group on the Digitalization of Qualified Vocational Training

Due to the current situation, which is characterized by limitations, the research process had to be adapted to actual conditions. The research methodology included a focus group on the digitalization of qualified vocational training, a focus group which eventually took place following all the rules of social distancing.

A focus group a discussion between people from similar backgrounds or experiences where they discuss a specific topic. It is a qualitative research where people are asked about their beliefs, opinion or ideas [9]. A focus group is a group of six to ten people led through by a skilled moderator. The group needs to be large enough to generate rich discussion but not so large that some participants are left out.

This focus group consisted of six professionals and a moderator who conducted the focus group. The participant were all teachers, from various technological high schools, amongst them: 3 headmasters, 1 teacher—senior member of the National Corps of Experts in Educational Management, and 2 engineers—one is the head of the engineering department and the other one is the coordinator of continuous training programs in one of the schools.

Obviously, all the participants were asked to share their opinion and ideas on the digitalization of qualified vocational training. The main question was related to how they see the development of education and vocational training in the context of digitalization. Participants shared their opinions, experience and challenges. A resume of the main expressed views is reported below:

- P1 “As a manager and engineer, I cannot help but consider digitalization to be essential in the development of education and training. The supply of vocational education in the 21st century must be based, to a greater extent, on the digital aspect. We want to become a regional technology center and one of the best ways is to exploit the potential of digitalization.”
- P2 “The digitalization of education seems to be a priority currently at EU level and I hope that we can take advantage of this wave of enthusiasm and attract important funds for the development of vocational education in Romania, education whose potential is far from being reached.”
- P3 “We are in the era of capitalism, so the economic environment dictates the necessary skills and competencies. We, the ones involved in the education system, need to create educational offers and programs in which the skills and competencies pursued, including digital ones, comply with the requirements. Cooperation with companies will be the new normal (it must be) because it is the most efficient way to keep up with rapid technological changes. This leads to the development of vocational education and training.”
- P4 “Our education system must develop and support the development of new educational programs better anchored to the reality of this era. The development of education and training must be enhanced by massive investments by the authorities, including in digitalization.”
- P5 “Digitalization is a very important issue in education and training because digitalization is synonymous with technology; the potential is enormous, but it depends a lot on future investments.”
- P6 “Training programs are about constant personal development. Moreover, we live in times when we must reinvent ourselves professionally. Digitization is the key that will help us become more efficient in the training process of the new generations.”

Other questions were discussed as well, all related to the main theme of digitalization. As a result of the discussion, the group reached a general consensus about the main aspects, pros and cons related to this consistent challenge named digitalization.

When speaking about challenges, the general agreement was that the vocational education and training cannot be entirely digitalized as qualified vocational development has to maintain its traditional approach in order remain attractive. The labour market dictates the implementation of skills and competences through different study programs, however, the accreditations of new educational programs cost money. Co-financing of new specializations must be done with the help of interested companies. Subsidizing participating companies by the state is essential, imperative. The local



companies are not interested in sustaining entire programs, unless motivated by the authorities. Efficiency is one of the big pros regarding digitalization, still, financing the rapid technological changes remains a big issue.

This study is one of the first conducted in Mureş County, Romania, on the topic of digitization. We would like to thank all the participants for their professionalism and dedication.

#### 4. Conclusions

In a such a dynamic economy, given the fact that the European Union wants to remain a sustainable and performant economy, vocational education and training must develop the skills and competences needed and demanded by the labour market. That is why vocational education and training, alongside the economy, have to become smart. Once the various economic sectors are updated from the technological point of view, the technological education must follow. A synergy has to be developed between the two. The major challenge of digitalization remains its cost and its constant need of updating. Also, at the moment, the technological gap between various economic sectors and the vocational education and training is vast.

Digitalization brings a series of advantages, making work easier, propelling technological improvement and innovation. The way we'll manage the future challenges may help us maintain the social and technological advantages. The appropriate adaptation of the qualified vocational training system to the new conditions is and will be essential in order to assure the trainee's employability and adaptability, qualities which are the most needed today and tomorrow. Sustainable development of a sector means not only considering the benefits but also the people, life and nature. Based on these aspects is appropriate to build various types of programs, including educational programs.

**Author Contributions:** M.M.V. enriched the article with bibliographical references. C.V. facilitated the writing of this research and approved some technical details, contributing with valuable input and ideas L.O.M. guided the research and approved the methodology. A.M.R. and A.S. organized the focus group while M.M.V. conducted the focus group and summarized the results. All authors have read and agreed to the published version of the manuscript.

**Funding:** This research received no external funding.

**Conflicts of Interest:** The authors declare no conflict of interest.

#### References

1. European Commission. A New Skills Agenda for Europe. Working Together to Strengthen Human Capital, Employability and Competitiveness. 2016. Available online: <https://ec.europa.eu/transparency/regdoc/rep/1/2016/EN/1-2016-381-EN-F1-1.PDF> (accessed on 9 August 2020).
2. Fleaca, E.; Stanciu, D.R. Digital-age Learning and Business Engineering Education—A Pilot Study on Students' E-skills. *Procedia Manuf.* **2019**, *32*, 1051–1057. [CrossRef]
3. ZF Corporate.ro. Available online: <https://www.zfcorporate.ro/business-legal/alexandru-reff-deloitte-modul-digital-de-lucru-nu-presupune-doar-adoptia-tehnologiilor-ci-presupune-noi-modele-de-business-18930533> (accessed on 9 August 2020).
4. European Commission. Available online: [https://ec.europa.eu/commission/presscorner/detail/en/ip\\_20\\_940](https://ec.europa.eu/commission/presscorner/detail/en/ip_20_940) (accessed on 14 August 2020).
5. ZF Corporate.ro. Available online: <https://www.zfcorporate.ro/mediafax-ro/economic/studiu-lucrand-acasa-angajatii-simt-lipsa-interactiunii-sociale-si-a-19169382> (accessed on 14 August 2020).
6. Prinz, C.; Kreggenfeld, N.; Kuhlenkötter, B. Lean meets Industrie 4.0—A practical approach to interlink the method world and cyber-physical world. *Procedia Manuf.* **2018**, *23*, 21–26. [CrossRef]
7. Windelband, L. Zukunft der Facharbeit im Zeitalter "Industrie 4.0". *JOTED* **2014**, *2*, 138–160.
8. Iivari, N.; Sharma, S.; Ventä-Olkkonen, L. Digital transformation of everyday life—How COVID-19 pandemic transformed the basic education of the young generation and why information management research should care? *IJIM* **2020**, *55*, 102183. [CrossRef]



9. Herd Organization. Available online: [https://www.herd.org.np/uploads/frontend/Publications/PublicationsAttachments/1485497050-Focus%20Group%20Discussion\\_0.pdf](https://www.herd.org.np/uploads/frontend/Publications/PublicationsAttachments/1485497050-Focus%20Group%20Discussion_0.pdf) (accessed on 30 August 2020).

**Publisher's Note:** MDPI stays neutral with regard to jurisdictional claims in published maps and institutional affiliations.



© 2021 by the authors. Licensee MDPI, Basel, Switzerland. This article is an open access article distributed under the terms and conditions of the Creative Commons Attribution (CC BY) license (<http://creativecommons.org/licenses/by/4.0/>).

# Anonymous Detection of Traveler Flows Employing Bluetooth Technologies <sup>†</sup>

Ionuț-Cosmin Chiva <sup>1,\*</sup>, Marius Minea <sup>1</sup>, Viviana-Laetitia Minea <sup>2</sup> and Augustin Semenescu <sup>3</sup>

<sup>1</sup> Telematics and Electronics for Transports, Faculty of Transports, University POLITEHNICA of Bucharest, 060042 Bucharest, Romania; marius.minea@upb.ro

<sup>2</sup> ORANGE S.A. Romania, 020334 Bucharest, Romania; viviana.minea@orange.com

<sup>3</sup> Engineering and Management of Metallic Materials, Faculty of Material Science and Engineering, University POLITEHNICA of Bucharest, Academy of Romanian Scientists, 060042 Bucharest, Romania; augustin.semenescu@upb.ro

\* Correspondence: ionut\_cosmin.chiva@upb.ro

<sup>†</sup> Presented at the 14th International Conference INTER-ENG 2020 Interdisciplinarity in Engineering, Mureș, Romania, 8–9 October 2020.

Published: 31 December 2020

**Abstract:** Intensive usage of public transportation represents a good solution to reduce traffic congestion. Dynamic allocation of vehicles enhances the service level and offers a more comfortable trip to travelers. Bluetooth (BT) has been used in some specific cases as a means of data collection regarding vehicle flow. However, it has been less employed for the anonymous detection of traveler flow, origin–destination, the density of travelers in public transport, etc. This paper analyzes the efficiency of different versions of BT for this type of application. Experiments were carried on for subway lines and stations, as well as in open space. Information regarding mobility dynamics represents an important factor to be considered in traffic management to improve the efficiency of existing systems. Conclusions and recommendations for future research are also provided.

**Keywords:** Bluetooth; anonymous detection; latency; robustness of communication; throughput

## 1. Introduction

Bluetooth (BT) version 5.0, issued approximately six years after the development of the BT 4.0 standard, allows for enhancements in short-range communications, with the perspective for inclusion in the deployment of the Internet of Things (IoT). This technology is one of the main pillars in IoT, including the transport domain. The medium access technique is frequency hopping, and BT promises the possibilities of anonymously detecting mobile carriers with such devices, helping in building intelligent transportation systems (ITS). A more efficient method to detect traffic flows is the usage of BT technology in terms of energy consumption reduction. The approach has been successfully applied in normal vehicle traffic measurements at surface road infrastructure but is less implemented in subway transportation. The proposed method is based on anonymous detection of BT/Wi-Fi devices carried by subway travelers. The method presents its advantages, as the infrastructure does not need expensive and hard to maintain dedicated sensors. Collecting relevant information about traveler flow may help information and public transport management systems better administer vehicle fleets, and guidance to relevant destinations, etc. The drawback of the methodology is that only a fraction of the real traveler flow is measurable since not all people may carry detectable BT/Wi-Fi devices. Installing BT/Wi-Fi sensors in specific station locations or in the subway wagons, an image of travelers' origin–destination (OD) flow, based on BT/Wi-Fi MACs detection, time stamping, and location, can also be built. It may be the goal of public transport administrations to obtain large amounts of data (spatiotemporal flow of travelers) without installing costly, physically invasive infrastructure of dedicated sensors. Moreover,

for surface public transport, the development of the proposed solution is also possible with a proper installation of BT/Wi-Fi detector configurations in buses or bus stops, and a similar image of passenger movements can be determined. The collected data can be useful in the dynamic distribution of public transport vehicles on the route (traveler demand-responsive public transportation). In the context of global warming and the increase in emissions, improving the attractiveness of public transportation represents a simple solution to greener cities worldwide.

## 2. Related Work

### 2.1. Employment of Indirect Measurement Techniques in Traffic and Traveler Detection

More recent advances in traffic and traveler detection employ indirect (anonymous) measurement techniques, which have the advantage of reduced infrastructure equipment over traditional implementations [1], such as the deployment of dedicated sensors in the field. Frequently, techniques, such as Floating Car Data (FCD) and Floating Car Observer (FCO), are employed to collect data from traffic and passenger flow. Some of these procedures use indirect detection of traffic elements (BT/Wi-Fi devices detection). The authors of [1] explained the BT technology particularities and concluded that even if two BT devices were used together for the inquiry process in a floating car data collection system, 1.919 s are needed for the complete inquiry in the worst case, which is 1.27 s (inquiry scan idle time) + 0.64 s (maximum back off time). This means that any BT device which is not in the cloaked mode can be identified, if in range. The authors of [2] also stated that for the detection of a mobile-carried BT device, two BT sensors are needed at both ends of the road segment. Since all travel time data collection methods do sampling on the travel time of individual travelers, it is important to determine the minimum appropriate sample size to have accurate traveler flow information. Some studies conclude that the minimum percentage of sampling rate should be about 5%. Another problem that will be addressed in this paper is the influence of the technology over measurement accuracy (e.g., BT version 5 over BT versions 4.x).

In paper [3], the authors compared BT versions and concluded that BT5 seems to offer significant performance improvements compared to the previous versions of BT in terms of speed, range, and broadcasting capacity. The authors of [4] evaluated BT and Wi-Fi technologies for scanning in road transportation. They noted that the usage of mobile-equipped BT devices was increasing with the improved availability of these and recommend employing Bluetooth Media Access Control Scanners (BMS) for traffic data collection. The authors also mention some disadvantages, e.g., the possibility of multiple detections of the same device in the range of a single detector (positive false) and the lower chance of detection for fast-moving BT nodes (negative false). In [5], Juan José Vinagre Díaz et al. performed a detailed analysis of the capabilities of Bluetooth technology for travel time estimation. For pedestrian detection at public transportation terminals, N. Shlayan et al. [6] looked for stochastic models specific to pedestrian movements within the experiments of traveler detection employing an in-house combined BT/Wi-Fi data collection methodology and system. They also proposed using anonymous and encrypted BT and Wi-Fi data obtained from the users of a pedestrian network to make real-time decisions. Other authors [7] explored technology-merging techniques to improve vehicle detection. The authors of [7] used BT detection and inductive loop sensors to improve data accuracy, and F. Mannering and D. Bullock [8] performed an analysis of freeway travel time variability using Bluetooth detection.

The authors of [9] tested the effect of the BT connection interval on the throughput and compared power efficiency relating to throughput for various BLE (Bluetooth Low Energy) versions and different transactions. They found that lowering channel interference (CI) will increase throughput for reads and writes, which is not the case for notifications and writes without response. Another finding was that energy consumption reduces with each newer BLE version.

### 2.2. Expected Improvements in BT 5.0 over BT 4.x and Threats of BT Communications

As specified by standards, BT 5.0 technology delivers better communication quality and experience, compared with its older versions. BT 5.0 continues the Low Energy version of BT 4.x, with speeds around 2 Mbps, communication distances up to 300 m, in the ISM band (industrial, scientific, and medical radio band) of 2.4–2.485 GHz. Version 5.0 also requires less energy than previous versions, thus increasing the battery usage of mobile devices, and the message capacity is around 255 bytes. Bluetooth 5.0 hardware is fully backward compatible with Bluetooth 4.2. Concerning the security of communication, BT 5.0 suffers from disadvantages specific to radio communications, including waves absorption, multiple reflections, multiple path propagation, interference, etc. However, as in many communication networks, one should not forget the potential for hacking the network, which may include bluejacking, bluebugging, bluesnarfing, bluesniping, or car whisperer, a technique for car handsfree devices attack. Considering the above, it was considered useful to test the capabilities of the two BT versions in real life, in similar conditions, with the target for future usage in transport and travel information systems, public transport management systems, and traveler on route guidance. With the expected increase in BT usage in the near future, this form of collecting information regarding traveler and passenger flow might be a promising technology for reducing sensor network complexity, energy consumption, and influence on the environment.

### 3. Concept of the System and Test Bed

#### 3.1. Concept of the System

The proposed solution tries to improve the public transport attractiveness by better satisfying the traveler demand, i.e., by dynamically allocating subway trains according to the transport demand. It may also help in determining the actual density of travelers per vehicle, line, or period of the day. Another benefit of anonymously collecting the presence and origin–destination information of travelers is that the information systems may also include route guidance in subway stations, better distribution of travelers in wagons of subways for reducing agglomeration and delay in stations, etc. The proposed configuration of the system architecture for a generic subway station is presented in Figure 1.

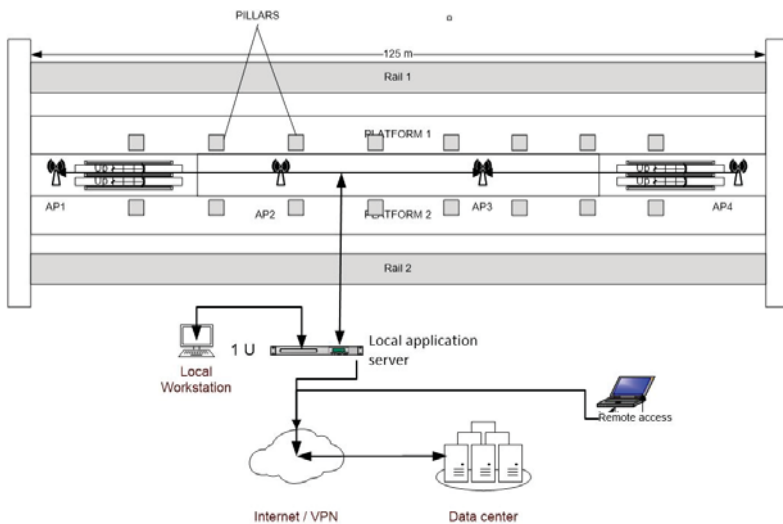


Figure 1. Proposed generic architecture for the subway setup of Bluetooth (BT) sensors.

In the previous schematic, specific Access Points (APs) are employed to detect nearby mobile BT devices. With respect to the received signal strength indicator (RSSI), the local application may detect the identity, position, and direction of travel of the nodes. The same setup can be installed in trains, indicating the estimated degree of passenger congestion and using the information to dispatch travelers to stations towards less agglomerated wagons, especially in rush hours. Due to the known position of APs, the travelers could also get location information and routing information to different destinations, other lines, and platforms, etc. However, there are some issues that must be considered when dealing with BT signal processing. Generally, the Bluetooth signal reception is shaped by the characteristics of the transmitter, receiver, and propagation medium. The propagation channel's effects are related to path loss due to the propagation medium and any obstacles on the propagation path. In subway stations, the effect of the walls and the platforms manifests in some way as a waveguide, but there are other obstacles, such as pillars, persons, etc., that obstruct the direct propagation of signals and create reflections and multiple propagation paths. In such cases, propagation may strongly depend on reflections, diffractions, penetration, or even scattering effects on the path. If there is a direct path between the transmitter (Master unit) and the receiver (Slave), then a free space loss model can be applied (for example, in a subway station where the two recipients are in direct sight):

$$P_L^{FS} = S_c + 20 \lg\left(\frac{f}{f_0}\right) + 20 \lg\left(\frac{d}{d_0}\right), \tag{1}$$

in which  $P_L^{FS}$  is the path loss for free space,  $S_c$  a scaling factor,  $f$  the frequency of signal,  $d$  the distance between the two recipients,  $f_0 = 1$  MHz,  $d_0 = 1$  km [9].

Path loss is usually represented by the path loss exponent, with a value ranging from 2 to 4 (2 for the free space propagation conditions and 4 for loss propagation conditions), reaching even values of 4 to 6 for extremely difficult propagation conditions. In subways, the tunnels usually act like a waveguide, and the value 2 is recommendable for estimating the path loss (only for linear sections), while in stations or in curved sections of tunnels, the loss exponent might reach values of 3 to 5.

Usually, in these conditions, the path loss is given by:

$$P_L = 10n \cdot \lg(d) + C, \tag{2}$$

in which  $P_L$  is the path loss [dB],  $n$  is the path loss exponent,  $d$  is the distance between the transmitter and the receiver [m], and  $C$  is a constant to express the local environment losses. A similar formula, derived from the Friis Transmission formula has the following expression:

$$P_L = 20 \lg\left(\frac{4\pi d}{\lambda}\right), \tag{3}$$

where  $P_L$  represents the path loss [dB],  $d$  is the distance between the radio recipients in meters, and  $\lambda$  the wavelength [m]. For more difficult environment configurations, a more appropriate model is Egli's, which predicts the total path loss for a point-to-point connection, usually suitable for cellular-type communications:

$$P_L = G_T G_R \cdot \left(\frac{h_T h_R}{d^2}\right)^2 \left(\frac{40}{f}\right)^2, \tag{4}$$

where  $G_T$  is the gain of the transmitter antenna,  $G_R$  is the gain of the receiver antenna,  $h_T, h_R$  are the heights of the transmitting, respectively receiving antennas,  $d$  is the distance between the two recipients, and  $f$  is the frequency [10].

### 3.2. Test Bed

The tests were performed in two different locations:

- Outdoors for testing the open field propagation conditions, in a comparison between the Bluetooth 4.x and Bluetooth 5.0 technologies;
- Indoors, in a subway station (“Politehnica” on M1 metro line in Bucharest, Romania).

In the first part of the tests, an outside environment was chosen in an open space to comparatively determine the performances of the two technologies in similar field of view (FOV) conditions. The location selected did have a direct view between the transmitter and the receiver, but it was also surrounded by trees—which caused additional signal power losses. The equipment employed was composed of two Samsung mobile phones (A5 2016 and S8), a Motorola One Vision, and a Nokia 8. Bluescan software was used for determining RSSI levels. A specific jpg file with 1.5 MB was also set for transmission between the master terminal and the slave, counting the total transmission time.

#### 4. Results of the Tests and Analysis

##### 4.1. Open Field Tests

The distance between the master unit and the slave was divided into steps of 10 m each, and measurements were performed for every step. To eliminate variations in signal level, sets of three measurements were performed for each distance slot. The results were considered for the average RSSI value at every distance slot. The first part of the experimental tests is presented in the diagrams below.

As shown in Figures 2 and 3, the signal strength decreased non-linearly with the distance from the transmitter, having a more abrupt near-field variation (usually the first 10–20 m), then maintaining a relatively constant (small decrease) on longer distances. However, here the advantages of the BT 5.0 technology became obvious, as the connection between the two devices could be maintained on considerably longer distances compared with BT4.x (almost twice the distance). Still, the BT 5.0 showed more variability in signal strength over the distance. For determining the latency of the connection in the two types of Bluetooth technologies, a specific jpg file with the length of 1.5 MB was sent from the master station to the slave, and the transmission time until completion was measured. The average data speed can be then computed by:

$$DS = \frac{Q}{t}, \tag{5}$$

where  $Q$  represents the amount of data transmitted and  $t$  the duration of the transmission.

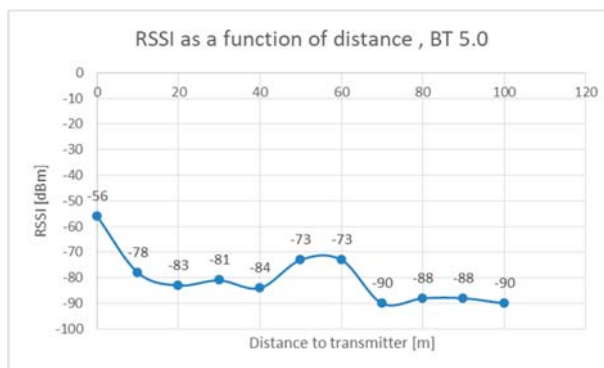


**Figure 2.** Received signal strength indicator (RSSI) average levels according to distance from the master device for Bluetooth 5.0.

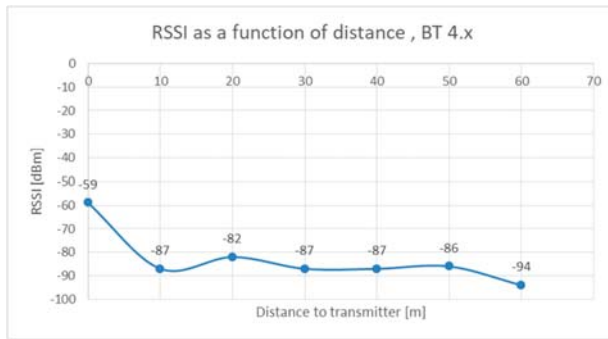
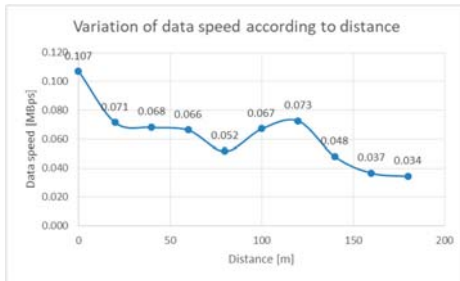
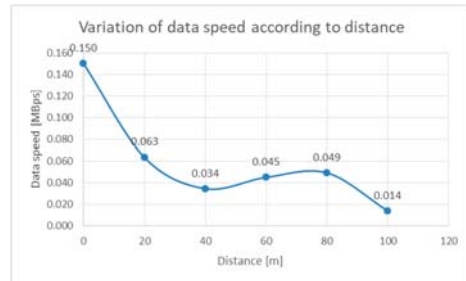


Figure 3. RSSI average levels according to distance from the master device for Bluetooth 4.x.

The results for BT5.0 technology are presented in Figure 4a and those for BT 4.x in Figure 4b. There was a more significant drop in speed for BT 4.x once the distance to the transmitter increased, which gave the BT 5.0 the advantage of a higher data rate at longer distances, reaching around 170 m from the transmitter. In addition, as in diagrams shown in Figure 5a,b, the variation of the file transmission time was less for the Bluetooth 5 than for its previous version. As the tests showed, it appeared that BT 4.0 experienced a more abrupt drop in speed over the first 40 m, then the slope was relatively constant for the next 40 m. Instead, the BT 5.0 showed better stability in data rate on much larger distances, passing over 100 m from the transmitter.

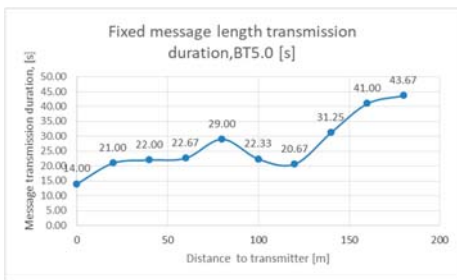


(a)

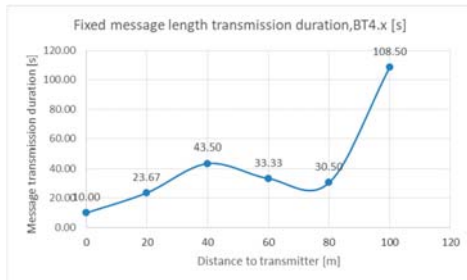


(b)

Figure 4. (a) Variation of data speed for BT5.0, according to the distance to the transmitter; (b) Variation of data speed for BT4.x, according to the distance to the transmitter.



(a)



(b)

Figure 5. (a) Variation of transmission time for BT5.0 technology; (b) Transmission time for BT4.x technology.

While there were, probably, some inherent specificities due to the test conditions, it appears from the open field measurements that the BT5.0 technology is capable of longer connections and is more reliable (Figure 6a), and it is able to deliver higher data rates than BT4.x. As it can be observed from Figure 6b, in the tests performed, on distances that exceed 80 m, the transmission duration varies very much, a fact which creates more instability of the data link. Due to its backward compatibility, this technology is recommendable for detecting nearby discoverable devices and for processing origin–destination information of the BT nodes.

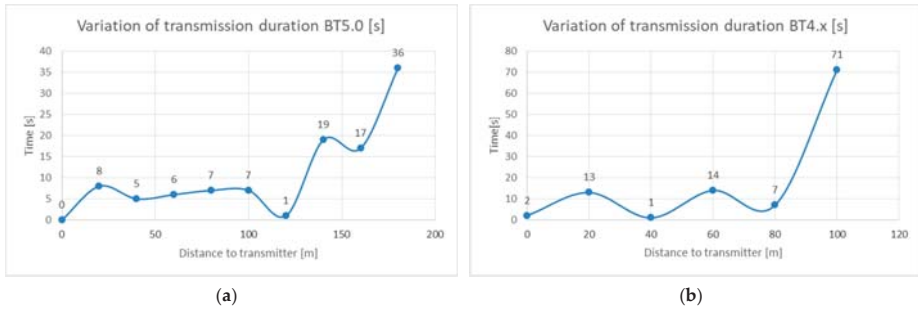


**Figure 6.** (a) Diagram showing the variation of transmission duration for BT5.0; (b) Diagram showing the variation of transmission duration for BT4.x.

#### 4.2. Tests Performed in the Subway Station

For consistency, the same tests have been carried on in the subway station “Politehnica” from the M1 line in Bucharest. The test conditions changed accordingly: This station has lateral pillars, and it has a rectangular shape. The length of the platforms in this station is 145 m, and it has two lateral rows of pillars, separated 12 m from each other. The tests performed indoors were affected by the configuration of the environment and by the sporadic presence of people on platforms or trains that arrived at the station. The set of employed equipment and software was the same as in the previous batch of outdoor tests. Results are presented in the following diagrams.

It appeared for tests performed in indoor conditions, the two versions of Bluetooth behaved in a comparable manner, in what concerns the attenuation of signals. The maximum length reached for a reliable communication was 60 m, even longer for BT4.x (Figure 7a,b). For the latency tests, the same jpg file was employed in both conditions. The results are presented in Figure 8a,b.

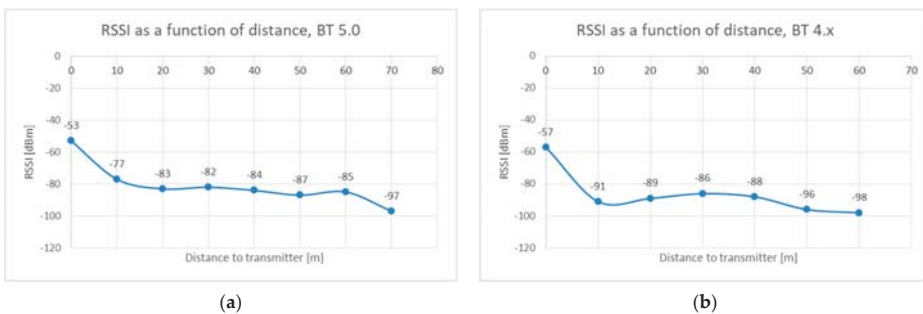


**Figure 7.** (a) RSSI average levels according to distance from the master device for Bluetooth 5.0, indoors test conditions; (b) RSSI average levels according to distance from the master device for Bluetooth 4.x, indoors test conditions.



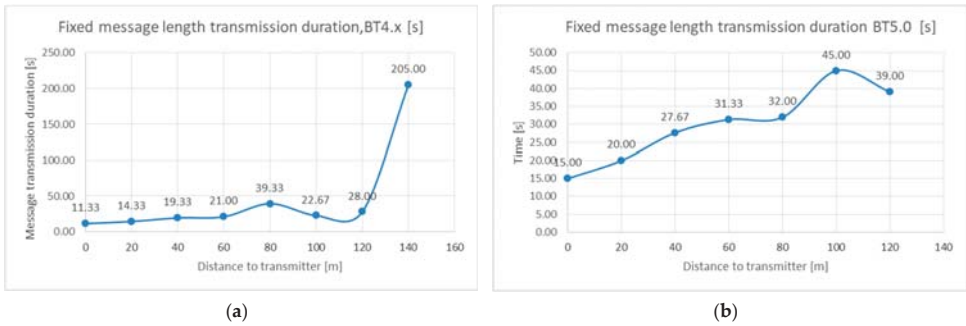


**Figure 8.** (a) Transmission time for BT4.x technology, fixed message length, indoor testing conditions; (b) Transmission time for BT5.0 technology, fixed message length, indoor testing conditions.

Bluetooth 5.0 kept decent values for transmitting the fixed-length message for approximately the same distances as the Bluetooth 4.x version, which even reached longer distances between the communicating devices while in difficult conditions (the transmission duration reached a whopping value of 205 ms for a 1.5 MB file).

For Figure 9, after a distance of 80 m to the transmitter, the reliability of the link drops significantly; however, messages could still be transmitted up to 120 m, with sporadic interruptions, depending on the presence of trains at the station and the number of travelers on platforms.

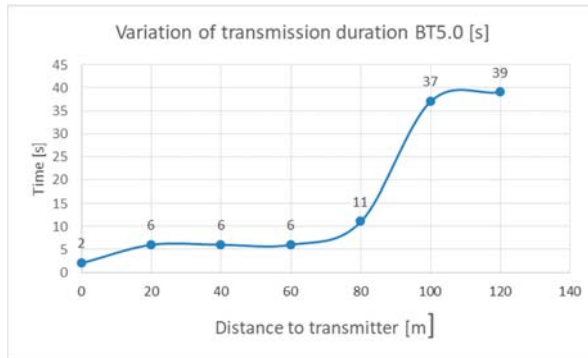


**Figure 9.** Variation of transmission time for BT5.0 technology, indoor testing conditions.

The Bluetooth 4.x technology appeared to behave better in indoor conditions (Figure 10), compared with BT5.0, having more constant transmission time for fixed-length messages. The link could be maintained up to 140 m.

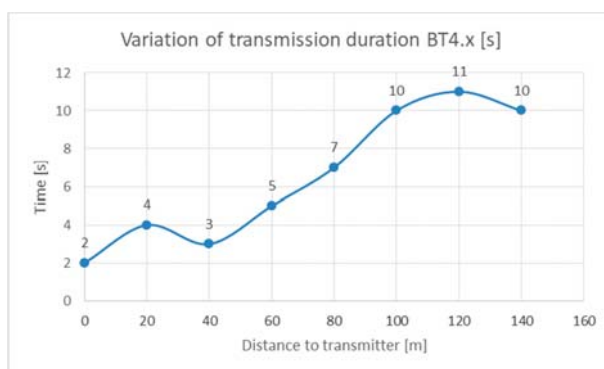


Figure 10. Variation of transmission time for BT4.x technology, indoor testing conditions.

## 5. Conclusions

For both Bluetooth technologies, the indoor environment created different conditions for the propagation of radio signals. It was even possible, in certain cases, for the propagation at longer distances, to create a sort of a “waveguide” effect, and the reception areas were separated into two zones: the so-called “near field” where the RSSI levels dropped on an exponential trend according to the open field path loss model, and a second, much longer zone, where RSSI levels had a variable, but constant within some limits, levels for longer distances, called “far field propagation”. For wide indoor areas, the Bluetooth 5.0 was more consistent in propagation distances and latency. Therefore, was more suitable for the detection of discoverable devices than Bluetooth 4.x. However, due to backward compatibility, the BT5.0 is also capable of detecting and communicating with BT4.x devices. In this case, considering the architecture of the proposed system, presented in Figure 1, it is recommendable that the Access Points should be provided with BT5.0 version for achieving better detection results.

**Funding:** This research received no external funding.

**Conflicts of Interest:** The authors declare no conflict of interest.

## References

1. Ruppe, S.; Junghans, M.; Haberjahn, M.; Troppenz, C. Augmenting the Floating Car Data Approach by Dynamic Indirect Traffic Detection. *Procedia Soc. Behav. Sci.* **2012**, *48*, 1525–1534. [\[CrossRef\]](#)
2. Sharifi, E.; Shamed, M.; Haghani, A.; Sadrsadat, H. Analysis of Vehicle Detection Rate for Bluetooth Traffic Sensors: A Case Study in Maryland and Delaware. In Proceedings of the 18th World Congress on Intelligent Transport Systems, Orlando, FL, USA, 16–20 October 2011.
3. Collotta, M.; Pau, G.; Talty, T.; Tonguz, O.K. Bluetooth 5: A Concrete Step Forward toward the IoT. *IEEE Commun. Mag.* **2018**, *56*, 125–131. [\[CrossRef\]](#)
4. Abbot-Jard, M.; Shah, H.; Bhaskar, A. Empirical Evaluation of Bluetooth and Wi-Fi Scanning for Road Transport. In Proceedings of the Australasian Transport Research Forum 2013 Proceedings, Brisbane, Australia, 2–4 October 2013.
5. Diaz, J.J.V.; Gonzalez, A.B.R.; Wilby, M.R. Bluetooth Traffic Monitoring Systems for Travel Time Estimation on Freeways. *IEEE Trans. Intell. Transp. Syst.* **2016**, *17*, 123–132. [\[CrossRef\]](#)
6. Shlayan, N.; Kurku, A.; Ozbay, K. Exploring Pedestrian Bluetooth and WiFi Detection at Public Transportation Terminals. In Proceedings of the 2016 IEEE 19th International Conference on Intelligent Transportation Systems (ITSC), Rio de Janeiro, Brazil, 1–4 November 2016.
7. Bachmann, C.; Roorda, M.J.; Abdulhai, B.; Moshiri, B. Fusing a Bluetooth Traffic Monitoring System with Loop Detector Data for Improved Freeway Traffic Speed Estimation. *J. Intell. Transp. Syst.* **2012**, *17*, 152–164. [\[CrossRef\]](#)

8. Manering, F.; Bullock, D.M. Analysis of Freeway Travel Time Variability Using Bluetooth Detection. *J. Transp. Eng.* **2011**, *137*, 697–704.
9. Akanni, A.O.; Odepian, K. Comparative Analysis of Propagation Pathloss and Channel Power of VHF and UHF Wireless Signals in Urban Environment. *Int. J. Res. Innov. Appl. Sci.* **2019**, *IV*. [[CrossRef](#)]
10. Mardeni, R.; Pey, L.Y. The Optimization of Okumura's Model for Code Division Multiple Access (CDMA) System in Malaysia. *Eur. J. Sci. Res.* **2010**, *45*, 508–528.

**Publisher's Note:** MDPI stays neutral with regard to jurisdictional claims in published maps and institutional affiliations.



© 2020 by the authors. Licensee MDPI, Basel, Switzerland. This article is an open access article distributed under the terms and conditions of the Creative Commons Attribution (CC BY) license (<http://creativecommons.org/licenses/by/4.0/>).

# Social Engineering—The Hidden Control <sup>†</sup>

Edina Albiné Budavári \* and Zoltán Rajnai

Doctoral School on Safety and Security Sciences, Obuda University, 1034 Budapest, Hungary;

rajnai.zoltan@bgk.uni-obuda.hu

\* Correspondence: budavari.edina@phd.uni-obuda.hu

<sup>†</sup> Presented at the 14th International Conference INTER-ENG 2020 Interdisciplinarity in Engineering, Mureş, Romania, 8–9 October 2020.

Published: 31 December 2020

**Abstract:** The former energy-wasting lifestyles of developed societies can no longer be sustained. In our age, efficiency is the key to continued sustainability. Increasing efficiency requires the use of infocommunication systems and their regulation. Regulatory modeling is based on the cybernetic loops model. The systems are not closed, so they are constantly suffering from environmental disturbances. External interference can also come from a human resource that covertly exploits the technological and psychic elements of the system to achieve its own goals. Social engineering is also such an intervention. The aims of the present study are to draw a parallel between cybernetic loops and social engineering, then to define social engineering on the cybernetic base.

**Keywords:** social engineering; cybernetic loop; hidden control; definition

---

## 1. Introduction

Throughout history, with the development of industry, humanity's energy needs have steadily increased. At the same time, humanity has scattered on the surface of Earth. The resources of the planet are finite. There is less opportunity for an energy-wasting lifestyle as the resources of the environment are depleted. Improving the quality of life requires long-term sustainability [1,2]. In terms of production, the new paradigm of advanced industry, Industry 4.0, targets environmental sustainability [3–5]. In terms of consumption, sustainability is also reflected in the design of the Smart City model [3,6–8]. The vital basis for all this is the operation of appropriate information technology systems [9,10] and their control [11,12]. The new generations of humanity must already grow up according to these principles. These principles need to be incorporated into the legal framework [13] and into the educational materials that define the daily approach [14–18].

One way to increase system efficiency is to increase the efficiency of system management. The implementation of the system control includes the monitoring and event management of the system [19–23]. These activities are consistent with the process model of cybernetic loops. The operation of real and virtual systems is always disturbed by external sources. External interference can also come from a human resource that covertly exploits the technology and psychic elements of the system to achieve its own goals.

The purpose of the intentional regulatory elements included in the model of the cybernetic loop is to implement the operation of the system over time. This also ensures the sustainability of the system. The purpose of social engineering is to interfere with the system in a covert way [24]. The intervention from a source unknown to the system operators is for an external purpose. This intervention serves its own purpose, not the sustainability of the system. The process leading to intervention is similar in both cases, which is why it is worth examining the parallels between the two methods.

## 2. Methods

The examination of social engineering can also be done with the applied methods and the used resources' technological and quality requirements groupings. In such an examination, distinction can be made between techniques that exploit people and those that exploit technical possibilities. Further distinction can be made according to whether these are techniques used in real physical space or techniques used in the virtual world. The techniques can be applied in a complementary manner. Furthermore, in terms of resource utilization, impacts can work in a direct or indirect way [24].

The control theory cybernetic loop model is based on modeling the control process. Thus, the parallelism between the process of social engineering and the model of the cybernetic loop is worth studying from the aspect of the cybernetic loop. The groupings mentioned above are not suitable for this. For this reason, a new approach must be taken. An approach can base on process modeling.

To achieve this,

1. It is worth simplifying the cybernetic loop model:
  - a. The processes that interact with and independently of the system must be identified;
  - b. The direction of signal flow for interacting with the system must be identified;
2. The processes of social engineering should be generalized from the aspect of the resulting simplified model:
  - a. The processes that interact with and independently of the system must be identified;
  - b. The social engineering toolkit needs to be typified in terms of interactivity;
  - c. The direction of signal flow for interacting with the system must be identified;
3. The process model of social engineering should be synthesized according to the model of the cybernetic loop.

This approach provides an opportunity to examine the parallels between the two models and to draw further conclusions.

## 3. Results

The steps identified for the methodology could be performed as follows:

- Based on the operational process of the cybernetic loop, the operational phases of social engineering can be identified;
- Based on the elements of the model of cybernetic loop, the toolbox of social engineering can be grouped and typified;
- Using the typified toolkit, the direction of signal flow could be determined;
- The process model of social engineering could be synthesized based on the model of the cybernetic loop.

The methodology used for the new theoretical approach made it possible to create a process model of social engineering. As the process model was synthesized on the basis of the cybernetic loop model, it was also suitable for standardization and further conclusions. The created model and the results achieved by its use are as follows:

- The logical process of social engineering can be paralleled with the process of regulation;
- Based on the parallelism, social engineering is a manifestation of regulation;
- As social engineering can be understood as a manifestation of regulation, it can be incorporated into the model of the cybernetic loop, which results in a unified process model;
- Based on the unified process model, a cybernetic definition of social engineering can be given.

#### 4. Discussion

The examination of the tools and process of social engineering from the cybernetic aspect included in the study reflects a new unique system of criteria. In this new system of criteria, the examination of the set of tools, intervention process and actors of social engineering is the same as the main elements of the information security approach system [3,5,7,8,25–27].

In accordance with the methodology of the examination, after the simplification of the scope of regulation, the processes of social engineering are examined and the set of tools is typified. After this, the parallelism of the two process models can be detected. As a further consequence, a combined model of the cybernetic loop and social engineering can be compiled.

##### 4.1. Cybernetic Loop

The regulation is a closed, continuous control process among the process models that can be used to control the system in control theory. The basic element of control modeling is the cybernetic loop model. This model represents the process of intervention in the system [5]. Its general structure contains a part-process regulated in the system. Negative feedback is associated with that part process, which realizes the control. The model also includes the effect of environmental disturbance. According to its operation, the control system receives feedback information about the state of the system from the starting point. Comparing the obtained state with the desired state, the control system produces the intervention that is at the end of the feedback.

The simplified general model of the cybernetic loop is shown in Figure 1.

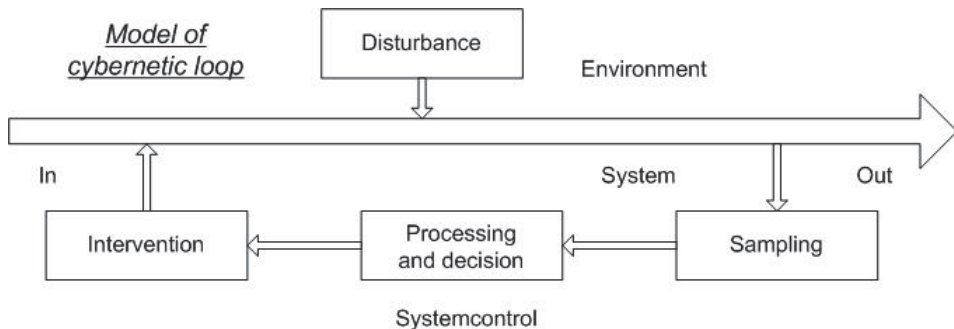


Figure 1. Simplified general model of cybernetic loop.

##### 4.2. Social Engineering

The goal of social engineering is to utilize system resources for system-independent external purposes in a way that is unobtrusive to system management. Throughout history, many techniques have emerged to accomplish this. According to the methodology included in the study, the techniques of social engineering should be typified on the model of the sub-processes included in the simplified model of the cybernetic loop. In this way, the basis of grouping is the interactivity with the system and its orientation.

Based on the grouping of information acquisition, processing and decision, the intervention can be as follows:

- Techniques for obtaining information: impersonation, shoulder surfing, dumpster diving, piggybacking, tailgating, scam, phishing, baiting, and OSINT (Open-source intelligence);
- As the method of data processing and decision making is completely independent of the implementation of the system, the same central technologies can be used to control system and social engineering. However, in the case of the use of distributed technologies, there is a high probability that the hidden state will disappear. Thus, manual correlation search technologies,

data warehousing solutions, the use of artificial intelligence, and central decision systems can also be mentioned here;

- Intervention techniques: asking for help, providing help, taking advantage of reciprocity, impersonation, piggybacking, tailgating, scam, phishing, DNS-based (Domain Name System based) attacks, whaling-type attacks, and baiting.

Some of the techniques listed can be used both to obtain the necessary information and to carry out the intervention. In such cases, the technique usually provides coverage in the system.

#### 4.3. The Parallell

The techniques in the palette of social engineering can be typified on the pattern of sub-processes in the simplified model of the cybernetic loop. Based on this, the parallel can be established. Sampling is a sub-process in the cybernetic loop model that aims to extract information from the system. This is equivalent of this information acquisition in social engineering. As information processing and decision making are present in both cases as separate subsystem processes in parallel with the operation of the system, the parallel of these is self-evident. In addition, these sub-processes require abstract processing, so both models have nearly the same palette. Finally, in both cases, the sub-processes implementing the intervention can be identified. The difference between the two models is that in the case of social engineering, the feedback of control is located outside the system and hidden. This is shown in Figure 2.

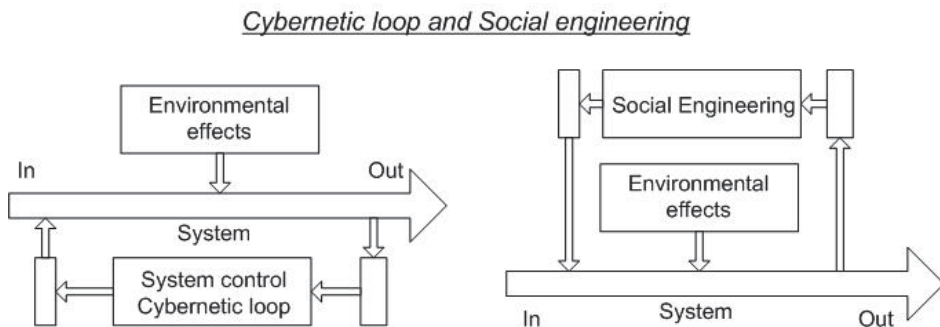


**Figure 2.** The parallel between the cybernetic loop and the operating scheme of social engineering.

#### 4.4. Model and Definition

As the parallel can be created between the two models, social engineering can be seen as a hidden external control of the system. The model and this recognition allow for a cybernetic definition of social engineering. Another emerging option is to merge the operating scheme of the cybernetic loop and social engineering. This is shown in Figure 3.

According to the above, the definition could be as follows: social engineering is the hidden external control of a system that seeks to exploit system resources to achieve its own goals.

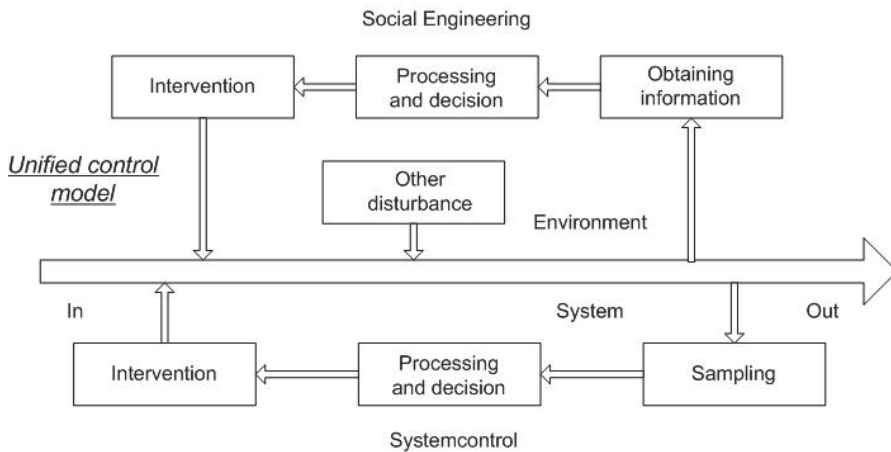


Figure 3. Unified model of cybernetic loop and social engineering.

## 5. Conclusions

In connection with industrial production, there is a need to cover the entire consumer spectrum of civilization. The industrial products appear in all walks of life. The process of population on our planet requires increasingly efficient use of energy [1,2]. This requirement appeared in all aspects of production. Automation helps increase efficiency. For this reason, the application of advanced infocommunication systems [9,10] is essential for the implementation of the next generation stage of the industry [3–5].

Increasing the management efficiency of the system also increases the efficiency of the operation of the system. The effectiveness of control is determined, among other things, by the application of appropriate cyber regulation. The purpose of this regulation is to ensure the adaptation of the system to external influences [11,12,19–23]. The social engineering is one of the external influences from human resources. This effect takes advantage of the system for an external purpose independent of the system and it is not for the sustainability of the system [24].

The basic element of control modeling is the cybernetic loop of the control theory. This study demonstrated a parallel between the cybernetic loop model and the social engineering process with a new approach. Based on this parallel, it can be stated that social engineering can be considered as a hidden version of cybernetic loop methods. The modeling of the processes ensured the creation of a combined model of the cybernetic loop and social engineering. The unified model, goals and methods made it possible to define social engineering in a cybernetic aspect.

**Conflicts of Interest:** The authors declare no conflict of interest.

## References

1. Albini, A.; Rajnai, Z. Modeling general energy balance of systems. *Procedia Manuf.* **2019**, *32*, 374–379. [CrossRef]
2. Kasac, J.; Stefancic, H.; Stepanic, J. Comparison of social and physical free energies on a toy model. *Phys. Rev. E* **2004**, *70*, 016117. [CrossRef]
3. Kiss, M.; Breda, G.; Muha, L. Information security aspects of Industry 4.0. *Procedia Manuf.* **2019**, *32*, 848–855. [CrossRef]
4. Tokody, D. Digitising the European industry—Holonc systems approach. *Procedia Manuf.* **2018**, *22*, 1015–1022. [CrossRef]
5. Kiss, M.; Muha, L. The Cybersecurity Capability Aspects of Smart Government and Industry 4.0 Programmes. *Interdiscip. Descr. Complex Syst.* **2018**, *16*, 313–319. [CrossRef]



6. Tokody, D.; Schusztar, G.; Papp, J. Study of How to Implement an Intelligent Railway System in Hungary. In Proceedings of the IEEE 13th International Symposium on Intelligent Systems and Informatics (SISY 2015), Subotica, Serbia, 17–19 September 2015.
7. Szabó, Z. The effects of globalization and cyber security on smart cities. *Interdiscip. Descr. Complex Syst.* **2019**, *17*, 503–510. [[CrossRef](#)]
8. Pető, R. Security of Smart City. *Interdiscip. Descr. Complex Syst.* **2019**, *17*, 13–19. [[CrossRef](#)]
9. Albin, A.; Rajnai, Z. General Architecture of Cloud. *Procedia Manuf.* **2018**, *22*, 485–490. [[CrossRef](#)]
10. Albin, A.; Tokody, D.; Rajnai, Z. Theoretical Study of Cloud Technologies. *Interdiscip. Descr. Complex Syst.* **2019**, *17*, 511–519. [[CrossRef](#)]
11. Mester, G. Obstacle Avoidance and Velocity Control of Mobile Robots. In Proceedings of the 6th International Symposium on Intelligent Systems and Informatics (SISY 2008), Subotica, Serbia, 26–27 September 2008.
12. Mester, G.; Rodic, A. Sensor-Based Intelligent Mobile Robot Navigation in Unknown Environments. *Int. J. Electr. Comput. Eng. Syst.* **2010**, *2*, 1–8.
13. Kovács, Z. Cloud Security in Terms of the Law Enforcement Agencies. *Hadmérnök* **2012**, *7*, 144–156.
14. Rodic, A.; Jovanovic, M.; Popic, S.; Mester, G. Scalable Experimental Platform for Research, Development and Testing of Networked Robotic Systems in Informationally Structured Environments. In Proceedings of the 2011 IEEE Workshop on Robotic Intelligence in Informationally Structured Space, Paris, France, 11–15 April 2011.
15. Mester, G. Rankings Scientists, Journals and Countries Using h-index. *Interdiscip. Descr. Complex Syst.* **2016**, *14*, 1–9. [[CrossRef](#)]
16. Dobrilovic, D.; Odadzic, B. Virtualization Technology as a Tool for Teaching Computer Networks. *Int. J. Educ. Pedagog. Sci.* **2008**, *13*, 41–45.
17. Mester, G. Academic Ranking of World Universities 2009/2010. *IPSI J. Trans. Internet Res.* **2011**, *7*, 44–47.
18. Szabó, A.; Szucs, E.; Berek, T. Illustrating Training Opportunities Related to Manpower Facility Protection through the Example of Máv Co. *Interdiscip. Descr. Complex Syst.* **2018**, *16*, 320–326. [[CrossRef](#)]
19. Mester, G.; Pletl, S.; Nemes, A.; Mester, T. Structure Optimization of Fuzzy Control Systems by Multi-Population Genetic Algorithm. In Proceedings of the 6th European Congress on Intelligent Techniques and Soft Computing (EUFIT '98), Aachen, Germany, 7–10 September 1998; pp. 450–456.
20. Mester, G.; Rodic, A. Simulation of Quad-rotor Flight Dynamics for the Analysis of Control, Spatial Navigation and Obstacle Avoidance. In Proceedings of the 3rd International Workshop on Advanced Computational Intelligence and Intelligent Informatics (IWACIII 2013), Shanghai, China, 18–21 October 2013; pp. 1–4.
21. Albin, A.; Mester, G.; Iantovics, B.L. Unified Aspect Search Algorithm. *Interdiscip. Descr. Complex Syst.* **2019**, *17*, 20–25. [[CrossRef](#)]
22. Zamfirescu, C.B.; Duta, L.; Iantovics, L.B. The Cognitive Complexity in Modelling the Group Decision Process. *Brain Broad Res. Artif. Intell. Neurosci.* **2010**, *1*, 69–79.
23. Mester, G.; Pletl, S.; Pajor, G.; Basic, D. Adaptive Control of Rigid-Link Flexible-Joint Robots. In Proceedings of the 3rd International Workshop of Advanced Motion Control, Berkeley, CA, USA, 20–23 March 1994; pp. 593–602.
24. Albiné Budavári, E.; Rajnai, Z. The Role of Additional Information in Obtaining information. *Interdiscip. Descr. Complex Syst.* **2019**, *17*, 438–443. [[CrossRef](#)]
25. Hell, P.M.; Varga, P.J. Drone systems for factory security and surveillance. *Interdiscip. Descr. Complex Syst.* **2019**, *17*, 458–467. [[CrossRef](#)]
26. Shatnawi, M.M. Applying Information Security Risk Management Standards Process for Automated Vehicles. *Bánki Rep.* **2019**, *2*, 70–74.
27. Tokody, D.; Flammini, F. Smart Systems for the Protection of Individuals. *Key Eng. Mater.* **2017**, *755*, 190–197. [[CrossRef](#)]

**Publisher's Note:** MDPI stays neutral with regard to jurisdictional claims in published maps and institutional affiliations.



© 2020 by the authors. Licensee MDPI, Basel, Switzerland. This article is an open access article distributed under the terms and conditions of the Creative Commons Attribution (CC BY) license (<http://creativecommons.org/licenses/by/4.0/>).

# Green Economy and Green Growth—Opportunities for Sustainable Development <sup>†</sup>

Lucreția Dogaru

Department of Law and Public Administration, Faculty of Economics and Law, University of Medicine, Pharmacy, Sciences and Technology “G.E. Palade” of Târgu Mureș, 540142 Târgu Mureș, Romania; lucretia.dogaru@umfst.ro

<sup>†</sup> Presented at the 14th International Conference INTER-ENG 2020 Interdisciplinarity in Engineering, Mureș, Romania, 8–9 October 2020.

Published: 22 January 2021

**Abstract:** Economic activities are increasingly carried out in modern conditions, a situation which is often linked to a negative impact on the environment. They have now reached such a level that they can be considered a real factor in climate formation and modeling. Such a trend has generated a lot of initiatives and strategies aimed at a green economy development. Thus, special public policy measures for the green economy and green growth have been developed and also implemented in the last few years. The analysis of the main challenges in the field of economic and environmental development, as well as the public policies for a green economy, is a real concern. More and more, the global trends for sustainable development are represented by green economy and green growth. The purpose of the present article is to present and analyze the issue of green economy and green growth, which is a new operating strategy both globally and European level. Green growth represents a practical tool for achieving the objective of sustainable development, as a timeless objective. This means fostering economic growth and development, while ensuring that the natural assets continue to provide environmental resources and services. We will try also to systematize the main challenges in the field of economic and environmental development, taking into account their specific characteristics, and to provide relevant suggestions for public policies related to reducing the impact of economic activities on the environment. Additionally, particular attention is focused here on establishing the kind of relationship that occurs between the green economy, green growth and sustainable development. In this regard, we will analyze the purpose of the simultaneous functioning of these three green ideas. We consider that the co-existence of the three green ideas (green economy, green growth and sustainable development) is reasonable due to the complementary and simultaneous nature of these concepts.

**Keywords:** green economy; green growth; sustainable development; economic activities

---

## 1. Introduction

Towards the end of the twentieth century, the so-called consumer society has been installed, which correlates with the population growth trend, the intensification of the urbanization process, the development and diffusion of information and communication technology, the progressive increase of the population's standard of living, but also with the significant reduction of natural resources and product life cycle ([1] pp. 22–24). These realities overlap with political and legislative initiatives and projects designed to contribute to the reduction of environmental risks and sustainable development without environmental degradation. Thus, the concept of ecological economy also known as the green economy begins to take shape and consolidate.

The complex, difficult and absolutely necessary process of transition to a green economy is correlated with the reconsideration of unsustainable consumption and production patterns, in order

to identify future development opportunities. In this sense, the adoption and implementation of the 2030 Agenda for Sustainable Development (which will be referred to in our paper as “The 2030 Agenda”) recently took place. In this regard, Goal 12 of the 2030 Agenda establishes the need for the integrated promotion of environmental, social and economic elements. It is aimed to ensure sustainable consumption and production patterns.

Developing global commitments and initiatives to reduce and manage waste, use resources efficiently, reduce pollution and combat the effects of climate change have been the main drivers of the green economy. The involvement of stakeholders in the consultations that took place in the High-Level Political Forum on Sustainable Development or in other international organizations, were synergistic actions with an important role in promoting and transitioning to the green economy. All the debates on the role of the green economy and, implicitly, of sustainable development in recent years, have ended with the approval at the European level of ambitious action plans and strategies, which have been the engine of the transition to a green economy.

The European path of the green economy is an ascending one, which came as a concrete answer to the complex environmental problems manifested in recent years. The challenges associated with the green economy involve political commitments to the green economy, the development of resource efficiency standards, the financing of innovation and research in the development of new technologies, and the promotion of information initiatives.

We can say that the green economy represents a system of economic activities of production, distribution and consumption associated with sustainability, a system correlated with the process of eliminating the dysfunctions generated by economic growth. It also indicates a type of economy that generates welfare and social equity, correlated with the significant reduction of environmental risks and ecological deficit. It is the type of low carbon economic progress conducive to environmental sustainability and inclusive social development, which defines green growth.

Most authors and specialists in the field, consider that the green economy phenomenon represents a field in economic science and also in economic practice which justifies the dependence of economic development on the environmental natural factors. So, in scientific terms, the green economy implies the development of new technologies and clean industries and, in practical terms this involves those types of activities that create and increase the natural capital and reduce environmental hazards and risks [2].

The concept of the green economy has an evolutionary character ([3] pp. 361–363), and it was used for the first time in 1989, in the *Blueprint for a Green Economy* report prepared for the United Kingdom Government by a group of economists in the field. Since October 2008, the United Nations Environment Program (UNEP) has launched the Green Economy Initiative, with the aim of supporting investment in the green sector as well as greening certain sectors, which is a real way to achieve sustainable development. Following the 2012 World Conference on Sustainable Development entitled Rio+20, the idea for an inclusive green economy was grounded. The term inclusive green economy and its associated concepts (green growth and sustainable development) have evolved from initial research to the present. This type of economy is based on efficient and low carbon consumption in the production process ([4] pp. 142–145), being an inclusive economy in terms of consumption and results that is based on sharing, circularity, collaboration, solidarity, adaptability, opportunity and interdependence.

In terms of the green growth, it can be said that this implies a concept which describes a form of economic growth that uses natural resources in a sustainable manner. In fact, this term is increasingly used globally to provide an alternative concept to classical industrial economic growth. This would lead to the green economy phenomenon, which is a real phenomenon of progress and a concept of environmental security ([5] p. 2, [6] pp. 1–10).

In the current global context generated by the Sars2 Covid-19 coronavirus pandemic, the concept of green growth is often used to describe those national, regional or international strategies, that promote economic recovery from the coronavirus recession ([7] pp. 3–5).

All debates and analyses on the opportunities of the green economy are directly associated with environmental protection, increasing competitiveness, innovation and technological research. Numerous initiatives have emerged on a European level in order to support the implementation of the green economy and green and sustainable development. Thus, The European Enterprise Network includes over 600 organizations from over 60 countries in order to support SMEs for the access of funding opportunities for eco-innovation, energy efficiency and access to resources. Concerning resource efficiency—using natural resources in a sustainable manner with a considerable reduction of the impact on the environment—a part of the Europe 2020 Strategy is represented by The Resource-Efficient Europe Flagship Initiative, which represents the European Union's growth strategy for a smart, inclusive and sustainable European economy.

Starting from the concept of the green economy, this implies by its definition, a direct reference to improving the quality of life and social equity and also the need to reduce environmental risks and the ecological deficit.

From this perspective, the transition to such an economy raises an interpretation in terms of resource efficiency through the implementation of innovative approaches designed to optimize resource consumption and reduce pollutant emissions. Alternatively, it requires a sustainable approach to resources, ensuring the preservation of natural capital, the resilience of ecosystems while also ensuring social inclusion.

Internationally, the concept of the green economy is frequently used in connection with a number of initiatives. In this regard, we recall the Paris Agreement, signed at the XXI Conference of the Parties (COP 21) to the United Nations Framework Convention on Climate Change, which marked a historic moment of global action to reduce global average temperature increase of 2 °C, being the first legally binding multilateral instrument in the field of climate change, starting in 2020. Additionally, the Batumi initiative in Georgia on the green economy (BIG-E) from 2016 (an initiative belonging to UNECE and carried out through the Green Growth Knowledge Platform) represents a pan-European strategic framework for the transition to an inclusive green economy, with thematic areas such as investment in innovation, the transfer of green technologies and products, and the stimulation of sustainable consumer behavior. At the same time, it proposes voluntary commitments until 2030, in order to contribute directly to the objectives of sustainable development. In this context we can mention other important initiatives in the area of the green economy, such as: The Green Growth Knowledge Platform (GGKP) (GGKP is a global network of international experts and organizations, established in January 2012 by the Global Green Growth Institute (GGGI), the Organization for Economic Co-operation and Development (OECD), the UN Environment and by the World Bank), which is a global network of international experts in the field of the green economy who meet annually at conferences that are dedicated to this platform; The Partnership of the United Nations for Action on Green Economy (PAGE), launched in 2013 to support countries involved in implementing a green economy approach; The Green Industry Platform, an international platform for green industry stakeholders, initiated by UNIDO at the Rio+20 Environment Conference; The Sustainable Technology Marketplace (WIPO Green), an initiative of the World Intellectual Property Organization to support the adoption and implementation of environmental technologies in emerging economies; the EaP GREEN regional program, to support the six Eastern Partnership countries towards a green economy by decoupling economic growth from environmental degradation and resource depletion, implemented in 2013–2017; The EU Switch to Green Facility, a platform that facilitates cooperation to increase international progress towards the transition to a green economy in the European Union and partner countries.

The perspectives offered by the green economy strengthen the comprehensive and unitary approach to sustainable development, with the common denominator of environmental protection, increasing the competitiveness and productivity of the resources available to an economy.

The transition to a green economy is a medium and long-term process that involves a political commitment of states that want to change the model of their economic development. This process involves initiatives related to public involvement in implementing a green approach in national policies

(renewable energy, energy efficiency of buildings, technologies and processes with low GHG emissions), the promotion of environmental footprint ([8] pp. 121–132) and the development of banking services and green investment.

Along with the final document of the Conference on Sustainable Development (Rio+20), which promoted the idea of green economy and sustainability [9], the 2030 Agenda for Sustainable Development adopted at the UN Summit on Sustainable Development (New York, September 2015) is a commitment to achieving sustainable development by 2030, worldwide. The implementation process of the 2030 Agenda prioritizes the need for integrated promotion of environmental, social and economic elements as well as the need to identify solutions to the challenges of the process of reconfiguring the classical economic model.

As far as we are concerned, we consider that Goal 17 of the 2030 Agenda has played an important role in raising public awareness regarding the green economy. Thus, the Ministerial Declaration elaborated on the occasion of the High-Level Political Forum on Sustainable Development (HLPF 2018) shows that decoupling economic growth from resource use continues to be a challenge. Therefore, promoting resource efficiency must be done following a cycle-based approach of product life, in order to reduce the use of resources, starting with the extraction and production phases, by reusing and recycling, through the implementation of technological innovations and standards (Declaration No. E/HLS/2018/1).

## **2. The European Framework of the Green Economy**

Since the beginning of 2015, an ambitious action plan on the green economy has been adopted at the EU level, with the aim of stimulating the transition to a competitive Community economy, so as to accelerate sustainable economic growth. The Communication of the European Commission of September 2017 entitled “Investing in a smart, innovative and sustainable Industry. A renewed EU Industrial Policy Strategy” (COM (2017) 479), is aimed to strengthen the capacity of industry to adapt to the requirements of developing new digital technologies that will allow the transition to a green economy [10,11]. The aforementioned document states that stimulating the use of smart technologies throughout industrial value chains linked to low carbon dioxide is essential for increasing competitiveness. Part of the European framework for the transition to the green economy is also the eco-design regulations (these are Directive 2009/125/EC (Directive 2009/125/EC establishing a framework for the setting of eco-design requirements for energy-related products, published in the Official Journal of the European Union No. L 285/10 from 31 October 2009) ([12] pp. 162–176) and subsequent vertical regulations), as well as the Eco-design Working Plan for 2016–2019.

According to Eurostat data (Eurostat 2018 a, Resource productivity statistics; Eurostat 2018 b, Resource productivity up in the European Union), at the level of the Member States of the European Union, the domestic consumption of raw materials in 2010 was of about 14 tons per capita, while in 2017 it decreased to 13 tons per capita. At the same time, at a European level, it is noted that resource productivity increased by about 40% in the period 2002–2018, even though domestic material consumption (DMC) decreased due to the economic crisis of 2008, which significantly affected the metallurgical industrial sector.

Regarding Romania, the official Eurostat data shows that, in 2017, the domestic consumption of materials used directly in the economy was about 485 thousand tons of materials, an almost twice lower consumption level than that of Germany. In other EU Member States, the highest resource productivity in 2018 was recorded in Italy, the Netherlands, Luxembourg and Spain, and the lowest resource productivity was scored in Bulgaria, Romania, Latvia and Finland. Definitely, the amount of resources used in an economy is essential in sustainable development, from the extraction of resources needed for production and consumption activities to materials released into the environment in the form of pollutants.

According to the EU Scoreboard on Resource Efficiency in 2017, our country has the largest increase in consumption of natural resources in Central and Eastern Europe (the per capita consumption

which has increased with 180% in the last 15 years). Of course, such a percentage, which indicates that we are deficient in increasing the productivity of resource use, requires both a reduction in the gap with other EU Member States and a boost to business development in the green economy. That is why, the challenge is firstly represented by minimizing the loss of resources that can be reintroduced into the economic circuit, and secondly, by changing the mentality of those interested in promoting ecological behavior. A successful economy requires the efficient use of natural resources and waste, and protection and sustainable development of the environment [13].

This relatively new concept, the green economy, associated also with social inclusion and low greenhouse gas emissions, involves certain categories of opportunities. Thus, we distinguish between the economic opportunities, materialized in the recycling capacity for certain fields and green acquisitions, the legislative opportunities, in the form of the community acquis that is required to be transposed at a national level, the social opportunities, which involve job creation, and last, but not least, the structural opportunities, involving applied education and innovation. Regarding this aspect, we feel obliged to specify that these opportunities are hit by a number of limitations, of an economic nature (such as the lack of funds for innovation and infrastructure and low purchasing power), legislative limitations (the incomplete transposition of European legislation the national legislation of the Member States), social constraints (poverty and the low level of awareness of the population), as well as structural limitations (uneven application of the legislation and the lack of specialized personnel in the public administration).

Considering these realities, certain public policy recommendations are required, especially regarding the legislative component, but also recommendations regarding the educational component. With regard to the legislative component, in our opinion, it is necessary to promote a national plan for efficient and sustainable production and consumption and to develop an appropriate legislative framework for the green economy, which requires the development of green economy plans at local or regional level (this has been done successfully by countries such as Finland, Sweden and Germany, which have adopted national resource efficiency programs). It is also necessary to initiate public debates on the appropriateness of developing new national standards for resource efficiency as well as an integrated approach to identify market opportunities and evaluate legislative initiatives. In the same direction, we appreciate that the promotion of ecological design principles is also needed. This can be accomplished by promoting sustainability models of products in the industry, correlated with modern taxation systems, as well as promoting operators' access to information on hazardous substances and establishing standards for the prevention and reduction of food and household waste (updating Law No. 217/2016, on reducing food waste, and supplementing it with a standard of clear definition of the criteria for cessation of waste status and transformation into a by-product, which can be composted and used later in agriculture or for biogas). It would also be relevant to promote the extension of the average duration of products through consumer protection legislation ([14] pp. 7–12) and also to revise the law on green public procurement and waste management regulations by promoting the concept of efficient and sustainable use of resources.

Now, humanity is facing a great problem that has become a real crisis. It is about the crisis caused by the Covid-19 pandemic, a topical issue that is aggressively transforming the way we live. We notice in this context that, while all interventions are largely focused on protecting people's lives and economies, for the moment, the big issue of waste management remains a secondary one. However, the management of this hazardous waste must be essential to minimize the long-term risks to environmental and human health. The global dynamics of solid waste generation is changing now, taking into account the fluctuations of the composition, quantity and high degree of contamination of those types of waste [15].

The current public policy recommendations include educational, research and communication components. In our opinion, the promotion of education for sustainable development ([16] pp. 9, 73–83), the adoption of sustainable lifestyles and the promotion of good international practices on the green economy is absolutely necessary and can be achieved by initiating specific steps (such as the development of an informative guide with good practices and resource consumption optimization



solutions; creating a national information platform on resource efficiency; initiating online information campaigns). It is also necessary, for example, to promote exchanges of experience or cross-border initiatives to implement best practices on the green economy at the level of local public authorities.

### 3. The National Framework of the Green Economy: Actualities and Perspectives

In regard to the green economy field, Romania has implemented at a national level relevant normative acts, which achieve synergies with this type of economy. In this context, we recall the implementation of the regulations contained in Directive 2012/27/European Parliament and of the Council on Energy Efficiency, consolidated in 2020 (Published in the *Official Journal of the European Union*, L 315 from 14 November 2012, pp. 1–56, it was transposed through Law No. 160/2016 for the amendment and completion of Law No. 121/2014 on energy efficiency) as well as those belonging to Directive 2009/125/EC establishing a framework for the setting of eco-design requirements of energy impact products, consolidated in 2012 (Published in the *Official Journal of the European Union*, L 285 from 31 October 2009, pp. 10–35, transposed into national legislation by GD No. 55/2011, completed by GD No. 580/2011 and GD 1090/2013). The mentioned regulations were also aimed at achieving an energy saving of 1.5% by the final consumers in the period between 2014 and 2020. Another relevant regulation in the field is the Emergency Ordinance No. 24/2017 on amending and supplementing the law establishing the system for promoting the production of energy from renewable energy sources transposing Directive 2009/28/EC on promoting the use of energy from renewable sources, consolidated in 2015 (Published in the *Official Journal of the European Union*, L 140 from 5 June 2009, pp. 16–62). Additionally, Regulation (EC) No. 834/2007 of the Council of Europe on organic production and labeling of organic products, amended and consolidated in 2013, was applied at the level of Romanian legislation.

We mention in this context the Government Decision No. 739/2016 for the approval of the National Strategy on Climate Change and Economic Growth based on low carbon emissions for the period 2016–2020 and the National Action Plan for the implementation of this Strategy, as well as Government Decision No. 594/2018 on the National Strategy for Green Jobs for the period 2018–2025. In our opinion, it is necessary to update Romania's industrial policy for the 2030 perspective, by updating the regulations on the bio economy as well as those contained in the law on green public procurement by including references on the circular economy.

However, in addition to the regulatory issues, we consider that for Romania, the structural and cohesion funds are important for the implementation of the concept of efficient use of resources and the concept of green economy. That is why the proposal for the new post-2020 multiannual financial framework is an opportunity, aiming at an 8% increase in cohesion funds in the future multiannual budget (respectively, from 25.2 billion euros in the period 2014–2020 to 27.2 billion euros for the period after 2020).

Certainly, the consideration of introducing new lines of financing for the green economy is an important step and a clear signal of political commitment at the national level.

### 4. Final Conclusions

It is a reality that, during periods of economic growth more resources and energy are consumed and more waste is produced, affecting the environment. Ideally, obtaining a higher economic value from a limited quantity of natural resources should generate a significantly higher economic growth than the percentage of the use of national resources. This resource efficiency is a topic related to the ability to generate cost savings and implement new technologies that are able to streamline economic processes.

This approach goes beyond the scope of environmental protection and becomes a holistic issue in synergy with industrial policy, competitiveness policy, research and innovation but also with education. The green economy can also be associated with the sharing economy, with peer-to-peer and mesh

economy, as well as with no-growth economy, as a policy strategy for responding to the limits of economic growth correlated with the decrease of natural resources.

In view of such issues, this paper seeks to provide some answers to the conceptual interrelationships between the green economy, green growth and sustainable development, through a harmonious blend with developments in the green economy at international, European and national levels. In order to better promote the green economy in Romania, we tried to advance some policy recommendations related to certain sectors.

The green economy is closely linked to the circular economy and increasing competitiveness, bringing with it not only benefits but also challenges for all stakeholders. In our opinion, the optimal use of natural resources also implies the existence of an electronic data transfer and reporting system based on an efficient infrastructure collection. Moreover, identifying sustainable solutions for optimizing resource consumption is an important goal at European level.

Developing collaborative partnerships and new sustainable business models that promote the efficient use of natural resources can also be the key to a green national economy. A positive signal that can be sent to the economic environment also aims to encourage the development of new skills as well as to consult stakeholders in promoting the transfer of human capital taxation to the taxation of natural resource consumption.

The green economy can determine opportunities for green and sustainable development, an aspect that implies an active involvement at the level of public policy and at the level of implementation in the territory. We have shown that, for the construction of a national model of green economy, the existing good practices at international and community level play an essential role.

We also consider other important issues as being important, such as the increase of decision-making transparency and the involvement of stakeholders through direct access to data and information, so that the creation of an electronic platform for industrial symbiosis could contribute as an example of good practice. At the same time, for the implementation of the green economy, a firm political commitment on several levels is required. In other words, a central coordination and an involvement of all public authorities and the private environment are necessary.

**Funding:** This research received no external funding.

## References

1. Kahle, L.R.; Gurel-Atay, E. *Communicating Sustainability for the Green Economy*, 1st ed.; Sharpe, M.E., Ed.; Routledge: New York, NY, USA, 2014; pp. 22–24.
2. Grima, S. Eleftherios Thalassinou. In *Contemporary Issues in Business and Financial Management in Eastern Europe*; Contemporary Studies in Economic and Financial Analysis; Emerald Publishing House: Bingley, UK, 2018; Volume 100, pp. 1–141.
3. Loiseau, E.; Saikku, L.; Antikainen, R.; Droste, N.; Hansjürgens, B.; Pitkänen, K.; Leskinen, P.; Kuikman, P.; Thomsen, M. Green Economy and Related Concepts: An Overview. *J. Clean. Prod.* **2016**, *139*, 361–363. [[CrossRef](#)]
4. Barbier, E.; Markandya, A. *A New Blueprint for a Green Economy*; Routledge: New York, NY, USA, 2013; pp. 141–145.
5. Pollin, R.; Garrett-Peltier, H.; Heintz, J.; Hendricks, B. *Green Growth: A U.S. Program for Controlling Climate Change and Expanding Job Opportunities*, Center for American Progress; Center for American Progress and Political Economy Research Institute, University of Massachusetts: Amherst, MA, USA, 2014; p. 2.
6. Albekov, A.U.; Parkhomenko, T.V.; Polubotko, A.A. *Green Economy: A Phenomenon of Progress and a Concept of Environmental Security*; Contemporary Studies in Economic and Financial Analysis; Emerald Publishing Limited: Bingley, UK, 2018; Volume 100, pp. 51–59.
7. Scott, M. *Green Growth 'Tigers' Can Help The Global Economy To Roar Once More*; Forbes Media LLC: New York, NY, USA, 2020; pp. 3–5.
8. Galli, A.; Wackernagel, M.; Iha, K.; Lazarus, E. *Ecological Footprint: Implications for Biodiversity*; Biological Conservation; Elsevier: Amsterdam, The Netherlands, 2014; Volume 173, pp. 121–132.



9. Bina, O. The Green Economy and Sustainable Development: An Uneasy Balance? Environment and Planning C: Politics and Space. *SAGE J.* **2013**. [[CrossRef](#)]
10. Vinuesa, R.; Azizpour, H.; Leite, I.; Balaam, M.; Dignum, V.; Domisch, S.; Felländer, A.; Langhans, S.D.; Tegmark, M.; Nerini, F.F. The role of artificial intelligence in achieving the Sustainable Development Goals. *Nat. Commun.* **2020**, *11*, 233. [[CrossRef](#)] [[PubMed](#)]
11. Kajcsa, A. The Influence of Compliance with Environmental Requirements on Commercial Competition. *Curentul Jurid. Jurid. Curr. Courant Jurid.* **2011**, *44*, 143–150.
12. Dalhammar, C. *Promoting Energy and Resource Efficiency through the Eco-Design Directive*; Scandinavian Studies in Law: Stockholm, Sweden, 2014; pp. 162–176.
13. Stahel, W.R. *The Performance Economy*, 2nd ed.; Palgrave MacMillan: London, UK, 2010; 350p.
14. Howels, G.; Ramsay, I.; Wilhelmsson, T. *Handbook of Research on International Consumer Law*, 2nd ed.; Edward Elgar Publishing: Cheltenham, UK, 2016; pp. 7–12.
15. Sharma, H.B.; Vanapalli, K.R.; Cheela, V.S.; Ranjan, V.P.; Jaglan, A.K.; Dubey, B.; Goel, S.; Bhattacharya, J. *Challenges, Opportunities, And Innovations For Effective Solid Waste Management During And Post COVID-19 Pandemic*; PMC Elsevier Public Health Emergency Collection: Amsterdam, The Netherlands, 2020; Volume 162. [[CrossRef](#)]
16. Diab, F.A.; Molinari, C. Interdisciplinarity: Practical approach to advancing education for sustainability and for the Sustainable Development Goals. *Int. J. Educ. Manag.* **2017**, *15*, 73–83. [[CrossRef](#)]

**Publisher's Note:** MDPI stays neutral with regard to jurisdictional claims in published maps and institutional affiliations.



© 2021 by the author. Licensee MDPI, Basel, Switzerland. This article is an open access article distributed under the terms and conditions of the Creative Commons Attribution (CC BY) license (<http://creativecommons.org/licenses/by/4.0/>).

Article

# About Sustainability between Responsible Production and Consumption <sup>†</sup>

Lucreția Dogaru

Department of Law and Public Administration, Faculty of Economics and Law, University of Medicine, Pharmacy, Sciences and Technology “G.E. Palade” of Tg-Mureș, 540142 Tg-Mureș, Romania; lucretia.dogaru@umfst.ro

<sup>†</sup> Presented at the 14th International Conference INTER-ENG 2020 Interdisciplinarity in Engineering, Mureș, Romania, 8–9 October 2020.

Published: 28 January 2021

**Abstract:** The concept of sustainable production and consumption is not only a complex one, but it is also one of great topicality and importance. It aims at the use of goods and services that meets basic needs and contributes to improving people’s living standards, correlated with reducing the use of natural resources and toxic materials as well as waste and polluting emissions during the lifecycle of products, in a way that is appropriate to the present generation’s needs but does not harm the needs of future generations. The current challenges of humanity have justified and determined a change in the way that goods are produced and consumed. Thus, it is necessary not only to create added value but also to reduce the use of natural resources related with reducing costs and minimizing the impact on the environment. In other words, we will have to do more and better with fewer resources. In the current national and European context, the integration of sustainable development objectives at the center of economic activities involves changing production and consumption standards. Starting from this reality, we will address in this paper the role that the promotion of sustainable production and consumption models has. We will also emphasize the role of European policy in promoting inclusive and sustainable industrialization as well as encouraging innovation.

**Keywords:** sustainable production; natural resources; sustainable consumption; eco-innovation

---

## 1. Considerations Regarding the Idea of Sustainable Consumption and Production

The modern world faces challenges that justify and determine changes in the production and consumption of goods. This context not only imposes the creation of more value but also demands the rational use of natural resources, conjugated with cost reduction and the attenuation of the overall impact on the environment.

It has been proven that efficient production processes, when associated with performant environment management systems, may result in a significant drop in waste and overall pollution, thus facilitating the conservation of natural resources while allowing enterprises to cut back on both exploitation costs and their dependence on raw materials.

The concepts of consumption and production are fundamental notions in the economy. Every time production and consumption become durable, economic growth dissociates from climate change.

On one hand, such a perspective includes the awareness of limited resources, and on the other hand, it involves applying sustainable measures that can safeguard a similar context to future generations. Obviously, this approach is meant to encourage more responsible conduct in the process of creating more efficient production and durable management of waste as a result of activities that must be consistent with the principles of environmental protection.

Consequently, the concepts of durable production and consumption are so intricate that they concern the use of goods and services that is in agreement with basic needs. Correlated with the

reduction in the use of natural resources, toxic materials, waste, and hazardous discharge in a sustainable manner, it contributes to the improvement of the living standards of the population.

Doubtless, approaching production and consumption in a durable manner, from the perspective of product management, concerns every domain, starting with the natural resources that are being used and continuing with the design stage, the manufacturing process, marketing, shipment, sale, and the use of the resulting waste.

The decrease in the impact of the production of goods may be accomplished through ecological design and eco-innovation. These two methods significantly contribute to the betterment of the ecological performance of products during their entire life cycle and to the increase in requests for more performant production technologies.

While our general consumption (which is composed of food, means of transport, housing, and other goods) is capable of generating negative impacts on resources and the quality of the environment, people could contribute by making the right choices when deciding what they consume. It has been proven that improving construction and the use of buildings could reduce the final energy and water consumption by 40%. The same thing can be said about GHG emissions.

Even if responsible production and consumption is considered able to ensure sustainability, at the doctrine level, this idea has generated controversial debates [1] (pp. 257–265). However, it has gradually become a social objective that is generally accepted on a global and on a regional level, despite the fact that a unanimous implementation is quite difficult [2] (pp. 93–94).

In Europe, the quantification of the current state of sustainable production and consumption is done through classical indicators of sustainable production and consumption (such as the consumption of materials and energetic intensity) as well as through emerging approaches (for example, green GDP (Green Gross Domestic Product, which represents an economic growth index that takes into account the consequences on the environment of that growth factored into a country's conventional domestic product), carbon footprint, and ecological footprint [3] (pp. 121–124)). Taking these into account, authorities and institutions with prerogatives of measuring economic performance and social progress have been set up (for example, the economic Stiglitz Commission made, in 2009, many recommendations aimed at detaching economic growth from the consumption of natural resources, recommendations that focused on the impact that green GDP can have in this regard).

Sustainable production and consumption pursues important objectives such as the implementation of a 10-year framework of programs for sustainable consumption and production models; the achievement of sustainable and efficient management and use of natural resources by 2030; the reduction by 50% of consumer-level food waste by 2030 [4] and reducing food loss in the production and supply processes; the achievement of ecological management of hazardous substances and workers while significantly reducing emissions; imposing the adoption of sustainable practices upon large and transnational companies, as well as making these companies integrate information regarding sustainability into the reporting cycle; promoting durable public acquisition practices.

An essential pillar of this process is eco-labeling, which can help consumers make informed choices about products and services. In this context, the European Union's eco-label policy aims to identify products and services that have a low impact on the environment throughout their life cycle. Of course, the role of public authorities in greening the economy of the community space is important and necessary. Thus, government spending on market sustainability has reached around 20% of the Union's GDP. We are convinced that by investing in green projects, public authorities have the opportunity to help increase the demand for more efficient products and services in terms of the use of natural resources.

Definitely, integrating sustainable development objectives at the core of economic activities involves changing production and consumption patterns. Surely, such a change can only take place through regulations and legal decisions, through appropriate tax measures, and with the aid of public requests. At the same time, an essential aspect of the approach of sustainable production and consumption is the accountability of the business environment and the awareness of civil society.

Public strategies and policies in the field must include the concept of sustainable production and consumption, with the involvement of both the productive branch and the services, in other words, with the contribution of the business environment.

A different approach in the way we produce and consume, namely the transition from unsustainable production and consumption to sustainable production and consumption, is a process that involves the following directions: reinforcement of the business environment's access to various tools towards sustainable production and consumption; making the business environment responsible for promoting and supporting sustainability; civil society awareness of the demand for products and services that are designed in accordance with sustainable production and consumption models.

Promoting sustainable production and consumption patterns and improving management and avoiding the overexploitation of natural resources while recognizing the value of ecosystem services are two important objectives of the EU's 2020 Sustainable Development Strategy. At the Romanian national level, the National Strategy for Sustainable Development, entitled "Horizons 2013–2020–2030", identified a series of medium- and long-term solutions with reference to sustainable production and consumption. These solutions are aimed at reducing the material consumption of natural resources in order to dynamically disconnect GDP from the material consumption of resources and energy and to reduce the impact on the environment.

The main guiding targets of the "Europe 2020" strategy for achieving energy and climate change targets are a 20% increase of the contribution of renewable sources in the total energy balance, a 20% decrease in GHG emissions, and a 20% improvement in energy efficiency.

The revised European Union Strategy for Sustainable Development aims to develop and identify actions to enable the European Union to improve quality of life by creating sustainable communities capable of managing and using resources efficiently while exploiting the potential of eco-innovation and the social development of the economy, with the purpose of ensuring prosperity, environmental protection, and social cohesion. The main objectives are the following: the conservation of biodiversity and compliance with the limits of natural resources while ensuring a high level of protection and improvement of the quality of the environment; prevention and reduction of environmental pollution, as well as the promotion of production and consumption in the spirit of sustainable development, in order to break the link between economic growth and environmental degradation; promoting a prosperous, innovative, rigorous, competitive, and eco-efficient economy [5] (pp. 11–20).

## **2. The Role of Ecolabeling, Energy Labeling, and Eco-Design in the Sustainable Use of Natural Resources and in Promoting Responsible Consumption**

An important pillar of this process is represented by eco-labeling (Regulation (EC) No 66/2010 of the European Parliament and of the Council, of 25 November 2009, on the EU Ecolabel, consolidated in November 2017), an approach able to provide a lot of information that can help consumers make informed choices about products and services. In other words, eco-labeling represents a modality of reducing the information gap between consumers and producers [6] (p. 2202). With eco-labeling, a good or a service is supposed to be green, and this implies a higher price for consumers, compared to a non-ecological good or service. It has been demonstrated that a conscious consumer (someone with a stronger ecological attitude) will usually demand ecological goods and services. On the other hand, consumers especially concerned about prices will demand less ecological goods and services. Therefore, the demand for environmentally friendly goods and services is conditioned by consumer awareness and declines for those categories of consumers oriented towards prices. Consumers of eco-labeled products prefer a subsidy for organic goods and services and a tax for non-ecological goods and services. Usually, consumers oriented only according to the price criterion will not take into account the environmental subsidy and they will be against taxes on non-ecological goods and services.

We believe that an important key to market uptake is represented by the sustainable communication related to the environmental benefits of bio or green products and services. In this regard, the use of ecolabels, in its new version of ISO 14024 Environmental labels and declarations—Type I environmental

labelling, is relevant (ISO 14024 Version 2018 was developed by technical committee ISO/TC 207, Environmental management, subcommittee SC 3, Environmental labelling). This document establishes the main principles and procedures for developing Type I environmental labeling programs, as well as the selection of product categories, product environmental criteria, and characteristic functions, and for assessing and demonstrating compliance with requirements. It also establishes the certification procedures for awarding an ecological label [7].

We recall in this context that the eco-label introduced by the European Union aims to identify those types of products and services that generate less impact on the environment throughout their life cycle. The eco-labeling criteria are established and reviewed periodically by the European Union Eco-Labeling Committee (EUEB) (European Commission Decision of 22 November 2010 establishing the European Union Ecolabelling Board (2010/709/EU)), which has related assessment and verification tasks. Of course, these criteria are based on studies to analyze the impact that certain products or services have on the environment.

Introduced in 1995, the EU Energy label has gradually become an important guide for producers and consumers. This Energy Labeling Directive was revised by Directive 2010/30/EU with a view to extending its scope to a wider range of products, including energy-using products and other categories of energy products. Thus, in 2015, the European Commission proposed a return to a single product labeling scale, from “A to G”. As a consequence, during 2017, the Regulation (EU) 2017/1369 was adopted for the purpose of establishing a new framework for energy labeling, as well as for repealing the provisions of Directive 2010/30/EU (Regulation (EU) 2017/1369 of the European Parliament and of the Council of 4 July 2017, setting a framework for energy labeling and repealing Directive 2010/30/EU, was published in Official Journal of the EU, L 198/28 July 2017, pp. 1–23). The revised EU Regulation simplifies and updates the energy efficiency labeling requirements for all kinds of products sold in the European Union. Starting with these new regulations, all products will be labeled on a new, updated, and much clearer scale, namely, from energy scale A (which is the most efficient) to the energy scale G (which is the least efficient). Under this new system, the system of A+++ to G labels will be gradually replaced as a result of the development of more energy-efficient products, in order to allow the consumers to clearly distinguish the most energy-efficient items. In this context, new energy labeling requirements have been created for specific product groups. Specifically, starting in 2021, five product groups will be reclassified, taking into account energy efficiency (these product groups include refrigerators, dishwashers and washing machines, televisions and lamps) [8] (pp. 1888–2000). Based on these provisions, a product belonging, for example, to the highest energy-efficiency class (A+++ ) will move to the class B after reclassification, but without any kind of change in its energy consumption. Moreover, although class A will remain empty at the beginning, it will later include more energy-efficient models. It is believed that such a procedure will allow consumers more clearly distinguish the most energy-efficient products. In the last period, the increased use of energy from renewable sources will also play a fundamental role in promoting sustainable energy, technological development, and innovation as well as technological and industrial leadership, providing at the same time a lot of environmental and social benefits. Such classifications justify the Directive (EU) 2018/2001 of the European Parliament and of the European Council of December 2018 regarding the promotion of the use of energy from renewable sources [9] (pp. 399–400).

Another tool with relevant implications in responsible production and consumption is represented by ecological design. This can be defined as any form of design that minimizes negative impacts on environmental factors and that puts the ecology in the foreground [10]. Its main role is to optimize the environmental performance of products by maintaining their functional qualities and providing new opportunities for producers, consumers, and society.

Taking into consideration that the eco-design of products represents a crucial factor in the Community strategy on Integrated Product Policy at the European level, the Directive 2005/32/EC on Eco-design was adopted to ensure the technical improvement of products. This document represents

an important regulation that establishes the framework for eco-design requirements for energy-using products [11].

It should be noted that, with the European Directive revision through Directive 2009/125/EC (Directive 2009/125/EC of the European Parliament and of the Council of 21 October 2009, establishing a framework for the setting of eco-design requirements for energy-related products, consolidated in December 2012), its scope was extended to other energy products besides energy-using products, namely products that, while not consuming energy during the use, still have an indirect impact on energy consumption (such as water-using devices or windows).

However, one of the controversial issues that have arisen in this sector is about the relationship between the standards and the taxes required, namely, if there is a balance between them [12].

### **3. Waste Reduction to Support Sustainable Production and Consumption Policies**

In a complex production process, there are many natural resources wasted, some of them limited and others non-renewable. This creates major pressures on the environment, especially the fact that some wastes are returned to nature, often in proportions that exceed the possibility of the environment to recycle them. For such reasons, waste has recently become a major environmental problem, in terms of both quantity and variety but also in terms of hazards [13]. More and more, at globally level, attention has been drawn to the increasingly alarming rates of waste and their contributions to the depletion of natural resources and rise in greenhouse gas emissions. Within the last ten years, the discovery of the rippling impacts of this interrelationship has generated increased urgency in efforts amongst global leaders, materialized in comprehensive plans and goals in addressing and reducing the rates of global waste. Waste lessens the quantity of available resources but also the availability of the many natural resources required to produce goods. This will certainly become an important factor as the entire world population will increase by more than 30% by the year 2050. For example, at present, approximately 1.4 billion tons of food are wasted every year due to various causes and challenges, which represents an increase in the usage of natural resources. In the EU, food and agriculture consume up to 15% of energy and account for 62% of freshwater use. The rate of natural resource depletion is not sustainable, and it endangers the ecosystem, involving both negative environmental consequences and the necessity of sustainability-compliant actions.

In this regard, many recommendations have been taken for primary production, manufacturing, and retail stages and for food services and consumer services (EC.2020: Communication from the Commission to the European Parliament, the Council, the European Economic and Social Committee and the Committee of the Regions; A Farm to Fork Strategy for a Fair, Healthy and Environmentally Friendly Food System, COM (2020) 381 Final). For example, the EU Platform on Food Losses and Food Waste has set many recommendations, which are common across various stages of the food value steps and are needed to achieve the global food loss and waste targets. The recommendations are addressed to both public and private entities, suggesting cooperation amongst the different actors concerned, to prevent food losses and food waste, as well as to provide important direction for all players, including European citizens.

Limiting food losses has been identified as representing an essential means of increasing food security while also reducing pressure on the natural resources of the environment. According to statistical data, in Romania, almost 25% of national food production is estimated to be lost or wasted. It is also estimated that each citizen throws away foods around 200 € per year.

At the European level, improving the food supply chain efficiency has also been identified as an important means to enhance food security and is correlated with reducing pressure on natural resources. However, these situations can be among the most unpredictable and difficult to manage for various reasons.

It is worth remembering that, due to the exceptional lockdown measures imposed by the Romanian government as a consequence of the emergence in this year of coronavirus pandemic, COVID-19, food production and consumption systems have undergone significant changes, which categorically

require urgent and effective plans and strategies. Statistics show that during the first weeks of the COVID-19 lockdown, there was no significant food loss on waste generation, but it increased by about 10% the reallocation of extra-domestic households' consumption. These measures, correlated with the economic impact (around +10%) and gas emissions (around +8%), complete the profile that the pandemic COVID-19 had on food loss waste generation and their management.

#### **4. Infringement Procedures as a Means towards Sustainable Development**

The European Commission published its July infringement package with some cases (on biodiversity, nuclear safety, energy efficiency, etc.) that show that some Member States (Romania, Croatia, Ireland, Spain) are not doing enough, especially in relation to sustainability.

In this context, the Commission is calling on Romania to combat illegal logging and better protect forests in its Natura 2000 sites. The European Commission is urging Romania to properly implement the European Union Timber Regulation (Regulation (EU) No. 995/2010 of the European Parliament and Council of 20 October 2010, laying down obligations of operators who place timber and timber products on the market, published on Official Journal of the European Union, L 295/2010, pp. 23–33), which forbids producing and placing on the European Union market products made from illegally harvested logs. European Commission shows that the Romanian authorities have been unable to effectively check the economic operators and to apply appropriate legal sanctions. It is also mentioned that the inconsistencies existing in national legislation do not allow Romanian authorities to check large amounts of illegally harvested timber. In addition, the Commission found that the Romanian authorities manage forests, including by authorizing logging, without evaluating beforehand the impacts on protected habitats as required under the Habitats Directive and Strategic Environmental Assessment Directives. The European Commission points out that if Romania does not act within one month, it will be able to refer the case to the Court of Justice of the European Union.

#### **5. Conclusions**

We consider that the role of public authorities in greening the economy of the communitarian space is an important and necessary one. This explains why the entire government spending on market sustainability has reached around 20% of the Union's GDP (High-Level Expert Group on sustainable finance (HLEG), Final Report 2018 by the High-Level Expert Group on Sustainable Finance Secretariat provided by the European Commission, Financing a Sustainable European Economy). We are also convinced that, by investing in green projects, public authorities will have the opportunity to contribute to increasing the demand for more efficient products and services in terms of sustainable use of natural resources.

The integration of sustainable development objectives at the center of economic activities involves changing production and consumption patterns. Of course, such a change could take place only through regulations and legal decisions as well as through appropriate tax measures. At the same time, an essential aspect of approaching sustainable production and consumption is the responsibility of the business environment and the awareness of civil society. Public strategies and policies in the field must include the concept of sustainable production and consumption, as well as involvement from the production and services sides, namely, from the business environment.

The change of attitude in the way of producing and consuming and the transition from unsustainable to sustainable production and consumption is a complex process that involves the following directions (United Nations 2019. Sustainable Development Goal 12: ensure sustainable consumption and production patterns. United Nations. Retrieved from <https://sustainabledevelopment.un.org/sdg12>): accountability of business environment to various tools towards sustainable production and consumption and awareness of civil society to have products and services designed according to sustainable production and consumption models.

In conclusion, to achieve sustainable production and consumption, a systems and life cycle approach is necessary, taking into consideration all economic, environmental, and social concerns of



the stakeholders. In order to facilitate this complex process, new decision-support frameworks have been developed that are able to incorporate such an approach. These frameworks include many tools regarding strategy analysis, life cycle costing and life cycle assessment, social sustainability assessment, and system optimization.

## References

1. Fontenelle, I.A. Global Responsibility through Consumption Resistance and assimilation in the anti-brand movement. *Strateg. Dir.* **2011**, *27*, 256–272. [CrossRef]
2. Azapagic, A.; Stamford, L.; Youds, L.; Barteczko-Hibbert, C. Towards sustainable production and consumption: A novel DEcision-Support Framework IntegRating Economic, Environmental and Social Sustainability. *Comput. Chem. Eng.* **2016**, *91*, 93–103. [CrossRef]
3. Galli, A.; Wackernagel, M.; Iha, K.; Lazurus, E. Ecological Footprint: Implications for biodiversity. *Biol. Conserv.* **2016**, *173*, 121–132. [CrossRef]
4. Kajcsa, A. Liability and responsibility of local public administration authorities in the field of waste management. Theoretical and practical study. *Jurid. Curr.* **2019**, *79*, 31–36.
5. Garcia-Herrero, I.; Hoehn, D.; Margallo, M.; Laso, J.; Bala, A.; Batlle-Bayer, L.; Fullana, P.; Vazquez-Rowe, I.; Gonzalez, M.J.; Durá, M.J.; et al. On the estimation of potential food waste reduction to support sustainable production and consumption policies. *Food Policy* **2018**, *80*, 24–38. [CrossRef]
6. Lewinson, A. Energy Efficiency Standards Are More Regressive Than Energy Taxes: Theory and Evidence. *J. Assoc. Environ. Res. Econ.* **2019**, *6*, S7–S36.
7. Dogaru, L. *The Relationship between Environmental Protection and Economic Growth from the Perspective of Sustainable Development*; Current Issues in Business Law; ADJURIS: Bucharest, Romania, 2018.
8. Wunderlich, S.M.; Martinez, N.M. Conserving natural resources through food loss reduction: Production and consumption stages of the food supply chain. *Int. Soil Water Conserv. Res.* **2018**, *6*, 331–339. [CrossRef]
9. Costa, I.; Massard, G.; Agarwal, A. Waste management policies for industrial symbiosis development: Case studies in European countries. *J. Clean Prod.* **2010**, *18*, 815–822. [CrossRef]
10. Schumacher, I. Ecolabeling, consumers' preferences and taxation. *Ecol. Econ.* **2010**, *69*, 2202–2212. [CrossRef]
11. van der Rhyn, S.; Cowan, S. *Ecological Design*, 10th ed.; Island Press Publisher: Washington, DC, USA, 2013.
12. Wurster, S.; Ladu, L.; Arisaktiwardhana, D. Bio-Based Products: Suggestions for Ecolabel Criteria and Standards in Line with Sustainable Development Goals. *Int. J. Stand. Res.* **2019**, *17*, 23–39. [CrossRef]
13. Mahlia, T.M.I.; Saidur, R. A review on test procedure, energy efficiency standards and energy labels for room air conditioners and refrigerator-freezers. *Renew. Sust. Energy Rev.* **2010**, *14*, 1888–1900. [CrossRef]

**Publisher's Note:** MDPI stays neutral with regard to jurisdictional claims in published maps and institutional affiliations.



© 2021 by the author. Licensee MDPI, Basel, Switzerland. This article is an open access article distributed under the terms and conditions of the Creative Commons Attribution (CC BY) license (<http://creativecommons.org/licenses/by/4.0/>).





# Research on Challenges and Prospects of Digital Agriculture <sup>†</sup>

Mihai Anitei <sup>1</sup>, Cristina Veres <sup>2,\*</sup> and Adrian Pisla <sup>3</sup>

<sup>1</sup> Department of Management and Economic Engineering, Faculty of Machine Building, Technical University of Cluj-Napoca, 400114 Cluj-Napoca, Romania; mihai.anitei@yahoo.com

<sup>2</sup> Department of Industrial Engineering and Management, Faculty of Engineering and Information Technology, George Emil Palade University of Medicine, Pharmacy, Science and Technology of Târgu-Mureș, 540139 Târgu-Mureș, Romania

<sup>3</sup> Department of Design Engineering & Robotics, Faculty of Machine Building, Technical University of Cluj-Napoca, 400114 Cluj-Napoca, Romania; adrian.pisla@muri.utcluj.ro

\* Correspondence: cristina.veres@umfst.ro

<sup>†</sup> Presented at the 14th International Conference INTER-ENG 2020 Interdisciplinarity in Engineering, Mureș, Romania, 8–9 October 2020.

Published: 19 January 2021

**Abstract:** The actual pandemic context highlighted once again the huge importance of agriculture in the society and create a path to a speeded-up digitalization. As soon as the virus crisis will end, countries will start reprioritizing their values and do investments accordingly; agriculture will regain focus. In order to get an overview image on the challenges and farmers needs in agriculture in the context of digitalization, a questionnaire-based research was made, collecting data from Romanian experienced farmers and business experts in agriculture.

**Keywords:** digital agriculture; farming; digitalization; farmers' challenges; EU green deal

## 1. Introduction

Agriculture plays an important role in providing food security and sustainability for the people in any country [1]. In the same time, nowadays agriculture faces several important challenges and limitations. In the latest decades, innovation significantly contributed to facilitate the fieldwork and to increase productivity.

As digitalization is impacting each component of our lives, different forms of digitalization started to be introduced in agriculture like: sensors, IoT (internet of things), big data, 3D printing, artificial intelligence, digital twins, augmented reality, system integration and the list may go on.

The aim of the research work is to identify the challenges and the prospects of agriculture in the context of digitalization, in the experts' and farmers' view. The data was collected from 19 experienced farmers and business experts in Romania within the month of August 2020. Of our best knowledge, this is the first research on Digital Agriculture, organized in Romania after pandemic Covid-19 expansion, whose effects can be considered key drivers to a future accelerated digitalization.

This research starts with a presentation of the actual global challenges that agriculture faces and a brief description of the Romania's agricultural profile. Then there are presented the questionnaire details and findings.

## 2. Digital Agriculture: Challenges and Prospects

### 2.1. Global Agriculture Challenges

Speaking about agriculture, we can't ignore the influence and impact of current global trends which are shaping the world development, as well as their inter-dependence: population growth,

urbanization process, population aging, climate change, economies' digitalization, advancement of globalization and liberalization processes. These trends may contribute in changing the pattern of agriculture and agri-food system and stimulating innovation capacity in the coming years [2].

One of the main challenges of tomorrow's agriculture is the growth of the population.

According to World Population Prospects, United Nations' projected in 2019 that the world's population would grow from 7.7 billion in 2019 to 8.5 billion in 2030, 9.7 billion in 2050 and 10.9 billion in 2100 [3].

How will be ensured the satisfaction of a vital physiological need of such rapid growth, providing food security for another two billion people in the next 30 years?

Because of the rural poverty, the lack of jobs and poor infrastructure the share of the urban population has grown steadily in recent decades. Together with the population aging, this will have an influence on food consumption behavior and may lead to issues related to logistics, which will need a rigorous planning.

Worldwide there is a movement towards more sustainable systems.

By now, the use of irrigation, fertilizers and expansion of agricultural land has made possible to face the rapid growth of population. Nevertheless, we should take into account the intensification of soil use, the deforestation, the land degradation, the water pollution, land losses by erosion, desertification, salinization, the rise of the sea level and other issues, which cumulated rise up new challenges to the long-term agricultural productivity.

The process of globalization, the free movement of goods, capital concentration, services availability, technology and information, influences the dynamic of agriculture. Increased investments in agriculture, the development of the food industry and the growth of the international trade of food are all effects of globalization and liberalization. The current pandemic caused a slowdown in the globalization process and people focused their attention to the local markets, at least for a determined period of time.

Digitalization, the socio-technical process of applying digital innovations, is an increasingly ubiquitous trend. Digitalization comprises phenomena and technologies such as big data, internet of things (IoT), augmented reality, robotics, sensors, 3D printing, system integration, ubiquitous connectivity, artificial intelligence, machine learning, digital twins and blockchain among others [4–7]. Digital technologies and new data analysis using artificial intelligence will influence each stage of the agri-food chain: primary production, processing, distribution, consumption.

Today, drones allow seeds planting in areas where tractors and people do not have access, thus erasing without trace specific limits in agriculture. New technologies can plant, irrigate soil according to its parameters, obtain real-time information about the state of crops, identify weeds and diseases, do pesticides application and precision harvesting, analyze data and take action.

## 2.2. Digital Agriculture in Romania

According to an analysis performed by professional services firm PwC, Romania is one of the European countries with the highest potential in agriculture, with the sixth biggest used agricultural area in EU, but with a low productivity due to several factors [8].

The country presents a huge development potential for Digital Agriculture, based on a series of facts and advantages.

Romania poses an important agricultural profile, rich soil, good environmental conditions, old tradition of working the land, ultra-high speed of internet (Romania has the 5th fastest internet in world, according to World Population Review, 2020 [9]), existence of highly appreciated IT specialists and software developers are all strong arguments to sustain its' agricultural digitalization potential. On the other hand, the predominantly small-farm structure of the country, fragmented land ownership and low levels of mechanization are palpable barriers to rapid system shift [10].

Globally, digitalization and Industry 4.0 will contribute to speed up innovations in agricultural field. It's a matter of time to reach up a new level of agricultural development in Romania.

### 2.3. Challenges and Prospects of Digital Agriculture in Farmers' View

In analyzing the challenges, it is important and interesting to notice how agriculture is seen in farmers' eyes in the context of digitalization, what limits and challenges do they face and what opportunities and future development they foreseen. To find out, a questionnaire survey, as one of the qualitative methods, was created and distributed. The questionnaire was sent online to targeted Romanian farmers and the collected data was analyzed.

Within the elaborated investigation to the questionnaire session participated 19 respondents from several counties of Romania, of which 17 farmers of small, medium and big farms and 2 business experts. The envisaged regions are: Călărași (CL), Olt (OT), Dolj (DJ), Suceava (SV), Iași (IS), Ialomița (IL), Tulcea (TL), Mureș (MS) and Ilfov (IF) (see Figure 1).

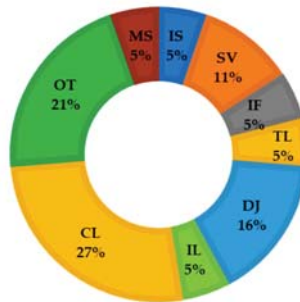


Figure 1. Distribution of respondents by county.

The questionnaire was formed of 4 identification questions and 9 open questions related to the digital agriculture.

From the survey 100% of the participants agreed that digitalization is an opportunity for their activity; none of them consider digitalization a threat. Digitalization in farmer's view is a real help, which will lead to maximum efficiency in the carried-out activity.

Participants were asked the express terms associated to Digital Agriculture. Most of them mentioned "indispensable" (26.3%), "efficiency" (26.3%) and "necessity" (21.1%), but also "future", "help for farmers", "evolution", "yield", "profitability", "development" and "maximum potential".

When they were asked about how they see digital agriculture today and in future all the participants gave a good feedback, and hereby are some relevant answers:

- Digital agriculture today is a delicate subject for Romanian farmers due to the costs. Only large farms can afford these costs. Today, everyone knows the benefits of digital systems, but very few have been able to financially support these investments.

In the future, I believe that digitalization must not be missing from any farm in order to be profitable;

- Today, it helps increase farm yield, helps the farmer decide when and how much to apply. In the future, we hope that digital agriculture can be put into practice on a larger scale;
- Digital agriculture is the tool that helps reaching the maximum of the production potential in conditions of economic efficiency;
- Digital agriculture will completely change the relationship between the farmer and the other players in near future.

When speaking about challenges and limits they face, 41.2% of the respondents claimed the lack of qualified staff, 31.6% mentioned the lack of financial funds, and 21.1%-the digitalization costs.

Figure 2 presents the Pareto chart of the mentioned challenges, distributed in descending order of their percentage.

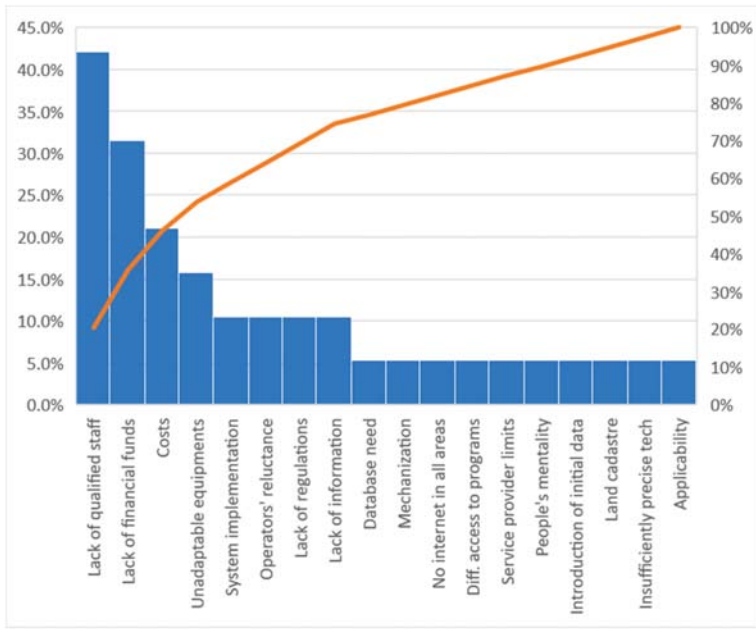


Figure 2. Challenges met by respondents.

An analysis on challenges and limits of digital agriculture wouldn't be complete without finding out what would help farmers to overcome the identified obstacles.

Here is what was found to be useful to speed up the digitalization in their activities:

- More information in this regard;
- Specialization courses and trainings in its use;
- Demo periods would be helpful;
- Friendlier interfaces;
- Easier access to digital farming programs;
- Targeted funds;
- Government investments;
- High quality services;
- Lower costs;

Expanding the number of respondents to the questionnaire would bring more value to the research and contribute to an improved overview.

### 3. Research and Methods

The bibliographical study method was used to study recent specialty literature, deepen knowledge and gain a good understanding of the field.

The questionnaire survey, as one of the qualitative methods, was used in the research. The questionnaire was sent to targeted people and the obtained data was analyzed.

The purpose of this research was to get an overview image of the challenges and prospects of digital agriculture, by collecting and analyzing data obtained from Romanian farmers and agricultural

experts. The aim of the research is to progress in the direction of the EU Green Deal that will mobilize the research and innovation potential to foster sustainable societal transition and to create a Project with visible results from research and innovation activities that can provide clear solutions for a better governance of the green and digital transition, social and value chain innovation. The actual research and the future Project, being anchored in the present pandemic situation, must help to the green and digital recovery, increasing societal resilience in agriculture.

Within the Green Deal, to agriculture is addressed a special call, the call no 6 “Farm to Fork: testing and demonstrating high impact innovations to address food system challenges in a place-based context.”, which aims to transform European food systems into a global standard for sustainability and find solutions to actual challenges.

The envisaged Project will be targeting the value chain components impact for the fertilizers’ and harmful nutrients’ reduction towards zero pollution by applying digital solutions within a demonstration pilot scenario, focused on three aspects:

- Align the three sustainability’s dimensions:
  - economic;
  - climate/environment;
  - social/health.
- Maximize synergies;
- Address to a specific challenge: to develop an appropriate mix of innovations.

As final scope can be considered the pilot demonstrating solution at TRL5 level (Technology Readiness Level) focused on systemic innovations that increase resilience of food systems to shock and stresses, considering:

- Reducing the GHG (Green House Gas) emissions and carbon blocking and/or storage;
- Reducing energy use and increasing energy efficiency in processing;
- Reducing the use and increasing the efficiency of fertilizers;
- Moving towards zero pollution by reducing the losses of nutrients from fertilizers;
- Reducing losses and waste, while avoiding unsustainable packaging [11];
- The potential to scale up the solution to national level by 2025 and EU level by 2030, including the presentation of obstacles and the stakeholder’s motivation;
- Identify, explain and quantify, the used KPI (Key Performance Indicators), about how the solution will deliver the expected impact.

#### 4. Conclusions

Agriculture, as one of the main pillars of society’s sustainability, has been shaped by digital era. Big data, internet of things (IoT), augmented reality, robotics, sensors, 3D printing and other high technology is changing the way we are feeding a growing world population.

After conducting a research among Romanian farmers on digital agriculture we discovered the limits and challenges they face, as well as their needs to speed up digitalization. The lack of qualified staff represents the biggest concern and challenge for farmers, as digital equipment and machines requires specific skills and competences. The second most important challenge is related to the lack of financial funds. High technology machines are expensive and difficult to maintain. The lack of funds affects especially small and medium-size farms, which should be extremely profitable to be able to afford expensive systems.

As a solution to these two and other challenges, government investments, specialized training, lower costs, an easier access to digital farming programs, a friendlier interface etc. are considered by farmers helpful to speed up digitalization of their activity.

In conclusion, farmers are aware of the benefits of digital agriculture and do want to digitalize their activities, but some challenges seem to limit them. As the technologization of farms is costly and many farms can't afford such revamping projects, perhaps in addition to the effort of farmers some future supported by authorities' programs could accelerate digitalization.

As a practical pilot demonstrator, the research group is envisaged to provide a Project proposal within the EU Green Deal Pact.

**Author Contributions:** M.A. defined the basic idea and direction of the research, contributed to developing the questionnaire and collecting data, C.V. facilitated the writing of the research, did the analysis of data and enriched the article with relevant bibliographical references and A.P. guided the research, approved the methodology and added valuable input on EU Green Deal Pact. All authors have read and agreed to the published version of the manuscript.

**Funding:** This research received no external funding.

**Conflicts of Interest:** The authors declare no conflict of interest.

## References

1. Anshari, M.; Almunawar, M.N.; Masri, M.; Hamdan, M. Digital Marketplace and FinTech to Support Agriculture Sustainability. *Energy Proc.* **2019**, *156*, 234–238. [CrossRef]
2. Fintineru, G. Tendințe și Perspective Globale în Agricultură. In *Agricultura. Concepte și Instrumente Operaționale. Caiet Documentar 4*; Stoian, M., Aniței, M., Eds.; Editura Club București: București, România, 2019; pp. 35–46.
3. United Nation. Population Facts. December 2019. Volume 6. Available online: [https://www.un.org/en/development/desa/population/publications/pdf/popfacts/PopFacts\\_2019-6.pdf](https://www.un.org/en/development/desa/population/publications/pdf/popfacts/PopFacts_2019-6.pdf) (accessed on 3 August 2020).
4. Klerkx, L.; Jakku, E.; Labarthe, P. A review of social science on digital agriculture, smart farming and agriculture 4.0: New contributions and a future research agenda. *NJAS-Wagening J. Life Sci.* **2019**, *90–91*, 100315. [CrossRef]
5. Alm, E.; Colliander, N.; Lind, F.; Stohne, V.; Sundström, O.; Wilms, M.; Smits, M. *Digitizing the Netherlands: How the Netherlands Can Drive and Benefit from an Accelerated Digitized Economy in Europe*; Boston Consulting Group: Stockholm, Sweden, 2016.
6. Smith, M.J. Getting value from artificial intelligence in agriculture. *Anim. Prod. Sci.* **2018**, *60*, 46–54. [CrossRef]
7. Tilson, D.; Lyytinen, K.; Sørensen, C. Research commentary—digital infrastructures: The missing IS research agenda. *Inf. Syst. Res.* **2010**, *21*, 748–759. [CrossRef]
8. Business Review. Available online: <https://business-review.eu/news/romania-has-significant-potential-in-agriculture-but-low-productivity-says-pwc-romania-study-132113> (accessed on 1 August 2020).
9. World Population Review. Available online: <https://worldpopulationreview.com/country-rankings/internet-speeds-by-country> (accessed on 3 August 2020).
10. Highclere Consulting. Available online: <https://highclere-consulting.com/en/digitalization-in-romanian-agriculture-three-solutions-to-bridge-two-eu-2030-agendas/> (accessed on 5 August 2020).
11. Tiko Pro. Available online: <https://www.tiko-pro.eu/success-stories-details/green-deal-call-area-6-farm-to-fork> (accessed on 5 August 2020).

**Publisher's Note:** MDPI stays neutral with regard to jurisdictional claims in published maps and institutional affiliations.



© 2021 by the authors. Licensee MDPI, Basel, Switzerland. This article is an open access article distributed under the terms and conditions of the Creative Commons Attribution (CC BY) license (<http://creativecommons.org/licenses/by/4.0/>).

# Streamlining the Work Process by Reducing Procedural Times in the Field of Electrostatic Powder Painting †

Jozsef Boer <sup>1</sup> and Petruta Blaga <sup>2,\*</sup> 

<sup>1</sup> SC ALLCOLORS SERV SRL, Parcul Industrial Târgu-Mureş, Platforma Industrială Nr. 1/G/5, 547612 Vidrasău, Romania; calitate@allcolors.ro

<sup>2</sup> Department of Management, “George Emil Palade” University of Medicine, Pharmacy, Science and Technology of Târgu Mureş, 540139 Târgu Mureş, Romania

\* Correspondence: petruta.blaga@umfst.ro; Tel.: +40-077-019-5200

† Presented at the 14th International Conference INTER-ENG 2020 Interdisciplinarity in Engineering, Mureş, Romania, 8–9 October 2020.

Published: 25 January 2021

**Abstract:** Many companies struggle to find the right balance between reducing costs and growing their business. It seems like an impossible equation for some, while for others it is a great challenge. The main purpose of a business is to make a profit, that is, to get money as a result of the investment and the work done. One of the means of reducing costs while increasing productivity is to make improvements based on new ideas. Companies tend to overlook one very important aspect of their daily activities when thinking about cost savings: use the old processes and avoid exploring and investing in one new and more practical solution. Based on this, we offer a tested and implemented solution to increase profits, which can be achieved by reducing the costs of the technological process in the field of electrostatic powder painting employed to give a brief introduction to your work.

**Keywords:** electrostatic power painting; qualitative and quantitative research; optimization; quality; production costs

## 1. Introduction

Electrostatic field painting with powder paint is a process by which a layer of decorative powder paint is applied to a metallic surface to color it and provide protection against the action of external factors. This process takes place in three main stages:

1. Chemical pretreatment—all unwanted factors and agents, foreign bodies and solutions are removed from the surface of the product, preparing it for painting;
2. Painting—the process by which the powder paint is transferred to the product using the electrostatic field created by a special installation;
3. Treatment—the process by which the powder paint is polymerized and stabilized on the surface of the product.

For these reasons, electrostatic powder coating is the most advanced surface treatment available, as it offers the following advantages:

- High adherence [1];
- High hiding power [2];
- High abrasion resistance;
- High wear resistance;



- High resistance to corrosive agents;
- Uniform fine coat of paint [3].

The paper presents the third stage of the electrostatic powder coating process—polymerization. The parts are sprayed with powder paint in the painting phase, hung on the chain of the conveyor in the process, and then are transported and suspended in the polymerization furnace. The time and temperature of polymerization are set depending on the type of powder, the temperature recommended by the paint manufacturer, and the customer's requirements. We work with the following parameters: temperatures between 160 °C and 200 °C, and working times between 7 and 30 min.

Correct polymerization involves setting the appropriate parameters, taking into account the material of which the product is made, the thickness of the material walls, its mass and volume, conveyor speed, polymerization oven capacity, powder paint polymerization performance, and storage space for cooling products after leaving the polymerization furnace.

## 2. Materials and Methods

By using a combined research methodology, we wanted to obtain results that strengthen the accuracy of the decision so as to reduce the polymerization time, creating the decision-making basis for obtaining the necessary settings for painting projects made after the implementation of polymerization reduction.

We started with thematic qualitative empirical research by observing the results obtained from the tests for measuring the temperature at different conveyor speeds, at respective polymerization times. Empirical research was followed by applied research aimed at finding a method or tool to reduce production costs.

Reducing production costs is one of the tools by which management can be made effective [4], and it contributes to the possibility of offering a lower price for the products made or services offered compared to the competition.

In this case, the polymerization time of the paint powder is reduced by 2 min compared to the usual process, without affecting the quality of the product. As such, the savings achieved by reducing processing times generate the possibility of making a larger quantity of products [5]. Consequently, more orders can be accepted, generating a higher profit return.

Schematically, the polymerization process in the furnace dedicated to this phase looks as follows (Figure 1).



Figure 1. The polymerization process before implementation.

After quality control at the workshop for the reception of raw products, they are placed on the painting line by hanging them on the conveyor in point A; the hanging systems are specially prepared for each type of product. They pass through the pre-treatment tunnel B where their surface, and then their inside if they have openings or open spaces, undergo a chemical attack by sprayers performed in several steps (Figure 2):

- Coarse washing with water;
- Degreasing using a strongly alkaline solution;
- Rinse with water;
- Rinse with demineralized water;
- Passivation with a nanoceramic multimetal solution;

- Rinse with recirculated demineralized water;
- Rinse with fresh demineralized water.

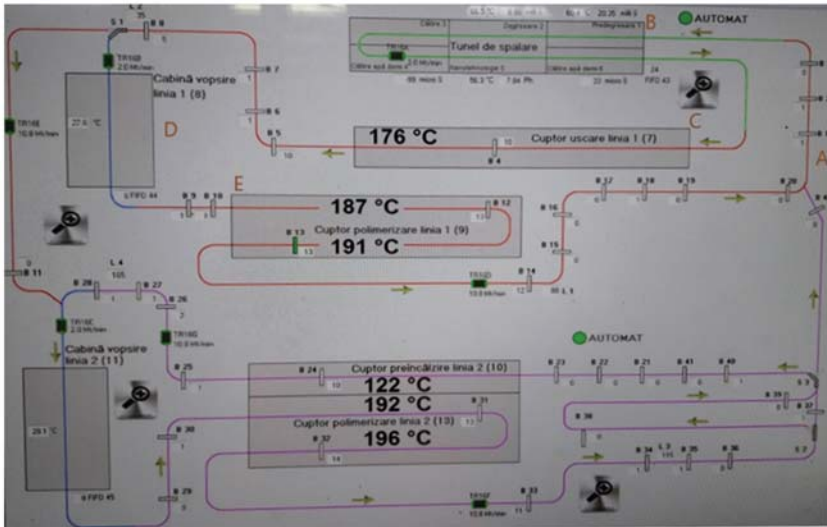


Figure 2. Painting line.

After the chemical pre-treatment [6], the products enter the drying oven C to dry and completely remove the water residue left on the surface and inside the products.

The painting step is the next step. This is done in a special booth D, ready to apply the powder paint on the surface of the products by means of automatic guns and, if necessary, manual guns. Everything is done in the electrostatic field created between the ends of the guns and the body of the paint product. Through the gun the powder passes onto the surface of the product and adheres to it thanks to the electronic loading of the paint powder, specific to the product in question.

The next stage is the polymerization stage, in which the polymerization of the paint layer on the surface of the product takes place. It takes place in the polymerization furnace E under the temperature conditions set according to the working procedures and instructions created on the basis of the customer’s requirements, the paint manufacturer’s recommendations and the standards in force.

This is the stage that has been studied in order to reduce the remaining times of the products in the polymerization furnace, reducing the working times and implicitly achieving a reduction in production costs [7].

After polymerization, the products are cooled, and after quality control they are sent for packaging and delivered to the customer.

The essence of the implementation consists of reducing the polymerization time from 27 min to 25, different from the one recommended by the paint powder manufacturer, without creating dysfunctions and taking away from the quality of the painted product.

In this case we are talking about the products on the hanging system no. 14 (Figure 3). Four to six or eight products can be suspended on this support, depending on their size, ranging from 0.3 to 0.7 m<sup>2</sup>/piece.



Figure 3. The polymerization process after implementation.

In the initial settings, support no. 14 remains in the oven for 27 min for curing. After the implementation settings, the remaining time decreased to 26 min, finally reaching 25 min in the oven (Table 1). Thus, for every 27 min of polymerization we have a gain of 2 min for the working process. Calculated at the actual working time of 7 h and 30 min (excluding breaks), a set of 18 cycles of 25 min is obtained, compared to the initial set of 16.66 cycles of 27 min. Therefore, the difference of 1.34 cycles  $\times$  25 min generates a saving of 33.5 min on an 8 h shift.

Table 1. Polymerization oven parameters.

Products Remaining Time in the Oven	Parameters	Air Temperature			No	Heaters Setting						
		Time (min)	27	26		25	1		2		2	
							27	26	25	27	26	25
Sensor 1	Temperature (°C)	187	189	197	PV	187	189	198	192	193	202	
Sensor 2		191	193	201	Min	194	195	198	194	195	197	
		Max	195	196	199	195	196	199	195	196	198	
		Setting point	195	196	198	195	196	198	195	196	198	
		Tolerance	1	1	2	1	1	2	1	1	2	

### 3. Results

As a result of the implementation of the optimization measures, a reduction in the polymerization time was obtained from 27 min to 25 min. With this time reduction calculated on a working day with two shifts of 8 h, you get twice the time, that is, 67 min, so a time saving of over an hour every 24 h will be made. Following an analysis of the 220 effective working days for 1 year, the time saving is  $220 \times 67$  min, which is 14,740 min or 245.66 h of actual work.

Turned into costs, this expression looks like this: the price paid by the customer for one system with four products per 1 h is EUR 10,176, given that the value of a painted product is EUR 2544. Multiplied by 15 effective working hours for 220 days per year, you get  $10,176 \times 15$  effective hours/day  $\times$  220 days/year = EUR 33,580.8 /year cost reduction or gain for the company.

If the calculation is made for a hanging system with six or eight products instead of four, the gain can be calculated very easily, the value of the economy achieved per year being obviously much higher.

The decision to implement the reduction of polymerization time was not taken without a very meticulous study and an analysis from all points of view of all data obtained.

The main idea of the implementation was to reduce the procedural time without affecting the quality of the product. The aim was to reduce the polymerization time to a minimum value, an aspect that ensures polymerization to the required quality and in conditions of satisfying the customer’s requirements, as well as with the observance of the implemented standards and the recommendations of the paint manufacturer [8]. The requirements of the paint manufacturer are presented in Figure 4.

Curing	180 C	×	20'
	190 C	×	15'
	200 C	×	10'

Figure 4. The requirements of the paint manufacturer.

Based on these criteria, the parameters of the curing oven must be set so as to reach the minimum temperature threshold for the paint to polymerize, guaranteeing the maximum adhesion of the paint to the surface of the product [9].

Starting from the possibility of increasing the polymerization temperature and thus reducing the polymerization time, the remaining time in the staggered polymerization furnace was reduced, from 27 min to 26 min and 25 min, increasing the polymerization temperature parallel to the degree of tolerance of ±1 min every 2 min (Figure 5).

Temp minim de remanență cuptor uscarea linia 1 (7)	9 Min
Temp minim de remanență cuptor polimerizare linia 1 (9)	27 Min
Temp minim de remanență cuptor preincalzire linia 2 (10)	9 Min
Temp minim de remanență cuptor polimerizare linia 2 (13)	27 Min

Temp minim de remanență cuptor uscarea linia 1 (7)	9 Min
Temp minim de remanență cuptor polimerizare linia 1 (9)	26 Min
Temp minim de remanență cuptor preincalzire linia 2 (10)	9 Min
Temp minim de remanență cuptor polimerizare linia 2 (13)	27 Min

Temp minim de remanență cuptor uscarea linia 1 (7)	9 Min
Temp minim de remanență cuptor polimerizare linia 1 (9)	25 Min
Temp minim de remanență cuptor preincalzire linia 2 (10)	9 Min
Temp minim de remanență cuptor polimerizare linia 2 (13)	27 Min

Figure 5. Reduction of polymerization time.

The result was not considered sufficient to justify a 100% safe decision after the temperature was monitored step by step for each time reduction step, which was done with the temperature measuring device (Datapack from TQC) directly on product surface (Figure 6).

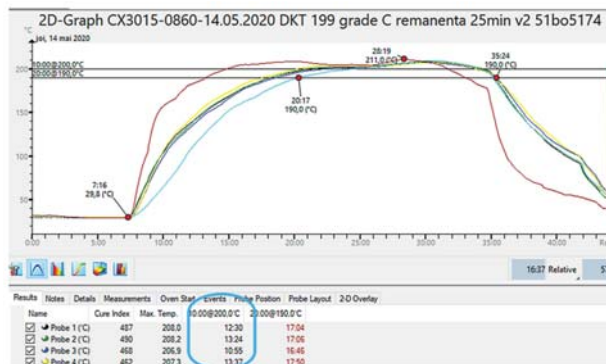


Figure 6. Temperature monitoring.

#### 4. Discussion

By using a combined research methodology, it was desired to obtain results that would strengthen the fairness of the decision to reduce the polymerization time, creating the decision basis for establishing a table with the necessary settings for painting projects after the implementation of polymerization reduction.

We started from a thematic qualitative empirical study by observing the results obtained from the temperature measurement tests at different speeds of the conveyor, at different polymerization times. The empirical research was followed by applied research aimed at finding a method or tool to reduce the production costs [10].

After data collection and information processing, the final conclusion was that the decrease in the polymerization time of 2 °C does not create quality and performance non-conformities in the painted product.

The polymerization time reduction tests have gone from qualitative to exploratory research to experimental research, this still being one of the research methods used.

Following the use of these tools, it was possible to implement a new polymerization time setting grid, reducing from 27 °C to 25, which in the long run leads to a EUR 33,580.8/year reduction in production costs [11,12], this being a real gain for the company.

#### 5. Conclusions

The monitoring reported in the paper is carried out for the entire painting process, starting from the hanging of the products on the pre-treatment line, up to the packing and final control after the painting and polymerization of the powder paint on the surface of the products.

Every step was monitored individually; these are parts of the whole painting process, so the obtained values after 3 months of monitoring are more significant in decreasing the costs over the whole process.

Even if using a developed and technologically advanced system of painting in an electrostatic field is not sufficient for purchase and for connecting the performant devices to the painting and pre-treatment system, the surveillance and monitoring must be carried out, namely to achieve continuous implementations so as to reduce the costs of production and to cope with the increasing competition in the market in the field, without forgetting the other important elements that make up the final price of the transaction cost of painting in an electrostatic field.

**Funding:** This research received no external funding.

#### References

1. Banerjee, S.; Mazumder, M.K. Surface microstructure of powder layers influenced by the forces of deposition and adhesion in electrostatic coating process. *IEEE Trans. Ind. Appl.* **2000**, *36*, 46–52. [\[CrossRef\]](#)
2. Barmuta, P.; Cywinski, K. Electrodeposition and efficiency of deposition during electrostatic powder coating. *J. Electrostat.* **2001**, *51*, 239–244. [\[CrossRef\]](#)
3. Cazaux, J. Critical thicknesses of electrostatic powder coatings from inside. *J. Electrostat.* **2007**, *65*, 764–774. [\[CrossRef\]](#)
4. Boer, J.; Blaga, P. Production cost optimization in industrial wastewater treatment. *Proc. Econ. Financ.* **2014**, *15*, 1463–1469.
5. Pop, L.D.; Nagy, E. Measuring System Optimization to Increase Productivity. *Procedia Eng.* **2017**, *181*, 1036–1042. [\[CrossRef\]](#)
6. Boer, J.; Blaga, P. The influence of the specific indicators of the chemical treatment on the production costs of painting in electrostatic field. *Proc. Econ. Financ.* **2015**, *32*, 514–519. [\[CrossRef\]](#)
7. Boer, J.; Blaga, P. Reducing production costs by monitoring the roughness of raw product surfaces. *Procedia Manuf.* **2018**, *22*, 202–208. [\[CrossRef\]](#)

8. Pop, L.D. Study on Creating a Simplified Model of Quality Management System in a SME from the Central Region of Romania. *Procedia Technol.* **2016**, *22*, 1084–1091. [[CrossRef](#)]
9. Glick, N.; Shareef, I. Optimization of electrostatic powder coat cure oven process: A capstone senior design research project. *Procedia Manuf.* **2019**, *34*, 1018–1029. [[CrossRef](#)]
10. Gabor, M.R.; Cimpian, L.; Oltean, F.D. Comparative Study concerning the Impact of IT&C Indicators on Performances of Organizations in the Industry. *Procedia Manuf.* **2019**, *32*, 627–633.
11. Boer, J.; Blaga, P. Optimizing production costs by redesigning the treatment process of the industrial waste water. *Procedia Technol.* **2016**, *22*, 419–424. [[CrossRef](#)]
12. Boer, J.; Blaga, P. Optimizing Production Costs with the Correct Setting of the Paint Thickness Parameters. *Procedia Eng.* **2017**, *181*, 1021–1027.

**Publisher's Note:** MDPI stays neutral with regard to jurisdictional claims in published maps and institutional affiliations.



© 2021 by the authors. Licensee MDPI, Basel, Switzerland. This article is an open access article distributed under the terms and conditions of the Creative Commons Attribution (CC BY) license (<http://creativecommons.org/licenses/by/4.0/>).



Proceedings

# Making Production More Efficient Using Analysis and Continuous Improvement Methods <sup>†</sup>

Petruta Blaga

Department of Management, “George Emil Palade” University of Medicine, Pharmacy, Science and Technology of Târgu Mureș, 38 Gheorghe Marinescu, 540139 Târgu Mureș, Romania; petruta.blaga@umfst.ro;  
Tel.: +40-077-019-5200

<sup>†</sup> Presented at the 14th International Conference INTER-ENG 2020 Interdisciplinarity in Engineering, Mureș, Romania, 8–9 October 2020.

Published: 25 January 2021

**Abstract:** This paper aims to present ways to increase the efficiency of the production activity implemented at the level of an important company of the Romanian car market producing car wiring, cables for photovoltaic panels, and industrial sensors. The company relies on state-of-the-art production processes to make its products and also develops innovative production concepts and products. In this regard, the company aims to continuously improve processes by ensuring quality standards at every stage of project management and the production process, as well as the correction and efficient elimination of errors or defects in the shortest possible time. The paper highlights at the company level a system that collects production data and allows the calculation of overall equipment efficiency, which becomes an important performance indicator of the company's production. Furthermore, the application of continuous improvement methods presented in the paper led to the improvement of some production indicators and, finally, to an increase in the company's production efficiency.

**Keywords:** production; management; analysis methods; continuous improvement; efficiency

## 1. Introduction

The production systems characteristic of the third millennium involve profound changes in their composition that affect both the technical basis and the methods and techniques of management, organization, and quality assurance. Thus, a company will need a high innovation capacity, because, without this element, even if it makes great efforts to capitalize on the material resources at its disposal, it will lag behind in terms of quality.

The customer orientation of a production organization, as a principle of quality management, is materialized by establishing quality objectives and adopting appropriate strategies to ensure competitive advantages. Improving quality must be a continuous and not sporadic action, a prevention of defects and not their remedy, and a systematic, professional approach.

Improving the production process frequently requires significant investments in time and financial resources to identify and implement improvements. It is necessary to carefully consider whether the improvement of the targeted process is the most appropriate for the business strategy, before making the investment.

Among the component management processes of quality management [1], continuous quality improvement has a dominant role in reducing costs and economic growth of organizations. Objectives of the improvement processes can be the following:

- obtaining customer satisfaction;
- continuous improvement of the quality of products/services;



- improving the effectiveness and efficiency of processes throughout the organization;
- reduction of losses due to non-quality.

Continuous quality improvement is a type of strategy that can be approached in two ways:

- in the classical vision—the strategy of technological innovation, which involves major technological changes, as a result of which the improvement of products is achieved with substantial investment efforts in order to obtain rapid economic effects;
- in the modern vision—the Kaizen strategy, which is considered an integrative strategy of the marketing, design-development, and production strategies of the company that pursues the gradual and continuous improvement of the quality of both products and services [2] and productivity and competitiveness, with the participation of the entire staff. This strategy adopts the principle of gradual improvement, through “small steps”, which can be achieved with small and continuous investment efforts, through conventional know-how, without major technological changes.

This paper aims to present ways to increase the efficiency of the production activity implemented at the level of an important company of the Romanian car market producing car wiring, cables for photovoltaic panels, and industrial sensors. The company relies on state-of-the-art production processes to make its products and also develops innovative production concepts and products. In this regard, the company aims to continuously improve processes by ensuring quality standards at every stage of project management and the production process, as well as the correction and efficient elimination of errors or defects in the shortest possible time.

## **2. Theoretical Foundations**

For a real image of the situation of a production company, it is necessary to use a key performance indicator that highlights as accurately as possible the level of performance of the company [3] at a given time. For predominantly automated activities, an optimal indicator is overall equipment efficiency (OEE). This indicator was created as part of the concept of total productive maintenance (TPM) and is a key performance indicator of the production department. As the machines take over much of the manual labor, it is important to know if these machines are working properly and at the desired efficiency. This aspect becomes even more important as the demand increases, and the question that arises is whether additional equipment is needed, which involves large investments for the company.

The OEE provides a measurement method that gives a correct perspective of the performance of the equipment. At the same time, the OEE shows where opportunities for improvement can be identified. Thus, this indicator is not only a tool that can compare the performance of one company with that of another company (benchmarking), but also a tool for continuous improvement. The parameters to be followed in the calculation of the OEE are availability, performance, and quality rate. The beauty of the OEE is that it does not provide a magic number, but offers three numbers that are useful and individual as the situation changes from day to day, and helps to visualize performance in simple terms—a very practical simplification [4].

## **3. Materials and Methods**

From the evolution of the OEE factors in 2016 at the level of the production department, presented in Figure 1, there was an average availability of 82.82%, a quality rate of 99.67%, and a lower performance of the machines, on average 70.43%. Compared to global performance, at that time, the possibilities for improvement were significant and actions were required to increase the efficiency of production activity.

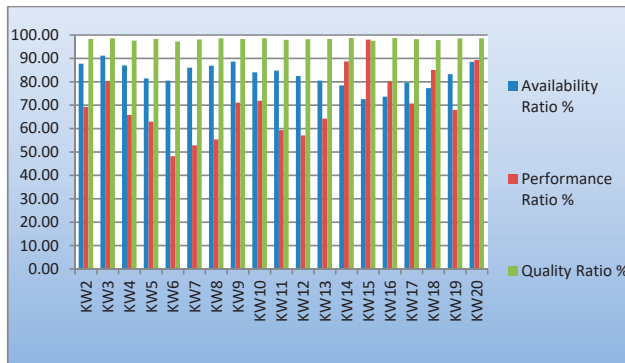


Figure 1. Evolution of overall equipment efficiency (OEE) factors in the first months of 2016.

Consequently, the management team set as a major objective the efficiency of the production activity by improving the OEE to 80% by the end of 2016 and 85% by the end of 2017.

In order to achieve the proposed objective, the main objective was cascaded into secondary objectives, all based on the implementation of the 5S method, standardization, and continuous improvement (Figure 2):

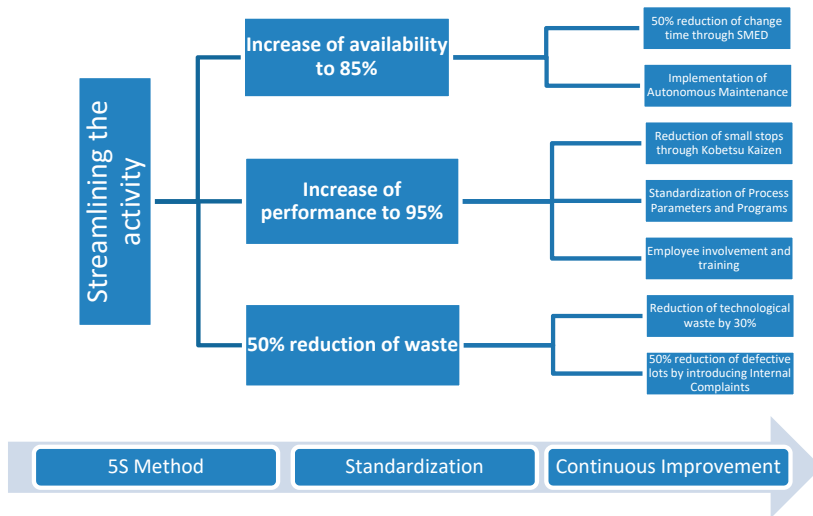


Figure 2. Cascading the main objectives set by the management team.

## 4. Results

### 4.1. Implementation of the 5S Method

Before any other improvement action, the implementation of the 5S method in the production department was started, with the 5S activities being considered the bases of any improvement project. The implementation was performed on different types of machines, following the replacement of the detected defective parts and the implementation of the ergonomic changes, after which a working standard was created, maintained, and audited periodically.

The implementation flow of the 5S Method (sort, set in order, shine, standardize, and sustain) on each workstation is represented in Figure 3:

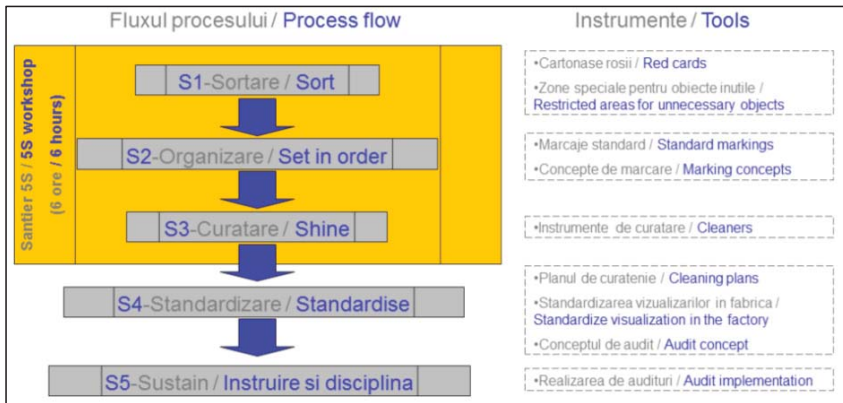


Figure 3. Implementation flow of the 5S method.

The actions and standards resulting from the implementation on each workstation were extended to the entire production department, in order to bring the entire area to a level satisfactory to the 5S method.

#### 4.2. Performance Improvement: Kobetsu Kaizen

Small machine stops for operator confirmations, small adjustments, product tub emptying, and low working speeds due to wear are all causes that can significantly reduce machine performance and cannot be recorded by the operator as downtime due to the fact that they take a little longer (on the order of tens of seconds) than their recording would take. They are the subject of a study for “Kobetsu Kaizen”, a method applied to increase the performance of machines.

To carry out the study, the following steps are followed:

- Two or three hours of activity of a machine are filmed, during which the operating parameters, the quantity produced, the qualitative problems, and the organizational problems that prevent the realization of the production in optimal conditions [5] are noted.
- The movie is watched, noting the duration of each production stop and grouping the stops by cause.
- The causes that lead to low stops/speeds are analyzed, and corrective and preventive actions are proposed.
- The causes are eliminated, and the filming is remade, comparing the obtained results.
- If the results are satisfactory, the corrective actions are extended to the remaining machines.

Following the analysis of the data resulting from the filming, the causes leading to the stops were grouped and their recurrence studied, resulting in 6.5% of the total stop time not being recorded. Thus, the total elimination of these causes could increase the performance of the car by about 2%.

The operating parameters of the machine with an impact on productivity [6] and quality were analyzed, studying their effect on quality when maximizing values to improve performance (Figure 4). In the 2 h of monitoring, the machine achieved, with the initial parameters, 1214 pcs/h. With the parameters set to maximum productivity, it would have been possible to achieve 1672 pcs/h; however, with these settings, the scrap rate increased by 34%. Following the analysis of the weight of the parameters on the quality, a set of optimized parameters was defined, parameters with which the production was 1400 pcs/h, obtaining a 0% rejection rate. Thus, a 15% increase in the machine's performance compared to the initial value was obtained.



**Figure 4.** Analysis of parameters and their influence on quality and productivity.

The set of parameters accordingly determined was standardized for the remaining machines with identical processes, thus ensuring the development of the concept of “best practice”.

#### 4.3. Reduction of Technological Waste: 6 Sigma

Only through the impact of selective collection and daily analysis, without taking other actions, the amount of technological waste decreased by 28%. Operators paid more attention to the correct setting of the machine and quickly intervened in the case of defective products.

Daily, the project team analyzed the defects and their mode of production, as well as their distribution by categories, taking actions to prevent recurrence. The resulting information was presented to all operators in the daily quality meeting (Figure 5), and the implemented technical solutions were distributed by conducting open punctual lessons (OPL).



**Figure 5.** The flow of information in the daily analysis of defects.

The evolution of the amount of technological waste was monitored daily and reported monthly, also being an indicator of the performance of the production department [7]. For any major deviation from the maximum permitted limit or for an unfavorable evolution of the quantity of waste, an analysis was performed, and corrective and preventive actions were taken.

The analysis was performed by the entire management team with the participation of experienced operators. Moreover, operators had an active role in solving quality problems, participating with ideas and solutions in the analysis of the situation.

The identified systematic technical problems leading to the production of technological waste (e.g., wear of stripping knives, nonlinearity of the storage tub to the machine, and nonlubricated applicator) were introduced in the daily checklist (autonomous maintenance sheet), so that the operator could check these points daily, thus preventing the production of waste.

Starting in 2017 from an average of 150 kg of waste/1,000,000 products made, at the end of 2018, a stable situation of 32 kg of waste/1,000,000 products was reached.

#### 4.4. Internal Delivery Performance

From a procedural point of view, the output elements of the production department are input elements for the other departments, with the production department being an internal supplier of semi-finished products for the other departments.

Thus, not only are internal improvement projects required, but also projects that directly satisfy the requirements of the client, with respect to the department for the client. For this, starting with 2018, the monitoring of the degree of satisfaction of the requirements was started, through the indicator “performance on delivery”, which was calculated as the ratio between the number of products delivered on time and the total number of products required.

From the analysis of the situation at that time, as can be seen in Figure 6, it emerged that the problem of delayed delivery of products was poor production planning.

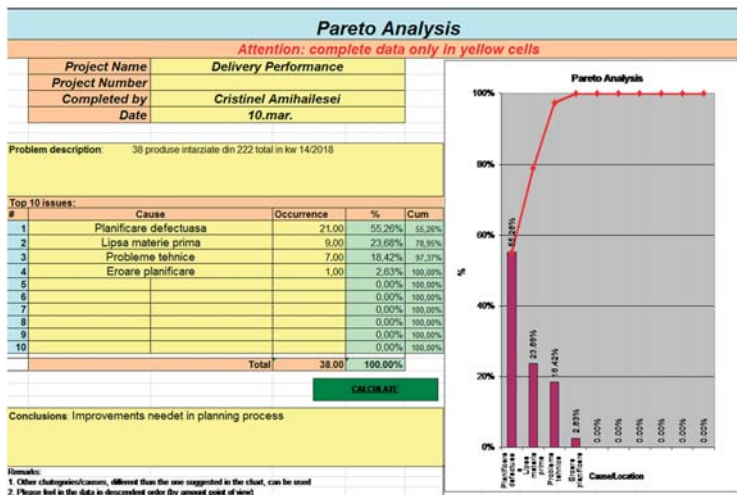


Figure 6. Analysis of the causes of the delay of the product’s parts

In this regard, analyses and actions were taken to achieve the goal of 95% delivery performance by mid-2019.

Initially, the planning of the products on cars was done manually, with the information written on a panel of considerable size and replaced weekly. The advantage of this method was that the panel was visual, centrally located, and accessible by anyone who needed information, even simple operators. Disadvantages were as follows:

- information could be easily lost;
- the allocation of parts on cars was done according to experience;
- the data from the previous weeks could be stored only in the form of a photograph, making their analysis extremely difficult;
- the process of allocating products on machines and prioritizing them took about 20 h a week.

As the first solution to improve the planning process, an Excel file for electronic planning management was proposed and developed, which, in addition to the much more accurate storage of information, allowed analysis of the planning process. Every day, the reason for delaying the delivery of a product was documented in the file. Some examples were the following:

- shortages of raw materials to the logistics department;
- technical issues to the maintenance department and the technical department.

The data were extracted weekly and their summary sent to the responsible persons.

As a result of this planning file being continuously supplemented with new data, one year after its implementation in production activity, the following improvements were made:

- prioritization of products was done automatically depending on the delivery date;
- the allocation of products on machines was assisted by the system by suggesting the machines capable of making the respective product;
- overloading or uneven loading of machines could be avoided by graphically displaying the capacity of the machine;
- by graphically viewing the orders per day, the peaks could be avoided and a leveling of the orders could be achieved;
- the production rules were updated automatically from the central information system (SAP);
- escalation of technical problems and lack of raw materials was done automatically by activating a macro that sent an email with the extract of information to the people involved;
- filling in the information in the file was done in real time, and, by sharing the support, departments could provide feedback to the problems reported directly in the file.

By optimizing the planning process [8], we obtained the following achievements:

- reducing the time required for planning from 20 h per week to a maximum of 8 h, in the context in which the number of products increased in 2018 by 43% compared to 2017;
- reduction of approximately 53% in human planning errors (from 15 misplaced landmarks in 2017 to seven landmarks in 2018) [9];
- improving delivery performance to 90% by the end of 2018.

## 5. Discussion

The effects of the continuous improvement actions carried out were visible in the evolution of the indicators at the level of the first semester of 2019.

The OEE not only reached the set target, but significantly exceeded it, with an average of 87.74% in 2018 and 94.36% in the first 4 months of 2019 (Figure 7).

Upon analyzing the OEE factors, a significant exceeding of the initial working norms was found, with the performance having an average of approximately 121% for the first 4 months of 2019, as well as a slight decrease in availability, partly due to the more precise way of collecting stop data compared to the initial period.

Following the improvement actions carried out, the performance of the cars increased in 2019 by 37% compared to 2016. Admitting a natural increase in this indicator by 12% resulted in a net improvement in performance by 25% following the actions.

In this context, the costs related to training and the implementation of improvement projects did not represent even 1% of the value of cost reductions obtained through performance increases [10].

If considering a reduction in the amount of technological waste to 25% of the initial quantities of waste or reaching a degree of 95% in delivery performance, the improvements could bring cost reductions [11] of hundreds of thousands of euros.

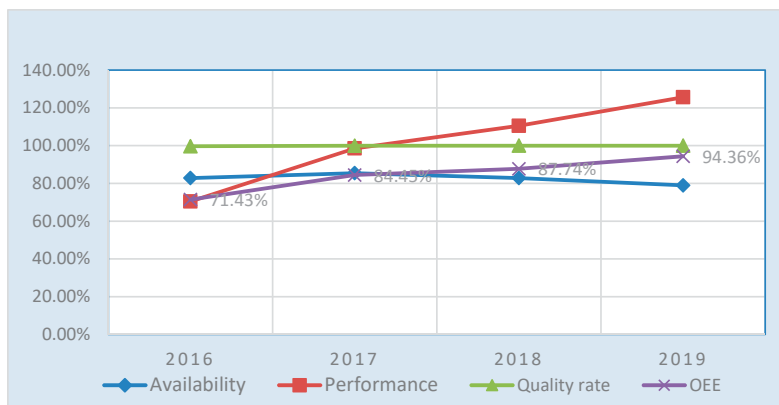


Figure 7. The evolution of the OEE and its factors.

## 6. Conclusions

A production company must represent the image of a well-oiled machine, perfectly organized and controlled, in order to meet customer expectations.

Using the right system for production management can help the organization meet and even exceed the expectations of business partners. It can also lead to better decision-making, improved quality standards, and increased production efficiency, all leading to an easier and faster response of the company to market challenges and ensuring competitive advantages.

A production management system that manages all aspects that easily lead to the improvement of the production activity offers the security of the smooth running of the company’s activity at low costs, giving the management team more time and information needed to develop the activity as it wishes.

**Funding:** This research received no external funding.

## References

1. Pop, L.D. Study on Creating a Simplified Model of Quality Management System in a SME from the Central Region of Romania. *Proc. Tech.* **2016**, *22*, 1084–1091. [CrossRef]
2. Wieslaw, U. Perceived quality versus quality process: A meta concept of service quality measurement. *Serv. Ind. J.* **2013**, *33*, 200–2017.
3. Gabor, M.R.; Cimpian, L.; Oltean, F.D. Comparative study concerning the Impact of IT&C indicators on performances of organizations in the industry. *Procedia Manuf.* **2019**, *32*, 627–633.
4. OEE.com. OEE Made Easy by Vorne. Free Resources and Fresh Perspectives on OEE. Master the Art and Science of OEE. Available online: <https://www.oee.com/#> and <https://www.oee.com/world-class-oee.html> (accessed on 17 July 2020).
5. Boer, J.; Blaga, P. Optimizing Production Costs with the Correct Setting of the Paint Thickness Parameters. *Procedia Eng.* **2017**, *181*, 1021–1027.
6. Pop, L.D.; Nagy, E. Measuring System Optimization to Increase Productivity. *Procedia Eng.* **2017**, *181*, 1036–1042. [CrossRef]
7. Boer, J.; Blaga, P. The influence of the specific indicators of the chemical treatment on the production costs of painting in electrostatic field. *Proc. Econ. Financ.* **2015**, *32*, 514–519. [CrossRef]
8. Boer, J.; Blaga, P. Optimizing production costs by redesigning the treatment process of the industrial waste water. *Proc. Tech.* **2016**, *22*, 419–424. [CrossRef]
9. Blaga, P.; Boer, J. Increasing human resource efficiency in the production process. *Proc. Tech.* **2014**, *12*, 469–475. [CrossRef]
10. Boer, J.; Blaga, P. Production cost optimization in industrial wastewater treatment. *Proc. Econ. Financ.* **2014**, *15*, 1463–1469.

11. Boer, J.; Blaga, P. Reducing production costs by monitoring the roughness of raw product surfaces. *Procedia Manuf.* **2018**, *22*, 202–208. [[CrossRef](#)]

**Publisher's Note:** MDPI stays neutral with regard to jurisdictional claims in published maps and institutional affiliations.



© 2021 by the author. Licensee MDPI, Basel, Switzerland. This article is an open access article distributed under the terms and conditions of the Creative Commons Attribution (CC BY) license (<http://creativecommons.org/licenses/by/4.0/>).





Proceedings

# Ways to Increase the Efficiency of Production Activity through the Active Involvement of the Human Factor †

Petruta Blaga 

Department of Management, “George Emil Palade” University of Medicine, Pharmacy, Science and Technology of Târgu Mureș, 38 Gheorghe Marinescu, 540139 Târgu Mureș, Romania; petruta.blaga@umfst.ro;  
Tel.: +40-077-019-5200

† Presented at the 14th International Conference INTER-ENG 2020 Interdisciplinarity in Engineering, Mureș, Romania, 8–9 October 2020.

Published: 26 January 2021

**Abstract:** This paper aims to present ways to streamline production by implementing methods of analysis and continuous improvement of an important company in the Romanian car market, based on technology which produces various components, especially car wiring used by many manufacturers of important cars. The production and processes within the company are designed from a lean and ergonomic point of view, taking into account the latest trends specific to the field. Supported by the company’s management, the continuous improvement activity, along with the basic methods, enjoys the involvement of all employees, trained in this process by various means. Employee involvement is not just about decision-making on the part of the staff, but starts with simple operators, who are encouraged and motivated to express their ideas for improvement and get involved in their implementation.

**Keywords:** production; management; human resources; analysis methods; continuous improvement

---

## 1. Introduction

Technological progress has streamlined the production process, lowered costs and put the human factor in difficulty—employees have always had to adapt to new technologies or change their specialization. The production line, machines and equipment of any kind that have brought a certain level of automation or computers and mobile devices are some of the most recent stages of technological progress in business. Beyond automation, there are also technologies that support employees and can fully contribute to employee efficiency.

The production company must represent the image of a well-oiled machine, perfectly organized and controlled in order to meet customer expectations. By choosing a suitable production management system, everything that happens in the factory can be found in real time, and you can intervene to adjust different production lines or solve any problems that may arise [1]. Once the production operations are automated, the quality level of the operations and products can be measured and tracked even during the manufacturing process, thus ensuring the automatic archiving of information in the system.

A modern system that supports communication and data transfer can improve the accuracy of information and visibility on all production processes, so as to reduce costs and respect delivery data [2]. Reducing manufacturing defects, order preparation time and operating with a minimum required stock synchronized with production are other elements that lead to lower costs, all of which can be achieved through the use of an efficient production management system.

A production management system can lead to a more efficient workflow, due to the reduction of human errors and the maximum use of resources. At the same time, it improves the accessibility of data that support better decision-making, increases quality standards, increases production efficiency and makes better use of equipment whose maintenance is automatically planned and managed [3].

Consequently, a system for production management provides real-time knowledge of the situation in the production area, allowing for immediate action when the situation requires adjustments. The improper management of production challenges often leads to irreparable situations.

This paper aims to present ways to streamline production by implementing methods of analysis and continuous improvement of an important company in the Romanian car market, based on technology which produces various components, especially car wiring used by many manufacturers of important cars. The production and processes within the company are designed from a lean and ergonomic point of view, taking into account the latest trends specific to the field. Supported by the company’s management, the continuous improvement activity, along with the basic methods, benefits from the involvement of all employees, trained in this process by various means. Employee involvement is not just about decision-making on the part of the staff, but starts with simple operators, who are encouraged and motivated to express their ideas for improvement and get involved in their implementation.

**2. Theoretical Foundations**

In order to have an overview of performance at a given time and to be able to analyze the evolution, it is necessary to monitor some key performance indicators, called in the business environment Key Performance Indicators (KPI). For the departments in which mainly automated activities are identified, it is necessary to introduce a performance indicator that reflects reality as fully as possible. One such indicator is Overall Equipment Efficiency (OEE) [3]. In order to be determined, it is necessary to establish a system that collects production data that allows for the calculation of the OEE, which has become the main performance indicator of the production department.

The OEE provides a measurement method that gives a correct perspective of the performance of the equipment. The OEE also shows where opportunities for improvement can be identified.

The parameters to be followed in the calculation of the OEE are:

1. availability—takes into account the time lost with the stops;
2. performance—takes into account the speed losses, in particular, and represents the ratio between the quantity of parts that should have been produced in the time interval (theoretical quantity) and the realized quantity (real quantity);
3. quality rate—takes into account the quality losses and is calculated as the ratio between the number of compliant parts and the total number of parts made.

The OEE provides three numbers that are useful and individual as the situation changes and help to visualize performance in simple terms—a very practical simplification [4].

Studies conducted worldwide show the following level of performance (Table 1), achieved by some of the most famous companies:

**Table 1.** World Class Overall Equipment Efficiency.

OEE Factors	World Class OEE
Availability	90.0%
Performance	95.0%
Quality	99.0%

Source: Vorne Industries, 2020 [4].

The needs for developing economic performance also refer to improving the skills of the human factor [5] in areas such as work organization, design–sizing–measurement–control–improvement–process management in companies, quality management [6], change management, risk management, project management, etc., with direct consequences on labor productivity [7] and performance competitiveness.

Whether it is a design process or an execution process, or whether it seeks to apply a technical or a non-technical process, the presence of the human factor is found in all, being substantially conditioned by its possibilities and interests. The successful initiation and development of activities within the company depends, to an overwhelming extent, on the degree to which the human factor is understood, motivated and coordinated, the only resource endowed with the ability to know and overcome its own limits [8].

### 3. Materials and Methods

Based on the data collected at the level of the production department, the OEE was calculated in the first 20 weeks of 2016, obtaining an average of 58.21% (Figure 1). Compared to the global performance at that time, the possibilities for improvement were significant, and actions were required to increase the efficiency of the production activity.

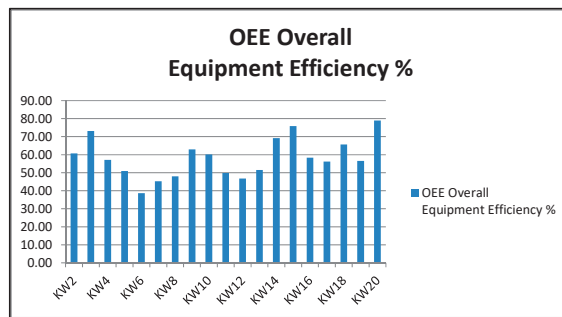


Figure 1. Evolution of the overall equipment efficiency (OEE) in the first months of 2016.

Consequently, the management team set as a major objective the efficiency of the production activity by improving the OEE to 80% by the end of 2016 and 85% by the end of 2017.

In order to achieve the objective proposed in the company, a series of methods for continuous improvement of the production activity were taken into account and implemented.

### 4. Results

#### 4.1. Analysis of Disturbing Factors

In order to improve all the factors that contribute to the evolution of the OEE, an analysis of the production department was carried out by the management team by making an Ishikawa Diagram. The analysis revealed the following causes:

- Machine: applicators with technical problems, wires attached to the pull rollers, loosening of the applicator discs while running;
- Method: cutting rules too high, unknown process parameters, long times to change products, wrong entries in the collection forms, incorrectly saved programs;
- Material: long threads;
- Worker: ignorance of the role of parameters by the operator, process parameters not observed, machine left unattended, programs not used by operators, when switching from long wires to short wires parameters remain set to minimum, incorrectly completed data leading to calculation errors;
- Environment: no cause was found.

The causes with significant impact were analyzed by the method of “5 Why?” to get to the root cause and be able to take action. For each case, up to 5 “why?” questions were asked.

For the identified causes, actions were taken, each being assigned to a team member, with a deadline. In order to assign actions and monitor the situation, an Action Plan (Figure 2) was used,

which allowed for the creation of graphs and monitoring actions (e.g., degree of closure of actions, distribution by areas, etc.) [9].

<b>Topic:</b> OEE improvement	<b>Department:</b> Production		<b>Attention:</b>			
	<b>Aria of interest:</b> Segment 5		blue - changes agreed since the last meeting	0	Actions without deadline	
	<b>Data:</b>	2.11.2018	green - changes proposed before the current meeting	0	O	Ongoing actions
	<b>Owner:</b>	C. Amihalesei		23	C	Closed actions
				0	I	Overdue actions

Action Plan									
Nr. crt.	Aria	Problem	Action	Responsible	Deadline	Made in	Status	Effective?	Remarks
1	ENG	Unknown process parameters	Conducting study on the influence of speed parameters on the length of the cut wires	L. Adorjani	30.11.2016	20.11.2016	C	Yes	Study conducted, parameters can be standardized by groups of lengths
2	PRD	Lack of standard method to change	SMED Workshop organization	C. Hanc	17.07.2017	02.07.2017	C	Yes	Workshop organized, work instruction created and saved on the network
3	PRD	Process parameters are not included in the specific training plan	Review specific training plan	S. Szente	20.11.2016	19.01.2018	C	Yes	Client segment (SG03) - boxes were ordered for new products
			Training for all operators with the new plan	S. Szente	15.05.2017	20.04.2017	C	No	Efficacy will be verified by written and practical testing

Figure 2. Action Plan.

4.2. Reducing Change Times: Pareto Analysis, SMED Method

Data on machine downtimes were analyzed using the Pareto Diagram. Thus, the main causes identified were product changes and settings. Figure 3 shows that product changes are responsible for 22.09% of the total downtime, which causes an average of 70 h of downtime per week for all cars.

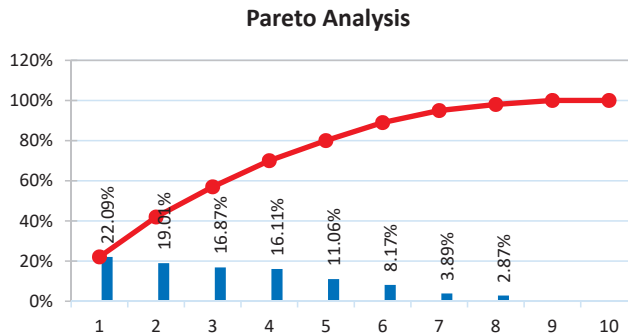
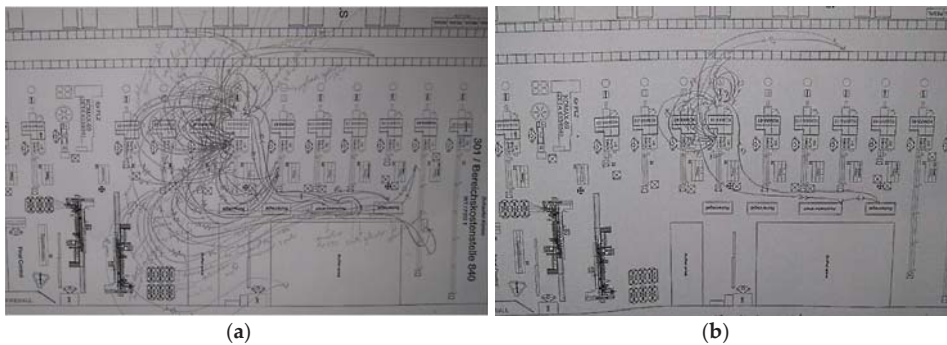


Figure 3. Pareto analysis of causes of stopping.

In order to reduce product change times, the SMED Method (Single Minute Exchange of Die) was also applied, the aim of which was to improve the method of changing tools/products so that the times when the machine does not produce are as short as possible. This method was then standardized.

The process of changing tools and materials on the machine to achieve a new part of the product was filmed for further analysis, because in real time certain aspects can escape observation. Moreover, all the movements of the operator in the change process were plotted using “Spaghetti Diagram” (Figure 4a).

After analyzing the filming of the process, a map of the value of the process was made—Value Stream Mapping (VSM), in which each movement, action or verification was quantified in meters and seconds (Figure 5). The internal operations (performed while the car is stationary) were also delimited from the external ones (performed while the machine was producing).



**Figure 4.** Spaghetti Diagram: (a) Spaghetti Diagram in the initial stage; (b) Spaghetti Diagram in the final stage.

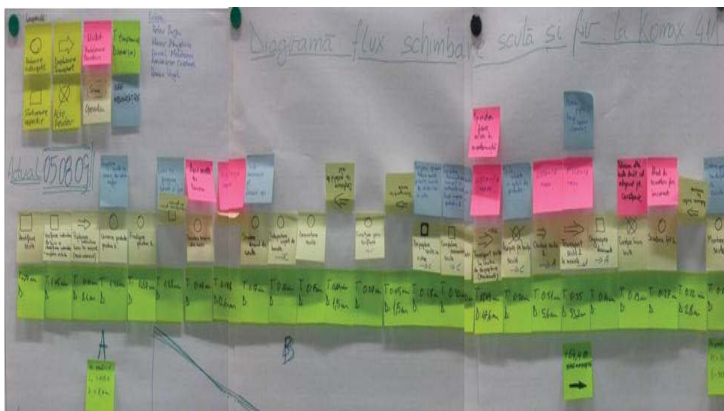


**Figure 5.** Value Stream Mapping (VSM).

The principle of Eliminate, Combine, Rearrange and Simplify (ECRS) was applied on VSM: each process step was analyzed, and unnecessary process steps were eliminated, operations that could be done at the same time were combined, the location of the tools was moved closer to the operator and difficult operations have been simplified. All operations that that did not require the machine to be stopped were performed either before the machine was stopped or after the machine was started.

Thus, the new VSM was transposed into a change procedure, which, applied on the same machine with the same operator, led to the results illustrated in Figure 4b and Table 2.

**Table 2.** Results obtained after applying the methods.

Factor	Before	After	Gain
Distance traveled [m]	429	151	284%
Total number of operations [pcs]	59	20	295%
Of which internal operations [pcs]	33	11	300%
Total time [min]	49.27	17.43	283%
From which internal time [min]	39.25	11.23	350%

#### 4.3. Improving the Technical Condition of Machines: Autonomous Maintenance

In order to reduce unplanned maintenance times (machine failures), the concept of “Autonomous Maintenance” has been implemented, making the machine operator responsible for a series of checks,

cleaning, lubrication and tightening, performed regularly, in order to eliminate the causes leading to machine failures and to provide specialized maintenance personnel with the time needed to carry out Preventive Maintenance activities.

Thus, the points that require daily verification were identified for each machine, and an Autonomous Maintenance form was created. Based on this, the operator performs daily checks and, depending on the situation, cleans, tightens or lubricates the machine parts. In order for the operators to be able to carry out these checks, it was obvious that they needed to be trained on the functional aspects of the machines.

An intensive training program was started within the department [10], the transfer of knowledge being done hierarchically, according to a weekly schedule in which the Process Engineer trains the Technician and the Regulators, and they in turn train the operators (Figure 6a).

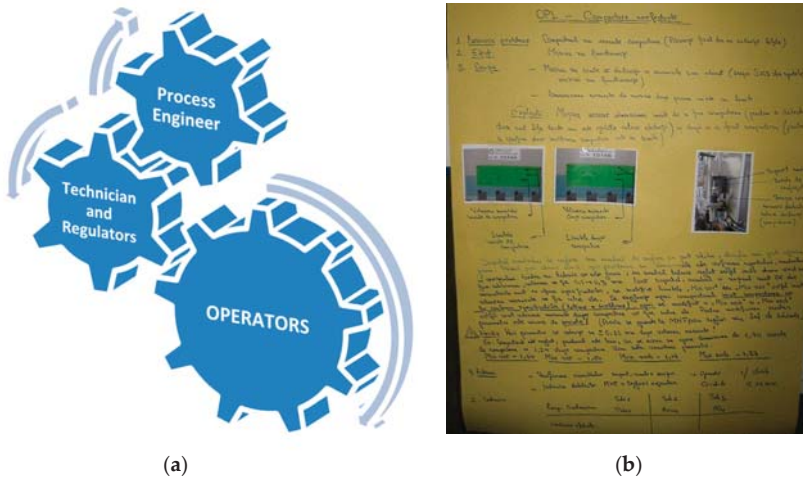


**Figure 6.** Autonomous Maintenance: (a) The process of knowledge transfer; (b) One-Point Lesson.

The information was grouped into thematic modules and presented in Power Point and on flipcharts. Where necessary, they were presented practically, on machines in production. Topics included both general concepts (5 Senses, Mechanical Assemblies, Lubrication, Pneumatics) and specific concepts of the machines on which the operators were working (Principles of operation, Cutting process, Crimping process, Tinning process, Critical parameters and their influence, etc.).

Following the remediation of some problems with machines, a One-Point Lesson (OPL) was created to standardize knowledge. It was originally made on the flipchart and contained the following required fields: Problem Description, Effect, Causes, Corrective/Preventive Actions, Trained People, Suggestive Photos. This OPL was presented to all those involved, explaining what the initial problem was, what effects it had on the machine, process or product, why this problem occurred and what actions to correct and prevent the recurrence of the problem were taken. An example of OPL made on paper is shown in Figure 6b. Subsequently, an Access database was created that allows the creation, distribution, storage and electronic management of these OPLs.

#### 4.4. Reducing Quality Losses Due to Human Error

The waste rate is composed of technological waste and non-compliant products. The main cause of the appearance of products made incorrectly is human error (wrongly set dimensions, mixed material, etc.).



Non-compliant products, expressed in pieces of non-compliant products per million products, were monitored. The results were reported monthly, and for deviations from the limit or unfavorable evolution analyses were performed and actions taken (Figure 7).

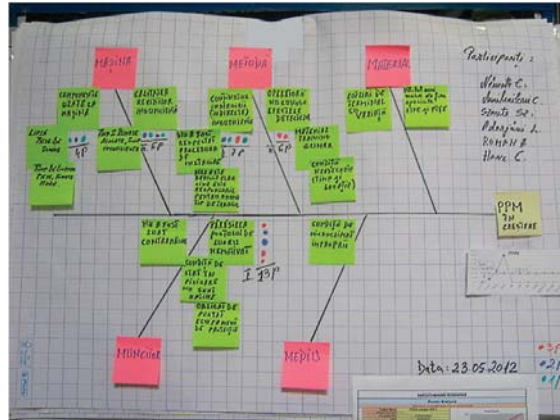


Figure 7. Analysis of the deviation from the allowed limit.

The actions applied after these analyses required both managerial and leadership skills, because they were focused not on the application of measures to sanction mistakes, but on the involvement of operators in the strategy “0 Defects” and their motivation in the desire to achieve product quality.

Some of the actions proposed and aimed at motivating operators to implement compliant products were:

- awarding the operator with the best quality performances;
- monthly ranking with the evolution of mistakes on work shifts;
- introduction for two days in the retraining activity of operators with repeated mistakes;
- entrusting the operator with the reprocessing of the non-compliant product.

5. Discussion

Following the actions taken to improve the three parameters of the OEE (Availability, Performance and Quality), the company managed to maintain a growing evolution of the OEE throughout 2017, repeatedly exceeding the proposed target of 87% by the end of the year (Figure 8).

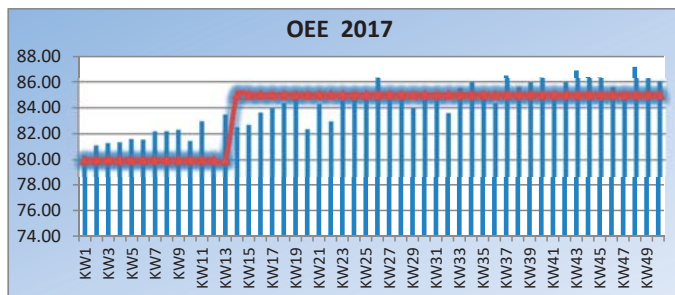


Figure 8. The evolution of the OEE in 2017 compared to the proposed objective.



The OEE not only provides a number, but also an overview of the situation, through its parameters. From the representation of the averages of the indicators for 2017 (Figure 9) it is possible to determine if the situation is the ideal one or if it deserves to be improved.



Figure 9. OEE factors in 2017.

The OEE not only reached the set target, but significantly exceeded it, with an average of 87, 74% in 2018 and 94.36% in the first four months of 2019. Consequently, the effects of the continuous improvement actions carried out were visible in the evolution indicators at the level of the first semester of 2019.

## 6. Conclusions

Today, important technologies are on the verge of making a major impact in production processes and the work environment. Thus, a company will need its own high innovation capacity, because without this element, even if it makes great efforts to capitalize on the material and human resources at its disposal, it will lag behind in terms of quality.

The profound changes in the composition of modern production systems will affect both the technical basis and the methods and techniques of management, organization and quality assurance. The performance of a production company, its ability to adapt to the rigors of the competitive market, to fully meet its requirements and at the same time to maximize its profit are dependent on investments in new technologies and in retraining people, as well as the effectiveness of their use.

This will considerably increase the role of human resources, which, at all levels, will have to face completely new problems regarding the continuous improvement of the production process and manufactured products.

**Funding:** This research received no external funding.

## References

1. Wang, L.; Liu, P.; Jiang, S.Q.; Xue, Y.M.; Wang, K.; Li, X.N. Production Management System for Small and Medium Sized Manufacturing Enterprises. In Proceedings of the 2018 IEEE International Conference on Industrial Engineering and Engineering Management (IEEM), Bangkok, Thailand, 16–18 December 2018; pp. 685–689.
2. Ameziane, F. An information system for building production management. *Int. J. Prod. Econ.* **2000**, *64*, 345–358. [CrossRef]
3. Phogat, S.; Gupta, A.K. Identification of problems in maintenance operations and comparison with manufacturing operations. A review. *J. Qual. Maint. Eng.* **2017**, *23*, 226–238. [CrossRef]
4. OEE.com. OEE Made Easy by Vorne. *Free Resources and Fresh Perspectives on OEE. Master the Art and Science of OEE*. Available online: <https://www.oee.com/#>; <https://www.oee.com/world-class-oee.html> (accessed on 17 July 2020).

5. Calabria, F.A.; de Melo, F.J.C.; de Albuquerque, A.P.G.; Jeronimo, T.D.; de Medeiros, D.D. Changing the training paradigm for learning: A model of human capital development. *Energy Environ.* **2018**, *29*, 1455–1481. [[CrossRef](#)]
6. Pop, L.D. Study on Creating a Simplified Model of Quality Management System in a SME from the Central Region of Romania. *Procedia Technol.* **2016**, *22*, 1084–1091. [[CrossRef](#)]
7. Pop, L.D.; Nagy, E. Measuring System Optimization to Increase Productivity. *Procedia Eng.* **2017**, *181*, 1036–1042. [[CrossRef](#)]
8. Blaga, P.; Boer, J. Increasing human resource efficiency in the production process. *Procedia Technol.* **2014**, *12*, 469–475. [[CrossRef](#)]
9. Blaga, P.; Boer, J. Human resources, quality circles and innovation. *Procedia Econ. Financ.* **2014**, *15*, 1458–1462. [[CrossRef](#)]
10. Blaga, P. Evaluating models of the human resources training programs. *Rev. Manag. Econ. Eng. I* **2015**, *14*, 702–711.

**Publisher's Note:** MDPI stays neutral with regard to jurisdictional claims in published maps and institutional affiliations.



© 2021 by the author. Licensee MDPI, Basel, Switzerland. This article is an open access article distributed under the terms and conditions of the Creative Commons Attribution (CC BY) license (<http://creativecommons.org/licenses/by/4.0/>).



Proceedings

# An Innovative Guide to Work-Based Learning in the Field of Industry 4.0 †

Liviu Moldovan

Faculty of Engineering and Information Technology, George Emil Palade University of Medicine, Pharmacy, Science, and Technology of Targu Mures, 1 Nicolae Iorga Street, 540088 Targu Mures, Romania; liviu.moldovan@umfst.ro; Tel.: +40-740-498-427

† Presented at the 14th International Conference INTER-ENG 2020 Interdisciplinarity in Engineering, Mures, Romania, 8–9 October 2020.

Published: 29 December 2020



**Abstract:** This paper presents a practical methodology for Work-Based Learning (WBL) as a research result of the iNduce 4.0 European project consortium. A training platform has been developed for the purpose of providing enterprises with affordable and flexible training which could be best adapted and customized to their specific needs. On the training platform, there are four training modules on the subject of Industry 4.0. The courses structure is the result of a large-scale survey within two target groups: manufacturing enterprises and vocational education and training stakeholders. Training begins with learning needs analysis designed to support the individual. The structure of the guide to quality WBL reveals the steps for an efficient WBL programme established by vocational education providers, which serves as a tool and requires them to commit to the quality standards and code of conduct dictated at the national level as well as to the ones stated in the European quality charter on internships and apprenticeships.

**Keywords:** work-based learning; industry 4.0; vocational education and training; manufacturing; smart production; training platform

---

## 1. Introduction

Work-Based Learning (WBL) is an educational strategy that provides students with real-life work experiences where they can apply academic and technical skills and develop their employability. Depending on the country and the type of agreement between the student and the company, it could be an internship, an apprenticeship, or a mentorship. Various innovative models can be used for training [1,2] and assessment [3]. WBL may take place on demand and during working hours, sometimes for a clearly defined problem [4], in various industrial fields [5,6] or services [7].

The learning materials need to be designed in order to facilitate learning by being effective and userfriendly [8], which can be on paper support or electronic [9,10]. In general, at the organizational level, the references regarding the advantages of electronic learning are superior to the disadvantages [11]. E-learning is just as effective as face-to-face training and awareness of the benefits is achieved six to eight weeks after the training [12]. A barrier to the use of electronic technologies in vocational education and training (VET) is the reluctance of some professional training institutions [13] as well as some teachers [14].

The purpose of this paper is to present an electronic training platform for WBL developed in the framework of the Erasmus project entitled Work-based training approach in the field of Industry 4.0 for competitive European Industry—iNduce 4.0 [15].

The research has started with a state-of-the-art analysis on the knowledge and skills gaps on the topic of Industry 4.0 and the requirements for WBL [16] as well as a review of the legislation framework in the field of WBL at a European level [17,18].

## 2. Methods

The iNduce 4.0 e-learning courses structure is the result of a large scale survey within two target groups: manufacturing small medium enterprises (SMEs) and VET providers/trainers/consultants. It was conducted in six European countries: Romania, Poland, Portugal, Germany, Bulgaria, and Cyprus. In total, 117 SMEs and 77 VET providers participated in the survey.

Based on the results of the survey, the iNduce 4.0 training course was developed on the ground of the following key points:

- The topic of Industry 4.0 is considered important but there is a low level of awareness of the subject at the company level;
- SMEs are better acquainted with the industry concept than VET providers' representatives;
- A comprehensive package of training materials is highly appreciated with focus put on "Introduction to Industry 4.0" and "Solutions for smart production environments in the manufacturing sector";
- Only one or two skills is not enough when it comes to Industry 4.0, but a set of skills is needed and is necessary to address as many skills as possible with focus on Complex Problem Solving Skills, Technical skills, and Systems skills;
- The iNduce 4.0 training course should be more practice-focused, with the option of being tailored to a different way of teaching, such as workplace training, blended learning, and online courses;
- The educational portal should have interactive evaluation tests, an option to download files, and discussion forums.

Important findings about Work-based learning that came out of the survey reveal that few of the participating VET organizations providing onsite training programmes to companies offer any training related to Industry 4.0. One reason for this might be the fact that the topic is still new and VET organizations have not yet managed to develop courses and they are not yet familiar enough with the topic. Other reasons are also linked to the lack of information resources, low demand/interest in educational services, and reluctance of employers and employees to engage with this new thematic. In comparison, SMEs pointed out two different obstacles in applying WBL programmes for new employees/students: lack of time and resources and lack of theoretical materials to combine with practical elements, such as legal regulations.

The level of awareness on the topic combined with the lack of information resources and theoretical and practical materials pointed out by SMEs and VET stakeholders as obstacles towards organizing WBL confirms the importance of the project and the need of such training materials and courses.

The training should start with learning needs to be analysed, which is a review of learning and development requirements that is designed to support the individual. It provides an opportunity to reflect on what skills/knowledge the trainee needs to succeed, what skills/knowledge the trainee already has, and what skills/knowledge the trainee needs to develop.

Skills analysis should reveal what skills the employee needs to know to carry out their role effectively and if the employee has any knowledge on the subject, which could range from having an understanding of a particular subject to more complex issues that require training, coaching etc. Expectations of the manager should reveal what is necessary for the employee to know for a better functioning of the organization and about fulfillment of organizational objectives. Identified gaps in learning, if the employee recognizes those gaps, indicate what is required in order to reach competence in that skill. Previous experience and training outlines volume of knowledge of the employee and what is required in order to reach competence in that task, the length of previous training on a particular matter and if this is still relevant and how this will be achieved, if there could be alternative ways

of learning than to send someone on a course and also how this is going to be evaluated, what processes are in place to ensure that it has been achieved, how it is going to be measured, and what the timescale are.

SMEs stakeholders for training, managers, consultants, and VET providers know that they need to keep up with the latest innovations and technologies if they want to live and thrive in a competitive global market. They need to develop their own skills and knowledge in Industry 4.0 and to make sure that their current and future workforce is up-to-date to succeed.

SMEs' managers need to ask themselves these questions before even considering their employees and their own training in Industry 4.0:

- Purpose of the training: Why do I need my employees to know more about Industry 4.0?
- Measurable objectives: What measurable results are desired over time?
- Identification of the needs: What competencies are needed for succeeding now and in the future?
- Measure potential and identify gaps: What are the Opportunities/Challenges?
- Evaluate results of training: How have the defined objectives been met?

### 3. Results

Based on these findings, the iNduce 4.0 e-learning platform [15] has been developed with the purpose of providing SMEs with affordable and flexible training which could be best adapted and customized to their specific needs (Figure 1). The iNduce 4.0 e-learning platform can be approached in different ways, depending on the specific needs of the user. Furthermore, it allows both SMEs' managers and employees to adapt the new disruptive tools and methodologies provided by e-learning to their best advantage, or any other kind of learning experience involving learning providers and companies.

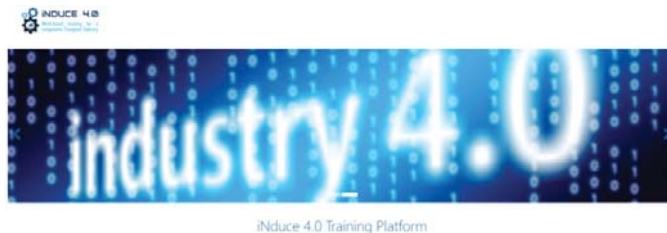


Figure 1. iNduce 4.0 e-learning platforms.

The iNduce 4.0 e-learning platform allows one to create new accounts and after registration, the user may choose a training course to enroll and then start studying. First, the user may select one of the languages: English, Romanian, Bulgarian, German, Greek, or Portuguese. There are four modules: Module 1—Introduction to industry 4.0; Module 2—Solutions for smart production environments in the manufacturing sector; Module 3—Smart robotics; Module 4—Applications of Cyber physical production systems/Internet of things across the process chain. Each of the four Modules include: Description and Outcomes; Subsections; Conclusion; The material in the pdf for download; Quiz (Figure 2).

The course facilities comprise: Dashboard: showing the courses that the user is enrolled in; Profile: settings of the profile; Messages: for exchange of messages with other participants and teachers; Preferences: change password, preferred language, etc.



Figure 2. Structure of training modules.

#### 4. Discussion

An efficient WBL programme established by SMEs’ Managers and VET providers with the support of the iNduce 4.0 e-learning platform requires them to commit to the quality standards and code of conduct dictated at a national level as well as to the ones stated in the European Quality Charter on Internships and Apprenticeships [19]. A comprehensive apprenticeship programme based on the INDUCE 4.0 course serves as a tool.

The structure of the Guide to quality WBL is presented in Figure 3. In the assessment phase, different departments of the company must be consulted to identify specific areas of work to which an intern could contribute.

The relations phase consists of approaching educational institutes like universities, technical schools, training centers, and other educational facilities that can equip the worker with the skills needed. This can create a solid bridge of skills between the company and the educational institutes.

The structured programme is a clearly defined programme which ensures that an apprenticeship/internship in the company is valuable and will help attract young talent. The programme should ensure that the intern: has clear written learning goals to be achieved; is given the opportunity to see different areas in the company; has planned and structured training using iNduce 4.0 onsite: an optimal “abstract/concrete” learning balance; is given a range of tasks to ensure the development of different skills foreseen in the programme; is given the opportunity to learn from other employees; has regular meetings with a supervisor to monitor progress.

The efficient recruitment increases the chances of getting the right person in the company. It should be based on: creation of a clear job description, including skills and competencies the company needs; stating in the job description that there is in-house training on Industry 4.0 will entice motivated people who are eager to improve their skills; ensure length of the apprenticeship/internship and the remuneration/reimbursements details are clearly stated; always give feedback to the interviewed people so they can improve their interview skills. This has the potential to create a positive image surrounding the company for young talent.

The introduction checklist is crucial for the intern to have a positive experience in the company. An example of a checklist for the first days in the company consists of: a good introduction to the company, its values, and missions, as well as to all the staff; a tour of the facilities; providing him with relevant health and safety information; giving him a copy of the working rules and the Code of Conduct; making him aware of available complaints channels; going through his desired learning

objectives, as well as tasks and duties stated in the job description; planning of training during his time with the company.

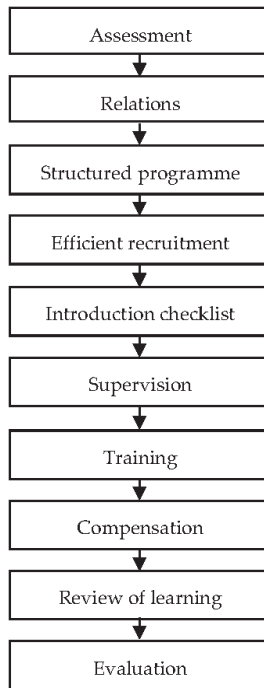


**Figure 3.** The Guide to quality Work-Based Learning (WBL).

The supervision is important for the intern in order to have supervisors who are trained in their responsibilities. This ensures that the intern feels supported and is part of a concrete learning process while the company is making the most of his skills and time. This could involve establishing monthly assessments to review progress and satisfaction and establishing a midterm review to assess progress against the written learning objectives.

Training gives interns the possibility to receive in-house training, which could enhance their professional skills. Training in Industry 4.0 is not only essential for the future of their career, but also for the company: it is important to go through iNduce 4.0 to select relevant modules for the intern as well as for the company. Good training must be well balanced between learning “abstracts” and applying them on-site and having a professional trainer is of course ideal but can be expensive. The alternative would be having an in-house trainer (e.g., the intern supervisor) who possesses pedagogical skills.

Compensation for interns means: no discrimination toward young people; incentive for motivation and commitment at work; making them part of the staff of the company, not just as cheap/free workforces.

Review of learning may consist of end-of-internship/apprenticeship presentation for the intern: what they have done; what they have learnt.

Evaluation of the internship/apprenticeship should include: How well the learning objectives are met? What projects have been completed or contributed to?; What knowledge and skills make the intern more prepared for the labor market?; What areas of improvement regarding the WBL process have been identified?



## 5. Conclusions

All levels of SMEs are going to benefit from the iNduce 4.0 training course. SME managers need to know about new technologies that can be applied to their companies in order to survive and develop in a competitive market. Acquiring skills and knowledge in Industry 4.0 can be key to the success of a business. This can be achieved in many efficient ways, including work-based learning by means of the e-learning platform iNduce 4.0.

Benefits and opportunities after upgrading to Industry 4.0 comprise: Increased productivity; Improved risk management; Real-time tracking, monitoring, and automation; Enhanced predictability of insights and actions; Optimized technology through the convergence of Information Technology and Operational Technology; Remote and predictive maintenance of machines; Optimized machine operations; Energy and environment monitoring and remote management; Self-sustained operations—machine learning-based robotic process automation of machines.

Benefits of the training using the iNduce 4.0 e-learning platform include benefits for the learner and benefits for the employer.

Benefits for the learner comprise: development of work-based learning and work-related skills simultaneously; exploiting the workplace as a learning resource; using existing knowledge activated as a foundation for new knowledge.

Benefits for the employer comprise: flexible, tailored to their needs; can lead to improved workforce performance and productivity; increases employee motivation—higher staff retention; meets skills shortages; work-based learning—little time off the job, minimal disruption.

iNduce 4.0 can be employed to best advantage its users thanks to its flexibility, which allows a customized adaptation of its learning tools to the specific needs of each user.

It is important to point out that even though e-learning presents many advantages, it is not exempt from some drawbacks. The most effective way to minimize the latter is to recur to blended learning: getting the most of an e-platform such as iNduce 4.0 by mixing online and face-to-face training [20].

**Funding:** This research was funded by the European Commission, Erasmus+ programme, grant number 2017-1-RO01-KA202-037222.

**Acknowledgments:** This publication reflects the views only of the author and the Commission cannot be held responsible for any use of the information contained therein. My acknowledgements go to project partners Dorina Scheidel and Samir Cheriaa who have participated in the iNduce 4.0 project outputs development.

**Conflicts of Interest:** The author declares no conflict of interest.

## References

1. Moldovan, L. Design and development of innovative tools and models for e-learning in central and western Romania. In Proceedings of the 6th International Seminar Quality Management in Higher Education—QMHE 2010, Tulcea, Romania, 8–9 October 2010; Book II, pp. 543–546.
2. Moldovan, L. Innovative tools and models for vocational education and training. *Rev. Manag. Econ. Eng.* **2010**, *9*, 282–290.
3. Moldovan, L.; Moldovan, A.-M. Green methodology for learning assessment. *Procedia Technol.* **2016**, *22*, 1176–1183. [[CrossRef](#)]
4. Wang, M.A. Framework of performance-oriented workplace e-learning. In *E-Learning in the Workplace. Explorations in the Learning Sciences, Instructional Systems and Performance Technologies*; Springer: Cham, Switzerland, 2018; pp. 95–103.
5. Moldovan, L. QFD employment for a new product design in a mineral water company. *Procedia Technol.* **2014**, *12*, 462–468. [[CrossRef](#)]
6. Ciobanu, I.; Stanculescu, D.I.; Iliescu, A.; Popescu, A.M.; Seiciu, P.L.; Mikolajczyk, T.; Moldovan, F.; Berteau, M. The Usability pilot study of a mechatronic system for gait rehabilitation. *Procedia Manuf.* **2018**, *22*, 864–871. [[CrossRef](#)]
7. Moldovan, F. New approaches and trends in health care. *Procedia Manuf.* **2018**, *22*, 947–951. [[CrossRef](#)]

8. Fleming, J.; Becker, K.; Newton, C. Factors for successful e-learning: Does age matter? *Educ. Train.* **2017**, *59*, 76–89. [CrossRef]
9. Mikolajczyk, T.; Moldovan, L.; Chalupczak, A.; Moldovan, F. Computer Aided Learning Process. *Procedia Eng.* **2017**, *181*, 1028–1035. [CrossRef]
10. Mikolajczyk, T.; Moldovan, F.; Ciobanu, I.; Chalupczak, A.; Marin, A.G. Brain research using computer test. *Procedia Technol.* **2016**, *22*, 1113–1120. [CrossRef]
11. Kimiloglu, H.; Ozturan, M.; Kutlu, B. Perceptions about and attitude toward the usage of e-learning in corporate training. *Comput. Hum. Behav.* **2017**, *72*, 339–349. [CrossRef]
12. Beinicke, A.; Bipp, T. Evaluating training outcomes in corporate e-learning and classroom training. *Vocat. Learn.* **2018**, *11*, 501–528. [CrossRef]
13. Schmidt, C. Innovation and structural change in German vocational education and training. *Int. J. Innov. Educ.* **2015**, *3*, 34–44. [CrossRef]
14. Callan, V.J.; Johnston, M.A.; Poulsen, A.L. How organisations are using blended e-learning to deliver more flexible approaches to trade training. *J. Vocat. Educ. Train.* **2015**, *67*, 294–309. [CrossRef]
15. Work-Based Training Approach in the Field of Industry 4.0 for Competitive European Industry—iNduce 4.0 Project. Available online: <http://induce-project.eu/ro> (accessed on 28 February 2020).
16. Moldovan, L. State-of-the-art analysis on the knowledge and skills gaps on the topic of Industry 4.0 and the requirements for work-based learning. *Procedia Manuf.* **2019**, *32*, 294–301. [CrossRef]
17. Moldovan, L. Review of legislation framework in the field of work-based learning. *Procedia Manuf.* **2019**, *32*, 302–308. [CrossRef]
18. Moldovan, L. State-of-the-art analysis on the knowledge and skills gaps on the topic of Industry 4.0 and the requirements for work-based learning in Romania. *Sci. Bull. “PetruMaior” Univ. TîrguMureş* **2018**, *15*, 32–35. [CrossRef]
19. European Quality Charter on Internships and Apprenticeships. Available online: <https://www.youthforum.org/quality-internships> (accessed on 28 February 2020).
20. Belaya, V. The Use of e-learning in vocational education and training (VET): Systematization of existing theoretical approaches. *J. Educ. Learn.* **2018**, *7*, 92–101. [CrossRef]

**Publisher’s Note:** MDPI stays neutral with regard to jurisdictional claims in published maps and institutional affiliations.



© 2020 by the author. Licensee MDPI, Basel, Switzerland. This article is an open access article distributed under the terms and conditions of the Creative Commons Attribution (CC BY) license (<http://creativecommons.org/licenses/by/4.0/>).



Proceedings

# Good Practices and Results for the Implementation of a Framework of Sustainable Development in Higher Education <sup>†</sup>

Liviu Moldovan

Faculty of Engineering and Information Technology, “George Emil Palade” University of Medicine, Pharmacy, Science, and Technology of Targu Mures, 1 Nicolae Iorga street, 540088 Targu Mures, Romania; liviu.moldovan@umfst.ro; Tel.: +40-740-498-427

<sup>†</sup> Presented at the 14th International Conference INTER-ENG 2020 Interdisciplinarity in Engineering, Mures, Romania, 8–9 October 2020.

Published: 29 December 2020

**Abstract:** Sustainability assessment implies a complex evaluation due to its multidisciplinary aspects. The new eQvet-us framework for sustainability evaluation was developed based on the principle that training contributes to the development of human capital, enhances social cohesion and should also pursue financial sustainability and environmental responsibility. This paper presents the testing and implementation results of the framework for sustainable development in a higher education institution. It highlights good practices and results that can be used by other similar institutions, which carry out continuous training programs.

**Keywords:** quality framework; sustainability evaluation; vocational education and training; social responsibility

---

## 1. Introduction

The increasing recognition of environmental values in our society and the changing nature of work have necessitated a shift in the way that we think and act in learning and in life. The recent integration of generic skills into vocational education and training has paved the way for the inclusion of sustainability skills and can be used to provide direction in this process [1].

Education for sustainability [2,3] is now a widely accepted concept, which seeks to promote and develop sustainability skills and awareness [4,5] throughout a learner’s educational pathway [6]. However, there is a lack of a comprehensive theoretical framework for understanding sustainable development and its complexities [7].

Sustainability assessment [8] implies a complex evaluation due to the multidisciplinary aspects [9] including environmental, economic and social, but also cultural factors [10], which has to be green [11]. Such an appraisal methodology supports decision making and institutional policy development. In this context, the assessment process requires an identification of the organizational aspects that contribute to a sustainable development and the ones that are not relevant for the purposes of the evaluation [12].

The new eQvet-us framework for sustainability evaluation [13] was developed based on the principle that training contributes to the development of human capital, enhances social cohesion and should also pursue financial sustainability and environmental responsibility.

The objective of this paper is to test and implement the framework for sustainable development in a higher education institution and to highlight good practice results that can be used by other similar institutions that carry out continuous training programs.

## **2. Method**

The research methodology consists of a series of steps that need to be taken by vocational education and training (VET) providers in order to: find out the state of the organization in the sense of eQvet-us; detect improvement possibilities; take measures for the improvement and monitor the results and the new state of the organization in the sense of continuous improvement [14].

eQvet-us quality framework establishes a series of indicators addressed at VET providers that already have quality management systems (QMS) incorporated in their organizations and wishes to continually improve the effectiveness of the quality management system, through the establishment of quality indicators in order to monitor and promote their sustainable development.

The eQvet-us framework is founded upon the 3 pillars of sustainable development: social, economic and environmental, embedded in the 7 social responsibility (SR) core subjects referenced in ISO26000, adapted to the training delivery context: organizational governance, human rights, labor practices, environment, fair operating practices, consumer issues, community involvement and development.

eQvet-us quality framework has been structured in 4 main phases, each of them corresponding to the 4 phases of the quality cycle, with respect to the training provision and delivery. For each correspondence with the core subjects of social responsibility eQvet-us framework establishes a specific indicator and a set of guiding questions, to support the self-evaluation process of VET providers with regard to the implementation of a sustainable model to continuously improve quality in VET. The list of indicators is presented in Table 1 according to each phase and respective activity.

In order to implement and use the eQvet-us framework in an organization, a practice set consisting of a self-diagnostic tool and implementation guide are elaborated [15].

Table 1. eQvet-us framework indicators matrix.

eQvet-Us Framework Indicators Matrix	1. Organizational Governance	2. Human Rights	3. Labor Practices	4. Environment	5. Fair Operating Practices	6. Consumer Issues	7. Community Involvement and Development	
P. Design of training provision	P.A. Training pathways planning and design	P.A.1 Decision making processes and structures	P.A.2 Accessibility of training programs addressed to disadvantaged groups	P.A.3 Health and Safety risk matrix	P.A.4 Environmental impact plan	P.A.5 Fair operational practices	P.A.6 Fair marketing & advertising practices	P.A.7 Community engagement actions
	P.B. Curriculums design	P.B.1 Existence of multicultural dimension	P.B.2 Training contents accessible and understandable	P.B.3 Definition of practical training materials	P.B.4 Environmental criteria to select the training materials	P.B.5 Commitment with property rights	P.B.6 Curriculums design for people with special educational needs	P.B.7 Training contents adapted to the community and company's needs.
I. Training delivery	I.A. Implementation of the training path	I.A.1 Attribution of training grants	I.A.2 Specific pedagogic approaches	I.A.3 Existence of health and safety conditions	I.A.4.1 Use of recycled materials I.A.4.2 Waste recycling	I.A.5 Ethical behavior practices	I.A.6 Use of stereotyped materials	I.A.7.1 Partnership and networking I.A.7.2 Work placements in community organizations
	I.B. Learning assessment	I.B.1 Assessment mechanisms	I.B.2 Tools for the assessment of the learning outcomes	I.B.3 Verification criteria of the working process	I.B.4 Environmental friend evaluation tools	I.B.5 Transparency and anticorruption practices	I.B.6 Nondiscriminatory assessment	I.B.7 Involvement and participation of companies and partners
E. Training evaluation	E.A. Evaluation of satisfaction	E.A.1 Assignment of monitoring mechanisms	E.A.2 Degree of learners satisfaction	E.A.3.1 Degree of staff satisfaction E.A.3.2 Degree of trainers satisfaction	N/A	N/A	E.A.6 Degree of clients satisfaction	E.A.7 Degree of satisfaction among enterprises, partners, stakeholders
	E.B. Evaluation of Training Impact	E.B.1 Evaluation monitoring mechanisms	E.B.2 Percentage of identified positive results	E.B.3 Improvement of the working conditions	E.B.4 Improvement of the environmental consumption	E.B.5 Long-term training partnerships	E.B.6 Training impact on trainees' job performance	E.B.7 Employability within the community
R. Continuous improvement	R.A. Self-evaluation	R.A.1 Self-evaluation tools	R.A.2 Assurance of freedom of expression	R.A.3.1 Consultation with all the staff R.A.3.2 Life balance mechanisms	R.A.4 Mechanisms to monitor energy consumption and waste	R.A.5 Feedback to VET provider staff	R.A.6 Handling complaints	R.A.7 Initiatives with the community
	R.B. Training pathways reengineering	R.B.1 Modifications made to the training pathways	R.B.2 N/A	R.B.3.1 Modifications of working processes relating to health and safety conditions R.B.3.2 Logistic changes	R.B.4 Environmental measures	R.B.5 Recognition and reputation strengthening	R.B.6 Pricing strategy re-evaluation	R.B.7 Good practices and transfer of experiences

### 3. Results

The VET provider Continuous Education Centre (CEC) from “George Emil Palade” University of Medicine, Pharmacy, Science, and Technology of Targu Mures (UMFST) conducted a pilot test for the implementation of a framework for sustainable development and the self-assessment tool over one week. The test involved a group of four staff members with different jobs: a training coordinator in charge of relations with companies, a trainer, a quality assurance specialist and administrative assistant. At the end of the self-assessment and diagnosis, the information was used in a common meeting for an internal improvement action plan proposal.

It was appreciated that the sustainability enforcement already exists in many different forms and diverse levels at UMFST in particular and throughout Romanian VET providers in general. The overall appreciation of the pilot implementation at UMFST is positive and revealed some results.

As regards environmental sustainability the outlined practices in each indicator are:

P.A.4 Environmental impact plan—the environmental connection of UMFST as a VET provider was not clear at first sight, but like in the case of every other institution or enterprise, it was concluded that the organization has to make decisions with an environmental impact on a daily basis. UMFST starts from the service delivery and consumption involving many factors, which are mentioned in the environmental pillar, such as the waste problem, resource productivity and consumption. Additionally, UMFST will encourage suppliers to improve the environment imposing relevant environmental requirements for their supplied products in order to reduce environmental impact.

P.B.4 Environmental criteria to select the training materials—the vision of the paperless class and office are still topical. “Going Paperless” can save money and space, produce electronic documentation and information easier to share, which minimize the environmental damage. On the other hand, it was showed that the introduction of the personal computer to offices increased paper usage instead of minimizing it, as it facilitated paper prints even if this was not necessary. Regarding the curricular content of the training materials, it is essential to highlight the importance of education for all trainees to achieve sustainable development. The competence-based model is the means of achieving educational and societal transformation towards sustainability, framed by a shared vision about quality education and a society that lives in harmony with the world’s natural capacity. Environmental education—in whatever form—actually supports and promotes more sustainable development in practice; its development is accompanied by the implementation of a problem-based learning approach, environmental impact assessment, environmental protection rules and integration of knowledge management.

I.A.4.1 Use of recycled materials—the main issue was to use digital documents in order to reduce paper consumption. Higher emphasis is placed on recycling printed paper, but also on the delivery of materials electronically rather than on paper. Another issue is related to the possibility that suppliers recover used products for recycling, such as toner cassettes for printers, copying machines and faxes. Another measure is the use of recycled plastic/paper garbage bags, reuse of printing and copying materials packaging materials, boxes, etc.

I.A.4.2 Waste recycling—the first step is to promote and ensure recycling, waste separation and circular economy. This approach is followed by issues related to the reuse of paper and separate waste collection.

I.B.4 Environmental friendliness evaluation tools—the main issue related to this topic is the use of assessment methods, which can be applied electronically rather than on paper. This approach will be extended via the use of software evaluations during classes and exams using computers, laptops, tablets and iPods, by extending the existing software such as: the student response system (SRS), peer learning evaluation (PeLe), One2act and also the learning management systems—Moodle. A supporting factor is that most of the students have mobile phones with touch sensitive screens that facilitate mobile learning in large course-rooms with Wi-Fi networks.

E.B.4 Improvement of the environmental consumption—regarding the use of raw materials, the main issue is the reduction of paper consumption due to electronic learning supports. The delivery

of materials in electronic rather than paper-based format is encouraged, in addition to printed paper recycling. The objective of water management aims to minimize consumption. Optimization is performed by developing awareness of staff members and participation in training courses. Additionally, sustainable consumption was promoted by providing course participants and employees with the possibility to purchase fair-trade products and locally produced fruits during course breaks. This reflects the idea of integrating environmental concerns into the decision making process of businesses, labeled as “Green Business”.

Another issue was that the production of electronic devices, such as tablets, computers, etc., consumes a lot of natural resources (water, raw materials such as Coltan, etc.) and the use of a “green computer” is a key requirement in this context.

R.A.4 Mechanisms to monitor energy consumption and waste—the starting point was climate change and energy and it was appreciated that energy efficiency is probably the most important aspect to which UMFST can contribute as a VET provider. This includes logistics, an evaluation of the course locations in terms of heating, water consumption and current supply, and “energy education”: this implies energy saving methods and staff training with regard to these measures (e.g., turn off the lights when leaving the office, avoid stand-by, etc.) using energy-saving controls. Additionally, UMFST aims to decrease electricity consumption by using energy-efficient equipment: fluorescent lamps, lighting control in rooms with low traffic by installment of detectors and signs for light turn-off. When buying new technological devices for the office (e.g., computers and mobile phones), an important factor is the energy consumption of the device and its energy-saving potential. While it is always possible to act efficiently from the perspective of energy consumption, it may be more complicated to promote clean energy. Then it was recommended that UMFST should search for providers who offer clean energy supply.

R.B.4 Environmental measures—in regards to water pollution, the chemicals are envisaged by reduction in the use of environmentally hazardous products: the chemicals risk phases are written down in plain text on a chemical list; good laboratory safety and chemical management is ensured in order to reduce the risk of injury on the environment and human health and non-chemical cleaning methods are used where it is possible. In regards to soil management and pollution, the use of products that respect the environment and have local origin is promoted and encouraged. By imposing relevant environmental requirements to suppliers to reduce their environmental impact and encourage suppliers to improve the environment, UMFST is committed to purchasing products, which cause as little environmental damage as possible, the ecolabels. The European ecolabel (ecolabel printing and copying paper and envelopes) is the guarantee of trust, which informs suppliers with regard to UMFST environmental requirements: a written environmental policy and a diploma or certification about the products. In the advertising and marketing process, all externally produced printed materials, etc., are ecolabeled, which implies an environmentally friendly printing process. Rechargeable small batteries are used. In regards to air pollution and greenhouse gas, efforts are concentrated on transport-related issues. Contacts, human encounters and communication are key elements of UMFST business. Meetings can be implemented in different ways. The active selection of environmentally friendly means of transportation can reduce the environmental impact. UMFST will promote holistic travel and transport, including avoiding unnecessary traveling by making use of various remote meeting systems: internet conference, Skype meeting, video laboratory meetings with codecs, etc.; leverage of own technology expertise to develop new ways of “remote working”; promoting and development of car-sharing practices; increasing information regarding public transports and greater use of trains and buses instead of cars and planes.

As regards the social sustainability, the relation between the UMFST added value and its social impact were analyzed. Efforts are concentrated towards minimizing negative social impact such as work accidents, human rights abuses, exploitation, mobbing of employees, etc., and maximizing positive ones, in relation to the added value.



Actions within the sphere of social responsibility include providing continuing education and training for staff in the framework of annual programs organized by UMFST, compatibility of career—work—and private life (e.g., by offering study facilities for member families), job safety and health assurance by a specialized service and equal opportunities for all human beings employed in UMFST.

UMFST has ensured that all employees have a health insurance according to the legal regulations of Romania. They work in an environment that promotes good health rather than causing health problems (through stress, mobbing, exhaustion, excessive demand, etc.). UMFST guarantee that basic human needs are met; this includes sufficient space and breaks, pleasant room temperatures, comfortable chairs, fresh air, etc. UMFST trainers and teachers are instructed annually in order to have the ability to give first aid and react adequately in situations of danger like: in the case of fire, earthquake and distress. UMFST is aware of its role as a health educator in the sense that it helps staff to improve their knowledge about health and hygiene and equips them with the skill to make provisions for their own health.

As regards social inclusion, the challenge resides in motivating “education resistant” groups to participate in educational activities and in including people who cannot afford to participate in VET courses due to their occupational duties and to economic constraints. For this purpose, we organized the Open Distance Learning Department, which offers distance learning for trainees who cannot attend daily courses.

As regards demography, UMFST is concerned with ensuring diversity by the employment of young people due to the fact that there are many teachers who are over 50 years old.

The economic sustainability is the central focus of socioeconomic sustainable development and sustainable consumption and production. We performed analyses regarding the number of trainers/teachers in relation to the number of trainees/students, but the perspective to expand is limited due to the demographic decrease.

The Counseling and Career Orientation Centre performs regular studies about the number of graduates who are able to enter the labor market after having completed a degree/training course.

The economic aspect is analyzed in terms of UMFST profitability regarding investments in research, development and innovation.

Sustainable consumption and production will be promoted by providing course participants and employees the possibility to purchase fair-trade products during course breaks in the university restaurant. A report about UMFST sustainability is posted on the institutional website [16].

#### **4. Conclusions**

The eQvet-us framework is different from others in terms of its objective, which consists of determining environmental impact improving the environmental, economic, social and quality of the training system.

The assessment tool helps training providers in order to: (a) check the level of performance for each area within the framework; (b) identify improvement possibilities for all categories and (c) make decisions and set priorities in relation to the three pillars, activities and business projects.

With this support, an innovative aspect of the framework is that it promotes the development of a strategy based on performance indicators that integrates sustainable development.

We consider that sustainable development strategy has a central role in the competitive strategy of the organization and we believe that it determines the other competitive strategies of a VET provider: marketing, training delivery, partnerships, etc. Such strategies describe how the VET provider plans to gain advantage over competitors, for example with the support of technology by using new educational technologies such as distance training, blended learning, learning management systems and video systems for the delivery of training with paperless support; strategies using the alternance model for training by working part-time with an employer; etc.

In regards to the methodological approach of the new framework for sustainable development, the multitude of indicators employed requires an assessment group of committed experts to accomplish the assessment.

The quality of the assessment depends on the availability of data at the assessed institution. In optimal conditions, the results of the assessment have to be objective and precision may be an issue that facilitates the progress of evaluations.

The results of self-evaluation are adequate to be used for establishing a sustainability baseline, to identify possibilities for improvement, and to prioritize the implementation.

Furthermore, the results can be used to develop sustainability policies and action plans, establish performance guidelines and improve internal sustainability performance of institutions in various fields of activity [17,18]. This will have direct relevance to improved economic and social performance, institutional effectiveness and an enhanced image of the organization [19,20].

Graduates of such institutions that implement the framework for sustainable development will naturally be sustainability driven.

**Funding:** This research was funded by the Erasmus+ European Programme, project number 2014-1-RO01-KA202-002758, project title “European Quality Assurance in VET towards new Eco Skills and Environmentally Sustainable Economy”.

**Conflicts of Interest:** The author declares no conflict of interest.

## References

1. Goldney, D.; Murphy, T.; Fien, J.; Kent, J. Finding the Common Ground: Is There a Place for Sustainability Education in VET? A National Vocational Education and Training Research and Evaluation Program Report. Available online: <https://files.eric.ed.gov/fulltext/ED499704.pdf> (accessed on 20 March 2020).
2. Moldovan, L. Design and development of innovative tools and models for e-learning in central and western Romania. In Proceedings of the 6th International Seminar Quality Management in Higher Education—QMHE2010, Tulcea, Romania, 8–9 July 2010; Volume II, pp. 543–546.
3. Moldovan, L. Innovative tools and models for vocational education and training. In *Review of Management and Economic Engineering-First Management Conference: Twenty Years after-How Management Theory Works*; Toderico Publishing House: Cluj-Napoca, Romania, 2010; Volume 9, pp. 282–290.
4. Moldovan, L. Innovative Models for Vocational Education and Training in Romania. *Procedia Soc. Behav. Sci.* **2012**, *46*, 5425–5429. [[CrossRef](#)]
5. Moldovan, L. Innovative Method of Peer Assisted Learning by Technology and Assessment of Practical Skills. *Procedia Technol.* **2014**, *12*, 667–674. [[CrossRef](#)]
6. Moldovan, L. Design of a New Learning Environment for Training in Quality Assurance. *Procedia Technol.* **2014**, *12*, 483–488. [[CrossRef](#)]
7. Jabareen, Y. A New Conceptual Framework for Sustainable Development. *Environ. Dev. Sustain.* **2006**, *10*, 179–192. [[CrossRef](#)]
8. Moldovan, L. Sustainability Assessment Framework for VET Organizations. *Sustainability* **2015**, *7*, 7156–7174. [[CrossRef](#)]
9. Moldovan, L. New Evaluation Model by Means of Mobile Technology. *Procedia Technol.* **2015**, *19*, 1094–1101. [[CrossRef](#)]
10. Moldovan, L. Training outcome evaluation model. *Procedia Technol.* **2016**, *22*, 1184–1190. [[CrossRef](#)]
11. Moldovan, L.; Moldovan, A.-M. Green Methodology for Learning Assessment. *Procedia Technol.* **2016**, *22*, 1176–1183. [[CrossRef](#)]
12. Sala, S.; Ciuffo, B.; Nijkamp, P. A systemic framework for sustainability assessment. *Ecol. Econ.* **2015**, *119*, 314–325. [[CrossRef](#)]
13. Moldovan, L. Framework Development for European Quality Assurance in VET Towards Environmentally Sustainable Economy. *Procedia Eng.* **2017**, *181*, 1064–1071. [[CrossRef](#)]
14. Moldovan, L. The Environmental Pillar Assessment in Vocational Education. *Environ. Eng. Manag. J.* **2017**, *16*, 739–750. [[CrossRef](#)]

15. Moldovan, L. Practical Implementation of a Framework for European Quality Assurance in VET towards Environmentally Sustainable Economy. *Procedia Eng.* **2017**, *181*, 1072–1079. [[CrossRef](#)]
16. Mikolajczyk, T.; Moldovan, L.; Chalupczak, A.; Moldovan, F. Computer Aided Learning Process. *Procedia Eng.* **2017**, *181*, 1028–1035. [[CrossRef](#)]
17. Sustainable Development Report of “George Emil Palade” University of Medicine, Pharmacy, Science and Technology of Târgu Mureş (UMFST). Available online: [https://green.umfst.ro/?pdf=En\\_UMFST\\_sustainability\\_report](https://green.umfst.ro/?pdf=En_UMFST_sustainability_report) (accessed on 8 July 2010).
18. Moldovan, F. New Approaches and Trends in Health Care. *Procedia Manuf.* **2018**, *22*, 947–951. [[CrossRef](#)]
19. Moldovan, L. QFD Employment for a New Product Design in a Mineral Water Company. *Procedia Technol.* **2014**, *12*, 462–468. [[CrossRef](#)]
20. Ciobanu, I.; Badea, D.I.S.; Iliescu, A.; Popescu, A.M.; Seiciu, P.L.; Mikolajczyk, T.; Moldovan, F.; Berteanu, M. The usability pilot study of a mechatronic system for gait rehabilitation. *Procedia Manuf.* **2018**, *22*, 864–871. [[CrossRef](#)]

**Publisher’s Note:** MDPI stays neutral with regard to jurisdictional claims in published maps and institutional affiliations.



© 2020 by the author. Licensee MDPI, Basel, Switzerland. This article is an open access article distributed under the terms and conditions of the Creative Commons Attribution (CC BY) license (<http://creativecommons.org/licenses/by/4.0/>).

Proceedings

# English for Specific Purposes in the Context of the Shifting Educational Paradigm Triggered by Industry 4.0 †

Dana Rus 

Department of Sciences and Letters, “George Emil Palade” University of Medicine, Pharmacy, Science, and Technology, 540142 Targu Mures, Romania; dana.rus@umfst.ro

† Presented at the 14th International Conference INTER-ENG 2020 Interdisciplinarity in Engineering, Mures, Romania, 8–9 October 2020.

Published: 8 January 2021

**Abstract:** The paper proposes a model for a prospective approach to the study of the English language for engineering students. This model is influenced and shaped by the consideration of the necessity of educating engineering students for the realities of Industry 4.0. Given the dramatically changing paradigm of language teaching and language teaching aims, a critical selection on the part of the teacher is indispensable when it comes to choosing the most adequate teaching resources. The paper includes theoretical and practical suggestions to approach the ESP (English for Specific Purposes) seminar, which can lead to the improvement and fine-tuning of students’ skills and attitudes in view of Industry 4.0 realities.

**Keywords:** English for Specific Purposes; Education 4.0; soft skills; oral communication; language education

---

## 1. Context: Industry 4.0 and Education 4.0

The huge technological advancements brought to humankind by Industry 4.0 cannot overlook any major sector of our world. The educational domain is definitely marked, reshaped, and influenced by these tremendous changes. “Education 4.0” is the umbrella term that encompasses the changes which educational systems must undergo to align with these technological changes. The reconfiguration of the role of education is natural under these circumstances; all great changes in human society—including all previous industrial revolutions—are bound to affect the sector responsible for education. Young generations must be educated in accordance with the new set of values brought about by industrial changes; they must develop, and exercise skills and aptitudes required by shifting technological realities. Lack of correlation between educational policies and objectives and the technological reality in which students will act leads to poor results, inability to adjust and fulfill obligations, and eventually professional failure.

The correlation between the 4th industrial revolution and education is approached in various studies. Bernard Marr [1] identifies a list of requirements that should be implemented in schools to prepare students for contemporary technological advancements. These requirements are a redefinition of the purpose of education, the improvement in STEM (science, technology, engineering, math) education, the development of human potential, the implementation of lifelong learning models, the alteration of education training, the transformation of schools into makerspaces, international mindfulness, and changes in higher education. Similarly, Brian E. Penprase holds that the 4th industrial revolution will affect deep changes in the way education is perceived and will trigger the necessity of more creative individuals, with an emphasis on collaborative work, interconnectivity, interdisciplinarity, and deep intercultural understanding [2]. Self-directed learning and thinking,

ethical thinking, intercultural awareness, critical thinking, and students' empowerment in the view of accomplishing their full potential are also trends favored by the new approach to education triggered by Industry 4.0. These are all commonly perceived as critical elements in students' ability to efficiently apply their knowledge in the technological world in rapid, unprecedented expansion. These new requirements bring about inevitable curricular changes. Schools must adapt to the realities of the day to produce well-informed and well-trained specialists.

Consequently, the concept of Career and Technical Education (CTE) has become increasingly popular, its main objective being that of providing students with specific tech-based and career-oriented skills. Within this framework, the emphasis is placed on developing human potential, boosting students' creativity, and the practice of soft skills, which are considered to be the essential elements to prepare students for the realities of the Industry 4.0 workplace [3].

Additionally, another way in which modern education may respond adequately to the challenges posed by Industry 4.0 represents the resort to hybrid teaching, combining online and on-site instruction. Blended learning, flipped courses, BYOD ("bring your own device") in the classroom, online activities may constitute more efficient learning tools, preparing students for the diversity of technological resources in contemporary workplaces. The current sanitary situation which humanity is currently facing has been a mere catalyst of an otherwise inevitable shift to modern, integrated, interconnected teaching resources.

Personalized learning is another feature of Education 4.0. With the huge amounts of information made possible by technology, mass learning is no longer the right technique for a generation characterized by intense heterogeneity in terms of knowledge and information. Therefore, education needs to be more and more a personal topic. Tailor-making learning objectives, techniques, and methods is an appropriate way of respecting individual differences and potential and taking them to a higher level.

Another educational priority imposed by Industry 4.0 in education is project-based learning. Learning information by heart and assimilating theory without practice does not work in the context of our technologically dominated world where every little thing is part of a larger practical concept. Schools will have to adapt this model and prepare students to learn by doing. Besides the practical value of such an approach, projects are also useful in learning organizational skills, management skills, collaborative skills—all fundamental aspects of a successful professional.

That education must change is beyond question. Such a huge technological revolution as Industry 4.0 ineluctably affects every aspect of human life, just as the other three revolutions which preceded it. In terms of education, we cannot teach students like in the past for a future that is so tremendously different. New types of professionals are needed, ones who are digitally literate, open to sudden change, versatile to perform tasks that appear overnight. Educational institutions must take this into account and align with this rapid technological development. "Education 4.0" is a concept derived from this necessity of alignment. The products of this new approach to education will enable people to explore the new possibilities of our modern times.

## **2. Industry 4.0 and English for Specific Purposes**

### *2.1. Background: Towards a New Approach to Teaching English*

To what extent can the features above be served in the context of English language education in universities? Professional communication is an important part in this respect. Students' fluency in a foreign language is essential in a world where the utilization of technology relies heavily on English language knowledge. Moreover, English language classes can help students develop inter-communication skills, technology literacy, and form positive attitudes regarding group dynamics through repeated practice.

To teach English for Specific Purposes in line with the requirements of Industry 4.0, an emphasis on soft skills is the right approach. Taking into account all the conditions presented above, triggered by the new industrial revolution which we are part of, English teachers should essentially reconsider their

role. We are no longer providers of information; this is so easily accessible nowadays. English grammar or technical vocabulary and the discrete point exercises practicing them in the language class are now rendered obsolete by the new realities: endless glossaries of extremely specific terminology, grammar explanations, and online translation tools at the tip of anyone's little finger. The traditional 'handout-based' approach is useless when there are huge resources of online material of the most diverse types. The once-fashionable emphasis on the traditional language skills and the adjacent subskills is only a good starting point, and a means to a higher end.

Which is then this higher end? Which should be the better approach for teaching English for Specific Purposes to students who will be full-time actors on the stage directed according to the requirements of Industry 4.0? In a world of interconnectivity, fast race technological developments, cyber-physical systems, and artificial intelligence, which is the role of English language seminars?

Besides the obvious answer that an interconnected world needs communication and English has the status of the universal language, the analysis goes deeper than this. In light of their specificity, English language seminars may have the objective of developing soft skills and attitudes. Soft skills may be defined as "character traits, attitudes, and behaviors rather than technical aptitude or knowledge, [ . . . ] intangible, non-technical, personality-specific skills that determine one's strength as a leader, facilitator, mediator and negotiator" [4].

The specific activities aimed at developing professional communicative competence can, therefore, achieve other objectives: They may be the opportunity for students to develop critical thinking, to express and defend opinions, to negotiate, to think creatively, to develop independent working routines, to collaborate, to work in groups, to reach agreement, to boost their versatile capacities and lower their resistance to change, to perform information transfer, to speak in public, to present professional information. These are but a few of the conditions which are expected from future employees if they are to perform successfully in a world dominated to a greater and greater extent by the philosophy behind the concept of Industry 4.0.

These educational scopes are recognized by many authors. Chamorro-Premuzic, among others, asserts the necessity that universities should implement "a set of non-academic attributes, such as the ability to cooperate, communicate and solve problems, often referred to as generic or soft skills in higher education", due to the fact that "unlike academic or disciplinary knowledge, which is subject-based, content-specific and formally assessed, soft skills comprise a range of competencies that are independent of, albeit often developed by formal curricula and rarely assessed explicitly" [5].

## *2.2. A Questionnaire Testing Student Perception*

Whenever changes are to be implemented, it is important to have a complete overview of all the stakeholders involved in the process. In the concrete case of any attempt to improve the outcomes of English language seminars for Engineering students, it is important to have an analysis of students' perceptions. Students are great and objective observers when it comes to course evaluation; they are perfectly capable of identifying their learning needs, their strong points, and deficiencies. Moreover, they are sometimes more connected to technical and professional realities than teachers are. They are "digital natives", while teachers are "digital immigrants" [6]. A reconsideration of the grounds on which teachers should reshape English language seminars should consider students' feedback as an essential factor.

To find an answer to the questions above, we applied a questionnaire to 1st- and 2nd-year students within the Department of Electrical Engineering and Information Technology (specializations: Automation and Medical Engineering) from "G.E. Palade" University of Medicine, Pharmacy, Sciences and Technology in Targu Mures, Romania. The questionnaire was applied in March 2020. During the previous semester, I attempted to include principles inspired by the requirements of Industry 4.0 presented above. This new approach included a predominant emphasis on oral communication and public speaking on a variety of topics, a greater resort to technology in the teaching process (by using a lot of educational websites and applications, but also by using genuine online

resources as teaching material), project-based assessment, peer assessment, self-assessment, blended learning, information transfer exercises, oral presentations, building effective visual support, debates, group work, teamwork, role-play, flipped classroom, etc.

The questionnaire consisted of 6 questions, both closed and open-ended, and was used to obtain students' perspective, in their capacity of end-users, of the way English language seminars should be conducted so that they serve the purposes of better preparing students for real-life professional situations. The questions were the following:

1. On a scale from 1–10, assess the importance of the English language seminar as part of the general engineering curriculum.
2. Which is the most important skill/aspect of language in your learning process?
  - Grammar
  - Vocabulary;
  - Pronunciation;
  - Reading skills;
  - Listening skills;
  - Writing skills;
  - Oral communication skills;
  - Other, namely.
3. Continue the sentence: "It is important for a future engineer to learn English because ... "
4. Continue the sentence: "What I like about studying English in university is ... "
5. Continue the sentence: "What I dislike about studying English in university is ... "
6. In order to be effective for engineering students and prepare us for real life, English should be taught:
  - In the traditional way, focusing on general language skills;
  - With an emphasis on technical vocabulary;
  - With an emphasis on grammatical accuracy;
  - With an emphasis on developing personal and inter-personal skills;
  - By resorting to technology as much as possible (web sites, apps, etc.);
  - Other, namely.

The questionnaire was answered anonymously by 40 students of the Faculty of Engineering. The first question is an acknowledgment of students' appreciation of the importance of the English language in the education of a future engineer, with 16 students (40%) considering that English has the highest importance.

The second question did not restrict students to only one answer; the intention of the question was to reveal to what extent students are aware of their personal priorities in terms of language acquisition. In addition, the question was intended to guide the teacher in setting the learning objectives of the future English classes so that a wider variety of learning styles are addressed. A great majority of students (95%) mentioned oral communication skills, which was the most popular answer. The next one in the order of students' preferences was language functions (40% of the answers mentioned this), writing (34%), vocabulary (28%), reading (27%), grammar (25%), pronunciation (20%), listening (16%). Two students chose "other" and wrote slightly similar answers referring to an integrated skills approach to languages.

Most of the answers to question 3 alluded to the importance of the English language in terms of finding a good job, understanding technical and other work-related documents, and keeping good interpersonal relations in the professional environment. This confirms the fact that students are aware of the conditions needed to perform on the labor market and how the English language seminar can be



the opportunity to develop essential skills, aptitudes, and attitudes. One of the students wrote that "Knowing a foreign language is essential for an engineer nowadays. We need English to communicate with our colleagues, with the clients, with suppliers. Documentation for the most modern equipment is in English, and so is all the specialized software. Most of the engineering companies are connected with the international business environment, so the knowledge of English can help our professional advancement."

Questions 4 and 5 were intended to provide objective feedback regarding the activity of the previous academic semester. Motivation is an essential factor in learning; one learns best when one is motivated to do so. It is important that the teacher know what students like doing in terms of activities, resources, patterns of interaction, assessment types, etc. Here are some of the students' answers, "I like that we focus on activities which develop our communicative abilities"; "I like that we learned and practiced how to express ourselves in public"; "It was useful for me to learn how to construct a communication strategy in English and deliver it in front of the class"; "I appreciate that we have to speak a lot, even if not everybody finds this comfortable"; "I particularly liked the online games, because I am a passionate gamer"; "I like the assessment through real-life projects instead of the typical exam"; "I enjoyed very much engaging into debates with my colleagues and the situations when we had to play roles". The negative feedback was limited. It mostly referred to situations in which some students' level of English was not good enough to enable them to understand everything. Furthermore, there were some suggestions on working more on technical vocabulary and one which would have appreciated more extensive grammar explanations. Overall, students' answers confirmed the expectation that building the course structure on criteria other than the classical ones, with a much higher emphasis on the development of personal skills, is a factor of success.

The last question had a similar purpose and students' answers confirmed this approach once more. Of the 40 students, no one thought that English should be taught in the traditional way. All of them (100%) consider that the best way to approach languages for engineering students is with an emphasis on developing personal and interpersonal skills and a vast majority (85%) agree on the importance of using technology in the classroom. Twenty students (50%) also acknowledge the importance of teaching technical vocabulary, while a smaller percentage (24%) consider that the focus on grammatical accuracy is the right approach.

### **3. Conclusions**

The findings of the questionnaire are encouraging and helpful for the author's attempt to align the English language seminar for engineering students with the requirements imposed by Education 4.0. The feedback was overwhelmingly positive, with a few exceptions which are extremely useful for future activities. Students' answers show that they are objective assessors of their learning style and priorities and that they acknowledge the benefits of the changes in terms of language learning for their personal and professional growth.

The reform process of the English language seminars falls within the much wider range of the educational system at large. It is an ongoing process in which teachers and students alike must try and adapt to new requirements, implement new methods and resources, and assimilate updated philosophies regarding the role of education and learning. At the same time, it is a trend that cannot be reversed because progress, innovation, and development cannot be reversed either. We live in an era of extraordinary, unprecedented changes that inescapably reflect upon every single aspect of human life, and educational actors will have to adjust accordingly.

**Funding:** This research received no external funding.



## References

1. Marr, B. 8 Things Every School Must Do to Prepare for the Industrial Revolution. *Forbes*, 22 May 2019. Available online: <https://www.forbes.com/sites/bernardmarr/2019/05/22/8-things-every-school-must-do-to-prepare-for-the-4th-industrial-revolution/#3666f65a670c> (accessed on 12 April 2020).
2. Penprase, B.E. The fourth industrial revolution and higher education. In *Higher Education in the Era of the Fourth Industrial Revolution*; Gleason, N.W., Ed.; Palgrave Macmillan: Singapore, 2018; pp. 207–229.
3. Rojewski, J.W.; Hill, R.B. A Framework for 21st-Century Career-Technical and Workforce Education Curricula. *Peabody J. Educ.* **2017**, *92*, 180–191. [[CrossRef](#)]
4. Robles, M.M. Executive perceptions of the top 10 soft skills needed in today's workplace. *Bus. Commun. Q.* **2012**, *75*, 453–465. [[CrossRef](#)]
5. Chamorro-Premuzic, T.; Arteche, A.; Bremner, A.J.; Greven, C.; Furnham, A. Soft skills in higher education: Importance and improvement ratings as a function of individual differences and academic performance. *Educ. Psychol.* **2010**, *30*, 221–241. [[CrossRef](#)]
6. Prensky, M. Digital Natives, Digital Immigrants Part 1. *Horizon* **2001**, *9*, 1–6. [[CrossRef](#)]

**Publisher's Note:** MDPI stays neutral with regard to jurisdictional claims in published maps and institutional affiliations.



© 2021 by the author. Licensee MDPI, Basel, Switzerland. This article is an open access article distributed under the terms and conditions of the Creative Commons Attribution (CC BY) license (<http://creativecommons.org/licenses/by/4.0/>).

Proceedings

# Translation, from Pen-and-Paper to Computer-Assisted Tools (CAT Tools) and Machine Translation (MT) †

Bianca Han

Faculty of Science and Letters “Petru Maior”, “George Emil Palade” University of Medicine, Pharmacy, Science and Technology of Târgu Mureş, 540139 Târgu Mureş, Romania; bianca.han@umfst.ro

† Presented at the 14th International Conference INTER-ENG 2020 Interdisciplinarity in Engineering, Târgu Mureş, Romania, 8–9 October 2020.

Published: 28 December 2020

**Abstract:** This paper reflects the technology-induced novelty of translation, which is perceived as a bridge between languages and cultures. We debate the extent to which the translation process maintains its specificity in the light of the new technology-enhanced working methods ensured by a large variety of Computer-Assisted Translation (CAT) and Machine Translation (MT) tools that aim to enhance the process, which includes the translation itself, the translator, the translation project manager, the linguist, the terminologist, the reviewer, and the client. This paper also hints at the topic from the perspective of the translation teacher, who needs to provide students with transversal competencies that are suitable for the digital area, supported by the ability to tackle Cloud-based translation tools, in view of Industry 4.0 requirements.

**Keywords:** translation process; CAT tools; machine translation; communication; applied linguistics

---

Published: 28 December 2020

## 1. Technology and Translation

The aim of the present paper lies in emphasising the necessity of adaptation to the intrinsic novelty imposed by the actual trend in the evolution of the world, brought about by the development of technology in all the arenas of human activity. Just like the industrial revolutions which preceded it, the fourth Industrial Revolution (commonly referred to as Industry 4.0) goes beyond the industry domain, affecting all spheres of human life. Theoreticians of the concept broadly define the specifics of Industry 4.0 as a fusion of technologies affecting all human activities, connecting the physical, digital, and biological levels. Since translation is perceived as a bridge between languages and cultures, it was only a matter of time until technology-induced novelty influenced the way in which we perform the sophisticated act of rendering words from one language to the other. Thus, we debate the extent to which the translation process still manages to maintain its specificity and particularity in light of the new technology-enhanced working methods ensured by a large (already) and increasing variety of CAT tools (computer assisted/aided translation) and MTs tools (machine translation) that aim to free-flow the entire process of translation, which includes the translation itself, the translator, the translation project manager, the linguist, the terminologist, the reviewer, and the end client. The approach of the author aims to link the use of technology in performing translations nowadays to the greater, more comprehensive phenomenon which we call Industry 4.0, which—although it started as an industrial concept—has now grown to influence every human endeavour. The paper will also hint at the topic from the point of view of the translation teacher, who needs to provide students with the necessary transversal skills and competences that are suitable for the digital area, supported by the ability to tackle the Cloud-based translation tools and software, in view of Industry 4.0 requirements.

The use of technology in translation teaching and, by extrapolation, the use of technology in education is one of the essential features characterizing Industry 4.0. The modern approach in performing translations implies the use of the same technologies and concepts which lie at the foundation of what Industry 4.0 stands for. The use of CAT tools is equivalent to the use of Big Data, artificial intelligence, automation, and digitalization. Moreover, by using CAT tools in the translation classroom, other major requirements of Industry 4.0 are met: the use of technology as a didactic means, the development of students' digital skills, and the integration of various technologies into the normal teaching flow as a basic ingredient.

The importance of translation in a (metaphorically speaking) 'post-Babel world' is already an understatement. The specialised literature on the topic consists of hundreds and thousands of pages, from the earliest over-2000-years-old approaches, attributed to Saint Jerome, acknowledged as the patron of translators, to contributions closer to our times, including those signed by Mona Baker, Roger T. Bell, Susan Bassnett, Umberto Eco, Eugene Nida, and George Steiner, to name only a few. Regardless of their preoccupations and approaches to translation studies—aiming to establish the relationship between word and meaning, the rapport among languages, the (im)possibility to express the intended message in the language of the Other, the precarity of the coding-decoding-recoding of the message, the fidelity towards the original, and the extent to which a translation is prone to lose and win (with)in the process—one of the coordinates that all seem to have agreed upon lies in the fact that translation is an important ingredient in the communication process. Translation enables the so-called cultural bridge, which empowers a perpetual communion of aesthetic values, a communication of the aesthetic identification factor among languages, and also the cognition and recognition of the universal in every language, contributing to the particularisation of a certain language in the general linguistic context, and to linguistic 'globalisation', as we stated in a book published in 2011 [1] (p. 45). In the same book, we read Titela Vîlceanu's opinion regarding the idea that translation appears to be a trans-cultural phenomenon enabling communication that goes beyond any territorial, linguistic, or cultural boundaries [2] (p. 91).

As we belong to a generation that learned how to type on an old typing machine before laying hands on a personal computer, it is only reasonable that we might understand the impact of technology to a greater extent than the generations that followed, who are often referred to as being 'digital-native'. Needless to say, former generations started their education with pen(cil) in hand to scribble on paper, which is still the start today; however, the jump towards the technology-enhanced devices seems to be happening sooner and quicker, and this is applicable to all fields of human activity, including translation, witnessing the evolution from pen-and-paper translation, or even PRAT (Pencil and rubber-assisted translation) [3] (p. 102), to MT and to the more sophisticated CAT tools.

In a broad and simplistic approach to the matter, one could endorse the idea that words were masterfully used and crafted by people first orally, then in (some sort of) writing. We might apply this to the production of original material, and to translation. Irrespective of this, as stated by Kingscott [4] (p.14), in past times, authors and translators would produce their work by hand, first writing a draft, then rewriting it. The portable typewriter came next, followed by the dictating machine as the next technological step, and it was adopted by in-house translation services.

## **2. On CAT Tools and MT**

The present article aims to raise the awareness of the presence and impact of technology upon the translation process, which is expanded to the idea that translation as a process manages not only to survive but also to blossom due to the input of technology. In order to achieve that, one should understand that the two main terms we are describing here, namely MT and CAT tools, are not to be confused or considered to refer to the same reality.

In her online course 'Trends and Reality in Translation Technology' [5], Emmanouela Patiniotaki regards the issue of translation technology as one that considers that all applications and software used by the translator in order to perform a translation project contain translation memories, glossaries,

terminology databases, terminology extraction tools, translation editors, machine translation, alignment, reference management, quality assurance, and review tools. The same author rightfully draws attention to the common misconceptions met in the matter, i.e., those which consider that Translation Technology only implies MT, or that Translation Technology is only intended for technical translation.

We read, in an online article [6], how Jemimah Rodriguez attempts to clarify the difference between the two terms; thus, we are aware of the fact that Computer-Assisted Translation software is a tool which helps translators to translate a text in the languages they work with. It may often be confused with machine translation, which only refers to feeding the text that gets translated without any human involvement. However, what CAT software does is to aid human translators in their translation of a text and saves that text into a database, which is known as Translation Memory (TM). Therefore, CAT tools help in the process of translating. This could be compared to a spell checker in word processing software, which ensures that the spellings in the content are correct. This type of CAT software facilitates the translation of documents without turning the translation process into an entirely automatic one, as Google Translate and other such machine translation tools might do.

Thus, according to A. Imre [3] (p. 210), MT is considered to be that procedure which stands behind analysis performed by an activated computer programme upon the source text in order to generate a target text without the intervention of the human translator. In his book, C.K. Quah [7] (p. 6) also admits that this was the initial goal of machine translation, i.e., to build a completely automatic high-quality translation machine that did not necessitate any human intervention. Nonetheless, in 1952, Bar-Hillel stated that this would be impractical and essentially unattainable.

We understand that MT was initially produced in order to automatise the translation process, as this process was, up to a certain extent, considered intuitive, repetitive, and mechanical, so much so that it was considered prone to customised matching, which may have resulted from possible equivalences between languages. The problems, of course, appeared the minute the language combination was not supported by the desired equivalence, which is often the case. Therefore, even if the rationale behind MT appears to be the simplification of the translation process in the case of formal or formulaic languages, by using artificial intelligence, still, human intervention cannot be substituted by any machine. Thus, it is the translator who needs to give the final touch to the machine-performed action in order to ensure the desired results.

Nevertheless, the subject of MT is a fascinating topic, since it aids the work of the human. That is why even the terminology on the matter seems to be rather generous: as shown in C.K. Quah [7] (p. 6), the terms commonly used to describe translation tools in the field of translation technology are:

- machine translation (MT);
- machine-aided/assisted human translation (MAHT);
- human-aided/assisted machine translation (HAMT);
- computer-aided/assisted translation (CAT);
- machine-aided/assisted translation (MAT);
- fully automatic high-quality (machine) translation (FAHQQT/FAHQMT).

It is evident that the distinctions between some of these terms are not always clear-cut, as we have already seen, but in order to maintain some order, specialists use the generic term ‘machine translation (MT)’ when referring to this issue. Some of the MT engines that are available now online are Google Translate, Babylon, Omniscien Technologies, Tauyou, Microsoft Translator, Kantan, CrossLang, Amplexor, Lingo24, Oneliner, Lionbridge GeoFluent, Systran, and DeepL.

On the other hand, ‘Computer-aided translation’ tools—with the variation ‘Computer-assisted translation tools’ (CAT tools)—seem to be more commonly used among professional translators. Since the topic at hand seems to have been amongst the preoccupation of the specialists in the field of translation technology, the terms used to explain the tools might appear to be rather complicated. These are tools that—just as their name suggests—assist/aid the translators in their job, i.e., the CAT tools segment and parse the text in the source language, which is fed into the software together with

other reference files, if they are necessary or relevant for the translation job; the variants offered to and decided upon by the translators are recorded as translation memories (TM), thus creating the translation database glossary (TB), to be later used by the translators in their future jobs. The more they translate, the larger the TM and TB. Needless to say, this entire process may seem sophisticated, and indeed, it takes time, practice, and patience to learn the rules of the game, but it is a rewarding, as well as a necessary procedure: the modern and up-to-date translator needs to adapt their approach to the new trends in translation and become much more than a mere carrier of meaning from one language to the other.

The current acceptance of the term 'translator' should also include the other tasks he/she needs to perform as a professional: besides that of a gifted and resourceful linguist, he/she also needs to have some knowledge in the field of computer software, in order to be able to deal with the CAT tools in the field of project management, in order to be able to manage his/her translation projects in the field of communication, so as to efficiently run the projects, etc. Out of the multi-layered facets incumbent upon the translation profession, our attention now focuses on the skills and competences from the computer software area. As we stated in an article, B.-O. Han [8] (p. 324), translators find themselves in a situation in which they need to adapt their work to the new tendencies in the field, being aware that this is the future, and that their survival, productivity, and efficiency in the translation market depends on their power of adaptation.

Our intention is not to suggest, or even imply, that the CAT tools perform the translator's job instead of translators. As we underlined in the same article [8] (p. 325), these tools should be understood, handled, and applied with caution in order to support the job of a translator in being achieved faster when facing, for instance, repetitive terms or terminology belonging to specialised fields. Some of the CAT tools that are already on the market are free, some others are not; some are more user-friendly and intuitive, while the others require more involvement on the part of the handler. This could be compared to the way in which one learns the steps of a new game and copes with the idea that, regardless of how one feels about it, evolution in this field is imminent.

According to an online article [9], the software programmes used in the context of translation are intended to hasten the translation process and ensure its efficiency. These programmes help to edit and store translations, translate projects segment by segment (while keeping their formatting), and ensure quality control (equivalence, consistency, spelling, etc.). Additionally, they help in simplifying terminology management, i.e., one can create, access, and use terms and translation memories while working on projects. The article also underlined the differences between MT and CAT tools: while CAT tools help translators to streamline their translation processes, without actually doing any of the translations instead of or for them, machine translation tools use artificial intelligence to translate texts directly. Nevertheless, translation software tools provide the same goal: to assist in and speed up the process of translation.

The CAT tools market has developed intensively lately, and it takes the form of a large variety of software. As such, there are translation software tools that can be downloaded on a PC desktop and used offline, and there are the cloud-based tools that allow the translator to work online. Furthermore, the variety extends to the market options regarding free or paid computer software; therefore, they are adapted to match different circumstances and needs.

When dealing with desktop (or offline) translation software, the advantages lie in the fact that they can be accessed without an internet connection, and that they work just as well as the computer they are installed on. The drawback to using them would be that they use space on a PC when they are installed, and can be used only on that particular PC. Some of the most well-known such pieces of translation software are: SDL Trados Studio, memoQ, Wordfast (Classic & Pro), Memsource (desktop), Déjà Vu, and Across (among the paid-for examples), and OmegaT and CafeTran Espresso (among the free examples).

The next generation of translation software is represented by Cloud-based translation tools, which are programmes accessed and used online through a web browser. There are many advantages

to using them, since they do not need to be installed on a PC, can be accessed on any device with an Internet connection, save translation in real time and do not lose data, and are updated and debugged frequently and immediately. On the other hand, as the Internet is prone to being hacked, this type of translation software stands at a certain risk. Some of the most well-known such pieces of translation software are: Memsourse (cloud-based), Wordbee, and XTM Cloud (among the paid-for examples) and Smartcat, MateCat, and Wordfast Anywhere (among the free examples).

Consequently, we observe that the translation software market is already fairly dense, and—judging by the way technology evolves—it is liable to become more populated. This is a natural process, and we need to adopt it and adapt to it. From the perspective of the translation teacher, this is ‘translated’—pun intended—into the effort of presenting this technology-enhanced reality to our students, the future translators, who need to be made aware of the tools they can use as professionals. Clearly, we ought to understand the benefits and the drawbacks that may result from using such tools, but it goes without saying that the future translators would be incomplete in their professional formation if they were deprived of the knowledge and implicit competences that back such technology-supported tools.

One might rightfully argue that the large number of such tools (and the future development of the ones to follow) would make it impossible for a translator to learn the insights of them all. Fortunately, even if they have a significant number of differences, the reality is that the *modus operandi* is essentially the same. The main features regarding, for instance, the text segmentation, the editor, the translation memory (TM), the translation base (TB) or glossary, and importing and exporting the files (to name just a few), are more or less similar, so that the translator finds the tool rather intuitive.

Wordfast Anywhere is the online version of Wordfast Classic and Pro (the offline CAT tool). Among its advantages are that it is user-friendly and convenient, totally free of charge, and permits cooperation with different users. Its weaknesses are that it is a somewhat slow tool and prone to bugs. Nevertheless, it makes a good tool for beginner translators. Smartcat is one of the quickest-developing web-based software translation options for Language for Specific Purposes translation (LSP), translation agencies, and freelance translators; it permits an unlimited number of users and access to continuously-updated translation memories (TMs), it allows the possibility to upload content in different formats, and it includes high-end terminology management. According to an online article [9], the benefits include the fact that it is free, user-friendly, and comprehensive, ensuring that one can transition from other CAT tools or start using it without any beforehand experience. Moreover, it has its own marketplace to collaborate with other professionals in the field.

Memsourse is a paid-for tool that provides a web-based translation editor as well as a desktop one. Despite the fact that some translators might consider that it is short of certain functionalities, and it works slower when involved in larger translation projects, it still has a simple, intuitive and user-friendly editor. Another paid-for cloud-based translation tool is XTM Cloud, a customer-oriented, well-organised, intuitive tool, with a solid support team.

Irrespective of the translation software we choose to use in the translation and translation management process, all of them need to have the following features, as pointed out by Jemimah Rodriguez in an online article [6], in which we read about segmentation as being the feature of a CAT tool which divides the content into several segments, thus simplifying the process of translation; instead of typing the translated text of the similar content once more, the translators can use the content segments from the existing database; next comes memorisation, which regards the situation of the specific content that was translated with the use of CAT tool, content which is memorised as source text into its memory; the next time the same content needs to be translated, the CAT tool offers auto-suggestions and permits translators to translate the text quickly. Another feature regards rectification, according to which translators can visualise both the source text and the translated content, and can rectify the translated content in order to ensure the quality. The centralisation feature of CAT tools allows a different translator to work on the same document, in order to ensure a better collaboration. Last, but not least, the import/export of different file formats feature allows the handling of files in varied formats, according to the clients’ requirements.

Unquestionably, the novelty implied by the use of any tool requires a certain amount of time to be dedicated to practice, but this does not exceed the working pattern a translator is used to. A translator's job is challenging and rewarding, including that of the translator of specialised texts, who deals with specific terminology, which is (considered) relatively limited or narrowed down. The multitude of tasks included by the job impose a new trend in the professional formation of the translator. The job of a professional translator no longer implies only the process of rendering words from one language to another, especially if we refer to the complete professional translator, who undertakes all of the jobs, i.e., contacting the client, collaboration with other professionals (linguists, terminologists, reviewers, etc.), thus performing the complex task of the translation project manager. Therefore, one can only embrace the aid offered by specialised software, that, if used appropriately, can only enhance and support the work. As underlined in S. Sachs [10] (p.13), if translators manage to learn how to use the proper translation software, they could benefit greatly from the aid of computers, as these can greatly increase the accuracy of texts. Moreover, computers can count words, guaranteeing accurate bills and saving the translator significant time.

### **3. Translation Technology into the Classroom**

As we have stated all along in our article, the technology-supported and -enhanced approach to our everyday life has already become a part of our activity; therefore, it was only natural that it got to shape the way in which we view and perceive the world, looking through a macro-lens, and the way in which we view education, looking through more specialised, micro-lens. As declared in a previous phase of our article, we are deeply preoccupied with the translation process per say, just as much as we are concerned with the training of our students into becoming good professionals. Our main aims are to raise the awareness of our students regarding translation software, and to provide the students with the necessary transversal skills and competences suitable for the digital area, supported by the ability to tackle the Cloud-based translation tools and software in view of Industry 4.0 requirements. This process was activated when we became aware that the translation market requires knowledge and practice in the software field, and that the traditional approach to teaching translation, if performed exclusively using the pen-and-paper technique, was already becoming obsolete. Consequently, we underwent professional training and benefited from the support of our university—by means of the INTECS (Internationalizarea Educației și a Cercetării Științifice) project ([http://proiect\\_intecs.upm.ro/ro/home/](http://proiect_intecs.upm.ro/ro/home/))—in purchasing the SDL Trados Studio 2015 for Translators software, to be used in teaching our students in the Applied Modern Languages specialisation. This helped us to ensure specific activities and provide our students with a professional approach to the translation process.

### **4. Conclusions**

The translation phenomenon appears to be versatile and sophisticated, adapting to the evolution of the rendering of meaning from one language into another. We owe it to ourselves to keep an open mind, to be ready to adapt, and to be able to adopt novelty in the fields in which we develop our activity. Technology has gained an essential role in our personal and professional environments, imprinting upon the perspective from which we see the world, which is undoubtedly forever technology-marked. From our point of view, education has proven to be an ecosystem which has fortunately managed to adapt to the technology-induced innovation, which enables us to believe that there is hope for a better future. The students we build today, will be able to build tomorrow.

**Funding:** This research received no external funding.

**Conflicts of Interest:** The author declares no conflict of interest.



## References

1. Han, B. *On Translation: Communication, Controversy, Cultural Globalisation*; Editura Universității "Petru Maior": Târgu Mureș, Romania, 2011; p. 45.
2. Vilceanu, T. *Fidelitate și alteritate lingvistică și culturală*; Universitaria Publishing House: Craiova, Romania, 2007; p. 91.
3. Imre, A. *Traps of Translation, A Practical Guide for Translators*; Editura Universității Transilvania: Brasov, Romania, 2013; pp. 102, 201.
4. Kingscott, G. Translator strategies for getting the most out of the word processing. In *Technology as Translation Strategy*; Muriel, V., Ed.; John Benjamins Publishing Company: Amsterdam, The Netherlands; Philadelphia, PA, USA, 2008; p. 14.
5. Patiniotaki, E. *Trends & Reality in Translation Technology*; Centre for Translation Studies at UCL University: London, UK, 2018.
6. The Top 10 Free and Open Source Computer-Assisted Translation Software. Available online: <https://www.goodfirms.co/blog/the-top-10-free-and-open-source-computer-assisted-translation-software> (accessed on 30 June 2020).
7. Quah, C.K. Bar-Hillel 1960/2003: 45. In *Translation and Technology*; Palgrave Macmillan: London, UK, 2006; p. 6.
8. Han, B. In Defence of the Human-Made Translation. In *Contemporary Perspectives on European Integration between Tradition and Modernity*; EITM 6; Editura Universității "Petru Maior": Târgu Mureș, Romania, 2016; pp. 324–325.
9. Top Translation Software Tools in 2020. Available online: <https://www.smartcat.ai/blog/top-translation-software-tools-in-2019-some-even-free/> (accessed on 28 June 2020).
10. Sachs, S. Word processing and the Independent translator. In *Technology as Translation Strategy*; Muriel, V., Ed.; John Benjamins Publishing Company: Amsterdam, The Netherlands; Philadelphia, PA, USA, 2008; p. 13.

**Publisher's Note:** MDPI stays neutral with regard to jurisdictional claims in published maps and institutional affiliations.



© 2020 by the author. Licensee MDPI, Basel, Switzerland. This article is an open access article distributed under the terms and conditions of the Creative Commons Attribution (CC BY) license (<http://creativecommons.org/licenses/by/4.0/>).





# Studies on the Use of ISO 7730 in Romanian Companies <sup>†</sup>

Mihaela Bucur

Department of Industrial Engineering and Management, “George Emil Palade” University of Medicine, Pharmacy, Science and Technology of Târgu Mureş, 540142 Târgu Mureş, Romania; mihaela.bucur@umfst.ro; Tel.: +40-074-239-4396

<sup>†</sup> Presented at the 14th International Conference INTER-ENG 2020 Interdisciplinarity in Engineering, Mures, Romania, 8–9 October 2020.

Published: 14 January 2021

**Abstract:** This paper aims to identify how the ISO 7730 Standard is perceived by manufacturing companies in Romanian industry. This paper aims to integrate the details of the ISO 7730 Standard into the research related to the level of comfort in manufacturing companies with high heat emissions. Furthermore, we hope to identify how the indices provided in the ISO 7730 Standard can influence the productivity and quality indicators in production.

**Keywords:** ISO 7730; IAQ; PMV; PPD

## 1. Introduction

Indoor air quality (IAQ) plays a major role in terms of employee health and comfort. Labor productivity can be disturbed by polluted environmental conditions and indoor air quality. In this article, we highlight the main factors that affect the daily productivity of employees in the workplace, without taking into consideration factors such as the effects of noise and lighting in large urban areas, previous health issues, personality, socio-economic status, and eating habits.

A company’s main objective should be related to raising awareness by assessing signs, such as health implications, workers’ complaints, absenteeism, and low productivity. The complexity of a real environment makes it very difficult to assess the impact of a single parameter on human performance; however, providing a superior environment can be an effective way to increase productivity [1]. Previous studies provide evidence that the quality of the environment influences the incidence of acute respiratory diseases, allergies, asthma, and disease symptoms.

Complaints from Dutch office workers have increased since the 1970s, when new office equipment and arrangements were implemented, such as new spatial concepts (open plan offices), advanced control equipment, and new materials. Table 1 presents the three acceptable perspectives of IAQ.

**Table 1.** The three acceptable perspectives of indoor air quality (IAQ) [2].

Point	Sensation
Building properties	No complaints, there are no requirements for ventilation, there is no polluting activity
US Environmental Protection (EPA)/Public health perspective	Minimizing toxin exposure, irritations, there are no adverse health effects, there are no comfort complaints
Building employees	Clean, dry, good ventilation, thermal comfort, there are no unfamiliar or unacceptable odors

Reports on holiday leave in Ireland and the UK show that most cases of leave among employees in public administration offices happen due respiratory problems that may be the result of IAQ [3].

The purpose of this paper derives from a previous study by the author [4], and consists in understanding the ISO 7730 Standard and identifying if Romanian companies know this standard, if they apply it, and if they consider that thermal conformity indicators influence the quality and quantity of their production.

Thus, the methodology used was based on a bibliographic study of the ISO 7730 Standard, followed by an investigation on a sample of 40 companies from Romania.

These companies have productive fields of activity, with heat release, in the automotive, metallurgy, and chemical industries, as well as industries in which thermal treatments are performed on metallic materials. Only 17 companies responded to our request, and the research was based on the interview method. The conclusions of the research are included in this paper.

## 2. How to Better Understand the Standard ISO 7730

The International Standard ISO 7730 was developed in order to measure and analyze the moderate and extreme conditions to which humans are exposed.

The thermal balance of the human body is obtained when internal heat production in the body is equal to the loss of heat to the environment. The main factors that influence this balance are physical activity, clothing, and the parameters: air temperature, mean radiant temperature, air velocity, and air humidity. When these parameters have been estimated and measured, the thermal sensation of the body can be predicted by calculating predicted mean vote (PMV).

PMV is intended for a large group of people exposed to the same environment.

It is applied in order to check if the given thermal environment complies with the comfort criteria and to establish requirements for different levels of acceptability, as shown in Table 2.

**Table 2.** Seven-point thermal sensation scale [2].

Point	Sensation
+3	Hot
+2	Warm
+1	Slightly warm
0	Neutral
-1	Slightly cool
-2	Cool
-3	Cold

The predicted percentage dissatisfied (PPD) index establishes a quantitative prediction (the number of thermal dissatisfied persons among a large group of people). The rest of the group will feel thermally neutral, slightly warm, or slightly cool. It can be calculated after the PMV value is determined as in (3):

$$PPD = 100 - 95 \times \exp(-0.03353 \times PMV^4 - 0.2179 \times PMV^2), \tag{1}$$

PMV and PPD express warm and cold discomfort for the body as a whole, and the Figure 1 shows the connection of these two indicators.

Thermal discomfort can also be caused by unwanted local/particular cooling or heating of the body. People with a sedentary activity are more sensitive than those who have a higher level of activity. The most common local discomfort factors are radiant temperature asymmetry (cold or warm surfaces), draught (defined as a local cooling of the body caused by air movement), vertical air temperature difference, and cold or warm floors [5].

Thermal comfort is that condition of mind that expresses satisfaction with the thermal environment. As a result of local or national priorities, technical developments, and climatic regions, these tools (PMV, PPD, the draught model, and the relations between these) may be used to determine different ranges of environmental parameters for the evaluation and design of the thermal environment [6].

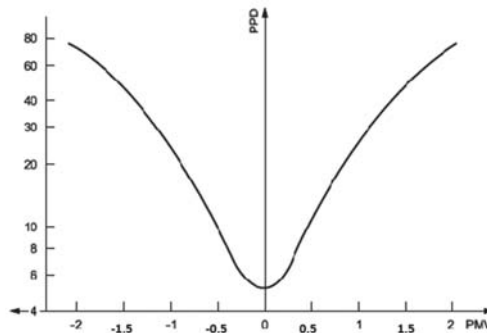


Figure 1. Predicted percentage dissatisfied (PPD) as a function of predicted mean vote (PMV) [2].

*Nonsteady State*

The thermal environment is often in a nonsteady state. There are three types of nonsteady state conditions that are often present: temperature cycles, temperature drifts or ramps, and transients.

Long-term evaluation of the general thermal comfort conditions.

Different categories of general comfort may be specified as ranges for the PMV–PPD, as shown in Table 3.

Table 3. Categories of thermal environment [4].

Category	Thermal State of the Body as a Whole			Local Discomfort		
	PPD %	PMV	DR %	PD % Caused by Vertical Air Temperature Difference	PD % Caused by Warm or Cold Floor	PD % Caused by Radiant Asymmetry
A	<6	-0.2 < PMV < +0.2	<10	<3	<10	<5
B	<10	-0.5 < PMV < +0.5	<20	<5	<10	<5
C	<15	-0.7 < PMV < +0.7	<30	<10	<15	<10

If these criteria are to be met, including extreme situations, the heating and/or cooling capacity of any heating, ventilation, air-conditioning (HVAC) installation should be relatively high. Economic and/or environmental considerations can lead to acceptable limited time intervals during which the PMV will be allowed to stay outside the specified ranges.

Using computer simulations or measurements, comfort conditions are often tested during longer periods for different types of building and/or HVAC design. The need here is to specify a characteristic value for the long-term comfort conditions for the comparison of designs and performance.

In determining the acceptable range of operative temperature according to this International Standard, a clothing insulation value that corresponds to the local clothing habits and climate should be used.

In warm or cold environments, there is often an influence due to adaptation. Apart from clothing, other forms of adaptation, such as body posture and decreased activity, which are difficult to quantify, can result in the acceptance of higher indoor temperatures. People used to working and living in warm climates can more easily accept and maintain a higher work performance in hot environments than those used to colder climates.

**3. Conclusions Regarding the Use of the Standard in the Romanian Production**

Because knowing the standard is very important to understanding the indicators of thermal comfort, I asked the production managers if they knew about the ISO 7730 Standard. Figure 2 shows that a significant percentage of these engineers were aware of the existence of this standard; however,

there were some who did not have information about the ISO 7730 Standard. This means that in these areas, there was potential for improving thermal comfort, if we assume that knowing the standard is a starting point for monitoring these indicators.

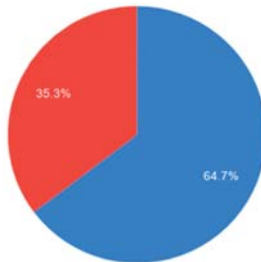


Figure 2. Have you heard about ISO 7730?

The most important indicators for measuring a given thermal environment, which meet the comfort criteria, are PMV, PPD, operative temperature, humidity, turbulence intensity, air velocity, thermal insulation, and draught. The designated managers from the companies I contacted for this research acknowledged that they were familiar with only some of these indicators. Thus, as shown in Figure 3, the best known indicators, and probably those that are the easiest relatively to monitor, were operative temperature and humidity; the least known indicators were thermal insulation, draught, and turbulence intensity.

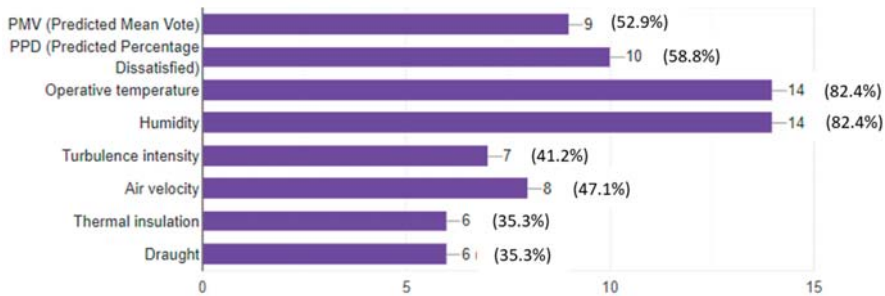


Figure 3. Which of the following indicators are you familiar with?

Given the results in Figure 3, I talked to the people responsible for the ergonomic part of the employees’ activity and asked if they considered that the indicators included in the ISO 7730 Standard influenced their productivity as well as the quality of production. Opinions changed as the discussions progressed, and this led me to believe that these interviews were more methods of raising awareness of the importance of these indicators. Thus, as shown in Figure 4, an extremely small percentage did not consider thermal comfort indicators to be able to influence their production, but only 58.8% were convinced of this. The present research has a significant role in demonstrating that in the future, the level of thermal comfort in the production halls has a direct influence on the quality indicators in production, in which the labor force is relatively important.

The reasons companies do not monitor thermal comfort indicators are complex, multiple, and depend on the management, financial support, the measuring tools (or lack of), responsibility, and other factors. We hope that these depend only on ignorance and the influence that these indicators have on financial losses due the poor quality of production in spaces with inappropriate thermal comfort being misunderstood. Thus, as a result of the multitude of reasons, Figure 5 clearly shows that very few companies are interested in monitoring the indicators in the ISO 7730 Standard.

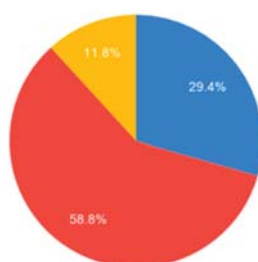


Figure 4. Do you think that these indicators could influence the quality of your production?

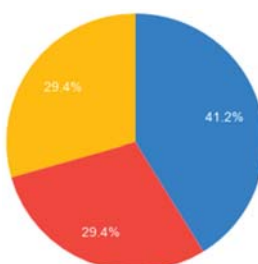


Figure 5. Would you be interested in monitoring the air quality in your production workspace?

#### 4. Conclusions

IAQ research shows that low indoor air quality significantly reduces productivity and performance among employees. In the future, there is a need to raise awareness of the work environment, especially in developing countries, as it may pose a major health hazard [7].

A healthy and safe environment includes listening and evaluating employees' complaints about the low or high temperature, humidity, and health symptoms that occur during office work. Defining a performance measurement system for public and private organizations that will provide accurate data, as well as an IAQ protocol that will promote the rapid assessment of IAQ issues is the future of employee-friendly jobs. Employers need to focus on creating healthy jobs and reducing productivity losses caused by low indoor air quality [8].

**Funding:** This research was funded by the University of Medicine, Pharmacy, Science and Technology "George Emil Palade" of Târgu Mureş Research Grant number 293/1/2020.

#### References

1. Mendell, M.J.; Adams, R.I. The challenge for microbial measurements in buildings. *Int. J. Indoor Environ. Health* **2019**, *29*, 523–526. [CrossRef]
2. ISO 7730:2005. Ergonomics of the Thermal Environment. Available online: <https://www.iso.org/standard/39155.html> (accessed on 1 November 2015).
3. Seguel, J.; Merrill, R.; Seguel, D.; Campagna, A.C. Indoor Air Quality. *Am. J. Lifestyle Med.* **2017**, *11*, 284–295. [CrossRef]
4. Bucur, M. Studies on the Need to Monitor IAQ Indicators in the Production Hall With Microclimate with Heat Release—Study on Companies from Mures County. *Acta Marisiensis Ser. Technol.* **2020**, *17*, 53–57. [CrossRef]
5. Isoda, N.; Tsuzuki, K.; Yoshioka, M. Importance of floor surface temperature in maintaining thermal comfort for people sitting directly on the floor. In Proceedings of the 10th ICEE, Fukuoka, Japan, 23–27 September 2002; pp. 821–824.
6. Toftum, J.; Melikov, A.; Tynel, A.; Bruzda, M.; Fanger, P.O. Human response to Air, Movement-Evaluation of ASHRAE's Draft Criteria (RP-843). *HVAC R Res.* **2003**, *9*, 187–202. [CrossRef]

7. Ole Fanger, P. Indoor Air Quality in the 21st Century: Search for Excellence. *Indoor Air* **2000**, *10*, 68–73. [[CrossRef](#)] [[PubMed](#)]
8. Ceravolo, L.S.; Mirakovski, D.; Polenakovik, R.; Ristova, E.; Sovreski, Z. Indoor Air Quality (IAQ) as a Parameter Affecting Workplace Productivity. *Air Pollut. Health* **1998**, *10*, 101–126.

**Publisher’s Note:** MDPI stays neutral with regard to jurisdictional claims in published maps and institutional affiliations.



© 2021 by the author. Licensee MDPI, Basel, Switzerland. This article is an open access article distributed under the terms and conditions of the Creative Commons Attribution (CC BY) license (<http://creativecommons.org/licenses/by/4.0/>).

Article

# Algorithm for Smart Home Power Management with Electric Vehicle and Photovoltaic Panels<sup>†</sup>

Lucian Ioan Dulău \* and Dorin Bică

Department of Electrical Engineering and Information Technology, Faculty of Engineering and Information Technology, “George Emil Palade” University of Medicine, Pharmacy, Science and Technology of Târgu Mureș, 540139 Târgu Mureș, Romania; dorin.bica@umfst.ro

\* Correspondence: lucian.dulau@umfst.ro; Tel.: +40-265-233-112

† Presented at the 14th International Conference INTER-ENG 2020 Interdisciplinarity in Engineering, Mureș, Romania, 8–9 October 2020.

Published: 25 December 2020

**Abstract:** In this paper is presented an algorithm for the power management of a smart home with electric vehicle and photovoltaic panels. The case study is performed considering the power demand of the household appliances, the charging/discharging of the electric vehicle, and the power supplied by the photovoltaic panels. The photovoltaic panels have a small installed power and benefit from the support scheme from the government for these types of generation sources, so it is a prosumer. The simulation is performed for a day. Additionally, the cost of power supplied to the consumer is also analyzed.

**Keywords:** electric vehicle; smart house; photovoltaic panels; power demand; prosumer

## 1. Introduction

In this paper will be presented an algorithm for the power management of a smart home with electric vehicle and photovoltaic panels.

The results will provide the management of power, the power cost for the consumer, and the possible profit for the consumer, respectively.

Other research focused on the following. In [1] it was determined an optimal schedule for the charging of EV based on predicted PV output and electricity consumption. In [2], the priority order between a PHEV, battery and imported power from the grid was determined and the overall cost of the imported grid energy and PEV charging cost was minimized. In [3], the optimal power management in a smart home with photovoltaic (PV) panel, battery, PHEV, thermal and electrical loads [3] was determined. In [4], the smart homes power management system that supports the grid and allows the optimal operation of the home (which has smart appliances, PV, storage and electric vehicle), so the total power costs are minimum. In [5] was performed an optimization of a community energy storage with heat and electricity storage.

In [6], a stochastic energy management of a smart home with PHEV energy storage and PV array was determined, resulting a lower electricity cost for the electric vehicles. In [7] was studied the interactions between electric vehicles and PV. In [8] was minimized the sum of energy costs and thermal discomfort costs for a long-term time horizon, for a sustainable smart home with a heating, ventilation, and air conditioning load. In [9], the design and implementation of a wireless PV powered home energy management system for a direct current environment allowed remote monitoring of appliances' energy consumptions and power rate quality. In [10], an algorithm was developed for the peak load management in commercial systems with electric vehicles. In [11], an energy management system for a smart house based on hybrid PV-battery and V2G was studied. In [12] a hybridized



intelligent home renewable energy management system that combines solar energy and energy storage services with smart home was planned considering the demand response and the power price.

Compared with these studies, in this paper, the analysis will be performed for a day, considering the power demand of the consumer, the electric vehicle charging/discharging, the power supplied by the photovoltaic panels and the support scheme from the government, and the power cost, respectively.

## 2. Algorithm Model

There are three types of electric vehicles: hybrid electric vehicles (HEV), plug-in hybrid electric vehicles (PHEV) and battery-powered electric vehicles (BEV). In this paper, we will consider a plug-in hybrid electric vehicle. When discharged, the batteries are recharged using the power grid, from a power outlet, but can also supply power to the household appliances if needed. The photovoltaic panels generate power and can be used to supply the house and/or to supply power to the grid. The photovoltaic panels have a small installed power and benefit from the support scheme from the government for these types of generation sources, so it is a prosumer.

The algorithm that is the base of the case study simulation is presented further, considering the cases when the PHEV is charging from the grid (case A), and is supplying power to the household appliances (discharging) (case B).

In case A, if the power supplied by the grid, the PV panels is higher than the power required by the load (household appliances), then the excess power of the PV panels is exported (sold) to the grid, resulting in a profit for the consumer.

$$P_{\text{grid}} + P_{\text{PV}} \geq P_{\text{L}} \quad (1)$$

where:

- $P_{\text{grid}}$ —power supplied by the grid [kW];
- $P_{\text{PV}}$ —power supplied by the PV panels [kW];
- $P_{\text{L}}$ —power demand of the load (household appliances) [kW].

The cost of the power supplied by the grid to the load is 0.55 lei/kWh.

$$\text{Consumer Profit} = P_{\text{PV}} \cdot \text{cost}_{\text{PV}} \quad (2)$$

where:

- $\text{cost}_{\text{PV}}$ —cost of power supplied by the PV panels to the grid [lei/kWh].

The cost of the power supplied by the PV panels to the grid is 0.22 lei/kWh.

In case B, if the power supplied by the grid, PV panels and electric vehicle is higher than the power required by the load (household appliances), then the excess power of the PV panels is also exported (sold) to the grid, resulting in a profit for the consumer.

$$P_{\text{grid}} + P_{\text{PV}} + P_{\text{PHEV}} \geq P_{\text{L}} \quad (3)$$

where:

- $P_{\text{PHEV}}$ —power supplied by the plug-in hybrid electric vehicle to the household appliances [kW].

## 3. Case Study

The smart house is placed in Târgu Mureş, Romania. The installed power of the PV panels, which are connected to the grid, is 15 kW, so it is a prosumer. The plug-in hybrid electric vehicle is a Toyota Prius. The battery capacity of the PHEV is 8.8 kWh, which requires a regular charging or discharging duration at home of 4 hours (it is considered 2.2 kWh for each hour). The PHEV is typically charged or discharged in the afternoon or during the night. The simulation is performed with the Matlab software.

In Figure 1 is presented the power demand of the household appliances, to which is added the power required to charge the PHEV between 17 and 21 (case A). This results in a total power demand of the load.

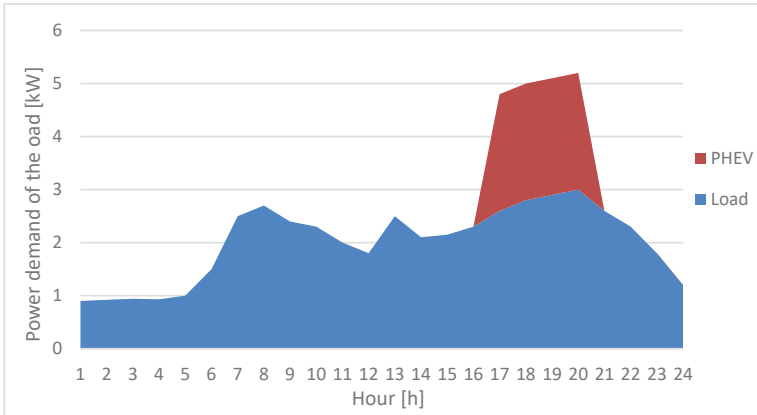


Figure 1. Power demand of the load (household appliances) and PHEV (case A).

The power supplied by the PV panels during a day is presented in Figure 2.

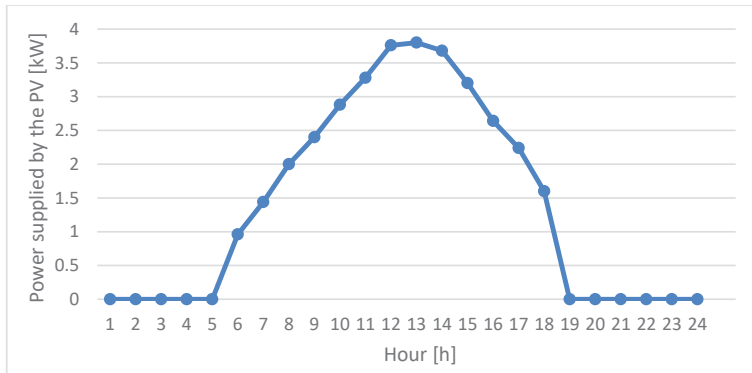


Figure 2. Power supplied by the PV panels.

In Figure 3 is presented the power demand of the household appliances, considering that the PHEV supplies power to the household appliances between 17 and 21 (case B). Therefore, the power demand of the load between 17 and 21 is smaller compared with the previous case.

Considering the algorithm presented in Section 2, the power cost for the consumer (Figure 4) and the profit for the consumer (Figure 5) is determined. Additionally, based on the results, the optimal management of power can be interpreted.

The total power cost for the consumer, for case A is 17.1325 lei/kWh, while for case B, it is 9.0145 lei/kWh. The profit for case A is 1.7798 lei, while for case B, it is 2.4046 lei.

Considering the results, it can be concluded that the case when the PHEV is discharging, supplying power to the household appliances is the best case, resulting in a lower power cost and higher profit.

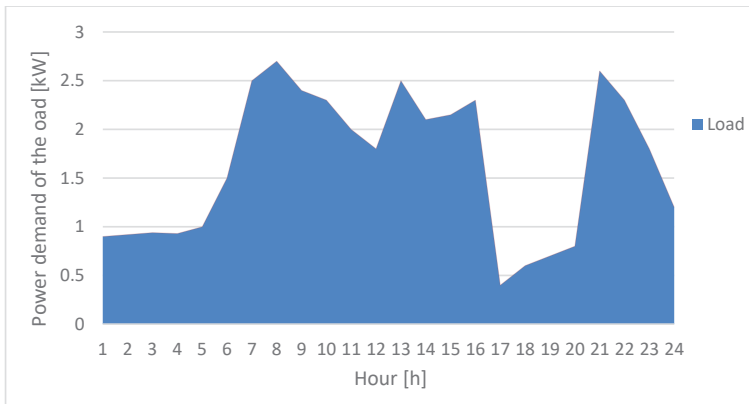


Figure 3. Power demand of the load (household appliances) (case B).

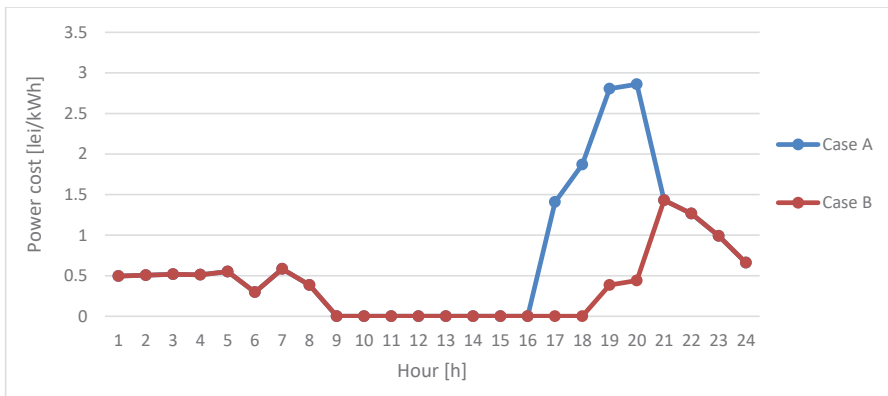


Figure 4. Power cost for the consumer.

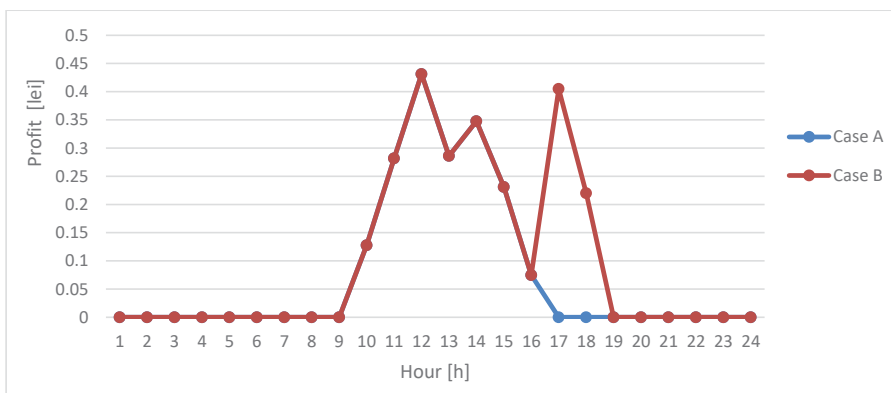


Figure 5. Consumer profit.

#### 4. Conclusions

In this paper was presented an algorithm for the power management of a smart home with electric vehicle and photovoltaic panels.

Compared to other studies, in this paper, the analysis was performed for a day, considering the power demand of the consumer, the cases of the electric vehicle charging/discharging, the power supplied by the photovoltaic panels and the support scheme from the government for prosumers, and the power cost, respectively.

The total power cost for the consumer was 17.1325 lei/kWh for the case when the PHEV was charging, compared with 9.0145 lei/kWh for the case when the PHEV was discharging. The profit for the first case is 1.7798 lei, compared to 2.4046 lei for the second case.

Considering the results, the case when the PHEV was discharging, results in a lower power cost and higher profit for the consumer.

**Funding:** This research received no external funding.

**Conflicts of Interest:** The authors declare no conflict of interest.

## References

1. Young-Min, W.; Jong-Uk, L.; Sung-Kwan, J. Electric vehicle charging method for smart homes/buildings with a photovoltaic system. *IEEE Trans. Cons. Electron.* **2013**, *59*, 323–328.
2. Sima, A.; Poria, F.; Arash, A. Smart home energy management considering real-time energy pricing of plug-in electric vehicles. In Proceedings of the 2018 IEEE Energy Conversion Congress and Exposition (ECCE), Portland, OR, USA, 23–27 September 2018; pp. 67–72.
3. Alireza, L.; Seyed, S.A.; Gevork, G.; Morteza, M.A. Energy management in smart home including PV panel, battery, electric heater with integration of plug-in electric vehicle. In Proceedings of the 2017 Smart Grid Conference (SGC), Tehran, Iran, 20–21 December 2017; pp. 1–7.
4. Lokesh, C.; Saurabh, C. Energy Management of Smart Homes with Energy Storage, Rooftop PV and Electric Vehicle. In Proceedings of the 2018 IEEE International Students' Conference on Electrical, Electronics and Computer Science (SCEECS), Bhopal, India, 24–25 February 2018; pp. 1–6.
5. Terlouw, T.; AlSkaif, T.; Bauer, C.; Sark, W. Optimal energy management in all-electric residential energy systems with heat and electricity storage. *Appl. Energy* **2019**, *254*, 1–20. [[CrossRef](#)]
6. Wu, X.; Hu, X.; Moura, S.; Yin, X.; Pickert, V. Stochastic control of smart home energy management with plug-in electric vehicle battery energy storage and photovoltaic array. *J. Power Sources* **2016**, *333*, 203–212. [[CrossRef](#)]
7. Hoarau, Q.; Perez, Y. Interactions between electric mobility and photovoltaic generation: A review. *Renew. Sust. Energ. Rev.* **2018**, *94*, 510–522. [[CrossRef](#)]
8. Yu, L.; Jiang, T.; Zou, Y. Online energy management for a sustainable smart home with an HVAC load and random occupancy. *IEEE Trans. Smart Grid* **2019**, *10*, 1646–1659. [[CrossRef](#)]
9. Sabry, A.H.; Hasan, W.Z.W.; Ab. Kadir, M.; Radzi, M.A.M.; Shafie, S. DC-based smart PV-powered home energy management system based on voltage matching and RF module. *PLoS ONE* **2017**, *12*, 1–22. [[CrossRef](#)] [[PubMed](#)]
10. Mahmud, K.; Hossain, M.J.; Ravishankar, J. Peak-load management in commercial systems with electric vehicles. *IEEE Syst. J.* **2019**, *13*, 1872–1882. [[CrossRef](#)]
11. Khoucha, F.; Benbouzid, M.; Amirat, Y.; Kheloui, A. Integrated energy management of a plug-in electric vehicle in residential distribution systems with renewables. In Proceedings of the 2015 IEEE 24th International Symposium on Industrial Electronics (ISIE), Buzios, Brazil, 3–5 June 2015; pp. 717–722.
12. Ma, Y.; Li, B. Hybridized Intelligent Home Renewable Energy Management System for Smart Grids. *Sustainability* **2020**, *12*, 2117. [[CrossRef](#)]

**Publisher's Note:** MDPI stays neutral with regard to jurisdictional claims in published maps and institutional affiliations.






© 2020 by the authors. Licensee MDPI, Basel, Switzerland. This article is an open access article distributed under the terms and conditions of the Creative Commons Attribution (CC BY) license (<http://creativecommons.org/licenses/by/4.0/>).



Article

# Solar Photovoltaic Cell Parameters Extraction Using Differential Evolution Algorithm <sup>†</sup>

Rachid Herbazi <sup>1,\*</sup>, Youssef Kharchouf <sup>2,‡</sup>, Khalid Amechnoue <sup>1</sup>, Ahmed Khouya <sup>1</sup>  
and Adil Chahboun <sup>2</sup>

<sup>1</sup> National School of Applied Sciences of Tangier, Abdelmalek Essaâdi University, Tangier BP 1818, Morocco; kamechnoue@uae.ac.ma (K.A.); ahmedkhouya3@yahoo.fr (A.K.)

<sup>2</sup> Faculty of Science and Technology of Tangier, Abdelmalek Essaâdi University, Tangier BP 416, Morocco; kharchouf-youssef@outlook.com (Y.K.); adchahboun@uae.ac.ma (A.C.)

\* Correspondence: r.herbazi@uae.ac.ma; Tel.: +212-660-000-166

<sup>†</sup> Presented at the 14th International Conference INTER-ENG 2020 Interdisciplinarity in Engineering, Mureş, Romania, 8–9 October 2020.

<sup>‡</sup> These authors contributed equally to this work.

Published: 22 December 2020

**Abstract:** This work presents a method for extracting parameters from photovoltaic (PV) solar cells, based on the three critical points of the current-voltage (I-V) characteristic, i.e., the short-circuit current, the open circuit voltage and the maximum power point (MPP). The method is developed in the Python programming language using differential evolution (DE) and a three-point curve fitting approach. It shows a good precision with root mean square error (RMSE), for different solar cells, lower than to those cited in the literature. In addition, the method is tested based on the measurements of a solar cell in the Faculty of Science and Technology of Tangier (FSTT) laboratory, thus giving a good agreement between the measured data and those calculated (i.e.,  $RMSE = 7.26 \times 10^{-4}$ ) with fewer iterations for convergence.

**Keywords:** differential evolution; photovoltaic; parameters extraction; single diode

## 1. Introduction

In recent decades, access to renewable energy (RE) sources has attracted a lot of attention. In fact, growing concerns over the environmental situation and the energy crisis due to the limited quantities of fossil fuel reserves have made the development and adoption of RE an urgent priority. The PV option has proven to be a leader among many promising renewable technologies to replace fossil fuels due to lower PV technology prices and improved efficiency of solar cells thus leading to a significant growth in the PV industry [1–3]. PV are mainly divided into three technologies; poly-crystalline, mono-crystalline and thin films. Since these technologies rely mostly on the PV effect in silicon P-N junctions, their behavior can be modeled using electric diode circuits [4,5]. These circuits include different components where each is representative of a certain physical mechanism within the cell such as exciton recombination and cell bulk resistance. Knowing the exact values of these parameters is important for many applications. The simulation and emulation of PV cells is crucial for energy yield prediction, quality control during manufacturing [2] and the study of PV cell degradation. However, the values of these parameters are not available in the manufacturers' technical data sheets. Open-circuit voltage, short-circuit current, and maximum power are given only under standard test conditions (STC). Obviously, the actual PV modules operation is generally far from these ideal conditions, which makes real-time fast parameter extraction necessary.

## 2. The Single Diode Model

The simplest model used for PV solar cells is the single diode model (SDM) [6] as shown in Figure 1. The current generator represents the photocurrent ( $I_{ph}$ ) that is due to the PV effect, the diode represents the P-N junction and its electric field through the diode ideality factor ( $n$ ) and the saturation current ( $I_0$ ), the series and shunt resistances ( $R_s$  and  $R_{sh}$ ) represent cell bulk resistance and leakage current, respectively. The SDM is used for the three dominant technologies in the PV industry (namely, mono-Si, poly-Si and thin films), but for other emerging technologies which do not rely on the electric field of the P-N junction for exciton separation [7,8], other more specialized models are necessary. This model is described by the Shockley diode equation for a PV module with  $N_s$  cells in series and  $N_p$  in parallel:

$$I = I_{ph}N_p - I_0N_p \left[ \exp\left(\frac{q(V + IR_sN_s/N_p)}{nkTN_s}\right) - 1 \right] - \frac{V + IR_sN_s/N_p}{R_{sh}N_s/N_p} \quad (1)$$

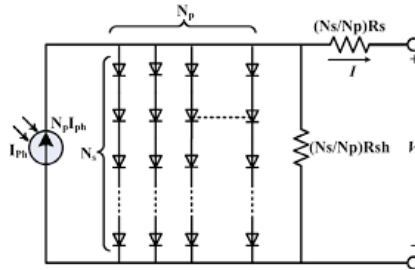


Figure 1. Equivalent circuit SDM of PV module.

## 3. Background

For the parameters extraction of the model, one can distinguish two main strategies. Firstly, the analytical approach based on information from several key points on the I-V curve such as the short-circuit current ( $I_{sc}$ ), the open circuit voltage ( $V_{oc}$ ), the maximum power point (MPP) as well as the gradient of the curve at those points. This approach is simple and allows rapid calculations, however, several assumptions and simplifications can be made, thus leading to incorrect results [3,9,10]. This approach is also sensitive to measurement noise since it only relies on a few selected points [11].

The second strategy is the numerical approach, the problem of which is formulated as an optimization problem by trying to minimize the error between the calculated and measured values. This approach allows for the usage of the wide array of well-studied deterministic and stochastic optimization algorithms. The deterministic algorithms include methods such as the Newton Raphson method [12], Iterative curve-fitting [13], Conductivity method [14], Levenberg Marquardt algorithm [15], etc. These are gradient-based methods, which adds continuity, differentiability and convexity requirements on the error functions. In contrast, stochastic methods provide global search capability and do not require gradient information, meaning the error function can be non-differentiable, and even non-continuous, which include; the genetic algorithms (GA) [2,6,16], particle swarm optimization (PSO) [17,18], DE [1], artificial bee swarm optimization (ABSO) [19]. The issues encountered by these stochastic methods are mainly related to the vastness of the search spaces, which cost a lot of time to cover and require a few thousand iterations before converging. They can also be trapped in local minima but are much less susceptible to this problem when compared to their deterministic counterparts.

In this context, this work is based on the DE algorithm for the extraction of SDM parameters, namely  $I_{ph}$ ,  $I_0$ ,  $a$ ,  $R_s$  and  $R_{sh}$ . The extraction method used is based on the three critical points ( $V_{oc}$ ,  $I_{sc}$ ,  $P_{mpp}$ ) of the I-V curve whose model is forced to pass through these cited points. Furthermore,

the method has been developed and implemented in the Python programming language, thus giving more precision and the need for few iterations for convergence.

#### 4. The Proposed Method

The DE algorithm application to the SDM would result in a five-dimensional search space. In this work, three points of the I-V characteristic are used to analytically calculate three of the parameters whose search space is reduced to two dimensions. The ideality factor ( $\alpha$ ) and the series resistance ( $R_s$ ) are the two parameters introduced into DE algorithm.

##### 4.1. Differential Evolution

The DE introduced by Storn and Price in 1995 [20] is a relatively recent stochastic and evolutionary algorithm. It is very similar to other evolutionary algorithms like GA in that it also has crossing and mutation operations as shown in Figure 2.

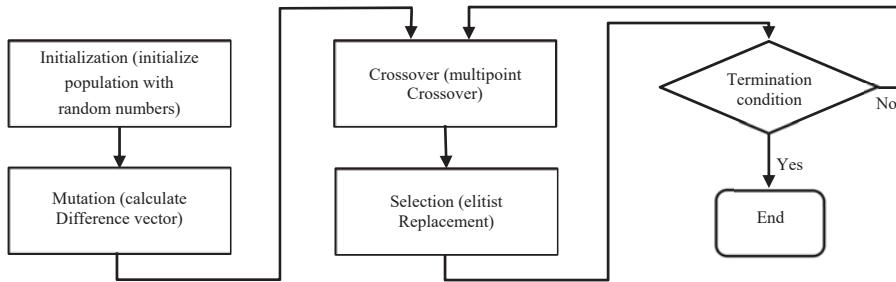


Figure 2. Main operations of DE algorithm.

##### 4.1.1. Initialization

First, we generate the initial population randomly trying to cover the entire search space. We may achieve this using Formula (2) assuming the  $rand(0, 1)$  term provides a uniform distribution of outputs.

$$V_j = V_{\min,j} + rand(0, 1)(V_{\max,j} - V_{\min,j}) \quad (2)$$

The initial population is spread uniformly over the entire search space, which helps the algorithm avoid being stuck in local minima. DE is very efficient, which means the algorithm converges well within  $Gen_{\max} = 100$  iterations, even with a small population  $NP = 50$ . The DE strategy is “DE/best/bin” which means that we choose the fittest vector in a population to generate mutants for the next generation, and that binomial crossover is performed on the trial vectors.

##### 4.1.2. Mutation

Next, we create a mutant vector by taking the fittest vector in the population and adding the difference of two other random vectors from the population. The difference is scaled with a mutation factor  $F \in [0, 1]$ . This is the key step that differentiates DE from other evolutionary methods according to the following formula:

$$M = V_{fittest} + F(V_{r1} - V_{r2}) \quad (3)$$

##### 4.1.3. Crossover

In this step, we created a trial vector by crossing over the elements from the mutant vector into the original. The probability of crossing over each element is set by the crossover rate, and we usually take



high values ( $CR = 0.8$ ) in order to promote diversity in the population [21]. A trial vector is generated as follows:

$$T_i = \begin{cases} M_i & \text{if } rand(0, 1) \leq CR \\ X_i & \text{otherwise, } X \text{ being the original vector} \end{cases} \quad (4)$$

#### 4.1.4. Penalty

One issue with DE is that unphysical values of the parameters can be obtained (i.e., negative  $R_s$ ). To circumvent this, we apply a penalty to any unphysical solution by assigning it a large fitness value.

#### 4.1.5. Selection

The last step is to select the vector based on whether or not its fitness value is superior to its previous generation counterpart. A possible method to achieve this is:

$$X_{gen+1} = \begin{cases} U & \text{if } J(U) < J(X) \\ X & \text{otherwise} \end{cases} \quad (5)$$

Note that, when the fitness function  $J$  is calculated, it evaluates to 100 for unphysical values as per the penalty phase. Storn and Price (2006) [21] recommend high crossover ( $CR = 0.7$ ) and mutation factor ( $F \geq 0.4$ ) values. The limits used to penalize solution vectors are  $a \in [1, 2]$ ,  $R_s \in [0, 0.5]$  as well as the previously stated negative values of currents and resistances. We should note that the method is very sensitive to the choice of the MPP; then, the proposed method includes different running of the algorithm times each with a slightly different MPP.

#### 4.2. Three-Point Curve Fitting

In order to minimize the complexity of the algorithm, it is possible to reduce the dimensionality of the problem using a few geometrically critical points in the I-V curve, namely the short-circuit, open-circuit and maximum power regions. These three points will allow us to determine three SDM parameters:

$$I_i = I_{ph}N_p - I_0N_p \left( e^{\frac{V_i + I_i R_s(N_s/N_p)}{aV_t}} - 1 \right) - \frac{V_i + I_i R_s(N_s/N_p)}{R_{sh}(N_s/N_p)}, \text{ where } i = 1, 2, 3 \quad (6)$$

Using algebraic manipulation, one can extract the three parameters  $I_{ph}$ ,  $R_{sh}$ , and  $I_0$ :

$$I_{ph} = \left[ I_0N_p \left( e^{\frac{V_1 + I_1 R_s(N_s/N_p)}{aV_t}} - 1 \right) + \frac{V_1 + I_1 R_s(N_s/N_p)}{R_{sh}(N_s/N_p)} + I_1 \right] \frac{1}{N_p} \quad (7)$$

$$R_{sh} = \frac{(V_1 - V_2)(N_p/N_s) + R_s(I_1 - I_2)}{I_2 - I_1 - I_0N_p \left( e^{\frac{V_1 + I_1 R_s(N_s/N_p)}{aV_t}} - e^{\frac{V_2 + I_2 R_s(N_s/N_p)}{aV_t}} \right)} \quad (8)$$

$$I_0 = \frac{\alpha(I_2 - I_1) - \beta(I_3 - I_1)}{N_p \left[ \alpha \left( e^{\frac{V_1 + I_1 R_s(N_s/N_p)}{aV_t}} - e^{\frac{V_2 + I_2 R_s(N_s/N_p)}{aV_t}} \right) + \beta \left( e^{\frac{V_1 + I_1 R_s(N_s/N_p)}{aV_t}} - e^{\frac{V_3 + I_3 R_s(N_s/N_p)}{aV_t}} \right) \right]} \quad (9)$$

where

$$\alpha = V_3 - V_1 + R_s \left( \frac{N_s}{N_p} \right) (I_3 - I_1) \quad (10)$$

and

$$\beta = V_2 - V_1 + \left( \frac{N_s}{N_p} \right) (I_2 - I_1) \quad (11)$$

Using this technique, the differential algorithm is executed in a two-dimensional search space, which considerably reduces the algorithm complexity.

## 5. Results and Discussion

### 5.1. The Schutten Solar STP6–120/36 Module

First, our code developed in Python gives a set of 22 data points of the I-V characteristic of the Schutten Solar STP6–120 module, which contains 36 solar cells, connected in series at a temperature of 55 °C. A comparison between the experimental dataset and the computed I-V curve is illustrated in Figure 3. We clearly see that the algorithm fits the dataset very well, despite most of the points being close the maximum power points and few being in the short-circuit and open-circuit regions. Table 1 compares the computed parameters using our code with those reported in [1].

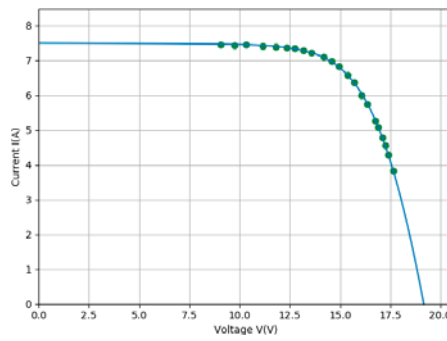


**Figure 3.** A comparison between the experimental data (green dots) and the calculated characteristic (blue line) for the Schutten Solar STP6–120/36 module.

**Table 1.** Parameter extraction results of the Schutten Solar STP6–120/36 module with those reported in [1].

Code	$I_{ph}$ (A)	$I_0$ ( $\mu$ A)	$a$	$R_s$ (m $\Omega$ )	$R_{sh}$ ( $\Omega$ )	RMSE
[1]	7.4830	0.8868	1.1872	5.3819	10.5309	0.0140
Present study	7.4738	0.5545	1.1571	5.9165	11.0491	0.0123

The fitness of a population is calculated by averaging each solution vector’s fitness in a specific generation. Its evolution is shown in Figure 4 where rapid convergence (within 30 iterations) is noticed towards the final value.

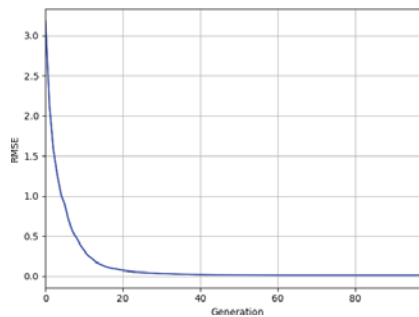


**Figure 4.** The evolution of average population fitness throughout the 100 iterations.

5.2. The R.T.C. France Commercial Silicon Solar Cell

For this case, we study the R.T.C France commercial silicon solar cell. The experimental dataset was taken at a temperature of 33 °C. Subsequently, the method used manages to extract very precise parameter values (Figure 5). A comparison between the computed values python DE algorithm and the proposed method in [1] is shown in Table 2. We can see the DE algorithm is slightly more accurate, and this could be explained by the absence of the constraints that are introduced in [1] by utilizing the three pivot points. It turns out that by giving up some precision on the pivot points; we can slightly gain in overall accuracy.

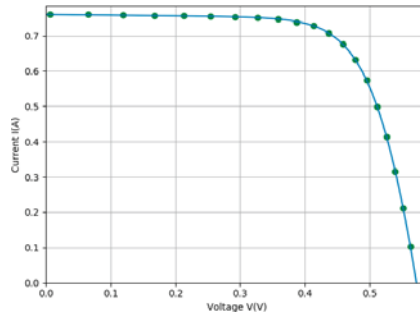


Figure 5. Comparison between experimental data (green dots) and calculated I-V curve (blue line) for the R.T.C France solar cell.

Table 2. Parameter extraction results of the R.T.C France commercial silicon solar cell with those reported in [1].

Code	$I_{ph}$ (A)	$I_0$ ( $\mu$ A)	$a$	$R_s$ (m $\Omega$ )	$R_{sh}$ ( $\Omega$ )	RMSE
[1]	0.7607	0.3191	1.4798	0.0362	54.1924	$8.12 \times 10^{-4}$
Present study	0.7607	0.3106	1.4772	0.0365	52.8897	$7.73 \times 10^{-4}$

5.3. FSTT Laboratory Silicon Cell

In this section, we tested in our FSTT laboratory, using RaRe Solutions solar simulator, the proposed method of the DE algorithm to extract the parameters values of a solar cell at a temperature of 30 °C.

A comparison between experimental data and the computed I-V curve is shown in Figure 6. The parameter values corresponding to this solution are laid out in Table 3 and are associated with a RMSE of  $7.26 \times 10^{-4}$ . The evolution of population fitness is shown in Figure 7.

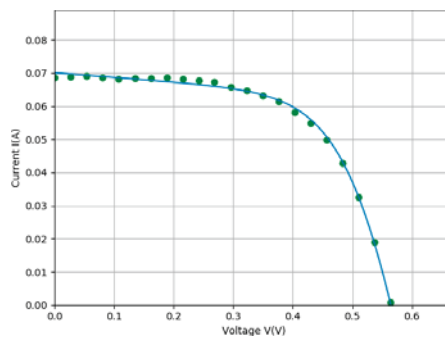
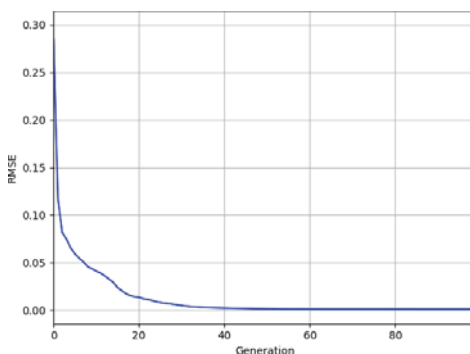


Figure 6. Comparison between experimental data (green dots) and the algorithm calculated I-V curve (blue line) for the FSTT solar cell.

**Table 3.** Extracted single diode parameter values for the FSTT cell.

Parameters	$R_{sh}$ ( $\Omega$ )	$R_s$ ( $\Omega$ )	$a$	$I_0$ ( $\mu A$ )	$I_{ph}$ (A)
Values	72.38	0.51	1.99	1.27	0.07



**Figure 7.** Evolution of average population fitness in the 100 iterations.

## 6. Conclusions

This work represents a developed method of extracting SDM parameters from PV solar cells using DE and the three-point curve fitting approach. The method is implemented in Python requires very few iterations for convergence and giving more precision compared to the results cited in the literature. Furthermore, the Python code developed gives very consistent results on several executions. However, the method seems very sensitive to choice of MPP in the experimental dataset, which makes it necessary to perform several executions, each with a different choice of MPP. It should be noted that the use of the three points seems to slightly reduce the method precision. Whereas a naive DE scheme implies a five-dimensional research space and requires a few hundred iterations, which is slightly higher in precision terms. This can probably be explained by the noise measurement in the pivot points constraining the proposed method.

**Author Contributions:** Conceptualization, R.H. and Y.K.; methodology, R.H. and Y.K.; software, R.H. and Y.K.; validation, A.C., K.A., A.K., Y.K. and R.H., formal analysis, R.H., Y.K., A.C., K.A. and A.K.; investigation, R.H. and Y.K.; writing—original draft preparation, R.H.; writing—review and editing, A.C., K.A. and A.K.; supervision, K.A., A.K. and A.C.; All authors have read and agreed to the published version of the manuscript.

**Funding:** This research received no external funding.

**Conflicts of Interest:** The authors declare no conflict of interest.

## References

- Chin, V.J.; Salam, Z. A New Three-point-based Approach for the Parameter Extraction of Photovoltaic Cells. *Appl. Energy* **2019**, *237*, 519–533. [[CrossRef](#)]
- Sellami, A.; Bouaïcha, A. Application of the Genetic Algorithms for Identifying the Electrical Parameters of PV Solar Generators. In *Solar Cells—Silicon Wafer-Based Technologies*; Kosyachenko, L.A., Ed.; IntechOpen Limited: London, UK, 2011; ISBN 978-953-307-747-5.
- Chin, V.; Salam, Z.; Ishaque, K. An accurate and fast computational algorithm for the two-diode model of PV module based on a hybrid method. *IEEE Trans. Ind. Electron.* **2017**, *64*, 6212–6222. [[CrossRef](#)]
- Oliva, D.; Aziz, M.A.E.; Hassanien, A.E. Parameter estimation of photovoltaic cells using an improved chaotic whale optimization algorithm. *Appl. Energy* **2017**, *200*, 141–154. [[CrossRef](#)]
- Chin, V.J.; Salam, Z.; Ishaque, K. An accurate modelling of the two-diode model of PV module using a hybrid solution based on differential evolution. *Energy Convers. Manag.* **2016**, *124*, 42–50. [[CrossRef](#)]

6. Zagrouba, M.; Sellami, A.; Bouaïcha, M.; Ksouri, M. Identification of PV solar cells and modules parameters using the genetic algorithms: Application to maximum power extraction. *Sol. Energy* **2010**, *84*, 860–866. [CrossRef]
7. Jiang, C.-S.; Yang, M.; Zhou, Y.; To, B.; Nanayakkara, S.U.; Luther, J.M.; Zhou, W.; Berry, J.J.; van de Lagemaat, J.; Padture, N.P.; et al. Carrier separation and transport in perovskite solar cells studied by nanometre-scale profiling of electrical potential. *Nat. Commun.* **2015**, *6*, 8397. [CrossRef] [PubMed]
8. Scharber, M.; Sariciftci, N.S. Efficiency of bulk-heterojunction organic solar cells. *Prog. Polym. Sci.* **2013**, *38*, 1929–1940. [CrossRef] [PubMed]
9. Ishaque, K.; Salam, Z.; Mekhilef, S.; Shamsudin, A. Parameter extraction of solar photovoltaic modules using penalty-based differential evolution. *Appl. Energy* **2012**, *99*, 297–308. [CrossRef]
10. Chin, V.J.; Salam, Z.; Ishaque, K. Cell modelling and model parameters estimation techniques for photovoltaic simulator application: A review. *Appl. Energy* **2015**, *154*, 500–519. [CrossRef]
11. Ishaque, K.; Salam, Z.; Taheri, H.; Shamsudin, A. A critical evaluation of EA computational methods for photovoltaic cell parameter extraction based on two-diode. *Sol. Energy* **2011**, *85*, 1768–1779. [CrossRef]
12. Easwarakhanthan, T.; Bottin, J.; Bouhouch, I.; Boutrit, C. Nonlinear Minimization Algorithm for Determining the Solar Cell Parameters with Microcomputers. *Int. J. Sol. Energy* **1986**, *4*, 1–12. [CrossRef]
13. Chan, D.S.H.; Phang, J.C.H. Analytical methods for the extraction of solar-cell single- and double-diode model parameters from I-V characteristics. *IEEE Trans. Electron Devices* **1987**, *34*, 286–293. [CrossRef]
14. Chegaar, M.; Ouennoughi, Z.; Hoffmann, A. New method for evaluating illuminated solar cell parameters. *Solid-State Electron* **2001**, *45*, 293–296. [CrossRef]
15. Ikegami, T.; Maezono, T.; Nakanishi, F.; Yamagata, Y.; Ebihara, K. Estimation of equivalent circuit parameters of PV module and its application to optimal operation of PV system. *Sol. Energy Mater. Sol. Cells* **2001**, *67*, 389–395. [CrossRef]
16. Jervase, J.A.; Bourdoucen, H.; Al-Lawati, A. Solar cell parameter extraction using genetic algorithms. *Meas. Sci. Technol.* **2001**, *12*, 1922–1925. [CrossRef]
17. Sandrolini, L.; Artioli, M.; Reggiani, U. Numerical method for the extraction of photovoltaic module double-diode model parameters through cluster analysis. *Appl. Energy* **2010**, *87*, 442–451. [CrossRef]
18. Soon, J.; Low, K.; Member, S. Photovoltaic Model Identification Using Particle Swarm Optimization with Inverse Barrier Constraint. *IEEE Trans. Power Electron.* **2012**, *27*, 3975–3983. [CrossRef]
19. Askarzadeh, A.; Rezaazadeh, A. Artificial bee swarm optimization algorithm for parameters identification of solar cell models. *Appl. Energy* **2013**, *102*, 943–949. [CrossRef]
20. Storn, R.; Price, K. *Differential Evolution—A Simple and Efficient Adaptive Scheme for Global Optimization over Continuous Spaces*; Technical Report TR-95-012; International Computer Science Institute: Berkeley, CA, USA, 1995.
21. Price, K.; Storn, R.M.; Lampinen, J.A. *Differential Evolution: A Practical Approach to Global Optimization*; Springer: Berlin, Germany, 2005.

**Publisher’s Note:** MDPI stays neutral with regard to jurisdictional claims in published maps and institutional affiliations.



© 2020 by the authors. Licensee MDPI, Basel, Switzerland. This article is an open access article distributed under the terms and conditions of the Creative Commons Attribution (CC BY) license (<http://creativecommons.org/licenses/by/4.0/>).

# Energetic Sustainability of Systems <sup>†</sup>

Attila Albini <sup>\*</sup>, Edina Albininé Budavári  and Zoltán Rajnai

Doctoral School on Safety and Security Sciences, Obuda University, 1034 Budapest, Hungary; budavari.edina@phd.uni-obuda.hu (E.A.B.); rajnai.zoltan@bgk.uni-obuda.hu (Z.R.)

<sup>\*</sup> Correspondence: attila.albini@gmail.com

<sup>†</sup> Presented at the 14th International Conference INTER-ENG 2020 Interdisciplinarity in Engineering, Mures, Romania, 8–9 October 2020.

Published: 25 December 2020

**Abstract:** An important problem in our world is that humanity's energy consumption is constantly rising. Therefore, nowadays there is an increasing emphasis on the problem of reusability and efficient energy management. The present paper studies the energy sustainability of systems by developing a unique test model. Using this test model, the theoretical problems of closed systems are investigated. With a theoretical experiment, the temporal motion of rigid systems is monitored and the behavior of flexible systems is analyzed. Finally, the study of the energy interaction of the general system and its environment shows the basic condition for the system's overall sustainability.

**Keywords:** closed system; dual system; ideal system; energetic model; long-term sustainability

---

## 1. Introduction

An important problem in our world is that humanity's energy consumption is constantly rising. Therefore, nowadays there is an increasing emphasis on the problem of reusability and efficient energy management [1–3]. Among other things, increasing efficiency is one of the requirements for the existence of long-term sustainable systems. Due to energy hunger, the need for sustainability is emerging in all areas of life. Demand is emerging everywhere from the industry's new paradigmatic concept to the smart city concept [4–7]. From other aspects, the need for sustainability must be emphasized in the underlying legal regulation [8] and in education [9–11].

The long-term sustainability of systems can be examined by the energy balance of the system. The aim of the present study is to examine the energy relationship between the ideal system and its environment in theoretical experiments, and to use this to demonstrate the energy conditions for the long-term sustainability of systems. The result can help to understand the relationship between the flexibility, efficiency and sustainability of systems. Furthermore, the result can help to show the dependence of the energy requirement of sustainability.

There are several arguments in favor of the energy aspect. The analysis of the movement of systems over time differs depending on the structural changes [12–14]. Structurally static motion can be modeled with the loops of cybernetics. This modeling leads to a system of differential equations with a static structure [15–21]. The result of organic change is a system of equations with a variable structure that cannot be handled easily. The study of such system changes is more based on textual modeling of human-based systems' change management. Long-term sustainability requires structural change. The energetic modeling of this is problematic because of the above. The series of theoretical experiments seeks a solution to this problem.

## 2. Methods

The study is based on the results of energy balance modeling according to [3]. Said modeling showed the energy relationship of the system components and the whole system and grouped the

energy issues. Theoretical experiments have analyzed the energy balance [1–3] of several types of system connections. As a first theoretical experiment, the problem of closed systems was investigated. Ideal dual relationships were modeled in the second series of theoretical experiments. In the third phase of the experiments, one of the actors in the dual relationship was replaced by the outside world. With this method, the operation of real systems can be deduced in several steps. It is also possible to formulate the energy conditions for long-term sustainability.

To achieve this:

1. one should create a system model to be used to investigate the problem;
2. the problem of closed systems should be investigated. Based on this, a conclusion can be drawn for singular cases;
3. a test model should be developed in which only two systems have an ideal relationship. This constitutes the general dual system testing model. It should examine the relationship between structurally different systems:
  - a. the dual relationship of rigid systems must be examined;
  - b. the dual relationship between fully flexible systems needs to be examined;
4. in the dual test model, one system must be replaced with the complement of the other system.

Thus, the two systems in the study are the same as the system and the world outside it. Generalization is the aim of this theoretical experimental step, from which conclusions can be drawn regarding the general sustainability requirements of systems.

### 3. Results

The structure of the model produced for the tests is the same as the general simplified model of the systems. In terms of energy balance, the behavior of the system can be characterized by the behavioral pattern of the general energy model. The mechanism of the interaction of the systems can be modeled with the model of cybernetic loops [15,16,19]. Theoretical experiments should be performed on the resulting system model.

Using the energy model of general systems, it can be shown that ideal closed systems are completely safe [22–25]. However, information on such systems cannot be obtained in reality, so their existence has not been proven. Thus, closed systems are only worth talking about at the level of a theoretical model. An examination of the pairwise interaction of the systems showed that rigid systems devour each other, while flexible systems are in balance with each other. Theoretical examination of the system and its environment has shown that the energetic condition for the long-term sustainability of the systems is that the stored energy of the system shows a continuous and unlimited increase. Summarizing the results:

- modeling of perfectly closed systems is only possible in theory, their existence cannot be proved,
- completely rigid systems engulf each other;
- perfectly flexible systems are balanced;
- the energy condition for sustainability is the continuous and unlimited growth of stored energy. This result is consistent with the experience that the energy of the long-life systems increases exponentially.

### 4. Discussion

The series of experiments is based on a modeling procedure not used so far. It uses the general energy and structural model of the systems simultaneously. The logical sequence of the series of theoretical experiments is also unique. The cases that resulted in anomalies are also examined during the experiments. For this reason, the sequence of experiments provides a way to answer the problem and get closer to real systems.

4.1. Model

Since the aim is to study the energy conditions, the application of the operating model used in the energy balance modeling of the systems may be expedient. According to this, the energy entering the system is equal to the sum of the change in stored energy and the energy leaving the system. The relevant equation is:

$$E(\text{in}) = \Delta E(\text{store}) + E(\text{out}). \tag{1}$$

In performing theoretical experiments, the logical separation of each experiment is based on the structure of the systems. For this reason, it is worth using the structure of the information system simplified system model [12–14] to model the structures of the systems. According to this, systems can be easily structurally modeled by defining the system, its properties, and the designation of its interface. In this case, the energy exchange of the system is only possible through its interface.

Finally, to model the interaction of systems, it is worth borrowing the mechanism of action of the cybernetic loops used in control theory [15–19]. According to this, negative feedback control loops were used to control the system according to the chain of action within the system. Based on the evaluation of the output, an intervention was made at the input of the chain to achieve the desired effect. This model assumes that the system is continuously exposed to external disturbances. The general model of the study is shown in Figure 1.

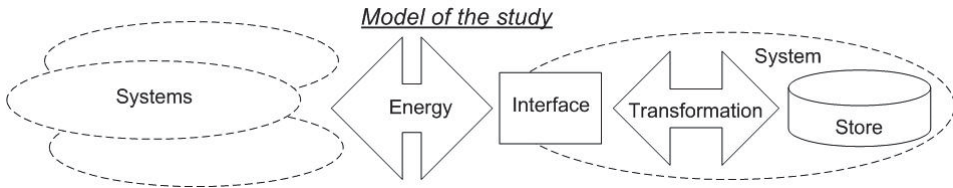


Figure 1. Model of the study. Based on [3].

4.2. Closed Systems

The interface of a perfectly closed system model is an empty set. This means that such systems are unsuitable for energy exchange. As a result, there is no exchange of information between the closed system and its environment. They know nothing about each other. Therefore, the discussion of closed systems is purely theoretical. In practice, such systems cannot be observed. A simplified structural model of closed systems is shown in Figure 2.

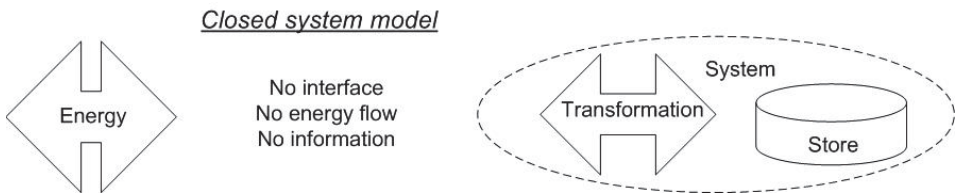


Figure 2. Simplified structural model of closed systems. Based on [3].

4.3. Dual Systems

At the beginning of the study of the interaction of systems, it is worth creating a general model. According to this model, there is no system in the imaginary world other than the two systems studied. The effect of one system is in interference with the other system and vice versa. Thus, the energy exchange also takes place only between the two systems. That is, systems only communicate energy to each other. The life of this dual system is determined by the variability of the energy transfer capacity



and the structure of each system. The relevant equations are (2) and (3). The system identifiers ( $E_1$  and  $E_2$ ) are in the lower index.

$$E_2(\text{out}) = E_1(\text{in}) = \Delta E_1(\text{store}) + E_1(\text{out}), \tag{2}$$

$$E_1(\text{out}) = E_2(\text{in}) = \Delta E_2(\text{store}) + E_2(\text{out}). \tag{3}$$

The model of the dual systems is shown in Figure 3.

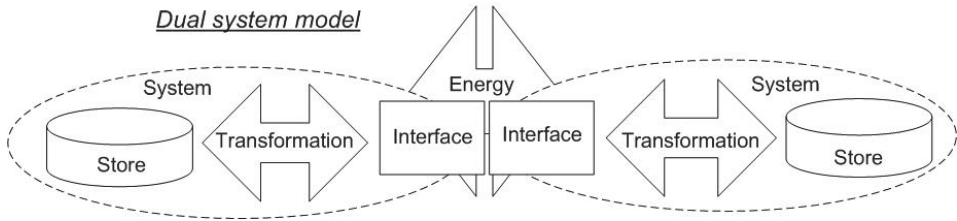


Figure 3. Model of the dual systems. Based on [3].

#### 4.4. Rigid Dual Systems

Rigid systems are systems in which it is not possible to flexibly change the energy storage capacity of the system. As a result, it is not possible to quickly change the structure of the system. Almost all of the energy entering the system serves the operation of the system, which energy leaves the system after work. In the case of a dual examination of these systems, systems that are the same in terms of energy balance operate in balance with each other. This is based on Equations (2) and (3). The consequence is Equation (4). Due to the rigidity of the structures, the equilibrium condition is Equation (5).

$$\Delta E_1(\text{store}) + \Delta E_2(\text{store}) = 0, \tag{4}$$

$$\Delta E_1(\text{store}) = \Delta E_2(\text{store}) = 0 \tag{5}$$

This balance is not ideal. Although a small deviation causes the excess energy to be absorbed by the other system without damage, the difference between the systems involved in the study gradually increases. As a result, the higher energy system swallows up the lower energy system. In the event of a high degree of difference in systems, this effect is immediate and severe. So, it is characteristic of rigid systems that they seek to achieve singularity.

#### 4.5. Flexible Dual Systems

Flexible structured systems are systems that are capable of rapid structural change. This is conditional on the possibility of storing a large part of the incoming energy. The energy demand for the operation of the system is much lower than the energy storage capacity. In the case of a dual examination of these systems, the identical systems are also in balance. Here, however, small differences are immediately offset because the ability of systems to change is rapid. The system can store the incoming excess energy without structural damage. The equilibrium condition is (6).

$$\Delta E_1(\text{store}) + \Delta E_2(\text{store}) = \Delta E_1(\text{out}) = \Delta E_2(\text{out}) \tag{6}$$

As a result, the energy balance of systems with different parameters and the amount of stored energy are balanced in the long run. So, flexible systems maintain a stable state of equilibrium with their environment.

#### 4.6. Complementary Dual Systems

During the complementary test, one of the dual systems must be replaced with the complement of the other system. This means that the interaction between the system and the outside world is studied as shown in Figure 4. This type of approach is already closer to real-world interactions than previous studies. The system under study has neither a perfectly rigid structure nor a perfectly flexible structure. Several conclusions can be drawn when conducting the theoretical experiment.

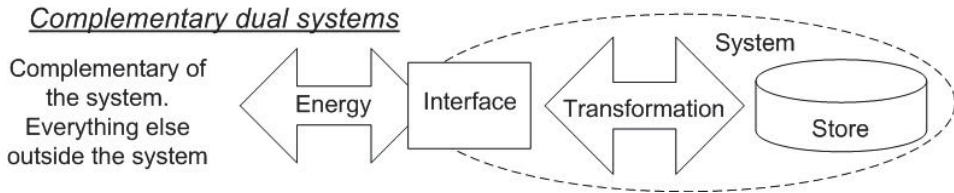


Figure 4. Model of the complementary dual systems. Based on [3].

The model of the complementary dual systems is shown in Figure 4.

The system is safe until a larger amount of energy arrives in its direction than it can store or pass. At higher energy doses, the system reacts as a rigid structure. Its structure is forced to change. The system then moves in the direction of the singularity. With a lower dose of energy, the system can store the excess. The structure of the system varies according to its own capabilities. In this case, the system moves towards balance with its environment. The general equation of the complementary dual system model is (7).

$$0 < E_{\text{system}}(\text{in}) = E_{\text{environment}}(\text{out}) < \infty. \quad (7)$$

The results of the study show the basic condition for the long-term energy sustainability of a general system. The system is most secure under the conditions if it is possible to ensure the storage and transmission of excess energy for all time intervals. This means that the change of the system must also be of this nature. All this suggests exponential behavior. This involves continuous flexibility. At the same time, the energy level of the environment can be characterized by infinity at the scale of the system. Therefore, the continuous flexibility of the system and thus its continuous sustainability can be increased by increasing the energy of the system continuously and unlimitedly.

#### 5. Summary

Industry 4.0 represents a new paradigm in terms of production. The smart city concept represents the same paradigm in terms of consumption, among other things. One of the most important features of this paradigm is to ensure long-term sustainability in all aspects [1–7].

In the present study, a unique test model has been developed to study the energy sustainability of systems. Using the test model, the theoretical problems of closed systems were first investigated. Subsequently, the temporal motion of rigidly structured systems was analyzed, which showed that such systems strive for singularity—they swallow up each other. Then, the study of flexible systems revealed that these systems strive for balance with their environment. Finally, a closer examination of the system showed that the basic condition for the energy sustainability of systems is that the system’s own energy should increase continuously and unlimitedly. This result is consistent with the experience that the energy of long-life systems increases exponentially.

**Funding:** This research received no external funding.

## References

1. Bernardi, D.; Pawlikowski, E.; Newman, J. A General Energy Balance for Battery Systems. *J. Electrochem. Soc.* **1985**, *132*, 5–12. [[CrossRef](#)]
2. Kasac, J.; Stefanic, H.; Stepanic, J. Comparison of social and physical free energies on a toy model. *Phys. Rev. E* **2004**, *1*, 16117–16124. [[CrossRef](#)] [[PubMed](#)]
3. Albini, A.; Rajnai, Z. Modeling general energy balance of systems. *Procedia Manuf.* **2019**, *32*, 374–379. [[CrossRef](#)]
4. Tokody, D.; Schuszter, G.; Papp, J. Study of How to Implement an Intelligent Railway System in Hungary. In Proceedings of the 2015 IEEE 13th International Symposium on Intelligent Systems and Informatics (SISY), Subotica, Serbia, 17–19 September 2015; Szakál, A., Ed.; IEEE: New York, NY, USA, 2015.
5. Kiss, M.; Breda, G.; Muha, L. Information security aspects of Industry 4.0. *Procedia Manuf.* **2019**, *32*, 848–855. [[CrossRef](#)]
6. Tokody, D. Digitising the European industry-holonic systems approach. *Procedia Manuf.* **2018**, *22*, 1015–1022. [[CrossRef](#)]
7. Szabó, Z. The effects of globalization and cyber security on smart cities. *Interdiscip. Descr. Complex Syst.* **2019**, *17*, 503–510. [[CrossRef](#)]
8. Kovács, Z. Cloud Security in Terms of the Law Enforcement Agencies. *Hadmérnök* **2012**, *7*, 144–156.
9. Mester, G. Rankings Scientists, Journals and Countries Using h-index. *Interdiscip. Descr. Complex Syst.* **2016**, *14*, 1–9. [[CrossRef](#)]
10. Dobrilovic, D.; Odadzic, B. Virtualization Technology as a Tool for Teaching Computer Networks. *Int. J. Educ. Pedagog. Sci.* **2008**, *13*, 41–45.
11. Mester, G. Academic Ranking of World Universities 2009/2010. *IPSI J. Trans. Internet Res. TIR* **2011**, *7*, 44–47.
12. Albini, A.; Tokody, D.; Rajnai, Z. Theoretical Study of Cloud Technologies. *Interdiscip. Descr. Complex Syst.* **2019**, *17*, 511–519. [[CrossRef](#)]
13. Albini, A.; Rajnai, Z. General Architecture of Cloud. *Procedia Manuf.* **2018**, *22*, 485–490. [[CrossRef](#)]
14. Albini, A.; Mester, G.; Iantovics, B.L. Unified Aspect Search Algorithm. *Interdiscip. Descr. Complex Syst.* **2019**, *17*, 20–25. [[CrossRef](#)]
15. Mester, G. Obstacle Avoidance and Velocity Control of Mobile Robots. In Proceedings of the 6th International Symposium on Intelligent Systems and Informatics SISY 2008, Subotica, Serbia, 26–27 September 2008; Catalog Number CFP0884C-CDR. IEEE: Piscataway, NJ, USA, 2008; pp. 97–101.
16. Mester, G.; Rodic, A. Sensor-Based Intelligent Mobile Robot Navigation in Unknown Environments. *Int. J. Electr. Comput. Eng. Syst.* **2010**, *1*, 55–66.
17. Szabó, A.; Szucs, E.; Berek, T. Illustrating Training Opportunities Related to Manpower Facility Protection through the Example of Máv Co. *Interdiscip. Descr. Complex Syst.* **2018**, *16*, 320–326. [[CrossRef](#)]
18. Mester, G.; Pletl, S.; Pajor, G.; Basic, D. Adaptive Control of Rigid-Link Flexible-Joint Robots. In Proceedings of the 3rd International Workshop of Advanced Motion Control, Berkeley, CA, USA, 20–23 March 1994; pp. 593–602.
19. Mester, G.; Pletl, S.; Nemes, A.; Mester, T. Structure Optimization of Fuzzy Control Systems by Multi-Population Genetic Algorithm. In Proceedings of the 6th European Congress on Intelligent Techniques and Soft Computing, EUFIT'98, Aachen, Germany, 7–10 September 1998; Verlag Mainz: Aachen, Germany, 1998; pp. 450–456.
20. Mester, G.; Rodic, A. Simulation of Quad-rotor Flight Dynamics for the Analysis of Control, Spatial Navigation and Obstacle Avoidance. In Proceedings of the 3rd International Workshop on Advanced Computational Intelligence and Intelligent Informatics (IWACIII 2013), Shanghai, China, 18–21 October 2013; pp. 1–4.
21. Zamfirescu, C.B.; Duta, L.; Iantovics, L.B. The Cognitive Complexity in Modelling the Group Decision Process. *BRAIN Broad Res. Artif. Intell. Neurosci.* **2010**, *1*, 69–79.
22. Shatnawi, M.M. Applying Information Security Risk Management Standards Process for Automated Vehicles. *Bánki Rep.* **2019**, *2*, 70–74.
23. Albininé Budavári, E.; Rajnai, Z. The Role of Additional Information in Obtaining information. *Interdiscip. Descr. Complex Syst.* **2019**, *17*, 438–443. [[CrossRef](#)]

24. Hell, P.M.; Varga, P.J. Drone systems for factory security and surveillance. *Interdiscip. Descr. Complex Syst.* **2019**, *17*, 458–467. [[CrossRef](#)]
25. Pető, R. Security of Smart City. *Interdiscip. Descr. Complex Syst.* **2019**, *1*, 13–19. [[CrossRef](#)]

**Publisher’s Note:** MDPI stays neutral with regard to jurisdictional claims in published maps and institutional affiliations.



© 2020 by the authors. Licensee MDPI, Basel, Switzerland. This article is an open access article distributed under the terms and conditions of the Creative Commons Attribution (CC BY) license (<http://creativecommons.org/licenses/by/4.0/>).



Article

# Challenges for the Large-Scale Integration of Distributed Renewable Energy Resources in the Next Generation Virtual Power Plants <sup>†</sup>

Adrian Gligor <sup>1</sup>, Piotr Cofta <sup>2</sup>, Tomasz Marciniak <sup>2</sup> and Cristian-Dragoş Dumitru <sup>1,\*</sup>

<sup>1</sup> Department of Electrical Engineering and Information Technology, Faculty of Engineering and Information Technology, "George Emil Palade" University of Medicine, Pharmacy, Sciences and Technology of Târgu Mureş, 540142 Târgu Mureş, Romania; adrian.gligor@umfst.ro

<sup>2</sup> Faculty of Telecommunications, Computer Science and Electrical Engineering, UTP University of Science and Technology, 85-796 Bydgoszcz, Poland; piotr.cofta@utp.edu.pl (P.C.); tomasz.marciniak@utp.edu.pl (T.M.)

\* Correspondence: cristian.dumitru@umfst.ro

<sup>†</sup> Presented at the 14th International Conference INTER-ENG 2020 Interdisciplinarity in Engineering, Mureş, Romania, 8–9 October 2020.

Published: 11 December 2020



**Abstract:** The proper power distribution systems operation is conditioned by its response to the consumers' energy demand. This is achieved by using predictable power sources supplemented by ancillary services. With the penetration of different alternative power sources especially the renewable ones, the grid increasingly becomes an active distribution network. In this context, the stability provided by ancillary services becomes increasingly important. However, providers of ancillary services are interested to benefit from the shift towards renewable energy. This leads to a complex scenario regarding the management of such service providers, specifically virtual power plants. In this regard, the aim of the paper was to investigate the strategies for improving the performance of virtual power plants by increasing the number of distributed renewable energy resources.

**Keywords:** virtual power plants; distributed renewable energy resources; ancillary services; optimization

## 1. Introduction

The shift from fossil fuel towards renewable energy has many environmental expected benefits and is within the long-term interest worldwide and clearly stated by regulations such as those issued by the EU or seven US states [1,2]. However, the negative impact on the stability and power quality of the grid has been already noticed in some countries [3,4]. With the penetration of different alternative energy sources and above all, the renewable ones, the grid increasingly becomes an active distribution network [5]. In this situation, provisioning of the stability provided by ancillary services becomes increasingly important [6] and the providers of ancillary services, specifically virtual power plants (VPPs), will be in a challenging situation, as they would also like to benefit from the shift towards renewable energy but without compromising their ability to deliver the service in a reliable and cost-effective way. This situation is somehow a paradox where the VPP would like to stabilize the unpredictable within the unpredictable. It is not helped by the fact that ancillary services may require a tight cooperation between distributed renewable energy resources (DERs) that are unlikely to be addressed by existing global optimization algorithms driven by the wealth of data.

The existing state-of-the-art in the field does not provide clear guidelines when it comes to such situations. Specifically, there are a few challenges listed below, related to different operational characteristics, increased competition and the complexity of inter-relationships. The challenge of helping VPPs to benefit from renewable energy requires a careful approach; therefore, the first step is

to look at the possibility to replace electrochemical storage with dispatchable renewables. It works on the assumption that the electrochemical storage, while very easy to control, is expensive and environmentally challenging. At the same time, variable-output renewables are deemed to be too unpredictable to be used in stabilizing the grid.

## 2. Main Challenges on DER Integration in VPP

The main challenges that arise in implementing DERs in VPPs are related, but not restricted, to one of the following categories [7]:

1. Poorer performance of dispatchable renewables, specifically in terms of response time. One of the main attractions of batteries is their rapid response time with minimal ramp-up time. It makes them particularly suitable for delivering unplanned and triggered services. Comparatively, dispatchable renewables, while offering more sustainable energy delivery, cannot be rapidly brought into action. If dispatchables are to be used to deliver more services, they must be combined with other forms of DER, forming hybrid solutions of complex characteristics. The other alternative would be to accept the energy loss due to pre-emptive deployment or accept the probabilistic nature of delivery. Thus, the solution must be able to provide some methods to compensate for the longer response and ramp-up time.
2. Increased competition on the ancillary service market, leading to decreasing prices for service provision. The market for ancillary services is financially attractive, but over the recent years it experienced a price pressure caused by the increased availability of batteries as well as by the aggregation of smaller DERs (e.g., electric vehicles, EVs) into VPPs that can offer at least some services. The price squeeze and the increased competition made providers look for more cost-effective solutions. Those solutions may arrive in the form of dispatchable renewables, but only if the final cost of using them will be favorable comparing to the battery-based solutions.
3. Complex inter-relation between DERs while delivering services as well as complex characteristics of hybrid DERs that make centralized optimization inapplicable. The use of distributed DERs, specifically the operation of the VPP relies on central optimization. As the VPP grows in complexity, such optimization increasingly must rely on the idealized model of the DER, doing away with intricate details of its operation. This approach may be acceptable for relatively homogeneous VPPs where the majority of DERs are of the same type and age. However, complex inter-relationships between heterogeneous DERs negatively impact on the ability to use centralized models. This situation calls for an alternative approach to the optimization.

All of these are in concordance with goals of decision factors such as in the EU [8].

## 3. Strategies and Methods for DERs Integration in Next Generation VPPs

VPPs tend to apply global optimization algorithms driven by the wealth of data, but these are unlikely to address the growing inter-relation between various DERs. This study focuses on the technical challenge of the VPP with high penetration of dispatchable renewables with no degradation to the delivery of ancillary services. Realistic assumptions about the grid expectations as well as about technical performances of various DERs, using both primary and secondary sources combined with extensive modeling are considered. In this case, appropriate control and optimization models for the VPP states and service delivery should be considered in order to overcome the limitations of centralized models, specifically when it comes to providing the real-time response. Further, this approach is required in order to model complex inter-connections between DERs that are characteristic to the delivery of ancillary services. Finally, such an approach should constitute the base for a decision-support tool that allows VPPs to determine the correct operation strategy.

In order for the VPP to increase the performance of its integrated portfolio through the substitution, it is necessary to equip VPPs with the decision-making tool that benefits from the technical insight into the best case feasibility yet allows VPPs to make their own commercial decisions. The way the

substitution conducted can be evaluated along the axis of substitution level and certainty, separately for each service and for each VPP, yielding the feasibility function for a give set of services. However, the complexity of inter-operation between different DERs makes it unlikely for traditional optimization models to address this challenge. It is likely that there is a trade-off between the level of substitution and the confidence it delivers. This implies that, instead of one common set of guidelines, it may be more feasible to construct the open model that can be perused by VPPs.

There is a need for a new model of the VPP and its DERs because it is expected that the operation of the VPP that is based on global multicriterial optimization will not be appropriate for this kind of challenge.

In order to develop the appropriate model of the grid, it is necessary to comprehend and express the operation of individual DERs. We anticipate some classes of DERs that represent different operational and physical constraints of the DER, such as wind, solar, hydro, biomass, electrochemical battery. We also anticipate that maybe DERs resemble the physical ones, but with more complex characteristics. For example, a fleet of electrical vehicles (EVs) does not satisfy the requirements of a typical battery DER, but it is rather an intelligent, distributed and statistical battery, being a class of a DER.

As the problem exhibits high complexity features, for simplifying the approach, some assumptions have to be identified and considered.

We consider it useful to assume at least the following aspects:

- the operation of the grid is essentially cyclic and statistically repeats itself at specific periods of time as shown in Figure 1a,b (e.g., daily, weekly, monthly or one-year cycles) [9]. The cyclical nature is defined by the sequence of seasons, which determine both the energy demand and the energy production;
- that there are some long-term trends that are visible across several cycles. Those trends may affect, e.g., service mix or the cost of use of various DERs;
- that services are demanded, and some of them are dispatched at fixed intervals throughout the day, with a most likely nowadays resolution of 15 min.

In order to achieve our goal, the following types of data are needed:

1. Annual demand for services, split into different serve types and services, including information about services that were used and those that were required yet not used. These data will be collected from public sources as well as from the grid operators. It would be beneficial to have this kind of information from few countries across the EU, as the market for service may vary. These data will be used to create the statistical model of service demand and delivery.
2. Technical characteristics of services, split into classes of services, describing technical specification of the service. Information's such delivery timeframe, trigger time and method, expected reaction time, expected delivery time, etc. This dataset contains only technical characteristics. They are well defined, usually in public domain (e.g., past calls for service delivery). The dataset will be used to construct the model.
3. Technical characteristics of three types of DERs: variable-output renewables, dispatchable renewables and battery storage. There are characteristics shared between all DERs from a given class and characteristics specific to a given DER and the project is interested in both. There is existing literature to gather some initial information, and there are technical specifications for DERs, available from manufacturers or users. These data will be used throughout the model.
4. Information about existing and planned VPPs, regarding objectives of their optimization (technical/commercial), size, type of DERs available, etc. These data come from public sources, contacts with VPPs as well as from the literature review. These data will be used to assess the range of parameters that the model should be able to handle.
5. Cost of various types of DERs, provisionally categorized into dispatchable renewables, variable-output renewables, electrochemical storage, other storage and other DERs. These data



are available at an aggregate level from public sources, with more detailed information available from operators and providers of various DERs. This data will be used to verify the assumption about commercial gains of the substitution of batteries with dispatchable renewables.

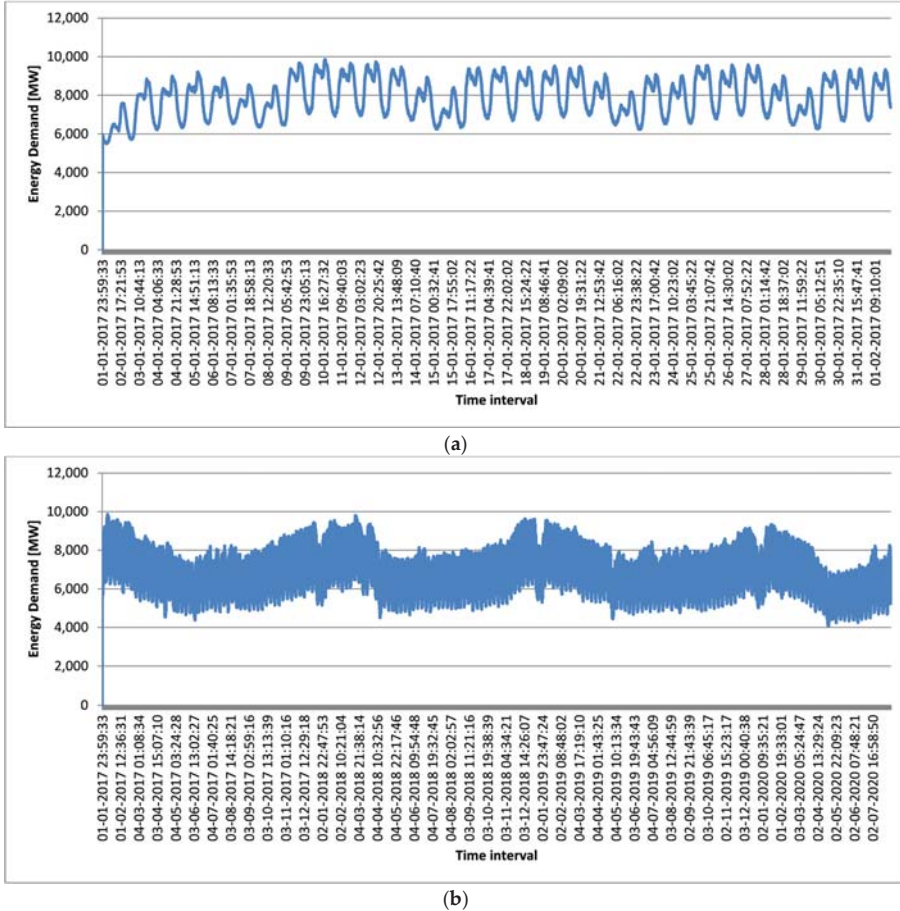


**Figure 1.** Cyclic evolution of the consumption: (a) over one month and (b) over three years (adapted from [10]).

In order to achieve the mentioned objectives, a provision and development of all or partial items presented in the following list depending on DERs involved is needed, starting from:

- delivering ancillary services while allowing dispatchable renewables penetration;
- developing weather analysis mechanisms for the most efficient use of renewable resources for DERs;
- development of a VPP distributed management and operation system;
- developing of a solution for estimating the effective operation of the use of renewable energy sources for the VPP;
- planning of the countermeasure recommender system for attack vectors on the grid.

## 4. Expected Outcomes

### 4.1. VPP Solution a Feasible Power Alternative

The number of used VPPs has been increasing over the past few years. Given the technological development, imposed requirements on RES adoption, certainly this trend will continue. For this reason, it makes perfect sense the development of solutions for managing increased RES as the primary option in VPPs. In support of this idea comes also the official prognosis at the international level, such as that presented in Figure 2 where it is shown the normalized Eurostat’s share of renewable energy sources in gross final energy demand, that market demand is growing, and everything indicates that it will continue to grow in the next years.

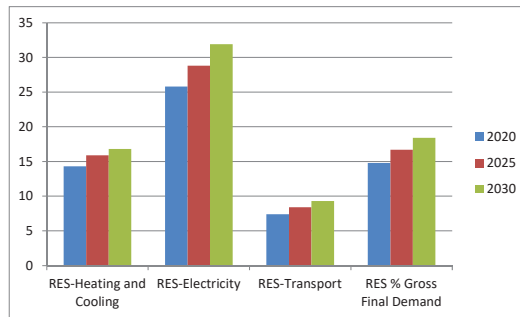


Figure 2. Green energy share prognosis at the EU level [11].

Currently, due to incentives provided by governments, micro-producers of energy namely prosumers knew a rapid growth [12]. Many people already have large solar sets or wind turbines in order to produce energy. In this context, electricity providers may opt for combining those micro producers together. This allows creation of an ecological power plant—a virtual power plant. Some of them which bring together many micro producers can even provide the same amounts of electricity as fossil fuel-based power plants or even nuclear power plants.

This scenario of DER-based VPPs is realistic and proved to be possible considering experiences of some countries that switched toward RES. Germany is one of the pioneer countries that are trying to increase the amount of produced green energy. In 2017, Germany produced more power from renewable sources than from coal.

In Norway, Statkraft began to work on its first VPP already in 2012. Its success encouraged others to develop other VPPs. Today there are more than 50 VPPs available. With the technical upgrades over the years, this solution seems to be more and more effective and this is proved by already known implementations. For example, Statkraft announced the 100 percent renewable-based VPP. The total capacity of Statkraft is as big as 10 nuclear power plants [13]. However, the planned 65% share of renewable energy is challenging and requires a lot of effort to reduce shares of other energy sources, but is not impossible.

### 4.2. VPP and Power Quality

The constantly growing demand for energy in the grid has a direct impact on its continuous and uninterrupted production. At present, with an unexpected reduction in consumption (load), some of the energy is wasted due to insufficient energy storage systems as well as poor use of renewable energy resources, which adds to the environmental footprint.

On the other hand, the unexpected increase in consumption may lead to the decrease of the quality of energy delivery and may impact system stability leading even to the disintegration of the grid. The optimal operation current operational approach of the power distribution system to its stability

is conditioned by the assurance of the energy demand. That is, the grid can cope with changing consumption patterns being assured that it can fully control energy production. Currently, the most important contribution to this request is provided by the classical dispatchable power generation systems. With the penetration of different alternative energy sources and above all, the renewable ones, the assurance of the system stability and power quality requires special measures. In addition, the situation becomes even more complex if consumer profiles change. Under these circumstances, the classical energy distribution network becomes an active distribution network that requires the use of collaborative distributed management and control systems which lead to the adoption of distributed generation solutions, VPPs and even of consumers with implemented management systems.

An option for these management and control structures is represented by decentralized optimization algorithms that while support the main functionality of VPPs to the distribution energy systems also ensure the power quality, minimize the operating costs, optimize the system reliability and provide increased flexibility and resilience. The success of these solution operations relies on popular information technologies able to cope with real-time data exchange, big data, smart data visualization, etc., but also on using them by all stakeholders, including both industrial and household consumers.

#### *4.3. VPP and Social Benefits*

Nowadays, energy systems can be seen as a bottom-up approach to energy self-sufficiency. The basic premise is that citizens (prosumers) are energy producers and have more control over how energy is produced and consumed.

Basically, local energy systems promote democratic decision-making, cost sharing and the benefits of shared responsibility and solidarity. Avoiding external costs, especially health costs, and the development of the local economy are significant benefits of the energy transformation, and to this should be added the increase in energy security and the development of a competitive economy 4.0. The climate policy defines civilization progress, encouraging the development of various services related to renewable energy installations and measures to improve energy efficiency. New job places are created, especially very interesting for young people. The use of local energy sources and their efficient use will lead to an increase in municipalities' revenues, remaining fees for electricity in the local economy, which will contribute to its development.

Energy efficiency provided by new VPPs translates into benefits for residents: healthier homes and cities, better transport, more efficient control of the energy system. The benefits of energy transformation and progressive climate policy can be seen especially at the local level. They relate to savings related to energy supply, introduction of sustainable mobility or lower costs of cities functioning, leading to the improvement of the quality of life.

## **5. Conclusions**

The last years have brought attention to RES as they can be as effective as other used energy sources and at the same time, they are ecological. An important task for all European countries is to increase the share of renewable energy.

The results arising from implementing of a system with features mentioned in the paper can represent innovative practices to maintain or improve the quality and performance of VPP. Due to the faster and faster climate change on Earth, the use of renewable energy sources seems to be the best possible solution. VPPs enable selling the renewable power and draw on the full flexibility of the renewable plants as if it were one large-scale reliable supplier. Moreover, the power producers do not have to sell the power themselves.

The management and control structures that involve the VPP operation can provide functionality to the distribution energy systems by using decentralized optimization algorithms which minimize the operating costs, optimize the system reliability and provide increased flexibility and resilience. All this control structures are possible due to new available technologies, including sensors, communication and computing technologies.

Adoption of DERs managed in VPPs exhibit many benefits such as being ecological but also at the economic and social levels. This is a developing domain that has to cope with many challenges mainly due to the RES availability.

**Author Contributions:** All authors equally contributed to the conceptualization, methodology, writing and editing the paper. All authors have read and agreed to the published version of the manuscript.

**Funding:** This research received no external funding.

**Conflicts of Interest:** The authors declare no conflict of interest.

## References

1. Official Journal of the European Union. Regulation (EU) 2018/1999 of the European Parliament and of the Council of 11 December 2018. Available online: [https://eur-lex.europa.eu/legal-content/EN/TXT/?toc=OJ:L:2018:328:TOC&uri=uriserv:OJ.L\\_:2018:328.01.0001.01.ENG](https://eur-lex.europa.eu/legal-content/EN/TXT/?toc=OJ:L:2018:328:TOC&uri=uriserv:OJ.L_:2018:328.01.0001.01.ENG) (accessed on 20 July 2020).
2. Erickson, P.; Lazarus, M.; Piggot, G. Limiting fossil fuel production as the next big step in climate policy. *Nat. Clim. Chang.* **2018**, *8*, 1037–1043. [CrossRef]
3. Pollitt, M.G.; Anaya, K.L. Can current electricity markets cope with high shares of renewables? A comparison of approaches in Germany, the UK and the State of New York. *Energy J.* **2016**, *37*, 69–88. [CrossRef]
4. Meyer, J.; Blanco, A.; Rönnberg, S.; Bollen, M.; Smith, J. CIGRE C4/C6.29: Survey of utilities experiences on power quality issues related to solar power. *CIREC-Open Access Proc. J.* **2017**, *2017*, 539–543. [CrossRef]
5. Karagiannopoulos, S.; Mylonas, C.; Aristidou, P.; Hug, G. Active distribution grids providing voltage support: The Swiss case. *IEEE Trans. Smart Grid* **2020**. [CrossRef]
6. Li, W.; Tesfatsion, L. A swing-contract market design for flexible service provision in electric power systems. In *Energy Markets and Responsive Grids*; Meyn, S., Samad, T., Hiskens, I., Stoustrup, J., Eds.; Springer: New York, NY, USA, 2018; Volume 162, pp. 105–127.
7. Silva, V.; Zulueta, M.L.B.; Wang, Y.; Fourment, P.; Hinchliffe, T.; Burtin, A.; Gatti-Bono, C. Anticipating Some of the Challenges and Solutions for 60% Renewable Energy Sources in the European Electricity System. In *Forecasting and Risk Management for Renewable Energy*; Drobinski, P., Mougeot, M., Picard, D., Plougonven, R., Tankov, P., Eds.; Springer: Cham, Switzerland, June 2017; Volume 254, pp. 169–184.
8. Official Journal of the European Union. L 328. 21 December 2018. Available online: <https://eur-lex.europa.eu/legal-content/EN/TXT/PDF/?uri=OJ:L:2018:328:FULL&from=EN> (accessed on 15 July 2020).
9. Gligor, A.; Vlasa, I.; Dumitru, C.D.; Moldovan, C.E.; Damian, C. Power Demand Forecast for Optimization of the Distribution Costs. *Procedia Manuf.* **2020**, *46*, 384–390. [CrossRef]
10. System Status in Real Time. Available online: <https://www.transelectrica.ro/en/web/tel/sistemul--energetic-national> (accessed on 15 September 2020).
11. EU Energy Trends to 2030. Available online: [https://ec.europa.eu/energy/sites/ener/files/documents/trends\\_to\\_2030\\_update\\_2009.pdf](https://ec.europa.eu/energy/sites/ener/files/documents/trends_to_2030_update_2009.pdf) (accessed on 10 July 2020).
12. Xiao, Y.; Wang, X.; Pinson, P.; Wang, X. Transactive Energy Based Aggregation of Prosumers as a Retailer. *IEEE Trans. Smart Grid* **2020**, *11*, 3302–3312. [CrossRef]
13. Virtual Power Plant: Europe's Biggest Power Plant Is 100 Per Cent Renewable. Available online: <https://www.statkraft.com/newsroom/news-and-stories/archive/2018/virtual-power-plant-europes-biggest-power-plant-is-100-renewable/> (accessed on 10 September 2020).

**Publisher's Note:** MDPI stays neutral with regard to jurisdictional claims in published maps and institutional affiliations.



© 2020 by the authors. Licensee MDPI, Basel, Switzerland. This article is an open access article distributed under the terms and conditions of the Creative Commons Attribution (CC BY) license (<http://creativecommons.org/licenses/by/4.0/>).



# Considerations Regarding the Negative Prices on the Electricity Market <sup>†</sup>

Pavel Atănăsoae \* , Radu Dumitru Pentiu and Eugen Hopulele

Faculty of Electrical Engineering and Computer Science, Stefan cel Mare University of Suceava, Universitatii 13, 720229 Suceava, Romania; radup@eed.usv.ro (R.D.P.); eugenh@eed.usv.ro (E.H.)

\* Correspondence: atanasoae@eed.usv.ro; Tel.: +40-721-246-229

<sup>†</sup> Presented at the 14th International Conference INTER-ENG 2020 Interdisciplinarity in Engineering, Mures, Romania, 8–9 October 2020.

Published: 16 December 2020



**Abstract:** Increasing of intermittent production from renewable energy sources significantly affects the distribution of electricity prices. In this paper, we analyze the impact of renewable energy sources on the formation of electricity prices on the Day-Ahead Market (DAM). The case of the 4M Market Coupling Project is analyzed: Czech-Slovak-Hungarian-Romanian market areas. As a result of the coupling of electricity markets and the increasing share of renewable energy sources, different situations have been identified in which prices are very volatile.

**Keywords:** electricity market; renewable energy; negative prices; price coupling of regions; day ahead market

## 1. Introduction

Electricity cannot be stored economically on a large scale and in appreciable quantities that would influence the operation of the power systems. Therefore, at all times, the supply injected into the network must be strictly equal to the demand and energy losses in the transmission and distribution networks. This explains why in the spot market, where prices are negotiated hourly, the price of electricity is very volatile [1].

Most European countries have chosen to accelerate the penetration of renewable energies into the electricity mix (20% by 2020). The production of electricity from renewable energy sources is supported by various support schemes [2–4]. To encourage the development of renewable energy sources, European countries have adopted a priority injection system that guarantees them access to the grid as soon as they produce electricity. This injection priority changes the way different means of production are used.

Increasing the production of electricity from renewable energy sources creates new challenges. The electricity generated by wind and solar energy is intermittent and difficult to predict, as it strongly depends on weather conditions [5]. Decision makers face various economic and technological challenges because renewable energy support instruments have a distortionary impact on electricity prices [6]. More specialized studies try through different models to anticipate the variation of prices on the energy markets in conditions of uncertainty. In the paper [7], the behavior of wind power producers adopting two different bidding modes in day-ahead electricity market is modeled and experimentally compared. The merit order effect for the Hellenic electricity market is analyzed in the paper [8]. Minimizing market risks and increasing profits are the main objectives of the market participants. Therefore, forecasting market prices is a challenge for all stakeholders [9–11]. As the supply and demand of electricity must be constantly balanced, the price varies depending on consumer behavior, climatic conditions or even compliance with the production schedules of

power plants. Prices fall in the event of a decrease in demand or a surplus of production compared to forecasts and an increase in the opposite case [12–14]. The issue of forecasting consumption and production levels is therefore crucial. Supply cannot always be adjusted to demand a few hours earlier, especially because electricity is difficult to store on a large scale. The increasing integration of intermittent production capacities, such as wind turbines and photovoltaic systems, makes this adjustment even more difficult to control.

## 2. Coupling of the Electricity Markets

Price Coupling of Regions (PCR) is based on a single price coupling solution to be used for the calculation of electricity prices between coupled energy markets. The Day Ahead Market (DAM) from Romania operates in a regime coupled with spot markets in Hungary (HU), Slovakia (SK) and the Czech Republic (CZ) inside the 4M Market Coupling project starting with 2014 (Figure 1a). As well, starting with 19 November 2019, the Intra-Day Market (IDM) from Romania operates in conjunction with the markets in the other 20 countries (Figure 1b) participating in the European project SIDC (Single Intra-Day Coupling).

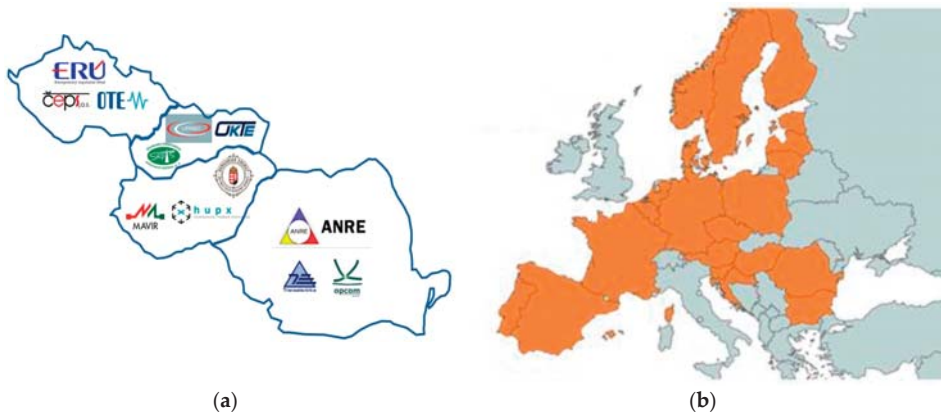


**Figure 1.** Coupling of the Electricity Markets: (a) The Day Ahead Market (DAM); (b) The Intra-Day Market (IDM); (Source: <http://www.opcom.ro>).

On the Day-Ahead Market are concluded on each trading day, firm transactions with electricity for each trading hour of the next delivery day, based on the offers submitted by the DAM participants. Transactions on the Intra-Day Market start with the day before delivery day, after the Day-Ahead Market trading has finished, and ends with an hour before starting the delivery.

## 3. Analysis of the Electricity Prices on DAM: Case of the 4M Market Coupling

Electrical network interconnections are a key element in regulating the European energy market, both for import and export. They allow for mutual assistance between the Member States of the Union, depending on the profiles of the respective consumers and their production capacities. This system makes it possible to strengthen the security of supply of the territory. At the same time, suppliers get the best price for energy at any time on the wholesale market.

The objective of the market coupling mechanism is to ensure the use of interconnections in the right direction, that is, from the market where energy is the cheapest to the most expensive. The only limit to the coupling of markets is given the import and export capacities at the borders. Network administrators set a limit to ensure security of supply. This limit cannot be exceeded by exporters.



Thus, based on flows, it makes it possible to provide the most useful exchanges in the service of the network, by finding the best solutions between the countries concerned. The establishment of this system, however, required the harmonization of national rules governing the various integrated networks [15–17].

Even after the coupling of the energy markets, a variation in very large limits of the electricity prices is observed. Thus, several situations were identified with very high prices (Figures 2 and 3), with very low prices (Figures 4 and 5) and even negative (Figures 6 and 7). These situations were analyzed in comparison with the electricity production of Romania and with the energy exchanges and available transmission capacities existing on the border (Tables 1–3).

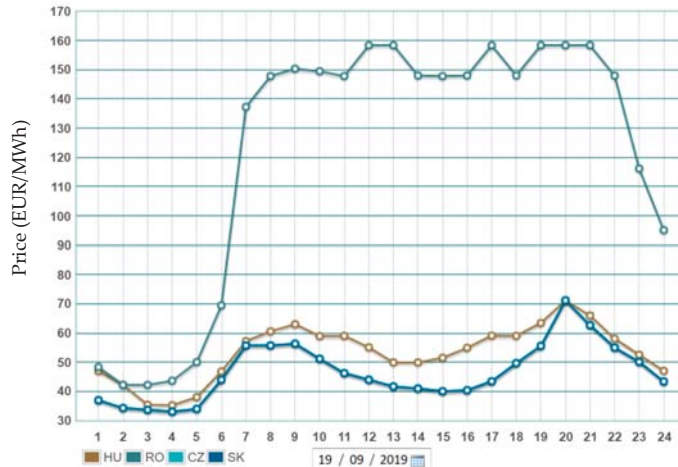


Figure 2. High prices on coupled electricity markets at the RO-HU border (data processed from website: <http://www.opcom.ro>).

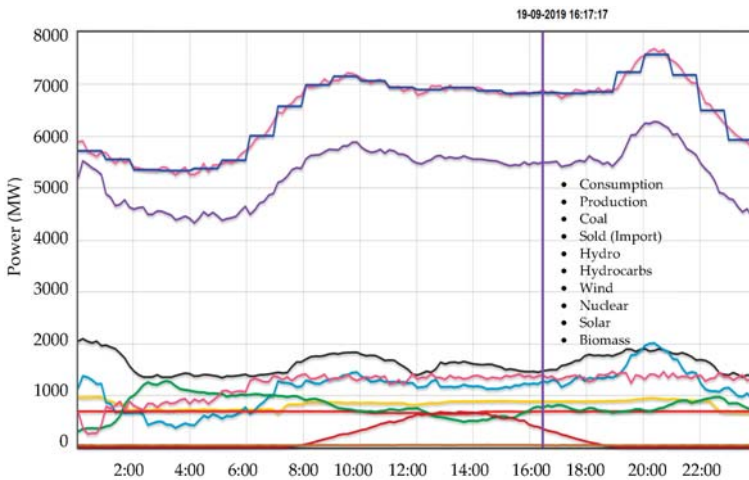
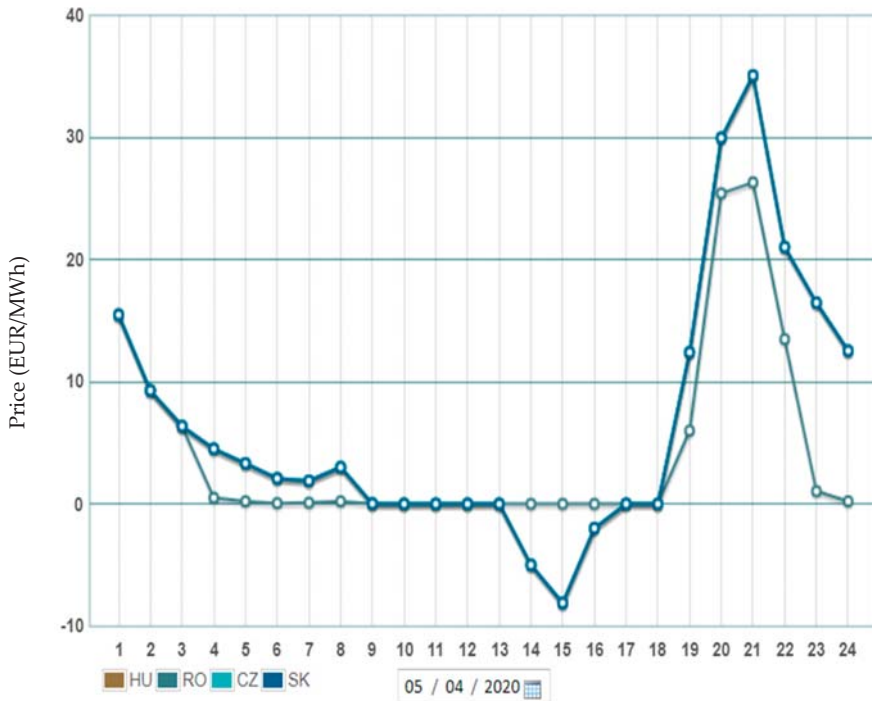
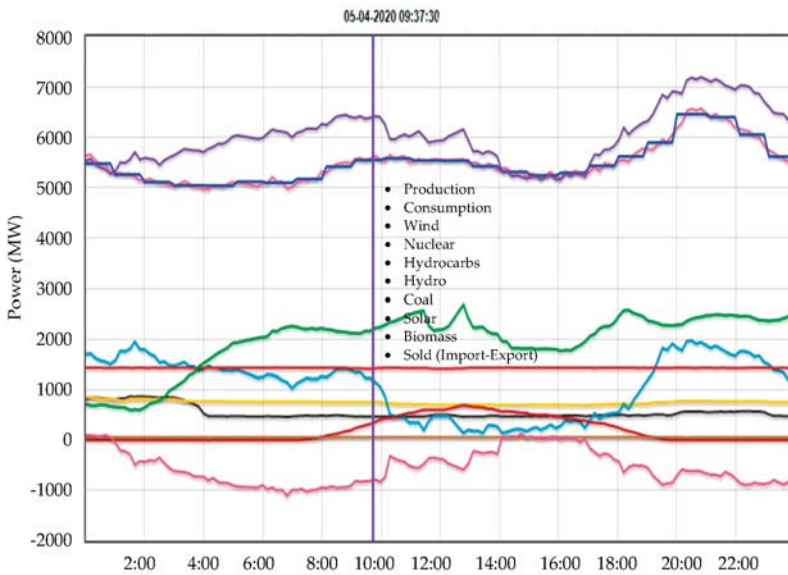


Figure 3. Electricity production in Romania on 19 September 2019 (data processed from website: <http://www.transelectrica.ro>).





**Figure 4.** Low prices on coupled electricity markets at the RO-HU border (data processed from website: <http://www.opcom.ro>).



**Figure 5.** Electricity production in Romania on 5 April 2020 (data processed from website: <http://www.transelectrica.ro>).

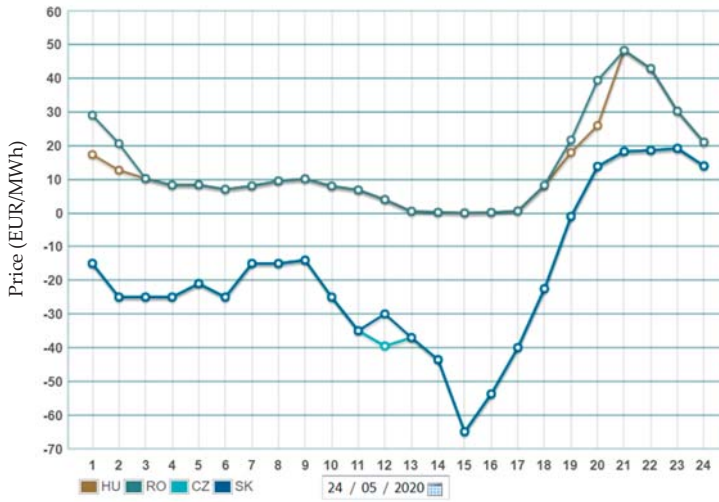


Figure 6. Negative prices on coupled electricity markets at the RO-HU border (data processed from website: <http://www.opcom.ro>).

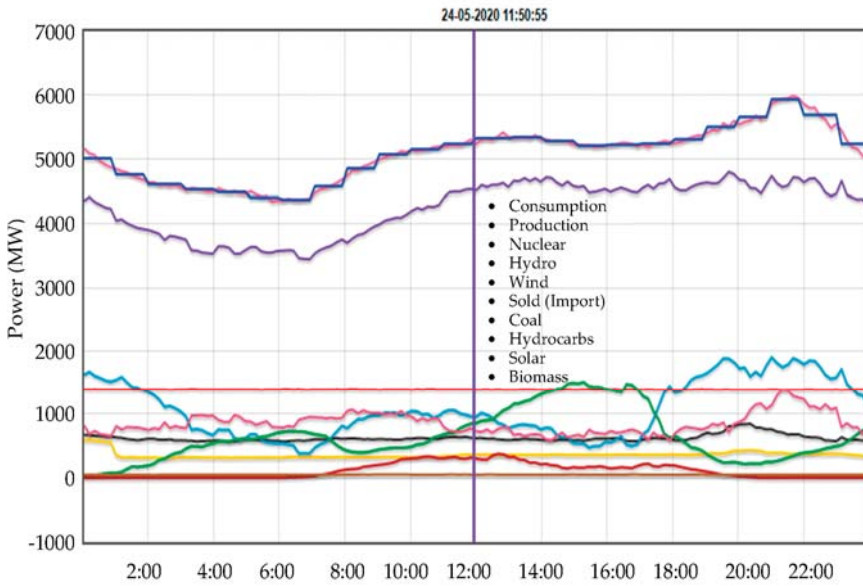


Figure 7. Electricity production in Romania on 24 May 2020 (data processed from website: <http://www.transelectrica.ro>).

**Table 1.** Characteristic values for coupling of the electricity markets on 19 September 2019.

Interval Time	Price DAM (EUR/MWh)				Cross-Border Flow (MWh)		Available Transmission Capacity (MW)	
	RO	HU	SK	CZ	RO_HU	HU_RO	RO_HU	HU_RO
...								
7	137.27	57.22	55.74	55.74	0	456	544	456
8	147.83	60.60	55.75	55.74	0	456	544	456
9	150.37	63.03	56.34	56.34	0	456	544	456
10	149.51	58.95	51.18	51.18	0	456	544	456
11	147.83	59.05	46.25	46.25	0	456	544	456
12	158.39	55.12	44.00	44.00	0	456	544	456
13	158.39	49.93	41.70	41.70	0	456	544	456
14	148.04	49.94	41.00	41.00	0	456	544	456
15	147.83	51.52	40.04	40.04	0	456	544	456
16	148.04	54.94	40.41	40.41	0	456	544	456
17	158.39	59.12	43.47	43.47	0	456	544	456
18	148.04	63.46	49.68	49.68	0	456	544	456
19	158.39	71.18	55.60	55.60	0	456	544	456
20	158.39	66.00	71.18	71.18	0	456	544	456
21	158.39	58.08	62.70	62.70	0	456	544	456
...								

**Table 2.** Characteristic values for coupling of the electricity markets on 5 April 2020.

Interval Time	Price DAM (EUR/MWh)				Cross-Border Flow (MWh)		Available Transmission Capacity (MW)	
	RO	HU	SK	CZ	RO_HU	HU_RO	RO_HU	HU_RO
...								
7	0.10	1.89	1.89	1.89	530.0	0.0	530	470
8	0.21	3.01	3.01	3.01	530.0	0.0	530	470
9	0.02	0.02	0.02	0.02	398.7	0.0	530	470
10	0.00	0.00	0.00	0.00	33.4	0.0	530	470
11	0.00	0.00	0.00	0.00	101.0	0.0	530	470
12	0.00	0.00	0.00	0.00	114.2	0.0	530	470
13	0.00	0.00	0.00	0.00	0.0	143.2	530	470
14	0.00	-5.00	-5.00	-5.00	0.0	470.0	530	470
15	0.00	-8.12	-8.12	-8.12	0.0	470.0	530	470
16	0.00	-1.99	-1.99	-1.99	0.0	470.0	530	470
17	0.00	0.00	0.00	0.00	0.0	176.4	530	470
18	0.00	0.00	0.00	0.00	50.2	0.0	530	470
19	6.00	12.42	12.42	12.42	530.0	0.0	530	470
20	25.45	30.00	30.00	30.00	530.0	0.0	530	470
21	26.35	35.11	35.11	35.11	530.0	0.0	530	470
...								

Electricity generation and consumption must be balanced so that the market is balanced and does not collapse. When there is too much production, short-term markets tend to lower their prices or even have negative prices to discourage producers from generating.

Prices on the wholesale electricity market result from the meeting of supply (production) and demand (consumption). Basically, the higher the supply compared to the demand, the lower the price of electricity.

In these periods of overproduction, producers who cannot shut down their power plants have to pay to sell their production, while some large buyers are encouraged to consume more. These short-term movements have little influence on the bill of small consumers, as most individuals have fixed-term contracts for long periods of time. On the other hand, for large industrial consumers who have short-term contracts, this is an advantage, because they can buy electricity very cheaply, even at a negative price.

**Table 3.** Characteristic values for coupling of the electricity markets on 24 May 2020.

Interval Time	Price DAM (EUR/MWh)				Cross-Border Flow (MWh)			Available Transmission Capacity (MW)		
	RO	HU	SK	CZ	RO_HU	HU_RO	SK_HU	RO_HU	HU_RO	SK_HU
...										
5	8.40	8.40	-21.00	-21.00	0	393.4	969.0	750	550	969
6	7.05	7.05	-24.99	-24.99	0	426.8	969.0	750	550	969
7	8.08	8.08	-14.99	-14.99	0	369.2	969.0	750	550	969
8	9.54	9.54	-15.00	-15.00	0	432.1	969.0	750	550	969
9	10.15	10.15	-14.02	-14.02	0	395.3	969.0	750	550	969
10	8.01	8.01	-25.00	-25.00	0	261.8	969.0	750	550	969
11	6.85	6.85	-35.00	-35.00	0	31.0	969.0	750	550	969
12	4.00	4.00	-30.00	-39.54	0	138.5	969.0	750	550	969
13	0.53	0.53	-37.04	-37.04	0	204.1	969.0	750	550	969
14	0.21	0.21	-43.59	-43.59	0	187.0	969.0	750	550	969
15	0.02	0.02	-65.00	-65.00	0	406.1	969.0	750	550	969
16	0.20	0.20	-53.79	-53.79	0	338.6	969.0	750	550	969
17	0.62	0.62	-40.00	-40.00	0	258.0	969.0	750	550	969
18	8.25	8.10	-22.50	-22.50	0	550.0	969.0	750	550	969
19	21.72	18.00	-1.00	-1.00	0	550.0	969.0	750	550	969
...										

Cross-border electricity exchanges use the available transmission capacity (ATC) on the border to reduce price differences between coupled electricity markets. Supply and demand are traded on the stock exchange until cross-border transmission capacity is exhausted or market prices are the same in both countries. These situations can be easily identified in Figure 2-Table 1 (on the SK-CZ border in time intervals 7–21); Figure 4-Table 2 (on the RO-HU-SK-CZ borders in the time intervals 10–13 and 17–18; on the HU-SK-CZ borders in the time intervals 7–9, 14–16 and 19–21); Figure 6-Table 3 (on the RO-HU border in time intervals 5–17; on SK-CZ borders in time intervals 5–21).

If the available transmission capacity on the border is reached before the price alignment, then electricity prices remain different: The other situations in Figure 2-Table 1; Figure 4-Table 2; Figure 6-Table 3.

Exports through interconnections and flexible consumption are not necessarily enough to reduce falling prices. If, at some point, electricity demand rises sharply and supply is difficult to maintain due to a lack of production supply, prices are rising because some suppliers are willing to pay a high price to avoid a blackout. If, on the other hand, demand is weak in the face of abundant supply, prices will fall.

Situations with negative prices certainly correspond to low marginal costs at a given time, but this does not mean that these prices make it possible to cover the total production costs of the installations concerned. This phenomenon can be amplified by the structure of certain support mechanisms for renewable production. Currently a large part of the production of electricity from renewable sources is supported by various schemes. Thus, support payments depend on the production of electricity achieved. Therefore, even when prices are negative it can be profitable for renewable producers to continue to operate.

#### 4. Conclusions

Radical changes have taken place in the energy sector in recent years, with a clear trend of increasing the production of electricity from renewable energy sources and new challenges for the market participants. Thus, some wholesale electricity markets have faced episodes of negative prices. In these single market situations, it is the producers who pay the suppliers. Negative prices occur especially in periods of abundant production of electricity from renewable sources and low demand, situations in which certain conventional energy sources cannot operate below a technical minimum. Negative values of electricity prices were recorded in the markets of Hungary, the Czech Republic and Slovakia (a record negative value of -65 EUR/MWh being registered on the SK-CZ border).

As well, the lack of the participants skills in developing adequate bidding strategies was one of the causes of the price increase.

The electricity prices on the Romanian Day Ahead Market are very variable between a minimum registered value (0 EUR/MWh) and a maximum registered value (158 EUR/MWh). No negative prices have been registered so far in Romania, however, the energy markets with which Romania operates in coupled regime register frequent situations with negative electricity prices.

However, negative wholesale prices are not good news. An increase in overproduction episodes creates uncertainty in the markets and reflects an imbalance. The main undesirable effect of these negative prices is that the market no longer sends the right signals to investors. This is equivalent to destroying value, as producers' revenues from the electricity market no longer cover real production costs. Electricity producers are no longer encouraged to invest in the renewal and expansion of new production capacity, and this can lead to a risk of shutdown during periods of high energy demand.

Coupling regional energy markets can partially solve these situations. Therefore, the imbalance of a system can be resolved by a neighboring system if the interconnections are not already used at their maximum capacity level.

After a strong period of development, it becomes necessary to review the mechanisms to support the development of electricity production from renewable energy sources. In the longer term and when renewable energy production systems reach a certain level of maturity, we can imagine that their development will depend much more on market mechanisms. For the time being, and because European targets are particularly ambitious, a first step towards avoiding these situations could be to stop paying support schemes in the event of negative wholesale prices or when renewable energies cause network congestion.

However, a positive effect of situations with lower or even negative prices in the electricity markets must be highlighted. The development of large-scale storage capacity will be able to be encouraged by such behavior of the electricity market. As well, more levers to increase the flexibility of electricity consumption will need to be activated. Some uses are easy to control, such as the thermal use of electricity (heating or cooling by heat pumps) or the recharging of electric vehicles.

Continuous improvement of electricity demand and supply forecasts, thanks to weather models, will make it possible to better predict imbalances in the electricity system and anticipate the use of levers to increase the flexibility of final energy consumption.

**Author Contributions:** Conceptualization, P.A. and R.D.P.; writing—review and editing, E.H. All authors have read and agreed to the published version of the manuscript.

**Acknowledgments:** This work was supported by a grant of the Romanian Ministry of Research and Innovation, CCCDI—UEFISCDI, project number PN-III-P1-1.2-PCCDI-2017-0404/31PCCDI/ 2018, within PNCDI III.

**Conflicts of Interest:** The authors declare no conflict of interest.

## References

1. Hinderks, V.J.; Wagner, A. Factor models in the German electricity market: Stylized facts, seasonality, and calibration. *Energy Econ.* **2019**, *85*, 104351. [[CrossRef](#)]
2. Balibrea-Iniesta, J. Economic Analysis of Renewable Energy Regulation in France: A Case Study for Photovoltaic Plants Based on Real Options. *Energies* **2020**, *13*, 2760. [[CrossRef](#)]
3. Xydis, G.; Vlachakis, N. Feed-in-Premium Renewable Energy Support Scheme: A Scenario Approach. *Resources* **2019**, *8*, 106. [[CrossRef](#)]
4. Conteh, A.; Lofly, M.E.; Adewuyi, O.B.; Mandal, P.; Takahashi, H.; Senjyu, T. Demand Response Economic Assessment with the Integration of Renewable Energy for Developing Electricity Markets. *Sustainability* **2020**, *12*, 2653. [[CrossRef](#)]
5. Maciejowska, K. Assessing the impact of renewable energy sources on the electricity price level and variability—A quantile regression approach. *Energy Econ.* **2019**, *85*, 104532. [[CrossRef](#)]
6. Pahle, M.; Schill, W.P.; Gambardella, C.; Tietjen, O. Renewable Energy Support, Negative Prices, and Real-time Pricing. *Energy J.* **2016**, *37*, 147–169. [[CrossRef](#)]

7. Zhao, H.; Wang, Y.; Zhao, M.; Tan, Q.; Guo, S. Day-Ahead Market Modeling for Strategic Wind Power Producers under Robust Market Clearing. *Energies* **2017**, *10*, 924. [CrossRef]
8. Loumakis, S.; Giannini, E.; Maroulis, Z. Merit Order Effect Modeling: The Case of the Hellenic Electricity Market. *Energies* **2019**, *12*, 3869. [CrossRef]
9. Pezzutto, S.; Grilli, G.; Zambotti, S.; Dunjic, S. Forecasting Electricity Market Price for End Users in EU28 until 2020—Main Factors of Influence. *Energies* **2018**, *11*, 1460. [CrossRef]
10. Rashidizadeh-Kermani, H.; Najafi, H.R.; Anvari-Moghaddam, A.; Guerrero, J.M. Optimal Decision-Making Strategy of an Electric Vehicle Aggregator in Short-Term Electricity Markets. *Energies* **2018**, *11*, 2413. [CrossRef]
11. Rounkvist, J.S.; Enevoldsen, P.; Xydis, G. High-Resolution Electricity Spot Price Forecast for the Danish Power Market. *Sustainability* **2020**, *12*, 4267. [CrossRef]
12. Genoese, F.; Genoese, M.; Wietschel, M. Occurrence of negative prices on the German spot market for electricity and their influence on balancing power markets. In Proceedings of the 7th International Conference on the European Energy Market, Madrid, Spain, 23–25 June 2010.
13. Filho, J.C.R.; Tiwari, A.; Dwivedi, C. Understanding the Drivers of Negative Electricity Price Using Decision Tree. In Proceedings of the 2017 Ninth Annual IEEE Green Technologies Conference (GreenTech), Denver, CO, USA, 29–31 March 2017.
14. Brijs, T.; De Vos, K.; De Jonghe, C.; Belmans, R. Statistical analysis of negative prices in European balancing markets. *Renew. Energy* **2015**, *80*, 53–60. [CrossRef]
15. Price Coupling of Regions (PCR). Available online: <http://www.epexspot.com/en/marketcoupling/pcr> (accessed on 30 June 2020).
16. Romanian Power Market Operator. Available online: <http://www.opcom.ro> (accessed on 30 June 2020).
17. Romanian Power Grid Company. Available online: <http://www.transelectrica.ro> (accessed on 30 June 2020).

**Publisher's Note:** MDPI stays neutral with regard to jurisdictional claims in published maps and institutional affiliations.



© 2020 by the authors. Licensee MDPI, Basel, Switzerland. This article is an open access article distributed under the terms and conditions of the Creative Commons Attribution (CC BY) license (<http://creativecommons.org/licenses/by/4.0/>).



# Overview on Efficient Naval Power Architecture †

Mariana Dumitrescu

Department of Automation and Electrical Engineering, “Dunarea de Jos” University of Galati, 80008 Galati, Romania; mariana.dumitrescu@ugal.ro

† Presented at the 14th International Conference INTER-ENG 2020 Interdisciplinarity in Engineering, Mureş, Romania, 8–9 October 2020.

Published: 14 December 2020



**Abstract:** Possible configurations for propulsion and electric power generation on vessels are an important field for the researcher in the naval area. The most important is electric power generation. Nowadays, diesel engines are the main prime movers, although all sorts of other electric power generating types are coming more and more. Apart from that, there are some specific high voltage/power applications that use steam or gas turbines. As well as this, wind power, either on a traditional sailing vessel or in a wind electric power generator, and also solar power, is gaining interest. The modern configuration is developing until the goal of zero carbon emissions is reached, using the electric power system configuration, introducing fuel cells as prime movers, and using batteries as energy storage devices, to increase the system’s safety.

**Keywords:** design; electric power generation; electric installation; ship; propulsion

## 1. Introduction

The future of ships is the electric propulsion, so more and more the ship designers are developing eco-friendly solutions (safe for the environment), with the goal of zero carbon emissions [1–4]. An electric ship is more than an electric drive system; it includes power generation, delivery, automation, and control. More and more naval applications require a larger amount of electric power generated and delivered (much more than the commercial ships), which can be used by high power consumers, high-power military loads, energy conversion systems, and a bigger delivery system. Other loads may include an electro-magnetic assistance launch system, communication, radar, sonar systems, and hospitality and service loads, as is shown in Figure 1.

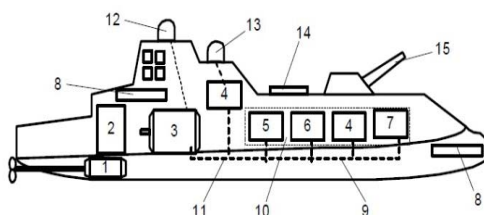


**Figure 1.** Power electric warship system: 1—advanced motor and propulsor, 2—motor drive, 3—advanced generators, 4—pulse forming network, 5—energy storage, 6—actuators and auxiliaries, 7—fuel cell stacks, 8—sensors, 9—distribution, 10—integrated power system, 11—integrated thermal and power management systems, 12 and 13—radar systems, 14—electromagnetic vertical launching system, 15—electromagnetic gun.

The synchronous electric generator driven by a gas turbine or diesel engines electrically connected with an electric propulsion motor is nowadays used in a large variety of vessels. According to [1],



the total installed electric propulsion power in marine vessels was in 2002 in the range of 6 to 7 GW. Azimuth thrusters and podded thrust units brought important maneuvering capabilities, control of the dynamic positioning, and intelligent applications [5–7]. Now, electric propulsion is applied mainly in the following types of marine vessels: cruise vessels, ferries, dynamic positioning drilling vessels, cargo vessels, moored floating production facilities equipped with thrusters, shuttle tankers, cable layers, pipe layers, icebreakers and other ice going vessels, supply vessels, submarines, combatant surface ships, and unmanned underwater vehicles.

The scientific literature [1,8–10] mentions that the expected compound annual increasing, for the electric engines and electric generators for ship propulsion systems, is expected to be around 20%. Today, almost all the cruise ships and a lot of cargo ships changed to electric motor propulsion systems. For example, the largest marine electric motors are installed on cruise vessel passenger liner Queen Elizabeth 2, which has a redundant system of propulsion—44 MW, 144 RPM, 60 Hz salient pole synchronous motors—driving the propeller shafts. The dimensions of the motors are 9 m in diameter, weighing more than 400 t each. The installed electric power is 95 MW, produced by nine three-phase 10.5 MW, 10 kV, 60 Hz salient pole synchronous generators—electric driven by diesel engines. The vessel is one of the largest, longest, tallest, widest, and most expensive passenger cruise vessels. Its power plant includes gas turbines and diesel engines that produce 118 MW of electricity, enough to power a city of 300,000 people. Most of the produced power is used for the propulsion system; each of the electric motors draws 21.5 MW during full power and it has Rolls Royce Mermaid pod propulsors, two fixed and two azimuths rotating 360°.

## 2. Propulsion and Electric Power Network

The naval system configurations for ship propulsion are presented below [4–6,11].

- Direct diesel propulsion, as shown in Figure 2a, uses electric power generated and distributed by a separated auxiliary system, gearbox reduction and fixed/controllable pitch propellers, and steerable thrusters with fixed/controllable pitch propellers.

The direct propulsion is the most common and basic configuration used still for many operating profiles because when the auxiliary power is a part of the propulsion power needed, there is no benefit in the combination of the propulsion and energy. Vessels like bulk, container carriers, or multipurpose have this direct configuration.

- Hybrid diesel electrical, as shown in Figure 2b,e, uses direct propulsion, integrated electric power generation and distribution, gearbox reduction and fixed/controllable pitch propellers, and steerable thrusters with fixed/controllable pitch propellers.

The hybrid configuration combines the advantages of combined propulsion and energy at a lower sailing speed, improving the carbon emissions goal and the efficiency (less power losses) of a diesel direct drive at higher speed.

- Electric diesel propulsion, as shown in Figure 2c,d, uses integrated electric power generation and distribution, gearbox reduction and fixed/controllable pitch propellers, and steerable thrusters with fixed/controllable pitch propellers.

The main switchboard power delivery system uses AC voltage, as shown in Figure 2c, or CC voltage, as shown in Figure 2d; in the second case, the power system is safer using the advantage of the energy storage system. There are many reasons for this type of system—better ship design, better power efficiency and reduction of emissions, better comfort from reduction of vibrations and noise, reduction of the maintenance of mechanical components, and more flexible operability.

- Direct diesel propulsion by shaft uses electric power, which can be also generated by driven shaft generators, as shown in Figure 2b,e, and a separated or integrated auxiliary system, with gearbox reduction and controllable pitch propellers, and steerable thrusters with controllable pitch propellers.

The propulsion with shaft configuration is mainly applied on vessels with an important power consuming process. When the process is not operated during sailing at maximum speed, then this mechanical combination of propulsion and power is more efficient for investment, fuel consumption, and emissions for container vessels or heavy lift ships. For separated or integrated main and auxiliary electrical power systems, the goal is the efficiency of the prime movers and the availability of the ship's electric network. The shaft generator is mostly operated at synchronous speed, but permanent magnet machines and power electronic converters allow generation at variable speed, so a hybrid diesel electrical configuration can be examined, allowing electric drive as well.

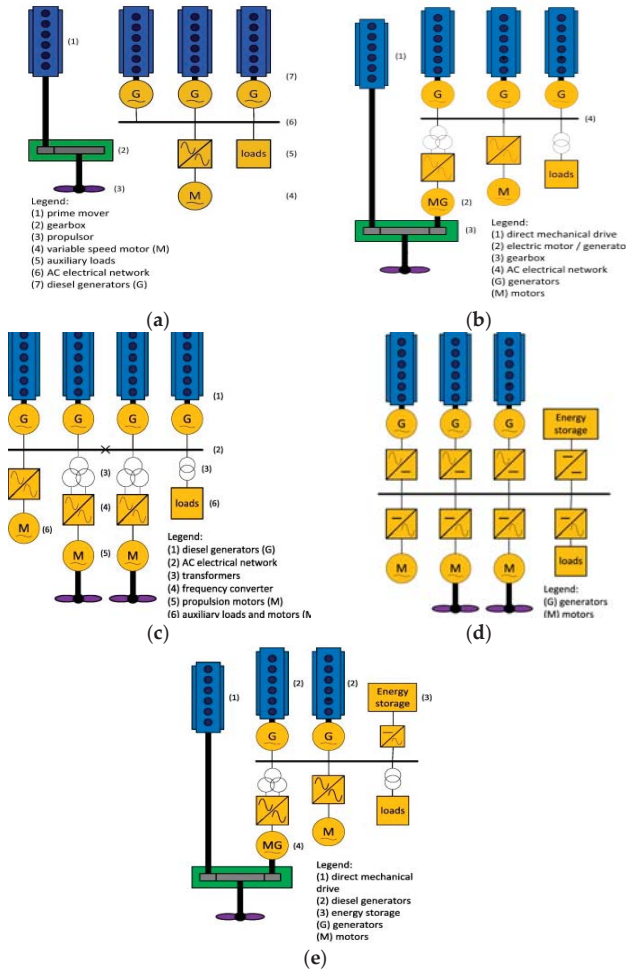


Figure 2. Naval configurations of the propulsion and electric power system, Direct diesel (a), Hybrid diesel electrical (b,e), Electric diesel (c,d).

Tables 1 and 2 give a synthetic overview of the naval system configurations for ship propulsion [12]. Presented are the types of ships that match with different types of propulsions, advantages and disadvantages of the propulsion and power systems on vessels, and installed power and parameters.

**Table 1.** Trends for configuration of propulsion and power supply architecture on vessel types.

Vessel Type (Voltage V, Frequency Hz, Power MW)	Frequency Converters	Supply Transformer	Type of Electric Propulsion Motors	Configuration Solutions
Offshore Support Vessels 690 V, 50/60 Hz, 13–15 MW	6-pulse Drive or Active Front End	-	Induction	Electric propulsion/Hybrid diesel electrical Transformer-less solution Less space and weight THD filter required
Cargo 6.6 kV, 50/60 Hz, 48 MW	VSI with PWM	24pulse	Synchronous 600 RPM/720 RPM	Direct diesel propulsion/Hybrid diesel electrical High propulsion power High drive and motor efficiency Low harmonics Heavy electric plant configuration
Cruise liner 11 kV, 50/60 Hz, 130 MW	VSI with PWM	24pulse	Synchronous slow speed 150 RPM	Electric diesel propulsion Highly redundant reliable High drive and motor efficiency Low noise and vibration Complex electric plant configuration
Ferry 690 V, 50/60 Hz, 13–15 MW	VSI-PWM technology	12pulse	Induction 900 RPM/1200 RPM	Electric diesel propulsion with hybrid power supply Robust and reliable technology No separate THD filters More space and weight compared to transformer-less solution
Carriers/Roll-on-roll-off 690 V, 50/60 Hz, 13–15 MW	Sinusoidal drive-Patented STADT AS	-	Induction (Two speeds)	Electrical propulsion with energy storage Highly reliable compact Very low losses Transformer-less solution Low THD (No THD filters needed) CP propeller

**Table 2.** Advantages and disadvantages of propulsion and power supply technologies on vessels [12].

Technology Type	Advantages	Disadvantages
Direct (Mechanical) propulsion	Low loss at design speed Low CO2 and NOx emissions at design speed Low conversion losses	Poor load efficiency and emissions High NOx at reduced speed Low redundancy Mechanical transmission noise
Electrical propulsion	Robustness Matching power load with generators High availability Reduced NOx emission at low speed Potentially low noise	Constant generator speed Losses at design speed
Hybrid propulsion	Low loss at design speed Robustness Matching load and engines at low speed Potentially low noise on electric drive	Constant generator speed System complexity
Hybrid power supply	Zero noise and emission mode Storing regenerated energy Efficient back-up power Reduced fuel consumption and emissions No NOx increase during acceleration	Constant generator speed System complexity Safety of the battery Battery cost

### 3. Aspects of the Air Emission Configuration Reduction

Only for the electric propulsion configuration the goal of zero carbon emissions is achievable if the diesel engine is replaced with the renewable power generation, like the fuel cell [12,13]. Hybrid fuel cell propulsion, and integrated electrical energy generation and distribution, with steerable thrusters with fixed pitch propellers, uses as the prime movers the fuel cells instead of diesel engines. There is a limited operating time, so for now it is used in the inland vessels.

The configuration is hybrid because of the direct online connected power battery. The advantages to the fuel cells are: zero emission for the power generation, all electric ship, and high redundancy because of the multi-functional power battery.

The air emissions coming from the combustion motors can be of different types. Substances, like NO<sub>x</sub>, SO<sub>x</sub>, and particulate matter (PM 2.5 and 10 μm), are regulated by the Maritime Environmental Pollution Committee—MEPC of the International Maritime Organization—IMO, the European Union, the Environmental Pollution Agency—EPA of the United States of America, and by local governments. The design is influencing only the PM type. For greenhouse gases, the IMO is involved in the reductions of CO<sub>2</sub> emissions. The issues are also economical, like improvement of fuel efficiency, future fuel prices may also include additional carbon prices, such as future capitalization of CO<sub>2</sub> emissions at a current approximate rate of EUR 22/t.

The ways to achieve the green ship power system goal, from a design point of view, are several. The traditional configurations for electric power generation, distribution, and consumption can be improved by the reduction of consumption, improving efficiency for the auxiliary equipment, LED lighting and intelligent consumption/control systems, and power management systems. For the electric propulsion design, changes involve the complete drive train and changing the hull shape, which are going to see the efficiency growing up to 40%. The potential for improvement of energy efficiency is clear from the efficiency diagram for the example of a container vessel sailing at 24 knots, as shown in Figure 3 [5,13]. We can consider that the prime mover can partially or completely be replaced by green renewable sources, wind or sun power, or by energy carriers like H<sub>2</sub>. When applying H<sub>2</sub>, the local energy conversion will be done with fuel cells.

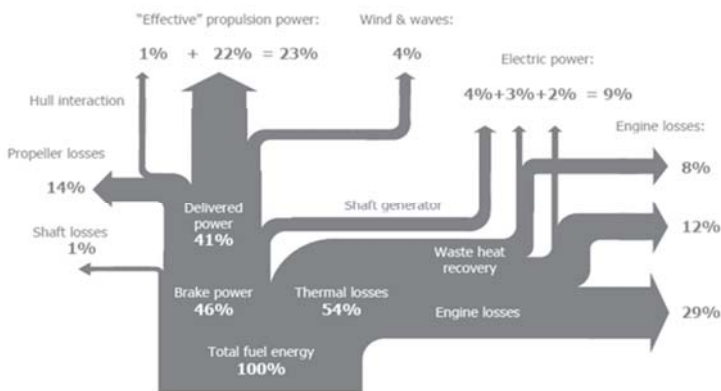
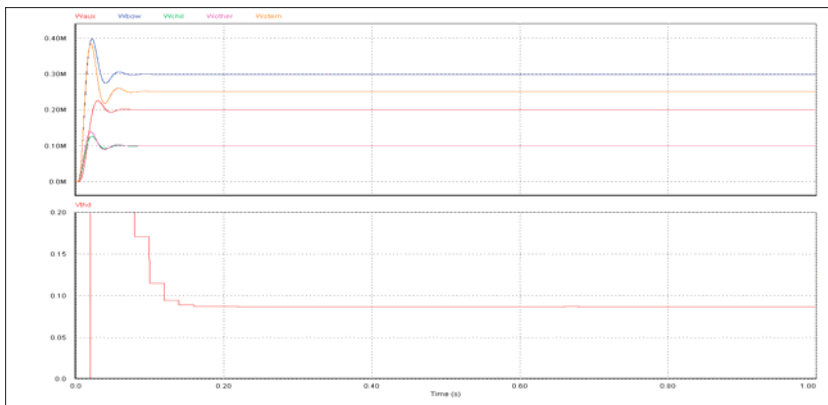


Figure 3. Efficiency diagram (Sankey diagram) for a container vessel, according to [13].

Electric diesel, hybrid electric diesel, and hybrid fuel cell power systems have a big power delivery system for the transportation and distribution of the main power [13,14]. The main delivery can use AC or DC voltage, low or medium voltage, with a maximum power rating; for example, an application of low voltage has 5 MWe. Selecting AC or DC is mainly a matter of energy losses; for example, if many frequency control power consumers are needed for gaining efficiency in power consumption,

a DC voltage power system implementation will prevent the double conversion AC-DC and DC-AC, saving up to 5% in efficiency. Because DC voltage power systems do not have reactive power, they can be a smaller size. They do not need phase synchronization during parallel operation of generators. As fuel cells and batteries produce DC voltage, it seems logical to select DC for the main power delivery of a fuel cell propulsion system. We also have to take into account that DC voltage systems are less easy to protect for overload and short-circuit, so ultra-rapid fuses are needed. Furthermore, DC voltage power systems need more care than AC voltage power systems, which concerns safety for humans and the machine.

The developing of hybrid diesel electric propulsion, power saving devices in the auxiliary grid like frequency converters, AC voltage switching power supplies, increasing application of LED lighting, and the electric network suffers more and more from current and voltage distortion and from increase of the zero sequence currents. Because the power system is an isolated one, it is more sensitive to the non-linear and the unbalanced loads, and for transient regimes caused by switching, so there is a need for extra attention to electric power systems design, to electromagnetic compatibility (EMC) and earthing. Figure 4 shows a simulation for switching on 950 kW in the electrical network of a mega yacht, presenting the total harmonic distortion on the system voltage, which is going to 9% and is too high. For preventing such a distortion, adding 12-pulse transformers supplying the frequency converter is a solution.



**Figure 4.** The total harmonic distortion on the system voltage by simulating the switching on of the auxiliary power system of a mega yacht, according to [13].

#### 4. Conclusions

The overview of the ship design architecture, for the isolated power system of a vessel, is pointing to the architecture with less air pollution effects, which is a feasible solution offered by the electric diesel with the total or partial fuel cell power supply. Fuel cell power generation can be considered from a shipbuilding point of view if the ship’s design process can provide an optimized system solution with a DC voltage electric network and a minimum of negative effects on the protection and safety on the network. Operating profiles have to give answers to the following questions: Does the operating speed profile justify the selection of an electrical diesel power system and propulsion? Can the electric power and energy system be supplied by fuel cells? The proposed solution depends also on the operating fuel consumption and the load characteristic of the prime movers with respect to the functional safety of the ship, but also to the maximal environmental pollution reduction.

**Conflicts of Interest:** The author declares no conflict of interest.

## References

1. Gieras, J. *Naval electric machine. Advancements in Electric Machines*; Springer: Dordrecht, The Netherlands, 2008; pp. 213–234.
2. Chalfant, J. Early-stage design for electric ship. *Proc. IEEE* **2015**, *103*, 2252–2266. [CrossRef]
3. Dennis, T. *Practical Marine Electrical Knowledge*, 3rd ed.; Witherby-Seamanship International: Livingston, Scotland, 2014.
4. International Maritime Organization. *SOLAS: Consolidated Text of the International Convention for the Safety of the Life at Sea*; Int. Maritime Org: London, UK, 2014.
5. Borstlap, R.; Ten Katen, H. *Ships' Electrical Systems*; Dokmar Maritime Publishers B.V.: Enkhuizen, The Netherlands, 2011.
6. Van Dokkum, K. *Ship Knowledge: A Modern Encyclopedia*, 1st ed.; Publisher Dokmar: Vlissingen, The Netherlands, 2003.
7. Van Dokkum, K. *Ship Knowledge: Types of Ships and Their Trades*; Publisher Dokmar: Vlissingen, The Netherlands, 2003.
8. Carlton, J. *Marine Propellers and Propulsion*; Elsevier: Amsterdam, The Netherlands, 2011.
9. Ferrante, M.; Chalfant, J.; Chryssostomidis, C.; Langland, G.; Dougal, R. Adding simulation capability to early-stage ship design. In Proceedings of the 2015 IEEE Electric Ship Technologies Symposium (ESTS), Alexandria, VA, USA, 21–24 June 2015; pp. 207–212.
10. Menis, R.; da Rin, A.; Sulligoi, G.; Vicenzutti, A. All electric ships dependable design: Implications on project management. In Proceedings of the 2014 AEIT Annual Conference—From Research to Industry: The Need for a More Effective Technology Transfer (AEIT), Trieste, Italy, 18–19 September 2014; pp. 1–6.
11. Maggioncalda, M.; Gualeni, P.; Notaro, C. Life Cycle Performance Assessment (LCPA) Tools. In *Optimisation of Ship Design and Operation for Life Cycle*; Springer: Berlin, Germany, 2014; Volume 1.
12. Geertsmaa, R.D.; Negenborna, R.R.; Vissera, K.; Hopmana, J.J. Design and control of hybrid power and propulsion systems for smart ships: A review of developments. *J. Appl. Energy* **2017**, *194*, 30–54. [CrossRef]
13. Krijgsman, B.M. Propulsion and energy optimization for ships an optimal propulsion and electrical energy concept. In Proceedings of the Second International Symp on Electrical and Electronics Engineering, Galati, Romania, 12–13 September 2008.
14. Nijland, M.; Van Beek, T. Efficiency improvement related to propeller-rudder interaction. In Proceedings of the 5th Annual Green Ship Technology Conference, Rotterdam, The Netherlands, 11–12 March 2008.

**Publisher's Note:** MDPI stays neutral with regard to jurisdictional claims in published maps and institutional affiliations.



© 2020 by the author. Licensee MDPI, Basel, Switzerland. This article is an open access article distributed under the terms and conditions of the Creative Commons Attribution (CC BY) license (<http://creativecommons.org/licenses/by/4.0/>).



# Isolated Power System Safety Analysis <sup>†</sup>

Mariana Dumitrescu

Department of Automation and Electrical Engineering, “Dunarea de Jos” University of Galati, 80008 Galati, Romania; mariana.dumitrescu@ugal.ro

<sup>†</sup> Presented at the 14th International Conference INTER-ENG 2020 Interdisciplinarity in Engineering, Mures, Romania, 8–9 October 2020.

Published: 14 December 2020

**Abstract:** For a specific vessel, the safety of the isolated power system is analyzed. Concerning the safety, the choice of propulsion system and the classification regulations have a major role for the power system design. The rules of SOLAS (International Convention for the Safety of Life at Sea), the flag state, and the harbor authorities are pointing to the basic level of safety, while the classification societies are pointing to the basic navigational regulations. A case study of the main switchboard and emergency switchboard safety, while taking into account different short circuits for the specific operational configuration of the electrical network, makes a comparative study possible.

**Keywords:** safety; design; power system; electric installation; ship

---

## 1. Introduction

Electric installations design of the ships is a very complete part of electrical engineering. Their safety is one of the main concerns of the specialists, as they are isolated power systems and they have to cover the complete spectrum from power generation to distribution and switchgear to all consumers [1,2]. The protections, the automations, the communication, and the nautical/navigation systems have to be included in the design. The electrical power for ships comes mainly from the synchronous generators [3,4]. The most common prime mover for an electric generator is often the diesel engine. Other smaller engines can be installed on a common base generator frame, but for diesel-electric important applications, it is possible that both have their own base frame and are connected with a flexible coupling [5,6]. For safety reasons an emergency diesel generator (EG) is always used to give main electrical power if the main source is in failure/blackout [7]. The emergency generator/source must be self-contained and built independent of the main engine room systems. It is completed with its own independent systems for starting, fuel oil, lubrication oil, cooling, and preheating, for an independent working purpose. The consumers supplied by the EG, as the regulations require, are the main consumers like: emergency lighting, navigation/communication devices, steering gear, fire and sprinkler pumps, bilge pump, water tight doors, and lifts.

When the emergency source of electrical network is an electric generator, it has to be provided with a transitional emergency electrical power source. The ship uses the selected uninterruptible power supply (UPS) application. A battery or an uninterruptible power supply must be used as a standby power supply with a capacity of 30 min. Navigation and safety aspects, required by the ship class, point to the use of the UPS, such as: automation system, navigation system, radio/safety announcement equipment, emergency lighting, watertight doors, etc.

## 2. Structure of the Electrical Network

Taking into account the isolated configuration nature of electrical power system onboard ship, several means are used to assure its safety and continuous availability. The main switchboard is divided into two or more sections power supplied by the main diesel generators (DG) [8,9]. The switchboard



supplied by an emergency generator as well as the uninterrupted (battery secured) power supply as Figure 1 shows is very important, both for reasons of safety and to ensure fault tolerant, redundant configuration. The EG must also be able to start automatically if the main source of electrical power fails to supply the emergency switchboard. In this case, the EG is automatically started and connected to the emergency switchboard by its automation power management system [9,10].

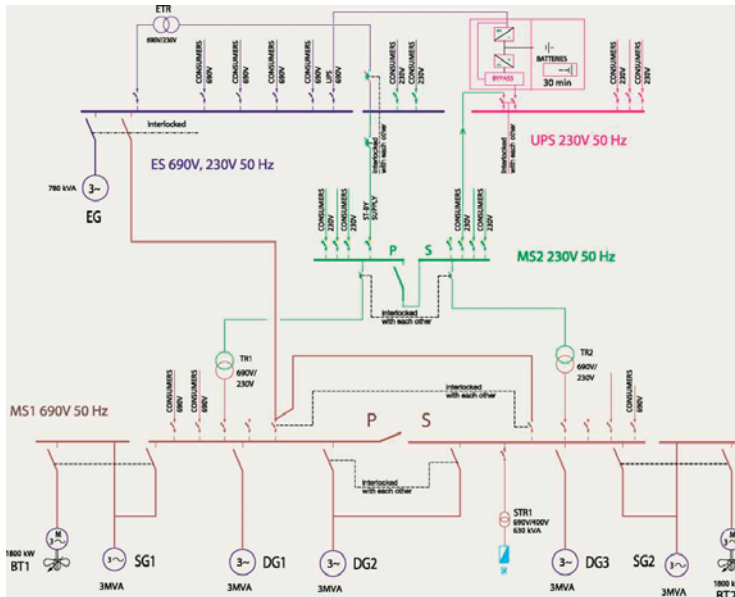


**Figure 1.** Low-voltage 690V electric network for an isolated power system, for a vessel with diesel-mechanical propulsion [10].

In addition to auxiliary generators an electrical network often has shaft generators (SG) driven by the main engine. Sometimes shaft generators are used only for driving the thrusters during maneuvers, while in other applications they are able also to supply the ship’s network. For this reason, some interconnections are required to avoid overload or damage to the network. The following feeder combinations, for example, are prohibited [5,10]:

- If the bus-tie breaker is closed, the SG breakers are interlocked in the open position;
- If the SG breaker is closed, the bus-tie breaker is interlocked in the open position;
- If the bow thruster breaker is closed, the SG breaker is interlocked in the open position;
- When synchronizing the SG in parallel with the diesel generator (DG), the DG breaker has to be open with a time delay;
- Interlocking every auxiliary power station (switchboard) must be defined separately.

When the SG is connected and is supplying the ship electrical installation, a constant speed mode for the main engine has to be chosen, meaning the network frequency. In constant speed mode, the propulsion will be controlled with the help of the pitch adjustments, using the controllable pitch propeller (CPP). The main engine can drive the SG when this is disconnected from the main propulsion line. In this case, the main engine runs as an auxiliary engine, for example to supply the big consumers in special regime like loading or unloading in the harbor.

First, the propulsion type has to be chosen, diesel-mechanic or diesel-electric, then other decisions are made, like the following [10,11]:

- Evaluation of the maximum electrical power needed to be generated (the load reservation is agreed with the customer);
- Given that information on the electrical loads/consumers, which can be based on relative values calculated from reference ships, taking into account different ship operating modes like: sailing, maneuvering, loading, harbor, dynamic positioning-DP this will affect the total load computing;
- Finding the generator number and its apparent power S [VA];
- Selection of main voltage and frequency;
- Computing the voltage drop;
- Computing of the short circuit regime and finding the network selectivity.

### 3. Designing the Electrical Network According to the Safety Rules

In the design stage, the first step is to define the ship type. The ship type, size, and purpose are key factors when dimensioning the electrical network. The following are expressing the different electrical needs of different types of ship [4]:

- For cargo ships, the handling equipment has the main role in containerships, and gives the requirement characteristics of the power electrical network;
- For tankers, the pumps and the compressors are mainly the significant factors;
- For passenger ships, the electrical consumers are mainly the air conditioning, the galley equipment, lighting installation, and the transverse thrusters for maneuvering in the harbor;
- For the ships with electric propulsion, the propulsion machinery itself is the dominating factor.

The choice of propulsion system and the classification regulations have an impact on the design of the power electrical network. The rules of SOLAS (International Convention for the Safety of Life at Sea), the flag state, and the harbor authorities specify the basic level of safety, while the classification societies specify the basic navigational regulations, like a redundant propulsion, an unmanned engine room, and a green power system.

For the study case configuration of the power system in Figure 2, the generators were already selected, and the short circuit safety analysis is presented, taking into account the functional alternatives:

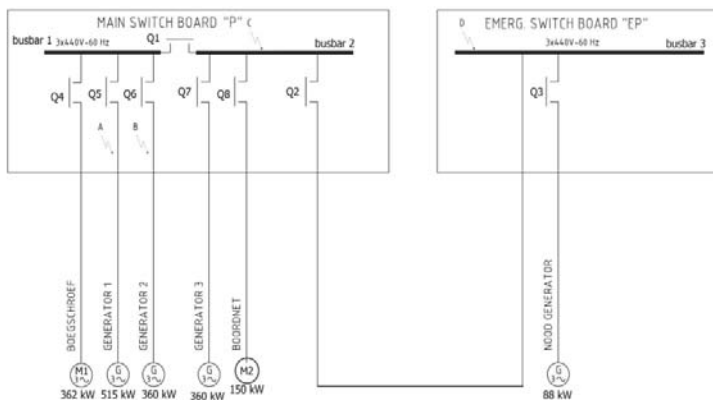


**Figure 2.** Configuration of the main switchboard and emergency switchboard for the power system study case.

Case 1—Generator 1 is in running mode, the rest of the generators are stopped. Generator 1 is supplying the thruster engine and the electrical system. Q1 is closed, Q2 and Q3 opened.

Case 2—Generators 2 and 3 are in running mode, the rest of the generators are stopped. Generators 2 and 3 are supplying the thruster engine and the electrical system. Q1 is closed, Q2 and Q3 opened.

Case 3—Generator 3 is in running mode, the rest of the generators are stopped. Generator 3 is supplying the electrical system. Q1, Q2, and Q3 are opened.

Case 4—Generator 2 is in running mode, the rest of the generators are stopped. Generator 3 is supplying the electrical system. Q1 is closed, Q2 and Q3 are opened.

Case 5—Emergency generator (EG) is in running mode, the rest of the generators are stopped. EG is supplying only the essential consumers from the electrical system, but not the thruster. Q1 is opened, Q2 and Q3 are closed.

The short circuit computation, with the help of the Germanischer Lloyd, Short Circuit Calculation Program and using its design safety rules [12,13], takes into account the short circuit locations A, B, C, and D. The calculation obtained the short circuit current values for the a.c. three phase system based on IEC 61363 standard. The short circuit current comprises three components, a.c component ( $I_{ac}$ ), d.c. component ( $I_{dc}$ ), and the peak current ( $I_p$ ). The results of the short circuit currents (in Ampere), for the location C on the main switchboard, are presented in Table 1.

**Table 1.** Alternatives comparison for the main switchboard (C point) short circuit computing, taking into account the functional variants in cases 1, 2, 3, and 4.

SC in point C	P (kW)	$I''_{kg}$	$I_{ng}$	$X_{d''}$	$\acute{I}_{km}$	$I_{mn}$	$I''_{kg_{tot}}$	$I''_{kmtot}$	$I''_{ktot}$	$I_{ptot}$
Case 1 Q1 open Q2 open	360	5681.09	624.92	0.11	1642.14	273.69	5681.09	1642.14	7323.23	16,843.43
Case 2 Q1 open Q2 close	360	5681.09	624.92	0.11	1642.14	273.69	6995.75	1642.14	8637.89	19,867.16
Case 3 Q1 close Q2 open	360	5681.09	624.92	0.11	1642.14	273.69	21,212.07	5091.12	26,303.19	60,497.34
Case 4 Q1 close Q2 close	360	5681.09	624.92	0.11	1642.14	273.69	22,526.77	5091.12	27,617.86	63,521.07
	88	1314.66	157.76	0.12						

These results give the overview of the needed information concerning the system safety and point to the protection equipment selection used to achieve the system safety goal. For comparison, of the system safety in all 4 analyzed cases, the peak current  $I_{ptot}$  is used, which has the biggest computed value in the case 4. This is a result of adding the generators' total current and the engines/motors total current, taking into account the equivalent reactance  $X_{d''}$ , the nominal generator current  $I_{gn}$ , the nominal motor current  $I_{mn}$ , and the multiplication factors 6 for the motors case and 2.3 for the  $I_{ptot}$  computing.

As Table 1 shows, the most dangerous case, from short circuit safety point of view, is case 4. Because case 4 is detected as the heaviest situation the system can deal with in the circuits design and equipment selection, the numerical results from case 4 will be used in design and equipment sizing. In Table 2 the nominal data computed for the electric circuits connected to the main switchboard, generator 1, generator 2, generator 3, emergency generator, and equivalent engine are presented. Table 2 also gives the selected circuit breakers data needed to achieve the operational security of the analyzed system for all the above-mentioned circuits.

**Table 2.** Electric circuits nominal data and circuit breakers selection for the heaviest operational state, represented by the case 4.

	P (kW)	In (A)	Ku	Is (A)	Kss	Iss (A)
Generator 1	515	886.49	0.9	797.84	1.12	900.76
Generator 2	360	624.92	0.9	562.42	1.1	618.67
Generator 3	360	624.92	0.9	562.42	1.1	618.67
Generator emergency	88	157.76	0.9	141.98	1.1	156.18
Thruster engine	362	574.83	0.9	517.34	1.1	569.08
Equivalent	150	273.79	0.9	246.32	1.1	270.95
Equipment		In (A)	Ir (A)	Irt (A)	tr (s)	Iinst (A)
Masterpact NT10H1/Micrologic 7.0A		1000	900	-	24	off
Compact NSX 630 N/ Micrologic 6.30A		630	630	618	0.5	945
Compact NSX 630 N/ Micrologic 6.30A		630	618	618	0.5	945
Compact NSX 160 N/ Micrologic 6.20A		160	160	156	0.5	240
Compact NSX 630 N/ Micrologic 6.30A		630	570	569	0.5	945
Compact NSX 400 N/ Micrologic 6.3 E-M		320	280	270	5	4800

#### 4. Conclusions

This paper presents a study case analysis of the operational safety for an isolated power system, in the situation of a vessel. Because the safety of the power system is the most important goal, especially for the ship’s electrical network, it is important to identify the design steps which can give the most suitable design architecture for the circuits. The marine special rules, which are mandatory, give more pressure when it comes to proposing the optimal design for the ship power system from a safety point of view. The main contribution of the paper is the proposed algorithm finding the most dangerous study case, from a short circuit safety point of view. The novelty is the procedure to select the study cases configuration which are subject for analysis by the Germanischer Lloyd, Short Circuit Calculation Program. The interpretation of the results and the conclusions of safety analysis are also a subject of the research proposed methodology. The alternatives analyzed in the paper for the operational power system specific situations help the specialist to find the most dangerous operational situation and the safest alternative possible. This gives the best confidence in the system response in case of the most dangerous short circuit possible, which can appear in the ship power electric network.

**Conflicts of Interest:** The author declares no conflict of interest.

#### References

1. Borstlap, R.; Ten Katen, H. *Ships’ Electrical Systems*; Dokmar Maritime Publishers: Enkhuizen, The Netherlands, 2011.
2. Van Dokkum, K. *Ship Knowledge: A Modern Encyclopedia*, 1st ed.; Dokmar Maritime Publishers: Enkhuizen, The Netherlands, 2003.
3. Van Dokkum, K. *Ship Knowledge: Types of Ships and Their Trades*; Dokmar Maritime Publishers: Enkhuizen, The Netherlands, 2003.
4. Chalfant, J. Early-stage design for electric ship. *Proc. IEEE* **2015**, *103*, 2252–2266. [[CrossRef](#)]
5. Dennis, T. *Practical Marine Electrical Knowledge*, 3rd ed.; Witherby-Seamanship International: Edinburgh, Scotland, UK, 2014.
6. Carlton, J. *Marine Propellers and Propulsion*; Elsevier: Amsterdam, The Netherlands, 2011.

7. SOLAS. *Consolidated Text of the International Convention for the Safety of the Life at Sea*; International Maritime Organization: London, UK, 2014.
8. Ferrante, M.; Chalfant, J.; Chryssostomidis, C.; Langland, G.; Dougal, R. Adding simulation capability to early-stage ship design. In Proceedings of the 2015 IEEE Electric Ship Technologies Symposium (ESTS), Alexandria, VA, USA, 21–24 June 2015; pp. 207–212.
9. Valkeejärvi, K. The ship's electrical network, engine control and automation. *Koninklijke Gallois Genootschap Magazine*, March/May 2006.
10. Menis, R.; da Rin, A.; Sulligoi, G.; Vicenzutti, A. All electric ships dependable design: Implications on project management. In Proceedings of the 2014 AEIT Annual Conference—From Research to Industry: The Need for a More Effective Technology Transfer (AEIT), Trieste, Italy, 18–19 September 2014; pp. 1–6.
11. Maggioncalda, M.; Gualeni, P.; Notaro, C.; Cau, C.; Bonazountas, M.; Stamatis, S. *Life Cycle Performance Assessment (LCPA) Tools: Volume 1: Optimisation of Ship Design and Operation for Life Cycle*; Springer: Cham, Switzerland, 2019.
12. International Electro Technical Commission. Publication 60909-0 Short-circuit Current in Three Phase A.C. Systems, Part: Calculation of Systems. 2016. Available online: <https://www.sis.se/api/document/preview/8018642/> (accessed on 1 January 2016).
13. Germanischer Lloyd. Short Circuit Calculation Program Version GL ES 1 98. Available online: [https://en.wikipedia.org/wiki/Germanischer\\_Lloyd](https://en.wikipedia.org/wiki/Germanischer_Lloyd) (accessed on 4 November 2020).

**Publisher's Note:** MDPI stays neutral with regard to jurisdictional claims in published maps and institutional affiliations.



© 2020 by the author. Licensee MDPI, Basel, Switzerland. This article is an open access article distributed under the terms and conditions of the Creative Commons Attribution (CC BY) license (<http://creativecommons.org/licenses/by/4.0/>).

Article

# Coal and Biomass Co-Combustion: CFD Prediction of Velocity Field for Multi-Channel Burner in Cement Rotary Kiln <sup>†</sup>

Zakia Ngadi \* and Mohamed Lhassan Lahlaoui

Faculty of Sciences of Tétouan, University Abdelmalek Essaadi, BP. 2121, Tetouan 93002, Morocco; hlhlaoui@hotmail.com

\* Correspondence: Zakia.ngadi@gmail.com

<sup>†</sup> Presented at the 14th International Conference INTER-ENG 2020 Interdisciplinarity in Engineering, Mureş, Romania, 8–9 October 2020.

Published: 11 December 2020



**Abstract:** This paper represents the medialization of alternative fuels co-combustion, in a cement rotary kiln, established on the commercial computational fluid dynamic (CFD) software ANSYS FLUENT. The focus is placed on the key issues in the flow field, mainly on how they are affected by turbulence models and co-processing conditions. Real data, from a Moroccan cement plant, are used for model input. The simulation results have shown a potential effect of the physics model on turbulent and gas-solid flow prediction. The CFD results can be taken as a guideline for improved co-processing burner design and reduce the effect of using alternative fuels.

**Keywords:** CFD; co-combustion; turbulence model; cement rotary kiln

## 1. Introduction

Alternative fuels (AF) have different chemical and physical properties compared to fossil fuels [1]. Thus, AF particles differ from coal in shape and size, their aerodynamics, and their heating up and combustion mechanism. Co-firing coal/OP (olive pomace) modeling in a cement kiln burner is an intricate process that includes gas and particle phases as well as a turbulence effect on the combustion mechanism and heat transfer.

Although much work [2–6] has been done on AF co-combustion, few researches on CFD (computational fluid dynamic) modeling of co-firing AF under rotary cement kiln burner conditions are available in the literature. Even though the efficiency of different K-epsilon models has been improved in recent years on predicting PF combustion, most improvements have been achieved by minimizing the calculation cost. Nonetheless, it is possible to further improve efficiency by comparing these models to choose a well-predicting model for novel alternative fuel. With this goal, this work seeks to develop a comparison between the three K-epsilon models (standard (STD), RNG (re-normalization group), and RKE (realizable K-epsilon)) combined with the eddy dissipation model, in a 2D modeling case of co-firing coal with olive pomace, under real rotary cement kiln burner conditions. The object is to explore how the flow field is affected by the turbulence models and how the co-processing environment can change the turbulence shape in the rotary kiln. The goal is to have a model that could well predict the turbulence behavior in the kiln environment, could take into account the difference in physical properties of AF versus coal, and could be able to give an overview of the kiln process parameters when changing the co-firing rate.

The remainder of the paper is organized as follows: The proposed mathematical models are presented in Section 2. The computational methodology is discussed in Section 3. Section 4 shows the results of different cases. Finally, Section 5 concludes with a summary.

## 2. Mathematical Models

The co-combustion in rotary cement kiln burner startup by carried combustibles particles, from the pulverizer to the furnace, using pressurized air. The flow in the rotary kiln is a gas-solid turbulent flow with chemical reactions. The Eulerian-Lagrangian approach is usually used and recommended for modeling dilute gas-solid flows in pulverized fuels (PF) combustion applications. In the Eulerian-Lagrangian approach, the motion of the continuous phase is modeled using the Eulerian framework, and the motion of dispersed-phase particles is modeled using the Lagrangian framework [7]. In this work, the focus was placed on the comparison of K-epsilon model varieties coupled with turbulence-chemistry interaction model (FR/ED (finite rate/eddy dissipation), i.e., how each model impacts the flow field).

### 2.1. Gas-Phase Governing Equations

The time-averaged steady-state Navier–Stokes equations, as well as the mass and energy conservation equations, are solved. The governing equations for the conservations of mass, momentum, energy, and species are given as:

$$\nabla \cdot (\rho \vec{u}) = S_m, \tag{1}$$

$$\nabla(\rho \vec{u} \vec{u}) = -\nabla P + \nabla \cdot (\bar{\bar{\tau}}) + \rho \vec{g} + \vec{F}, \tag{2}$$

$$\nabla \cdot (\vec{u}(\rho E + P)) = \nabla \cdot \left( k_{eff} \nabla T - \sum_i h_i \vec{J}_i + (\bar{\bar{\tau}} \cdot \vec{u}) \right) + S_h, \tag{3}$$

$$\nabla \cdot (\rho \vec{u}_i Y_i) = -\nabla \cdot \vec{J}_i + R_i + S_i, \tag{4}$$

The source  $S_m$  in Equation (1) is the mass added to the continuous phase due to the combustion of particles. Equation (2) is the steady-state momentum equation, where  $P$  is static pressure,  $\bar{\bar{\tau}}$  is the shear forces, and it is called a stress tensor. The third term on the right-hand side (RHS) represents the gravitational body force and the last term is the drag force source term. The first three terms on the RHS of the energy equation in Equation (3) represent the energy transfer due to conduction, species diffusion, and viscous dissipation, respectively.  $S_h$  is a source term including the heat of chemical reaction and radiation. Radiation heat transfer is calculated using the P1 model, and the absorption coefficient is evaluated by the weighted sum of the gray gas model (WSGG) [8,9]. Equation (4) is the species mass fraction conservation equation for the  $i^{th}$  species.  $R_i$  is the chemical reaction production rate of species  $i$  (this rate will be calculated by the FR/ED turbulence-chemistry interaction models) and  $S_i$  is the source term added from the dispersed phase.  $\vec{J}_i$  is the turbulent diffusion flux of species  $i$  [10].

### 2.2. Particle-Phase Governing Equations

Alternative fuels are bigger, lighter in density, and are less spherical compared to coal, which affects the motion of particles in the furnace. In the present work, for simplification, we considered AF as a spherical particle; also, the AF and coal particles were modeled separately with two discrete phases following a Rosin-Rammler size distribution [11]. The particles were tracked in Lagrangian frame reference using a stochastic model [12] as shown in Equation (5).

$$\frac{du_p}{dt} = \frac{3\rho C_D}{4d_p\rho_p} |u_p - u| (u - u_p) + g \frac{\rho_p - \rho}{\rho_p}, \tag{5}$$

where  $g$  is the gravitational force, and  $C_D$  is the drag coefficient, which is an empirical function of  $Re$  as described by Morsi and Alexander [13]. Here  $Re$  is the relative Reynolds number, and it's written as,

$$Re = \frac{\rho d_p |u_p - u|}{\mu}, \tag{6}$$

In this work, the combustion of solid particle conversion is treated as heating, devolatilizing, and char burning process. For computing volatilization, the single kinetic rate model [14] was used. The kinetic-diffusion limited model [15] was used for char combustion modeling. For both volatilization and char combustion, only convection and heat released by reactions were computed.

### 3. Numerical Computation and Strategy

#### 3.1. Geometry and Grid Description

The rotary kiln used in this paper was assimilated to a real kiln with 46 m in length and 3.8 m in diameter, and it was specially equipped with a multichannel burner (see Figure 1). For simplification, the calculation was started from the fuel injection (i.e., from the burner nozzle end). Therefore, the domain of calculation considered was a 2D axisymmetric rectangle with a multi-entry for fuels and airs. Also, the burner entry geometry was modified for modeling facilities (for more details, see [16]).

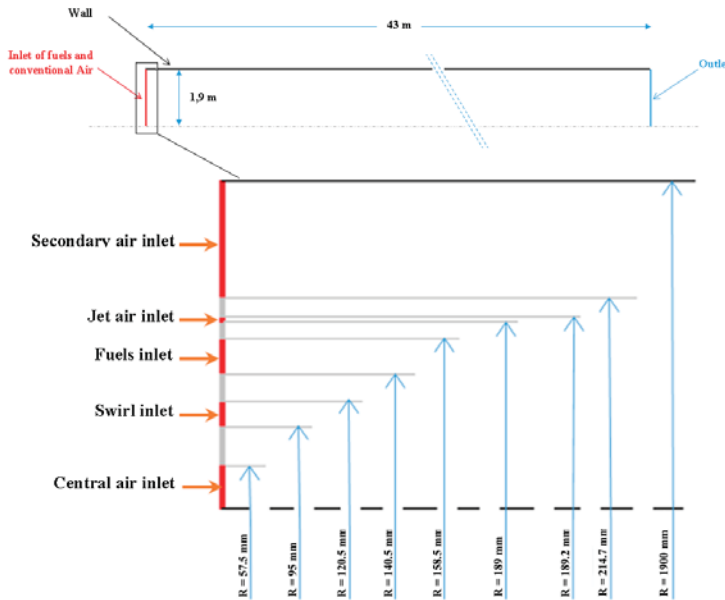


Figure 1. Scheme of the 2D axisymmetric geometry and the simplified burner details.

Based on the geometric and calculation purposes, a structured non-uniform mesh was used, and a fine grid with 14,040 elements was selected, based on the mesh independence. To optimize convergence, the mesh had a higher density near to the burner and on the axial direction, and was coarse at the rest of the domain.

#### 3.2. Numerical Method and Boundary Condition

The simulation of the 2D domain was implemented on the commercial CFD tool, ANSYS Fluent, based on the finite volume method. A pressure-based coupled algorithm (Coupled) was used to solve the Lagrangian-Eulerian model for gas and particle equations. To achieve numerical stability, the under-relaxation factors were carefully modified for each k-epsilon model. The limited residuals values were taken as  $10^{-3}$  for continuity,  $10^{-5}$  for energy and radiation, and  $10^{-4}$  for all the rest of the parameters.

To be consistent with the real kiln operating condition, the inlet for temperature and velocity was similar to the real case data (see Table 1). A velocity inlet was specified at all the inlet boundaries with



direction normal to boundary except for the swirl inlet that had two velocity components inlet. All the walls were treated as adiabatic and no-slip walls. The outlet was set as a pressure outlet condition. The K and epsilon inlet conditions were computed from the turbulent intensity and hydraulic diameter.

**Table 1.** Operating condition data.

Boundaries	Velocity m/s	Temperature °K
Secondary air inlet	5	1126
Jet air inlet	218	500
Fuels inlet	Transport air 30 Coal and AF 30	500
Swirl inlet	Axial 212 Tangential 45	500
Central air inlet	200	500

### 3.3. Case Study

As mentioned earlier, this paper discusses the effect of the different K-epsilon turbulence models on the velocity field prediction in a cement rotary kiln under co-combustion parameters. To this aim, six different cases were investigated and are summarized in Table 2.

**Table 2.** Investigated cases details.

Case	Turbulence Model	Turbulence Chemistry Interaction Model	Discrete Phase Model (DPM)
1		OFF	OFF
2	STD	ON	ON
3		OFF	OFF
4	RNG	ON	ON
5		OFF	OFF
6	RKE	ON	ON

## 4. Results and Discussion

To investigate the effect of the turbulence model on the flow field, we started with an initial test without the DPM model and species reaction for the three k-epsilon models. Figure 2 shows the axial velocity streamlines without the DPM model and species reaction simulations. One can observe that the STD and RNG models predict the overall flow field similarly, however, the velocity field in RKE simulation extends further into the rotary kiln than STD and RNG, before taking a uniform distribution (see Figure 3).

The three models differ in the capture of the recirculation zone length. The RNG has a wide inner bubble recirculation zone compared to the STD and RKE at around 6.8–10.6 m. The RKE simulation gives a small inner bubble recirculation zone but a longer recirculation circle at around 9.7–14 m. The recirculation zone given by the STD is around 4.5 m. The difference comes from the epsilon equation forms and the solution method.

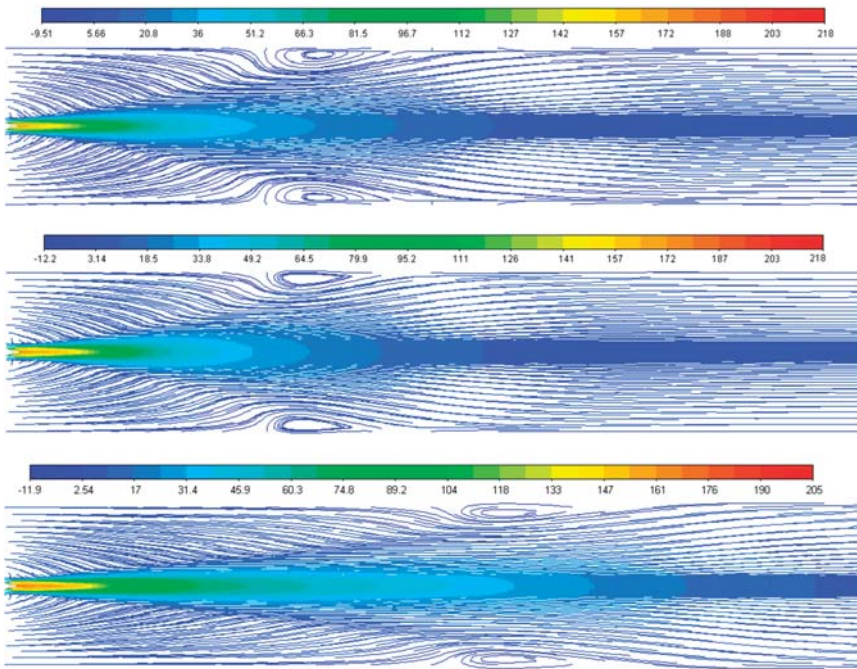


**Figure 2.** Streamlines of axial velocity without DPM (STD, RNG, and RKE respectively from the top).

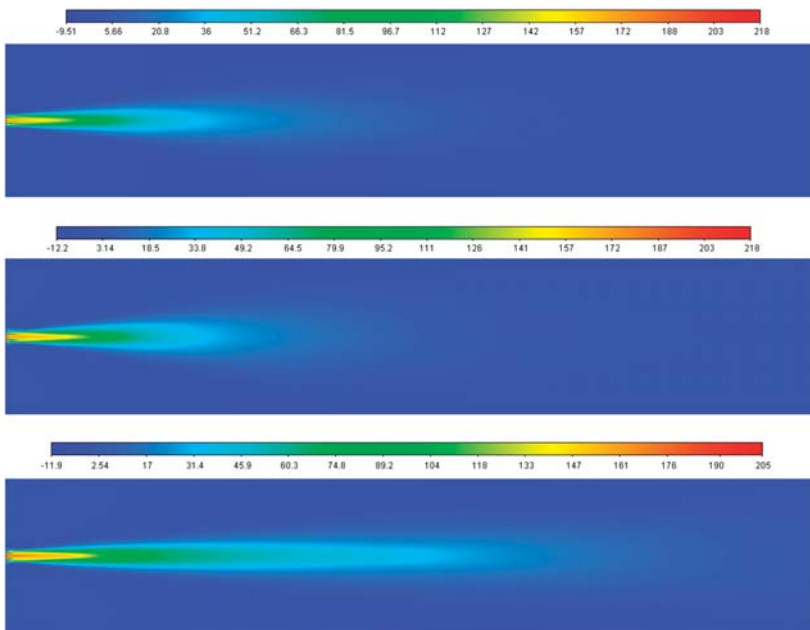


**Figure 3.** Axial velocity contours without DPM (STD, RNG, and RKE respectively from the top).

From Figure 4, for the STD and RNG cases, it can be seen that when the pulverized particles mix into the flow, the uniform velocity field is deteriorated from 13.24 to 9.21 m/s for STD and from 10.8 to 8.58 m/s for RNG. Also, the recirculation zone is smaller than the cases without DPM as shown in Figure 5; this is due to the interaction of particle-flow.

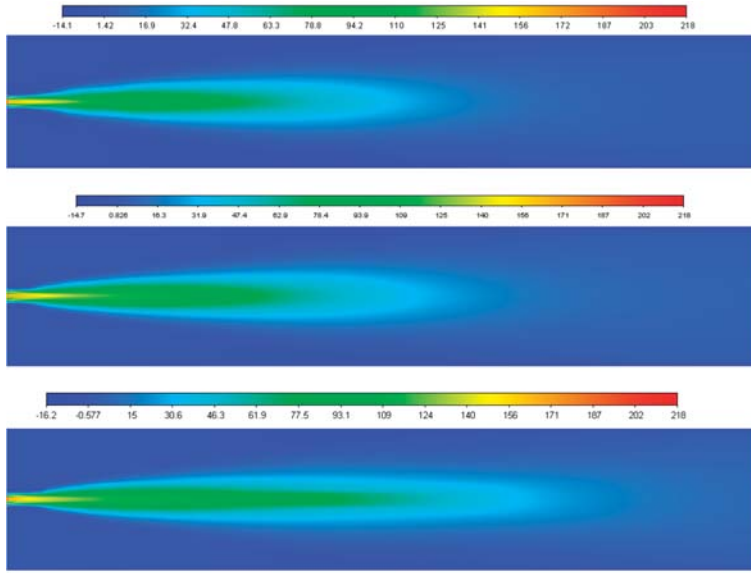


Figure 4. Axial velocity contour with particle injection (STD, RNG, and RKE respectively from the top).

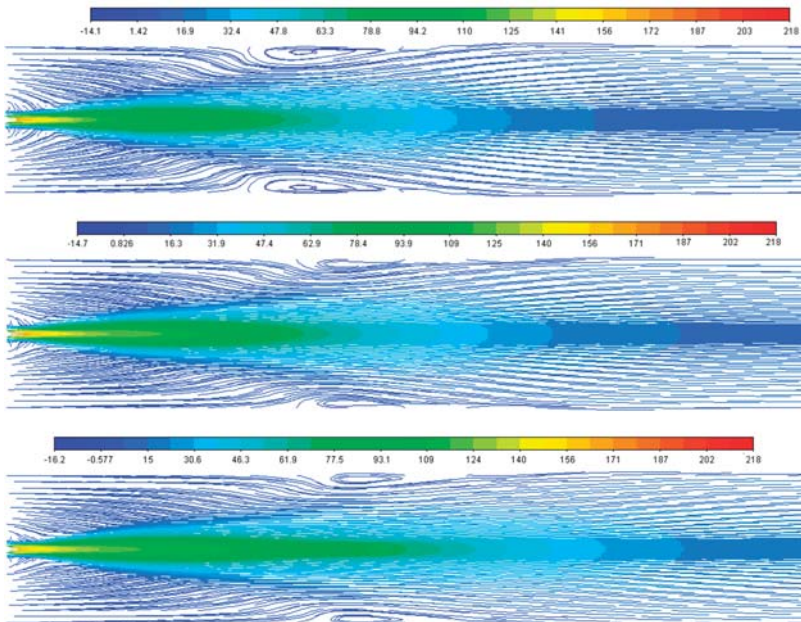


Figure 5. Streamlines of axial velocity with particle injection (STD, RNG, and RKE respectively from the top).

Generally, particles interact with the flow through the drag forces and thermodynamics effect, causing a reduction in the gas turbulence and an increase in the dissipation rate of that energy which explain the decay of velocity; for more details, see [17]. For the RKE model case, we remark that the uniform velocity is higher in the case with particle injection than the DPM-off case (7.22 m/s vs. 2.54 m/s).

From the results illustrated, it is clear that the RKE model in both test cases gives the lower velocity compared to the RNG and STD models, which may be due to the dissipative nature of the RKE model. Another important point is that the STD and RNG give the lower reverse velocities, as shown in Figure 5, ensuring a speedy mixture of the hot gases with cold burner stream and the stabilization of the flame in the kiln compared to the RKE cases, which impacts the species and temperature distribution that will be discussed in another paper. Current numerical simulations of AF co-combustion are compared with the numerical results obtained by [18,19] who have investigated the simulation of oxy-coal combustion with RANS (Reynolds averaged Navier stokes) and LES (Large eddy simulation) models. The results obtained for the standard and RNG models show the same trend.

## 5. Conclusions

The effect of the turbulence model (i.e., STD, RNG, and RKE K-epsilon models) on the prediction of the velocity field of the real rotary kiln case was investigated.

Six different cases were simulated and predicted results were verified with available literature study. Results of the size and the position of the recirculation zone closer to the wall showed the sensitivity of the velocity field to the particle-flow interaction, especially in the RKE cases. A longer recirculation circle at around 9.7–14 m was remarked in RKE case and the recirculation zone given by the STD was around 4.5 m. Nevertheless, the STD and RNG models gave a good estimation of the flow field and recirculation zone size and length, while the RKE model performed best.

## References

1. Ngadi, Z.; Lahlaoui, M.L. Impact of Using Alternative Fuels on Cement Rotary Kilns: Experimental Study and Modeling. *Procedia Eng.* **2017**, *181*, 777–784. [[CrossRef](#)]
2. Guessab, A.; Aris, A.; Bounif, A. Simulation of turbulent piloted methane non-premixed flame based on combination of finite-rate/eddy-dissipation model. *Mechanika* **2013**, *19*, 657–664. [[CrossRef](#)]
3. Collazo, J.; Porteiro, J.; Míguez, J.L.; Granada, E.; Gómez, M.A. Numerical simulation of a small-scale biomass boiler. *Energy Convers. Manag.* **2012**, *64*, 87–96. [[CrossRef](#)]
4. Yang, Y.B.; Newman, R.; Sharifi, V.; Swithenbank, J.; Ariss, J. Mathematical modelling of straw combustion in a 38 MWe power plant furnace and effect of operating conditions. *Fuel* **2007**, *86*, 129–142. [[CrossRef](#)]
5. Djurović, D.; Nemoda, S.; Repić, B.; Dakić, D.; Adzić, M. Influence of biomass furnace volume change on flue gases burn out process. *Renew. Energy* **2015**, *76*, 1–6. [[CrossRef](#)]
6. Tumsa, T.Z.; Chae, T.Y.; Yang, W.; Paneru, M.; Maier, J. Experimental study on combustion of torrefied palm kernel shell (PKS) in oxy-fuel environment. *Int. J. Energy Res.* **2019**, *43*, 7508–7516. [[CrossRef](#)]
7. Ranade, V.V.; Gupta, D.F. *Computational Modeling of Pulverized Coal Fired Boilers*; CRC Press: Boca Raton, FL, USA, 2015; ISBN 9781482215359.
8. ANSYS Fluent theory guide. In *ANSYS Fluent Theory Guide 15.0*; Ansys Inc.: Canonsbourg, PA, USA, 2013; p. 193.
9. Cassol, F.; Brittes, R.; França, F.H.R.; Ezekoye, O.A. Application of the weighted-sum-of-gray-gases model for media composed of arbitrary concentrations of H<sub>2</sub>O, CO<sub>2</sub> and soot. *Int. J. Heat Mass Transf.* **2014**, *79*, 796–806. [[CrossRef](#)]
10. Spalding, D.B. Mixing and chemical reaction in steady confined turbulent flames. *Symp. (Int.) Combust.* **1971**, *13*, 649–657. [[CrossRef](#)]
11. Rosin, P.; Rammler, E. The laws governing the fineness of powdered coal. *J. Inst. Fuel* **1933**, *7*, 29–36.
12. Shuen, J.-S.; Chen, L.-D.; Faeth, G.M. Evaluation of a stochastic model of particle dispersion in a turbulent round jet. *AIChE J.* **1983**, *29*, 167–170. [[CrossRef](#)]

13. Morsi, S.A.; Alexander, A.J. An investigation of particle trajectories in two-phase flow systems. *J. Fluid Mech.* **1972**, *55*, 193. [[CrossRef](#)]
14. Badzioch, S.; Hawksley, P.G.W. Kinetics of Thermal Decomposition of Pulverized Coal Particles. *Ind. Eng. Chem. Process Des. Dev.* **1970**, *9*, 521–530. [[CrossRef](#)]
15. Baum, M.M.; Street, P.J. Predicting the Combustion Behaviour of Coal Particles. *Combust. Sci. Technol.* **1971**, *3*, 231–243. [[CrossRef](#)]
16. Hiromi Ariyaratne, W.K.W.K.; Malagalage, A.; Melaaen, M.C.; André Tokheim, L. CFD Modeling of Meat and Bone Meal Combustion in a Rotary Cement Kiln. *Int. J. Model. Optim.* **2014**, *4*, 263–272. [[CrossRef](#)]
17. Vaillancourt, P.A.; Yau, M.K. Review of Particle–Turbulence Interactions and Consequences for Cloud Physics. *Bull. Am. Meteorol. Soc.* **2000**, *81*, 285–298. [[CrossRef](#)]
18. Yilmaz, H.; Cam, O.; Tangoz, S.; Yilmaz, I. Effect of different turbulence models on combustion and emission characteristics of hydrogen/air flames. *Int. J. Hydrogen Energy* **2017**, *42*, 25744–25755. [[CrossRef](#)]
19. Chen, L.; Yong, S.Z.; Ghoniem, A.F. Oxy-fuel combustion of pulverized coal: Characterization, fundamentals, stabilization and CFD modeling. *Prog. Energy Combust. Sci.* **2012**, *38*, 156–214. [[CrossRef](#)]

**Publisher's Note:** MDPI stays neutral with regard to jurisdictional claims in published maps and institutional affiliations.



© 2020 by the authors. Licensee MDPI, Basel, Switzerland. This article is an open access article distributed under the terms and conditions of the Creative Commons Attribution (CC BY) license (<http://creativecommons.org/licenses/by/4.0/>).

# Thermoelectric Generator Based on $\text{CuSO}_4$ and $\text{Na}_2\text{SiO}_3$ †

Mihail Chira <sup>1,\*</sup>, Andreea Hegyi <sup>1</sup>, Henriette Szilagyi <sup>1</sup>  and Horațiu Vermeșan <sup>2</sup> 

<sup>1</sup> NIRD URBAN-INCERC Cluj-Napoca Branch, 117 Calea Florești, 400524 Cluj-Napoca, Romania; andreea.hegyi@incerc-cluj.ro (A.H.); henriette.szilagyi@incerc-cluj.ro (H.S.)

<sup>2</sup> Faculty of Material Science and Environment, Technical University of Cluj-Napoca, 103-105 Muncii Bld., 400641 Cluj-Napoca, Romania; horatiu.vermesan@imadd.utcluj.ro

\* Correspondence: mihail.chira@incerc-cluj.ro

† Presented at the 14th International Conference INTER-ENG 2020 Interdisciplinarity in Engineering, Mureș, Romania, 8–9 October 2020.

Published: 18 December 2020

**Abstract:** Thermoelectric generators can operate at small temperature differences providing enough electricity for low-power electronics, sensors in distribution networks, and biomedical devices. The article presents the obtaining of a thermoelectric generator and its electrical characteristics using usual substances. Experimental research was carried out using a mixture consisting of several substances (copper sulfate, calcium hydroxide, silicon dioxide, and sodium silicate) in different proportions. The mixture was inserted between two plates, one graphite (hot plate) and the other aluminum (cold plate), thus obtaining a thermoelectric generator. Electrical voltage, output current, and electrical power were measured at different temperatures.

**Keywords:** thermoelectric generators; output current; electrical power; copper sulfate; sodium silicate

## 1. Introduction

The technology-based age we are in today has brought great advantages for a more comfortable and intelligent life and leads the way for even faster development in all areas of science and engineering, but at the same time brings a very high demand for energy. Current and future energy consumption requires alternative energy sources with low environmental impact. Easily available solar and wind energy have led to the use of fossil fuels as alternative energy sources [1]. Moreover, due to more recent developments in thermoelectric materials and devices (TE), the possibility of efficient use of heat energy, usually wasted, has become a feasible alternative [2]. More importantly, thermal waste has become a very important and environmentally friendly source of wasted energy [3,4]. There are already many studies explaining the mechanism of conversion of heat into electricity [5–8]. Such studies were the starting point for the development and optimization of new materials using the resources of rising nanotechnologies [9,10].

Thermoelectric devices are an attractive solution, due to their passive operation and simplicity and lack of moving parts. A thermoelectric generator is based on the Seebeck effect that generates tension in materials in the presence of a temperature gradient. Although many materials exhibit the Seebeck effect, the energy generation efficiency is based on a complex interaction between temperature, temperature gradient, Seebeck coefficient, and electrical and thermal conductivity [9]. Often, these properties do not extend in the same direction, which leads to challenges in the efficient generation of thermoelectric energy. Altenkirch derived the thermoelectric efficiency,  $ZT$ , better known as the thermoelectric figure of merit [11], to describe the thermoelectric energy conversion capacity of a material. This value is given as

$$ZT = \frac{\alpha^2 \sigma T}{\lambda} \quad (1)$$



where  $\alpha$  is the Seebeck coefficient,  $\sigma$  is the electrical conductivity,  $T$  is the absolute temperature, and  $\lambda$  is the thermal conductivity.

The maximum conversion efficiency of thermoelectric energy is given by the relationship:

$$\eta_{max} = \frac{T_h - T_c}{T_h} \left[ \frac{\sqrt{1 + ZT_{avg}} - 1}{\sqrt{1 + ZT_{avg}} + \frac{T_c}{T_h}} \right] \quad (2)$$

Materials that offer an intrinsically high ZT value are rare and are generally composed of rare earth-based substances, in particular selenes and telluride-based alloys. SiGe alloys [4], skutterudites [12], clathrates [13], and semi-heusler alloys [14] are other promising systems, among them skutterudite, for example. p-Zn<sub>4</sub>Sb<sub>3</sub>, P-CeFe<sub>3</sub>Co<sub>0.5</sub>Sb<sub>12</sub>, and N-CoSb<sub>3</sub> are actively studied by numerous research groups, providing a high value of merit in the intermediate temperature range from 500 to 973 K with conversion efficiency of 9.5% [9,15]. One approach to improving the ZT is by nano-structuring, by introducing superlattices [16] or nanostructures [17,18], since it has been recognized that it has a reduction in phononic thermal conductivity. Venkatasubramanian et al. [16] reported that the P-type Bi<sub>2</sub>Te<sub>3</sub>/Sb<sub>2</sub>Te<sub>3</sub> superstructures exhibit an exceptionally high ZT of 2.4 at room temperature with a remarkably low thermal conductivity of 0.22 Wm<sup>-1</sup>K<sup>-1</sup>. There are other references to Si/Ge [19], GaAs/AlAs [20], and PbTe/PbSe [21] superstructures that have lower thermal conductivity than their alloy counterparts. However, many of these materials have low thermal and chemical stability, difficult to produce in useful forms, and are expensive, with low availability and in some cases high toxicity. There are many studies around the world to find thermoelectric potential alloys and oxides and to create multifunctional properties through microstructural engineering. The expansion of thermoelectric applicability will require the development of low-cost, abundant materials as well as the viability or applicability of scalable manufacturing technologies. A potential source of scalable thermoelectric materials is those based on transition metal oxides, which provide reasonable electrical conductivity and a Seebeck coefficient, while being cost-effective and environmentally friendly. Oxides based on Ti, Mg, W, Zn, Cu, V, Co, Rh, and Mo represent a wide range of materials, less investigated than TE materials [22]. Metal oxides can provide a wide range of electronic properties, from insulators to semiconductors.

TEG are divided into two types, large (or bulk) and micro-TEG. The first category has a millimeter size and provides the output power from several to hundreds of watts in a high heat range. This category is usually used for industrial purposes. The second category operates with low dissipated heat and generates electricity in the range of  $\mu$ W up to a few mW [23].

Waste heat temperature, arrangement of TE modules, enhancing heat transfer co-efficient and parasitic loss plays an important role to maximize the net electric power [24].

In many articles, the thermoelectric material properties are assumed to be constant for easy calculation, but in fact the three properties of thermoelectricity, electrical resistivity, thermal conductivity, and Seebeck coefficient, are temperature dependent. The thermal resistance model, whose properties are assumed to be constant, overestimates the output power and efficiency of the TEG. It can be attributed to the underestimation of electrical resistance and does not solve the temperature distributions within the TEG. Assuming the properties of thermoelectric materials as a constant can induce a numerical deviation at high temperatures [25].

Waste heat recovery is very important in terms of reducing energy costs and environmental impacts. The method used for waste heat recovery must be feasible [26].

## 2. Materials and Methods

For the realization of the thermoelectric generator, the following materials and substances were used: graphite plate, aluminum strip, copper sulfate, sodium silicate solution of 30% concentration, calcium hydroxide, and silicon dioxide.

1.2 g  $\text{CuSO}_4$  with 0.18 g  $\text{CaOH}$  and 0.08 g  $\text{SiO}_2$  were mixed until homogenized, after which 2 mL of 30%  $\text{Na}_2\text{SiO}_3$  solution was added. A homogeneous paste was obtained, which was applied to a graphite plate of 5 mm thickness, and over it was placed an aluminum strip of thickness 0.5 mm and width 30 mm. The graphite/mixture/aluminum overlap area is  $50 \times 30 \text{ mm}^2$ .

The obtained thermoelectric generator and the schematic representation of the layers that make up it are shown in Figure 1.

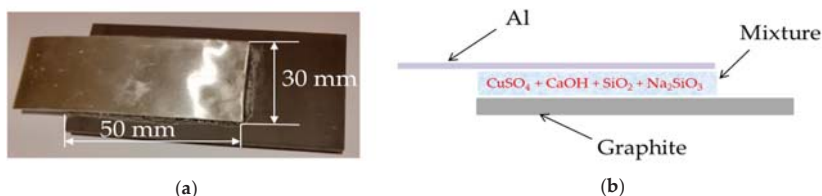


**Figure 1.** Thermoelectric generator made: (a) photo; (b) schematic representation.

Temperature ( $T_c$  and  $T_h$ ) and electrical measurements (voltage, current, and resistivity) were performed using the digital multimeter (Peaktech P4090) from room temperature to 393 K to calculate the Seebeck coefficient, electrical conductivity, and electrical power. The Seebeck coefficient was calculated using the measured voltage generated from the temperature gradient. The temperature difference between the hot and cold part of the sample was generated by heating the graphite plate and cooling the aluminum strip, using an 800 W thermostat hob as a heater and cold air gun as a cooler.

Electrical resistivity was measured by the four-point probe technique, from room temperature to 393 K. The Open circuit was made to measure voltage and current as a temperature function to calculate power.

The thermal conductivity of the TE material was measured using a flash laser analyzer from room temperature up to 393 K.

### 3. Results and Discussion

The dimensions characterizing the thermoelectric generator are presented in Table 1 and Figure 2.

**Table 1.** Parameters of the thermoelectric generator at 393 K.

Properties at 393 K	$\alpha$ (mV/K)	$\sigma$ (S/m)	$\lambda$ (W/mK)	ZT	$\eta$ (%)
Graphite/mixture/aluminum	4.3	3.3	0.875	0.027	0.129

Analyzing the data in the table, a high Seebeck coefficient is observed due to the possible p–n junctions formed between the elements of the mixture and a reasonable thermoelectric performance. Further experimental research will make it possible to improve TEG parameters by changing the percentages of substances that make up the mixture.

The Seebeck coefficient allows us to calculate the merit factor ZT and determine the efficiency of the thermoelectric generator  $\eta$ .

The heat source touches the graphite plate, which becomes the positive electrode, and the aluminum plate becomes the negative electrode (Figure 3).



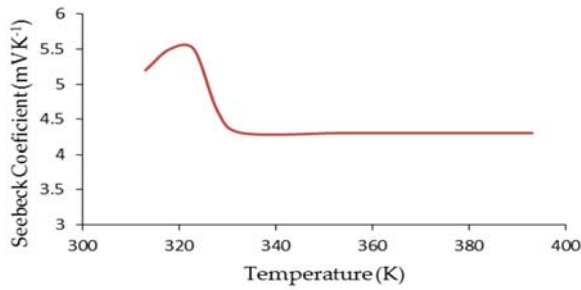


Figure 2. Seebeck coefficient of graphite/mixture/aluminum system as a function of temperature.

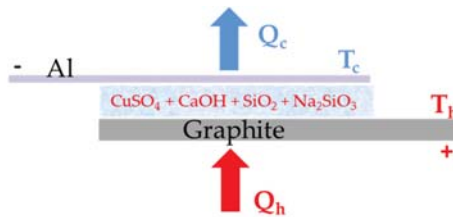


Figure 3. Schematic representation of the mode of operation of the thermoelectric generator.

The temperature of the graphite plate was increased from 297 to 393 K, and at the same time, the voltage and the output current were measured. The graphic representation of the voltage and current variation as a function of temperature can be seen in Figure 4.

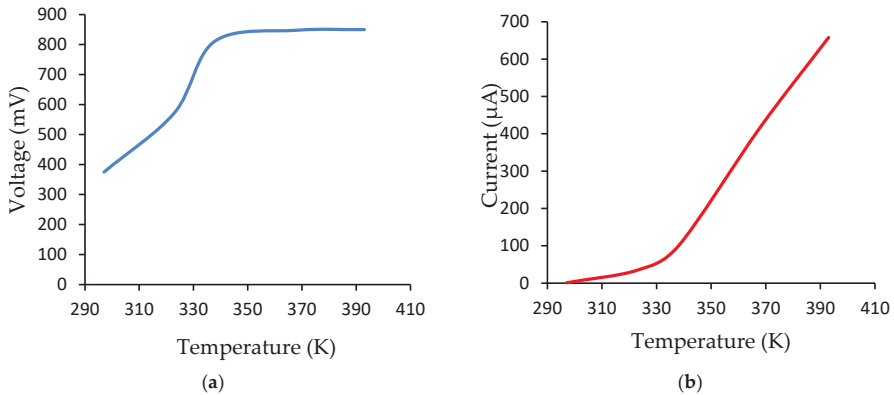


Figure 4. Thermoelectric generator: (a) the voltage; (b) the output current.

The output voltage ranges from 375 to 850 mV in the range 297–393 K, and the output current ranges from 1 to 658  $\mu\text{A}$  in the same temperature range.

Analyzing Figure 4, it is found that from 330 K, the system is activated so that the output voltage reaches a maximum value around 850 mV and remains constant, and the output current has a linear increase, the slope of the line being high.

A doubling of the amount of calcium hydroxide in the mixture between the graphite and aluminum plates causes a decrease in the current three times, and a doubling of the amount of silicon dioxide causes a decrease in the current two times.

It was found that the lack of calcium hydroxide in the mixture causes a fluctuation of the generated electric current and voltage.

Serial connection of thermoelectric generators causes the Seebeck voltage to increase, while parallel connections allow the output current to increase. The combination of Serial and parallel connections should lead to an increase in both voltage and electric current.

The output voltage and current were represented according to the number of modules connected in series, respectively, in parallel to a temperature gradient of 96 K in Figure 5.

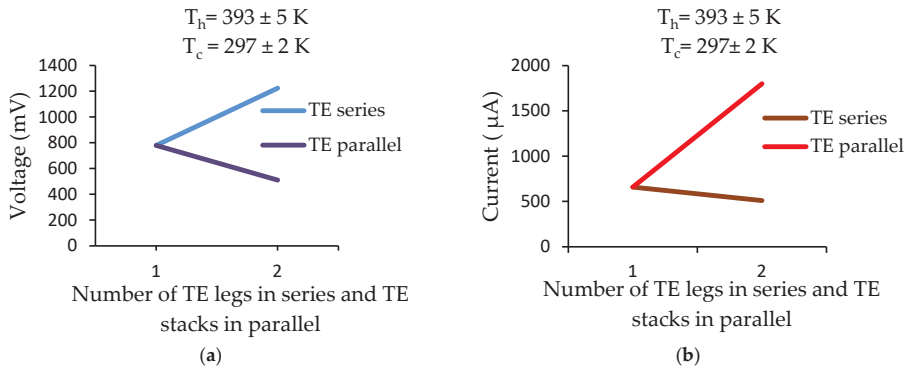


**Figure 5.** (a) The output voltage of the thermoelectric generator for serial and parallel connection; (b) the output current of the thermoelectric generator for serial and parallel connection.

When the modules were connected in series, the increase in the output voltage was from 780 mV (one module) to 1224 mV (two modules). The simultaneous decrease in current was measured from 658 µA (single module) to 510 µA (two modules), because the serial connection increased the internal resistance of the thermoelectric generator and as a result decreased the power of the electric current.

To reduce the internal resistance and increase the output current of the thermoelectric generator, the modules were connected in parallel. In this case, the output voltage has changed from 780 mV (single module) to 510 mV (two modules). The simultaneous increase in current was measured from 658 µA (one module) to 1800 µA (two modules), because the parallel connection decreased the internal resistance of the thermoelectric generator and as a result increased the power of the electric current.

For a given heat energy supplied, the temperature difference and the values of the output sizes (voltage, current, electric power) are influenced by the area of the common section—graphite/mixture/aluminum, by the thickness of the layer forming the mixture, and by the number and mode of connection of the thermoelectric generators. As the joint area increases, the output power also increases. An increase in the thickness of the intermediate layer increases the temperature gradient, but also the internal resistance of the thermoelectric generator. The output power of the thermoelectric generator according to the temperature of the hot plate is shown in Figure 6.

Even if the output power is small, the realization of this mixture of substances with thermoelectric properties represents a step for further research on improving the properties of the thermoelectric generator realized.

The materials used have an advantage over those commonly used, namely, they have thermal and chemical stability, are found in abundance, are cheap, have low toxicity, and are easy to process in order to obtain the thermoelement and low cost.

Figure 7 shows a graph from the technical data sheet of the commercial thermogenerator 1MD03-024-04/1, in which the variation of the electrical voltage and the electrical output power according to the temperature of the hot plate is observed [27].

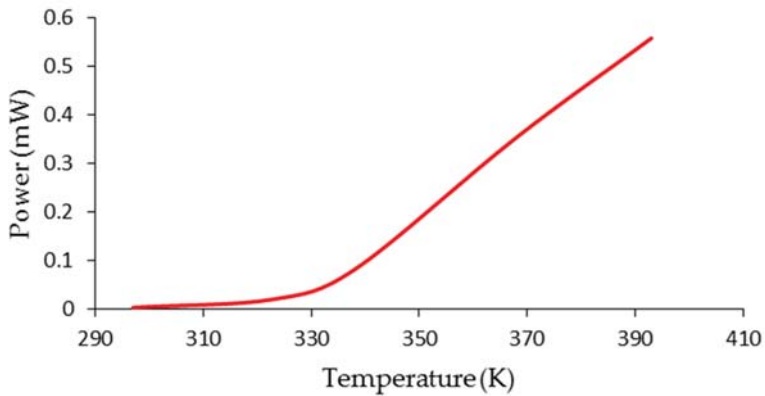


Figure 6. Output power of the thermoelectric generator.

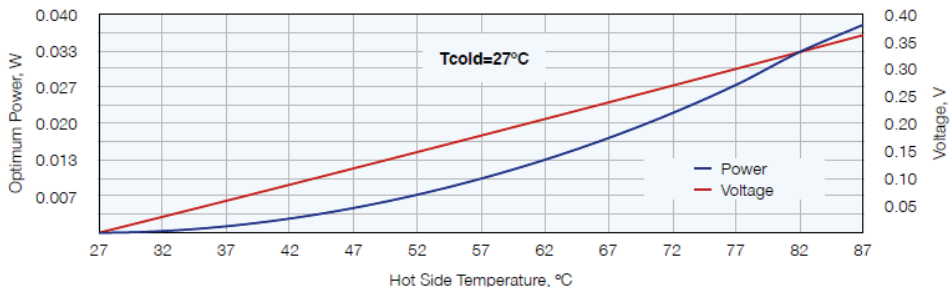


Figure 7. Voltage and power output for commercial thermoelectric generator 1MD03-024-04/1.

By connecting the thermoelectric modules in series and in parallel, it is possible to obtain values of electrical voltage and output power comparable to commercial ones.

#### 4. Conclusions

This paper demonstrates by experimental data that the thermoelectric generator made is comparable to those produced industrially and found on the market. The originality of this research is given by the novelty of substances used to generate electric current under the action of the thermal factor.

Experimental results indicated:

- The output current and output power depends on the nature of the mixture of substances used.
- The lack of calcium hydroxide in the mixture causes fluctuations in the output current, and too much of it causes the current to decrease.
- Too much silicon dioxide causes the electric current to decrease.
- The optimum operating temperature is around 393 K.
- If an aluminum electrode is used in which a network of holes with a diameter of 0.2 mm is practiced, and it is in an environment with high humidity, then the current generated by the thermoelement increases three times.

**Author Contributions:** Conceptualization: M.C., A.H., H.S., and H.V.; methodology: M.C. and H.V.; validation: M.C., A.H., and H.V.; formal analysis: A.H. and H.S.; investigation: M.C.; data curation: M.C.; writing—original draft preparation: M.C.; writing—review and editing: M.C., A.H., H.S., and H.V.; visualization: A.H. and H.S.; supervision: H.V. and H.S. All authors have read and agreed to the published version of the manuscript.

**Funding:** This research received no external funding.

**Conflicts of Interest:** The authors declare no conflict of interest.

## References

1. Akella, A.K.; Saini, R.P.; Sharma, M.P. Social, economical and environmental impacts of renewable energy systems. *Renew. Energy* **2009**, *34*, 390–396. [[CrossRef](#)]
2. Zheng, X.F.; Liu, C.X.; Yan, Y.Y.; Wang, Q. A review of thermoelectrics research—Recent developments and potentials for sustainable and renewable energy applications. *Renew. Sustain. Energy Rev.* **2014**, *32*, 486–503. [[CrossRef](#)]
3. Rowe, D.M. Thermoelectrics, an environmentally-friendly source of electrical power. *Renew. Energy* **1999**, *16*, 1251–1256. [[CrossRef](#)]
4. Ismail, B.I.; Ahmed, W.H. Thermoelectric Power Generation Using Waste-Heat Energy as an Alternative Green Technology. *Recent Pat. Electr. Eng.* **2009**, *2*, 27–39. [[CrossRef](#)]
5. Riffat, S.B.; Ma, X. Thermoelectric: A review of present and potential applications. *Appl. Therm. Eng.* **2003**, *23*, 913–935. [[CrossRef](#)]
6. Bulusu, A.; Walker, D.G. Review of electronic transport models for thermoelectric materials. *Superlattices Microstruct.* **2008**, *44*, 1–36. [[CrossRef](#)]
7. Elsheikh, M.H.; Shnawah, D.A.; Sabri, M.F.M.; Said, S.B.M.; Hassan, M.H.; Bashir, M.B.A.; Mohamad, M. A review on thermoelectric renewable energy: Principle parameters that affect their performance. *Renew. Sustain. Energy Rev.* **2014**, *30*, 337–355. [[CrossRef](#)]
8. Gould, C.A.; Shammass, N.Y.A.; Grainger, S.; Taylor, I. A comprehensive review of thermoelectric technology, micro-electrical and power generation properties. In Proceedings of the 2008 26th International Conference on Microelectronics, Nis, Serbia, 10–14 May 2008; pp. 329–332.
9. Snyder, G.J.; Toberer, E.S. Complex thermoelectric materials. *Nat. Mater.* **2008**, *7*, 105–114. [[CrossRef](#)]
10. Alam, H.; Ramakrishna, S. A review on the enhancement of figure of merit from bulk to nano-thermoelectric materials. *Nano Energy* **2013**, *2*, 190–212. [[CrossRef](#)]
11. Telkes, M. The efficiency of thermoelectric generators. *I. J. Appl. Phys.* **1947**, *18*, 1116–1127. [[CrossRef](#)]
12. El-Genk, M.S.; Saber, H.H.; Caillat, T. Performance tests of skutterudites and segmented thermoelectric converters. *AIP Conf. Proc.* **2004**, *699*, 541–552.
13. Shi, X.; Yang, J.; Bai, S.; Yang, J.; Wang, H.; Chi, M. On the design of high efficiency thermoelectric clathrates through a systematic cross-substitution of framework elements. *Adv. Funct. Mater.* **2010**, *20*, 755–763. [[CrossRef](#)]
14. Yang, J.; Li, H.; Wu, T.; Zhang, W.; Chen, L.; Yang, J. Evaluation of half-Heusler compounds as thermoelectric materials based on the calculated electrical transport properties. *Adv. Funct. Mater.* **2008**, *18*, 2880–2888. [[CrossRef](#)]
15. Sales, B.C.; Mandrus, D.; Williams, R.K. Filled skutterudite antimonides: A new class of thermoelectric materials. *Science* **1996**, *272*, 1325–1328. [[CrossRef](#)] [[PubMed](#)]
16. Venkatasubramanian, R.; Siivola, E.; Colpitts, T.; O’quinn, B. Thin-film thermoelectric devices with high room-temperature figures of merit. *Nature* **2001**, *413*, 597–602. [[CrossRef](#)] [[PubMed](#)]
17. Hicks, L.; Dresselhaus, M. Thermoelectric figure of merit of a one-dimensional conductor. *Phys. Rev. B* **1993**, *47*, 16631. [[CrossRef](#)] [[PubMed](#)]
18. Hicks, L.; Dresselhaus, M. Effect of quantum-well structures on the thermoelectric figure of merit. *Phys. Rev. B* **1993**, *47*, 12727. [[CrossRef](#)] [[PubMed](#)]
19. Liu, W.; Borca-Tasciuc, T.; Chen, G.; Liu, J.; Wang, K. Anisotropic thermal conductivity of Ge quantum-dot and symmetrically strained Si/Ge superlattices. *J. Nanosci. Nanotechnol.* **2001**, *1*, 39–42. [[CrossRef](#)]
20. Capinski, W.S.; Maris, H.J. Thermal conductivity of GaAs/AlAs superlattices. *Physica B* **1996**, *219*, 699–701. [[CrossRef](#)]
21. Caylor, J.; Coonley, K.; Stuart, J.; Colpitts, T.; Venkatasubramanian, R. Enhanced thermoelectric performance in PbTe-based superlattice structures from reduction of lattice thermal conductivity. *Appl. Phys. Lett.* **2005**, *87*, 023105. [[CrossRef](#)]
22. Walia, S.; Balendhran, S.; Nili, H.; Zhuiykov, S.; Rosengarten, G.; Wang, Q.H. Transition metal oxides—Thermoelectric properties. *Prog. Mater. Sci.* **2013**, *58*, 1443–1489. [[CrossRef](#)]
23. Liu, S.; Hu, B.; Liu, D.; Li, F.; Li, J.; Li, B.; Li, L.; Nan, Y.L.C. Microthermoelectric generators based on through glass pillars with high output voltage enabled by large temperature difference. *Appl. Energy* **2018**, *225*, 600–610. [[CrossRef](#)]
24. Rana, S.; Orr, B.; Iqbal, A.; Ding, L.C.; Akbarzadeh, A.; Date, A. Modelling and optimization of low-temperature waste heat thermoelectric generator system. *Energy Procedia* **2017**, *110*, 196–201. [[CrossRef](#)]

25. Chen, W.H.; Lin, Y.X. Performance comparison of thermoelectric generators using different materials. *Energy Procedia* **2019**, *158*, 1388–1393. [[CrossRef](#)]
26. Omera, G.; Yavuzb, A.H.; Ahiskac, R.; Calisald, K.E. Smart thermoelectric waste heat generator: Design, simulation and cost analysis. *Sustain. Energy Technol. Assess.* **2020**, *37*, 100623. [[CrossRef](#)]
27. RMTLtd Thermoelectric Cooling Solutions. Available online: <http://www.rmtltd.ru/applications/temicrogenerators> (accessed on 5 February 2020).

**Publisher's Note:** MDPI stays neutral with regard to jurisdictional claims in published maps and institutional affiliations.



© 2020 by the authors. Licensee MDPI, Basel, Switzerland. This article is an open access article distributed under the terms and conditions of the Creative Commons Attribution (CC BY) license (<http://creativecommons.org/licenses/by/4.0/>).

Article

# A Review over Electromagnetic Shielding Effectiveness of Composite Materials <sup>†</sup>

Cezar Afilipoaei \*  and Horatiu Teodorescu-Draghicescu

Faculty of Mechanical Engineering, Transilvania University of Brasov, 500024 Brasov, Romania; draghicescu.teodorescu@unitbv.ro

\* Correspondence: cezar.afilipoaei@unitbv.ro or afilipoaei\_cezaru@yahoo.ro

<sup>†</sup> Presented at the 14th International Conference INTER-ENG 2020 Interdisciplinarity in Engineering, Mures, Romania, 8–9 October 2020.

Published: 14 December 2020



**Abstract:** The aim of this paper is to review and compare the response to the electromagnetic radiation of different structural or non-structural composites on absorption, reflections and re-reflection grades. The area of interest has been reduced to the carbon allotropy and conducting non-magnetic/magnetic fillers (inclusions, metallic powders, granular ferrites) in dielectric hosts characterized by existing mixing rules. The results could be grouped in distinctive ranges,  $SE \leq 10$  dB corresponding to a poor shielding, 10–30 dB describing an acceptable effectiveness and  $SE \geq 30$  dB exceeding the acceptable range for industrial and commercial applications of 20 dB.

**Keywords:** composites; carbon; shielding; electromagnetic; interference; frequency

## 1. Introduction

In the space around us, the presence of electromagnetic waves is observed as a matter of course phenomenon. The light itself is theoretically an unlimited electromagnetic radiation which could be detected by human eye, defining the visible spectrum, or could be invisible for human eye as ultra-violet (UV) or infra-red spectrums. Beside the aforementioned source, there are a lot of artificial sources of electromagnetic waves created by different electric or electronic equipment travelling under different polarization forms illustrated by Figure 1a. The electromagnetic interferences (EMI) thus are unavoidable.

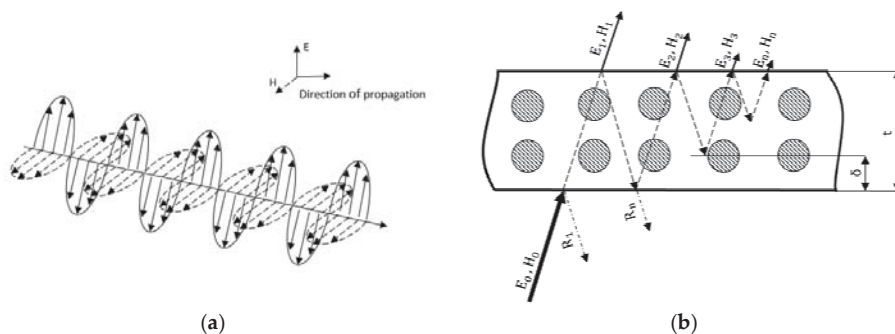


**Figure 1.** (a) The electromagnetic wave field propagation through space, vertical polarization; (b) the mechanism of shielding effectiveness through a given composite section.

The possibility of combining two or more materials with different electrical and mechanical properties in order to obtain an enhanced material with a high grade of homogeneity, aligns with actual trends of economical and environment global strategies. The materials resulted in aforementioned process are known as composites, having a well-defined structure characterized by two phases: one continuous, depicted as host or matrix medium and one discontinuous, described by reinforced elements or fillers. The aerospace industry was coupled many years with composite materials due to lightweight and particular structural efficiency, nowadays being widely spread in different industry fields from automotive to medical equipment. Generally, the composites are structured by association of two different material types; based on the atomic structure and chemical composition, materials are classified in three major classes: metals, ceramics and polymers (compounds resulted by hydrocarbons refining) [1].

Confining the composite classification to the domain of electromagnetic shielding effectiveness (SE) has delineated two major properties which the material should possess, high electric conductivity  $\sigma$  and low specific weight  $g$ . In Table 1 are presented values of conductivity for different kind of materials. Some materials are characterized by a high electric conductivity given intrinsically by its structure: magnetic metals, ferrites, carbon compounds or conducting polymers. For example, the electric conductivity of carbon structures, regardless of type, could be controlled by carbonization temperatures; high temperatures corresponding to top graphitization degree, therefore, to an enhanced  $\sigma$  value. A large interest in carbon and in its allotropic nature is observed since almost half of scientific articles written in the last decade on electromagnetic interference shielding topics contained “carbon” as a keyword [2].

**Table 1.** Electric conductivity for different classes of materials [3].

Material	Conductivity [ $\sigma$ ]		Relative
	[S/m]	[S/cm]	
Cu	$5.81 \times 10^7$	$5.81 \times 10^5$	1
Al	$3.48 \times 10^7$	$3.48 \times 10^5$	$6.01 \times 10^{-1}$
S/S	$1.16 \times 10^6$	$1.16 \times 10^4$	$2 \times 10^{-2}$
S/S in polymer	$5 \times 10^2$	5	$8.62 \times 10^{-6}$
GRFP	$1.16 \times 10^4$	$1.16 \times 10^2$	$2 \times 10^{-4}$
40%CF	1	$1 \times 10^2$	$1.72 \times 10^{-8}$
20%Ni coated	$9.09 \times 10^2$	9.09	$1.57 \times 10^{-5}$

One particular form of carbon emerged in this review article it is represented by the carbon fibers under various forms: continuous fibers (CF), long fibers (LF) and short fibers (SF) embedded usually in polymer matrices being grouped in a well-defined category CFRP (carbon fibers reinforced polymers matrix) or ACM (advanced composite materials).

## 2. The Fundamentals of Shielding Effectiveness (EMC/EMI)

The shielding effectiveness mechanism  $SE$  is described in the relation (1) as a sum of three particular losses: wave reflection losses  $R$ , wave absorption losses  $A$  and wave re-reflection losses  $B$  caused by the molecular structure of the material.

When an initial transmitted electromagnetic wave, as shown in Figure 1b characterized by an electric field intensity  $E_0$  and a magnetic field intensity  $H_0$ , meets the shielding material surface a certain grade of reflection occurs, followed closely by material absorption and an attenuation of wave intensity caused by  $n$  wave internal re-reflections. Mathematically, the shielding effectiveness is given by relation (2) as a logarithmic ration between the plane field intensity of radiated wave  $P_0$  and plane

field intensity of transmitted wave  $P_n$ . Similarly, the reflection, absorption and multiple reflections are described logarithmically by formulas given in relations (3)–(5).

$$SE = A + R + B[\text{dB}] \tag{1}$$

$$SE = 20 \log\left(\frac{E_0}{E_n}\right) = 20 \log\left(\frac{H_0}{H_n}\right) = 10 \log\left(\frac{P_0}{P_n}\right)[\text{dB}] \tag{2}$$

$$R = -10 \log\left(\frac{\sigma_{ac}}{16\omega\epsilon_0\mu_r}\right)[\text{dB}] \tag{3}$$

$$A = -20\left(\frac{t}{\delta}\right) \log_{10} e[\text{dB}] \tag{4}$$

$$B = 20 \log_{10}(1 - e^{-2t/\delta})[\text{dB}] \tag{5}$$

Shielding effectiveness  $SE$  depends on a series of constants and variables, such as complex permittivity  $\epsilon_r$  and permeability  $\mu_r$ , material type, material thickness  $t$ , dielectric properties  $\sigma_{ac}$ , frequency  $\omega$ , free space permittivity  $\epsilon_0$ , skin depth  $\delta$ . The skin depth  $\delta$  is defined as being the material thickness where the electromagnetic field intensity is reduced with approximate 37% (examples given  $\partial_{Cu} = 2.09 \mu\text{m}$ ,  $\partial_{Ni} = 0.47 \mu\text{m}$ , at a frequency of 1 GHz).

When high grades of wave reflection are permitted a suitable solution for shielding it is represented by metals, but in general many applications require a high grade of absorption through material, the reflected waves compromising the normal functionality of electronic and electric equipment. Therefore, ways are sought of converting the radiated or conducted wave energy in thermal energy, very often as heat.

### 3. Composites Used in Shielding Application

Radiated electromagnetic emissions have been measured around an electric vehicle in real drive conditions. These measurements were accomplished between the 30 MHz and 1 GHz frequency spectrum and revealed the highest interference between 30 MHz and 54 MHz when the peak detector was placed at the right and left of the vehicle being at a constant speed. Full scans of the vehicle at a constant speed were performed showing that the peak electric field are 5 dB higher than those measured at the right and left of the vehicle. The measurement techniques proved that the electromagnetic radiations varied significantly during a driving cycle [4].

The 2/2 twill weave carbon fabric with different specific weights was used to form composite laminates. Both dry carbon fibers and laminates were subjected to a frequency spectrum of 30 MHz to 1.5 GHz to measure the electromagnetic shielding effectiveness parameter in a coaxial device according to ASTM D4935 standard. In the case of a 1 mm thick composite laminate (four layers) with 2/2 twill weave carbon fabric, the shielding effectiveness parameter varied between 63.7 dB to 82.3 dB in the domain from 30 MHz to 450 MHz frequency. For a 3 mm thick laminate with eight layers of 2/2 twill weave carbon fabric, the SE shows variations between 70.9 dB to 88.2 dB in the range of 30 MHz to 401.28 MHz spectrum. The dry carbon fabric increases its shielding properties due to the lack of the resin as well as increasing the contact between fibers. On the other hand, the fiberglass allows the electromagnetic radiation to act without any compulsion. Sandwich PVC foam core specimens with one layer of carbon fabric and one layer of fiberglass on both sides as skins present shielding effectiveness values up to 122 dB measured within the 30 MHz to 500 MHz frequency range [5].

Carbon nanotubes paste was prepared and then printed on this plastic film. Measurements of the shielding effectiveness were accomplished in the frequency domain from 15 MHz to 1 GHz with a signal generator according to ASTM D4935. All carbon-based films presented an electromagnetic shielding effectiveness between 12 dB and 28 dB in the frequency range from 30 Hz to 50 Hz; this parameter drops significantly between 3 dB and 6 dB for a frequency domain from 50 Hz to 100 Hz, remaining almost constant until 1000 Hz frequency [6].



In many situations when an enclosure is needed to protect an equipment against EMI, the design of composite material and of the structure are developed virtually using various wave tool simulation as EZ-FDTD (finite difference time-domain process tool) developed by EMC Laboratory of MS&T and IBM, or CST Microwave studio. Koledintseva et al. studied, using a genetic algorithm optimization GA, the performance of Teflon carbon fiber filled composite shielding enclosures in a single layer/multilayer in terms of SE, in the microwave band 100 MHz–10 GHz. The Maxwell–Garnett rule has been used to determine the material effective electromagnetic parameters at given frequency ranges and the afferent carbon fiber properties (aspect ratio, percolation threshold, volume fraction, alignment). Using FDTD simulation at frequencies between  $10^{-1}$ – $10^1$  GHz the SE of a composite single layer box is situated at 10–50 dB, while the same box with composite multilayers the peak of SE reaches 90 dB. In the same study it was proven that composites materials have superior properties compared with metals when enclosures contains various geometrical apertures [7].

In the automotive industry, various technical solutions have been developed in order to suppress EMI. There is a wide range of conductive elastomers in molded or extruded shapes reinforced with conductive fillers, such as carbon C, passivized aluminum IA, silver plate aluminum Ag/Al, Nickel-coated carbon Ni/C evidenced a shielding effectiveness up to 120 dB at 10 GHz. Thermoformed polycarbonate foils have been coated with conductive metals molded in different shapes, as covers or caps, shown an effectiveness of 60–80 dB in frequency spectrum 30 MHz up to 2 GHz [8].

Neruda et al. tested two types of textile plain weave woven fabrics composite; the first was waved with silver-coated yarns and the second with a mix between non-conductive PES (polyamide) yarns (60%) and silver-coated yarns (40%) characterized by a high electrically conductivity  $\sigma = 244$  S/m, noticing a reduction of electromagnetic field intensity with 25–50 dB in a frequency range of 0.03–1.5 GHz. Testing was based on ASTM 4935-10, using the coaxial transmission line method [9].

The attenuation of electromagnetic field, the power of the absorbed wave field and the shielding effectiveness were determined for composites materials reinforced with carbon black (TN150 and TN300), graphite (GR150/GR300), ferrites (FT150) and micro particles of iron (FE300) in the frequency spectrum of 10MHz up to 1 GHz, with thicknesses of material varying in the range of 2.3–3 mm. An enclosed plain waved TEM (Transverse Electro-Magnetic) cell with a high grade of isolation from exterior perturbations was used, the electromagnetic field being separated in two components, electric and magnetic as plain waves. Values of shielding effectiveness were observed from 0.5 to 2.13 dB, emerging on the variation plot the highest values at the end of frequency range, near 1 GHz. Among all types of tested materials GR300, 2.6 mm thickness possesses superior shielding properties which puts the graphite on the top of the list with materials with high electromagnetic absorption properties [10]. The same testing technology of TEM cell according to ASTM D4935 has been applied on a composite material with a conductive coating developed by Freudenberg Sealing Technologies GmbH & Co. KG reaching a top sealing of 115 dB at 10 MHz [11].

Petru Ogrutan et al. using the wave guide-based method shown in Figure 2a,b, which presents similarities with MIL-STD-285 and EN 50147 standard specifications, measured the shielding effectiveness for different composites materials and validated the wave power attenuation using a Pspice model simulation. Cardboard sheets, glass fabric phenolic sheets, 3 mm and 5 mm sheets of synthetic graphite and FE300 (Butadiene styrene rubber matrix reinforced with ferrites) with 3 mm thickness were appropriate for testing. The results shown at 10 GHz describe an electromagnetic power attenuation of 1 dB in case of cardboard sheet, 2 dB for glass fabric phenolic screen and 6 dB when FE300 was used [12].

Erhan Sancak et al. investigated the electromagnetic shielding effectiveness of polyamide (PA6) membranes filled with AgNP (Silver nanoparticles, 20 nm, spherical shape on metal basis) at different concentrations (0 wt%, 1 wt%, 2 wt%). The polymer membranes have been obtained combining electro spun nanofibers (sizes from 174 nm up to 238 nm) using the electrospinning technique. The ASTM D4935-10 coaxial transmission line method was used in the frequency domain of 15 MHz–3 GHz.

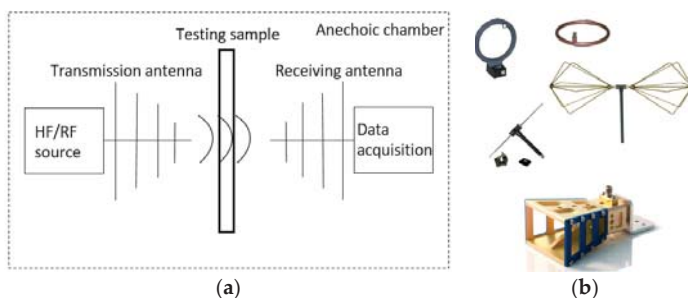


**Figure 2.** (a) Shielding effectiveness wave guide-based method schematic test set-up; (b) types of antennas, constructive solutions.

The results show a constant attenuation of 2.5 dB on the entire frequency domain when specimens contained 2 wt% AgNP, approximately 1 dB in the case of 1 wt% and no attenuation in the pure PA6 samples. The shielding effectiveness performance is influenced directly by material electric conductivity. The polyamide, as pure material, exhibits a non-conducting behavior, while the percentages of AgNP have enhanced the material electric conductivity, hence have increased the shielding effectiveness [13].

A wide range of studies have been conducted on the evaluation of electromagnetic compatibility and radiated emissions in the case of high voltage electric vehicles in various operating ways. Anca-Alexandra Săpunaru et al. measured the electromagnetic radiation values for an electric vehicle in charging mode, driving mode and ready-to-drive mode in a frequency spectrum of 30 MHz–1 GHz.

It was found that in driving mode, at 40 km/h, the level of radiated emissions, peaks level exceeded 45 dB $\mu$ V/m, the quasi-peak detector limit for an antenna at 3 m distance being 42 dB $\mu$ V/m [14].

A separate category of composites encompassing textiles were tested to fields suppression; considering IEEE STD-299 (using two horn antennas and a shielded structure with an opened window) instrumental set-up various structures containing natural fibers (wool and cotton), polymeric fibers (as nylon and polyester) and conductive fibers (Cu, SS, C) were checked for shielding effectiveness in a frequency domain of 1 GHz to 18 GHz. The samples tested were split based on used conductive fibers in two categories: textiles with copper and stainless-steel wires and textiles which were woven with carbon fibers, in percentages of 4.5–7.5%. It has been remarked that samples knitted with stainless steel threads exhibit an SE of 54.7 dB at 2.7 GHz, while Cu fibers reinforced textiles have reached 20.18 dB at 2.4 GHz. The efficiency of carbon fibers in technical textiles have been issued on a narrow band frequency (13 GHz–18 GHz) ranging between 2–8 dB. Therefore, the study conclusion is confining the shielding efficiency of the carbon yarns in the technical textile in specific frequency domain of 16–18 GHz [15].

Long and short carbon fibers LCF/SCF (7  $\mu$ m, L/D = 300; 100) were mixed into a cellulose blend in percentages of 5%, 10%, 15%, 20% and dried freeze. Obtained samples were supposed to have electromagnetic radiation in a frequency spectrum of 30 to 1500 MHz, with top values of SE being noted of 25 dB (30–200 MHz) when the material contained SFC and 60 dB (400–700 MHz) when the filler was LCFs [16]. Hao-Kai Peng et al. measured the suppression grade of a sandwich composite formed by a rigid polyurethane (PUR) foam covered by a nylon nonwoven fabric with aluminum foil. The samples were geometrically defined as having a diameter of 80 mm and a thickness of 20 mm. By applying ASTM D4935 test setup, the sandwich composite material reached 45 dB in the range of 600 MHz up to 2.5 GHz. Samples made by pure PUR barely reached 10 dB which is reasonable, given the fact that PUR is naturally an insulator [17]. By applying in situ polymerization method, Nina Joseph et al. developed flexible films of materials based on nanofibers of polyaniline and graphite on nylon and cotton fabric supports. The waves absorption rate given by the 1 mm thin composite sheet had reached 83–89 dB in the 8.2–18 GHz frequency interval [18]. Co-doped barium hexaferrites BaFe<sub>11</sub>CoO<sub>19</sub>, 3 mm thickness, toroid shape samples were obtained by using ceramic sintering powder processing

technique. Using ASTM D 4935 standard setup in the frequency range of 2–18 GHz, an approximately flat curve of SE was observed, 34 dB attenuation in 4–18 GHz spectrum. The obtained measurements were compared with theoretical calculations made based on each material constituent properties using Nicholson–Ross–Weir (NRW) rule. The complex permittivity was measured in same frequency domain showing values of 5–6 for  $\epsilon'_r$  and 0–1 for  $\epsilon''_r$ . The two plots describe a high grade of similarity, the calculated SE showing a constant tier of 35 dB in the 4–16 GHz domain [19].

Muhammad H. Zahari et al. manufactured composite structures samples based on in-situ polymerization of aniline mixed with barium ferrite  $\text{BaFe}_{12}\text{O}_{19}$  and multi-wall carbon nanotubes MWCNT in different percentages (0 wt%, 5 wt%, 10 wt%, 15 wt%, 20 wt% and 25 wt%). The reflection and absorption wave losses were determined in the frequency range of 8–12 GHz. The measurements shown reflections losses of 1–5 dB in the aforementioned frequency domain while the absorption losses reached a top of 35 dB at 12 GHz. The real  $\epsilon'_r$  and imaginary  $\epsilon''_r$  parts of complex permittivity were determined, plots marking values of 22.5–17.3 for energy storage and 15.3–10.8 for dielectric losses. Among all the samples tested, 20 wt% MWCNT registered the best shielding efficiency [20].

A relatively new material which can fulfil the requirements of shielding mechanism in the Ku-band is represented by graphene, as an allotrope form of carbon. On sheets of reduced graphene oxide were applied nano particles of barium ferrites  $\text{BaFe}_{12}\text{O}_{19}$  (20–30  $\mu\text{m}$ ) in 3 mm thickness samples. It was observed that in the frequency range of 12.4–18 GHz the nanocomposite behaved an SE of 32 dB [21].

Ranjivai Ram et al. proposed as composite material for shielding application polyvinylidene fluoride matrix (PVDF) doped with MWCNT and SCF (short carbon fibers) in certain weight percentages (0.5 wt%, 1 wt%, 2 wt%, 5 wt%). The results were compared in the frequency range of 8–12.5 GHz. The direct influence of the filler in the EMI SE properties was observed, MWCNT presenting enhanced results compared with SCF. A SE at 5 wt% of 35 dB was established at 12.5 GHz while SCF 5 wt% reached approximately 20 dB at the same peak frequency [22].

#### 4. Conclusions

The increasing number of engineering applications which are using electric and electronic systems led to the creation of new material requirements regarding the electromagnetic interferences. In Table 2 are reviewed some proposed composites materials which were developed to counteract the effect of interference in functioning. It was proved that the allotropy of carbon suits mostly when the balance between electrical and mechanical performances is sought. The weight percentage included in the matrix plays a crucial role in the shielding effectiveness, the more the better, but always considering also the mechanical and thermal properties.

Table 2. Composites materials shielding effectiveness overview (\*ns, not specified).

	Matrix	Filler	Sample Thickness [mm]	Frequency [GHz]	Shielding Effectiveness [dB]	Ref.
1	Polymer	CNT	*ns	0.15–1	3–28	[6]
2	Teflon	CF	3/9	0.1–10	10–50	[7]
3	PC	Metallic inclusion	*ns	0.03–2	60–80	[8]
4	Elastomer	C/I/Ag/Al	*ns	10	120	[8]
5	Textile	Ag/PES	*ns	0.03–1.5	25–50	[9]
6	*ns	TN150/300/GR150/GR300/FT150/FT300	2.3–3	0.01–1	0.5–2.13	[11]
7	GR/Glass/Cardboard	*ns	3/5	10	1–6	[12]
8	PA6	AgNP	*ns	0.15–3	1–2	[13]
9	PET/Cotton/Wool	Cu/SS/C	*ns	1–18	20.18–54.7	[15]
10	Cellulose	LCF/SCF	*ns	0.03–1.5	25–60	[16]
11	Nylon/Al	PUR	20	0.6–2.5	45	[17]
12	Nylon/Cotton	PANI/GR NT	1	8.2–18	83–89	[18]
13	BaFe <sub>12</sub> O <sub>19</sub>	Co	3	4–16	35	[19]
14	PANI	BaFe <sub>12</sub> O <sub>19</sub> /MWCNT	*ns	8–12	35	[20]
15	RGO	BaFe <sub>12</sub> O <sub>19</sub>	3	12.4–18	32	[21]
16	PVDF	MWCNT/SCF	5	8–12.5	35–20	[22]

**Funding:** This research received no external funding.

**Conflicts of Interest:** The authors declare no conflict of interest.

## References

1. Callister, W.D., Jr.; Rethwisch, D.G. *Materials Science and Engineering an Introduction*, 8th ed.; John Wiley & Sons, Inc.: Hoboken, NJ, USA, 2009.
2. Wang, C.; Murugadoss, V.; Kong, J.; He, Z.; Mai, X.; Shao, Q.; Chen, Y.; Guo, L.; Liu, C.; Angaiah, S.; et al. Overview of carbon nanostructures and nanocomposites for electromagnetic wave shielding. *Carbon* **2018**, *140*, 696–733. [CrossRef]
3. Evans, R.W. *Design Guidelines for Shielding Effectiveness, Current Carrying Capability, and the Enhancement of Conductivity of Composite Materials*; Tec-Masters, Inc.: Huntsville, AL, USA, 1997.
4. Pliakostathis, K.; Zanni, M.; Trentadue, G.; Scholz, H. Vehicle Electromagnetic Emissions: Challenges and Considerations. In Proceedings of the 2019 International Symposium on Electromagnetic Compatibility—EMC EUROPE, Barcelona, Spain, 2–6 September 2019; pp. 1106–1111. [CrossRef]
5. Munalli, D.; Chronopoulos, D.; Greedy, S. Electromagnetic shielding effectiveness of fiber-reinforced composites: A preliminary study. In Proceedings of the 9th European Workshop on Structural Health Monitoring (EWSHM 2018), Manchester, UK, 10–13 July 2018.
6. Wang, L.L.; Tay, B.K.; See, K.Y.; Sun, Z.; Tan, L.K.; Lua, D. Electromagnetic interference shielding effectiveness of carbon-based materials prepared by screen printing. *Carbon* **2009**, *47*, 1905–1910. [CrossRef]
7. Koledintseva, M.Y.; Drewniak, J.; DuBrof, R. Modeling of shielding composite materials and structures for microwave frequencies. *Prog. Electromagn. Res.* **2009**, *5*, 197–215. [CrossRef]
8. Noto, J.; Fenical, G.; Tong, C. Automotive EMI Shielding—Controlling Automotive Electronic Emissions and Susceptibility with Proper EMI Suppression Methods. 2010. Available online: <https://www.streakwave.com> (accessed on 5 January 2020).
9. Neruda, M.; Vojtech, L. Electromagnetic Shielding Effectiveness of Woven Fabrics with High Electrical Conductivity: Complete Derivation and Verification of Analytical Model. *Materials* **2018**, *11*, 1657. [CrossRef] [PubMed]
10. Nicolae, G. Measurement method for determining electromagnetic field attenuation in nanomaterials using the TEM cell (2nd part). *Recent* **2009**, *10*, 26.
11. Jedrowicz, G.; Morgenstern, S.; Nuško, M.; Schroiff, V. Efficient Development of Seal and Shielding Concepts for Electrified Powertrains. *MTZ Worldw.* **2018**, *10*, 44–49. [CrossRef]
12. Ogrušan, P.; Aciu, L.E. Electromagnetic Shielding Effectiveness Evaluation for Materials. *Int. J. Eng. Res. Appl.* **2013**, *3*, 2329–2334.
13. Sancak, E.; Ozen, M.S.; Erdem, R.; Yilmaz, A.C.; Yuksek, M.; Soin, N.; Shah, T. PA6/silver blends: Investigation of mechanical and electromagnetic shielding behaviour of electrospun nanofibers. *J. Text. Appar./Tekstil Konfeksiyon* **2018**, *28*, 229–235.
14. Săpunaru, A.A.; Ionescu, V.M.; Popescu, M.O.; Popescu, C.L. Study of Radiated Emissions Produced by an Electric Vehicle in Different Operating Modes. In Proceedings of the 2019 Electric Vehicles International Conference (EV), Bucharest, Romania, 3–4 October 2019; pp. 1–5. [CrossRef]
15. Telipan, G.; Morari, C.; Moasa, B. Electromagnetic shielding characterization of several conductive textiles. *Bull. Transilv. Univ. Braş.* **2017**, *10*, 1.
16. Li, R.; Lin, H.; Lan, P.; Gao, J.; Huang, Y.; Wen, Y.; Yang, W. Lightweight Cellulose/Carbon Fiber Composite Foam for Electromagnetic Interference (EMI) Shielding. *Polymers* **2018**, *10*, 1319. [CrossRef] [PubMed]
17. Peng, H.K.; Wang, X.X.; Li, T.T.; Huang, S.Y.; Lin, Q.; Shiu, B.C.; Lou, C.W.; Lin, J.H. Effects of hydrotalcite on rigid polyurethane foam composites containing a fire retarding agent: Compressive stress, combustion resistance, sound absorption, and electromagnetic shielding effectiveness. *RSC Adv.* **2018**, *8*, 33542–33550. [CrossRef]
18. Joseph, N.; Varghese, J.; Sebastian, M.T. In situ polymerized polyaniline nanofiber-based functional cotton and nylon fabrics as millimeter-wave absorbers. *Polym. J.* **2017**, *49*, 1–9. [CrossRef]
19. Araz, İ. The measurement of shielding effectiveness for small-in-size ferrite-based flat materials. *Turk. J. Electr. Eng. Comput. Sci.* **2018**, *26*, 2997–3007. [CrossRef]

20. Zahari, M.H.; Guan, B.H.; Cheng, E.M.; Che Mansor, M.F.; Lee, K.C. EMI Shielding Effectiveness of Composites Based on Barium Ferrite, PANI, and MWCNT. *Prog. Electromagn. Res.* **2016**, *52*, 79–87. [[CrossRef](#)]
21. Verma, M.; Singh, A.P.; Sambyal, P.; Singh, B.P.; Dhawan, S.K.; Choudhary, V. Barium ferrite decorated reduced graphene oxide nanocomposite for effective electromagnetic interference shielding. *Phys. Chem. Chem. Phys.* **2018**, *17*, 1610–1618. [[CrossRef](#)] [[PubMed](#)]
22. Ram, R.; Khastgir, D.; Rahaman, M. Physical properties of polyvinylidene fluoride/multi-walled carbon nanotube nanocomposites with special reference to electromagnetic interference shielding effectiveness. *Adv. Polym. Technol.* **2018**, *37*, 3287–3296. [[CrossRef](#)]

**Publisher's Note:** MDPI stays neutral with regard to jurisdictional claims in published maps and institutional affiliations.



© 2020 by the authors. Licensee MDPI, Basel, Switzerland. This article is an open access article distributed under the terms and conditions of the Creative Commons Attribution (CC BY) license (<http://creativecommons.org/licenses/by/4.0/>).



# Thermal Dynamic Behavior in Bi-Zone Habitable Cell with and without Phase Change Materials †

Hanae El Fakiri \*, Lahoucine Ouhsaine and Abdelmajid El Bouardi

Energetic Laboratory, Thermal, Solar Energy and Environment Team (ETEE), Physics Department, Faculty of Sciences, Abdelmalek Essaâdi University, Tetouan 93000, Morocco; ouhsaine.la@gmail.com (L.O.); a\_bouardi@yahoo.fr (A.E.B.)

\* Correspondence: hanaefakiri@gmail.com; Tel.: +212-(0)671-53-80-04

† Presented at the 14th International Conference INTER-ENG 2020 Interdisciplinarity in Engineering, Mureş, Romania, 8–9 October 2020.

Published: 21 December 2020

**Abstract:** The thermal dynamic behavior of buildings represents an important aspect of the energy efficiency and thermal comfort of the indoor environment. For this, phase change material (PCM) wallboards integrated into building envelopes play an important role in stabilizing the temperature of the human comfort condition. This article provides an assessment of the thermal behavior of a “bi-zone” building cell, which was built based on high-energy performance (HEP) standards and heated by a solar water heater system through a hydronic circuit. The current study is based on studying the dynamic thermal behavior, with and without implantation of PCMs on envelope structure, using a simplified modeling approach. The evolution of the average air temperature was first evaluated as a major indicator of thermal comfort. Then, an evaluation of the thermal behavior’s dynamic profile was carried out in this study, which allowed for the determination of the PCM rate anticipation in the thermal comfort of the building cell.

**Keywords:** thermal comfort; phase change materials (PCMs); HEP building; thermal performance

## 1. Introduction

The sustained growth in the energy demand’s dependence on fossil fuel and fluctuating prices, as well as environmental constraints, have prompted African countries to explore potential sources of energy savings. One of the promising responses is energy efficiency. In Morocco, since the launch of the national energy strategy in 2009, energy efficiency has become one of the main pillars for the sustainability and energy independence policy of the kingdom.

The building sector is among the most energy-demanding sectors in Morocco, with an energy consumption of up to 33% of the total energy in the country, including 26% for the residential sector and 7% for the tertiary sector. The building sector today has the greatest potential for improving energy efficiency by representing an energy-saving potential of 40% [1]. An important rate is dominated by heating, ventilation, and air conditioning (HVAC) systems. The Moroccan thermal standard was launched in 2015 to reduce the energy bill and environmental impact. Thus, high-energy performance (HEP) in building standards is a key element to achieve the Moroccan thermal regulation of buildings (RTCM) [2]. The thermal performances required in the RTCM differ according to the type of building (residential or tertiary) and according to the climatic zone by location [3].

Besides, several research works have been developed to improve building energy efficiency, the thermal performance of buildings, and energy consumption savings. In this context, several solutions have been presented, among them the incorporation of phase change materials (PCMs) as promising systems with the ability to improve the imbalance between energy supply and demand and provide high-energy storage density using latent heat.



PCMs are substances that release or absorb energy during melting and freezing processes at a constant or semi-constant temperature based on the phase change temperature of the material.

Therefore, one of the uses of variable phase materials is the storage of latent thermal energy, whereby the variable phase materials combined with building materials can increase the thermal breakdown of buildings to contribute to reducing fluctuations in internal temperature and achieving internal thermal comfort, reducing the energy consumption needed for heating and air conditioning.

In the Mediterranean context, Mandilaras et al. [4] thermally characterize a typical two-story family house embedded with PCM gypsum pasteboard panels. They analyze the building walls orientation effect for meteorological conditions and with conducted experimental measurements, the authors conclude that the thermal mass enhancement for early summer and autumn results in a decrease in decrement factor by 30 to 40% and an increase in time lag by approximately 100 min. These two cited factors are key output parameters to evaluate thermal performance inside buildings; they were also determined and discussed in the works of Kharbouch et al. [5] who investigated the thermal performance of PCM-enhanced walls and roofs in northern Moroccan buildings.

Most supplementary studies have also shown that PCM integration into building envelopes has major benefits. Mourid et al. [6,7] have been experimentally concluding that the application of PCMs on the envelope of a cavity living space is an effective technique for improving thermal comfort by storing heating losses, which reduces the electrical energy consumption, compared to a similar cavity without PCMs. Other research works [8,9] revealed experimentally that the optimal site to achieve greater efficiency by integrating PCMs was located closer to the interior surface of the wall. In addition, Li et al. [10] construed that building envelopes containing PCMs manifest different levels of enhancement by reducing peak temperature and temperature fluctuations. Li et al. [11] improved heat transfer reduction in multi-layer walls of conventional buildings by using PCMs.

This work aims to numerically investigate the thermal dynamic behavior of all the components of a whole building partially covered by PCMs and that of one without PCMs. The outcomes of the study may contribute to clearing the way for energy analysis and comparison with standard and conventional buildings in matters of thermal conditioning.

In the presented paper, the first part describes the thermal model and the proposed bi-zone building description, while the second part discusses briefly the developed scheme of numerical dynamic simulation as well as the different adopted scenarios that were shown to evaluate the use of PCMs in the building envelope. Finally, the results obtained from the dynamic simulation are developed to discover the optimal scenario in the proposed building.

## 2. Thermal Model

### 2.1. Building Description

The building studied is a prototype that was built at the Abdelmalek Essaadi University Faculty of Sciences in Tetouan (Figure 1), located in the climate Z2 zone [2], which is characterized by moderate climate in the Tangier-Tetouan region in the north of Morocco (N 35°34' W 5°22'). For Moroccan conditions, the location is relatively rain-laden and is located on a plateau, about 90 m above mean sea level and 10 km south of the Mediterranean Sea. The city is surrounded by the Rif Mountains in the northern and southern directions.

The building has an entire area of 53 m<sup>2</sup> and consists of two rooms, which are connected by a simple wooden door (4 cm thick, 83 cm × 210 cm) as illustrated by Figure 2. The entrance door on the north side of the building has a heat transfer coefficient of 1.627 W/m<sup>2</sup> K; its structural characteristics are the same as those of the internal door. Furthermore, the building has six simple windows (76 cm × 117 cm, 4 mm thick) with aluminum frames. Two are located in the south of the building, while four face westward. The thermo-physical characteristics of the building are summarized in Table 1.



Figure 1. Perspective prototype of the bi-zone building.

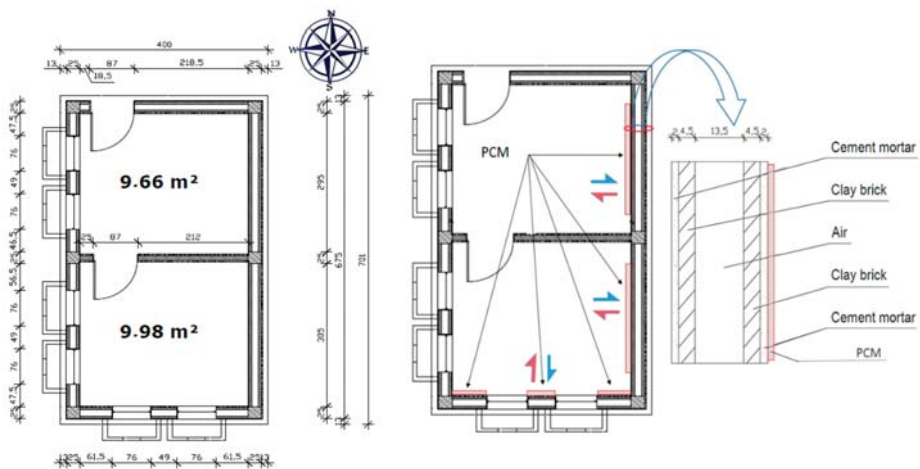


Figure 2. Bi-zone model prototype with and without phase change material (PCM) cases.

Table 1. Thermo-physical characteristics of the building.

Components	Sub-Component	Thickness (mm)	Thermal Cond. $Wm^{-1} K^{-1}$	Specific Heat Capacity $(J/kg^{-1} m^{-3})$	Density $(kg/m^3)$	Heat Transfer Coefficient U
External wall	Cement mortar	2	0.42	1000	1800	Heat transfer coefficient: $U = 1.43 W/(m^2 K)$
	Clay brick	4.5	0.34	1000	1784	
	Air (static)	13.5	0.03	1000	1.29	
	Clay brick	4.5	0.34	1000	1784	
	Cement mortar	2	0.42	1000	1800	
Floor	Gravel	5	0.70	1000	1800	Heat transfer coefficient: $U = 0.81 W/(m^2 K)$
	Reinforced concrete	35	1.65	880	2150	
	Cork	4	0.05	1800	155	
	Screed	5	1.0	1000	2000	
	Tile	0.7	1.4	1000	2500	
Entrances	Window: single glazing + frame	4	-	-	-	$U = 1.627 W/(m^2 K)$
	Doors wood	4	-	-	-	
Roof	Tile	0.7	1.4	1000	2500	Heat transfer coefficient: $U = 1.43 W/(m^2 K)$
	Cement mortar	2	0.42	1000	1800	
	Reinforced concrete	3.5	1.62	880	2150	
	Hollow block ceiling/toe board	15.5	0.60	880	1000	
	Cement mortar	2	0.42	1000	1800	

In this work, the PCM wall board was proposed to be embedded in the inside part of the eastern and southern building faces, because those faces were assumed to receive the highest amount of daily solar radiation. Furthermore, this study intended to limit the integration of the PCM in the whole building for economic reasons and to investigate firstly the partial PCM integration in building walls (Figure 2).

2.2. Heat and Mass Transfer Modeling

The chosen mathematical approach to model the thermal behavior in the bi-zone cell was the heat capacity and thermal conductivity variation concerning the PCM temperature method [12].

The heat equation in the solid-state is defined by the Laplace equation and reduced to the developed form described by the equation; this model describes formally the thermal balance in a transient regime without heat term sources for different sub-layers of the system in a wall sample.

$$\rho_i C_i e_i \frac{dT_i}{dt} = \frac{k_i}{e_i} (T_{i-1} - T_i) - \frac{k_{i+1}}{e_{i+1}} (T_i - T_{i+1}) \text{ for } i = 1 \dots N \tag{1}$$

where  $\rho_i$ ,  $C_i$ ,  $k_i$ , and  $e_i$  are respectively the density, the heat capacity, the thermal conductivity, and the thickness of the layer  $i$ , while  $i + 1$  leads to the adjacent layer. It can be noted in this work that the reference for the indoor chosen direction is from indoor to outdoor. The integration of the PCM layer can be modeled by the following equation:

$$\rho_\phi C_\phi (T_\phi) e_\phi \frac{dT_\phi}{dt} = \frac{k_\phi(T_\phi)}{e_\phi} (T_{\phi-1} - T_\phi) - \frac{k_{\phi+1}}{e_{\phi+1}} (T_\phi - T_{\phi+1}) \tag{2}$$

where  $\phi$  subscript denotes the phase change material layer, while  $\phi - 1$  and  $\phi + 1$  corresponds to the adjacent layers in front (indoor air) and behind the PCM layer, respectively.

The approach used in this work consists to extend the wall model with and without PCM pasteboard into full-building bi-zone scale. Figure 3 represents the multi-scale process RC (resistance capacity) equivalent network modeling for a 1D single wall to a mono and then for a full bi-zone dynamic model with and without PCMs. The heat capacity and thermal conductivity variation were developed in the work of Kharbouch et al. [5]; the PCM used in this work was composed of paraffin-wax microcapsule material and its phase change temperature was 21 °C, which is near thermal comfort conditions.

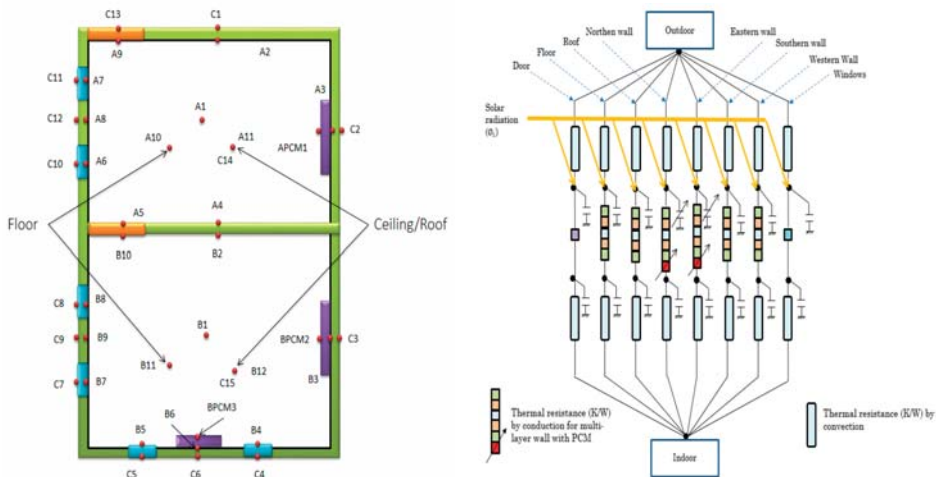


Figure 3. The multi-scale process RC equivalent network modeling.

The heat transfer between the building envelopes and its outdoor and indoor environments is realized by convection and radiation. The thermo-physical parameters are estimated by referring to

the literature and physical assumptions. Figure 4 represents 38 thermal points' predictions that are determined by the simplified dynamic model in the case of PCM integration.

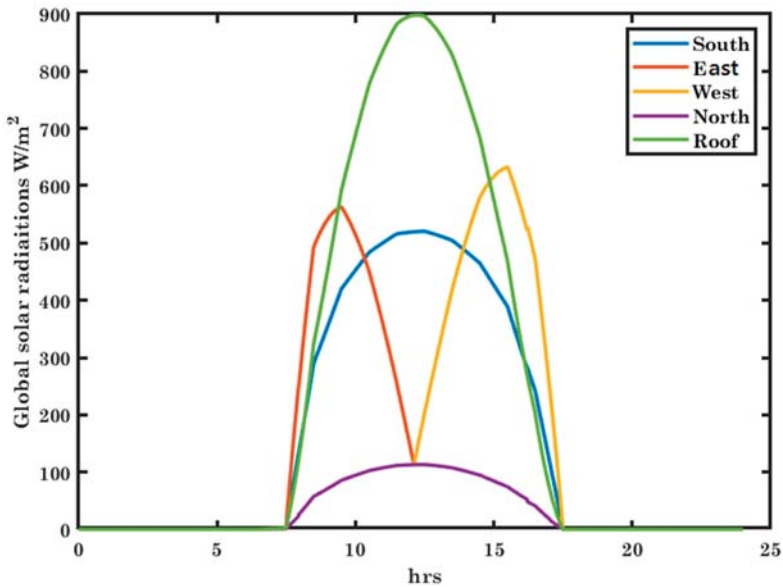


Figure 4. Solar radiation density issued in different surfaces for the first day in January.

### 3. Dynamic Simulation

#### 3.1. Meteorological Data (Hourly TMY)

The meteorological data used were extracted from the hourly typical meteorological years (TMY) Meteornorm database where different levels of global solar radiation that rose into the four facades (north, south, east, and west) were checked. Additionally, the ambient temperature and the wind speed were also useful in this work [13].

#### 3.2. Finite Difference Method

The finite difference method (FDM) is one of the performing numerical simulation methods that were employed to resolve differential equations, by substituting the derivatives in the equation using differential quotients, principally approximating the boundary conditions value problems by appropriate finite-difference operators [14]. FDM consists of approximating the derivatives of the heat equation-employing Taylor expansions and is deducted directly from the definition of the derivative [15].

The governing equation was solved along with the corresponding boundary and initial conditions using a finite difference method. The simulations were performed using MATLAB Software. The thermal transfer and storage processes of PCMs were taken into account by employing a one-dimensional conduction finite-difference solution as the heat balance algorithm. To account for phase change energy, this algorithm gives an implicit finite difference scheme combined with heat capacity and thermal conductivity function.

### 4. Results and Discussion

Dynamic simulation was conducted to determine the thermal behavior in the unheated bi-zone habitable cell with and without phase change materials (PCMs). It is worthwhile to know that the

modeling approach predicted the temperature dynamics state for about 41 components of the system with PCMs and 38 components for the non-PCM case.

#### 4.1. Thermal Profile in Winter Period

Figure 5 represents the temperature dynamic behavior with PCM integration phase for the 10th to the 12th day of January 2012. It can be seen that the PCMs amplify the natural heat sources in the indoor area. The southern side of the building that is most exposed to the sun causes high thermal behavior in indoor surfaces.

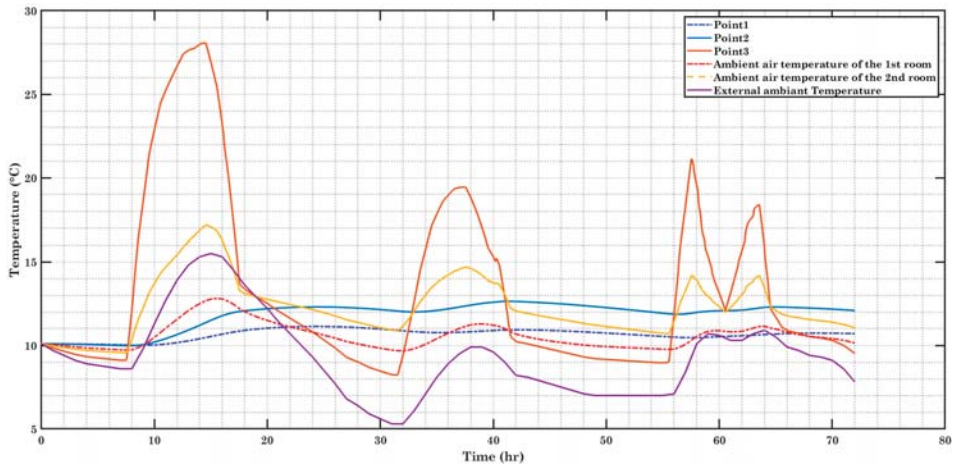


Figure 5. The temperature dynamic behavior with PCM integration phase in winter period.

Figure 6 represents the temperature dynamic behavior without the PCM integration cases, and it can be seen that the temperature profile is lower than the temperature profile of the PCM case integration.

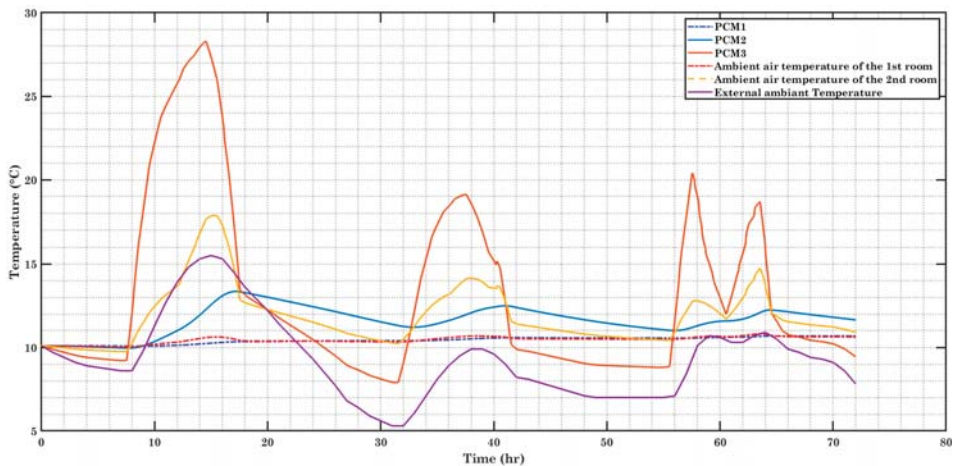


Figure 6. The temperature dynamic behavior without PCM integration phase in winter period.



#### 4.2. Thermal Profile in Summer Period

In this section, we show temporal evolutions of the temperature for the cells with and without PCMs. During the trees first day of July in the summer period, it can be seen from Figures 7 and 8 that the PCMs reduce significantly the thermal behavior in the building cells for the first room and has negative impact for the second room in the summer period.

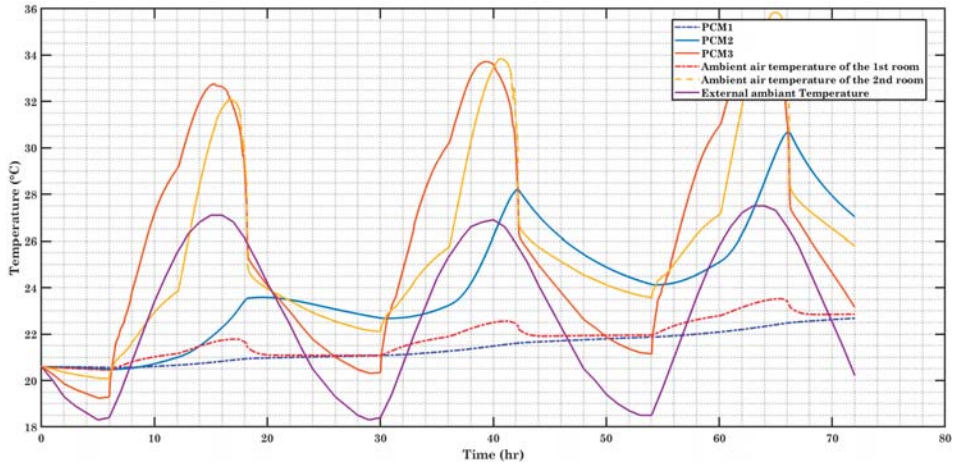


Figure 7. Time evolution of the temperatures of the cells without PCMs in Summer Period.

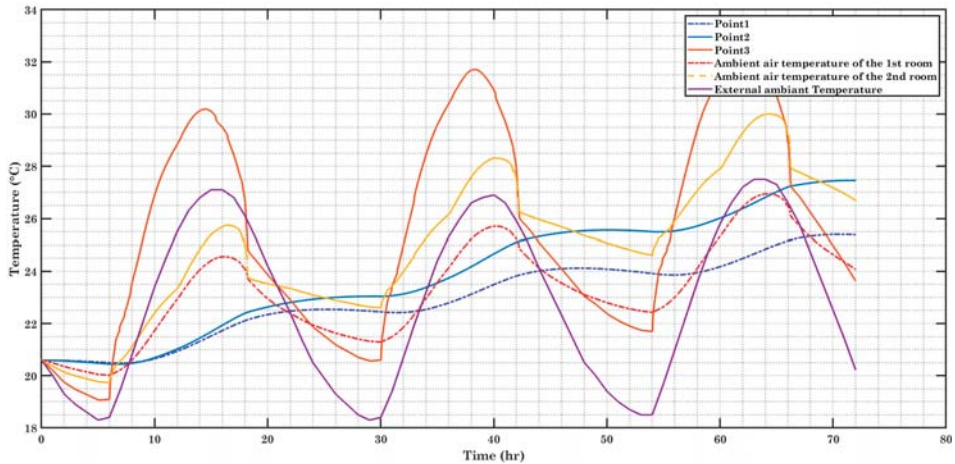


Figure 8. Time evolution of the temperatures of the cells with PCMs in Summer Period.

### 5. Conclusions

The aim of this study was to investigate the thermal behavior of PCM integration in a bi-zone building cells. The dynamic simulation was conducted for 31 subcomponents. The represented results show the dynamic thermal profile along the daytime period. The study was limited to the dynamic simulation and the comparison with the partial PCM integrations into the indoor walls. The prospect of this study was to investigate deeply the effect of the parameters that control the mathematical model, and to optimize the PCM integration in the buildings.

**Author Contributions:** Conceptualization, methodology, validation, original draft preparation, review, and editing by H.E.F. and L.O.; supervision by A.E.B. All authors have read and agreed to the published version of the manuscript.

**Conflicts of Interest:** The authors declare no conflict of interest.

## References

1. AMEE. Moroccan Agency for Energy Efficiency: Energy Efficiency in Buildings. Available online: <https://www.amee.ma/en/node/118> (accessed on 10 June 2020).
2. AMEE. Moroccan Agency for Energy Efficiency: La Réglementation Thermique Dans le Bâtiment (RTCM). Available online: <https://www.amee.ma/reglementation-thermique> (accessed on 10 June 2020).
3. AMEE. *Construction Building Thermal Regulation Code in Morocco (TRCM), Zonage Climatique du Maroc Adapté au Règlement Thermique de Construction au Maroc*; AMEE: Dundee, Finland, 2018.
4. Mandilaras, I.; Stamatiadou, M.; Katsourinis, D.; Zannis, G.; Founti, M. Experimental thermal characterization of a Mediterranean residential building with PCM gypsum board walls. *Build. Environ.* **2013**, *61*, 93–103. [[CrossRef](#)]
5. Kharbouch, Y.; Ouhaine, L.; Mimet, A.; El Ganaoui, M. Thermal performance investigation of a PCM-enhanced wall/roof in northern Morocco. *Build. Simul.* **2018**, *11*, 1083–1093. [[CrossRef](#)]
6. Mourid, A.; Alami, M.E. Experimental analysis of the thermal behavior of two cavities kind of living space with and without PCM on envelopes. *Int. J. Mod. Embed. Syst.* **2017**, *5*, 7.
7. Mourid, A.; Alami, M.; Kuznik, F. Experimental investigation on thermal behavior and reduction of energy consumption in a real scale building by using phase change materials on its envelope. *Sustain. Cities Soc.* **2018**, *41*, 35–43. [[CrossRef](#)]
8. Jin, X.; Hu, H.; Shi, X.; Zhou, X.; Yang, L.; Yin, Y.; Zhang, X. An improved heat transfer model for building phase change material wallboard. *J. Therm. Anal. Calorim.* **2018**, *134*, 1757–1763. [[CrossRef](#)]
9. Li, M.; Gui, G.; Lin, Z.; Jiang, L.; Pan, H.; Wang, X. Numerical Thermal Characterization and Performance Metrics of Building Envelopes Containing Phase Change Materials for Energy-Efficient Buildings. *Sustainability* **2018**, *10*, 2657. [[CrossRef](#)]
10. Arıcı, M.; Bilgin, F.; Nižetić, S.; Karabay, H. PCM integrated to external building walls: An optimization study on maximum activation of latent heat. *Appl. Therm. Eng.* **2020**, *165*, 114560. [[CrossRef](#)]
11. Li, Z.X.; Al-Rashed, A.A.; Rostamzadeh, M.; Kalbasi, R.; Shahsavari, A.; Afrand, M. Heat transfer reduction in buildings by embedding phase change material in multi-layer walls: Effects of repositioning, thermophysical properties and thickness of PCM. *Energy Convers. Manag.* **2019**, *195*, 43–56. [[CrossRef](#)]
12. Meteonorm Software Worldwide Irradiation Data, Weather Stations and Satellites, NREL TMY Dataset Downloads. Available online: <http://www.meteonorm.com/en/> (accessed on 13 July 2020).
13. Akeiber, H.; Nejat, P.; Majid, M.Z.; Wahid, M.A.; Jomehzadeh, F.; Famileh, I.Z.; Calautit, J.K.; Hughes, B.R.; Zaki, S.A. A review on phase change material (PCM) for sustainable passive cooling in building envelopes. *Renew. Sustain. Energy Rev.* **2016**, *60*, 1470–1497. [[CrossRef](#)]
14. Košny, J. Short History of PCM Applications in Building Envelopes. In *PCM-Enhanced Building Components*; Springer: New York, NY, USA, 2015; pp. 21–59.
15. Voller, V.R. Fast implicit finite-difference method for the analysis of phase change problems. *Numer. Heat Transf. Part B Fundam.* **1990**, *17*, 155–169. [[CrossRef](#)]

**Publisher's Note:** MDPI stays neutral with regard to jurisdictional claims in published maps and institutional affiliations.



© 2020 by the authors. Licensee MDPI, Basel, Switzerland. This article is an open access article distributed under the terms and conditions of the Creative Commons Attribution (CC BY) license (<http://creativecommons.org/licenses/by/4.0/>).

# Numerical Investigation of a Novel Heat Pipe Radiant Floor Heating System with Integrated Phase Change Materials <sup>†</sup>

Marius Brănoaea \*, Andrei Burlacu, Vasilică Ciocan, Marina Verdeș and Robert Ștefan Vizitiu

Faculty of Civil Engineering and Building Services, “Gheorghe Asachi” Technical University of Iasi-Romania, Blvd. Mangeron, No. 1, 700050 Iasi, Romania; andrei.burlacu@academic.tuiasi.ro (A.B.);

vasilica.ciocan@academic.tuiasi.ro (V.C.); marina.verdes@academic.tuiasi.ro (M.V.);

robert.vizitiu@tuiasi.ro (R.S.V.)

\* Correspondence: marius.branoaea@tuiasi.ro; Tel.: +40-751-299-671

<sup>†</sup> Presented at the 14th International Conference INTER-ENG 2020 Interdisciplinarity in Engineering, Mures, Romania, 8–9 October 2020.

Published: 11 December 2020

**Abstract:** The subject of buildings energy efficiency has gained increased interest in modern society. Recently, researchers aiming to reduce the energy demand of buildings have studied the implementation of phase change materials (PCMs) in various building elements. At the same time, researchers studied the implementation of unconventional technologies such as heat pipes (HP) in the buildings’ heating system. This paper combines both of these technologies in order to take advantage of the thermal storage properties of PCMs and overcome their reduced conductivity with heat pipes. Through computational fluid dynamics (CFD) simulations, this paper studies and highlights that with the implementation of a PCM, a reduction of the daily energy demand is achieved through the increase in the discharge phase time.

**Keywords:** phase change material; floor heating; heat pipe; computational fluid dynamics

## 1. Introduction

Worldwide, energy consumption is increasing, and buildings require over 40% of the global energy demand. In terms of emissions, buildings produce over 30% of the global net greenhouse gas emissions as a result of the increase in the indoor residence time and subsequently the surge in the requirements for indoor thermal environments and the heavy increase in urbanization, deforestation, and global climate change [1].

The increase in the global energy demand is one of the key reasons for the degradation and unstable development of our planet. This increase in the worldwide energy demand is a result of the rise in population coupled with better accessibility to energy of developing countries. Currently, a big portion of the global energy production is represented by fossil fuels; this has a drastic impact on the environment due to the greenhouse gas emissions. Since energy demand and the gross domestic product (GDP) growth of a country are linked, a policy towards the reduction of the energy demand would have a negative impact towards the GDP, and since the growth of renewable energies is slower than the rise in energy demand, an increase in energy efficiency can have a significant impact [2–4].

On a European scale, in order to overcome the drawbacks and to reduce the impact energy has on the climate, the European Parliament adopted a legislation in 2012 with the aim to reduce CO<sub>2</sub> emissions by 20% by 2020 in comparison to the values recorded in 1990. Studies showed that this goal would not be met by the proposed deadline, and as a result, the target year was set to 2030, but the required reductions values were imposed to 27% for the energy demand and 40% for the CO<sub>2</sub> emissions [5].



PCMs are special materials that are capable of storing increased quantities of thermal energy in comparison to other materials through the phase transition process. There are two main ways of storing thermal energy, in the form of sensible heat, when the temperature of the material increases, the material phase being unchanged during this process, and in the form of latent heat, when the material receives thermal energy, changing its phase in the process, the materials that store latent heat being called phase change materials. PCMs can be classified in three categories: solid–liquid PCMs, solid–gas PCMs and liquid–gas PCMs, but among these categories, solid–liquid PCMs are the most commonly used [6–8].

In order to address the global concerns regarding topics such as energy consumption, energy efficiency, and sustainable buildings, researchers interest towards PCM has increased drastically in the last decades, highlighted by the number of publications and research articles, Figure 1.

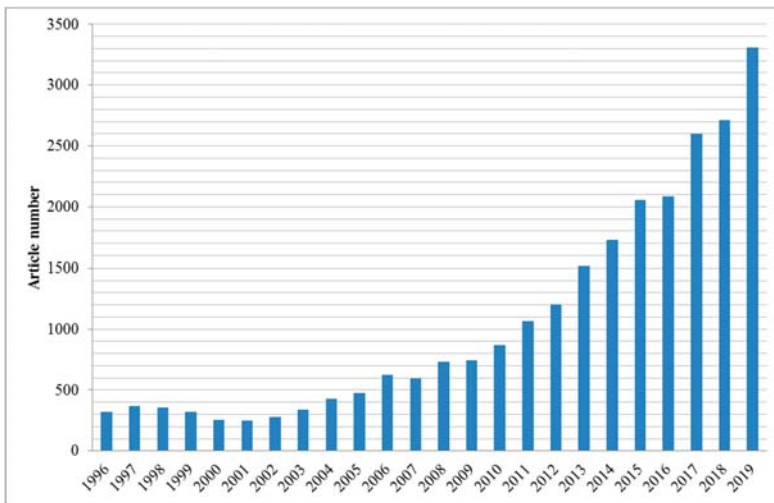


Figure 1. Worldwide PCM research articles between 1996 and 2019.

The interest in phase change materials in the scientific community is highlighted by the increased interest towards their applications in buildings and their integration in various building elements such as walls [9–13], windows [14,15], ceilings [16,17], floors [18–23].

Heat pipes are highly efficient heat exchangers, being able to rapidly transfer high quantities of thermal energy across a small temperature gradient. A key advantage of heat pipes is their capability to quickly transfer heat from one of their ends to the other one with a reduced heat loss in comparison to other materials; thus, heat pipes can be regarded as “superconductors” [24].

Heat pipe applications in buildings also include the possibility to integrate them in glazed facades to take advantage of the solar radiation [25] to recover the waste heat [26].

The objective of this research is the study of a HPHS with an original design and analyzing the advantages and disadvantages obtained through integrating a PCM into this system.

## 2. Research Methodology

To achieve the objective of the research paper, studies for an originally designed heat pipe floor heating system were performed using the ANSYS Fluent CFD software in order to simulate the correct operation of two floor heating systems, a floor heating system that uses heat pipes as heat exchangers, and the same heat pipe heating system with an integrated phase change material layer.

For the study, a floor heating system with heat pipes was designed; the heat pipes heat the floor from two opposing sides in order to ensure a uniform distribution of the temperature for the floor.

As a primary agent, water was chosen, being the most commonly used working fluid for floor heating systems. After using this system, two cases were analyzed, the system heating a regular concrete floor and the system heating a concrete floor with an integrated PCM layer; the PCM layer is represented between two layers of concrete, because due to the phase transition process, shape stabilization is a problem that needs to be resolved.

The research is based on multiple CFD simulations using the ANSYS STUDENT 2019 R3 package and addressed the heat transfer of both cases during the heating and cooling cycles in order to demonstrate the system feasibility. The 3D modelling was realized with the DesignModeler part of the package, as highlighted in the horizontal and vertical sections in Figures 2 and 3.

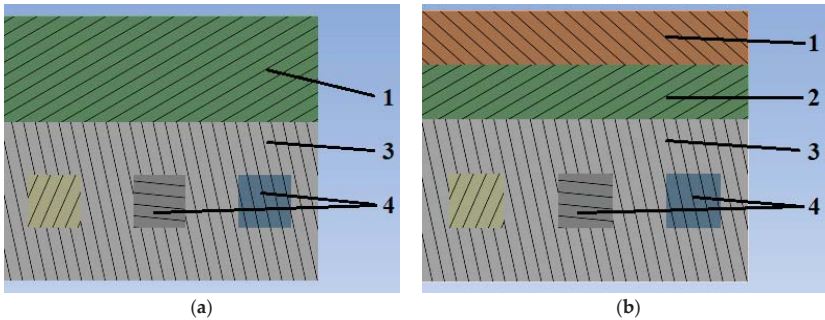


**Figure 2.** A vertical section of the models highlighting the different layers of both models: (a) The HPHS (b) The PCMHPHS: 1. First concrete layer. 2. PCM layer. 3. Second concrete layer. 4. Rectangular heat pipes.

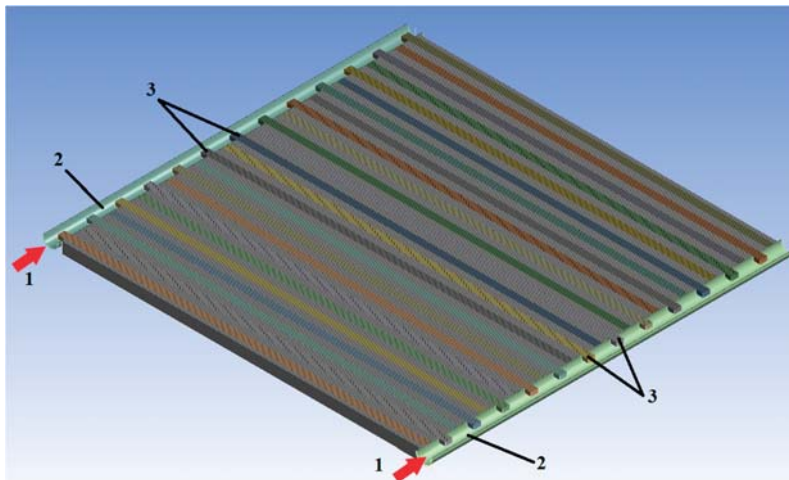


**Figure 3.** A horizontal section through the heat pipes and distributor. 1. Hot water inlet. 2. Distributors. 3. Rectangular heat pipes.

The analyzed models' geometry and dimensions are as follows:

- first concrete layer  $500 \times 500 \times 20/10$  mm
- PCM layer  $500 \times 500 \times 10$  mm
- second concrete layer  $500 \times 500 \times 30$  mm
- rectangular heat pipes  $10 \times 10$  mm, 510 mm in length

- two-circular distributors 22 mm in diameter, 500 mm in length.

In terms of mesh initialization, sizing, and quality, linear element order with a 5 mm element size was imposed, and for the mesh quality, a target skewness of 0.8 was set, as presented in Figure 4.

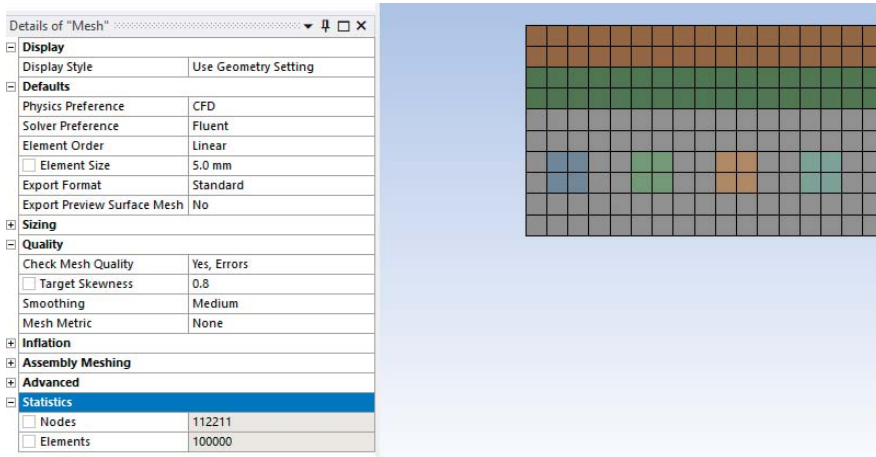


Figure 4. Model mesh sizing and initialization.

To have an accurate representation of CFD simulation for the models in the case of the PCM model apart from the energy equation, the solidification/melting model was used.

For the phase change material, a paraffin, RT 21 HC, produced by Rubitherm Technologies GmbH [27] was considered, because it presents impressive purity and specific composition, which translates to increased latent heat capacity with a small temperature range, the performance of the material remaining high for the phase change cycles as a result of the long lifetime of the material. The paraffin properties are shown in Table 1.

Table 1. RT 21 HC Material properties.

Characteristics	Value	Units
Melting area	20–23	[°C]
Solidification area	19–21	[°C]
Heat storage capacity	190	[kJ/kg]
Specific heat capacity	2	[kJ/kg·K]
Density solid (at 15 °C)	0.88	[kg/L]
Density liquid (at 25 °C)	0.77	[kg/L]
Heat conductivity	0.2	[W/(m·K)]
Max. operation temperature	45	[°C]

The reference temperature for the water inlet was considered to be 35°C, because it is a standard operating temperature for the working fluid in an underfloor heating system.

The initial temperature during the heating phase of the system was considered 10 °C.

In terms of the cooling phase, the temperature of 10 °C was imposed on the upper surface.

### 3. Results and Discussion

In order to analyze the thermal storage capacity of both systems, complete charging/discharging cycles were simulated.

The numerical simulation shows that in this case, the heating phase of the HPHS reached a convergence temperature after 30 min and 40 s. The heat pipes' thermal properties are highlighted

through the second section, presenting that the heat pipes start heating the concrete layer in less than 1 min (Figure 5). The cooling phase for the HPHS lasted 68 min (Figure 6).

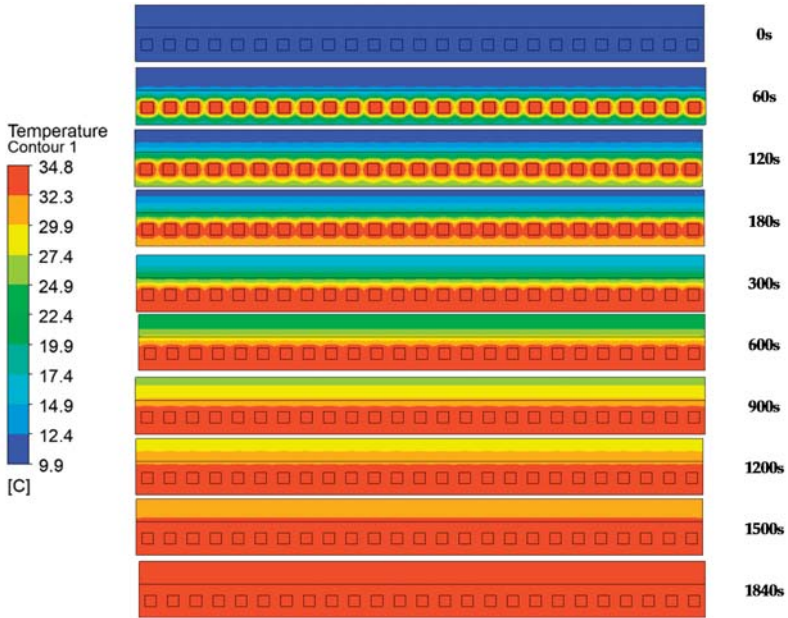


Figure 5. A section through the HPHS during the heating phase.

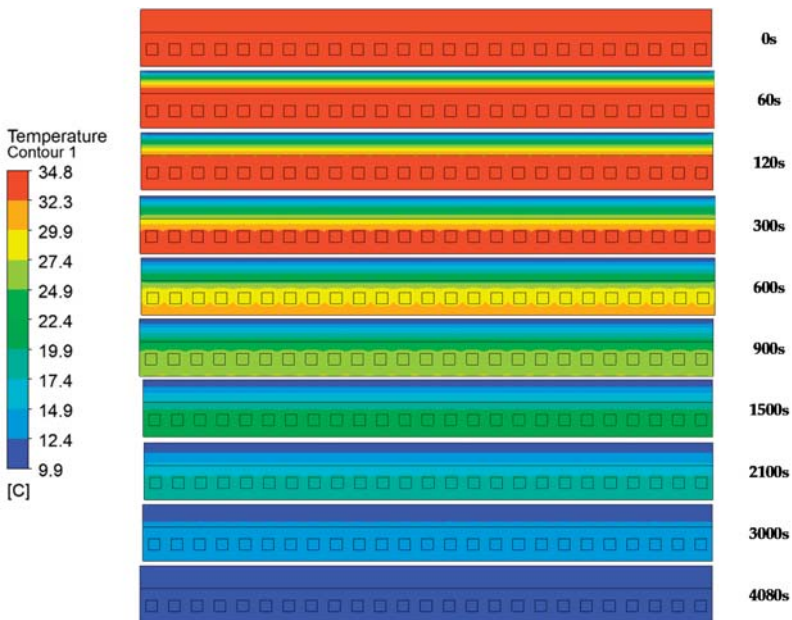


Figure 6. A section through the HPHS during the cooling phase.

In the case where a PCM layer was integrated, from the liquid fraction during the heating phase the PCM melting can be viewed; the PCM started melting around after 500 s, and it is fully melted after 4800 s; from the point the PCM starts melting, it takes almost 72 min for the PCM to fully melt (Figure 7). The system is fully heated after 127 min (Figure 8).

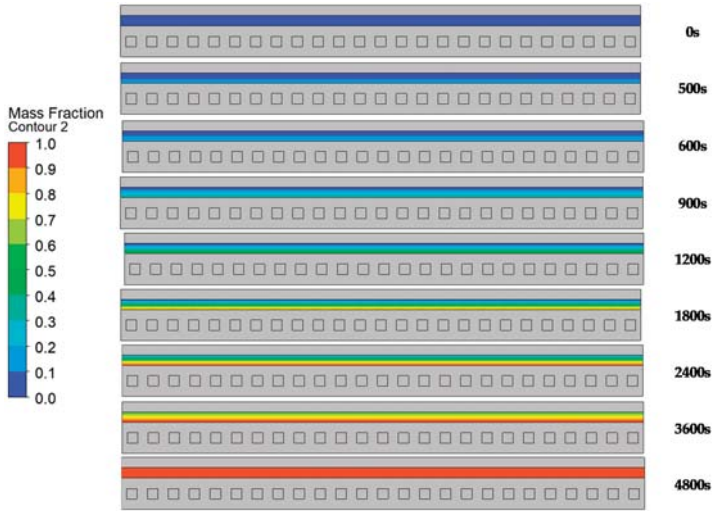


Figure 7. A section through the PCMHPHS during the heating phase, displaying the PCM liquid fraction over time.

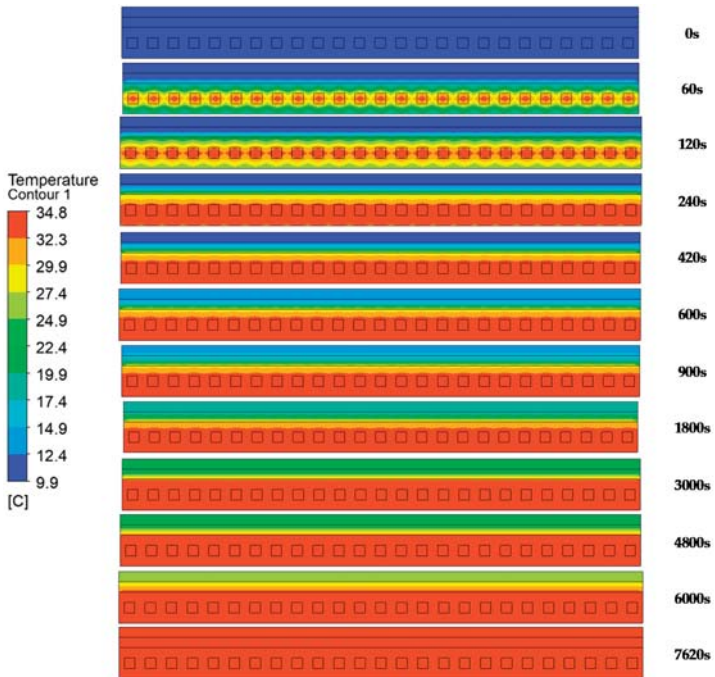
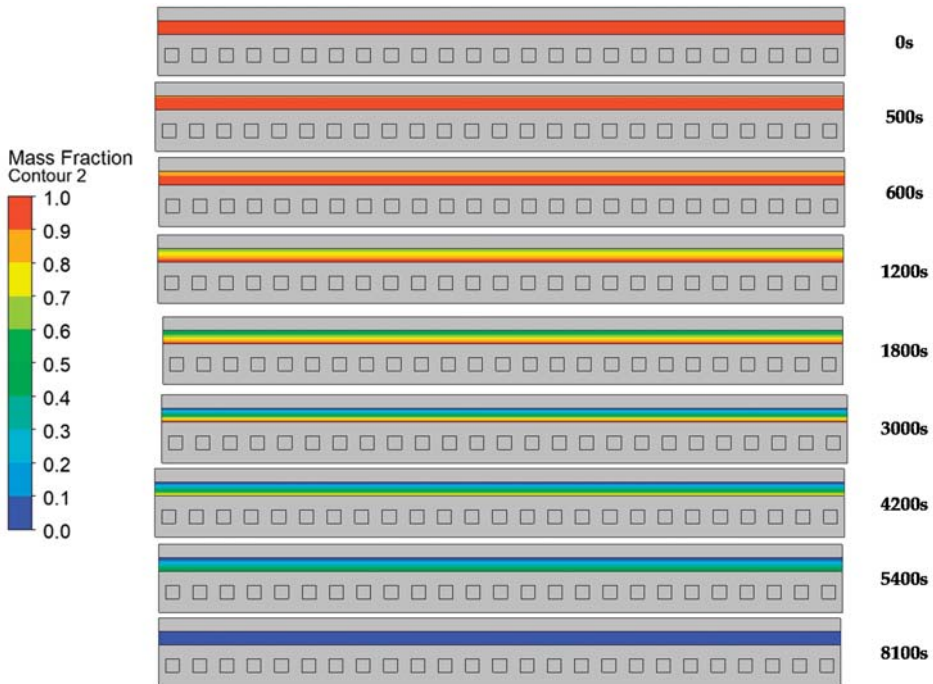


Figure 8. A section through the PCMHPHS during the heating phase.

During the cooling process, the PCM properties are evidenced through the liquid fraction; the PCM starts melting solidifying in under 10 min, but the solidification period is prolonged, reaching a fully solid state, 99.7%, after 135 min (Figure 9).



**Figure 9.** A section through the PCMHPHS during the cooling phase, displaying the PCM liquid fraction over time.

In case of the second heating system, with a layer of PCM, the discharge period is drastically prolonged in comparison to the system without the PCM; the system is fully cooled down after over 290 min, proving that PCMs can be used in buildings to increase the thermal energy storage (Figure 10).

From the figures, the thermal properties of the HPHS can be observed during the heating and cooling phase, and through adding a PCM layer, the thermal properties of the PCMHPHS change, the second system having a greatly increased discharge phase, but as a result, the heating phase is also increased. Due to an increase in both the heating and cooling time for the second system in comparison to the HPHS, a direct comparison of the heating and cooling time was not used; thus, an analysis on the number of cycles in a 24 h period was used, while recording the charging and discharging time.

Following the numerical simulations, the time for each case was recorded for the heating and cooling cycles (Figure 11) and used to make a comparison between the two systems.

Considering the heating and cooling time for both systems to make a comparison in terms of energy consumption, 24 h uninterrupted cycles were analyzed; thus, the HPHS would require 14.59 cycles over a 24 h period, and the PCMHPHS required 3.45 cycles.

Afterwards, knowing the number of cycles and the heating time, the number of daily hours the heating source would operate is 7.46 h/day for the heat pipe floor heating system and 7.30 h/day for the PCM integrated heat pipe floor heating system.

The results highlight that the HPHS can be a viable alternative to a classic heating system; furthermore, by integrating a PCM into the structure of the floor, a further reduction in the number of working hours for the heating source can be achieved.



In order to further verify these results, further research will be realized through studying the system in comparison to various classic floor heating systems on real scale models and an analysis on the efficiency of different types of PCMs in floor heating systems.

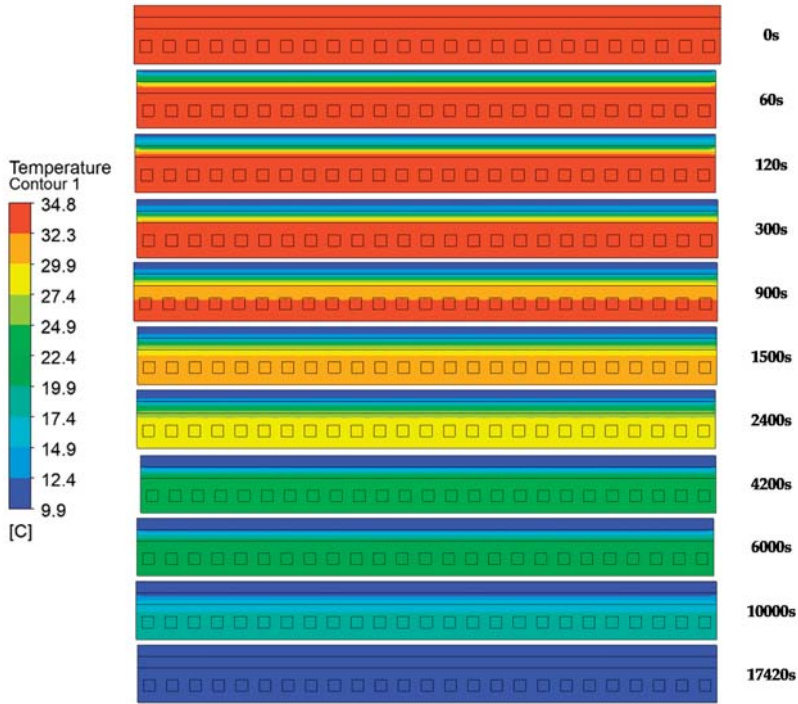


Figure 10. A section through the PCMHPHS during the cooling phase.

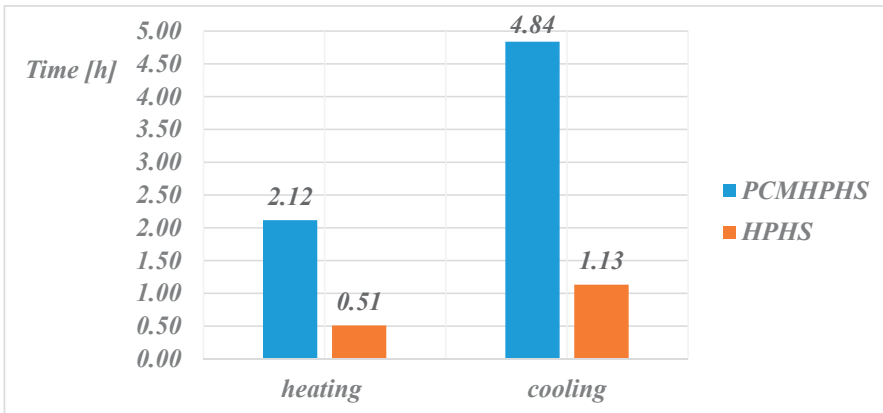


Figure 11. The results for the heating/cooling cycles.

#### 4. Conclusions

The originally designed heat pipe floor heating system harnesses the properties of heat pipes in order to heat the floor in an efficient way and through integrating a PCM in this system a prolonged

discharge period can be achieved, highlighting that both technologies have great potential to reduce the energy consumption in buildings.

The proposed heat pipe floor heating system requires a number of 7.46 h/day for heating, while the PCM integrated system requires 7.30 h/day. Apart from the reduction in the required time for heating through integrating a PCM, a further reduction in costs can be achieved through programming and automation if the heating cycles are set during off-peak periods, taking advantage of the PCM thermal energy storage properties.

**Conflicts of Interest:** The authors declare no conflict of interest.

## Nomenclature

HP	Heat Pipe
PCM	Phase Change Material
HPHS	Heat Pipe Heating System
PCMHPHS	Phase Change Material integrated Heat Pipe Heating System
T	Temperature, [°C]

## References

1. Cao, X.; Dai, X.; Liu, J. Building energy-consumption status worldwide and the state-of-the-art technologies for zero-energy buildings during the past decade. *Energy Build.* **2016**, *128*, 198–213. [CrossRef]
2. Akalpler, E.; Shingil, M.E. Statistical reasoning the link between energy demand, CO<sub>2</sub> emissions and growth: Evidence from China. *Procedia Comput. Sci.* **2017**, *120*, 182–188. [CrossRef]
3. Fotis, P.; Karkalakos, S.; Asteriou, D. The relationship between energy demand and real GDP growth rate: The role of price asymmetries and spatial externalities within 34 countries across the globe. *Energy Econ.* **2017**, *66*, 69–84. [CrossRef]
4. IEA. Global Energy Review 2020. IEA. Paris. Available online: <https://www.iea.org/reports/global-energy-review-2020> (accessed on 7 February 2020).
5. Cambeiro, F.P.; Armesto, J.; Bastos, G.; López, J.I.P.; Barbeito, F.P. Economic appraisal of energy efficiency renovations in tertiary buildings. *Sustain. Cities Soc.* **2019**, *47*, 101503. [CrossRef]
6. Belz, K.; Kuznik, F.; Werner, K.F.; Schmidt, T.; Ruck, W. Thermal energy storage systems for heating and hot water in residential buildings. In *Advances in Thermal Energy Storage Systems*; Woodhead Publishing: Sawston, UK, 2015; pp. 441–465.
7. Lin, Y.; Jia, Y.; Alva, G.; Fang, G. Review on thermal conductivity enhancement, thermal properties and applications of phase change materials in thermal energy storage. *Renew. Sustain. Energy Rev.* **2018**, *82*, 2730–2742. [CrossRef]
8. Magendran, S.S.; Khan, F.S.A.; Mubarak, N.M.; Vaka, M.; Walvekar, R.; Khalid, M.; Abdullah, E.C.; Nizamuddin, S.; Karri, R.R. Synthesis of organic phase change materials (PCM) for energy storage applications: A review. *Nano-Struct. Nano-Obj.* **2019**, *20*, 100399. [CrossRef]
9. Kong, X.; Wang, L.; Li, H.; Yuan, G.; Yao, C. Experimental study on a novel hybrid system of active composite PCM wall and solar thermal system for clean heating supply in winter. *Sol. Energy* **2020**, *195*, 259–270. [CrossRef]
10. Wang, H.; Lu, W.; Wu, Z.; Zhang, G. Parametric analysis of applying PCM wallboards for energy saving in high-rise lightweight buildings in Shanghai. *Renew. Energy* **2020**, *145*, 52–64. [CrossRef]
11. Rathore, P.K.S.; Shukla, S.K. Potential of macroencapsulated pcm for thermal energy storage in buildings: A comprehensive review. *Constr. Build. Mater.* **2019**, *225*, 723–744. [CrossRef]
12. Pirasaci, T. Investigation of phase state and heat storage form of the phase change material (PCM) layer integrated into the exterior walls of the residential-apartment during heating season. *Energy* **2020**, *207*, 118176. [CrossRef]
13. Bejan, A.S.; Catalina, T. The implementation of Phase Changing Materials in energy-efficient buildings. Case Study: EFdeN Project. *Energy Procedia* **2016**, *85*, 52–59. [CrossRef]
14. Li, S.; Zou, K.; Sun, G.; Zhang, X. Simulation research on the dynamic thermal performance of a novel triple-glazed window filled with PCM. *Sustain. Cities Soc.* **2018**, *40*, 266–273. [CrossRef]



15. Hu, Y.; Heiselberg, P.K. A new ventilated window with PCM heat exchanger—Performance analysis and design optimization. *Energy Build.* **2018**, *169*, 185–194. [CrossRef]
16. Weinsläder, H.; Klinker, F.; Yasin, M. PCM cooling ceilings in the Energy Efficiency Center—Regeneration behaviour of two different system designs. *Energy Build.* **2017**, *156*, 70–77. [CrossRef]
17. Yasin, M.; Scheidemantel, E.; Klinker, F.; Weinsläder, H.; Weismann, S. Generation of a simulation model for chilled PCM ceilings in TRNSYS and validation with real scale building data. *J. Build. Eng.* **2019**, *22*, 372–382. [CrossRef]
18. Yun, B.Y.; Yang, S.; Cho, H.M.; Chang, S.J.; Kim, S. Design and analysis of phase change material based floor heating system for thermal energy storage. *Environ. Res.* **2019**, *173*, 480–488. [CrossRef]
19. Lu, S.; Xu, B.; Tang, X. Experimental study on double pipe PCM floor heating system under different operation strategies. *Renew. Energy* **2020**, *145*, 1280–1291. [CrossRef]
20. Faraj, K.; Faraj, J.; Hachem, F.; Bazzi, H.; Khaled, M.; Castelain, C. Analysis of underfloor electrical heating system integrated with coconut oil-PCM plates. *Appl. Therm. Eng.* **2019**, *158*, 113778. [CrossRef]
21. Guo, J.; Jiang, Y.; Wang, Y.; Zou, B. Thermal storage and thermal management properties of a novel ventilated mortar block integrated with phase change material for floor heating: An experimental study. *Energy Convers. Manag.* **2020**, *205*, 112288. [CrossRef]
22. Mays, A.E.; Ammar, R.; Mahamad, H.; Akroush, M.A.; Hachem, F.; Khaled, M.; Ramadan, M. Using phase change material in under floor heating. *Energy Procedia* **2017**, *119*, 806–811. [CrossRef]
23. Devaux, P.; Farid, M.M. Benefits of PCM underfloor heating with PCM wallboards for space heating in winter. *Appl. Energy* **2017**, *191*, 593–602. [CrossRef]
24. Reay, D.A.; McGlen, R.J.; Kew, P.A. *Heat Pipes, Theory, Design and Applications*, 6th ed.; Elsevier: Oxford, UK, 2014.
25. Burlacu, A.; Lăzărescu, C.D.; Ciocan, V.; Verdeş, M.; Balan, M.C.; Şerbănoiu, A.A. CFD Heat Transfer Analysis for Heat Pipes Integration into Buildings with Glazed Façades. *Procedia Eng.* **2017**, *181*, 658–665. [CrossRef]
26. Burlacu, A.; Sosoi, G.; Vizitiu, R.Ş.; Bărbuţă, M.; Lăzărescu, C.D.; Ciocan, V.; Şerbănoiu, A.A. Energy efficient heat pipe heat exchanger for waste heat recovery in buildings. *Procedia Manuf.* **2018**, *22*, 714–721. [CrossRef]
27. PCM RT-LINE. Wide-Ranging Organic PCM for Your Application. Available online: <https://www.rubitherm.eu/en/index.php/productcategory/organische-pcm-rt> (accessed on 7 February 2020).

**Publisher's Note:** MDPI stays neutral with regard to jurisdictional claims in published maps and institutional affiliations.



© 2020 by the authors. Licensee MDPI, Basel, Switzerland. This article is an open access article distributed under the terms and conditions of the Creative Commons Attribution (CC BY) license (<http://creativecommons.org/licenses/by/4.0/>).

Article

# Technical-Economic Analysis of a Hybrid Thermal Energy Supply System Based on Renewable Energy Sources <sup>†</sup>

Roxana Pătraşcu <sup>\*</sup>, Constantin Ionescu, Mihai Rareş Sandu  and Diana Ban (Tuţica)

Department of Energy Generation and Use, Power Engineering Faculty, University POLITEHNICA of Bucharest, 060042 Bucharest, Romania; ionescu.constantin@upb.ro (C.I.); mihai\_rares.sandu@upb.ro (M.R.S.); dianatutica@yahoo.fr (D.B.)

\* Correspondence: op3003@yahoo.com

† Presented at the 14th International Conference INTER-ENG 2020 Interdisciplinarity in Engineering, Mureş, Romania, 8–9 October 2020.

Published: 14 December 2020

**Abstract:** The technical-economic analysis represents a decisional factor in the implementation of a new thermal energy supply system and is a key part of the feasibility study. In the present paper, the economic performance indicators, used as evaluation instruments within the analysis, highlight the economic efficiency of each proposed scenario and offer an establishment of hierarchy for them. Based on this analysis, the optimal scenario can be recommended, such that the benefits are maximized. The sensibility analysis, performed for the optimal scenario at the end of the paper, shows an estimation of the effects throughout the lifespan of the new system. This is beneficial to pre-empt negative effects or to stimulate the factors that can increase the efficiency of the system throughout the entire lifespan.

**Keywords:** renewable energy sources; thermal energy supply; technical-economic efficiency; performance indicators; optimisation

---

## 1. Introduction

Mainly, through a technical-economic analysis, the effects of an investment project are assessed together with the implementation profitability of the project throughout the entire lifetime. The analysis within the feasibility study is holistically performed, combining technical and economic aspects, on which the optimal solution is determined. The economic performance indicators are strictly dependent on the equipment of the technical solution and its characteristics. The calculations performed within the economic analysis, throughout a relatively long period of time, take into account considerations, premises, and a set of hypotheses compatible with the analysed project, which are lowering the uncertainty degree of the analysis.

In the present paper, a comparative analysis from an economical perspective is performed for a hybrid thermal energy supply system with different operating scenarios, in order to identify the optimal solution.

Defining and determining the financial-economic performance indicators associated with the proposed scenarios for the hybrid thermal energy supply system offers the possibility to identify the optimal operating scenario. For given conditions, this scenario will minimize the financial effort and risks while increasing the benefits.

The main purpose of the project that will be implemented is to cover the thermal energy demand of a building from the campus of University Politehnica of Bucharest (UPB) using a hybrid thermal

energy supply system based on renewable energy sources, and to inject the overproduction of heat into UPB's district heating network. Therefore, the following objectives are proposed:

- Generate three forms of energy (electricity, heat, and cold) based on a hybrid renewable energy source (geothermal and solar), in which the electricity produced will cover at least the consumption of the thermal energy generation unit (on a yearly basis).
- Fully cover the heating and cooling demand for the target building (TB) using thermal energy produced from 100% renewable energy sources [1].
- The reintegration of the TB into the UPB heat distribution network (UPB DH) to inject the overproduction of heat.
- Develop a modular concept that will ease the process of replication and scaling.

## 2. Description of Hybrid Thermal Energy Supply System

The energy audit of the target building (TB) and the UPB DH led to the development of a new solution for the thermal supply of the building, which ensures heating, cooling, and domestic hot water. It integrates technologies based on renewable sources, namely a ground-to-water heat pump (HP), solar hybrid photovoltaic panels (PVT), and photovoltaic panels (to cover the power consumption of the thermal installation). The proposed solution also involves the replacement of the heat and cold distribution system of the building, as well as the implementation of a new internal hot/cold water distribution system (pipelines, appliances, and final consumers). The structure of the hybrid system is presented in Figure 1 [2].

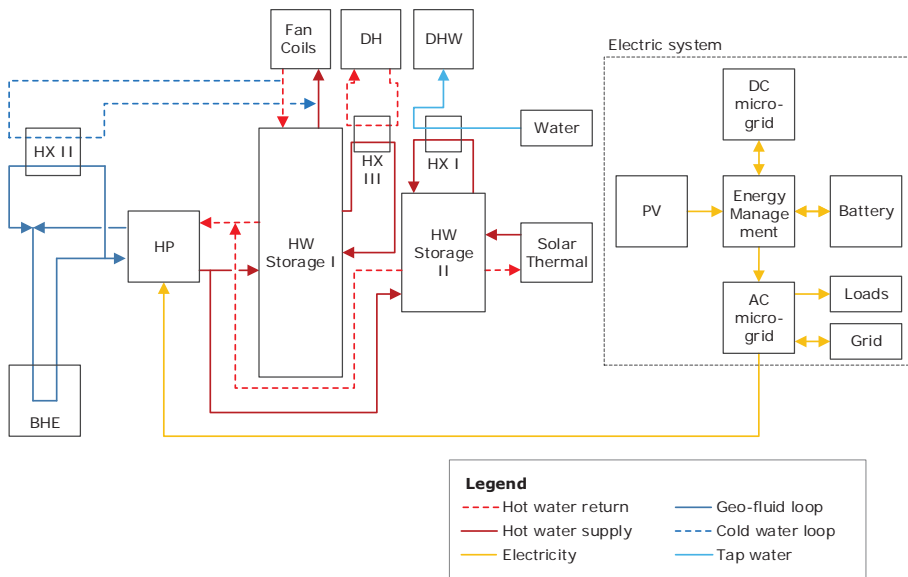


**Figure 1.** Structure of hybrid thermal energy supply system. BHE—borehole heat exchanger; HX—heat exchanger; DH—district heating; HP—heat pump; HW—hot water; DHW—domestic hot water; PV—photovoltaic panels; DC—direct current.

The energy capacity of the proposed solution will allow ensuring the indoor comfort in the target building's spaces, safety, and flexibility in the supply of thermal energy, as well as the delivery in the DH system of UPB of a share of thermal energy produced from renewable sources.

The design of the hybrid system and sizing of the equipment is based on the thermal energy demand of the analysed building. An oversize of about 30–40% was considered in order to achieve the

injection of heat into the local district heating network. In Table 1, the consumption of thermal and electrical energy of the target building and the production ensured by the proposed hybrid solution are summarized.

**Table 1.** Consumption of thermal and electrical energy of target building and the productions related to the hybrid solution.

Energy Consumption/Energy Production	UM	Value
- thermal energy production—heating	MWh	281.00
- thermal energy consumption—heating	MWh	127.00
- thermal energy consumption injection—DH	MWh	154.00
- electricity consumption for cold production	MWh	4.43
- electricity consumption for production—DHW	MWh	0.69
- electricity production from PV + PVT	MWh	50.00
- electricity consumption for building heating (related to GT-S scheme)	MWh	42.33
- electricity consumption for heat injection (related to GT-S scheme)	MWh	51.33
- total electricity consumption (related to GT-S scheme)	MWh	93.67
- reduced CO <sub>2</sub> through the GT-S scheme for the building	t/year	31.88
- reduced CO <sub>2</sub> through the GT-S scheme for the network	t/year	32.00
- building heating gas consumption	MWh/year	138.00
- combined heat power plant heating gas consumption (equivalent to injection)	MWh/year	192.50
- total gas consumption	MWh/year	330.50

### 3. Definitions of Scenarios, Characteristics, and Considerations

The technical-economic analysis was performed for three scenarios, in which functioning, economical, and marketing aspects were considered.

In the definitions of the scenarios the followings were considered:

- The thermal energy demand of the building
- Its reintegration into the centralized heat supply system of UPB by injecting a quantity of heat [3,4].

The aspects considered in the technical-economic analysis, valid for all scenarios, were the following:

- As a reference, the current heat supply of the building from a local thermal power plant, which uses natural gas, was considered.
- The production of electricity resulting from photovoltaic panels, as well as from PVT, covers a part of the electrical consumption of the thermal scheme, namely the one related to ensuring the necessary heat and cold of the building [5].
- By implementing the new solution, based on renewable sources, the CO<sub>2</sub> emissions were reduced both at the level of the building frame and the analysed system, this reduction being directly proportional to the reduction of the consumption of primary resources (saved natural gas) [6].
- The value of CO<sub>2</sub> certificates related to reducing the amount of CO<sub>2</sub> by implementing the new energy supply solution were considered as revenues, or *virtual receipts*.
- The share provided by UPB was considered as the value of the investment from its own funds. The difference up to the total value of the investment that the analysed solution implies is considered non-reimbursable from European funds (grants).
- The calculations were performed in two ways:
  1. The value of the investment was equal to the insured quota from the UPB budget.
  2. The value of the investment was equal to the total investment costs assumed by the implementation of the new solution.

Characteristic aspects of Scenario 1:

- By implementing the thermal energy supply solution of the building based on the integration of geothermal-solar systems, it is considered that natural gas saving is achieved both for the building

and the centralized heat supply system of UPB (corresponding to the production of heat injected into the system). This economy is quantified economically by the *annual saving of expenses with the fuel (natural gas) saved*.

- The total annual expenses include both the maintenance and operation expenses related to the solution, as well as the expenses related to the annual electricity consumption, in addition to the production provided by the photovoltaic panels.

Characteristic aspects of Scenario 2:

- The virtual receipts of “virtual sales” of the entire amount of heat produced by the implementation of the proposed scheme were considered as income.
- The price of the “sold” heat was considered equal to the price in the UPB invoice.

Characteristic aspects of Scenario 3:

- The virtual receipts of “virtual sales” of the share of the heat produced by the new system, related to the injection into the centralized UPB system, were considered as income.
- It was considered that a natural gas saving is achieved at the level of the building, corresponding to the coverage of the heat demand for its heating. This economy was quantified economically by the *annual saving of expenses with the fuel (natural gas) saved*.

#### 4. Methodology of Technical-Economic Analysis

The technical-economic analysis of the proposed scenarios was mainly based on three economic efficiency indicators with present values, which were determined for each described scenario considering the above-mentioned conditions and maintaining, at the same time, the hypothesis and general considerations [7,8].

##### 4.1. Net Present Value (NPV)

The NPV represents the algebraic amount of annual net income updated over the entire period of activity considered (lifetime). The analytical form of the indicator depends essentially on the reference point considered for the update.

In the case of the present economic analysis, the moment of starting the investment project was considered as a reference moment.

The net present value is given by the following equation:

$$NPV = \sum_{i=1}^n \frac{IN_i - C_i - I_i}{(1 + a)^i} \quad (1)$$

where

$IN_i$  are the receipts made in the year “ $i$ ”;

$C_i$  are the operating expenses for the year “ $i$ ”, excluding depreciation;

$I_i$  are the investments made from European non-reimbursable funds (grant) in the year “ $i$ ” (the investment is made in one year, in the year “1”)

$a$  is the discount rate considered, and  $n$  is the duration of the study. The time period for which the discounted net income was calculated was  $n = 20$  years.

An analysed solution is economically efficient if  $NPV \geq 0$ , and in the case of comparing several solutions, the optimal solution corresponds to the condition  $NPV = \max [9,10]$ .

#### 4.2. Internal Rate of Return

The internal rate of return (IRR) of an investment is the discount rate ( $a_0$ ) for which the net present value is cancelled, respectively:

$$NPV = \sum_{i=1}^n \frac{IN_i - C_i - I_i}{(1 + a_0)^i} = 0 \tag{2}$$

$$IRR = a_0 \tag{3}$$

The solution of Equation (2) results from attempts of an iterative calculation, due to the fact that the equation cannot be solved analytically.

The IRR value was interpreted as the percentage interest that could be accepted for both the investment and the working capital so that the proposed investment project does not produce losses.

It is worth noting the following:

- The internal rate of return (IRR) was used to estimate the economic efficiency of each solution proposed and analysed individually. The IRR cannot be used to compare several solutions as it may lead to false conclusions.
- The profitability of a project (solutions) was interpreted in relation to the IRR value, as follows: if the IRR has a unique value (in this analysis, only this situation is taken into account), the project is profitable if  $a \geq IRR$  (the comparison was made with values of the discount rate in the range of 5–10%).

#### 4.3. Payback Period

The payback period ( $PP$ ) is defined as the number of years ( $n_r$ ) for which the condition is met:

$$NPV = \sum_{i=1}^{n_r} \frac{IN_i - C_i - I_i}{(1 + a)^i} = 0 \tag{4}$$

$$PP = n_r \tag{5}$$

where  $PP$  represents the objective duration of exploitation, at the end of which the initial investment can be covered and an additional income corresponding to the considered discount rate can be achieved [9,10].

Defining the payback period requires establishing an origin of time. The accepted convention is to calculate this duration starting from the moment of implementation of the respective objective.

The decision to accept or eliminate an investment project should be taken by comparing the recovery period of the capital " $n_r$ " with the lifetime of the objective " $n$ " (in the analysed case, 20 years). Theoretically, if  $n_r \leq n$ , the investment project can be accepted, bringing net updated incomes, and if  $n_r > n$ , the project must be rejected; it will not bring net incomes over the lifetime of the proposed solution.

In practice, the project is considered economically efficient based on this indicator, if the value calculated for the  $PP$  is compared with a reference value ( $T_r$ ), called the standard return of investment. From the literature, it results that the standard term is in the following range:

$$T_r \leq \left(\frac{1}{2} \div \frac{1}{3}\right) \cdot n \tag{6}$$

A particular case is the gross value of the payback period ( $GPP$ ), which does not take into account the discount rate ( $a$ ). The value for the  $GPP$  is determined at the beginning of the investment and is defined as the following:

$$GPP = \frac{I}{IN - C} \tag{7}$$

## 5. Results of the Analysis

The technical-economic comparison of the proposed solutions was made over a study period equal to a lifetime of 20 years for both proposed solutions, based on the calculation of economic performance indicators with updated values: the net present value (NPV), the internal rate of return (IRR), and the payback period (PP) [11,12]. The considerations and hypotheses mentioned in the previous paragraphs were taken into account.

The components of the income and expenditure flows related to the analysed solutions are presented in Table 2.

**Table 2.** Income and expenditure flows for the analysed scenarios.

Type of Cost [EUR]	Scenario 1		Scenario 2		Scenario 3	
	UPB Investment Share	Total Investment	UPB Investment Share	Total Investment	UPB Investment Share	Total Investment
Total investment [EUR]	52,000	279,747	52,000	279,747	52,000	279,747
Specific investment [EUR/kW]	812.5	4371	812.5	4371	812.5	4371
Total annual expenses [EUR/year]	-5992	-5992	5609	5609	765	765
Specific expenses [EUR/kW year]	93.7	93.7	87.7	87.7	12	12
Sales receipts [EUR/year]	1916	1916	19,801	19,801	11,718	11,718
Annual revenue [EUR/year]	7909	7909	14,192	14,192	10,953	10,953

Note: Negative values indicate cost savings.

The values of the economic performance indicators calculated for the analysed solutions, in the “University Politehnica of Bucharest (UPB) Investment option”, are summarized in Table 3.

**Table 3.** Performance indicators values.

Economic Performance Indicator	Scenario 1	Scenario 2	Scenario 3
NPV [EUR]	55,482	140,877	96,857
PP [years]	7.80	4	5.2
GPP [years]	6.58	3.66	4.75
IRR [%]	14.13%	27.07%	20.56%

The optimal solution is one in which the following occurs:

- Virtual receipts of annual costs related to “virtual sales” of the entire amount of heat produced by the implementation of the proposed scheme are considered as income.
- The price of the “sold” heat is considered equal to the price in the UPB invoice.
- The value of the investment is equal to the quota provided by the UPB budget.

The summary of the results of the technical-economic analysis is presented in Table 4, while in Figure 2, the evolution curve of the payback period for all analysed scenarios is shown.

**Table 4.** Technical-economic analysis results.

Economic Performance Indicator	Scenario 1		Scenario 2		Scenario 3	
	UPB Investment Share	Total Investment	UPB Investment Share	Total Investment	UPB Investment Share	Total Investment
NPV [EUR]	55,482	-172,265	140,877	-86,870	96,857	-130,890
PP [years]	7.80	>lifetime	4	>lifetime	5.2	>lifetime
GPP [years]	6.58	35.37	3.66	19.71	4.75	25.54
IRR [%]	14.13%	-5.57%	27.07%	0.14%	20.56%	-2.22%

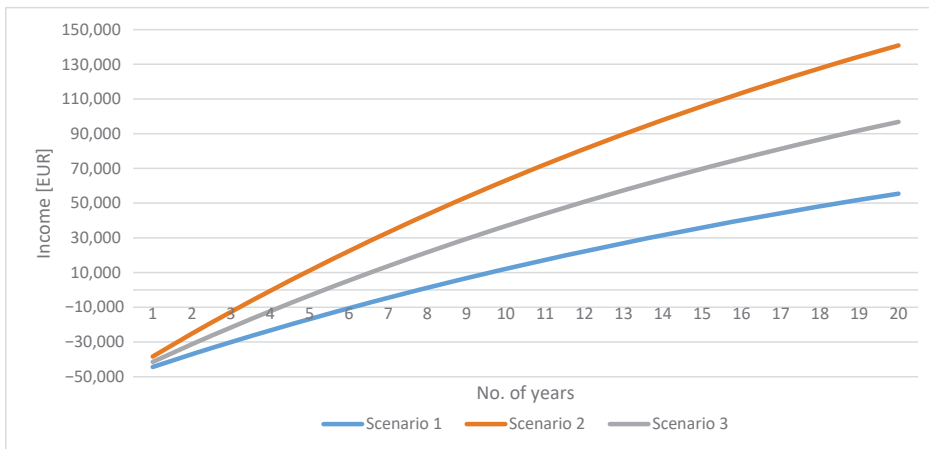


Figure 2. Payback period evolution for all scenarios.

## 6. Conclusions and Sensibility Analysis for Optimal Scenario

In all the analysed scenarios, when the integral value of the investment related to the new heat supply system is considered, the economic performance indicators are below the profitability limit [13]. This conclusion is highlighted by all the calculated indicators:

- NPV < 0
- GPP and PP > analysed system lifetime (20 years)
- IRR < 4%

This aspect was predictable due to the current high investment cost of the new technologies, but also due to small installed capacities, which do not allow significant compensation from high investments, with savings in energy costs and/or revenues resulting from “selling” the heat injected into the UPB centralized heat supply system.

To financially support the implementation of projects through which new technologies are implemented, which use renewable sources, the application of financial levers, such as non-reimbursable grants, are practised at the European level that allows the amortization of the investment in an acceptable period of time during the life of the objective. Considering this fact, the technical-economic calculation was used the share of the investment that returns as the investment effort of UPB, while the difference (up to the value of the total investment) being ensured by the WEDISTRICT H2020 project, Grant agreement ID: 857801, which aims to demonstrate that District Heating and Cooling systems can be built on a combination of renewable energy sources and waste heat recovery solutions.

Under these conditions, in all three analysed scenarios, the proposed solution is efficient from the technical-economic point of view, a conclusion resulting from the determined values of the economic performance indicators.

- NPV > 0
- GPP and PP < analysed system lifetime (20 years)
- IRR > 4%

The scenario in which the maximum values of the technical-economic indicators are obtained is Scenario 2, namely income, the “virtual receipts” of annual costs, related to “virtual sales” of the entire amount of heat produced by the implementation of the proposed scheme (Table 5).



**Table 5.** Results of the sensibility analysis.

Variable Factor	Solution 1			
	NPV [EUR]	DR [years]	PP [years]	IRR [%]
<b>a [%]</b>				
4	140,877	3.66	4	27.07
5	124,867	3.66	4	27.07
6	110,784	3.66	4	27.07
<b>e<sub>p</sub> [EUR/MWh]</b>				
100	150,966	3.48	4	28.53
117	140,877	3.66	4	27.07
140	127,228	3.94	4.1	25.07
<b>q<sub>p</sub> [EUR/MWh]</b>				
55	107,854	4.42	5	22.21
63.65	140,877	3.66	4	27.07
75	184,231	2.99	3.2	33.32
<b>CO<sub>2p</sub> [EUR]</b>				
25	136,537	3.75	4.1	26.43
30	140,877	3.66	4	27.07
35	145,218	3.58	4	27.70

To eliminate the degree of uncertainty of the prediction of certain quantities that intervene in the calculation of economic indicators for the entire analysed period (20 years), it is opportune to conduct a sensitivity analysis on the economic efficiency indicators to the variation of quantities that are relatively difficult to predict [14]. In this sense, the variation of NPV, IRR, PP were analysed for the optimal solution from a technical-economic point of view, depending on the following:

- discounting rate (4, 6, 8%)
- fuel price (natural gas), ( $\pm 5$ ,  $\pm 10\%$ ): to determine the extent to which the decrease in fuel price no longer allows recovery of the investment (pessimistic scenario—the limit of economic profitability of the proposed solution)
- electricity price: e<sub>p</sub> ( $\pm 5$ ,  $\pm 10\%$ )
- the price of the delivered heat: q<sub>p</sub> ( $\pm 5$ ,  $\pm 10\%$ )
- the value of CO<sub>2</sub> certificates: CO<sub>2p</sub> (30–35 EUR)
- annual maintenance expenses (biannual growth of  $\pm 1\%$ )

Only one size varied, the others remaining constant, at a value equal to that of the reference option. The sensitivity analysis was done only for the selected solution as the optimal one.

The increase in the discounted net revenue of the optimal solution was influenced by the increase in the annual revenue, depending on the following:

- the amount of heat injected into the centralized system
- the fluctuation of the related thermal energy price
- the value of carbon certificates

**Acknowledgments:** This work has received funding from the European Union’s Horizon 2020 research and innovation program, under grant agreement No 857801. This text reflects only the author’s views and the Commission is not liable for any use that may be made of the information contained therein.

## References

1. Acciona Engineering. *Project Management (Work) Plan, Internal Project Document*; Acciona Engineering: Madrid, Spain, 2019.
2. Acciona Engineering. *Pre-Assessment of Demo-Sites, Internal Project Document*; Acciona Engineering: Madrid, Spain, 2020.
3. Ecoheat4cities. Guidelines for Technical Assessment of District Heating Systems. Available online: [https://www.euroheat.org/wp-content/uploads/2016/04/Ecoheat4cities\\_3.1\\_Labelling\\_Guidelines.pdf](https://www.euroheat.org/wp-content/uploads/2016/04/Ecoheat4cities_3.1_Labelling_Guidelines.pdf) (accessed on 5 July 2020).
4. UNE-EN 15603:2008. Energy Performance of Buildings—Overall Energy Use and Definition of Energy Savings. 2008. Available online: <https://www.iso.org/standard/56226.html> (accessed on 1 January 2020).
5. ISO 52000-1:2017. Energy Performance of Buildings—Overarching EPB Assessment. Available online: <https://www.iso.org/standard/65601.html> (accessed on 1 January 2020).
6. Danish Energy Agency. *Finding You Cheapest Way to a Low Carbon Future—The Danish Levelized Cost of Energy Calculator*; Danish Energy Agency: København, Denmark, 2016.
7. Athanasovic, V.; Dumitrescu, I.S.; Pătrașcu, R.; Bitir, I.; Minciuc, E.; Alexe, F.; Cenuse, V.; Raducanu, C.; Coman, C.; Constantin, C. *Tratat de inginerie termică. District Heating—Cogeneration*; Agir, Academia de Științe Tehnice Publisher: Bucharest, Romania, 2010; ISBN 978–973-720-314–4.
8. Ea Energy Analyses. Renewable Energy Cost and Benefits for Society (RECABS). Final Technical Report. 2007. Available online: <http://iea-retd.org/wp-content/uploads/2011/09/RECABS-final-report.pdf> (accessed on 1 January 2020).
9. ExternE. External Cost of Energy. Available online: [http://www.externe.info/externe\\_d7/](http://www.externe.info/externe_d7/) (accessed on 7 July 2020).
10. NREL. Simple Levelized Cost of Energy (LCOE) Calculator Documentation. Available online: <https://www.nrel.gov/analysis/tech-lcoe-documentation.html> (accessed on 8 July 2020).
11. Evaluation Unit DG Regional Policy European Commission. *Guide to Cost-Benefit Analysis of Investment Projects*; European Union: Luxembourg, 2015.
12. DOE. Levelized Cost of Energy (LCOE). Available online: <https://www.energy.gov/sites/prod/files/2015/08/f25/LCOE.pdf> (accessed on 7 July 2020).
13. CEZ. Applicable Procedures for Design. Available online: [https://www.cez.ro/ckfinder/userfiles/files/cez/despre-noi/cez/d/proceduri-aplicabile-pentru-proiectare/metcalcularalindiceficielucrinvest\\_rev04.pdf](https://www.cez.ro/ckfinder/userfiles/files/cez/despre-noi/cez/d/proceduri-aplicabile-pentru-proiectare/metcalcularalindiceficielucrinvest_rev04.pdf) (accessed on 10 July 2020).
14. Diaconescu, I.; Pătrașcu, R.; Tuțică, D.; Ionescu, C.; Minciuc, E. Influence of technical and economic factors in the assessment of energy efficiency projects in industry. In Proceedings of the 2019 International Conference on ENERGY and ENVIRONMENT (CIEM), Timișoara, Romania, 17–18 October 2019.

**Publisher's Note:** MDPI stays neutral with regard to jurisdictional claims in published maps and institutional affiliations.



© 2020 by the authors. Licensee MDPI, Basel, Switzerland. This article is an open access article distributed under the terms and conditions of the Creative Commons Attribution (CC BY) license (<http://creativecommons.org/licenses/by/4.0/>).



# Technical-Economic Analysis of a Hybrid Energy Systems Composed of PV and Biomass Obtained from Municipal Solid Waste Connected to the Grid <sup>†</sup>

Daniel-Cornel Balan <sup>1,\*</sup>, Sorina-Mihaela Balan <sup>2</sup> and Juliana Szakacs <sup>3</sup>

<sup>1</sup> Doctoral School, Technical University from Cluj Napoca, 400114 Cluj-Napoca, Romania

<sup>2</sup> Strategies, Programs and Projects Department, Dimitrie Cantemir University from Targu Mures, 540139 Targu Mures, Romania; bsoinamihaela@yahoo.com

<sup>3</sup> Pharmacy, Science and Technology of Targu Mures, George Emil Palade University of Medicine, 540139 Targu Mures, Romania; szjulianna@gmail.com

\* Correspondence: bdsrl@yahoo.com; Tel.: +40-724-551-156

<sup>†</sup> Presented at the 14th International Conference INTER-ENG 2020 Interdisciplinarity in Engineering, Mures, Romania, 8–9 October 2020.

Published: 10 December 2020

**Abstract:** This paper describes the technical-economic analysis of a hybrid renewable energy systems (HRES) connected to the grid, consisting of photovoltaic (PV) source and municipal solid waste (MSW), taking into account economic and technical criteria. Photovoltaic energy and the new technology used for MSW processing have a lower cost and lower environmental impact. The sensitivity analysis shows that improving the rate of return on investment in HRES can be a measure to encourage the use of renewable energies for electricity production, both in terms of costs and environmental impact.

**Keywords:** solar photovoltaic power; biomass; grid-connected hybrid renewable energy system; prosumer

## 1. Introduction

Renewable Energies (RE) are an alternative worth exploring, as they are effective means of preventing and mitigating climate change, with undeniable external benefits in terms of environmental quality and economic value, especially in the case of photovoltaic (PV), wind, and biomass [1]. The main benefits of RE are in terms of environmental performance, as these sources are carbon-free (photovoltaic) or carbon-neutral (biomass), thus being a viable alternative to de-carbonizing energy generation. Another notable benefit of using RE is the re-evaluation of resources currently misused as well as the creation of local job opportunities. Energy waste technologies are beginning to capture the attention of developing countries as a sustainable source of energy in response to the worsening problem of municipal solid waste management. Waste-to-energy refers to the recovery of the energy from waste materials into usable heat, electricity, or fuel. Various WtE approaches are categorized into landfill, thermal treatment, and biological treatment [2]. Investments in waste-to-energy (WtE) technologies are widely discussed in the literature using the traditional valuation methods such as life cycle analysis (LCA), net present value (NPV), internal rate of return (IRR), payback period (PBP), and returns on investment (ROI). These methods do not cover some characteristics for assessing the project in WtE, the level of risk, such as the irreversibility of the investment project, investment risks, and uncertainty in future cash flows. WtE investment decisions are influenced by waste supply, legal and governmental risks, those related to technology, infrastructure, and socio-political and environmental risks [3]. We must not forget that the biomass has the merit of dispatching, which means that biomass energy is controllable and available when it is needed. Combining the photovoltaic system

with the biomass system could be an efficient way to create a reliable and cost-effective hybrid energy system. Photovoltaic systems are clean, environmentally friendly, and safe energy sources, and their installation has played an important role worldwide. Grid-connected photovoltaic systems can be Building Integrated Systems (BiPV), Distribution Generation (DGPV), and centralized photovoltaic plants. BiPV systems usually provide a specific load and inject the excess energy into the grid. On the other hand, DGPV systems inject all produced energy into the grid without supplying any local load. Grid-connected systems may consist of a PV array only as an energy source or another energy source may be incorporated with the PV array, such as a wind turbine, diesel generator, biomass, or a storage unit. The third type of grid-connected photovoltaic systems is centralized large photovoltaic systems connected to the utility distribution system. The size and performance of photovoltaic systems depend on meteorological data, and the productivity of the PV system is a location-dependent variable that varies depending on the climatic nature of the area. A good knowledge of climatic parameters, such as solar radiation and ambient temperature, is very important to understanding the total energy available for use in a photovoltaic system. The hybridized RE sources (HRES) are usually photovoltaic and wind, combined with battery storage, or diesel engine-generator set to ensure safety in power supply. The alternative of connecting to the electricity grid of HRES with municipal solid waste (MSW) source has been observed in a few cases [4].

This study focuses on a technical-economic analysis of a hybrid energy system for electricity supply to a consumption center, where the electricity grid is available. The grid can be used both for the sale of locally generated surplus energy and for the purchase of electricity depending on the load curve (load demand). If the load demand cannot be met by the hybrid energy system, then the rest of the electricity can be purchased from the grid at purchase price, and if there is an excess of electricity available due to low energy consumption at a certain time in the village, it can be sold to the grid at sell-back price rate to obtain additional income. Thus, the consumption center becomes a center for energy generation, called a prosumer.

This paper proposes to use the MSW, which is a locally available source and the authorities pay for its processing. The novelty of this paper can be justified by the presentation of the solution for obtaining electricity from the technology used in the processing of MSW and the PV system connected to the electricity grid, which is not always 100% available.

## 2. System Description

The hybrid system connected to the distribution system operator (DSO) of grid is according to Figure 1, with the advantages of the flexibility provided by connection of HRES to the grid (on-grid) and the MSW generator, which can be used as a back-up to the PV system. Components of system include PV module and a biomass system consisting of a gasifier coupled with an internal combustion engine (ICE) generator group.

The MSW processing subsystem has a 250 kW<sub>e</sub> gasifier-ICE generator to partially cover the average hourly energy demand. The goal is to recycle waste efficiently and use it optimally for energy for solution *Waste to energy or Energy generation from waste*.

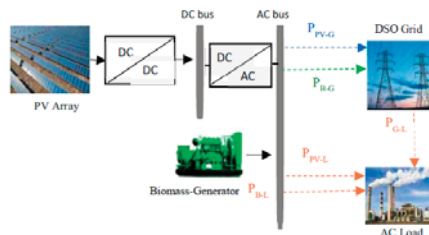


Figure 1. Proposed Photovoltaic (PV)-Biomass Generator on-grid system.

Through the gasification process, MSW is a raw material for the chemical conversion process, which at high temperature is transformed into a usable gas or syngas, which can be transformed into transport fuel, fertilizer, or can substitute natural gas. The clean syngas obtained by gasification can be used in reciprocating motors or turbines to generate electricity for producing chemicals and liquid fuels [5].

The Waste2Energy plant also has an environmentally friendly advantage: it enables safe disposal at every location and avoids large-scale transport and the storage of large and hazardous waste, as well as noise and smell harassment, and also generates new revenue. By optimizing the hybrid system from a technical and economic point of view, the model can be extended to 1 MW and used in different places, adapting environmental factors, energy demand, component performance, and cost variables to the constraints imposed.

For environmental reasons, this paper proposes to prioritize the use of photovoltaic energy in the time interval 8–16, before the generation of energy from biomass, which is used to support PV whenever it is not available. When total photovoltaic and biomass production is insufficient to match the overall demand, the HRES will consume electricity from the public electrical grid. When photovoltaic energy is sufficient to match the demand, the biomass engine will be reduced to 30% coefficient of functionality. An intermediate situation occurs when photovoltaic energy exceeds the demand, or when they are not sufficient to supply demand, but starting the biomass subsystem at load generates electricity surplus, and the excess electricity produced is sold to the grid at the market price.

### 3. System Component Modeling

#### 3.1. Mathematical Model of Biomass Generator

Biomass, as an energy resource, has a variety of forms, such as municipal solid waste (MSW). A biomass-based generation system consists of biomass preparation unit, biomass gasifier, gas cooling and cleaning system, internal combustion engine, and electric generator. The producer gas obtained from MSW is a feedstock for a high temperature chemical conversion process, as shown in Figure 2.

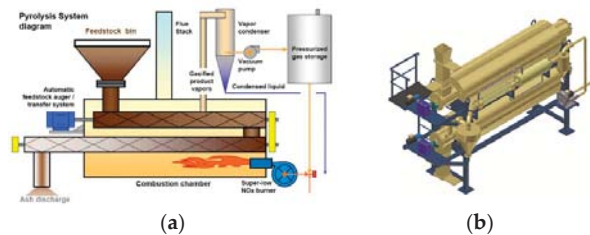


**Figure 2.** (a) Schematic of a municipal solid waste (MSW) gasifier and pyrolysis reactor; (b) Pyrolysis reactor.

The annual (8760 h) delivered electricity production ( $E_{year}$ ) of an energy system from MSW gasifier (MSWG), with nominal power of electricity generator is dependent on capacity utilization factor ( $CUF$ ).

$$E_{year} = P_{MSW} * CUF * 8760 \tag{1}$$

where  $P_{MSW}$  is the rated power of MSW gasifier (MSWG) system. The maximum size of a MSW gasifier depends on the amount of MSW available, calorific value of MSW, number of hours of usage, and efficiency gasifier system. Following [6], the maximum rating of biomass gasifier can be calculated as Equation (2), where  $M_{MSW}$  is the total biomass (Tons/y) available for power generation,  $\eta_{MSWG}$  is the efficiency of the MSW gasifier system,  $t_{MSWG}$  is the number of operating hours of MSWG system in a day, and  $CV_{MSW}$  is the calorific value of the MSW available.

$$P_{MSW}^{max} = \frac{M_{MSW} * 1000 * CV_{MSW} * \eta_{MSWG}}{365 * 860 * t_{MSWG}} \tag{2}$$

### 3.2. Mathematical Model of PV Generator

According to [7] and using the solar radiation available on the tilted surface of photovoltaic panel, the hourly energy output of the PV generator ( $E_{PV}$ ) can be calculated according to hourly irradiance ( $G$ ) and the following Equation (3), considering the PV system power output (DC) approximately a linear relationship to the insolation.

$$E_{PV} = G(t) * A * \eta_{PV} \tag{3}$$

where  $E_{PV}(t)$  is the hourly energy output from PV;  $G(t)$  is the hourly irradiance in kWh/m<sup>2</sup>,  $A$  is surface area of the PV modules in m<sup>2</sup>,  $\eta_{PV}$  is the efficiency of PV, and the temperature effects on PV cells are ignored.

## 4. Methodology Description

The following subsections show the steps for choosing the components of the hybrid system connected to the public electrical grid. First, a sample location is selected and then the data needed is determined for the model to identify the optimal compromise between cost and technical constraints and impact in terms of CO<sub>2</sub> emissions. Currently, there is no hybrid solar-MSW-pyrolysis plants operating in our country.

### 4.1. Sample Selection

The sample location is a urban township in central Transylvania, with precise geographical coordinates of 46°28' North and 24°25' East, a region with high availability of municipal solid waste and a moderate solar irradiation averaging around 1550 kWh/m<sup>2</sup>/year. The hourly electricity load averages approximately 1.6 MWh and the hourly peak demand is 2200 kWh.

### 4.2. Input Data

Input data are considered as follows: weather-related and demand data, cost and financial variables, equipment efficiency, and performance variables. The data come from trustworthy sources. The solar radiation at ground level, horizontal level was obtained from JRCs' website (European Joint Research Center). This was a starting value to calculate radiation in the modules according to the method indicated by standard UNI 8477/1. Considering the monthly and annual average values for the modules with an inclination of 30° orientated to south and based on the standards that were mentioned above, the following values were obtained (Table 1).

**Table 1.** Radiation study.

Month	Days	$\rho$	Average Daily Horizontal Radiation	Average Daily Radiation at Tilt Angle 30°	Total Monthly Horizontal Radiation	Total Monthly Radiation at Tilt Angle 30°
			[Wh/m <sup>2</sup> day]	[kWh/m <sup>2</sup> day]	[kWh/m <sup>2</sup> ]	[kWh/m <sup>2</sup> ]
January	31	0.25	1.33	21.813	41.23	67.62
February	28	0.25	2.1	29.987	58.80	83.96
March	31	0.25	3.29	40.790	101.99	126.45
April	30	0.25	4.58	49.415	137.40	148.25
May	31	0.25	6.08	59.757	188.48	185.25
June	30	0.25	6.39	60.071	191.70	180.21
July	31	0.25	6.42	61.550	199.02	190.80
August	31	0.25	5.92	62.008	183.52	192.22
September	30	0.25	4.47	53.814	134.10	161.44
October	31	0.25	2.94	41.965	91.14	130.09
November	30	0.25	1.56	24.895	46.80	74.69
December	31	0.25	1.12	19.099	34.72	59.21

Table 1. Cont.

Month	Days	$\rho$	Average Daily Horizontal Radiation	Average Daily Radiation at Tilt Angle 30°	Total Monthly Horizontal Radiation	Total Monthly Radiation at Tilt Angle 30°
			[Wh/m <sup>2</sup> day]	[kWh/m <sup>2</sup> day]	[kWh/m <sup>2</sup> ]	[kWh/m <sup>2</sup> ]
Total					1408.9	1600.19
Average per day					3.86 [kWh/m <sup>2</sup> /day]	4.38 [kWh/m <sup>2</sup> /day]

The MSW processing pilot project supplies a 250 kW power generation plant. The aim is to expand MSW processing so that a power of 1 MW can be generated. Processing of fresh municipal waste—at collection points—eliminates air, water, and soil pollution by transforming biomass into pellets. This is done by drying, chopping, and compression into unalterable granules that can be stored for recovery energy by burning there and when needed. For approximately 120,000 inhabitants that collect at least 0.5 Kg of garbage per day, that means 120,000 pers.  $\times$  0.5 Kg/day  $\times$  365 days = 21,900 tons of household waste/year. From this amount of biomass, by drying, about 35% is lost, although the following can be achieved: 21,900 t  $\times$  0.65 = 14,235 tons of pellets obtained from municipal waste. Therefore, by processing biomass from municipal waste, the community not only gets rid of the storage of 21,900 tons of garbage but also recovers energy from it 14,235 t  $\times$  4.2 Mw/t = 59,787 Mwh/year.

4.3. Efficiency and Performance Variables

Here we include the efficiency of PV modules, auxiliary equipment of PV, and biomass gasification internal combustion engine (ICE) system. The technical characteristics of the PV module (Jinko JKM-250P-60) and SMA Sunny Central SMA 850CP XT-10 inverter used in the studied project are listed in Tables 2 and 3. The PV warranted efficiency curve is used to estimate the PV power output decrease over modules lifetime due to aging (Figure 3).

Table 2. Specifications of the PV module.

Type	Voc (V)	Isc (A)	Vmax (V)	Imax (A)	Pmax (W)
JKM250P	37.6	8.81	30.4	8.23	250

Table 3. Efficiency and performance variables.

Data	Value
PV module reference efficiency	15.27%
PV inverter efficiency	98.4%
PV module mismatch factor	98.00%
PV connections efficiency	99.50%
PV DC wiring losses factor	98.00%
PV AC wiring losses factor	99.00%
PV soiling derating factor	95.00%
PV system availability O&M	99.00%
Nominal DC system efficiency	83.9%
Nominal AC system efficiency	97.4%
Biomass gasifier operation efficiency	95%

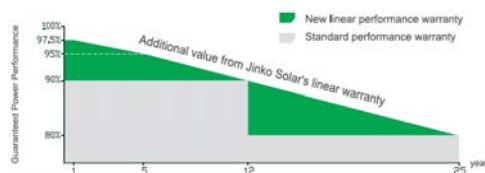


Figure 3. Premium performance warranty [8].



The device processes 24 t per day; the municipal waste is shredded by an integrated shredder. Energy recovery: with dry waste about 1 t = 1 MWh and with wet waste approx.  $(2.5-3) \text{ t} = 500 \text{ m}^3/\text{h} = 1 \text{ MWh}$ . Another advantage of the system is that its operation requires no significant expertise and has a small footprint (plant  $150 \text{ m}^2$ , arrival and departure and storage area  $850-1350 \text{ m}^2$ ).

#### 4.4. Cost and Financial Components

The cost components include the purchasing cost of PV modules, invertors, biomass gasifier and gas cleaning systems, and the ICE-generator equipment. The implementation of an investment project shall undoubtedly generate expenses that shall have to be exigently and pertinently analyzed. Some of these expenses are exclusively generated by the operation of the investment objective, and others by the legislation in force, especially with regard to the taxes and impositions owed to the state budget or local budget.

##### 4.4.1. Operating Expenses

The group of expenses regarding materials and raw materials comprises sub-groups according to the structure analyzed, cash-flow, and budget of revenues and expenses:

- expenses regarding raw materials
- expenses regarding fuels
- expenses regarding spare parts
- expenses regarding other consumable materials
- expenses regarding inventory objects.

Expenses related to personnel, including the expenses related to social security, refers to the necessary personnel that serve the operation under good conditions of the electric energy production equipment, with the mention that we have also considered the fact that this equipment shall operate 24 h a day. To the operational expenses is added expenses related to social insurance (social security contribution  $-20.80\%$ ; health social insurance contribution  $-5.20\%$ ; medical leave fund contribution  $-0.85\%$ ; unemployment fund contribution  $-0.50\%$ ; contribution for accident and professional disease insurance  $-0.80\%$ ), expenses related to rent and concession, expenses related to utilities, expenses related to transport, to fees and charges, to commercial and advertising, expenses regarding maintenance and repairs, to insurance, related to the amortization of fixed assets, and expenses related to impositions and taxes.

##### 4.4.2. Financial Expenses

The financial expenses are made up of the interests corresponding to the credit, the interest taken into consideration, here being  $4.00\%/year/balance$ . The applicant does not pay in year 1 any interest and any installment, the obligations towards the employer running from year 2 of the investment operation. The expenses regarding interests have been appropriately taken over both in year 2 as well as in years 3-8 of the time interval plotted into the analysis. The key variables determined with regard to the financial results of this project are:

- update rate
- credit interest
- cost of the machines purchased by the project
- cost of salaries of the employed personnel following the project implementation
- revenues achieved from the support schemes.

## 5. Case Study

This case study presents the results obtained at the moment for the promotion of a hybrid electricity generation system consisting of PV and biomass (MSW). A 250 kW power generation plant from MSW

processing was built. Presented also are the technical and financial elements related to the 2.5 MW photovoltaic power plant, which can supply part of the energy demand.

### 5.1. Biomass System, Pyrolysis Capital, and Operating Costs

Household waste brought to the platform is introduced into a grinding system (Figure 4a) using a conveyor belt. The grinding system has a capacity of 3000 kg/hour, from which 3000 kg/h shredded waste is obtained. The ground waste is placed in a rotary dryer (Figure 4b) to obtain the necessary moisture for pelletizing.

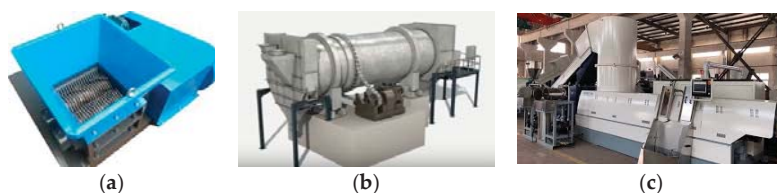


Figure 4. (a) Grinding plant; (b) Rotary dryer; (c) Pelletizer.

A quantity of 2983.05 kg/h of ground waste is introduced, with an average humidity of 53.46%, from which 1500 kg/h of ground and dried waste, with a humidity of 9.25%, is obtained. The ground and dried waste is introduced into the pelletizer (Figure 4c), obtaining 1500 kg/h pellets. After pelleting, the pellets are introduced into the pyrolysis reactor (Figure 4b). The pellets are introduced by means of a conveyor belt into a reactor heated to the temperature required for pyrolysis. With the high temperature, the thermal decomposition is achieved, and the resulting gases are passed through a complex purification system. The hot gases are first passed through a fine cyclone separating the carbon dust and then directed to a cooling system, where it is cooled to 50 °C. The gases pass through an alternative wet and dry filtration system and are stored in a pressure vessel using a high-performance compressor. It is obtained 500 m<sup>3</sup> syngas/hour and max. 12% coal (ash), 166.62 kg/hour. The pyrolysis reactor is a major energy consumer, as the reactor must be maintained at 550–600 °C in the continuous processing of MSW wet raw material. Continuous heat supply is achieved by burning secondary coal, which is a conventional approach used in most industrial pyrolysis systems. From 500 m<sup>3</sup> of resulting gases, 1 MWh of electricity can be obtained, from which a power of 80–120 kW is used for the operation of the equipment. The investment cost for a 1 MW electrical power are 4.821.880 euro with 19%VAT, as shown in Table 4.

Table 4. MSW investment cost.

Costs of Basic Investment (Euro with 19% VAT)	
Buildings, constructions, installations	35,700
Buildings, constructions and installations related to operation of machinery	23,800
Buildings, constructions, installations related to labor safety and protection	11,900
Assembly of technological machinery	11,900
Machinery, equipment with assembly	4,760,000
Machinery land transportation	2380
Software for technological machinery	11,900
Total Cost	4,857,580

Consistent with the known daily energy demand, the solar photovoltaic installation is dimensioned so that the maximum power of PV to generate electricity is equal to the maximum daily energy demand minus the amount of electricity that can be generated by the MSW-based biomass installation (pyrolysis unit). This then sets the proportion of the total energy demand that will be supplied by the solar PV plant, as well as the solar PV output for each hour in the day. The pyrolysis unit can operate

continuously, generating syngas that can be stored in a tank and used to power the engine/generator unit when required (Figure 5).

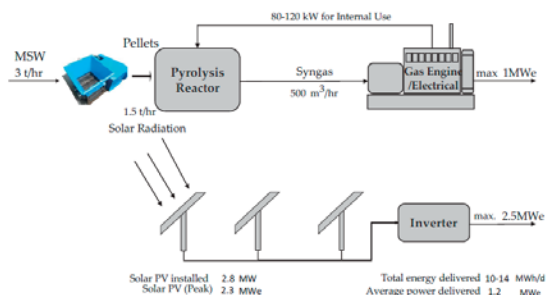


Figure 5. Integration of syngas production and solar PV.

### 5.2. Solar PV Unit Capital and Operating Costs

The generator of the power plant consists of 11.976 single polycrystalline solar modules, each with an electrical peak power of 250 watts, in total 2994 kilowatts. The modules are mounted on a substructure, which is founded on poles rammed into the earth. Twenty-four modules are connected in series to reach higher DC voltages up to max. 1000 V. Two of these module strings are connected parallel to reduce cabling. The PV power plant consists of three inverters in total with an AC output power up to max. 935 kVA each. The type of the inverter is SMA Sunny Central 850CP-10 [9]. The inverters are housed in weatherproofed steel cabinets. These steel cabinets are founded on metal poles rammed into the earth. Six string combiners are connected to one inverter. The inverters are converting the DC current into three-phase AC current with a voltage of 386 volts. For monitoring and control reasons, there will be installed a fiberoptic ethernet to connect all monitoring components (SMA SC-COM/Webbox/Cluster Controller) with the router located in transformer station one. In Romania, starting with 2013, the average leveled costs of electricity from photovoltaic energy decreased from 1.1 euro/W to 0.80 euro/W in 2020, being in continuous decrease due to the decrease of prices for photovoltaic modules, inverters, and cost-effective project management and execution. The first two factors that are contributors to the total cost of the PV installation are the photovoltaic modules and mounting system, to which are added the inverters, the substation connection, and the construction labor (Table 5). The operating and maintenance (OPEX) costs of the PV solar power plant are estimated at 2% of the capital per year and also include insurance, administration, and monitoring PV costs.

Table 5. PV total installed capital cost.

Item	Cost (Euro/W)
Modules	0.45
Mounting system	0.08
Electrical system	0.09
Inverters	0.26
Construction labour	0.08
Spares	0.01
Owners engineering	0.03
Contingency	0.08
Total installed capital cost	1.08

## 6. Techno-Economic Results

The energy generated by the Photovoltaic Power Plant (2.5 MW) located in the coordinates specified in Section 4.1 (Table 6) and the 250 kW installation obtained from the MSW processing inside

the consumer lead to the promotion of a hybrid PV-MSW on grid system to ensure energy demand, as shown in Table 7. The environmental conditions are favorable for the operation of the photovoltaic installation, as evidenced by the energy production recorded over the period 2013–2020 (Table 6) [10].

**Table 6.** Total yield (MWh).

	Jan.	Feb.	Mar.	Apr.	May	Jun.	Jul.	Aug.	Sep.	Oct.	Nov.	Dec.	Total
2013							423.8	453.1	316.18	294.7	170.8	112.42	1770.9
2014	88.92	208.1	373.9	353.21	471.9	455.8	447.4	467.9	400.38	277.7	150	105.61	3800.9
2015	118.9	233.7	330.2	388.35	435.2	459.7	517	458.2	296.06	248.5	133.8	78.48	3698.1
2016	116.1	182.3	294.3	400.67	422.5	466.1	494.7	443.6	374.87	189.7	151.4	102.38	3638.7
2017	150.6	171.8	356.6	392.26	441.3	478.7	496.8	470.1	337.89	255.1	97.9	66.92	3715.8
2018	141.5	128.1	238.5	420.44	487.6	407.6	415.9	484	349.31	304.5	160.2	64.64	3602.2
2019	90.21	185.8	369.7	387.87	379.1	472.8	440.2	447.2	370.75	310.1	150.9	100.04	3704.7
2020	95.83	182.9	297.5	464.76	380.4	332	435.6	441.9	360.59	199.7	80.78	38.12	3310.2

**Table 7.** The evolution of power.

P	2020	2021	2022	2023	2024
MW	1.6	2.5	3.2	3.6	4

The techno-economic analysis for the photovoltaic and MSW-based installation is undertaken using a discounted cash flow (DCF) model. In the technical and economic analyzes, the increase of energy consumption was taken into account. Thus, from a power of 1.6 MW, it will reach a power of 4 MW (Table 7). The feasibility study prepared showed that from MSW installation and according to the sale price agreed by both parties (DSO electric operator and beneficiary) of 45.00 euro/MWh and taking into account the fact that the equipment can operate 24 h a day, it results in a power of 24 MW that can be generated per day, some of which are distributed locally and the surplus energy will be delivered on the grid. Following the processing of biomass and achievement of electric energy, the result is a quantity of residual product (ashes) in a percentage of 16% of the processed biomass quantity. The residual product achieved, in combination with other additives, represents raw material for obtaining cement; consequently it can be valorized as such. Furthermore, the applicant may opt for an association for producing cement and this can be subsequently valorized. In calculating the performed analysis, we have opted for the valorization in raw condition of the residual product, the sale price being established as being 20–25 euro/ton. The resulting financial indicators for a 1 MW plant generating electricity from MSW processing lead to a favorable investment and the investment can support its own cost, the operation cost and, more than that, also generate a profit.

### 7. Conclusions

The hybrid system described, consisting of photovoltaic sources and municipal solid waste connected to the electricity network of the distributor, is a feasible source that can provide energy at competitive prices. For the power required in the next period, it will be necessary to analyze the technical options for expanding the processing capacity of MSW and providing electricity from the biomass plant. In this regard, it would be advisable to analyze the heat recovery solution and its use to power a motor for electricity generation, when the situation requires it. The development of the solar PV and MSW energy systems will require a stable and reasonably priced supply of biomass in areas where the solar yield is attractive. While the solar PV and MSW system analyzed in this work will likely be a niche solution, it offers a credible starting point for the development of larger-scale bio-energy value chains, with the longer term goal of converting MSW materials into renewable transportation fuels and chemicals.

## References

1. Zhao, H.; Guo, S. External benefit evaluation of renewable energy power in China for sustainability. *Sustainability* **2015**, *7*, 4783–4805. [CrossRef]
2. Kumar, A.; Samadder, S.R. A review on technological options of waste to energy for effective management of municipal solid waste. *Waste Manag.* **2017**, *69*, 407–422. [CrossRef] [PubMed]
3. Ferdan, T.; Šomplák, R.; Zavíralová, L.; Pavlas, M.; Frýba, L. A waste-to-energy project: A complex approach towards the assessment of investment risks. *Appl. Therm. Eng.* **2015**, *89*, 1127–1136. [CrossRef]
4. González, A.; Riba, J.R.; Rius, A. Optimal sizing of a hybrid grid-connected photovoltaic–wind–biomass power system. *Sustainability* **2015**, *7*, 12787–12806. [CrossRef]
5. Vishal, S.; Vatsal, N. Gasification—A Process for Energy Recovery and Disposal of Municipal Solid Waste. *Am. J. Mod. Energy* **2016**, *2*, 38–42.
6. Gupta, A.; Saini, R.P.; Sharma, M.P. Steady-state modelling of hybrid energy system for off grid electrification. *Renew. Energy* **2010**, *35*, 520–535. [CrossRef]
7. Diaf, S.; Diaf, D.; Balha, M.; Hahhadi, M. A methodology for optimal sizing of autonomous hybrid PV/wind system. *Energy Policy* **2007**, *35*, 5708–5718. [CrossRef]
8. Available online: <https://keysolar.com.au/wp-content/uploads/2014/07/Jinko-Poly250W.pdf> (accessed on 11 June 2012).
9. Available online: <http://files.sma.de/dl/18859/SC800CP-900CP-DEN1751-V23web.pdf> (accessed on 11 June 2012).
10. Balan, D. Behavior of photovoltaic systems connected to the distribution network. Case study, photovoltaic power plants in the distribution network of the SDEE Mureş operator. *Procedia Manuf.* **2018**, 803–810. [CrossRef]

**Publisher's Note:** MDPI stays neutral with regard to jurisdictional claims in published maps and institutional affiliations.



© 2020 by the authors. Licensee MDPI, Basel, Switzerland. This article is an open access article distributed under the terms and conditions of the Creative Commons Attribution (CC BY) license (<http://creativecommons.org/licenses/by/4.0/>).

# Stochastic Models of Particle Trajectories in Turbulent Atmosphere Flows by Using the LANGEVIN Equations <sup>†</sup>

Yousra El Qasemy <sup>1,\*</sup>, Abdelfatah Achahbar <sup>1</sup> and Abdellatif Khamlichi <sup>2</sup>

<sup>1</sup> Department of Physics, Faculty of Science Tetouan, University Abdelmalek Essaadi, Tetouan 93030, Morocco; acfetah@gmail.com

<sup>2</sup> Department STIC, National School of Applied Sciences at Tetouan, BP 2121, Tetouan 93030, Morocco; khamlichi@yahoo.es

\* Correspondence: youssraelqasemy@gmail.com or elqasemy@correo.ugr.es; Tel.: +34-692188770 or +212-668618610

<sup>†</sup> Presented at the 14th International Conference INTER-ENG 2020 Interdisciplinarity in Engineering, Mureş, Romania, 8–9 October 2020.

Published: 17 December 2020

**Abstract:** The stochastic behavior of wind speed is a particular characteristic of wind energy production, which affects the degradation mechanism of the turbine, resulting in stochastic charging on the wind turbine. A model stochastic is used in this study to evaluate the efficiency of wind turbine power of whatever degree given fluctuating wind turbulence data. This model is based on the Langevin equations, which characterize, by two coefficients, drift and diffusion functions. These coefficients describe the behavior of the transformation process from the input wind speed to the output data that need to be determined. For this present work, the computation of drift and diffusion functions has been carried out by using the stochastic model to assess the output variables in terms of the torque and power curves as a function of time, and it is compared by the classical method. The results show that the model stochastic can define the efficiency of wind turbine generation more precisely.

**Keywords:** wind speed; stochastic model; Langevin equation; wind turbine; power curve

## 1. Introduction

Wind energy has become one of the most encouraging responses to global energy troubles. This is due to recent advances and intense research activities in engineering, meteorology, and physical sciences. However, there are still important difficulties to overcome, such as the following: firstly, the predictability and optimization of power production; and secondly, the high cost of constructing wind turbines by optimizing their control and monitoring [1]. In fact, the devices dedicated to the measure of some load types are expensive. Moreover, the unpredictable manner of wind makes it primordial to place more than one device at each turbine, in order to prevent the loss of load measurement accuracy. The estimation of loads applied to the wind turbine is important to estimate the life expectancy of the turbine. The arrangement of wind speed measurements at different wind turbines was used for generating the torque. This can serve to assess fatigue analysis of the wind turbine and the blades.

The pioneering work of Peinke and Friedrich in 1997 [2] was at the origin of the development of the Langevin approach, which consists of a direct method for extracting the evolution equation of a stochastic series of measurements. Improving the methods necessary for predicting the electrical power produced by wind farms is essential to increase the wind energy contribution to electrical and

power production. In this context, several studies were conducted during the last decennary [3,4]. The framework developed by Milan et al. [5] consists of deriving a stochastic differential equation describing the evolution of the torque at one wind turbine. It shows through this method that, using only the load measurements at one single turbine and the set of wind speed measurements, the fatigue loads in any wind turbine within one wind park can be accurately estimated. In another study [6], and in order to establish a new stochastic modeling approach for the wake of a wind turbine, data were generated and analyzed by the turbulence-resolving large-eddy simulation (LES) PALM model. A procedure to derive stochastic wake models from costly computational fluid dynamics (CFD) was also presented. Lind, and her. [7] presented a stochastic approach to model the conversion process operated by a wind energy converter (WEC) used to convert wind fluctuations and wind gusts into electrical power fluctuations and power gusts fed into the grid. The result of the study they conducted shows the effect of turbulence on wind power production, as well as the importance of turbulence research to completely convert more wind energy into electrical networks. A more emphasized and detailed study conducted by the same researchers [8] had as an objective the development of a new stochastic approach in order to describe and remodel the conversion process of a wind farm considering the wind farm as a dynamical system described as a stochastic drift/diffusion model [9]. The Langevin equation was then used and adapted to the current system to model a synthetic signal of power output for any given wind speed/direction signals.

In this study, we carried out a stochastic analysis to model wind fluctuations created by a turbulent wind flow. A Langevin equation-based procedure was used. At that point, the electric power derived from wind was assessed by taking into account the dynamic response of a standard wind turbine under these wind field speed fluctuations. Then, the differential equations of the stochastic model were implemented by using Matlab simulation. The numerical simulation allowed the power variance to be extracted, based on wind velocity. Therefore, we conclude by showing that the results of stochastic modeling and the classical formula used for estimating the power are coherent. However, for reliable prediction of wind energy potential in a given site where wind speed is recorded instantaneously, the stochastic model is suggested. In future work, a comparative study of experimental data will be performed.

## 2. Features of the Wind Energy Converter Dynamics

One of the biggest issues in wind energy development is to properly estimate the output characterization of the wind turbine. Data estimation is needed to determine the power curve of a given machine. After all, it is certain that the wind speed  $u(t)$  and the power output  $P(t)$  are needed. It can also use the wind direction  $\vec{u}(t)$  as theory relates the following:

The study of wind is an essential step before any wind turbine installation project. Wind is a variable element and its change can depend on many phenomena, such as temporal phenomena and phenomena related to altitude. Typically, wind speed is measured by using an anemometer, as shown in Figure 1. The most common types are cup anemometers and ultrasonic anemometers. However, these sensors should be used for more than a year to characterize wind farms.

### *Measure Requirements*

To simulate a wind energy converter’s power output properly, the stochastic model must be parameterized. Effective parameters can be derived from a calculation of interest taken out in advance at the WEC.

The variables to be evaluated are the WEC’s simultaneous wind speed  $u(t)$  and power output  $P(t)$  time signals. The sampling frequency of the time series must be of the order of 1 Hz, as shown in Figure 2.

Over most important features, the irregular tasteful essence of the wind is observed. This reflects the need for high-frequency measurements containing extensive information on the rapid variability, which is not available with the generic ten-minute average measurement technique.

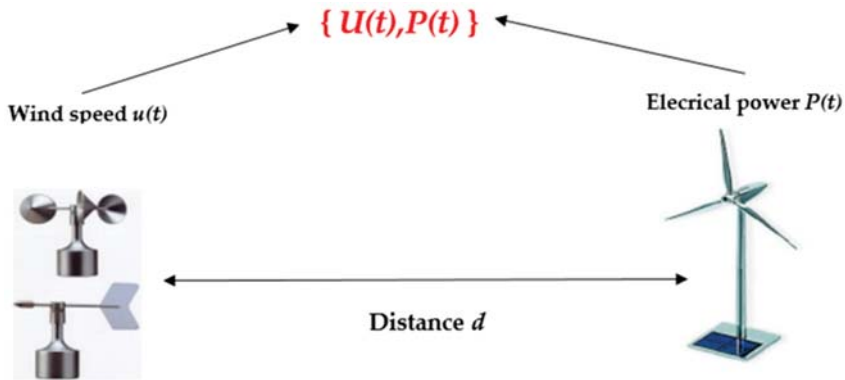


Figure 1. Measuring equipment of the wind speed and electrical power [10].

This basically motivated us to study this aspect, as the most important aim to present this method is to model the complex statistics.

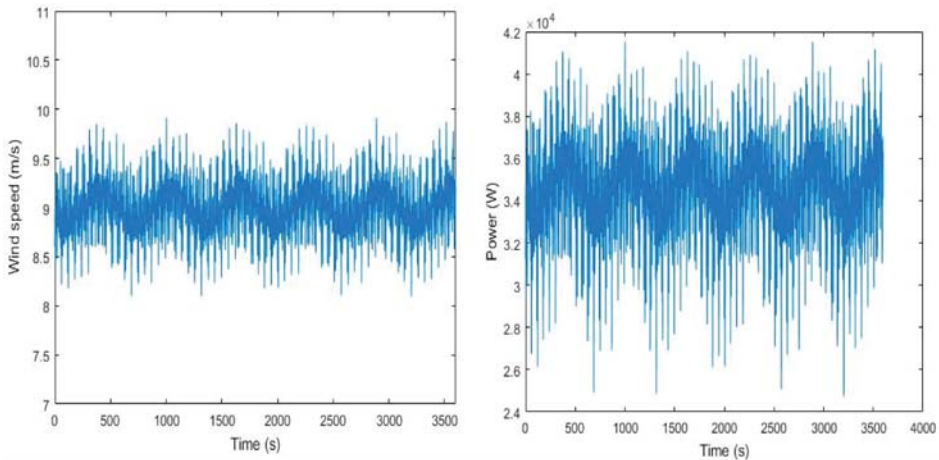


Figure 2. Schematization of the wind speed  $u(t)$  (right) and power output  $P(t)$  (left) at a frequency of 1 Hz.

For an accurate display of the dynamics of the WEC, the original measurement should be sufficiently long to cover all the necessary wind conditions. Therefore, the wind speed  $u(t)$  should be estimated from the mast at hub height approach, as defined in the standard International Electrotechnical Commission power curve. For optimal performance, actual data requirements and corrections as defined in the IEC standard could be applied here [11]. Only the reported data sampling frequency must be in the range of 1 Hz instead of the average of ten minutes specified in the IEC standard.

For that reason, by definition, the stochastic model is applicable to power curve methods, since it attempts to transform wind velocity into power output. This intrinsic possible connection makes it a versatile tool that could be applied to any WEC design showing a clearly defined power curve. The measurement data used in this work contain 100 points, and the frequency takes the value of 25 Hz [12].



### 3. Mathematical Formulation

#### 3.1. Basic Model

The equation of the kinetic energy of the wind is

$$P_{wind} = \frac{1}{2} \times S_{windTurbine} \times \rho \times u^3, \tag{1}$$

The recovered power for a wind turbine is

$$P_{windTurbine} = C_p \times P_{wind}, \tag{2}$$

where  $C_p$  represents the power coefficient,  $S_{windTurbine}$  indicates the surface swept by the wind turbine ( $m^2$ ),  $\rho$  is the air density ( $1.225 \text{ kg/m}^3$ ), and  $u$  represents the wind speed ( $m/s$ ).

#### 3.2. Stochastic Model

Differential equations are widely used to describe dynamic complex, nonlinear systems. Regardless of the ensemble averages, the focus is only on the instantaneous electric wind turbine power output [13–15]. This work covers the analysis stochastic based on a current model for rebuilding the increment statistics of the torque in single wind turbines as a tool for estimating fatigue loads of one wind turbine as well as of its neighbors. The condition of the Langevin equation used here as the model is defined as

$$\frac{dT}{dt} = D^{(1)}(T, u) + \sqrt{D^{(2)}(T, u)}\Gamma_t, \tag{3}$$

where  $T$  represents the torque at the wind turbine,  $u$  is the wind speed,  $\Gamma_t$  is a Gaussian,  $\delta$  is the correlated white noise,  $D^1$  is the drift function, and  $D^2$  is the diffusion function.

$D^1$  and  $D^2$ , appearing in Equation (3), can be calculated by using a time record of torque by means of the first and second statistical conditional moments, respectively:

$$M_{u^*}^1(T, \tau) = \langle T(t + \tau) - T(t) \rangle_{|T(t)=T, u(T)=u^*}, \tag{4}$$

$$M_{u^*}^2(T, \tau) = \langle (T(t + \tau) - T(t))^2 \rangle_{|T(t)=T, u(T)=u^*}, \tag{5}$$

where  $\langle \cdot \rangle_{|T(t)=T}$  indicates the average over the full time series, whenever  $T(t)$  takes the value  $T$  and wind speed  $u = u^*$  [7].

In order to stochastically model the torque, we use the Langevin Equation (3) referred to above to produce the torque by coordinating wind speed measurements at various wind turbines. It will serve to test wind turbine power performance.

### 4. Results and Discussion

From Figure 3 that represents the values of torque 1 and torque 2 calculated using the classical instantaneous method, the coefficients  $D^{11}$ ,  $D^{12}$ ,  $D^{21}$ , and  $D^{22}$  are calculated from Equations (4) and (5), respectively. These coefficients are shown in Table 1.

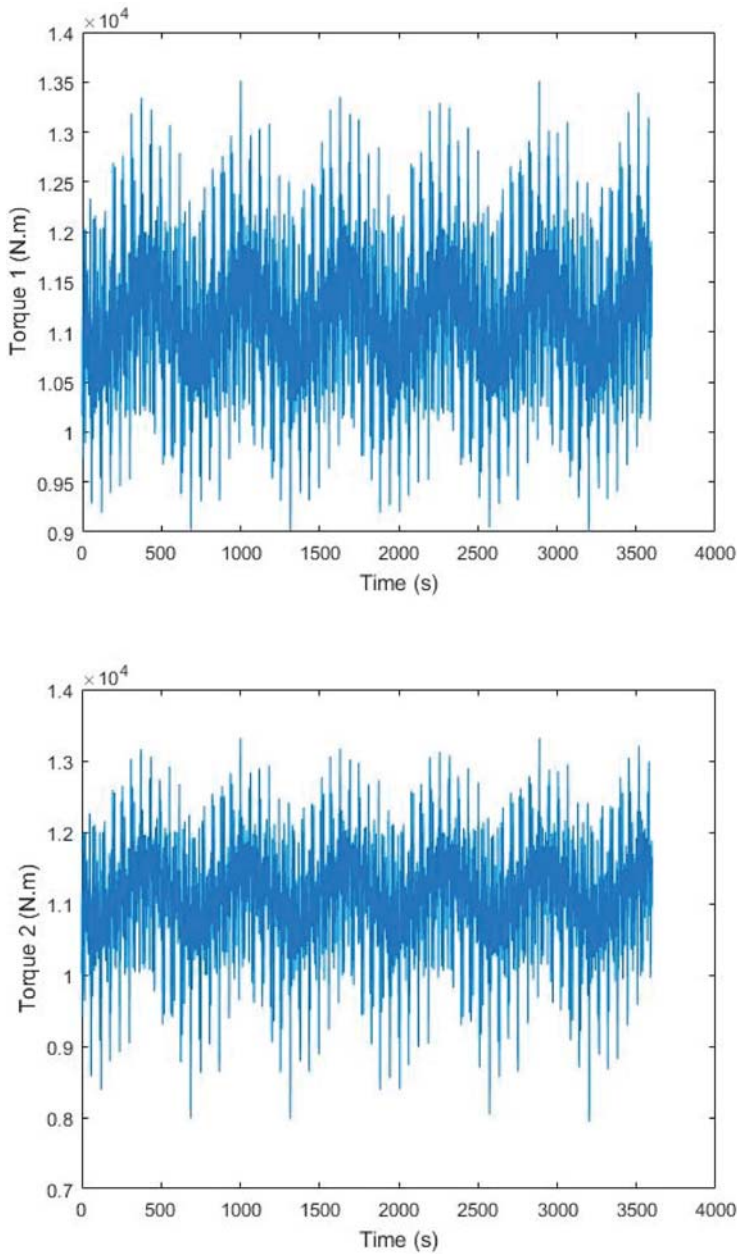


**Figure 3.** Representations of torque 1  $T(t)$  (line 1) and torque 2  $T(t)$  (line 2), which were used to calculate  $D^1$  and  $D^2$ .

**Table 1.** Coefficients values used as inputs in the Matlab code.

$D^{11}$	$D^{12}$	$D^{21}$	$D^{22}$
1.3829	$1.7395 \times 10^5$	1.6116	$1.9925 \times 10^5$

The results obtained by the implemented Equation (3) in the Matlab code using the coefficients indicated in Table 1 are shown in Figure 4. As we can see clearly in Figure 4 (left), which presents the distribution curves of the torque, there is a good coherence between the classical mechanical model (blue line) and the stochastic model that we proposed (red line). This model, as it gives us a large interval of torque values for a single wind speed value, helps us to control, more precisely, the value of the torque and, therefore, the value of the extracted power, which is clearly a significant advantage of using the stochastic model.

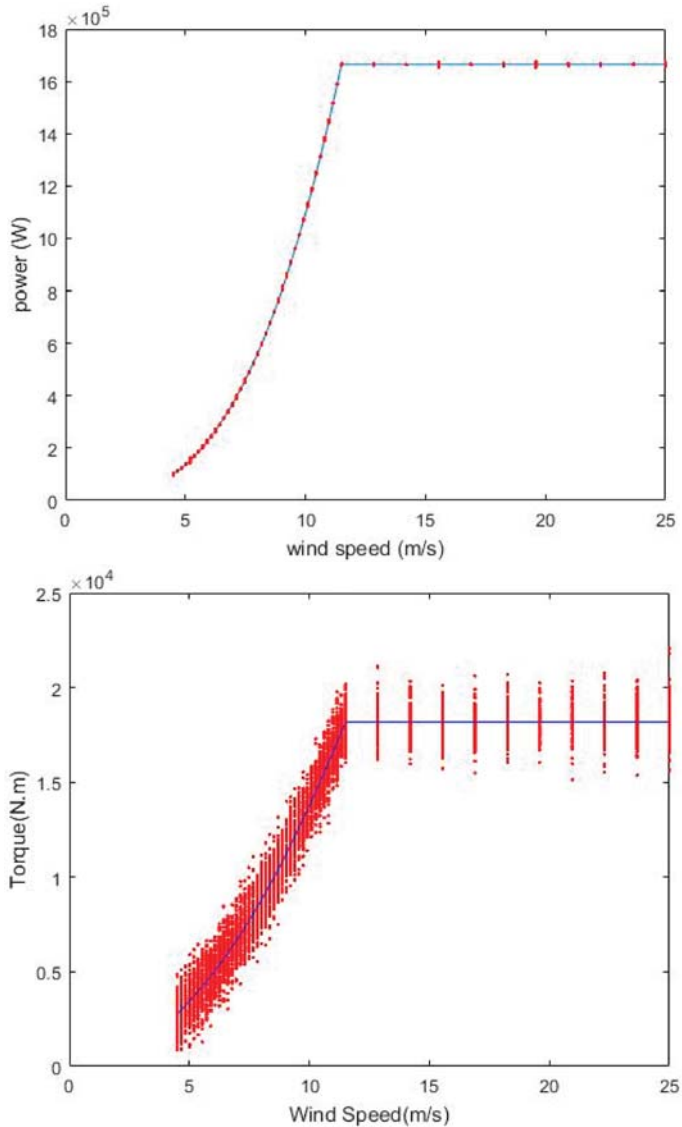


**Figure 4.** Representations of the numerical computation power (w) (**up**) and torque (N.m) (**down**) curves at a frequency of 25 Hz containing 100 points; the frequency is similar to [12].

We can also see that the torque spectrum has an upper limit, which gives us a more real picture of the wind turbine's operation. Since wind is very dynamic in nature, the resulting forces are also dynamic in nature. A stochastic approach is proposed not only for modeling, but also for accessing and extracting most of the information available in the torque and power dynamics.

In the operation of the wind turbine, we find that the torque probability density functions are limited to extreme wind speeds, which helps to explain the effect of turbulence on the quality and quantity of aerodynamic torque.

## 5. Conclusions

This paper had as an objective the development of a stochastic analysis to help predict the capacity of wind energy given the instantaneous records of wind speed. To do so, our approach consists of using a stochastic drift/diffusion model based on the Langevin equation to describe the attraction towards the power curve and the additional turbulent fluctuations, respectively.

This method characterizes wind turbine power curves and torque more accurately and independently of specific parameters of the site such as intense turbulence. This approach can be used to conduct numerical simulation in order to estimate the wind velocity and, therefore, it seems to be fully capable of treating the turbulent field. In addition, it can be used to re-estimate, more reliably, the expected amount of electric energy that is available for a given implementation site in a wind farm. It can be concluded that the stochastic approach can improve the accuracy of the standard determined approach.

With these objectives in mind, we are going to focus on the application of the presented approach in this article on real generated data in our future work.

**Conflicts of Interest:** The author declare no conflict of interest.

## References

1. Joaquin, M.A. *Curso de Energía Eólica*; Universidad de Zaragoza: Zaragoza, Spain, 2009; ISBN 84-95050-07-2.
2. Friedrich, R.; Peinke, J. Description of a Turbulent Cascade by a Fokker-Planck Equation. *Phys. Rev. Lett.* **1997**, *78*, 863–866. [[CrossRef](#)]
3. Bechrakis, D.A.; Deane, J.P.; McKeogh, E.J. Wind resource assessment of an area using short term data correlated to a long term data set. *Sol. Energy* **2004**, *76*, 725–732. [[CrossRef](#)]
4. Celik, A.N. Weibull representative compressed wind speed data for energy and performance calculations of wind energy systems. *Energy Convers. Manag.* **2003**, *44*, 3057–3072. [[CrossRef](#)]
5. Patrick, M.; Allan, M.; Matthias, W.; Joachim, P. Wind Energy: A Turbulent, Intermittent Resource. In *Wind Energy—Impact of Turbulence*; Springer: Berlin, Germany, 2014; Volume 2, pp. 73–78. [[CrossRef](#)]
6. Bastine, D.; Vollmer, L.; Wächter, M.; Peinke, J. Stochastic wake modelling based on POD analysis. *Energies* **2018**, *11*, 612. [[CrossRef](#)]
7. Lind, P.G.; Herráez, I.; Wächter, M.; Peinke, J. Fatigue load estimation through a simple stochastic model. *Energies* **2014**, *7*, 8279–8293. [[CrossRef](#)]
8. Milan, P.; Peinke, J. Stochastic modeling and performance monitoring of wind farm power production. *J. Renew. Sustain. Energy* **2014**, *6*. [[CrossRef](#)]
9. Cremona, C.; Arnaud, G. *Développement d'algorithmes de simulation de champs de vitesse de vent*; Laboratoire Centrale des Ponts et Chaussées: Paris, France, 1997; ISBN 2-7208-2620-0.
10. Patrick, F.; Peinke, J.; Gottschall, J.; Laurent, C.; Patrick, M. *The Stochastic Power Curve Analysis of Wind Turbines*; University of Oldenburg Institute of Physics: Oldenburg, Germany, 2008.
11. Milan, P.; Wächter, M.; Peinke, J. Stochastic modeling of wind power production. In Proceedings of the European Wind Energy Conference & Exhibition 2011, EWEC 2011, Brussel, Belgium, 14–17 March 2011; pp. 176–180.
12. Anahua, E.; Barth, S.; Peinke, J. Markovian power curves for wind turbines. *Wind Energy* **2008**, *11*, 219–232. [[CrossRef](#)]

13. Anahua, E.; Barth, S.; Peinke, J. Characterisation of the Power Curve for Wind Turbines by Stochastic Modelling. *Wind Energy* **2007**, 173–177. [[CrossRef](#)]
14. Chen, X.; Li, L.Q.S. *Stochastic Evolutions of Dynamic Traffic Flow Modeling and Applications*; Springer: Beijing, China, 2015; ISBN 9783662445716.
15. Rodean, H.C. *Turbulent Diffusion as a Stochastic Lagrangian Process*; American Meteorological Society: Boston, MA, USA, 1996; Volume 26, ISBN 9781878220233.

**Publisher's Note:** MDPI stays neutral with regard to jurisdictional claims in published maps and institutional affiliations.



© 2020 by the authors. Licensee MDPI, Basel, Switzerland. This article is an open access article distributed under the terms and conditions of the Creative Commons Attribution (CC BY) license (<http://creativecommons.org/licenses/by/4.0/>).

# Computational Fluid Dynamics Simulation to Predict the Airflow and Turbulence in a Wind Farm in Open Complex Terrain <sup>†</sup>

Amahjour Narjisse <sup>1,\*</sup>  and Abdellatif Khamlichi <sup>2</sup>

<sup>1</sup> Department of Physics, Faculty of Science Tetouan, Abdelmalek Essaadi University, Tetouan 93 030, Morocco

<sup>2</sup> Department TITM, National School of Applied Sciences at Tetouan, Abdelmalek Essaadi University, Tetouan 93 030, Morocco; khamlichi7@yahoo.es

\* Correspondence: narjisse.amahjour@gmail.com

<sup>†</sup> Presented at the 14th International Conference INTER-ENG 2020 Interdisciplinarity in Engineering, Mureş, Romania, 8–9 October 2020.

Published: 18 December 2020

**Abstract:** The performance of a wind turbine depends on the characteristics of the airflow as well as the conditions of the atmospheric boundary layer (ABL). To evaluate accurately the amount of wind energy, it is required to have the exact height distribution of wind speed for the considered implementation site of a wind turbine. In this paper, computational fluid dynamics (CFD) simulation predictions provided by the standard  $k-\varepsilon$  turbulence model under neutral conditions were examined. The objective is to investigate the influence of hill slopes in the microscale wind farm on the airflow velocity to optimize the location of wind turbines. The results were validated by RUSHIL wind tunnel data and were compared with flat terrain.

**Keywords:** airflow; atmospheric boundary layer; CFD; RANS; turbulence model; wind turbine

## 1. Introduction

Wind energy is one of the most prominent renewable energy sources today. The increasing concerns with environmental issues are driving the search for more sustainable electrical sources. Wind energy along with solar energy, biomass, and wave energy is possible solutions for environmentally friendly energy production. The initialization of wind power installation, which started at the beginning of the 1980s, is very much related to the oil crises of the mid-1970s. During the 1980s, most wind power installations were limited to a few hundred kilowatts. The small size of those installations did not threaten the power system stability. The 1990s marked an important breakthrough in the industry. New concepts emerged because of the demand for more efficient power production and because of the necessity to comply with power quality requirements [1].

The production of wind energy potential for a given site often involves uncertainties due to the stochastic nature of wind speeds and the variation of the power curve [2]. Wind velocity distribution corresponds to the effect of airflow turbulent in the atmospheric boundary layer according to a complex pattern that depends hugely on associating peeling occurring on the airflow due to the roughness of the ground surface, local Reynolds number, and obstacles. It varies as a function of the altitude and the site topography. The wind farm performance affected by the presence of macroscopic obstacles on the surface of a plate modifies the flow characteristics of wind and the wind speed profile normal to that plate is changed. To evaluate the amount of wind energy, it is necessary to have the accurate height distribution of wind speeds on that location.

In this study, computational fluid dynamics (CFD) modeling is used to solve the turbulent airflow equations that consist of the Navier–Stokes equations coupled to the  $k-\varepsilon$  turbulence model and to

simulate the turbulent flow over different slopes of the two-dimensional hills that are presented on the ground.

The major advantage of CFD is that it is a very compelling, non-intrusive, virtual modeling technique with powerful visualization capabilities, and engineers can evaluate the performance of a wide range of system configurations on the computer without the time, expense, and disruption required to make actual changes onsite; it has seen dramatic growth over the last several decades. This technology has widely been applied to various engineering applications such as automobile and aircraft design, weather science, civil engineering, and oceanography.

The main objective of this research is to perform a comprehensive CFD analysis in hilly terrain to optimize the siting of the turbines by considering their obstruction effect. While several studies have shown that complex terrain affects the wake flow of wind turbines [3–5], few research papers have focused on studying its effect on the velocity profile approaching the leading edge of the turbine, which may be an area for further research. Additionally, this work was carried out to assess the efficiency of the CFD model on the airflow distribution in the neutral atmospheric boundary layer (ABL) to describe the impact of topography in the micro-scale wind farms in open hilly terrain, which was considered by the implementation of four wind turbines aligned with two different hill slopes.

In this work, COMSOL Multiphysics software package [6] which is based on the Finite Element (FE) method was used to solve the fluid dynamics equations. This software allows to couple different equations in order to describe general Multiphysics phenomenon. Appropriate boundary layer conditions were applied. In the other hand, the precision of the standard  $k-\epsilon$  turbulence model was examined by comparison with experimental data for the “Russian Hill” (RUSHIL) wind-tunnel study [7]. The velocity profile in different positions of the terrain are compared with those of flat plate without obstacle. The numerical results obtained show good agreement with experimental data. Thus, they indicate that the velocity profiles were highly affected by the presence of the hill, especially, on the steep slope.

## 2. Mathematical Formulation and Numerical Techniques

Choosing a particular CFD model mainly depends on the characteristics of the physical process to be simulated. It further depends on the goals of the numerical simulation and the available computational facilities. To achieve an accurate representation at the targeted turbulence scale, the whole comprehensive of the mathematical model was required. However, the computational cost is one of the important factors that should be taken into account.

In the present work, the Navier–Stokes equations coupled with the  $k-\epsilon$  turbulence model in the case of the incompressible steady-state fluid flow are implemented by using COMSOL Multiphysics software package.

### 2.1. Reynolds-Averaged Navier–Stokes (RANS) Equations

The partial differential equations that present the average steady-state incompressible flow are described from continuity (Equation (1)) and momentum (Navier–Stokes) (Equation (2)), which simplifies to:

$$\rho(\nabla \cdot \bar{v}) = 0 \tag{1}$$

$$\rho(\bar{v} \cdot \nabla) \bar{v} = \nabla[-p + g + \mu(\nabla \bar{v} + (\nabla \bar{v})^T)] - \rho \bar{v}_r(\nabla \bar{v}_r) + F \tag{2}$$

where  $v$  is the velocity,  $\rho$  the density,  $p$  the pressure,  $F$  the density of volumetric forces acting in the fluid, and  $\nabla$  the gradient operator.  $\mu$  is the dynamic viscosity that depends only on the physical properties of the fluid and  $\mu_T$  is the turbulent eddy viscosity which is supposed to simulate unresolved velocity fluctuations  $u'$ .

The system of the equations has an additional term that means the turbulent Reynolds stress  $-\rho \bar{v}_r(\nabla \bar{v}_r)$  representing the influence of the fluctuation on the average flow. In order to close its system,

this term must be determined. To achieve this condition, the standard  $k - \epsilon$  turbulence model was chosen in the following section.

### 2.2. Standard $k - \epsilon$ Turbulence Model

The most common model used in CFD simulation for the turbulent applications is the standard  $k - \epsilon$  turbulence model [8], which was introduced by [9]. The model solves for two transport equations, the turbulence kinetic energy  $k$  (Equation (3)); and the turbulence dissipation energy  $\epsilon$  (Equation (4)), respectively [10]. The recommended values of standard closure constants implement in both of the transport equations given in Table 1. In the present work, these constants have been adjusted according to the features of the surface boundary layer in neutral atmospheric conditions suggested by [11].

$$\rho(\bar{v} \cdot \nabla)k = \nabla \cdot \left[ \left( \mu + \frac{\mu_t}{\sigma_k} \right) \nabla k \right] + P_k - \rho \epsilon \tag{3}$$

$$\rho(\bar{v} \cdot \nabla)\epsilon = \nabla \cdot \left[ \left( \mu + \frac{\mu_t}{\sigma_\epsilon} \right) \nabla \epsilon \right] + C_{\epsilon 1} \frac{\epsilon}{K} P_K - C_{\epsilon 2} \rho \frac{\epsilon^2}{K} \tag{4}$$

$$P_K = \mu_t \left[ \nabla \bar{v} + (\nabla \bar{v})^T \right] : \nabla \bar{v}, \mu_t = \rho C_\mu \frac{K^2}{\epsilon} \tag{5}$$

**Table 1.** Overview of the closure constants used for the standard  $k - \epsilon$  turbulence model.

	$C_\mu$	$C_{\epsilon 1}$	$C_{\epsilon 2}$	$\sigma_k$	$\sigma_\epsilon$	$\kappa$
Standard	0.09	1.44	1.92	1.0	1.3	0.41
Neutral ABL	0.033	1.176	1.92	1.0	1.3	0.42

### 2.3. Boundary Conditions

The full model to specify the turbulence airflow is mentioned above. The presence of the linear term in momentum equation produce some difficulty in the solving process of the equations. On the other hand, the hypothesis of the standard  $k - \epsilon$  turbulence model is not applicable near the surface. However, an accurate specification of the boundary conditions on the various sides is needed. It is summarized in Table 2.

**Table 2.** Summary of the boundary conditions.

Boundary Conditions	Inlet	Outlet	Wall	Open Boundary
Standard $k - \epsilon$	$U_{(y)} = \frac{u_\tau}{\kappa} \ln\left(\frac{y+z_0}{z_0}\right)$ $k(y) = \frac{u_\tau^2}{\sqrt{C_\mu}} \left(D_1 - \frac{y}{D_2}\right)^2$ $\epsilon(y) = \frac{C_\mu^{3/4} k^{3/2}}{\kappa_\epsilon y}$	$P = P_{atm}$	Scalable Wall function	$\frac{\partial}{\partial n}(u, v, k, \epsilon) = 0$

The boundary condition of the wall surface was fixed by scalable wall function condition that requires the standard  $k - \epsilon$  turbulence model, which is presented in COMSOL Multiphysics by the following equations [12]:

- Velocity was applied as a no-slip condition

$$\bar{u} \cdot n = 0 \tag{6}$$

- Shear stress condition



$$n \cdot \bar{\sigma} - (n \cdot \bar{\sigma} \cdot n)n = -v_\tau \frac{\bar{u}}{\|\bar{u}\|} \max(C_\mu^{1/4} \sqrt{k}, v_\tau) \tag{7}$$

with

$$\bar{\sigma} = \nu(\nabla \bar{u} + (\nabla \bar{u})^T), v_\tau = \frac{\kappa \|\bar{u}\|}{\ln(\delta_w^+ + \kappa B)} \tag{8}$$

- Turbulent kinetic energy and dissipation energy

$$n \cdot \nabla k = 0, \varepsilon = \frac{C_\mu^{3/4} k^{3/2}}{\kappa \delta_w} \tag{9}$$

The scalable wall function is assumed to be positioned at a distance from the wall  $\delta_w$  as shown in the Figure 1. This distance refers to the intersection of the logarithmic layer and viscous sublayer in the value of the dimensionless distance from  $\delta_w^+$  equal to 11.06, where  $\delta_w^+ = \rho u_\tau \frac{\delta_w}{\mu}$  and  $u_\tau = C_\mu^{1/4} \sqrt{k}$  is the friction velocity. The scalable wall function means that the dimensionless distance from the wall is limited from below so that it never become smaller than half of the height of the boundary mesh cell  $\delta_w^+ = \{11.06, \frac{h^+}{2}\}$  [6].

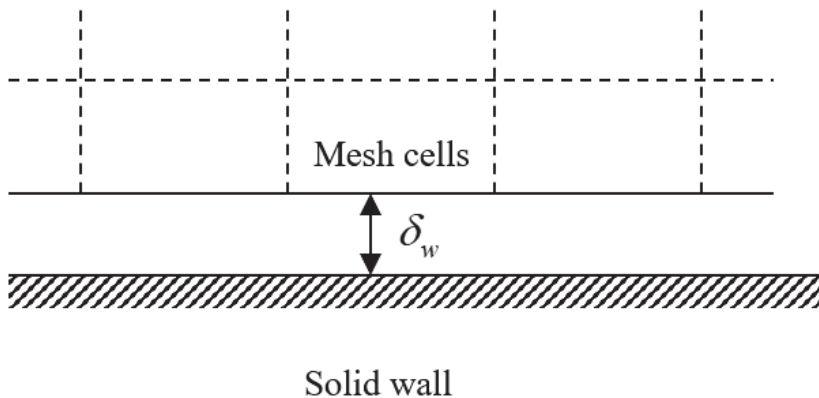


Figure 1. Distance from the wall to the computational domain.

### 3. Computational Domain and Mesh Configuration

In this work, simulation was considered via a 2D airflow approximation of the problem. In addition, the implementation of four wind turbines aligned with two different hills slopes was performed. The wind turbines were separated by distances in x-direction such as  $x = -10D, x = 0D, x = 2D, x = 10D$ , respectively from the center of domain, where  $D = 125$  mm is the rotor diameter and the hub height was  $y_{hub} = 100$  mm from  $y = 0$ .

Assuming the wind tunnel data of the RUSHIL experiment [7], the computational domain was indicated as the same configuration mentioned in [13]. The surface is considered to be a horizontal plane with a hill as shown in Figure 2. The dimensions of the surrounding domain correspond to the length  $\pm 40$  H up and downstream of the top of the hill to vertical height of  $\pm 13.7$  H.

The slopes of the hills are defined by the parametric equation specified in [13]. They are called here Hill3 and Hill5 as function to their  $a/H$  ratios and according to their maximum hill slopes which are  $26^\circ$  and  $16^\circ$ , respectively. The hill height H was fixed by 0.117 m. The uniform velocity and the friction velocity were fixed by  $U_0 = 4$  m/s and  $u_* = 0.188$  m/s, respectively. On the other hand, the boundary layer depth takes a value equal to  $D = 1$  m with a roughness length fixed by  $z_0 = 0.157$  mm.

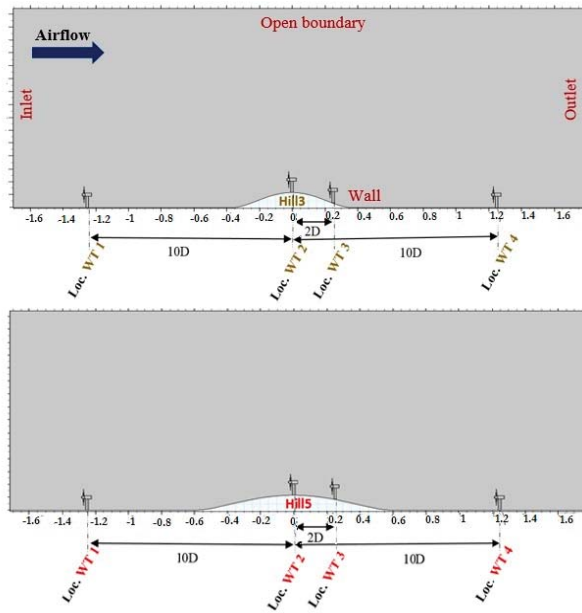


Figure 2. Schematic of the computational domain: (Top) Hill3+ Wind farm, (Bottom) Hill5+ Wind farm.

At the practical level, CFD simulation typically faces the challenge of creating an initial mesh that is sufficiently accurate to produce a solution for the real problem and in particular for the required wall law resolution. In this case, a parametric study was also performed in order to identify a suitable mesh. The ground surface was meshed using the properties of the boundary layer mesh, then, a free triangle mesh elements was used for the whole of the computational domain. The complete domain contains 15,065 mesh elements and it was definite with the maximum elements growth rate fixed at 1.2. The configuration of the obtained mesh until convergence was shown in Figure 3.

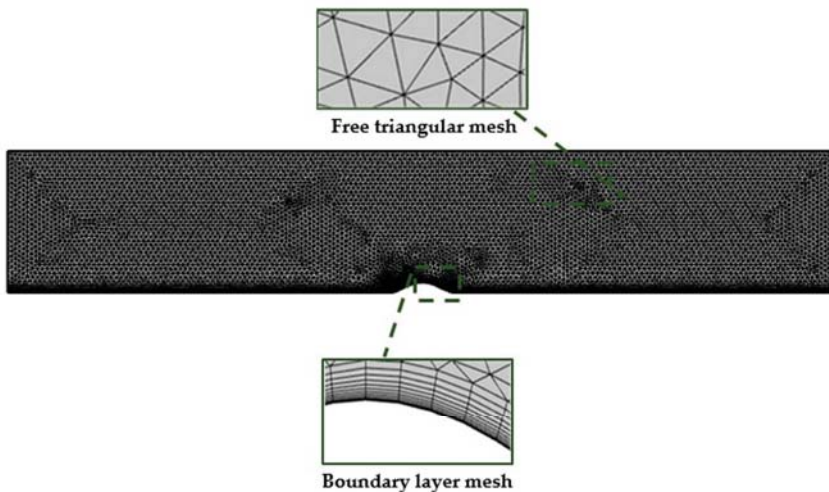
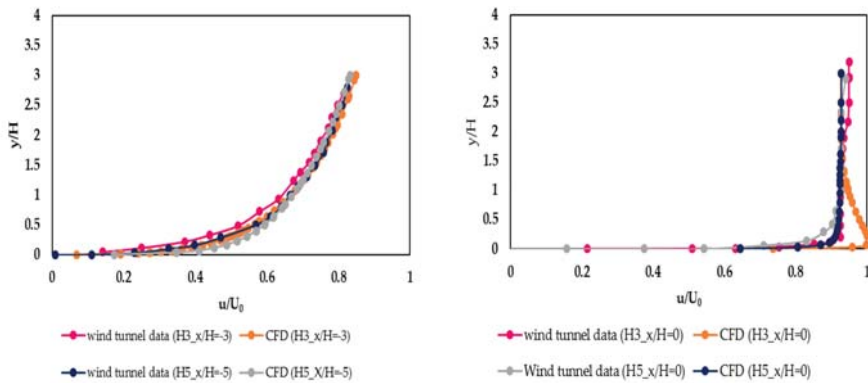


Figure 3. Detail of the mesh elaborated with free triangle elements and the boundary layer mesh near the ground surface.

#### 4. Results and Discussion

To study the surface flow over hilly terrain further, three cases are analyzed below. The first considers the streamwise velocity profile implementation in Figure 4, which show the agreement with wind tunnel data measurement. The third case considers the presence of the Hill3 and Hill5 with the installation of the wind turbines in several locations (hilly terrain + wind farm). First location at  $x = -10D$  in the upstream of both hills. Therefore, the second location is presented and placed on top of both hills (Hill3 and Hill 5) at  $x = 0D$ , while the third involves the turbine placed at  $x = 2D$  of both hills. Finally, the fourth contains the turbine placed far away from both hills and at distance  $x = 10D$  from the symmetry of the hills. Then, the streamwise velocity profile was measured at the hub height for four positions, as shown in Figure 5.



**Figure 4.** Mean streamwise profiles of velocity component: (left) Hill3+ Hill5+ Wind tunnel data (upstream  $x/H = -3$  for H3 and  $x/H = -5$  for H5), (right) Hill3+ Hill5+ Wind tunnel data (summit  $x/H = 0$ ).

Further, to study the distribution of the flow over wind farm in complex terrain, the simulation was done at four selected locations, as illustrated in Figure 5. The mean streamwise velocity profiles for two cases (with and without wind turbines) around hilly terrain with various slope are schemed in Figure 6. The wind-speed curves of inflow on flat terrain are plotted too for comparison purposes. All the velocities presented in Figure 6 are normalized with hub height velocity  $U_{hub}$ . The wind-speed profile was taken at  $1D$  before of the center of the wind turbines.

Figure 6a treats the horizontal stream-wise velocity along of the wind turbine for the Case 1, which is placed at the distance of  $-10D$  in the upstream of the hill. Firstly, it can be seen that under the hill height ( $y/D < 1$ ), the velocity distribution on hilly terrain without wind turbine is depressed when compared with the upstream on flat plate. The little discrepancies between complex terrain without wind turbine and flat terrain from close the ground to the hill summit. Therefore, it is due to the blockage effect on the flow situated in lee side of the hill. Hence, it is necessary to consider this effect because it can decrease the extractable kinetic energy from the air by wind turbine.

Then, above ( $y/D > 1$ ) the horizontal velocity increase with the elevation, these discrepancies reduce continuously and finally disappear after the top of the hill. Thus, if the wind turbine moves by the distance higher than  $10D$ , it can decrease this blockage effect. On the other hand, the important difference of stream-wise velocity distributions on  $x$ - $y$  planes of hilly terrain with wind turbine can be seen when compared with hilly terrain without wind turbine. However, this difference is caused by obstruction of the wind turbine. Consequently, in order to ensure noble studies and results as assessment of wind farms, all these effects cannot be ignored.

Case 2 describes the behavior of the flow on the crest of the hill, with the wind turbine placed at this location.

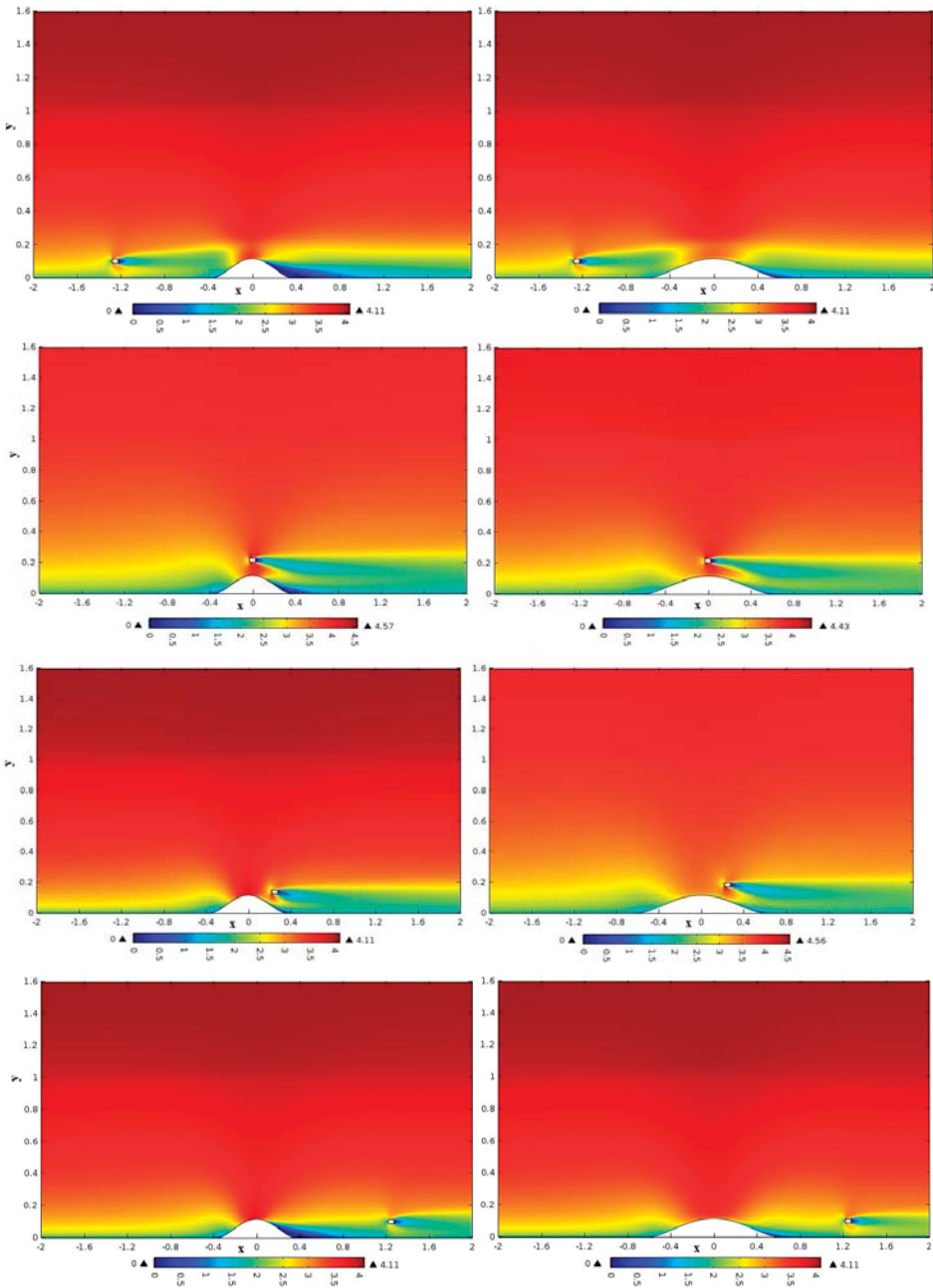


**Figure 5.** Contours of average velocity in the x-y direction for four location of wind turbine with two slopes of the hills (H3 and H5): (line 1)  $x = -10D$ , (line 2)  $x = 0D$ , (line 3)  $x = 2D$ , (line 4)  $x = 10D$ .

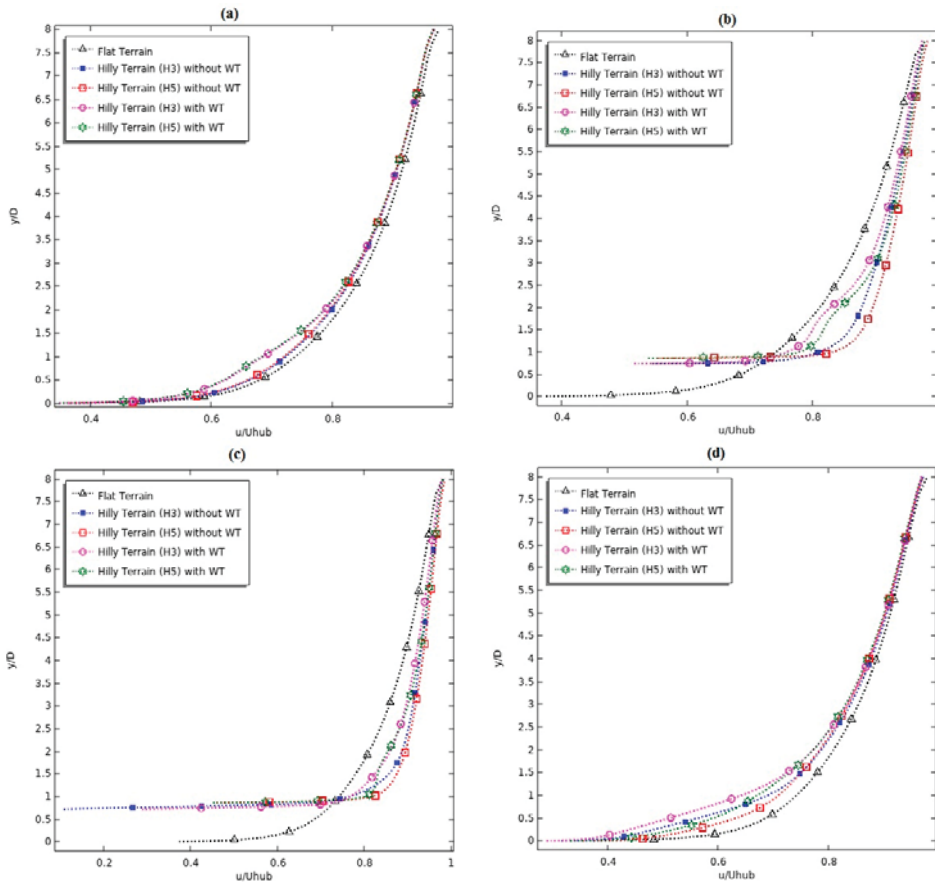


**Figure 6.** Comparison of the normalized mean streamwise of velocity component for four location of wind turbine with two slopes of the hills (H3 and H5): (a)  $x = -10D$  (cut-line at  $1D$  before center of WT); (b)  $x = 0D$  (cut-line at  $1D$  before center of WT); (c)  $x = 2D$  (cut-line at  $1D$  before center of WT); (d)  $x = 10D$  (cut-line at  $1D$  before center of WT).

In this section, the position is analyzed of horizontal-spanwise curves of the normalized averaged streamwise velocity on the top hill for the both of the hill slopes. It can be observed from Figure 6b, that when the cut-line is placed at  $1D$  before center of wind turbine, the effect of the acceleration on the hill was clearly presented. An interesting observation that might be drawn from Figure 6b, is that the maximum speed is on the top of the hill for H3 and H5 without installed wind turbine due to the compression on this location depending on the wind side and leeward slope of the hill and the influence of change distribution of the flow caused by different positions at all of the length hill. Then, we can observe the increase of velocity from the hill height to the hub height ( $0.73 < y/D < 2$ ) for H3 and ( $0.86 < y/D < 2$ ) for H5 when compared by flat terrain  $y/D = 0$  ( $u/U_{hub} = 0.78$ ). However, the velocity for high slope H3 reaches the value of  $u/U_{hub} = 0.87$  and  $u/U_{hub} = 0.9$  for low slope H5. Therefore, the local acceleration of the hilly terrain can reproduce the increase of power ratio in wind farms and adjust the distribution of the wind speed to decrease the fatigue loads acting on the wind turbine. On the other hand, when installing the wind turbine on the top of the both of hill, it can be seen from Figure 5 (line 2) the distribution of velocity and from Figure 6b the streamwise velocity curves for Hill3 and Hill5 by the presence of wind turbine are lower than complex terrain without

turbine, especially when compared with the velocity from the hill height until upper limit of the wind turbine rotor ( $0.73 < y/D < 2.25$  for H3 and  $0.86 < y/D < 2.25$  for H5). Thus, the difference for the H3 high slope is about 2.5% and for the H5 low slope is about 3.5%. Then, the speed-up surface is choked by the presence of nacelle and the hub in our computational domain, that is to say, the presence of wind turbine in reality. In other way, it can be positive for increased lifetime of the rotor blades.

Figure 6c gives the horizontal velocity profile for case 3 in which wind turbine is installed at downside of the hill (2D at the down of the hill). It is based on the comparison of five curves, which include the two hilly terrains for the high and low slope H3 and H5, respectively, with and without wind turbine and the curve of flat terrain. The important effect of the slope hill can clearly be observed over downhill in Figure 5a and in wind profile of H3 and H5 presented in Figure 5c for hilly terrain without wind turbine that the high slope produce steep detachment and separation of the boundary layer compared to that of the low slope. However, its steep detachment and separation produce the strong adverse pressure gradient in this region, which contributes to the large decreasing of wind speed, so that the wind turbine cannot extract a significant quantity of kinetic energy. In addition, the rotor blades can be affected by the reversed flow in the developed recirculation region at downwind of the obstacle. The two other wind profiles show the distribution of velocity of H3 and H5 with location wind turbine. At this point, the little decrease of velocity for the range  $0.9 < y/D < 2$  can be shown due to the obstructing wind turbine that increases the adverse pressure gradient leeward of the obstacle. In addition, the velocity of the high slope H3 at this position is lower than H5 due to the difference steep of the separation. Furthermore, the uniform distribution of velocity continued in this location due to the previous effect of acceleration on the crest of the hill.

Comparison of wind-speed curves at a distance 10D far from the hill for flat terrain and hilly terrain for both hills with the absence of wind turbine, and speed curves at the similar location with wind turbine is plotted in Figure 6d. Whereas, as mentioned above, the velocity with turbine is lower than the absence of the wind turbine, it can see from Figure 6d that there are little discrepancies between the two cases, therefore its effects on the rotating blades can be ignored. However, the effect that cannot be neglected is the decrease of velocity that is shown clearly in Figure 6d when compared with flat terrain. Its thrust is such that the velocity profile returns to take original form of the atmospheric boundary layer profile, but the impact of the hill largely degrades the wind speed. The slope of hill affects the developing of the scale of separation, which can be seen from the Figure 5 (line 4) and Figure 6d the wind turbine in the case 4 affect by the large separation of the H3 hill by comparison with H5. Moreover, the large separation can produce the increase of turbulence intensity, which increases the fluctuations loads acting on the blades of wind turbine. To reduce the most significant impact on results and to increase the power ratio in this location, it would be necessary to adjust the distance between hill and installed wind turbine.

The results show that the presence of the hills in wind farm have a positive influence on the performance of the wind-turbine, but then again, it would be necessary to take account the change of velocity results in the implementation of the wind turbine for the given respectable conditions of micro-siting. On the other hand, choosing the location that contribute significantly the increase of the lifetime of the wind turbines is important.

## 5. Conclusions

A CFD simulation was proposed and applied to examine the impact of micro-scale wind turbines on wind farms within both flat and hilly configurations, on two different slopes in this study. However, it was based on the simulation of the implementation of four various positions of the wind turbine. The changes and distributions of wind speed were discussed. The main findings of this study can be summarized as follows:

1. Hill slopes are an important element for flow characteristics and disturbing effect. The steep slope and the separation of the flow due to the high adverse pressure gradient will considerably decrease the average speed.

2. The velocity distribution of modelling the wind turbine in the simulation process is more likely than for the absence of the wind turbine.
3. In the crest of the hill, the average speed on two positions highly increases, which leads to an extractable maximum power rate. In addition, reduced fatigue loads, which act on wind turbines on the crest of hill caused by the decrease in turbulence at these locations, yield to increase the lifetime of the rotor blade.
4. The velocity profile in the wind turbine located at the down of the hill is still higher for low slope due to the small effect of the separation than the high slope. Therefore, the wind speed profile returns to the form of the boundary layer profile for both cases before and after the hill. The velocity of a wind turbine located at some distance before and after the hill is even lower than that of flat terrain due to the separation and interaction airflow effect in the windward side, which can be caused by choosing a small distance.

On another hand, for the accuracy of siting of the wind farms, the accurate study of the affecting the two lateral of the hill, the increase of turbulence, the characteristics of the flow affected by the change topography and obscurity of the implement wind turbines should be considered. Nevertheless, the numerical solutions achieved indicate that the wind farm siting in the hilly ground is appropriate.

**Conflicts of Interest:** The authors declare no conflict of interest.

## References

1. Bhattacharya, P. *Wind Energy Management*; Smiljanic, T., Ed.; IntechOpen: Rijeka, Croatia, 2011; ISBN 9533073365.
2. Jin, T.; Tian, Z. Uncertainty analysis for wind energy production with dynamic power curves. In Proceedings of the 2010 IEEE 11th International Conference on Probabilistic Methods Applied to Power Systems, Singapore, 14–17 June 2010; IEEE: New York, NY, USA, 2010; pp. 745–750.
3. Alfredsson, P.H.; Segalini, A. Introduction Wind farms in complex terrains: An introduction. *Philos. Trans. A Math. Phys. Eng. Sci.* **2017**, *375*. [[CrossRef](#)] [[PubMed](#)]
4. Choudhry, A.; Mo, J.-O.; Arjomandi, M.; Kelso, R. Effects of Wake Interaction on Downstream Wind Turbines. *Wind Eng.* **2014**, *38*, 535–547. [[CrossRef](#)]
5. Yan, S.; Shi, S.; Chen, X.; Wang, X.; Mao, L.; Liu, X. Numerical simulations of flow interactions between steep hill terrain and large scale wind turbine. *Energy* **2018**, *151*, 740–747. [[CrossRef](#)]
6. COMSOL Multiphysics. *Introduction to COMSOL Multiphysics*; COMSOL Inc.: Stockholm, Sweden, 2016.
7. Khurshudyan, L.H.; Snyder, W.H.; Nekrasov, I.V. (Eds.) *Flow and Dispersion of Pollutants over Two-Dimensional Hills: Summary Report on Joint Soviet-American Study*; Version Details—Trove; Environmental Protection Agency: Washington, DC, USA, 1982.
8. Pope, S.B. *Turbulent Flows*; Cambridge University Press: Cambridge, UK, 2000; ISBN 9780511840531.
9. Jones, W.; Launder, B. The prediction of laminarization with a two-equation model of turbulence. *Int. J. Heat Mass Transf.* **1972**, *15*, 301–314. [[CrossRef](#)]
10. Ferziger, J.H.; Peric, M. *Computational Methods for Fluid Dynamics*, 3rd ed.; Springer: Stanfrod, CA, USA, 2002.
11. Panofsky, H.A.; Dutton, J.A. *Atmospheric Turbulence. Models and Methods for Engineering Applications*, 1st ed.; John Wiley & Sons: New York, NY, USA, 1984.
12. COMSOL Multiphysics. *Multiphysics COMSOL Modeling Guide*; COMSOL Inc.: Stockholm, Sweden, 2007; ISBN 1781273332.
13. Castro, I.P.; Apsley, D.D. Flow and dispersion over topography: A comparison between numerical and laboratory data for two-dimensional flows. *Atmos. Environ.* **1997**, *31*, 839–850. [[CrossRef](#)]

**Publisher's Note:** MDPI stays neutral with regard to jurisdictional claims in published maps and institutional affiliations.



© 2020 by the authors. Licensee MDPI, Basel, Switzerland. This article is an open access article distributed under the terms and conditions of the Creative Commons Attribution (CC BY) license (<http://creativecommons.org/licenses/by/4.0/>).



# Modeling of Wind Turbines Based on DFIG Generator <sup>†</sup>

Sabra Ahyaten \*  and Jalal El Bahaoui

Department of Physics, Faculty of science Tetouan, Abdelmalek Essaadi University, 93 030 Tetouan, Morocco; jelbahaoui@yahoo.com

\* Correspondence: ahyatensabra@gmail.com or sabra.ahyaten@etu.uae.ac.ma; Tel.: +212-669681292

† Presented at the 14th International Conference INTER-ENG 2020 Interdisciplinarity in Engineering, Mureş, Romania, 8–9 October 2020.

Published: 16 December 2020

**Abstract:** The role of wind energy is so promising as a source of future energy all over the world. However, whether the unpredictable nature of wind speed fluctuations and the stability of the power systems be affected by a high penetration of wind power remains an unanswered question. Therefore, an accurate analysis study of the effectiveness and robustness performance of the doubly fed induction generator (DFIG) is one of the challenges in wind turbine applications. The present works tackle the issue of grid connection of DFIG modeling and the dynamic operation to evaluate the capabilities and their impact on the pitch angle, current and voltage stability. The model is simulated using MATLAB/Simulink software, and the curves' results are indicated based on the system that was connected to eight wind turbines in the wind farm. The results show the dynamic features of the DFIG response to the necessary output variables. On the other hand, its show us a view of the waveforms obtained, which means that an adequate study for choosing the type of control suitable for the DFIG is necessary.

**Keywords:** doubly fed induction generator (DFIG); grid; power system; renewable energy; wind turbine

## 1. Introduction

At the global scale, the improvement of renewable energy in modern production power systems has exponentially increased due to the increase in greenhouse gas concentrations in the atmosphere, which are extremely destructive to our planet. Wind energy has become a suitable answer for producing clean energy and is currently the quickest developing source when correlated with other sustainable power sources. Nonetheless, the use of available energy depends on weather conditions (wind speed) and its integration produces volatility in the power system. Integrating renewable energies with network connection, intelligent control, and storage systems could result in a change in generating electricity and reducing CO<sub>2</sub>. The demand for a 100% renewable electricity supply by the global energy storage has already analyzed [1,2]. According to the author of International Electrotechnical Commission, the need for energy storage arises as a result of the increasing use of renewable energy and innovations in smart grids [3]. For 2050, it is foreseen that renewable energy sources (RESs) will be able to meet 70% of the world's energy needs. Wind, solar energy, and storage systems will be the most important. The investment in these energy alternative sources reduces in the electricity sector greenhouse gas emissions and also decreases fossil fuel dependence [4]. Wind energy will probably be the most dominant and will be the first immediate practical power of a global energy system, and the bulk of most nuclear and fossil fuel sources will also be replaced completely. At present, efforts to increase and improve the wind sector's participation in the electricity generation market have aroused the interest of numerous researchers [5]. It is important to mention that the development of power electronic technologies (power semiconductor devices, converters, pulse width modulation



(PWM) techniques) has played an enormous role in the improvement of wind turbine efficiency. Therefore, this strong problem of wind energy in the electrical system has been strictly linked to the enhancement of wind turbine conversion and control technology [6]. These systems can be operated in order to encounter the network requirements since they can supply frequency, and active/reactive power. Essentially, there are several types of generators used in the wind power fields such as the squirrel-cage induction generator (SCIG), doubly fed induction generator (DFIG) and a direct-drive synchronous generator (DDSG) [7–9]. However, the doubly fed induction generator (DFIG) is the most frequently chosen. The reason behind this popularity is the fact that DFIG is based on the operation and independent control of active and reactive power. One of the examples of using this kind of generator in power systems application is presented by Raúl in [10], who investigated the DFIG-based hybrid system by modeling the different battery and ultra-capacitor energy storage systems. This modeling has been performed by using intelligent control techniques such as fuzzy logic to generate a compensating active power term that is changed between both energy storage systems (ESSs) to adjust their state of charge (SOC) according to the operating conditions. The impact of the wind turbines on the dynamic behavior of the system experiencing a fault and how the wind turbines behave in the system when it experiences a transient fault have also been analyzed [11]. Furthermore, it has also been found that if a transient fault in the system lead to considerable excursions in voltage and/or frequency the wind turbines were to disconnect and reconnect only once the system has returned to stable operation [12–14]. While increasing wind power penetration leads to the problem that a considerable amount of generation might disconnect in case of a transient fault in the system, this causes the system to become unstable from an otherwise harmless fault situation [15]. According to this, the grid-connected DFIG wind turbines was used in the present work. This paper indicates how the study of the dynamic behavior of the DFIG characteristic analysis and its effectiveness and optimal performance can assess the impact on the output variables of a wind farm encompassing many wind turbines. The purpose of this research was to have an exact view of the distribution and degree of fluctuations presented in the pitch angle, current, and voltage curves. In order to choose a suitable DFIG-t type control based on a series-connected wind farm by the conjunction a hybrid system consisting of several wind turbines, an energy storage system must be selected in future work to avoid such situations.

## **2. Power System Model Integrated with Wind Farm Using DFIG**

A dynamic model of a DFIG wind turbine can be indicated in terms of the equations of a piece system. The stator winding is connected directly to the grid, while a bidirectional power converter feeds the rotor windings, allowing variable frequency operation in the rotor currents. This power converter is made up of two back-to-back insulated gate bipolar transistor (IGBT) bridges (rotor side converter, or RSC; and grid side converter, or GSC) linked by a DC bus. The wind turbine is also equipped with a blade pitch angle controller that limits wind power capture and rotational speed for high winds. Figure 1 represents its configuration.

The output power of the turbine is controlled to follow a determined power–speed characteristic, called tracking characteristic. The electrical output power on the network the wind turbine terminals are added to the power losses is compared to the reference power obtained from the tracking feature. In the converter system on the rotor side, AC voltage and Volt Ampere Reactive (VAR) are regulated. The DC–DC intermediate circuit contains two converters: first converter AC to DC and second converter DC to AC. The intermediate DC to DC circuit consists of current regulation, DC voltage and pitch control system. The last one is adjusted at zero degrees by the regulator of pitch angle to the extent that the speed is required to follow the characteristics of the control system. The DC voltage output from intermediate circuit was applied to the grid side converter which consists of an insulated gate bipolar transistor (IGBT) two-level inverter, generating an AC voltage at 60 Hz. A 12 MW wind farm consisting of eight 1.5 MW wind turbines connected to a 25 kV distribution system exports power to a 120 kV grid through a 30 km, 25 kV feeder. The wind speed is maintained constant at 15 m/s.

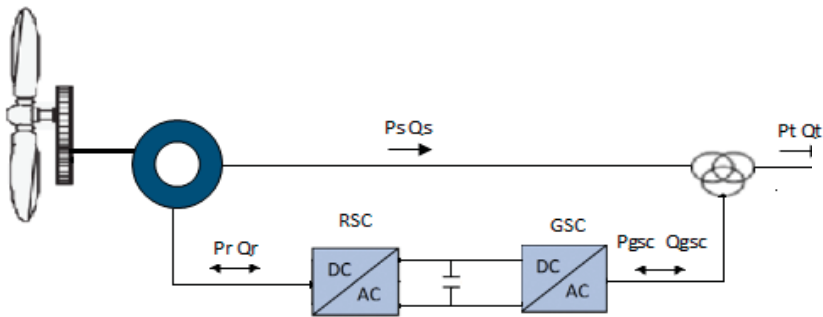


**Figure 1.** Doubly fed induction generator (DFIG) wind turbine scheme by Rotor side converter (RSC) and grid side converter (GSC).

2.1. Mechanical System Model

The system mechanic contains the drive train and aerodynamic rotor. The model of the rotor expresses the mechanical torque extracted from the wind, defined by the actuator disk theory. This torque is transmitted to the DFIG rotor through the drive train, represented by the well known two masses model. In this model, two rotating masses—the aerodynamic rotor and the DFIG rotor—are elastically connected via springs, characterized by the stiffness and damping factor of the coupling [9].

2.2. Electrical System Model

The DFIG and its power converter are two important factors that can be indicated in the electrical system model. The DFIG system can be implemented under a fifth-order model to define its behavior. The four electrical equations are indicated in a direct (*d*)-quadrature (*q*) for the rotor and stator voltage coordinates, which include the synchronous turning speed in this wind farm. The equations are determined by

$$U_{ds} = R_s i_{ds} + \frac{d}{dt} \varphi_{ds} - \omega \varphi_{qs} \tag{1}$$

$$U_{qs} = R_s i_{qs} + \frac{d}{dt} \varphi_{qs} - \omega \varphi_{ds} \tag{2}$$

$$U_{dr} = R_r i_{dr} + \frac{d}{dt} \varphi_{dr} - (\omega - \omega_r) \varphi_{qr} \tag{3}$$

$$U_{qr} = R_r i_{qr} + \frac{d}{dt} \varphi_{qr} + (\omega - \omega_r) \varphi_{dr} \tag{4}$$

where *U* represents the voltage, *i* represents the current,  $\omega$  is the rotating speed,  $\varphi$  denotes the magnetic flux, *R* represents resistance and *L* inductance, indexes *d* and *q* stand for the direct and quadrature components, and indexes *s* and *r* refer to the stator and rotor, respectively.

Furthermore, the mechanical power available from a wind turbine is typically given by (5) [9]:

$$P_w = 0.5 \rho \pi R^2 V_w^3 C_p(\lambda, \beta) \tag{5}$$

$$C_p = \frac{1}{2} (\lambda - 0.022 \beta^2 - 5.6) e^{-0.17 \lambda} \tag{6}$$

$$\lambda = \frac{V_w}{\omega \beta} \tag{7}$$

where *P<sub>w</sub>* is the extracted power from the wind,  $\rho$  is the air density, *R* is the blade radius and  $\omega \beta$  is the wind speed. *C<sub>p</sub>* is called the ‘power coefficient’ and is given as a nonlinear function of the parameters’

tip speed ratio  $\lambda$  and blade pitch angle  $\beta$ . The calculation of the performance coefficient requires the use of blade element theory.  $\omega_\beta$  is the rotational speed of the turbine. Usually,  $C_p$  is approximated as [12]:

$$C_p = \alpha\lambda + \beta\lambda^2 + \gamma\lambda^3 \tag{8}$$

### 3. Simulation and Results

The Figure 2 define the model based on the doubly fed induction generator. This model consists of eight 1.5 MW wind turbines connected to a 25 kV distribution system which exports power to a 120 kV grid through a 30 km, 25 kV feeder. The eight 1.5 MW wind turbines form a wind farm of 12 MW of power.

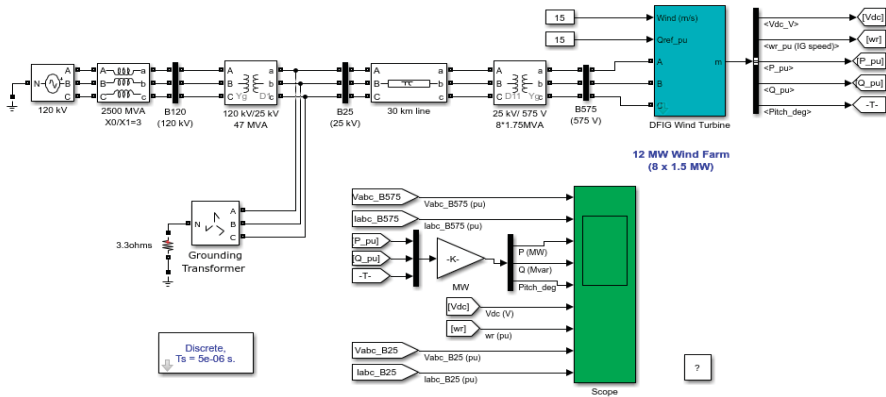


Figure 2. Schematic of the doubly fed induction generator model of MATLAB/Simulink.

In the following, we will represent and analyze simulation 1 over a period of 60 s by showing the graphs of the rotational speed, pitch angle, active power and DC link capacitor voltage and the current of wind turbines. Most of the variables of interest cited above were represented in pu values where the base power is the nominal power of each wind turbine (1.5 MW). The value 1 pu delimits the nominal power of the wind turbine. We will start by representing two important mechanical parameters, which are the rotational speed and the pitch angle of wind turbine. As we can see, the rotational speed of the rotor is regulated through the angle of the blades. From Figure 3a, the pitch angle starts to oscillate right after the disturbance. Nevertheless, it can be seen the oscillation decays after 5 seconds and the system is stable. Moreover, it is clear in Figure 3b that the rotational speed of the wind turbine starts at 1.2 pu during the first 10s of the simulation. However, the rotational speed decreases as well to a value below (1pu), which means the generator rotor of the wind turbine does not rotate at its rated value anymore. This behavior shows that the rotational speed is highly dependent on wind power. From Figure 3c, it can be seen that the DC link capacitor voltage shows small fluctuations on rotor active power and output power caused by wind speed variations. The voltage and currents considerably change the generator’s active and reactive powers, which are shown in Figure 3d. It also remarks in Figure 3e,g, that the wind farm DC voltage is the sum of the DC voltages of wind turbines, which means that the GSC is controlling the wind farm DC voltage by maintaining it to a set constant value and also assuring the active power exchange from the generator to the grid . It can also be seen from Figure 3f, h that the active power and reactive power diminution of the wind turbine fluctuates until the end of the simulation. The other parameter that is necessary to verify in order to check that our Simulink model is working perfectly is the DC voltage.

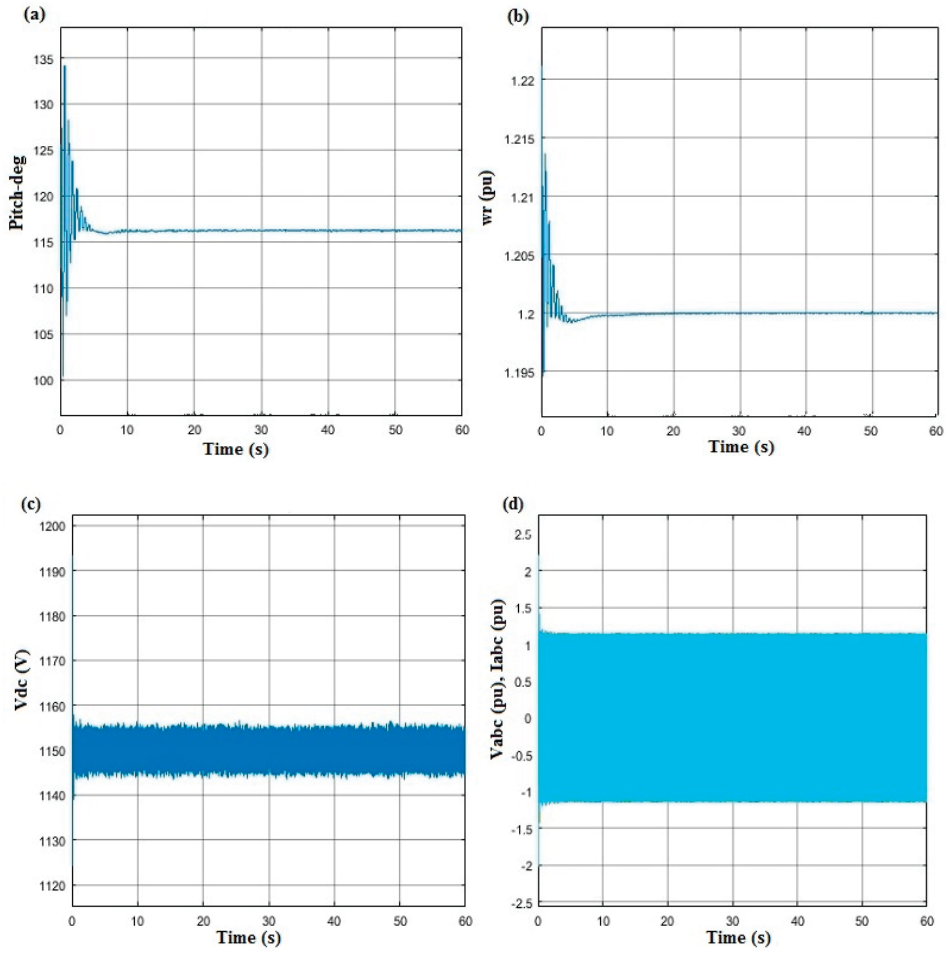
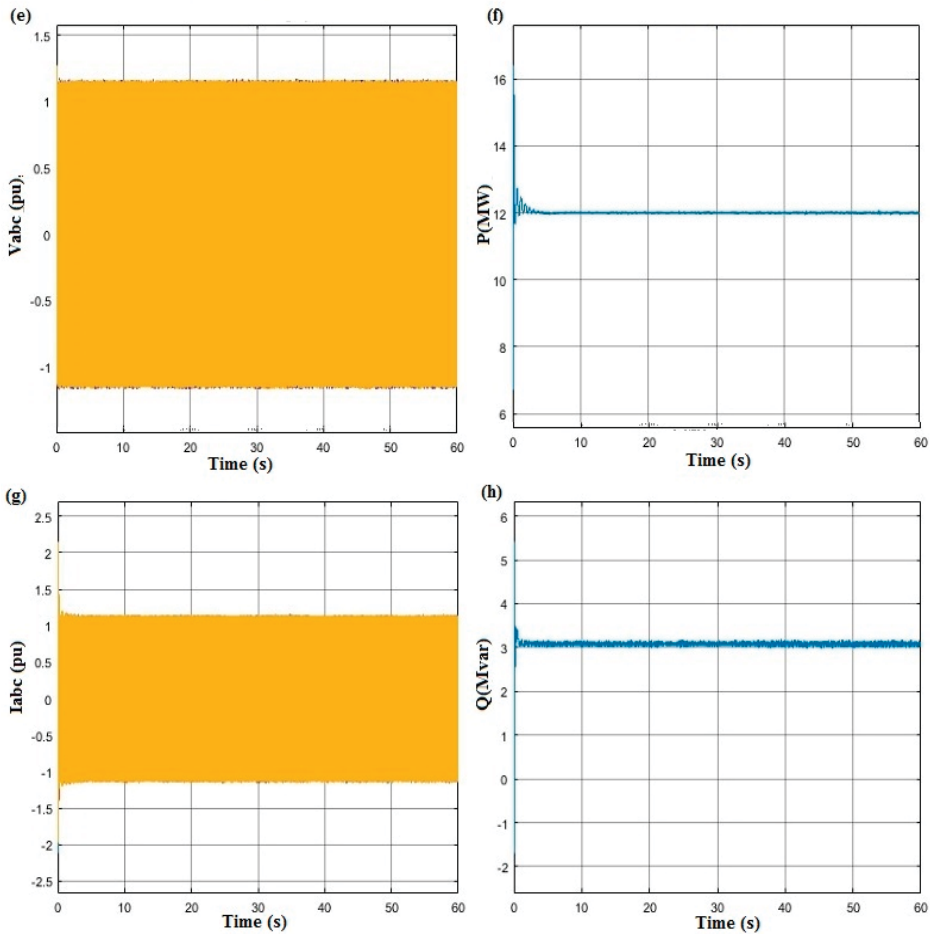


Figure 3. Cont.



**Figure 3.** Schematization of the set output variables of DFIG: (a) pitch-deg; (b)  $W_r$  (pu); (c)  $V_{dc}$  (V); (d)  $V_{abc}$  (pu)  $I_{abc}$  (pu); (e)  $V_{abc}$  (pu); (f)  $I_{abc}$  (pu); (g) P (MW); and (h) Q (Mvar).

#### 4. Conclusions

In this research, the DFIG and the dynamics operation were modeled to evaluate the responses and to assure the electrical distribution with the wind in terms of grid voltage and frequency fluctuations. Moreover, the main objective of this paper is the study on the dynamic behavior of the DFIG characteristic analysis and its effectiveness and optimal performance to assess the impact on the output variables of a wind farm contain many wind turbines. For this reason, the continuation of the proposal of this research is to make a hybrid system consisting of several wind turbines and an energy storage system will be selected to provide a clear idea and exact view of the distribution and degree of fluctuations as presented in the analysis and simulation in the pitch angle, current, and voltage curves to prevent such fluctuation situations and others. Each subsystem will be controlled via non-isolated power converters, and then coupled with grid or local load through the inverter. Simulations of the intelligent control system will also be improved through energy management among all the components of the hybrid system. Therefore, it is not enough to claim that one energy storage device is the best among all the others for each generator, but it is more appropriate to state that each of them has a better performance and is the most suitable for certain applications. Different

configurations will be studied to eliminate the weaknesses of DFIG generator wind turbines that will allow the use of electronic power converters. The storage devices comprised in the hybrid system add the flexibility and capacity to the control and regulate the active power generation of the hybrid system, which yield to adapt the changes on the grid demand.

**Conflicts of Interest:** The authors declare no conflict of interest.

## Abbreviations

The following abbreviations and notations are used in this manuscript:

DFIG	Doubly fed induction generator
RES	Renewable energy sources
PWM	Pulse width modulation
WECS	Wind energy conversion systems
$\omega_\beta$	Rotational speed of turbine
$V_w$	Wind speed
$\Lambda$	Tip speed ratio
$\beta$	Blade pitch angle
U	Voltage
R	Resistance
$P_w$	Power wind turbine
$C_p$	Polynomial function of $\lambda$ and $\beta$
GSC	Grid source converter

## References

1. Pleßmann, G.; Erdmann, M.; Hlusiak, M.; Breyer, C. Global energy storage demand for a 100% renewable electricity supply. *Energy Procedia* **2014**, *46*, 22–31. [[CrossRef](#)]
2. Bussar, C.; Moos, M.; Alvarez, R.; Wolf, P.; Thien, T.; Chen, H.; Cai, Z.; Leuthold, M.; Sauer, D.U.; Moser, A. Optimal allocation and capacity of energy storage systems in a future European power system with 100% renewable energy generation. *Energy Procedia* **2014**, *46*, 40–47. [[CrossRef](#)]
3. IEC White Paper Energy Challenge:2010. *Coping with the Energy Challenge The IEC 's Role from 2010 to 2030*; IEC: Geneva, Switzerland, 2010.
4. IRENA. *Global Energy Transformation: A Roadmap to 2050*, 2018th ed.; IRENA: Abu Dhabi, UAE, 2018.
5. Sun, Z.; Wang, H.; Li, Y. Modelling and simulation of doubly-fed induction wind power system based on Matlab/Simulink. *IET Conf. Publ.* **2012**, *2012*. [[CrossRef](#)]
6. Jami, H. *World Wind Resource Assessment Report*, 2014th ed.; World Wind Energy Association: Bonn, Germany, 2014.
7. Rolán, A.; Pedra, J.; Córcoles, F. Detailed study of DFIG-based wind turbines to overcome the most severe grid faults. *Int. J. Electr. Power Energy Syst.* **2014**, *62*, 868–878. [[CrossRef](#)]
8. Fernández, L.M.; García, C.A.; Saenz, J.R.; Jurado, F. Equivalent models of wind farms by using aggregated wind turbines and equivalent winds. *Energy Convers. Manag.* **2009**, *50*, 691–704. [[CrossRef](#)]
9. Krim, Y.; Abbes, D.; Krim, S.; Mimouni, M.F. Intelligent droop control and power management of active generator for ancillary services under grid instability using fuzzy logic technology. *Control Eng. Pract.* **2018**, *81*, 215–230. [[CrossRef](#)]
10. Precup, R.; Kamal, T.; Hassan, S.Z. *Advanced Control and Optimization Paradigms for Wind Energy Systems*; Springer: Singapore, 2019; ISBN 978-981-13-5994-1.
11. Shi, G.; Zhang, J.; Cai, X.; Zhu, M. Decoupling control of series-connected DC wind turbines with energy storage system for offshore DC wind farm. In Proceedings of the 2016 IEEE 7th International Symposium on Power Electronics for Distributed Generation Systems (PEDG), Vancouver, BC, Canada, 27–30 June 2016. [[CrossRef](#)]
12. Mu, W.; Wang, J.; Feng, W. Fault detection and fault-tolerant control of actuators and sensors in distributed parameter systems. *J. Franklin Inst.* **2017**, *354*, 3341–3363. [[CrossRef](#)]

13. Li, W.; Chao, P.; Liang, X.; Sun, Y.; Qi, J.; Chang, X. Modeling of complete fault ride-through processes for DFIG-Based wind turbines. *Renew. Energy* **2018**, *118*, 1001–1014. [[CrossRef](#)]
14. Nazir, M.S.; Wu, Q.H.; Li, M.; Luliang, Z. Lagrangian-Based Approach for Non-linear Dynamic Control of an Islanded Power System Short title: Non-linear dynamic control of power system. *Int. J. Comput. Sci. Inf. Secur.* **2017**, *15*, 24–29.
15. Sarrias-Mena, R.; Fernández-Ramírez, L.M.; García-Vázquez, C.A.; Jurado, F. Improving grid integration of wind turbines by using secondary batteries. *Renew. Sustain. Energy Rev.* **2014**, *34*, 194–207. [[CrossRef](#)]

**Publisher's Note:** MDPI stays neutral with regard to jurisdictional claims in published maps and institutional affiliations.



© 2020 by the authors. Licensee MDPI, Basel, Switzerland. This article is an open access article distributed under the terms and conditions of the Creative Commons Attribution (CC BY) license (<http://creativecommons.org/licenses/by/4.0/>).

# Designing an Artificial Intelligence Control Program Model to be Tested and Implemented in Virtual Reality for Automated Chevrolet Camaro <sup>†</sup>

Lavinia Andrei <sup>1</sup>, Doru-Laurean Baldean <sup>2,\*</sup> and Adela-Ioana Borzan <sup>2</sup>

<sup>1</sup> Public Health and Management, Faculty of Medicine, University of Medicine and Pharmacology, Cluj-Napoca, Victor Babeş, 400012 Cluj, Romania; andreilavinialavinia@yahoo.com

<sup>2</sup> Automotive Engineering and Transportation Department, Faculty of Automotive Engineering, Mechatronics and Mechanics, Technical University of Cluj-Napoca, Muncii 103-105, Cluj-Napoca, 400641 Cluj, Romania; adela.borzan@auto.utcluj.ro

\* Correspondence: doru.baldean@auto.utcluj.ro; Tel.: +40-26-420-2790

<sup>†</sup> Presented at the 14th International Conference INTER-ENG 2020 Interdisciplinarity in Engineering, Mureş, Romania, 8–9 October 2020.

Published: 22 December 2020

**Abstract:** A control program was designed with Unity 5 virtual reality application in the automotive and robotics field. Thus, a virtual model of a robotic car was tested in a virtual reality program. After optimization, the smart controller was implemented on a specific model of the automated Chevrolet Camaro. The main objective of the present paper is to design a control program model to be tested in virtual reality and in a real-size car. Results concerning the virtual modeling of an automated car and its artificial intelligence controls have been presented and discussed, outlining the forces, torques, and context awareness capabilities of the car.

**Keywords:** artificial intelligence; automated car; automotive; robotic vehicle; virtual reality

## 1. Introduction

Design and research are some of the most important sequences in the production protocol [1,2]. Defining the shapes, instruments, and methods used for production and optimization is inherent for design sequences [3]. The purpose of this paper is to outline the design sequences and manufacturing of an operational model. Additionally, it features the capability of automated driving, being controlled by a digital written program. It was first tested in virtual reality. Preparing the model for further development makes the progress in the automotive and robotic sector susceptible for convergence and accelerated unification. Communication technologies and mobile virtual fence systems are contributing to the topological object recognition process [4,5].

Automation and robotics are applied more and more in many industries, including automotive technology [6]. Robotization of transmission and gear shift mechatronics are popular applications [7]. Converging the automotive industry and robotics with complex mechatronics systems will provide the possibility for autonomous or automated driving in the near future [8]. The current problem is the integration and optimization of all the given systems and interdisciplinary efforts for one direction effort, which is road traffic safety [9]. Mechatronic systems should be precisely programmed like automated robots to perform safely in complex traffic scenarios [10]. Artificial intelligence may be implemented in electric cars to improve performance and responses [11–14]. Standards and measures are provided by different entities regarding self-driving cars to solve safety problems and to optimize road traffic flows [9,15–18]. An optimized model of a control program was designed, tested, and implemented in virtual reality for an automated robotic car. Specific targeted objectives



were the following: define the technical data concerning the robotic vehicle; use the support of driver-assistance system capabilities in a real-size model; create a virtual environment to match the challenges from real-world driving situations; program an automated model of the Chevrolet Camaro to follow different tracks in predefined scenarios; use different technologies (such as a mobile virtual fence and a context awareness mechanism) to improve communications of the automated vehicle with the traffic and infrastructure; configure the car control script in Unity 5 application; define the car dynamic parameters (forces and torque) and kinematic; and prepare the experimental testing of the real-size car. It was an important achievement to complete the model and test it in Unity 5 (as an artificial intelligence application) for validating the first step of research. It also used mobile virtual fence technology and vehicular network capabilities to increase safety and communication. Graphic design and programming were provided. The second step consisted of transferring the know-how to a real-size model car. In this case, the dynamics and detail aspects were more complex. Smart robot cars bring benefits and opportunities, but, at the same time, vulnerabilities and threats. More investigations should be made regarding automated cars in road traffic conditions.

## 2. Materials and Methods

The research methodology was based on simulation and testing, first in virtual reality and secondly, step by step, in a practical set up on a real-size model to highlight all the problems and limits of the automated driving process. Unity 5 digital application was used to generate shapes and simulate the robotic vehicle behavior. Multiple driving scenarios were studied to acquire the most significant actual values regarding the kinematics and dynamics of the simulated vehicle in virtual and real scenarios.

Materials used for the research were the Unity 5 program and Chevrolet Camaro model, for testing and investigating automated driver capabilities, with technical data given in Table 1. These requirements were matched in the experimental testing of the automated vehicle.

**Table 1.** Technical data regarding the robotic vehicle materials used for research.

Basic System	Value 1	Value 2
Propulsion	V6 engine	335 HP
Wheels	245/45R20 (front axle)	275/35R20 (rear axle)
Transmission	automatic	8L45 <sup>1</sup>

<sup>1</sup> Supporting driver-assistance system capabilities.

Virtual reality environment, known as Unity 5, allows the implementation of a program based on artificial intelligence in order to control the vehicle model, both in start-stop procedures and on the track following and collision avoidance, with a simplified schematic of the complex connections, shown in Figure 1.

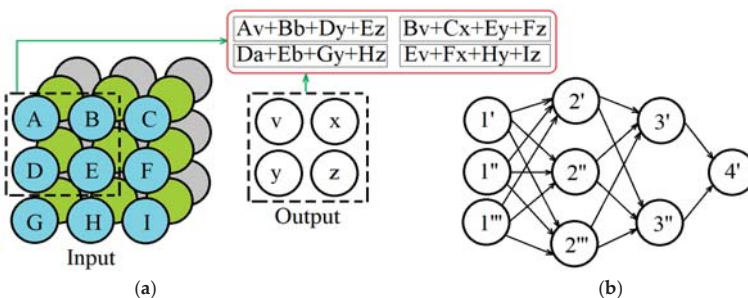


**Figure 1.** Simplified design of controlling methodology for the artificial intelligence (AI) program with neural networks: (a) applied method for machine learning; (b) artificial intelligence neural network combinations [1].

### 3. Investigation and Results

Results obtained by the virtual modeling in the Unity 5 simulation environment were compared with real-time testing data. The main findings of the robotic engineering research show that there were some kinematic limits for the designed vehicle model. Thus, the optimal safety was obtained for an alternative curving track at velocities under the value of 35 km/h. Sinusoidal driving of the tested vehicle with the value above was susceptible to safety hazards.

#### 3.1. List of Smart Robotic Automotive Applications and a Technological Investigation

##### 3.1.1. Smart Car versus Robotic Vehicle

The list of distinctive classes of smart vehicle applications:

- Genuine smart features on-board implemented by manufacturer
- Old vehicle with up-graded smart technologies
- Context-aware computing inside car
- Mobile virtual fences
- Mutual awareness mechanism
- Research or prototype smart cars

The list of automated or robotic car prototypes may be structured as follows:

1. Apple self-driving vehicles
2. Connected car with autopilot
3. Tesla autopilot
4. Volvo's autonomous concept vehicle
5. Waymo self-driving autonomous cars

##### 3.1.2. Investigating the Integration of Innovative Technologies

It is considered appropriate and factual to investigate the integration of new features and technologies to address conventional problems and risks, such as road events and traffic accidents. Virtual fence technology supports the inter-connection of mobile robots to enhance the mutual awareness factor. Vehicle-to-vehicle, vehicle-to-infrastructure, and vehicle-to-everything types of communication were considered and used to facilitate and implement the connected car feature in robotic vehicle development. Car-to-car connectivity facilitates implementation of the mutual awareness mechanisms.

#### 3.2. Virtual Reality Modelling and Design Results

Virtual reality program Unity 5 was used for environment generation and other testing components assembling, as shown in Figure 2. Results obtained in the designing process of the artificial intelligence control program consisted of digital content used for environment and track creation in virtual reality (VR), as well as the automated robotic Chevrolet Camaro vehicle, implemented in Unity 5 for drive testing.

Virtual robotic car Chevrolet Camaro in Unity 5 had automated driving features, and the real car supported the validation of the concept, with a driver assistance system, as shown in Figure 3. Air force ( $F_a$ ), force of gravity ( $F_g$ ), road reactions ( $R_f$ ,  $R_r$ ), and velocity were the main kinematic and dynamic parameters considered in the digital program, besides the engine's torque and power output.

Mobile virtual fence (MVF) was used by the automated robotic car, Chevrolet Camaro, in the Unity 5 testing scenario when self-driving to support the safety program and accident avoidance, as shown in Figure 4. Wireless communication capability and MVF make vehicular networking a possibility.



**Figure 2.** Basic programming results in virtual reality program Unity 5: (a) Environment used for track generation for digital testing of the robotic car; (b) sequence of the program used for automation of the Chevrolet Camaro robotic model.

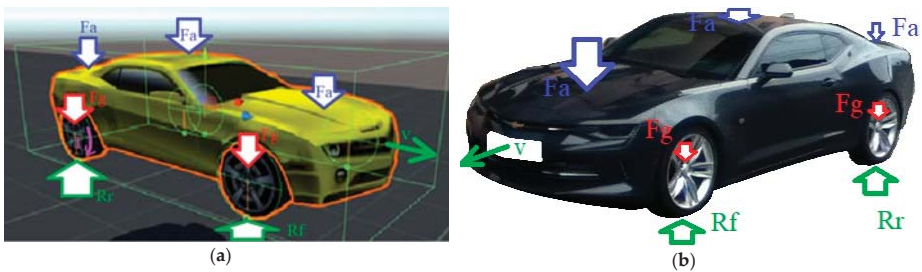


**Figure 3.** Virtual reality Chevrolet Camaro model in Unity 5: (a) Digital model of tested robotic car; (b) actual Chevrolet Camaro model with the driver assistance program used for road testing conditions.



**Figure 4.** Robotic Chevrolet Camaro model supported by mobile virtual fence (MVF) in the Unity 5 virtual reality drive test: (a) Digital model of tested robotic vehicle is self-driving away from an obstacle; (b) vehicular mobile networking when both cars communicate and interact through their MVFs.

The design of the car engine and the vehicle system output performance was made in a virtual reality program, known as Unity 5, by using a script and dialog boxes for input data, as shown in Figure 5. Results are supported by an artificial intelligence control program, which used vehicle-to-infrastructure and context-aware technologies. An automated robotic Chevrolet Camaro, implemented and tested in Unity 5 for situation-aware capability and obstacle avoidance maneuvers, was designed for the task.

The context awareness mechanism, with the mobile virtual fence system, allowed the virtual reality program to adjust the maneuvers for avoiding the obstacles and to reconfigure the trajectory through artificial intelligence, as shown in Figure 6. The virtual automated car, Chevrolet Camaro, had AI program features in Unity 5 to use a speed-reactive mobile virtual fence system with physical object-aware computing and accident-avoidance capacity.



**Figure 5.** Basic digital support in configuring the car control program script in Unity 5 application: (a) Car engine script used to define maximum motor torque; (b) kinematic parameter definition.

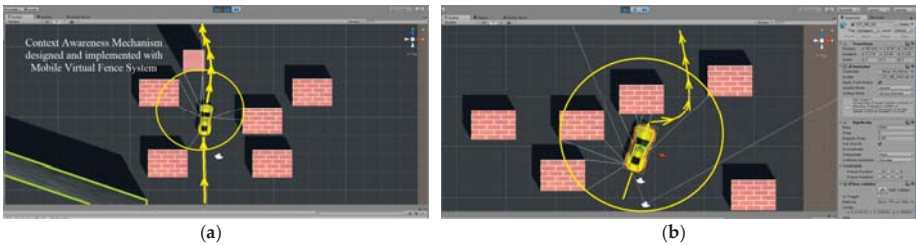


**Figure 6.** Artificial intelligence control program of the robotic vehicle model in Unity 5 virtual reality: (a) Context aware computing applied to self-driving optimization for avoiding a few physical objects; (b) vehicle-about-everything type of sensing for object avoidance program and track re-defining.

Application of the mobile virtual fence technology (MVFT), both in Unity 5 and the driver assistance system used by the Chevrolet Camaro vehicle, was useful for performance optimization, as shown in Figure 7. Any physical object could trigger the proximity detection sensors and context-aware system. A real-road scenario allowed the detection of physical objects and mutual awareness in vehicular networks through wireless communication technologies. The auto-driving was made by cruise-control.



**Figure 7.** The Chevrolet Camaro was equipped with MVF both in the digital and actual drive test environment: (a) Robotic virtual modeled vehicle using the self-driving optimization capacity to avoid objects; (b) driver assistance system was applied to validate the virtual distilled model of the robotic car.

Using the mobile virtual fence technology (MVFT) and Wi-Fi connectivity with a smart vehicle, in addition to previously presented data, the research scenario was completed with accessibility to environmental data for road route optimization [15], as shown in Figure 8. The vehicle is connected to the infrastructure and reads the pollution map, thus reconfiguring the street route to follow.

Through available connectivity, the smart device accessed the data concerning the red spots of the pollution level and highlighted the peaks, as shown in Figure 9.

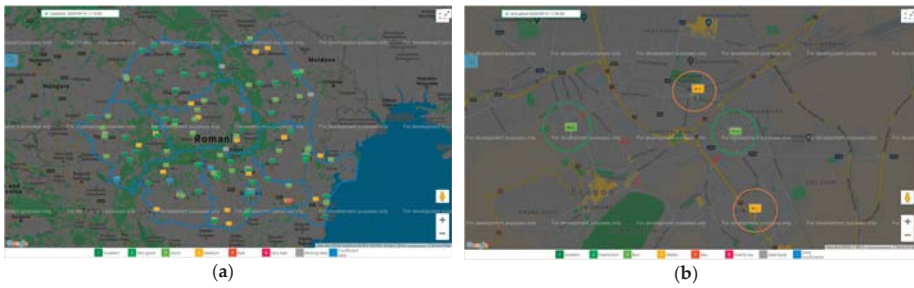


**Figure 8.** Environmental checking maps when configuring the route scenarios to be followed by car: (a) Overall map of the entire country showing the monitoring stations placed in different points for air quality measurement; (b) close view of the city map with environment checkpoints for pollution.



**Figure 9.** The environmental data accessed a Wi-Fi connection and was made available on the local area network: (a) Accessing the synoptic view of the pollutants panel from a red spot to determine the value; (b) graphical representation of the hourly evolution and the peak value for the spotted pollutant.

Tropospheric ozone (O<sub>3</sub>) actual values and its peak point, as well as wind direction data, were also accessed from a virtual cloud to perform better optimization of the road route in traffic, actual values being numerically available and graphically represented, as shown in Figure 10.

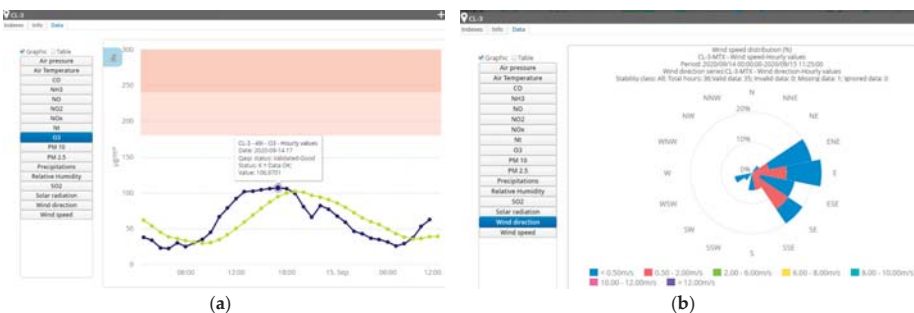


**Figure 10.** Cloud data regarding the environmental check for tropospheric ozone (O<sub>3</sub>) and windy conditions in road route configuration: (a) Ozone (O<sub>3</sub>) level variation and its peak value, accessed from a virtual cloud; (b) wind direction and speed distribution for a 36 h total interval.

The artificial intelligence program model was designed to test and implement both the virtual reality and actual vehicle, Chevrolet Camaro, as shown in Table 2. Wireless networks and hot spot function allowed the creation of a mobile digital sphere. The latter could be assimilated to the more popular mobile virtual fence (MVF), which was considered as the basis of vehicular networking.

Context-aware mechanisms consist of sensors and an electronic control unit that processes signals from all sides of the vehicle to properly command the steering and powertrain. Investigation and analyze of strengths, weaknesses, opportunities, and threats outlines some of the most interesting results and vulnerabilities, as presented and centralized in Table 2.

**Table 2.** Results of strength, weakness, opportunity, and threat (SWOT) investigation.

1 Strength	2 Weakness	3 Opportunity	4 Threat
Stored knowledge	Complexity	More creativity	Digital blockage
Self-driving	Limited sensing	Context aware study	Inadequate response
Internet of things	Easy interception	Connected car service <sup>1</sup>	Lack of privacy

<sup>1</sup> All the revisions and vehicle failures are digitally planned and followed precisely by maintenance staff.

### 3.3. Programming Artificial Intelligence with Bayes Theorems

The primary probability used by the AI was defined using a group for training, as follows:

$$A_I(c|d) = [A_I(d|c) \cdot A_I(c)] / A_I(d) = [A_I(c) \cdot \prod_{i=1}^N A_I(d_i|c)] / A_I(d), \tag{1}$$

where  $A_I(c)$  is the prime probability;  $A_I(d)$  is the post probability; and  $A_I(d|c)$  is the training group probability.

## 4. Discussion and Comparative Relation with Other Contributions in the Field

Specific contributions in the process of designing and manufacturing of a control model program, destined to be implemented in an automated car, consisted of defining the track to be followed by the robotic vehicle during virtual reality testing. Specification of the vehicle model chosen for simulation and real-time testing contributed to the innovative character of the study. Thus, original aspects of the developed research comprised a modern Chevrolet Camaro (a virtual model) adapted to autonomous driving on a defined track and real-time testing with an adapted similar vehicle model.

Manufacturing of physical systems and complex virtual environments corelates quite intimately with the recent published works in the field [1–5]. Production of those elements and connections between components allowed complete programing of a robotic vehicle to operate in alternate dynamic and kinematic regimes, including the usage of the data, not only the display of some information [6]. Using virtual reality in the manufacturing/development process of the specific operating environment for the robotic vehicle is a complex task, which places the present study in a symbiotic relation with the rest of the research [8–12]. With the VR program, three important scenarios for applying AI in a robotic car should be considered as the following: 1. environmental inspection automated vehicle, 2. as a taxi, and 3. as an ambulance. In the present paper, the first scenario was considered.

In addition, the authors developed some advanced algorithms/applications for improving the road route optimization by considering multiple factors (physical and chemical, some of them accessed from the cloud, other determined directly). The first part of the study was supported by some features of a software application, but the second phase was originally proposed and developed in a cross-reference participatory act with the road traffic and environmental management discipline.

## 5. Conclusions

Designing, testing, and implementation of a control program in VR for automated driving of robotic Chevrolet Camaro was successful and allowed us to gain insight in the problems that are necessary to be considered in further investigations, both in simulations and practical tests. The applied testing in real-size conditions on the actual road is still a problem because there is not any completely developed robotic car yet. The existing driver assistance systems are optimal for the partial kinematic control of the car, but still do not allow full dynamic programming.



The most important aspects covered in the present paper were designing the phase and implementation of a control program for the Chevrolet Camaro passenger car with automated driver assistance in VR and on the actual road. The first step of investigation was the simulation program and the second phase actually tested driver assistance and MVF on the road.

**Author Contributions:** Conceptualization, D.-L.B. and A.-I.B.; methodology, D.-L.B.; software, D.-L.B.; validation, L.A., D.-L.B., and A.-I.B.; formal analysis, A.-I.B.; investigation, D.-L.B.; resources, A.-I.B.; data curation, D.-L.B.; writing—original draft preparation, A.-I.B.; writing—review and editing, D.-L.B.; visualization, A.-I.B.; supervision, A.-I.B.; project administration, D.-L.B.; funding acquisition, L.A. All authors have read and agreed to the published version of the manuscript.

**Funding:** This research received no external funding.

**Acknowledgments:** Technical support was given by Florin Covaciu from Robotics Department and by Justinian Berindei from Advanced Techniques in the Automotive Engineering; Faculty of Automotive Engineering, Mechatronics and Mechanics; Technical University of Cluj-N.; Romania.

**Conflicts of Interest:** The authors declare no conflict of interest.

## References

1. Bec, P.; Borzan, A.I.; Frunză, M.; Băldean, D.L.; Berindei, I. Study of Vulnerabilities in Designing and Using Automated Vehicles based on SWOT method for Chevrolet Camaro. In *The IOP Conference Series: Materials Science and Engineering, Proceedings of the Annual Session of Scientific Papers "IMT ORADEA 2020"*, Oradea, Romania, 28–29 May 2020; Grebenisan, G., Ed.; IOP Publishing: Philadelphia, PA, USA, 2020; pp. 1–6.
2. Covaciu, F.A.; Băldean, D. Contribution to Research the Applied Engineering Protocol to Implement a Fuzzy Regulator for Autonomous Driving of an Automotive Model Implemented in Virtual Reality. In *Proceedings of the SMAT 2019, the 30th SIAR International Congress of Automotive and Transport Engineering*, Craiova, Romania, 23 October 2019; Dumitru, I., Covaciu, D., Racila, L., Rosca, A., Eds.; Springer: Cham, Switzerland; Basel, Switzerland, 2020; pp. 468–476.
3. Covaciu, F.A. Developing the communication of autonomous vehicles controlled with the aid of artificial intelligence for person and capital safety. In *Safety of the Person and Building the Social Capital*, 1st ed.; Nechita Iancu, E.A., Ed.; Universul Juridic: Arad, Romania, 2020; Volume 1, pp. 478–484.
4. Ferenti, I.; Băldean, D.L. Artificial intelligence implemented in rally vehicles for increasing energetic efficiency in competitions. *Stiinta si Inginerie* **2018**, *34*, 1–10.
5. Hyun, E.Y.; Hwang, G.; Lee, M.; Choi, Y.G.; Cho, S.; Jeon, B. Topological Sequence Recognition Mechanism of Dynamic Connected Cars using the Connected Mobile Virtual Fence (CMVF) System for the Connected Car Technology. *Appl. Sci.* **2020**, *10*, 4347.
6. Jovrea, S.; Borzan, A.I.; Băldean, D.L. Researching on-board display of essential information concerning technical conditions in operation and fuel-economy of a motor-vehicle in operation. *Stiinta si Inginerie* **2017**, *31*, 1–10. Available online: <http://stiintasiinginerie.ro/31-67> (accessed on 1 December 2020).
7. Mitroi, M.F.; Chiru, A. Aspects Regarding the Identification of Optimum Driver Comfort Level by Virtual Analysis of the Vertical Oscillations Generated by Road. In *Proceedings of the SMAT 2019, the 30th SIAR International Congress of Automotive and Transport Engineering*, Craiova, Romania, 23 October 2019; Dumitru, I., Covaciu, D., Racila, L., Rosca, A., Eds.; Springer: Cham, Switzerland; Basel, Switzerland, 2020; pp. 221–230.
8. Moldovan, A.; Borzan, A.I.; Băldean, D.L. Experimental research of the management system from the Peugeot 4007 Sport Utility Vehicle. *Stiinta si Inginerie* **2017**, *31*, 1–10.
9. NHTSA, Federal Motor Vehicle Safety Standards, V2V Communications. 2017. Available online: <https://www.federalregister.gov/documents/2017/01/12/2016-31059/federal-motor-vehicle-safety-standards-v2v-communications> (accessed on 1 December 2020).
10. Ollero, A.; Simon, A.; Garcia, F.; Torres, V.E. Integrated mechanical design and modelling of a new mobile robot. In *IFAC Intelligent Components and Instruments for Control Apps*; Elsevier: Amsterdam, The Netherlands, 1992; pp. 461–466.

11. Pappalardo, C.M.; Lombardi, N.; Dašić, P.V.; Guida, D. Design and development of a virtual model of an electric vehicle of category L7. In *The IOP Conference Series: Materials Science and Engineering, Proceedings of the Annual Session of Scientific Papers "IMT Oradea 2019", Oradea, Romania, 30–31 May 2019*; Grebenisan, G., Ed.; IOP Publishing: Philadelphia, PA, USA, 2019; pp. 1–6.
12. Park, C.; Chung, S.; Lee, H. Vehicle-in-the-Loop in Global Coordinates for Advanced Driver Assistance System. *Appl. Sci.* **2020**, *10*, 2645. [[CrossRef](#)]
13. SAE J2735, *Dedicated Short Range Communications (DSRC) Message Set Dictionary*; SAE Internat: Troy, MI, USA, 2016.
14. Thrun, S. Toward Robotic Cars. *Commun. ACM* **2010**, *53*, 99–106. [[CrossRef](#)]
15. RNMCA. Air Quality. *Air Quality Assessment*. Available online: <http://www.calitate aer.ro/public/assessment-page/> (accessed on 5 June 2020).
16. Baldean, D.; Andrei, L.; Borzan, A.I. Research of NOx and PM10 pollutants in Cluj-Napoca with the mobile system for mitigating public health risks. In *IOP Conference Series: Materials Science and Engineering*; Grebenisan, G., Ed.; IOP Publishing: Philadelphia, PA, USA, 2020; Volume 898, p. 012003.
17. Baldean, D.; Andrei, L.; I Borzan, A. Investigation of NOx emissions for mitigating public health risk with Mercedes E Coupe. In *IOP Conference Series: Materials Science and Engineering*; Grebenişan, G., Ed.; IOP Publishing: Philadelphia, PA, USA, 2020; Volume 898, p. 012006.
18. Self-Driving Car. Available online: [https://en.wikipedia.org/wiki/Self-driving\\_car](https://en.wikipedia.org/wiki/Self-driving_car) (accessed on 5 June 2020).

**Publisher's Note:** MDPI stays neutral with regard to jurisdictional claims in published maps and institutional affiliations.




© 2020 by the authors. Licensee MDPI, Basel, Switzerland. This article is an open access article distributed under the terms and conditions of the Creative Commons Attribution (CC BY) license (<http://creativecommons.org/licenses/by/4.0/>).





# Developing and Researching a Robotic Arm for Public Service and Industry to Highlight and Mitigate Its Inherent Technical Vulnerabilities <sup>†</sup>

Florin Covaciu <sup>1</sup>, Persida Bec <sup>2</sup> and Doru-Laurean Băldean <sup>1,\*</sup> 

<sup>1</sup> Design Engineering and Robotics Department, Faculty of Machines Building, Technical University of Cluj-Napoca, 103-105 Muncii, 400641 Cluj-Napoca, Romania; florin.covaciu@muri.utcluj.ro

<sup>2</sup> Ethics of Vulnerabilities Group, Faculty of Philosophy, Babes-Bolyai University, Kogălniceanu 1, 400084 Cluj-Napoca, Romania; bec.persida@gmail.com

\* Correspondence: doru.baldean@auto.utcluj.ro or dorubaldean@yahoo.com; Tel.: +40-264-202-790

<sup>†</sup> Presented at the 14th International Conference INTER-ENG 2020 Interdisciplinarity in Engineering, Mureş, Romania, 8–9 October 2020.

Published: 15 December 2020

**Abstract:** The present study highlights the design and testing of a robotic arm and its vulnerabilities. The purpose of this paper is to develop, manufacture, test, and improve the robotic arm as a separate system. Additionally, its actuators in operation and the evaluation of challenges in Strengths, Weaknesses, Opportunities, and Threats (SWOT) analysis (or vulnerability assessment) are considered. The specific objective consists in designing the robot's actuators to generate effective work and torque in operational conditions of the external environment in which are found objects that have a resistance force. Another secondary specific objective is to realize an automatic loop with a corresponding architecture based on a previously stressed actuator configuration.

**Keywords:** robotic arm; automatics; controls; manufacturing; vulnerability

## 1. Introduction

When introduced to robotics [1] and automation [2], some individuals are convinced that these kinds of applications are destined only for the industry field or just for technological research and development [3]. Anyway, the purpose and objective of robotics and automation [4,5] consists in assisting human activities [6,7] both working in the industry and in performing daily tasks at home, the office, or in public areas [8,9]. To merge the limits of the common knowledge and the actual reality of robotics, an internet connection must be introduced and used [10]. One robotic arm has been created [3] in the Swiss Federal Laboratories for Materials Testing and Research to highlight its capacity to work based on a specific technology [11]. Thus, an actuator with a dielectric elastomer (DE) was implemented in a robotic arm. It allowed the system to benefit from a few of the material's unique properties which outlined a special parameter [12]. These groups were among the few organizations which made, in a contest, the pioneering act of matching electro-active polymeric material (EAPM) in a robotic arm to be like a hand. This event was held during a scientific event in San Diego, in 2005. Arm robots placed and exploited within the International Space Station were constructed to perform some important tasks, as follows: building or construction, servicing and maintenance of the station, sustaining some tests and experiments in outer space, capturing free moving systems, performing activities on the station's exterior, and supporting specific research and development. The mobile robotic arm [13] equipment can perform multiple common activities and operations, as follows: video equipment aligning, vehicle positioning, door opening, and recipient moving, as well as displacing, replacing,

and installing a 100-tonne module [14–16]. Security measures and advanced programming are some of the most significant aspects to be treated to achieve the optimal application and operation of robotic arms in inhospitable environments [17–20].

## 2. Materials and Methods

Mathematical equations of the simulation and the practical determinations are nothing but linear. The method for controlling the robotic arm is partitioned in a dual sequence approach: on the first level is coarse control and, on the second level, is fine management. On the basis of the advanced control hypothesis, one linear regulator is built to get superior control. Large spaces and outer space represent some challenges for the operational procedures of robotic arms. It is a problem to locate objects in a finite volume without physical boundaries. The important question is how to search for something in a limited environment with no material walls? To solve the mentioned challenge, it is recommended to use a chromatic code represented upon the space ground. It will be necessary to read the chromatic panel using a light-detecting sensor facing toward the floor. Another method is by using a bumper as a reference, and thus allowing the robotic arm to move randomly in the working space or in a more precise manner to follow a predefined schematic. The scientific approach may be realized quite efficiently by applying a funnel to move the manipulated components in relation to the bumper. Another approach is by using powerful antennas coupled to touch sensors to support object detection for public health services in open spaces. For locating and finding large objects in the working space, ultra-sonic sensors (USSs) or wireless sensors are used, with the effect of improving operational accuracy, as shown in Figure 1. The static platform (1) is the main support for the main arm, which is the TTLinker board (2), and wireless positioning sensors (3) are controlled by Feetech SCS 15 servomotors (4) to command the displacement of the detection sensor (5). An alternative to a static robotic arm may be developed with a mobile platform (6), with an ESP 32 microcontroller (8) (placed in a safety case), and a Lipo accumulator (9). In this case, a programming and remote-control station (7) is also provided. ESP 32 (with Xtensa 32-bit LX6 CPU) has the role of operating the robotic arm at 160 MHz.

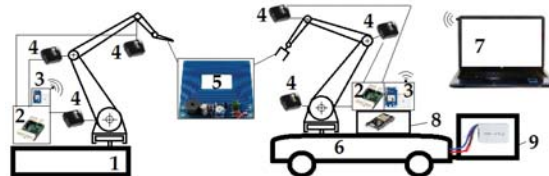


Figure 1. Schematic representation of components linked in the robotic arm assembly for industry.

An Arduino connection to the SCServo needs the TTLinker board. This provides signal conversion. Arduino also converts the universal asynchronous receiver-transmitter (UART) signal into half duplex. The TTLinker has multiple interfaces to receive signals from more sensors (to detect suspicious objects), as shown in Figure 2.



Figure 2. Schematic presentation of Feetech mini-board TTLinker used for connecting SCS15 servos.

Material components and a GPS module may be linked to a computer, notebook, or mobile device with a USB to UART converter. It may be accessed with the U-center app and is compatible with many flight control modules that have GPS virtual testing programs. Pin connections are given in Table 1.

**Table 1.** Centralized data regarding the pin connections between the GPS module and ESP 32.

Transmitter	Receiver	Observations
ESP 3.3V	GPS VCC	NEO-6M U-Blox chip
ESP GND	GPS GND	-----  -----
ESP RX	GPS TX	-----  -----
ESP TX	GPS RX	-----  -----

### 3. Development and Results

The results consist in the findings from the simulation and experimental testing of controls for a dual-tasking robot arm. The mathematical equations for a dual-tasking experimental robotic arm have been verified thoroughly. This robotic arm has two rotation degrees of freedom and one degree of freedom in translation, which results in a three-dimensional workspace. The workload is specified by adding auxiliary mass to the robotic arm end. The numerical and experimental results are highlighted in the present paper, consisting in design plans, dimensioning, and digital modeling with Computer Aided Design (CAD) programs, as presented in Figure 3.

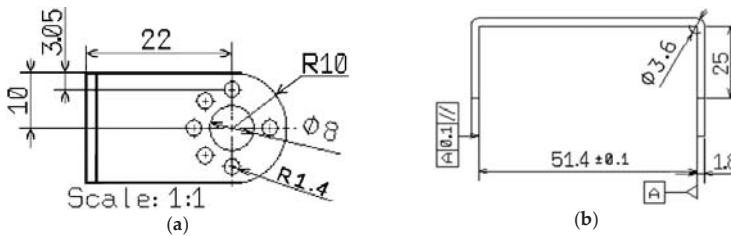


**Figure 3.** CAD virtual model of servo bracket to present and define the geometric parameters: (a) 2D drawing in the front view of the bracket; (b) bottom view of the servo bracket for the robotic arm.

The following step is the virtual modeling of the sensor holder in a 2D drawing and 3D representation, as shown in Figure 4.

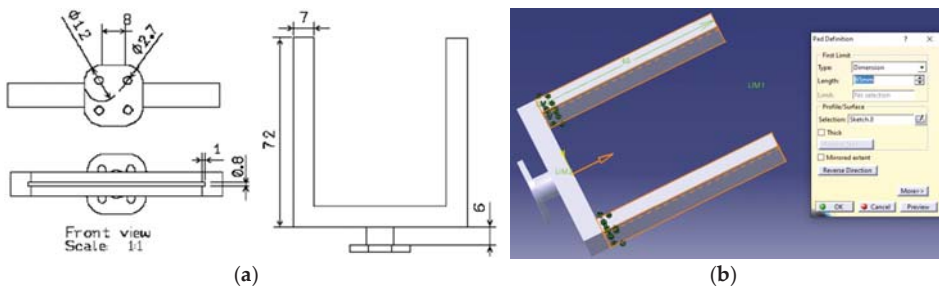


**Figure 4.** Virtual development of the end part of the robotic arm sensor holder with Computer Aided Design (CAD): (a) 2D drawing of the sensor holder; (b) representation of a 3D model designed as a mine detection sensor holder.

The next step of the research and development process for a robotic arm for public health service and industry consists in coupling the electric accumulator to the structure, as shown in Figure 5.

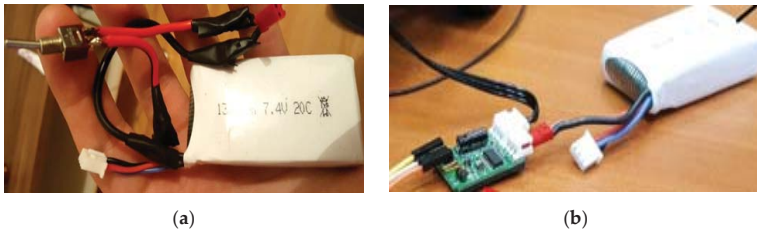


**Figure 5.** Different types of electric accumulator connection to the robotic arm application for testing: (a) accumulator connected to the robotic arm through a switcher; (b) connection to the TTLinker board.

For testing the operational capability of the robotic arm in the public health service and industry, it was installed on a mobile platform, as shown in Figure 6.

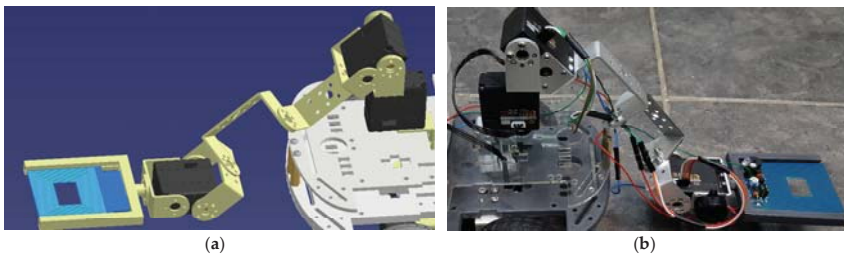


**Figure 6.** Robotic arm in laboratory-stage development: (a) CAD version; (b) practical test version.

The final stages of the robotic arm development consist in programming the control interface and user commands, through which the servo motors may be actuated or stopped, as shown in Figure 7.

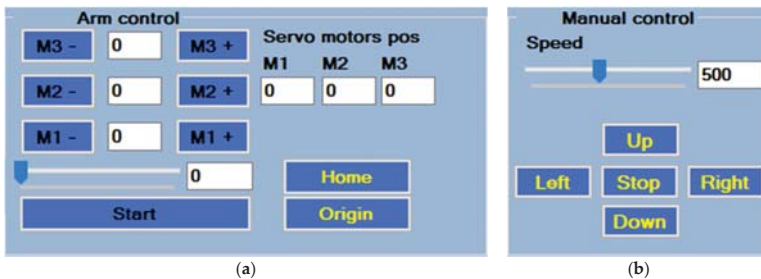


**Figure 7.** Configuring the control panel: (a) robotic arm control with servo motors; (b) manual control.

The general interface developed in a Microsoft package with Visual Studio is shown in Figure 8.



**Figure 8.** User control interface and the saving tool for coordinates: (a) general view; (b) reset button.

Required torque may be calculated with the following mathematical relations (1) and (2):

$$M = (m \cdot a \cdot v \cdot k) / \omega, \tag{1}$$

$$M = (F_i \cdot v \cdot k) / \omega, \tag{2}$$

where M is the calculated torque requirement; m—mass of the load, in kg; a—acceleration of the robot  $a = 2 \text{ m/s}^2$ ;  $F_i$ —inertial force, in N; v—velocity, in m/s;  $\omega$ —angular velocity, in rad/s; k—operation factor ( $k = 1.5$ ). Forces are simulated for low-carbon steel, known as mild steel, that has a  $0.05 \div 0.3$  carbon content.

To build the actual size model of the crane/spatial structure, for implementing the sensor’s support of the robotic arm, a frame with nodes and constraints which facilitated the analysis of the assembly’s behavior and validation of the model was designed, as shown in Figure 9.

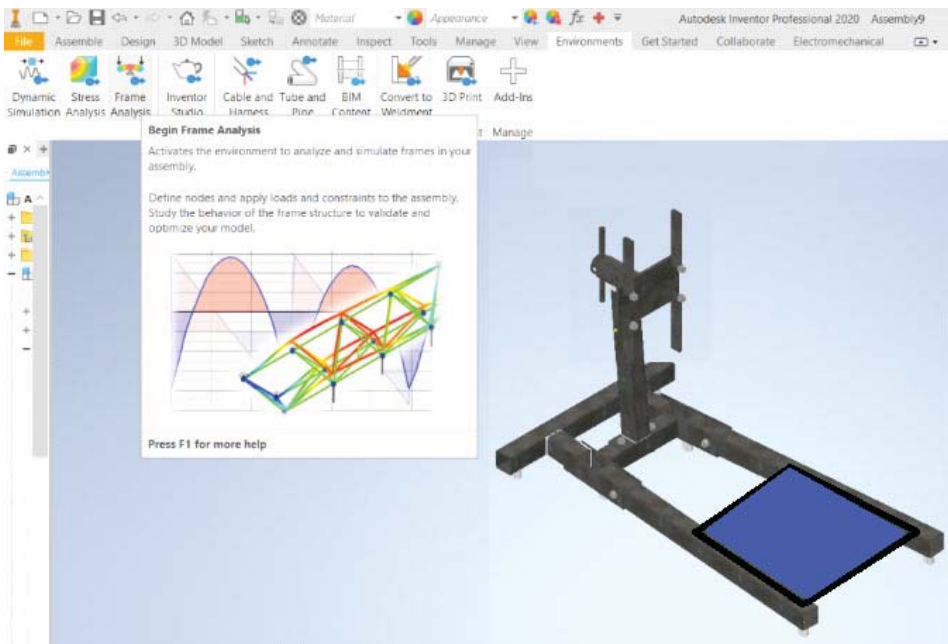


Figure 9. Mechanical structure of the arm developed in CAD stage to begin stress frame analysis.

The design and virtual modeling of the sensor’s supporting structure activates the simulation possibilities of the environment to study stresses of the frame in the assembly. To test the resistance and displacement capability of the mechanical assembly low-end arm, a force was placed on the structure, as shown in Figure 10. The red line indicates the most vulnerable area of the assembly.

Additional stages in the study of the structural stresses of the robotic arm consist in the determination of the vertical force effects on the individual components and the bending stress on the spatial wire frame, as shown in Figure 11. The sensor support may take a bending stress of 3.5 MPa on the joint.

Some important observations regarding the robotic arm analysis and development consist in highlighting strengths, weaknesses, opportunities, and threats in implementing and using such structures. The robotic arm is designed and proposed to be tested on a mobile platform for service.

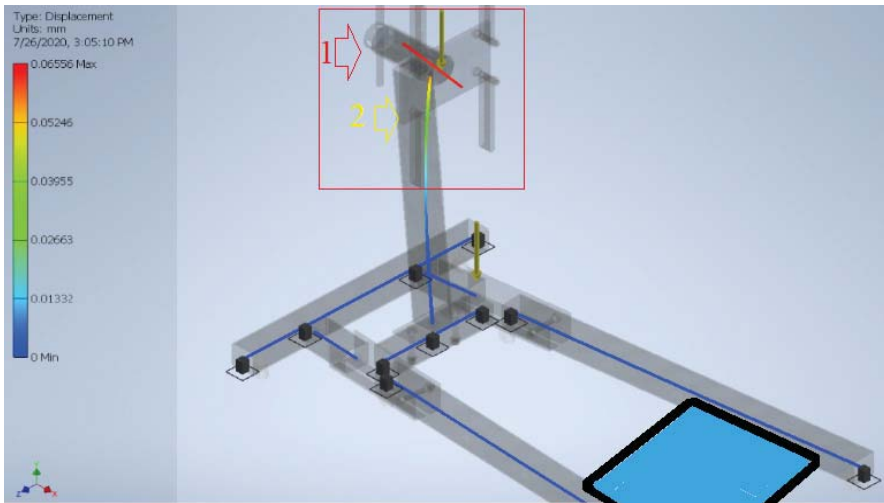


Figure 10. Robotic arm in displacement analysis stage: (a) critical area; (b) second-level displacement.

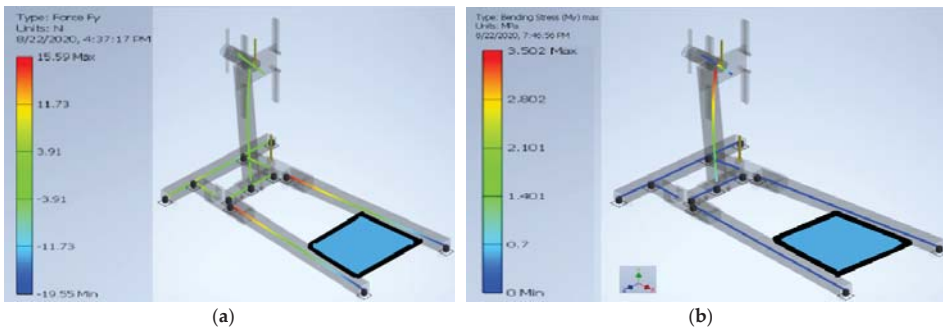


Figure 11. Virtual analysis of the sensor's support regarding: (a) vertical force; (b) bending stress.

#### 4. Discussions and Conclusions

The practical research through the design and development of a robotic arm for public service and industry in order to highlight and mitigate its inherent vulnerabilities is supported on a specific presentation of strengths, weaknesses, opportunities, and threats (SWOT), facts given in Table 2. To analyze these problems, specialized testing procedures were applied to the robotic arm. Considering this statement, it is also postulated that aspects around the topic are handled in a practical engineering manner. Vulnerabilities of the robotic arm influence the overall operation of the system.

Table 2. Practical data regarding the strengths, weaknesses, opportunities, and threats (SWOT) analysis for assessing vulnerabilities.

Strengths	Weaknesses	Opportunities	Threats
Complete force control	Complex programs	More jobs	Failures and events
Selfless intel	No empathy	Escaping arrogance	Hacking
Performance in operation	Volatile memory	Rapid connection	Data losses
Remote operation	Intercepting incidents	Improving efficiency	Cyber hacks



Applying the SWOT analysis method for defining the vulnerabilities concerning the robotic arm equipment in operation has allowed us to assess the stringent problems and to optimize the use of automated and intelligent systems for public service and for industrial applications.

The contributions consist in designing the robotic arm and modeling in simulation programs to validate the proposed solution. Additionally, an experimental laboratory model has been designed and created to check vulnerabilities and faults in the project before serial production and further development. ESP 32 runs properly on the lab mini model and must be replaced with a stronger CPU.

The comparison between the present paper’s achievements and other studies is given in Table 3.

**Table 3.** Comparative parameters of the robotic arm analyzed in the present paper and other studies.

Research Paper	Robot Type	Platform	Transmission
Aboulissane et al. 2019	Parallel	Mobile	Parallelograms and joints
David Alejo et al. 2019	Six-wheeled	Drivable robotic platform	Mechanical
Kadir et al. 2012	Robotic arm	Static platform	Mechanical
Present study	Robotic arm	Mobile platform	Spatial assembly and joints

The present research contributes to the field of robotic arms by increasing the experience and knowledge regarding the process of the design, development, optimization, and control of these instruments. Quantitatively, the sensor support takes a 15 N force on the y direction in operation.

Automation and robotics in manufacturing and servicing are some of the most important research topics in engineering and technology today. The present paper deals with the automatic processes and control procedures of a robotic arm designed and tested in robotics laboratory.

In the present paper were underlined the sequences of developing and researching a robotic arm intended to be used in the health service and industry to highlight and mitigate its inherent technical vulnerabilities. Thus, the components linked together in the robotic arm assembly were represented.

The vulnerabilities consist in detection sensor safety in operation and the arm’s flexible joints’ effect upon electric wires. They must be protected and secured from numerous alternative displacements or movements. Bending stress, reaching more than 3.5 MPa, also has a negative effect on the arm.

The most important technical concerns are the control and performance of the robotic arm during operation. It is an actual problem to control and limit the accurate displacement.

Robotic arm tools may be useful to enhance the productivity and safety of some workers due to the remote access at some sites and more time can be reserved for research and study in non-operational tasks. Anyway, this situation leads to some specific problems and vulnerabilities, such as failures, complex programs, data losses, and eventual cyber hacks.

The most notable vulnerabilities that were highlighted by the present development were found firstly in the design process and secondly in the testing of the robotic arm. In the primary phase of the research and development of the robotic arm for hazardous environments, the outlined vulnerabilities are the factual aspects that actual operational data are hardly able to be recreated and implemented in the beginning. The important considered data are related considerably to the kinematics and dynamical aspects of the robotic arm. The second set of vulnerabilities are the highly complicated programmed learning of artificial intelligence, that consists in a finite phase by a phase sequence and leads to variable results during operation time. The applied tests have shown many other vulnerabilities because there is no human operator involved continuously and the machine learning program must adapt to the task via a training session. Anyway, in the present industry, there are operational static robotic arms, but mobile robots (placed on moving platforms, such as the presented one from this paper) are a work in progress and need to be further studied and optimized.



**Author Contributions:** Conceptualization, F.C. and D.-L.B.; methodology, D.-L.B.; software, F.C.; validation, P.B., D.-L.B., and F.C.; formal analysis, D.-L.B.; investigation, P.B.; resources, P.B.; data curation, D.-L.B.; writing—original draft preparation, F.C.; writing—review and editing, D.-L.B.; visualization, D.-L.B.; supervision, P.B.; project administration, D.-L.B.; funding acquisition, P.B. All authors have read and agreed to the published version of the manuscript.

**Funding:** This research project was co-funded by the European Social Fund.

**Acknowledgments:** This paper was supported by the project “Entrepreneurial competences and excellence research in doctoral and postdoctoral programs-ANTREDOC” co-funded by the European Social Fund.

**Conflicts of Interest:** The authors declare no conflict of interest.

## References

1. Aboulissane, B.; El Haiek, D.; El Bakkali, L.; El Bahaoui, J. On the Workspace Optimization of Parallel Robots Based on CAD Approach. In Proceedings of the 12th International Conference Interdisciplinarity in Engineering (INTER-ENG 2018), Targu Mures, Romania, 4–5 October 2018; Moldovan, L., Gligor, A., Eds.; Elsevier: Amsterdam, The Netherlands, 2019; Volume 32, pp. 1085–1092.
2. Alejo, D.; Mier, G.; Marques, C.; Caballero, F.; Merino, L.; Alvito, P. SIAR: A Ground Robot Solution for Semi-autonomous Inspection of Visitable Sewers. In *Advances in Robotics Research: From Lab to Market*; Grau, A., Morel, Y., Puig-Pey, A., Cecchi, F., Eds.; Tracts in Advanced Robotics; Springer: London, UK, 2019; Volume 132, pp. 275–296.
3. Andrei, L.; Bâldean, D.; Borzan, A.I. Applied Measurements and Instrumentation for Improving Diagnostic Devices and Systems in Metropolitan Polluted Environments with Nitric and Carbon Oxides. In Proceedings of the 6th International Conference on Advancements of Medicine and Health Care through Technology, Cluj-Napoca, Romania, 17–20 October 2018; Vlad, S., Roman, N., Eds.; Springer: London, UK, 2019; Volume 46, pp. 45–49.
4. Bar-Cohen, Y. *Biomimetics: Biologically Inspired Technologies*; Taylor & Francis: New York, NY, USA, 2006.
5. Bâldean, D.L.; Covaciu, F. Developing the communication of autonomous vehicles controlled with the aid of artificial intelligence for person and capital safety. *Saf. Person Constr. Soc. Cap.* **2020**, *1*, 478–484.
6. Bâldean, D.L.; Covaciu, F.A. Robotic Art in Creation and Development of Innovative Shapes and Programs for Automated Driven Cars with Artificial Intelligence. *J. Soc. Media Inq.* **2020**, *2*, 22–39. [[CrossRef](#)]
7. Bec, P.; Borzan, A.I.; Frunză, M.; Bâldean, D.L.; Berindei, I. Study of Vulnerabilities in Designing and Using Automated Vehicles based on SWOT method for Chevrolet Camaro. In Proceedings of the IOP Conference Series: Materials Science and Engineering, Oradea, Romania, 28–29 May 2020; Grebeni, G., Roman, N., Eds.; IOP Publishing: Bristol, UK, 2020. [[CrossRef](#)]
8. Borzan, A.I.; Bâldean, D.L. The Development of a New Interface for Intelligent Control of Energy Supply in Dynamic Environment with Process Digitization. In Proceedings of the 13th International Conference Interdisciplinarity in Engineering (INTER-ENG 2019), Targu Mures, Romania, 3–4 October 2019; Procedia Manufacturing; Moldovan, L., Gligor, A., Eds.; Elsevier: Amsterdam, The Netherlands, 2020; Volume 46, pp. 1–6.
9. Gao, Z.; Wanyama, T.; Singh, I.; Gadhri, A.; Schmidt, R. From Industry 4.0 to Robotics 4.0-A Conceptual Framework for Collaborative and Intelligent Robotic Systems. *Procedia Manuf.* **2020**, *46*, 591–599. [[CrossRef](#)]
10. Kadir, W.M.H.W.; Samin, R.E.; Ibrahim, B.S.K. Internet Controlled Robotic Arm. *Procedia Eng.* **2012**, *41*, 1065–1071. [[CrossRef](#)]
11. Kobayashi, Y.; Harada, K.; Takagi, K. Automatic controller generation based on dependency network of multi-modal sensor variables for musculo skeletal robotic arm. In *Robotics and Autonomous Systems*; Elsevier: Amsterdam, The Netherlands, 2019; Volume 118, pp. 55–65. [[CrossRef](#)]
12. Mroziak, D.; Mikolajczyk, T.; Moldovan, L.; Pimenov, D.Y. Unconventional Drive System of a 3D Printed Wheeled Mobile Robot. In Proceedings of the 13th International Conference Interdisciplinarity in Engineering (INTER-ENG 2019), Targu Mures, Romania, 3–4 October 2019; Procedia Manufacturing; Moldovan, L., Gligor, A., Eds.; Elsevier: Amsterdam, The Netherlands, 2020; Volume 46, pp. 509–516.

13. Oltean, S.E. Mobile Robot Platform with Arduino Uno and Raspberry Pi for Autonomous Navigation. In Proceedings of the 12th International Conference Interdisciplinarity in Engineering (INTER-ENG 2018), Targu Mures, Romania, 4–5 October 2018; Procedia Manufacturing; Moldovan, L., Gligor, A., Eds.; Elsevier: Amsterdam, The Netherlands, 2019; Volume 32, pp. 572–577.
14. Syreyshchikova, N.V.; Pimenov, D.Y.; Mikolajczyk, T.; Moldovan, L. Automation of Production Activities of an Industrial Enterprise based on the ERP System. In Proceedings of the 13th International Conference Interdisciplinarity in Engineering (INTER-ENG 2019), Targu Mures, Romania, 3–4 October 2019; Procedia Manufacturing; Moldovan, L., Gligor, A., Eds.; Elsevier: Amsterdam, The Netherlands, 2020; Volume 46, pp. 525–532.
15. Shah, R.; Pandey, A.B. Concept for Automated Sorting Robotic Arm. In Proceedings of the 2nd International Conference on Materials Manufacturing and Design Engineering, Tg. Mures, Romania, 4–5 October 2018; Procedia Manufacturing; Elsevier: Amsterdam, The Netherlands, 2018; Volume 20, pp. 400–405.
16. Tokody, D.; Ady, L.; Hudasi, L.F.; Varga, P.J.; Hell, P. Collaborative Robotics Research: Subiko Project. In Proceedings of the 13th International Conference Interdisciplinarity in Engineering (INTER-ENG 2018), Targu Mures, Romania, 3–4 October 2019; Procedia Manufacturing. Moldovan, L., Gligor, A., Eds.; Elsevier: Amsterdam, The Netherlands, 2020; Volume 46, pp. 467–474.
17. Industrial Robot. Available online: [https://en.wikipedia.org/wiki/Industrial\\_robot](https://en.wikipedia.org/wiki/Industrial_robot) (accessed on 16 June 2020).
18. Mechanical Arm. Available online: [https://en.wikipedia.org/wiki/Mechanical\\_arm](https://en.wikipedia.org/wiki/Mechanical_arm) (accessed on 16 June 2020).
19. Robotic Arm. Available online: [https://en.wikipedia.org/wiki/Robotic\\_arm](https://en.wikipedia.org/wiki/Robotic_arm) (accessed on 16 June 2020).
20. Autonomous Robot. Available online: [https://en.wikipedia.org/wiki/Autonomous\\_robot](https://en.wikipedia.org/wiki/Autonomous_robot) (accessed on 8 June 2020).

**Publisher's Note:** MDPI stays neutral with regard to jurisdictional claims in published maps and institutional affiliations.



© 2020 by the authors. Licensee MDPI, Basel, Switzerland. This article is an open access article distributed under the terms and conditions of the Creative Commons Attribution (CC BY) license (<http://creativecommons.org/licenses/by/4.0/>).



# Development of an Automated System for Fuel Tank Level Checking and Machinery Location Management to Optimize Remote Accessibility and Mobile Tracking <sup>†</sup>

Daniela Popescu <sup>1</sup> , Adela-Ioana Borzan <sup>2</sup> and Doru-Laurean Băldean <sup>2,\*</sup> 

<sup>1</sup> Research Department, SC JIDVEI SRL Company, 45 Garii Street, 517385 Jidvei, Romania; daniela.popescu@jidvei.ro

<sup>2</sup> Automotive Engineering and Transportation Department, Faculty of Automotive Engineering, Mechatronics and Mechanics, Technical University of Cluj-Napoca, 400114 Cluj-Napoca, Romania; adela.borzan@auto.utcluj.ro

\* Correspondence: doru.baldean@auto.utcluj.ro or dorubaldean@yahoo.com; Tel.: +40-26-420-2790

<sup>†</sup> Presented at the 14th International Conference INTER-ENG 2020 Interdisciplinarity in Engineering, Mureş, Romania, 8–9 October 2020.

Published: 11 December 2020

**Abstract:** The present article shows the most significant steps to be taken in the process of the development of an automated system for fuel tank level monitoring and machinery location checking to optimize accessibility and mobile tracking. Fuel or energy consumption is converted with money spending and machinery in operation during different tasks. The maintenance and service costs add up to the final price of the product making it less attractive if the customer must pay more for each acquired unit of produce. Thus, optimization is required in the production system to lower the costs of energy and operation of working machinery. The main objective of the present paper is the research, development, and testing the process of an automated system designed with the purpose of controlling fuel tank level and machinery location management to improve accessibility and to optimize mobile tracking. The secondary objective consists of the installation of a volumetric sensor in the fuel tank.

**Keywords:** automation; fuel tank level sensor; machinery; smart control; vehicles

## 1. Introduction

The automation field has increased with each year passed in the last decades. It helped in the production and manufacturing process. With the support of automatic systems for food production, feeding capability has increased significantly and its availability tends to sustain large populations. With highly automatized production systems, energy efficiency is optimized and costs are diminished. Automation and remote control of production have increased the manufacturing capability in every sector. It also has improved location tracking, efficiency, and production costs.

Applied measurement and instrumentations for optimizing scanning devices [1] and digital controllers for highly complex systems (with fuzzy controllers) [2] are based on electronic equipment and use software programs [3]. The development of software automated systems for fuel level control supports the investigation of fuel economy and emissions [4] and the design for supply-to-engine [5]. Smart control in fuel systems [6,7] facilitates powertrain operations [8], on-board data display [9], intra-vehicular communication [10], and economy management [11]. Vehicular networks may use antennas with multi-sources signals [12] in transferring data from the electronic control module (ECM)

from multiple sources [13,14]. With internet services, multiple applications are made available [15] and specific reports may be structured in Titan Farmis [16]. Smart control is based on mobile access.

The objective of the paper is the automation of fuel control and data report creation for specific tasks.

## 2. Material and Method

The paper discusses much more than a system used for monitoring the fuel consumption of agriculture machinery via a software application. It is the greatest opportunity to implement and to test the cloud data transfer for an entire fleet of machinery and vehicles which support remote monitoring and accessibility. In the present paper, the approach of the subject is based on experimental testing and development. Knowing that electronic control may offer a considerable advance in improving the production process efficiency, we are defining here an applied methodology for monitoring the fuel level inside the machineries' reservoirs to assess values of consumption and energy distribution, using remote accessibility and mobile tracking.

Basic materials and their connections which are applied in the present research are shown in Figure 1. It offers the implementation details, with specific connections of the Fuel Level Sensor (FLS), as well as the digital graphic interfaces. The applied research presents a practical engineering part, on the one hand, and a substantial scientific or analytical content, on the other hand. This is going to clarify what the present paper intends to show. The schematics and the figures contain some of the captures made when implementing and using the hardware with the software application for the remote control of the machinery. In the present case, the fuel level is not only monitored as a simple measurement to be displayed on board during operation. The study goes further to monitor the actual fuel flow, fuel level, consumption, and efficiency related to the work done by the specific machinery from a remote location. The Fuel Level Sensor (FLS) (1) is the energy supplied from a battery (12–24 V) and placed in the fuel tank (2). It is supported by a volumetric method of determining the fuel level. Through the analog RS 232 interface (3), the signals are sent via electrical linkages (4) to the system's control unit (5), which transfers the location and operational data to the server (6), to be stored (8) and analyzed (9).

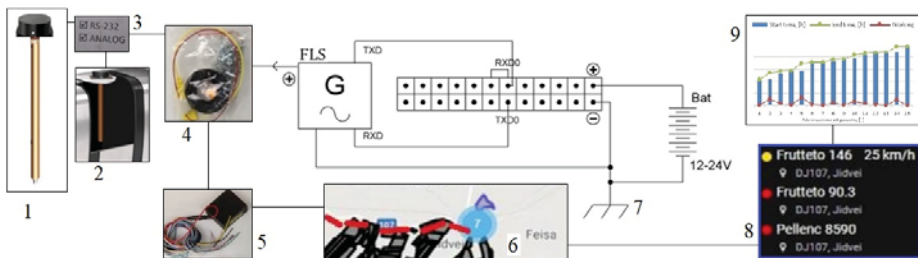


Figure 1. Materials used for implementing the automated system for remote check of fuel tank level.

Grounding (7) is important to close the circuit. The methodology is based on the map available in the Titan Farmis application. The latter one is a digital platform that allows the control of an entire fleet of vehicles and machinery in real-time, regarding both kinematic-dynamic aspects and energetic parameters. The methodology is based upon the proper operation of the automated system with a micro-controller, as shown in Figure 2. These images show and support the implementation methods, communication topologies, software technologies, and services (databases) used during the research.

The first basic step in the development of an automated system for fuel tank level control is to set up the specific sensor on the vehicle and connect it to the control unit. Data transfer via a wireless connection is put into practice by using S7 Technology with a Bluetooth Low Energy (BLE) channel. Later ones have a specific type of signal from the DUT-E S7 fuel level sensor. It can be transferred and received by a compatible machinery tracking unit (the one that supports also telematic features) and

by any Android equipment. GPS machinery tracking components relate to the fuel level sensors to support precise fuel accounting and to indicate drainages/accidents related to the fuel tank. The fuel level sensors are used for level monitoring in mobile and in stationary units. To realize the machinery location management a web connection is defined and used, as shown in Figure 3.

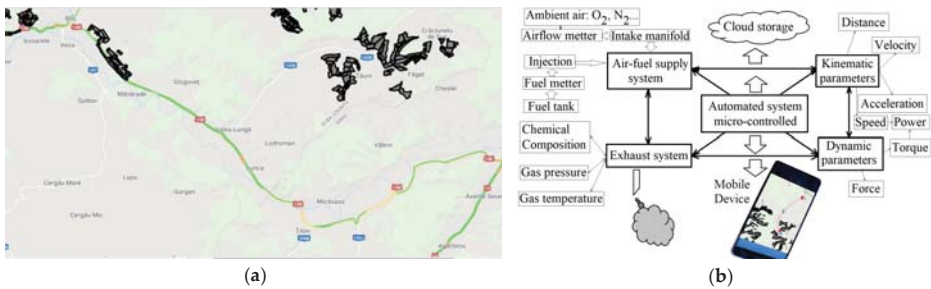


Figure 2. Support map for the operational site (a) and cloud-based mobile tracking methodology (b).



Figure 3. Preparing the research materials (a) and setting networking software application (b) [16,17].

Firstly, the components in the machinery supply scheme are configured properly and filled with fuel to cover all the requirements for a specific task and to facilitate at least 8 h of program operation. The method consists of the electro-mechanical engineering practical approach of assembling.

Secondly, the mobile internet connection is established, and actual data are generated to be transferred toward the central server. Basic service set (BSS) and wireless LAN (WLAN) are used.

The total area of operational testing and data generation consists of more than 10 hectares of land which is prepared for the practical campaigns. Support technologies consist of magnetic, conductive, or hall effect for the measuring sensors. Materials and research components are defined in Table 1.

Table 1. Actual values regarding implemented machinery and operational characteristics.

Parameter	Actual Values	Unit Measurement
Machinery type	Frutteto 146	-
Total surface	12.83	ha
Overall consumption	40.57	L
Average consumption	3.16	L/ha
Operating time	6:25	h
Hourly efficiency	30	min/ha

Frutteto machinery is used to control the fuel system with the automatic system that is realized for this study. The method applied is experimental-digital fuel level monitoring and database creation.

### 3. Applied Part and Results

The applied part and acquired results of the present work were the experimental data and the electronic management system for remote control of the fuel level measurement. The actual values recorded by the monitoring system in practice are valuable assets for the engineering endeavor validation. The testing protocol for the automatic measuring system of fuel tank level was developed, tested and numerical results were meanwhile acquired for the machinery used in the applied study. The main findings thus consisted of the capability and utility of fast-tracking of every machinery movement and fuel level status. Numerical results were centralized in digital databases and put on post-processing actions.

The first step of the system scanning consisted of the login sequence, followed by an activity log check and machine status evaluation, as shown in Figure 4. Following these steps allowed for the possibility to generate the data files for each machine.

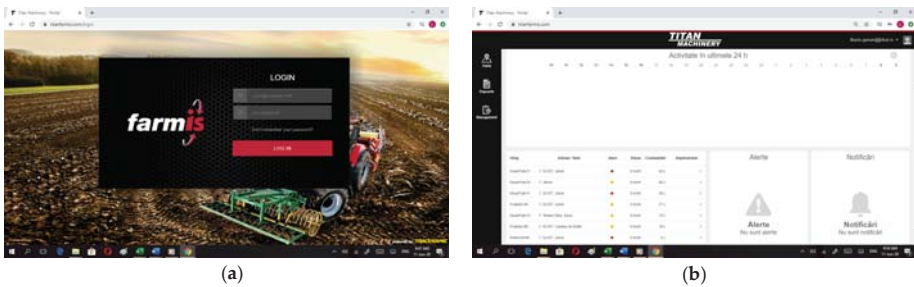


**Figure 4.** Titan Farmis application interface and available machines for operational monitoring in exploitation: (a) Titan Farmis login interface; (b) Titan Machinery activity log page [16].

The follow-up steps consisted of detailing the activity available data and actual values monitoring. After the login phase in Titan Farmis and activity brief check, the following sequences were considered to control the consumption and operation status, as shown in Figure 5.

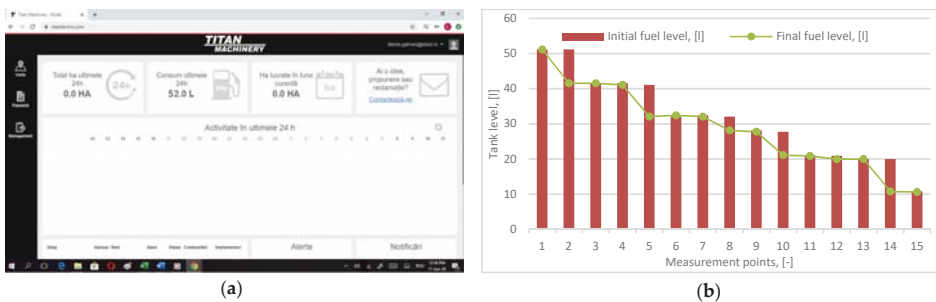


**Figure 5.** Titan Machinery application interface used for accessing data for consumption and fuel level: (a) Titan Machinery interface; (b) Tank fuel level data points.

The third step in data digging consisted of fuel measurement and mapping the operating time, as shown in Figure 6. Graphical representation of data, and mapping, offered an added quality level in process of machine monitoring and management, which was a real scientific contribution.

Differences between the start time and end time somewhat correspond to the bars which represent the fuel consumption in operation. All the data generated within the implemented system were available for post-processing operations to draw maps or to create surfaces.

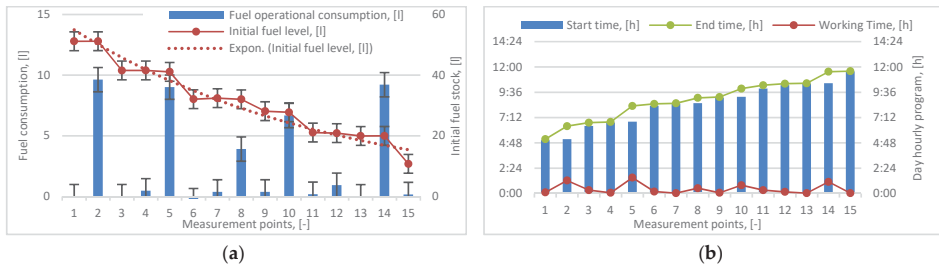


**Figure 6.** Actual values variation and correlations of data acquired during testing in operating conditions: (a) Fuel consumption values and tank level variation; (b) Graphical map of operating time.

Line variations for fuel level and working time in the field were essential in understanding the evolution and differences between the initial and final values, as shown in Figure 7.

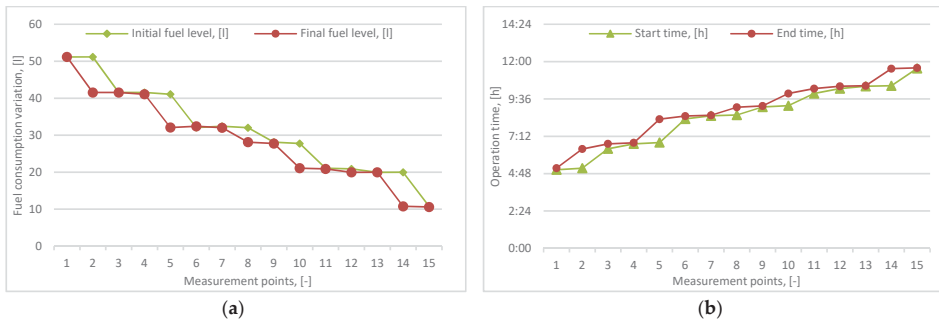


**Figure 7.** Correlation and variation of fuel level and operating time: (a) Evolution of initial fuel level and final fuel level during the measurement program; (b) Start time/end time evolution.

The measurement of the final fuel level and operating time allowed for other calculations such as autonomy and fuel consumption, as shown in Figure 8.

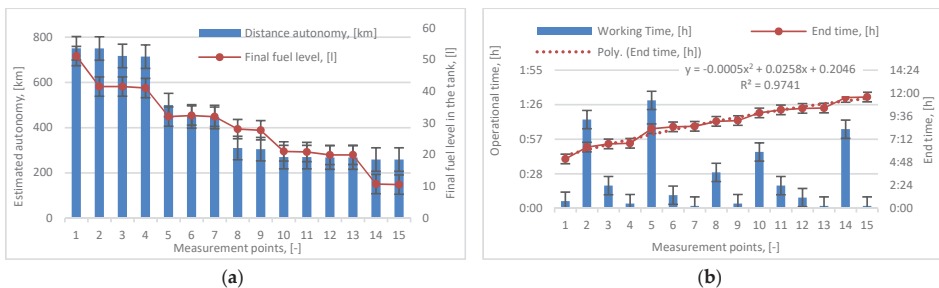


**Figure 8.** Correlation of reachable distance autonomy and final fuel level: (a) Representation of standard error bars and evolution of fuel level and autonomy; (b) Operating time and hourly interval.

Appreciation of distance into the reach of fuel autonomy is very important in operation and transport logistics due to optimal programming of routes and travel. The Titan Farmis application and its implements were providing valuable data regarding the real values, as shown in Figure 9.

Fuel consumption may be also consequently appreciated from the investigation of INITIAL FUEL LEVEL (IFL) evolution curve, which represents the recorded values in the electronic database.



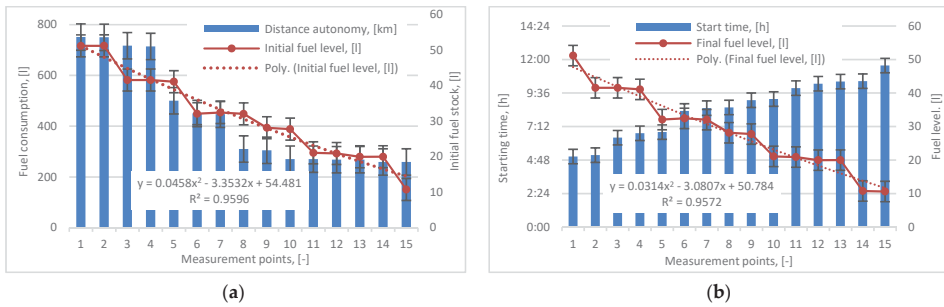


**Figure 9.** Some parameters related to fuel consumption and operating time interval for testing and mapping: (a) Fuel consumption level and autonomy prediction; (b) Fuel level variation vs. time of machinery operation.

Operating end time (OET) is mathematically defined by the following equation to gain the trendline actual values based on a polynomial model:

$$OET = -5 \times 10^{-4} x^2 + 2.6 \times 10^{-2} x + 0.2, [I], \quad (1)$$

where OET is the operating end time during the applied tests;  $x$ —specific measurement coefficient (1 ... 15).

Initial fuel level (IFL) is mathematically described by the following equation in order to retrieve the trendline numerical values based on the polynomial model:

$$IFL = 45 \times 8 \times 10^{-3} x^2 - 3.35x + 54.5, [I], \quad (2)$$

where IFL is the initial fuel level inside the fuel tank;  $x$ —specific measurement coefficient (1 ... 15).

Final fuel level (FFL) is mathematically described by the Equation (3) in order to retrieve the trendline numerical values based on the polynomial model:

$$FFL = 31 \times 4 \times 10^{-3} x^2 - 3.1x + 50.8, [I], \quad (3)$$

where FFL is the final fuel level inside the fuel tank;  $x$ —specific measurement coefficient (1 ... 15).

#### 4. Discussions and Contributions

The important contributions of the authors consist of designing the system that supported the integration of the physical components in the existing machinery fleet, as well as testing the client's remote access to the database on the server. Other contributions are the specific optimization sequences required for the complete implementation of the system on mobile equipment. Installation of fuel level sensors was also very important for the main objective of the research, and it requested a proper calibration and quality check. In addition, the manufacturing of electrical infrastructure, electronic connections, and digital testing represents a specific contribution. Thus, the most important contribution of the present research is the design and development of an automated system for fuel level control and machinery location tracking which optimized remote accessibility and telematics, as is shown by Figure 10. Each vehicle from the fleet (1) is sending a data package through a wireless connection (3) to the world wide web (4). The mainframe server (5) stores the data and provides access for the client units. An extensive research unit works with LAN (6) on the Jidvei plant factory for retrieving and processing data recorded from the fleet. A remote researcher unit (7) elsewhere is participating in post-processing the data package. Finally, the remote client unit (8) inspects and verifies the overall results. In this manner, the remote accessibility and up to date telematic system is

created. Thus, mobile tracking in a global network is developed and put in operation, providing actual values in real-time.

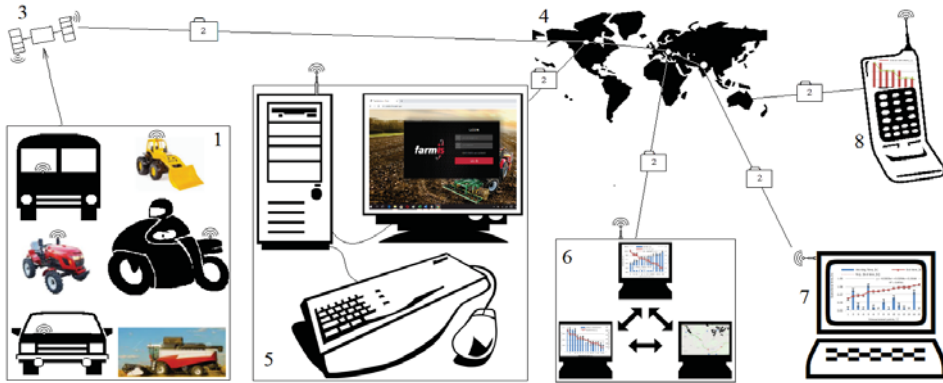


Figure 10. Synoptic view of the system for fuel tank level remote control and machinery geo-tracking.

The significant technical features put into the system are supported by the RS232 interfaces (Fruitteto RS), customizable analog and frequency outputs (AF), as well as the CAN J1939 interface. The sensors have a Kline interface, used to configure the complete interaction between them. The RS and CAN sensors have an “alarm” feature for signaling a fuel leak incident. The signal provided by the low-level “alarm” turns on whenever the fuel level drops below a preset value. The sensors determine the level of fuel as well as other liquids (if necessary, such as cooling liquid). These solid-state fuel, coolant, or oil level sensors generate a continuous signal regarding the monitored tank content level and operate either voltage or resistance formats. The sensor unit will be automatically re-calibrated every time the fuel tank is refilled. It can work properly even when mixtures of conventional fuels and additives are included. Available sizes are suitable for every tank depth in a range between 190 mm and 1000 mm. The length of the sensor may also be adjusted to the proper size adapted for each practical application. In addition, there is provided a built-in display and accelerometer to facilitate measurements on all types of rough terrains. Compared to other achievements, such as [9–13], this one is offering both remote tracking, fuel monitor, and kinematic recording at distance. The discussion over the main contributions and achievements of the present research creates the opportunity for issuing conclusive ideas regarding the practical implements and the recorded results.

## 5. Final Observations and Conclusions

Automatic systems and smart interfaces in production and logistics are key factors for development. They constitute some of the most significant research subjects in mechatronics and robotics nowadays. The applied research and testing are supporting the automatic system development with a high level of control and monitoring procedures for speed, location, tilled area, fuel economy, and energy efficiency integrated into a smart program available on mobile devices.

It may be quite easily observed that the implemented system has the operational capacity and provides actual data in real-time for multiple geo-locations regarding fuel level monitoring and precise global positioning. Tank fuel level sensors transmit data through GPS connections during operation and stationary periods. The accurate measurement of the level inside the fuel tank contributes to the optimization of the time and geo-location of re-fills, as well as the prevention of fuel leaks. The fuel level sensor makes accurate measurements of the amount of fuel in the tank, and it is compatible with the machinery telematics systems and data managing equipment (both hardware and software). Accessing databases of different pieces of machinery may support a better assessment of their performance and energy consumption in order to define energy costs and financial impact.

The automation of data recording about tank fuel levels and of the data storage system allows the admin account to have remote access to the controlled machinery, including checking their status.

The development of the automated system for fuel tank level control has been realized according to the initially proposed objective and it allowed the practical setups on specific machinery, as well as manufacturing the technical solutions for integrating all necessary components.

Actual data have been received remotely by the WLAN connection supported by the machinery location management system that was put in place during the experimental setup operation. Thus, these were taken into consideration and optimization procedures were realized for accessibility level and mobile tracking, showing the precise location, GPS coordinates, tilled area for tractors, and traveling speed.

Further research is expected to define more accurately the topic of automation for remote machinery operation. As other similar technologies will be used more, comparison studies will be done.

**Author Contributions:** Conceptualization, D.P. and D.-L.B.; methodology, A.-I.B.; software, D.P.; validation, D.P., D.-L.B. and A.-I.B.; formal analysis, D.-L.B.; investigation, D.P.; resources, A.-I.B.; data curation, D.-L.B.; writing—original draft preparation, D.P.; writing—review and editing, D.-L.B.; visualization, D.-L.B.; supervision, D.P.; project administration, A.-I.B.; funding acquisition, A.-I.B. and D.P. All authors have read and agreed to the published version of the manuscript.

**Funding:** This research received funding from the Research and Innovation Ministry, CCCDI-UEFISCDI, through PN-III-P2-2.1-CI-2018-1227 Grant—PNCDI III.

**Acknowledgments:** Lab support was provided by SC Maria Turism SRL, Jidvei Company.

**Conflicts of Interest:** The authors declare no conflict of interest.

## References

1. Andrei, L.; Băldean, D.L.; Borzan, A.I. Applied Measurements and Instrumentation for Improving Diagnostic Devices and Systems in Metropolitan Polluted Environments with Nitric and Carbon Oxides. In Proceedings of the 6th International Conference on Advancements of Medicine and Health Care through Technology, Cluj-Napoca, Romania, 17–20 October 2018; Vlad, S., Roman, N., Eds.; Springer: Singapore, 2019; Volume 46, pp. 45–49. [CrossRef]
2. Baghli, F.Z.; El bakkali, L.; Lakhal, Y. Multi-input Multi-output Fuzzy Logic Controller for Complex System: Application on Two-links Manipulator. In Proceedings of the 8th International Conference Interdisciplinarity in Engineering, INTER-ENG 2014, Tirgu Mures, Romania, 9–10 October 2014; pp. 607–614. [CrossRef]
3. Băldean, D.L. Software for the study of some parameters of gasoline injection process in Otto engines. *J. Acta Tech. Napoc. Appl. Math. Mech.* **2018**, *6*, 70–78.
4. Borza, E.V.; Băldean, D.L.; Borzan, A.I. Research Concerning Fuel Economy Coefficient and Carbon Footprint in Various Conditions for a City Compact Size Vehicle with Digital Control for a Green Solution and Method at Technical University from Cluj-Napoca. In Proceedings of the 4th International Congress of Automotive and Transport Engineering, Cluj-Napoca, Romania, 30 September 2018; Burnete, N., Varga, B., Eds.; Springer: Cham, Switzerland, 2018; Volume 46, pp. 181–189. [CrossRef]
5. Borzan, A.I.; Băldean, D.L. Experimental design for Diesel supply control in order to improve fuel efficiency. *IOP Conf. Ser. Mater. Sci. Eng.* **2019**, *568*. [CrossRef]
6. Borzan, A.I.; Băldean, D.L. The Development of a New Interface for Intelligent Control of Energy Supply in Dynamic Environment with Process Digitization. In Proceedings of the 13th International Conference Interdisciplinarity in Engineering, INTER-ENG 2019, Tirgu Mures, Romania, 4 October 2019; Volume 46, pp. 1–6. [CrossRef]
7. Chereches, A.I.; Băldean, D.L.; Borzan, A.I. Research of Intelligent Control of Injection Systems for Subaru Competition Car. In Proceedings of the 30th SIAR International Congress of Automotive and Transport Engineering, SMAT 2019, Craiova, Romania, 14 October 2019. [CrossRef]
8. Jovrea, S.; Băldean, D.L. Experimental Research of Electronic Diesel Control (EDC) System Operation in Relation with N47 Engine Load from BMW 320D (E90) Automobile at Constant Temperature and Speed. 2018, Volume 33. Available online: <http://stiintasiinginerie.ro/33-43> (accessed on 15 June 2020).

9. Jovrea, S.; Borzan, A.I.; Băldean, D.L. Researching on-Board Display of Essential Information Concerning Technical Conditions in Operation and Fuel-Economy of a Motor-Vehicle in Operation. *Știință și Inginerie* 2017, 31. Available online: <http://stiintasiinginerie.ro/31-67> (accessed on 15 June 2020).
10. Jovrea, S.; Băldean, D.L. Researching the Implementation at on-Board Level of Mercedes e Class Coupe Vehicles of Essential Information Concerning Fuel-Economy in Operation. 2018, Volume 33. Available online: <http://stiintasiinginerie.ro/33-62> (accessed on 15 June 2020).
11. Jovrea, S.; Jovrea, D.L.; Crisan-Lupa, L.V. Researching the Economy of Mercedes e Class Coupe Limo in Operation. 2019, Volume 35. Available online: <http://stiintasiinginerie.ro/35-42> (accessed on 16 June 2020).
12. Kaabal, A.; El halaouia, M.; El Jaafarib, B.; Ahyoudc, S.; Asselman, A. Design of EBG antenna with multi-sources excitation for high directivity applications. In Proceedings of the 11th International Conference Interdisciplinarity in Engineering, Tirgu Mures, Romania, 5–6 October 2017; Volume 22, pp. 598–604. [[CrossRef](#)]
13. Marinaș, C.; Băldean, D.L.; Kocsis, L.B.; Borzan, A.I. Contribuții la cercetarea experimentală a funcționalității modului electronic diesel control (EDC) în raport cu alimentarea de la motorul N47 de la automobilul BMW 320D (E90). 2017. Available online: <http://stiintasiinginerie.ro/31-82> (accessed on 16 June 2020).
14. Moldovan, A.; Băldean, D.L. Borzan, Experimental Research of the Management System from the Peugeot 4007 Sport Utility Vehicle. 2017; Volume 31. Available online: <http://stiintasiinginerie.ro/31-71> (accessed on 16 June 2020).
15. Turc, T. Using WEB Services in SCADA Applications. In Proceedings of the 8th International Conference Interdisciplinarity in Engineering, Tirgu Mures, Romania, 9–10 October 2014; Volume 19, pp. 584–590. [[CrossRef](#)]
16. Titan Farmis. Available online: <https://titanfarmis.com/> (accessed on 16 June 2020).
17. Bosch—Bessere Luftqualität und Individuelle Mobilität. Available online: <https://www.youtube.com/watch?v=XU23yfb780> (accessed on 16 June 2020).

**Publisher’s Note:** MDPI stays neutral with regard to jurisdictional claims in published maps and institutional affiliations.



© 2020 by the authors. Licensee MDPI, Basel, Switzerland. This article is an open access article distributed under the terms and conditions of the Creative Commons Attribution (CC BY) license (<http://creativecommons.org/licenses/by/4.0/>).



# Robotic Arms with Anthropomorphic Grippers for Robotic Technological Processes <sup>†</sup>

Ionel Staretu <sup>1,2</sup>

<sup>1</sup> Design, Mechatronics and Environment Department, Transilvania University of Brasov, 500036 Brasov, Romania; rectorat@unitbv.ro; Tel.: +40-744309186

<sup>2</sup> Technical Sciences Academy of Romania, 030167 Bucharest, Romania

<sup>†</sup> Presented at the 14th International Conference INTER-ENG 2020 Interdisciplinarity in Engineering, Mureş, Romania, 8–9 October 2020.

Published: 28 January 2021

**Abstract:** The robotic arms of the human arm type, so-called collaborative robots, have been improved, optimized, and diversified greatly in recent years. However, most of them are still equipped with mechanical grippers with plier-like jaws. Equipping these robotic arms with anthropomorphic grippers is currently hampered by variants of these grippers on the market that are far too complex and at inaccessible prices to be used on a large scale. As an alternative to the familiar anthropomorphic grippers, I presented an anthropomorphic gripper with five fingers, made under my coordination, constructive, and functional, including briefly the coupling solution with a robotic arm.

**Keywords:** robotic arm; human arm; direct kinematic; collaborative robot; anthropomorphic gripper

## 1. Introduction

After the advent of industrial robots in technological processes, for a long time, industrial robots have been and are equipped for parts transfer operations, with mechanical grippers with jaws. These grippers can only be used for one type of parts or a set of similar parts. There are also multi-grippers that can be used for more types of parts. The main disadvantage of these grippers is the limited range of use and the need to change the gripper in the case of another type of part in shape or size [1]. In parallel with the mechanical grippers with jaws, anthropomorphic grippers, similar to the human hand, with three to five fingers, were continuously developed and perfected. Robotic arms similar to the human arm were also developed and perfected, which became compact, precise, and reliable [2,3]. Thus, in the robotic technological processes, the classic industrial robots got to be replaced, as an increasingly obvious trend, with robotic arms/collaborative robots (cobots) equipped with anthropomorphic grippers, fixed or mounted on mobile platforms, to the more complex shape of humanoid robots. In this way, it is possible to replace human operators with these variants of humanoid arms or robots.

This paper presents a unit of robotic arm/ anthropomorphic gripper that can be widely used in the robotization of technological processes for industrial products' manufacturing.

## 2. Types of Collaborative Robotic Arms

In the industrial robot, the robotic arm had from the beginning as a model the human arm, with the mention that the initial variants of industrial robots had large dimensions and some disproportions compared to the human arm. Anatomically and cinematically, the human arm represented in Figure 1 is characterized by several elements and seven independent movements (in  $xyz$  coordinate axis): three rotations in the shoulder ( $\omega_1$ ;  $\omega_2$ ;  $\omega_3$ ), one rotation in the elbow ( $\omega_4$ ), one rotation around the forearm ( $\omega_5$ ), and two rotations at the wrist level ( $\omega_6$ ;  $\omega_7$ ).

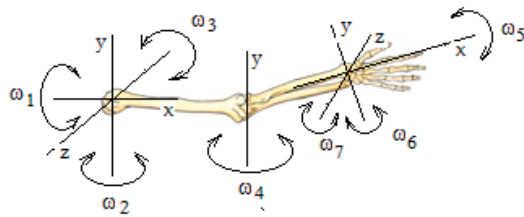


Figure 1. Anatomically and cinematically the human arm.

As we have already mentioned, the first variants of industrial robots only tried to copy the structure and kinematics of the human hand, a direction in which they were partially successful. However, in the last 10–15 years, robotic arm structures have appeared that are much more similar to the human arm and have comparable performance. Some of these variants will be presented (for each variant the independent movements are highlighted:  $\omega_1, \dots, \omega_7$ , corresponding to the number of degrees of freedom, an original contribution of this paper, useful for the easier understanding of the operation of these robots). The Barrett Arm (Figure 2a) has been made since the early 2000s and is particularly accurate. The main features of this robotic arm are a height of 42 cm, length of 72 cm, width of 34 cm, weight 27 of kg, high speed, and very good accuracy [4]. Figure 2b shows the Universal Robot UR 10 robotic arm. Its main features are: it safely works alongside employees or separately; it automates tasks up to 22 lbs (10 kg); its reach radius is up to 51.2 in (1300 mm); it has 360-degree rotation on each wrist joint, 6-axis capability, and 0.1 mm repeatability; and it is lightweight and mountable at only 24.3 lbs and easily programmed to switch tasks [5].

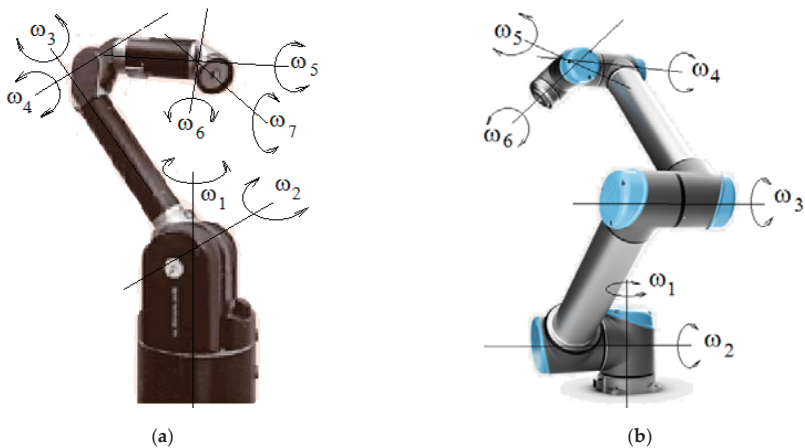
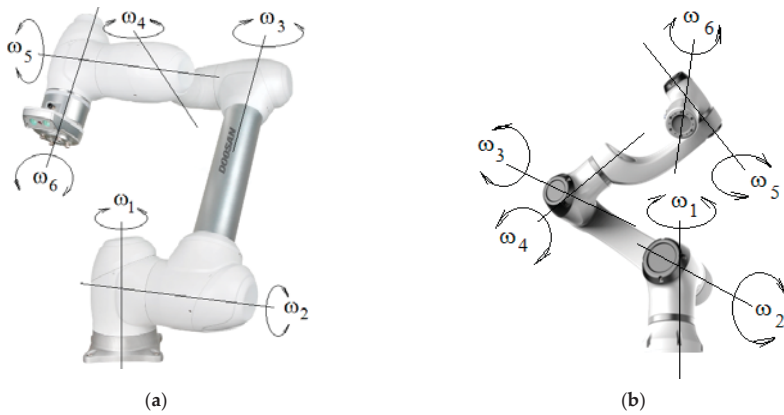


Figure 2. Collaborative robots: (a) WAM Barrett robotic arm; (b) Universal Robot UR 10 robotic arm.

Doosan M 1013 Robotic Arm (Figure 3a) is characterized by: degrees of freedom: 6; payload: 10 kg; reach: 1300 mm; tool speed: 1 m/s; repeatability:  $\pm 0.1$  mm; operating temperature: 5–45 °C; weight: 33 kg; installation position: floor, ceiling, and walls; protection rating: IP54, I/O ports: configured with 6 I/Os; and power supply: 24 V/Max. 3 A, joint movement (range/speed): J1; J2:  $\pm 360^\circ/120^\circ/s$ ; J3:  $\pm 160^\circ/180^\circ/s$ ; J4, J5, J6:  $\pm 360^\circ/225^\circ/s$  [6]. Figure 3b shows the robotic arm type Elfin, which has the following features: control mode: continuous path control; drive mode: electric; application loading, pick and place, condition: new; CE certification; trademark: Han’s Robot [7].



**Figure 3.** Collaborative robots: (a) Doosan M 1013 Robotic Arm; (b) Elfin Robotic Arm.

Another variant of robotic arm of this type is ROZUM Robotics (Figure 4a) characterized by being ultra-lightweight and mobile (8 kg weight), strong and dexterous (3 kg payload, 700 mm reach), precise ( $\pm 0.1$  mm repeatability), and fast (30 rpm/2 m/s) [8]. The KUKA robotic arm (Figure 4b), made after a long period of improvement and optimization of KUKA classic robots, in which we can also remark upon the great difference between the traditional industrial robots and articulated robotic arms of the last generation, is characterized by a 7-DOF robotic arm and adaptation algorithms; the robot is equipped with torque sensors, allowing us to perform torque control and by extension impedance control, allowing for compliant interaction and motion-adaptation [9].

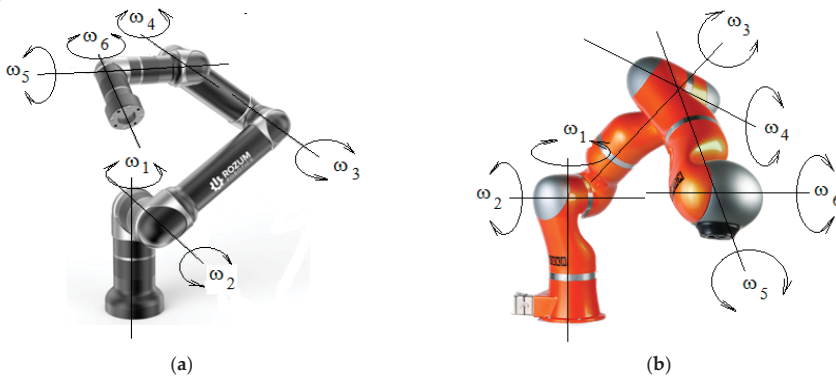


**Figure 4.** Collaborative robots: (a) ROZUM robotic arm; (b) KUKA robotic arm.

The Rebel Arm 1–2 robotic arm (Figure 5a) is characterized by 6 DOF, with integrated control system and motor; an outer chassis that consists entirely of polymers and is therefore cost-effective and light; an articulated arm that enables applications involving human–machine collaboration; lightweight, internal cables; joints that are suitable for service robotics applications; and brushless DC motors instead of stepper motors [10]. The Panda robotic arm (Figure 5b) is characterized by a easy-to-program robotic arm designed for small businesses and ability to move in seven axes, designed with a smart sense of “touch”; the Panda can help conduct science experiments, build circuit boards, or pretest equipment (two Panda arms can even work together to build a third) [11].



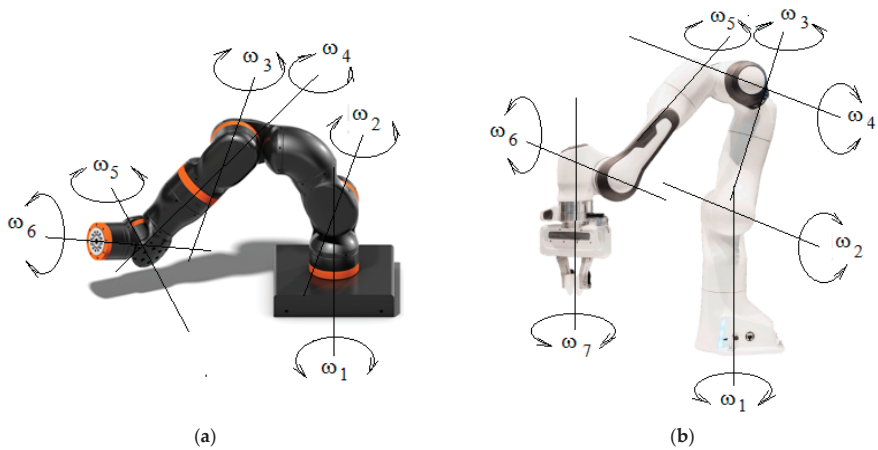


**Figure 5.** Collaborative robots: (a) Rabel robotic arm; (b) Panda robotic arm.

All types of robotic arms presented are part of the so-called class of collaborative robots designed to interact in a friendly manner and very efficiently with the human operator. These robotic arms typically have six or more degrees of mobility and can be used individually or in pairs, as human arms. Two examples are given for illustration of the structure equipped with two robot arms each (Figure 6a,b).



**Figure 6.** Robotic structure with two robotic arms: (a) Yaskawa type [12]; (b) ABB type [13].

In most cases, these robotic arms, used individually or in pairs, have been equipped and are still equipped, as already mentioned, on a large scale with grippers with jaws, pliers, or sporadically with articulated finger grippers (3, 4, or 5 fingers). This situation is explained by the still low performance and affordable variants of anthropomorphic finger grippers.

It is time for this situation to be overcome and to move broadly to the endowment of robotic arms of the collaborative type with anthropomorphic grippers with five articulated fingers [2,3].

### 3. Solving the Direct Kinematic Problem with the Method of Homogeneous Operators

A problem of particular importance for robotic arms of the human arm type is the solution of direct kinematics. The following is a brief example of solving direct kinematics for a robot of this type, for which the method of homogeneous operators is applied [14,15]. This method application involves the use of homogeneous operators of rotation, translation, and rotation–translation compound operators, respectively, for translation–rotation. In Figure 7a, we show the form of the homogeneous elementary translation operator of the reference system  $O_m x_m y_m z_m$  to the reference system  $O_n x_n y_n z_n$ , by the axis  $x_m = x_n$ :

$$A_{mn} = T_{mn}^x = \begin{bmatrix} 1 & 0 & 0 & 0 \\ d_{nm} & 1 & 0 & 0 \\ 0 & 0 & 1 & 0 \\ 0 & 0 & 0 & 1 \end{bmatrix}, \tag{1}$$

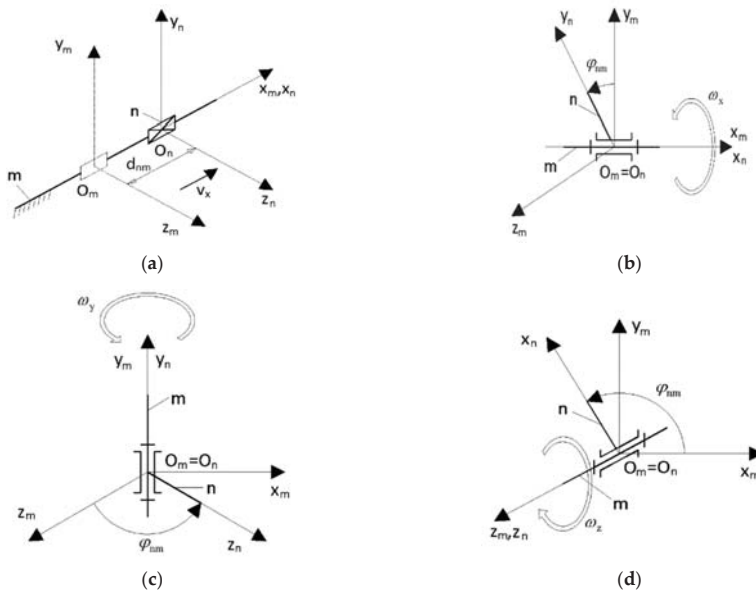


Figure 7. Appropriate kinematic schemes for homogeneous elementary operators: (a) translation; (b) rotation by x axis; (c) rotation by y axis; (d) rotation by z axis.

In the same form, the matrix of elementary homogeneous rotation operators by x-axis, y-axis, and z-axis, according to Figure 7b–d, are:

$$A_{mn} = R_{mn}^x = \begin{bmatrix} 1 & 0 & 0 & 0 \\ 0 & 1 & 0 & 0 \\ 0 & 0 & C_{nm} & -S_{nm} \\ 0 & 0 & S_{nm} & C_{nm} \end{bmatrix}, \quad A_{mn} = R_{mn}^y = \begin{bmatrix} 1 & 0 & 0 & 0 \\ 0 & C_{nm} & 0 & S_{nm} \\ 0 & 0 & 1 & 0 \\ 0 & -S_{nm} & 0 & C_{nm} \end{bmatrix}, \tag{2}$$

$$A_{mn} = R_{mn}^z = \begin{bmatrix} 1 & 0 & 0 & 0 \\ 0 & C_{nm} & -S_{nm} & 0 \\ 0 & S_{nm} & C_{nm} & 0 \\ 0 & 0 & 0 & 1 \end{bmatrix},$$

In these matrices,  $S_{nm} = \sin\varphi_{nm}$  and  $C_{nm} = \cos\varphi_{nm}$  are sines, respectively, cosines of rotation angles. Rotation is around the respective axes, from the reference system  $m$  to the reference system  $n$ . If we use two elementary homogeneous rotation and translation operators, translation and rotation ones, respectively, we can obtain compound homogeneous operators corresponding to matrices resulted by multiplying the matrices corresponding to homogeneous elementary operators. Compounds operators ease, to some extent, the kinematic calculation, by reducing the number of operations of multiplication of the matrices corresponding to rotations around axes in kinematic couplings and translations between the two axes of two successive couplings. Below, we exemplify the direct kinematic problem solving for the kinematic structure with 6 axes (0,1,2,3,4,5) analyzed and represented in Figure 8.

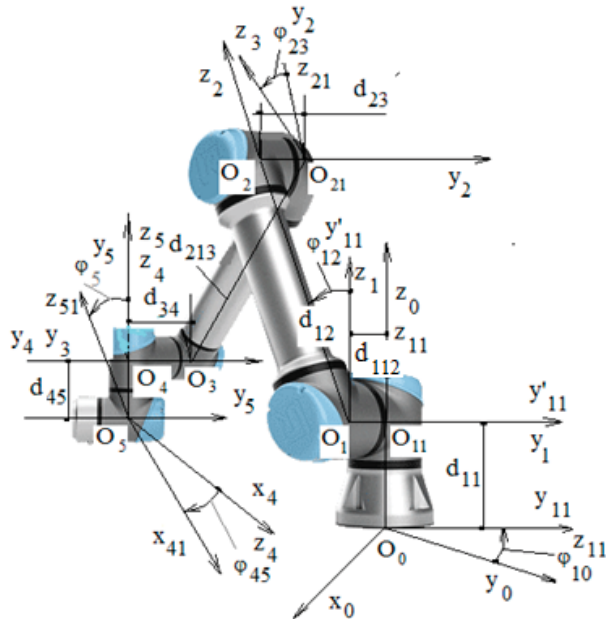


**Figure 8.** The necessary notations for solving the direct kinematics with the method of homogeneous operators.

To obtain the reference system coordinates  $O_5x_5y_5z_5$  reported to the reference system  $O_0x_0y_0z_0$  (the direct kinematics problem), we write matrix forms of the rotation or translation operators of successive passage from the reference system  $m$  to the reference system  $n$ :  $m = 0, 1, 2, 3, 4, 5$ ;  $n = 0, 1, \dots, 5$ . The matrix of the reference system coordinates  $O_5x_5y_5z_5$ , as compared to the reference system  $O_0x_0y_0z_0$ , which is a product of the transfer matrices above matrix, under the form:

$$A_{05} = A_{01} \cdot A_{11} \cdot A_{12} \cdot A_{22} \cdot A_{23} \cdot A_{33} \cdot A_{34} \cdot A_{44} \cdot A_{45}, \tag{3}$$

The kinematic analysis presented may be extrapolated to any other structure of the robotic arm type human arm.

#### 4. Five-Finger Anthropomorphic Gripper for Robotic Arms

Furthermore, I describe an anthropomorphic five-finger gripper, designed under the coordination of the author, with a high degree of resemblance to the human hand made under my coordination, a type of gripper that is recommended to be used to equip the robotic arms described above. Figure 9

shows such a robotic arm and the gripper that will be mounted on it, real variant and the CAD model [16].

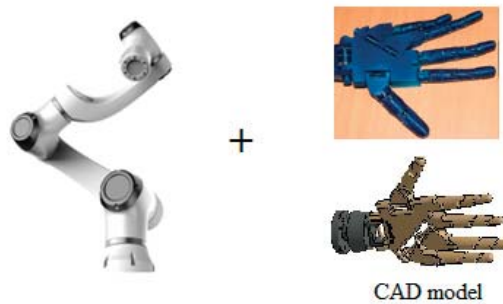


**Figure 9.** Recommendation for coupling a human arm robot with an anthropomorphic five-finger grip.

This gripper, according to Figure 10a, has five degrees of mobility and is driven by five stepper motors (Figure 10b). The implementation of the gripper is being carried out, having solved the first part of the problem by ensuring the compatibility between the robot and the gripper.

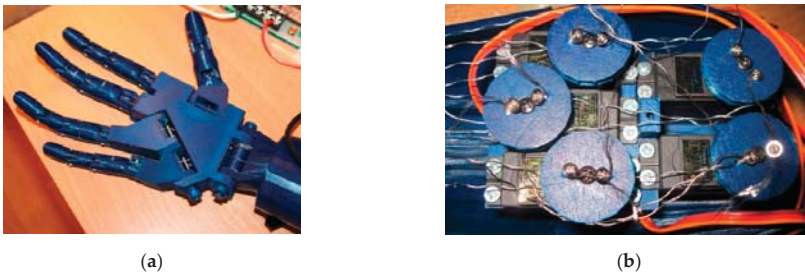


**Figure 10.** Anthropomorphic gripper with five fingers: (a) Constructive version; (b) The stepper motors.

An example of use is the simulation of a mounting and transfer operation of a metal shaft. According to Figure 11a,b, a bearing is mounted on a shaft.

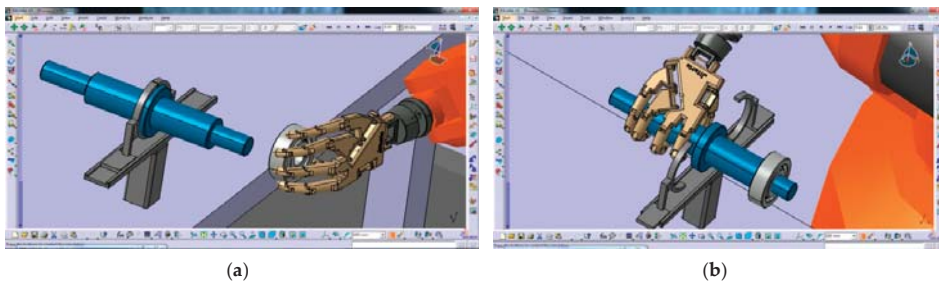


**Figure 11.** Simulation operations: (a) A bearing is mounted on a shaft; (b) Transfer operation.

After mounting, the shaft is taken and stored in a box on a suitable support (Figure 12).

The robotic workstation can be optimized by using a Kinect sensor, which takes over the movements of a human arm and transmits them to the robotic arm, the anthropomorphic gripper being configured to grip various parts using a Motion Leap sensor (Figure 13).

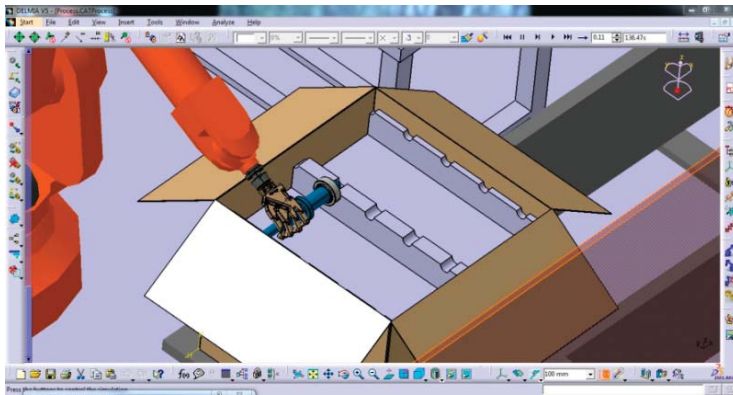


Figure 12. The shaft is stored in a box.

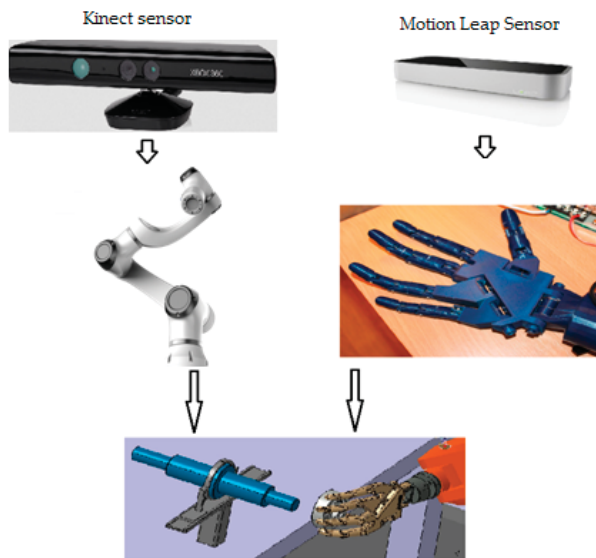


Figure 13. Control solution for the robotic structure with robotic arm and anthropomorphic finger grip.

The presentation of this solution seeks to encourage the widespread use of robotic arms equipped with anthropomorphic grippers with five fingers of average complexity achievable at low cost, which really contributes to the quasi-total robotization of technological processes of manufacture and assembly.

## 5. Conclusions

Based on what is presented in this paper, the following conclusions can be drawn:

- Human arm type robotic arms, also called collaborative robots or cobots if their shapes are more complex, have greatly improved and diversified in recent times; even one of the big companies brought to market industrial robots and such structures.
- These robotic arms, more efficient than the robotic arms from the traditional industrial robots, are further equipped especially with jaw grippers of the pliers type that do not highlight all their constructive and operational possibilities.

- The maximum efficiency of collaborative robotic arms use can be achieved by equipping them with anthropomorphic grippers, still difficult to access because of high costs, and a sometimes unnecessary complexity;
- As an alternative to the familiar anthropomorphic gripper, to equip robotic arms, I briefly present an anthropomorphic gripper with five fingers, sufficiently advanced and feasible at a lower cost, made under my supervision, including a solution for coupling a robotic arm, and exemplification of use in the case of assembly and transfer operations; this is a solution that has advantages in terms of cost and operation for current applications compared to other very expensive and unjustifiably complex anthropomorphic grippers.

## References

1. Staretu, I. *Gripping Systems*; Derc Publishing House: Tewksbury, MA, USA, 2011.
2. El Zaatari, S.; Marei, M.; Li, W.; Usman, Z. Cobot programming for collaborative industrial tasks: An overview. *Rob. Auton. Syst.* **2019**, *116*, 162–180. [CrossRef]
3. Schou, C.; Andersen, R.S.; Chrysostomou, D.; Bøgh, S.; Madsen, O. Skill-based instruction of collaborative robots in industrial settings. *Robot. Comput. Integr. Manuf.* **2018**, *53*, 72–80. [CrossRef]
4. Robots Your Guide to the World of Robotics. Available online: <https://robots.ieee.org/robots/wam/> (accessed on 24 April 2020).
5. Automation Distribution! Available online: <https://automationdistribution.com/universal-robots-ur10-collaborative-industrial-robot-arm/> (accessed on 26 April 2020).
6. Generation Robots. Available online: <https://www.generationrobots.com/en/403413-dooan-m1013-robotic-arm.html> (accessed on 20 April 2020).
7. Made-in-China. Available online: <https://www.made-in-china.com/showroom/hansrobot/product-detail0CKEAFvTEScF/China-6-Axis-Universal-Robot-for-Pick-and-Place-Competitor-Price.html> (accessed on 20 April 2020).
8. ROZUM ROBOTICS. Available online: <https://www.f6s.com/rozumrobotics> (accessed on 26 April 2020).
9. Laurens, A.; Khoramshahi, M.; Billard, A. *Adaptive Human-Robot Interaction: From Human Intention to Motion Adaptation Using Parameterized Dynamical Systems*; Technical Report; Ecole Polytechnique Federal de Lausanne: Lausanne, Switzerland, 2018.
10. IGUS Plastics for Longer Life. Available online: <https://www.igus.ro/info/news-2018-20852> (accessed on 24 April 2020).
11. TIME-BEST INVENTION 2018. Available online: <https://time.com/collection/best-inventions-2018/5454734/panda/> (accessed on 24 April 2020).
12. YASKAWA. Available online: <https://www.yaskawa.eu.com/products/robots> (accessed on 20 June 2020).
13. ABB. Available online: <https://new.abb.com/products/robotics/industrial-robots/irb-14000-yumi> (accessed on 20 June 2020).
14. Dudita, F.; Diaconescu, D.; Gogu, G. *Linkages Mechanisms (in Romanian)*; Editura Tehnica: Bucharest, Romania, 1989.
15. Staretu, I. The Structure, Work Space and Direct Kinematic of the Robots with 8 Axes of Type T Normal R Parallel (PM) (OM). *Appl. Mech. Mater.* **2014**, *658*, 718–723. [CrossRef]
16. Moldovan, C. Theoretical and Experimental Researches Regarding the Diversification of a Virtual Hand Interaction with Objects from a Virtual World with Applications in Industrial Engineering (in Romanian). Ph.D. Thesis, Transilvania University of Brasov, Brasov, Romania, 2014.

**Publisher's Note:** MDPI stays neutral with regard to jurisdictional claims in published maps and institutional affiliations.



© 2021 by the author. Licensee MDPI, Basel, Switzerland. This article is an open access article distributed under the terms and conditions of the Creative Commons Attribution (CC BY) license (<http://creativecommons.org/licenses/by/4.0/>).



# A Wire Rod Rolling Mill Digital Twin for the Simulation of the Rolls Replacement Process <sup>†</sup>

Ana María Valdeón Junquera, Javier García González, Joaquín Manuel Villanueva Balsera  and Vicente Rodríguez Montequín \* 

Project Engineering Area, University of Oviedo, C/Independencia 3, 33004 Oviedo, Spain; valdeonana@uniovi.es (A.M.V.J.); garciagjavier@uniovi.es (J.G.G.); jmvillanueva@uniovi.es (J.M.V.B.)

\* Correspondence: montequi@uniovi.es; Tel.: +34-985-104-272

<sup>†</sup> Presented at the 14th International Conference INTER-ENG 2020 Interdisciplinarity in Engineering, Mures, Romania, 8–9 October 2020.

Published: 11 December 2020

**Abstract:** Smart Manufacturing is a goal to be achieved, and the most advanced manufacturing approaches are being used to pursue this objective. Within this context, industry development aims to attain an intelligent manufacturing using, for example, virtual models that simulate production lines. This paper presents the architecture of a Digital Twin for emulating the rolls replacement process within a wire rod rolling mill. The model is developed in Python, using a backtracking algorithm to select the suitable set of rolls as a first basic approach for the validation of the system. It may be used in the future to improve the production system automating the decision for the replacement of rolls as alternative to the current human-decision process.

**Keywords:** Digital Twin; Digital Shadow; smart manufacturing; rolling mill

## 1. Introduction

Nowadays, companies are employing the most advanced technologies, such as Artificial Intelligence (AI) and Internet of Things (IoT), to meet the demands of a worldwide marketplace. This inevitably entails an automation of the industrial processes [1–3] that improves their competitiveness and efficiency, which increases the quality of the organizations and paves the way for the fourth industrial revolution, noted as Industry 4.0.

Smart manufacturing [4–7] is a term used to refer to that future state of manufacturing, which is characterized by a range of interconnected automated systems that merge the physical and digital worlds. One way of developing smart manufacturing systems and processes is using Digital Twin technologies.

Digital Twins [8–10], also named Digital Shadows, are a way of recreating physical entities virtually based on models of its behaviors. A Digital Twin is never a target by itself, but a way of achieving the organization goals. They are used in several industrial sectors to analyze the data generated, visualize the processes, or optimize the business operations by optimizing the operation and maintenance of industrial installations and manufacturing processes. In the next years, Digital Twins are expected to be implemented by countless industries for multiple purposes such as supply chains, logistics, or production lines.

The rolling process is the most common industrial process in steel manufacturing, which is used for making large length cross section like sheets and plates of steel and aluminum for structures. Rolling mills are used for performing the rolling process. Wire rod is one of the resulting products from the rolling process, which is mostly used as a quality raw material to produce screws, tires, or construction materials among others. It has a hot rolled round section that is turned into wire through cold rolling processes or wire drawing.



Multiple elements are involved during the wire rod mill operation. The raw material is passed through regular rolls until the required cross-section profile is achieved. Rolls work usually in pairs (at least for the configuration noted as “two high rolling mills,” where the rolls rotate in the opposite direction to the movement of the work piece, and the work piece is fed between the rolls) and they are assembled in stands. Every roll in the process has a specific function in the making of the piece. At every stage, there are minor changes in the configuration of the metal. The size of the roll depends on the metal type, thickness, and formability. One of the most important tasks in the wire rod mill case is to determine the set of rolls to be used in the drawing process for a specific set of orders. Rolls are replaced frequently (every several days), because of the wear. Wear depends on various parameters, the most important being the tons of raw material rolled. Once a set of rolls is worn, they must be disassembled. The rolls are usually changed as a whole, or at least all of them in the same area of the rolling mill at the same time. The rolls are not discarded when disassembled, they are reconditioned in a maintenance workshop located in the same facility by grinding the roll and reshaping their tracks. There is also a warehouse where all the rolls of the plant are stored. Each roll is an expensive asset that is carefully managed through its life cycle, since it is provided by the seller until it is finally disposed. The wire rod mill has a series of determining factors which make this process complex: the number of assembled rolls is high (more than one hundred for this kind of rolling mill) and there are several sections, each one with specific requirements depending both on the track where they are going to be assembled and the kind of product to be rolled. There are also diameter restrictions for the rolls, being the fulfillment of those restrictions one of the most important parameters to take into account when changing the rolls. When the rolls are disassembled, they need to be grinded in order to be used again, reducing its diameter, and therefore, its lifetime.

The aim of this paper is to present a new Digital Twin model for the wire rod rolling mill that will allow to develop and simulate autonomous systems as alternative to the current human-decision process. The paper is structured as follows: first, the wire rod process is introduced, paying special attention to the rolls replacement operation. Then, the architecture of the simulator is presented. Finally, the conclusions and future research are featured. The work presented here constitutes a first approach, so only preliminary results are presented.

## 2. Theoretical Background: The Behavior of the Wire Rod Mill and the Rolls Exchange Process

A wire rod mill uses billets that are heated in a reheating furnace (around 1.115 °C) as raw materials; these are long products that have a square section whose length is variable. The rolling process has at its beginning a first roughing mill, consisting of three rolling stands, whose goal is to reduce the square section of the billet (150 × 150 mm) to a square section of approximately 112 × 112 mm. Afterwards, the rolling process is divided in two parallel streams, named veins, as it is depicted in Figure 1. Each vein starts with a second roughing mill formed by seven roll stands, which is followed by the intermediate section, with eleven additional rolling stands. Following this, the finishing area is equipped with two sections of rolling stands, the first one named “block” and the last one named “RSM” (Reducing Sizing Mill). These sections are in charge of providing the final quality to the rolled product. The process ends with a pair of rolls for keeping the traction. Finally, the coils of wire rod are formed. Figure 1 shows the outline of the process.

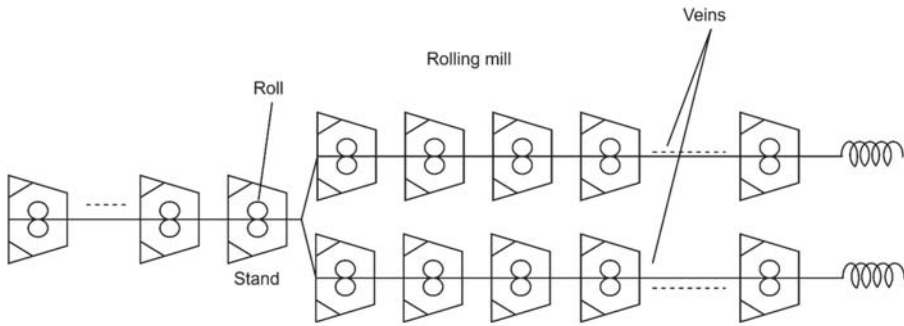


Figure 1. Schema of the wire rod rolling mill.

The stock of managed rolls in the factory is particularly high, having usually more than 4000 registered rolls, each with its specific features such as dimension, alloys, geometry, etc. The rolls are grinded and shaped with several tracks, as depicted in Figure 2, each having its own state, which can be working, used, or unused, and its properties, such as the number of tons rolled since it was assembled. Each track is used independently of the others of the same roll for a specific assembly and once the track is worn, the roll is disassembled and that track is marked as used, being the roll able to be assembled again if it still has unused tracks. Each time new rolls are received and whenever all the tracks of a roll are used, its tracks are prepared, that is they are grinded, textured, and chromed, resting ready to be used.

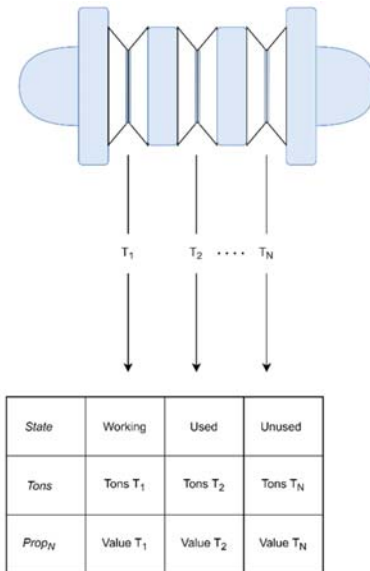


Figure 2. Schema of the main roll parts.

The rolls always work in pairs, as it is depicted in Figure 1, so when the manager must choose the suitable track of a roll for a stand, that whose geometry and shape are compatible with the stand, two rolls with equal tracks must be chosen for each vein. In those cases, the manager must take into account the roll service life, the number of accumulated rolled tons, and the location in the warehouse of the roll, turning the problem into a highly dimension one that cannot be handled manually. A database is

used for registering all the information as it is of great importance to keep track of the roll’s life cycle. There are different restrictions; for example, some rolls only suit in a particular section of the rolling mill and there is a diameter difference constraint between the rolls assembled on several rolling stands.

Currently, the operators of these facilities simplify the problem working with predefined roll pairs and using families and groups of similar rolls that are likely to work together. This is inefficient and reduces the flexibility of the roll changing process.

### 3. Digital Twin Design Approach

A simulator of the rolling mill has been developed in order to test further different approaches for selecting the appropriate rolls for the stands. The simulator is developed using Python. It is currently running in a Windows 10 operating system, although it could run in any Linux system. A backtracking algorithm is used to find the suitable set of rolls for each scheduled batch of orders, being a batch the set of jobs that the mill performs before the rolls are disassembled.

The general schema of the simulator can be seen in Figure 3. As it is depicted, at the beginning, the variables are initialized. To do that, the simulator receives a JSON file as input with the required values and using them the roll dataset that will be used as the rolls warehouse’s stock is created (1). Next, the simulation starts, and, for each scheduled batch of orders, it requests a group of rolls (2) to replace the assembled ones. In order to do this, it has to read the rolls status (3) and once known, it proposes a roll set to be used (4). This part is designed as a separate module, because one of the main goals of this simulator is testing different approaches and comparing results among them. In order to try a first approach that could be used for validation of the present work, a backtracking algorithm has been implemented. The backtracking algorithm is executed for each vein and takes the compatible rolls for each of the stands, that are those which meet the geometry and shape requirements. Then, it checks for each stand its constraints: the two rolls of the same vein must have the same diameter and the diameter restrictions among the rolls of the current stand and the rolls of the previous stand have to be met. If not, it backtracks to the previous stand.

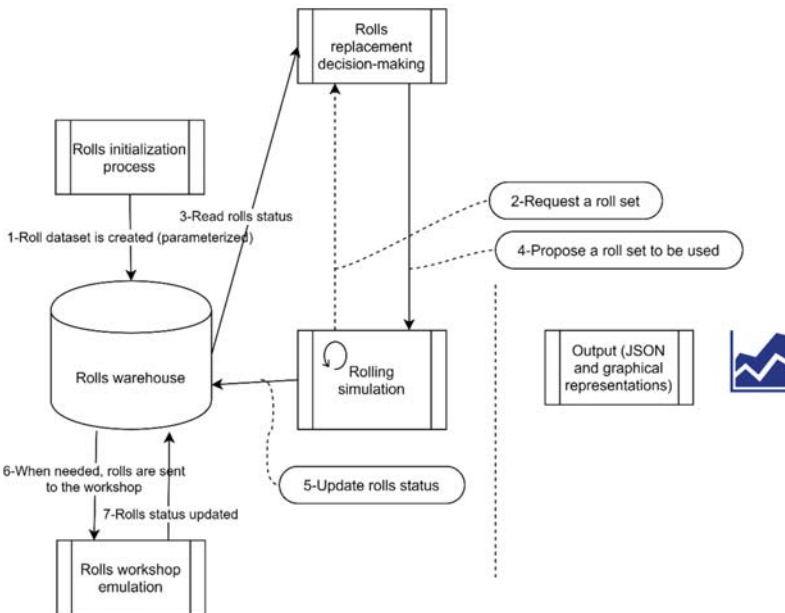


Figure 3. Simulator schema.

A flow chart of the backtracking algorithm is shown in Figure 4. The number of rolls that are checked for each stand is restricted to prevent it from taking too much time. After simulating the rolling of a specific number of tons, the rolls are disassembled because the wear of the tracks that are working and those tracks are marked as used (5). When all the tracks of a roll are marked as used, the roll is sent to the rolls workshop (6), where it is grinded and left ready to work again, reducing the rolls diameter (7) (as consequence of the grinding operation). Otherwise, while the roll has some track available for rolling, it could be assembled again. When all batches of a simulation are performed, the simulator creates several JSON files as outputs with the results and they are displayed graphically. The wear of rolls (and as consequence the reduction of the diameter) is simulated using a model trained with historical data collected from the process.

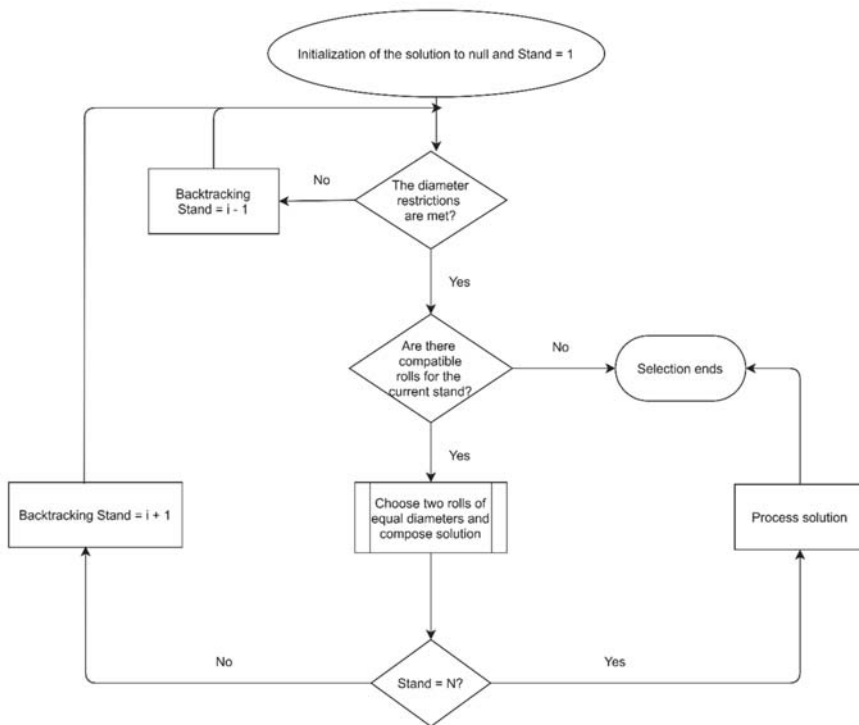


Figure 4. Backtracking algorithm flow chart.

There are N stands from 1 to N. At each step the diameter restrictions for the rolls that have been selected are checked and if they are fulfilled, it checks whether it has compatible rolls for the current stand (i) and goes to the previous stand otherwise (i - 1). If there are not compatible rolls for the current stand, the selection algorithm ends and no set is proposed, but if there are, two rolls of equal diameters are chosen and added to the solution. Then, it checks whether there have been chosen rolls for all the stands (stand = N), and if so, the solution is processed and the algorithm ends. If not, it continues with the next stand (i + 1). Each of the stages of the simulator is described in more detail below.

### 3.1. Algorithm Inputs: Initial Set of Rolls, Batches, and Restrictions

The system generates a set of rolls simulating the situation that could be found in the warehouse. In order to reproduce different scenarios, this initialization is parametrized. The JSON configuration file that the simulator has as input has defined the different types of rolls that are in the sections of

the rolling mill (its geometry, the number of positions, and the shape of each of them), the batches scheduled to be done, and its restrictions. The simulator generates a set of rolls that suit that types and the user must choose the algorithm that wants to be used in order to find a set of rolls that can be employed to perform each batch. Here, the users can design their own strategies for selecting the rolls, hence enabling the evaluation of different approaches and comparing the results.

### 3.1.1. Types of Rolls

The types of rolls are defined indicating the quantity of each, the geometry, shapes of its tracks, number of tracks, and initial and final diameter. The actual diameter of the rolls is generated randomly.

### 3.1.2. Batches, Jobs Performed with the Same Set of Rolls, and How They Are Defined

Changing the rolls is not an easy or quick operation, so it is avoided as much as possible. That is why the operators group the jobs that the mill has to do (batch) before performing them, reducing the number of replacements. For this very reason, the works that the simulator has to do are not single jobs but compositions (batches) of those that can be performed with the same set of rolls. The simulator is given a set of batches to perform and every batch received consists on each single job that has to be done before the rolls are disassembled. The batches are defined indicating the stands which take part, giving its number, geometry, shape and, for each of the single jobs that are part of it, the quality of the material and the number of tons rolled.

### 3.1.3. Restrictions Involved in the Rolls Exchange: Diameter Restrictions

Although this type of installation has several types of restrictions, the most important to be considered here are the restrictions between rolls diameters. These restrictions entail that the diameters of the rolls assembled in two consecutive stands must accomplish some constraints. A restriction between two stands with a given diameter ( $D_A$ ,  $D_B$ ) is applied in a factor ( $k$ ) and is constrained to a given value (*limit*) using a relational operator (*op*). The evaluation of the restriction is performed evaluating the expression  $(D_B - D_A)/k \text{ op } \textit{limit}$ , where, as stated before,  $D_B$  and  $D_A$  are the diameters of the rolls,  $k$  is the factor, *op* is the relational operator (usually  $\pm$ ), and *limit* is the value to which the expression is constrained.

## 3.2. Outputs

The batches defined in the configuration file are launched a certain amount of times defined previously and, for each batch, the diameter of the rolls is reduced according to a simple model which has been developed taking into account the number of tons laminated, the initial diameter of the roll, its geometry, and the shape of the track that works. Finally, the results are written to a JSON file and to observe them, they can be shown graphically by plotting the average, median, mode, and range diameters for each geometry and shape as well as the percentage of rolls grinded for each batch. In Figure 5a, the evolution of the average diameter for a particular type of roll, with a particular geometry, number of positions, and shapes of each of them is shown. This measure is an indicator of the remaining life of this set of rolls, and some indicators, as the tons rolled by millimeter could be derived. In Figure 5b, the evolution of the diameter of a particular roll is shown, as it is seen it has been assembled twice, and then the roll was no longer used.

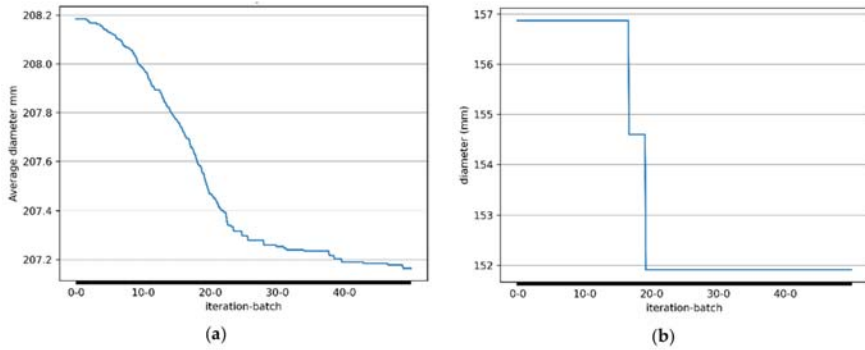


**Figure 5.** (a) Evolution of the average diameter for a particular type of roll; (b) evolution of the diameter of a particular roll.

In Figure 6, a set of eight batches has been launched fifty times (iterations) and the cumulative percentage of rolls grinded after each batch has been plotted. This is an indicator of how many rolls in the set have been grinded, and thus, their diameter has been reduced. The goal is to reduce diameters in a homogeneous way, to avoid that the differences in diameters in the collection or rolls are enlarged, which would imply a higher difficulty to find compatible rolls, forcing larger diameter reductions, with the consequent reduction in cylinder life. It is indicated in the X axe as iteration—batch, that is number of the execution—number of batch executing.

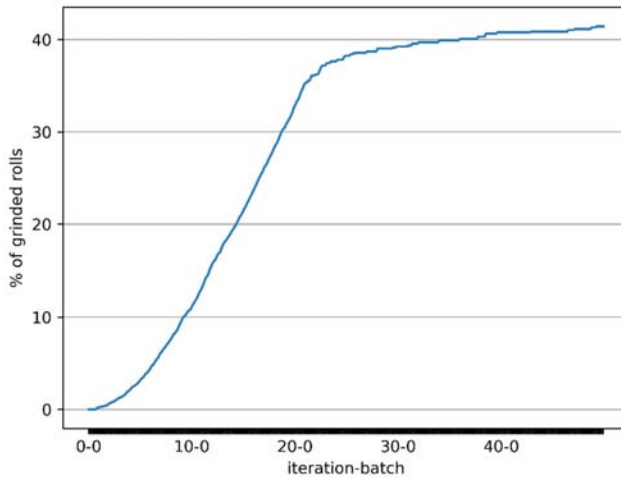


**Figure 6.** Percentage of rolls grinded.

In order to accelerate the process, a filtering strategy is applied first, selecting for each stand just only those rolls that have positions ready to be assembled and whose geometry and shape are compatible with the roll stand. In this way, the number of rolls that are checked for each stand is limited, having also a maximum number of checked rolls for each pair of each stream. In Figure 7, a set of 5600 rolls has been launched without time restriction and the number of pairs of rolls checked for each stream has been limited to ten, as it is seen, when there are no compatible solutions, the execution time boosts significantly, being the number of rolls checked for each stand very small the time it lasts as maximum is about twenty five seconds, and this would increase exponentially with the number

of rolls checked. Future rolls reduction approaches must take into account the maintenance of rolls diameter compatibility.

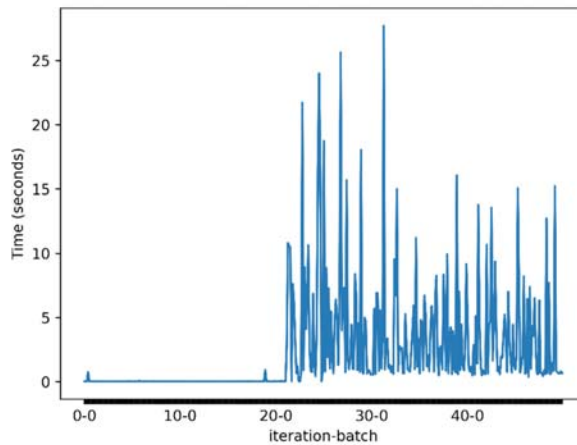


Figure 7. Execution times.

If no solution is found, it is considered that it does not exist. The tests performed have been done with a small set of rolls, around 2800, in a Windows 10 desktop computer powered by an Intel Core i5-8500 processor of 3.00 GHz with 8.00 GB of DDR4 RAM, but more accurate tests will be done in the future. The time it lasts in finding a solution is very variable, from 2/100 s to more than three seconds or even not finding one. The results have proved that the probability of the algorithm finding a solution decreases with the generated rolls actual diameters difference; for example, if the randomly generated actual diameter for the rolls is generated between the initial diameter and the final diameter plus eighty percent of the difference, the algorithm usually finds a solution for every batch (higher probabilities of meeting the diameter restrictions among rolls); however, if the actual diameter is generated among the final and half the initial diameter, it can last three seconds or more and usually it does not find a solution at all before ending its execution. If the number of rolls is increased, it is easier to find suitable rolls, as the possibilities of finding compatibles ones are greater; for example, with 5600 rolls, solutions are found when the randomly generated actual diameter is among the initial and the final diameters, being the times very variable, from 2/100 s to more than three.

#### 4. Conclusions

The developed Digital Twin, although it could be improved, is an accurate representation of the wire rod rolling mill, however, as we stated at the beginning, Digital Twins are never a target by themselves, but a way of achieving the organization goals. In this case, the organization goal that wants to be achieved is an upgrading of the rolls selection system by increasing its efficiency.

Future research could compare the performance of several selection algorithms in order to choose that of greater efficiency. This problem is an example of Constraint Satisfaction Problem, whose natural way of solving is some kind of Domain-pruning strategy such as the current backtracking algorithm implemented in the simulator. First approaches could be performed using asynchronous backtracking algorithm (ABT) [11], an agents distributed algorithm. Following this approach, each stand will be implemented as an intelligent agent. The method needs a total order among agents, each holding exactly one variable. In this case, the order is given by the sequence of stands along the rolling mill, and the variable would be the rolls to be assembled for each stand. During the computation, the agents sent their assigned values to the agents that are connected to them by outgoing links. This approach

would give a reference standard to compare with more sophisticated further approaches such as Reinforcement Learning methods.

**Author Contributions:** Conceptualization, V.R.M. and J.M.V.B.; methodology, V.R.M.; software, A.M.V.J. and J.G.G.; validation, A.M.V.J. and J.V.B.; formal analysis, A.M.V.J.; investigation, V.R.M.; writing—original draft preparation, A.M.V.J. and V.R.M. All authors have read and agreed to the published version of the manuscript.

**Funding:** This research was funded by AGENCIA ESTATAL DE INVESTIGACION (Spain), grant number MCIU-19-PCI2019-103443.

**Acknowledgments:** The authors acknowledge CHIST-ERA SOON (Social Network of Machines) project for supporting this work.

**Conflicts of Interest:** The authors declare no conflict of interest.

## References

1. Erol, S.; Jäger, A.; Hold, P.; Ott, K.; Sihn, W. Tangible Industry 4.0: A scenario-based approach to learning for the future of production. *Procedia CiRp* **2016**, *54*, 13–18. [[CrossRef](#)]
2. Oztemel, E.; Gursev, S. Literature review of Industry 4.0 and related technologies. *J. Intell. Manuf.* **2020**, *31*, 127–182. [[CrossRef](#)]
3. Alcácer, V.; Cruz-Machado, V. Scanning the Industry 4.0: A Literature Review on Technologies for Manufacturing Systems. *Eng. Sci. Technol. Int. J.* **2019**, *22*, 899–919. [[CrossRef](#)]
4. Tao, F.; Cheng, J.; Cheng, Y.; Gu, S.; Zheng, T.; Yang, H. SDMSim: A manufacturing service supply–demand matching simulator under cloud environment. *Robot.-Comput.-Integr. Manuf.* **2017**, *45*, 34–46. [[CrossRef](#)]
5. Tao, F.; Cheng, J.; Qi, Q. IIHub: An industrial Internet-of-Things hub toward smart manufacturing based on cyber-physical system. *IEEE Trans. Ind. Inform.* **2017**, *14*, 2271–2280. [[CrossRef](#)]
6. Davis, J.; Edgar, T.; Porter, J.; Bernaden, J.; Sarli, M. Smart manufacturing, manufacturing intelligence and demand-dynamic performance. *Comput. Chem. Eng.* **2012**, *47*, 145–156. [[CrossRef](#)]
7. Mittal, S.; Khan, M.A.; Romero, D.; Wuest, T. Smart manufacturing: Characteristics, technologies and enabling factors. *Proc. Inst. Mech. Eng. Part B J. Eng. Manuf.* **2017**. [[CrossRef](#)]
8. Grieves, M.; Vickers, J. Digital twin: Mitigating unpredictable, undesirable emergent behavior in complex systems. In *Transdisciplinary Perspectives on Complex Systems*; Springer: Berlin/Heidelberg, Germany, 2017; pp. 85–113.
9. Glaessgen, E.; Stargel, D. The digital twin paradigm for future NASA and US Air Force vehicles. In Proceedings of the 53rd AIAA/ASME/ASCE/AHS/ASC Structures, Structural Dynamics and Materials Conference 20th AIAA/ASME/AHS Adaptive Structures Conference 14th AIAA, Honolulu, HI, USA, 23–26 April 2012; p. 1818.
10. Lu, Y.; Liu, C.; Wang, K.I.-K.; Huang, H.; Xu, X. Digital Twin-driven smart manufacturing: Connotation, reference model, applications and research issues. *Robot.-Comput.-Integr. Manuf.* **2020**, *61*, 101837. [[CrossRef](#)]
11. Yokoo, M. Asynchronous Backtracking. In *Distributed Constraint Satisfaction: Foundations of Cooperation in Multi-Agent Systems*; Yokoo, M., Ed.; Springer Series on Agent Technology; Springer: Berlin/Heidelberg, Germany, 2001; pp. 55–68, ISBN 978-3-642-59546-2.

**Publisher's Note:** MDPI stays neutral with regard to jurisdictional claims in published maps and institutional affiliations.



© 2020 by the authors. Licensee MDPI, Basel, Switzerland. This article is an open access article distributed under the terms and conditions of the Creative Commons Attribution (CC BY) license (<http://creativecommons.org/licenses/by/4.0/>).





# Machining Quality Prediction Using Acoustic Sensors and Machine Learning <sup>†</sup>

Stefano Carrino <sup>1,\*</sup>, Jonathan Guerne <sup>1</sup>, Jonathan Dreyer <sup>1</sup>, Hatem Ghorbel <sup>1</sup>, Alain Schorderet <sup>2</sup> and Raphael Montavon <sup>1</sup> 

<sup>1</sup> Haute Ecole Arc Ingénierie, University of Applied Sciences and Arts Western Switzerland (HES-SO), CH-2610 St. Imier, Switzerland; jonathan.guerne@gmail.com (J.G.); jonathan.dreyer@he-arc.ch (J.D.); hatem.ghorbel@he-arc.ch (H.G.); raphael.montavon@he-arc.ch (R.M.)

<sup>2</sup> HEIG-VD, University of Applied Sciences and Arts Western Switzerland (HES-SO), CH-1401 Yverdon-les-Bains, Switzerland; alain.schorderet@heig-vd.ch

\* Correspondence: stefano.carrino@he-arc.ch

<sup>†</sup> Presented at the 14th International Conference INTER-ENG 2020 Interdisciplinarity in Engineering, Mures, Romania, 8–9 October 2020.

Published: 17 December 2020



**Abstract:** The online automatic estimation of the quality of products manufactured in any machining process without any manual intervention represents an important step toward a more efficient, smarter manufacturing industry. Machine learning and Convolutional Neural Networks (CNN), in particular, were used in this study for the monitoring and prediction of the machining quality conditions in a high-speed milling of stainless steel (AISI 303) using a 3mm tungsten carbide. The quality was predicted using the Acoustic Emission (AE) signals captured during the cutting operations. The spectrograms created from the AE signals were provided to the CNN for a 3-class quality level. A promising average f1-score of 94% was achieved.

**Keywords:** condition monitoring; machine learning; acoustic emission; milling machines; micro-manufacturing; quality prediction

## 1. Introduction

In this paper, we investigate the automatic detection of quality degradation during a milling machining process by analyzing the acoustic signature of the machining process using neural networks. Such a degradation is often due to the inevitable tool wear resulting from any metal cutting process. Typical tool wear is characterized by three stages: break-in, steady state, and failure [1]. Break-in indicates the rapid process that transforms and wears the tool when it is first used. Afterwards, and for most of the tool's lifespan, the tool's wear increases gradually; here, the tool is in a steady-state condition. Finally, failure represents a rapidly deterioration phase at the end of the tool's life.

Reliable continuous quality monitoring would allow real-time decision-making to adjust the machining process when the process is about to produce an undesired surface quality in the workpiece (e.g., replacing a machining tool, changing cutting parameters, etc.). In this paper, we investigate Acoustic Emission (AE) sensors for the indirect monitoring of machining quality. AE sensors are used to detect the high-frequency waves that are provoked by the metal-cutting process. AEs typically include a frequency range from 100 to 1 MHz [2]. The analysis of the AE allows the characterization of the process without a direct observation of the workpiece, thereby possibly avoiding the wasting of material, tools breaking, and unplanned production stops (unplanned equipment downtime).

## Theoretical Background

The usage of sensors for the monitoring of cutting processes has been studied for several years. In this context, previous research has demonstrated that the acoustic signals analyzed during an industrial process can contain features which could be used to automatically estimate the quality of the process itself [3,4]. If this is compared to traditional manual interventions, AE signals can be acquired without interfering with the cutting process, and the sensed frequency range is much higher compared to other sensors such as accelerometers. The previous works used AE (often in combination with other sensors) for the prediction and monitoring of the state of the surface, gear grinding [5–7], turning [8,9] and the analysis of scuffing [10]. The surface quality and the tool wear are the variables that are typically monitored. AE sensors have also been studied in other manufacturing processes, such as additive manufacturing [3].

Our study is focused on milling machining for high-precision industry (the watch and automotive industries). Specifically, milling is a machining process that aims to remove material using rotating cutters. For the analysis of different manufacturing operations, AE sensors have been often used in combination (or compared with) other sensors, such as simpler microphones [11], force and power measurements [12], vibration acceleration sensing [13,14], and infrared cameras [15] (for a general survey of data-driven monitoring in the manufacturing process, a reader can refer to the survey of Xu et al. [16]).

The usage of Acoustic Emission sensors for the monitoring of machining processes has been investigated for several years, but the recent availability of data-driven learning solutions based on Machine Learning opens the path to the analysis of larger amounts of data from sensors that have higher dynamics. Machine Learning approaches have shown potential for making better decisions to monitor and, finally, to automate the machining process. Different algorithms are used in the literature, such as Support Vector Machines [11,17], Hidden Markov Models [18], decision trees [14], and (deep) neural networks (such as Convolutional Neural Networks, Long Short-Term Memory networks, etc.) [9].

In this study, we want to investigate the machine learning performances that can be achieved by reducing—at the bare minimum—the pre-processing and feature extraction steps, using only the information from AE sensors. In a similar work, Krishnan et al. [18] extracted the milling process signature and used Hidden Markov modelling for the prediction of the tool conditions. Their study showed a promising correlation between the AE signal features and the tool conditions. In their study, the features were manually extracted. We focus our study on the usage of Convolutional Neural Networks (CNN) [19] for the automatic extraction of the relevant features.

The rest of the paper is organized as follows: Section 2 will describe the materials and the methodology used to acquire the dataset, including the data labeling approach. Section 3 will present the realized data processing and machine learning architecture. Finally, Section 4 will discuss the results achieved.

## 2. Materials, Methods and Data Acquisition

### 2.1. Materials

A milling machine, called ‘Micro5’ (Figure 1), was used for the cutting process. The Micro5 machine belongs to a novel category of milling machines characterized by their small size and the related improved efficiency.

The sensor used for the acquisition was a Vallen VS45-H. This sensor is a piezoelectric AE-sensor with a wide frequency response. This sensor can be used in a frequency range between 40 kHz and 450 kHz. For this project, we limited the maximum sampling rate to 200 kHz. Resulting from our use of the Nyquist–Shannon sampling theorem, we limited our study to frequencies between 40 kHz and 100 kHz. The AE sensor was placed in direct contact with the raw material, as displayed in the figure below (Figure 2).



**Figure 1.** The Micro5, the milling machine used in this study.



**Figure 2.** Acoustic emission sensor positioning. As highlighted by the red circle, the AE sensor is glued to the material that is being machined.

## 2.2. Methodology: Data Acquisition, Labeling and Classification

For the experimentation, we used a milling machine working with stainless steel (AISI 303) and no lubrication. A tungsten carbide tool with a 3 mm diameter was used for the machining. The cutting process consisted in simple linear passes at different heights (creating a stair-shaped workpiece, as illustrated in Figure 3). Once half of the material was machined, the process was repeated symmetrically. Figure 4 shows the resulting part.

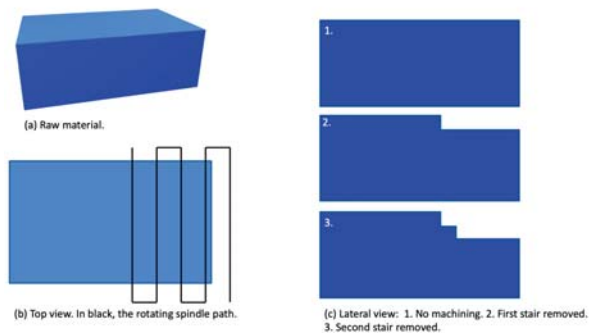


**Figure 3.** A visual representation of the milling operation investigated in this study. (a) The raw material before the machining; (b) in black, from the right to the left, the path of the cutting tool. In the representation, we can observe 5 passes, of which 1 is outside the material, and 4 are in the material—top view. (c) Removal of the first 2 levels of the material—lateral view.

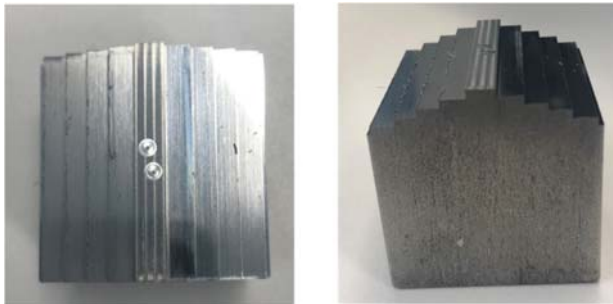


**Figure 4.** Pictures of one of the resulting workpieces.

At the beginning of each experience, the tool is new. The machining ends and the tool is replaced if one of the following conditions is verified:

1. the tool breaks;
2. the tool is considered ‘too used’ by an expert human;
3. the workpiece is completely machined (6 stairs).

### 2.3. Milling Dataset

In order to train the supervised machine learning algorithms, the creation of a labeled dataset is needed. The materials presented in the previous sections were used to realize multiple workpieces; the acquired data represent the dataset used for the study. Table 1 summarizes the conditions and the different experiences realized.

**Table 1.** Summary of the different experiences realized. Only the data from experiences 4, 5 and 6 were used to train the evaluating Machine Learning solutions.

Experience ID	Spindle Rotation Speed (Revolutions per Minute)	Number of Stairs Machined	Quality Label: 0 (Good), 1 (Intermediate), 2 (Bad)
1	0 RPM	0×	-
2	29k RPM	0×	-
3	35k RPM	0×	-
4	29k RPM	6×	0, 0, 0, 1, 1, 1
5	33k RPM	6×	1, 1, 1, 1, 1
6	35k RPM	3×	1, 2, 2

Experiences 1, 2, and 3 did not involve any actual machining. The tool was mounted on the machine, but the material was not processed. In experience 1, the milling machine was turned on and the spindle was not turning. In experiences 2 and 3, the spindle was turning at 29,000 and 35,000 revolutions per minute respectively, but the cutting tool was not touching the material. This allows the characterization of the signal ‘noise’ generated by the machine, rather than by the contact between the tool and the material. Actual machining with the tool cutting the material was recorded for experiences 4, 5, and 6. The last column presents the encoding of the observed labels: 0 stands for ‘good quality’, 1 for ‘intermediate quality’, and 2 for ‘bad quality’.

A simple observation of the dataset allows us to notice the impact of the spindle’s rotation speed on the machining quality degradation. In the given configuration, a lower RPM allowed the process to maintain a better machining quality for a longer time. A higher RPM quickly degraded the machining quality (due to faster tool wear).

#### 2.4. Labeling Approach

In order to label the dataset, the quality of the machining was computed with the help of the observed surface roughness. As mentioned in the previous paragraph, in this project, we considered three different quality labels (good, intermediate and poor quality). It is important to highlight that the process quality was observed and measured only at the end of the machining of the resulting parts. This implies that the quality of the machining and the related label (used as the ground truth and labels in the analyses) can be assessed only for the particular steps of the process on the surface of the remaining material (see Figure 5).

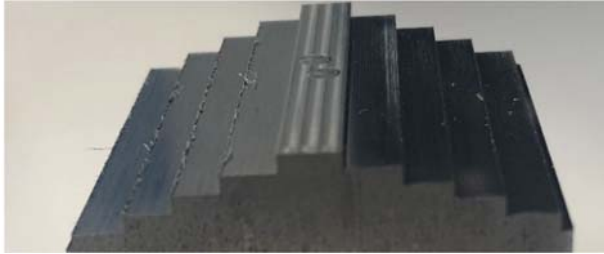


**Figure 5.** This figure shows the details of a workpiece. The left side was machined with a tool at the end of its lifespan. The presence of multiple chips in the material indicates that the quality of the stair edges has deteriorated.

As shown in Table 1, the acquired database is relatively small. The labeling approach generated only 15 labels, one per stair. In order to augment the labels in the dataset and to make it suitable for the Machine Learning approach, we decided to extend the labels to each pass through the material (multiple passes are required to machine one stair). The stair labels were extended to each pass of the spindle on the material through a linear interpolation. The passes outside the material, when the tool is moving but it is not touching the material, were removed. This allowed us to increase the number of labels from 15 to 544.

#### 2.5. Feature Extraction

Instead of using the raw acoustic data directly as our model input, we converted the value of these sensors into the frequency domain. Several time/frequency transformation approaches were evaluated (wavelet transformation, constant Q-transformation, etc.); in this paper, we present the results achieved with a spectrogram based on the Fast Fourier Transform (FFT) approach (1024 FFTs with a window overlap of 512).

Figure 6 shows an example of 1 minute of the acoustic signal (top part of the figure) and the resulting spectrogram (bottom part). On the first passes on the left, the tool is not touching the material. The periodic pattern shows the different passes in the material. Figure 7 zooms in on the spectrogram generated by one pass.

In the middle of the spectrogram, we can observe a clearer area. This section represents when the tooling machine is actively machining the material and more frequencies are being captured. The darker areas represent the machining portions when there is no contact between the tool and the workpiece. An interesting approach to exploit this data could be to subtract the machine noise signature from the machining noise; however, this approach has not been explored in this paper.

Finally, before providing the spectrograms to the neural network, the inputs were resized to a constant size of  $126 \times 126$  points.

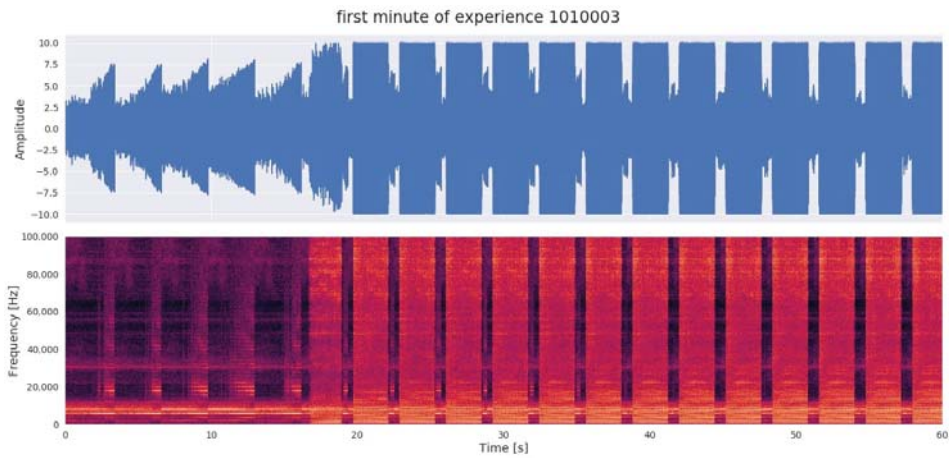


**Figure 6.** Transformation of the signal from the time domain to the related spectrogram. On the left, we can observe that the first 5 passes are outside the material (no-machining), the sixth touches the material only partially, and the following passes characterize the normal machining behavior.

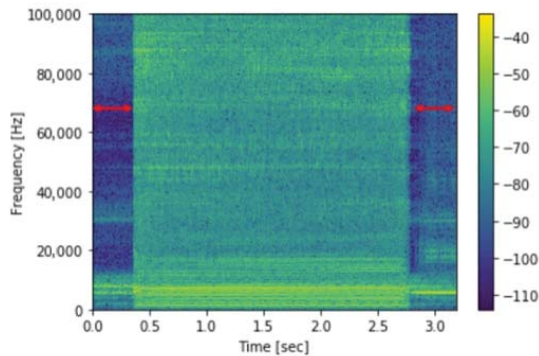


**Figure 7.** A typical spectrogram of one pass. In the dark blue vertical areas, highlighted by the red arrows, the tool is outside of the machining area. The color, in log scale, represents the intensity of the signal.

## 2.6. Classification

The spectrograms generated by the feature extraction preprocessing can be used as image-like inputs for the classification task. Image classification is a well-documented problem; today, one of the most frequently-used approaches for such tasks is the Convolutional Neural Network (CNN). This deep learning model is trained to automatically recognize patterns in images, and to associate such patterns with the appropriate label. The architecture of our CNN is as follows: two convolutional layers, the purpose of which is to extract features from the inputted images, followed by two dense layers for the classification itself. For the convolutions, 32 and 64 filters,  $3 \times 3$ , were used respectively for the first and second layers. The max pooling and dropout layers were used to reduce the computational cost of the learning, and to reduce the risk of overfitting (a model with high variance and low bias [20]). The details of the implementations are presented in Appendix A.

In order to assess the training process quality, we decided to adopt a cross-validation approach. Cross-validation is used in applied machine learning to estimate the quality of a machine learning model, and it is particularly relevant for small datasets. The goal is to estimate how the model is

expected to perform when it is used to make predictions on data that are not seen during the training of the model. The approach used here is a k-folds cross-validation with  $k = 5$ . The idea behind the k-fold validation is to split  $k$  times the dataset into training and validation sets. As the name implies, for each fold, the newly created training set will be used to train the model, while the validation set (unseen by the model) will be used to evaluate its classification performance. Then, 138 sur 544 images were used in the test set. Among other parameters (such as network complexity), the number of epochs used to train a dataset affects the bias and variance of a classifier. In particular, the more epochs are used to train the dataset, the higher the risk of overfitting. A common approach to limit overfitting is to observe the behavior of the training and validation loss after each epoch during the whole training process. If the training loss tends to get smaller and smaller while the validation loss increases, then we can clearly see that the model is starting to memorize the training set instead of learning general patterns: it is overfitting. The observation of training and validation loss allows for a deeper understanding of the model's behaviors; it not only gives insight about whether or not the model is overfitting, but also about when it started to happen. The knowledge of when the model starts to overfit allows the use of a technique called early stopping. As the name implies, this will shorten the training process if necessary. The stopping condition is based on the validation loss and how it behaves: if—after converging for a while—it starts going back up, then we know the model is starting to overfit. Categorical cross-entropy was used as the loss function, using Adam as the optimizer.

### 3. Results

Our classification performances were computed over multiple runs using a confusion matrix (displayed in Figure 8) and an f1-score on a test set that was unseen during the training phase. The f1-score (also called the f-measure) is the harmonic mean of the Precision and Recall [21]. Overall, on these runs, the model achieved an average f1-score of 94% and, as mentioned in the previous section, we reduced the overfitting risk with the help of a 5-fold cross-validation approach, regularization, and dropout layers. Since the dataset is unbalanced (labels 0 and 1 are more represented than label 2), we preferred the f1-score over other metrics, such as accuracy.

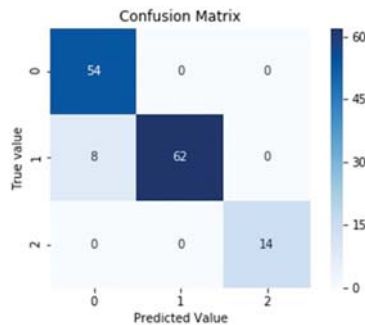


Figure 8. Classification performance of the model for one run.

### 4. Discussion

As shown in the confusion matrix (Figure 8), only a few data points were misclassified by the neural network solution. In addition, the misclassified points belong to the middle class 1, indicating an intermediate quality of the machining: the classifier never confuses 'good' quality with 'bad' quality. All of the misclassified points were classified with the 0 label; this could be due to the unbalanced dataset, but further analysis is needed to assess this point.

Concerning the computational performances, the filtering of the signal directly after the acquisition and the generation the spectrogram can be achieved in pseudo-real time. Considering the typical length of a machining process (from a few seconds to several minutes), the proposed classifier can



predict the quality of the machining directly during the process. The AE sensor's high sampling frequency leads to a rapidly-growing dataset, even for rather short cutting operations. In this study, we collected data during the whole processing. However, most of the data are redundant: for instance, the data at the beginning of a pass are quite similar to the data at the end of the same pass. In order to shorten the computation time, it can be opportune to reduce the time windows used to generate the spectrogram to few milliseconds. Instead of collecting data for a whole pass, just a significant fraction of the data can be collected. These results are extremely promising because they show that it is possible to detect the quality of a machining process without directly observing the realized workpiece. This observation has several practical consequences:

- Additional machines to assess the quality can be removed from the production line.
- If the quality estimation can be performed on the fly during the machining, tool breakage and material and time wastage can be avoided.

Nevertheless, the presented results were achieved in a particular set of conditions, and further analyses are needed in order to validate these results in a more general context. The current limitations include:

- The small dataset.
- The fact that realized milling process is simple, as it consists of linear passes repeated at different heights. More complex cutting operations can generate noise that could be more difficult to analyze.
- Only one type of material was used, along with one type of tool and one type of lubrication (no lubrication).

In order to address these limitations, we plan to evaluate the model's performance on a larger dataset acquired in different machining conditions. The presented 3-class classification problem will be adapted into a multi-objective regression formulation in order to directly predict the surface roughness and dimensional quality (given nominal values to achieve for a specific task). From an applied perspective, the novel approach has the advantage of being easier to adapt to different scenarios. According to the context of utilization, it will be possible to decide for each specific use case what can be considered to be 'good' or 'bad' machining by fixing the appropriate thresholds. For instance, for a precision workpiece used in the watchmaking industry, minimal variations can have a huge impact on the functioning of a watch, whereas such strict requirements are not required in other domains, and the machining constraints can be relaxed.

**Author Contributions:** S.C. coordinated the research, conceived the presented approach and extracted the features from the raw signals. J.G. conceived and developed the machine learning solution (CNN); J.D. worked on the results analyses together with H.G., A.S. contributed with the sensor selection, their installation on the machine and a data validation step. R.M. coordinated the mechanical tasks with the Micro5: from the conception to the parts to the actual machining of the parts. All authors have read and agreed to the published version of the manuscript.

**Funding:** This research was internally funded by the University of Applied Sciences and Arts Western Switzerland (HES-SO) and the CHIST-ERA program (SOON project).

**Acknowledgments:** These results could not have been achieved without the help of the technical team involved in the instrumentation of the machine; the design and implementation of the machining plan; and the data retrieval, storing and pre-processing. In particular, the authors want to thank Jeshon Assunção, Damien Heiniger, Jérémy Terrier, Adrien Limat, Nima Pakpoor Gilani, Nicolas Jacquod and Célien Donzé.

**Conflicts of Interest:** The authors declare no conflict of interest. The funders had no role in the design of the study; in the collection, analyses, or interpretation of data; in the writing of the manuscript, or in the decision to publish the results.

## Appendix A

The convolution architecture is detailed with the following summary (generated using Keras API, <http://keras.io/> and then adjusted for publication).

**Table A1.** CNN model summary.

Layer (Type)	Output Shape	Param #
Conv2D (relu)	(None, 126, 126, 32)	320
Conv2D (relu)	(None, 124, 124, 64)	18496
MaxPooling2D	(None, 62, 62, 64)	
Dropout	(None, 62, 62, 64)	
Flatten	(None, 246016)	
Dense	(None, 128)	31490176
Dropout	(None, 128)	
Dense (softmax)	(None, 3)	387
Total params: 31,509,379		
Trainable params: 31,509,379		
Non-trainable params: 0		

## References

- Dou, J.; Xu, C.; Jiao, S.; Li, B.; Zhang, J.; Xu, X. An unsupervised online monitoring method for tool wear using a sparse auto-encoder. *Int. J. Adv. Manuf. Technol.* **2020**, *106*, 2493–2507. [CrossRef]
- Dornfeld, D.A.; Lee, Y.; Chang, A. Monitoring of Ultraprecision Machining Processes. *Int. J. Adv. Manuf. Technol.* **2003**, *21*, 571–578. [CrossRef]
- Shevchik, S.A.; Masinelli, G.; Kenel, C.; Leinenbach, C.; Wasmer, K. Deep Learning for In Situ and Real-Time Quality Monitoring in Additive Manufacturing Using Acoustic Emission. *IEEE Trans. Ind. Inf.* **2019**, *15*, 5194–5203. [CrossRef]
- Inasaki, I. Application of acoustic emission sensor for monitoring machining processes. *Ultrasonics* **1998**, *36*, 273–281. [CrossRef]
- Mouli, D.S.B.; Rameshkumar, K. Acoustic Emission-Based Grinding Wheel Condition Monitoring Using Decision Tree Machine Learning Classifiers. In *Advances in Materials and Manufacturing Engineering*; Li, L., Pratihari, D.K., Chakrabarty, S., Mishra, P.C., Eds.; Lecture Notes in Mechanical Engineering; Springer: Singapore, 2020; pp. 353–359. ISBN 9789811513060.
- Sachin Krishnan, P.; Rameshkumar, K. Grinding wheel condition prediction with discrete hidden Markov model using acoustic emission signature. *Mater. Today Proc.* **2020**. [CrossRef]
- Arun, A.; Rameshkumar, K.; Unnikrishnan, D.; Sumesh, A. Tool Condition Monitoring of Cylindrical Grinding Process Using Acoustic Emission Sensor. *Mater. Today Proc.* **2018**, *5*, 11888–11899. [CrossRef]
- Li, X. A brief review: Acoustic emission method for tool wear monitoring during turning. *Int. J. Mach. Tools Manuf.* **2002**, *42*, 157–165. [CrossRef]
- Ibarra-Zarate, D.; Alonso-Valerdi, L.M.; Chuya-Sumba, J.; Velarde-Valdez, S.; Siller, H.R. Prediction of Inconel 718 roughness with acoustic emission using convolutional neural network based regression. *Int. J. Adv. Manuf. Technol.* **2019**, *105*, 1609–1621. [CrossRef]
- Saeidi, F.; Shevchik, S.A.; Wasmer, K. Automatic detection of scuffing using acoustic emission. *Tribol. Int.* **2016**, *94*, 112–117. [CrossRef]
- Zhang, K.; Yuan, H.; Nie, P. A method for tool condition monitoring based on sensor fusion. *J. Intell. Manuf.* **2015**, *26*, 1011–1026. [CrossRef]
- Chung, K.T.; Geddam, A. A multi-sensor approach to the monitoring of end milling operations. *J. Mater. Process. Technol.* **2003**, *139*, 15–20. [CrossRef]
- Cao, X.; Chen, B.; Yao, B.; Zhuang, S. An Intelligent Milling Tool Wear Monitoring Methodology Based on Convolutional Neural Network with Derived Wavelet Frames Coefficient. *Appl. Sci.* **2019**, *9*, 3912. [CrossRef]
- Krishnakumar, P.; Rameshkumar, K.; Ramachandran, K.I. Tool Wear Condition Prediction Using Vibration Signals in High Speed Machining (HSM) of Titanium (Ti-6Al-4V) Alloy. *Procedia Comput. Sci.* **2015**, *50*, 270–275. [CrossRef]

15. Luiz Lara Oliveira, T.; Zitoune, R.; Ancelotti, A.C., Jr.; Cunha, S.S., Jr. da Smart machining: Monitoring of CFRP milling using AE and IR. *Compos. Struct.* **2020**, *249*, 112611. [[CrossRef](#)]
16. Xu, K.; Li, Y.; Liu, C.; Liu, X.; Hao, X.; Gao, J.; Maropoulos, P.G. Advanced Data Collection and Analysis in Data-Driven Manufacturing Process. *Chin. J. Mech. Eng.* **2020**, *33*, 43. [[CrossRef](#)]
17. Krishnakumar, P.; Rameshkumar, K.; Ramachandran, K.I. Machine learning based tool condition classification using acoustic emission and vibration data in high speed milling process using wavelet features. *IDT* **2018**, *12*, 265–282. [[CrossRef](#)]
18. Sachin Krishnan, P.; Rameshkumar, K.; Krishnakumar, P. Hidden Markov Modelling of High-Speed Milling (HSM) Process Using Acoustic Emission (AE) Signature for Predicting Tool Conditions. In *Advances in Materials and Manufacturing Engineering*; Li, L., Pratihar, D.K., Chakrabarty, S., Mishra, P.C., Eds.; Lecture Notes in Mechanical Engineering; Springer: Singapore, 2020; pp. 573–580. ISBN 9789811513060.
19. Krizhevsky, A.; Sutskever, I.; Hinton, G.E. ImageNet Classification with Deep Convolutional Neural Networks. In *Proceedings of the 25th International Conference on Neural Information Processing Systems-Volume 1*; Curran Associates Inc.: Red Hook, NY, USA, 2012; pp. 1097–1105.
20. Hawkins, D.M. The Problem of Overfitting. *J. Chem. Inf. Comput. Sci.* **2004**, *44*, 1–12. [[CrossRef](#)] [[PubMed](#)]
21. Hripcsak, G. Agreement, the F-Measure, and Reliability in Information Retrieval. *J. Am. Med Inform. Assoc.* **2005**, *12*, 296–298. [[CrossRef](#)] [[PubMed](#)]

**Publisher's Note:** MDPI stays neutral with regard to jurisdictional claims in published maps and institutional affiliations.



© 2020 by the authors. Licensee MDPI, Basel, Switzerland. This article is an open access article distributed under the terms and conditions of the Creative Commons Attribution (CC BY) license (<http://creativecommons.org/licenses/by/4.0/>).

Article

# Control Strategies for Thermal Processes in Chemical Industry <sup>†</sup>

Mircea Dulău

Department of Electrical Engineering and Information Technology, George Emil Palade University of Medicine, Pharmacy, Science, and Technology of Târgu Mureş, Gh. Marinescu Street, No. 38, 540139 Târgu Mureş, Romania; mircea.dulau@umfst.ro

<sup>†</sup> Presented at the 14th International Conference INTER-ENG 2020 Interdisciplinarity in Engineering, Mureş, Romania, 8–9 October 2020.

Published: 18 December 2020

**Abstract:** In the current context, the control of the industrial processes continues to be very important, due to the rapid modification of the economic conditions, the development of production and the tightening of environmental and safety conditions. This paper presents the technological scheme for obtaining the saturated steam from superheated steam and proposes Proportional–Integral–Derivative (PID) controller options based on an internal model, Integral of Time Multiplied by Absolute Error (ITAE) criterion and Ziegler–Nichols criterion. The simulation tests are performed using the Matlab software.

**Keywords:** PID control; internal model control; thermal process; chemical plant

## 1. Introduction

Due to the existence of an important chemical factory in the Mureş industrial area, the students and the academic staff have the opportunity to carry out technological installation studies and test the control possibilities for processes with parameters such as: temperature, level, pressure, flow, pH etc.

Additionally, the chemical engineers require technical knowledge and tools to facilitate their work in modern technological installations.

Thus, the use of well-defined mathematical modeling methods and advanced monitoring systems for the industrial process allows high performance analysis. Moreover, an advanced approach involves the understanding of the dynamic regimes and the feedback and stability concepts used in control systems analysis.

Such topics are addressed by the specialists in the field of control systems in collaboration with technological and chemical engineers.

Thus, the mathematical modeling principles for the first-order and high-order systems, the closed-loop control mechanisms, as well as the tuning techniques for Proportional–Integral–Derivative (PID) controllers, are developed with significant examples in [1,2].

The mathematical modeling of processes with flow, level, pressure, temperature control, and the control loops for these parameters is detailed in [3]. In [4], simple and advanced techniques for choosing and tuning of the PID controllers are presented, including the method based on the internal model.

In [5], the implementation results of an internal model control (IMC), with set-point tracking, for flow control applications are presented. An internal model control for unstable processes, based on a standard IMC, is proposed in [6], while [7] presents an IMC system for level control applications implemented for two interconnected tanks.

An IMC structure for a Multi-Input Multi-Output (MIMO) system, which simultaneously ensures the decoupling and rejection of the disturbance, is developed in [8]. The sensitivity analysis with IMC PID controllers, based on the Nyquist stability criterion, is detailed in [9].

The IMC procedure for Single-Input Single-Output (SISO) systems, which leads to PID controllers and to variants for nonlinear systems, is detailed in [10,11]. Other tuning algorithms and tuning techniques are suggestively presented in [12]. The control strategies study can be performed using dedicated programs and environments, such as Matlab. Significant usage examples are those in [13].

This paper aims to analyze, using simulation, the behavior of a technological installation that produces saturated steam from superheated steam, with various PID control structures. Section 2 presents the mathematical modeling of a thermal process, and Section 3 details the practical schema of the steam temperature control in a chemical saturator and the equivalent block diagrams in which the transfer functions are highlighted. The control principles based on the internal model and the tuning relations for the automatic controller are detailed in Section 4. The behavior of the process with IMC, Integral of Time Multiplied by Absolute Error (ITAE) and Ziegler–Nichols controllers is presented in Section 5, followed by conclusions regarding the obtained performances (Section 6).

## 2. Mathematical Modeling of a Thermal Process

This is considered the thermal system consisting of a tank with a product which has the input parameters:  $F, T_i$ . The following situations are considered for the output [1–3]:

- The product is delivered for use immediately at the outlet of the tank (Figure 1a);
- The product is delivered for use with a time delay, after passing a pipe of length  $l$ , with speed  $v$  (Figure 1b).

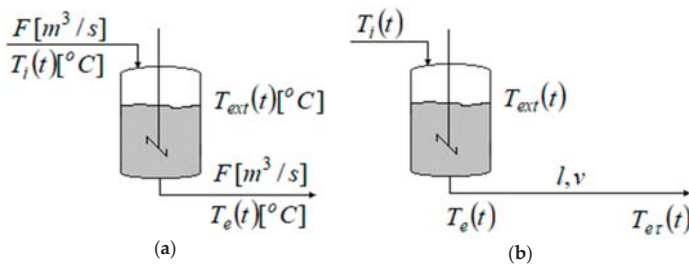


Figure 1. The thermal system: (a) without delay; (b) with delay.

The mathematical modeling involves determining the relationship between the outlet temperature,  $T_e(t)$  and the inlet temperature,  $T_i(t)$ , considering that there is a heat exchange between the tank and the environment.

The dynamic equation has the following form:

$$F\rho_i h_i(t) - F\rho_e h_e(t) - q(t) = \frac{d}{dt}[V\rho_e u(t)], \tag{1}$$

where:  $F$  is the volumetric flow [ $\text{m}^3/\text{s}$ ];  $\rho_i, \rho_e$ —the input/output density of the fluid [ $\text{kg}/\text{m}^3$ ];  $h_i, h_e$ —the input/output enthalpy of the fluid [ $\text{J}/\text{kg}$ ];  $q(t)$ —the heat exchange with the environment;  $V$ —the volume [ $\text{m}^3$ ];  $u(t)$ —the internal energy of the fluid [ $\text{J}/\text{kg}$ ].

Considering the constant pressure, in terms of temperature, it results in:

$$F\rho_i c_i T_i(t) - F\rho_e c_e T_e(t) - K_T A [T_e(t) - T_{ext}(t)] = V\rho_e c_v \frac{d}{dt} T_e(t), \tag{2}$$

where:  $T_i(t), T_e(t)$  are the input/output temperatures of the fluid/product [ $^{\circ}\text{C}$ ];  $c_i, c_e$ —the input/output caloric capacity (at constant pressure) [ $\text{J}/\text{kg}^{\circ}\text{C}$ ];  $c_v$ —the specific heat (at constant volume) [ $\text{J}/\text{kg}^{\circ}\text{C}$ ];  $K_T$ —the thermal transfer coefficient (constant);  $A$ —the thermal transfer area [ $\text{m}^2$ ];  $T_{ext}(t)$ —the environment temperature [ $^{\circ}\text{C}$ ].

For the control strategy, the steady state relation:  $F\rho_i c_i T_{i0} - F\rho_e c_e T_{e0} = 0$  is considered and the following infinitesimal variations are defined:

$$\begin{aligned} \Delta T_i(t) &= T_i(t) - T_{i0} \\ \Delta T_e(t) &= T_e(t) - T_{e0} \end{aligned} \tag{3}$$

The dynamic equation becomes:

$$F\rho_i c_i [T_i(t) - T_{i0}] - F\rho_e c_e [T_e(t) - T_{e0}] - K_{TA} [T_e(t) - T_{e0} - (T_{ext}(t) - T_{ext0})] = V\rho_e c_v \frac{d}{dt} [T_e(t) - T_{e0}], \tag{4}$$

$$V\rho_e c_v \frac{d}{dt} \Delta T_e(t) + (K_{TA} + F\rho_e c_e) \Delta T_e(t) = F\rho_i c_i \Delta T_i(t) + K_{TA} \Delta T_{ext}(t), \tag{5}$$

$$\frac{V\rho_e c_v}{K_{TA} + F\rho_e c_e} \cdot \frac{d}{dt} \Delta T_e(t) + \Delta T_e(t) = \frac{F\rho_i c_i}{K_{TA} + F\rho_e c_e} \cdot \Delta T_i(t) + \frac{U A}{K_{TA} + F\rho_e c_e} \cdot \Delta T_{ext}(t), \tag{6}$$

$$T \cdot \frac{d}{dt} \Delta T_e(t) + \Delta T_e(t) = k_1 \cdot \Delta T_i(t) + k_2 \cdot \Delta T_{ext}(t), \tag{7}$$

where:  $T = \frac{V\rho_e c_v}{K_{TA} + F\rho_e c_e}$  is the time constant [sec.];  $k_1, k_2$ —non-dimensional constants.

Any change in the  $V, F, c_e, c_v, \rho_e$  values will affect the value of the time constant  $T$  and will be seen in the response speed.

Based on the Laplace transformation, it results in:

$$(Ts + 1) \cdot \Delta T_e(s) = k_1 \cdot \Delta T_i(s) + k_2 \cdot \Delta T_{ext}(s), \tag{8}$$

$$\Delta T_e(s) = \frac{k_1}{Ts + 1} \cdot \Delta T_i(s) + \frac{k_2}{Ts + 1} \cdot \Delta T_{ext}(s). \tag{9}$$

If the external temperature variation is  $\Delta T_{ext}(s) = 0$ , it results in:  $H_1(s) = \frac{k_1}{Ts + 1}$ , and if  $\Delta T_i(s) = 0$ , it results in:  $H_2(s) = \frac{k_2}{Ts + 1}$ , with  $k_1, k_2 < 1; k_1 \gg k_2$ , which means that the  $T_i$  signal influences  $T_e$  much more than  $T_{ext}$  does.

If the output product passes through a pipe section, the mathematical model is augmented with the transport time (time delay),  $\tau = l/v$ , as follows:

$$H_1(s) = \frac{k_1}{Ts + 1} \cdot e^{-\tau s}, \tag{10}$$

respectively:

$$H_2(s) = \frac{k_2}{Ts + 1} \cdot e^{-\tau s}. \tag{11}$$

### 3. Temperature Control Diagram

The practical control diagram (Figure 2) involves the measurement and transmission of the product’s output temperature (TT—temperature transmitter), processing this information according to the control law (TIC—temperature controller) and generating the command signal to the actuator (TV—temperature valve). In addition, the installation is provided with temperature, pressure and level indicators (TI, PI, LI) and with a level control loop (LT, LIC, LV) [1,2,4–10,14].

The associated block diagram highlights the transfer functions for:  $H_{TC}$ —controller;  $H_{TV}$ —actuator;  $H_P$ —process with delay time;  $H_{TT}$ —temperature transducer/sensor;  $K_{SP}$ —gain on the set-point path and the signals  $T_{SP}; T_e$ —set-point and output temperatures;  $\varepsilon$ —error;  $u_{TC}$ —command;  $u_{TV}$ —manipulation signal;  $d$ —disturbance (Figure 3).

The closed-loop transfer function is:

$$H_0(s) = \frac{T_e(s)}{T_{SP}(s)} = K_{SP} \frac{H_{TC}H_{TV}H_P}{1 + H_{TC}H_{TV}H_P H_{TT}} = \frac{H_{TC}H_F}{1 + H_{TC}H_F}, \tag{12}$$

considering the hypothesis:  $H_{TT} = K_{SP}$  și  $H_F = H_{TV}H_P H_{TT}$  (Figure 4).

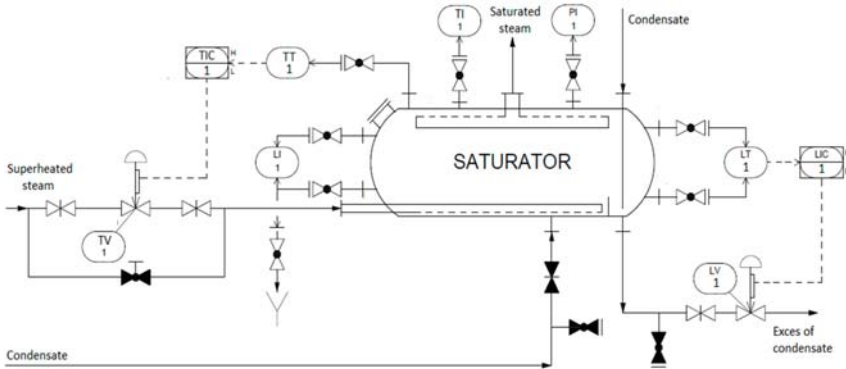


Figure 2. The practical diagram implemented for the temperature control [14].

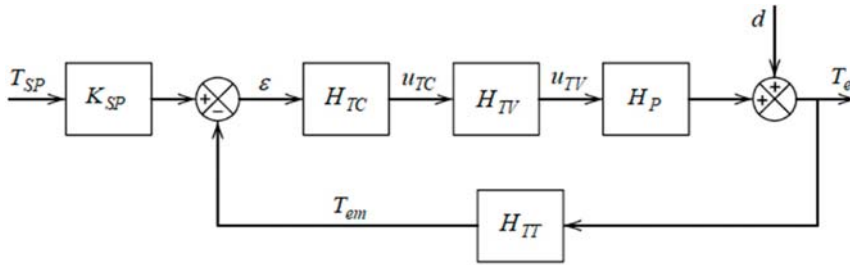


Figure 3. The control block diagram.

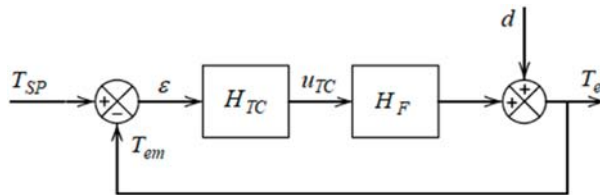


Figure 4. The conventional control block diagram.

#### 4. Design of the IMC Controller

A control solution takes into consideration the uncertainties which affect the process and involves determining the controller’s structure based on the internal model (IMC) of the process, (Figure 5) [10,11].

The conventional control diagram (Figure 4) and the IMC diagram (Figure 5) are equivalent if the controllers  $H_{TC}$  and  $H_{TC}^*$  meet the following condition:

$$H_{TC} = \frac{H_{TC}^*}{1 - H_{TC}^* H_{Fm}}. \tag{13}$$

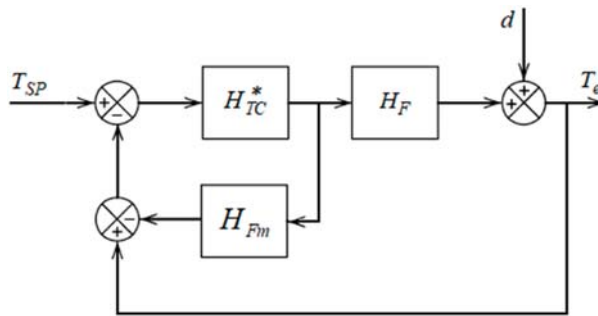


Figure 5. The internal model control (IMC) control block diagram.

In order to determine the IMC controller:

- the process model,  $H_{Fm}$  is factored:

$$H_{Fm} = H_{Fm+}H_{Fm-}, \tag{14}$$

where:  $H_{Fm+}$  contains the time delay and the zeros situated in the right half of the complex plane;

- the IMC controller is designed as:

$$H_{TC}^* = \frac{1}{H_{Fm-}}H_{fil}, \tag{15}$$

where:

$$H_{fil} = \frac{1}{T_{fil}s + 1}, \tag{16}$$

is a low-pass filter, which reduces the sensitivity of the control system to modeling errors;  $T_{fil}$  is a design parameter.

Considering the transfer function of the process:

$$H_F(s) = \frac{k_F}{T_Fs + 1} \cdot e^{-\tau s}, \tag{17}$$

designing the IMC controller depends on the approximation expression of the time delay.

If  $H_{Fm} \equiv H_F$ , meaning that the model and the process model are identical and the Pade approximation is used as:

$$e^{-\tau s} \cong \frac{-\frac{\tau}{2}s + 1}{\frac{\tau}{2}s + 1}, \tag{18}$$

after replacing it in relationship (17), it results in:

$$H_{Fm}(s) = \frac{k_F}{T_Fs + 1} \cdot \frac{-\frac{\tau}{2}s + 1}{\frac{\tau}{2}s + 1} = \left(-\frac{\tau}{2}s + 1\right) \cdot \frac{k_F}{(T_Fs + 1)\left(\frac{\tau}{2}s + 1\right)} = H_{Fm+}H_{Fm-}. \tag{19}$$

The transfer function of the controller (15) becomes:

$$H_{TC}^* = \frac{(T_Fs + 1)\left(\frac{\tau}{2}s + 1\right)}{k_F(T_{fil}s + 1)}, \tag{20}$$



and the equivalent controller (13) has the form:

$$H_{TC} = \frac{(T_F s + 1) \left( \frac{\tau}{2} s + 1 \right)}{k_F (T_{fii} + \frac{\tau}{2}) s}, \tag{21}$$

with the PID standard expression:

$$H_{TC} = k_P \left( 1 + \frac{1}{T_i s} + T_d s \right), \tag{22}$$

where the tuning parameters are:

$$k_P = \frac{1}{k_F} \cdot \frac{2 \frac{T_F}{\tau} + 1}{2 \frac{T_f}{\tau} + 1}; T_i = \frac{\tau}{2} + T_F; T_d = \frac{T_F}{2 \frac{T_F}{\tau} + 1}. \tag{23}$$

If the Taylor approximation is used:

$$e^{-\tau s} \cong -\tau s + 1, \tag{24}$$

the transfer function of the PI controllers is:

$$H_{TC} = k_P \left( 1 + \frac{1}{T_i s} \right), \tag{25}$$

where the tuning parameters are:

$$k_P = \frac{T_F}{k_F (T_{fii} + \tau)}; T_i = T_F. \tag{26}$$

### 5. Experimental Results and Discussions

Considering the practical diagram implemented for the temperature control (Figure 2) with the transfer function:  $H_F(s) = \frac{1}{100s+1} \cdot e^{-10s}$ , different control structures were determined and the performances were analyzed. Thus, with a PID controller (22) and the tuning parameters described by (23), respectively, with a Proportional-Integral (PI) controller (25) and the tuning parameters (26), the indicial responses in Figure 6 were obtained [13].

Using a PI controller (25) and the ITAE criterion for tuning the parameters (set-point tracking), where, according to [12]:  $k_P = \frac{0.586}{k_f} \left( \frac{\tau}{T_f} \right)^{-0.916}$ ;  $T_i = \frac{T_f}{1.030 - 0.165(\tau/T_f)}$ , the indicial response in Figure 7a was obtained, presented in comparison to the indicial response obtained with IMC PI controller. According to Ziegler-Nichols criterion, the tuning parameters of the PI controller are [4]:  $k_P = \frac{0.9}{k_f} \left( \frac{\tau}{T_f} \right)^{-1}$ ;  $T_i = 3.3 \cdot \tau$ .

The indicial responses of the closed loop system, obtained with IMC PI controller and with Ziegler-Nichols controller, are shown in Figure 7b, while the noise and error sensitivity functions are presented Figure 8.

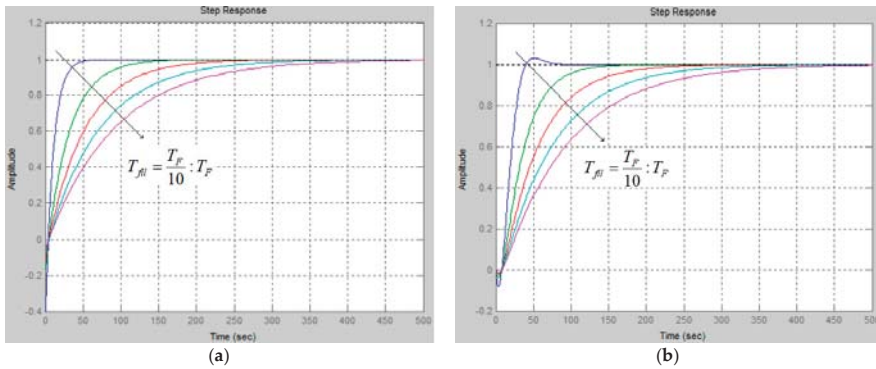


Figure 6. The indicial responses with IMC: (a) Proportional–Integral–Derivative (PID); (b) pressure indicator (PI).

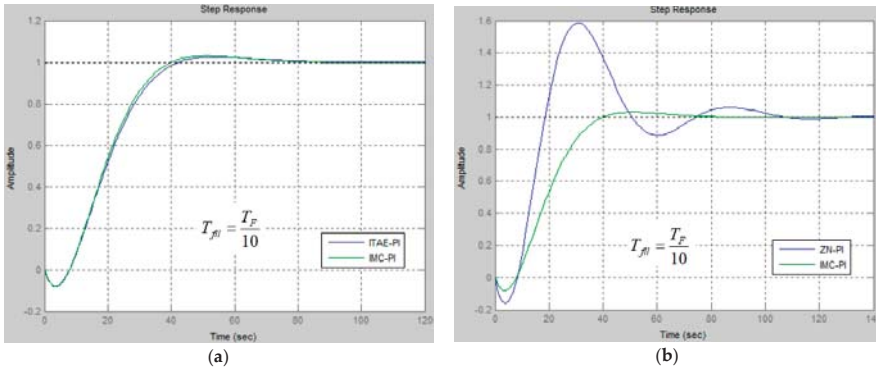


Figure 7. The indicial responses with PI controllers: (a) IMC and Integral of Time Multiplied by Absolute Error (ITAE); (b) IMC and Ziegler–Nichols.

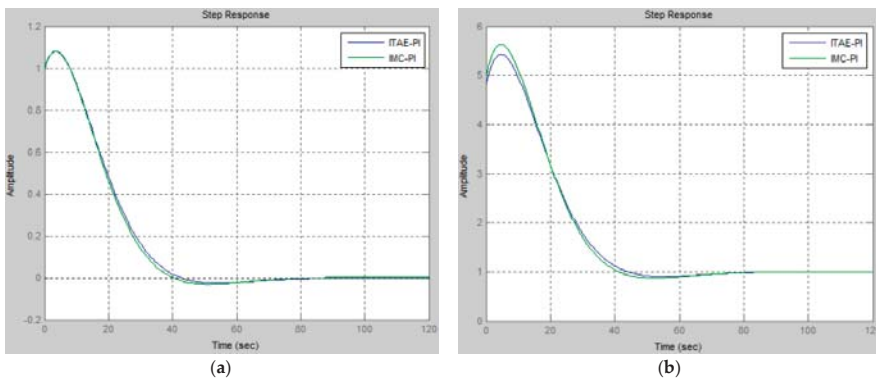


Figure 8. The sensitivity functions: (a)  $S = 1/(H_R H_F)$ ; (b)  $R = H_R S$ .

## 6. Conclusions

The paper presents a mathematical model of the tank used in a chemical plant for obtaining the saturated steam from superheated steam and proposes different PID controllers, implemented for the temperature control.

Due to a very large overshoot, the use of the Ziegler–Nichols determined controller is not recommended. The controller designed by the ITAE criterion offers good performances, both in steady state and in transient regimes.

In the case of designing the IMC controllers described by (22) with approximation (18) for time delay and (25) with approximation (24) for time delay, the  $T_{fil}$  parameter influences the transient regime performances of the closed loop system. By varying the parameter  $T_{fil}$ , the time response can be changed relatively easily, adequately influencing the overshoot of the control system.

**Conflicts of Interest:** The author declares no conflict of interest.

## References

1. Smith, C.; Corripio, A. *Principles and Practice of Automatic Process Control*; John Wiley & Sons, Inc.: New York, NY, USA, 1997.
2. Seborg, D.E.E.T.; Edgar, T.F.; Mellichamp, D.A. *Process Dynamics and Control*; John Wiley & Sons, Inc.: New York, NY, USA, 2011.
3. Dulău, M. *Sisteme de Conducere a Proceselor Continue*; “Petru Maior” University of Târgu Mureș: Târgu Mureș, România, 2013.
4. Lazăr, C.; Vrabie, D.; Carari, S. *Sisteme Automate cu Reglatoare PID*; MatrixRom: Bucharest, Romania, 2004.
5. Khimani, D.; Mane, S.; Patil, M.D. Implementation of internal model control for flow control application. In Proceedings of the IEEE 9th International Conference on Industrial and Information Systems (ICIIS), Gwalior, India, 15–17 December 2014; pp. 1–6.
6. Touati, N.; Saidi, I.; Soudani, D. Modified internal model control for unstable systems. In Proceedings of the IEEE International Conference on Advanced Systems and Electric Technologies (IC\_ASET), Hammamet, Tunisia, 22–25 March 2018; pp. 352–356.
7. Indirapriyadharshini, J.; Sivaranjani, T.; Gokila, R. Performance Analysis of Internal Model Control and Modified Internal Model Control for Two Tank Interacting and Non-Interacting Liquid System. *Int. J. Innov. Technol. Explor. Eng.* **2019**, *8*, 712–716.
8. Dasgupta, S.; Sadhu, S.; Ghoshal, T.K. Internal Model Control based controller design for a Stirred Water Tank. In Proceedings of the IEEE India Conference (INDICON), Kolkata, India, 17–19 December 2010; pp. 1–4.
9. Pathiran, A.; Jagadeesan, P. Design of internal model control dead-time compensation scheme for first order plus dead-time systems. *Can. J. Chem. Eng.* **2018**, *96*, 2553–2563. [[CrossRef](#)]
10. Rivera, D.E.; Morari, M.; Skogestad, S. Internal Model Control. PID Controller Design. *Process Des. Dev.* **1986**, *25*, 252–265. [[CrossRef](#)]
11. Garcia, C.; Morari, M. Internal model control. A unifying review and some new results. *Ind. Eng. Chem. Process Des. Dev.* **1982**, *21*, 308–323. [[CrossRef](#)]
12. Rovira, A. Control Algorithm Tuning, and Adaptive Gain Tuning in Process Control. LSU Historical Dissertations and Theses. Ph.D. Thesis, Louisiana State University, Baton Rouge, LA, USA, 1981.
13. Xue, D.; Chen, Y.; Atherton, D.P. *Linear Feedback Control. Analysis and Design with MATLAB*; SIAM: Philadelphia, PA, USA, 2007.
14. Engineers Guide. Flow Diagram of Urea Production Process from Ammonia and Carbon-Dioxide. Available online: <http://enggyd.blogspot.com/2010/09/flow-diagram-of-urea-production-process.html> (accessed on 1 October 2020).

**Publisher’s Note:** MDPI stays neutral with regard to jurisdictional claims in published maps and institutional affiliations.



© 2020 by the author. Licensee MDPI, Basel, Switzerland. This article is an open access article distributed under the terms and conditions of the Creative Commons Attribution (CC BY) license (<http://creativecommons.org/licenses/by/4.0/>).

Article

# The Effects of Weighting Functions on the Performances of Robust Control Systems †

Mircea Dulau and Stelian-Emilian Oltean \* 

Department of Electrical Engineering and Information Technology, George Emil Palade University of Medicine, Pharmacy, Science, and Technology of Targu Mures, Gh. Marinescu Street, no. 38, 540139 Targu Mures, Romania; mircea.dulau@umfst.ro

\* Correspondence: stelian.oltean@umfst.ro

† Presented at the 14th International Conference INTER-ENG 2020 Interdisciplinarity in Engineering, Mures, Romania, 8–9 October 2020.

Published: 25 December 2020

**Abstract:** An important stage in robust control design is to define the desired performances of the closed loop control system using the models of the frequency sensitivity functions  $S$ . If the frequency sensitivity functions remain within the limits imposed by these models, the control performances are met. In terms of the sensitivity functions, the specifications include: shape of  $S$  over selected frequency ranges, peak magnitude of  $S$ , bandwidth frequency, and tracking error at selected frequencies. In this context, this paper presents a study of the effects of the specifications of the weighting functions on the performances of robust control systems.

**Keywords:** H-infinity synthesis; robust control; robust performances; sensitivity functions; weighting functions

## 1. Introduction

In general, the design objectives of any control system are defined using different models which implement the desired responses to a specified reference. So, the closed-loop control system becomes stable, achieves the imposed performances, rejects the disturbances and measurement noise, and avoids the saturation of actuators, even in the presence of modeling uncertainties or change in the operating point [1–5].

In the H-infinity synthesis, the objectives refer to the optimization of the H-infinity norm of the closed-loop system, considering all the external input variables (references, disturbances, noises) and all the output variables according to the block diagram from Figure 1, where:  $H_p(s)$  and  $H_R(s)$  are the plant and controller transfer functions,  $r$ —reference input,  $e$ —control error,  $y_r$ —feedback signal,  $y$ —the plant output,  $u$ —control signal,  $v, l$ —disturbances, and  $\eta$ —measurement noise.

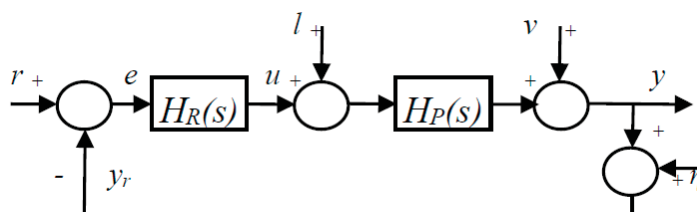


Figure 1. Block diagram of the closed-loop system.

The input–output behavior of the system is characterized by the energy transfer from the external variables  $r, v, \eta, l$  to the output variable  $y$  (and sometime to the control variable  $u$ ). Considering the relation  $H_d(s) = H_R(s)H_p(s)$ , there are four important transfer functions to fully describe the system:

- The sensitivity function  $S(j\omega) = [1 + H_d(j\omega)]^{-1}$ ;
- The complementary sensitivity function  $T(j\omega) = H_d(j\omega) \cdot [1 + H_d(j\omega)]^{-1} = H_d(j\omega)S(j\omega)$ ;
- The noise sensitivity function  $R_S(j\omega) = H_R(j\omega) \cdot [1 + H_d(j\omega)]^{-1} = H_R(j\omega)S(j\omega)$ ;
- The load sensitivity function  $P_S(j\omega) = H_p(j\omega)[1 + H_d(j\omega)]^{-1} = H_p(j\omega) \cdot S(j\omega)$ .

If  $l = 0$ , the relations between  $y$  and  $r, v, \eta$ , respectively, between  $e$  and  $r, v, \eta$  are given by:

$$y = \frac{H_d(s)}{1 + H_d(s)} \cdot r - \frac{H_d(s)}{1 + H_d(s)} \cdot \eta + \frac{1}{1 + H_d(s)} \cdot v = T \cdot r - T \cdot \eta + S \cdot v, \tag{1}$$

$$e = \frac{1}{1 + H_d(s)} \cdot r - \frac{1}{1 + H_d(s)} \cdot v + \frac{H_d(s)}{1 + H_d(s)} \cdot \eta = S \cdot r - S \cdot v + T \cdot \eta \tag{2}$$

The sensitivity function  $S$  describes the input–output behavior from input  $v$  to the output  $y$ , if the other input variables are  $r = 0, \eta = 0, l = 0$ . In (1), if  $\eta = 0, T = 1, S = 0$ , the reference tracking and disturbance rejection result.

In the block diagram from Figure 1, it is often necessary to include some weighting cost functions, chosen to reflect the design objectives and information about noise and disturbance [5]. The modified block diagram including these weighting functions is presented in Figure 2.

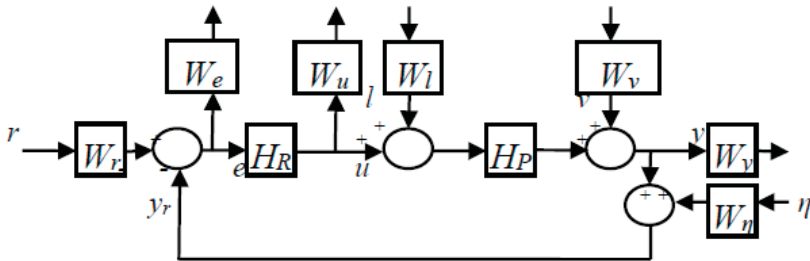


Figure 2. Block diagram of the closed-loop system including the weighting functions.

Although there are some recommendations for choosing the weighting functions, these depend on the designer skills and involves several iterations until a final form is achieved, which guarantees the control performances imposed to the closed loop system.

The paper [6] presents the robust analysis of a positioning control system where the weighting-functions-based tuning method simplifies the H-infinity design procedure. In [7], the  $\mu$ -synthesis robust design method is used for a multi-model control problem. The selection of the weighting functions is made for low, medium and high frequencies. The studies from [8] presents the disadvantages of the H-infinity design method. At the same time, the authors had chosen the weighting functions for the  $\mu$ -synthesis of a Proportional-Integrative (PI) controller, in order to improve the performances of the robust system.

A theoretical guide for choosing the weighting functions and the design procedure which assures the system gains are developed in the paper [1].

The paper [9] is focused on determining the weighting functions under two aspects: initial selection and tuning procedure which improves the performances of the closed-loop system. An interesting procedure for choosing the weighting functions for the optimal H-infinity design formulated as an optimization problem is presented in [10]. The paper [11] contains the synthesis issue for a nominal

controller with unstable weighting functions. The authors proposed a simplification of the robust controller design procedure.

The papers [2,12,13] present some techniques for choosing the weighting functions, reducing the order of the transfer functions and designing the robust controllers using the Matlab Toolbox. Robust control methods are developed in [3,4] for both linear and nonlinear systems, and approaches of robust control theory based on weighting functions are also addressed in [5].

In [14], the authors proposed a weighting function modeling method which is used in H infinity loop-shaping design and tested in the numerical simulation. Other methodologies for selecting the sensitivity functions are shown in [15]. For multiple input multiple output (MIMO) systems, an application of choosing the reduced order weighting function is developed in [16].

The paper presents in Sections 2 and 3 the models for choosing the weighting functions in accordance with the robust theory, a short analysis of two of these models ( $S$  and  $R_S$ ) and the influence of some parameters (magnitude, bandwidth frequency, tracking error). Section 4 contains the analysis of the performances of the closed-loop control system which depend on the parameters of the weighting functions. The conclusions are highlighted in Section 5.

## 2. Recommendations for Choosing the Models for the Weighting Functions

The robustness performance requirements depend on the sensitivity functions, whose specifications are included in the frequency behavior models. If these sensitivity functions remain inside the imposed limits, the robustness objectives are met [2–5].

So, for a standard second order model, the sensitivity function depends on the damping ratio and natural frequency according to Figure 3a and relation:

$$S(s) = \frac{s^2 + 2\xi\omega_n s}{s^2 + 2\xi\omega_n s + \omega_n^2} \tag{3}$$

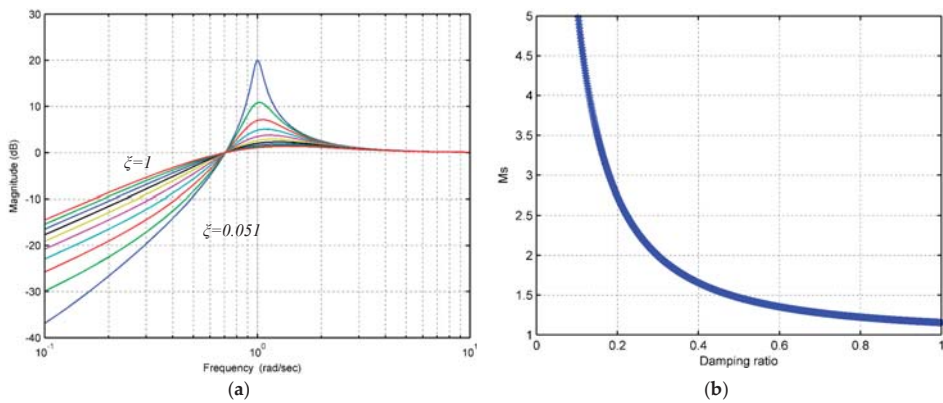


**Figure 3.** Damping ratio effect on: (a) sensitivity function; (b) magnitude (peak sensitivity).

On the other hand, the magnitude  $M_S$  depends on the damping ratio, according to the relation:

$$M_S := \|S\|_{\infty} = \frac{x \sqrt{x^2 + 4\xi^2}}{\sqrt{4x^2\xi^2 + (1 - x^2)^2}}, x = \sqrt{0.5 + 0.5\sqrt{1 + 8\xi^2}} \tag{4}$$

As a result, the performance specifications can be given by:

$$|S(s)| \leq \left| \frac{s}{s/M_S + \omega_{bs}} \right|, s = j\omega, \forall \omega, \omega_{bs} \text{ is the bandwidth.} \tag{5}$$

In the ideal case, relation  $|W_e S| \leq 1$  provides the reference tracking to a step input signal (and a zero steady state control error), meaning:

$$W_e \leq \frac{s/M_S + \omega_{bs}}{s}. \tag{6}$$

Important for the practical situations is to have a steady state error less than an imposed value ( $|S(0)| \leq \epsilon_S$ ). Thus, it is sufficient to choose  $|W_e(0)| \geq 1/\epsilon_S$  ( $\epsilon_S$  is the tracking error), which can be achieved by correcting Function (6) with the modified form:

$$W_e(s) = \frac{\frac{s}{M_S} + \omega_{bs}}{s + \omega_{bs}\epsilon_S} \tag{7}$$

A proper design in terms of the sensitivity function is obtained if both conditions imposed to  $\omega_{bs}$  and  $M_S$  are satisfied according to the relations:

$$\|W_e(j\omega)S(j\omega)\|_\infty \leq 1, \|S(j\omega)\|_\infty \leq \frac{1}{W_e(j\omega)}, \tag{8}$$

where the upper limit (Figure 4a) is:

$$\frac{1}{W_e(s)} = \frac{s + \omega_{bs}\epsilon_S}{\frac{s}{M_S} + \omega_{bs}}. \tag{9}$$

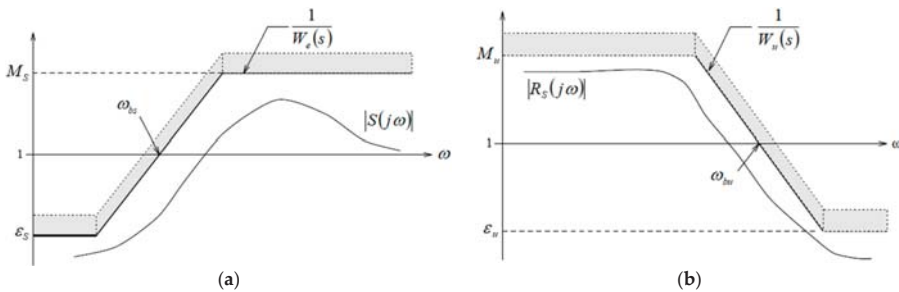


Figure 4. Design models for: (a)  $S(j\omega)$ ; (b)  $R_S(j\omega)$ .

For improved performances, Model (7) may have a higher order, as follows:

$$W_e(s) = \left( \frac{\frac{s}{M_S} + \omega_{bs}}{s + \omega_{bs}\epsilon_S} \right)^k, k \geq 1. \tag{10}$$

For the noise sensitivity function, the weighting function  $W_u(s)$  is chosen, which influences the control signal,  $u$ , according to the relations:

$$W_u(s) = \frac{s + \frac{\omega_{bu}}{M_u}}{\epsilon_u s + \omega_{bu}}, \|W_u(j\omega)R_S(j\omega)\|_\infty \leq 1, \|R_S(j\omega)\|_\infty \leq \frac{1}{W_u(j\omega)}. \tag{11}$$

where  $M_u$ ,  $\omega_{bu}$ ,  $\epsilon_u$  are the maximum gain, the bandwidth and the error. The upper limit is:

$$\frac{1}{W_u(s)} = \frac{\epsilon_u s + \omega_{bu}}{s + \omega_{bu}/M_u} \tag{12}$$

The magnitude of  $|R_S|$  on low frequency is essential to limit the control signal.

The procedure is similar for the complementary sensitivity function and the load sensitivity function.

### 3. The Effect of the Parameters on the Weighting Functions

Several possibilities may be used in order to design the weighting functions. One possible choice is to consider a combination of cost functions providing the mixed-sensitivity formulation.

Figures 5 and 6 show the behaviors imposed using the functions  $1/W_e(s)$ , Equation (9), and  $1/W_u(s)$ , Equation (12), considering different values of the parameters  $M_S$ ,  $\omega_{bs}$ ,  $\epsilon_S$ ,  $M_u$ ,  $\omega_{bu}$ ,  $\epsilon_u$  [8,16].

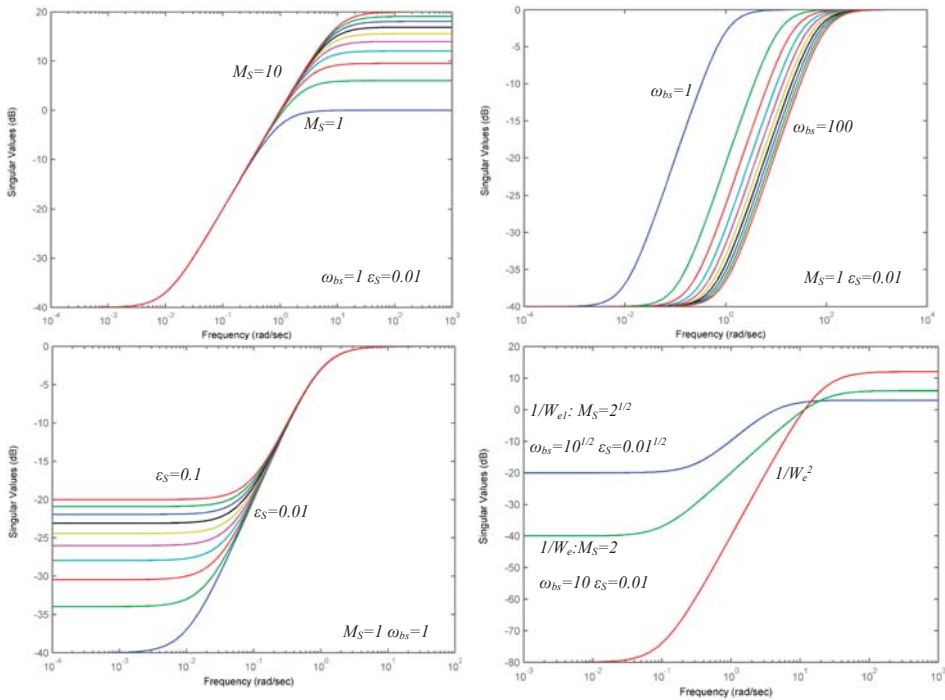


Figure 5. Models imposed with function  $1/W_e(s)$ .



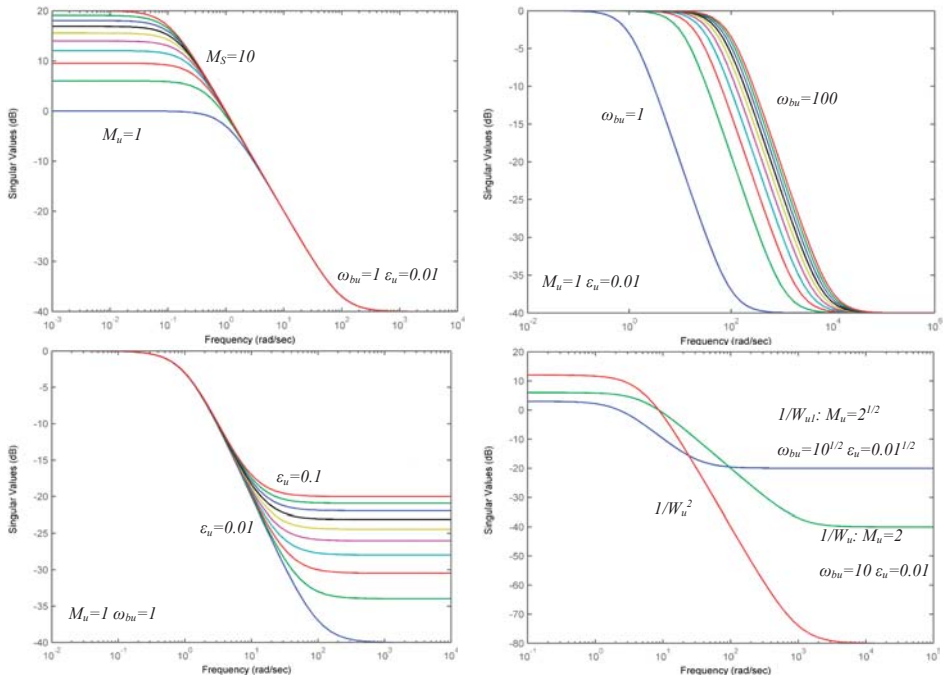


Figure 6. Models imposed with function  $1/W_u(s)$ .

The study of the dependencies on the shape of the weighting functions  $W_e(s)$  and  $W_u(s)$  highlights the importance of the following values for the magnitude  $M_S, M_u = 1, 2, 3$ , bandwidth  $\omega_{bs}, \omega_{bu} = 1, 2$  and errors  $\epsilon_S, \epsilon_u > 0.01$ .

4. Results of the Analysis of the Closed-Loop Control System

The main objectives required in the control system (defined by the block diagram with the weighting functions from Figure 7) are: good reference tracking and a limited control signal [1–5].

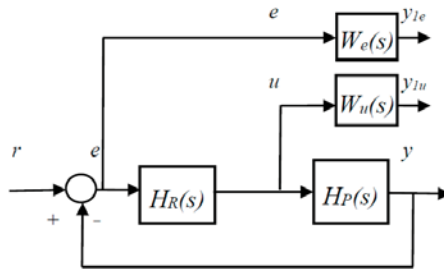


Figure 7. Control diagram with the weighting functions.

The robust design consists in determining the controller  $H_R$  so that the H-infinity norm of the closed-loop transfer function is less than a positive number ( $\gamma$ ):

$$\left\| \begin{matrix} W_e S \\ W_u H_R S \end{matrix} \right\|_{\infty} < \gamma \tag{13}$$

The plant model used for the case study of the closed-loop system from Figure 7 is described by the transfer function  $H_p(s) = \frac{2}{s^2+0.05s+0.2}$ .

The block diagram also includes the weighting functions and the controller designed using the H-infinity synthesis. The simulations from Figures 8 and 9 show the behaviors of the system [13].

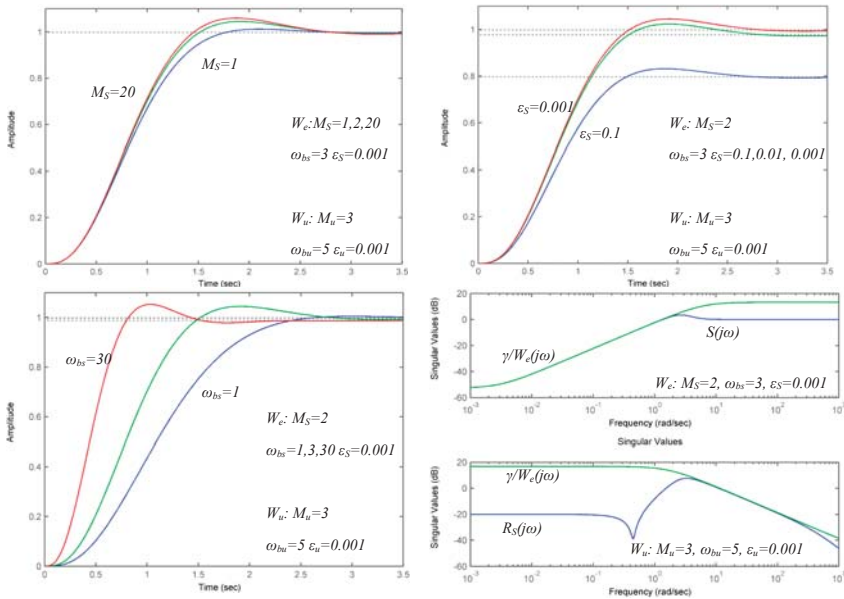


Figure 8. Responses to the step input considering different weighting functions  $1/W_e(s)$ .

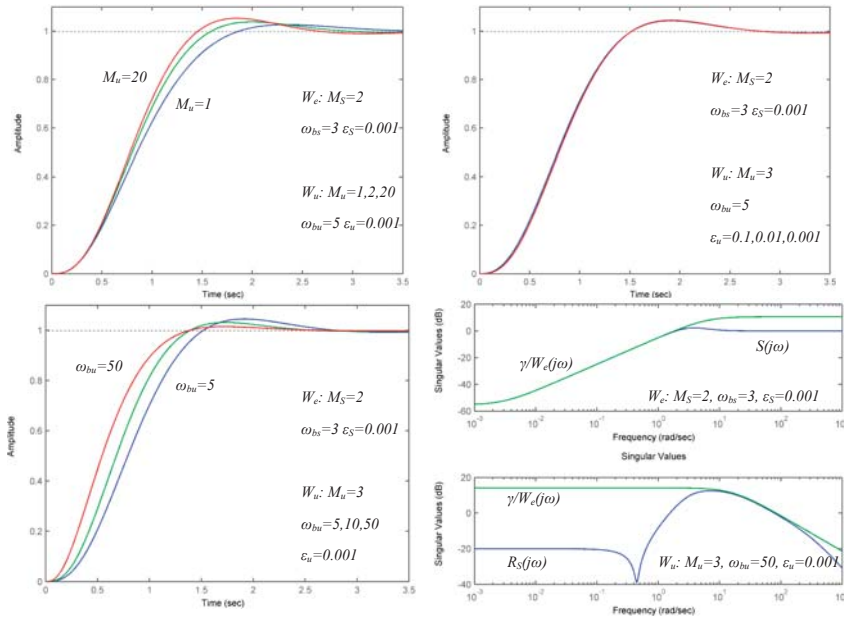


Figure 9. Responses to the step input considering different weighting functions  $1/W_u(s)$ .

## 5. Conclusions

In this paper, a short study of the effects of the weighting functions on the performances of the robust control systems was presented.

In this context, the basic requirements imposed to the control system (from Figure 1) were:

- Reducing the control error, rejecting the disturbances and ensuring the desired performances;
- Reducing the effect of the variations of the parameters in the open-loop system on the transition to the closed-loop system, i.e., ensuring the robustness of the control system in case of uncertainties.

In the robust control diagram (Figure 2), the performances regarding the reference tracking, disturbances and measurement noise rejection and control signal effort should be achieved for each external input  $r$ ,  $v$ ,  $\eta$ ,  $l$ , whose energy does not exceed a predetermined value. As a result, weighting functions must be properly designed and used.

So, for the weighting function  $W_e(s)$ :

- Increasing the  $M_S$  leads to a higher overshoot; reasonable values for the overshoot and for the gain (robustness) margin are obtained for  $M_S \leq 2$ ;
- Increasing the  $\omega_{bs}$  leads to a lower transient time, meaning a faster response of the closed-loop system and a quick rejection of the disturbances; a higher value for  $\omega_{bs}$  highlights a closed-loop system which is more sensitive to disturbances and parameter variations; a low value for  $\omega_{bs}$  indicates a longer response time and a more robust system;
- A low value imposed to the  $\varepsilon_S$  (e.g.,  $\varepsilon_S = 0.1$ ) leads to a high steady state error; so, the recommended value is  $\varepsilon_S > 0.01$  (e.g.,  $\varepsilon_S = 0.001, 0.0001$ ). At the same time, for the weighting function  $W_u(s)$ :
- $M_u$  it is chosen according to the restrictions imposed to the actuator; increasing the  $M_u$  leads to a higher overshoot and a reasonable value is obtained for  $M_u \leq 2$ ;
- Increasing the  $\omega_{bu}$  leads to a lower response time of the closed-loop system; a lower value of  $\omega_{bu}$  assures a better limitation of the measurement noise;
- The value of  $\varepsilon_u$  does not significantly influence the performances of the closed-loop system.

**Author Contributions:** Conceptualization, M.D. and S.-E.O.; methodology, M.D.; software, validation, M.D. and S.-E.O.; formal analysis, S.-E.O.; investigation, resources, and data curation, M.D.; writing—original draft preparation, M.D.; writing—review and editing, S.-E.O.; visualization, supervision, M.D.; project administration, M.D.; funding acquisition, M.D. and S.-E.O. All authors have read and agreed to the published version of the manuscript.

**Funding:** This research received no external funding.

**Conflicts of Interest:** The authors declare no conflict of interest.

## References

1. Grimble, M.J.; Biss, D. Selection of optimal control weighting functions to achieve good H/sub infinity/robust designs. In Proceedings of the IEEE International Conference on Control, Oxford, UK, 13–15 April 1988; pp. 683–688.
2. Gu, D.W.; Petkov, P.H.; Konstantinov, M.M. *Robust Control Design with MATLAB*; Springer: London, UK, 2005.
3. Ionescu, V.; Varga, A. *Systems Theory. Robust Synthesis. Numerical Methods (Romanian Version, Teoria Sistemelor. Sinteza Robusta. Metode Numerice de Calcul)*; ALL Publishing: Bucharest, Romania, 1994.
4. Popescu, D. *Analysis and Synthesis of Robust Systems (Romanian Version, Analiza si Sinteza Sistemelor Robuste)*; Universitaria Publishing: Craiova, Romania, 2010.
5. Zhou, K. *Essentials of Robust Control*; Prentice Hall: Upper Saddle River, NJ, USA, 1999.
6. Raafat, S.M.; Akmeliawati, R. Bounded constrained optimization of performance weighting function for precise robust positioning control system. In Proceedings of the IEEE 4th International Conference on Mechatronics, Kuala Lumpur, Malaysia, 17–19 May 2011; pp. 1–7.
7. Qinghai, H.; Jing, L.; Qingzhu, H.; Wen, Z.; Hai, Z. The selections of nominal plant and weighting functions for robust control design. In Proceedings of the IEEE 8th World Congress on Intelligent Control and Automation, Jinan, China, 7–9 July 2010; pp. 771–775.

8. Heng, Q.; Lu, J.; Lu, Y.; Zhou, H.  $\mu$ -synthesis robust control of a boiler combustion system. In Proceedings of the IEEE 30th Chinese Control Conference, Yantai, China, 22–24 July 2011; pp. 2331–2334.
9. Beaven, R.W.; Wright, M.T.; Seaward, D.R. Weighting function selection in the  $H_{\infty}$  design process. *Control Eng. Pract.* **1996**, *4*, 625–633. [[CrossRef](#)]
10. Munawa, P.; Folly, K.A. Selection of weighing functions in  $H_{\infty}$  controller design using PBIL. In Proceedings of the IEEE International Joint Conference on Neural Networks, Beijing, China, 6–11 July 2014; pp. 1733–1738.
11. Veenman, J.; Lahr, M.; Scherer, C.W. Robust controller synthesis with unstable weights. In Proceedings of the IEEE 55th Conference on Decision and Control, Las Vegas, NV, USA, 12–14 December 2016; pp. 2390–2395.
12. Balas, G.; Chiang, R.; Packard, A.; Safonov, M. *Robust Control Toolbox. Getting Started Guide R2013b*; The MathWorks, Incorporations: Natick, MA, USA, 2013.
13. Mathworks. Matlab Control System Toolbox. Available online: [https://ch.mathworks.com/products/robust.html?s\\_tid=srchtitle](https://ch.mathworks.com/products/robust.html?s_tid=srchtitle) (accessed on 10 August 2020).
14. Geng, L.; Yang, Z.; Zhang, Y. A Weighting Function Design Method for the H-infinity Loop-shaping Design Procedure. In Proceedings of the Chinese Control and Decision Conference, Shenyang, China, 9–11 June 2018; pp. 4489–4493.
15. Pathak, D.; Sambariya, D.K. Methodologies for the Selection of Weighting Function. In Proceedings of the IEEE 2nd International Conference on Power Energy, Greater Noida, India, 18–19 October 2019; pp. 347–350.
16. Usami, T.; Yubai, K.; Yashiro, D.; Komada, S. Low-order multivariable weighting function design for  $H_{\infty}$  loop shaping method based on  $\nu$ -gap. In Proceedings of the IEEE International Conference on Industrial Technology, Lyon, France, 20–22 February 2018; pp. 223–228.

**Publisher’s Note:** MDPI stays neutral with regard to jurisdictional claims in published maps and institutional affiliations.



© 2020 by the authors. Licensee MDPI, Basel, Switzerland. This article is an open access article distributed under the terms and conditions of the Creative Commons Attribution (CC BY) license (<http://creativecommons.org/licenses/by/4.0/>).



# Concept Lattice-Based Classification in NLP<sup>†</sup>

László Kovács

Department of Information Science, University of Miskolc, 3515 Miskolc, Hungary; kovacs@iit.uni-miskolc.hu; Tel.: +36-20-3319765

<sup>†</sup> Presented at the 14th International Conference INTER-ENG 2020 Interdisciplinarity in Engineering, Mureş, Romania, 8–9 October 2020.

Published: 24 December 2020

**Abstract:** Classification in discrete object space is a widely used machine learning technique. In this case, we can construct a rule set using attribute level implication rules. In this paper, we apply the technique of formal concept analysis to generate the rule base of the classification. This approach is suitable for cases where the number of possible attribute subsets is limited. For testing of this approach, we investigated the problem of the part of speech prediction in natural language texts. The proposed model provides a better accuracy and execution cost than the baseline back-propagation neural network method.

**Keywords:** machine learning; morphological classification; formal concept analysis; natural language processing

## 1. Introduction

In the area of machine learning, classification is the most widely used technology. In the case of classification, we have an object space  $O$ , where every object  $o \in O$  is given by a set of attribute–value pairs, and the objects are assigned to a category/class value:

$$O = \{ \{ (a, v), c \} \mid a \in A, v \in Dom_a, c \in C \}, \quad (1)$$

where  $A$  denotes the attribute set and  $C$  is the category set. The main goal of the classifier is to generate a prediction function:

$$f_C : \{ \{ (a, v) \} \} \rightarrow C, \quad (2)$$

where  $f_C$  assigns a category value for every attribute–value pair set of the problem domain.

A special case of the classification problem is when the  $Dom_a$  sets contain only discrete values. Such discrete domains can be found among others in assignment problems, permutation to perform efficient classification in discrete domain space. Among the most widely known candidates, we can mention the decision tree classifier and the neural network classifier.

Neural network (NN) [1] classifiers are based on composition of elementary binary perceptron classifiers using separation hyperplanes. The elementary classification nodes are structured into a network where the nodes are connected by weighted directed edges. In the simplest case, the output of a node is given by:

$$\text{sigmoid} \left\{ \sum_i w_i s_i + b \right\} \quad (3)$$

where  $w_i$  denotes the edge weight values,  $s_i$  is the notation for signal strength and  $b$  is a bias value. During the training process, the weight values are adjusted to produce a minimal misclassification error. In the case of Back-propagation NN, the input is given by a feature vector and the output is a category vector. The network contains only one hidden layer. Besides this simple classification network, many other special complex network structures were developed in recent years. For the

classification of multi-dimensional objects, the convolutional NN models provide an efficient solution. For the handling of sequences such as words or transaction events, the family of recurrent networks is the suitable tool. The LSTM (long-term short-term memory) NN are very popular in the domain of natural language processing.

In the case of decision trees [2], each child node corresponds to a distinct attribute value. As the child node set is discrete, thus also the attribute value set is assumed to be discrete. In the ID3 decision tree construction methods, the attribute with the smallest weighted entropy is selected:

$$\operatorname{argmin}_a \left\{ \operatorname{entropy} \left( \left\{ p_{(i,a)} \right\} \right) \right\} \tag{4}$$

where the entropy refers to the homogeneity level of the category (class label) distribution.

The decision process of a decision tree can be represented by a set of logical formulas of the form:

$$\text{If } a_1 = v_1 \wedge a_2 = v_2 \wedge \dots \wedge a_m = v_m \text{ then category} = c \tag{5}$$

If we consider all formulas related to a decision tree, we can see that attribute  $a_1$  is contained in all formulas, while the last attribute is used only in few formulas. The decision tree constructs a priority order of the attributes.

A more general ruleset can be constructed if we consider not a decision tree, but a decision lattice. The theory of Formal Concept Analysis (FCA) can be used to construct a decision lattice as generalization of the decision tree.

In the next section, the basic concepts of formal concept analysis are presented. This formalism is used to generate the frequent attribute patterns in the training set. Section 3 introduces a morphological classification model based on the concept lattice approach. The results of the experimental tests on efficiency comparison are analyzed in Section 4.

## 2. Classification with FCA

The theory of Formal Concept Analysis (FCA) [3] provides a tool for conceptualization in an object–attribute relational context. A formal concept corresponds to a pair of related closed sets. The first component containing objects is called the extent part, while the second component containing attributes is the intent part. Formal concepts created from the context can be structured into a concept lattice based on the set containment relationship. The ordering among the lattice elements can be considered as a specialization and generalization relationship among the concepts. The roots of FCA originate in the theory of Galois connections [4] and in the applied lattice and order theory developed later by Birkhoff [5]. The terminology and theoretical foundation of FCA was introduced and built up in the 1980s by Rudolf Wille and Bernhard Ganter [6].

In FCA, two special, partially ordered sets are considered, namely,  $G$  is the set of objects and  $M$  is the set of attributes. The corresponding fixpoints are called formal concepts, which are built up from a matching pair of object and attribute sets. Using the notations defined in [7], the terminology of FCA can be summarized in the following way:

A formal context is defined as a triplet  $\langle G, M, I \rangle$ , where  $I$  is a binary relation between  $G$  and  $M$ . The condition  $(x, y) \in I$  is met if and only if the attribute  $y$  is true for the object  $x$ . Two derivation operators are introduced as mappings between the powersets of  $G$  and  $M$ . For  $A \subseteq G, B \subseteq M$ :

$$\begin{aligned} f(A) &= A^I = \{m \in M \mid \forall g \in A : (g, m) \in I\} \\ f(A) &= A^I = \{m \in M \mid \forall g \in A : (g, m) \in I\} \end{aligned} \tag{6}$$

For a context  $\langle G, M, I \rangle$ , a formal concept is defined as a pair  $(A, B)$ , where  $A \subseteq G, B \subseteq M, A = B^I, B = A^I$  are met. The composition of these derivations is closure operator. Regarding this derivation, the components of a formal concept satisfy the  $A = A^{II}, B = B^{II}$  conditions, too. The  $A$  component is called the extent of the concept, while  $B$  is the intent part.

On the set of formal concepts,  $C$ , generated from the context  $\langle G, M, I \rangle$ , a partial ordering relation is defined in the following way:

$$(A_1, B_1) \leq (A_2, B_2) \Leftrightarrow A_1 \subseteq A_2 \tag{7}$$

FCA can be used also as a classification tool in Machine Learning [8,9]. In classification problems, the context is extended with a category attribute and the lattice is used similarly to a decision tree, where the tree leaves correspond to the maximal consistent concepts of the lattice. A pioneer work on the application of concept lattices in retrieval of semantic information is presented in [10]. The area of FCA-based classification is nowadays an active research problem domain [11,12].

Taking an object  $(\{(a, v)\}, c)$  from the training set, we can convert the information on the object into the following implication rule:

$$a_1 = v_1 \wedge a_2 = v_2 \wedge \dots \wedge a_m = v_m \Rightarrow c \tag{8}$$

Thus, the training set can be considered as a ruleset. The objects usually correspond to the atomic nodes in the FCA lattice. Every node in the lattice can be constructed as the intersection of some object-level nodes of the lattice, resulting a node of the following form:

$$a_1 = v_1 \wedge a_2 = v_2 \wedge \dots \wedge a_m = v_m \Rightarrow c_1 \vee c_2 \vee \dots \vee c_k \tag{9}$$

where  $a_1 = v_1, a_2 = v_2, \dots, a_m = v_m$  are present in every operand node of the intersection. If the right side of the rule contains only one class label, then this node is called the consistent node.

$$a_1 = v_1 \wedge a_2 = v_2 \wedge \dots \wedge a_m = v_m \Rightarrow c \tag{10}$$

Among the consistent nodes of the lattice, a special role is assigned to the maximal consistent nodes having a minimal attribute set. A consistent node

$$a_1 = v_1 \wedge a_2 = v_2 \wedge \dots \wedge a_m = v_m \Rightarrow c \tag{11}$$

is maximal if none of the attribute–value pairs can be removed without breaking the rule.

The set of maximal consistent nodes is considered as the core ruleset for the classification process. The concept lattice structure can be used to generate the elements of the core ruleset. The naive way to generate the lattice is to perform all intersections on the lattice elements. The main bottleneck of this approach is that the size of the lattice and the number of required intersections can be very huge. In the survey paper of [13], the efficiency of two popular methods, CbO and the NextClosure, is investigated. It is shown that the most efficient lattice construction methods have a theoretical complexity of  $O(N^2MC)$  (see Figure 1). Theoretically, the value of  $C$  is bound by  $2^M$ , but usually the density of the training set is lower, yielding a smaller lattice. A sharper theoretical upper bound was shown by Prisner in [14] and by Albano Chornomaz in [15]. They investigated a special type of context, the contranomial scale free context involving both theoretical analysis and test experiments. They could show that the execution cost is in general of polynomial shape and in the worst case of exponential shape.

Based on these cost properties, the processing of all possible intersections is implausible in acceptable time. Thus, to apply an FCA-based classification for problem domains with several millions of objects, we need an optimized and simplified method to determine the maximal consistent elements.



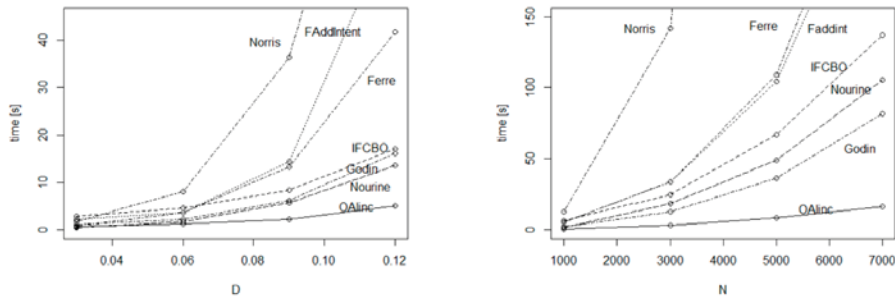


**Figure 1.** Execution cost function ( $N = 1000, M = 100$ ) for left side; ( $M = 150, \text{density level} = 7$ ) for right side.

### 3. Cost Reduction Methods for FCA-Based NLP POS Classifiers

In FCA, the main goal is to construct all possible formal concepts from the input object set. In the prediction task, we do not need all implication rules—one matching rule may be enough to determine the related class label. Thus, in the construction of FCA-based classifiers, we require only a subset of the all possible concept nodes. The relevance of a node can be given with the following three parameters:

- Support level (the size of the extension component, the number of matching objects);
- Heterogeneity level (regarding the class labels);
- Generalization ability (length of the generalization path).

In the classic approach, the engine builds up first the whole concept lattice. The maximal consistent nodes are selected from this lattice using a top-down traversing approach. In the lattice, the top node is usually inconsistent while the atomic nodes are usually consistent. The standard way of lattice construction is to process the atomic nodes first and generate the more general concepts later. This process corresponds to a bottom-up approach.

In the proposed method, the support level is also an important factor, as we need such rules that can cover a larger set of objects. Using rules with large support values results in a reduced ruleset.

We allow also inconsistent nodes in the lattice as in some cases only the atoms are consistent. Thus, the method yields a probability distribution of the different classes.

In the case of part of speech classifiers (NLP POS) [16], the classifier engine determines the grammatical category of the input words. We have analyzed the POS prediction for the Hungarian language, where we use eight basic POS units (noun, verb, adjective, adverb, article, conjunction, number, date) and 42 compound POS units. The composite POS labels are coming from the fact that some word forms have different meaning with different POS labels. For example, the word *vár* can be a verb (*to wait*) or a noun (*castle*).

For the representation of the words, we have used the character sequence format, thus for the word *almákat*, the corresponding letters (*a, l, m, á, k, a, t*) are the description attributes. A special constraint is used in our model, namely, we allow only a subset of the word subsequences as attribute tuples used in the generalization process. For example, for the word *almákat*, only the following strings are valid attribute subsets:

$$\#, \text{at}\#, \text{kat}\#, \text{ákat}\#, \text{mákat}\#, \text{lmákat}\#, \text{almákat}\#$$

where symbol # denotes the terminal symbol.

With this kind of simplification, for a word with a length of  $n$  characters, the number of possible subsets is equal to  $O(n)$ , instead of the usual subset count  $O(2^n)$ . Thus, the number of concept nodes is linear with total number of characters in the word set. This means that we can process all

candidate nodes in a linear time to generate the maximal consistent nodes. Based on this consideration, we constructed the following algorithm to generate all maximal consistent nodes.

```

SDict = dictionary()
For all word (w) in the training set:
    S = generate all substrings of w
    for each s in S:
        h = class_homogeneity (s)
        f = support(s)
    merge (s,h,f) into SDict
    
```

In the merge process, the cost frequency distribution of s is aggregated to the existing (h,f) values in the dictionary.

In the purging process, we can eliminate nodes having a weaker relevance value.

```

for all (s,h,f) in SDict:
    w = w(h,f)
    if w < w_limit:
        remote (s,h,f) from SDict
    
```

The reduced dictionary can be used as rule space, every node as separate role of the form

$$f_c : \{(a, v)\} \rightarrow C \tag{12}$$

In the prediction phase, we perform a nearest neighbor classification process. In the first step, the set of subset stings is generated for the query word on the standard way mentioned previously. Then, for each substring s, the entry for s in the dictionary is located. Every entry contains also a class distribution vector; thus, we can calculate an aggregated class distribution for the query word. The winner category is the class with the highest probability.

#### 4. Experimental Results

For the tests, we have used a training set containing 2,200,000 word-entries with POS value. For the baseline method, we have selected the back-propagation neural network and the LSTM neural network engine. In the tests, first we used a character-level representation of the words to compare to baseline neural network classifiers: standard back-propagation network and the LSTM recurrent network. Both NN units were implemented in Python Keras framework. The test results were a bit surprising as both NN engines provided very similar accuracy, near 70% for the case when the size of training set was 250,000. For the test, we have used a disjoint sample of 250,000 items. This experiment has shown that the sequence approach is not superior to the standard classification approach for our problem domain.

Later, we have introduced a different representation approach, where an extended character representation form was used. In this approach, the feature vector also contained the phonetical attributes of the characters. Using this approach, the NN engines could achieve 86% accuracy, while the combined pattern matching, the NN method, could reach a 96% accuracy. The test results are summarized in Table 1. In the table, PM denotes our proposed method and symbol NN is for the neural network approach.

**Table 1.** Efficiency comparison of the proposed method (PM) with neural network (NN) classifiers.

Method	NN t-Time	PM t-Time	NN Accuracy	PM Accuracy
90% train, 10% test	130 min	6 min	86%	96%
60% train, 10% test	80 min	4 min	86%	96%
3% train, 10% test	2 min	0.7 min	86%	95%
1% train, 10% test	1.5 min	0.5 min	85%	93%
0.3% train, 10% test	1 min	0.4 min	84%	91%
0.1% train, 10% test	0.6 min	0.3 min	82%	87%

In the tests, we have investigated two factors:

- Accuracy;
- Model construction time.

Based on the performed test experiments, we experienced two surprising results:

- The proposed model provides a significantly better classification accuracy;
- The model's construction in the proposed method is significantly faster than in the NN approach.

## 5. Conclusions

The FCA concept–lattice-based structure can be used also in classification problems where the maximal consistent nodes are basic rules for the prediction process. The FCA-based approach is suitable for cases where the number of possible attribute subsets is limited. In this paper, we introduced the adaptation of the FCA-based classifier to solve an NLP-POS classification problem. Based on the test experiments, the proposed model provides a better accuracy and execution cost than the baseline back-propagation neural network method.

**Funding:** This research received no external funding.

**Acknowledgments:** The described article/presentation/study was carried out as part of the EFOP-3.6.1-16-2016-00011 “Younger and Renewing University—Innovative Knowledge City—institutional development of the University of Miskolc aiming at intelligent specialisation” project implemented in the framework of the Szechenyi 2020 program. The realization of this project is supported by the European Union, co-financed by the European Social Fund.

**Conflicts of Interest:** The author declares no conflict of interest.

## References

1. Féraud, R.; Clérot, F. A methodology to explain neural network classification. *Neural Netw.* **2002**, *15*, 237–246. [[CrossRef](#)]
2. Safavian, S.R.; Landgrebe, D. A survey of decision tree classifier methodology. *IEEE Trans. Syst. Man Cybern.* **1991**, *21*, 660–674. [[CrossRef](#)]
3. Ganter, B.; Wille, R. *Formal Concept Analysis: Mathematical Foundation*; Springer: Heidelberg, Germany; New York, NY, USA, 1999.
4. Oystein, O. Galois Connexions. *Trans. Am. Math. Soc.* **1944**, *55*, 493–513.
5. Birkhoff, G. *Lattice Theory*; American Mathematical Society: Providence, RI, USA, 1940; Volume 25.
6. Wille, R. Restructuring lattice theory: An approach based on hierarchies of concepts. In *Ordered Sets*; Springer: Dordrecht, The Netherlands, 1982; Volume 83.
7. Piskova, L.; Horvath, T. Comparing Performance of Formal Concept Analysis and Closed Frequent Itemset Mining Algorithms on Real Data. In Proceedings of the CLA 2013, La Rochelle, France, 15–18 October 2013; pp. 299–308.
8. Zhao, Y.; Yao, Y. Classification based on logical concept analysis. In Proceedings of the Computational Studies of Intelligence, Quebec, QC, Canada, 7–9 June 2006; pp. 419–430.
9. Makhalova, T.; Kuznetsov, S. On Overfitting of Classifiers Making a Lattice. In Proceedings of the ICFCA 2017, Rennes, France, 13–16 June 2017; pp. 184–197.
10. Carpineto, C.; Romano, G. A Lattice Conceptual Clustering System and Its application to Browsing Re-trieval. *Mach. Learn.* **1996**, *24*, 95–122. [[CrossRef](#)]
11. Hao, J.; Zheng, Y.; Xu, C.; Yan, Z.; Li, H. Feature assessment and classification of diabetes employing concept lattice. In Proceedings of the International Conference on Computer Supported Cooperative Work in Design, Porto, Portugal, 6–8 May 2019; pp. 333–338.
12. Telcian, A.S.; Cristea, D.M.; Sima, I. Formal concept analysis for amino acids classification and visualization. *Acta Univ. Sapientiae Inform.* **2020**, *12*, 22–38. [[CrossRef](#)]
13. Ignatov, D. Introduction to formal concept analysis and its applications in information retrieval and related fields. In *Russian Summer School in Information Retrieval*; Springer: Cham, Switzerland, 2014; pp. 42–141.
14. Prisner, E. Biclques in graphs I: Bounds on their number. *Combinatorica* **2000**, *20*, 109–117. [[CrossRef](#)]

15. Albano, A.; Chornomaz, B. Why concept lattices are large. In Proceedings of the CLA 2015, Clermont-Ferrand, France, 13–16 October 2015; pp. 73–91.
16. Morton, T.S. Coreference for NLP applications. In Proceedings of the 38th Annual Meeting of the Association for Computational Linguistics, Hong Kong, China, 1–8 October 2000.

**Publisher’s Note:** MDPI stays neutral with regard to jurisdictional claims in published maps and institutional affiliations.



© 2020 by the authors. Licensee MDPI, Basel, Switzerland. This article is an open access article distributed under the terms and conditions of the Creative Commons Attribution (CC BY) license (<http://creativecommons.org/licenses/by/4.0/>).



# Assessing the Capability of KELM Meta-Model Approach in Predicting the Energy Dissipation in Different Shapes Channels <sup>†</sup>

Seyed Mahdi Saghebain <sup>1,\*</sup>, Daniel Dragomir-Stanciu <sup>2</sup> and Roghayeh Ghasempour <sup>3</sup>

<sup>1</sup> Department of Civil Engineering, Ahar Branch, Islamic Azad University, 54511 Ahar, Iran

<sup>2</sup> Department of Electrical Engineering and Information Technology, "George Emil Palade" University of Medicine, Pharmacy, Science and Technology of Targu Mures, 540142 Targu Mures, Romania; daniel.dragomir-stanciu@umfst.ro

<sup>3</sup> Department of Water Resource Engineering, Faculty of Civil Engineering, University of Tabriz, 51666 Tabriz, Iran; ghasempourroghy@gmail.com

\* Correspondence: smsaghebain@iau-ahar.ac.ir; Tel.: +98-9143136057

<sup>†</sup> Presented at the 14th International Conference INTER-ENG 2020 Interdisciplinarity in Engineering, Mures, Romania, 8–9 October 2020.

Published: 23 December 2020

**Abstract:** For transition of a supercritical flow into a subcritical flow in an open channel, a hydraulic jump phenomenon is used. Different shaped channels are used as useful tools in the extra energy dissipation of the hydraulic jump. Accurate prediction of relative energy dissipation is important in designing hydraulic structures. The aim of this paper is to assess the capability of a Kernel extreme Learning Machine (KELM) meta-model approach in predicting the energy dissipation in different shaped channels (i.e., rectangular and trapezoidal channels). Different experimental data series were used to develop the models. The obtained results approved the capability of the KELM model in predicting the energy dissipation. Results showed that the rectangular channel led to better outcomes. Based on the results obtained for the rectangular and trapezoidal channels, the combination of  $Fr_1$ ,  $(y_2 - y_1)/y_1$ , and  $W/Z$  parameters performed more successfully. Also, comparison between KELM and the Artificial Neural Networks (ANN) approach showed that KELM is more successful in the predicting process.

**Keywords:** energy dissipation; different shapes channels; KELM; strip rough elements

## 1. Introduction

For transition of a supercritical flow into a subcritical flow in an open channel, a hydraulic jump phenomenon is used. Hydraulic jumps can occur downstream of hydraulic structures, such as normal weirs, gates, and ogee spillways. It is considered as rapidly varying flow, and this type of flow regime transformation is associated with severe turbulence and flow energy dissipation [1]. Based on the energy dissipating action of hydraulic jumps, the stilling basin is one of the possible solutions which may be adopted. In order to design an optimal hydraulic structure, different devices such as sills, baffle blocks, end sills, roughness elements, and roller buckets are used in hydraulic structures. However, modeling hydraulic jump characteristics is of great importance since it plays an important role in designing hydraulic structures. Thus far, various studies have been done to explain the complex phenomenon of the hydraulic jump and to estimate its characteristics. Bhutto et al. developed a semi-empirical equation for calculating the sequent depth and relative energy loss ratio in sloping and horizontal rectangular channels [2]. Finnemore et al. stated that the Froude number has significant impact on the characteristics of the hydraulic jump [3]. The impact of wall friction on the sequent

depth ratio was studied by Hager and Bremen [4]. Ayanlar investigated the hydraulic jump properties in channels with corrugated beds [5]. Bilgin collected some experiments in a channel with smooth bed in order to investigate the distribution of shear stress for turbulent flow [6]. However, due to the complexity and uncertainty of the hydraulic jump phenomenon, the results of the classical models are not general and under variable conditions do not present the same results. Therefore, it is essential to use other methods that show more accuracy in predicting the energy dissipation in channels with different shapes and rough elements.

The Meta model approaches such as Artificial Neural Networks (ANNs), Neuro-Fuzzy models (NF), Genetic Programming (GP), Kernel extreme Learning Machine (KELM), and Support Vector Machine (SVM), have been applied in investigating the hydraulic and hydrologic complex phenomena in recent decades. Prediction of total bedload [7], urban flash flood forecast [8], precipitation forecasting [9], modeling flow resistance in open channels with dune bedform [10], developing stage-discharge curves [11], and predicting of bedload in sewer pipes [12], are some examples of the applications of Meta model approaches.

The aim of the present study is to assess the capability of KELM as an effective kernel-based approach in modeling energy dissipation in channels with different shapes (i.e., rectangular channel with strip and staggered elements and trapezoidal channel with strip elements). Different inputs combinations were considered, and the impact of hydraulic characteristics and channels geometry was assessed. In addition, the capability of the KELM approach was compared with the ANN meta-model approach.

## 2. Materials and Methods

### 2.1. Used Data Sets

In this study, the experimental data of Simsik (2006) and Evcimen (2012) studies were used for prediction goals [13,14]. Simsik used prismatic roughness elements with different arrangements in a rectangular channel to investigate the impact of these elements on hydraulic jump characteristics. Two types of roughness elements with stripe and staggered arrangements were used during experiments. The experiments of Evcimen were done at the hydraulic laboratory of the Middle East Technical University, which were intended for hydraulic jump in trapezoidal channels, and the impact of prismatic roughness on hydraulic jump was assessed. The used experimental data ranges are given in Table 1. To compare the performance of applied models, the total data were divided into two sets: the training and testing sets. Seventy-five-percent of the whole data were used for training the models and the last 25% of data were used for testing the models. The training set trains the scheme on the basis of a minimization criterion and the testing set is used to evaluate the generated model and assess its generalization capability

**Table 1.** The experimental data used in the study.

Researcher	Channel Shape	Rough Element Arrangement	Fr <sub>1</sub> (Froude Number)	W (cm) Space between Elements	Y Sequence Depth	Z (cm) Height of Elements
Simsik (2006)	Rectangular	Strip and staggered	2.13–11.92	3–9	2.5–14.8	1
Evcimen (2012)	Trapezoidal	Strip	3.92–13.28	2–10	4.15–14.9	1–3

### 2.2. Kernel Extreme Learning Machine (KELM)

ELM is a Single Layer Feed Forward Neural Network (SLFFNN) preparing method initially introduced by Huang et al. [15]. SLFFNN is a straight framework where information weights linked to hidden neurons and hidden layer biases are haphazardly chosen, while the weights among the hidden nodes are resolved logically (see Figure 1). This strategy likewise has preferred execution and adapts

progressively over the bygone era learning methods [15]. In light of the fact that, unlike traditional techniques, which involve numerous variables to set up, demonstrating a complex issue utilizing this technique does not need much human intercession to accomplish ideal parameters. The standard single-layer neural system with  $N$  random information  $(x_i, y_i)$  (where  $x_i = [x_{i1}, x_{i2}, \dots, x_{in}]^T \in R^n$ ,  $y_i = [y_{i1}, y_{i2}, \dots, y_{im}]^T \in R^m$ ),  $M$  hidden neurons, and the active function  $f(a)$  is shown as follow:

$$\sum_{i=1}^M \varphi_i f(w_i x_j + c_i) = O_j \quad j = 1, 2, \dots, N \tag{1}$$

where  $w_i = [w_{i1}, w_{i2}, \dots, w_{in}]^T$  is the weight vector that joins the input layer to the hidden layer,  $\varphi_i = [\varphi_{i1}, \varphi_{i2}, \dots, \varphi_{im}]^T$  is the weight vector that joins hidden layer to the target layer.  $c_i$  shows the hidden neuron biases. The general SLFFNN network aim is minimizing the difference between the predicted ( $O_j$ ) and target ( $t_j$ ) values which can be expressed as below:

$$\sum_{i=1}^M \varphi_i f(w_i x_j + c_i) = T_j \quad j = 1, 2, \dots, N \tag{2}$$

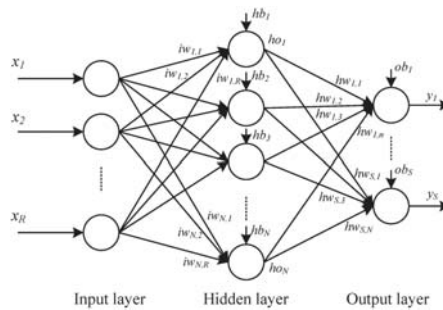


Figure 1. Single hidden Layer Feedforward Neural network.

The Equation (2) can be summarized as:

$$H\varphi = T \tag{3}$$

where

$$H(w_1, \dots, w_M, c_1, \dots, c_M, x_1, \dots, x_N) = \begin{bmatrix} f(w_1 x_1 + c_1) \dots f(w_M x_M + c_M) \\ \dots \\ f(w_1 x_N + c_1) \dots f(w_M x_N + c_M) \end{bmatrix} \tag{4}$$

$$T = \begin{bmatrix} T_1^T \\ \vdots \\ T_M^T \end{bmatrix}, \quad \varphi = \begin{bmatrix} \varphi_1^T \\ \vdots \\ \varphi_M^T \end{bmatrix} \tag{5}$$

The matrix  $T$  is identified as the target matrix of the hidden layers of the neural network.  $H$  is considered as output matrix of neural network. Huang et al. also introduced kernel functions in the design of ELM [16]. Now number of kernel functions is used in the design of ELM such as Linear, radial basis, Normalized polynomial, polynomial kernel functions. Kernel function-based ELM design is named Kernel extreme Learning Machine (KELM). For more detail about KELM, readers and researchers are referred to [16].



### 2.3. Artificial Neural Networks

Artificial Neural Network (ANN) is learning systems that have solved a large amount of complex problems related to different areas (classification, clustering, regression, etc.) and is a system loosely modeled on the human brain [17]. The field goes by many names, such as connectionism, parallel distributed processing, neuro-computing, neural intelligent system, machine learning algorithms and Artificial Neural Networks. It is an attempt to simulate within specialized hardware or sophisticated software. This simulation is achieved through multiple layers of simple processing elements called neurons. Each neuron is linked to certain neighbors with varying coefficients of connectivity that represent the strengths of these connections. Learning is accomplished by adjusting these strengths to cause the overall network to output appropriate results. The parameters to be found by training are the weight vectors connecting the different nodes of the input, hidden, and output layers of the network by the so-called error-back propagation method (a specialized version of the gradient-based optimization algorithm). During training, the values of the parameters (weights) are varied so that the ANN output becomes similar to the measured output on a known data set. There are two Artificial Neural Network topologies—Feed Forward and Feedback. In the first type, the information flow is unidirectional. A unit sends information to other unit from which it does not receive any information. There are no feedback loops. They are used in pattern generation/recognition/classification. They have fixed inputs and outputs. In the second type, feedback loops are allowed. They are used in content addressable memories. In this study, feed forward neural networks (FFNNs) are used. FFNNs with one sigmoidal hidden layer and a linear output layer have been proven to be capable of approximating any function with any desired accuracy if the associated conditions are satisfied. In this study, a two-layer feed forward neural network (one hidden layer and one output layer) is used for predicting monthly flows. The number of neurons in the hidden layer, along with the weights and biases, are obtained, based on the errors in the predicted values. Sigmoid and linear activation functions are used for the hidden layer and output layer, respectively.

### 2.4. Performance Criteria

Three statistical criteria named Determination Coefficient (DC), Correlation Coefficient (R), and Root Mean Square Error (RMSE) were used for assessing the proposed model’s efficiency. The used criteria equations are as follows:

$$DC = 1 - \frac{\sum_{i=1}^N (l_o - l_p)^2}{\sum_{i=1}^N (l_o - \bar{l}_p)^2}, R = \frac{\sum_{i=1}^N (l_o - \bar{l}_o) \times (l_p - \bar{l}_p)}{\sqrt{\sum_{i=1}^N (l_o - \bar{l}_o)^2 \times (l_p - \bar{l}_p)^2}}, RMSE = \sqrt{\frac{\sum_{i=1}^N (l_o - l_p)^2}{N}} \tag{6}$$

where  $l_o, l_p, \bar{l}_o, \bar{l}_p, N$  are the observed values, predicted values, mean observed values, mean predicted values and number of data samples, respectively.

## 3. Simulation and Models Development

### 3.1. Input Variables

Appropriate selection of input combination has significant impact on the accuracy of developed models. In Figure 2, the quantities measured for jumps in channels with different shape are shown. Based on [18–20], the important variables which affect the energy dissipation are:

$$f(y_1, y_2, V_1, L_j, \Delta E, \mu, g, \rho, Z, W) = 0 \tag{7}$$

where  $y_1$  and  $y_2$ : sequent depth of upstream and downstream,  $V_1$ : upstream flow velocity,  $\mu$ : water dynamic viscosity,  $g$ : gravity acceleration,  $L_j$ : length of jump,  $\rho$ : density of water,  $\Delta E (=E_1 - E_2)$  in

which  $E_1$  and  $E_2$  are energy per unit weight before and after the jump,  $Z$ : rough element height, and  $W$ : space between rough elements.

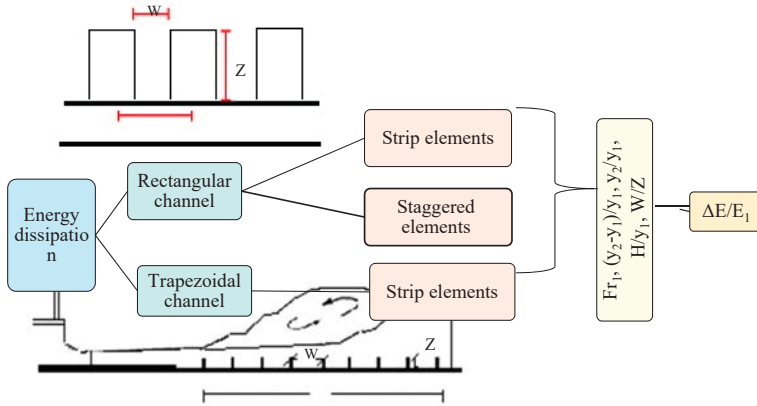


Figure 2. The schematic view of different types of channels used in this study.

From dimensional analysis and considering  $y_1$ ,  $g$  and  $\mu$  as repeating variables, these parameters of Equation (7) can be expressed as follows:

$$f\left(\frac{y_2}{y_1}, \frac{\Delta E}{E_1}, \frac{L_j}{y_1}, \frac{v_1^2}{gy_1}, \frac{\rho v_1 y_1}{\mu}, \frac{Z}{y_1}, \frac{W}{y_1}\right) = 0 \tag{8}$$

Equation (8) can be expressed as:

$$f\left(\frac{y_2}{y_1}, \frac{\Delta E}{E_1}, \frac{L_j}{y_1}, Fr_1, Re, \frac{Z}{y_1}, \frac{W}{y_1}\right) = 0. \tag{9}$$

where  $Fr_1$  is flow Froude number and  $Re$  is flow Reynolds number.

Experimental studies by several researchers (i.e., [21,22]) revealed that hydraulic jump characteristics only depend on Froude number, and the Reynolds number has no effective role in the predicting process. Also, Hager showed that the height of jump can affect the characteristics of the hydraulic jump [1]. Therefore, in this study, based on upstream hydraulic data and geometric data, the models of Table 2 were considered for modeling energy dissipation due to the hydraulic jump in different types of channels with different rough elements. It should be noted that the modeling process was done using developed cods for KELM and ANN approaches in MATLAB software.

Table 2. Kernel Extreme Learning Machine (KELM)-developed Models.

Input Variable(s)	Models
$Fr_1$	M (I)
$Fr_1, (y_2-y_1)/y_1$	M (II)
$Fr_1, Z/y_1$	M (III)
$Fr_1, W/Z$	M (IV)
$Fr_1, (y_2-y_1)/y_1, W/Z$	M (V)

### 3.2. KELM Parameters Setting

It should be noted that each artificial intelligence method has its own parameters. To achieve the desired results, the optimized amount of these parameters should be determined. For example, in designing the KELM approach, the selection of the appropriate type of kernel function is needed.

There are various kernel functions which can be used based on the nature of the studied phenomenon. In this research, the model  $M(V)$  of the rectangular channel with strip elements was predicted using different kernel types. In this regard, the  $Fr_1, (y_2 - y_1)/y_1, W/Z$  parameters were used as inputs for KELM approach and considering different kernel types this model was run. Then, for each kernel the amount of the RMSE was calculated and compared with the others. According to Figure 3a, the RBF kernel function ( $e^{-\gamma|x-y|^2}$ ) in which  $\gamma$  is the kernel parameter) was defined as the best kernel function. Figure 3b shows the RMSE statistic parameter via  $\gamma$  values for comparing the impact of RBF kernel parameter of  $\gamma$  on performance of employed algorithm for testing set of the model  $M(V)$  for rectangular channel with strip elements. In this study, optimization of  $\gamma$  was performed by a systematic grid search of the parameter using cross-validation. It could be seen that  $\gamma = 5$  (the optimum amount) led to the least RMSE value. On the other hand, in ANN modeling the network topology has direct effects on its computational complexity and generalization capability. Therefore, the appropriate structure of ANN should be selected. In this study, various networks were tried for determining the hidden layer node numbers. For this aim, different numbers of neurons (i.e., 2, 3, 5, and 7) in the hidden layer were tested. Also, it was found that the tangent sigmoid and pure linear functions are suitable for the hidden and output node activation functions, respectively. The model training was done using the scheme of back propagation approach.

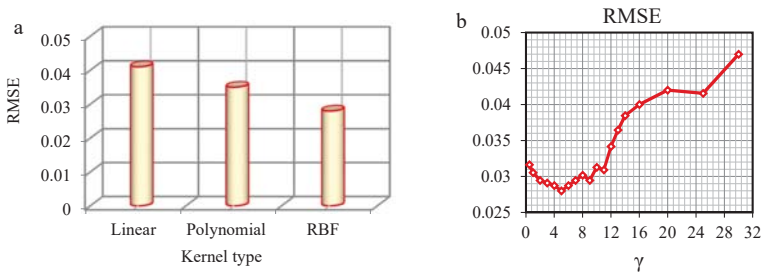


**Figure 3.** Root Mean Square Error (RMSE) statistics parameter via (a) KELM kernels function types and (b)  $\gamma$  values to find KELM optimums of testing set for the model  $M(V)$ .

#### 4. Results and Discussion

##### 4.1. Results Obtained for Rectangular Shape Channels

For rectangular shape channel, two states were considered. In the first state the efficiencies of the developed models were investigated in the channel with strip rough elements and in the second state channel with staggered rough elements. In developing models, the flow condition and geometry of the applied rough elements were considered. The developed models were analyzed with KELM model to carry out the energy dissipation ratio prediction in these channels. Table 3 and Figure 4 show the results of the KELM models. Based on the results of the RMSE, R, and DC statistical parameters, it was observed that, between two types of channels, the developed models for the case of the channel with strip elements in modeling the energy dissipation performed more successfully. For both cases, the model  $M(V)$  with input parameters of  $Fr_1, (y_2 - y_1)/y_1, W/Z$  led to more accurate outcome than the other models. A comparison between the results of the models showed that, for prediction the relative energy dissipation in rough bed channels, using parameter  $Z/y_1$  and  $W/Z$  as the input parameters caused an increment in the models' efficiency and the  $Z/y_1$  parameter is more efficient.

**Table 3.** Statistical parameters of the KELM models for the rectangular shape channels.

Performance Criteria						Models
Test			Train			
RMSE	DC	R	RMSE	DC	R	
Strip elements						
0.067	0.892	0.934	0.038	0.914	0.959	M (I)
0.055	0.942	0.982	0.032	0.968	0.983	M (II)
0.058	0.935	0.975	0.038	0.964	0.981	M (III)
0.062	0.922	0.973	0.039	0.963	0.978	M (IV)
0.049	0.944	0.986	0.025	0.973	0.991	M (V)
Staggered elements						
0.075	0.818	0.841	0.043	0.859	0.863	M (I)
0.062	0.847	0.884	0.036	0.871	0.885	M (II)
0.065	0.842	0.878	0.043	0.868	0.883	M (III)
0.07	0.83	0.876	0.044	0.867	0.88	M (IV)
0.055	0.868	0.927	0.031	0.886	0.969	M (V)

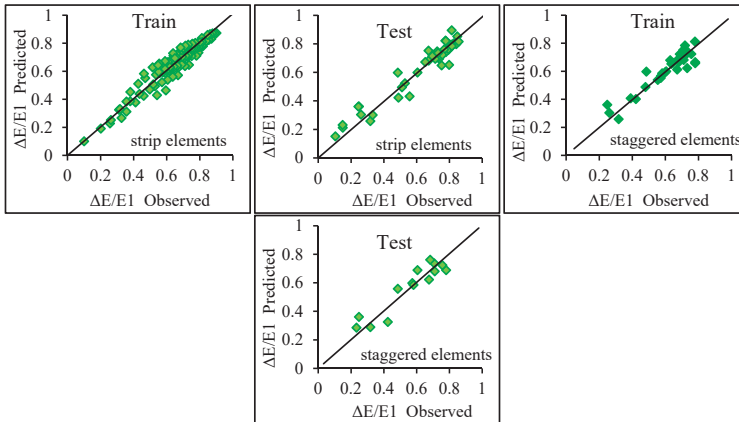


**Figure 4.** Comparison of observed and predicted energy dissipation for the rectangular shape channels superior models.

4.2. Results Obtained for Trapezoidal Shape Channel

The obtained results for trapezoidal shape channel are listed in Table 4 and shown in Figure 5. In this case, the model M (V) with input parameters of  $Fr_1$ ,  $(y_2 - y_1)/y_1$ ,  $W/Z$  was the superior model. According to the results, it could be seen that adding parameters  $(y_2 - y_1)/y_1$ ,  $Z/y_1$ , and  $W/Z$  as an input parameter caused an increment in the models' efficiency. However, for this state, the variable  $W/Z$  was more effective than variables  $(y_2 - y_1)/y_1$  and  $Z/y_1$  in improving the model accuracy. This issue shows the impact of the rough elements' geometry on predicting the relative energy dissipation. From the comparison between the results of Tables 3 and 4, it could be stated that the model developed for a rectangular channel with rough elements performed more successfully in predicting the energy dissipation than that of a trapezoidal channel with rough elements.

**Table 4.** Statistical parameters of the KELM models for the trapezoidal shape channels.

Performance Criteria						Models
Test			Train			
RMSE	DC	R	RMSE	DC	R	
0.086	0.804	0.904	0.072	0.822	0.909	M (I)
0.082	0.811	0.909	0.067	0.831	0.912	M (II)
0.084	0.809	0.906	0.069	0.825	0.91	M (III)
0.073	0.827	0.927	0.059	0.849	0.938	M (IV)
0.072	0.858	0.935	0.057	0.885	0.942	M (V)

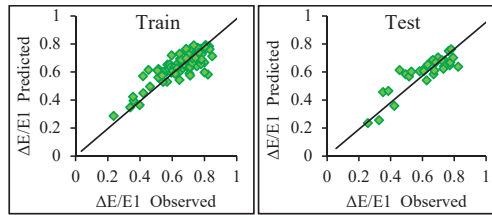


**Figure 5.** Comparison of observed and predicted relative energy dissipation for the trapezoidal shape channel superior model.

4.3. Validation of Proposed Best KELM Models Using ANN Method

The experimental data of both applied channels were used to evaluate the performance of the best-KELM model compared with the other data driven model. In this regard, for each channel the superior model was run using ANN method and the results were compared with the KELM. Table 5 shows the results of this comparison. As it can be seen from Table 5, ANN led to the desired accuracy, and the efficiency of this model was good at energy dissipation modeling. However, the KELM model yielded slightly better results in comparison with the ANN method.

**Table 5.** Statistical parameters of the KELM and Artificial Neural Network (ANN) methods for the superior models.

Structure of KELM and ANN	Performance Criteria						Models
	Test			Train			
	RMSE	DC	R	RMSE	DC	R	
Rectangular shape channels with strip elements							
$\gamma = 5$ (3, 7, 1) *	0.049	0.944	0.986	0.025	0.973	0.991	M (V), KELM
	0.053	0.938	0.978	0.03	0.961	0.981	M (V), ANN
Rectangular shape channels with staggered elements							
$\gamma = 4$ (3, 7, 1)	0.055	0.868	0.927	0.031	0.886	0.969	M (V), KELM
	0.061	0.851	0.915	0.035	0.87	0.935	M (V), ANN
Trapezoidal shape channel							
$\gamma = 6$ (3, 9, 1)	0.072	0.858	0.935	0.057	0.885	0.942	M (V), KELM
	0.076	0.833	0.905	0.062	0.867	0.931	M (V), ANN

\* (inputs number, neurons number, output number).

5. Conclusions

In this study, the KELM method was used to predict the relative energy dissipation in two rectangular and trapezoidal channels with different rough elements. The KELM was applied for

different models based on flow conditions and geometry of channels and rough elements. The obtained results showed that, in predicting the energy dissipation in rectangular and trapezoidal channels, the model M (V) with input parameters of  $Fr_1$ ,  $(y_2 - y_1)/y_1$ , and  $W/Z$  performed more successfully than the other models. It was observed that  $Z/y_1$  and  $W/Z$  parameters increased the models' efficiency; therefore, it could be stated that the height and space of applied elements were important factors in the energy dissipation prediction. Between two types of rectangular channels, the developed models for the case of channel with strip elements were more accurate than the staggered elements. Comparison between the results of two channels revealed that the models developed in the case of the rectangular channel led to more accurate outcomes. A comparison was also done between the KELM results and ANN method and the results verified the superior performance of the KELM method.

**Author Contributions:** S.M.S.: Conceptualization, Methodology, Review & Editing; D.D.-S.: Investigation, Resources, Data Curation; R.G.: Project administration, Methodology, Writing. All authors have read and agreed to the published version of the manuscript.

**Funding:** This research received no external funding.

**Conflicts of Interest:** The authors declare no conflict of interest.

## References

- Hager, W.H. *Energy Dissipators & Hydraulic Jumps*; Kluwer Academic Publication: Dordrecht, The Netherlands, 1992; pp. 151–173.
- Bhutto, H.; Mirani, S.; Chandio, S. Characteristics of free hydraulic jump in rectangular channel. *Mehran Univ. Res. J. Eng. Technol.* **1989**, *8*, 34–44.
- Finnemore, J.E.; Franzini, B.J. *Fluid Mechanics with Engineering Applications*; McGraw-Hill: New York, NY, USA, 2002; p. 790.
- Hager, W.H.; Bremen, R. 1989 Classical Hydraulic Jump: Sequent Depths. *J. Hydraul. Res.* **1989**, *7*, 565–585. [[CrossRef](#)]
- Ayanlar, K. Hydraulic Jump on Corrugated Beds. Master's Thesis, Middle East Technical University, Department of Civil Engineering, Ankara, Turkey, 2004.
- Bilgin, A. Correlation and Distribution of Shear Stress for Turbulent Flow in a Smooth Rectangular Open Channel. *J. Hydraul. Res.* **2005**, *43*, 165–173. [[CrossRef](#)]
- Chang, C.K.; Azamathulla, H.M.; Zakaria, N.A.; Ghani, A.A. Appraisal of soft computing techniques in prediction of total bed material load in tropical rivers. *J. Earth Syst. Sci.* **2012**, *121*, 125–133. [[CrossRef](#)]
- Yan, J.; Jin, J.; Chen, F.; Yu, G.; Yin, H.; Wang, W. Urban flash flood forecast using support vector machine and numerical simulation. *J. Hydroinform.* **2018**, *20*, 221–231. [[CrossRef](#)]
- Kisi, O.; Shiri, J. Precipitation forecasting using wavelet-genetic programming and wavelet-neuro-fuzzy conjunction models. *J. Water Resour. Manag.* **2011**, *25*, 3135–3152. [[CrossRef](#)]
- Roushangar, K.; Alami, M.T.; Saghebian, S.M. Modeling open channel flow resistance with dune bedform via heuristic and nonlinear approaches. *J. Hydroinform.* **2018**, *20*, 356–375. [[CrossRef](#)]
- Azamathulla, H.M.; Ghani, A.A.; Leow, C.S.; Chang, C.K.; Zakaria, N.A. Gene-expression programming for the development of a stage-discharge curve of the Pahang River. *J. Water Resour. Manag.* **2011**, *25*, 2901–2916. [[CrossRef](#)]
- Roushangar, K.; Ghasempour, R. Estimation of bedload discharge in sewer pipes with different boundary conditions using an evolutionary algorithm. *Int. J. Sediment Res.* **2017**, *32*, 564–574. [[CrossRef](#)]
- Simsek, C. Forced Hydraulic Jump on Artificially Roughened Beds. Master's Thesis, Middle East Technical University, Department of Civil Engineering, Ankara, Turkey, 2006.
- Evcimen, T.U. Effect of Prismatic Roughness on Hydraulic Jump in Trapezoidal Channels. Ph.D. Thesis, Middle East Technical University, Department of Civil Engineering, Ankara, Turkey, 2012.
- Huang, G.B.; Zhu, Q.Y.; Siew, C.K. Extreme learning machine: Theory and applications. *Neurocomputing* **2006**, *70*, 489–501. [[CrossRef](#)]
- Huang, G.B.; Zhou, H.; Ding, X.; Zhang, R. Extreme Learning Machine for Regression and Multiclass Classification. *IEEE Trans. Syst. Man Cybern. Part B (Cybern.)* **2012**, *42*, 513–529. [[CrossRef](#)] [[PubMed](#)]

17. Haykin, S.; Cybenko, G. *Approximation by Superposition of a Sigmoidal Function Neural Networks*, 2nd ed.; Prentice Hall: Englewood Cliffs, NJ, USA, 1999; Volume 2, pp. 303–314.
18. Rajaratnam, N.; Subramanya, K. Hydraulic Jump below Abrupt Symmetrical Expansions. *J. Hydraul. Div. ASCE* **1968**, *94*, 481–503.
19. Hager, W.H. Hydraulic Jumps in Non-Prismatic Rectangular Channels. *J. Hydraul. Res.* **1985**, *23*, 21–35. [[CrossRef](#)]
20. Gandhi, S. Characteristics of Hydraulic Jump. *Int. J. Math. Comput. Phys. Electr. Comput. Eng.* **2014**, *8*, 692–697.
21. Wu, S.; Rajaratnam, N. Transition from hydraulic jump to open channel flow. *J. Hydraul. Eng.* **1996**, *122*, 526–528. [[CrossRef](#)]
22. Elevatorski, E.A. *Hydraulic Energy Dissipators*; McGraw-Hill: New York, NY, USA, 2008.

**Publisher's Note:** MDPI stays neutral with regard to jurisdictional claims in published maps and institutional affiliations.



© 2020 by the authors. Licensee MDPI, Basel, Switzerland. This article is an open access article distributed under the terms and conditions of the Creative Commons Attribution (CC BY) license (<http://creativecommons.org/licenses/by/4.0/>).

Proceedings

# A Machine Learning Approach for DDoS (Distributed Denial of Service) Attack Detection Using Multiple Linear Regression †

Swathi Sambangi \* and Lakshmeeswari Gondi \* 

Department of Computer Science and Engineering, GITAM University, Visakhapatnam, Andhra Pradesh 530045, India

\* Correspondence: ssambangi555@gmail.com (S.S.); gondi.lakshmeeswari@gmail.com (L.G.)

† Presented at the 14th International Conference INTER-ENG 2020 Interdisciplinarity in Engineering, Mures, Romania, 8–9 October 2020.

Published: 25 December 2020



**Abstract:** The problem of identifying Distributed Denial of Service (DDoS) attacks is fundamentally a classification problem in machine learning. In relevance to Cloud Computing, the task of identification of DDoS attacks is a significantly challenging problem because of computational complexity that has to be addressed. Fundamentally, a Denial of Service (DoS) attack is an intentional attack attempted by attackers from single source which has an implicit intention of making an application unavailable to the target stakeholder. For this to be achieved, attackers usually stagger the network bandwidth, halting system resources, thus causing denial of access for legitimate users. Contrary to DoS attacks, in DDoS attacks, the attacker makes use of multiple sources to initiate an attack. DDoS attacks are most common at network, transportation, presentation and application layers of a seven-layer OSI model. In this paper, the research objective is to study the problem of DDoS attack detection in a Cloud environment by considering the most popular CICIDS 2017 benchmark dataset and applying multiple regression analysis for building a machine learning model to predict DDoS and Bot attacks through considering a Friday afternoon traffic logfile.

**Keywords:** DDoS attack; multiple linear regression; traffic packet; classification; Cloud

## 1. Introduction

Historically, Denial of Service (DoS) attacks are intended primarily to disrupt computing systems in a network. Fundamentally, these attacks are initiated from a single machine with the illegitimate intention of targeting a server system through an attack. A simple DoS attack could be a PING Flood attack in which the machine sends ICMP requests to the target server and a more complex DoS attack example could be Ping of death attack. DDoS (Distributed Denial of Service) attacks are postcursor to DoS attacks, i.e., DoS attacks are forerunner to DDoS attacks. DDoS attacks are the attacks which are carried in distributed environments. Fundamentally, a DDoS attack is an intentional attack type which is usually made in a distributed computing environment by targeting a website or a server so as to minimize their normal performance. To achieve this, an attacker uses multiple systems in a network. Now, using these systems, the attacker makes an attack on the target website or server by making multiple requests to the target system or server. As these types of attacks are carried out in distributed environments, hence, these are also called distributed DDoS attacks.

The conventional way of DDoS attacks is the brute force attack that is triggered using Botnet wherein the devices of the network environment are infected with malware. Based on the target and the behavior, we may classify DDoS attacks into three categories. Thus, though DDoS attacks could be categorized into several types, usually these attacks are mainly classified into three classes. They are



(i) Traffic/fragmentation attack, (ii) Bandwidth/Volume attack and (iii) Application attack as shown in Figure 1. In traffic-based attacks, voluminous UDP or TCP packets are sent to the target system by the attacker and these huge UDP or TCP packets reduce the system performance. In the second type of attack called bandwidth or volumetric attacks, the attacker creates congestion in bandwidth through consuming excessive bandwidth than required legitimately and they also try to flood the target system through sending large amounts of anonymous data. The last type of attack are also specialized attacks as they are aimed at attacking only a specific system or a network. These types of attacks are also difficult to mitigate and throw greater challenges in recognizing them.

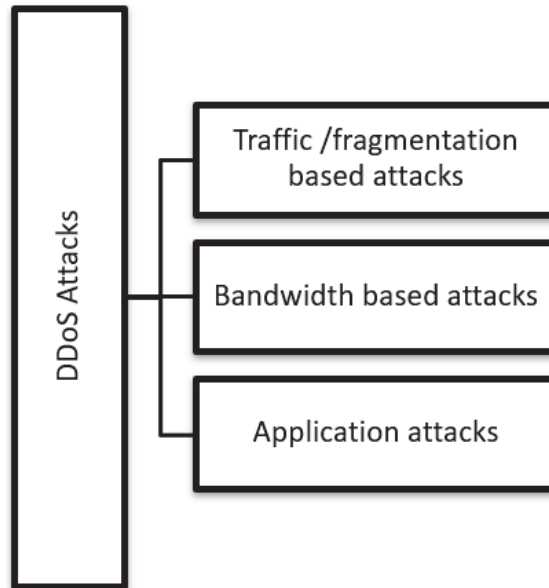


Figure 1. Classification of DDoS ((Distributed Denial of Service) attacks.

In general, a Denial of Service attack, which is usually called a DoS attack, is a purposeful attempt which is initiated so as to make an application or website unavailable to its legitimate users. This is achieved usually by flooding the website or application through network traffic. In order to achieve this, usually, one of the several choices of attackers is to apply diversified techniques that intentionally consume huge network bandwidth, thus causing inconvenience to legitimate users. Alternately, attackers also achieve this by handling system resources in an illegitimate manner. DoS attack is also called Non-distributed Directed attack wherein an attacker initiates DoS attack on the target system. The concept of DDoS attack is similar to DoS attack but the fundamental difference is that in DDoS attacks there are multiple attack sources which are implicitly involved, i.e., in DDoS attacks, the attacker makes an attack by using multiple sources which may include routers, IoT devices, and computers in a distributed environment infected by malware. To make this possible, an attacker looks for availability of any compromised network. By utilizing such compromised networks, an attacker usually attacks the target system through continuously generating packet floods or requests to conquer the target system. The DDoS attacks are common in the Network layer, Transport layer, Presentation and Application layer of the 7-layer OSI reference model. Network layer and Transport layer attacks are usually called Infrastructural attacks whereas the Presentation layer and Application layer attacks are commonly known as Application layer attacks.

## 2. Related Works

At an abstract level, one may view a DDoS attack as a clogged unexpected traffic on the highway so as to prevent the regular traffic flow arrival at its destination. DDoS attacks are usually performed through the use of a network of connected machines which are all connected via internet. The main problem with these types of attacks is the difficulty in discriminating between normal traffic and attack traffic as each Bot acts as if it is a legitimate one. DDoS attacks not only affect servers in distributed environments but also do not leave Cloud environments. DDoS attacks take the advantage of the services provided by Cloud environment such as (i) pay-as-you-go (ii) auto scaling and (iii) multi-tenancy. In a typical Cloud infrastructure, Virtual machines (VMs) are run in large numbers by Cloud servers to provide uninterrupted services to legitimate users of the Cloud environment. Now, in an event of an attack by attackers, the server can consider this situation as an event of higher resource utilization. The result would be the server trying to utilize an auto scaling feature in Cloud computing. The result of auto scaling feature could be allocation of resources, and migration of resources so as to solve the server overloading problem. Now, assume that resource allocation and process migration continues as a result of an attack, then, the attacker eventually becomes successful in DDoS attack that was initiated and that such an attack affects either directly or indirectly the Cloud services and eventually implicates the financial revenues. Some of the DDoS attacks in Cloud environment are Buffer overflow, SYN flooding, Ping of death, IP spoofing and land attack. DDoS attack defence in Cloud environments may be achieved by using three methods which include (i) Preventing attacks in the first place, (ii) Detecting the attacks and (iii) Mitigation of attacks. Anomaly detection and Botnet detection techniques are used for preventing and detecting a DDoS attack.

Denial of Service and Distributed Denial of Service attacks are the important sources that make internet services vulnerable. Attack detection is not new in using machine learning techniques. Some of the attacks that are identified through machine learning techniques are signature-based and anomalies-based. From ref. [1], it is learnt that signatures are used for signature-based Intrusion detection system, while detecting unknown attacks are the part of anomaly detection, whereas data flows generated by the unknown patterns gives the scope for studying DDoS. DDoS attacks can be prevented. Attacks are defined as violations of security policies of the network. Usually the attacks are classified into passive and active attacks. Passive attacks never affect the system but active attacks take control of system. The most frequent attacks in real-time network are Denial of Service (DoS) attacks. When a DoS attack is deployed into legitimate systems in a distributed environment, it is further considered as a Distributed Denial of Service (DDoS) attack. Distributed Denial of Service attack is where multiple systems try to target one single system. By flooding the messages to the target system, the services in the systems are denied and considered as zombies [1]. Some of the types of DDoS attacks are Flooding, IP Spoofing, TCP SYN Flood, PING Flood, UDP Flood, and Smurf attacks. Multiple machines are used to construct flooding in DDoS attacks.

- TCP SYN Flood attacks—The attack that spoofs the IP addresses is called TCP SYN Flood attack. This attack is more vulnerable as this is based on 3-way handshake protocol [2].
- PING Flood attacks—PING attacks are based on packets of ICMP request. As the PING attack targets the system, the connection slows down and reply request packets cannot be communicated from the end users.
- UDP Flood attacks—Target system cannot handle authorized connection once the threshold limit is reached. As the servers reach the threshold limits, the other packet requests are discarded.
- SMURF attacks—This attack occurred because of spoofed PING messages. By pinging the IP address, huge ICMP requests are received, further, more bandwidth will be consumed which slows down the computer to work.

The detections are divided into two steps: IP Entropy and Traffic collection module to extract entries and messages to detect DDoS attacks. Over the recent years, it has notified that many DDoS attacks incurred losses in heavy downtime, business loss, etc. One of the recent attacks where Amazon

EC2 Cloud servers attacked were by DDoS attacks [3]. The present hot topic across the area of research is to mitigate the DDoS attacks using machine learning techniques. Some of the recent works also have used Support Vector Machine technique to mitigate the DDoS [4]. Many machine learning methods like Naïve Bayes, SVM, and Decision trees were proposed to detect Distributed Denial of Service attacks. However, to detect this DDoS attacks using machine learning methods requires prerequisites on the network to identify the suitable data from the datasets [5,6]. Most of the common machine learning methods used in detecting the DDoS attacks are Convolutional Neural Networks [7], Long Short-term memory neural networks [8], Recurrent neural networks [9], etc. Over the years, the most widely used methods to detect Intrusion detection with DoS and DDoS attacks are based on machine learning algorithms. One such algorithm where the results were accurate and efficient in detecting the DDoS attack was using Decision Tree C4.5 algorithm [10]. Liao et al. [11] proposed a scheme based on SVM to detect the DDoS attacks using detection scheme base algorithm. Xiao et al. [12] proposed the most frequently used kNN algorithm for detecting the different types of anomalies in the network. By using the kNN algorithm, a maximum number of bots in the network were identified. Accuracy was improved compared to any algorithm in detecting the unknown attacks. In ref. [12], the author proposes a new method to detect the DDoS attack using Radial basis function (RBF) using neural networks algorithms. This RBF algorithm is used to classify the attacks as normal and abnormal. From the past study, it is identified that many clustering algorithms and a priori association algorithms are used to extract network traffics and packets [13,14]. Ref. [15] describes the detection of attacks using classification algorithms to monitor the incoming and outgoing packets in the network and also to compile the TCP SYN and ACK flags in the network. Ref. [16] used Artificial Neural networks to detect the DDoS attacks by comparing Decision Tree, Entropy, ANN and Bayesian algorithms. Further, in ref. [17], many researchers discovered that to detect different DDoS attacks, the separation of Flash Crowd event from Denial of Service attack is to be performed. One of the important approaches towards the DDoS attacks are SNORT and configurable firewall. Additionally, in ref. [18], it is shown that SNORT is used to reduce the false alarm rates to improve the accuracy in Intrusion prevention system. By having an impact on the real-time networks using Cloud Environment, the security services are blocked if the valid document is not used to detect intrusions. The proposed method in ref. [19] aims to detect DDoS attacks by statistical analysis of network traffic and Gaussian Naïve Bayes method is applied on training data for classification. The DDoS attacks are performed on various machines with two main methods. The first method is by sending the malformed packets to the victim and the second method is by performing either by exhausting the bandwidth or applying application level flooding [20]. In 2011, Lee et al. [21] proposed DoS attacks using Hadoop Framework. Ref. [21] used a counter-based detection algorithm to detect HR attacks using MapReduce algorithm. Many researchers have been using the Hadoop clusters in the Cloud computing platforms. Hadoop framework's job is only to monitor the data or packets. Many researchers have used the machine learning methods in order to create and view the DDoS attacks. Most often from the research, FireCol is the algorithm that is used to protect from flooding the DDoS attacks [22]. To detect the intrusion in DDoS attacks in the system, different classifiers like Ensemble reducing features, Heterogeneous and Homogeneous, are used for Ensemble methods [23]. Machine learning methods can also use to detect the DDoS in software-defined network. The study says that some of the issues were identified in the large network dataset for abnormal traffic using feature selection method to detect DDoS attacks. The most widely used approaches are feature ranking, scalability, and distributed approach.

### 3. Emerging Need for DDoS Attack Detection in Cloud Environments

The problem of DDoS attack prevention, detection and mitigation has received significant importance in relevance to Cloud computing environment. Of these three issues, the problem of DDoS attack detection has received primary importance from researchers. Researchers across the globe have been continuously working on proposing various methods and approaches to address detection of DDoS attacks. In spite of the availability of various contributions that addressed methods

and techniques to put a stop to DDoS attacks, unfortunately, even today the deployment of the available methods could not resist the DDoS attacks affecting the Cloud environments. In fact, they are substantially increasing over time in terms of the frequency of attacks and also the attack size. One of the most common reasons is there is no consensus among various end points in a distributed internet network as one cannot enforce cooperation globally. The second reason could be the socioeconomic factors involved which makes the global cooperation enforcement difficult. The third point comes from the nature of DDoS attacks, i.e., there is no way of ensuring and enforcing a single point deployment so as to best ensure the defence against the DDoS attacks.

As per reports by Amazon Web Services, to date, the biggest DDoS attack that took place is in the month of February in the year 2020. The peak incoming traffic of this attack is seen to be 2.3 Tbps. The choice of attackers for making this attack was hijacked CLDAP web servers (Connection-less Lightweight Directory Access Protocol web servers) which is alternative to LDAP and is also a protocol used for handling user directories. Before this 2.3 Tbps DDoS attack in February of 2020, the second largest DDoS attack was the 1.3 Tbps DDoS attack—the one which targeted GitHub through sending 126.9 million traffic packets per second. Thus, there is an emerging immediate need to properly study, identify and figure out the reasons for failure of the available methods in the research literature.

#### 4. DDoS Attack Detection Framework Using Multiple Linear Regression

The fundamental research objective behind the proposed method is to design a machine learning model based on multiple linear regression analysis and also perform data visualization by considering residual plots and fit charts. The idea behind the proposed approach is to study the possibility of applying multiple linear regression analysis to the CICIDS 2017 dataset which is the benchmark dataset widely used in some of the most significant recent research studies. The objective is to first apply the feature selection technique and determine the important attributes that are better deliverables for the prediction model. In the present approach shown in Figure 2, we have used the Information Gain approach method for carrying feature selection. Information Gain approach is a widely applied model in several data mining-based applications. The selected features are then considered for carrying multiple linear regression analysis, and the behavior of chosen and retained important attributes of the CICIDS 2017 dataset is studied by analyzing the fit charts and residual plots. The next subsection gives the experiment result analysis using the proposed approach by considering Friday log files of the most popular CICIDS 2017 research dataset.

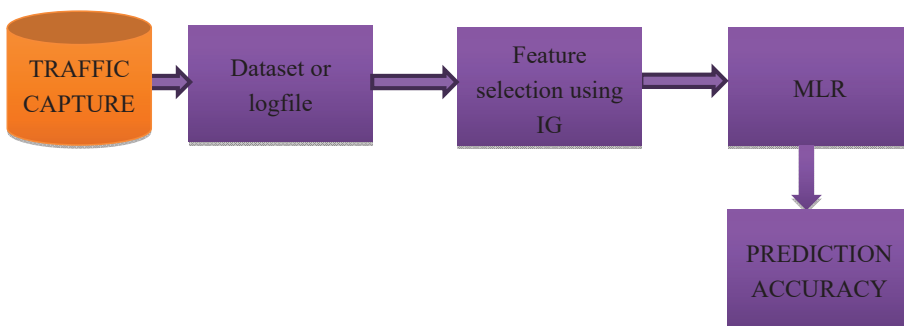


Figure 2. Proposed Machine Learning approach for DDoS attack detection.

#### 5. Experiment Result Analysis

The dataset chosen for experimentation consisted of five-day log records from Monday to Friday in csv format. For experiment analysis, we have considered the log file of Friday afternoon which also consisted of two class labels. The class labels are Benign (Normal) and DDoS (attack). The total number of traffic packets in the log file included 225,746 traffic packets.

Experiment Analysis for the Log File of Friday Afternoon with Class Labels as Benign (Normal) and DDoS (Attack)

Initially, the number of attributes in the Friday afternoon logfile are 78 with the last attribute being the class label, i.e., there are 79 dimensions along with class label. Initially, the modeling process started by application of feature selection algorithm which is based on computation of information gain for each of the attributes in the dataset. The top 16 attributes have been considered for retention and other attributes in the attribute set are removed. Figure 3 depicts the entire details of ANOVA model and the list of the top 16 attributes with higher information gain are listed in Figure 4. For mathematical modeling, we chose to perform multiple linear regression analysis by running regression analysis on the logfile with these 16 attributes. After initial analysis is carried, the attributes that are retained include the attributes at dimensions 1, 5, 6, 7, 9, 11, 13, 35, 36, 53, 54, 55, 56, 64,66 and 67. The analysis is thus performed using the reduced dimensionality log file with these 16 attributes as mentioned above. The mean absolute percentage error for the linear regression model is obtained as 0.2621. Hence, the percentage accuracy of the multiple linear regression model is obtained as equal to 73.79%, i.e., 0.7379.

Figure 5 shows the residual plot obtained for each of the 16 attributes of the CICIDS 2017 dataset w.r.t Friday afternoon log file. Figure 6 shows the residual plot and Figure 7 shows the fit chart for the overall multiple linear regression model. After the initial model is developed, then, we have eliminated 10 attributes which are not statistically significant and retained the remaining six attributes. So, the number of attributes is now reduced to six attributes. The attribute dimensions are 1, 9, 13, 53, 54, and 64. Then, the multiple regression analysis is performed once again on these statistically significant attributes. Figure 8 depicts the fit chart, visualizing the actual label and predicted label. Figure 9 shows these six attributes’ residual plots and finally, Figure 10 depicts the residual plot for the model. Thus, the machine learning model accuracy obtained using these six attributes is 71.6% which also clearly shows that the first model with 16 attributes is comparatively better.

ANOVA					
	df	SS	MS	F	Significance F
Regression	16	29778.18946	1861.136841	23832.54328	0
Residual	225733	25640.72297	0.113588722		
Total	225749	55418.91243			

	Coefficients	Standard Error	t Stat	P-value	Lower 95%	Upper 95%	Lower 95.0%	Upper 95.0%
Intercept	1.480163181E0	1.214964E-3	1.218277377E3	0	1.477781883E0	1.48254448E0	1.477781883E0	1.48254448E0
Destination Port	-7.95866E-06	5.07513E-08	-1.568157955E2	0	-8.05807E-06	-7.85913E-06	-8.05807E-06	-7.85913E-06
Total Length of Fwd Packets	0	0	6.5535E4	#NUM!	0	0	0	0
Total Length of Bwd Packets	3.09845E-06	6.49544E-08	4.770183338E1	#NUM!	2.97114E-06	3.22576E-06	2.97114E-06	3.22576E-06
Fwd Packet Length Max	8.64604E-06	1.1702E-06	7.388505992E0	1.48996E-13	6.35248E-06	1.09396E-05	6.35248E-06	1.09396E-05
Fwd Packet Length Mean	0	0	6.5535E4	#NUM!	0	0	0	0
Bwd Packet Length Max	2.86673E-06	7.00377E-07	4.093126063E0	#NUM!	1.49401E-06	4.23945E-06	1.49401E-06	4.23945E-06
Bwd Packet Length Mean	7.06531E-05	3.26813E-06	2.161880723E1	1.5235E-103	6.42476E-05	7.70585E-05	6.42476E-05	7.70585E-05
Fwd Header Length	0	0	6.5535E4	#NUM!	0	0	0	0
Bwd Header Length	-5.97066E-4	5.71258E-06	-1.045177417E2	#NUM!	-6.08262E-4	-5.85869E-4	-6.08262E-4	-5.85869E-4
Average Packet Size	2.81867E-4	4.07743E-06	6.912847606E1	n	2.73875E-4	2.89858E-4	2.73875E-4	2.89858E-4
Avg Fwd Segment Size	-1.49379E-4	4.89145E-06	-3.053887974E1	2.0805E-204	-1.58966E-4	-1.39792E-4	-1.58966E-4	-1.39792E-4
Avg Bwd Segment Size	0	0	6.5535E4	#NUM!	0	0	0	0
Fwd Header Length	4.1925E-4	7.04326E-06	5.952493054E1	#NUM!	4.05445E-4	4.33054E-4	4.05445E-4	4.33054E-4
Subflow Fwd Bytes	-3.81369E-06	4.82535E-07	-7.903452827E0	2.72494E-15	-4.75944E-06	-2.86793E-06	-4.75944E-06	-2.86793E-06
Subflow Bwd Bytes	0	0	6.5535E4	#NUM!	0	0	0	0
Init_Win_bytes_forward	-1.24761E-05	9.91958E-08	-1.257727911E2	#NUM!	-1.26706E-05	-1.22817E-05	-1.26706E-05	-1.22817E-05

Figure 3. p-value and confidence intervals—ANOVA for CICIDS2017 Dataset.

S.NO	ATTRIBUTE NAME	INFORMATION GAIN	ATTRIBUTE DIMENSION IN CICIDS2017 DATASET
1	TotalLengthofFwdPackets	0.939343	5
2	SubflowFwdBytes	0.939343	64
3	AveragePacketSize	0.80995	53
4	TotalLengthofBwdPackets	0.782456	6
5	SubflowBwdBytes	0.782456	66
6	BwdPacketLengthMean	0.781841	13
7	AvgBwdSegmentSize	0.781841	55
8	forwardheaderLength	0.778016	56
9	forwardheaderLength1	0.778016	35
10	DestinationPort	0.77582	1
11	BwdPacketLengthMax	0.760317	11
12	Init_Win_bytes_forward	0.708411	67
13	AvgFwdSegmentSize	0.706064	54
14	FwdPacketLengthMean	0.706064	9
15	FwdPacketLengthMax	0.701009	7
16	BwdHeaderLength	0.682524	36

Figure 4. Attributes along with their information gains.

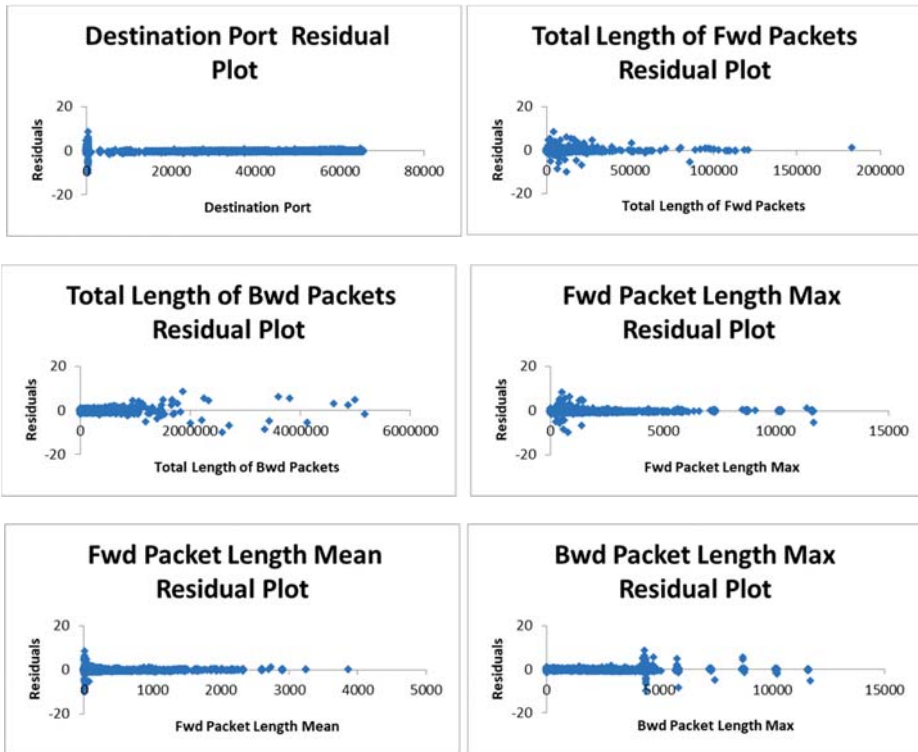


Figure 5. Cont.

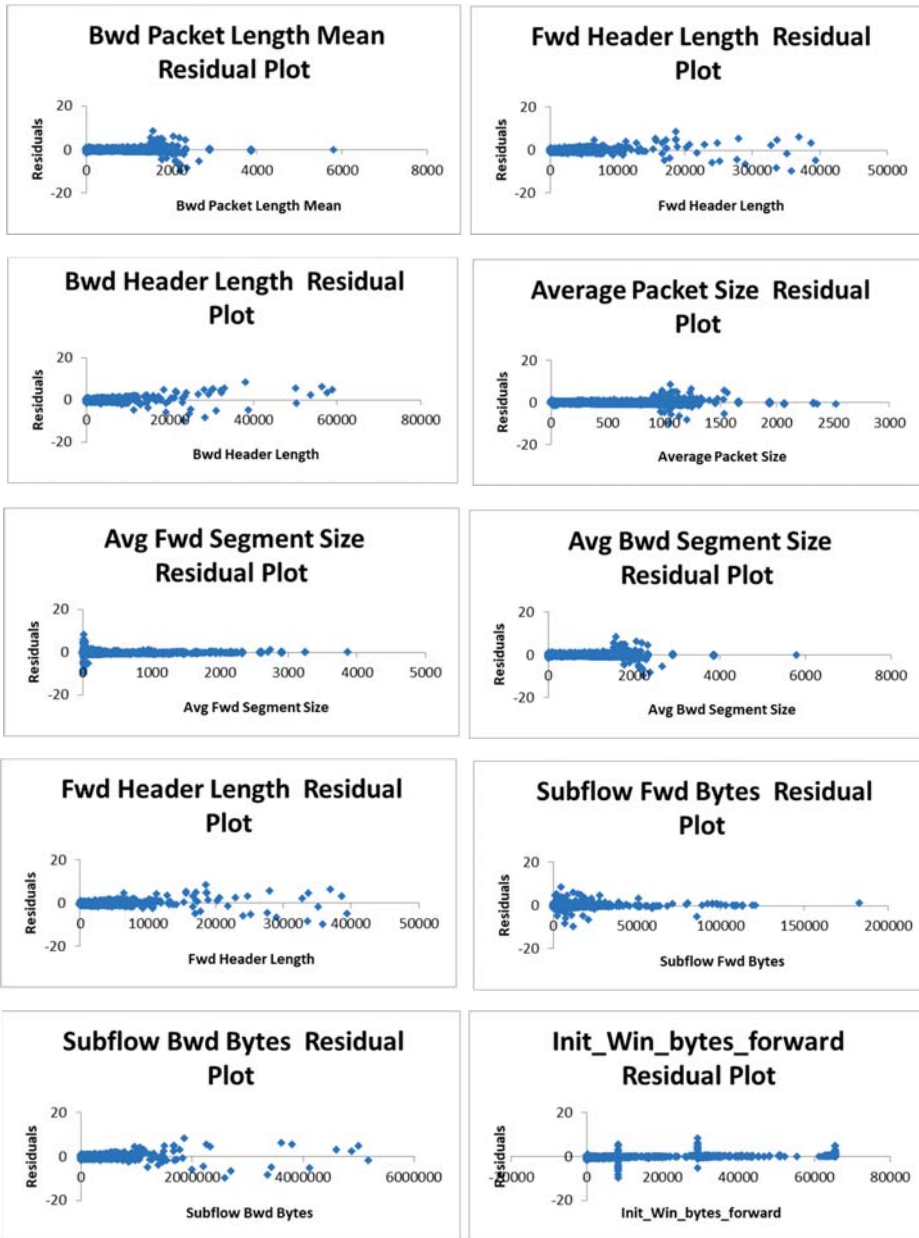


Figure 5. Residual plots for 16 attributes of Friday afternoon log of CICIDS 2017 dataset.



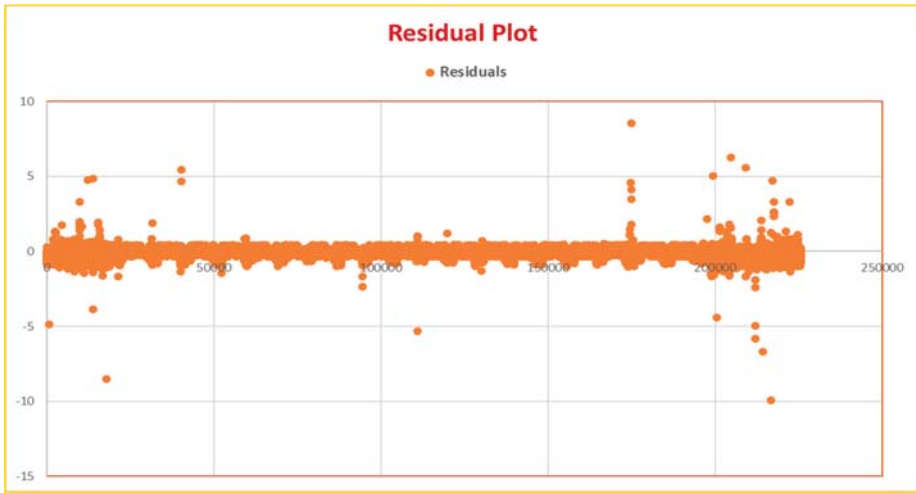


Figure 6. Residual plot obtained for multiple linear regression model for CICIDS 2017 dataset.

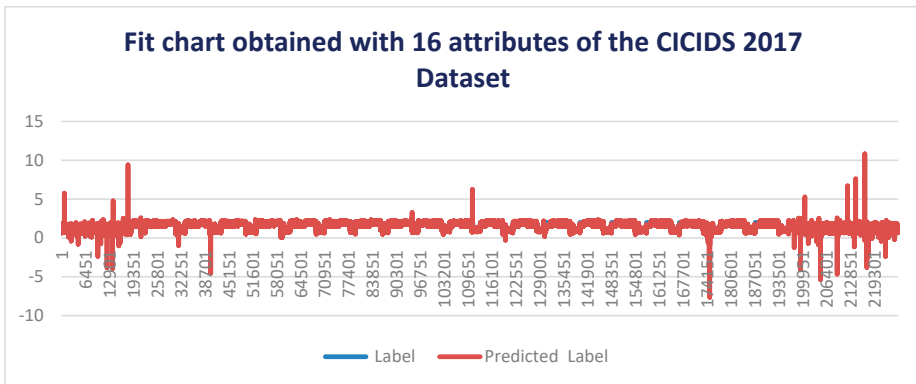


Figure 7. Fit chart obtained for Friday afternoon logfile of CICIDS 2017 dataset.

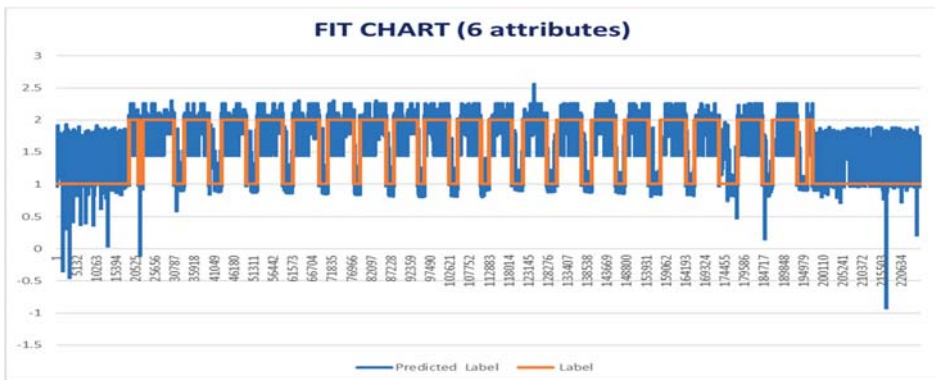


Figure 8. Fit chart obtained for Friday afternoon logfile of CICIDS 2017 dataset by considering 1, 9, 13, 53, 54, and 64 attributes.



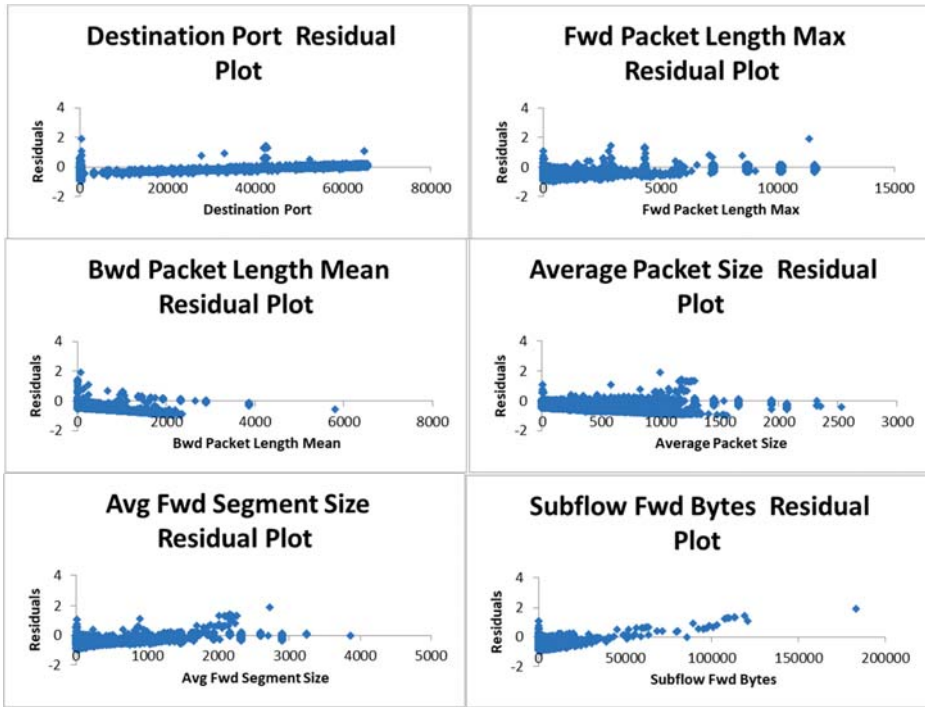


Figure 9. Residual plots for six attributes of Friday afternoon log of CICIDS 2017 dataset.

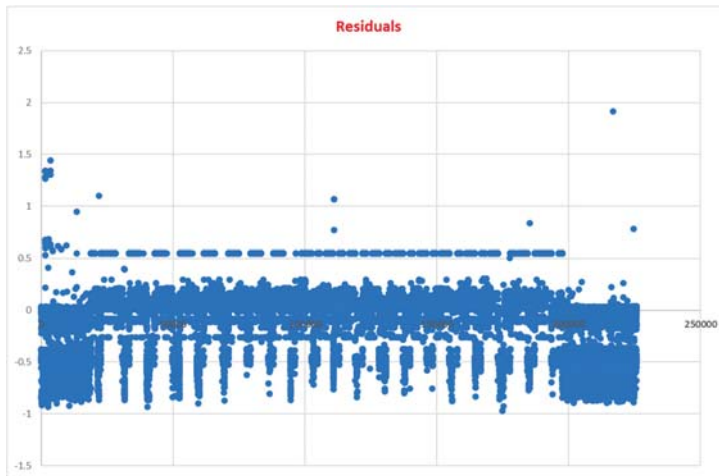


Figure 10. Residual plot obtained for multiple linear regression model for CICIDS 2017 dataset by considering six attributes of the dataset.

It can be seen from the experiment result analysis that the fit chart obtained by carrying multiple regression analysis on CICIDS 2017 dataset with the top 16 attributes obtained through information gain-based feature selection method is better than the fit chart obtained through considering six attributes of the CICIDS 2017 dataset. This is because of the fact that in the later fit chart, the difference between

actual label and predicted label is clearly visible. Hence, the first model considered with 16 attributes is better for carrying the detection of DDoS attacks.

## 6. Conclusions

As detection of DDOS attack has become more common in a distributed environment like Cloud, it is essential to detect the attacks which cause service unavailability of Cloud. To identify such attacks, machine learning models can be used to train and test the attack detection datasets. Alternately, we can use the regression analysis technique by applying one of its important variants known as multiple linear regression analysis. The research objective behind this study is to build a machine learning model that is an ensemble of feature selection using information gain and regression analysis. For experimental study, the dataset considered was in the popularly known CICIDS 2017 dataset. Specifically, the Friday logfile of morning and afternoon are considered which has Benign, Bot and DDoS classes. It has been observed that through this ensemble model for Friday morning dataset, a prediction accuracy of 97.86% is achieved. Similarly, for the Friday afternoon log file, the prediction accuracy is obtained as 73.79% for 16 attributes obtained through information gain-based feature selection and regression analysis-based ML model. This paper thus paved a way to show the importance of regression analysis in building an ML model and also shows some of the important visualizations such as residual plots and fit chart which proves the importance of the model and its suitability of considering the model for prediction. In this work, we have limited our analysis for one-day log file and in future, this research may be extended to consider all traffic log files of fivedays and come out with a consensus-based machine learning model.

## References

- Dayanandam, G.; Reddy, E.S.; Babu, D.B. Regression algorithms for efficient detection and prediction of DDoS attacks. In Proceedings of the 2017 3rd International Conference on Applied and Theoretical Computing and Communication Technology (iCATecT), Tumkur, India, 21–23 December 2017; pp. 215–219. [\[CrossRef\]](#)
- Sharma, N.; Mahajan, A.; Mansotra, V. Machine Learning Techniques Used in Detection of DOS Attacks: A Literature Review. *Int. J. Adv. Res. Comput. Sci. Softw. Eng.* **2016**, *6*, 100.
- Somani, G.; Gaur, M.S.; Sanghi, D.; Conti, M.; Buyya, R. DDoS attacks in cloud computing: Issues, taxonomy, and future directions. *Comput. Commun.* **2017**, *107*, 30–48. [\[CrossRef\]](#)
- Perera, P.; Tian, Y.-C.; Fidge, C.; Kelly, W. A Comparison of Supervised Machine Learning Algorithms for Classification of Communications Network Traffic. In *International Conference on Neural Information Processing*; Springer: Cham, Switzerland, 2017; pp. 445–454.
- Zammit, D. A Machine Learning Based Approach for Intrusion Prevention Using HoneyPot Interaction Patterns as Training Data. Bachelor’s Thesis, University of Malta, Msida, Malta, 2016.
- Doshi, R.; Apthorpe, N.; Feamster, N. Machine Learning DDoS Detection for Consumer Internet of Things Devices. *arXiv* **2018**, arXiv:1804.04159.
- Hochreiter, S.; Schmidhuber, J. Long Short-Term Memory. *Neural Comput.* **1997**, *9*, 1735–1780. [\[CrossRef\]](#) [\[PubMed\]](#)
- Chung, J.; Gulcehre, C.; Cho, K.; Bengio, Y. Empirical evaluation of gated recurrent neural networks on sequence modeling. In Proceedings of the NIPS 2014 Deep Learning and Representation Learning Workshop, Montreal, QC, Canada, 12 December 2014.
- Breitenbacher, D.; Elovici, Y. N-BaIoT—Network-Based Detection of IoT Botnet Attacks Using Deep Autoencoders. *IEEE Pervasive Comput.* **2018**, *17*, 12–22.
- Zekri, M.; El Kaffali, S.; Hanini, M.; Aboutabit, N. Mitigating Economic Denial of Sustainability Attacks to Secure Cloud Computing Environments. *Trans. Mach. Learn. Artif. Intell.* **2017**, *5*, 473–481. [\[CrossRef\]](#)
- Liao, Q.; Li, H.; Kang, S.; Liu, C. Application layer DDoS attack detection using cluster with label based on sparse vector decomposition and rhythm matching. *Secur. Commun. Netw.* **2015**, *8*, 3111–3120. [\[CrossRef\]](#)
- Xiao, P.; Qu, W.; Qi, H.; Li, Z. Detecting DDoS attacks against data center with correlation analysis. *Comput. Commun.* **2015**, *67*, 66–74. [\[CrossRef\]](#)

13. Karimazad, R.; Faraahi, A. An anomaly-based method for ddos attacks detection using rbf neural networks. In Proceedings of the International Conference on Network and Electronics Engineering, Hong Kong, China, 25–27 November 2011; pp. 16–18.
14. Zhong, R.; Yue, G. Ddos detection system based on data mining. In Proceedings of the 2nd International Symposium on Networking and Network Security, Jinggangshan, China, 2–4 April 2010; pp. 2–4.
15. Wu, Y.-C.; Tseng, H.-R.; Yang, W.; Jan, R.-H. Ddos detection and traceback with decision tree and grey relational analysis. *Int. J. Ad Hoc Ubiquitous Comput.* **2011**, *7*, 121–136. [[CrossRef](#)]
16. Li, H.; Liu, D. Research on intelligent intrusion prevention system based on Snort. In Proceedings of the International Conference on Computer, Mechatronics, Control and Electronic Engineering (CMCE), Changchun, China, 24–26 August 2010; Volume 1, pp. 251–253.
17. Chen, J.-H.; Zhong, M.; Chen, F.-J.; Zhang, A.-D. DDoS defense system with turing test and neural network. In Proceedings of the IEEE International Conference on Granular Computing (GrC), Hangzhou, China, 11–13 August 2012; pp. 38–43.
18. Ibrahim, L.M. Anomaly network intrusion detection system based on distributed time-delay neural network (dtdnn). *J. Eng. Sci. Technol.* **2010**, *5*, 457–471.
19. Fadil, A.; Riadi, I.; Aji, S. Review of Detection DDOS Attack Detection Using Naive Bayes Classifier for Network Forensics. *Bull. Electr. Eng. Inform.* **2017**, *6*, 140–148. [[CrossRef](#)]
20. Zargar, S.T.; Joshi, J.B.; Tipper, D. A Survey of Defense Mechanisms Against Distributed Denial of Service (DDoS) Flooding Attacks. *IEEE Commun. Surv. Tutor.* **2013**, *15*, 2046–2069. [[CrossRef](#)]
21. Gupta, B.B.; Misra, M.; Joshi, R.C. FVBA: A combined statistical approach for low rate degrading and high bandwidth disruptive DDoS attacks detection in ISP domain. *IEEE Int. Conf. Netw.* **2008**, 1–4. [[CrossRef](#)]
22. Francois, J.; Aib, I.; Boutaba, R. FireCol: A Collaborative Protection Network for the Detection of Flooding DDoS Attacks. *IEEE/ACM Trans. Netw.* **2012**, *20*, 1828–1841. [[CrossRef](#)]
23. Jia, B.; Huang, X.; Liu, R.; Ma, Y. A DDoS Attack Detection Method Based on Hybrid Heterogeneous Multiclassifier Ensemble Learning. *J. Electr. Comput. Eng.* **2017**, *2017*, 1–9. [[CrossRef](#)]


**Publisher's Note:** MDPI stays neutral with regard to jurisdictional claims in published maps and institutional affiliations.



© 2020 by the authors. Licensee MDPI, Basel, Switzerland. This article is an open access article distributed under the terms and conditions of the Creative Commons Attribution (CC BY) license (<http://creativecommons.org/licenses/by/4.0/>).

Article

# UWB-MMIC Matrix Distributed Low Noise Amplifier †

Moustapha El Bakkali \* , Said Elkhaldi, Intissar Hamzi, Abdelhafid Marroun and Naima Amar Touhami

Faculty of Sciences, Abdelmalek Essaâdi University, BP.2121 M'Hannech II, Tetuan 93030, Morocco; saidelkhaldi@gmail.com (S.E.); Hamzi.intissar@gmail.com (I.H.); abdelhafid.marroun@gmail.com (A.M.); Nai\_amar@yahoo.fr (N.A.T.)

\* Correspondence: moustapha.elbakkali@etu.uae.ac.ma; Tel.: +212-628-725-127

† Presented at the 14th International Conference INTER-ENG 2020 Interdisciplinarity in Engineering, Mureş, Romania, 8–9 October 2020.

Published: 25 December 2020

**Abstract:** In this paper, a 3.1–11 GHz ultra-wideband low noise amplifier with low noise figure, high power gain  $S_{21}$ , low reverse gain  $S_{12}$ , and high linearity using the OMMIC ED02AH process, which employs a 0.18  $\mu\text{m}$  Pseudomorphic High Electron Mobility Transistor is presented. This Low Noise Amplifier (LNA) was designed with the Advanced Design System simulator in distributed matrix architecture. For the low noise amplifier, four stages were used obtaining a good input/output matching. An average power gain  $S_{21}$  of 11.6 dB with a gain ripple of  $\pm 0.6$  dB and excellent noise figure of 3.55 to 4.25 dB is obtained in required band with a power dissipation of 48 mW under a supply voltage of 2 V. The input compression point 1 dB and third-order input intercept point are  $-1.5$  and 23 dBm respectively. The core layout size is  $1.8 \times 1.2 \text{ mm}^2$ .

**Keywords:** Matrix Distributed LNA; MMIC; GaAs; pHEMT; Noise Figure

---

Published: 25 December 2020

## 1. Introduction

With the growth of technological needs, especially in wireless communication, it was imperative for researchers to find and develop more structures compatible with modernity and which are aligned with global standards. In this context, we mention ultra-wideband (UWB) systems which were a source of interest for the most important industrial companies and institutes during the sixties of the previous century. As for recent years, these systems have several advantages, such as, high data rate transmission [1], high flexibility [2,3], low power spectra density [4], security [5], single chip architecture with small size, low cost and low power requirements [6]. Thus, systems performances are enhanced. According to Federal Communication Commission (FCC), UWB can be used in the field imaging systems (medical systems, Global Positioning Systems (GPS) and surveillance systems) or communications and measurement systems or vehicular Radar systems, allocating them a frequency domain of 3.1 to 10.6 GHz [7]. A critical component of UWB system is the Low Noise Amplifier, which aims to reduce the noise figure with large gain, low power consumption and stability necessary for eliminating self-oscillation [8].

The first distributed amplifier was studied in 1948 from pentode tubes [9]. The originality of principle lies in the fact that we got to take this advantage by the active elements in parallel while avoiding the disadvantages of reducing the input and output impedances. In distributed amplifiers, the active elements are placed between two propagation lines which carry out both an addition of the currents and adaptation to the source and to the load.

Today, distributed amplifiers have become good candidates for providing flat gain in a sufficiently wide band [10]. Monolithic microwave integrated circuit or MMIC technology seems a priori, the best suited to achieve this objective.

This paper is organized as follows. In Section 2, the characteristics of the ED02AH transistor device and the MMIC process will be presented. Section 3 gives a description of the proposed circuit and design considerations. Section 4 will discuss the results of a post-implementation simulation of proposed design techniques and compare them with those recently performed. The conclusion of this work will be presented in Section 5.

## 2. Device Characteristics and MMIC Process

OMMIC ED02 commercial foundry provides several models for pseudomorphic High Electron Mobility transistors (pHEMTs) in the ED02AH technology. This uses six gate segments of 15  $\mu\text{m}$  width each ( $6 \times 15 \mu\text{m}$  ED02AH) as shown in Figure 1. Small signal linear models are given by scattering parameters versus bias points of a transistor. Nonlinear models include noises sources usually developed by manufacturers (Kacprzak and Materka model [11], Triquint foundry model [12], etc.).

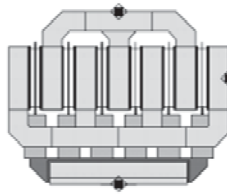


Figure 1. ED02AH  $6 \times 15 \mu\text{m}$  layout.

The typical results of the data comparison between the non linear and small signal model are shown in Figure 2 for the bias point  $I_D = 16 \text{ mA}$  and  $V_{DS} = 2 \text{ V}$ .

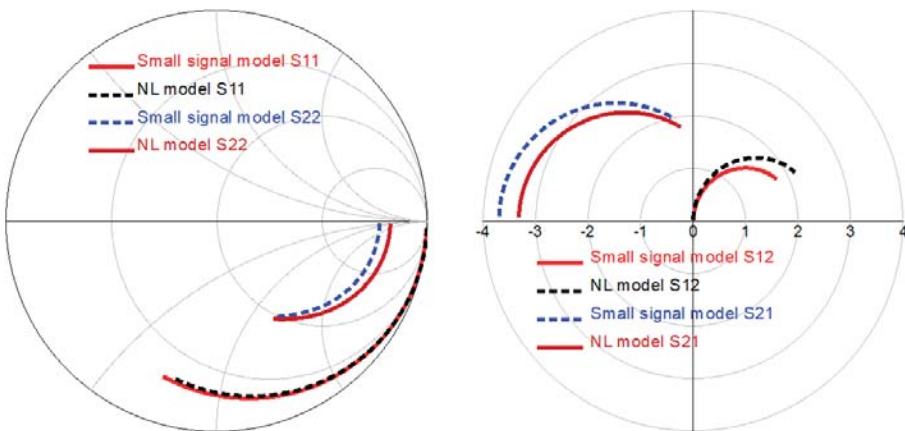


Figure 2. Scattering parameters comparison of linear and NL ED02AH models transistor in frequency range of 0.5 to 30 GHz ( $V_{gs} = -0.3 \text{ V}$  and  $V_{ds} = 2 \text{ V}$ ).

The error of the input and output reflection coefficients ( $S_{11}$  and  $S_{22}$ ) of the two models is weak compared to the direct and inverse gain parameters ( $S_{21}$  and  $S_{12}$ ) which can be as high as 30% when the frequency becomes larger. These Monolithic Microwave Integrated Circuit (MMIC) chips are fabricated with 0.18  $\mu\text{m}$  pseudomorphic GaAs based HEMT technology, carried out by commercially available foundry. Table 1 summarizes the different characteristics of transistor ED02AH.

**Table 1.** The physical characteristics of transistor ED02AH.

Process	Tech	Gate Length	Thickness	$F_t$	$F_{max}$	$G_m$
ED02AH pHEMT	GaAs	0.18 $\mu\text{m}$	100 $\mu\text{m}$	60 GHz	110 GHz	450 $\text{ms/mm}$
	$V_{bgd}$ (V)	$V_{dsmax}$ (V)	$I_{dss}$ (mA/mm)	$I_{dss}$ max(mA/mm)	NF (dB)	Power Density
	8	7	250(on)/140(off)	400(on)/180(off)	0.8(18GHz)	330 (mW/mm)

### 3. Circuit Description

Figure 3 shows Ultra-Wideband Low Noise Amplifier (LNA) using MMIC technology. This LNA was designed in distributed matrix architecture. The noise resistor of transistor ED02AH depends on several parameters, which can be reduced using several short fingers ( $6 \times 15 \mu\text{m}$ ) or by increasing the number of stages. The amplifier that meets these criteria consists of six cells.

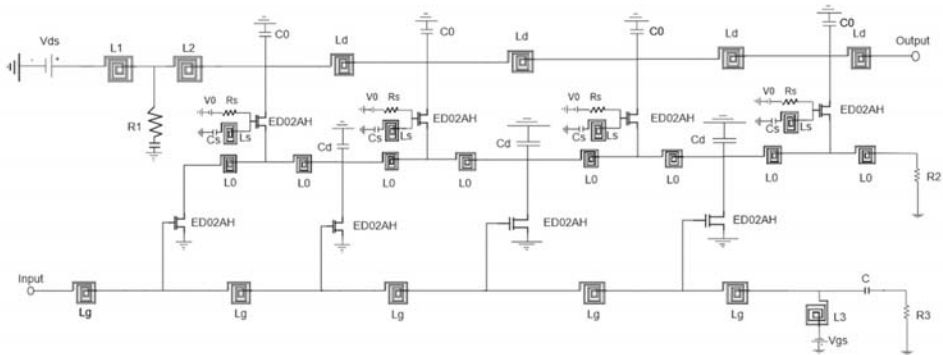


**Figure 3.** Schematic of the Low Noise Amplifier (LNA).

This Matrix architecture presents a very important gain for an ultra-wide frequency band. The resistive stability of the amplifier at high frequencies increases the value of the output conductance of the structure and at the same time degrades the gain of the amplifier [13]. Adjusting the reactive stability is an appropriate solution achieved by the means of the  $L_s C_s$  components of the gate of the transistor. A parallel resistor  $R_s$  is put in place to ensure the polarization of the circuit. The polarizations are fed via drain and gate lines. Inductances  $L_1$  and  $L_3$  must be dimensioned in order to have high impedance with respect to the Radio-Frequency RF signals. The module of the impedances  $Z_{Ld}$  and  $Z_{Lg}$  of these inductances is written as:

$$|Z_{Ld}| = 2\pi f L_1 \tag{1}$$

$$|Z_{Lg}| = 2\pi f L_3 \tag{2}$$

In order to ensure good RF signal transmission, the  $Z_{Ld}$  and  $Z_{Lg}$  impedance module must be greater than the characteristic impedance of the  $50 \Omega$  drain and gate lines at the minimum operating frequency. The Capacitors  $C_0$  and  $C_d$  are optimized to ensure a good adaptation in the frequency range studied. The values of different LNA parameters are shown in Table 2:

**Table 2.** Optimization result of different LNA parameters.

$L_1$ (nH)	$L_2$ (nH)	$L_3$ (nH)	$L_d$ (nH)	$L_g$ (nH)	$L_s$ (nH)	$L_o$ (nH)
4.212	2.088	2.67	0.3948	0.488	0.3	0.7835
$R_1$ ( $\Omega$ )	$R_2$ ( $\Omega$ )	$R_3$ ( $\Omega$ )	$R_s$ ( $\Omega$ )	$C_d$ (pF)	$C_s$ (pF)	$C_0$ (ff)
57	100	49	100	0.3	0.247	10

#### 4. Results and Discussion

The proposed wideband LNA was simulated with a 0.18  $\mu\text{m}$  GaAs-pHEMT ED02AH transistor. The performances of gain, noise, input/output matching, linearity, and power consumption are specified in order to regulate the values of the circuit components.

The final MMIC layout of the proposed wideband LNA is shown in Figure 4. The LNA is compact with the dimensions of  $1.8 \times 1.2 \text{ mm}^2$ .

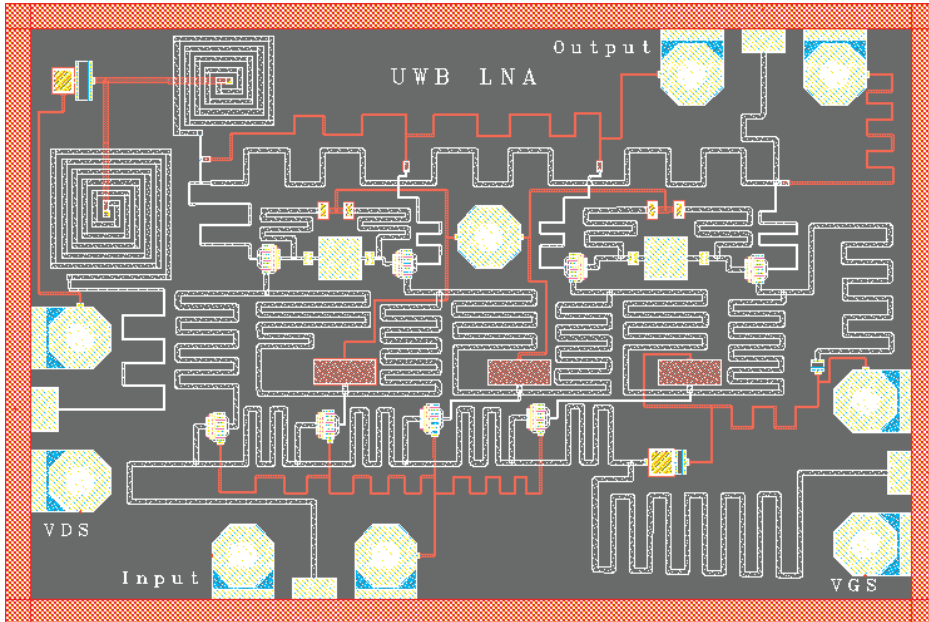


**Figure 4.** Photograph of the Monolithic Microwave Integrated Circuit (MMIC) Low Noise Amplifier ( $1.8 \times 1.2 \text{ mm}^2$ ).

The simulated input and output reflections of LNA are shown in Figure 5a. Input and output reflections are less than  $-10 \text{ dB}$  at all frequencies. The stability of LNA can be verified using Rollet’s K factor defined as in expression (3):

$$K = \frac{1 - |S_{11}|^2 - |S_{22}|^2 - |\Delta|^2}{2|S_{12}S_{21}|} \quad (3)$$

where,  $|\Delta| = |S_{11}S_{22} - S_{21}S_{12}|$ .



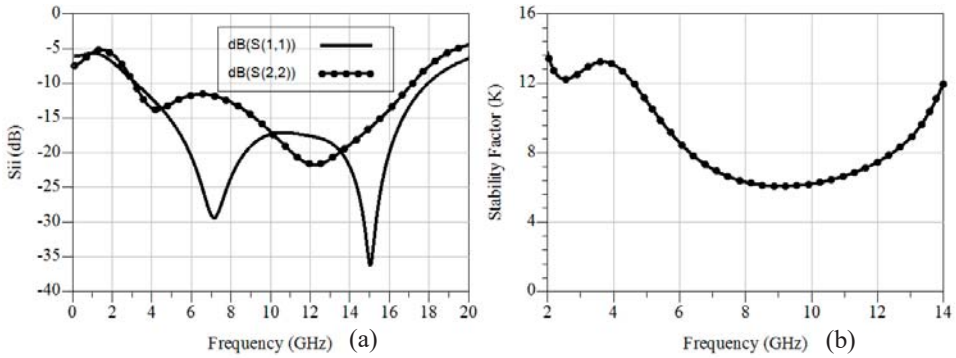


Figure 5. Simulated results of: (a) input/output reflection coefficients and, (b) LNA Stability.

For unconditional stability, the condition  $K > 1$  and  $\Delta < 1$  must be satisfied. Figure 5b shows the value of  $K$  of LNA, which proves the unconditional stability over the entire band. It can be seen from Figure 6a that reverse gain  $S_{12}$  is less than  $-33$  dB. Figure 6b proves an excellent noise figure (NF) as low as 3.65–4.35 dB in the required band with flat power gain of  $\{11\text{--}12.2$  dB and a consumption of 48 mW under a supply voltage of 2 V. Linearity is another important LNA parameter. The 1 dB compression point and third-order intercept point (IP3) represent the non linear operating domain of RF circuits that helps in proving a circuit’s linearity and dynamic range. By generating a two-tone input signal with a separation frequency of 10 MHz, the intermodulation point IM is the point of intersection between the fundamental spectrum and the third-order intercept point IP3. The output IP3 was calculated with Equation (4).

$$OIP3 = P_1 + \frac{1}{2}(P_1 - P_3) \tag{4}$$

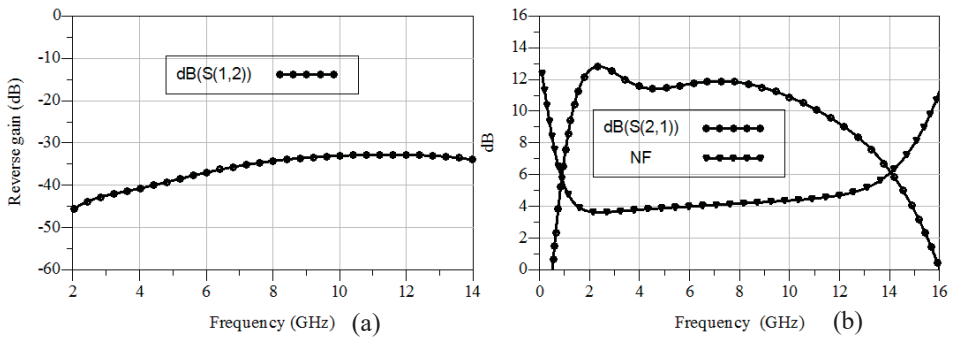


Figure 6. Simulated results of: (a) isolation, and (b) Simulated results of power gain and noise figure (NF).

Figure 7 shows that the compression point occurs for  $-1.5$  dBm and the third-order input interception point (IIP3) is about 20 dBm for input RF power.



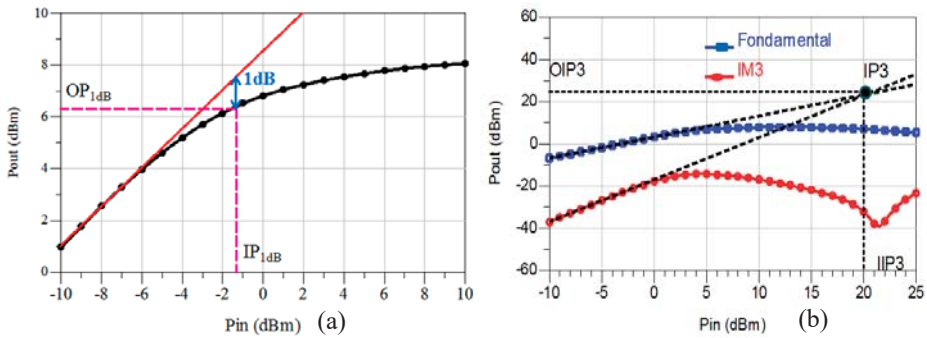


Figure 7. Simulated results of: (a) compression point 1 dB, and (b) Interception point (IP3).

The performance analysis with comparison of current works with recent literature was shown in Table 3.

The MMIC Matrix Distributed Low Noise Amplifier presents a high gain and low noise compared to the work of [14,15]. The linearity of this amplifier is very high compared to [14–16] and reaches up to 20 dBm.

Table 3. UWB LNA performance comparison.

	[14]	[15]	[16]	This Work
Technology( $\mu\text{m}$ )	0.18-CMOS	0.13-CMOS	0.18-CMOS	0.2-pHEMT
Supply voltage (V)	N/A	N/A	N/A	2
Bandwidth (GHz)	3.1–10.6	3.1–10.6	3.1–10.6	3.1–11
$P_{dc}$ (mW)	N/A	17.92	13.6	48
$S_{11}$ (dB)	<−8.8	<−8	<−9.5	<−10
$S_{22}$ (dB)	N/A	N/A	N/A	<−10
$S_{21}$ (dB)	11 max	10.24 max	12.1±0.7	11.6 ± 0.6
NF (dB)	3.95 ± 0.75	0.9–4.1	4.56–4.7	3.9 ± 0.35
$S_{12}$ (dB)	N/A	−31	N/A	−33
$P_{1dB}$ (dBm)	N/A	N/A	N/A	−1.5
IIP3 (dBm)	6	6.8	−12.5	20
Die area ( $\text{mm}^2$ )	0.7 × 0.8	N/A	N/A	1.8 × 1.2

## 5. Conclusions

An Ultra-wideband LNA using MMIC technology with 0.18  $\mu\text{m}$ - pHEMT ED02AH transistor was designed in distributed matrix architecture. The input/output matching conditions were satisfied by parallel capacitance. Stability was enhanced by an LC resonant circuit used in series with the transistor gate. From 3.1 to 11 GHz and with 2 V supply voltage, the amplifier’s noise figure is  $3.9 \pm 0.35$  dB. The average power gain is 11.9 dB. The power consumption is 48 mW. Due to wideband and high linearity, the proposed LNA is a suitable choice for multi-standard and UWB applications.

## References

1. Intel White Paper. *Ultra-Wideband (UWB) Technology: Enabling High-Speed Wireless Personal Area Networks*; Intel: Santa Clara, CA, USA, 2004.
2. Chong, C.C.; Yong, S.K.; Kim, Y.-H.; Kim, J.-H.; Lee, S.-S. Samsung Electronics (SAIT) CFP Presentation for IEEE 802.15.4a Alternative PHY: UWB Direct Chaotic Communication System. In Proceedings of the IEEE 802.15-05- 0030-02-004a, Monterey, CA, USA, 26 January 2005.
3. Chong, C.-C.; Yong, S.K. On the performance of non-coherent and differential-coherent UWB-DCC system. In Proceedings of the IEEE Wireless Commun. and Networking Conf., Las Vegas, NV, USA, 3–6 April 2006.

4. Giuliano, R.; Mazzenga, F. On the coexistence of power-controlled ultra wide-band systems with UMTS, GPS, DCS1800, and fixed wireless systems. *IEEE Trans. Veh. Technol.* **2005**, *54*, 62–81. [[CrossRef](#)]
5. McKinstry, D.R.; Buehrer, R.M. Issues in the performance and covertness of UWB communications systems. In Proceedings of the 45th Midwest Symposium on Circuits and Systems, Tulsa, OK, USA, 5–7 August 2002; Volume 3, pp. 601–604.
6. Namgoong, W. A channelized digital ultrawideband receiver. *IEEE Trans. Wirel. Commun.* **2003**, *2*, 502–510. [[CrossRef](#)]
7. Federal Communications Commission. *Revision of Part 15 of the Commission's Rules Regarding Ultra-Wide Band Transmission Systems*; First Report and Order (ET Docket 98–153); Federal Communications Commission: Washington, DC, USA, 2002.
8. Lei, Y.; Viktor, K.; S'ebastien, D.; Vitaliy, Z.; Tom, K.J.; Chenhui, J. GaAs Wideband Low Noise Amplifier Design for Breast Cancer Detection System 978-1-4244-2802-1/09/2009 IEEE. *IEEE Micro* **2010**, *8*, 357–360.
9. Percival, W.S. Thermionic Valve Circuits. British Patent 460562, 25 January 1937.
10. Moustapha, E.B.; Hanae, E.; Naima, A.T.; Elhamadi, T. 2.3–21 GHz broadband and high linearity distributed low noise amplifier. *Integration* **2020**, *76*, 61–68. [[CrossRef](#)]
11. Materka, A.; Kacprzak, T. Computer calculation of large-signal GaAs FET amplifier characteristics. *IEEE Trans. MTT* **1985**, *MTT-33*, 129–135. [[CrossRef](#)]
12. Smith, D. *TOM-2: An Improved Model for GaAs MESFET*; Internal Memorandum; Triquint Semiconductor Inc.: Hillsboro, OR, USA, 1995.
13. Ming, D.T.; Kuo, L.D.; Huei, W.; Chun, H.C.; Chih, S.C.; Chern, J.G.J. A miniature 25-GHz 9-dB CMOS cascaded single-stage distributed amplifier. *IEEE Microw. Wirel. Compon. Lett.* **2004**, *14*, 554–556. [[CrossRef](#)]
14. Chen, C.C.; Wang, Y.C. 3.1–10.6 GHz ultra-wideband LNA design using dual-resonant broadband matching technique. *Int. J. Electron. Commun.* **2013**, *67*, 500–503. [[CrossRef](#)]
15. Rastegar, H.; Ryu, J.Y. A broadband Low Noise Amplifier with built-in linearizer in 0.13- $\mu$ m CMOS process. *Microelectron. J.* **2015**, *46*, 698–705. [[CrossRef](#)]
16. Saberkari, A.; Kazemi, S.; Shirmohammadli, V.; Yagoub, M.C.E. gm-boosted flat gain UWB low noise amplifier with active inductor-based input matching network. *Integr. VLSI J.* **2016**, *52*, 323–333. [[CrossRef](#)]


**Publisher's Note:** MDPI stays neutral with regard to jurisdictional claims in published maps and institutional affiliations.



© 2020 by the authors. Licensee MDPI, Basel, Switzerland. This article is an open access article distributed under the terms and conditions of the Creative Commons Attribution (CC BY) license (<http://creativecommons.org/licenses/by/4.0/>).



# Dual-Band 28/38 GHz Inverted-F Array Antenna for Fifth Generation Mobile Applications <sup>†</sup>

Mustapha El Halaoui <sup>1,2</sup>, Laurent Canale <sup>1,\*</sup> , Adel Asselman <sup>2</sup> and Georges Zissis <sup>1</sup>

<sup>1</sup> LAPLACE, Université de Toulouse, CNRS, INPT, UPS, 31000 Toulouse, France;

mustapha.halaoui@gmail.com (M.E.H.); georges.zissis@laplace.univ-tlse.fr (G.Z.)

<sup>2</sup> Optics and Photonics Laboratory, Faculty of Sciences, Abdelmalek Essaadi University, 93000 Tetouan, Morocco; adelasselman@gmail.com

\* Correspondence: laurent.canale@laplace.univ-tlse.fr

<sup>†</sup> Presented at the 14th International Conference INTER-ENG 2020 Interdisciplinarity in Engineering, Mureş, Romania, 8–9 October 2020.

Published: 28 December 2020

**Abstract:** The development of 5G (fifth generation) mobile communication systems was initiated to meet the expected need for higher data rates. In this article, a new 28/38 GHz dual-band “inverted-F” array antenna for 5G applications is proposed. This antenna can be integrated in OLEDs (Organic Light Emitting Diodes) panels which can be used both for lighting or display. This 5G antenna, composed of 32 elements, has the advantage of a dual-band and compact structure. Each element of the array antenna has the shape of an “inverted-F” antenna. This array antenna can cover the 28 GHz band (27.94–28.83 GHz) and the 38 GHz band (37.97–38.96 GHz) with mutual coupling between the elements less than –35 dB. The characteristics of the end fire radiation beams were obtained by employing an array of 32 “inverted-F” antenna elements on the upper and lower portions of the PCB (Printed Circuit Board). The suggested design has a gain of approximately 16.52 dB at 28.38 GHz and 15.35 dB at 38.49 GHz, which is suitable for 5G mobile communications.

**Keywords:** antenna; array antenna; fifth generation; millimeter wave; OLEDs light sources

## 1. Introduction

Since the beginnings of consumer wireless telephony in the early 1980s with the first Generation “1G”, which gives the user the freedom to make and receive phone calls, mobile communication systems go through different evolution stages [1,2]. This development is mainly based on the increase in data transfer rate, which achieved 100 Mbit/s for fourth generation systems, and it can be improved to 1 Gbit/s. The goal for the fifth generation systems is determined to reach up to 10 Gbps and a latency of about 1 ms, which results in a reduction in the energy consumption [3].

The antennas for the fourth generation operate in the 0.5–3 GHz frequency band, while the antennas for the fifth generation operating in the 28 GHz and 38 GHz bands [4–6]. The new cellular technology uses the millimeter wavelength spectrum, which permits the use of larger bandwidths, wireless broadband access, the use of large numbers of antennas in the transmission and reception, and reduces the mutual coupling between the antennas [7]. For the spectrum of millimeter-wave, the use of antennas with high gain and directional radiation patterns is necessary [8].

For the mobile phone applications, the antennas must be compact, small size, with low SAR value and compatible with other RF components [9,10]. Therefore, the use of millimeter wave spectrum automatically reduces the electrical length of the antenna, which complicates task of this antenna design, and allows for the use of array antenna to improve the antenna gain to overcome excessive path loss in the millimeter wave band [11,12]. In addition, the dual band antennas solutions are desirable

for 5G applications. Several works of literature have proposed dual-band 28/38 GHz antennas for mobile phones through several techniques [13–22].

The aim of this article is to design a dual band patch array antenna, for 5G mobile phone communication, with: high gain, radiation pattern beams characteristics, wide bandwidth, and a simple geometry which is formed by using the “Inverted-F” element. To improve the antenna gain, the array antenna technique is applied and gives us gains of 16.52 dB at 28.38 GHz and 15.35 dB at 38.49 GHz for an array of 32 elements.

## 2. The Single Element “Inverted-F” Antenna

### 2.1. Antenna Geometry

The aim is to design an antenna with a high gain and a directional radiation pattern for mobile phones in next generation mobile communication. Since the millimeter wave band is reserved for future 5G systems, the antennas that operate in this band are of small sizes. The dimensions and the geometry of the antenna are given in Figure 1. This antenna is designed on a FR4 substrate with permittivity  $\epsilon_r = 4.4$ , loss tangent  $\tan \delta = 0.025$  and thickness  $h_s = 0.2$  mm. The ground plane dimensions are  $5.5 \times 4$  mm<sup>2</sup>. To obtain two distinct operating bands, the antenna has the shape of an “inverted-F”. The configuration of the “inverted-F” antenna comprises two L-strip branch: one for the 28 GHz band and the other for the 38 GHz band. The parameter values of the antenna are shown in Figure 1. The antenna was designed and optimized using CST Microwave Studio.

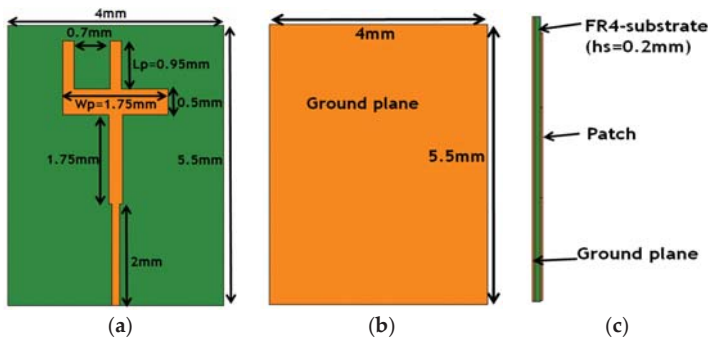


**Figure 1.** The geometry of the antenna: (a) ground plane, (b) bottom view and (c) side view.

### 2.2. Parametric Study

To understand the operating behavior of the 5G antenna, a parametric study is performed by CST microwave studio. Figure 2 shows the effect of the variation of patch length  $L_p$  on the reflection coefficient of the antenna ( $L_p = 1.45$  mm, 1.5 mm, 1.55 mm). This figure shows that the resonance frequencies for the two bands 28/38 GHz shift to lower frequency with increasing  $L_p$ . The results of the reflection coefficient for the variation of patch width  $W_p$  ( $W_p = 1.65$  mm, 1.7 mm, 1.75 mm) are shown in Figure 3. We notice, with increasing  $W_p$ , the resonance frequencies in the two bands, 28/38 GHz, shift to lower frequencies.

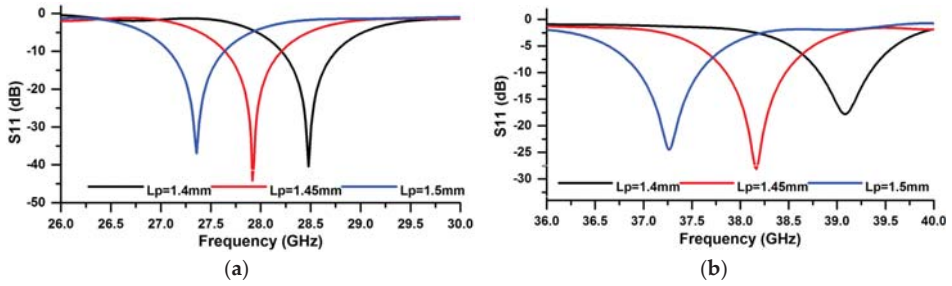


Figure 2. The reflection coefficient with variation of  $L_p$ : (a) at 28 GHz band and (b) at 38 GHz band.

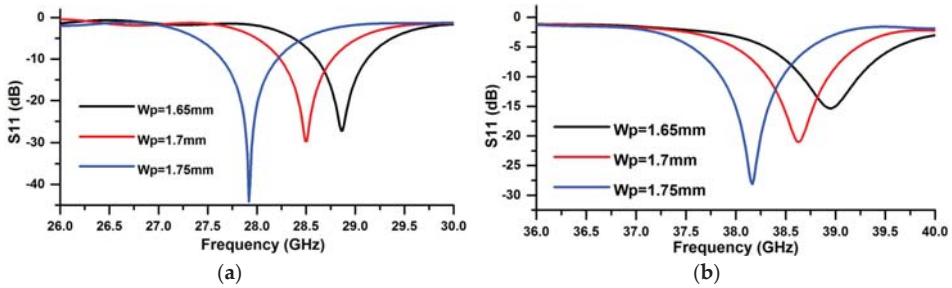


Figure 3. The reflection coefficient with variation of  $W_p$ : (a) at 28 GHz band and (b) at 38 GHz band.

### 2.3. Reflection Coefficient

The reflection coefficient for the single element of the 5G antenna is shown in Figure 4. The two operating bands of the antenna are obtained: the first band ( $S_{11} < -6$  dB) from 27.94 to 28.83 GHz with a width of 890 MHz and the second band from 37.97 to 38.96 GHz with a width of 990 MHz. The two bands obtained cover millimeter-wave frequency bands for future mobile cellular devices.

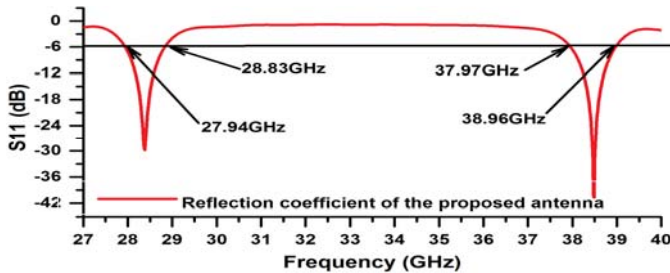


Figure 4. The reflection coefficient of the antenna.

### 2.4. Current Distribution

To understand the operating mechanism of the antenna, the surface current distribution at both operating bands was studied. The surface current distributions of the 5G antenna at 28.38 and 38.49 GHz are shown in Figure 5a,b, respectively.

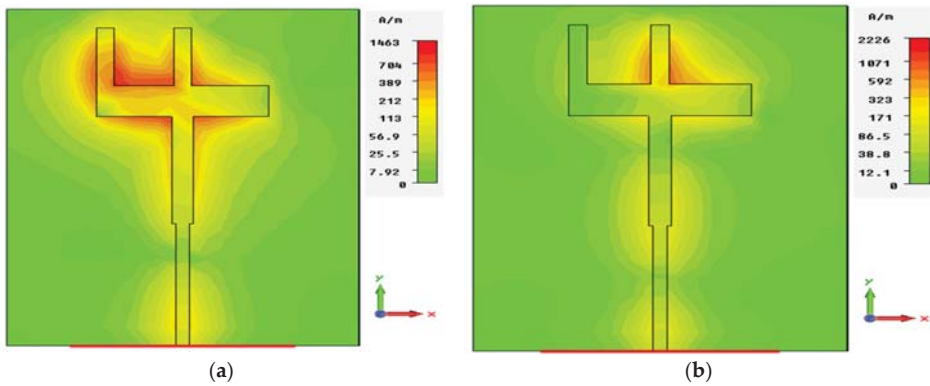


Figure 5. Surface current distribution: (a) at 28 GHz band and (b) at 38 GHz band.

Figure 5a shows the simulated current distribution for the “inverted-F” antennas at 28.38 GHz. From this figure, we notice a large current is excited in the L-strip branch left of the “inverted-F”. In Figure 5b, the surface current at 38.49 GHz is distributed in the L-strip branch right of “inverted-F” and has a maximum intensity around this strip.

### 2.5. Radiation Pattern

The 3D radiation pattern of the single element “inverted-F” antenna at 28.38 and 38.49 GHz are illustrated in Figure 6a,b, respectively. The obtained results showed that the “inverted-F” antenna had a good end-fire radiation behavior and a gain of 6.22 dB at 28.38 GHz and 6.33 dB at 38.49 GHz.

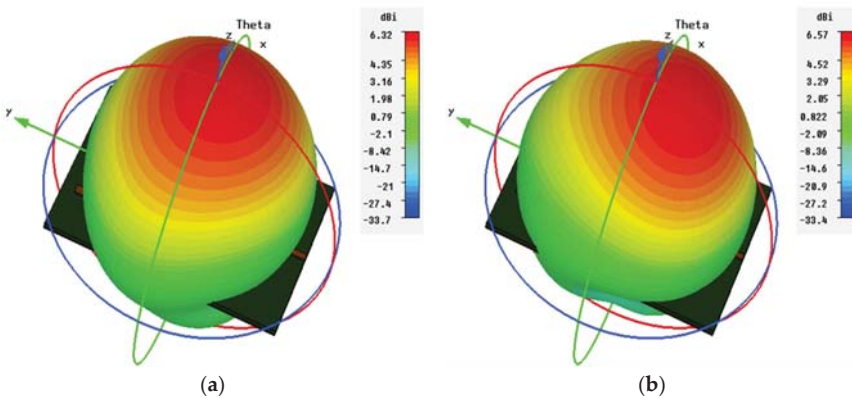


Figure 6. The 3D radiation pattern: (a) at 28 GHz band and (b) at 38 GHz band.

## 3. The “Inverted-F” Array Antenna

### 3.1. The Antenna Array Geometry

The chosen configuration for the application is a 32 array element with identical elements. Figure 7 shows the geometry of the linear array with 32 elements of the “inverted-F” antennas. The 16 array elements are chosen to be placed in the top portion of PCB, while the other 16 elements are placed in the bottom portion of the PCB. For uniformly spaced linear arrays, the elements have 4 mm spacing between them ( $0.795\lambda$  at 28.38 GHz and  $1.076\lambda$  at 38.49 GHz). The PCB size is  $133 \times 64 \times 0.2 \text{ mm}^3$ . The array antenna has been designed, optimized, and simulated using the CST microwave studio.

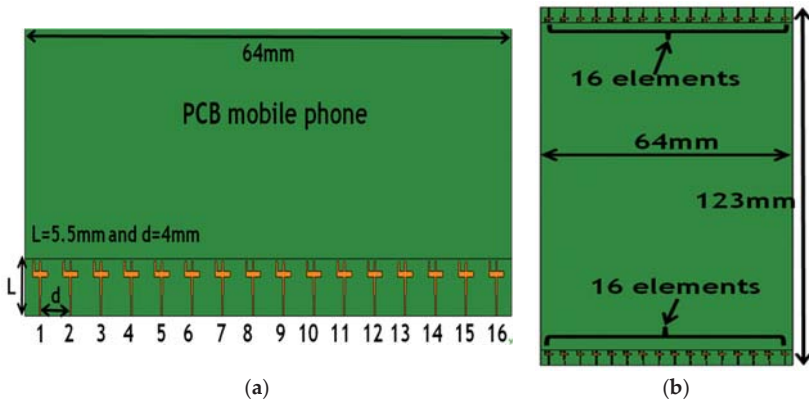


Figure 7. The geometry of the array antenna: (a) bottom portion of the PCB and (b) top view.

3.2. The S-Parameters of the Array Antenna

The simulated S-parameters for the array antenna are illustrated in Figure 8. From this figure, we can see that the array antenna exhibits good impedance matching in the 28/38 GHz frequency bands and the mutual-coupling characteristics between the elements are less than  $-35$  dB.

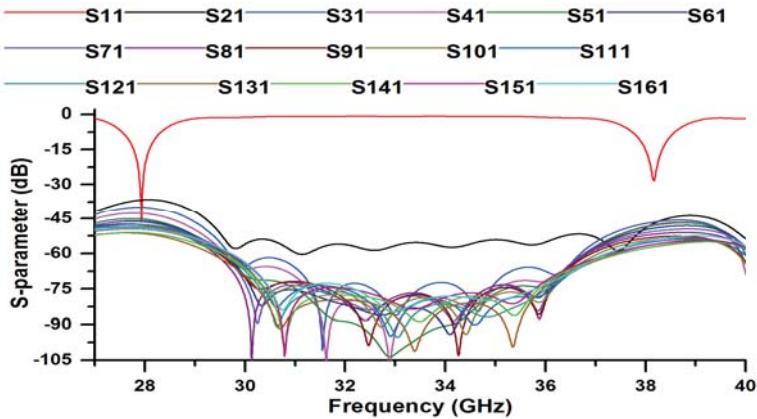


Figure 8. The S-parameters of the array antenna.

3.3. The Cartesian Gains

The Cartesian gains of the array antenna in  $x-z$  plane are displayed in Figure 9. As illustrated, the array antenna has a good beam steering characteristic with end-fire mode and sufficient gains at different scanning angles.

A stable gain with a value of 16.52 dB (+10 dB compared to a single antenna element) at 28.38 GHz is observed in Figure 9a. Additionally, from Figure 9b, we notice that the antenna gain decreases with the increase in the angle; and it is about 15.35 dB in  $0^\circ$  (+9 dB compared to a single antenna element) at 38.49 GHz.



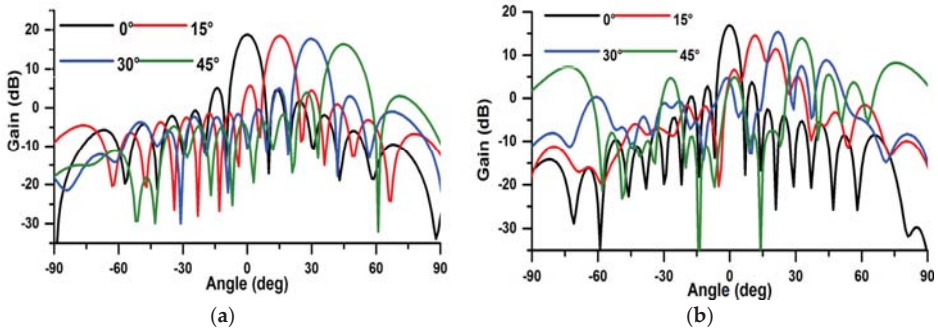


Figure 9. The cartesian gains of the 5G array antenna: (a) at 28.38 GHz and (b) at 38.49 GHz.

### 3.4. The Radiation Pattern of the Array Antenna

The beam steering characteristic of the simulated radiation patterns of the 5G antenna in different scanning angles ( $0^\circ$  to  $45^\circ$ ) is also studied. Figures 10 and 11 show the 3D radiation pattern beams of the array antenna at 28.38 and 38.49 GHz, respectively. The beam steering characteristic of the 5G antenna for plus/minus scanning angles are symmetric [16]. We observe, the array antenna has a good beam steering property which is highly effective to cover the range of  $\pm 45^\circ$  [17].

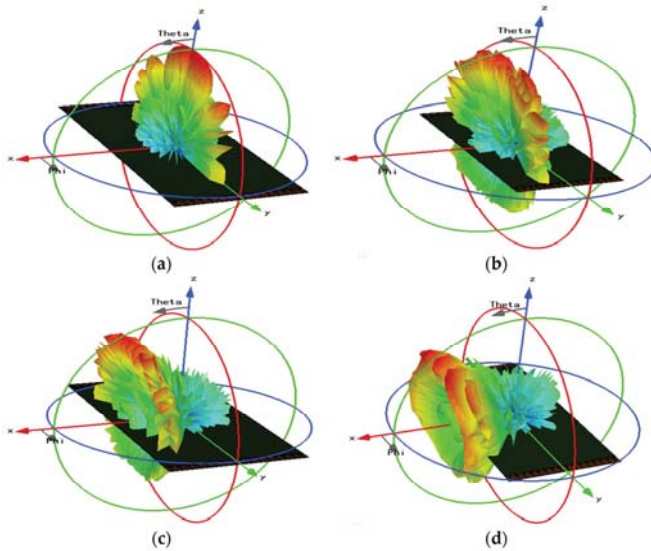
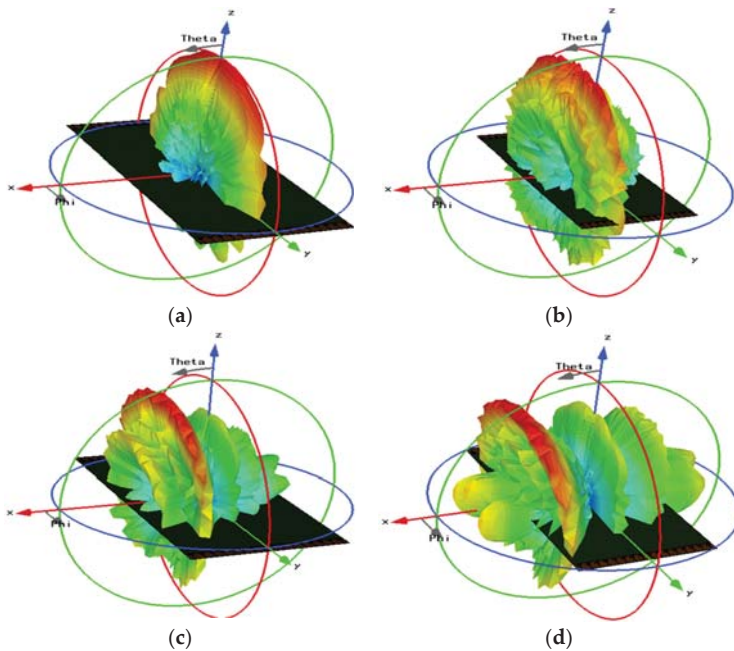


Figure 10. The 3D radiation beams in 28 GHz band at different scanning angles; (a)  $0^\circ$ , (b)  $15^\circ$ , (c)  $30^\circ$  and (d)  $45^\circ$ .



**Figure 11.** The 3D radiation beams in 38 GHz band at different scanning angles; (a)  $0^\circ$ , (b)  $15^\circ$ , (c)  $30^\circ$  and (d)  $45^\circ$ .

#### 4. Conclusions

In this paper, a new compact dual-band (28/38 GHz) “inverted-F” array antenna for the future fifth generation (5G) mobile networks have been demonstrated. The 5G antenna is worked in the 28 GHz mm-wave band (27.94–28.83 GHz) and the 38 GHz mm-wave band (37.97–38.96 GHz) with a bandwidth 890 and 990 MHz, respectively. Since the proposed antenna is of small size and simple geometry with the simplicity of reaching the desired frequency bands, it is easy to manufacture and integrate in the case of the OLEDs. The mutual-coupling characteristics between the elements are less than  $-35$  dB. To improve the gain of the antenna, we used the antenna array technique. Therefore, we have reached a high gain of 16.52 dB in the first band and 15.35 dB in the second band. End-fire radiation beams were achieved by employing 32 elements of “inverted-F” antennas on the top and bottom portions of the OLEDs display. With 5G communications, the bandwidth and data rate will be higher, but the distance between receiver and transmitter will be shorter. This makes it necessary to multiply the antennas across an extended network, for example, such as the public lighting network. In this context, this antenna is a good candidate for 5G applications and can be integrated in OLED panels for display as well as in street lighting.

**Acknowledgments:** This work is granted by PHC Maghreb (Program Hubert Curien) MELINA (Mastering Efficient Lighting In North Africa) funded by Ministry of Europe and Foreign Affairs and supported by Campus France and, in Morocco, by the Ministry of National Education, Professional Training, Higher Education and Scientific Research, in partnership with the National Center for Scientific and Technical Research (CNRST).

#### References

1. Roh, W.; Seol, J.Y.; Park, J.; Lee, B.; Lee, J.; Kim, Y.; Cho, J.; Cheun, K.; Aryanfar, F. Millimeter-wave beam forming as an enabling technology for 5G cellular communications: Theoretical feasibility and prototype results. *IEEE Commun. Mag.* **2014**, *52*, 106–113. [[CrossRef](#)]

2. Gupta, A.; Jha, R.K. A Survey of 5G Network: Architecture and Emerging Technologies. *IEEE Access* **2015**, *3*, 1206–1232. [[CrossRef](#)]
3. Rappaport, T.S.; Sun, S.; Mayzus, R.; Zhao, H.; Azar, Y.; Wang, K.; Wong, G.N.; Schulz, J.K.; Samimi, M.; Gutierrez, F. Millimeter Wave Mobile Communications for 5G Cellular: It Will Work! *IEEE Access* **2013**, *1*, 335–349. [[CrossRef](#)]
4. Rappaport, T.S.; Qiao, Y.; Tamir, J.I.; Murdock, J.N.; Ben-Dor, E. Cellular broadband millimeter wave propagation and angle of arrival for adaptive beam steering systems (invited paper). In Proceedings of the 2012 IEEE Radio and Wireless Symposium (RWS), Santa Clara, CA, USA, 15–18 January 2012; pp. 151–154.
5. Akdeniz, M.R.; Liu, Y.; Rangan, S.; Erkip, E. Millimeter wave picocellular system evaluation for urban deployments. In Proceedings of the 2013 IEEE Globecom Workshops (GC Wkshps), Atlanta, GA, USA, 9–13 December 2013; pp. 105–110.
6. El Halaoui, M.; Canale, L.; Asselman, A.; Zissis, G. An Optically Transparent Antenna Integrated in OLED Light Source for 5G Applications. In Proceedings of the 2020 IEEE International Conference on Environment and Electrical Engineering and 2020 IEEE Industrial and Commercial Power Systems Europe (EEEIC/I&CPS Europe), Madrid, Spain, 9–12 June 2020; pp. 1–5. [[CrossRef](#)]
7. Hong, W.; Baek, K.-H.; Lee, Y.; Kim, Y.; Ko, S.-T. Study and prototyping of practically large-scale mm Wave antenna systems for 5G cellular devices. *IEEE Commun. Mag.* **2014**, *52*, 63–69. [[CrossRef](#)]
8. Tatomirescu, A.; Oprian, A.; Zhekov, S.; Pedersen, G.F. Beam-steering array for handheld devices targeting 5G. In Proceedings of the 2015 International Symposium on Antennas and Propagation (ISAP), Hobart, Tasmania, Australia, 9–12 November 2015; pp. 1–4.
9. El Halaoui, M.; Kaabal, A.; Asselman, H.; Ahyoud, S.; Asselman, A. Multiband Planar Inverted-F Antenna with Independent Operating Bands Control for Mobile Handset Applications. *Int. J. Antennas Propag.* **2017**, *2017*, 1–13. [[CrossRef](#)]
10. Helander, J.; Zhao, K.; Ying, Z.; Sjoberg, D. Performance Analysis of Millimeter-Wave Phased Array Antennas in Cellular Handsets. *IEEE Antennas Wirel. Propag. Lett.* **2015**, *15*, 504–507. [[CrossRef](#)]
11. Ashraf, N.; Haraz, O.M.; Ali, M.M.M.; Ashraf, M.A.; Alshebili, S.A.S. Optimized broadband and dual-band printed slot antennas for future millimeter wave mobile communication. *AEU Int. J. Electron. Commun.* **2016**, *70*, 257–264. [[CrossRef](#)]
12. Bisharat, D.J.; Liao, S.; Xue, Q. High Gain and Low Cost Differentially Fed Circularly Polarized Planar Aperture Antenna for Broadband Millimeter-Wave Applications. *IEEE Trans. Antennas Propag.* **2016**, *64*, 33–42. [[CrossRef](#)]
13. Ojaroudiparchin, N.; Shen, M.; Pedersen, G.F. Multi-layer 5G mobile phone antenna for multi-user MIMO communications. In Proceedings of the 2015 23rd Telecommunications Forum Telfor (TELFOR), Belgrade, Serbia, 24–26 November 2015; pp. 559–562.
14. Li, W.-Y.; Chung, W.; Wong, K.-L. Highly-Integrated Dual-Band mm Wave Antenna Array for 5G Mobile Phone Application. In Proceedings of the 2020 14th European Conference on Antennas and Propagation (EuCAP), Copenhagen, Denmark, 15–20 March 2020; pp. 1–5.
15. Wang, Y.; Huang, H.-C.; Jian, X. Integrated Design of a Cable-Fed Dual-Band Dual-Polarization 5G mm-Wave Antenna Array with a U-Slotted Full-Metal Casing for a Cellular Phone. In Proceedings of the 2019 International Conference on Microwave and Millimeter Wave Technology (ICMMT), Guangzhou, China, 19–22 May 2019; pp. 1–3.
16. Huang, H.-C.; Wang, Y.; Jian, X. Novel Integrated Design of Dual-Band Dual-Polarization mm-Wave Antennas in Non-mm-Wave Antennas (AiA) for a 5G Phone with a Metal Frame. In Proceedings of the 2019 International Workshop on Antenna Technology (iWAT), Miami, FL, USA, 3–6 March 2019; pp. 125–128.
17. Mahmoud, K.R.; Montaser, A.M. Design of dual-band circularly polarised array antenna package for 5G mobile terminals with beam-steering capabilities. *IET Microw. Antennas Propag.* **2018**, *12*, 29–39. [[CrossRef](#)]
18. Li, Y.; Sim, C.-Y.-D.; Luo, Y.; Yang, G. Multiband 10-Antenna Array for Sub-6 GHz MIMO Applications in 5-G Smartphones. *IEEE Access* **2018**, *6*, 28041–28053. [[CrossRef](#)]
19. Marzouk, H.M.; Ahmed, M.I.; Shaalan, A.A. A Novel Dual-band 28/38 GHz Slotted Microstrip MIMO Antenna for 5G Mobile Applications. In Proceedings of the 2019 IEEE International Symposium on Antennas and Propagation and USNC-URSI Radio Science Meeting, Atlanta, GA, USA, 7–12 July 2019; pp. 607–608.

20. Deckmyn, T.; Cauwe, M.; Ginste, D.V.; Rogier, H.; Agneessens, S. Dual-Band (28,38) GHz Coupled Quarter-Mode Substrate-Integrated Waveguide Antenna Array for Next-Generation Wireless Systems. *IEEE Trans. Antennas Propag.* **2019**, *67*, 2405–2412. [[CrossRef](#)]
21. Rahayu, Y.; Hidayat, M.I. Design of 28/38 GHz Dual-Band Triangular-Shaped Slot Microstrip Antenna Array for 5G Applications. In Proceedings of the 2018 2nd International Conference on Telematics and Future Generation Networks (TAFGEN), Kuching, Malaysia, 24–26 July 2018; pp. 93–97.
22. Ullah, H.; Tahir, F.A.; Khan, M.U. Dual-band planar spiral monopole antenna for 28/38 GHz frequency bands. In Proceedings of the 2017 IEEE International Symposium on Antennas and Propagation USNC/URSI National Radio Science Meeting, San Diego, CA, USA, 9–14 July 2017; pp. 761–762.


**Publisher's Note:** MDPI stays neutral with regard to jurisdictional claims in published maps and institutional affiliations.



© 2020 by the authors. Licensee MDPI, Basel, Switzerland. This article is an open access article distributed under the terms and conditions of the Creative Commons Attribution (CC BY) license (<http://creativecommons.org/licenses/by/4.0/>).



# Wideband Reconfigurable Antenna with Beams Switching for Wireless Systems Applications <sup>†</sup>

Faouzi Rahmani <sup>1,\*</sup>, Naima Amar Touhami <sup>1</sup>, Abdelmounaim Belbachir Kchairi <sup>2</sup> and Nihade Taher <sup>3</sup>

<sup>1</sup> Faculty of Sciences, Abdelmalek Essaadi University, Tetuan 93030, Morocco; nai\_amar@yahoo.fr

<sup>2</sup> Faculty of Sciences and Techniques, Hassan II University of Casablanca, Casablanca 20006, Morocco; belbachir.kochairi@gmail.com

<sup>3</sup> National School of Applied Sciences, Abdelmalek Essaadi University, Tetuan 93030, Morocco; nihade.thr@gmail.com

\* Correspondence: mr.fauzi.rahmani@gmail.com; Tel.: +212-671-307-689

<sup>†</sup> Presented at the 14th International Conference INTER-ENG 2020 Interdisciplinarity in Engineering, Mures, Romania, 8–9 October 2020.

Published: 18 December 2020

**Abstract:** In this paper, a new wideband reconfigurable antenna with beams switching for wireless systems applications is presented and studied. The radiation pattern of the proposed antenna can be changed using the PIN diodes. The designed antenna has a bandwidth of 26.75% from 5.31 to 6.95 GHz and can steer the beam in the azimuth plane. The simulated realized gain of the antenna obtained is 5.9 dB at 5.8 GHz. The proposed antenna can operate for various wireless systems, such as Wi-Fi, WiMAX, Intelligent Transportation System (ITS) and C-band satellite. The simulated results are also presented and investigated.

**Keywords:** reconfigurable antenna; PIN diode; radiation pattern; wideband; Wi-Fi; WiMAX; ITS

## 1. Introduction

With the rapid development of electronic and wireless communication, performance is important in any antenna system. The reconfigurable antennas have gained more attention due to their flexibility in operating frequency, polarization and radiation pattern reconfiguration [1–4]. This makes them highly suitable for different wireless communication systems. This antenna type can electronically change its parameters in response to different environments, which has been studied extensively. This means it can satisfy the diverse requirements and strict standards of advanced wireless communication systems due to its numerous merits such as reducing size, expanding capacity and wide cover. Optical, mechanical or electronic switching can be used to accomplish reconfiguration. Electronic switching is achieved using lumped components, for example, varactor diodes [5], PIN diodes [6–14], RF MEMS switches [15] or FET transistors.

The reality that distinct wireless applications, such as Wi-Fi, WiMAX and ITS, use various operating bands and the exigency of Wideband reconfigurable antennas for wireless terminals is also rising. Multifunction in antennas is an important characteristic that has currently generated more interest in antenna design development. Contrast with accustomed antennas, multifunctional antennas offers the capability to dynamically alter several antenna parameters.

In recent years, this antenna type has been proposed and developed more and more. To realize the pattern reconfigurability, there are various main technical and methods in the literature. The antenna in [15] performed six operating states by monitoring the states of MEMS switches. The antenna in [16] achieved two states by controlling the state of two PIN diodes between the feed line and patch elements. Based on a circular monopole patch and three ship-shaped parasitic patches, the radiation pattern of

the antenna in [17] would be reconfigured in two modes in the azimuth plane by steering the state of two PIN diodes. In Ref. [18], by shifting the states of the four PIN diodes, four pattern reconfigurable states were obtainable. To increase the antenna performance, we propose to use four radiation cells connected to a central circular patch by using PIN diodes. The PIN diodes are very reliable since there are no moving parts and are extremely low cost. Patch antenna can be integrated easily with PIN diode switches to form reconfigurable patch antennas [18,19]. In addition to the pattern reconfigurability, the objective is to increase the bandwidth and miniaturize the antenna size.

In this work, we propose a new reconfigurable radiation pattern antenna using four fan-shaped radiation cells that operate either as reflector(s) or director(s) according to the PIN diodes states, and a square planar ground. The radiation pattern can be changed into four states using four switches. The antenna main beam can be switched to four directions in the azimuth plane by controlling the states (ON or OFF) of four Microsemi MPP4203 PIN diodes [20]. The designed antenna has a bandwidth of 5.31–6.95 GHz and can operate for various wireless systems, such as Wi-Fi, WiMAX and ITS.

This work will begin by describing the wideband reconfigurable antenna design and operation principle to realize the reconfigurability of the radiation patterns. The design evolutions process for the proposed antenna and parametric study will be presented in Sections 3 and 4, respectively. The simulation results of the proposed antenna at operating states will be presented in Section 5. Finally, the conclusion is given in Section 6.

## 2. Antenna Design

The proposed antenna consisted of a central circular patch and four radiation cells graved on  $h = 0.8$  mm thick Rogers RT5880 substrate with a relative dielectric constant of 2.2 and a dissipation factor of 0.0009. A square-shaped ground plane is printed on the bottom surface of the substrate as shown in Figure 1. The first (yellow area) part is a circular patch located at the center of the proposed antenna, which is connected to the inner pin of the coaxial cable. The second (red area) parts are four fan-shaped radiation cells, which distribute around the antenna center symmetrically as shown in Figure 1a.

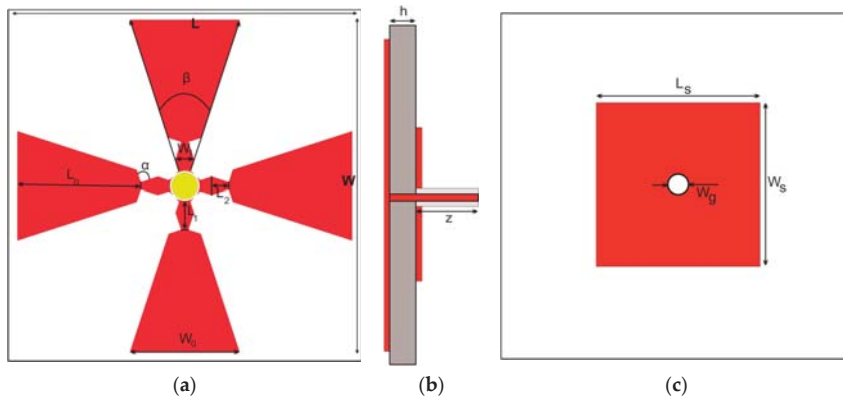


**Figure 1.** The designed reconfigurable antenna: (a) Top view; (b) side view; (c) bottom view.

The size of the substrate is  $(W \times L \times h) = (60 \text{ mm} \times 60 \text{ mm} \times 0.8 \text{ mm})$ . The radiation elements are connected to the central circular patch using four switches in the gap between them, the width of this gap is 0.3 mm. The four PIN diodes are mounted in the gap between the circular patch and the four parasitic patches as shown in Figure 2. This antenna was obtained after many optimizations using an electromagnetic simulator (CST Microwave Studio). The optimized parameter values of the proposed wideband reconfigurable radiation pattern antenna are given in Table 1.

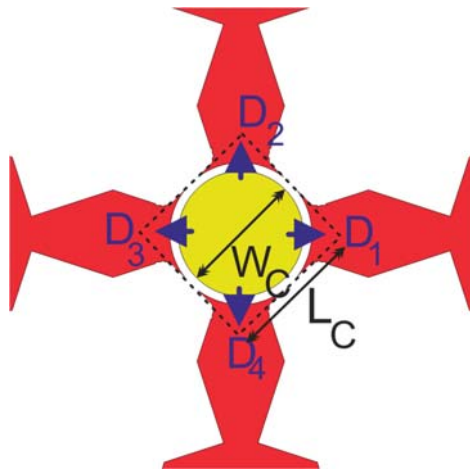


Figure 2. The proposed enlarged antenna center: Top view.

Table 1. Dimensions of the proposed antenna.

Parameter	W	W0	W1	W <sub>C</sub>	W <sub>S</sub>	W <sub>G</sub>	L	L0
Dimension	30 mm	20.2 mm	3 mm	4.4 mm	34 mm	4.1 mm	30 mm	21 mm
	L1	L2	L <sub>C</sub>	L <sub>S</sub>	z	h	$\beta$	$\alpha$
	4.5 mm	2.8 mm	4.95 mm	34 mm	5 mm	0.8 mm	40°	90°

### 3. Design Evolution Procedure

Figure 3 shows the design evolution of the proposed antenna, with corresponding results of simulated reflection coefficient S11 (dB) as shown in Figure 4a, and simulated gain realized over frequency of each step as shown in Figure 4b. The simulation results are obtained when the antenna operates in state 1. This study gives the same results for the other operation states.

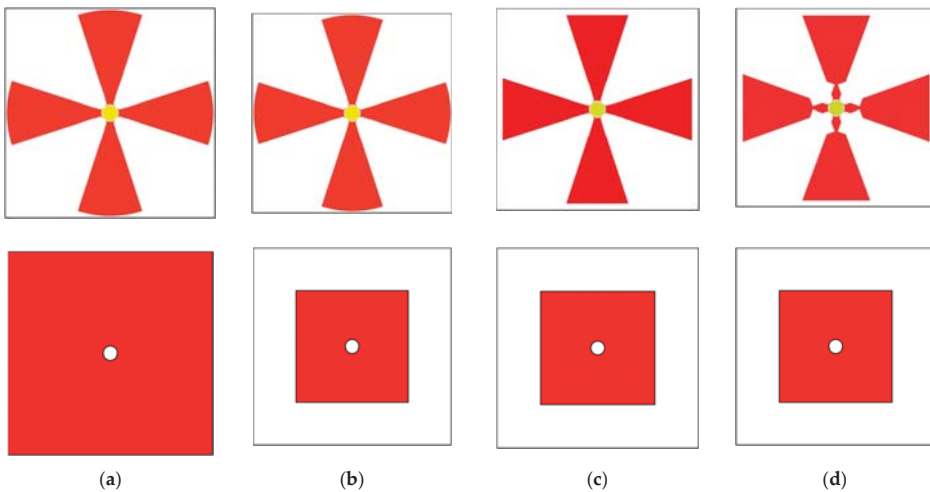
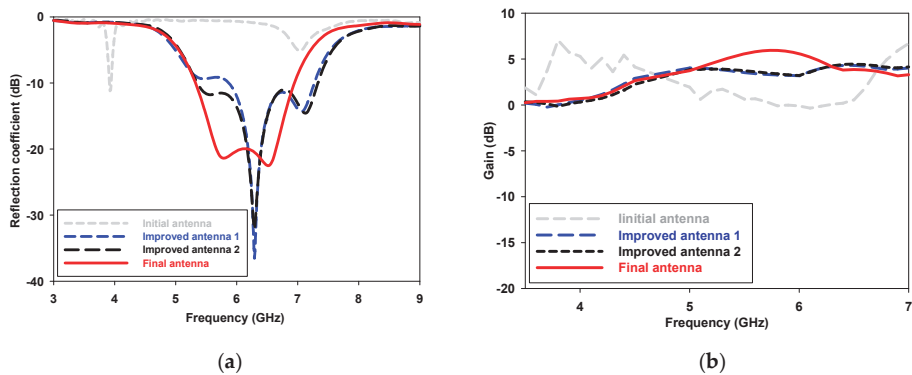


Figure 3. Design evolution of the proposed antenna: (a) initial antenna; (b) Improved antenna design 1; (c) Improved antenna design 2; (d) Final antenna.





**Figure 4.** Simulated reflection coefficient and max gain of different antennas: (a) Reflection coefficient, (b) Max gain.

The first step in the design of the proposed reconfigurable antenna is presented in Figure 3a. As can be seen from this figure, on the top side of the substrate four symmetrical circular-shaped microstrip parasitic patches are placed one opposite the other, and a circular-shaped patch is located at the center of the antenna, which is connected to the inner pin of the coaxial. On the bottom surface of the substrate, a square-shaped ground plane is printed. A resonant frequency at 3.93 GHz is created with  $-10$  dB impedance bandwidth that ranges from 3.91 to 3.95 GHz as shown in Figure 4a. However, the maximum simulated gain value is 6.90 dB for the initial antenna at 3.93 GHz frequency as shown in Figure 3b.

In order to enhance the impedance bandwidth, a change in the ground plane was implemented as shown in Figure 3b. Meanwhile, as in the case of the previous step, on the top side of the substrate, the antenna geometry remains unchanged. As given in Figure 4a, the improved antenna 1 resonates at 6.29 GHz with  $-10$  dB impedance bandwidth that ranges from 5.83 to 7.27 GHz. Note that the improved antenna 1 has a bandwidth greater than that of the initial antenna. On the other hand, the maximum simulated gain value is around 4.30 dB as shown in Figure 4b.

In order to improve the impedance bandwidth, a change in the parasitic patch geometry is implemented. The circular side of the radiating cells becomes rectilinear as shown in Figure 3c. As illustrated in Figure 4a, the improved antenna 2 resonates at 6.29 GHz with  $-10$  dB impedance bandwidth that ranges from 5.35 to 7.33 GHz. Note that the improved antenna 2 has a bandwidth greater than that of the improved antenna 1. Meanwhile, the maximum simulated gain value is around 4.21 dB as shown in Figure 4b.

To make the antenna more adapted, deformation at the entry of the parasitic patches was carried out with slots in the form of triangles as shown in Figure 3d. The proposed reconfigurable antenna becomes more adapted. The designed antenna has a bandwidth of 5.31–6.95 GHz as shown in Figure 4a. Note that the final antenna has a gain greater than that of the other antennas. Meanwhile, the maximum simulated gain value at 5.8 GHz is around 6.0 dB as shown in Figure 4b. The choice of the fan-shaped design is intended to cover the whole azimuthal plane and to have a new antenna capable of yielding directive gain patterns in the azimuth plane.

#### 4. Parametric Study

A parametric study was achieved to comprehend the influence on the proposed antenna performance. Taking state 1 as an example, the parameters are optimized for antenna performance and tabulated in Table 1. In this section, we study the effects of the main geometric parameters on reflection coefficient (S11) and antenna gain. We present a parametric study of the proposed antenna

that is used to obtain the optimal values and the best performance by tuning one parameter at a time while other parameters are left invariable.

4.1. The Effect of the Length  $L_0$

The antenna reflection coefficient ( $S_{11}$ ) (dB) and the gain are simulated for different values of the length ( $L_0$ ) of fan-shaped radiating cells and the other dimensions remaining constant are presented in Figure 5. It can be seen that the impedance bandwidth of the proposed antenna remains stable and that the frequency resonances are shifted. As illustrated in Figure 5a, when  $L_0 = 21$  mm, the antenna becomes more adapted. On the other hand, the antenna gain remains almost stable for the 5.31–6.95 GHz band when the length  $L_0 = 21$  mm as shown in Figure 5b. Therefore, the optimal value of length is  $L_0 = 21$  mm.

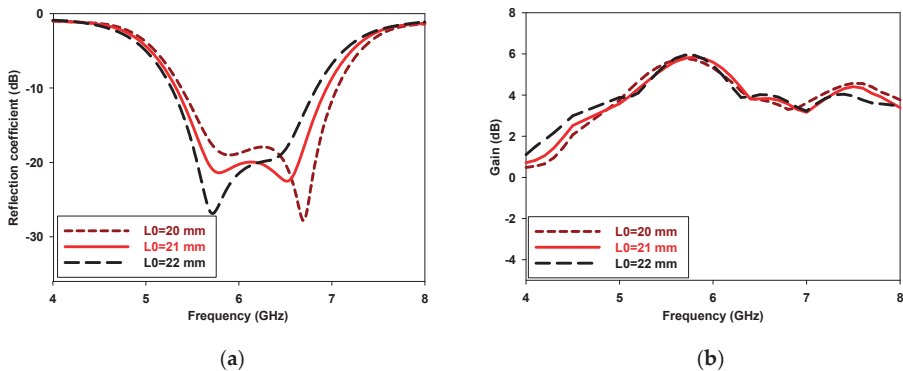


Figure 5. Simulated reflection coefficient and max gain versus the length  $L_0$ : (a) Reflection coefficient, (b) Max gain.

4.2. The Effect of the Angle  $\beta$

The antenna gain and parameter ( $S_{11}$ ) (dB) are also simulated as a function of the angle  $\beta$  variation. As presented in Figure 6a, the frequency resonances are shifted. Meanwhile, the antenna becomes more adapted when  $\beta = 40^\circ$ . Likewise, the antenna gain is larger at the 5.8 GHz frequency when the angle  $\alpha$  increases from  $36^\circ$  to  $44^\circ$  as shown in Figure 6b. Therefore, the optimum value of this angle is  $\beta = 40^\circ$ .

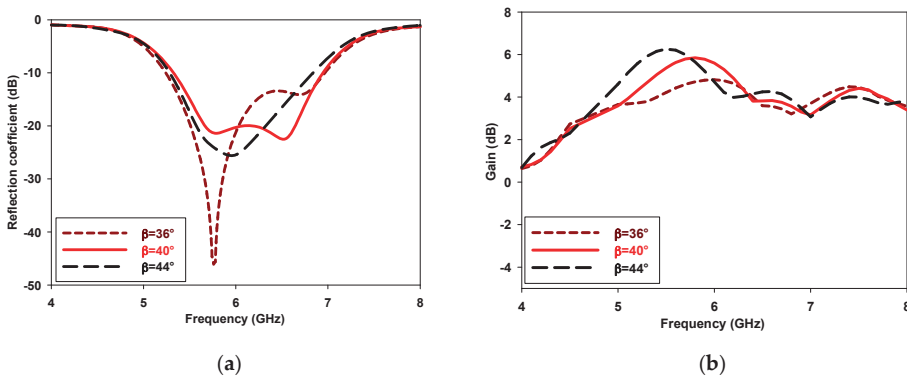


Figure 6. Simulated reflection coefficient and max gain versus the angle  $\beta$ : (a) Reflection coefficient, (b) Max gain.

### 5. Simulation Results and Discussion

Based on the PIN diode states, the different radiating elements of the antenna can be selectively powered by the circular patch. Therefore, a series of simulations was performed as given in Table 2. The PIN diode resistance and capacitance in the ON and OFF conditions are  $3 \Omega$ ,  $0 \text{ pF}$ , and  $25 \text{ k}\Omega$ ,  $0.8 \text{ pF}$ , respectively [18,19]. By controlling the biasing of the PIN diodes, the distribution of the antenna surface current will be modified; this will deflect the direction of the antenna radiation. The radiating cells operate either as reflector(s) or director(s) according to the switches states. This shows that the proposed antenna has four operating states named as state 1 (S1), state 2 (S2), state 3 (S3) and state 4 (S4).

Table 2. The antenna operating states.

Operating States	PIN Diode 1	PIN Diode 2	PIN Diode 3	PIN Diode 4
State 1	ON	ON	OFF	ON
State 2	ON	ON	ON	OFF
State 3	OFF	ON	ON	ON
State 4	ON	OFF	ON	ON

The reflection coefficient (S11) (dB) of the proposed wideband reconfigurable antenna is presented in Figure 7. The simulated results show that the proposed antenna has a bandwidth of 26.75% from 5.31 to 6.95 GHz with (S11) less than  $-23 \text{ dB}$ . The simulated results are obtained when the antenna operates in state 1. The same results are given for the other three operation states.

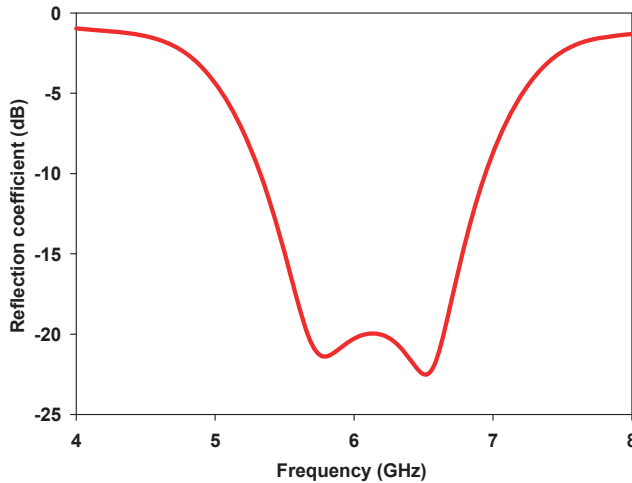
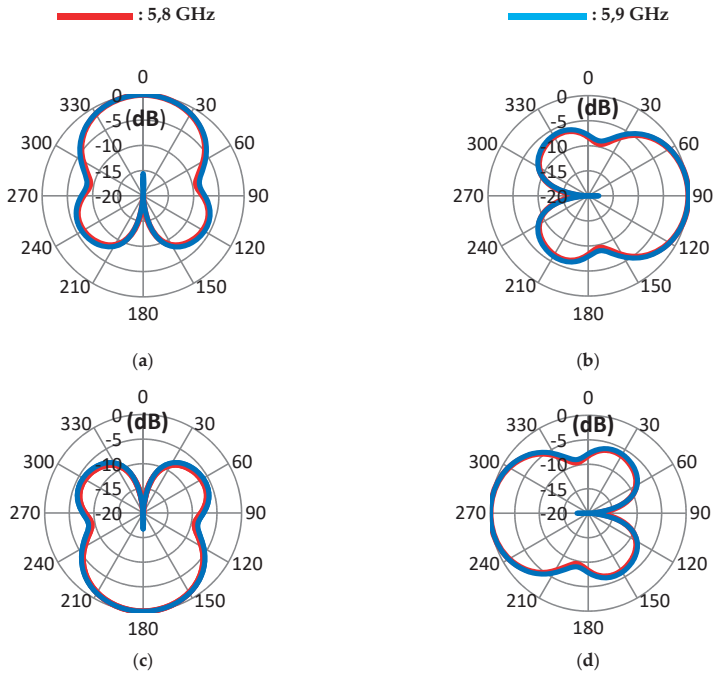
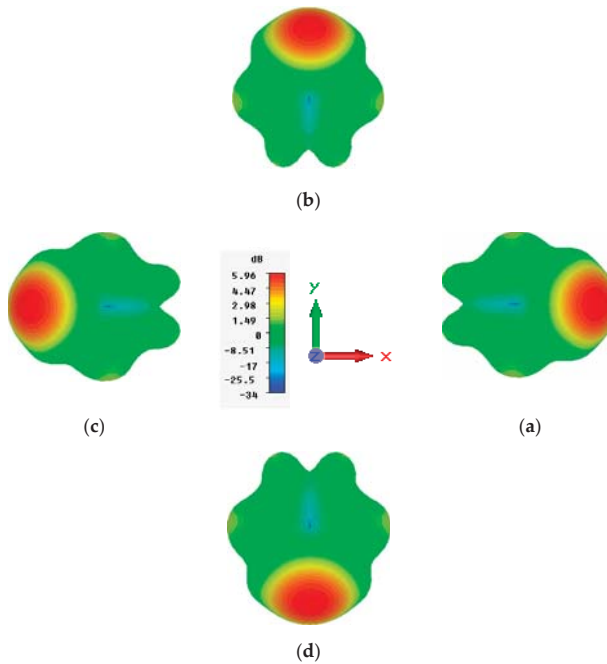


Figure 7. Simulated reflection coefficient S11 (dB).

Far-field radiation patterns of the proposed antenna are simulated using an electromagnetic simulator. Figure 8a–d show the simulated radiation patterns in the azimuth plane (XOY plane). The main beam of the proposed antenna can be steered to approximate  $\phi = 0^\circ$ ,  $\phi = 90^\circ$ ,  $\phi = 180^\circ$  and  $\phi = 270^\circ$ , for State 1 to State 4, respectively. The radiation patterns in elevation are similar and the main beam directions all point at  $\theta = 36^\circ$ . Far-field radiation patterns at frequencies 5.8 GHz and 5.9 GHz in the azimuth plane show that the proposed wideband reconfigurable pattern antenna radiates in four different directions as shown in Figures 8 and 9.



**Figure 8.** Simulated radiation patterns of the proposed wideband reconfigurable antenna in azimuth Plane: (a) State 1, (b) State 2, (c) State 3, (d) State 4.



**Figure 9.** Simulated 3D radiation patterns at 5.8 GHz: (a) State 1, (b) State 2, (c) State 3, (d) State 4.

To validate the proposed design, Table 3 presents a comparison between our wideband reconfigurable antenna and other previously reported designs. It is clear that the impedance bandwidth of this antenna is higher than that of all published patterns reconfigurable antenna. According to Table 3, the proposed antenna not only has pattern-reconfigurability and an enhanced bandwidth, but also possesses additional advantages—notably its smaller size.

**Table 3.** Comparison between recently proposed antennas and the proposed wideband reconfigurable antenna.

Ref. No.	Impedance Bandwidth	S11  (dB)	Peak Gain	Azimuth Plane Beam-Scanning	Switch No.	Size ( $\lambda_0^*$ )
[7]	18.6%	22	6–6.5 dBi	360°	4	$1.37 \times 1.37 \times 0.02$
[18]	4.7%	40	8.22 dB	360°	4	$0.94 \times 0.94 \times 0.03$
[19]	5.6%	20	4.7–7.3 dBi	180°	8	$1.17 \times 1.17 \times 0.08$
This work	26.7%	23	5.95 dB	360°	4	$1.14 \times 1.14 \times 0.01$

$\lambda_0^*$  is the wavelength of the free space.

## 6. Conclusions

In this work, a new wideband reconfigurable radiation pattern antenna using four fan-shaped radiation elements is simulated and studied. Based on the four PIN diode biasing, the nominated antenna can operate at four basic different modes and achieve radiation pattern reconfigurable characteristics. When the operation states of the proposed antenna steer sequentially, the main radiation beam can be changed in four different directions and can cover the whole azimuth plane. The designed antenna can supply a wideband ranging from 5.31 to 6.95 GHz. As is known, this band is exactly reserved for Wi-Fi, WiMAX, ITS and C-band satellite. Therefore, the proposed design fulfills the goal of this work absolutely.

**Conflicts of Interest:** The authors declare no conflict of interest.

## References

- Xie, P.; Wang, G.-M.; Li, H.-P.; Wen, T.; Kong, X. Frequency Reconfigurable Quasi-Yagi Antenna with a Novel Balun Loading Four PIN Diodes. *Frequenz* **2018**, *72*, 189–195. [\[CrossRef\]](#)
- Saeed, S.M.; Balanis, C.A.; Birtcher, C.R. Inkjet-Printed Flexible Reconfigurable Antenna for Conformal WLAN/WiMAX Wireless Devices. *IEEE Antennas Wirel. Propag. Lett.* **2016**, *15*, 1979–1982. [\[CrossRef\]](#)
- Kim, J.; Sung, Y. Dual-Band Microstrip Patch Antenna with Switchable Orthogonal Linear Polarizations. *J. Electromagn. Eng. Sci.* **2018**, *18*, 215–220. [\[CrossRef\]](#)
- Ramli, N.; Ali, M.T.; Islam, M.T.; Yusof, A.L.; Muhamud-Kayat, S. Aperture-Coupled Frequency and Patterns Reconfigurable Microstrip Stacked Array Antenna. *IEEE Trans. Antennas Propag.* **2015**, *63*, 1067–1074. [\[CrossRef\]](#)
- Nguyen-Trong, N.; Hall, L.; Fumeaux, C. A Frequency- and Polarization-Reconfigurable Stub-Loaded Microstrip Patch Antenna. *IEEE Trans. Antennas Propag.* **2015**, *63*, 5235–5240. [\[CrossRef\]](#)
- Rahmani, F.; Touhami, N.A.; Kchairi, A.B.; Taher, N. Circular Planar Antenna with Reconfigurable Radiation Pattern using PIN Diodes. *Procedia Manuf.* **2020**, *46*, 760–765. [\[CrossRef\]](#)
- Cheng, Y.-F.; Ding, X.; Wang, B.-Z.; Shao, W. An Azimuth-Pattern-Reconfigurable Antenna with Enhanced Gain and Front-to-Back Ratio. *IEEE Antennas Wirel. Propag. Lett.* **2017**, *16*, 2303–2306. [\[CrossRef\]](#)
- Li, H.; Wu, M.; Yuan, S.; Zhou, C. Design of Off-Center Fed Windmill Loop for Pattern Reconfiguration. *IEEE Antennas Wirel. Propag. Lett.* **2019**, *18*, 1626–1630. [\[CrossRef\]](#)
- Tran, H.H.; Park, H.C. Wideband Reconfigurable Antenna With Simple Biasing Circuit and Tri-Polarization Diversity. *IEEE Antennas Wirel. Propag. Lett.* **2019**, *18*, 2001–2005. [\[CrossRef\]](#)
- Liu, B.-J.; Qiu, J.-H.; Wang, C.-L.; Li, G.-Q. Pattern-Reconfigurable Cylindrical Dielectric Resonator Antenna Based on Parasitic Elements. *IEEE Access* **2017**, *5*, 25584–25590. [\[CrossRef\]](#)
- Jin, G.; Li, M.; Liu, D.; Zeng, G. A Simple Planar Pattern-Reconfigurable Antenna Based on Arc Dipoles. *IEEE Antennas Wirel. Propag. Lett.* **2018**, *17*, 1664–1668. [\[CrossRef\]](#)

12. Chen, S.-L.; Qin, P.; Lin, W.; Guo, Y. Pattern-Reconfigurable Antenna with Five Switchable Beams in Elevation Plane. *IEEE Antennas Wirel. Propag. Lett.* **2018**, *17*, 454–457. [[CrossRef](#)]
13. Tawk, Y.; Costantine, J.; Makhoul, F.; Nassif, M.; Geagea, L.; Christodoulou, C.G. Wirelessly Automated Reconfigurable Antenna with Directional Selectivity. *IEEE Access* **2017**, *5*, 802–811. [[CrossRef](#)]
14. Tang, M.-C.; Zhou, B.; Duan, Y.; Chen, X.; Ziolkowski, R.W. Pattern-Reconfigurable, Flexible, Wideband, Directive, Electrically Small Near-Field Resonant Parasitic Antenna. *IEEE Trans. Antennas Propag.* **2018**, *66*, 2271–2280. [[CrossRef](#)]
15. Ma, W.D.; Wang, G.M.; Wang, Y.W.; Zong, B.F. Compact Microstrip Antenna with Pattern-Reconfigurable Characteristic. *Radioengineering* **2017**, *26*, 662–667. [[CrossRef](#)]
16. Khan, M.S.; Iftikhar, A.; Capobianco, A.-D.; Shubair, R.M.; Ijaz, B. Pattern and frequency reconfiguration of patch antenna using PIN diodes. *Microw. Opt. Technol. Lett.* **2017**, *59*, 2180–2185. [[CrossRef](#)]
17. He, X.; Gao, P.; Zhu, Z.; You, S.; Wang, P. A flexible pattern reconfigurable antenna for WLAN wireless systems. *J. Electromagn. Waves Appl.* **2019**, *33*, 782–793. [[CrossRef](#)]
18. Rahmani, F.; Touhami, N.A.; Kchairi, A.B.; Taher, N.; El Ouahabi, M. Reconfigurable Radiation Pattern Antenna Using Kite-Shaped Parasitic Patches for Wireless Access Applications. *Int. J. Microw. Opt. Technol.* **2020**, *15*, 187–195.
19. Deng, W.-Q.; Yang, X.-S.; Shen, C.-S.; Zhao, J.; Wang, B.-Z. A Dual-Polarized Pattern Reconfigurable Yagi Patch Antenna for Microbase Stations. *IEEE Trans. Antennas Propag.* **2017**, *65*, 5095–5102. [[CrossRef](#)]
20. Datasheet of Microsemi MPP4203 PIN Diodes. Available online: <http://www.microsemi.com> (accessed on 1 March 2020).

**Publisher’s Note:** MDPI stays neutral with regard to jurisdictional claims in published maps and institutional affiliations.



© 2020 by the authors. Licensee MDPI, Basel, Switzerland. This article is an open access article distributed under the terms and conditions of the Creative Commons Attribution (CC BY) license (<http://creativecommons.org/licenses/by/4.0/>).



# Effect of the Variation in Humidity of the Medium on the GPR Radar Response <sup>†</sup>

Aye Mint Mohamed Mostapha <sup>1,\*</sup>, Gamil Alsharahi <sup>2</sup>, Ahmed Faize <sup>2</sup> and Abdellah Driouach <sup>1</sup>

<sup>1</sup> Faculty of Sciences, Abdelmalek Essaâdi University, Tetouan 93000, Morocco; adriouach@hotmail.com

<sup>2</sup> Faculty Polydisciplinarily, Mohammed 1st University, Nador 60000, Morocco; alsharahigamil@uae.ac.ma (G.A.); ahmedfaize6@hotmail.com (A.F.)

\* Correspondence: aye.muhamed@gmail.com

<sup>†</sup> Presented at the 14th International Conference INTER-ENG 2020 Interdisciplinarity in Engineering, Mures, Romania, 8–9 October 2020.

Published: 18 December 2020

**Abstract:** This work presents research on the influence of the variation in humidity of the medium on the Ground-penetrating radar GPR response. During this research, we used a GPR SIR 3000 system coupled with a 400 MHz frequency antenna, and GprMax and Reflexw software, which are based on the numerical method known as finite difference in time domain (FDTD). The results obtained (experimental and by simulation) have shown that the reflection force and the penetration depth of GPR waves are strongly related to the physical properties of the objects and the medium inspected. The increase in the conductivity of the inspected medium causes a reduction in the depth of the GPR waves, which causes the non-detection of objects.

**Keywords:** electromagnetic wave; Snell's law; conductivity; ground penetrating radar; object detection; humidity; Reflexw and GprMax simulation

## 1. Introduction

Ground penetrating radar is a non-destructive technique used to assess the location and depth of underground targets [1,2]. It is based on the emission, by an antenna coupled to the ground, of short electromagnetic pulses, of harmonic waves confined to a certain frequency band. Once the transmitted signal is returned, by deep-buried objects, it will be picked up by the GPR receiving antenna and will be transformed into a response signal, which is in the form of an image called a radargram. This image radargram will be processed with specialized software to collect information from the subsoil [3]. Its wide range of sampling frequency combined with its non-destructive nature and its ease of implementation have enabled it to find a large number of applications [4] such as archeology, the construction of buildings, the detection of antipersonnel mines, shallow geological research or the criminal science sector, where it can be used to find corpses or buried weapons, etc. [5–8]. GPR provides the precise spatial location of targets from high-resolution images over short periods. These images can be affected by several factors such as the nature of the ground, internal and external noise, etc. The interest of this work focuses on the influence of the variation in soil humidity on the quality of the radargram.

## 2. Snell–Descartes Laws

When an electromagnetic wave strikes the interface between two media with different dielectric properties, part of its energy is reflected and the rest is transmitted to the lower medium (Figure 1). The incident, reflected and transmitted wave directions are linked together by Snell's law [9–11].

$$\theta_i = \theta_r \text{ (Snell's law of reflection)} \quad (1)$$



$$\beta_1 \sin \theta_i = \beta_2 \sin \theta_t \tag{2}$$

$\beta_1$ : medium1 wave number;  $\beta_2$ : medium2 wave number.

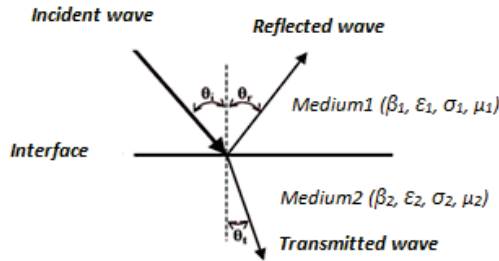


**Figure 1.** Diagram representing the phenomena of reflection and transmission at the interface between two media which represent different dielectric contrasts.

If several interfaces are present, this rule must be applied to each limit and the wavefront or rays must bend or change direction at each limit. If the speed or the materials vary continuously, this relationship still applies. In GPR, medium 1 can easily be considered as an atmospheric environment and medium 2 considered as the soil or material to be probed [12,13].

### 3. Methodology

In this work, we have used a GPR SIR3000, Gprmax and Reflexw software.

- GPR SIR3000

The SIR3000 is a lightweight, portable, single-channel (Figure 2), ground-penetrating radar system that is ideal for a wide variety of applications.



**Figure 2.** GPR SIR3000.

- Reflexw

This is a processing software program for GPR and seismic wave propagation based on the Finite-difference time-domain FDTD. Field data as well as synthetic data can be processed in two and three dimensions. In our case, we used the Reflexw 2D [14].

- GprMax2d

GprMax is based on FDTD and is available free of charge for both academic and commercial use; it has been successfully employed in many situations. The tool can be downloaded from [www.gprmax.org](http://www.gprmax.org) or by contacting the author [14].

## 4. Results and Discussion

### 4.1. Simulation Results

The purpose of this paragraph is to show the influence of the humidity of the medium on the GPR operation. We simulated the detection of a conductive object (circular) buried in a medium of wet sand by varying each time the conductivity of the medium and the depth of the object.

- With a conductivity of 0.001 s/m, the targets are easily detectable by the GPR in the two depths chosen for this study: 0.3 and 0.7 m.
- We also note that with a conductivity of 0.01 s/m, the GPR detects objects but with less visible hyperbolas than for the previous case.
- Meanwhile, for a conductivity of 0.1 s/m, and at a depth of 0.3, the presence of the object is indicated by an almost invisible hyperbola, and at a depth of 0.7 m, the object is invisible.

Following the results obtained, it is clear that the change in conductivity affects the quality of the GPR results.

#### 4.1.1. Simulation of a Medium with a Conductivity of 0.001 s/m

Figure 3a,b present two models of two conductive objects buried in a medium of wet sand with a conductivity of 0.001 s/m at two different depths, 0.3 and 0.7 m, while Figure 3c,d present the radargrams obtained. We note the detection of two objects in this case; the presence of each object is indicated by the presence of a clearly visible hyperbola.

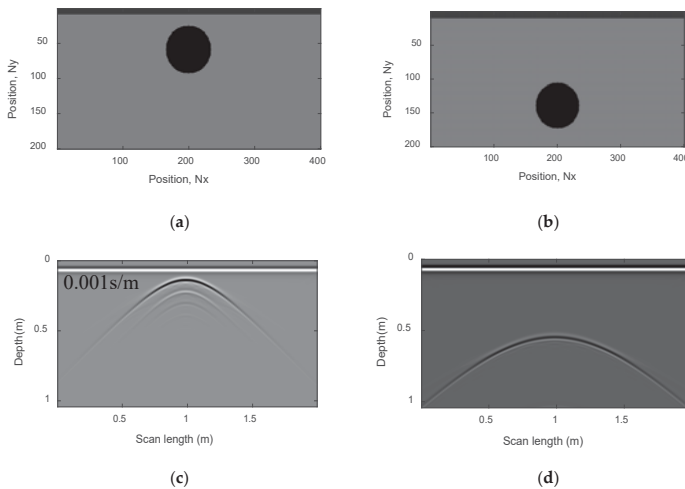


**Figure 3.** Simulation results (a,b) models of two conductive objects buried in a medium of wet sand at a depth of 0.3 and 0.7 m (c,d) object detection radargrams.

#### 4.1.2. Simulation of a Medium with a Conductivity of 0.01 s/m

In this case, we simulated the detection of the same previous objects in the medium of wet sand with a conductivity of 0.01 s/m. On the obtained radargrams (Figure 4c,d), we note that the hyperbolas

indicating the presence of objects are less clear than the previous case due to the increase in the conductivity of the medium.

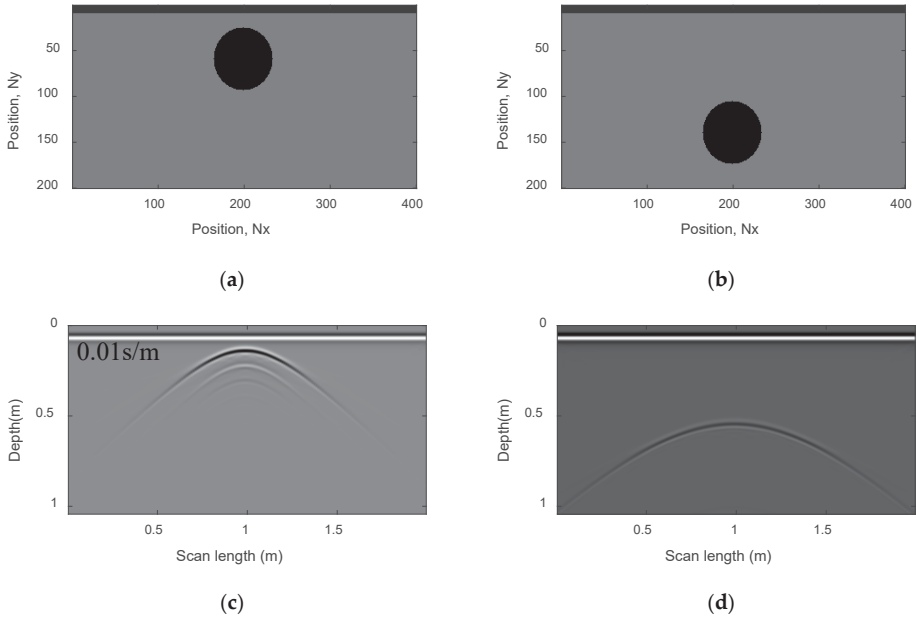


**Figure 4.** Simulation results(a,b) two conductive objects buried in a wet sand medium at a depth of 0.3 and 0.7 m (c,d) object detection radargrams.

#### 4.1.3. Simulation of a Medium with a Conductivity of 0.1 s/m

In the case where the conductivity of the medium is 0.1 s/m, we note the detection of the object at a depth of 0.3 m, with a hyperbola that is almost invisible, while at a depth of 0.7 m, the object is invisible due to the increased conductivity of the medium and the depth of the target (Figure 5c,d).

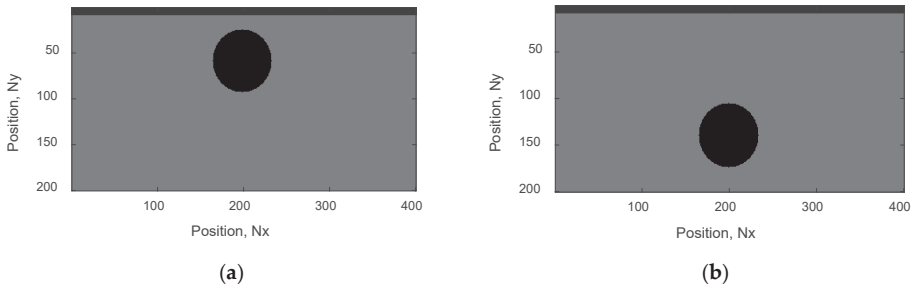


**Figure 5.** Cont.

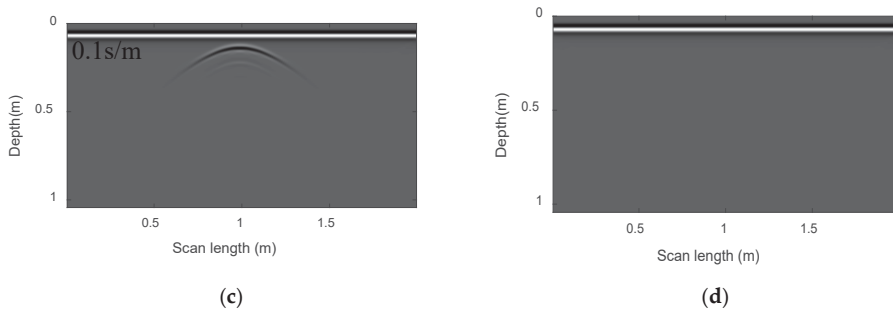


**Figure 5.** Simulation results(a,b) two conductive objects buried in a wet sand medium at a depth of 0.3 and 0.7 m (c,d) object detection radargrams.

#### 4.2. Experimental Results (by GPR Radar)

This section presents experiments carried out on the beach in the city of Martil (located 12 km from Tétouan), in order to detect buried objects of different types using our GPR radar system (model SIR3000), equipped with an antenna of 400 MHz. For this experimental study, we used:

- A conductive object,
- A container (empty and filled with sea water) and
- A rocky object.

The results obtained experimentally by the GPR were processed by the Reflexw software; with this same software, and using the same objects mentioned above, we carried out simulations of the GPR measurements and we found good agreement between them.

##### 4.2.1. Conductive Object

For the detection of the buried conductive object (Figure 6), we chose two depths: 0.3 and 0.5 m:

- Depth 0.3 m



**Figure 6.** Image of a conductive object with dimensions  $0.61 \times 0.35$  m.

Figure 7a shows the radargram obtained at this depth; we can see the presence of the hyperbola indicating the object in question. It is clearly visible, due to strong reflections by the conductive object. Figure 7b shows the result of the same object and under the same conditions as those of the experiment.

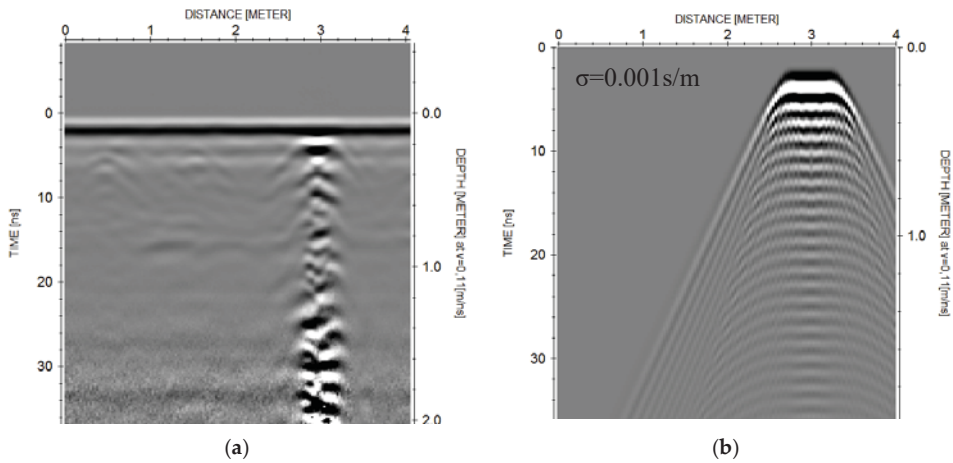


Figure 7. (a) Result obtained by GPR, and (b) result obtained by simulation.

- Depth of 0.5 m

At a depth of 0.5 m, we noticed that the hyperbolas which represent the conductive object seem less visible than for the previous case (depth of 0.3 m), due to the increase in depth, which decreases the intensity wave reflection. We also observed this difference in the results obtained by simulation, shown in Figure 8b.

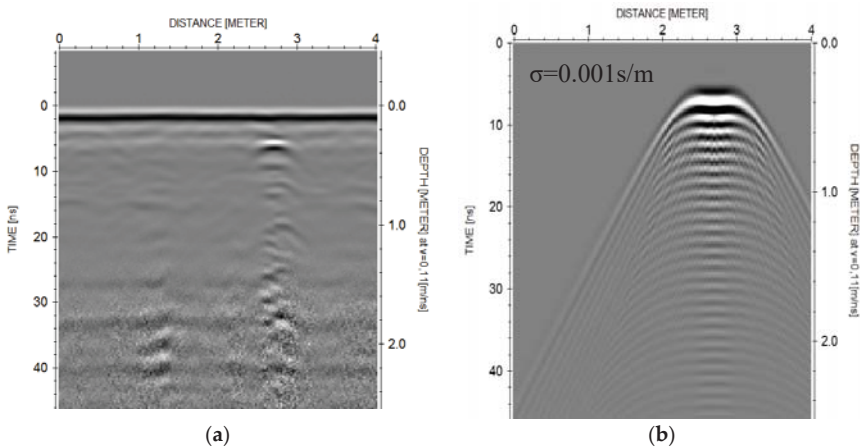
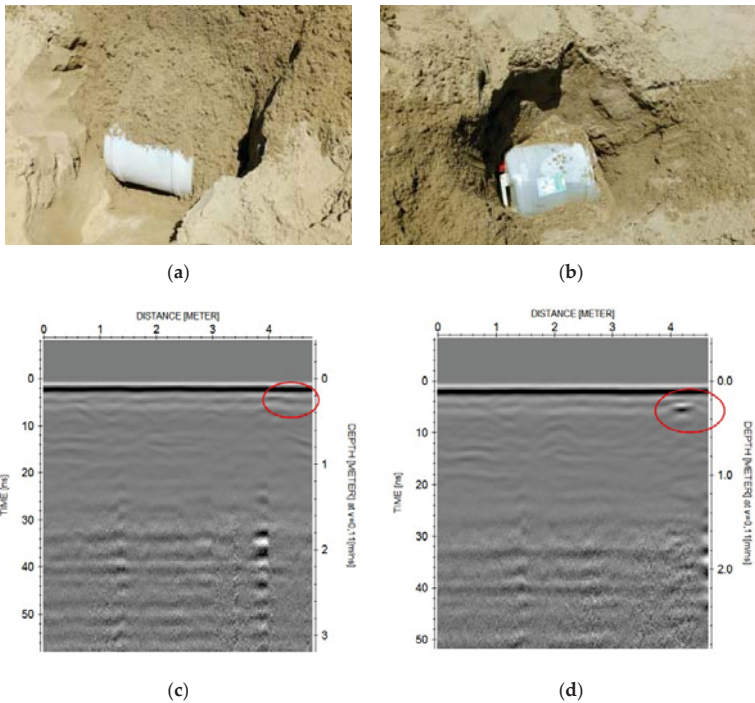


Figure 8. (a) Result obtained by GPR, (b) result obtained by simulation.

#### 4.2.2. Use of Dielectric Objects: A Plastic Container (Empty Then Filled with Seawater)

During this experiment, we proceeded as follows:

- First, we tested the GPR with an empty underground container (Figure 9);
- Then, in a second step, we used the same container but this time the container was filled with sea water (see Figure 9b).



**Figure 9.** (a) Image of an empty container, (b) image of a container filled with water, (c,d) the resulting radargrams.

We found that the GPR could not detect the presence of the empty container (Figure 9c). On the other hand, when the container was filled with sea water, which has a high conductivity, the visibility of the object was better (Figure 9d). This is due to the significant difference in permittivity between the water inside the container and the medium, which created strong signal reflection.

#### 4.2.3. Use of a Rocky Object

In this case, we buried a rocky object at a depth of 0.2 m (Figure 10a); despite this small depth, the GPR was unable to detect the object, which was due to the humidity of the environment and the poor reflection of the rocky object.

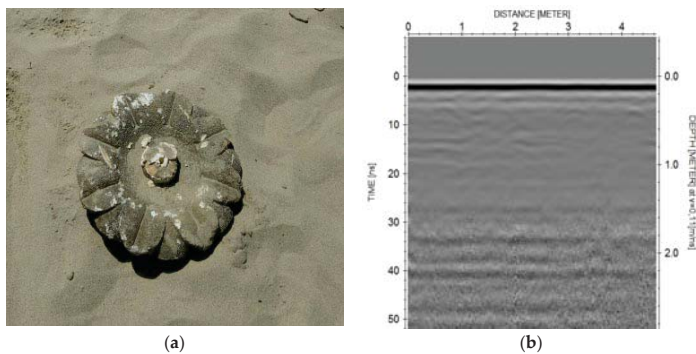


**Figure 10.** (a) Image of a rock, (b) radargram obtained.

## 5. Conclusions

The study presented in this work allowed us to gain a global idea of the GPR response for targets with different physical properties and shapes, buried in a wet sand medium.

The results obtained showed that:

- The conductive objects are easily detectable by GPR due to their high conductivities, which cause total reflection of the signal.
- The higher the difference in permittivity between the object and the medium, the greater the reflection strength of the signal.
- The humidity of the medium reduces the penetration depth of GPR waves, which causes the non-detection of targets.

## References

1. Kanli, A.I.; Taller, G.; Nagy, P.; Tildy, P.; Pronay, Z.; Toros, E. GPR survey for reinforcement of historical heritage construction at fire tower of Sopron. *J. Appl. Geophys.* **2015**, *112*, 79–90. [[CrossRef](#)]
2. Boubaki, N. Détection de Cavités Par Deux Méthodes Géophysiques: Radar de Sol et Mesures de Résistivités Électriques. Ph.D. Thesis, Université Paris Sud-Paris XI, Orsay, France, 2013.
3. Mostapha, A.M.M.; Alsharahi, G.; Driouach, A. Effect of External Noise on Ground Penetrating Radar Ability to Detect Objects. *Int. J. Microw. Opt. Technol.* **2019**, *14*, 124–131.
4. Alsharahi, G.; Faize, A.; Louzazni, M.; Mostapha, A.; Bayjja, M.; Driouach, A. Detection of cavities and fragile areas by numerical methods and GPR application. *J. Appl. Geophys.* **2019**, *164*, 225–236. [[CrossRef](#)]
5. Heggy, E. Etude et Modélisation des Performances des Radars Sondeurs Basse Fréquence Pour la Recherche de l'eau Dans le Sous-Sol de Mars. Ph.D. Thesis, Université Pierre et Marie Curie-Paris VI, Paris, France, 2002.
6. Potin, D. Traitement des Signaux Pour la Détection de Mines Antipersonnel. Ph.D. Thesis, Ecole Centrale de Lille, Villeneuve-d'Ascq, France, 2007.
7. Faize, A.; Alsharahi, G.; Hamdaoui, M. Radar GPR Application to Explore and Study Archaeological Sites: Case Study. *Int. J. Adv. Comput. Sci. Appl.* **2020**, *11*, 179–182. [[CrossRef](#)]
8. Alsharahi, G.; Faize, A.; Maftai, C.; Bayjja, M.; Louzazni, M.; Driouach, A.; Khamlichi, A. Analysis and Modeling of GPR Signals to Detect Cavities: Case Studies in Morocco. *J. Electromagn. Eng. Sci.* **2019**, *19*, 177–187. [[CrossRef](#)]
9. Zhao, W.; Forte, E.; Fontana, F.; Pipan, M.; Tian, G. GPR imaging and characterization of ancient Roman ruins in the Aquileia Archaeological Park, NE Italy. *Measurement* **2018**, *113*, 161–171. [[CrossRef](#)]
10. Annan, P. *Ground Penetrating Radar Principles, Procedures and Applications*; Sensors and Software: Mississauga, ON, Canada, 2003; 278p.
11. Hamdaoui, M. Effect of electromagnetic parameters of the medium on the GPR data. *Int. J. Emerg. Trends Eng. Res.* **2020**, *8*, 1749–1755. [[CrossRef](#)]
12. Perez, R. Contribution à l'analyse Théorique et Expérimentale de Bscan GPR: Performances des Antennes: Apports d'une Configuration Multistatique. Ph.D. Thesis, Université de Limoges, Limoges, France, 2005.
13. Mehennaoui, N. Etude Théorique de la Propagation des Ondes Électromagnétiques Dans les Milieux Hétérogènes-Application au Radar Sol. Master's Thesis, Université Ferhat Abbas-Setif, Sétif, Algeria, 2018.
14. Mostapha, A.M.M.; Alsharahi, G.; Driouach, A. Simulation effect of polarization of targets on the Ground Penetrating Radar response. In Proceedings of the 2017 International Conference on Wireless Technologies, Embedded and Intelligent Systems (WITS), Fez, Morocco, 19–20 April 2017.

**Publisher's Note:** MDPI stays neutral with regard to jurisdictional claims in published maps and institutional affiliations.



© 2020 by the authors. Licensee MDPI, Basel, Switzerland. This article is an open access article distributed under the terms and conditions of the Creative Commons Attribution (CC BY) license (<http://creativecommons.org/licenses/by/4.0/>).



# Design of Transparent Antenna for 5G Wireless Applications <sup>†</sup>

Sanae Azizi <sup>1</sup>, Laurent Canale <sup>2,\*</sup>, Saida Ahyoud <sup>3</sup>, Georges Zissis <sup>2</sup> and Adel Asselman <sup>1</sup>

<sup>1</sup> Optics and Photonics Laboratory, Abdelmalek Essaadi University, 93030 Tetouan, Morocco; sanae.azizi5@gmail.com (S.A.); adelasselman@gmail.com (A.A.)

<sup>2</sup> LAPLACE, Université de Toulouse, CNRS, INPT, UPS 31000 Toulouse, France; georges.zissis@laplace.univ-tlse.fr

<sup>3</sup> Information Technology and System Modeling Team, Abdelmalek Essaadi University, 93030 Tetouan, Morocco; sa\_ahyoud@yahoo.fr

\* Correspondence: Laurent.canale@laplace.univ-tlse.fr

<sup>†</sup> Presented at the 14th International Conference INTER-ENG 2020 Interdisciplinarity in Engineering, Mureş, Romania, 8–9 October 2020.

Published: 28 December 2020

**Abstract:** This paper presents the design of a compact size band patch antenna for 5G wireless communications. This wideband antenna was designed on a glass substrate ( $12 \times 11 \times 2 \text{ mm}^3$ ) and is optically transparent and compact. It consists of a radiation patch and a ground plane using AgHT-8 material. The antenna design comprises rectangular shaped branches optimized to attain the wideband characteristics. The calculated impedance bandwidth is 7.7% covering the frequency range of 25 to 27 GHz. A prototype of the antenna and various parameters such as return loss plot, gain plot, radiation pattern plot, and voltage standing wave ratio (VSWR) are presented and discussed. The simulated results of this antenna show that it is well suited for future 5G applications because of its transparency, flexibility, light weight, and wide achievable frequency bandwidth near the millimeter wave frequency band.

**Keywords:** transparent antenna; 5G communications; AgHT material; glass substrate; optical antenna

## 1. Introduction

Over recent decades, wireless mobile communication technology has developed significantly despite its relatively recent establishment. The fifth generation (5G) mobile communication system will be deployed on a large scale in the next decade, and it will bring us many advantages such as higher transmission rate, high bit rate with lower battery consumption, and shorter latency than the current 4G system [1,2].

Today, the modern telecommunication industries are already moving towards 5G enabled devices, and some are working on fully transparent and flexible devices [3]. Such cases create the need for flexible and transparent antennas to be designed in the 5G and millimeter wave frequency band.

Transparent antennas operating in the wireless frequency regions are useful in glass-mounted applications including automobiles, homes, and businesses where transmission and reception through or from a window is desired. Transparent antennas have been fabricated with AgHT materials, indium tin oxide (ITO) [4,5], and fluorine doped tin oxide on glass and polyimide. The use of a transparent conductor can pose challenges in fabrication and in application [6].

Among them are losses in films with lower conductivities, film thicknesses less than skin depth, and other complications, specifically additional losses and lower radiation efficiency posed by the presence of a transparent ground plane on thin substrates in standard, planar antennas.



The main objective of this work was to design and analyze a transparent antenna operating in the wide frequency band of 26 GHz. The frequency range extends from 25 to 27 GHz, which covers the band for 5G applications. The size of the compact antenna is  $(12 \times 11 \times 2 \text{ mm}^3)$ .

The article is organized as follows. Section 2 summarizes a literature review, and Section 3 describes the antenna design and its initial calculation. Results and discussion are presented in Section 4 followed by the conclusion in Section 5.

## 2. Literature Review

The antenna design is one of the most important factors to be considered in order to fully utilize the 5G technology. However, a few design issues can affect an antenna’s performance. Aside from that, in fabrication process, mechanical inaccuracies and errors can affect the antenna performance [7]. As presented in Table 1, a number of transparent antenna designs have been proposed in literature such as dual-band [8,9] and ultra-wideband [10–13] characteristics, but very few cover millimeter wave applications. In Ref. [14], a semi-transparent flexible antenna working in the range of 7 to 13 GHz is proposed for 5G applications using polyethylene terephthalate (PET) and silver nanoparticles.

**Table 1.** Comparison of the proposed transparent antenna with other existing antennas.

Ref	Operating Bands (GHz)	Return Loss at Resonance (dB)	Gain (dB)	Transparent	Size (mm <sup>2</sup> )
[14]	7–13	<10	5	Semi-transparent	60 × 75
[12]	2.2–12.1	<10	3–5	Yes	17 × 33.5
[11]	2–13	<10	1.5–3	Yes	20 × 20
Proposed antenna	25–27	40	5.5	Yes	12 × 11

This paper proposes a transparent patch microstrip antenna working at 26 GHz frequency with compact size, simple shape, and good performance.

## 3. Antenna Design and Parameters

This section describes in detail the geometrical configuration and a procedure for designing the transparent compact antenna for 5G applications. The concept of designing this antenna is based on the square ring monopole antenna structure.

### 3.1. Design of Transparent Antenna for 5G

Figure 1 shows the stepwise design evolution of the proposed antenna, which was designed and optimized using CST Microwave Studio software simulator.

The optically transparent antenna comprises transparent glass with a dielectric constant of 4.82 and 2 mm thickness as the substrate material. Transparent conductive oxide AgHT-8 with a surface resistivity of  $8 \Omega/\text{m}$ , which is equivalent to the conductivity of 125,000 S/m, constitutes the patch radiator and ground. A feed line with a width of 3.58 mm is used to achieve  $50 \Omega$  impedance matching.

Front and rear views of the proposed antenna are shown in Figure 1a,b. A partial ground plane is used to increase the performance of the antenna and ensure the impedance matching. The optimized dimensions of the proposed transparent antenna are listed in Table 2.

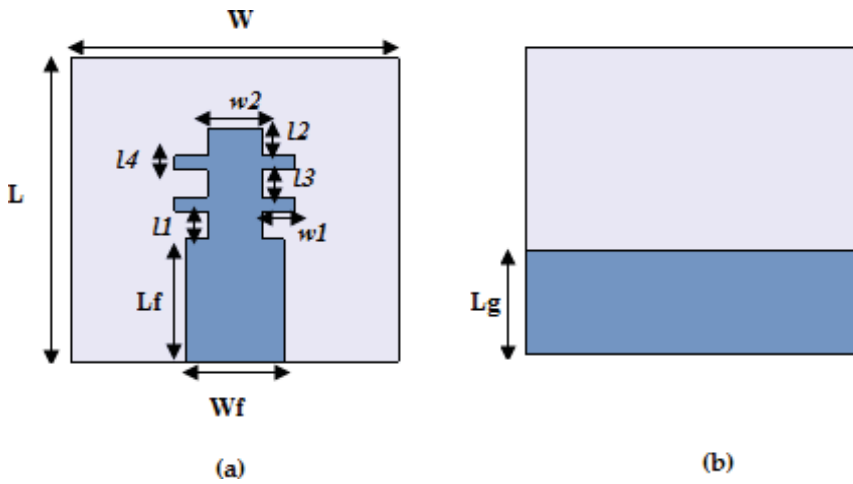


Figure 1. Geometry of proposed transparent antenna. (a) Front view; (b) rear view.

Table 2. Dimensions of the proposed antenna.

Parameters	Dimension (in mm)
$L$	11
$W$	12
$W_f$	3.58
$L_f$	4.45
$L_1$	1
$L_2$	1
$L_3$	1
$L_4$	0.5
$w_1$	1.2
$w_2$	2
$L_g$	4.4
$tm$	0.0177
$hs$	2

### 3.2. Parametric Study

Parametric investigation of the rectangular arm widths was performed to investigate the performance of the proposed antenna. In this study, rectangular arm width variations are given as terms  $w_1$  and  $w_2$ .

Figures 2 and 3 show the performance of the proposed transparent antenna with the variations of  $w_1$  and  $w_2$ . From Figure 2, it is seen that the return-loss performance is better for  $w_1 = 1.2$  mm. When  $w_1$  increases from 0.8 to 1.2 mm, the wide bandwidth ranges from 25 to 27 GHz, supporting the bandwidth requirements for 5G. The  $-10$  dB reflection coefficient performance degrades with further decrease in the rectangular arm's width. From Figure 3, it can be seen that the best impedance matching is obtained as  $w_2 = 2$  mm. The center frequency is around 26 GHz, and the bandwidth covered is from 25 to 27 GHz.

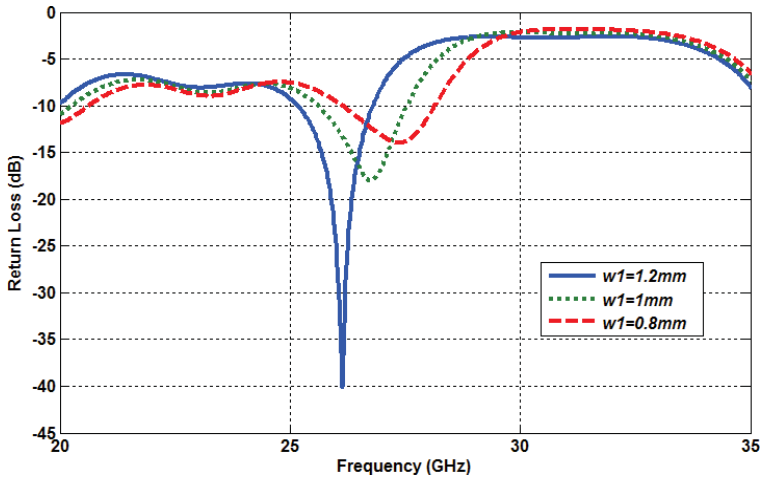


Figure 2. Antenna performance with the variations in term  $w_1$ .

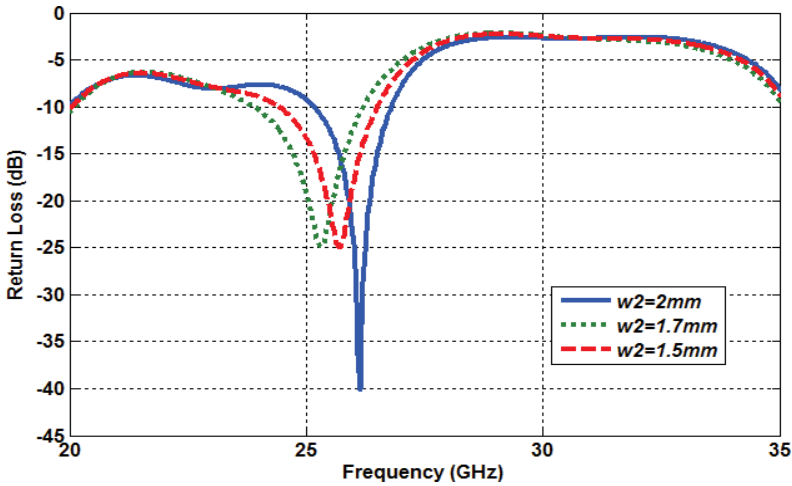


Figure 3. Antenna performance with the variations in term  $w_2$ .

The optimum values of  $w_1$  and  $w_2$  were selected as 1.2 and 2 mm, respectively.

#### 4. Simulation Results and Analysis

Simulations of the proposed antenna were performed using Computer Simulation Technology (CST) Microwave Studio. An antenna parameter of significant importance in the antenna is the reflection coefficient ( $S_{11}$ ), which defines the bandwidth and the impedance matching characteristic. The simulated result of the return loss for transparent antenna is depicted in Figure 4. The simulated results show that the single element antenna has a reflection coefficient ( $S_{11}$ ) of  $-40$  dB, less than  $-10$  dB in the frequency range of 25 to 27 GHz. More than 2 GHz of impedance bandwidth was obtained.

Another imperative parameter beside the reflection coefficient and input impedance that reflects the antenna performance is the voltage standing wave ratio (VSWR). The antenna is only able to operate at frequencies where the values of VSWR are less than 2 (Figure 5).

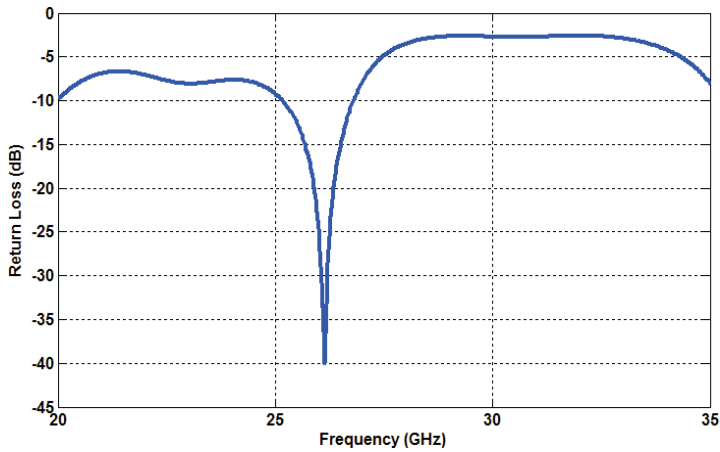


Figure 4. Simulated return loss (S11) for proposed antenna.

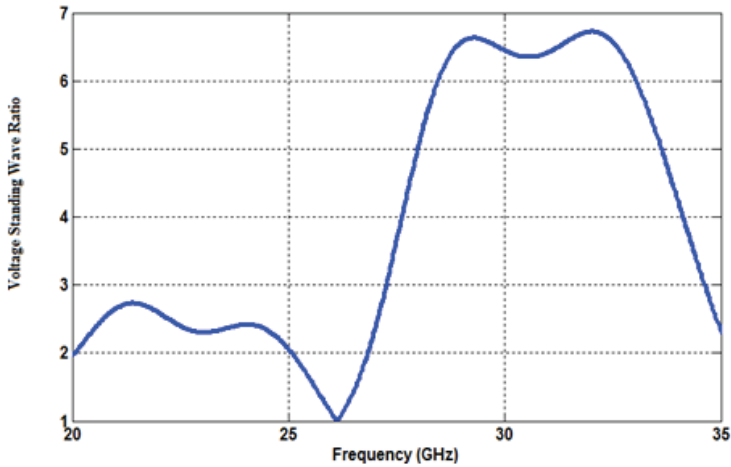


Figure 5. Voltage standing wave ratio (VSWR) values of the single element antenna.

The gain performance of the proposed transparent antenna is shown in Figure 6. The high positive gain performance is observed all over the working frequency band. The peak gain of about 5.5 dB is observed at 26 GHz. This positive gain and widespread radiation pattern ensure the stable performance of the antenna for 5G applications.

The radiation patterns in terms of E-plane and H-Plane are shown in Figure 7. It can be noticed that the E plane radiation pattern appears bi-directional at 26 GHz, and the H plane pattern covers a wide aperture angle with three main orientations.

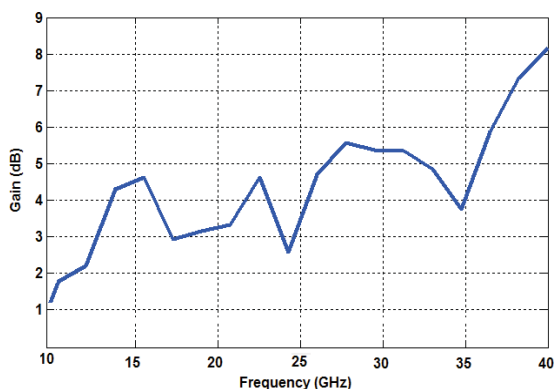


Figure 6. Simulated peak gain of the proposed antenna.

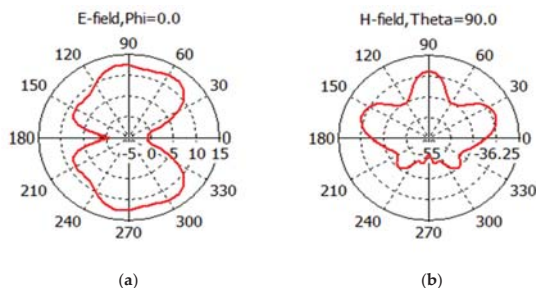


Figure 7. (a) E-plane radiation pattern at 26 GHz; (b) H-plane radiation pattern at 26 GHz.

### 5. Conclusions

With the development of 5G communication, the integration of transparent antennas on glass surfaces or OLED lighting sources will become a necessity in the next decade. In this study, transparent antennas of simple shape and miniaturized structure were investigated. The proposed antenna is potentially a good option for fifth generation (5G) wireless systems that require high gain topology and low profile. The simulated results show a reflection coefficient of  $-40$  dB with an S11 of less than  $-10$  dB in the frequency range 25 to 27 GHz and an impedance bandwidth of more than 2 GHz. In the future, we will try to manufacture the proposed antenna and compare the radiation pattern and reflection coefficient of the simulated and measured results.

**Author Contributions:** Conceptualization, S.A. (Sanae Azizi) and S.A. (Saida Ahyoud); methodology, S.A. (Sanae Azizi) and A.A.; validation, L.C., S.A. (Sanae Azizi) and A.A.; formal analysis, S.A. (Sanae Azizi); investigation, S.A. (Sanae Azizi); resources, S.A. (Sanae Azizi); data curation, S.A. (Sanae Azizi), S.A. (Saida Ahyoud) and A.A.; writing—original draft preparation, S.A. (Sanae Azizi), S.A. (Saida Ahyoud), L.C.; writing—review and editing, S.A. (Sanae Azizi), L.C., S.A. (Saida Ahyoud), G.Z. and A.A.; visualization, S.A. (Sanae Azizi), L.C.; supervision, L.C., A.A.; project administration, L.C., A.A.; funding acquisition, L.C. All authors have read and agreed to the published version of the manuscript.

**Funding:** This research was funded by PHC Maghreb 2020 “MELINA” (Mastering Efficient Lighting in North Africa), grant number 43981ZG—Campus France and supported by the French Ministry of Europe and Foreign Affairs and, in Morocco, by the Ministry of National Education, Professional Training, Higher Education and Scientific Research, in partnership with the National Center for Scientific and Technical Research (CNRST).

**Acknowledgments:** This work is granted by PHC Maghreb (Program Hubert Curien) MELINA (Mastering Efficient Lighting in North Africa) by the French Ministry of Europe and Foreign Affairs and supported by Campus France and, in Morocco, by the Ministry of National Education, Professional Training, Higher Education and Scientific Research, in partnership with the National Center for Scientific and Technical Research (CNRST).

**Conflicts of Interest:** The authors declare no conflict of interest. The funders had no role in the design of the study; in the collection, analyses, or interpretation of data; in the writing of the manuscript, or in the decision to publish the results.

## References

1. Haraz, O.M.; Mohamed, M.A.; Saleh, A.; Abdel-Razik, S. Design of a 28/38 GHz dual-band printed slot antenna for the future 5G mobile communication Networks. In Proceedings of the 2015 IEEE International Symposium on Antennas and Propagation & USNC/URSI National Radio Science Meeting, Vancouver, BC, Canada, 19–24 July 2015; pp. 1532–1533. [\[CrossRef\]](#)
2. Haraz, O.; Mohamed, M.A.; Ayman, E.; Abdel-Razik, S. Four-element dual-band printed slot antenna array for the future 5G mobile communication networks. In Proceedings of the 2015 IEEE International Symposium on Antennas and Propagation & USNC/URSI National Radio Science Meeting, Vancouver, BC, Canada, 19–24 July 2015; pp. 1–2. [\[CrossRef\]](#)
3. Büschel, W.; Viergutz, A.; Dachselt, R. Towards Interaction with Transparent and Flexible Displays. In Proceedings of the Workshop on ‘Displays Take New Shape: An Agenda for Interactive Surfaces’, Paris, France, 28 April 2013.
4. Guan, N.; Furuya, N.; Delaune, D.; Ito, K. Antennas made of transparent conductive films. *PIERS Online* **2008**, *4*, 116–120.
5. Sun, G.; Badar, M.; Qi, Z. A study of microstrip antenna made of transparent ITO films. In Proceedings of the 2014 IEEE Antennas and Propagation Society International Symposium (APSURSI), Memphis, TN, USA, 6–11 July 2014; pp. 1867–1868. [\[CrossRef\]](#)
6. Saberlin, J.R.; Furse, C. Challenges with Optically Transparent Patch Antennas. *IEEE Antennas Propag. Mag.* **2012**, *54*, 10–16. [\[CrossRef\]](#)
7. Outerelo, D.A.; Alejos, A.A.; Sanchez, M.G.; Isasa, M.V. Microstrip antenna for 5G broadband communications: Overview of design issues. In Proceedings of the 2015 IEEE International Symposium on Antennas and Propagation & USNC/URSI National Radio Science Meeting, Vancouver, BC, Canada, 19–25 July 2015; pp. 2443–2444. [\[CrossRef\]](#)
8. Upadhyaya, T.; Arpan, D.; Riki, P.; Upesh, P.; Kanwar, P.K.; Killol, P. Compact transparent conductive oxide based dual band antenna for wireless applications. In Proceedings of the 2017 Progress in Electromagnetics Research Symposium-Fall (PIERS-FALL), Singapore, 19–22 November 2017; pp. 41–45. [\[CrossRef\]](#)
9. Desai, A.; Trushit, U.; Merih, P.; Riki, P.; Upesh, P. Dual band optically transparent antenna for wireless applications. In Proceedings of the 2017 IEEE Asia Pacific Microwave Conference (APMC), Kuala Lumpur, Malaysia, 13–16 November 2017; pp. 960–963. [\[CrossRef\]](#)
10. Katsounaros, A.; Hao, Y.; Collings, N.; Crossland, W.A. Optically Transparent Ultra-Wideband Antenna. *Electron. Lett.* **2009**, *45*, 722–723. [\[CrossRef\]](#)
11. Peter, T.; Yuk, T.I.; Nilavalan, R.; Cheung, S.W. A novel technique to improve gain in transparent UWB antennas. In Proceedings of the 2011 Loughborough Antennas & Propagation Conference, Loughborough, UK, 14–15 November 2011; pp. 1–4. [\[CrossRef\]](#)
12. Peter, T.; Tharek, A.R.; Cheung, S.W.; Rajagopal, N.; Hattan, F.A.; Antonio, V. A Novel Transparent UWB Antenna for Photovoltaic Solar Panel Integration and RF Energy Harvesting. *IEEE Trans. Antennas Propag.* **2014**, *62*, 1844–1853. [\[CrossRef\]](#)
13. Hakimi, S.; Sharul, K.A.R.; Mohammad, A.; Noghabaei, S.M.; Khalily, M. CPW-Fed Transparent Antenna for Extended Ultrawideband Applications. *IEEE Antennas Wirel. Propag. Lett.* **2014**, *13*, 1251–1254. [\[CrossRef\]](#)
14. Tighezza, M.; Rahim, S.K.A.; Islam, M.T. Flexible Wideband Antenna for 5G Applications. *Microw. Opt. Technol. Lett.* **2018**, *60*, 38–44. [\[CrossRef\]](#)

**Publisher’s Note:** MDPI stays neutral with regard to jurisdictional claims in published maps and institutional affiliations.



© 2020 by the authors. Licensee MDPI, Basel, Switzerland. This article is an open access article distributed under the terms and conditions of the Creative Commons Attribution (CC BY) license (<http://creativecommons.org/licenses/by/4.0/>).



Article

# Design and Development of a Low-Cost Automated All-Terrain Intelligent Robotic Vehicle for Detection to Study Its Faults and Vulnerabilities from SWOT Perspective <sup>†</sup>

Florin Covaciu <sup>1</sup>, Persida Bec <sup>2</sup> and Doru-Laurean Bâldean <sup>1,\*</sup> 

<sup>1</sup> Design Engineering and Robotics Department, Faculty of Machines Building, Technical University of Cluj-Napoca, 103-105 Muncii, 400641 Cluj-Napoca, Romania; florin.covaciu@muri.utcluj.ro

<sup>2</sup> Ethics of Vulnerabilities Group, Faculty of Philosophy, Babes-Bolyai University, Kogălniceanu 1, 400084 Cluj-Napoca, Romania; bec.persida@gmail.com

\* Correspondence: doru.baldean@auto.utcluj.ro or dorubaldean@yahoo.com; Tel.: +40-26-420-2790

<sup>†</sup> Presented at the 14th International Conference INTER-ENG 2020 Interdisciplinarity in Engineering, Mureş, Romania, 8–9 October 2020.

Published: 18 December 2020

**Abstract:** This scientific article highlights the development of an all-terrain intelligent robotic vehicle (ATIRV) platform, its overall structure, virtual modeling and simulation programs (such as Unity 5), electronic controls, and corresponding modules. This paper also shows the physical structure developed for the all-terrain intelligent vehicle and some of its components, which allow other modern robotic vehicles to operate autonomously and automatically in uncharted and dangerous environments. The practical part of the project has been developed by using state-of-the-art features like tele-metrics, tele-operation, drive assist modules, and autonomous navigation using the physical model of the all-terrain intelligent vehicle as structural model in the research experiment and for validating the initial hypothesis (of automatic ATIRV). Other scientific contributions consist in the determination of operational (kinematic and dynamic) parameters. Their comparison with reference values guides the paper's discussions and conclusions.

**Keywords:** automation; intelligent systems; design; manufacturing; robotic vehicles; vulnerability

## 1. Introduction

Design and development, supported by computational power, are already applied in the optimization of robotic systems [1]. Hazardous environments involve the usage of robotic applications for the detection of combat-mines, explosives, and dangerous materials to save lives and to protect the health of civilians and personnel engaged in decontamination. Applied solutions concerning robotic systems for quasi-autonomous inspections [2], dangerous material detection/measurement [3], harshness assessment [4], personal safety [5], automated controlled vehicles [6], and Strengths, Weaknesses, Opportunities, and Threats (SWOT) analysis of the development processes [7] have been partially approached, and applied in laboratory research. They also have been field-tested in given conditions to some extent [8,9]. Dangerous fields, such as postwar areas, roads, agricultural terrains, and accident sites with fatal casualties, are seen to be the beneficiaries of remotely controlled robotic applications. If combat-mines or sharp or cutting metals exist in the surface soil, then that field has a high degree of risk potential in other civil applications (injury may occur and fatalities and bodily integrity threats are possible). Analyzing applied data from cross-sectional testing of operational parameters is a request in the fields of vehicle use, terrain exploration, and other utility equipment [10].



Studies of smart control of the operational systems installed on the utility vehicles [11], and the optimal planning of displacement, in the case of mobile robots, using mathematical algorithms [12] as well as Arduino and other platforms [13–15], were applied for specific propulsion and robot-in-the-loop coordination [16]. Resource protection and security are two of the main objectives for these kinds of developments. Enhanced power sources are a key factor [17] for autonomous robotic vehicles [18] in hazardous scenarios [19].

The primary objectives of the present paper include designing an all-terrain intelligent robotic vehicle (ATIRV); developing a low-cost model for metal detection; studying the faults, challenges, and vulnerabilities of the laboratory model; extending the capabilities of the laboratory work to the real-size vehicle; and presenting the first test results. The ATIRV design process, development, and testing sequences cover aspects regarding multiple operating modes (such as accelerate, drive, brake, decelerate, and detect), as well as engineering innovation solutions for reaching the primary objective of research. This research addresses problems and aspects related to designing, programming, sensor installation, remote digital management, vehicle electronic control, actuator structures, and multiple practical testing (both in laboratory conditions with a low-cost mini-model and in the field scenario with a real-size all-terrain vehicle). These scenarios have been made to verify the physical platform and the predefined algorithms for automated driving. Challenges, faults, and vulnerabilities of the robotic models were also closely monitored during the design and development process. The intelligent components installed in this application consist in fuzzy regulators which are used in the vehicle's control part. First, a virtual reality model for an experimental mobile robot with field exploration and detection capabilities was created. Second, the mini-model for laboratory testing was realized. The third phase presented the real-size vehicle dynamic field testing in which the programming and digital control were applied to an actual All-Terrain Vehicle (ATV) for data recording and scientific study of the problem. The main tasks of ATIRVs are field exploration and the detection of metal objects (like combat-mines).

## 2. Materials and Designing Method

The applied scientific work is supported by an adaptable design of an automated robotic all-terrain vehicle that is designed to detect specific objects in broken or hazardous terrains. Considering these aspects is a quite often debated and defined problem in robotics and mechatronics, especially when high mobility or autonomy is required. Significant demands for this kind of robotic applications are also taken into consideration in domains regarding victim assistance, complex fires, atomic hazards, and space exploration. During the sequence of ATIRV designing and project development, engineering-specialized programs (such as Unity 5, MATLAB/Simulink, AutoCAD, and SolidWorks) were used to study both the one-degree model and the all-terrain-wheeled robot with mathematical equation systems.

A series of calculations and programming were done to determine and control the operational dynamic parameters related to robotic vehicles by using a digital platform. A simple diagram with the connections of the components is shown in Figure 1.

Virtual reality (VR) is the cutting edge of technology development. Using VR tools facilitates the experimentation of a new reality (that does not exist in material world). It is used in important applications (such as the ones mentioned and proposed in the present paper). Part of the design for ATIRVs is supported by the Siemens NX program. In the first place, the robot's platform was generated. This was provided with "home position" for the robotic arm, headlights, energy source, and antenna. After the virtual creation of the robot's platform, the wheel train was designed. Then the components were assembled and a format conversion was made to facilitate implementation in the virtual reality. After the 3D construction and virtual modeling of the mobile robot, it was imported into the Unity 5 environment, which supports specific formats and extensions such as "3ds", "dae", "dxf", "fbx", "obj", and "skp". The next step was to assign material properties to the components of the mobile robot in the Keyshot program. The main challenge was the size of the resulting file, which was considerably large. Due to the problems in using such a volume-demanding format, the alternative

3ds Max program became appealing. This software solution allowed complex 3D modeling, animation, rendering, and graphical composition in motion. All the components must be verified in 3ds Max to have a correct load. Other faults and challenges were found in the fact that the 3ds Max program did not keep the restraints from Siemens NX. The positions of the axles were, at this point, misplaced. Beside all the designing process, one specific innovation was the solution for aligning all the axles in the correct positions. We assigned coordinates to each part of axis. Then we replaced all the axles of components according to the topological data from Siemens NX, obtaining in this manner the correct positions of the corresponding components. This was done by selecting the specific part from 3ds Max, entering the pivot menu, and changing the axis position. After assigning physical material to each component, the importation process needed to be realized into the Unity 5 application.

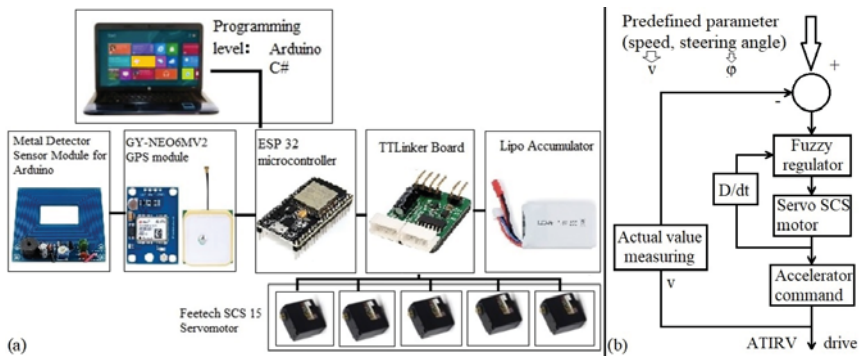


**Figure 1.** Simplified structure of the physical components (a) and the control algorithm (b) for all-terrain intelligent robotic vehicles (ATIRVs).

An important step in the design and virtual development of the ATIRV consisted in material assignment and rendering from wireframe and coating parameter definition, as shown in Figure 2.

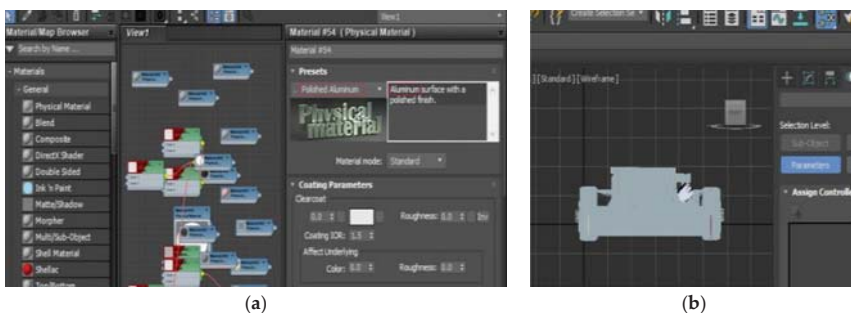


**Figure 2.** Virtual modeling with material map browser: (a) assigning materials to virtual components; (b) rendering of robotic vehicle from wireframe after the components were “materialized”.

The Unity 5 environment is used for 3D games and VR simulators, allowing 3 programming codes (C#, JavaScript, and Boo) and exporting capabilities for multiple operating systems. Prior to ATIRV import into the Unity 5 application, a textured environment was generated using the Gaia program, which allows the creation of vegetation, water, and rocks (of different sizes and shapes), as shown in Figure 3.



**Figure 3.** Virtual modeling of the sustaining environment in the Gaia program for implementation into Unity 5.

The Unity 5 application may be generated for different types of operating systems (Android, iOS, Linux, Mac, PC, PS4, Xbox, etc.), as shown in Figure 4.



**Figure 4.** Importing the Gaia environment in Unity 5 and the Operating System (OS) selection.

With the support of the developed virtual model, a laboratory mobile mini-robot was realized to test similar features, such as detection and exploration, for the ATIRV. The software application facilitated the virtual modeling of different robotic mechanisms. Robotic design allowed an improved control of the automation suitable processes. The design and development of the lab model was strongly facilitated by the virtual construction of the automated vehicle. The virtual model may be designed and simulated on the same computer station, but the physical model has two distinctive control units, one being the server (at the programming level) and the other being the client Espressif Systems Part (ESP 32 micro-controller).

The electronic control unit acquires all the signals and information from the transferring module once the transfer procedure is complete and will send the signals toward the powertrain assembly to drive the ATIRV to the new defined location. In relation to the physical road track, the method of detecting and following the magnetic material lane is very efficient and reliable in this type of robotic application for reaching the expected outcome and proper results. The optimal driving track lane is realized when taking into consideration all the aspects and vulnerabilities that may occur. The ATIRV was a battery-propelled electric vehicle which could charge with electricity automatically. To improve the ATIRV operational performance, inductive power transfer methods were applied.

Material components used by the present work consist in electronic software programs, command units, and physical actuators for controlling the automated vehicle (specific data regarding technical features are offered in Table 1).

**Table 1.** Specific data regarding the robotic vehicle materials used for research.

Programming Level	Command Level	Actuator Level
Operating system	Metal detector	Feetech
Arduino	GPS module; TTLinker Board	SCS 15
C++	ESP 32; Lipo Accumulator	Servomotor

### 3. Development and Results

Proximity sensing transducers were installed in the robotic ATIRV driveway in order to gain information about the vehicle's surrounding obstacles, kinetic actions, distances, and empty paths, the kinds of data which practically impose the starting and stopping sequences. Photometric transducers were set up to gain information concerning obstacles or objects on the track. A predefined object detection module was also provided, and a physical transfer system facilitated detection and deactivation of hazardous materials with a package of special mechatronic equipment, in which all electric and electronic connections were interdependent.

The first phase of development consisted in design, calculus of dimensions, and virtual development using Computer Aided Design (CAD) tools, as shown in Figure 5.

The second important phase consisted in material acquirement and wire connections. Electronic circuits and sensor connections were made to develop the detection system, which was provided with LED signaling lamp 1, for object presence, and signal amplifier 2, as shown in Figure 6.

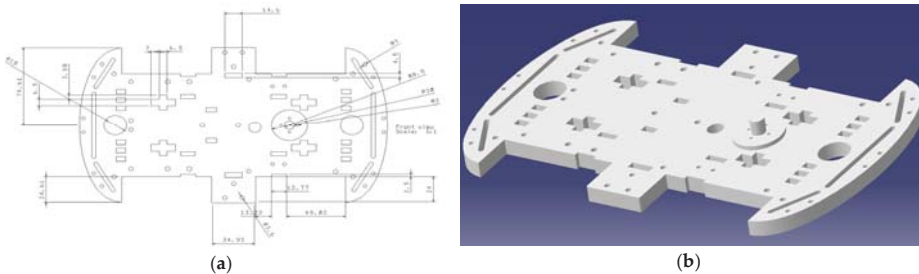


**Figure 5.** Virtual model of the platform for mini robotic vehicle: (a) 2D drawing of the robot platform; (b) 3D model of ATIRV main platform based on a commercial kit of 4-wheeled remote controlled car.

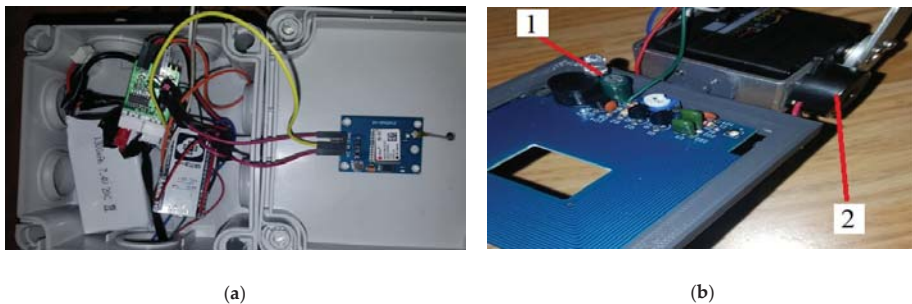


**Figure 6.** Electronic connection between the GPS module and the microcontroller, as well as additions to the metal sensor: (a) wiring of the GPS structure with the microcontroller board; (b) detector.

The third phase of the design and development process consisted in vehicle assembly (servomotor 1, TTLinker board 2, conversion board 3) and detection testing. For the power supply of the robot, a Lipo 7.4 V/1300 mA accumulator 4 was provided. The hardware structure was manufactured and assembled for ATIRV complete development and for power supply testing, as shown in Figure 7.

A switch was added to turn the robot on whenever required and to turn it off when the detection task was completed, for energy conservation in the accumulator. One fault of the GPS module, which was outlined during the tests, consisted in the duration of about 15 min it took to establish satellite connection outdoor. Indoor, the connecting process became even harder, and it could take up to one hour. This made robot testing a challenge because we had to make the connection first, prior to running the detection program. In light of the above-mentioned problem, the robot's antenna was

installed above the plastic case of the electronic components, to facilitate satellite connection, as shown in Figure 8.

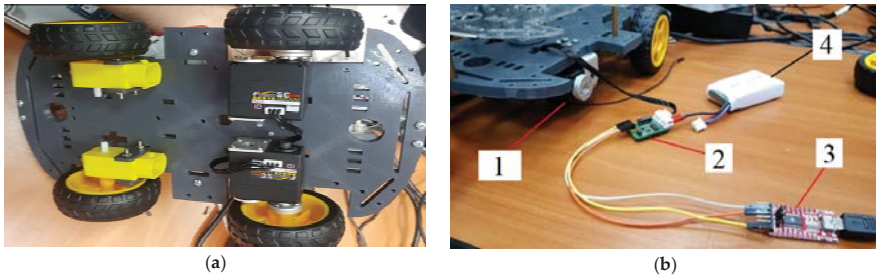


**Figure 7.** Platform development of an automated all-terrain digitally controlled vehicle for detection: (a) basic platform assembly; (b) testing of energy supply system and digital command.

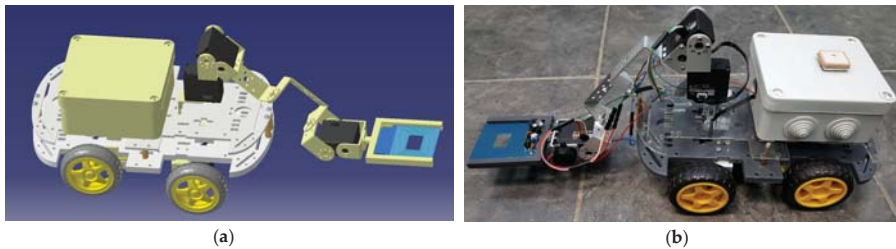


**Figure 8.** All-terrain intelligent robotic vehicle model for detection ready for testing and optimization: (a) virtual model; (b) laboratory prototype model for testing and development.

The hardware platform we received with the Arduino kit and initially used had some major issues, a fact which contributed to the personalized design of the mobile robot. Thus, additional pockets were created in the platform to attach the servomotors for the front D65X28 wheels. Another adjustment we had to make was the creation of a section where we could attach the robotic detector tool, since the standard design version of the kit did not include such equipment. The final challenge was the acrylic plastic material of structural platform from the standard assembly because it would collapse under the weight and stress of the detector equipment. The power consumption was calculated using Equation (1).

Using a software interface, the user can define specific IDs to each servomotor. The default ID is 0. To change the ID with this program the “unlock” checkbox on top must be clicked, the ID value in the corresponding field written, “set” pressed, and then “WRITE” hit. Additionally, the servo type may be set to servo-mode or to wheel mode, and many other pre-testing specifications may be set, by using script-fields and selection boxes for data input, as shown in Figure 9.

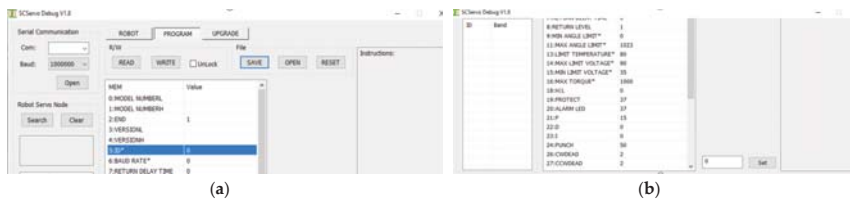


**Figure 9.** Feetech FD-v1.8 software application: (a) defining the ID of servo motor; (b) menu for kinematic and dynamic parameters definition.



Microsoft Visual Studio 2017 was used for the design and development of the graphical user interface with map display system and client-server communication, as shown in Figure 10.

The server in this case is on the PC station inside the control room and the client is on the mobile robot that is remotely driven through the smart application.



**Figure 10.** User-adapted graphic interface and the communication tool between the client and server: (a) coordinates definition; (b) data saving tool in the user interface and map location monitoring.

For experimental testing of the proposed idea was considered a research-prepared ATIRV, as shown in Figure 11.

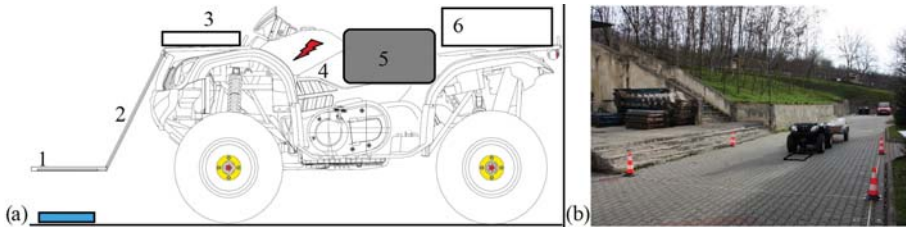


**Figure 11.** Simplified schematic (a) of the experimental proposed ATIRV (b) consisting of the following main components: (1) front sensor; (2) sensor support; (3) conversion board and wire assembly box; (4) experimental configured ATIRV; (5) GPS module safety box; (6) accumulator safety box.

The hardware assembly we received with the experimental ATV kit and first used in testing had multiple major issues, a fact which contributed to the specialized design of the ATIRV. Thus, additional components were created and placed in the front of the vehicle to attach the metal detecting sensor, the wiring box, the GPS protection case, and the accumulator safety cover. Additionally, the ABS (Antilock Braking System) needed to be programmed as BAS (Braking Assist System) to improve stopping control of the wheels. Another contribution we had to make consisted of an adjustment where the metal detector sensor was attached, since the standard design version of the kit did not include such equipment. After solving the practical challenges, tests were performed.

During the experimental testing, kinematic data were obtained by using GPS data and acceleration sensor, which are significant data of ATIRV operation.

Longitudinal accelerations and speed variations on horizontal terrain were graphically represented for two distinctive testing scenarios ((a) without any added load; (b) with a load of 1000 N), as shown in Figure 12.

The actual values obtained in the process of experimental testing of the practically prepared ATIRV, without any added load, are offered in Table 2.

The real values gained in the process of experimental testing of the practically configured ATIRV, with 1000 N added load, are offered in Table 3.

The required power was defined using the following mathematical model to gain values:

$$P = F_i \cdot v \cdot k, \tag{1}$$

where  $P$  is power consumption;  $F_i$  is inertial force, in Newtons;  $v$  is speed; and  $k$  is correction factor ( $k = 1.5$ ).

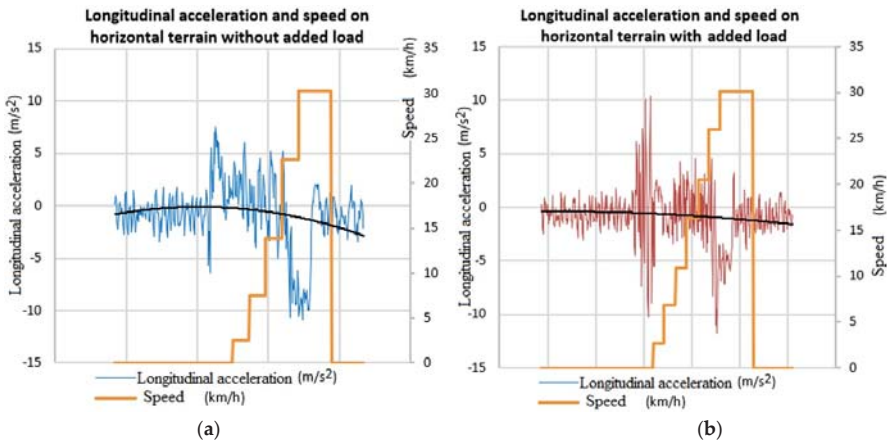


**Figure 12.** Graphics for longitudinal accelerations and speeds for the ATIRV in practical testing conditions: (a) without any attached load on the vehicle; (b) with 1000 N load attached on the vehicle.

**Table 2.** Real values gained in practical testing of the experimental ATIRV without added load.

Road's Configuration, [-]	Surface, [-]	Speed, [km/h]	Max. Deceleration, [m/s <sup>2</sup> ]	Max. Acceleration, [m/s <sup>2</sup> ]
Horizontal terrain	Irregular surface	10	11.42	10.91
		20	10.21	09.48
		30	08.82	08.55

**Table 3.** Actual values recorded in practical tests of the experimental ATIRV with added load.

Road's Configuration, [-]	Surface, [-]	Speed, [km/h]	Max. Deceleration, [m/s <sup>2</sup> ]	Max. Acceleration, [m/s <sup>2</sup> ]
Horizontal terrain	Irregular surface	10	12.22	09.92
		20	11.19	08.47
		30	09.52	07.91

#### 4. Discussions and Conclusions

One of the significant innovative contributions of the present research consists in the physical developed vehicle, which is highly adaptable and has a great degree of flexibility, thus making it suitable to be implemented in multiple robotic applications and automotive architectures. The connectors, communication pathways, technical vulnerabilities, and safety aspects were also considered and evaluated. This work presented the design and results of control protocol for an all-terrain intelligent vehicle robot which may be applied in a multitude of scenarios, such as surveillance, hazardous transports, and metal detection, in both muddy and snowy surfaces. The ATIRV was designed to be electrically powered from a rechargeable battery package (to be used with a solar photo-voltaic panel charger) and most of the implemented actuators were electric motors. All the latter components were electronically controlled by integrated microprocessors monitored by the vehicle's control unit. The ATIRV was equipped with eight high-resolution digital camera sensors, 3D scanners with laser technology, a special Inertial Control Unit (ICU), a digital compass, a GPS unit, a radio transceiver kit, and long-range wireless communication capability. The primary model of the ATIRV focused on

first-level objectives such as specific detection, 3D all-terrain surveillance and mapping (on-road and off-road), basic driving styles, basic starting and stopping styles, avoiding obstacles like large rocks or stone blocks, and driving over off-road surfaces like highly fractured ground and hilly terrains. The detection tool performed specific maneuvers such as precise locating, searching, removing, or neutralizing if there were applied additional components. In relation to other research, such as on semi-autonomous robots [2], this was intended to perform fully automated, even if there was a limit regarding the complete automation of the experimental kit to the present moment.

Still, the know-how transfer from laboratory mini-model to the real-size field ATIRV was a significant challenge. It required a precise control of kinematics and dynamics of the robotic vehicle. The propulsion and the braking needed to be properly managed and precisely monitored. A display and graphic presentation [14] of the actual values were important in fast monitoring process.

Some descriptors in the process of designing the automated vehicle and from the SWOT analysis to study its faults and vulnerabilities are offered by Table 4.

**Table 4.** SWOT analysis descriptors used in faults-and-vulnerabilities mapping of the application.

Strengths	Weaknesses	Opportunities	Threats
Controllable memory	Storage volatility	Defining standards	Buffer failure
Remotely controlled	Complex protocols	Programming	Program hacks
Internet communication	Potential privacy risks	Extensive reach	Data leaks

Development and research of automatic ATIRVs, using VR simulation and laboratory models, has significant importance in automation and robotics, Computer Aided Design/Computer Aided Manufacturing/Computer Aided Engineering (CAD/CAM/CAE) integrated systems, sensing and control, information systems technology, advanced software technology, intelligent systems and technologies, parallel and distributed computing technology, automotive engineering and transportation due to improvement of road and traffic safety, data processing techniques, and operational reliability in the coming years. In the present case, the proposed and tested ATIRV with an automatic guided driving program had a metal object detection system placed in the front part, a powertrain, and a steering system inside the vehicle’s structure to drive it optimally in a given scenario. The researched robot in the present study was a customized all-terrain intelligent guided vehicle that had the capacity to detect magnetic materials, but it could also be reconfigured for other specialized tasks. The ATIRV robot acted and drove independently and automatically on its own data as soon as the program was downloaded inside the electronic control unit. The electronic control unit was used for both powertrain and detecting system, which were interconnected. The electronic control unit drove the robotic vehicle and sustained the working process of the automated ATIRV. Compared to Havlik’s robotic tools for de-mining operations, the present work is still a progressing project, but there are some expectations for development.

**Author Contributions:** Conceptualization, F.C. and D.-L.B.; methodology, D.-L.B.; software, F.C.; validation, P.B., D.-L.B., and F.C.; formal analysis, D.-L.B.; investigation, P.B.; resources, P.B.; data curation, D.-L.B.; writing—original draft preparation, F.C.; writing—review and editing, D.-L.B.; visualization, D.-L.B.; supervision, P.B.; project administration, D.-L.B.; funding acquisition, P.B. All authors have read and agreed to the published version of the manuscript. Authorship must be limited to those who have contributed substantially to the work reported.

**Funding:** This research project was co-funded by the European Social Fund.

**Acknowledgments:** This paper was supported by the “Entrepreneurial competences and excellence research in doctoral and postdoctoral programs—ANTREDOC” project, co-funded by the European Social Fund.

**Conflicts of Interest:** The authors declare no conflict of interest.



## References

1. Aboulissane, B.; Haiek, D.; Bakkali, L.; Bahaoui, J. On the Workspace Optimization of Parallel Robots Based on CAD Approach. *Procedia Manuf.* **2019**, *32*, 1085–1092. [CrossRef]
2. Alejo, D.; Mier, G.; Marques, C.; Caballero, F.; Merino, L.; Alvito, P. SIAR: A Ground Robot Solution for Semi-autonomous Inspection of Visitable Sewers. In *Advances in Robotics Research: From Lab to Market*; Grau, A., Morel, Y., Puig-Pey, A., Cecchi, F., Eds.; Springer: Berlin/Heidelberg, Germany, 2020; Volume 132, pp. 275–296.
3. Andrei, L.; Băldean, D.; Borzan, A.I. Applied Measurements and Instrumentation for Improving Diagnostic Devices and Systems in Metropolitan Polluted Environments with Nitric and Carbon Oxides. In Proceedings of the 6th International Conference on Advancements of Medicine and Health Care through Technology, Cluj-Napoca, Romania, 17–20 October 2018; Vlad, S., Roman, N., Eds.; Springer: Berlin/Heidelberg, Germany, 2019; Volume 46, pp. 45–49. [CrossRef]
4. Băldean, D. Comparative Analysis of Three Distinct Porsche Models Concerning N.V.H. Aspects. In Proceedings of the 30th SIAR International Congress of Automotive and Transport Engineering, Craiova, Romania, 22–25 October 2019; Volume 1, pp. 209–213. [CrossRef]
5. Baldean, D.L.; Covaciu, F. Developing the communication of autonomous vehicles controlled with the aid of artificial intelligence for person and capital safety. In *Safety of the Person and the Construction of Social Capital*; Nechita Iancu, E.-A., Ed.; Universul Juridic: Arad, Romania, 2020; Volume 1, pp. 478–484. ISBN 978-606-39-0579-7.
6. Baldean, D.-L.; Covaciu, F.-A. Robotic Art in Creation and Development of Innovative Shapes and Programs for Automated Driven Cars with Artificial Intelligence. *J. Soc. Media Inq.* **2020**, *2*, 22–39. [CrossRef]
7. Bec, P.; Borzan, A.I.; Frunză, M.; Băldean, D.L.; Berindei, I. Study of Vulnerabilities in Designing and Using Automated Vehicles based on SWOT method for Chevrolet Camaro. In *IOP Conference Series Materials Science and Engineering*; IOP Publishing: Bristol, UK, 2020; Volume 898.
8. Borzan, A.I.; Băldean, D. Application of advanced engineering methods in studying a road traffic event between a 12-wheeler truck and a small tourism in a local junction from Cluj-Napoca. *Univ. Pitesti. Sci. Bull. Automot. Ser.* **2017**, *27*, 97–106. [CrossRef]
9. Borzan, A.-I.; Băldean, D. The Development of a New Interface for Intelligent Control of Energy Supply in Dynamic Environment with Process Digitization. *Procedia Manuf.* **2020**, *46*, 914–921. [CrossRef]
10. Cărăușan, H.; Baldean, D.-L.; Borzan, A.-I. Analysis of Experimental Cross-Sectional Tests by Telemetry of Load Parameters in Relation to the Charge on a Mitsubishi Lancer. In *National Bibliometric Instrument*; IDSI: Chisinau, Moldova, 2018; Volume 51, pp. 217–220. Available online: [https://ibn.idsi.md/sites/default/files/imag\\_file/217-220\\_4.pdf](https://ibn.idsi.md/sites/default/files/imag_file/217-220_4.pdf) (accessed on 10 June 2020).
11. Chereches, I.A.; Baldean, D.-L.; Borzan, A.-I. Research of Intelligent Control of Injection Systems for Subaru Competition Car. In Proceedings of the 30th SIAR International Congress of Automotive and Transport Engineering, Proceedings of the SMAT 2019, Craiova, Romania, 23 October 2019; Dumitru, I., Covaciu, D., Racila, L., Rosca, A., Eds.; Springer: Berlin/Heidelberg, Germany, 2020; pp. 82–87. [CrossRef]
12. Haiek, D.; Aboulissane, B.; Bakkali, L.; Bahaoui, J. Optimal Trajectory Planning for Spherical Robot Using Evolutionary Algorithms. *Procedia Manuf.* **2019**, *32*, 960–968. [CrossRef]
13. Havlik, S. Robotic tools for de-mining and risky operations. In *Using Robots in Hazardous Environments*; Woodhead Publishing: Sawston, UK, 2011; pp. 327–352.
14. Jovrea, S.; Băldean, L.D.; Borzan, I.-A. Researching on-board display of essential information concerning technical conditions in operation and fuel-economy of a motor-vehicle in operation. In *Science and Engineering*; AGIR: Bucharest, Romania, 2017; Volume 31, Available online: <https://stiintasiinginerie.ro/31-67> (accessed on 4 May 2017).
15. Oltean, S.-E. Mobile Robot Platform with Arduino Uno and Raspberry Pi for Autonomous Navigation. *Procedia Manuf.* **2019**, *32*, 572–577. [CrossRef]
16. Park, C.; Chung, S.; Lee, H. Vehicle-in-the-Loop in Global Coordinates for Advanced Driver Assistance System. *Appl. Sci.* **2020**, *10*, 2645. [CrossRef]
17. Yatimi, H.; Ouberrri, Y.; Aroudam, E. Enhancement of Power Production of an Autonomous PV System Based on Robust MPPT Technique. *Procedia Manuf.* **2019**, *32*, 397–404. [CrossRef]
18. Thrun, S. Toward robotic cars. *Commun. ACM* **2010**, *53*, 99–106. [CrossRef]

19. Autonomous Robot. Available online: [https://en.wikipedia.org/wiki/Autonomous\\_robot](https://en.wikipedia.org/wiki/Autonomous_robot) (accessed on 8 June 2020).

**Publisher's Note:** MDPI stays neutral with regard to jurisdictional claims in published maps and institutional affiliations.



© 2020 by the authors. Licensee MDPI, Basel, Switzerland. This article is an open access article distributed under the terms and conditions of the Creative Commons Attribution (CC BY) license (<http://creativecommons.org/licenses/by/4.0/>).



MDPI  
St. Alban-Anlage 66  
4052 Basel  
Switzerland  
Tel. +41 61 683 77 34  
Fax +41 61 302 89 18  
[www.mdpi.com](http://www.mdpi.com)

*Proceedings* Editorial Office  
E-mail: [proceedings@mdpi.com](mailto:proceedings@mdpi.com)  
[www.mdpi.com/journal/proceedings](http://www.mdpi.com/journal/proceedings)





MDPI  
St. Alban-Anlage 66  
4052 Basel  
Switzerland

Tel: +41 61 683 77 34  
Fax: +41 61 302 89 18

[www.mdpi.com](http://www.mdpi.com)



ISBN 978-3-0365-0717-0